Chemical Engineering Methods and Technology

Activated Carbon

Classifications, Properties and Applications



James F. Kwiatkowski
Editor

NOVA

CHEMICAL ENGINEERING METHODS AND TECHNOLOGY

ACTIVATED CARBON

CLASSIFICATIONS, PROPERTIES AND APPLICATIONS

No part of this digital document may be reproduced, stored in a retrieval system or transmitted in any form or by any means. The publisher has taken reasonable care in the preparation of this digital document, but makes no expressed or implied warranty of any kind and assumes no responsibility for any errors or omissions. No liability is assumed for incidental or consequential damages in connection with or arising out of information contained herein. This digital document is sold with the clear understanding that the publisher is not engaged in rendering legal, medical or any other professional services.

CHEMICAL ENGINEERING METHODS AND TECHNOLOGY

Additional books in this series can be found on Nova's website under the Series tab.

Additional E-books in this series can be found on Nova's website under the E-books tab.

MATERIALS SCIENCE AND TECHNOLOGIES

Additional books in this series can be found on Nova's website under the Series tab.

Additional E-books in this series can be found on Nova's website under the E-books tab.

CHEMICAL ENGINEERING METHODS AND TECHNOLOGY

ACTIVATED CARBON

CLASSIFICATIONS, PROPERTIES AND APPLICATIONS

JAMES F. KWIATKOWSKI
EDITOR

Nova Science Publishers, Inc.
New York

Copyright © 2012 by Nova Science Publishers, Inc.

All rights reserved. No part of this book may be reproduced, stored in a retrieval system or transmitted in any form or by any means: electronic, electrostatic, magnetic, tape, mechanical photocopying, recording or otherwise without the written permission of the Publisher.

For permission to use material from this book please contact us:
Telephone 631-231-7269; Fax 631-231-8175
Web Site: http://www.novapublishers.com

NOTICE TO THE READER

The Publisher has taken reasonable care in the preparation of this book, but makes no expressed or implied warranty of any kind and assumes no responsibility for any errors or omissions. No liability is assumed for incidental or consequential damages in connection with or arising out of information contained in this book. The Publisher shall not be liable for any special, consequential, or exemplary damages resulting, in whole or in part, from the readers' use of, or reliance upon, this material. Any parts of this book based on government reports are so indicated and copyright is claimed for those parts to the extent applicable to compilations of such works.

Independent verification should be sought for any data, advice or recommendations contained in this book. In addition, no responsibility is assumed by the publisher for any injury and/or damage to persons or property arising from any methods, products, instructions, ideas or otherwise contained in this publication.

This publication is designed to provide accurate and authoritative information with regard to the subject matter covered herein. It is sold with the clear understanding that the Publisher is not engaged in rendering legal or any other professional services. If legal or any other expert assistance is required, the services of a competent person should be sought. FROM A DECLARATION OF PARTICIPANTS JOINTLY ADOPTED BY A COMMITTEE OF THE AMERICAN BAR ASSOCIATION AND A COMMITTEE OF PUBLISHERS.

Additional color graphics may be available in the e-book version of this book.

Library of Congress Cataloging-in-Publication Data

Activated carbon : classifications, properties and applications / editor,
James F. Kwiatkowski.
p. cm.
Includes index.
ISBN978-1-62081-666-0 (eBook)
1. Carbon, Activated. I. Kwiatkowski, James F.
TP245.C4A36 2011
662'.93--dc22

2011001139

Published by Nova Science Publishers, Inc. † New York

CONTENTS

Preface		**vii**
Chapter 1	Environmental Applications of Activated Carbon and Carbon Nanotubes *A. R. Khataee, S. Aber, M. Zarei and M. Sheydaei*	**1**
Chapter 2	Catalytic Ozonation of Organics with Loaded Activated Carbon *Luo Hanjin and Rao Yifei*	**93**
Chapter 3	Surface Chemistry of Activated Carbons *Sónia A. C. Carabineiro, M. Fernando R. Pereira, José J. M. Órfão and José L. Figueiredo*	**125**
Chapter 4	Activated Carbons as Catalyst Supports *M. E. Gálvez, S. Ascaso, A. Boyano, R. Moliner and M. J. Lázaro*	**169**
Chapter 5	Conventional and Non-Conventional Thermal Processing for the Production of Activated Carbons from Agro-Industrial Wastes *Leandro S. Oliveira and Adriana S. Franca*	**205**
Chapter 6	Activated Carbons: Classifications, Properties and Applications *John U. Kennedy Oubagaranadin and Z. V. P. Murthy*	**239**
Chapter 7	Carbon Nanofibers: Synthesis, Types, Properties and Chemical Activation *Vicente Jiménez, Paula Sánchez, Mª Luz Sánchez, Antonio Nieto-Márquez, José Luís Valverde and Amaya Romero*	**267**
Chapter 8	Activated Carbon as a Metal Oxide Support: A Review *A. Barroso-Bogeat, C. Fernández-González, M. Alexandre-Franco and V. Gómez-Serrano*	**297**
Chapter 9	Using Activated Carbon from Bagasse for Color Removal *Paitip Thiravetyan and Parinda Suksabye*	**319**

Chapter 10 Use of Activated Carbon as Pre-Separation Agent in NAA of Selenium, Cobalt and Iodine **347**
M. Navarrete and T. Martínez

Chapter 11 Virtual Porous Carbon (VPC) Models: Application in the Study of Fundamental Activated Carbon Properties by Molecular Simulations **355**
Artur P. Terzyk, Sylwester Furmaniak, Piotr A. Gauden, Peter J. F. Harris, Radosław P. Wesołowski and Piotr Kowalczyk

Chapter 12 Activated Carbonaceous Materials Based on Thermosetting Binder Precursors **377**
J. Simitzis and Z. Ioannou

Chapter 13 Platinum Catalysts on Activated Carbon Supports Prepared from Mononuclear and Polynuclear Precursors: Influence of Porous Structure of the Support **393**
L. B. Okhlopkova and S. Yu. Troitskii

Chapter 14 Planting Soybean in Cd-, Cu-, or Zn-Contaminated Soils to Assess Its Feasibility in Further Producing Biodiesel **409**
Hung-Yu Lai, Bo-Ching Chen, Hsuen-Li Chen, Chih-Jen Lu and Zueng-Sang Chen

Chapter 15 Adsorptive Removal of Residual Sulfur Compounds in Commercial Fuel Oil by Means of Biomass-Derived Activated Carbons **421**
Seiji Kumagai

Chapter 16 Combination of Ozone and Activated Carbon for Water and Wastewater Treatment **433**
F. J. Beltrán and P. M. Álvarez

Chapter 17 Strategies for Optimizing the Development of Cellulose-Based Activated Carbon Cloths by the Chemical Activation Process **475**
M. E. Ramos, P. R. Bonelli and A. L. Cukierman

Chapter 18 Self Assembled Ordered Mesoporous Carbon: Synthesis, Characterization and Applications **509**
Dipendu Saha and Shuguang Deng

Index **539**

PREFACE

This new book presents topical research in the study of activated carbon, which includes topics such as the surface chemistry of activated carbons and as catalyst supports; thermal processing of activated carbons from agro-industrial wastes; activated carbon as a metal oxide support; Virtual Porous Carbon (VPC) models and combining ozone and activated carbon for water and wastewater treatment.

Chapter 1 – In the past decade, research and development in the area of environmental remediation processes have become tremendous. The tunable physical, chemical, and electrical properties of activated carbon and carbon nanotubes inspire innovative solutions to persistent environmental challenges. This book describes the environmental applications of activated carbon and carbon nanotubes. It begins with explanations about preparation methods of the activated carbon. Then, examples of early environmental applications of different activated carbons (e.g. powdered activated carbon (PAC), granulated activated carbon (GAC), activated carbon fibers (ACF), and impregnated carbon) have been discussed. Applications of carbon nanotubes in the fields of filtration, adsorption, electrochemical water treatment processes and photocatalysis are subsequently reviewed. Finally, adverse and side effects of application of activated carbon and carbon nanotubes are discussed.

Chapter 2 – It is important to increase the efficiency of producing hydroxyl radicals with ozone during the process of treating wastewater containing toxic and refractory organic pollutants. In the present study, nickel oxide-loaded activated carbon (NiO/AC) and copper oxide-loaded activated carbon (CuO/AC) were prepared with an incipient wetness impregnation method at low temperatures. The effectiveness for degradation of phenol and oxalic acid by the combination of NiO/AC or CuO/AC and ozone at different pH values and concentrations of tert-butyl alcohol (*t*-BuOH) was investigated. The composition and surface morphology of activated carbon (AC) and catalyst were characterized by XRD, SEM, BET and AAS, which showed that copper and nickel were loaded on the surface of AC in the form of rod-like copper oxide and nickel oxide. The specific, micropore, and external surface areas and micropore volume of Cu/AC and Ni/AC decreased by 50.7%, 62.9%, 34.8%, and 62.4% and 47.9%, 60.6%, 31.0%, and 60.7%, respectively. Compared to those of AC, in the systems of O_3/Cu/AC and O_3/Ni/AC, the mechanism of degradation of phenol and oxalic acid by ozone was achieved mainly by molecular ozone oxidation, while the mechanism with O_3/AC was primarily due to molecular ozone oxidation and absorption of AC. The removal efficiencies of phenol and oxalic acid by O_3/Cu/AC were 29% and 30.4% while those by O_3/Ni/AC were 52% and 59%. The efficiencies of both methods were higher than those by ozone only. The degradation process occurred during the formation of hydroxyl radicals and

the reaction of Cu/AC or Ni/AC with ozone demonstrates the strong synergy effect. The catalytic performance of Cu/AC and Ni/AC were stable, and both catalysts were reusable for further catalyzation.

Chapter 3 – Activated carbons have a disordered graphitic structure, which has been described as compared to to wrinkled paper sheets. The presence of heteroatoms (such as O, N, H, S, etc) bound to the edges of the graphene layers originates a variety of surface functional groups. Oxygenated functionalities have been most extensively studied, since they are formed spontaneously by exposure of the carbon material to the atmosphere; however, nitrogen, sulfur and phosphorous groups can also be found. The nature and concentration of surface functional groups may be modified by suitable thermal or chemical treatments. Treatments in the gas or liquid phase can be used to increase the concentration of surface groups, while heating under inert atmosphere may be used to selectively remove some of those functionalities. A variety of experimental techniques has been used to characterise functional groups, such as chemical titration methods, temperature-programmed desorption, X-ray photoelectron spectroscopy and infra-red spectroscopy methods. The results obtained by temperature-programmed desorption agree quantitatively with the elemental and proximate analyses of the oxidized materials, and qualitatively with the observations by infra-red spectroscopy. Some applications of functionalised activated carbons in adsorption and catalysis for several reactions are mentioned.

Chapter 4 – Among their many interesting applications, activated carbons have been considered over the last decades for their utilization in several processes involving heterogeneous catalytic reactions. In these processes the catalyst increases the reaction rate and controls the selectivity of the reactions involved towards the generation of desired products. Most of these catalysts consist of metals or metallic compounds supported on several materials which role is not only to maintain the catalytic phase in a well dispersed state but also affect the catalytic activity, by means of direct participation in any of the steps of the reaction mechanism, or by favouring the interactions between active phase and support. This participation and their interaction with the active phase make catalyst supports more than just simple active phase carriers.

Chapter 5 – Adsorption is currently the most prospective technology being used for the removal of organic and inorganic pollutants from waters and wastewaters. Although there are many adsorbents in use, activated carbon is the most widely used adsorbent for the removal of a variety of contaminants from waters. However, there is a major disadvantage associated with it, which is the strict necessity to regenerate the activated carbon, due to its inherent high cost, to allow for further use, thus, imparting additional costs to the adsorption process. Another negative aspect is the loss of adsorption capacity during the regeneration process which restricts its application even further. Although synthetic resins present a longer working life than activated carbons as adsorbents, their use is still costly for they also require regeneration after use. These aspects have greatly stimulated research interests into the production of alternative low-cost adsorbents to replace the costly activated carbons and synthetic resins. Attention has been focused on preparation and use of low-cost adsorbents, which present adequate adsorption capacities and are able to remove unwanted pollutants from contaminated waters without the need for regeneration and, thus, doing so at a low-cost. Industrial wastes and agricultural byproducts are classes of materials that are being considered the most promising precursors for the production of low-cost adsorbents for they are renewable, locally available in large quantities, inexpensive and require little processing

to turn them into activated carbons and increase their adsorption capacities toward a specific adsorbate (pollutant). The majority of potential precursor materials being studied is of biological origin and, thus, fit into the categories of carbonaceous or lignocellulosic materials. As such, these materials contain a variety of chemical functional groups at their surfaces (e.g., carboxylic, phenolic, amino and others) and upon thermal and chemical treatment these groups can be manipulated, transforming the material into a more functionally selective activated carbon. These surface modifications will contribute to a variety of adsorption mechanisms, such as chemisorption, complexation, ion exchange and others, depending on the possible spectrum of interactions between adsorbent and adsorbate. Thus, the objective of this essay is to present a critical overview on conventional and non-conventional thermal and chemical treatments that are being employed in the preparation of activated carbons using residues of biological origin as precursors, discussing their effects on both physical and chemical characteristics of the produced adsorbents and on the performance of the prepared activated carbon for the removal of wastewater pollutants.

Chapter 6 – Activated carbons are processed forms of carbon and are one of the most significant adsorbent materials due to their highly developed porosity, large surface area ranging from 500 to 3000 m^2/g, variable characteristics of surface chemistry, and high degree of surface reactivity. Most of the activated carbons are produced by a two-stage process, viz., carbonization followed by activation. The first-stage, carbonization, is to enrich the carbon content and to create an initial porosity and the second-stage, activation process, helps in enhancing the pore structure. Precursors to activated carbons are either of botanical origin (e.g., wood, coconut shells and nut shells) or of degraded and coalified plant matter (e.g., peat, lignite and all ranks of coal). Agricultural by-products are also considered as very important source material for the production of activated carbons as they are renewable and low-cost materials. Utilization of wastes as raw materials in the preparation of activated carbon is an interesting alternative to the expensive commercial activated carbons. Activated carbons may be obtained by physical activation (with steam or gaseous CO_2) or chemical activation by strongly reacting chemicals, such as $ZnCl_2$, H_3PO_4 and alkali-metal hydroxides (NaOH and KOH). Chemically activated carbons have good thermal stability, characteristic porous structure, and large internal surface area and porous volume. Activated carbons are classified in many ways, although a general classification can be made based on their physical characteristics, as powdered activated carbon, granular activated carbon, extruded activated carbon, impregnated carbon, polymer coated carbon and other types, such as cloths and fibers. They are used in specific applications. Powdered activated carbons are added directly to process units, granulated carbons are used for deodorization and for the separation of components in flow systems, extruded activated carbons are mainly used for gas phase applications, impregnated carbons are used for specific applications in air pollution control and polymer coated carbons are useful for hemoperfusion. Properties of activated carbon are: its specific surface area, iodine index, molasses index, tannin index, methylene blue index, butane index, carbon tetrachloride index, dechlorination half-value length, density, hardness number, ash content, porosity and particle size distribution. The indexes give an idea of the kind of pore a certain carbon has. Activated carbons are used in a wide range of applications that include medicinal uses, gas storage, pollutant and odor removal, gas separations, catalysis, gas purification, metal extraction, water purification, chromatographic separation, chemical purification, trapping mercury, fuel cells and many other applications. Carbon adsorption has numerous applications in industrial processes; such as spill cleanup,

groundwater remediation, drinking water filtration, air purification, volatile organic compounds removal, gasoline dispensing operations, and other processes. With the development of technology, the applications of activated carbons keep expanding, with newer applications such as super-capacitors, electrodes, gas storage, and so on. This chapter deals with a short review of preparation of activated carbons from various raw materials reported in published literature in the recent past. In this chapter the various classifications, significance of various properties and applications of activated carbons are treated in detail with cross reference to a number of relevant publications.

Chapter 7 – Carbon materials are found in a variety of forms such as graphite, diamond, fullerenes, carbon nanofibers (CNFs), and carbon nanotubes (CNTs). Within the five, the nanostructured carbon materials have sparked an increasing interest for chemists, physicists, and material scientists worldwide. Carbon nanofibers have been recently innovated due to their unique properties, which have generated an interest in applications, including selective adsorption, hydrogen storage, polymer reinforcement and catalysts support. To produce carbon nanostructures, three main techniques are generally used: arc discharge, laser ablation, and chemical vapor deposition. In general, chemical vapor deposition (CVD) results in carbon nanostructures that have a large diameter range, which can be poorly controlled. There are mainly three types of carbon nanofibers: the herringbone, in which the graphene layers are stacked obliquely with respect to the fiber axis; the platelet, in which the graphene layers are perpendicular to the fiber axis; and the ribbon, in which the graphene layers are parallel to the growth axis. High surface area, controlled pore size and pore size distribution are necessary for the application of those materials in a specific end use. Thus, the specific surface area and porosity of carbons nanofibers can be significantly modified by an activation process that removes the most reactive carbon atoms from the structure, increasing the surface area and porosity. The porous texture of the activated carbons depends strongly on both the activation process (chemical or physical) and the nature of the precursor. It has been shown that some experimental variables have great influences on the porosity of the activated carbons prepared by chemical activation: nature of the metal hydroxide, nature of the inert gas, the mass ratio activating agent/CNFs, activation temperature and time, and the inert gas flow rate during the carbonization.

Chapter 8 – There is increasing interest in semiconductor oxides supported on activated carbon because of their variety of applications, such as photocatalytic degradation of many pollutants in wastewaters, catalysis of important organic reactions, adsorption of inorganic ions and gas sensors. These oxides include TiO_2, Fe_2O_3, ZnO, SnO_2, WO_3 and Al_2O_3. Because of their applications, these materials have been widely studied and researched, specially the first one. This paper is a critical review of the published reports of the latest investigations for each of these materials. Particular attention is paid to the preparation methods, applications and results of the applications.

Chapter 9 – Activated carbons have always become interesting materials due to their continuous usages in many areas. These materials have been synthesized from many types of carbonaceous precursors. Formerly, coal has become the major precursor for activated carbon production. Since coal is more valuable to be used for energy generation, people started to study many type of biomass such as coconut shell as the precursors. The utilization of several type of biomass for activated carbon production has a positive impact in reducing organic solid wastes.

Chapter 10 – The position of pre-irradiation separations in neutron activation analysis is shortly discussed. Special attention is given to separations for purification and/or concentration of analyte elements, either complexed or uncomplexed, via sorption on activated carbon. It was shown for a number of trace elements that the blank value introduced due to the use of activated carbon is small or mostly even negligible. The NAA determination via pre-separations based on activated carbon is highlighted for selenium, cobalt and iodine.

Chapter 11 – Due to progress in the development of computers, molecular simulations have become the major theoretical technique in chemistry and physics. In the field of activated carbons the so called Virtual Porous Carbon (VPC) models are becoming more and more popular. As stated by Biggs and Buts (who are the authors of this term) "we use the term Virtual Porous Carbon (VPC) to describe computer-based molecular models of nanoporous carbons that go beyond the ubiquitous slit pore model and seek to engage with the geometric, topological and chemical heterogeneity that characterizes almost every form of nanoporous carbon. We differentiate these from the many other complex models that have been proposed for nanoporous carbons since the early 20th century by requiring them to be computer-based and, thus, open to further analysis or use in molecular simulations". Therefore, the major properties of VPC models are a well defined absolute (geometric) pore size distribution (PSD), as well as known chemical composition of carbon surface layer, exactly known density etc. It is obvious that a PSD, as well the chemical composition of the carbon surface determine adsorption properties from the gaseous phase as well as from solutions. Because the geometry of pores and the composition of surface layers are hard to determine in the case of real activated carbons the authors still use more or less trivial approaches (for example one can use the BET model for calculation of surface area or one can assume the slit - like pore geometry to calculate the PSD curve, or use the Boehm's titration method for calculation of surface functionalities concentration). All those properties and characteristics are well known for VPC. Moreover, in contrast to real experiments, we also know carbon ring statistics, the number of edge carbon atoms etc. Therefore using VPC models one can easily and systematically determine the influence of different factors on carbon adsorption properties, and then compare the results with experimental data. In this chapter the authors review recent progress in the field of simulation of gas and liquid adsorption on VPC models. The authors will start from two basic older VPC models i.e. the model proposed by Biggs et al. and the model proposed by Do et al. Next the authors will discuss the VPC model proposed, based on HRTEM measurements, by Harris et al. The authors will show that some empirically observed correlations that were not simply explained become clear if one performs a series of molecular simulations using those VPC models. The same can be stated about the methods of PSD curve calculation, or about the mechanisms of adsorption from liquid phase. The authors will demonstrate that the application of a simulation technique and VPCs leads to an explanation of the mechanism of phenol adsorption from aqueous solutions on activated carbons. In simulations which agree with the real experiment, introduction of oxygen groups on an activated carbon surface leads to a decrease in phenol adsorption, but because in the simulation the authors use well defined VPCs the authors can explain the reason of this decrease. Additionally in this chapter other examples of VPC application will be given and discussed.

Chapter 12 – There are many raw materials available for preparing activated carbons which can be divided into two kinds: a) grade low coal (such as peat and lignite), waste pulp solution, waste plastics and various agricultural by-products and b) synthetic resins and fibers.

Coal and lignocellulosic materials are the most commonly used starting materials for the production of commercial activated carbons (ACs). The latter are also prepared from various agricultural by-products and polymeric materials because of their low cost and high carbon yield. The pores in carbon materials play an important role in their functions and characteristics. Glass-like carbon (GC) is prepared by heat-treatment on thermosetting resins in inert atmosphere. They show various unique properties such as great hardness compared with other carbon materials and gas impermeability. Phenol-formaldehyde resins are being increasingly used to replace pitch as bonding agents for refractory materials. Starting from such precursors, various carbons in the form of fibers, particles, membranes and preforms have been produced. Carbonised phenolic resins are usually highly microporous, with the amount of open micropores passing through a maximum at a carbonisation temperature of 700 to 800 ^{o}C. Molecular sieving carbon (MSC) or carbon molecular sieves (CMSs) are carbonaceous adsorbents with almost uniform micropores of a few angstroms in diameter having the ability to selectively separate molecules, mainly of a gas mixture. Carbon molecular sieve membrane (CMSM) is usually prepared by carbonisation of polymeric films, which conducts to the formation of a thin carbon layer or thin film of CMS with pores smaller than 1 nm. In order to prepare CMSM, the polymeric precursor needs to have thermosetting property in order to avoid melting when heated and thus retain structure shape during heating and pyrolysis. Mesoporous carbons, due to their high surface area and periodic arrays of uniform pores, are utilized as catalysis and electrode materials for different purposes such as protection of environment and improvement of energy efficiency. Mesoporous carbons with high surface area, large porosity and fine electric-conductivity have been regarded as an advanced material for many potential applications in nanotechnology. Monomers such as furfuryl alcohol, acrylonitrile, and phenol-aldehyde monomers mixture were usually used as the precursors to prepare mesoporous carbons. Other carbonaceous forms includes carbon brushes prepared from proper thermosetting resin binder and monolithic activated carbons prepared from resin impregnated expanded graphite, from isotropic fibers or prepared as carbon aerogels. Nanostructured carbon materials are potentially of great technological interest for the development of electronic, catalytic and hydrogen-storage systems.

Chapter 13 – A number of catalysts have been prepared by adsorption of platinum precursors on activated carbons of different origin followed by reduction in flowing hydrogen. They were characterized by CO chemisorption, TEM and liquid-phase hydrogenation of cyclohexene. Porous structure of the support and the nature of platinum precursor proved to have a profound influence on the properties of catalysts. The metal dispersion of catalysts prepared from platinum (IV) chloride can be controlled in the range from 10 to 90%. Activity of the catalysts reached a maximum in the range of intermediate metal dispersion, with the limit being dependent on the support used. It has been suggested that a part of the supported metal became inaccessible to the organic substrate due to localization of metal particles in narrow pores of the support. The extent of blocking proved to be higher for highly dispersed Pt particles and on the supports with smaller pores. An alternative route to preparing supported Pt catalysts is the synthesis of polynuclear hydroxochloride complexes from Pt(II) chloride that is followed by their deposition on carbon. The catalysts prepared from polynuclear precursor showed high activity even in the range of high metal dispersion and for microporous carbons. Structure of product of Pt(II) chloride hydrolysis was established by means of NMR Pt, O.

Chapter 14 – There are many farmlands been contaminated with heavy metal (HM) in central Taiwan resulted from the irrigation using river water contaminated with HMs. According to the Soil and Groundwater Pollution Remediation Act (SGWPR Act) of Taiwan, these lands can not planting edible crops until suitable techniques are conducted to decrease the total concentration of HM in soils to conform to the Soil Control Standard (SCS). However, some of the foliar crops still accumulated high concentration of HM in the edible parts even the concentration of HM of the remediated sites is below the SCS. Planting suitable crop species is especially important in this situation and these contaminated sites after remediation can be reused. Soybean, a biomass crop further used to produce biodiesel, seems feasible to plant in the farmlands in this situation. This manuscript reports previous results used pot experiments to investigate the accumulation of HM by various parts of soybean planted in the artificially cadmium- (Cd-), copper- (Cu-), or zinc (Zn-) contaminated soils with different concentrations. The aim is to assess the feasibility of planting soybean in the HM-contaminated soils to produce biodiesel.

Chapter 15 – Micro- and mesoporous granular rice husk activated carbon (RHAC) and microporous granular coconut shell activated carbon (CSAC) were evaluated as adsorptive desulfurization agents to remove residual sulfur in forms of benzothiophenes (BTs) and dibenzothiophenes (DBTs) in commercial kerosene. Fixed-bed flow desufurization tests were conducted, providing the breakthrough curves for BTs and DBTs. The adsorption isotherms for BTs and DBTs were also obtained in a batch-mode, correlating with the results of the fixed-bed flow test. RHAC and CSAC are found to be useful to remove BTs and DBTs. RHAC showed a lower selectivity for DBTs and a higher selectivity for BTs than CSAC did. A larger adsorption capacity of DBTs in volume basis was observed on CSAC, which was attributed to its higher bed density, higher carbon content and larger volume of ultramicropores. Although RHAC had lower carbon content and smaller volume of ultramicropores, it showed a larger adsorption capacity of BTs and acceptable adsorption capacity of DBTs in volume basis. This was explained by a larger volume of mesopores contributing to efficient transportation of BTs and DBTs towards their adsorption sites of ultramicropores.

Chapter 16 – One the major problems wastewater and drinking water treatment plants, (WWTPs and DWTPs, respectively) will likely have to face in the near future is the removal of emergent contaminants coming from the abundant use of pharmaceutical and personal care products (PPCPs). These compounds, as well as others already catalogued as priority pollutants, are usually encountered in influents and effluents of WWTPs and even of DWTPs at low but potentially hazardous concentrations for humans and other living beings. It has been clearly established that many of these pollutants go through the classical primary and secondary treatments in water plants without being properly removed and only most costly tertiary treatments technologies are able to completely remove them from water. Among these treatments chemical oxidation, particularly advanced chemical oxidation (ACO), and activated carbon adsorption processes (ACAPs) present high efficiency to remove these pollutants. Also, among ACO processes, those involving ozone have already shown their applicability in this field.

Chapter 17 – The present chapter deals with strategies for optimizing the development of activated carbon cloths (ACC) through the chemical activation process with ortho-phosphoric acid solutions, as activating reagent, focusing on two unexplored cellulosic fabrics as precursors, denim and lyocell. The latter is a novel form of regenerated cellulose

manufactured from wood pulp by an environmentally-friendly process, and is commercialized through the brand Tencel®. The influence of main variables involved in the chemical activation process, acid concentration (5-15 %wt), temperature (600-950 ºC), thermal treatment time (0-3 h), and N_2 flow rate (100-300 mL min^{-1}), on yield and physico-chemical characteristics of the resulting ACC is examined. Characterization of the ACC is carried out by elemental analysis, total acidity determination, X-ray diffraction, N_2 (77 K) adsorption, and scanning electronic microscopy. Phosphoric acid impregnation of the precursors occasions significant modifications in their thermal behavior, as evidenced from dynamic thermogravimetic analysis of untreated and impregnated samples. It leads to shift thermal degradation onset and maximum rate to lower temperatures, and to increase residual weight fractions, their intensity depending upon the precursor and acid concentration. Despite substantial changes taking place during the activation process, all the ACC preserve the original structure of the fabrics and integrity of the constituting fibres. Process conditions affect appreciably elemental composition, crystalline structure, surface chemistry and textural properties of the resulting ACC. In particular, activation of denim demonstrates to promote formation of acidic functional groups on the surface of the resulting ACC, as evidenced from enhancement of total acidity. The effect of these functionalities, which are relevant to the potential use of ACC for toxic metals uptake from wastewater, is verified from assays involving Zn(II) ions removal from model dilute solutions. Among the process variables, the thermal treatment temperature exerts a key role on the development of the ACC. For both precursors, increasing the temperature leads to ACC of higher specific surface area and total pore volume, although at the expense of lower yields. Nevertheless, the Tencel-based ACC show a more pronounced development of porosity than those obtained from denim. At the highest temperature investigated (950 °C) and for the same acid concentration (10 wt%), keeping otherwise constant conditions, maximum values of 2011 m^2/g and 0.67 cm^3/g characterize the ACC developed from Tencel, whereas the ACC obtained from denim show maximum surface area and total pore volume of 1055 m^2/g and 0.53 cm^3/g, respectively. Moreover, although all the ACC are essentially microporous, those derived from Tencel show a pronounced development of a fairly narrow microporosity, suggesting that they are potentially suited for gaseous effluents treatment. Prolongation of the thermal treatment time induces an enhanced development of porous structures for the Tencel-based ACC, whereas increase of the gas flow rate leads to the opposite effect. The latter might be due to the relatively less oxidative activation atmosphere generated as a consequence of shorter residence times of the volatile compounds released. Overall, present results contribute to the tailoring of cellulose-based activated carbon cloths in terms of desired properties and/or specific end uses through the strategic selection of main variables involved in the chemical activation process.

Chapter 18 – Controlled and ordered mesoporosity in carbon-based materials has gained a lots interests and applications in the present technology. Conventionally, ordered mesoporous carbon was nanocasted by doping a suitable inorganic scaffold or template (mostly silica) with an organic carbon precursor followed by carbonization at high temperature. Due to the presence of several associated drawbacks of the nanocasting method, different researchers attempted to insert mesoporosity in carbon based materials without employing any inorganic scaffold. In this so called “soft template” or self-assembly process, an organic block copolymer has been employed as a structure dictating agent and a phenol-formaldehyde type of resin as carbon source held together by hydrogen bonding or

occasionally by with an external cross-linking agent. During carbonization, the resin converted to pure carbon where as the copolymer decomposes from the system leaving its contribution as the monitor of the structure of porosity in the resultant carbon. Pluronic P123, Pluronic F127 or polystyrene-*block*-ploy(4-vinylpyridine) are most common structure dictating copolymers where as phenol, resorcinol or phloroglucinol-formaldehyde resins are most widely used as a suitable source of carbon precursors. Literature value revels that these ordered mesoporous carbon possesses the BET specific surface area in the range of 280-1300 m^2/g based on the reagents and synthesis procedures. Depending on the processing and aging conditions, the morphology of OMC can be tuned within monolith, fiber or sheets in order to meet the specific demands of the applications.

In: Activated Carbon
Editor: James F. Kwiatkowski
ISBN: 978-1-61209-684-1
©2012 Nova Science Publishers, Inc.

Chapter 1

ENVIRONMENTAL APPLICATIONS OF ACTIVATED CARBON AND CARBON NANOTUBES

A. R. Khataee*, S. Aber, M. Zarei and M. Sheydaei
Department of Applied Chemistry, Faculty of Chemistry,
University of Tabriz, Tabriz, Iran

ABSTRACT

In the past decade, research and development in the area of environmental remediation processes have become tremendous. The tunable physical, chemical, and electrical properties of activated carbon and carbon nanotubes inspire innovative solutions to persistent environmental challenges. This book describes the environmental applications of activated carbon and carbon nanotubes. It begins with explanations about preparation methods of the activated carbon. Then, examples of early environmental applications of different activated carbons (e.g. powdered activated carbon (PAC), granulated activated carbon (GAC), activated carbon fibers (ACF), and impregnated carbon) have been discussed. Applications of carbon nanotubes in the fields of filtration, adsorption, electrochemical water treatment processes and photocatalysis are subsequently reviewed. Finally, adverse and side effects of application of activated carbon and carbon nanotubes are discussed.

1. INTRODUCTION

All the elements are important in the world but carbon is the most important one and has a vital role, because it is used widely in living tissues. Carbon can be called "living element" because it has a basic role in the life of all microorganisms, plants, animals, humans and any kind of living bodies. Carbon is cycled between living bodies and the other parts of the world. When a living organism is grown it consumes carbon for the construction of its body mass

* Corresponding author: Department of Applied Chemistry, Faculty of Chemistry, University of Tabriz, Tabriz, Iran, Tel: (+ 98) (411) (3393165), Fax: (+ 98) (411) (3340191), E-mail address: a_khataee@tabrizu.ac.ir (ar_khataee@yahoo.com)

and when it dies carbon gets back to the environment. So carbon is the source of life in the world. When elemental carbon atoms aggregate they can construct materials like carbon black (CB), activated carbon (AC) and carbon nanotubes (CNTs) that have their own characteristics and a wide range of applications. ACs are carbon structures with high porosity and surface area which capture the pollutants from surrounding environment, a process called adsorption. It is an effective technique for the remediation of the environment. The adsorption capacity of ACs is different according to the preparation method and the used precursors. CNTs are manufactured using special techniques and have a lot of different applications in the fields such as electronics, optics, materials science, and architecture. They can be used as field emitters, conductive plastics, conductive adhesives and connectors, thermal materials, structural composites, fibers and fabrics, catalyst supports, and for energy storage and biomedical applications. This book discusses the different aspects of ACs and CNTs majorly from the view point of environmental applications. In this book we present a detailed review of synthesis, properties and application of ACs and CNTs. At first we explain preparation methods of the activated carbons. Then, examples of early environmental applications of different activated carbons have been discussed. The next parts of this report are devoted to discussions on the properties and environmental applications of CNTs which include in: filtration, adsorption, electrochemical and photocatalytic water and wastewater treatment processes.

2. PREPARATION OF AC

Since increasing consumption of AC in industries, especially in wastewater treatment units, production of this adsorbent grows recently. In order to decrease the cost of AC production and applications, different works have been done including: production of AC with high adsorption ability and use cheaper precursors and methods.

Adsorption ability of AC is mostly affected by its surface area, porosity and surface functional groups. As can be seen in Figure 2.1, AC pores are classified into three basic groups including: pores with diameters less than 2 nm (micropores), pores with diameters more than 50 nm (macropores) and pores between these values (mesopores) [1]. Among ACs, micropore AC is the most effective adsorbent. AC with high micropores content shows large surface area and adsorption ability [2]. Analysis of N_2 adsorption/desorption isotherm at 77 K using Brunauer, Emmet and Teller (BET), Barrett, Joyner and Halenda (BJH) and micropore analysis (MP) methods is the common used test for determination of AC surface area and pores distribution. Infrared absorption spectroscopy is also used for determination of surface functional groups such as oxygen content on the surface of AC. In addition to these tests, CO_2 adsorption/desorption, iodine number, molasses number and methylene blue (MB) adsorption measurements are used for the determination of surface characteristics and adsorption ability of AC.

The AC preparation processes are categorized to physical, chemical and physicochemical activation methods [3]. The basic aim of all AC preparation methods is generation of pores with appropriate internal diameter and adsorption-effective chemical groups such as ketones, carboxyls, phenols, ethers, or lactones on the surface of AC [4]. In this section, the preparation methods of activated carbons are explained.

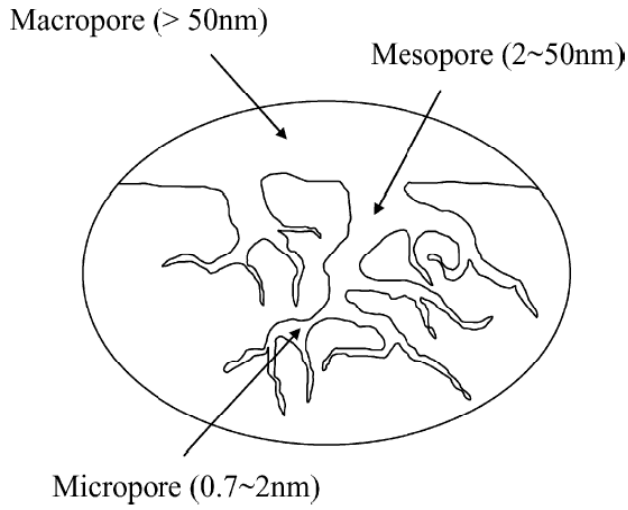


Figure 2.1. Pore structure of activated carbon. (Adapted from Eom et al. [1] with permission from publisher, Elsevier. License Number: 2567610963921).

2.1. Physical Activation

In physical activation method, gaseous agents such as CO_2, steam and air are used to generate pores on the surface of char. In the presence of these gaseous activation agents at high temperatures, some carbon atoms of char are oxidized and left the char surface, which lead to production of pores. Also some superficial carbon atoms of char are oxidized incompletely and converted to adsorption effective chemical groups [5, 6].

Using physical activation method, usually the AC is prepared in two steps. The first step is carbonization process. In this step the precursor is pyrolyzed at atmosphere of inert gases such as nitrogen or argon, which leads to formation of solid char as principal product. In addition to solid char, other solids, liquids and gaseous products are also produced [7, 8]. Depending on precursor, the temperature of pyrolyze is varied from 200 to 950 ^{o}C [9, 10]. In the case of precursors like nutshells, which have high contents of volatile compounds, removing of these compounds from surface of precursor needs a higher pyrolysis temperature [5]. As can be seen in Table 2.1, in some other matters such as rubber wood sawdust [10] and acrylic textile fibers [11], respectively low temperatures are adequate for removing the volatile compounds from surface. The obtained char surface became appropriate for reception of gaseous activation agents in activation step.

In the second step, the obtained char is activated in the atmosphere of CO_2, steam or other gaseous activation agents. In the presence of these gases, some of carbon atoms of char are oxidized. Complete carbon oxidation leads to pores development (decrease in C content) and partial oxidation leads to the generation of oxygen-containing functional groups on the surface of AC (increase in O content) [5].

In addition to prevalent two-step preparation methods, one-step process can be used for AC production via physical activation, too. In this process, the carbonization and activation are done simultaneously. One-step preparation process with steam activation is used for

production of AC from lignocellulosic materials such as apricot and cherry stones or almond, walnut and coconut shells, and grape seeds (see Table 2.1). One-step production process is simple and need short time and low energy in comparison with two-step one [12, 13]. Yang et al. [12] have prepared AC with BET surface area of 1410 $m^2 g^{-1}$ using one-step preparation using CO_2 procedure from coconut shells which is appropriate in comparison with other ACs.

AC characteristics are mostly specified by precursor nature, and carbonization and activation procedures variables. In the next sub-sections, effects of precursor, and carbonization and activation procedures on the final characteristics of AC are explained.

2.1.1. Effect of Precursor on AC Preparation

Precursor properties such as carbon content, availability, cost, mechanical properties and bulk density influences on AC characteristics [13]. Various natural and synthetic carbonaceous materials are used for preparation of AC such as: used tyres [14], peanut shells [15], rice straw [16], oil-palm-shell [17], date pits [18] and oil palm wood [19] for GAC and PAC preparation, and acrylic textile fibers [11], viscous rayon [20] and phenolic resin [21] for ACF production. The AC preparation precursors and conditions with obtained AC characteristics are summarized in Table 2.1.

As can be seen in Table 2.1, preparation of AC from acrylic textile fibers needs low carbonization temperature (300 ^oC) and the obtained AC has high surface area (1535 $m^2 g^{-1}$). But the most important disadvantage of this precursor is its high burn off (94%) in AC preparation.

The AC, which is prepared using precursors like bituminous coal by steam and CO_2 has high surface area (1369 and 1404 $m^2 g^{-1}$), with relatively low burn off (54 and 63%). But these precursors need high carbonization and activation temperatures (850 ^oC). In the case of AC preparation from rice bran with CO_2 activation, burn off value is appropriate (33%), but the obtained AC has low surface area (652 $m^2 g^{-1}$).

2.1.2. Effect of Carbonization Step Variables on AC Preparation

Pyrolysis of precursor in carbonization step leads to the removal of volatile materials from precursor surface. Some variables of this step such as, carbonization temperature and time, flow rate of inert gas and heating rate affect on characteristics of produced char and final AC [7]. Increasing the carbonization temperature leads to decrease the content of volatile matters in the char and enhance char quality and AC surface area and pore volume, but at the same time the char yield decreases [22]. Using excessive pyrolysis temperature, the volatile fractions of carbon are softened to form a molten intermediate in the char structure. These process leads to decrease the AC surface area and char yield, simultaneously. Lua et al. [23] have reported the effect of pyrolysis temperature on the properties of AC prepared from pistachio-nut shells. Results of their work show that increasing the pyrolysis temperature from 250 to 500 ^oC enhances AC surface area, but more increasing to 800 ^oC leads to surface area reduction.

Inert gas flow on the surface of carbonizing precursor prevents carbon burn off and helps removing the evaporated matter from the surface of precursor. High inert gas flow rate accelerates the volatiles releasing by cleaning the surface from previously evaporated matters [23]. Lua et al. [23] have investigated the effect of nitrogen flow rate (50 to 250 $cm^3 min^{-1}$) in the carbonization step on properties of ACs prepared from pistachio-nut shells. The obtained

results show that among investigated nitrogen flow rates, 150 cm^3 min^{-1} is optimum condition for carbonization of pistachio-nut shells.

The percentage of precursor burn-off is calculated using Eq. 2.1 [24].

$$Burn\text{-}off\ (\%) = \frac{(A-B)}{A} \times 100 \tag{2.1}$$

where *A* and *B* are weights of precursor and obtained AC, respectively.

Evaporation of the volatiles is increased with lengthening the carbonization time. But like carbonization temperature, prolonged carbonization causes negative effect on AC pore structure and AC yield due to melt some matters in the char structure [17]. Lua et al. [17] have investigated the effect of carbonization time on pore development of oil-palm-shell ACs. With increasing the carbonization time to 2 h, BET surface area, micropore area and micropore volume of the AC are increased (see Figure 2.2). But more lengthening of carbonization time leads to decrease of AC pore development [17].

Table 2.1. ACs produced by physical activation method under different conditions

Precursor	Activating gas	Carbonization temperature (^oC)	Activating temperature (^oC)	Surface area (m^2 g^{-1})	Burn-off (wt%)	Ref.
Used tyres	Steam	800	900	1317	87	[14]
Used tyres	CO_2	800	850	496	61	[14]
Bituminous coal	Steam	850	850	1369	54	[25]
Bituminous coal	CO_2	850	850	1404	63	[25]
Acrylic textile fibers	CO_2	300	900	1535	94	[11]
Acrylic textile fibers	CO_2	300	800	1397	-	[26]
Viscous rayon	CO_2	230	850	1850≈	-	[20]
Apricot stones	Steam	-	800 (one-step AC preparation)	1092	91	[13]
Coconut shells	CO_2	-	900 (one-step AC preparation)	1667	87	[12]
Rice bran	CO_2	850	850	652	33	[27]
Phenolic resin	Steam	800	800	1663	62	[28]
Phenolic resin	Steam	400	600	727.62	64	[21]
Peanut shells	Steam	800	800	757	84	[15]
Rice straw	CO_2	800	800	790	-	[16]
Oil-palm-shell	CO_2	600	900	519	-	[17]
Date pits	CO_2	825	800	1669		[18]
Oil palm wood	Air	390	806	1084	86	[19]
Olive-tree	Air	600	400	481	58	[29]

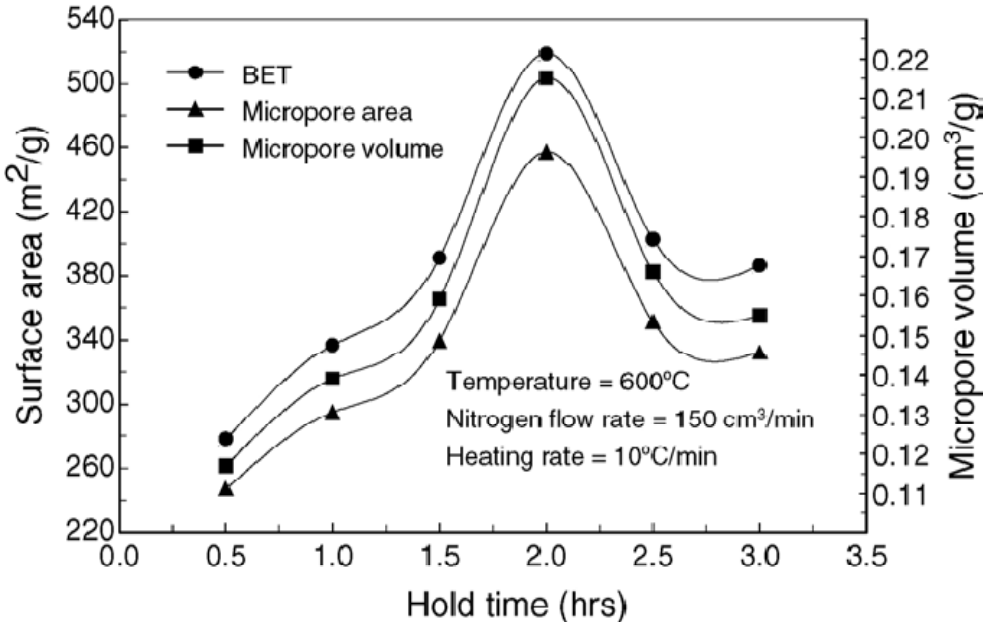


Figure 2.2. Effect of pyrolysis hold time on the BET surface area, micropore area and micropore volume of the activated carbons. (Adapted from Lua et al. [17] with permission from publisher, Elsevier. License Number: 2567601287445).

Finally, accelerating the carbonization heating rate increases the volatiles evaporation, by prompting the removal of the evaporated matters from the char surface.

2.1.3. Effect of Activation Step Variables on AC Preparation

In activation step, variables such as activation gas and its flow rate, heating rate, activation temperature and time affect on AC characteristics.

Activation gas and its flow rate significantly alter the prepared AC properties. Reaction of activation gas with precursor leads to preparation of pores and functional groups on the surface of AC. CO_2 and steam are the most used activation agents for preparation of AC. Reaction of CO_2 with char is endothermic [7]. The AC, which is prepared using CO_2 gas activation method, has larger microporous volume than steam activation [30]. The principal reaction between CO_2 and char is:

$$C_{(s)} + CO_{2\,(g)} \rightarrow 2\,CO_{(g)} \tag{2.2}$$

which leads to gasification of carbon contents of char and pore development [31].

As well as CO_2, the reaction of steam and char is endothermic. The most probable reactions between char and steam are [32]:

$$C_{(s)} + H_2O_{(g)} \rightarrow CO_{(g)} + H_{2\,(g)} \tag{2.3}$$

$$CO_{(s)} + H_2O_{(g)} \rightarrow CO_{2\,(g)} + H_{2\,(g)} \tag{2.4}$$

Flow rate of activation gas in the preparation reactor also affects on properties of final AC. Increasing the flow rate causes acceleration of gasification rate and discarding the volatile gases from the surface of carbon. More increase in flow rate may decrease the reactor temperature or reduce the contact time between the molecules of activation gas and the char [33]. Reducing reactor temperature and contact time decreases AC pore volume and adsorption ability. Yang et al. [33] have reported the effect of CO_2 flow rate on the surface area and yield of AC prepared from pistachio-nut shells. It has been indicated that with increasing CO_2 flow rate from 50 to 100 $cm^3\ min^{-1}$ surface area and yield of AC is increased and decreased, respectively. Flow rate increase to 150 $cm^3\ min^{-1}$ leads to surface area reduction but does not have significant effect on AC yield.

Since the char reaction with CO_2 or steam is endothermic, the porosity of resulting AC increases with activation temperature until an optimum amount. Further increase in the temperature leads to destruction of the porous wall and conversion to large pores. In addition, activation temperature affects on development of AC surface functional groups. At lower activation temperatures (200-400 ^oC), acidic surface groups are mostly developed on the surface of AC. This kind of AC mostly is used for adsorption of basic matters. On the other hand, the presence of basic oxides on the surface of AC, which are activated at higher temperatures (800-1000 ^oC), is considerable. This AC is appropriate to remove acids [34].

The contact time between char and activation gas as well as their characteristics and activation temperature, affect on AC properties. Increasing the activation time increases contact time between char and activation gas, so results in pore development. Longer activation time would result in more enlargements of pores and higher burn-off, which is calculated using Eq. 2.1, due to excessive oxidation [2].

2.2. Chemical Activation

Another AC preparation process is chemical activation method. This method involves precursor carbonization in the presence of alkali hydroxides such as KOH and NaOH and inorganic acids like H_3PO_4, HNO_3 and H_2SO_4. Preparation of AC using chemical activation method includes:

1) Impregnation of precursor by chemical activation agent: in this stage the precursor is soaked in solution of activation agent and then dried. The amount of Impregnation ratio is determined using Eq. 2.5.

$$\text{Impregnation ratio} = \frac{(W_f - W_i)}{W_i} \tag{2.5}$$

where W_i and W_f are weights of precursor and impregnated precursor, respectively [35]

2) Carbonization of impregnated sample in inert atmosphere: the carbonization stage in chemical activation method is same as that of physical activation. In this stage the impregnated sample is heated in inert atmosphere for appropriate time.

Diaz-Diez et al. [36] have prepared AC from different woods through chemical activation method. They have used chestnut, cedar and walnut woods as precursors and phosphoric acid as chemical activation agent. In their methods, the precursors have been washed by acid and water for removal of darts and dried. Then, the dried precursors have been impregnated with solution of 36 wt.% H_3PO_4 at 85 ^oC for 4 h. The impregnated precursors have been carbonized at temperature 850 ^oC for 4 h under nitrogen stream with flow rate of 100 mL min^{-1}. Finally, the prepared AC has been washed with distilled water and dried. Specific surface areas of AC prepared from chestnut, cedar and walnut are 777, 812 and 769 $m^2 g^{-1}$, respectively.

The main advantages of chemical activation method in comparison with physical activation process are:

1. The preparation yield of AC prepared with chemical activation method is usually higher than AC prepared with physical activation [37]: In physical activation method, the development of AC pores is mainly due to removal of carbon atoms by gasification. But, in chemical procedure, activation agents dehydrogenate the precursor, which leads to form the cross-link between carbons and finally causes to create the pores on the surface of AC [38, 39].
2. Unlike physical activation process, preparation of AC using chemical activation method usually is done in one stage (carbonization and activation are done simultaneously).
3. AC preparation by chemical activation method needs lower temperature than physical activation process [37, 40].
4. Chemical activation method usually develops pore structure better than the physical activation process [39]. Surface area and pore volume of ACs which are prepared using chemical activation method are relatively high in comparison with ACs prepared using physical activation method. Phan et al. [9] have prepared AC from jute and coconut with chemical and physical activation methods. Surface areas of ACs which prepared from jute and coconut with physical activation method are 912 and 1088 $m^2 g^{-1}$, respectively. Using chemical activation method, Surface areas of prepared ACFs from jute and coconut are 959 and 1303 $m^2 g^{-1}$, respectively, which are relatively higher than surface area of ACs, prepared by physical activation.
5. Chemical activation method usually is done at shorter time than physical activation [41].
6. In chemical activation method, the variety of activation agents is more than physical activation. In physical activation procedure, limited types of agents such as CO_2 and steam are used, but different kinds of alkali hydroxides, inorganic acids or other chemicals are applied in chemical activation.

Chemical activation method has some shortcoming in comparison with physical activation. For example, the incorporation of activating agent on the surface of AC may change the chemical properties of the activated carbon [42].

Using chemical activation method, different variables affect on final properties of prepared AC. The most effective variables are precursor, activating chemical, heating rate, impregnation ratio between precursor and activation chemical, activation temperature and time. In the following sections, effects of different variables on the final characteristics of AC are discussed.

2.2.1. Effect of Precursor on AC Preparation

As well as physical activation method, in chemical activation method precursor characteristics affect on final properties of AC. Different kinds of carbonaceous matters are used for AC production with this method such as woods [36], coffee bean husks [43], cotton stalks [44], coconut shells [45], chestnut wood [42] and petroleum coke [46]. Table 2.2 presents activation agents and temperatures for AC production and obtained surface area of some ACs using chemical activation. As can be seen in Table 2.2, precursors like coffee bean husks and bamboo are appropriate for the preparation of AC with high surface area by H_3PO_4 activation method. But in the case of bituminous coal and woods, the surface areas of ACs resulted from H_3PO_4 activation are relatively low. On the other hand, bituminous coal is very appropriate precursor for preparation of AC using KOH activation.

Table 2.2. ACs produced by chemical activation method under different conditions

Precursor	Activating Agent	Carbonization temperature (^oC)	Surface area ($m^2\ g^{-1}$)	Ref.
Coffee bean husks	H_3PO_4	450	1402	[43]
Bamboo	H_3PO_4	600	1432	[39]
Bituminous coal	H_3PO_4	500	770	[47]
Bituminous coal	$ZnCl_2$	600	960	[47]
Bituminous coal	KOH	800	3300	[47]
Coconut shells	$ZnCl_2$	560 W (Microwave radiation)	794.84	[48]
Olive-mill waste water	KOH	800	1768	[49]
Cotton stalks	H_3PO_4	420	834	[44]
Petroleum coke	KOH	800	1798	[46]
Antibiotic waste	K_2CO_3	900	1170	[50]
Chestnut wood	H_3PO_4	500	783	[42]

2.2.2. Effect of Impregnation Step Variables on AC Preparation

Among the chemicals for activation of precursors, H_3PO_4, $ZnCl_2$ and alkaline metal compounds such as KOH are common chemicals for preparation of commercial ACs [10]. Phosphoric acid shows some advantages over other chemicals such as lower toxicity and simple recovery by washing with water [48]. Alkali hydroxides such as KOH and NaOH are hazardous, corrosive and costly. $ZnCl_2$ also shows some disadvantages such as unfriendly to the environment, corrosion and inefficient chemical recovery, which leads to create waste disposal problem [42]. Therefore, in the production of AC for food and pharmaceutical industries, H_3PO_4 is commonly used [51].

Two possible activation mechanisms for cellulose precursors are suggested in the presence of H_3PO_4. Phosphoric acid, as an acidic catalyst, accelerates dehydration and dehydrogenation reactions leading to the formation of cross-links in carbon skeleton and creation of pores. In addition, H_3PO_4 reacts with organic species and is converted to phosphate and polyphosphate esters, which work as bridges to link organic species to each other and produce pores on the surface of prepared AC [47, 52]. Due to these reactions, the H_3PO_4 activated AC yield is higher in comparison with prepared AC using CO_2 activation [37, 38].

Although, H_3PO_4 is known as low toxic and friendly to the environment, $ZnCl_2$ is much effective and widely used activation chemical for AC preparation [34]. Using this chemical, AC pores are formed by cellulose degradation and carbon skeleton aromatization. $ZnCl_2$ increases the AC yield by decomposition of carbonaceous material and restricting the tar formation at high temperatures [53].

KOH is also used as activation agent of AC. This chemical is mainly used for AC production from coal precursors or chars such as bituminous coal [47]. KOH activation mechanism is partially different from H_3PO_4 and $ZnCl_2$. This difference is due to the participation of the gasification mechanisms in the pore development processes using KOH. Due to the effect of gasification reactions in KOH activation, this method needs higher activation temperature than that of H_3PO_4 and $ZnCl_2$. The probable reaction between KOH and precursor is [34]:

$$2KOH_{(s)} + C_{(s)} \rightarrow 2K_{(s)} + H_2O_{(g)} + 3CO_{(g)} \quad (2.6)$$

In the chemical activation method, presence of agent on the surface of precursor contributes the development of porosity. Therefore, impregnation ratio between activation agent and precursor is one of the effective preparation variables.

Chemical agents enhance the condensation reactions between carbon containing compounds to create pores. Therefore with impregnation ratio, the surface area and yield of AC increase [54]. But, excessive impregnation ratio causes further dehydration, which might leads to destruction of AC micropore walls and turning them to larger pores [3, 55].

2.2.3. Effect of Carbonization Step Variables on AC Preparation

The required energy for reaction between precursor and activation agent is supplied in the carbonization step. Heat treatment by electrical furnaces is the conventional method for supplying reaction energy and development of pores on the surface of prepared AC. In carbonization step, different variables such as carbonization temperature and time affect on properties of prepared AC.

Carbonization temperature is the most important variable in this step. At low carbonization temperatures (temperatures lower than 300 ^oC), mainly pyrolysis reactions are occurred and rate of activation reactions is very low. With increasing the carbonization temperature, activation reactions are accelerated which leads to create the pores on the surface of AC. Excessive carbonization temperatures lead to reduction of AC surface area with two probable mechanisms including [3, 50]:

1) Evaporating the activation agent from the surface of AC or carbonized precursor.
2) Enlarging the created pores by burning off the pores structure carbon and converting them to larger pores.

Aber et al. [3] have reported the effect of activation temperature on adsorption ability of AC prepared from kenaf with chemical activation method. The results indicate that with increasing the activation temperature up to 700 ^oC, the adsorption ability of prepared AC is increased. With more increase in the activation temperature to 750 ^oC, the adsorption ability of AC is decreased.

Chemical activation using electrical furnaces or other conventional heating methods needs high temperature (300-1200 ^{o}C). In recent years, microwave heating technology is used instead of routine furnaces for heating of precursors [39]. The most important advantage of microwave heating technology is to apply uniform and rapid heat treatment [48]. Microwave power, radiation time, and impregnation ratio of activation agent to precursor affect on prepared AC properties. Enhancing the microwave power until precise level (e.g. 560 W in the case of AC preparation from cotton stalk using microwave assisted chemical activation (see Figure 2.3) [48]) leads to input more energy to activation reaction. Overfull microwave power **(**e.g. more than 560 W in the case of AC preparation from cotton stalk using microwave assisted chemical activation (see Figure 2.3) [48]**)** causes destroying the pores structure by carbon burnt [48]. As well as microwave power, the pore generation increases with lengthening the microwave radiation time, but prolonged radiation leads to burning off the pores structure carbon.

Chemical activation usually is faster than physical one. Therefore, it is commonly done in shorter time [50]. With excessive increasing the activation time, the walls of pores collapse and the pores are enlarged, so the adsorption ability of AC is reduced [3]. In the work of Aber et al. [3] the optimized activation time is 2 h and with more increasing the activation time up to 4 h, the adsorption ability of AC is decreased.

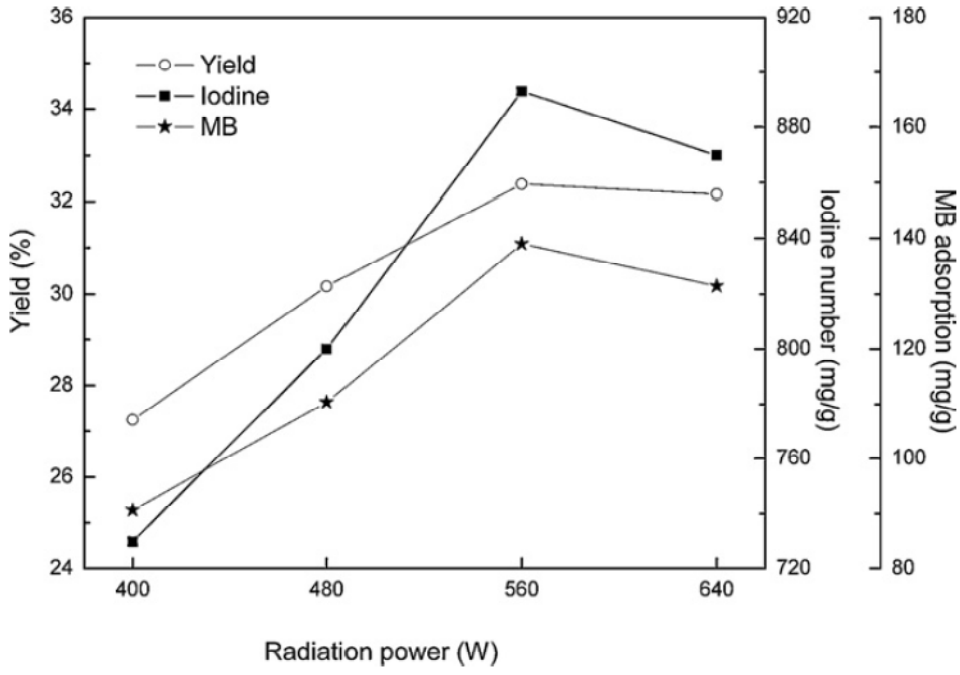


Figure 2.3. Effect of microwave radiation power on yield and adsorption capacities of activated carbon (XZn = 1.2 g g^{-1}, radiation time=8min). (Adapted from Deng et al. [48] with permission from publisher, Elsevier. License Number: 2573060857566).

2.3. Physicochemical Activation

Recently, physicochemical activation, as a new activation method is used for AC preparation, which is combination of chemical and physical activation methods. In this method the pore development is done with both of previously described activation procedures. Therefore surface area of physicochemically prepared AC is higher than chemically or physically prepared ones [3, 34]. In order to optimize the AC production using physicochemical activation, both of physical and chemical activation effective variables should be considered.

Salman et al. [56] have prepared AC from oil palm fronds using physicochemical activation by KOH and CO_2 as chemical and physical activation agents, respectively. The preparation method including: 1) Carbonization at 700 ^oC for 2 h with heating rate of 10 ^oC min^{-1} under N_2 flow. 2) Soaking in KOH solution with different KOH to carbonized precursor impregnation ratios. 3) Activation under CO_2 atmosphere at different temperatures and times. These researchers have optimized the impregnation ratio, activation temperature and activation time using central composite design of response surface methodology. According to the results, 3.75:1, 850 ^oC and 1 h are the optimum values of KOH:carbonized precursor impregnation ratio, activation temperature and activation time, respectively. BET surface area and carbon yield of AC prepared at optimum conditions are 237.13 m^2 g^{-1} and 21.6 %, respectively.

Hu et al. [57] have prepared of ACs from pistachio shells with chemical and physicochemical activation methods using KOH and KOH-CO_2, respectively. Surface area of AC, prepared using chemical activation at 780 ^oC for 1 h, is 1013 m^2 g^{-1}. More activation of chemically activated sample by CO_2 gasification at 780 ^oC for 1 h leads to increase the AC surface area up to 2145 m^2 g^{-1}. These results indicate that the surface area of AC prepared with physicochemical activation method is two times higher than that of AC prepared with chemical activation.

3. ADSORPTION BY ACTIVATED CARBON AND ITS ENVIRONMENTAL APPLICATIONS

Nowadays, contamination of the environment by various chemicals is a worrying topic and the human uses his all capabilities to solve this problem. There are many processes which can be used for the purification of contaminated environment. Common purification methods are different oxidation-based ones including advanced oxidation processes (AOPs) [58, 59], coagulation-flocculation [60], aerobic and anaerobic biological treatment [61], electro-chemical [62] and adsorption [63, 64] processes. Adsorption is the safest among other methods since chemical or electrochemical processes produce intermediates which may be more harmful than the primary pollutant, while adsorption captures the pollutants and releases no dangerous intermediate into the environment. This advantage is the main reason for the widespread applications of different adsorbents in the remediation of water, air and soil.

AC is the most common adsorbent. Other common types of adsorbents which have found commercial applications are zeolites, silica gel and activated alumina. According to Weber [65], adsorption is a process in which a component is concentrated in the interface of two

phases. This can be liquid-liquid, gas-liquid, gas-solid or liquid-solid interface [65] but liquid-solid and gas-solid interfaces are the most common.

The usage of AC dates back to ancient period. Ancient Egyptians used it for medicinal purposes about 1550 B.C. [66]. Ancient Hindus used it in drinking water purification and Egyptians in mummification [66, 67].

There are two major types of adsorption studies. The first type is kinetic studies in which the concentration of adsorbate (pollutant) with time is followed up in contact with adsorbent. Pseudo-first-order (Eq. 3.1), pseudo-second-order (Eq. 3.2), simplified Elovich (Eq. 3.3), intraparticle diffusion (Eq. 3.4) and diffusion (Eq. 3.5) equations are common kinetic models used in adsorption studies in aqueous solutions [3, 68-70].

$$\log(q_e - q_t) = \log(q_e) - \frac{k_1}{2.303}t \tag{3.1}$$

$$\frac{t}{q_t} = \frac{1}{k_2 q_e^2} + \frac{1}{q_e}t \tag{3.2}$$

$$q_t = \frac{1}{\beta}\ln(\alpha\beta) + \frac{1}{\beta}\ln(t) \tag{3.3}$$

$$q_t = k_i t^{0.5} \tag{3.4}$$

$$-\log\left(1-(\frac{q_t}{q_e})^2\right) = (\frac{4\pi^2 D}{2.3d^2})t \tag{3.5}$$

In these equations, q_t and q_e are the amounts of adsorbate adsorbed on adsorbent (mg g^{-1}) at time t and equilibrium, respectively. k_1 (L min^{-1}), k_2 (g mg^{-1} min^{-1}) and k_i (mg g^{-1} $min^{-0.5}$) are the rate constants of pseudo-first-order, pseudo-second-order and intraparticle diffusion equations, respectively. α is the initial rate of adsorption (mg g^{-1} min^{-1}) and β is the constant of desorption (g mg^{-1}) in any one experiment. D is a coefficient which covers surface and pore diffusion (cm^2 s^{-1}) and d is the mean diameter of particle (cm). The constants of pseudo-first-order (q_e, k_1), pseudo-second-order (q_e, k_2) and diffusion (D) kinetic models are calculated using the linear plots of $\log(q_e - q_t)$, $\frac{t}{q_t}$, and $-\log\left(1-(\frac{q_t}{q_e})^2\right)$, respectively versus t. Also, the linear plots of q_t versus $\ln(t)$ and $t^{0.5}$ gives the constants of Elovich (α, β) and intraparticle diffusion (k_i) equations, respectively.

Isotherm studies are the second type of investigations related to adsorption in which the equilibrium concentration of pollutant at constant temperature is measured. The results of isotherm studies create knowledge about partitioning the pollutant between contaminated environment and adsorbent after reaching the equilibrium. The isotherm studies are performed by the contact between a constant amount of adsorbent and different

concentrations of adsorbate at constant temperature and solution volume in a continuously-shaking system (e.g. shaker-incubator). Experiments also can be done with constant concentration of adsorbate and different adsorbent dosages. The most common isotherm models which are used widely in adsorption studies in aqueous solutions are explained here.

Langmuir model is one of the isotherm models used in adsorption studies. Original form of Langmuir isotherm is Eq. 3.6 which can be linearized as Eq. 3.7 [71]. Langmuir model assumes that adsorption sites have uniform energy and adsorption takes place on a homogenous surface as monolayer coverage without any interaction between adsorbed molecules [72].

$$\frac{q_e}{Q} = \frac{bC_e}{1+bC_e} \tag{3.6}$$

$$\frac{1}{q_e} = \frac{1}{Qb}\frac{1}{C_e} + \frac{1}{Q} \tag{3.7}$$

where q_e is the amount of adsorbate adsorbed on adsorbent (mg g^{-1}) at equilibrium, C_e is the equilibrium concentration of adsorbate in the solution (mg L^{-1}), Q is a constant showing the maximum amount of adsorbate adsorbed on adsorbent (mg g^{-1}) as monolayer coverage, and b is the isotherm constant related to free adsorption energy (L mg^{-1}). Using the linear plot of $\frac{1}{q_e}$ versus $\frac{1}{C_e}$ the isotherm constants (Q, b) can be obtained. There is a separation factor, R_L, which is defined as Eq. 3.8.

$$R_L = \frac{1}{1+bC_0} \tag{3.8}$$

where C_0 is the initial concentration of adsorbate in the solution. $R_L>1$, $R_L=1$ and $0<R_L<1$ indicate unfavorable, linear and favorable adsorptions, respectively [73].

The original form of Langmuir equation (Eq. 3.6) can be linearized at least in 4 different ways, producing Langmuir type I (Eq. 3.9), type II (Eq. 3.10), type III (Eq. 3.11) and type IV (Eq. 3.12) [72]. It is important to note that the isotherm constants and regression coefficients (R^2) obtained from the fitting of various types of Langmuir isotherm to experimental data are different.

$$\frac{C_e}{q_e} = \frac{1}{bQ} + \frac{C_e}{Q} \tag{3.9}$$

$$\frac{1}{q_e} = \frac{1}{bQC_e} + \frac{1}{Q} \tag{3.10}$$

$$q_e = Q - \frac{1}{b}\frac{q_e}{C_e} \tag{3.11}$$

$$\frac{q_e}{C_e} = bQ - bq_e \tag{3.12}$$

Freundlich isotherm assumes that adsorption takes place as multilayer on a heterogeneous solid surface. Stronger adsorption sites uptake the adsorbate first and binding strength is weakened when the occupation of adsorption sites increases [72]. Freundlich isotherm is as follows:

$$q_e = K_F (C_e)^{1/n} \tag{3.13}$$

that can be linearized as Eq. 3.14:

$$\ln q_e = \ln K_F + \frac{1}{n}\ln C_e \tag{3.14}$$

where K_F (mg g^{-1}(L mg^{-1})$^{1/n}$) is a Freundlich constant related to adsorption capacity and $\frac{1}{n}$ shows the intensity of adsorption. The constants are calculated using the intercept and the slope of the linear plot of $\ln q_e$ versus $\ln C_e$. According to Behnamfard and Salarirad [72], n>1 or 0<$\frac{1}{n}$<1, shows that adsorptive forces on the surface of adsorbent are weak. But, according to Omar et al. [74] this implies that it is a result of strong adsorptive forces.

Temkin or Tempkin isotherm can be expressed as Eq. 3.15 [72]:

$$q_e = q_m \ln K_T + q_m \ln C_e \tag{3.15}$$

where K_T (L mg^{-1}) and q_m (mg g^{-1}) are isotherm constants. q_m is a constant related to heat of adsorption. In this model heat of adsorption decreases linearly by increasing the coverage because of adsorbate-adsorbate interactions, and binding energies distribute uniformly up to a maximum amount.

Dubinin-Radushkevich isotherm is as Eq. 3.16 which can be linearized to Eq. 3.17 [72, 75].

$$q_e = q_m \exp(-D\varepsilon^2) \text{ that } \varepsilon = RT\ln(1 + C_e^{-1}) \tag{3.16}$$

$$\ln q_e = \ln q_m - D\varepsilon^2 \tag{3.17}$$

In this isotherm, the linear plot of $\ln q_e$ versus ε^2 gives the monolayer adsorption capacity, q_m (mg g^{-1}), and the constant related to sorption energy, D (mol^2 kJ^{-2}). ε is Polanyi potential, R (kJ mol^{-1} K^{-1}) is universal gas constant and T (K) is temperature. The mean free energy of sorption per molecule of sorbate when it is transferred from infinity to solid surface in the solution, E (kJ mol^{-1}), can be calculated using D and Eq. 3.18.

$$E = \frac{1}{\sqrt{2D}} \tag{3.18}$$

BET isotherm is expressed as Eq. 19 and can be linearized as Eq. 20 [76].

$$q_e = \frac{q_m K_b C_e}{(C_s - C_e)[1 + (K_b - 1)\frac{C_e}{C_s}]} \tag{3.19}$$

$$\frac{C_e}{(C_s - C_e)q_e} = \frac{1}{K_b q_m} + (\frac{K_b - 1}{K_b q_m})(\frac{C_e}{C_s}) \tag{3.20}$$

In these equations q_e and q_m are the equilibrium amount and the amount of adsorbate adsorbed on adsorbent as complete monolayer (mg g^{-1}), respectively. K_b is a constant related to the energy of interaction with surface. C_e is the equilibrium concentration of the adsorbate in the solution (mg L^{-1}), and C_s is the saturation concentration of adsorbate in solution (mg L^{-1}) which is dependent on temperature [77]. Using the linear plot of $\frac{C_e}{(C_s - C_e)q_e}$ versus $\frac{C_e}{C_s}$ the constants of the isotherm, K_b and q_m, are calculated.

The three-parameter Redlich-Peterson isotherm is a combination of Langmuir and Freundlich models and can be used in both homogenous and heterogeneous systems. This model can be expressed as Eq. 3.21 [72, 76].

$$q_e = \frac{K_R C_e}{1 + \alpha_R C_e^{\beta}} \tag{3.21}$$

Eq. 3.21 can be converted to linear form as Eq. 3.22.

$$\ln\left(K_R \frac{C_e}{q_e} - 1\right) = \ln \alpha_R + \beta \ln C_e \tag{3.22}$$

K_R (L g^{-1}), α_R (L$^{\beta}$ mg$^{-\beta}$) and β are isotherm constants. β is in the range of 0 and 1. Other parameters are like the previous isotherm models. The constants of Redlich-Peterson model

are calculated using a minimization method by maximizing the agreement between the experimental and calculated amounts of q_e.

Main thermodynamic studies in adsorption processes include the calculation of change in standard Gibbs free energy (ΔG°) (J mol^{-1}), standard enthalpy (ΔH°) (J mol^{-1}) and standard entropy (ΔS°) (J mol^{-1} K^{-1}) of adsorption which are calculated using Eqs. 3.23-3.25 [75, 78].

$$\ln K_L = \frac{\Delta S^0}{R} - \frac{\Delta H^0}{RT} \tag{3.23}$$

In this equation, R (J mol^{-1} K^{-1}) is universal gas constant and T (K) is absolute temperature. K_L (L mol^{-1}) is the equilibrium constant which can be calculated using this equation: $K_L = 1000bM$ in which M is the molecular weight of the adsorbent and b (L mg^{-1}) is the Langmuir isotherm constant. The values of ΔH° and ΔS° are calculated using the linear plot of $\ln K_L$ versus $\frac{1}{T}$. ΔG° is calculated by Eq. 3.24 or 3.25.

$$\Delta G^0 = \Delta H^0 - T\Delta S^0 \tag{3.24}$$

$$\Delta G^0 = -RT \ln K_L \tag{3.25}$$

$\Delta G^\circ<0$ indicates the spontaneous nature of the adsorption while $\Delta G^\circ>0$ shows that the adsorption is not spontaneous (desorption is spontaneous) and the conditions must be changed to make feasible the adsorption. $\Delta G^\circ=0$ shows the adsorption in equilibrium. The negative and positive values of ΔH° imply exothermic and endothermic adsorption, respectively. ΔS° values show the change in randomness in the adsorption interface which increases with positive values of ΔS° and vice versa.

From the above-mentioned explanations, it can be concluded that kinetic, isotherm and thermodynamic studies provide us some information about the adsorption processes and their feasibility, rate, distribution of adsorbate between its solution and adsorbent, and some other useful data necessary to compare the performance of different adsorbents. This leads to the right selection of an adsorbent for a certain application.

AC can be used as four major forms in environmental remediation. These forms are PAC, GAC, ACF, and any kind of AC forms which are doped with other agents to gain new functionalities and called impregnated carbon (IC). We explain the environmental applications of ACs in the following subsections.

3.1. Powdered Activated Carbon

PAC is a form of AC typically with particle size smaller than 80 mesh or 0.177 mm [79]. It cannot be used as fixed bed in adsorption columns, because its fine particles produce a large amount of pressure drop between the top and the bottom of the column. PAC is mainly used as dispersed in polluted phase. It has a lot of applications in the removal of contaminants

from aqueous, gaseous, and even solid environment. The following paragraphs introduce some environmental applications of PAC.

PAC is used to improve the performance of membranes and increase their life time. In hybrid systems of PAC-membrane, PAC adsorbs organic pollutants in the solution. This, results in a decrease in the amount of organics loaded to the membrane and therefore the fouling problem in membranes is reduced. Gai and Kim have reported the role of PAC in the performance of membrane water treatment systems [80]. They have used a hybrid system including PAC with mesh size between 100 and 325 and surface area about 1500 m^2 g^{-1} and a polyethersulfone (PES) membrane with a pore size of 0.2 μm. In this system total organic carbon (TOC) removal of 66.2 and 69.8% in the absence and the presence of PAC can be obtained, respectively and the corresponding removal of UV absorbance at 254 nm (UV_{254}) is 70.6 and 82.4%. The trans-membrane pressure (TMP) in the presence of PAC reaches 16 kPa after 65 days while in the absence of PAC it is 61 kPa after 48 days. It is obvious that hybrid system extends the life time of the membrane, considerably. The results show that in the hybrid system the number of the bacteria, naturally present in the system, is one hundred times more than simple membrane system since PAC adsorbs the bacteria and holds them in the system. So, it is logical to have more biological activity in hybrid systems which results in the biodegradation of organic pollutants. Also in hybrid systems, PAC decreases the adverse effects of high organics loading via adsorption of them [80]. This study indicates the positive enhancing effect of PAC in the performance of membrane systems and the quality of produced filtrate.

PAC has been used for adsorption of polyvinyl alcohol (PVA) from aqueous solution [81]. PVA is a recalcitrant pollutant which is used as sizing agent in textile industries. It is also used to prepare adhesives, paper coatings, emulsion paints, detergents and drugs. Its high discharge rate and stability pollute the environment and raise health hazards because it can accumulate in human body. PVA can dissolve heavy metals from sediments and increase their concentration in water streams. PAC with specific surface area of 1050 m^2 g^{-1} and mean particle size of 4.5 nm was used to remove PVA from solution [81]. PVA adsorption on PAC follows pseudo-second-order kinetics and external mass transfer is the step which controls the rate of the adsorption. The results show that adsorption isotherm is H-shaped (Figure 3.1). This kind of isotherm is appeared when the adsorbate species are large or ionic and there is high affinity between adsorbent and adsorbate [81]. In this situation, the most of adsorption sites are occupied in low adsorbate concentrations and by increasing its concentration, a decreasing number of adsorption sites are available for adsorption [81]. Freundlich isotherm best fits the equilibrium adsorption data in the adsorption of PVA on PAC and the values obtained for ΔG^0, ΔH^0 and ΔS^0 propose that the adsorption process is spontaneous and endothermic and the randomness increases by the adsorption. A PVA removal of 92% in the common conditions of pH 6.3 and adsorbent dose of 5 g L^{-1} after 30 min contact time shows that adsorption on PAC is a good method to remove PVA from aqueous solutions without production of intermediate species. Production of intermediates is common in the procedures based on chemical, electrochemical and photochemical reactions.

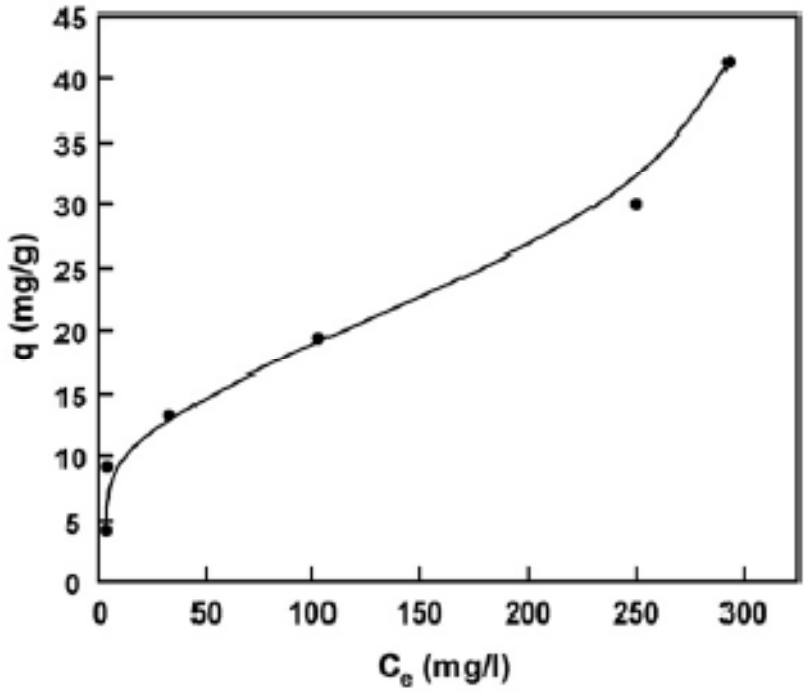


Figure 3.1. H-shaped isotherm curve found for the adsorption of PVA on PAC. (Adapted from Behera et al. [81] with permission from publisher, Elsevier. License Number: 2575950783715).

Ozonation in combination with AC adsorption process is used for the removal of some pollutants from aqueous solutions. Beltran et al. [82] removed diclofenac as a nonsteroidal antiinflammatory drug from water using single ozonation and its combination with AC adsorption process. Single ozonation rapidly removes the drug from water but it is inefficient in TOC removal. The results show that adding AC to the process reduces ozone consumption from 28 to 7 mg per mg TOC removed and increases TOC removal from 30 to 80% after 60 min contact time [82]. The combined process is often considered as AOPs since it produces the hydroxyl radicals in the solution. Ozone consumes some basic oxygen groups on carbon surface and so, it is not correct if AC is considered as a catalyst. Beltran et al. [82] have been studied the ozonation of diclofenac in aqueous solutions in the presence of PAC for mechanistic and kinetic purposes. They have investigated the effect of operational parameters such as gas flow rate, ozone concentration and initial TOC of the solution on its removal rate and found that the application of PAC decreases liquid-solid and internal diffusion mass transfer resistance. The elimination of mass transfer resistance has an important role in the promotion of diclofenac removal rate.

In the production of potable water, natural organic matter (NOM) and organic contaminants must be removed from water sources. Dissolved organic matter (DOM) causes some problems in water treatment industries. It increases the amount of coagulant necessary for water treatment, produces harmful disinfection byproducts (DBP) and makes the water proper for bacterial growth in water distribution system. DOM also competes with targeted pollutants in their adsorption on AC which reduces pollution adsorption capacity. It is the major problem present in the application of AC in natural water sources. The removal of

NOM in water treatment plants is usually not complete especially when a large portion of small-molecular-size NOM is present. Anion exchange resins are proper alternatives to coagulation/flocculation process in the removal of NOM. PAC is a good choice to remove trace organic pollutants from water but its adsorption capacity significantly reduces in the presence of NOM. The reduction in adsorption capacity is affected by NOM characteristics, AC pore size distribution and the ratio between NOM and targeted organic compounds [83]. The adversary compounds either compete for adsorption sites of the adsorbent (low–molecular-weight compounds) or block the pores (high–molecular-weight compounds). It is believed that the most of competition is made by small-size NOM compounds, which are greatly captured by anion exchange resins [83]. So, the application of AC-anion exchange resin systems can reduce the competition and keep the inherent adsorption capacity of carbon. Humbert et al. [83] have reported the removal of NOM and pesticides (i.e. atrazine and isoproturon) using a combination of ion exchange resin and PAC from surface water with high concentration of DOC about 6.0 mg L^{-1}. Anion exchange resins remove DOC up to 75% after 30 min contact time. Application of PAC after resin step, only slightly improves DOC removal efficiency. Experiments with high (200 mg L^{-1}) and low (1 mg L^{-1}) pesticide concentrations show the increased removal of both pesticides using simultaneous or successive (first resin then PAC) combination of anion exchange resin and PAC compared to PAC alone.

Jia et al. [84] have studied the effect of air bubbling agitation on the adsorption of atrazine from aqueous solutions by PAC. The adsorption of a solute on an adsorbent has four successive steps: first, diffusion in the bulk of solution; second, diffusion across the liquid film surrounding the adsorbent particles; third, pore diffusion in the adsorbent surface; and finally bonding the adsorbate to the active sites on adsorbent [84]. The bubbling of solution can influence on the first two steps mentioned above via agitation of bulk of solution, reducing the thickness of diffusion layer in solid-liquid interface, and detachment of bubbles from surface of the adsorbent. Air bubbling is a good mixing method and the mixing resulted from just a few bubbles can improve adsorption efficiency. There is a linear relation between liquid film mass transfer coefficient and bubbling rate until an ultimate constant value. The researchers have also studied the effect of intermittent bubbling and found that intermittent high intensity bubbling more increases the adsorption efficiency than continuous low intensity one, in constant flow rate per unit time. So, intermittent high intensity sparging is better than continuous one, because it helps in better adsorption while the air and energy consumption is reduced.

Acrylic acid is an organic acid with serious toxicity. It can enter the body via skin, inhalation and ingestion. It is very dangerous for aquatic environment and can irritate skin, eyes, respiratory and gastrointestinal systems [85]. Acrylic acid has wide application in various industries such as the production of paints, synthetic fibers, adhesives, papers and detergents [85]. Adsorption is one of the good choices to treat effluents containing acrylic acid. Kumar et al. [85] have studied the isotherm and kinetics of the removal of acrylic acid (initial concentration=50-500 mg L^{-1}) using PAC from synthetic aqueous solution. They have worked at the temperature range of 303-348 K and found that the decrease of temperature increases the adsorption efficiency because of the exothermic nature of the adsorption. Kumar et al. [85] have reported that Freundlich isotherm best fits the equilibrium experimental data and that the equilibrium is reached after 6 h contact time. According to their results, 1 g of the used PAC adsorbs the maximum amount of acrylic acid equal to 36.23 mg. Optimum PAC

dosage is 20 g for 1 L of solution at 303 K and initial acrylic acid concentration of 100 mg L^{-1}. Their kinetic study shows that pseudo-second-order rate equation is the right choice for the process. Thermodynamic calculations give negative amounts for ΔG^{o}_{ads} between −16.60 to −18.18 kJ mol^{-1}, which shows that adsorption takes place spontaneously. These results indicate that PAC is an effective adsorbent material to remove acrylic compounds from aqueous environments.

Öztürk and Köse [86] have studied nitrite adsorption kinetics on PAC. Nitrogenous compounds like ammonia, nitrites and nitrates often are present in drinking water and wastewaters from agricultural, domestic and industrial sources. Nitrogen compounds can be appeared in water sources due to the application of fertilizers, animal excretions and industrial effluents. Nitrogen compounds can cause the eutrophication of rivers and lagoons and have health hazards for human [86]. The presence of high concentrations of these compounds in drinking water causes cyanosis in babies and the cancer of gastrointestinal system [86]. Therefore, it is so important the reduction of nitrate and nitrite to the values below standard limits. Öztürk and Köse [86] in their research have used the PAC originated from plant with particle size between 71 and 80 μm and surface area of 866.25 m^2 g^{-1}. Their results show that among three well-known kinetic models including pseudo-first-order, pseudo-second-order and intraparticle diffusion models, adsorption on PAC follows pseudo-second-order model. The results show that the initial nitrite adsorption rate on PAC is lower than another adsorbent called sepiolite but the final adsorption capacity of PAC is about twice of sepiolite after 200 min contact time (1.2 versus 0.65 mg g^{-1}). The results obtained in a 50-mL $NaNO_2$ solution with the concentration of 25 mg L^{-1} containing 0.5 g adsorbent (PAC or sepiolite) show that equilibrium nitrite removal by PAC needs more time compared to sepiolite (120 versus 30 min).

In another work, Qu et al. [87] have studied the adsorption of perfluorooctanoic acid in aqueous solutions on PAC. Perfluorinated acids and their salts are used as surfactant in the synthesis of polymers; in photolithography; as fire retardant and carpet cleaner agent; and for paper coating. Perfluorooctanoic acid is bioaccumulative and has been detected in water sources, animals, human, even in the zooplankton. These compounds are probably carcinogen agents in human, and have toxicity for reproductive and immune systems [87]. Perfluorooctanoic acid has high stability and is not biodegradable. So, PAC has been used for the removal of perfluorooctanoic acid from aqueous solutions. The used PAC has particle size lower than 100 mesh and a specific surface area of 1000 m^2 g^{-1}. The obtained data show that Langmuir isotherm better describes the equilibrium conditions which are established within 60 min. The maximum removal of perfluorooctanoic acid is mostly equal to 99%. The positive amounts of change in standard enthalpy and entropy show that the adsorption is endothermic and the randomness in the interface of PAC and solution is increased when the adsorption takes place. The negative amounts of change in standard Gibbs free energy show that the adsorption is spontaneous, too. Increasing the temperature from 293 to 323 K decreases the change in standard Gibbs free energy. It causes to an increase in the adsorption capacity of PAC. The kinetics of adsorption follows pseudo-second-order model and the adsorption mainly is controlled by particle diffusion. The results of Qu et al. [87] totally show that PAC is an effective, economic and favorable adsorbent for perfluorooctanoic acid removal in aqueous environment.

Ranganathan [88] has studied the adsorption of Hg (II) ions from aqueous solutions using PAC. Hg is very toxic and irreversible neurological hazards can be produced by its

compounds [88]. So, it is very interesting to find a proper method for the removal of mercury from polluted wastewater. Ranganathan [88] has reported the preparation of PAC from *Casurina equisetifolia* leaves with particle size ranging from 45 to 75 μm. The experiments has been done in batch mode in 100-mL solutions with Hg (II) concentration of 5-40 ppm agitated in contact with 25-250 mg of prepared PAC at pH 2.1-10.5. It has been found that the equilibrium adsorption of Hg (II) fits well the Langmuir equation. The results show that the higher concentration of NaCl in the solution decreases Hg (II) removal. This method is capable to remove mercury from aqueous solution up to 99.9%, resulting in a conclusion that the adsorption is a promising method for the removal of very toxic mercury ions in aqueous environments.

Aber et al. [63] have studied the removal of acid orange 7 as a mono azo dye, which is widely used in dyeing synthetic fibers, wool, and cotton and in paper industries, using PAC. The researchers have also simulated the adsorption process using artificial neural network (ANN). Azo dyes contain –N=N– chromophore and aromatic groups and can cause unwanted health effects. Dyes produce aesthetic problems in water sources, can be poisonous and carcinogen, may be toxic for aqueous ecosystems, stop the photosynthesis by absorbing the sun light, and reduce the oxygen content of water bodies [63]. It is important to find a proper method to remove dyes from aqueous environments. More than 95% of acid orange 7 can be adsorbed at equilibrium on PAC at pH about 3 where the initial dye concentration is 150 mg L^{-1}. The required contact time to reach full equilibrium is at least 24 h. The adsorption of acid orange 7 follows second order kinetic model. Experimental data better fits Freundlich equation compared with Langmuir model. The results show that the adsorption of acid orange 7 on PAC can be well simulated by ANN. Feed forward backpropagation ANN has been used with 3 layers including 3, 2 and 1 neurons in first, second and third layers, respectively.

Some endocrine disrupting compounds such as bisphenol A, 17b-estradiol, and/or 17a-ethynyl estradiol are found in drinking water, surface water, groundwater and wastewater [89]. Yoon et al. [89] have studied PAC capability in the removal of these compounds. The results show that all these endocrine disrupting compounds are removed by PAC in the range of 31-99% depending on type and dosage of PAC and presence or absence of NOM in water sample. The removal order is as follows: 17b-estradiol, 17a-ethynyl estradiol and bisphenol A. Freundlich isotherm model fits well to the experimental data. This study shows that PAC can remove more than 99% of the three estrogenic compounds. So, it can be resulted that PAC can be used in removal of endocrine disrupting compounds from contaminated water.

PAC has widely used in removal of various gaseous pollutants that are going to be discharged into the atmosphere through flue gases. There are a variety of pollutants which enter the environment through gaseous streams, including zero valent metals (e.g. mercury and lead), and organic compounds (e.g. dioxins, furans, polychlorobenzenes (PCBs)) and polycyclic aromatic hydrocarbons (PAHs). Bais et al. [90] have used PAC for the removal of persistent organic pollutants including fluoranthene (belongs to PAHs family) and hexachlorobenzene (belongs to PCBs family) from gas stream. They have found an adsorption capacity up to 1.6 and 2.5 mmol g^{-1} for fluoranthene and hexachlorobenzene, respectively.

Municipal waste incinerators are one of the largest dioxin emission sources in the environment. Dioxins have serious health effects and must be removed before the discharge into the atmosphere. One of effective methods to remove dioxins in gas streams is the

application of a proper adsorbents like PAC. It can be injected to the gas stream where adsorbs the pollutants before the separation of gas and PAC takes place. Chang et al. [91] have characterized the emission of dioxins from municipal waste incinerators in Taiwan. They have analyzed flue gas samples to characterize the efficiency of air pollution control devices. Their records show that the emission of dioxin has decreased significantly after PAC injection to gas stream. This is corresponding to an increase in dioxin removal efficiency from 5.9 to about 90% in the gas stream discharged to the atmosphere. They have also reported that continuous PAC injection increases dioxin removal efficiency to 98.6%**.** These results show that AC injection technology can effectively remove dioxins from incinerators' flue gas.

Installing a PAC injection unit before particulate control devices such as electrostatic precipitators or fabric filters is a method to remove or reduce mercury concentration in flue gases. This can adsorb mercury in gas phase, and even in fly ash+PAC deposits. So, mercury-containing PAC is collected along with fly ash in particulate control devices. Therefore, fly ash is contaminated with mercury-containing PAC. This may affect on the properties of the fly ash which will be sent to landfill or can have other applications. Therefore, it is necessary to study the release of mercury from PAC+fly ash mixtures. Senior et al. [92] have studied the release of mercury by performing leaching analyses on fly ash. Two types of fly ash have been studied in this work: one produced from bituminous and another from a subbituminous coal. Their results show that little or no Hg can be detected in the leachate solution and so the resulted fly ashes can be buried in engineering landfills.

The results of other researches which have used PAC for treatment of contaminated aqueous and gaseous phases have been summarized in Table 3.1.

Table 3.1. Some of the PAC applications in the removal of contaminants

Removal agent/process	Treated phase	Pollutant(s)	Removal capability (proximate)	Ref.
PAC+Microfiltration	Aqueous	Cetyl trimethyl ammonium bromide (CTAB), Linear alkyl benzene sulfonate (LABS)	CTAB: 98% LABS: 93%	[93]
PAC	Aqueous	Geosmin**	0.17 $\mu g\ g^{-1}$	[94]
PAC	Aqueous	Turquoise Blue-G	95%	[95]
PAC	Aqueous	Metsulfuron-methyl (a herbicide)	330 $mg\ g^{-1}$	[96]
PAC	Aqueous	Malachite green	99.9%	[38]
PAC, s-PAC*	Aqueous	Geosmin**	s-PAC: 90% PAC: 30%	[97]
PAC+Ozonation	Aqueous	A surfactant: sodium dodecylbenzenesulphonate	Only O_3: 18% O_3/PAC: 70%	[98]
PAC+Submerged anaerobic membrane bioreactor	Aqueous	Dissolved organic carbon (DOC)	89%	[99]
PAC	Gaseous	Volatile organic compounds (VOCs)	85%	[100]
PAC	Gaseous	Polychlorinated dibenzodioxins (PCDD), Polychlorinated dibenzofurans (PCDF)	-	[101]
PAC	Gaseous	Mercury	25-95%	[102]

* Super powdered activated carbon: has much finer particle size than PAC.

** A compound responsible to water taste and odor

3.2. Granulated Activated Carbon (GAC)

GAC has particle size larger than PAC. At least 90% of its weight is retained on a 180-μm (80 mesh) standard sieve [103]. GAC is suitable for column adsorption. Although it has lower specific surface area compared with PAC, it is widely used in the treatment of aqueous and gaseous polluted streams. The most of potentially active adsorption sites are confined in the inside of carbon particles of GAC, and so it has lower surface area compared with PAC and ACF.

Ahmad and Hameed [104] have studied the adsorption of C.I. Reactive Black on a fix bed of GAC prepared from bamboo waste. They have reported the effect of various operational parameters including dye concentration, feed flow rate and GAC bed height on the adsorption efficiency. They have obtained a bed adsorption capacity of 39.02 mg g^{-1} and found that the adsorption process fits well to the fixed bed adsorption models of Thomas and Yoon–Nelson. The results show that the GAC prepared from bamboo waste can be a suitable adsorbent in dye removal using fixed bed adsorption columns.

2,4-dichlorophenoxy-acetic acid (2,4-D) is a herbicide which is widely used to control the growth of broad-leaved weeds. Its low cost and good selectivity makes it preferable between various herbicides. It is toxic and poorly degradable [105] and can cause wide environmental pollution. Aksu and Kabasakal [105] have reported the batch adsorption of 2,4-D from aqueous solution by GAC. They have studied the process at different pH values, temperatures and initial herbicide concentrations. The results indicate that GAC has an uptake capacity of 518.0 mg g^{-1}. Freundlich and Koble-Corrigan isotherms fit well to the experimental data. They found that both the boundary layer and intraparticle diffusion have important role in adsorption process and the kinetics of adsorption follows first-order kinetic model. They believe that the application of GAC for the removal of 2,4-D from wastewater can be suitable in wastewater treatment plants.

Álvarez et al. [106] have used ozonated GAC to adsorb phenolic compounds from aqueous solutions. The researchers have studied the ability of GAC in the adsorption of phenol, *p*-nitrophenol, and *p*-chlorophenol from aqueous solutions after the treatment of carbon by ozonation. The results show that ozonation can not change considerably the porous structure of GAC, but it modifies the chemical surface and hydrophobicity of carbon. They have found that the ozonation of GAC increases the surface acidic oxygen groups. At 25 °C carboxylic acid group is the major acidic group while at 100 °C, various acidic groups such as carboxylic, lactonic, carbonyl and hydroxyl are resulted. The ozonation of GAC at room temperature decreases its ability in the adsorption of phenol, *p*-nitrophenol, and *p*-chlorophenol, but if ozonation temperature increases to 100 °C in some cases adsorption capacity even increases.

Azizian and Yahyaei [107] have studied the kinetic modeling of 18-crown-6 adsorption from aqueous solutions on to GAC. 18-crown-6 is a phase transfer catalyst which makes possible the reaction between species in two immiscible phases. This kind of catalysts is used in organic reactions; synthesis of pharmaceuticals, agricultural chemicals, and perfumes; polymerization reactions etc [107]. 18-crown-6 is used for the phase transfer of sodium cyanide or $KMnO_4$. Crown ethers are toxic and must be removed before the discharge into the environment. One of effective methods to remove crown ethers is adsorption. Azizian and Yahyaei [107] have studied the effect of temperature and crown concentration on its adsorption on GAC. They have found that the adsorption process follows pseudo-second-

order kinetic model. The results confirm that GAC is a suitable adsorbent for 18-crown-6 in aqueous solutions. They have also found the room temperature (about 25 ^{o}C) as the best one for adsorption of 18-crown-6 on GAC.

Bansode et al. [108] have reported the adsorption of VOCs by pecan shell and almond shell based GAC. They have studied the adsorption of bromo-dichloromethane, benzene, carbon tetrachloride, 1,1,1-trichloromethane, chloroform, and 1,1-dichloromethane. They have found that GAC samples adsorb benzene better than the other VOC compounds. The results confirm that adsorption on GAC can be an alternative method for the removal of VOCs from aqueous solutions.

Daneshvar et al. [64] have studied the adsorption of insecticide imidaclopride from aqueous solutions by adsorption on GAC. They have used an on-line spectrophotometric analysis system. This system is a batch experimental set up with a line of adsorbate solution passing through a spectrophotometer cuvette for on-line sampling. Imidaclopride is widely used in agriculture. They have studied on imidaclopride adsorption and its kinetics at various pH values and temperatures. They have studied over a 90-min time span and introduced the second order kinetic model as the best one which fits the experimental data. According to their results rate constant of the adsorption decreases with an increase in temperature. The studied GAC sample decreases the concentration of imidaclopride from 25 to around 5 mg L^{-1} and this means that the method has the capability of removal efficiency at least equal to 80%.

Lead is one of the toxic heavy metals and can cause some disease. An important problem about lead is that it can accumulate in the body and concentrated through food chain. It is a metabolic poison and enzyme inhibitor. Lead can be released in the environment through very different ways such as lead acid batteries; pulp and paper industries; petrochemicals, refineries, printing industries; pigments; photographic materials; manufacturing of explosives; ceramic, glass, paint, oil and metal industries; phosphate fertilizers; electronics and wood production; combustion of fossil fuels; forest fires; mining activities; and automobile emissions [109]. Considering the health risks of lead, it should be removed from wastewater streams before discharge to the environment. Dwivedi et al. [109] have reported the removal of lead using GAC packed bed and batch system. The adsorption process follows Langmuir and Freundlich adsorption isotherms and packed bed can adsorb 2 mg of lead per gram of GAC which is very lower than batch results. According to the Langmuir isotherm the maximum capacity of the GAC in the adsorption of Pb (II) ions is about 26.5 mg g^{-1}. Pb (II) removal depends on its concentration and hydraulic loading rate. The used GAC can be regenerated using a mineral acid solution such as nitric acid with the concentration of 0.5 M and can be applied for further applications.

Lataye et al. [110] have used commercial grade GAC for the sorption of pyridine from aqueous solution. They have studied the sorption process from kinetic, thermodynamic and isotherm aspects. Pyridine is a volatile and flammable toxic chemical with pungent and unpleasant odor. Its unpleasant odor can be detectable in a concentration as low as 0.82 mg dm^{-3} in wastewater [110]. Lataye et al. [110] have studied the effect of adsorbent dose, initial pH of solution, contact time, temperature and initial concentration of pyridine on its removal efficiency using GAC. At low pyridine concentrations (<50 mg L^{-1}) removal efficiency is about 97% while in high pyridine concentrations (600 mg L^{-1}) the efficiency decreases to about 84%. These data are obtained at GAC dosage of 30 kg m^{-3} at 30 ^{o}C. Pyridine adsorption is endothermic and obeys Toth or Radke–Prausnitz isotherms. Because of the

endothermic nature of pyridine adsorption, its removal increases by increasing the temperature.

In another work, Lataye et al. [111] have studied the adsorption of α-picoline onto GAC from equilibrium and thermodynamic aspects. The particle size of used commercial GAC is in the range of 500-1700 μm. The other name of α-picoline is 2-picoline and it is a derivative of pyridine. It is a hazardous and colorless liquid with unpleasant odor. It is the precursor of various chemicals used in the manufacturing of polymers, textiles, fuels, agrochemicals, pharmaceuticals and colorants [111]. Lataye et al. [111] have reported the adsorption capacity of GAC. Initial pH, adsorbent dose, contact time, initial concentration and temperature have been studied as impacting parameters on the adsorption efficiency. The maximum α-picoline adsorption onto GAC is 4.55 mg g^{-1} at low concentration (50 mg L^{-1}) and 36 mg g^{-1} at high concentration (600 mg L^{-1}) at GAC dosage of 10 kg m^{-3} at normal temperature. Radke–Prausnitz, Toth and Redlich–Peterson isotherms fits adequately to experimental data. Like pyridine the adsorption process is endothermic. The used GAC is regenerated by acidic water and acids. The results show that GAC can be used for the adsorption of α-picoline from aqueous solutions. Another advantage of this process is that α-picoline adsorption is almost independent on pH and so, conducting the adsorption in neutral range of pH is feasible. Also, producing the wastewater with low or high pH values cannot extensively affect the process efficiency.

Di Natale et al. [112] have worked on the removal of chromium ions by adsorption on GAC in aqueous solution. Chromium is a dangerous metal especially in Cr (VI) form. Trivalent chromium has much less toxicity. Di Natale et al. [112] have studied the chromium adsorption isotherms in aqueous solutions. They have shown that chromium adsorption capacity on GAC depends on salinity and pH of solution. Its maximum amount is around 7 mg g^{-1} at low salinity and neutral pH. The results show that at pH values lower than 3 the mechanism of chromium removal is first its reduction to Cr (III) by carbon surface groups and then the adsorption of Cr (III). At pH values higher than 7, there is a competition between Cr (VI), OH^- and Cl^- for adsorption on GAC. Langmuir isotherm model well fits the equilibrium experimental data.

Yang et al. [113] have studied removal of organic compounds in drinking water using GAC in a pilot plant. Organic compounds cause odor and taste problems in water sources. Organic compounds react with chorine used in water disinfection and produce harmful DBPs. DBPs include compounds such as trihalomethanes (THMs) and haloacetic acids (HAAs) which are resistant to traditional water treatment methods. GAC reduces the haloacetic acid formation potential more than that of trihalomethanes. The presence of bromide in the water body produces some brominated DBPs. 2-methylisoborneol (2-MIB) and geosmin are two major organic compounds giving taste and odor to water. These two compounds are easily removed by GAC but bromo-THMs cannot. Yang et al. [113] have found GAC as a promising tool to resolve odor problem in water sources.

GAC also has a lot of applications in the treatment of gas streams in fixed bed columns. The polluted gas stream, for example air, goes through a GAC column which adsorbs the pollutants and purifies the stream which leaves the column. Abumaizar et al. [114] have treated contaminated air streams by a biofilter containing compost and AC. The contaminants have been benzene, toluene, ethylbenzene, and o-xylene (BTEX). A biofilter is a filter bed with natural constituents such as soil and compost or peat in wet status which makes active the biofilm layer around the filter particles. Biofiltration of air streams with low pollutant

concentration has high removal efficiency, low capital and operational costs, higher degree of safety, low energy consumption and produces harmless products such as water and carbon dioxide [114]. The researchers have used three laboratory-scale biofilter columns to remove BTEX from a waste gas stream. Two of the three biofilters have comprised of a mixture of yard waste, sludge compost and GAC. The different amounts of GAC have been used to evaluate its effect in the promotion of the biofilter efficiency. The columns have utilized the BTEX with this order: benzene, toluene, ethylbenzene, and o-xylene. They have found that each of BTEX compounds can be removed with the removal efficiency greater than 90%. GAC increases the removal efficiency and makes stable the operation conditions when a shock appears in the system by increasing the gas flow rate or BTEX concentration. The results show that compost is a suitable biofilteration media to remove BTEX from gas streams but its ability increases after mixing with relatively small amounts of GAC. Using GAC, as a constituent of biofilter, the pressure drop in the column decreases.

Chung et al. [115] have removed the high concentration of NH_3 in gas streams containing H_2S using a biological filter containing GAC. H_2S and NH_3 are simultaneously emitted from processes like food and fish processing, rubber and leather industries, and wastewater treatment plants [115]. Biotreatment processes normally consist of two steps. In the first step, the pollutants are adsorbed on an adsorbent and then, in the second step, they are degraded using microorganisms living in the liquid phase or packing material. Type and amount of inoculated microorganisms, biofilter materials and operational conditions are very important in the performance of the filters. Biofilter materials must adsorb the pollutants, act as a support for microorganisms, have good water holding capacity, provide good air diffusion possibility, and have high pH buffer capacity and good mechanical characteristics [115]. AC can be used as a support material in biofilters. AC has good mechanical resistance, adsorbs water and provides sufficient surface area for the microorganisms. Chung et al. [115] have found high NH_3 and H_2S removal efficiencies from waste gases using biofilters. They have inoculated the GAC with *Arthrobacter oxydans CH8* for NH_3 removal and *Pseudomonas putida CH11* for H_2S removal. The results show that physical adsorption of NH_3 by GAC is efficient in first 10 days. After this period, ammonia gas is biodegraded by inoculated microorganisms. Average ammonia and H_2S removal efficiencies are greater than 96% and 100%, respectively over an operating period of 140 days without a need to pH adjustment. The results show that the pH remains between 6.5 and 8.0 after physical adsorption step. Coexistence of H_2S does not affect NH_3 removal efficiency. Gas retention time has an important role in the performance of the system. The efficient removal of high concentrations of NH_3 in its mixtures with H_2S and high adaptability of the system to loading and temperature shocks are advantages of the used GAC-based biofilter. In this system, NH_3 removal is not inhibited by H_2S and the pH is almost constant.

Gaur et al. [116] have studied the processing of landfill gas (LFG) using adsorption and alkanolamine absorption. Considering the energy crisis in the world, the recovery of LFG is very important. Methane is one major constituent of LFG, so it has high energetic potential. The application of LFG as an energy source reduces the green house gases emissions from landfills and reduces the consumption of fossil fuels. LFG is composed of CH_4 (35 to 60%), CO_2 (35 to 55%), and other trace components such as aromatics, chlorinated organic hydrocarbons, siloxanes and sulfur compound [116]. Adsorption is an economical and safe method. It is a good choice to remove impurities from gas streams. The impurities can be harmful for human and can cause problems like corrosion in boilers and combustion engines.

CO_2 can be efficiently removed from LFG using absorption by alkanolamine solutions. Gaur et al. [116] have converted the LFG to pure methane by adsorption on GAC and absorption by a mixed alkanolamine solution containing monoethanolamine and diethanolamine. In the work, toxic aromatic and chlorinated compounds were adsorbed on GAC in this order: carbon tetrachloride > toluene > chloroform > xylene > ethylbenzene > benzene > trichloroethylene ≈ tetrachloroethylene; Then, the gas stream was fed to a mixed solution of monoethanolamine and diethanolamine to absorb CO_2. The methane gas produced after adsorption and absorption steps can be used in domestic applications.

Jo and Yang [117] have used GAC adsorption followed by a photocatalytic system to control indoor aromatic compounds. VOCs are harmful compounds which are appeared in indoor environments and have dangerous health effects. BTEX is a category of VOCs produced from indoor sources like building materials and consumer products. GAC adsorbs VOCs and so, the pollutants transfer from a phase to another one and convert the GAC to a hazardous waste. Therefore, there is a need to find a method to regenerate the used GAC and degrade the adsorbed contaminants. Photocatalytic process can degrade the hydrocarbons to carbon dioxide and water after complete oxidation. So, photocatalytic processes can be considered as a proper GAC regeneration method. Adsorption capacity of GAC for BTEX compounds is low because of their low concentration in indoor air (< 1 ppm for each of BTEX constituents). Therefore, it is better to couple the GAC with photocatalytic degradation process to increase BTEX removal efficiency. Jo and Yang [117] have studied a hybrid system (Figure 3.2) containing a GAC step which its output stream passes through a thin TiO_2 film photocatalytic oxidation step. This arrangement regenerates the used GAC and control the concentration of BTEX in indoor air. The researchers have shown that the hybrid system has higher removal efficiency (about 100%) compared with the process containing GAC alone. Hybrid system does not have significant dependence on humidity and BTEX concentration. The results show that the photocatalytic oxidation unit degrades more than 70% of the BTEX desorbed from GAC unit. So this work shows that a photocatalytic oxidation step after a GAC adsorption unit can help to control the indoor concentration of BTEX compounds and to regenerate the used GAC.

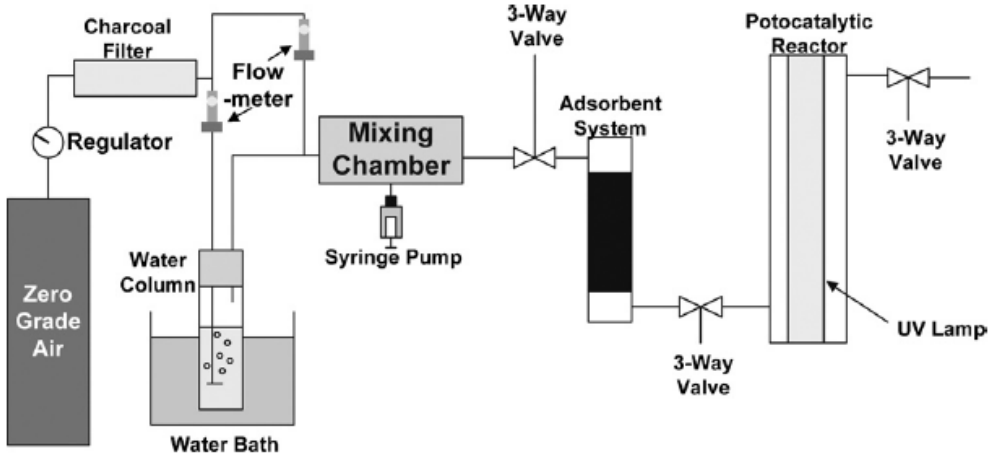


Figure 3.2. Schematic of the hybrid system used to remove BTEX compounds in indoor air. (Adapted from Jo and Yang [117] with permission from publisher, Elsevier. License Number: 2575950325875).

Sutherland et al. [58] removed methyl tert-butyl ether (MTBE) from ground waters using GAC and compared the results with air stripping and O_3/H_2O_2 and UV/H_2O_2 advanced oxidation processes. MTBE is widely used to improve the fuel combustion and to decrease the amount of pollutants emitted from vehicles. It enters the environment by leakage from underground storage tanks, spills, boats, etc. This leads to the pollution of ground water sources [58]. Since MTBE is highly soluble in water (43,000–54,300 mg L^{-1}), it easily transfers in the environment. The results show that GAC is mostly effective in MTBE removal but is more costly compared to air stripping and the advanced oxidation processes.

The results of other researches which have used GAC for treatment of contaminated aqueous and gaseous phases have been summarized in Table 3.2.

Table 3.2. Some of the GAC applications in the removal of contaminants

Removal agent/process	Treated phase	Pollutant(s)	Removal capability (proximate)	Ref.
GAC	Aqueous	Methyl violet	0.095 g g^{-1}	[118]
GAC	Aqueous	p-nitrophenol	5.5 mol kg^{-1}	[119]
GAC	Aqueous	Benzene	180 mg g^{-1}	[120]
Ozonation+GAC	Aqueous	C.I. Reactive Red 194, C.I. Reactive Yellow 145	95% COD removal	[121]
GAC	Aqueous	Cu (II), Co (II)	Cu (II): 28 mg g^{-1}, Co (II): 250 μmol g^{-1}	[122]
GAC+Ultrasound	Aqueous	Phenol	1.8 mol kg^{-1}	[123]
GAC	Aqueous	Phenol, Resorcinol	97% for each pollutant	[124]
GAC	Aqueous	Perfluorinated surfactants	230 mg g^{-1}	[125]
GAC	Aqueous	Trinitro-toluene (TNT), dinitro-toluene (DNT), nitrobenzene (NB)	400 mg g^{-1}	[126]
GAC	Aqueous	Lindane	300 mg g^{-1}	[127]
GAC	Aqueous	Phenolic compounds	0.252 g g^{-1} $h^{-0.5}$ for 2,4-Dichlorophenol	[128]
GAC	Gaseous	1,1-dichloro-1-fluoroethane (HCFC- 141 b)	560 mg g^{-1}	[129]
GAC	Gaseous	Benzene, chlorobenzene	Benzene: 320 mg g^{-1}, chlorobenzene: 450 mg g^{-1}	[130]
GAC bioreactor	Gaseous	H_2S	> 98%	[131]
GAC	Gaseous	Toluene	90%	[132]
GAC	Gaseous	SO_2, NO	SO_2: > 99% NO: 55%	[133]
GAC	Gaseous	Toxic compounds like aromatics and chlorinated compounds from LFG	-	[134]
GAC	Gaseous	Elemental mercury (Hg^0)	505 ng mg^{-1}	[135]
GAC	Gaseous	Dibenzofuran	0.28 g g^{-1}	[136]

3.3. Activated Carbon Fibers (ACF)

ACF is the newest form of AC and commonly used as felt and Cloth. ACF has some advantages compared with GAC and PAC, including:

- Adsorption rate of ACF is relatively higher than GAC. The diameter of carbon fibers is smaller than that of granules. Therefore, diffusion path in ACF pores is shorter and the adsorption rate is higher than that of GAC [137].
- ACF pores are mainly in micropore range, but in GAC, there are micropores, mesopores and macropores, together. Considering that high micropore content shows large surface area and adsorption ability, the adsorption ability of ACF is higher than that of GAC [137].
- Due to its monolithic form, handling of ACF in batch adsorbers and separation of used ACF is simpler than PAC and GAC [138].
- Unlike PAC, ACF has monolithic form and causes low pressure drop when used in adsorption column.
- Unlike PAC and GAC, ACF has monolithic form and high conductivity, so can be used as porous electrode in various environmental applications such as electroadsorption, electrooxidation and electroreduction processes.

Recently, the application of ACF in the environmental remediation, because of its advantages, increases. Various works are done in the removal of organic and inorganic pollutants from aqueous and gaseous phases using ACF [3, 139-142].

Aber et al. [3] have prepared ACF from natural Kenaf fibers using K_2HPO_4 as chemical activator and investigated its application in the removal of phenolic compounds from contaminated water. Phenolic compounds are a group of toxic chemicals which exist in wastewaters. The researchers have optimized the preparation of ACF by Taguchi experimental design method, and then studied the kinetics and the isotherms of phenol and p-nitrophenol adsorption on ACF. According to the results of equilibrium adsorption experiments, the adsorption of phenol and p-nitrophenol follows Langmiur model. The maximum adsorption capacity of the prepared ACF for phenol and p-nitrophenol has been found to be 140.84 and 136.99 mg g^{-1}, respectively. The results of kinetic adsorption experiments also indicate that the adsorption process follows the pseudo-first-order kinetic model.

Ayrancy and Hoda [139] have reported the ability of ACF with a surface area of 2500 m^2 g^{-1} in the removal of pesticides ametryn, aldicarb, dinoseb and diuron from contaminated water. The results of equilibrium adsorption experiments show that adsorption of ametryn, aldicarb, dinoseb and diuron on ACF fits reasonably the Langmuir and Freundlich isotherm models. The maximum adsorption capacity of ACF for pesticides is as the following: ametryn > diuron > aldicarb > dinoseb. Results obtained from adsorption kinetic studies show that the adsorption of ametryn follows the pseudo-first-order model but the adsorption of aldicarb, dinoseb and diuron follows the pseudo-second-order one. According to the results obtained from both pseudo-first-order and pseudo-second-order models, adsorption rate constants of pesticides are in the following order: dinoseb > ametryn > diuron > aldicarb.

Nabais et al. [140] have removed mercury from aqueous solutions and flue gas by adsorption on commercial and laboratorial prepared ACF. They have prepared ACF from commercial acrylic textile fibers. Before the adsorption experiments, powdered sulfur or H_2S gas have used to modify the surface of ACF samples. The removal of mercury has been investigated using 0.1 g of modified ACF and 50 mL $HgCl_2$ solution (1500 mg L^{-1}) at pH 6.0. The $HgCl_2$ concentration in solution was measured by ultraviolet spectrophotometry at 230 nm, after 24 h contact time. The results show that the modified ACF samples can adsorb $HgCl_2$ favorably (290–710 mg g^{-1}). Among modified ACF samples, prepared ACF modified with H_2S gas shows better performance. They have also used ACF, which modified by powdered sulfur, to prepare a filter for the removal of mercury species from flue gases produced via fossil fuel combustion. They have found that the filter can remove all the mercury from flue gas.

Mohan et al. [141] have used commercial and laboratorial prepared ACF for the removal of trivalent chromium from tannery effluents. First, they have prepared ACF from coconut shell fibers using chemical activation method, and then, investigated the kinetic and the equilibrium of Cr (III) adsorption on both commercial and prepared ACF samples. The results of kinetic studies show that the adsorption of Cr (III) on ACF samples follows pseudo-second-order model. Also, according to the results obtained from equilibrium adsorption experiments, the Langmuir model better describes the adsorption of trivalent chromium. On the basis of Langmuir model, the maximum adsorption capacity of commercial and prepared ACF samples for the removal of trivalent chromium at 25 ^{o}C is 12.2 and 39.56 mg g^{-1}, respectively. The adsorption capacity of ACF samples is enhanced with increasing the adsorption temperature. Finally, Mohan et al. have compared the adsorption ability of commercial and prepared ACF samples with other adsorbents or biosorbents in the removal of Cr (III). The results show that commercial and prepared ACF samples are appropriate adsorbents in the removal of trivalent chromium from aqueous environments.

ACF has high electrical conductivity and adsorption ability, so it can be used in electroadsorption, electrochemical degradation and photoelectro-Fenton methods for the removal of pollutants from contaminated waters. Electroadsorption is a non-faraday process, in which the surface of adsorbent is electrically polarized. Therefore, the adsorbents with high surface area and conductivity are appropriate to be used in electroadsorption process [142]. The polarization of adsorbent surface accelerates the adsorption of ions and polar molecules from electrolyte solution and as a result, the adsorption capacity of adsorbent for polar and ionic adsorbates increases. According to Foo and Hameed [143], electroadsorption was introduced by Grahame in 1946 when he studied on the potential-controlled adsorption of *n*-octanol. The application of this method rapidly developed and now is used in various applications. The most important advantages of electroadsorption process are [144, 145]:

1) Low energy consumption,
2) Selectivity,
3) Be friendly to the environment,
4) Safety,
5) Versatility, and
6) Cost effectiveness.

Han et al. [146] have studied the removal of phenol from basic aqueous solution using electroadsorption on ACF with surface area of 1335 m^2 g^{-1}. Cyclic voltammetry has been used to determine the range of electric potential, in which the phenol is not electroactive. This is very important step to prohibit the reduction or oxidation of phenol during electroadsorption process. They have investigated the effect of bias potential on the electrosorption of phenol from a solution containing 2 mmol L^{-1} phenol and 0.05 mol L^{-1} NaOH. The adsorption ability of ACF after 10 h contact time enhances from 0.2 mmol g^{-1} to 2.3 mmol g^{-1} using a bias potential between 0 and 700 mV. The researchers have also investigated the effect of electrolyte concentration on the electroadsorption ability of ACF. The obtained results show that with increasing electrolyte concentration, electroadsorption rate is enhanced due to an increase in solution conductivity, but the equilibrium adsorption capacity decreases because electrolyte ions occupy some of ACF pores. Thermodynamic results show that the electroadsorption of phenol on ACF is exothermic.

Park et al. [147] have treated ACF, electrochemically and used it for the removal of Cr (VI) from aqueous solutions. As mentioned previously, surface functional groups of AC as well as its surface area and porosity affect its adsorption ability. They have used phenol-based ACF with the surface area of 1646 mg g-1 and treated it with anodic oxidation in the aqueous solution of sodium hydroxide at 25 ^oC and current density of 0-450 mA m^{-2}. According to obtained results, anodic oxidation enhances the acidity of ACF and increases the presence of functional groups on ACF surface. They have investigated the adsorption capacity and the rate of treated ACF in the removal of Cr(VI) from aqueous solutions. The results show that increasing current density from 0 to 450 mA m^{-1}, increases the equilibrium amount of adsorbed Cr (VI) on ACF from 293 to 372 μmol g^{-1}. Anodic oxidation not only enhances the adsorption rate and capacity of ACF, but also improves its mechanical strength.

The electrical polarization of ACF surface not only enhances adsorption rate and capacity, but also helps the regeneration of ACF after electroadsorption. Han et al. [142] studied on the electrochemical adsorption and desorption of acid orange 7 on ACF. The electrosorption experiments were done using 30.0±0.5 mg ACF in 1 mmol L^{-1} acid orange 7 solution at polarized potential of 0 (open circuit), 200, 400 and 600 mV. The results indicate that the polarization potential of 600 mV shows better performance and enhances the adsorption rate and capacity by 120% and 115%, respectively. After electroadsorption, the electrochemical regeneration of ACF has been performed with 80 mL of 2% NaCl solution for 2 h. According to obtained results using a potential of −5 V, more than 90% of ACF pores are regenerated. After 10 cycles of electrosorption and regeneration, more than 70% of initial ACF pores are remained. These results show the positive effect of electrochemical polarization on adsorption performance and reducing its costs.

Fan et al. [148] have studied the application of ACF as an electrode for the electro-chemical degradation of amaranth, an azo dye, under galvanostatic conditions. They have used a cell with two separated compartments connected through a cation selective membrane. The cell contains three electrodes including a piece of ACF as working electrode, a Pt wire as counter electrode and a saturated calomel electrode (SCE) as reference electrode. Potentials of oxidation and reduction of amaranth on ACF are 0.6 and -0.4 V, respectively. According to the obtained results, with the current density in the range of −1.1 to 0.50 mA cm^{-2}, electroreduction, adsorption and electrooxidation have influence on the dye removal. Results show that adsorption has the lowest influence. The color and COD removal efficiencies by applying the current density of 0.50 mA cm^{-2} after 8 h contact time are 99.1% and 52%,

respectively. The current density of −1.0 mA cm^{-2} results in 100% color and 61% COD removal. The results show that the performance of electroreduction is a little higher than electrooxidation in the removal of amaranth.

Wang et al. [149] have used ACF as cathode for the removal of acid red 14 (AR14) by photoelectro-Fenton process. They have used an electrochemical cell containing a 20-cm^2 RuO_2/Ti anode and a 20-cm^2 ACF cathode for the electrochemical generation of H_2O_2. Heptahydrated ferrous sulfate was used as ferrous ion source. Before photoelectro-Fenton process, the ACF was saturated with AR14 using 400 mg L^{-1} dye solution for 12 h. According to obtained results, this process can remove more than 94% of TOC from 450 mL contaminated solution with initial AR14 concentration of 200 mg L^{-1}. They have also investigated the ACF cathode ability in the repetitive degradation of AR14 in 6-h cycles. The results show the stability of ACF cathode in the electrogeneration of H_2O_2 after 4 cycles.

ACF can be used to remove pollutants from gas phase, too. Das et al. [150] have used ACF in the removal of VOCs from gaseous stream. Benzene, toluene, xylene, dichloromethane, and trichloroethylene have been selected as the examples of VOCs. Das et al. [150] have used two types of ACF with surface area of 1000 and 1700 m^2 g^{-1} prepared from viscous rayon, and investigated the effect of inlet VOC concentration, gas flow rate, bed temperature and ACF dosage on the dynamic adsorption of VOCs on ACF. According to the results, the adsorption is exothermic and the bed temperature of 50 ^oC is suitable for adsorption. It is also observed that the adsorption performance of ACF with the surface area of 1700 m^2 g^{-1} is higher than that with 1000 m^2 g^{-1}. The adsorption ability of ACF in the removal of VOCs has been compared with that of GAC, 5A zeolites and silica gel. In the same operational conditions, the adsorption ability of ACF is the highest compared with the other adsorbents. The used ACFsamples have been appropriately regenerated by DC electrical heating at 150 ^oC. The obtained results show that the reoccurrence of adsorption and regeneration for 25–30 cycles does not change the adsorption capacity of ACF, considerably.

ACFs in some conditions have catalyst role in the removal of pollutants from gas phase. Muniz et al. [151] have used the ACF samples derived from coal and petroleum pitch, polyacrilonitrile, and phenolic resin and applied them to catalyze the reduction of NO to NH_3 at temperatures between 100 – 400 ^oC. A mixture of 700 ppm_v (ppm in terms of volume) NO, 800 ppm_v NH_3, 3 $\%_{vol.}$ O_2 and He has been used as a model flue gas. In this condition, NO reacts with NH_3 and O_2 which results in the production of N_2 and H_2O. The results indicate that polyacrilonitrile-based ACF exhibits the highest catalytic activity among all studied ACF samples. This is due to the presence of nitrogen containing functional groups on its surface. Due to the negative effect of H_2O, the activity of ACF is low at temperatures below 250 ^oC in the presence of H_2O. The results of kinetic studies also show that the NO reduction reaction has first-order and zero-order dependence on NO and NH_3, respectively.

The results of other researches which have used ACF for treatment of contaminated aqueous and gaseous phases have been summarized in Table 3.3.

Table 3.3. Some of the ACF applications in the removal of contaminants

Removal agent/process	Treated phase	Pollutant(s)	Removal capability (proximate)	Ref.
ACF	Aqueous	2,4-dichlorophenol	347 mg g^{-1}	[152]
ACF	Aqueous	Acid Blue 45, Acid Blue 92, Acid Blue 120, Acid Blue 129	1.3×10^{-4} 6.5×10^{-5} 3.6×10^{-5} 1.2×10^{-4} mol g^{-1}	[153]
ACF	Aqueous	Humic acids	15.3 mg g^{-1}	[154]
ACF	Aqueous	*p*-nitrophenol	450 mg g^{-1}	[138]
ACF	Aqueous	Lead (II)	0.064 kg kg^{-1}	[155]
ACF	Aqueous	1,1-Dichloroethene, Trichloroethene, Tetrachloroethene, 1,1,2-Trichloroethane	18.91, 42.75, 88.41, 27.48 mg g^{-1}	[156]
ACF (electroadsorption)	Aqueous	Catechol, Resorcinol	2.3×10^{-3} 1.9×10^{-3} mol g^{-1}	[157]
ACF	Aqueous	Benzyltrimethylammonium chloride	0.07 mmol g^{-1}	[158]
		Benzyltriethylammonium chloride	0.33 mmol g^{-1}	
		Benzyltributylammonium chloride	0.68 mmol g^{-1}	
		Benzyldimethyldecylammonium chloride	0.94 mmol g^{-1}	
		Benzyldimethyltetradecyl ammonium chloride	0.87 mmol g^{-1}	
		Benzyldimethylhexadecylammonium chloride	0.86 mmol g^{-1}	
		N-dodecylpyridinium chloride	1.28 mmol g^{-1}	
		N-cetylpyridinium chloride	1.10 mmol g^{-1}	
ACF	Gaseous	SO_2	92%	[159]
ACF	Gaseous	Cr, Cd, Pb species	20, 12.8, 28.6 mg g^{-1}	[160]

3.4. Impregnated Carbon (IC)

New science and technology combine other remediation methods with the adsorption so that contaminants can be removed in a more efficient manner. ICs are ACs promoted by doping of active agents on their surface. Doping agent can be a metal, or an organic or an inorganic compound which give new traits to AC or promote its adsorption capacity and rate. Doping (impregnating) agent is selected according to the type of pollution which is under treatment. All previously mentioned types of AC including PAC, GAC and ACF can be impregnated with proper doping agents.

Yuan et al. [161] have prepared TiO_2/ACF composite and investigated its ability in the removal of methylene blue (MB) in aqueous solution. TiO_2/ACF composite has been prepared by mixing TiO_2 and ACF with epoxy, followed by calcination at 460 ^oC in N_2 atmosphere. Then, the prepared composite has been repeatedly used for the removal of MB with initial concentration of 85 mg L^{-1}. Finally its ability has been compared with that of fresh

P25 TiO_2. After six photocatalytic degradation cycles, not only the photocatalytic ability of TiO_2/ACF composite is not reduced, but also its amount is higher than fresh P25 TiO_2.

Liu et al. [162] have used ACF to prepare chitosan/ACF/TiO_2 membrane and investigated the adsorption, filtration and photocatalytic properties of the membrane in the removal of 2,4-dichlorophenol (2,4-DCP) from water. Dynamic filtration of 2,4-DCP solution with the concentrations of 1–50 mg L^{-1} with flow rates of 25-100 L m^{-2} h^{-1} has been investigated using the prepared composite. According to the results, under dynamic filtration with low 2,4-DCP concentration and low flow rates the removal rate of pollutant is relatively acceptable. The effect of in-situ and off-site UV/TiO2 oxidation on the regeneration of composite has been compared. The results show that off-site regeneration is more effective than in-situ one. The reason is thought to be the fact that the concentration of pollutants is low and the loaded photocatalyst on the membrane does not have good contact with the pollutants in in-situ regeneration method.

Alves and Clark [163] have reported the adsorption of hydrogen cyanide (HCN) and cyanogens ($(CN)_2$) with ACs impregnated by Cu (II) and Cr (V). The proper protective masks used for the protection of workers against HCN have canisters filled with GAC impregnated with Cu (II), Cr (VI) and Ag and called Whetlerite [163]. These species enhance the chemisorption of HCN and prevent it's desorption during the usage of the mask. The following reaction (Eq. 3.26) takes place on the surface of AC doped with Cu (II) [163]:

$$Cu^{2+} + 2CN^{-} \rightarrow CuCN + \frac{1}{2}(CN)_2 \tag{3.26}$$

Alves and Clark [163] have reported the copper impregnation and soaking the substrate AC in a solution of Cu $(NO_3)_2$ for 1 h. The soaked AC has been filtered and dried at 373 K. The AC then has been heated at 870 K for 1 h in a furnace under N_2 stream to decompose the nitrate. The impregnation of chromium has been done on ACs impregnated and non-impregnated with copper, using a solution of $Na_2Cr_2O_7$. They have compared the ability of prepared ICs with commercial IC called Whetlerite in gas phase and found that these two types of ICs have comparable properties.

Cao and Shiraishi [164] have studied the photocatalytic and adsorptive treatment of 2,4-dinitrophenol (DNP) in aqueous solution using GAC with particles covered by TiO_2 film. DNP is a compound which is used in the preparation of black dyes, as the inhibitor of polymerization and as wood preservative [164]. The photocatalysts such as TiO_2 can be combined with AC to increase the reaction rate of contaminants removal. In hybrid systems, AC is covered with a thin layer of photocatalyst and this increases the adsorption of the contaminants and takes them to reaction surface. Hybrid systems also increase the surface to volume ratio of the photocatalyst. Both of these changes increase the efficiency of the process in the removal of contaminants. Cao and Shiraishi [164] have used polyethylene terephthalate (PET) films as a support for AC+TiO_2 system. Their results show that the presence of AC enhances the photocatalytic decomposition rate. Also, the presence of TiO_2 decreases the loading of AC since some of DNP molecules are degraded by TiO_2.

The application of metal impregnation of GAC in the removal of cyanide from aqueous solution has studied by Deveci et al. [165]. They have prepared the ICs by contacting GAC samples with $CuCl_2$ or $AgNO_3$ solutions for three days. The results show that the cyanide

removal capacity of GAC considerably increases by impregnation with copper and silver (up to 6.3 fold). The analysis show that the loading of silver on GAC is more successful than copper (5.07 % against 0.43%). The silver impregnated GAC removes 5.7–92.3% of cyanide while copper impregnated GAC and plain GAC remove 4.4–35.4% and 1.5–14.3%, respectively. The results confirm that the adsorption of cyanide by prepared ICs follows pseudo-second-order kinetic and Langmuir isotherm models. They have stated that metal impregnation increases the adsorption capacity of AC because of the formation and adsorption of metal cyanide complexes on AC surface.

Duman and Ayranci [166] have studied the attachments of benzo-crown ethers onto ACF to adsorb Cr(III), Co(II) and Ni(II) from aqueous phases. Chromium, cobalt and nickel are important environmental pollutants. Chromium is discharged from metal finishing, electroplating, leather tanning, and mineral color production industries and nickel is distributed from pigments, battery, mining, ceramic, and electroplating industries [166]. These metal ions produce serious health problems and are not degradable in the environment, so they must be removed before discharge in to the environment. Crown ethers form complexes with certain metallic positive ions depending on the size of ion and the size of their cavity. Duman and Ayranci [166] have used two groups of crown ethers to modify the surface of ACF. Monobenzo-crown ethers are in the first group including benzo-12-crown-4, benzo-15-crown-5 and benzo-18-crown-6. Second group comprises dibenzocrown ethers such as dibenzo-15-crown-5, dibenzo-18-crown-6, dibenzo-21-crown-7, dibenzo-24-crown-8 and dibenzo-30-crow-10. They have reported that ACF better adsorbs the monobenzo-crown ethers than dibenzo-crown ones. They have also reported that in each group, increasing the size of crown ether increases its adsorption on the ACF surface. The results show the better adsorption of Cr (III) on modified or unmodified ACF than Co (II) and Ni (II). The adsorption of studied ions onto ACF has been enhanced after modification with monobenzo-crown ethers. The ACF modified with benzo-18-crown-6 shows the highest adsorption capacity for chromium. While the benzo-12-crown-4 modified ACF shows the highest adsorption capacity for cobalt and nickel ions.

ICs can be used in the degradation of sulfur mustard in air stream. Sulfur mustard, also known as mustard gas or mustard agent, is a dangerous chemical used in World Wars I and II. Considering the dangers of sulfur mustard, Prasad et al. [167] have studied its degradation kinetics and the effect of moisture on its degradation on IC systems like $NaOH/CrO_3/C$, $NaOH/CrO_3/EDA/C$ and $RuCl_3/C$. They have prepared the ICs via the impregnation of AC in aqueous solutions containing 4% sodium hydroxide and 3% Cr(VI) as CrO_3, with or without 5% ethylene diamine (EDA) and 5% ruthenium chloride. They have shown that the degradation follows first-order kinetics and degradation rate constants decrease with the increase in humidity. They have revealed that the prepared ICs can be used in personal protection filters against sulfur mustard. These filters are better than the ones act only upon adsorption, because the later desorption of pollutants is possible when adsorption is the only mechanism. But, the filters based on ICs degrade the pollutants which decreases the possibility of later pollutant desorption. The degradation of sulfur mustard has been studied by Sharma et al. [168], too. They have used carbons impregnated by polyoxometalates. The used polyoxometalates are 11-molybdo-1-vanadophosphoric acid (V1/C), phosphotungstic acid (PTA/C), sodium phosphotungstic acid (PTANa/C), phosphomolybdic acid (PMoA/C), sodium phosphomolybdic acid (PMoANa/C) and silicotungstic acid (SiTA/C). They contacted the ICs and the sulfur mustard solution in chloroform. The degradation reaction of

sulfur mustard follows the pseudo-first-order kinetics. The researchers have reported the V_1/C as a promising system for sulfur mustard degradation.

Ramos et al. [169] have used aluminum-impregnated carbon to adsorb fluoride from aqueous solutions. Drinking waters with fluoride concentrations higher than permitted limit cause fluorosis. The researchers have combined the high surface area of activated carbon with the high affinity of aluminum towards fluoride anion. They have contacted activated carbon with a solution of aluminum nitrate for 5 days followed by drying at 100 ^oC for 24 h and calcination in N2 atmosphere at a temperature between 300-1000 ^oC for 1 h. They have shown that aluminum-impregnated carbon capacity for fluoride removal is 3 to 5 times of plain AC.

Gu et al. [170] have used TiO_2 supported by GAC to remove 2, 4-dichlorophenol (DCP) from aqueous solution. DCP has some applications in the production of insecticides, herbicides, preservatives, antiseptics and disinfectants. Immobilization of TiO_2 on GAC makes easier its separation from reaction environment and also increases the surface area which brings more photocatalytic active sites. Using GAC as the support of TiO_2 increases the adsorption capacity of the system and this, concentrates the pollutants near TiO_2 particles, which lead to an increase in the efficiency and rate of oxidation of pollutants. It also can adsorb the oxidation intermediates for further and complete mineralization. Gu et al. [170] have used a pilot scale reactor to study the effect of air flow rate, initial pH, annealing temperature, catalyst loading, and DCP concentration on its removal. Their results show that the synergistic effect of adsorption by GAC and photocatalytic degradation by TiO_2 increases the DCP removal efficiency up to about 100% after 60 min contact time while it is about 48% for GAC adsorption alone.

There are a lot of reports about the applications of ICs in decontamination of gas phase (see Table 3.4). In these works continuous fixed or fluidized bed systems, and desiccators containing ICs and vaporized adsorbate are used for decontamination of gas phase. For instance, Lee et al. [171] have used a fixed bed system to study the ability of GAC impregnated with iodide and chloride in the removal of mercury (Hg^0) from gas phase. In their work, HCl and KCl solutions have been used to impregnate the GAC samples. The results show that GACs impregnated with I^- and Cl^- have reasonable capacity to remove elemental mercury. The results also show that Hg^0 adsorption efficiency for I-impregnated GAC increases with temperature (680.2, 703.3, 847.5 μg g^{-1} at 80, 120, 140 ^oC after 4 h contact time, respectively). But, increasing the temperature has reverse effect on Cl-impregnated GAC (645.9, 577.7, 537.4 μg g^{-1} at 80, 120, 160 ^oC after 4 h contact time, respectively).

Mei et al. [172] have studied the removal of elemental mercury from vapor phase by AC impregnated with N-doped $CuCoO_4$. Commercial GAC has been impregnated with $CuCoO_4$ (AC–C), $CuCoO_4$+NH_4Cl (AC–Cl), and $CuCoO_4$+NH_4Br (AC–Br). The results show that AC-Cl and AC-Br have higher Hg^0 oxidation ability compared to AC-C at a wide temperature range (350-530 K). They have found that for the all three types of ICs, the increase of impregnation degree increases Hg^0 oxidation ability. The results show that the impregnation of AC increases its ability to oxidize and to capture the elemental mercury. The Hg capturing ability of AC, AC-C, AC-Cl and AC-Br is equal to 0, 63.4, 87.6 and 91.5%, respectively and their Hg oxidation ability is equal to 0, 65.2, 90.3 and 94.2%, respectively. These results approve that the proper impregnation of AC samples significantly increases the removal efficiency of elemental mercury from vapor phase. The oxidation of elemental mercury to its

cation is important because Hg^{+} and Hg^{2+} are soluble in water and are less volatile, so they can be controlled in easier way than elemental mercury.

Table 3.4. Some of the ICs applications in the removal of contaminants

IC type	Treated phase	Pollutant(s)	Removal capability (proximate)	Ref.
GAC impregnated with sulfur using Na_2S solution	Aqueous	Pb (II)	Removal efficiency of Pb (II) with IC was 35% higher than non-impregnated carbon	[175]
ACF impregnated with Cu using copper nitrate solution	Aqueous	Ammonia	Ammonia conversion of 95% by wet oxidation in the presence of Cu-ACF catalyst. IC acts as an oxidation catalyst.	[176]
GAC loaded with ZnO	Aqueous	Pb (II)	0.043 mmol g^{-1} for GAC, 0.221 mmol g^{-1} for ZnO-GAC	[177]
GAC coated with MnO_2	Aqueous	Fluoride anion (F^-)	2.1 mg g^{-1} for MnO_2-GAC, 0.8 mg $g^{-1}$for GAC	[178]
TiO_2 nanoparticles immobilized on ACF	Aqueous	Phenol, Methyl orange	Phenol: 31% by ACF against 93% by TiO_2-ACF Methyl orange: 19% by ACF against 98% by TiO_2-ACF	[179]
GAC coated with Iron	Aqueous	Selenite (SeO_3^{2-})	97.3% for IC, 7% for non-impregnated carbon	[180]
Zinc-impregnated AC	Gaseous	H_2S	5.16%wt sulfur	[181]
Co_3O_4 (AC-Co) , MnO_2 (AC-Mn) and $CuCoO_4$ (AC-CC) loaded activated carbon	Gaseous	Mercury	91% Hg^o removal for AC-Co, 63% Hg^o removal for AC-Mn, 69% Hg^o removal for AC-CC	[182]
AC impregnated with 5 wt.% ruthenium chloride	Gaseous	Diethyl sulphide	-	[183]
GAC impregnated with copper chloride (BPL-C), b-aminoanthraquinone (BPL-A), 2-(aminomethyl)pyridine (BPL-P), and 2-aminoethanethiol (BPL-T)	Gaseous	Mercury	515 μg $g^{-1}Hg^0$ removal by BPL-C, 297 μg $g^{-1}Hg^0$ removal by BPL-A, 1247 μg $g^{-1}Hg^0$ removal by BPL-T, 0.3 μg $g^{-1}Hg^0$ removal by BPL-P	[184]
AC impregnated with Cu(II) 1,1,1,5,5,5-hexafluoroacetylacetonate, Cu(II) 1,1,1-trifluoroacetylacetonate, 1-phenylbute-1,3-dione-2-oxime plus Cu(II)	Gaseous	Dimethyl methylphosphonate	68.5% wt removal by Cu hexafluoro acetylacetonate IC, 59% wt removal by Cu trifluoro acetylacetonate IC	[185]
ACF impregnated with NH_3	Gaseous	SO_2	100%	[186]
Zinc chloride impregnated AC	Gaseous	Mercury	880 μg $g^{-1}Hg^0$ removal for IC, 110 μg $g^{-1}Hg^0$ removal for non-impregnated carbon	[187]

In another work, Peterson et al. [173] have used triethylene diamine (TEDA) impregnated carbon for the removal of methyl bromide (CH_3Br) from air stream. The adsorption capacity of ACs for methyl bromide is low and their surface should be modified for better adsorption. Peterson et al. [173] have impregnated GAC by TEDA through contacting them as solid in a V-blender at 60 ^oC for 2 h. At this temperature TEDA sublimes and penetrates GAC pores.

They have found that the prepared IC removes CH_3Br from dry and humid air streams (up to 100 mg g^{-1}). Bulushev et al. [174] have used gold impregnated ACF to oxidize carbon monoxide (CO) at low (room) temperatures. AC supports compared to oxide supports (e.g. Al_2O_3, SiO_2, TiO_2, MgO, and Fe_2O_3) have advantages such as high specific surface area, stability in acidic and basic conditions, and ability to burn the catalyst for the recovery of supported metal [174]. Bulushev et al. [174] have reported that ACF impregnated with gold nanoparticles (2-5 nm) can effectively oxidize CO at low (room) temperature. They have used the aqueous solution of gold complex with ethylenediamine, $[Au(en)_2]Cl_3$. Gold deposition has been done on the ACF surface through ion exchange mechanism between Au and the protons of carboxylic and phenolic groups on the ACF surface. They have achieved CO to CO_2 conversions up to 44% by 0.02 g gold impregnated ACF with 4.8% gold and activated in H_2 at 673 K, in a gas stream with 1 vol% CO, O_2 to CO ratio equal to 5 and total gas flow rate of 100 mL min^{-1}. The results of other researches which have used ICs for treatment of contaminated aqueous and gaseous phases have been summarized in Table 3.4.

3.5. Application of AC in Soil Remediation Processes

Surfactant solutions can be used for the washing of polluted soils. The application of surfactants increases the cost of soil remediation process so it is necessary to have a proper method to reuse the surfactant. The adsorption of contaminants by AC helps to reuse the surfactants. Ahn et al. [188] have studied the adsorption of Triton X-100 as a nonionic surfactant and phenanthrene as a soil pollutant on GAC samples. They have studied the adsorption of these two compounds in their separate solutions and also in their mixtures. The results show that phenanthrene can be separated from surfactant via adsorption on GAC and this helps to reuse the surfactant in soil washing processes. In another work, Ahn et al. [189] have investigated the application of selective adsorption for separation of phenanthrene from Tween 40, Tween 80, Brij 30 and Brij 35 nonionic surfactants. They achieved an effective recovery of 85-89% for all studied surfactants.

Polluted soils can be treated using supercritical fluid extraction (SFE) technology. One of the most advantages of this technology is the preservation of the structure and nutrients of soil. After extraction process using a supercritical solvent, the pressure above the solvent decreases and solvent and solute are separated, but the recompression of the solvent for further use is costly. This costly separation step can be replaced by a cheaper alternative which is the adsorption of solute from solution. Alonso et al. [190] have used a pilot plant to remediate polluted soil through extraction of pollutant by supercritical CO_2 and then the pollutant adsorption on AC. They have optimized the operational parameters such as extraction temperature, soil particle size and solvent ratio. They have found that good results are achieved by controlling the conditions at 26 MPa and 40 ^oC in extraction step and at 50 ^oC in adsorption step when treating the soil polluted by gasoil. According to the results the application of supercritical extraction combined with adsorption is possible in commercial scale.

Bes and Mench [191] have studied the immobilization of copper in contaminated topsoil using AC. They have believed that the excavation of the large amounts of polluted soil and its disposal in landfills or exposing it to washing processes has different economical, ecological and environmental problems. Therefore, in-situ treatment of soil is preferred by the

techniques such as addition of AC to polluted soil to adsorb the contaminants. The researchers have found that the addition of AC, as single or combined with zero valent iron (ZVI), to polluted soil results in the lowest concentration of copper (0.04 mg L^{-1}). This means that AC successfully adsorbs and immobilizes copper. Brändli et al. [192] have used a similar method for in-situ remediation of soil and fixing native polyaromatic hydrocarbons (PAH) in soil using AC and CB. They have added 2% PAC to a moderately polluted urban soil and found that the concentration of native PAH in soil solution decreases up to 99%. For the same soil with higher PAH pollution, GAC reduces PAH concentration in soil solution about 64%. They found that the reduction of pollution in heavily contaminated creosote soil was about 63% and 4% using PAC and GAC, respectively.

Gong et al. [193] have used AC to regenerate the vegetable oil used in the remediation of contaminated soils. Vegetable oil is a non-toxic, economic and biodegradable solvent to extract PAHs from contaminated soils. The resulting vegetable oil can be reused by the separation of extracted PAHs. Gong et al. [193] have performed batch and column adsorption tests on oil-AC systems. They have run equilibrium isotherm studies and investigated the effect of operational parameters such as initial concentration of PAHs and AC dosage. They have found that AC is effective in the regeneration of the used vegetable oil.

Koran et al. [194] have used an anaerobic GAC fluidized bed bioreactor to treat a synthetic solution. The pollutants in this study have been pentachlorophenol (PCP) and four PAHs including naphthalene, acenaphthene, pyrene and benzo(b)fluoranthene. The synthetic solution has simulated the effluent of a soil washing process used for the soils of a wood preserving site. The results show that PCP removal efficiency from washing effluent is higher than 99.8% with 46.5% conversion to its dechlorination intermediates. Naphthalene and acenaphthene are removed from the washing effluent with 86% and 93% efficiency, respectively. The concentration of pyrene and benzo(b)fluoranthene is very low in treated phase owing to the high adsorption of these compounds on GAC. The results indicate that these two compounds cannot be converted biochemically in the reactor. The anaerobic GAC fluidized bed bioreactor is a good choice for the treatment of soil washing effluents.

Liang et al. [195] have studied the effect of biocarriers on the biodegradation of crude oil as a remediation process for the soils polluted with crude oil. Biodegradation is an economic choice for the remediation of soils polluted with crude oil but its slow degradation rate is a major problem. It is due to the low number of hydrocarbon degrading bacteria and the low bioavailability of contaminants which is consumed by bacteria. Biocarriers are porous materials such as ACs and zeolites which immobilize hydrocarbon degrading bacteria. In the experiments of Liang et al. [195], the number of bacteria have reached 10^{10} cell per gram on AC. The intrinsic biodegradation removes 13% crude oil while the addition of AC to the samples increases the removal percent to 48.89%. The results indicate that addition of biocarrier increases the bacterial population in the soil to 10^8 cells per gram of dry soil. The increase in biodegradation efficiency and microbial population in the soil is due to the improvement of oxygen and nutrient mass transfer and water holding capacity of the soil. These improvements result from the adsorption property of biocarrier**.**

Liu and Yu [196] have used microwaves along with GAC to treat polychlorinated biphenyl (PCB) contaminated soil. They have studied the removal of 2,4,5-trichlorobiphenyl (PCB29) with the combination of microwave irradiation and GAC. The role of GAC in this method is the absorption of microwave so that high temperatures are obtained. It also acts as reductant in the dechlorination reaction. The experiments show that GAC effectively

increases the temperature of soil and PCB removal rate is dependent on microwave power, soil moisture content, and GAC amount. The addition of 1.0 g GAC to the soil increased the temperature from 220 ^{o}C to 550 ^{o}C after 900 s microwave irradiation with the power of 700 W in a soil with 50 mg kg^{-1} initial PCB29. In this case, the addition of GAC increased the PCB29 degradation rate constant from 0.024 to 0.148 min^{-1}.

Liu et al. [197] have studied the adsorption of PCB29 from simulated soil washing solution by GAC in a continuous flow column and regenerated the used GAC by 2450 MHz 700 W microwave irradiation for 5 min. They have found that after several adsorption and regeneration cycles, the adsorption rate of GAC increases but its capacity decreases which are probably due to the changes in textural properties of GAC. The results show that the most of adsorbed PCB29 is degraded during 3 min irradiation via dechlorination mechanism.

Park et al. [198] have studied the impact of PAC on the capacity of landfill cover soil in methane removal. Landfill gases mainly are constituted of methane (CH_4) and are emitted in to the atmosphere. Landfill cover soil can act as a biofilter to oxidize methane to carbon dioxide and water. Park et al. [198] have performed column and batch studies and found that the landfill cover soil amended with PAC is similar to the soil amended with earthworm with methane removal rate of 14.6 mol m^{-2} d^{-1}. But the methane removal rate is 7.4 mol m^{-2} d^{-1} for the landfill cover soil without any amendment. The results indicate that earthworm amendment increases the oxidation of methane while PAC acts by its adsorption. According to their results the amendment of landfill cover soil with earthworm and PAC causes to a major decrease in methane emission into the atmosphere.

It can be concluded that AC is an adsorbent material with three major forms of PAC, GAC, and ACF and so it has enough flexibility for application in various systems with different shapes and operational parameters. AC also removes pollutants almost without releasing harmful chemicals to the environment. It has the ability of improving its adsorption capability through the doping of proper organic and inorganic compounds and metals. All these advantages introduce AC as a promising and well known adsorbent to remediate the environment including air, water and soil.

4. CARBON NANOTUBES AND THEIR PROPERTIES

Carbon nanotubes (CNTs) have been first discovered in 1991, by Sumio Iijima [199]. The nanotubes consist of up to several tens of graphitic shells (so-called multi-walled carbon nanotubes (MWCNTs)) with adjacent shell separation of ~0.34 nm, diameters of ~1 nm and large length/diameter ratio. CNTs are a completely new type of carbon fibers that comprises coaxial cylinders of graphite sheets, which range from 2 to 50 sheets [200]. Two years later, Iijima and Ichihashi [201] and Bethune et al. [202] synthesized single-walled carbon nanotubes (SWCNTs) [203].

The name CNT is derived from their size which is only a few nanometers wide. By definition, CNTs are cylindrical carbon molecules with properties that make them potentially useful in extremely small scale electronic and mechanical applications. These tubes consist of rolled up hexagons, 10,000 times thinner than a human hair. Ideal nanotubes can be described as a seamless cylinder of rolled up hexagonal networks of carbon atoms, which is capped with half a fullerene molecule at the end [204, 205].

Nanotubes are suitable as electron field emitters because of their nanosize, structural perfection, high electrical conductivity and chemical stability with an application in flat panel displays [206]. CNTs are consist of honeycomb lattices, which built from sp^2 carbon units and have a seamless structure. They are tubular having a diameter of a few nanometers but lengths of many microns. MWCNTs are closed graphite tubules rolled like a graphite sheet. Diameters usually range between 2 and 25 nm, and the distance between sheets is about 0.34 nm. SWCNT is made of a single seamlessly rolled graphite sheet with a typical diameter of about 1.4 nm which is similar to a buckyball (C60). They have a tendency to form in bundles which are parallel in contact and consist of tens to hundreds of nanotubes. Depending on how the grapheme walls of the nanotube are rolled together they can result in an armchair, zigzag or chiral shapes [205–207].

4.1. Properties

CNTs are unique nanostructures which are known to have remarkable electronic and mechanical properties. These characteristics have sparked great interest in their possible uses for nano-electronic and nanomechanical devices. Properties of CNTs can also be expanded to thermal and optical properties as well. CNTs are predicted to have high stiffness and axial strength as a result of the carbon–carbon sp^2 bonding [203, 205]. In this section, the properties of CNT-based materials are considered. Adverse effects of application of carbon-based nanomaterials and their toxicity has been explained in detail in section 8.

4.1.1. Strength

Experimental and theoretical results have shown an elastic modulus of greater than 1 TPa (that of a diamond is 1.2 TPa) for CNTs. It has been reported that CNTs strength is 10–100 times higher than the strongest steel at a fraction of the weight. It has been predicted that CNTs have the highest Young's modulus of all different types of composite tubes such as BN, BC_3, BC_2N, C_3N_4, CN, etc. This strength results from the covalent sp^2 bonds formed between the individual carbon atoms [205, 208, 209] (Table 4.1).

Table 4.1. Comparison of mechanical properties of CNTs and other materials [200]

Material	Young's modulus (GPa)	Tensile strength (GPa)
SWCNT	1054	150
MWCNT	1200	150
Stainless steel	208	0.4
Epoxy	3.5	0.005
Wood	16	0.008

4.1.2. Hardness

Diamond is considered to be the hardest material. A new superhard phase SWCNT (SP-SWCNT) composed of single-wall CNTs has been studied which exhibits a bulk modulus exceeding or comparable with diamond and hardness belongs to the range between cubic boron nitride (BN) and diamond. The SP-SWCNT has been synthesized by applying a shear

deformation under load in a diamond-anvil cell; the procedure of stress tensor variation. After intermediate phase transitions, single-wall carbon nanotubes have been transformed to SP-SWCNT at pressure of 24 GPa. SWCNT do not collapse under pressure of at least 55 GPa, since the SWCNT band positions are not changed (only are broaden). Bulk modulus of 462 to 546 GPa has been found out for SP- SWCNT. This value exceeds the bulk modulus of diamond (420 GPa for single diamond crystal). These hardness measurements have been performed using nanoindentation technique [210].

The superlative mechanical properties of CNTs make them the filler material of choice for composite reinforcement. For example, polyvinyl alcohol (PVA) has been applied as a matrix material by Cadek et al. [211]. Nanohardness tests on spun cast films of arc-discharge MWCNT in both PVA and polyvinyl carbazole (PVK) have been carried out. Increases in modulus from 7 GPa to 12.6 GPa with 0.6 vol.% MCWNT in PVA and from 2 GPa to 5.6 GPa with 4.8 vol.% in PVK has been observed. Li et al. [212] have studied SWCNT–epoxy composites by nanohardness testing. An increase in modulus from 4 to 7 GPa with 5 wt.% SWCNT has been observed. Increases in hardness from 0.35 to 0.45 GPa has also been observed [213].

4.1.3. Electrical

Theoretical and experimental results show superior electrical properties of carbon nanotubes. CNTs can produce electric current carrying capacity 1000 times higher than copper wires [205, 214, 215]. The amazing mechanical and electrical properties of CNTs stem in their quasi one-dimensional (1D) structure and the graphite-like arrangement of the carbon atoms in the shells. Electrical transport through carbon nanotubes has attracted considerable interest due to the many possible applications in nanoscale electronic devices. The nanotubes are nearly perfect 1D conductors in which at low temperatures a number of interesting mesoscopic phenomena has been observed such as single-electron charging, resonant tunneling through discrete energy levels and proximity-induced superconductivity [203].

4.1.4. Optical

The optical properties of CNTs refer specifically to the absorption, photoluminescence and Raman spectroscopy of carbon nanotubes. Optical absorption in carbon nanotubes differs from absorption in conventional 3D materials by presence of sharp peaks instead of an absorption threshold followed by an absorption increase. The three peaks at 0.68, 1.2 and 1.7 eV have been found to correspond to the density of states (DOS) peaks of two semiconducting and one metallic tube in the optical absorption spectrum of purified SWNT thin films [216]. Additionally, the large absorption band at 4.5 eV has been ascribed to the π-plasmon of SWCNTs observed also in the energy-loss spectrum [203, 216]. Photoluminescence (PL) is one of the important tools for CNTs characterization. Photoluminescence is widely used to deduce (n, m) indices. The integers n and m denote the number of unit vectors along two directions in the honeycomb crystal lattice of graphene. First CNTs are dispersed using an appropriate chemical agent (dispersant) to reduce the intertube quenching. Then PL is measured, scanning both the excitation and emission energies and thereby producing a PL map [217].

4.1.5. Thermal

All nanotubes are expected to be very good thermal conductors along the tube, exhibiting a property known as "ballistic conduction", but good insulators laterally to the tube axis. Measurements show that a SWCNT has a room temperature thermal conductivity along its axis of about 3500 W m^{-1} K^{-1}; compare this to copper, a metal well-known for its good thermal conductivity, which transmits 385 W m^{-1} K^{-1}. A SWCNT has a room temperature thermal conductivity across its axis of about 1.52 $Wm^{-1}K^{-1}$, which is about as thermally conductive as soil [218, 219]. The specific heat and thermal conductivity of CNTs are determined primarily by phonons. In physics, a phonon is a quasi particle characterized by the quantization of the modes of lattice vibrations of periodic, elastic crystal structures of solids. At low temperatures, the phonon contribution to these quantities dominates and is due primarily to acoustic phonons. The measurements of the specific heat of MWCNTs from 10 to 300 K have revealed linear dependence of the specific heat on the temperature over the entire temperature span. This behavior has been attributed to the acoustic branches of the separate layers [203, 220]. Mizel et al. [221] have measured the specific heat of MWCNTs and bundles of SWCNTs with average diameter of 1.3 nm in the temperature range $1 < T < 200$ K. The MWCNT data has graphite-like behavior while the bundle data has rather steep temperature dependence at low temperatures.

4.2. Synthesis of Carbon Nanotubes

A variety of methods have been developed for the synthesis of CNTs including chemical vapor deposition (CVD), arc discharge, laser ablation, solar energy technique, chemical methods, plasma torch method, and so on. In this section the techniques of CNTs production are reviewed.

4.2.1. Arc Discharge

During this process, the carbon contains in the negative electrode sublimates because of the high discharge temperatures. Historically, the electric arc discharge is the first technique that has been used for the production of both multi-walled [199] and single-walled CNTs. This method is the most widely-used method of nanotube synthesis. The yield for this method is up to 30 percent by weight and it produces both SWCNTs and MWCNTs with lengths of 50 micrometers with few structural defects. Using suitable catalysts and buffer gases, this technique has been improved such that it can be used for the production of bundles of SWCNTs in large numbers [222]. The arc discharge technique generally involves the use of two high-purity graphite rods as the anode and cathode. A graphite anode is dipped into an open container of liquid nitrogen containing a short nonconsumable copper or graphite cathode. The electrodes are momentarily brought into contact and an arc is struck. As the anode is consumed, a constant gap between the anode and cathode is maintained by adjusting the position of the anode (see Figure 4.1). Then four kinds of products are formed in different parts of the reactor: (1) large quantities of rubbery soot on reactor walls; (2) web-like structures between the cathode and the chamber walls; (3) hard deposit at the end of cathode; and (4) spongy collaret around the cathodic deposit. To produce SWCNTs, the electrodes are doped with a small amount of metallic catalyst particles such as nickel and cobalt [201, 202,

222-224]. Different preparation conditions of carbon nanotubes by arc discharge method have been summarized in Table 4.2.

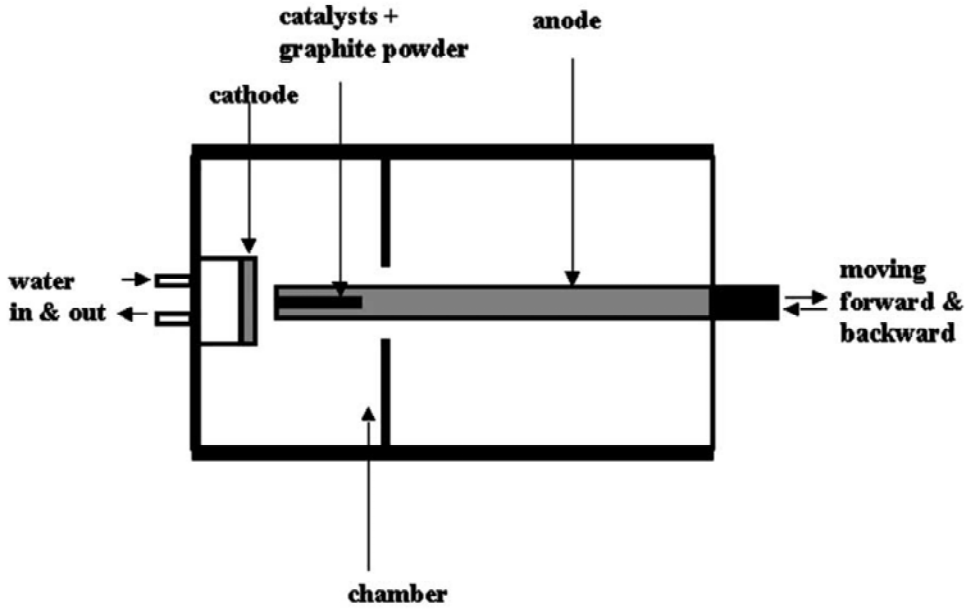


Figure 4.1. The scheme of the arc discharge method. (Adapted from Park et al. [225] with permission from publisher, Elsevier. License Number: 2540260991346).

Table 4.2. Preparation conditions of CNTs by arc discharge method

Preparation conditions or kinds of arc discharge methods	Product	Ref.
Hollow graphite cathode discharge CVD technique	Aligned carbon nanofibers	[226]
Thick, hollow graphite as the cathode in the arc discharge process	Silk like SWCNT materials	[227]
Hydrogen arc discharge method	Long SWCNT ropes	[228]
Decomposition of methane (CH_4) using an arc-jet plasma	Continuous high-purity synthesized CNTs	[229]
Small gaps between electrodes (>1 mm), high current (100 A), plasma between the electrode at about 4000 K, voltage range of 30–35 V	SWCNTs	[202]
Production o CNTs by a 12-phase AC arc discharge among carbon electrodes in helium gas	MWCNTs of 20–40nm in diameter	[230]
Using Y–Ni–C composite rod as anode and a tungsten rod as cathode and exchanging the electrodes after each discharge	Yielding about 10 g soot with about 50% SWCNTs with the diameter of the bundles about 10–20 nm in less than half an hour discharging time	[231]

Table 4.2. (continued)

Preparation conditions or kinds of arc discharge methods	Product	Ref.
Cathodic micro-arc discharge in aqueous solution	CNTs and carbon nanofibres with 20–30 nm in diameter and 0.5–1 μm in length	[232]
Arc discharge plasma method in hydrocarbon solvent (toluene) as carbon source of CNTs with nickel electrodes	Tube-like nanocarbons with several graphite sheets and hollow inside of its structure, similar to MWCNTs	[233]
Arc discharge technique in an atmosphere of Ar and H_2 mixture (1:1 / v:v) at 350 Torr, using a mixture of Ni, Co, Fe and S powders heated in an inert gas atmosphere at 500 ^oC for 1 h as catalyst	Double walled carbon nanotubes with outer diameter in the range of 1.9–5 nm and inner tube diameters in the range of 1.1–4.2 nm	[234]
Arc discharge method using graphite anode filled with a mixture of polyvinyl alcohol as an additional carbon source and iron group catalysts such as $Fe_2(SO_4)_3.nH_2O$ or $Fe(NO_3)_3.9H_2O$	MWCNTs with diameter in the range of 30–340 nm	[235]
Binary mixtures of the platinum-group metals as catalysts by arc evaporation in helium gas	SWCNTs with the distribution of diameters of 1.28±0.07 nm	[236]
Arc discharge method using chloride as a promoter and iron sulfide as catalyst	Double walled CNTs with ~2.5–3.5 nm inner tubes and ~3.5–4.5 nm outer tubes	[237]
Using pulsed arc discharge after preheating the catalyst (Y_2O_3, Ni powder) in reduced pressure air	SWCNTs with diameter of 1.5–2 nm and several micrometers length	[238]
DC arc discharge under N_2 atmosphere (200–300 Torr)	MWCNTs	[239]
Using a graphite rod with a hole filled with the powder of a mixture of Y–Ni alloy and graphite or calcium carbide and nickel as anode	SWCNTs	[240]
DC arc discharge evaporation of a carbon electrode including 1% Fe catalyst in hydrogen mixed gas [H_2–inert gas (Ne, Ar, Kr, Xe), or H_2–N_2]	SWCNTs with purity higher than 90%	[241]
DC arc discharge under low pressure of helium gas with small amount of a mixture of nickel and iron powders	SWCNTs bundles and nanoparticles with 10-20 nm in diameter	[225]
Y–Ni alloy composite graphite rod as anode for DC arc discharge	Cloth-like soot containing about 40% SWCNTs	[242]
Arc-discharge in a mixture of Ar and H_2 (2:1, v/v) at 300 Torr	Fullerene waste soot-derived double walled carbon nanotubes	[243]
Hydrogen arc discharge method using graphite powders or MWCNTs/carbon nanofibers as carbon feedstock	Double walled CNTs with the yield about 4g/h	[244]
DC arc-discharge in the presence of hydrogen and copper catalysts	Branched MWCNTs	[245]
Polycyclic aromatic hydrocarbons as carbon sources in helium arc discharge	CNT columns with diameter in the range of 10–50 μm	[246]
DC arc discharge in H_2–Ar gas atmosphere with Fe_3O_4 as catalyst	SWCNTs with diameters of 10 to 50 nm	[247]
Arc discharge performed in liquid environments (liquid nitrogen and deionised water) between pure graphite electrodes	MWCNTs	[248], [249]
Arc discharge with Ho/Ni as catalyst	Long SWCNT ribbons consisting of roughly aligned bundles	[250]

4.2.2. Laser Ablation

The laser ablation method is another technique for producing CNTs. This process is known to produce CNTs with the highest quality and high purity of single walls. Laser ablation is the first technique used to generate fullerenes in clusters. In laser ablation process, a piece of graphite is vaporized by laser irradiation under inert atmosphere of helium or argon. A very high temperature is obtained which allows the sublimation of the carbon. Two kinds of products are possible: MWCNTs or SWCNTs. For this process a purification step by gasification is also needed to eliminate carbonaceous material. The effect of the gasification depends on the type of reactant used [205, 251-253]. Both arc-discharge and laser ablation techniques have the advantage of high (>70%) production yields of SWCNTs. These techniques also have the drawbacks that are: (1) they rely on evaporation of carbon atoms from solid targets at temperatures >3000 ^{o}C, and (2) the nanotubes are tangled which makes difficult the purification and application of the samples [203]. Figure 4.2 shows schematic diagram of a pulse laser ablation apparatus. Different preparation conditions of carbon nanotubes by laser ablation method have been summarized in Table 4.3.

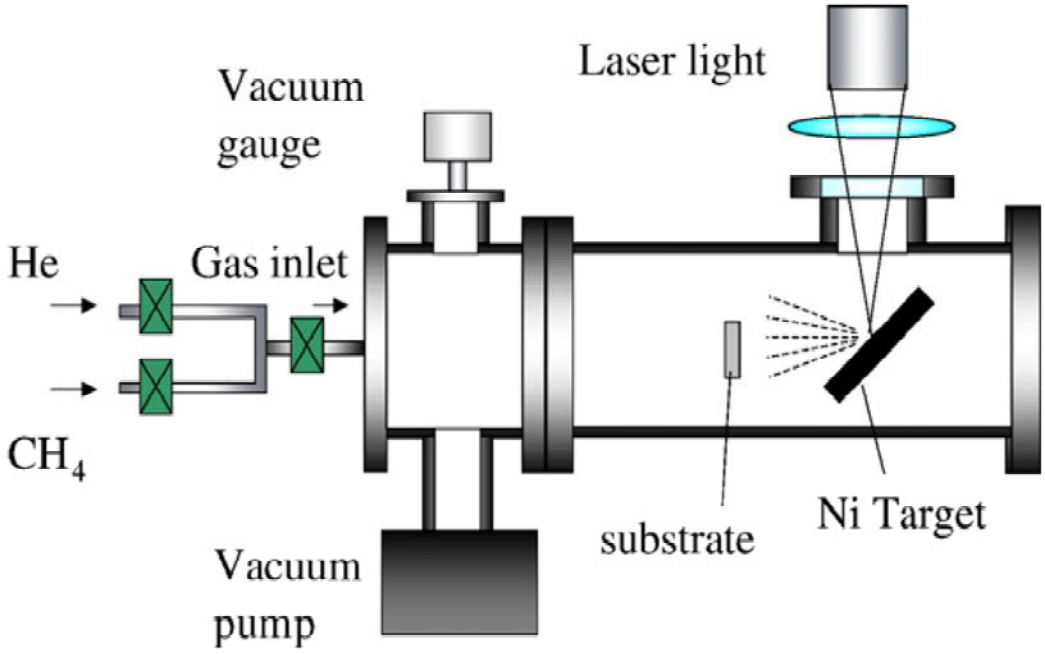


Figure 4.2. Schematic diagram of a pulse laser ablation apparatus. (Adapted from Ou et al. [254] with permission from publisher, Elsevier. License Number: 2539371450261).

Table 4.3. The preparation conditions of CNTs by laser ablation method

Preparation conditions or methods	Type of prepared CNT	Ref.
Vaporization of a piece of graphite by laser irradiation under inert atmosphere	MWCNTs or SWCNTs	[252]
Laser ablation (vaporization) of graphite rods with small amounts of Ni and Co at 1200 ^{o}C	SWCNTs	[255]
Pulsed laser vaporization technique	Large-scale production of SWCNTs	[256]
XeCl excimer laser ablation. Irradiation onto a graphite target containing Co and Ni at the temperatures of 1273 K, 1373 K, 1473 K and 1623 K under the atmosphere (0.1 MPa) of Ar gas with the flow rate of 12 mL/min	SWCNTs with the diameter distribution of 1.2~1.7 nm and the length of >2 μm	[257]
Plasma plume produced by KrF excimer laser ablation of graphite in O_2 atmosphere	Carbon nanofibers with a diameter of 10–50 nm	[258]
Laser ablation of a crude-tube target containing SWCNTs (20-30%), particles of graphite (about 10-20%), amorphous carbon (50-60%) and a little of Ni and Co (about 0.6%)	SWCNTs	[259]
Nanosecond Nd:YAG (yttrium aluminium garnet)-laser ablation of a C–Ni–Co target inside a high-temperature laser vaporization reactor by controlling and restricting the growth times	SWCNTs	[260]
CO_2 continuous wave at laser power of 400–900 W of C/Ni/Co at room temperature	SWCNTs bundles	[261]
CO_2 continuous and pulsed wave with gas conditions of Ar, He and N_2 of 50–500 Torr	SWCNTs	[262]

4.2.3. Chemical Vapor Deposition (CVD)

In the CVD process growth involves heating a catalyst material to high temperatures (500–1000 ^{o}C) in a tube furnace using a hydrocarbon gas through the tube reactor over a period of time. Figure 4.3 shows schematic diagram of a CVD apparatus. The basic mechanism in this process is the dissociation of hydrocarbon molecules catalyzed by the transition metal and saturation of carbon atoms in the metal nanoparticle. Precipitation of carbon from the metal particle leads to the formation of tubular carbon solids in a sp^2 structure. The characteristics of the carbon nanotubes produced by CVD method depend on the working conditions such as the temperature and the pressure of operation, the volume and concentration of methane, the size and the pretreatment of metallic catalyst, and the time of reaction [205, 263]. In the CVD process, single wall nanotubes are found to be produced at higher temperatures with a well-dispersed and supported metal catalyst while multi wall nanotubes are formed at lower temperatures and even with the absence of a metal catalyst [205]. The synthesis of SWCNTs using plasma-enhanced chemical vapor deposition (PECVD) is a novel, attractive technique for carbon nanotube synthesis because it can independently control synthesis variables such as substrate temperature, local gas composition, plasma power density and operating pressure. Recently, SWCNT synthesis has been accomplished using radio frequency PECVD and shielded microwave PECVD [222, 264, 265]. Different preparation conditions of CNTs by CVD process have been summarized in Table 4.4.

Table 4.4. Different preparation conditions of carbon nanotubes by CVD process

Preparation conditions or methods	Type of prepared CNT	Ref.
CVD process using ethanol as carbon source and several substrate materials (such as quartz, conductive glass (SnO_2:F film deposited on soda-lime glass), porous alumina and nickelplates) at 750 ^oC and cobalt and iron particles as catalyst	MWCNTS with diameters ranging from 25 to 90 nm	[266]
CVD technique and iron as catalyst	Large-scale synthesis of aligned carbon nanotubes	[267]
CVD method using porous silicon wafer	Regular array of MWCNTs	[268]
Silicon wafers patterned with micrometerscale islands of catalytic material by the CVD technique	High-quality SWCNTs	[269]
Catalytic CVD method using alumina plate-supported nickel as catalyst and acetylene as carbon source at 450–800 ^oC	Carbon nanofibers with the fiber diameters ranging from 35 to 70 nm and the average diameter of ~50 nm	[270]
CVD of methane on iron floating catalyst in situ deposited on MgO in a fluidized bed reactor	CNTs (CWCNTs and MWCNTs) bundles with diameters of ~10–20 nm	[271]
CVD method for preparation of SWCNTs with high productivity using a novel aerogel supported Fe/Mo catalyst	Large-scale preparation of SWCNTs (greater than 200% the weight of the catalysts)	[272]
Thermal CVD performed directly on stainless steel substrates of various geometries without the addition of an external catalyst	MWCNTs with diameters ranging from 20 to 70 nm	[273]
Ethanol CVD, different catalyst preparations, based on organometallic salts (Co, Fe, Mo, Ni acetate, and bimetallic mixtures), have been spin coated onto thermally grown silicon dioxide on silicon chips to perform tests in a temperature range between 500 and 900 ^oC.	SWCNTs with diameter ranging from 0.9 to 2.1 nm	[274]
Activated Cu catalysts for alcohol CVD	non-magnetic bamboo-like carbon nanotubes and branched bamboo-like carbon nanotubes	[275]
Thermal CVD at atmospheric pressure using Co as catalyst with NH_3 as reactive gas	Aligned carbon nanotubes with diameters ranging from 30 to 60 nm	[276]
Thermal CVD with palladium as catalyst and ammonia (NH_3) for pretreatment	MWCNTs with Average diameter ranging from 20 to160 nm	[277]
Iron supported catalyst by catalytic CVD in a fluidized bed reactor	MWCNTs with mean diameter about 17 nm and the inner diameter around 8 nm	[278]
Hot filament CVD method using CH_4 and H_2 as reaction gases	MWCNTs	[279]
Catalytic CVD with Catalysts prepared by the combustion route using either urea or citric acid as the fuel	Double and triple-walled CNTs	[280]
Catalytic CVD of methane over Fe–Co/MgO catalyst	Double-walled CNTs (DWCNTs) with inner and outer diameters of 0.6–1.2 and 1.3–2 nm, respectively	[281]
Using perovskites $LaFe_xMo_yMn_zO_3$ (x = 0.27–0.90, y = 0.00–0.09 and z = 0.01–0.10) as catalyst precursors for the CVD synthesis of CNTs from CH_4 between 900 and 1100 ^oC	SWCNTs, DWCNTs and MWCNTs	[282]
Fabrication of CNTs on 5 cm×5 cm borosilicate glass substrate by using capacitive coupled radio frequency plasma-enhanced infrared thermal CVD equipment, at substrate temperature of 580 ^oC and inborn $Fe(OH)_3$ sol as catalyst	CNTs film with uniform diameter of 40–80 nm	[283]
CVD process using $Co_xMg1-xMoO_4$ as catalyst and a methane–hydrogen–ammonia mixture as precursor	High-purity (over 95%) nitrogen-doped MWCNTs with average diameter of 25 nm	[284]

Table 4.4. (continued)

Preparation conditions or methods	Type of prepared CNT	Ref.
Graphite antenna CVD at the low temperature of 390 ^{o}C in a hydrogen-free atmosphere	Vertically aligned MWCNTs with the outer diameter of 5–13 nm (mean, 8 nm)	[285]
RF plasma CVD method with an additional RF-substrate power at 490 ^{o}C and Ni-based catalyst	Vertically aligned MWCNTs	[286]
CVD process using Ni–Y/Mo as catalyst	MWCNTs with a narrow inner diameter (below 3 nm for most of the tubes) and outer diameters ranging from 5 to 20 nm	[287]
Using Fe as the catalyst and a mixture of CO and H_2 as feeding gas	SWCNTs with diameters from 1.3 to 2.1 nm and large diameter DWCNTs (outer diameter: 5.9–7.5 nm; inner diameter: 5.0–6.8 nm)	[288]
Thermal CVD with acetylene (C_2H_2) and hydrogen at 750 ^{o}C and $(Fe,Si)_3O_4$ catalyst particles	Aligned and uniform film of MWCNTs	[289]
CCVD on FeMo/MgO catalyst using acetylene as carbon source	SWCNTs	[290]
Hot Filament assisted CVD	SWCNTs with heights? ranging from 1 to 3 nm	[291]
CVD of ferrocene–ethanol mist at atmospheric pressure (~ 1 atm)	Uniform web-like films consisting SWCNTs bundles with a tube diameter of ~ 1 nm	[292]
H_2–CH_4 mixtures on a MgO-supported bimetallic Mo/Co catalyst using microwave plasma-enhanced CVD	SWCNTs	[293]
Thermal CVD on Ni/Cr coated glass substrate at 550 and 500 °C by low pressure (8 Torr)	Vertically aligned-MWCNTs	[294]
CVD process using Single phase $MgMoO_4$ as catalyst	Bundled MWCNTs with diameter distribution of 10–20 nm	[295]
CVD process using aluminum powder as transition metal catalyst	MWCNTs with the diameters ranging from 10 to 20 nm	[296]
Electron cyclotron resonance CVD (ECR-CVD) on porous silicon and without any bias application on the substrate, using CH_4 and H_2 as source gases and Fe_3O_4 nanoparticles as the catalyst	Large area, well-aligned CNTs with outer diameters varying from 10 to 90 nm and uniform length over 10 μm	[297]
CVD process using a Ni/Y catalyst supported on copper at different reduction and reaction temperature (500–700 ◦C)	Bamboo-shaped CNTs with a diameter of about 7–18 nm and carbon onions with sizes ranging from 10 to 90 nm	[298]
Hot filament assisted CVD at the atmospheric pressure at a substrate temperature of 550 ^{o}C	MWCNTs with emission current densities of 6.5 mA/cm^2 and 2.5 mA/cm^2 at 1 V/mm for 5–8 nm and 20 nm size, respectively	[299]
CVD process with titanate-modified palygorskite as catalyst and acetylene as carbon source at high temperature (600-900 ^{o}C)	MWCNTs	[300]
Direct current plasma enhanced CVD method with submicron-sized dot-catalyst array (dot size of 400 nm and dot intervals varying from 0.3 μm to 10 μm)	Vertically aligned CNTs with diameter of 80–100 nm and length of about 3 μm	[301]
Radio frequency plasma enhanced CVD on the Fe deposited substrate in the radio frequency powers of 10-50 W, substrate temperatures of 600 ^{o}C and C_2H_2: H_2=1:9	Well-aligned CNTs with a length of 2 μm and diameter approximately 10-15 nm	[302]

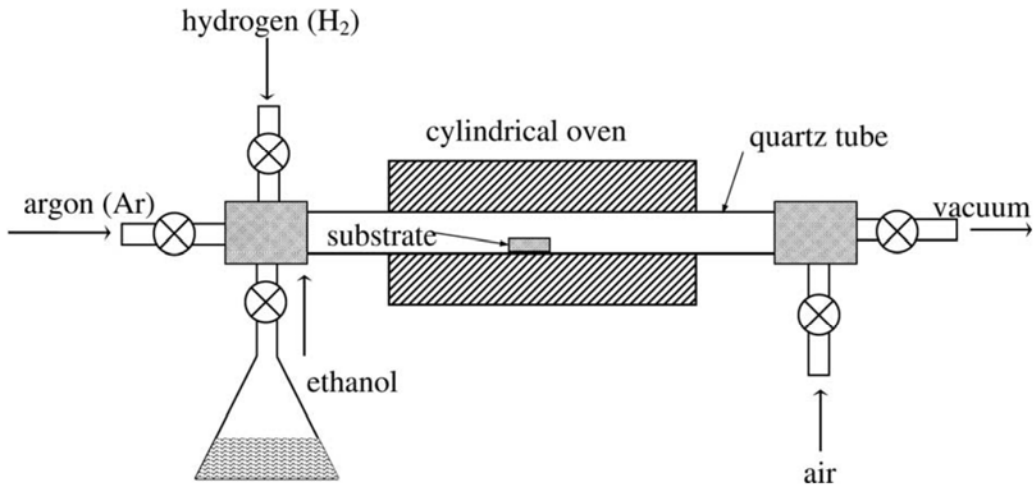


Figure 4.3. Schematic diagram of the CVD apparatus. (Adapted from Ortega-Cervantez et al. [266] with permission from publisher, Elsevier. License Number: 2539390889777).

4.2.4. Other Methods

Table 4.5 summarizes some other methods that have been used for CNTs production.

Table 4.5. Some other methods that have been used for CNTs production

Name of method	Description	Ref.
Solar energy technique	The sunlight is focused on a graphite sample and vaporizes the carbon. Soot containing the nanotube is then condensed in a dark zone of a reactor, which is collected in a filter and water cooled.	[252]
Chemical methods	The catalytic decomposition of hydrocarbons is performed in a flow furnace at high temperatures.	[252]
Plasma torch method	CNTs would naturally grow in any environment in which both appropriate metal atoms and carbon atoms are present.	[303]
AC electric arc method	Combines the underwater growth with the use of an AC controlled power supply.	[303]
Electrolytic formation of CNTs	Carbon nanotubes have been generated by electrolysis in molten alkali halide salts using carbon electrodes under argon atmosphere.	[304]

4.3. Applications

The unique mechanical and electronic properties of both the single-walled and multi-walled varieties of CNTs have led to applications in a wide variety of materials and devices [222]. The application of CNTs most widely has been employed so far is the construction of various detection devices, such as gas sensors, electrochemical detectors and biosensors with immobilized biomolecules. Their application in voltammetric methods is especially favorable,

but they are also employed for sorption of different analytes and in electrochemical stripping methods [305]. CNTs are attractive candidates for electrode materials of microbattery systems or microcapacitors due to their superb characteristics of chemical stability, low mass density, low resistivity, and large surface area. Composite materials with CNTs as fillers are expected to show similar superior properties [306]. Potential practical applications have been reported such as chemical sensors and probes [307], gas sensors [308], biosensors [309], field emission materials [310], catalyst support [311], electronic devices [312], nanotube-based lamps [313], high sensitivity nanobalance for nanoscopic particles [314], nanotweezers [315], reinforcements in high performance composites, and as nanoprobes in meteorology and biomedical and chemical investigations, anode for lithium ion in batteries [315], nanoelectronic devices [316], supercapacitors [317], voltammetry [318], solid-phase extraction [319], chromatographic applications [320], and hydrogen storage [223]. New applications are likely in the diamond industry since experiments have shown the conversion of carbon nanotubes to diamond under high pressure and high temperatures with the presence of a certain catalyst [321]. These are just a few possibilities that are currently being explored. As research continues, new applications will also develop [205]. In the following sections, the environmental applications of CNTs are considered.

5. FILTERS AND ADSORBENTS BASED ON CARBON NANOTUBES

Carbon-based materials typify a class of significantly and widely used engineering adsorbents. Using new and advanced carbon-based materials as the adsorbents often yields a physical adsorption system with high adsorptive capabilities. In recent years, efforts targeting adsorbent development have turned to nano-structured carbon-based materials because of their extraordinary mechanical, electrical, thermal, and structural properties [322]. CNTs, including both the multi-walled [199] and the single-walled types [201, 202], represent a fascinating new member in the family of carbon-based materials. CNTs are a novel and interesting carbon materials first found in 1991 by Iijima [199]. CNTs are cylindrically shaped, graphite-like, sp^2-bonded, entirely carbon materials. Their large specific surface areas and sharper curvatures together with their high thermal and chemical stabilities make them ideal for application to the adsorption of pollutant chemicals, especially chemicals with aromatic backbones [322]. The unique properties of CNTs are highly porous and hollow structure, large specific surface area, light mass density, and strong interaction between carbon and hydrogen molecules. These properties have led CNTs to interest in the potential applications as quantum nano-wires, electron field emitters, catalyst supports, chemical sensors and adsorbents for hydrogen and other gas storages [307, 323–326]. CNTs are found efficient for the removal of dioxin, fluoride and metal ions [327–339]. There are number of publications on the sorption of various divalent metal ions (Cd^{2+}, Cu^{2+}, Ni^{2+}, Pb^{2+}, Zn^{2+}) from aqueous solutions by raw and surface-oxidized CNTs which discuss their sorption capacities, mechanisms, process parameters, desorption and other research works [328, 330-340]. Li et al. [328, 340] have reported exceptional adsorption capacity and high adsorption efficiency of oxidized CNTs in removal of lead and cadmium from water. Chen and Wang [334] have investigated the adsorption of nickel on the oxidized MWCNTs. Table 5.1 summarizes different compounds adsorbed by CNTs.

CNTs have been considered useful in pollution prevention strategies and are known to have widespread applications as environmental adsorbents and high flux membranes [341]. CNTs are also potentially important for in situ environmental remediation due to their unique properties and high reactivity [342]. Investigations dealing with the sorption of organic contaminants, such as dioxin [333], 1,2-dichlorobenzene [343], trihalomethanes [344], polycyclic aromatic hydrocarbons (PAHs) [345], *o*-xylene, *p*-xylene [346] and reactive dye (Procion Red MX-5B) [347] on CNTs suggest that CNTs may also be suitable candidates for the pre-concentration and solidification of pollutants from wastewater. Strong adsorptive interaction between CNTs and polycyclic aromatic hydrocarbons are ascribed to π-π electron–donor–acceptor (EDA) interactions between aromatic molecules (electron acceptors) and the highly polarizable graphene sheets (electron donors) of CNTs [345, 348]. In addition, hydrophobic effect, dispersion and weak dipolar forces as well as micropore diffusion are also considered to be responsible for adsorption [345, 346, 349, 350].

Application of CNTs has the potential to make important advancements in water security and protection from biothreat agents. CNTs can potentially concentrate bacterial pathogens from contaminated water [351-353]. After surface modification, CNTs also have the capability of detecting pathogens [354, 355]. One major advantage of CNTs is that they have strong antimicrobial activity [356, 357]. The antimicrobial activity of modified and unmodified CNTs has been tested on vegetative cells [356, 357] as well as on spores [358, 359]. Once the cells contact with CNTs they act as ‘‘nanosyringes’’ [360] and cause highly localized disruption of bacterial cell wall [356, 357, 360]. This unique feature is not seen in other carbon-based adsorbents where the nature of the material actually facilitates the growth of the bacteria [361-363]. There is evidence of reduction of disinfection efficiencies in water treatment plants [361, 363], due to the growth and persistence of bacteria on AC filters that are used upstream in the treatment plant. CNTs do not permit the growth of the bacteria [356]. Installing a nanotube filter at certain points in the distribution systems not only prevents the bio-film formation in the system but also traps the natural dissolved organic matter that might be increased due to the bacterial growth [364].

5.1. Modification of CNTs

The large adsorption capacity of pollutants by CNTs is mainly attributable to their pore structure and the existence of a wide spectrum of surface functional groups which can be achieved by chemical modification or thermal treatment to make CNTs that possess optimum performance for particular purposes [365]. Numerous approaches for purification or enhancement of functional groups on CNTs that involve separation and elimination processes have been developed [366-370]. They fall into two groups according to the general mechanism of functionalization of CNTs. In the first group, some C=C bonds are fully opened, forming defects within the CNT wall. In the second group, some C=C bonds are broken and single bonds are used for functionalization, yielding some sp^3 character of particular C atoms. The oxidation of carbon surfaces is known to generate not only more hydrophilic surface structures but also more oxygen-containing functional groups and to increase the ion-exchange capacity [368]. The first type of functionalization typically involves oxidation using acids or oxidants [368–370], causing carboxyl groups to functionalize the defects and the ends of the CNTs [367]. The second type CNT wall

functionalization is generally an addition of a C=C double bond by alkylation, arylation, oxycarbonyl nitrene, and 1,3 dipolar cyclo-addition [371-374].

5.2. Difficulties with the Use of CNTs

Two major difficulties have arisen with the use of CNTs in adsorption applications. Immobilization is an initial problem, which is commonly overcome using the traditional packing technique; for instance, by packing the agglomerates of MWCNTs into a column. A column packed with MWCNTs can provide a flow system for continuously treating the liquid and/or gaseous effluents, but such a system often requires a high-pressure pumping system, which in turn diminishes the overall treating capacity of the adsorptive system. Enlargement of the effective surface areas of CNTs has been another important step in producing CNT-based adsorbents with high adsorptive efficiency. CNTs, because of the high aspect ratio of each tube and the strong Van der Waals attractions among the tubes, often occur as large-sized agglomerates (often up to few mm) of many individual tubes. Adsorption of chemicals with high molecular weights, such as the water-soluble organic dyes, occurs mainly over the outermost surfaces of the CNT agglomerates. In other words, the innermost tubes often make no contribution to the adsorption of such chemicals. Dispersion of the agglomerates of CNTs into individual tubes can maximize the adsorptive surfaces; however, difficulties persist in keeping the CNTs in the individual forms while the tubes are packed or immobilized [323].

A way for overcoming these difficulties has been reported by H. Yu and B. Fugetsu [323]. A novel approach has been established for the creation of a CNT-based adsorbent with high adsorptive efficiency and high mechanical strength. This goal has been achieved by using diatomite (diatomaceous earth) as a micro-reverser (container of microsize) and polyurethane polymers as binders. The agglomerates of MWCNTs have been first dispersed into individual tubes in water using sodium n-dodecyl glyceryl itaconate, an anionic type of surfactant, in combination with 3-(N,N-dimethylmyristylammonio)-propanesulfonate, a zwitterionic type of surfactant, as the dispersant. These dispersed-MWCNTs have been then packed into the cavities of diatomite. The resulting diatomite/MWCNT composites have been finally immobilized on the cell walls of polyurethane foams. The prepared foam-like and ternary type of adsorbent has been used for adsorption of water-soluble dyes [323].

5.3. Application of CNTs in Solid Phase Extraction

Solid phase extraction (SPE) is one of the important places at the preconcentration–separation studies for trace metal ions and other pieces in environmental samples due to its simplicity and easy adaptation of automatic procedures [375, 376]. In SPE studies, the suitable adsorbent usage is a critical factor to get high enrichment efficiency [377]. Nanoparticles including maghemite nanoparticles [378], nano mesoporous silica [379], nano-barium–strontium titanate microspheres [380], modified nanometer titanium dioxide [381] and magnetic nanoparticle [382] have been used for the enrichment of trace metal ions. CNTs have been also used for solid phase extraction of inorganic and organic traces in various media [383-385]. Their strong binding affinity for hydrophobic molecules, internal tube cavity and surface area as well as their ability to establish π–π electrostatic interactions are the

main characteristics that have attracted their use in SPE. The main advantage of CNTs compared to conventional carbon sorbents is that they are relatively non-porous. Consequently, the solute is retained on the surface by Van der Waals type forces which eliminates the mass transfer resistance related to the diffusion into the pore structures [386, 387]. Table 5.1 shows some compounds extracted by CNTs and SPE method.

Table 5.1. Preparation conditions and environmental applications of CNTs as adsorbent

Type of CNT	Preparation method	Application	Ref.
Composites of diatomite/ MWCNTs	Agglomerates of MWCNTs are dispersed into individual tubes using sodium n-dodecyl itaconate mixed with 3-(N,N-dimethylmyristyl ammonio)-propanesulfonate as the dispersants and the resultant dispersed-MWCNTs are inserted into cavities of diatomite to form composites of diatomite/MWCNTs	Removal of Organic dyes (Ethidium bromide, acridine orange, methylene blue, eosin B, and eosin Y) from water	[323]
MWCNTs	Pyrolysis of methane gas on Ni particles via CVD method	Removal of direct dyes (C.I. Direct Yellow 86 and C.I. Direct Red 224) from water	[388]
MWCNTs	Pyrolysis of methane gas on Ni particles via CVD method	Removal of a reactive dye (Procion Red MX-5B) from water	[347]
Magnetic MWCNTs (MMWCNTs) nanocomposite	MWCNTs are dispersed in concentrated nitric acid at 60 ^{o}C for 12 h under stirring and washed by copious water and ethanol subsequently, then dried at 110 ^{o}C for 4 h. Purified MWCNTs are suspended in mixed solution of ammonium ferrous sulfate and ammonium ferric sulfate following by the slow addition of NH_4OH solution at 50 ^{o}C under nitrogen atmosphere with the aid of ultrasonic stirring. MMWCNTs are isolated from the mixture by a permanent magnet	Removal of cationic dyes (methylene blue, neutral red and brilliant cresyl blue) from water	[389]
Magnetic chitosan enwrapping nanosized γ-Fe_2O_3 and MWCNTs	Chitosan is dissolved in acetic acid aqueous solutions under ultrasonic stirring for 1.5 h at room temperature then magnetic nanosized γ-Fe_2O_3 and MWCNTs are added into the colloidal solution and stirred for 1 h. The prepared mixture is dispersed in paraffin oil containing Span under stirring. After 30 min of emulsification, glutaraldehyde is added to crosslink chitosan and is stirred for 90 min in a water bath at 40 ^{o}C. Black products (m-CS/c-Fe_2O_3/MWCNTs) are washed with N,N-dimethylformamide, ethanol and double distilled water and collected by the aid of an adscititious magnet and dried	Removal of methyl orange from water	[390]
MWCNTs	Catalytic decomposition of CH_4	Hydrogen storage medium (adsorption of supercritical hydrogen)	[391]
MWCNTs	Modification of MWCNTs by 3-aminopropyl-triethoxysilane	Adsorption of CO_2 from gas streams	[365]

Table 5.1. (continued)

Type of CNT	Preparation method	Application	Ref.
SWCNTs and MWCNTs	-	Adsorption of polycyclic aromatic hydrocarbons (naphthalene, phenanthrene and pyrene)	[345]
MWCNTs	-	Adsorption of ^{243}Am(III)	[327]
Oxidized MWCNTs	MWCNTs are prepared using CVD of acetylene in hydrogen flow at 760 ^{o}C using Ni–Fe nanoparticles as catalysts. Oxidized MWCNTs are prepared by oxidization with 3 M HNO_3	Adsorption of Th(IV) from water	[392], [393]
Oxidized MWCNTs	MWCNTs are synthesized from the CH_4/H_2 mixture by CVD method at 700 ^{o}C using Ni particles as catalyst.	Adsorption of atrazine (2-chloro-4-ethylamino-6-isopropylamino-s-triazine)	[349]
MWCNTs	Modified MWCNTs following microwave/chemical treatment	Removal of cadmium (II) from water	[366]
SWCNTs	-	Adsorption of *Bacillus subtilis*	[351]
NaOCl-oxidized MWCNTs	MWCNTs are purified via NaOH solution at the boil for 2 h and then oxidized by 30% NaOCl solution	Adsorption of benzene, toluene, ethyl benzene and p-xylene	[394]
Surface oxidized CNTs with H_2O_2, $KMnO_4$ and HNO_3	CNTs are prepared by thermal decomposition of the methane in hydrogen flow at temperature 750 ^{o}C using Ni nanoparticles as catalysts. The as-grown CNTs are added into the solutions of H_2O_2, $KMnO_4$, and nitric acid, respectively	Adsorption of cadmium (II) from water	[328]
Aligned carbon nanotubes (ACNTs)	Catalytic decomposition of xylene using ferrocene as catalyst	Adsorption of fluoride from water	[329]
Amorphous Al_2O_3 supported on CNTs (Al_2O_3/CNTs)	CNTs and $Al(NO_3)_3$ are dispersed into deionized water and magnetically agitated, then dried up at 100 ^{o}C. The dried sample is heated at 500 ^{o}C under N_2 atmosphere to yield Al_2O_3 supported on CNTs	Adsorption of fluoride from water	[395]
SWCNTs and MWCNTs	CNTs are synthesized by the CVD method and purified by mixed HNO_3 and H_2SO_4 solutions	Adsorption of fulvic acid from water	[396]
MWCNTs	CVD method	Adsorption of heavy metal ions (Cu, Co, Cd, Zn, Mn, Pb) from water	[397], [398]
MWCNTs	-	Adsorption of natural organic matter (NOM) from water	[399]
Oxidized MWCNTs	Production by CVD method using acetylene gas in the presence of ferrocene and oxidizing with concentrated nitric acid	Adsorption of Ni(II) from water	[400], [401]
Oxidized CNTs	CNTs are fabricated by catalytic pyrolysis of the propylene in a ceramic tube with Fe particles as the catalysts and oxidized with concentrated nitric acid	Adsorption of nicotine and tar from the mainstream smoke of cigarettes	[402]
MWCNTs	Catalytic decomposition of the CH_4/H_2 mixture at 700 ^{o}C using Ni particles as catalyst	Adsorption of trihalomethanes from water	[344]
MWCNTs	CVD method	Adsorption of Triton X-series surfactants	[403]
SWCNTs and MWCNTs	SWCNTs and MWCNTs are purified by sodium hypochlorite solutions	Adsorption of zinc(II) from water	[367]
CNTs	Prepared on Ni nanoparticle catalyzed pyrolysis of propylene in a hydrogen flow at 750 ^{o}C	Adsorption of Pb^{2+} from water	[330], [340]
SWCNTs	SWCNTs are synthesized by arc discharge method	Capture of bacteria *Streptococcus mutans*	[404]

Type of CNT	Preparation method	Application	Ref.
Aligne CNTs Supported ceria nanoparticles (CeO_2/ACNTs)	ACNTs are prepared by catalytic decomposition of hydrocarbon. The CeO_2/ACNTs is prepared by adding $CeCl_3$ solution into ACNTs solution	Adsorption of Cr(VI) from drinking water	[331]
SWCNTs	-	Solid phase extraction of Fe(III) and Cr(III)	[383]
MWCNTs	-	Solid phase extraction of pesticides	[386], [405]
MWCNTs	-	Solid phase extraction of heavy metal ions	[406], [407]
Ethylenediamine-modified MWCNTs	Purified MWCNTs is suspended in concentrated HNO_3 and refluxed. The product (MWCNTs-COOH) is suspended in EDA	Selective solid-phase extraction and pre-concentration of metal ions (Cr(III), Fe(III) and Pb(II))	[408]
Oxidized MWCNTs	MWCNTs are prepared by using CVD of acetylene in hydrogen flow at 760 ^oC using Ni-Fe nanoparticles as catalyst and oxidized with concentrated HNO_3	Removal of Pb (II) from water	[409]
Manganese oxide-coated CNTs	CNTs are suspended in deionized water and the solution containing Mn(II) acetate is added. Then, $KMnO_4$ solution is added under continuous stirring	Removal of lead (II) from water	[410]
Nitric acid treated MWCNTs	MWCNTs are prepared by dissociating methane in a hydrogen flow at 900 K using Ni nanoparticles supported on diatomites as catalysts and treated with concentrated HNO_3	Competitive adsorption of Pb^{2+}, Cu^{2+} and Cd^{2+} ions from water	[332]
Oxidized MWCNTs	Oxidization of MWCNTs with 1:3 (v:v) concentration nitric acid–sulfuric acid	Adsorption of anionic surfactant (sodium dodecylbenzene sulfonate (SDBS)) and nickel (metal) from water	[411]
Oxidized CNTs	Oxidized CNTs with concentrated nitric acid	Adsorption of nickel, copper, zinc and cadmium from water	[412]
MWCNTs	-	Removal of parts per billion levels of hexavalent chromium from aqueous solution	[413]
MWCNTs	-	Removal of chlorophenol from water	[414]
Oxidized CNTs	Oxidization of CNTs by HCl, H_2SO_4, HNO_3 and NaOCl solutions	Adsorption of benzene, toluene, ethyl benzene and p-xylene (BTEX) from water	[415]
MWCNTs	Electrostatic interaction between magnetic iron-oxide nanoparticles and the surface of microwave-assisted acidified MWCNTs	Adsorption of volatile organic compounds including benzene, toluene, ethyl benzene, xylene, and styrene	[416]
MWCNTs	MWCNTs treated by concentrated HNO_3	Adsorption of resorcinol and other phenolic derivatives from water	[417]
MWCNTs	CNTs were treated by citric acid, potassium permanganate and nitric acid	Adsorption of aniline from water	[418]
Open ended SWCNTs (o-SWCNTs)	-	Adsorption of Xenon (Xe) gas	[419]

6. ELECTROCHEMICAL WATER TREATMENT PROCESSES BASED ON CARBON NANOTUBES

Water is essential for the subsistence of living beings. Unfortunately, water pollution remains a pervasive threat, with water quality being merely a concept reflecting the kind and quantity of contaminants [420]. It is well known that large amounts of various synthetic organic pollutants, including industrial chemicals, pesticides, dyes and pharmaceuticals and personal care products (PPCPs), are released daily into natural water channels where they accumulate in the aquatic environment. This contamination arises from urban, industrial and agricultural human activities and cannot be significantly reduced in conventional wastewater treatment plants because the vast majority of these compounds are persistent organic pollutants (POPs) [421-431]. Different technological processes such as physical adsorption [432], biodegradation [433, 434], chemical methods (chlorination, ozonation [435]), electrocoagulation, electrochemical reduction and oxidation, indirect electro-oxidation with strong oxidants and photocatalytic degradation [436–439] for the removal of pollutants have been recently developed. In recent years, advanced oxidation processes (AOPs) have been described as efficient procedures for obtaining high oxidation yields from several kinds of organic compounds [439, 440]. AOPs are based on the generation of very reactive nonselective transient oxidizing species such as the hydroxyl radicals ($OH^{\bullet}$), which are identified as the dominant oxidizing species [439–441]. Among AOPs, electrochemical advanced oxidation processes (EAOPs) like anodic oxidation and indirect electro-oxidation methods based on H_2O_2 electrogeneration are very attractive for wastewater decontamination. It is because of their low cost and high effectiveness for POPs removal, without needing addition of toxic chemical reagents and without producing dangerous wastes [442]. More potent indirect electro-oxidation methods with hydrogen peroxide electrogeneration are also being developed for wastewater remediation. In these techniques, H_2O_2 is continuously supplied to the contaminated solution from the two-electron reduction of O_2 usually at carbon-felt [443–448] and carbon-polytetrafluoroethylene (PTFE) O_2-diffusion [449, 450] cathodes:

$$O_2 + 2H^+ + 2e^- \rightarrow H_2O_2 \tag{6.1}$$

The oxidizing power of the hydrogen peroxide is highly enhanced by the addition of Fe^{2+} generating the Fenton reaction [451]:

$$Fe^{2+} + H_2O_2 \rightarrow Fe^{3+} + OH^{\bullet} + OH^- \tag{6.2}$$

It is worthwhile stressing that the treatment of aqueous solutions of toxic organic pollutants by advanced oxidation processes is not necessarily accompanied by a decrease of the toxicity, since the oxidation reaction might lead to the formation of intermediates more toxic than the initial pollutant. Generally, the efficiency of pollutants degradation would depend on the concentration of H_2O_2 in Fenton reaction [452, 453]. Therefore, to promote pollutants degradation, a highly efficient cathode system for efficient production of H_2O_2 seems to be important [454]. CNTs, possessing unique properties such as high electrical

conductivity, high surface area, chemical stability and significant mechanical strength, are considered to be the promising electrode material [455].

Electro-Fenton degradation of Rhodamine B based on a composite cathode of Cu_2O nanocubes and CNTs has been reported by Ai et al. [456]. This oxygen-fed gas diffusion electrode has been prepared by combining Cu_2O nanocubes and MWCNTs with poly tetrafluoroethylene (Cu_2O/CNTs/PTFE). The electro-Fenton system produces copper ions in situ from Cu_2O nanocubes and simultaneously electrochemically reduces oxygen into hydrogen peroxide. These two Fenton reagents further react together to produce hydroxyl radicals to degrade Rhodamine B effectively at neutral pH. More importantly, the electro-Fenton system with the Cu_2O/CNTs/PTFE cathode can efficiently degrade Rhodamine B without losing activity after several processes (6 run).

Zhang et al. [455] have prepared a nitrogen-functionalized CNTs (N-CNT) cathode for highly efficient electrocatalytic generation of H_2O_2 in electro-Fenton system. N-CNT is obtained by nitrogen functionalization of CNTs by pulsed high voltage discharge in a gas–liquid hybrid reactor. It has been found that nitrogen functionalities are pyridine, pyrrol and quaternary species. H_2O_2 formation rate on the CNT electrode is greatly improved by the presence of nitrogen functionalities due to the acceleration of electron transfer of O_2 reduction. For the electro-Fenton degradation of methyl orange, the N-CNT electrode has shown faster removal of methyl orange compared to the CNT electrode. No significant current response decrease has been observed after replacing the electrolyte used for 20 repetitive cycles. This test suggests that the stability of the N-CNT electrode is noticeable.

Zarei et al. [457] have studied peroxi-coagulation degradation of the dye C.I. Basic Yellow 2 using carbon-PTFE and CNT-PTFE electrodes as cathode. The researchers have mixed appropriate amounts of AC or CNT, PTFE, distilled water and n-butanol in an ultrasonic bath to create a highly dispersed mixture. The resulting mixture has been heated at 80 ^oC until it resembled an ointment in appearance. The ointment has been bonded to 50% PTFE-loaded carbon papers and sintered at 350 ^oC for 30 min under inert conditions (N_2). The resulting electrode then has been cut to obtain operational carbon-PTFE or CNT-PTFE cathodes of 25 mm diameter and about 0.6 mm thickness. The cathode has been placed at the bottom of a cylindrical holder of polypropylene with an inner graphite ring as current collector in contact with a copper wire as electrical connection. The H_2O_2 concentration produced on the graphite felt, carbon-PTFE and CNT-PTFE has been determined when the electrodes have fed with O_2 (Figure 6.1). As can be seen from Figure 6.1, the concentration of H_2O_2 obtained via graphite felt, carbon-PTFE and CNT-PTFE electrodes is 0.47, 5.9 and 14.3 mM, respectively at 300 min electrolysis. The amount of electrogenerated H_2O_2 obtained with CNT-PTFE electrode is nearly three and thirty times higher than that of carbon-PTFE and graphite felt electrodes, respectively.

The different abilities of H_2O_2 electro-generation of carbon and CNT-PTFE electrodes can be related to the large surface area of CNT-PTFE. Figure 6.2 shows atomic force microscopy (AFM) images of carbon-PTFE and CNT-PTFE electrodes. It is obvious that CNT-PTFE has more active sites for generation of H_2O_2 than carbon-PTFE (Figure 6.2a and b).

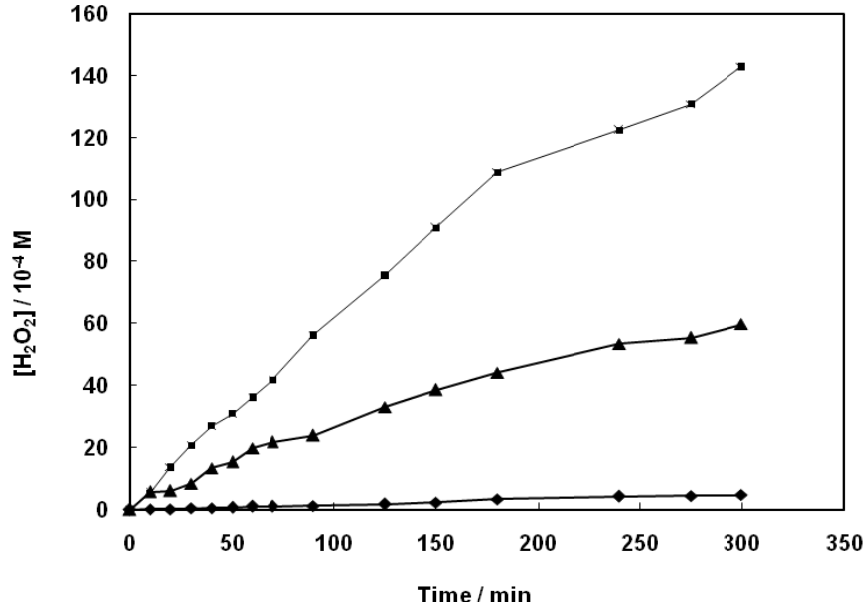


Figure 6.1. The amount of electrogenerated H_2O_2 as a function of time at room temperature, [Na_2SO_4] = 0.05 M, Applied current = 100 mA, pH=3. (♦) graphite felt; (▲) carbon-PTFE; (■) CNT-PTFE. (Adapted from Zarei et al. [457] with permission from publisher, Elsevier. License Number: 2539391425351).

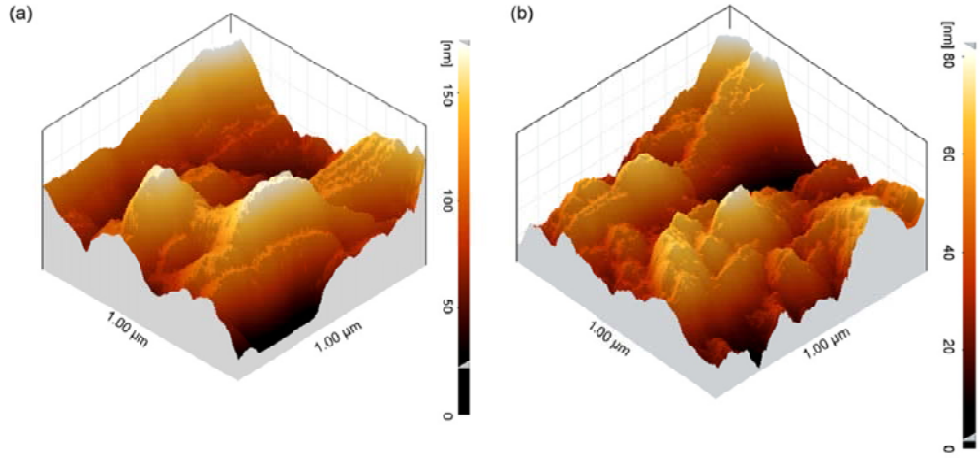
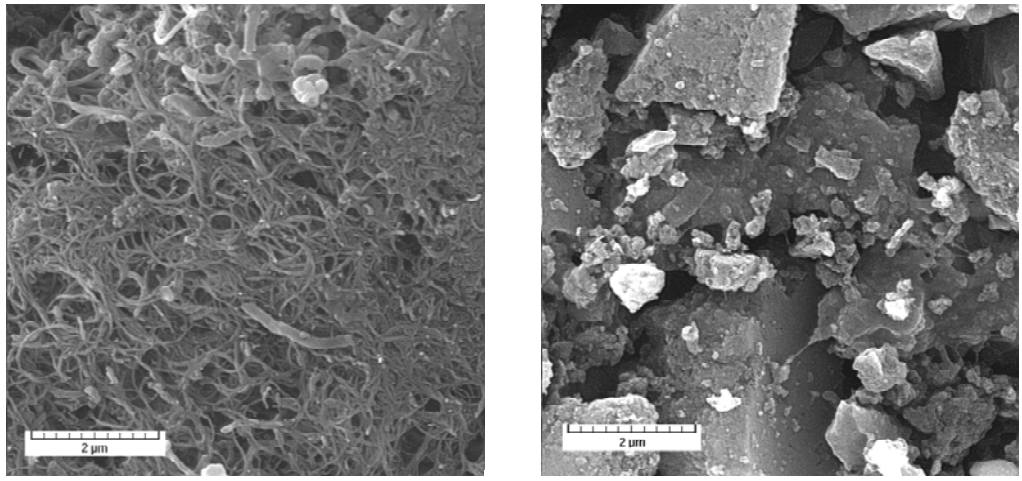


Figure 6.2. Three-dimensional (3D) AFM images of (a) carbon-PTFE, (b) CNT-PTFE electrodes. (Adapted from Zarei et al. [457] with permission from publisher, Elsevier. License Number: 2539391425351).

Figure 6.3 shows SEM images of the surface of carbon-PTFE and CNT-PTFE electrodes. As can be seen in Figure 6.3a the surface of CNT-PTFE electrode is rough and many nanoscaled pores have been formed, whereas the surface layer of carbon-PTFE electrode (Figure 6.3b) has many clods and it is not flat. Such a porous surface of CNT-PTFE electrode can allow fast diffusion of O_2 achieving high mass transfer rate and highly efficient production of H_2O_2. The decolorization efficiency of 20 mg/L C.I. Basic Yellow 2 in peroxi-

coagulation process has reached 62% and 96% in the first 10 min by carbon-PTFE and CNT-PTFE electrodes at 100 mA, respectively. [457].



(a) (b)

Figure 6.3. SEM images of (a) CNT-PTFE electrode and (b) carbon-PTFE electrode. (Adapted from Zarei et al. [457] with permission from publisher, Elsevier. License Number: 2539391425351).

CNTs commonly have a strong tendency to agglomerate due to their nanosize and respective high surface energy. Therefore, their vast applications have remained extremely limited because of the difficulty in dissolving them in the solution (water or organic solvent). CNTs can oxidize with hydroxyl radical by pulsed high voltage discharge (PHVD) with the goal of enhancing their solubility [458]. The oxidation of CNTs has been achieved in a novel gas–liquid hybrid reactor where O_2 has been bubbled through the holes of the needle electrodes forming pulsed O_2 plasma, while CNTs have been fluidized [459]. The molecular O_2 readily scavenges electrons, forming hydroxyl radical. The reactions are expressed by the following equations [460, 461, 462]:

$$O_2 + e^- \rightarrow O + {}^*O(^1D) \tag{6.3}$$

$${}^*O(^1D) + H_2O \rightarrow 2^{\bullet}OH \tag{6.4}$$

where O is atomic oxygen and $*O(^1D)$ is oxygen atom in excited state.

CNTs before and after oxidation have been characterized by various techniques such as XRD, Raman, FT-IR, and XPS. The results show that oxygen bearing groups (C-OH, -COO, COOH, -C=O) are introduced on the surface of CNTs. The oxidized CNTs are easily dispersed in ethanol. Zhang et al. [458] have reported the oxidation of CNT samples which called as CNT-n, where n is the treatment time (min). The H_2O_2 yield on the original CNT is 102 mg/L at −0.85 V after 90 min. In contrast, H_2O_2 yield on CNT-15 has reached 146 mg/L at the same conditions, resulting from the enhancement of the accessibility of O_2 on CNT.

In the electro-Fenton, the removal of Methyl Orange on the original CNTs is around 40%, and it has increased to 95% on oxidized CNTs [458].

Zhang et al. [463] have studied the characterization of the CNT/TiO_2 composite electrodes prepared using CNT, anatase typed TiO_2 and phenolic resin binder. The adsorption effects, structural variations, surface state and elemental compositions have been investigated through preparation of three kinds of CNT/TiO_2 composites. In order to fabricate of electrodes, ethyl alcohol has been used as solvent for the melting of phenol resin. After dissolving phenol resin in the alcohol solution, TiO_2 powder and CNTs have been mixed with resin-alcohol solution. Then, the mixtures have been pressed into 9.95 × 39.5 × 5.95 mm hexagonal pellets in a mould. The curing temperature of the pelletized CNT/TiO_2 matrix is about 423 K. The cured samples then have been pyrolyzed at 673 K for 1 h in order to completely cure the binder. The electro-photocatalytic decomposition of methylene blue has been performed with CNT/TiO_2 electrode.

Table 6.1. Different organic pollutants treated by electrochemical water treatment processes based on CNTs

Type of electrode (cathode)	Electrochemical process	Organic pollutant	Ref.
CNT-PTFE	Peroxi-coagulation	C.I. Basic Yellow 2	[457], [464]
CNT-PTFE	Peroxi-coagulation	C.I. Basic Blue 3, Malachite green and C.I. Basic red 46	[465]
CNT-PTFE	Photoelectro-Fenton combined with photocatalytic process	C.I. Acid Red 17 and C.I. Basic Red 46	[466], [467]
Cu_2O/CNTs/PTFE	Electro-Fenton	Rhodamine B	[456]
CNT-PTFE	Oxalate catalyzed photoelectro-Fenton	C.I. Basic Blue 3 and C.I. Basic Red 46	[468], [469]
Gas diffusion electrode	Electro-Fenton	Methyl Orange	[458]
CNTs/TiO_2 composite	Electro-photocatalytic decomposition	Methylene Blue	[463]

7. PHOTOCATALYTIC PROCESSES BASED ON CARBON NANOTUBES

In this section, the environmental applications of CNT-based materials in the field of photocatalysis are considered.

Photocatalytic chemistry involving semiconductor materials has grown from a subject of esoteric interest to one of central importance in both academic and technological research. In this context, environmental pollution and its control through nontoxic treatments and easy recovery processes is a serious matter. The number of publications concerning mineralization of dyes, pesticides, fungicides and hazardous compounds, etc., increased tremendously in the last decade [439, 470-473].

Photocatalysis covers the range of reactions proceeding under the action of light. Among these, we find catalysis of photochemical reactions, photo–activation of catalysts, and photochemical activation of catalytic processes. Photocatalysis is defined by the IUPAC. “Photocatalysis is the catalytic reaction involving light absorption by a catalyst or a substrate”

[474-476]. A more precise definition may be that "photocatalysis is a change in the rate of chemical reactions or their generating under the action of light in the presence of the substances (photocatalysts) that absorb light quanta and are involved in the chemical transformations of the reaction participants, repeatedly coming with them into intermediate interactions and regenerating their chemical composition after each cycle of such interactions" [475]. The most typical processes covered by photocatalysis are the photocatalytic oxidation (PCO) and the photocatalytic decomposition (PCD) of substrates such as organic compounds. The PCO process employs the gas–phase oxygen as a direct participant to the reaction, while the PCD takes place in the absence of O_2 [476].

Several semiconductors possess band gaps suitable to catalyze chemical reactions. Titanium dioxide has become a ''gold standard'' semiconductor in the field of photocatalysis. TiO_2 is chemically and biologically inert as well as cheap to manufacture and apply. In recent years, applications of nanostructured TiO_2 materials in environmental remediation have been one of the most active areas in research [476-479]. In addition to TiO_2 [480, 481], there is a wide range of metal oxides and sulfides that have been successfully tested in photocatalytic reactions. Among these are ZnO [482], WO_3 [483], WS_2 [484], Fe_2O_3 [485], V_2O_5 [486], CeO_2 [487], CdS [488], and ZnS [489]. Interaction of these semiconductors with photons that possess energy equal or higher than the band gap may cause separation of conduction and valence bands. This event is known as electron–hole pair generation. For TiO_2, this energy can be supplied by photons with energy in the near ultraviolet range. This property promotes TiO_2 as a promising candidate in photocatalysis where solar light can be used as the energy source [476]. Some of the beneficial characteristics of nanostructured TiO_2 materials include high photocatalytic efficiency, physical and chemical stability, low cost and low toxicity.

When TiO_2 is illuminated with $\lambda < 390$ nm light, an electron excites out of its energy level and consequently leaves a hole in the valence band. As electrons are promoted from the valence band to the conduction band, they generate electron–hole pairs (Eq. 7.1) [481, 490, 491]:

$$TiO_2 + h\nu(\lambda < 390nm) \rightarrow e^- + h^+ \tag{7.1}$$

Valence band (h^+) potential is positive enough to generate hydroxyl radicals ($^\bullet OH$) at TiO_2 surface and the conduction band (e^-) potential is negative enough to reduce molecular oxygen as described in the following equations:

$$e^- + O_{2(ads)} \rightarrow {}^\bullet O^-_{2(ads)} \tag{7.2}$$

$$e^- + H^+_{(ads)} \rightarrow {}^\bullet H_{(ads)} \tag{7.3}$$

$$h^+ + OH^-{}_{(ads)} \rightarrow {}^\bullet OH_{(ads)} \qquad (\text{in alkaline solutions}) \tag{7.4}$$

$$h^+_{VB} + H_2O_{(ads)} \rightarrow H^+ + {}^\bullet OH_{(ads)} \ (\text{in neutral solutions}) \tag{7.5}$$

The hydroxyl radical is a powerful oxidizing agent which may attack the organic matters (OM) present at or near the surface of TiO_2. It is capable to degrade toxic and bioresistant

compounds into harmless species (e.g. CO_2, H_2O, etc). This decomposition can be explained through the following reactions [492, 493]:

$$h^{+}_{VB} + OM \rightarrow OM^{\bullet+} \rightarrow Oxidation\,of\,OM \quad (7.6)$$

$$^{\bullet}OH_{(ads)} + OM \rightarrow Degradation\ of\ OM \quad (7.7)$$

Nanostructured TiO_2 materials are successfully used for the photocatalytic removal of a variety of organic pollutants such as hydrocarbons and chlorinated hydrocarbons (e. g. CCl_4, $CHCl_3$, C_2HCl_3, phenols, chlorinated phenols, surfactants, pesticides, dyes) as well as reduction deposition of heavy metals such as Pt^{4+}, Pd^{2+}, Au^{3+}, Rh^{3+} and Cr^{3+} from aqueous solutions. Nanostructured TiO_2 materials have also been affective in the destruction of biological organisms such as bacteria, viruses, and molds [494–500].

An appropriate method for increasing the photocatalytic efficiency of TiO_2 consists in adding a co–adsorbent such as carbon based materials (e.g. AC and CNTs). This synergy effect has been explained by the formation of a common contact interface between different solid phases. Carbon based materials act as an adsorption trap for the organic pollutants which are then efficiently transferred to the TiO_2 surface. The organic pollutants are immediately degraded by the photoactivated TiO_2. For this reason, carbon grain coated with activated nano–TiO_2 (20–40 nm) (TiO_2/AC) was prepared and used for the photodegradation of methyl orange dyestuff in aqueous solution [501]. Some of the benefits that take place in the application of the carbon based materials are summarized below [502, 503]:

1) The adsorbent makes a high concentration environment of target organic substances around the loaded TiO_2 particles by adsorption. Therefore, the rate of photodegradation is enhanced.
2) The adsorbed organic substances are oxidized on the photocatalyst surfaces. The resultant intermediates are also adsorbed and then further oxidized. Toxic intermediates, if formed, are not released in the air and/or in solution thus preventing secondary pollution.
3) Since the adsorbed substances on the adsorbent supports are finally oxidized to give CO_2, the high adsorption ability of the hybrid photocatalysts for organic substances is maintained for a long time. The amount of TiO_2 as catalyst may play a significant role on the photo–efficiency of hybrid catalysts.

Recently, attention has been called to the fact that CNTs are attractive and competitive catalyst supports compared to AC due to the combination of their electronic, adsorption, mechanical and thermal properties [504]. The unique electronic property of CNT is that they can be either metallic or semiconducting, depending on their geometry [505].

Considering the unique electrical properties and high chemical stability of MWCNTs, it is expected that the combination of MWCNTs with TiO_2 may induce charge transfer and thus improve the photocatalytic activity of TiO_2 under visible light. MWCNTs as adsorbent and conductive materials can absorb the visible light irradiation and transfer the photogenerated electron into the conduction band of TiO_2 particles efficiently. When MWCNTs–TiO_2 composite is illuminated with visible light, electrons are promoted from the valence band via

MWCNTs to the conduction band of TiO_2 to produce electron (e^-)–hole (h^+) pairs (Eqs. 7.8 and 7.9). This electron transfer between MWCNTs and TiO_2 semiconductor enhances the photocatalytic activity of the composite. The potential of electrons (e^-) is negative enough to reduce molecular oxygen (Eq. 7.10) and the potential of holes (h^+) is positive enough to generate hydroxyl radicals at the surface (Eq. 7.11). Therefore, the role played by MWCNTs can be explained by injecting electrons into TiO_2 conduction band under visible light illumination and triggering the formation of very reactive radicals super-oxide radical ion ($O_2^{-\bullet}$) and hydroxyl radical ($^{\bullet}OH$), which are responsible for the degradation of the organic compounds (Eqs. 7.6 and 7.7) [506].

$$MWCNT - TiO_2 + Visible\ ligh \rightarrow MWCNT^+ - TiO_2(e^-) \tag{7.8}$$

$$MWCNT^+ - TiO_2(e^-) + (O_2)_{ads} \rightarrow MWCNT^+ - TiO_2 + O_2^{-\bullet} \tag{7.9}$$

$$MWCNT^+ - TiO_2 \rightarrow MWCNT - TiO_2(h^+) \tag{7.10}$$

$$MWCNT - TiO_2(h^+) + H_2O \rightarrow MWCNT - TiO_2 + H^+ + {}^{\bullet}OH \tag{7.11}$$

Preparation conditions and environmental applications of hybrid CNT-photocatalyst nanomaterials have been summarized in Table 7.1. For instance, Wang et al. [506-508] have reported the preparation of MWCNTs–TiO_2 composite photocatalysts by a modified sol–gel method for photocatalytic degradation of phenol under visible light irradiation. The researchers have synthesized high purity MWCNT by a catalytic chemical vapor deposition (CCVD) method in fluidized bed reactor on a Fe/Al_2O_3 catalyst. MWCNT-TiO_2 composites have been prepared by a modified acid-catalyzed sol–gel method from alkoxide precursors. The preparation has been performed at room temperature as following: 0.1 mol of $Ti(OC_3H_7)_4$ has been dissolved in 200 mL of ethanol. The solution has been stirred magnetically for 30 min, and then 1.56 mL of nitric acid (65 wt.%) has been added. Subsequently, certain amount of MWNT has been introduced into the $Ti(OC_3H_7)_4$ ethanol solution. The mixture has been loosely covered and kept stirring until a homogenous MWNT-contained gel formed. The gel has been aged in air for several days. Then, the xerogel has been crushed into a fine powder and dried at room temperature. The powder has been calcined at 400 ^oC in a flow of nitrogen for 2 h to obtain MWCNT-TiO_2 composite. Material characterization has indicated a more homogeneous MWCNT dispersion in TiO_2 matrix and less agglomeration of TiO_2 particles on MWCNT surface, suggesting a strong interphase structure effect between MWCNT and TiO_2, so as to increase the surface area of the composite catalysts. The BET surface areas of composite catalysts vary from 114 to 163 m^2/g, increasing with the initial MWCNT/TiO_2 ratio from 5 to 40%. Then, the synthesized MWCNT-TiO_2 composite has been used for photocatalytic degradation of phenol under visible light irradiation (see Table 7.1). The complete elimination of phenol from the solution on the irradiated MWCNT–TiO_2 composite catalyst has been achieved within 4 h. By contrast, neat TiO_2 can only reach 44.2% of phenol conversion within the same reaction time.

Table 7.1. Preparation conditions and environmental applications of hybrid CNT-photocatalyst nanomaterials

Type of photocatalyst	Type of CNT	Preparation method of hybrid nanomaterial	Application	Irradiation light and wavelength (nm)	Ref.
TiO_2 (anatase phase)	MWCNTs	Acid-catalyzed sol-gel method using $Ti(OC_3H_7)_4$ and synthesized MWCNTs	Photocatalytic degradation of phenol in water	Visible light, 366-546	[506]
TiO_2 (anatase phase)	MWCNTs	Sol-gel method using titanium (IV) butoxide and MWCNTs	Photocatalytic degradation of 2,6-dinitro-*p*-cresol in water	Solar light	[507]
TiO_2 (anatase phase)	MWCNTs	Modified acid-catalyzed sol-gel method using $Ti(OC_3H_7)_4$ and synthesized MWCNTs	Photocatalytic degradation of phenol in water	UV light, the radiation source is a low-pressure mercury vapor lamp	[508]
C-N-doped TiO_2 (anatase and rutile phases)	Carbon nanorods	CVD	Photocatalytic degradation of methyl orange in water	High-pressure xenon short arc lamp	[509]
TiO_2 (anatase phase)	Two-dimensional carbon nanowalls	CVD	Photoelectrochemical removal of phenol in water	UV-A, 365	[510]
TiO_2 (anatase phase)	MWCNTs	Sol-gel method using titanium (IV) butoxide and MWCNTs	Photoelectrochemical removal of phenol in water	Visible light	[511]
CdS–TiO_2	MWCNTs	Sol-gel method using $Cd(NO_3)_2{\cdot}4H_2O$, $Ti(OC_4H_9)_4$ and MWCNTs	Photocatalytic degradation of toluene in gaseous phase	UV-C, 254	[512]
TiO_2 (Degussa P25)	SWCNTs	Mechanically mixing of TiO_2 and CNTs	Photocatalytic H_2 gas production from water/alcohol mixtures	Super high-pressure mercury lamp (500 W)	[513]
TiO2 (anatase phase)	CNT arrays	Two-step thermal CVD	Photocatalytic degradation of phenol in water	UV-A, 365	[514]
TiO2 (anatase phase)	MWCNTs	Mechanically blending	Anode materials for Li-ion batteries	-	[515]
TiO2 (anatase phase)	MWCNTs	MWCNTs as a starting material, and titanium(IV) isopropoxide, titanium(IV) propoxide and titanium(IV) n-butoxide as titanium sources and benzene as a solvent	Photocatalytic degradation of methylene blue in water	UV-A, 356	[516]
TiO2 (anatase phase)	MWCNTs	Conventional and the surfactant wrapping sol-gel	Photocatalytic degradation of methylene blue in water	UV-A, 365	[517]
TiO2 (anatase phase)	MWCNTs	Dip-coating sol-gel method using TiCl4 and synthesized MWCNTs	Photoinactivation of Escherichia coli bacteria in water	Visible light, >400	[518]
TiO2 (anatase and brookite phases)	MWCNTs	Sonochemical and calcination methods	Photocatalytic oxidation of acetone in air	UV-A, 365	[519]

Type of photocatalyst	Type of CNT	Preparation method of hybrid nanomaterial	Application	Irradiation light and wavelength (nm)	Ref.
TiO_2 nanotubes (anatase, rutile or a mixture of both)	MWCNTs	Sol–gel and then heat treatment	Photocatalytic oxidation of propene in gaseous phase	UV-C, 257.7	[520]
TiO_2 (rutile phase)	MWCNTs	Hot CVD process	Photocatalytic decomposition of gaseous acetaldehyde	UV-B	[521]
TiO_2 (anatase phase)	MWCNTs	Adding TiO_2 and CNTs in weight ratios of 10:1, 10:2 and 10:3 to solution	Photocatalytic degradation of an azo dye, C.I. Reactive Red 2 in water	254, 365 and 410	[522]
TiO_2	Fe-CNTs	Sol-gel process using CNTs as support, titanium sulphate as TiO_2 precursors, and $Fe(NO_3)_3 \cdot 9H_2O$ as additive.	Photocatalytic degradation of rhodamine B in water	UV light	[523]
ZnS nanocrystals	MWCNTs	Reaction between $Zn(NO_3)_2$ and Na_2S in an aqueous suspension of MWCNTs	Photocatalytic degradation of methylene blue in water	UV-A, 365	[524]
ZnO nanoparticles	MWCNTs	Sol-gel process using $Zn(CH_3COO)_2 \cdot 2H_2O$ and treated MWCNTs	Photocatalytic degradation of methyl orange in water	High pressure Hg lamp (375 W)	[525]
ZnO nanocrystals	MWCNTs	ZnO nanocrystals-coated MWCNTs composite is fabricated through noncovalent modification of MWCNTs with the dispersant of sodium dodecyl sulfate	Photocatalytic degradation of methylene blue in water	Medium pressure Hg lamp (300 W)	[526]

Liu et al. [509] have reported the photocatalytic degradation of methyl orange in water using C-N-doped TiO_2 nanotube array/carbon nanorod composite. The C-N-doped TiO_2/carbon nanorod composite is fabricated by CVD. The cleaned titanium ribbon is anodized at 15 V for 3 h in an electrolyte containing 0.1 M NaF and 0.5 M $NaHSO_4$ at room temperature. Then, the anodized TiO_2 nanotubes are annealed at 450 °C in air atmosphere for 3 h. The sintered samples are put in a graphite trough in which 5 mg polyvinyl alcohol and/or 20 mg urea are added as the carbon and nitrogen source, respectively, and then annealed at 600 °C in N_2 atmosphere. The C-N doping shifts the absorption edge of TiO_2 nanotubes to the visible light region. Under the simulated solar light irradiation using High-pressure xenon short arc lamp, the C-N-doped TiO_2 nanotubes show higher photocatalytic activity in the degradation of methyl orange than the undoped TiO_2 nanotubes. The enhanced photocatalytic activity has been attributed to the carbon and nitrogen doping which extends the absorption of TiO_2 into the visible light region. The formed carbon nanorods facilitate the photogenerated charge transferring from TiO_2 interface.

In the same work, a two-dimensional TiO_2/carbon nanowall composite has been fabricated by growing carbon nanowalls on a Ti sheet with hot filament CVD, followed by metal-organic CVD using titanium isopropoxide as TiO_2 precursor and argon as carrier gas [510]. The prepared TiO_2/carbon nanowall composite has showed a higher photocatalytic activity than TiO_2 nanotubes for the photoelectrocatalytic degradation of phenol under UV-A

light irradiation. The enhanced photocatalytic activity has been attributed to the improvement of the separation of photogenerated electrons and holes. Photoelectrochemical measurements have been performed in a three-electrode configuration with the TiO_2/CNWs on a Ti sheet as photoanode, a platinum foil as counter electrode and a saturated calomel electrode (SCE) as reference electrode. The electrolyte is 0.01 M Na_2SO_4 aqueous solution. A 300W high-pressure mercury lamp has been used as the UV light source with a principal wavelength of 365 nm. Chen et al. [511] have also reported the enhanced visible light-induced photoelectrocatalytic degradation of phenol by CNT-doped TiO_2 electrodes. Modified sol–gel method has been used to prepare TiO_2 and MWCNT composites that subsequently deposited onto indium tin oxide (ITO) conductive glass plates. The photoelectrochemical activity of the prepared electrodes has been evaluated in terms of the degradation of phenol under visible light using a reactor operated in a standard three-electrode mode. Platinum wire and Ag/AgCl have been used as the counter and reference electrodes, respectively.

Having explained the preparation and applications of CNTs-TiO_2 composites, let's proceed to investigate synthesis and environmental applications of the hybrid CNT-ZnO nanomaterials (see Table 7.1). Zinc oxide (ZnO) nanoparticles are also the important semiconductor materials applied in conventional catalysis [482]. For photocatalytic reactions, ZnO nanoparticles with a wide band-gap have several advantages such as high optical activity and stability, high sensitivity for UV–Vis light and low fabrication cost [527]. Jiang and Gao [526] have reported the preparation and characterization of ZnO-coated MWCNTs with enhanced photocatalytic activity through noncovalent modification of MWCNTs with the dispersant of sodium dodecyl sulfate. ZnO nanoparticles have been also coated on the MWCNTs through a sol process using $Zn(CH_3COO)_2{\cdot}2H_2O$ and treated MWCNTs as raw materials [525]. The synthesis progress includes two steps. In the first step, 1.10 g $Zn(CH_3COO)_2{\cdot}2H_2O$ is dissolved in 250 mL diethyleneglycol. Subsequently, 10 mL deionized water is added into the above solution. After that, the mixture is magnetically stirred at 160–180 °C for 5 min and then placed in the air for 2 h to get ZnO sol. In the second step, certain amount of purified MWCNTs is dispersed into the above sol with sonication for 30 min. Then, the solution is slowly heated to 160–180 °C with vigorous stirring for 1.5 h. ZnO–MWCNTs nanocomposites are obtained after being cooled to the room temperature, centrifuging, washing by absolute ethanol and deionized water and drying the suspension at 110 °C for 12 h. The synthesized nanocomposites exhibits blue-shift absorption compared with pure ZnO nanomaterials [525, 526]. The prepared nanocomposites have been used for photocatalytic decolorization of methyl orange [525] and methylene blue [526] solution under UV light irradiation. The photocatalytic experiments exhibit that the composite has a higher photocatalytic activity than that of both the ZnO nanoparticles and the mechanical mixture of MWCNTs and ZnO. The reason of these observations is thought to be the fact that the enhanced photocatalytic activity of ZnO–MWCNTs composite may result from the electron transfer processes. Under UV light irradiation, the valence band electrons of ZnO are excited to its conduction bands, giving rise to the formation of electron and hole pairs. CNTs are relatively good electron acceptors, while semiconductor ZnO can be considered as good electron donor under UV light irradiation. CNT which acts as a photogenerated electron acceptor, promotes interfacial electron-transfer processes from the attached ZnO to the CNT. Thus the photocatalytic property of ZnO-coated MWCNTs composite is improved [525, 526].

In conclusion, there are three predominant explanations for the enhanced photocatalytic activity of hybrid CNT-photocatalyst nanomaterials under visible light irradiation. First, the CNTs absorb almost the entire visible light spectrum and act as photosensitizers, endowing the CNT–TiO_2 composites with an electron transfer mechanism similar to that of dye-sensitized TiO_2. Therefore, the CNT–TiO_2 samples can transfer excited electrons from the CNTs to the conduction band of TiO_2 when illuminated with visible light, thereby increasing the photocurrent. Second, the conductivity of CNTs is superior to that of TiO_2; therefore, it can be expected a high transport rate of electrons in the CNT–TiO_2 film and a lower possibility of e^-/h^+ recombination. Third, the CNT–TiO_2 samples presumably possess high surface areas, pore sizes, and pore volumes that enhance visible light absorption and interfacial charge transfer, thereby improving the efficiency.

8. Adverse Effects of Application of Carbon-Based Nanomaterials

Carbon-based nanomaterials, especially CNTs, has a wide range of applications in electronics, solar and fuel cells, energy storage, biomedical engineering, tissue engineering, drug delivery, nanoinjectors, neuroengineering, gene therapy, bio and chemical sensor technology, cosmetics, ceramic and metallic CNT composites, polymer CNT composites and environmental purification [528-531]. In spite of such attractive features, the adverse effects of carbon-based nanomaterials are the prime concern investigated by several research groups [532-534]. There are still many open questions regarding the effects of human or ecological exposure. The results of toxicological studies suggest that CNTs may affect human health and the environment. In this section, the adverse effects and toxicity of carbon-based nanomaterials are briefly presented.

As a consequence of widespread applications, human and environmental exposure to CNTs is likely to increase. The adverse effects and toxicity issues of CNTs are highly relevant for two reasons: firstly, as more products containing CNTs come to market, there is a chance that free CNTs get released during their life cycles, most likely during production or disposal, and find their way through the environment into the body. Secondly, and much more pertinent with regard to potential health risks, is the use of CNTs in biological and medical settings. CNTs interesting structural, chemical, electrical and optical properties are explored by numerous nanomedicine research groups around the world with the goal of improving performance and efficacy of biological detection, imaging and therapy applications. In many of these applications, CNTs would be deliberately injected or implanted in the body.

Adverse effects of CNTs is related to their properties, such as their structure (SWCNT or MWCNT), length and aspects ratio, surface area, degree of aggregation, extent of oxidation, bound functional group(s), method of manufacturing (which can leave the catalytic residues and produced impurities) and their concentration and dose. CNTs are in the nanometer size range and hence easily enter into the lungs via the respiratory tract with air inhalation. After entering the lungs they distribute rapidly in the central nervous system, peripheral nervous system, lymph and blood (see Figure 8.1). They show rapid distribution in heart, spleen, kidney, bone marrow and liver. Depending upon size and physical structure of CNTs, they are deposited in the different regions of the respiratory tract. After deposition, CNTs are

transferred to the extrapulmonary site and reach the target organ site by various transfer routes and mechanisms [532]. Adverse effects of CNTs on animals and human cells have been summarized in Table 8.2 and 8.3. The interactions between CNT and various cells have been induced nutrient deprivation anti-proliferative effects, decreased cell adhesion, apoptosis and necrosis and oxidative stress (see Table 8.2 and 8.3). These results suggest that carbon based nanomaterials are potentially toxic to humans and that strict industrial hygiene measures should to be taken to limit exposure during their manipulation.

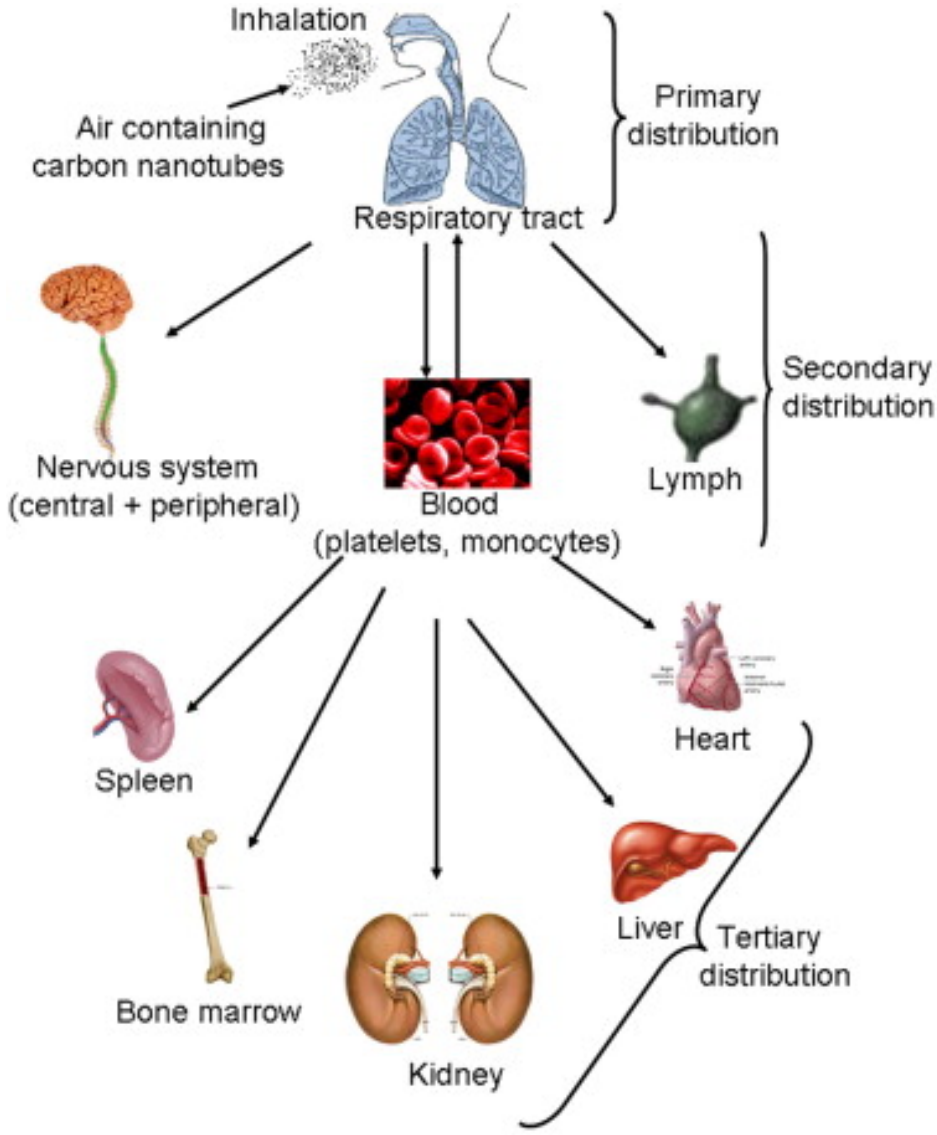


Figure 8.1. Distribution of CNTs in the body. (Adapted from Tekade et al. [532] with permission from publisher, Elsevier. License Number: 2496941097499).

Table 8.2. Adverse effects of CNTs on animals cells

Type of CNT	Animal species/ cells	Exposure conditions	Objective	Outcomes or results	Ref.
98% MWCNT and the remaining consisted of traces of cobalt and iron	Female Wistar rats/ epithelial cells	*In vivo,* micronuclei are assessed in type II pneumocytes 3 days after a single intra-tracheal administration of MWCNT (0.5 or 2 mg). *In vitro,* cytokinesisblock micronucleus assay in rat lung epithelial cells exposed to MWCNT (10, 25, 50 mg/mL)	Determining whether MWCNT elicit genotoxic effects in rat lung cells, specifically in type II pneumocytes (AT-II)	*In vivo*, significant and dose-dependent increase in micronucleated pneumocytes after a single administration of MWCNT. *In vitro*, significant increase of micronuclei in epithelial cells after exposure to MWCNT	[534]
Water soluble MWCNT (S-MWCNT)	Female Kunming mice	*In vi*vo, the mice are randomly assigned to the S-MWCNT (six mice per group). Two S-MWCNT groups are injected twice with total S-MWCNT dose of 60 or 100 mg/kg body weight on day 0 and 4 h after the first injection. After the injection, behavior and abnormal symptom of mice are monitored. The mice are sacrificed 1, 7, 15, 30, or 60 days post-exposure	The influences of S-MWCNTs on mouse spleen by carbon clearance measurements, oxidative injury and histopathologic examination	Phagocytic activity of reticuloendothelial system, activity of reduced glutathione, superoxide dismutase and malondialdehyde in splenic homogenate do not change significantly in 2 months. No observable sign of damage in spleen; however, the accumulated S-MWCNTs gradually transfer from the red pulp to the white pulp over the exposure time and might initiate the adaptive immune response of spleen	[533]
MWCNT	Female Sprague–Dawley rats	MWCNTs administer intratracheally (0.5, 2 or 5 mg/animal) to the rats	Estimation of lung persistence, inflammation and fibrosis	MWCNTs are present in the lung after 60 days and induce inflammatory and fibrotic reactions	[535]
MWCNT	Erythrocytes isolated from the heparinized rat blood	*In vitro*	Estimatation of MWCNT cytotoxicity *in vitro*	MWCNT at concentrations up to 25 µg/mL do not show toxic effects on rat erythrocytes and thymocytes, while at concentration 50 µg/mL cause the acceleration of erythrocyte hemolysis, decrease of the number of viable thymocytes and inhibition of mitochondrial electron-transporting chain	[536]
Acid treated and carboxylated SWCNTs	Rat/aortic smooth muscle cells	The impact of SWCNT (0.0–0.1 mg/mL) on rat aortic smooth muscle cells over a 3.5-day time-course	Evaluation of the time-, dosage-, and aggregation-dependent influence of purified SWCNT on the growth of rat aortic smooth muscle cells	At 0.1 mg/mL, similar decrease in cell number relative to the control medium is observed	[537]

Table 8.2. (continued)

Type of CNT	Animal species/ cells	*Exposure conditions*	Objective	Outcomes or results	Ref.
MWCNT contained 0.41% sodium and 0.32% iron	Male C57BL-6J mice	*In vivo,* MWCNT are dispersed in dispersion medium and the mice receives 10, 20, 40 or 80 μg MWCNT by aspiration exposure. At 1, 7, 28 and 56 days post-exposure, MWCNT-induced pulmonary toxicity is investigated	Pulmonary toxicity of MWCNT	MWCNT exposure rapidly produces significant adverse health outcomes in the lung	[538]
SWCNTs (purity of 95%)	Male CD-ICR mice	Each mice is exposed to SWCNTs by three times of injection every 4 h (330μg SWCNTs/0.33 mL). At 90 days post-exposure, mice are sacrificed and blood/organ samples are collected for accumulation determination and toxicological assays	The toxicity of SWCNTs to main organs, including liver, lung and spleen	Slight inflammation and inflammatory cell infiltration occur in lung, but the serum immunological indicators remain unchanged. No apoptosis is induced in the main organs. The decreasing glutathione level and increasing malondialdehyde level suggest that the toxicity of SWCNTs might be due to the oxidative stress	[539]
SWCNTs and acid-functionalized SWCNTs (AF-SWCNTs)	Adult pathogen free female CD-1 mice	Mice are exposed by oropharyngeal aspiration to 10 or 40 μg of SWCNTs and AF-SWCNTs. 24 h later, pulmonary inflammatory responses and cardiac effects are assessed	Evaluation of whether acid functionalization enhanced the cardiopulmonary toxicity of SWCNT	Instillation of 40 μg of AF-SWCNTs, increases percentage of pulmonary neutrophils. Isolated perfused hearts from mice exposed to 40 μg of AF-SWCNTs have significantly lower cardiac functional recovery, greater infarct size, and higher coronary flow rate. Acid functionalization increases the pulmonary toxicity of SWCNTs	[540]
HCl-treated MWCNT contained 0.12 wt.% cobalt	Young adult male Wistar rat	Utilization of a 1× 6 h inhalation exposure protocol follows by a 3 months post-exposure period. The rats are nose-only exposed to 11 and 241mg/m^3 MWCNT of respirable, solid aerosol	Pulmonary toxicity of MWCNT following a single 6 h inhalation exposure of rats and a 3 months post-exposure period	Pulmonary inflammogenicity following exposure to MWCNT is concentration-dependent with evidence of regression over time. The predominant response to inhaled MWCNT is principally related to the assemblage structure and not catalyst impurities	[541]

Table 8.3. Adverse effects of CNTs on human cells

Type of CNT	Type of human cells	Exposure conditions	Objective	Outcomes or results	Ref.
MWCNT	Pulmonary cells: epithelial A549 and mesothelial MeT5A cell lines	*In vivo*; cells were exposed for 6, 24, 48 or 72 h to serum-free medium, 0.1 to 100 μg/ml (0.02–20 μg/cm^2) of MWCNT	Evaluation of toxicological effects (cell viability, apoptosis and oxidative stress) as well as cellular internalization of CNT	Incubation with 100 μg/mL MWCNT induces a decrease in metabolic activity without changing cell membrane permeability or apoptosis; MWCNT produces for industrial purposes exert adverse effects without being internalized by human epithelial and mesothelial pulmonary cell lines	[542]
Raw and annealed MWCNTs contained 4.24 and 0.08 wt.% iron, respectively	Human lung cell: epithelial A549 cell line	*In vitro*; Cells were exposed to 100 μL of MWCNTs suspensions, from 0.25 to 100 μg/mL during 1 to 72 h	Toxicity and intracellular accumulation of MWCNTs in A549 human pneumocytes	MWCNTs are able to rapidly enter into cells, and distribute in the cytoplasm and intracellular vesicles; The length does not influence cytotoxicity, neither the presence of metal catalyst impurities	[543]
SWCNT contained 10 wt.% iron	Human lung cell: epithelial A549 cell line	*In vitro*	Assessment of cytotoxicity of SWCNT on A549 cells; Cytotoxicity parameters: the metabolic, lysosomal, and mitochondrial activities of the cells	SWCNT have very low acute toxicity to the A549 cells; No intracellular localization of SWCNT in A549 cells following 24 h exposure; Increased numbers of surfactant storing lamellar bodies in exposed cells	[544]
SWCNT and C_{60}-fullerene	Murine and human macrophages	*In vitro*	The ability of purified SWCNTs and C_{60} to elicit an inflammatory response by murine and human macrophage cells *in vitro*	SWCNTs and C-fullerenes uptaken by human macrophage cells is very low, and they possess a very low toxicity against human macrophage cells	[545]
Unpurified and purified MWCNTs contained 6.2 and 0.0005 wt.% iron, respectively	Human monocyte-derived macrophage cells	Human monocyte-derived macrophage cells were exposed to MWNTs for 4 h and 4 days at concentrations of 0.31–20.00 mg/mL at 37 °C	(i) to determine whether MWNTs are toxic and if the toxicity is an effect of residual iron; (ii) To ascertain the uptake and distributions of MWNTs within exposed cells; (iii) To assess the localized effects of ingested MWNTs on cell viability and structure	(i) A decrease in cell viability is correlated with uptake of unpurified MWNTs due to mainly necrosis; (ii) Toxicity is yielded only from the nanotubes and not from Fe_2O_3; (iii) Unpurified MWNTs entere the cell both actively and passively frequently inserting through the plasma membrane into the cytoplasm and the nucleus and result in oxidative stress and cell death	[546]

Table 8.3. (Continued)

Type of CNT	Type of human cells	*Exposure conditions*	Objective	Outcomes or results	Ref.
Three different samples of MWCNT: 97%, 99% and 97% purity	Cultured human neuroblastoma cells	*In vitro*; For short-term assays, cells incubated with the MWCNT for 3 days; for long-term assays, cells cultured with the MWCNT-modified culture medium for 2 weeks	The effect of various physicochemical features of MWCNTs on toxicity and biocompatibility with cultured human neuroblastoma cells	(i) After 3 days of incubation with three different types of CNTs, 0.01% cell viability is not affected and apoptosis are not induced in the cells; (ii)After 2 weeks, the loss of cell viability is minimal for pure MWCNTs (99% purity), but cell proliferation decreases significantly for 97% purity MWCNTs and acid treated MWCNTs (97% purity); (iii) no intracellular reactive oxygen species; (iv) ED_{25} is 48, 34.4, and 18.4 μg/mL, respectively, for 99%, 97%, and acid-treated 97% purity MWCNTs	[547]
SWCNT and MWCNT contained 8.8% and 0.27 wt.% iron, respectively	Human aortic endothelial cells	*In vitro;* human aortic endothelial cells were seeded 20,000 cells per well in a 24-well plate and exposed to SWCNT, MWCNT in concentrations of 10–150 μg/106 cells. Then the cells are cultured for 3 or 24 h	Evaluation of potential direct toxicity of CNT on human endothelial cells, with special emphasis on the evaluation of dose-dependent effects	Marked actin filament and VE-cadherin disruption, cytotoxicity, and reduced tubule formation occurred consistently at 24 h post-exposure to the highest concentrations of CNTs [50–150 μg/106 cells (1.5–4.5 μg/mL)]; These effects are not observed with lower concentrations of CNTs [1–10 μg/106 cells (0.04–0.4 μg/mL)]	[548]
MWCNT, size: 90–150 nm and MWCNT, size: 60–80 nm	Human embryonic kidney HEK293 cell line	*In vitro;* The stock suspensions of MWCNTs are freshly diluted to different concentrations in the cell culture medium without serum. After cells have attached for 12 h in the full medium, it is replaced with low serum to prevent particle agglomeration. Freshly dispersed particle suspensions are immediately applied to the cells and allowed to incubate for 48 h	Evaluation of cytotoxicity of MWCNT and the eventuality of kidney toxicity	Exposure of different sizes of two MWCNTs at dosage levels between 3 and 300 μg/mL decrease cell viability in a concentration dependent manner; The IC_{50} values (concentration of nanoparticles to induce 50% cell mortality) of two MWCNTs are 42.10 and 36.95μg/mL. Exposure of MWCNT (10–100μg/mL) to HEK cells result in concentration dependent cell membrane damage; The cytotoxicity and oxidative stress is significantly more in MWCNT2 exposed cells than MWCNT1	[549]
MWCNT1, size: 90–150 nm	Human epidermal keratinocytes (HEK)	*In vivo;* Celles were exposed to 0.1, 0.2, and 0.4 mg/mL of MWCNT for 1, 2, 4, 8, 12, 24 and 48 h	Assessment the interaction between MWCNT and HEK	MWCNT induces the release of the proinflammatory cytokine interleukin 8 from HEKs in a time dependent manner. MWCNT are capable of both localizing within and initiating an irritation response in a target epithelial cell	[550]

ACKNOWLEDGMENTS

We are grateful to the University of Tabriz, Iran for all their support.

REFERENCES

[1] Eom, S-W; Lee, C-W; Yun, M-S; Sun, Y-K; *Electrochim. Acta*., 2006, 52, 1592-159
[2] Zabaniotou, A; Madau, P; Oudenne, PD; Jung, CG; Delplancke, MP; Fontana, A; *J. Anal. Appl. Pyrolysis*, 2004, 72, 289-297.
[3] Aber, S; Khataee, A; Sheydaei, M; *Bioresour. Technol.*, 2009, 100, 6586-6591.
[4] Afkhami, A; Madrakian, T; Karimi, Z; *J. Hazard. Mater.*, 2007, 144, 427-431.
[5] Schroder, E; Thomauske, K; Weber, C; Hornung, A; Tumiatti, V; *J. Anal. Appl. Pyrolysis*, 2007, 79, 106-111.
[6] Wang, Z-M; Kanoh, H; Kaneko, K; Lu, GQ; Do, D; *Carbon*, 2002, 40, 1231-1239.
[7] Chattopadhyaya, G; Macdonald, DG; Bakhshi, NN; Soltan Mohammadzadeh, JS; Dalai, AK; *Fuel Process. Technol.*, 2006, 87, 997-1006.
[8] Wigmans, T; *Carbon*, 1989, 27, 13-22.
[9] Phan, NH; Rio, S; Faur, C; Le Coq, L; Le Cloirec, P; Nguyen, TH; *Carbon*, 2006, 44, 2569-2577.
[10] Srinivasakannan, C; Abu Bakar, MZ; *Biomass and Bioenergy*, 2004, 27, 89-96.
[11] Carrott, PJM; Nabais, JMV; Carrott, MMLR; Pajares, JA; *Carbon*, 2001, 39, 1543-1555.
[12] Yang, KB; Peng, JH; Xia, HY; Zhang, LB; Srinivasakannan, C; Guo, SH; *J. Taiwan Inst. Chem. E.*, 2010, 41, 367-372.
[13] Sentorun-Shalaby, L; Uçak-AstarlIoglu, MG; Artok, L; SarIcI, L; *Micropor. Mesopor. Mat.*, 2006, 88, 126-134.
[14] Gonzalez, JF; Encinar, JM; Gonzalez-Garcia, CM; Sabio, E; Ramiro, A; Canito, JL; Ganan, J; *Appl. Surf. Sci.*, 2006, 252, 5999-6004.
[15] Wilson, K; Yang, H; Seo, CW; Marshall, WE; *Bioresour. Technol.*, 2006, 97, 2266-2270.
[16] Yun, CH; Park, YH; Park, CR; *Carbon*, 2001, 39, 559-567.
[17] Lua, AC; Lau, FY; Guo, J; *J. Anal. Appl. Pyrolysis*, 2006, 76, 96-102.
[18] Belhachemi, M; Rios, RVRA; Addoun, F; Silvestre-Albero, J; Sepúlveda-Escribano, A; Rodriguez-Reinoso, F; *J. Anal. Appl. Pyrolysis*, 2009, 86, 168-172.
[19] Ahmad, AL; Loh, MM; Aziz, JA; *Dyes Pigm.*, 2007, 75, 263-272.
[20] Rodriguez-Reinoso, F; Pastor, AC; Marsh, H; Huidobro, A; *Carbon*, 2000, 38, 397-406.
[21] Zhao, X; Lai, S; Liu, H; Gao, L; *J. Environ. Sci.*, 2009, 21, S121-S123.
[22] Ioannidou, O; Zabaniotou, A; *Renew. Sust. Energ. Rev.*, 2007, 11, 1966-2005.
[23] Lua, AC; Yang, T; Guo, J; *J. Anal. Appl. Pyrolysis*, 2004, 72, 279-287.
[24] Ariyadejwanich, P; Tanthapanichakoon, W; Nakagawa, K; Mukai, SR; Tamon, H; *Carbon*, 2003, 41, 157-164.
[25] Linares-Solano, A; Martín-Gullon, I; Salinas-Martínez de Lecea, C; Serrano-Talavera, B; *Fuel*, 2000, 79, 635-643.
[26] Gryglewicz, G; Grabas, K; Lorenc-Grabowska, E; *Carbon*, 2002, 40, 2403-2411.

[27] Suzuki, RM; Andrade, AD; Sousa, JC; Rollemberg, MC; *Bioresour. Technol.*, 2007, 98, 1985-1991.
[28] Yang, JB; Ling, LC; Liu, L; Kang, FY; Huang, ZH; Wu, H; *Carbon*, 2002, 40, 911-916.
[29] Ould-Idriss, A; Stitou, M; Cuerda-Correa, EM; Fernández-González, C; Macías-García, A; Alexandre-Franco, MF; Gómez-Serrano, V; *Fuel Process. Technol.*, 2011, 92, 266-270.
[30] Min, A; Harris, AT; *Chem. Eng. Sci.*, 2006, 61, 8050-8059.
[31] Aworn, A; Thiravetyan, P; Nakbanpote, W; *J. Anal. Appl. Pyrolysis*, 2008, 82, 279-285.
[32] Cai, Q; Huang, ZH; Kang, FY; Yang, JB; *Carbon*, 2004, 42, 775-783.
[33] Yang, T; Lua, AC; *J. Colloid Interf. Sci.*, 2003, 267, 408-417.
[34] El Qada, EN; Allen, SJ; Walker, GM; *Chem. Eng. J.*, 2008, 142, 1-13.
[35] Hayashi, J; Kazehaya, A; Muroyama, K; Watkinson, AP; *Carbon*, 2000, 38, 1873-1878.
[36] Díaz-Díez, MA; Gómez-Serrano, V; Fernández González, C; Cuerda-Correa, EM; Macías-García, A; *Appl. Surf. Sci.*, 2004, 238, 309-313.
[37] Shi, QQ; Zhang, J; Zhang, CL; Li, C; Zhang, B; Hu, WW; Xu, JT; Zhao, R; *J. Environ. Sci-China*, 2010, 22, 91-97.
[38] Malik, R; Ramteke, DS; Wate, SR; *Waste Manag.*, 2007, 27, 1129-1138.
[39] Liu, QS; Zheng, T; Wang, P; Guo, L; *Ind. Crop. Prod.*, 2010, 31, 233-238.
[40] Lillo-Ródenas, MA; Marco-Lozar, JP; Cazorla-Amorós, D; Linares-Solano, A; *J. Anal. Appl. Pyrolysis*, 2007, 80, 166-174.
[41] Karacan, F; Ozden, U; Karacan, S; *Appl. Therm. Eng.*, 2007, 27, 1212-1218.
[42] Gómez-Serrano, V; Cuerda-Correa, EM; Fernández-González, MC; Alexandre-Franco, MF; Macías-Garcia, A; *Mater. Lett.*, 2005, 59, 846-853.
[43] Baquero, MC; Giraldo, L; Moreno, JC; Suárez-García, F; Martínez-Alonso, A; Tascón, JMD; *J. Anal. Appl. Pyrolysis*, 2003, 70, 779-784.
[44] Girgis, BS; Smith, E; Louis, MM; El-Hendawy, A-NA; *J. Anal. Appl. Pyrolysis*, 2009, 86, 180-184.
[45] Azevedo, DCS; Araújo, JCS; Bastos-Neto, M; Torres, AEB; Jaguaribe, EF; Cavalcante, CL; *Micropor. Mesopor. Mat.*, 2007, 100, 361-364.
[46] Kawano, T; Kubota, M; Onyango, MS; Watanabe, F; Matsuda, H; *Appl. Therm. Eng.*, 2008, 28, 865-871.
[47] Hsu, L-Y; Teng, H; *Fuel Process. Technol.*, 2000, 64, 155-166.
[48] Deng, H; Yang, L; Tao, G; Dai, J; *J. Hazard. Mater.*, 2009, 166, 1514-1521.
[49] Moreno-Castilla, C; Carrasco-Marín, F; López-Ramón, MV; Alvarez-Merino, MA; *Carbon*, 2001, 39, 1415-1420.
[50] Budinova, T; Petrov, N; Parra, J; Baloutzov, V; *Journal of Environmental Management*, 2008, 88, 165-172.
[51] Adinata, D; Daud, WMAW; Aroua, MK; *Bioresour. Technol.*, 2007, 98, 145-149.
[52] Jagtoyen, M; Derbyshire, F; *Carbon*, 1998, 36, 1085-1097.
[53] Gurses, A; Dogar, C; Karaca, S; Acikyildiz, M; Bayrak, R; *J. Hazard. Mater.*, 2006, 131, 254-259.
[54] Mohanty, K; Jha, M; Meikap, BC; Biswas, MN; *Chem. Eng. Sci.*, 2005, 60, 3049-3059.
[55] Kim, JW; Sohn, MH; Kim, DS; Sohn, SM; Kwon, YS; *J. Hazard. Mater.*, 2001, 85, 301-315.
[56] Salman, JM; Hameed, BH; *J. Hazard. Mater.*, 2010, 175, 133-137.
[57] Hu, C-C; Wang, C-C; Wu, F-C; Tseng, R-L; *Electrochim. Acta.*, 2007, 52, 2498-2505.

[58] Sutherland, J; Adams, C; Kekobad, J; *Water Res.*, 2004, 38, 193-205.
[59] Friedmann, D; Mendive, C; Bahnemann, D; *Appl. Catal.*, 2010, 99, 398-406.
[60] Aber, S; Salari, D; Parsa, MR; *Chem. Eng. J.*, 2010, 162, 127-134.
[61] Selvamurugan, M; Doraisamy, P; Maheswari, M; *Ecol. Eng.*, 2010, 36, 1686-1690.
[62] Aber, S; Amani-Ghadim, AR; Mirzajani, V; *J. Hazard. Mater.*, 2009, 171, 484-490.
[63] Aber, S; Daneshvar, N; Soroureddin, SM; Chabok, A; Asadpour-Zeynali, K; *Desalination*, 2007, 211, 87-95.
[64] Daneshvar, N; Aber, S; Khani, A; Khataee, AR; *J. Hazard. Mater.*, 2007, 144, 47-51.
[65] Weber, WJ; *Physicochemical processes for water quality control,* John Wiley and Son Inc., 1972.
[66] *Evaluation of activated carbon for use in cigarette filter*s, Philip Morris USA, Version 1.0, 2002. Retrieved on 16 Oct. 2010 from the web site of University of California, San Francisco, Legacy Tobacco Documents Library: <*http://legacy.library.ucsf.edu/tid/ady31c00/pdf*>.
[67] A brief history of activated carbon and a summary of its uses. Retrieved on 2 Feb. 2011 from the web site of Department of Civil and Environmental Engineering, University of Virginia Teck: <*http://www.cee.vt.edu/ewr/environmental/teach/gwprimer/group23/achistory.html*>.
[68] Demirbas, E; Dizge, N; Sulak, MT; Kobya, M; *Chem. Eng. J.*, 2009, 148, 480-487.
[69] Yang, X; Al-Duri, B; *J. Colloid Interf. Sci.*, 2005, 287, 25-34.
[70] Barkat, M; Nibou, D; Chegrouche, S; Mellah, A; *Chem. Eng. Process.*, 2009, 48, 38-47.
[71] Daneshvar, N; Salari, D; Aber, S; *J. Hazard. Mater.*, 2002, B94, 49-61.
[72] Behnamfard, A; Salarirad, MM; *J. Hazard. Mater.*, 2009, 170, 127-133.
[73] Tseng, R-L; Wu, F-C; *J. Taiwan Inst. Chem. E.*, 2009, 40, 197-204.
[74] Omar, HA; Moloukhia, H; *J. Hazard. Mater.*, 2008, 157, 242-246.
[75] Senthil Kumar, P; Ramalingam, S; Senthamarai, C; Niranjanaa, M; Vijayalakshmi, P; Sivanesan, S; *Desalination*, 2010, 261, 52-60.
[76] Arami, M; Yousefi Limaee, N; Mahmoodi, NM; *Chemosphere*, 2006, 65, 1999-2008.
[77] Juang, R-S; Shiau, J-Y; *J. Hazard. Mater.*, 1999, B70, 171-183.
[78] Chakravarty, S; Pimple, S; Chaturvedi, HT; Singh, S; Gupta, KK; *J. Hazard. Mater.*, 2008, 159, 396-403.
[79] ASTM-D5158; *Standard Test Method for Determination of Particle Size of Powdered Activated Carbon by Air Jet Sieving*, ASTM International, Vol: 15.01.
[80] Gai, XJ; Kim, HS; *Desalination*, 2008, 225, 288-300.
[81] Behera, SK; Kim, JH; Guo, XJ; Park, HS; *J. Hazard. Mater.*, 2008, 153, 1207-1214.
[82] Beltran, FJ; Pocostales, JP; Alvarez, PM; Jaramillo, J; *J. Hazard. Mater.*, 2009, 169, 532-538.
[83] Humbert, H; Gallard, H; Suty, H; Croué, J-P; *Water Res.*, 2008, 42, 1635-1643.
[84] Jia, Y; Wang, R; Fane, AG; *Chem. Eng. J.*, 2006, 116, 53-59.
[85] Kumar, A; Prasad, B; Mishra, IM; *J. Hazard. Mater.*, 2010, 176, 774-783.
[86] Öztürk, N; Köse, TE; *Desalination*, 2008, 223, 174-179.
[87] Qu, Y; Zhang, C; Li, F; Bo, X; Liu, G; Zhou, Q; *J. Hazard. Mater.*, 2009, 169, 146-152.
[88] Ranganathan, K; *Carbon*, 2003, 41, 1087-1092.
[89] Yoon, Y; Westerhoff, P; Snyder, SA; Esparza, M; *Water Res.*, 2003, 37, 3530-3537.

[90] Bais, N; Bouzaza, A; Guernion, PY; Laplanche, A; *Chem. Eng. Process.*, 2008, 47, 316-322.
[91] Chang, MB; Lin, J-J; Chang, S-H; *Atmos. Environ.*, 2002, 36, 279-286.
[92] Senior, C; Bustard, CJ; Durham, M; Baldrey, K; Michaud, D; *Fuel Process. Technol.*, 2004, 85, 601-612.
[93] Basar, CA; Karagunduz, A; Cakici, A; Keskinler, B; *Water Res.*, 2004, 38, 2117-2124.
[94] Ng, C; Losso, JN; Marshall, WE; Rao, RM; *Bioresour. Technol.*, 2002, 85, 131-135.
[95] Kargi, F; Ozmihci, S; *Process Biochem.*, 2005, 40, 2539-2544.
[96] Kim, SH; Ngo, HH; Shon, HK; Vigneswaran, S; *Sep. Purif. Technol.*, 2008, 58, 335-342.
[97] Matsui, Y; Ando, N; Sasaki, H; Matsushita, T; Ohno, K; *Water Res.*, 2009, 43, 3095-3103.
[98] Rivera-Utrilla, J; Mendez-Diaz, J; Sanchez-Polo, M; Ferro-Garcia, MA; Bautista-Toledo, I; *Water Res.*, 2006, 40, 1717-1725.
[99] Vyrides, I; Conteras, PA; Stuckey, DC; *J. Hazard. Mater.*, 2010, 177, 836-841.
[100] Archer, ED; Allen, RWK; MacInnes, JM; *Filtr. Sep.*, 2000, 37, 32-39.
[101] Lee, VKC; Cheung, WH; McKay, G; *Chemosphere*, 2008, 70, 682-688.
[102] Liu, Y; Bisson, TM; Yang, H; Xu, Z; *Fuel Process. Technol.*, 2010, 91, 1175-1197.
[103] ASTM-D2862-10; *Standard Test Method for Particle Size Distribution of Granular Activated Carbon*, ASTM International, Vol: 15.01.
[104] Ahmad, AA; Hameed, BH; *J. Hazard. Mater.*, 2010, 175, 298-303.
[105] Aksu, Z; Kabasakal, E; *Sep. Purif. Technol.*, 2004, 35, 223-240.
[106] Álvarez, PM; García-Araya, JF; Beltrán, FJ; Masa, FJ; Medina, F; *J. Colloid Interf. Sci.*, 2005, 283, 503-512.
[107] Azizian, S; Yahyaei, B; *J. Colloid Interf. Sci.*, 2006, 299, 112-115.
[108] Bansode, RR; Losso, JN; Marshall, WE; Rao, RM; Portier, RJ; *Bioresour. Technol.*, 2003, 90, 175-184.
[109] Dwivedi, CP; Sahu, JN; Mohanty, CR; Mohan, BR; Meikap, BC; *J. Hazard. Mater.*, 2008, 156, 596-603.
[110] Lataye, DH; Mishra, IM; Mall, ID; *J. Hazard. Mater.*, 2008, 154, 858-870.
[111] Lataye, DH; Mishra, IM; Mall, ID; *Chem. Eng. J.*, 2009, 147, 139-149.
[112] Di Natale, F; Lancia, A; Molino, A; Musmarra, D; *J. Hazard. Mater.*, 2007, 145, 381-390.
[113] Yang, J-S; Yuan, D-X; Weng, T-P; *Desalination*, 2010, 263, 271-278.
[114] Abumaizar, RJ; Kocher, W; Smith, EH; *J. Hazard. Mater.*, 1998, 60, 111-126.
[115] Chung, YC; Lin, YY; Tseng, CP; *Bioresour. Technol.*, 2005, 96, 1812-1820.
[116] Gaur, A; Park, J-W; Maken, S; Song, H-J; Park, J-J; *Fuel Process. Technol.*, 2010, 91, 635-640.
[117] Jo, WK; Yang, CH; *Sep. Purif. Technol.*, 2009, 66, 438-442.
[118] Azizian, S; Haerifar, M; Bashiri, H; *Chem. Eng. J.*, 2009, 146, 36-41.
[119] Chern, J-M; Chien, Y-W; *Water Res.*, 2002, 36, 647-655.
[120] Choi, JW; Choi, NC; Lee, SJ; Kim, DJ; *J. Colloid Interf. Sci.*, 2007, 314, 367-372.
[121] Gul, S; Ozcan, O; Erbatur, O; *Dyes Pigm.*, 2007, 75, 426-431.
[122] Jaramillo, J; Gomez-Serrano, V; Alvarez, PM; *J. Hazard. Mater.*, 2009, 161, 670-676.
[123] Juang, RS; Lin, SH; Cheng, CH; *Ultrason. Sonochem.*, 2006, 13, 251-260.

[124] Kumar, S; Zafar, M; Prajapati, JK; Kumar, S; Kannepalli, S; *J. Hazard. Mater.*, 2011, 185, 287-294.
[125] Ochoa-Herrera, V; Sierra-Alvarez, R; *Chemosphere*, 2008, 72, 1588-1593.
[126] Rajagopal, C; Kapoor, JC; *J. Hazard. Mater.*, 2001, 87, 73-98.
[127] Sotelo, JL; Ovejero, G; Delgado, JA; Martinez, I; *Chem. Eng. J.*, 2002, 87, 111-120.
[128] Zogorski, JS; Faust, SD; Haas, JH; *J. Colloid Interf. Sci.*, 1976, 55, 329-341.
[129] Lin, SH; Chen, YW; *J. Hazard. Mater.*, 1998, 57, 193-207.
[130] Long, C; Li, Q; Li, Y; Liu, Y; Li, A; Zhang, Q; *Chem. Eng. J.*, 2010, 160, 723-728.
[131] Ma, Y; Zhao, J; Yang, B; *Int. Biodeterior. Biodegrad.*, 2006, 57, 93-98.
[132] Mohan, N; Kannan, GK; Upendra, S; Subha, R; Kumar, NS; *J. Hazard. Mater.*, 2009, 168, 777-781.
[133] Qiang, T; Zhigang, Z; Wenpei, Z; Zidong, C; *Fuel*, 2005, 84, 461-465.
[134] Shin, HC; Park, JW; Park, K; Song, HC; *Environ. Pollut.*, 2002, 119, 227-236.
[135] Skodras, G; Diamantopoulou, I; Pantoleontos, G; Sakellaropoulos, GP; *J. Hazard. Mater.*, 2008, 158, 1-13.
[136] Xiang, L; Zhong, L; Lingai, LUO; *Chin. J. Chem. Eng.*, 2008, 16, 203-208.
[137] Leyva-Ramos, R; Diaz-Flores, PE; Leyva-Ramos, J; Femat-Flores, RA; *Carbon*, 2007, 45, 2280-2289.
[138] Tang, D; Zheng, Z; Lin, K; Luan, J; Zhang, J; *J. Hazard. Mater.*, 2007, 143, 49-56.
[139] Ayranci, E; Hoda, N; *Chemosphere*, 2005, 60, 1600-1607.
[140] Nabais, JV; Carrott, PJM; Carrott, MMLR; Belchior, M; Boavida, D; Diall, T; Gulyurtlu, I; *Appl. Surf. Sci.*, 2006, 252, 6046-6052.
[141] Mohan, D; Singh, KP; Singh, VK; *J. Hazard. Mater.*, 2006, B135, 280-295.
[142] Han, Y; Quan, X; Ruan, X; Zhang, W; *Sep. Purif. Technol.*, 2008, 59, 43-49.
[143] Foo, KY; Hameed, BH; *J. Hazard. Mater.*, 2007, 142, 506-511.
[144] Huang, CC; Su, YJ; *J. Hazard. Mater.*, 2010, 175, 477-483.
[145] Wang, L; Balasubramanian, N; *Chem. Eng. J.*, 2009, 155, 763-768.
[146] Han, Y; Quan, X; Chen, S; Zhao, H; Cui, C; Zhao, Y; *J. Colloid Interf. Sci.*, 2006, 299, 766-771.
[147] Park, SJ; Park, BJ; Ryu, SK; *Carbon*, 1999, 37, 1223-1226.
[148] Fan, L; Zhou, Y; Yang, W; Chen, G; Yang, F; *J. Hazard. Mater.*, 2006, B137, 1182-1188.
[149] Wang, AM; Qu, JH; Liu, HJ; Ru, J; *Appl. Catal., B.*, 2008, 84, 393-399.
[150] Das, D; Gaur, V; Verma, N; *Carbon*, 2004, 42, 2949-2962.
[151] Muniz, J; Marban, G; Fuertes, AB; *Appl. Catal., B.*, 2000, 27, 27-36.
[152] Wang, JP; Chen, YZ; Feng, HM; Zhang, SJ; Yu, HQ; *J. Colloid Interf. Sci.*, 2007, 313, 80-85.
[153] Hoda, N; Bayram, E; Ayranci, E; *J. Hazard. Mater.*, 2006, B137, 344-351.
[154] Starek, J; Zukal, A; Rathousky, J; *Carbon*, 1994, 32, 207-211.
[155] Xiu, GH; Li, P; *Carbon*, 2000, 38, 975-981.
[156] Yu, JJ; Chou, SY; *Chemosphere*, 2000, 41, 371-378.
[157] Bayram, E; Hoda, N; Ayranci, E; *J. Hazard. Mater.*, 2009, 168, 1459-1466.
[158] Duman, O; Ayranci, E; *J. Hazard. Mater.*, 2010, 174, 359-367.
[159] Li, KX; Ling, LC; Lu, CX; Qiao, WM; Liu, ZY; Liu, L; Mochida, I; *Carbon*, 2001, 39, 1803-1808.
[160] Liu, ZS; Ayranci, E; *J. Hazard. Mater.*, 2010, 174, 359-367.

[161] Yuan, RS; Guan, RB; Shen, WZ; Zheng, JT; *J. Colloid Interf. Sci.*, 2005, 282, 87-91.
[162] Liu, LF; Zhang, PH; Yang, FL; *Sep. Purif. Technol.*, 2010, 70, 354-361.
[163] Alves, BR; Clark, AJ; *Carbon*, 1986, 24, 287-294.
[164] Cao, X; Shiraishi, F; *Chem. Eng. J.*, 2010, 160, 651-659.
[165] Deveci, H; YazIcI, EY; Alp, I; Uslu, T; *Int. J. Miner. Process.*, 2006, 79, 198-208.
[166] Duman, O; Ayranci, E; *J. Hazard. Mater.*, 2010, 176, 231-238.
[167] Prasad, GK; Singh, B; Suryanarayana, MVS; Batra, BS; *J. Hazard. Mater.*, 2005, 121, 159-165.
[168] Sharma, A; Singh, B; Saxena, A; *Carbon*, 2009, 47, 1911-1915.
[169] Ramos, RL; Ovalle-Turrubiartes, J; Sanchez-Castillo, MA; *Carbon*, 1999, 37, 609-617.
[170] Gu, L; Chen, Z; Sun, C; Wei, B; Yu, X; *Desalination*, 2010, 263, 107-112.
[171] Lee, SJ; Seo, Y-C; Jurng, J; Lee, TG; *Atmos. Environ.*, 2004, 38, 4887-4893.
[172] Mei, Z; Shen, Z; Yuan, T; Wang, W; Han, H; *Fuel Process. Technol.*, 2007, 88, 623-629.
[173] Peterson, GW; Rossin, JA; Smith, PB; Wagner, GW; *Carbon*, 2010, 48, 81-88.
[174] Bulushev, DA; Yuranov, I; Suvorova, EI; Buffat, PA; Kiwi-Minsker, L; *J. Catal.*, 2004, 224, 8-17.
[175] Goel, J; Kadirvelu, K; Rajagopal, C; Garg, VK; *J. Hazard. Mater.*, 2005, 125, 211-220.
[176] Hung, C-M; *J. Hazard. Mater.*, 2009, 166, 1314-1320.
[177] Kikuchi, Y; Qian, Q; Machida, M; Tatsumoto, H; *Carbon*, 2006, 44, 195-202.
[178] Ma, Y; Wang, S-G; Fan, M; Gong, W-X; Gao, B-Y; *J. Hazard. Mater.*, 2009, 168, 1140-1146.
[179] Yao, SH; Li, JY; Shi, ZL; *Particuology*, 2010, 8, 272-278.
[180] Zhang, N; Lin, L-S; Gang, D; *Water Res.*, 2008, 42, 3809-3816.
[181] Cal, MP; Strickler, BW; Lizzio, AA; Gangwal, SK; *Carbon*, 2000, 38, 1767-1774.
[182] Mei, Z; Shen, Z; Zhao, Q; Wang, W; Zhang, Y; *J. Hazard. Mater.*, 2008, 152, 721-729.
[183] Prasad, GK; Singh, B; *J. Hazard. Mater.*, 2005, 126, 195-197.
[184] Vidic, RD; Siler, DP; *Carbon*, 2001, 39, 3-14.
[185] Saxena, A; Singh, B; Sharma, A; Dubey, V; Semwal, RP; Suryanarayana, MVS; Rao, VK; Sekhar, K; *J. Hazard. Mater.*, 2006, 134, 104-111.
[186] Xu, L; Guo, J; Jin, F; Zeng, H; *Chemosphere*, 2006, 62, 823-826.
[187] Zeng, H; Jin, F; Guo, J; *Fuel*, 2004, 83, 143-146.
[188] Ahn, CK; Kim, YM; Park, JM; Woo, SH; Hyun-Ku Rhee, I-SN; Jong Moon, P; *Selective adsorption of phenanthrene on activated carbons for surfactant reuse in soil washing process, Surface Science and Catalysis*, Elsevier.2006.
[189] Ahn, CK; Kim, YM; Woo, SH; Park, JM; *J. Hazard. Mater.*, 2008, 154, 153-160.
[190] Alonso, E; Cantero, FJ; Garcia, J; Cocero, MJ; *J. Supercrit. Fluid.*, 2002, 24, 123-135.
[191] Bes, C; Mench, M; *Environ. Pollut.*, 2008, 156, 1128-1138.
[192] Brändli, RC; Hartnik, T; Henriksen, T; Cornelissen, G; *Chemosphere*, 2008, 73, 1805-1810.
[193] Gong, ZQ; Alef, K; Wilke, BM; Li, PJ; *J. Hazard. Mater.*, 2007, 143, 372-378.
[194] Koran, KM; Suidan, MT; Khodadoust, AP; Sorial, GA; Brenner, RC; *Water Res.*, 2001, 35, 2363-2370.
[195] Liang, Y; Zhang, X; Dai, D; Li, G; *Int. Biodeterior. Biodegrad.*, 2009, 63, 80-87.
[196] Liu, X; Yu, G; *Chemosphere*, 2006, 63, 228-235.
[197] Liu, X; Yu, G; Han, W; *J. Hazard. Mater.*, 2007, 147, 746-751.

[198] Park, S; Lee, I; Cho, C; Sung, K; *Chemosphere*, 2008, 70, 1117-1123.
[199] Iijima, S; *Nature*, 1991, 354, 56–58.
[200] Yamabe, T; *Synthetic Met.*, 1995, 70, 1511–1518.
[201] Iijima, S; Ichihashi, T; *Nature*, 1993, 363, 603–605.
[202] Bethune, DS; Kiang, CH; De Vries, MS; Gorman, G; Savoy, R; Vazquez, J; Beyers, R; *Nature*, 1993, 363, 605–607.
[203] Popov, VN; *Mater. Sci. Eng.*, 2004, R 43, 61–102.
[204] Biro, LP; Horvath, ZE; Szlamas, L; Kertesz, K; Weber, F; Juhasz, G; *Chem. Phys. Lett.*, 2003, 372, 399–402.
[205] Paradise, M; Goswami, T; *Mater. Design*, 2007, 28, 1477–1489.
[206] Rinzler, AG; Hafner, JH; Nikolaev, P; Lou, L; Kim, SG; Tomanek, D; Nordlander, P; Colbert, DT; Smalley, RE; *Science*, 1995, 269, 1550–1553.
[207] Zhao, Q; Gan, Z; Zhuang, Q; *Electroanal.*, 2002, 23, 1609–1613.
[208] Thoteson, E; Ren, Z; Chou, T; *Compos. Sci. Technol.*, 2001, 61, 1899–1912.
[209] Delmotte, JP; Rubio, A; *Carbon*, 2002, 40, 1729–1734.
[210] Popov, M; Kyotani, M; Nemanich, RJ; Koga, Y; *Phys. Rev. B*, 2002, 65, 033408.
[211] Cadek, M; Coleman, JN; Ryan, KP; Nicolosi, V; Bister, G; Fonseca, A; Nagy, JB; Szostak, K; Béguin F; Blau, WJ; *Nano Letters*, 2004, 4, 353–356.
[212] Li, XD; Gao, HS; Scrivens, WA; Fei, DL; Xu, XY; Sutton, MA; Reynolds, AP; Myrick, ML; *Nanotechnology*, 2004, 15, 1416–1423.
[213] Colema, JN; Khan, U; Blau, WJ; Gun'ko, YK; *Carbon*, 2006, 44, 1624–1652.
[214] Collins, PG; Avouris, P; *Sci. Am.*, 2000, 283, 62–69.
[215] Dresselhaus, M; Dresselhaus, G; Saito, R; *Carbon*, 1995, 33, 883–891.
[216] Kataura, H; Kumazawa, Y; Maniwa, Y; Umezu, I; Suzuki, S; Ohtsuka, Y; Achiba, Y; *Synth. Metals*, 1999, 103, 2555–2558.
[217] Weisman, RB; Bachillo, SM; *Nano Letters*, 2003, 3, 1235–1238.
[218] Pop, E; Mann, D; Wang, Q; Goodson, K; Dai, H; *Nano Lett.*, 2005, 6, 96–100.
[219] Sinha, S; Barjami, S; Iannacchione, G; Schwab, A; Muench, G; *J. Nanopart. Res.*, 2005, 7, 651–657.
[220] Yi, W; Lu, L; Zhang, DL; Pan, ZW; Xie, SS; *Phys. Rev. B*, 1999, 59, R9015–R9018.
[221] Mizel, A; Benedict, LX; Cohen, ML; Louie, SG; Zettl, A; Budraa, NK; Beyermann, WP; *Phys. Rev. B*, 1999, 60, 3264–3270.
[222] Zeng, Q; Li, Z; Zhou, Y; *J. Nat. Gas Chem.*, 2006, 15, 235–246.
[223] Journet, C; Maser, WK; Bernier, P; Loiseau, A; De La Chapells, ML; Lefrant, S; Deniard, P; Lee, R; Fischer, JE; *Nature*, 1997, 388, 756–758.
[224] Journet, C; Alvarez, L; Micholet, V; Guillard, T; De La Chapelle, ML; Anglaret, E; Sauvajol, JL; Lefrant, S; Bernier, P; Laplaze, D; Flamant, G; Loiseau, A; *Synth. Met.*, 1999, 103, 2488–2494.
[225] Park, YS; Kim, KS; Jeong, HJ; Kim, WS; Moon, JM; An, KH; Bae, DJ; Lee, YS; Park, G; Lee, YH; *Synth. Metals*, 2002, 126, 245–251.
[226] Huczko, A; Lange, H; Sioda, M; Zhu, YQ; Hsu, WK; Kroto, HW; Walton, DRM; *J. Phys. Chem. B*, 2002, 106, 1534–1536.
[227] Zhu, HW; Xu, CL; Wu, DH; Wei, BQ; Vajtai, R; *Science*, 2002, 296, 884–886.
[228] Liu, C; Cheng, HM; Cong, HT; Li, F; Su, G; *Mater. Res. Adv. Tech.*, 2000, 91, 306–311.

[229] Choi, SI; Nam, JS; Lee, CM; Choi, SS; Kim, J; Park, JM; Hong, SH; *Curr. Appl. Phys.*, 2006, 6, 224–229.
[230] Matsuura, T; Taniguchi, K; Watanabe, T; *Thin Solid Films*, 2007, 515, 4240–4246.
[231] Wang, M; Wang, X; Li, Z; Liu, Z; He, P; *Mater. Chem. Phys.*, 2006, 97, 243–246.
[232] Zhao, HP; He, YD; Kong, XH; Gao, W; *Mater. Lett.*, 2007, 61, 4916–4919.
[233] Okada, T; Kaneko, T; Hatakeyama, R; *Thin Solid Films*, 2007, 515, 4262–4265.
[234] Hutchison, JL; Kiselev, NA; Krinichnaya, EP; Krestinin, AV; Loutfy, RO; Morawsky, AP; Muradyan, VE; Obraztsova, ED; Sloan, J; Terekhov, SV; Zakharov, DN; *Carbon*, 2001, 39, 761–770.
[235] Wang, Y; Chiu, S; Lin, K; Li, Y; *Carbon*, 2004, 42, 2535–2541.
[236] Saito, Y; Tani, Y; Miyagawa, N; Mitsushima, K; Kasuya, A; Nishina, Y; *Chem. Phys. Lett.*, 1998, 294, 593–598.
[237] Qiu, H; Shi, Z; Guan, L; You, L; Gao, M; Zhang, S; Qiu, J; Gu, Z; *Carbon*, 2006, 44, 516–521.
[238] Li, Z; Liu, P; Zhao, B; Wang, H; Zhang, Y; *Carbon*, 2008, 46, 1792-1828.
[239] Cui, S; Scharff, P; Siegmund, C; Schneider, D; Risch, K; Klotzer, S; Spiess, L; Romanus, H; Schawohl, J; *Carbon*, 2004, 42, 931–939.
[240] Shi, Z; Lian, Y; Liao, FH; Zhou, X; Gu, Z; Zhang, Y; Iijima, S; Li, H; Yue, KT; Zhang, S; *J. Phys. Chem. Solids*, 2000, 61, 1031–1036.
[241] Zhao, X; Ohkohchi, M; Inoue, S; Suzuki, T; Kadoya, T; Ando, Y; *Diam. Relat. Mater.*, 2006, 15, 1098–1102.
[242] Shi, Z; Lian, Y; Zhou, X; Gu, Z; Zhang, Y; Iijima, S; Zhou, L; Yue, KT; Zhang, S; *Carbon*, 1999, 37, 1449–1453.
[243] Qiu, J; Chen, G; Li, Z; Zhao, Z; *Carbon*, 2010, 48, 1312–1320.
[244] Li, L; Li, F; Liu, C; Cheng, H; *Carbon*, 2005, 43, 623–629.
[245] Durbach, SH; Krause, RW; Witcomb, MJ; Coville, NJ; *Carbon*, 2009, 47, 635–644.
[246] Lai, HJ; Lin, MCC; Yang, MH; Li, AK; *Mater. Sci. Eng. C*, 2001, 16, 23–26.
[247] Sun, X; Bao, W; Lv, Y; Deng, J; Wang, X; *Mater. Lett.*, 2007, 61, 3956–3958.
[248] Antisari, MV; Marazzi, R; Krsmanovic, R; *Carbon*, 2003, 41, 2393–2401.
[249] Gang, X; Shen-li, J; Zong-qian, S; *New Carbon Mater.*, 2007, 22, 337–341.
[250] Yao, M; Liu, B; Zou, Y; Wang, L; Li, D; Cui, T; Zou, G; Sundqvist, B; *Carbon*, 2005, 43, 2894–2901.
[251] Chiang, M; Liu, K; Lai, T; Tsai, C; Cheng, H; Lin, I; *J. Vac. Sci. Technol. B*, 2001, 19, 1034–1039.
[252] Journet, C; Bernier, P; *Appl. Phys. A*, 1998, 67, 1–9.
[253] Srivastava, D; Brenner, DW; Schall, JD; Ausman, KD; Yu, M; Ruoff, RS; *J. Phys. Chem. B*, 1999, 103, 4330–4337.
[254] Ou, Q; Tanaka, T; Mesko, M; Ogino, A; Nagatsu, M; *Diam. Relat. Mater.*, 2008, 17, 664–668.
[255] Thess, A; Lee, R; Nikolaev, P; Dai, H; Petit, P; Robert, J; Xu, C; Lee, YH; Kim, SG; Rinzler, AG; Colbert, DT; Scuseria, GE; Tomanék, D; Fischer, JE; Smalley, RE; *Science*, 1996, 273, 483–487.
[256] Dresselhaus, MS; Dresselhaus, G; Eklund, PC; *Nature*, 1996, 381, 678–680.
[257] Kusaba, M; Tsunawaki, Y; *Thin Solid Films*, 2006, 506–507, 255–258.
[258] Nakajima, K; Furusawa, M; Yamamoto, T; Tashiro, J; Sasaki, A; Chikyow, T; Ahmet, P; Yamada, H; Yoshimoto, M; *Diam. Relat. Mater.*, 2002, 11, 953–956.

[259] Zhang, M; Yudasaka, M; Iijima, S; *Chem. Phys. Lett.*, 2001, 336, 196–200.
[260] Puretzky, AA; Geohegan, DB; Schittenhelm, H; Fan, X; Guillorn, MA; *Appl. Surf. Sci.*, 2002, 197–198, 552–562.
[261] Zhang, H; Ding, Y; Wu, Ch; Chen, Y; Zhu, Y; He, Y; Zhong, S; *Physica B*, 2003, 325, 224–229.
[262] Maser, WK; Muñoz, E; Martínez, MT; Benito, AM; De La Fuente, GF; *Opt. Mater.*, 2001, 17, 331–334.
[263] Dai, H; *Surface Sci.*, 2002, 500, 218–241.
[264] Kato, T; Jeong, GH; Hirata, T; Hatakeyama, R; *Chem. Phys. Lett.*, 2003, 381, 422–426.
[265] Wang, YY; Gupta, S; Nemanich, RJ; *Appl. Phys. Lett.*, 2004, 85, 2601–2603.
[266] Ortega-Cervantez, G; Rueda-Morales, G; Ortiz-López, J; *Microelectr. J.*, 2005, 36, 495–498.
[267] Li, WZ; Xie, SS; Qian, LX; Chang, BH; Zou, BS; Zhou, WY; Zhao, RA; Wang, G; *Science*, 1996, 274, 1701–1703.
[268] Fana, S; Liang, W; Dang, H; Franklin, N; Tombler, T; Chapline, M; Dai, H; *Physica E*, 2000, 8, 179–183.
[269] Kong, J; Soh, HT; Cassell, AM; Quate, CF; Dai, H; *Nature*, 1998, 395, 878–881.
[270] Zheng, G; Kouda, K; Sano, H; Uchiyama, Y; Shi, Y; Quan, H; *Carbon*, 2004, 42, 635–640.
[271] Maghsoodi, S; Khodadadi, A; Mortazavi, Y; *Appl. Surf. Sci.*, 2010, 256, 2769–2774.
[272] Su, M; Zheng, B; Liu, J; *Chem. Phys. Lett.*, 2000, 322, 321–326.
[273] Baddour, CE; Fadlallah, F; Nasuhoglu, D; Mitra, R; Vandsburger, L; Meunier, J; *Carbon*, 2008, 47, 313–347.
[274] Ansaldo, A; Haluška, M; Čech, J; Meyer, JC; Ricci, D; Gatti, F; Zitti, ED; Cincotti, S; Roth, S; *Physica E*, 2007, 37, 6–10.
[275] Borowiak-Palen, E; Rümmeli, MH; *Superlattice. Microst.*, 2009, 46, 374–378.
[276] Wei, S; Kang, WP; Davidson, JL; Huang, JH; *Diam. Relat. Mater.*, 2006, 15, 1828–1833.
[277] Wong, YM; Wei, S; Kang, WP; Davidson, JL; Hofmeister, W; Huang, JH; Cui, Y; *Diam. Relat. Mater.*, 2004, 13, 2105– 2112.
[278] Corrias, M; Caussat, B; Ayral, A; Durand, J; Kihn, Y; Kalck, Ph; Serp, Ph; *Chem. Eng. Sci.*, 2003, 58, 4475 – 4482.
[279] Sun, Y; Gu, CZ; Liu, W; Jin, ZS; *Diam. Relat. Mater.*, 2004, 13, 1187–1190.
[280] Flahaut, E; Laurent, Ch; Peigney, A; *Carbon*, 2005, 43, 375–383.
[281] Liu, BC; Yu, B; Zhang, MX; *Chem. Phys. Lett.*, 2005, 407, 232–235.
[282] Moura, FCC; Tristão, JC; Lago, RM; Martel, R; *Catal. Today*, 2008, 133–135, 846–854.
[283] Xinghui, L; Changchun, Z; Weihua, L; Fanguang, Z; Changhui, T; *Mater. Chem. Phys.*, 2005, 93, 473–477.
[284] Tao, XY; Zhang, XB; Sun, FY; Cheng, JP; Liu, F; Luo, ZQ; *Diam. Relat. Mater.*, 2007, 16, 425–430.
[285] Yokoyama, D; Iwasaki, T; Ishimaru, K; Sato, S; Nihei, M; Awano, Y; Kawarada, H; *Carbon*, 2010, 48, 825–831.
[286] Furuta, H; Ikunoc, T; Shikina, N; Honda, S; Hirao, T; Oura, K; *Physica B*, 2002, 323, 299–302.

[287] Pérez-Mendoza, M; Vallés, C; Maser, WK; Martínez, MT; Langlois, S; Sauvajol, JL; Benito, AM; *Carbon*, 2005, 43, 3002–3039.
[288] Queipo, P; Nasibulin, AG; Gonzalez, D; Tapper, U; Jiang, H; Tsuneta, T; Grigoras, K; Duenas, JA; Kauppinen, EI; *Carbon*, 2006, 44, 1581–1616.
[289] Yao, Y; Falk, LKL; Morjan, RE; Nerushev, OA; Campbell, EEB; *Carbon*, 2007, 45, 2065–2071.
[290] Kukovecz, Á; Méhn, D; Nemes-Nagy, E; Szabó, R; Kiricsi, I; *Carbon*, 2005, 43, 2842–2849.
[291] Iaia, A; Marty, L; Naud, C; Bouchiat, V; Loiseau, A; Di Muoio, E; Fournier, T; Bonnot, AM; *Thin Solid Films*, 2006, 501, 221–223.
[292] Chaisitsak, S; Nukeawb, J; Tuantranont, A; *Diam. Relat. Mater.*, 2007, 16, 1958–1966.
[293] Maschmann, MR; Amama, PB; Goyal, A; Iqbal, Z; Gat, R; Fisher, TS; *Carbon*, 2006, 44, 10–18.
[294] Li, CH; Tseng, SC; Lo, SC; Chen, KF; Juang, ZY; Leou, KC; Tsai, CH; *Surf. Coat. Tech.*, 2006, 200, 3220–3223.
[295] Li, Y; Zhang, XB; Tao, XY; Xu, JM; Chen, F; Shen, LH; Yang, XF; Liu, F; Van Tendeloo, G; Geise, HJ; *Carbon*, 2005, 43, 1317–1339.
[296] He, C; Zhao, N; Han, Y; Li, J; Shi, C; Du, X; *Mater. Sci. Eng. A*, 2006, 441, 266–270.
[297] Wang, Z; Ba, D; Liu, F; Cao, P; Yang, P; Gu, Y; Gao, H; *Vacuum*, 2005, 77, 139–144.
[298] Kang, J; Li, J; Du, X; Shi, C; Zhao, N; Nash, P; *Mater. Sci. Eng. A*, 2008, 475, 136–140.
[299] Jayatissa, AH; Guo, K; *Vacuum*, 2009, 83, 853–856.
[300] Cheng, J; Zhang, X; Liu, F; Tu, J; Ye, Y; Ji, Y; *Carbon*, 2003, 41, 1965–1970.
[301] Matsuda, T; Mesko, M; Ogino, A; Nagatsu, M; *Diam. Relat. Mater.*, 2008, 17, 772–775.
[302] Yabe, Y; Ohtake, Y; Ishitobi, T; Show, Y; Izumi, T; Yamauchi, H; *Diam. Relat. Mater.*, 2004, 13, 1292–1295.
[303] Alford, JM; Mason, GR; Feikema, DA; *Formation of carbon nanotubes in a microgravity environment*, Sixth international microgravity combustion workshop, NASA Glenn Research Center, Cleveland, OH, 2001, May 22–24, 293–296.
[304] Hsu, WK; Terrones, M; Hare, JP; Terrones, H; Kroto, HW; Walton, DRM; *Chem. Phys. Lett.*, 1996, 262, 161–164.
[305] Trojanowicz, M; *Tr. Anal. Chem.*, 2006, 25, 480–489.
[306] Zhang, Z; Dewan, C; Kothari, S; Mitra, S; Teeters, D; *Mater. Sci. Eng.* B, 2005, 116, 363–368.
[307] Kong, J; Franklin, NR; Zhou, C; Chapline, MG; Peng, S; Cho, K; Dai, H; *Science*, 2000, 287, 622–625.
[308] Ahn, KS; Kim, JH; Lee, KN; Kim, CO; Hong, JP; *J. Korean. Phys. Soc.*, 2004, 45, 158–164.
[309] Dai, L; He, P; Li, S; *Nanotechnology*, 2003, 14, 1081–1097.
[310] Tans, SJ; Verschueren, RM; Dekker, C; *Nature*, 1998, 393, 49–52.
[311] Planeix, JM; Coustel, N; Coq, B; Brotons, V; Kumbhar, PS; Dutartre, R; Geneste, P; Bernmier, P; Ajayan, PM; *J. Am. Chem. Soc.*, 1994, 116, 7935–7936.
[312] Saito, S; *Science*, 1997, 278, 77–78.
[313] Baugham, R; Zakhidov, A; Heer, W; *Science*, 2002, 297, 787–792.
[314] Kim, P; Lieber, CM; *Science*, 1999, 286, 2148–2150.

[315] Che, G; Lakshmi, BB; Fisher, ER; Martin, CR; *Nature*, 1996, 384, 147–150.
[316] Collins, PG; Zettle, A; Bando, H; Thess, A; Smally, RE; *Science*, 1997, 278, 100–103.
[317] Che, G; Lakshmi, BB; Fisher, ER; Martin, CR; *Nature*, 1998, 393, 346–349.
[318] Britto, PJ; Santhanam, KSV; Ajayan, PM; *Bielectrochem. Bioenerg.*, 1996, 41, 121–125.
[319] Cai, YQ; Jiang, GB; Liu, J; Zhou, Q; *Anal. Chem.*, 2003, 75, 2517–2521.
[320] Xu, J; Wang, Y; Xian, Y; Jin, L; Tanaka, K; *Talanta*, 2003, 60, 1123–1130.
[321] Wang, WK; Cao, LM; *Russ. Phys. J.*, 2001, 44, 178–182.
[322] Yu, H; Fugetsu, B; *J. Hazard. Mater.*, 2010, 177, 138–145.
[323] Ma, R; Bando, Y; Zhu, H; Sato, T; Xu, C; Wu, D; *J. Am. Chem. Soc.*, 2002, 124, 7672–7673.
[324] Kim, C; Choi, YS; Lee, SM; Park, JT; Kim, B; Lee, YH; *J. Am. Chem. Soc.*, 2002, 124, 9906–9911.
[325] Collins, PG; Bradley, K; Ishigami, M; Zettl, A; *Science*, 2000, 287, 1801–1804.
[326] Hilding, J; Grulke, EA; Sinnott, SB; Qian, D; Andrews, R; Jagtoyen, M; *Langmuir*, 2001, 17, 7540–7544.
[327] Wang, XK; Chen, CL; Hu, WP; Ding, AP; Xu, D; Zhou, X; *Environ. Sci. Technol.,* 2005, 39, 2856–2860.
[328] Li, Y; Wang, S; Luan, Z; Ding, J; Xu, C; Wu, D; *Carbon*, 2003, 41, 1057–1062.
[329] Li, Y; Wang, S; Zhang, X; Wei, J; Xu, C; Luan, Z; Wu, D; *Mater. Res. Bull.*, 2003, 38, 469-476.
[330] Li, Y; Di, Z; Ding, J; Wu, D; Luan, Z; Zhu, Y; *Water Res.*, 2005, 39, 605–609.
[331] Di, Z; Ding, J; Peng, X; Li, Y; Luan, Z; Liang, J; *Chemosphere*, 2006, 62, 861–865.
[332] Li, Y; Ding, J; Luan, Z; Di, Z; Zhu, Y; Xu, C; Wu, D; Wei, B; *Carbon*, 2003, 41, 2787–2792.
[333] Long, RQ; Yang, RT; *J. Am. Chem. Soc.*, 2001, 123, 2058–2059.
[334] Chen, CL; Wang, XK; *Ind. Eng. Chem. Res.*, 2006, 45, 9144–9149.
[335] Rao, GP; Lu, C; Su, F; *Sep. Purif. Technol.*, 2007, 58, 224–231.
[336] Lu, C; Chiu, H; Liu, C, *Ind. Eng. Chem. Res.*, 2006, 45, 2850–2855.
[337] Lu, C; Liu, C; *J. Chem. Technol. Biotechnol.*, 2006, 81, 1932–1940.
[338] Li, YH; Zhu, Y; Zhao, Y; Wu, D; Luan, Z; *Diam. Relat. Mater.*, 2006, 15, 90–94.
[339] Liang, P; Liu, Y; Guo, L; Zeng, J; Lu, H; *J. Anal. Spectrom.*, 2004, 19, 1489–1492.
[340] Li, Y; Wang, S; Wei, J; Zhang, X; Xu, C; Luan, Z; Wu, D; Wei, B; *Chem. Phys. Lett.*, 2002, 357, 263–266.
[341] Mauter, MS; Elimelech, M; *Environ. Sci. Technol.*, 2008, 42, 5843–5859.
[342] Fugetsu, B; Satoh, S; Shiba, T; Mizutani, T; Lin, Y; Terui, N; Nodasaka, Y; Sasa, K; Shimizu, K; Akasaka, T; *Environ. Sci. Technol.*, 2004, 38, 6890–6896.
[343] Peng, X; Li, Y; Luan, Z; Di, Z; Wang, H; Tian, B; Jia, Z; *Chem. Phys. Lett.*, 2003, 376, 154–158.
[344] Lu, C; Chung, Y; Chang, K; *Water Res.*, 2005, 39, 1183–1189.
[345] Yang, K; Zhou, Xing, L; *Environ. Sci. Technol.*, 2006, 40, 1855–1861.
[346] Chin, CJM; Shih, LC; Tsai, HJ; Liu, TK; *Carbon*, 2007, 45, 1254–1260.
[347] Wu, C; *J. Hazard. Mater.*, 2007, 144, 93–100.
[348] Chen, W; Duan, L; Zhu, D; *Environ. Sci. Technol.*, 2007, 41, 8295–8300.
[349] Chen, G; Shan, X; Zhou, Y; Shen, X; Huang, H; Khan, SU; *J. Hazard. Mater.*, 2009, 169, 912–918.

[350] Pan, B; Lin, D; Mashayekhi, H; Xing, B; *Environ. Sci. Technol.*, 2008, 42, 5480–5485.
[351] Upadhyayula, VKK; Deng, S; Smith, GB; Mitchell, MC; *Water Res.*, 2009, 43, 148–156.
[352] Srivatsava, A; Srivatsava, ON; Talapatra, S; Vajtai, R; Ajayan, PM; *Letters to Nature*, 2004, 3, 610–614.
[353] Deng, S; Upadhyayula, VKK; Smith, GB; Mitchell, MC; *IEEE Sens. J.*, 2008, 8, 954–962.
[354] Gu, L; Elkin, T; Jiang, X; Li, H; Lin, Y; Qu, L; Rong, T; Tzeng, J; Joseph, R; Sun, YP; *Chem. Commun.*, 2004, 7, 874–876.
[355] Huang, TS; Tzeng, Y; Liu, YK; Chen, YC; Walker, KR; Guntupalli, R; Liu, C; *Diam. Relat. Mater.*, 2004, 13, 1098–1102.
[356] Kang, S; Pinault, M; Pfefferle, LD; Elimelech, M; *Langmuir*, 2007, 23, 8670–8673.
[357] Lee, SB; Koepsel, R; Stolz, DB; Warriner, HE; Russell, AJ; *J. Am. Chem. Soc.*, 2004, 126, 13400–13405.
[358] Krishna, V; Pumprueg, S; Lee, HS; Zhao, J; Sigmund, W; Koopman, B; Moudgil, BM;. *Process Saf. Environ.*, 2005, 83, 393–397.
[359] Wang, H; Gu, L; Lin, Y; Lu, F; Meziani, JM; Luo, PG; Wang, W; Cao, L; Sun, YP; *J. Am. Chem. Soc.*, 2006, 128, 13364–13365.
[360] Narayan, RJ; Berry, CJ; Brigmon, RL; *Mater. Sci. Eng. B*, 2005, 123, 123–129.
[361] Camper, AK; LeChevallier, MW; Broadway, SC; McFeters, GA; *Appl. Environ. Microb.*, 1985, 50, 1378–1382.
[362] Pimenov, AV; Mitilenos, AG; Pendinen, GI; Chernov, VE; Liberman, AI; Schimidt, JL; Cheh, HY; *Separ. Sci. Technol.*, 2001, 36, 3385–3394.
[363] Shimp, RJ; Pfaender, FK; *Appl. Environ. Microb.*, 1982, 44, 471–477.
[364] Su, F; Lu, C; *J. Environ. Sci. Health A*, 2007, 42, 1543–1552.
[365] Su, F; Lu, C; Cnen, W; Bai, H; Hwang, JF; *Sci. Total Environ.*, 2009, 407, 3017–3023.
[366] Kuo, C; Lin, H; *Desalination*, 2009, 249, 792–796.
[367] Lu, C; Chiu, H; *Chem. Eng. Sci.*, 2006, 61, 1138 – 1145.
[368] Liu, J; Zubiri, MR; Vigolo, B; Dossot, M; Fort, Y; Ehrhardt, JJ; McRae, E; *Carbon*, 2007, 45, 885–891.
[369] Wu, CH; *J. Colloid. Interf. Sci.,* 2007, 311, 338–346.
[370] Kuo, CY; *J. Hazard. Mater.*, 2008, 152, 949–954.
[371] Liang, F; Sadana, AK; Peera, A; Chattopadhyay, J; Gu, Z; Hauge, RH; Billups, WE; *Nano Lett.*, 2004, 4, 1257–1260.
[372] Dyke, CA; Tour, JM; *J. Am. Chem. Soc.*, 2003, 125, 1156–1157.
[373] Holzinger, M; Abraham, J; Whelan, P; Graupner, R; Ley, L; Hennrich, F; Kappes, M; Hirsch, A; *J. Am. Chem. Soc.*, 2003, 125, 8566–8580.
[374] Georgakilas, V; Konstantinos, K; Prato, M; Guldi, DM; Holzinger, M; Hirsch, A; *J. Am. Chem. Soc.,* 2002, 124, 760–761.
[375] El-Sheikh, AH; Sweileh, JA; Saleh, MI; *J. Hazard. Mater.*, 2009, 169, 58–64.
[376] Narin, I; Soylak, M; Elci, L; Dogan, M; *Talanta*, 2000, 52, 1041–1046.
[377] Thurman, EM; Mills, MS; *Solid Phase Extraction: Principles and Practice*, John Wiley and Sons, New York, 1998.
[378] Afkhami, A; Norooz-Asl, R; *Colloids Surf. A,* 2009, 346, 52–57.
[379] Heidari, A; Younesi, H; Mehraban, Z; *Chem. Eng. J.*, 2009, 153, 70–79.
[380] Zhang, D; Li, N; Gao, D; *Chin. J. Anal. Chem.*, 2009, 37, 1188–1192.

[381] Weijuan, L; Yiran, X; Yun, D; Yaming, W; Qiufen, H; *Asian J. Chem.*, 2009, 21, 5403–5408.
[382] Khajeh, M; *J. Hazard. Mater.*, 2009, 172, 385–389.
[383] Soylak, M; Unsal, YE; *Food Chem. Toxicol.*, 2010, 48, 1511–1515.
[384] Pacheco, PH; Gil, RA; Smichowski, P; Polla, G; Martinez, LD; *Anal. Chim. Acta*, 2009, 656, 36–41.
[385] Soylak, M; Unsal, YE; *J. AOAC Int.*, 2009, 92, 1219–1224.
[386] Asensio-Ramos, M; Hernandez-Borges, J; Borges-Miquel, TM; Rodriguez-Delgado, MA; *Anal. Chim. Acta*, 2009, 647, 167–176.
[387] Sae-Khow, O; Mitra, S; *J. Chromatogr. A,* 2009, 1216, 2270–2274.
[388] Kuo, C; Wu, C; Wu, J; *J. Colloid. Interf. Sci.*, 2008, 327, 308–315.
[389] Gong, J; Wang, B; Zeng, G; Yang, C; Niu, C; Niu, Q; Zhou, W; Liang, Y; *J. Hazard. Mater.*, 2009, 164, 1517–1522.
[390] Zhu, HY; Jiang, R; Xiao, L; Zeng, GM; *Bioresource Technol.*, 2010, 101, 5063–5069.
[391] Zheng, QR; Gu, AZ; Lu, XS; Lin, WS; *J. Supercrit. Fluid.*, 2005, 34, 71–79.
[392] Chen, CL; Li, XL; Wang, XK; *Radiochim. Acta*, 2007, 95, 261–266.
[393] Chen, C; Li, X; Zhao, D; Tan, X; Wang, X; *Colloids and Surfaces A: Physicochem. Eng. Aspects*, 2007, 302, 449–454.
[394] Su, F; Lu, C; Hu, S; *Colloids and Surfaces A: Physicochem. Eng. Aspects*, 2010, 353, 83–91.
[395] Li, Y; Wang, S; Cao, A; Zhao, D; Zhang, X; Xu, C; Luan, Z; Ruan, D; Liang, J; Wu, D; Wei, B; *Chem. Phys. Lett.*, 2001, 350, 412–416.
[396] Yang, K; Xing, B; *Environ. Pollut.*, 2009, 157, 1095–1100.
[397] Stafiej, A; Pyrzynska, K; *Sep. Purif. Technol.*, 2007, 58, 49–52.
[398] Pyrzyńska, K; Bystrzejewski, M; *Colloids and Surfaces A: Physicochem. Eng. Aspects,* 2010, 362, 102–109.
[399] Lu, C; Su, F; *Sep. Purif. Technol.*, 2007, 58, 113–121.
[400] Yang, S; Li, J; Shao, D; Hu, J; Wang, X; *J. Hazard. Mater.*, 2009, 166, 109–116.
[401] Kandah, MI; Meunier, J; *J. Hazard. Mater.*, 2007, 146, 283–288.
[402] Chen, Z; Zhang, L; Tang, Y; Jia, Z; *Appl. Surf. Sci.*, 2006, 252, 2933–2937.
[403] Bai, Y; Lin, D; Wu, F; Wang, Z; Xing, B; *Chemosphere*, 2010, 79, 362–367.
[404] Akasaka, T; Watari, F; *Acta Biomater.*, 2009, 5, 607–612.
[405] Al-Degs, YS; Al-Ghouti, MA; El-Sheikh, AH; *J. Hazard. Mater.*, 2009, 169, 128–135.
[406] Duran, A; Tuzen, M; Soylak, M; *J. Hazard. Mater.*, 2009, 169, 466–471.
[407] Tuzen, M; Saygi, KO; Soylak, M; *J. Hazard. Mater.*, 2008, 152, 632–639.
[408] Zang, Z; Hu, Z; Li, Z; He, Q; Chang, X; *J. Hazard. Mater.*, 2009, 172, 958–963.
[409] Xu, D; Tan, X; Chen, C; Wang, X; *J. Hazard. Mater.*, 2008, 154, 407–416.
[410] Wang, S; Gong, W; Liu, X; Yao, Y; Gao, B; Yue, Q; *Sep. Purif. Technol.*, 2007, 58, 17–23.
[411] Tan, X; Fang, M; Chen, C; Yu, S; Wang, X; *Carbon*, 2008, 46, 1741–1750.
[412] Gao, Z; Bandosz, TJ; Zhao, Z; Han, M; Qiu, J; *J. Hazard. Mater.*, 2009, 167, 357–365.
[413] Pillay, K; Cukrowska, EM; Coville, NJ; *J. Hazard. Mater.*, 2009, 166, 1067–1075.
[414] Abdel Salam, M; Mokhtar, M; Basahel, SN; Al-Thabaiti, SA; Obaid, AY; *J. Alloy. Compd.*, 2010, 500, 87–92.
[415] Lu, C; Su, F; Hu, S; *Appl. Surf. Sci.*, 2008, 254, 7035–7041.
[416] Lee, P; Chiu, Y; Sun, Y; Ling, Y; *Carbon*, 2010, 48, 1397–1404.

[417] Liao, Q; Sun, J; Gao, L; *Colloids and Surfaces A: Physicochem. Eng. Aspects,* 2008, 312, 160–165.
[418] Xie, X; Gao, L; Sun, J; *Colloids and Surfaces A: Physicochem. Eng. Aspects,* 2007, 308, 54–59.
[419] Jalili, S; Vaez, A; *Chem. Phys. Lett.*, 2007, 437, 233–237.
[420] Daughton, CG; *Environ. Impact Assess. Rev.*, 2004, 24, 711–732.
[421] Daughton, CG; Jones-Lepp, TL; Pharmaceuticals and Personal Care Products in the Environment. Scientific and Regulatory Issues; ACS Symposium Series: Washington, DC, 2001.
[422] Kümmerer, K; Pharmaceuticals in the Environment. Sources, Fate and Risks; Springer-Verlag: Berlin, Germany, 2001.
[423] Albrechtsen, HJ; Mills, MS; Aamand, J; Bjerg, PL; *Pest. Manag. Sci.*, 2001, 57, 341–350.
[424] Ternes, TA; Meisenheimer, M; McDowell, D; Sacher, F; Brauch, HJ; Haist-Gulde, B; Preuss, G; Wilme, U; Zulei-Seibert, N; *Environ. Sci. Technol.*, 2002, 36, 3855–3863.
[425] Gerecke, AC; Scharer, M; Singer, HP; Müller, SR; Schwarzenbach, RP; Sagesser, M; Ochsenbein, U; Popow, G; *Chemosphere*, 2002, 48, 307–315.
[426] Bound, JP; Voulvoulis, N; *Chemosphere*, 2004, 56, 1143–1155.
[427] Carballa, M; Omil, F; Lema, JM; Llompart, M; García-Jares, C; Rodríguez, I; Gómez, M; Ternes, T; *Water Res.*, 2004, 38, 2918–2926.
[428] Ródenas-Torralba, E; Morales-Rubio, A; De La Guardia, M; *Anal. Bioanal. Chem.*, 2005, 383, 138–144.
[429] Wu, Y; Lerner, DN; Banwart, SA; Thornton, SF; Pickup, RWJ; *Environ. Qual.,* 2006, 35, 2021–2025.
[430] Khetan, SK; Collins, TJ; *Chem. Rev.*, 2007, 107, 2319–2364.
[431] Brillas, E; Sirés, I; Oturan, MA; *Chem. Rev.*, 2009, 109, 6570–6631.
[432] Safarik, I; Nymburska, K; Safarikova, M; *J. Chem. Tech. Biotechnol.*, 1997, 69, 1–4.
[433] Patil, SS; Shinde, VM; *Environ. Sci. Technol.*, 1988, 22, 1160–1165.
[434] Daneshvar, N; Ayazloo, M; Khataee, AR; Pourhassan, M; *Bioresource Technol.*, 2007, 98, 1176–1182.
[435] Slokar, YM; Le Marechal, AM; *Dyes Pigments*, 1998, 37, 335–356.
[436] Karkmaz, M; Puzenat, E; Guillard, C; Herrmann, JM; *Appl. Catal. B- Environ.*, 2004, 51, 183–194.
[437] Kasiri, MB; Aleboyeh, H; Aleboyeh, A; *Appl. Catal. B- Environ.,* 2008, 84, 9–15.
[438] Martinez-Huitle, CA; Brillas, E; *Appl. Catal. B- Environ.*, 2009, 87, 105–145.
[439] Khataee, AR; Vatanpour, V; Amani Ghadim, AR; *J. Hazard. Mater.*, 2009, 161, 1225–1233.
[440] Daneshvar, N; Rasoulifard, MH; Khataee, AR; Hosseinzadeh, F; *J. Hazard. Mater.*, 2007, 143, 95–101.
[441] Masten, SJ; Davies, SHR; *Environ. Sci. Technol.*, 1994, 28, 180A–185A.
[442] Daneshvar, N; Aber, S; Vatanpour, V; Rasoulifard, MH; *J. Electroanal. Chem.*, 2008, 615, 165–174.
[443] Drogui, P; Elmaleh, S; Rumeau, M; Bernard, C; Rambaud, A; *Water Res.*, 2001, 35, 3235–3241.
[444] Oturan, MA; Oturan, N; Lahitte, C; Trevin, S; *J. Electroanal. Chem.*, 2001, 507, 96–102.

[445] Gözmen, B; Oturan, MA; Oturan, N; Erbatur, O; *Environ. Sci. Technol.*, 2003, 37, 3716–3723.
[446] Hanna, K; Chiron, S; Oturan, MA; *Water Res.*, 2005, 39, 2763–2773.
[447] Irmak, S; Yavuz, HI; Erbatur, O; *Appl. Catal. B- Environ.*, 2006, 63, 243–248.
[448] Diagne, M; Oturan, N; Oturan, MA; *Chemosphere*, 2007, 66, 841–848.
[449] Brillas, E; Calpe, JC; Casado, J; *Water Res.*, 2000, 34, 2253–2262.
[450] Brillas, E; Boye, B; Síres, I; Garrido, JA; Rodríguez, RM; Arias, C; Cabot, PL; Comninellis, C; *Electrochim. Acta*, 2004, 49, 4487–4496.
[451] Pignatello, JJ; *Environ. Sci. Technol.*, 1992, 26, 944–951.
[452] Zhou, MH; Yu, QH; Lei, LC; Barton, G; *Dyes Pigments*, 2008, 77, 129–136.
[453] Liu, H; Li, XZ; Leng, YJ; *Water Res.*, 2007, 41, 1161–1167.
[454] Qiang, ZM; Chang, JH; Huang, CP; *Water Res.*, 2002, 36, 85–94.
[455] Zhang, X; Fu, J; Zhang, Y; Lei, L; *Sep. Purif. Technol.*, 2008, 64, 116–123.
[456] Ai, Z; Xiao, H; Mei, T; Liu, J; Zhang, L; Deng, K; Qiu, J; *J. Phys. Chem. C*, 2008, 112, 11929–11935.
[457] Zarei, M; Salari, D; Niaei, A; Khataee, A; *Electrochim. Acta*, 2009, 54, 6651–6660.
[458] Zhang, X; Lei, L; Xia, B; Zhang, Y; Fu, J; *Electrochim. Acta*, 2009, 54, 2810–2817.
[459] Lei, LC; Zhang, Y; Zhang, XW; Du, YX; Dai, QZ; Han, S; *Ind. Eng. Chem. Res.*, 2007, 46, 5469–5477.
[460] Sun, B; Sato, M; Clements, JS; *Environ. Sci. Technol.*, 2000, 34, 509–513.
[461] Joshi, AA; Locke, BR; Arce, P; Finney, WC; *J. Hazard. Mater.*, 1995, 41, 3–30.
[462] Imasaka, K; Suehiro, J; Kanatake, Y; Kato, Y; Hara, M; *Nanotechnology*, 2006, 17, 3421–3427.
[463] Zhang, F; Chen, M; Oh, W; *Bull. Korean Chem. Soc.*, 2009, 30, 1798–1804.
[464] Zarei, M; Niaei, A; Salari, D; Khataee, AR; *J. Hazard. Mater.*, 2010, 173, 544–551.
[465] Zarei, M; Niaei, A; Salari, D; Khataee, AR; *J. Electroanal. Chem.*, 2010, 639, 167–174.
[466] Khataee, AR; Zarei, M; Khameneh Asl, S; *J. Electroanal. Chem.*, 2010, 648, 143–150.
[467] Zarei, M; Khataee, AR; Ordikhani-Seyedlar, R; Fathinia, M; *Electrochim. Acta*, 2010, 55, 7259–7265.
[468] Khataee, Ali R; Zarei, M; Khataee, Amir R; *CLEAN - Soil, Air, Water*, 2011, In prees.
[469] Khataee, AR; Zarei, M; Moradkhannejhad, L; *Desalination*, 2010, 258, 112–119.
[470] Pirkanniemi, K; Sillanpaa, M; *Chemosphere*, 2002, 48, 1047–1060.
[471] Konstantinou, IK; Albanis, TA; *Appl. Catal. B-Environ.*, 2004, 49, 1–14.
[472] Blake, DM; *National Renewable Energy Laboratory*, Update Number 4 to October 2001.
[473] Khataee, AR; Aleboyeh, A; Aleboyeh, H; *J. Exper. Nanosci.*, 2009, 4, 121–137.
[474] Verhoeven, JW; *Pure. Appl. Chem.*, 1996, 68, 2223–2286.
[475] Parmon,V; Emeline, AV; Serpone, N; *Int. J. Photochem.*, 2002, 4, 91–131.
[476] Richards, R; *Surface and nanomolecular catalysis*, Published by CRC Press, Taylor and Francis Group, 2006.
[477] Khataee, AR; Fathinia, M; Aber, S; *Ind. Eng. Chem. Res.,* 2010, 49, 12358–12364.
[478] Fathinia, M; Khataee, AR; Zarei, M; Aber, S; *J. Mol. Catal. A: Chem.,* 2010, 333, 73–84.
[479] Khataee, AR; Kasiri, MB; *J. Mol. Catal. A: Chem.,* 328, 8–26.
[480] Mills, A; Hunte, SL; *J. Photoch. Photobio. A*, 1997, 108, 1–35.
[481] Daneshvar, N; Salari, D; Khataee, AR; *J. Photoch. Photobio. A*, 2003, 157, 111–116.

[482] Daneshvar, N; Salari, D; Khataee, AR; *J. Photoch. Photobio. A*, 2004, 162, 317–322.
[483] Cheng, XF; Leng, WH; Liu, DP; Zhang, JQ; Cao, CN; *Chemosphere*, 2007, 68, 1976–1984.
[484] Jing, D; Guo, L; *Catal. Commun.*, 2007, 8, 795–799.
[485] Bandara, J; Klehm, U; Kiwi, *J; Appl. Catal. B: Environ*., 2007, 76, 73–81.
[486] Teramura, K; Tanaka, T; Kani, M; Hosokawa, T; Funabiki, T; *J. Mol. Catal. A: Chem*., 2004, 208, 299–305.
[487] Zhai, Y; Zhang, S; Pang, H; *Mater. Lett*., 2007, 61,1863–1866.
[488] Kanade, KG; Baeg, JO; Mulik, UP; Amalnerkar, DP; Kale, BB; *Mater. Res. Bull.,* 2006, 41, 2219–2225.
[489] Torres–Martínez, CL; Kho, R; Mian, OI; Mehra, RK; *J. Colloid. Interf. Sci.*, 2001, 240, 525–532.
[490] Daneshvar, N; Salari, D; Niaie, A; Rasoulifard, MH; Khataee, AR; *J. Environ. Sci, Heal. A*, 2005, 40, 1605–1617.
[491] Khataee, AR; Fathinia, M; Zarei, M; Aber, S; *J. Hazard. Mater.,* 2010, 181, 886–897.
[492] Khataee, AR; Kasiri, MB; *J. Mol. Catal. A: Chem.,* 331, 86–100.
[493] Khataee, AR; Pons, MN; Zahraa, O; *Water Sci. Technol.,* 2010, 62, 1112–1120.
[494] Hoffmann, MR; Martin, ST; Choi, W; Bahnemannt, DW; *Chem. Rev*., 1995, 95, 69–96.
[495] Wang, X; Yu, JC; Liu, P; Wang, X; Sua, W; Fua, X; *J. Photoch. Photobio. A*, 2006, 179, 339–347.
[496] Zheng, M; Gu, M; Jin, Y; Jin, G; *Mat. Sci. Eng. B*, 2000, 77, 55–59.
[497] Daneshvar, N; Salari, D; Niaei, A; Khataee, AR; *J. Environ. Sci. Heal. B*, 2006, 41, 1273–129.
[498] Tennakone, K; Wijayantha, KGU; *J. Photoch. Photobio. A*, 1998, 113, 89–92.
[499] Pons, MN; Alinsafi, A; Evenou, F; Abdulkarim, EM; Zahraa, O; Benhammou, A; Yaacoub, A; Nejmeddine, A; *Dyes. Pigments*, 2007, 74, 439–445.
[500] Keller, N; Rebmann, G; Barraud, E; Zahraa, O; Keller, V; *Catal. Today*, 2005, 101, 323–329.
[501] Li, L; Zhu, W; Zhang, P; Chen, Z; Han, W; *Water Res.,* 2003, 37, 3646–3651.
[502] Mansoori, GA; Rohani-Bastami, T; Ahmadpour, A; Eshaghi, Z; "Environmental applications of nanotechnology", *Annual Review of Nano Research*, 2008, 2, 1–73.
[503] Li, Y; Li, X; Li, J; Yin, *J; Water Res.*, 2006, 40, 1119–1126.
[504] Serp, P; Corrias, M; Kalck, P; *Appl. Catal. A*, 2003, 253, 337-358.
[505] M.S. Dresselhaus, G. Dresselhaus, P.C. Ecklund, *Science of Fullerenes and Carbon Nanotubes*, Academic Press, San Diego, 1996.
[506] Wang, W; Serp, P; Kalck, P; Faria, JL; *J. Mol. Catal. A: Chem.*, 2005, 235, 194–199.
[507] Wang, H; Wang, HL; Jiang, WF; *Chemosphere,* 2009, 75, 1105–1111.
[508] Wang, W; Serp, P, Kalck, P; Faria, JL; *J; Appl. Catal. B: Environ*., 2005, 56, 305–312.
[509] Liu, S; Yang, L; Xu, S; Luo, S; Cai, Q; *Electrochem. Commun*., 2009, 11, 1748–1751.
[510] Wang, H; Quan, X; Yu, H; Chen, S; *Carbon*, 46, 2008, 1126-1132.
[511] Chen, LC; Ho, YC; Guo, WS; Huang, CM; Pan, TC; *Electrochim. Acta*, 2009, 54, 3884–3891.
[512] Huang, B; Yang, Y; Chen, X; Ye, D; *Catal: Commun.,* 2010, 11, 844–847.
[513] Ahmmad, B; Kusumoto, Y; Somekawa, S; Ikeda, M; *Catal: Commun.*, 2008, 9, 1410–1413.

[514] Yu, H; Quan, X; Chen, S; Zhao, H; Zhang, Y; *J. Photoch. Photobio. A*, 2008, 200, 301–306.
[515] Huang, H; Zhang, WK; Gan, XP; Wang, C; Zhang, L; *Mater. Lett*., 2007, 61, 296–299.
[516] Chen, ML; Zhang, FJ; Oh, WC; *New Carbon Mater.,* 2009, 24, 159-166.
[517] Gao, B; Chen, GZ; Puma, GL; *J; Appl. Catal. B: Environ*., 2009, 89, 503-509.
[518] Akhavan, O; Abdolahad, M; Abdi, Y; Mohajerzadeh, S; *Carbon*, 47, 2009, 3280-3287.
[519] Yu, Y; Yu, JC; Yu, JG; Kwok, YC; Che, YK; Zhao, JC; Ding, L; Ge, WK; Wong, PK; *Appl. Catal. A: Gen.,* 2005, 289, 186-196.
[520] Bouazza, N; Ouzzine, M; Lillo-Rodenas, MA; Eder, D; Linares-Solano, A; *J; Appl. Catal. B: Environ*., 2009, 92, 377383.
[521] Tsubota, T; Ono, A; Murakami, N; Ohno, T; *J; Appl. Catal. B: Environ*., 2009, 91, 533-538.
[522] Kuo, CY; *J. Hazard. Mater.*, 2009, 163, 239–244.
[523] Kan, Z; Zeda, M; Wonchun, O; *Chinese J. Catal.,* 2010, 31, 751-758.
[524] Shou-ai, F; Jiang-hong, Z; Zhen-ping, Z; *New Carbon Mater.,* 2008, 23, 228-234.
[525] Zhu, LP; Liao, GH; Huang, WY; Ma, LL; Yang, Y; Yu, Y; Fu, SY; *Mat. Sci. Eng. B*, 2009, 163, 194-198.
[526] Jiang, L; Gao, L; *Mat. Chem. Phys*., 2005, 91, 313-316.
[527] Lee, KR; Park, S; Lee, KW; Lee, JH; *J. Mater. Sci. Lett.,* 2003, 22, 65-67.
[528] Zhu, L; Tian, C; Zhai, J; Yang, R; *Sensor. Actuat. B: Chem.,* 2007, 125, 254-261.
[529] Foldvari, M; Bagonluri, M; *Nanomedicine: Nanotechnology, Biology and Medicine*, 2008, 4, 183-200.
[530] Sharma, T; Reddy, ALM; Chandra, TS; Ramaprabhu, S; *Int. J. Hydrogen Energ*., 2008, 33, 6749-6754.
[531] Ji, SR; Liu, C; Zhang, B; Yang, F; Xu, J; Long, J; Jin, C; Fu, DL; Ni, QX; Yu, XJ; *Biochim. Biophys. Acta*, 2010, 1806, 29-35.
[532] Kayat, J; Gajbhiye, V; Tekade, RK; Jain, NK; *Nanomedicine: Nanotechnology, Biology and Medicine*, 2011, 7, 40-49.
[533] Deng, X; Wu, F; Liu, Z; Luo, M; Li, L; Ni, Q; Jiao, Z; Wu, M; Liu, Y; Carbon, 2009, 47, 1421-1428.
[534] Muller, J; Decordier, I; Hoet, PH; Lombaert, N; Thomassen, L; Huaux, F; Lison, D; Kirsch-Volders, M; *Carcinogenesis*, 2008, 29, 427-433.
[535] Muller, J; Huaux, F; Moreau, N; Misson, P; Heilier, JF; Delos, M; Arras, M; Fonseca, A; Nagy, JB; Lison, D; *Toxicol.Appl. Pharm*., 2005, 207, 221- 231.
[536] Prylutska, SV; Grynyuk, II; Matyshevska, OP; Yashchuk, VM; Prylutskyy, YI; Ritter, U; Scharff, P; *Physica E*, 2008, 40, 2565–2569.
[537] Raja, PMV; Connolley, J; Ganesan, GP; Ci, L; Ajayan, PM; Nalamasu, O; Thompson, DM; *Toxicol. Lett*., 2007, 169, 51-63.
[538] Porter, DW; Hubbs, AF; Mercer, RR; Wu, N; Wolfarth, MG; Sriram, K; Leonard, S; Battelli, L; Schwegler-Berry, D; Friend, S; Andrew, M; Chen, BT; Tsuruoka, S; Endo, M; Castranova, V; *Toxicology*, 2010, 269, 136-147.
[539] Yang, ST; Wang, X; Jia, G; Gu, Y; Wang, T; Nie, H; Ge, C; Wang, H; Liu, Y; *Toxicol. Lett*., 2008, 181, 182-189.
[540] Tong, H; McGee, JK; Saxena, RK; Kodavanti, UP; Devlin, RB; Gilmour, MI; *Toxicol. Appl. Pharm.,* 2009, 239, 224-232.
[541] Ellinger-Ziegelbauer, H; Pauluhn, J; *Toxicology*, 2009, 266, 16-29.

[542] Tabet, L; Bussy, C; Amara, N; Setyan, A; Grodet, A; Pairon, JC; Boczkowski, J; Lanone, S; *J. Toxicol. Environ*. *Health A*, 2009, 72, 60-73.
[543] Simon-Deckers, A; Gouget, B; Mayne-L'Hermite, M; Herlin-Boime, N; Reynaud, C; Carrière, M; *Toxicology*, 2008, 253, 137-146.
[544] Davoren, M; Herzog, E; Casey, A; Cottineau, B; Chambers, G; Byrne, HJ; Lyng, FM; *Toxicol. in Vitro*, 2007, 21, 438-448.
[545] Cheng, C; Muller, KH; Koziol, KKK; Skepper, JN; Midgley, PA; Welland, ME; Porter, AE; *Biomaterials*, 2009, 30, 4152-4160.
[546] Fiorito, S; Serafino, A; Andreola, F; Bernier, P; *Carbon*, 2006, 44, 1100-1105.
[547] Vittorio, O; Raffa, V; Cuschieri, A; *Nanomedicine: Nanotechnology, Biology, and Medicine,* 2009, 5, 424-431.
[548] Walker, VG; Li, Z; Hulderman, T; Schwegler-Berry, D; Kashon, ML; Simeonova, PP; *Toxicol. Appl. Pharm*., 2009, 236, 319-328.
[549] Narsimha Reddy, AR; Narsimha Reddy, Y; Krishna, DR; Himabindu, V; *Toxicology*, 2010, 272, 11-16.
[550] Monteiro-Riviere, NA; Nemanich, RJ; Inman, AO; Wang, YY; Riviere, JE; *Toxicol. Lett*., 2005, 155, 377-384.

In: Activated Carbon
Editor: James F. Kwiatkowski
ISBN: 978-1-61209-684-1
©2012 Nova Science Publishers, Inc.

Chapter 2

CATALYTIC OZONATION OF ORGANICS WITH LOADED ACTIVATED CARBON

Luo Hanjin* *and Rao Yifei*
College of Environmental Science and Engineering,
South China University of Technology, Guangzhou, China

ABSTRACT

It is important to increase the efficiency of producing hydroxyl radicals with ozone during the process of treating wastewater containing toxic and refractory organic pollutants. In the present study, nickel oxide-loaded activated carbon (NiO/AC) and copper oxide-loaded activated carbon (CuO/AC) were prepared with an incipient wetness impregnation method at low temperatures. The effectiveness for degradation of phenol and oxalic acid by the combination of NiO/AC or CuO/AC and ozone at different pH values and concentrations of tert-butyl alcohol (*t*-BuOH) was investigated. The composition and surface morphology of activated carbon (AC) and catalyst were characterized by XRD, SEM, BET and AAS, which showed that copper and nickel were loaded on the surface of AC in the form of rod-like copper oxide and nickel oxide. The specific, micropore, and external surface areas and micropore volume of Cu/AC and Ni/AC decreased by 50.7%, 62.9%, 34.8%, and 62.4% and 47.9%, 60.6%, 31.0%, and 60.7%, respectively. Compared to those of AC, in the systems of O_3/Cu/AC and O_3/Ni/AC, the mechanism of degradation of phenol and oxalic acid by ozone was achieved mainly by molecular ozone oxidation, while the mechanism with O_3/AC was primarily due to molecular ozone oxidation and absorption of AC. The removal efficiencies of phenol and oxalic acid by O_3/Cu/AC were 29% and 30.4% while those by O_3/Ni/AC were 52% and 59%. The efficiencies of both methods were higher than those by ozone only. The degradation process occurred during the formation of hydroxyl radicals and the reaction of Cu/AC or Ni/AC with ozone demonstrates the strong synergy effect. The catalytic performance of Cu/AC and Ni/AC were stable, and both catalysts were reusable for further catalyzation.

* Corresponding author: Dr. Luo Hanjin, E-mail: luohj@scut.edu.cn

Keywords: catalytic ozone oxidation, hydroxyl radical, loaded activated carbon, phenol, oxalic acid.

1. INTRODUCTION

As a strong oxidant, ozone has greater advantage in removing odor and color, and be widely used in the field of drinking water disinfection. However, there are certain limitations of ozone [1], such as strong selectivity, sometimes can not completely mineralize organic matter and has low solubility in water. These make certain restrictions for the application of ozone in wastewater treatment. In recent years, advanced oxidation combined with a variety of techniques, such as the contribution of catalysts, resulting in low selective and strong oxidizing HO• to improve the oxidative capacity of the system.

According to the state of the catalyst species in the reaction, catalyzed ozonation technology can be divided into two categories [2]: homogeneous catalytic ozonation and heterogeneous catalytic ozonation. In the research of Hewes and Davison [3], they observed that the addition of some salts in the process ozone oxidation of phenolic compounds will increase the organic matter mineralization. Some studies [4] pointed out that the generated HO• (the decomposition of ozone) can improve the degradation rate of the matrix. However, it is difficult to summarize heterogeneous catalytic reaction mechanism when comparing with other advanced oxidation technologies. The reason was that the effectiveness of homogeneous catalytic ozonation reaction systems vary greatly to different pollutants. Addition of different types of metal into the homogeneous system will cause more difficulties of liquid waste treatment. In heterogeneous catalytic systems, the most common combined techniques are solid catalysts with gas or liquid reactants. Recently, researchers have launched other methods using liquid phase reactions. Since Chen [5] firstly published a research article about Fe_2O_3 heterogeneous catalytic ozonation of pollutants, experiments of catalysts such as metal oxides [6-13], mesoporous material catalysts [14], activated carbon [15-19], metal-alumina loaded solid catalyst [20-25], supported honeycomb ceramics catalyst [26-29] and activated carbon supported catalysts [30-36] have been carried out. In general, the catalytic activity is mainly achieved by free radical species such as HO•. Therefore, in the heterogeneous catalysis system the decomposition of ozone is largely depended on the solution properties (pH, temperature, ionic strength, etc.) and the surface characteristics of catalyst [1].

Researchers have tried to increase the surface area of catalyst, and then loaded it onto the alumina, clay, silica gel or zeolite, and then strengthen the reactivity of catalyst for transforming ozone into HO•. The research of loading metal on a variety of carriers was reported more frequently. Catalysts used in water treatment were Al_2O_3, honeycomb ceramic, activated carbon, zeolite and metal oxides.

Activated carbon is a porous material, with a large surface area, high security, high-performance catalyst, which is insoluble in water and organic solvents, easily to be recycled and so on. As an ideal catalyst, activated carbon has good physical and chemical properties, stability in acidic and alkaline conditions, and easy for recycling. Therefore, the activated carbon which loaded with metal can significantly improve the efficiency of catalytic oxidation. Studies have shown that [29] the active carbon which catalyst complex compounds

was in the form of ligand exchange. For example sulfide can be oxidized to sulfate. Research showed that the catalytic activity was related to porous structure of activated carbon.

In recent years, the metal which was loaded on activated carbon (as a carrier) for preparing metal catalyst was FeOOH [30], Mn [31], Ce [32-34], Ni [35], Ru [36] and so on. The studies of Faria [32] have shown that AC and CeO showed strong combined effect during the process of oxalic acid removal by Ce/AC, which achieved the greatest degree of mineralization and HO• was produced simultaneously. During the process of dye removal using O_3/Ce/AC [34], the activity of the catalyst with Ce was weakened due to the deplete of HO• by carbonate and bicarbonate ions. Research has proved that catalytic ozonation was effective for the three levels of biochemical waste treatment. Li [35] studied the petroleum coke prepared Ni/AC applied in aqueous for chloride acid catalytic ozonation. It showed that the addition of petroleum coke did not improve the ozonation for the removal of parachlorobenzoic-acid, but was beneficial for mineralization of parachlorobenzoic-acid. In the solution which HO• was generated, Ni/AC catalyst showed good activity and stability. Wang et al. [36] studied the Ru/AC catalytic ozonation of dimethyl phthalate and its disinfection by-products. The results indicated that Ru was not detected in treated water samples. Compared to ozonation, O_3/Ru/AC was effective for removal of TOC in natural water and reduction the possible formation of disinfection by-products.

Previous researchers mainly focused on the degradation of pollutants, catalytic activity and reaction mechanism. However, the comparative study about the process of catalytic reaction kinetics of ozone and a variety of metal loaded onto activated carbon catalyst were rare. In this study, the synthesis of the supported of copper and nickel catalyst were prepared in low temperature, and the catalysts were characterized by XRD, SEM, BET and other analytical methods. Meanwhile, the comparative study of the process of degradation and reaction mechanism between ozonation of phenol and oxalic acid were carried out to study the chemical reaction kinetics mechanism.

2. TEST EQUIPMENT, MEDICINES, TESTING AND ANALYSIS

2.1. Materials and Chemicals

A granulated coal-based AC purchased from Xinhua Carbon Corp., Shanxi Province, China, was crushed to 0.20-0.45 mm. Chemicals were all analytical grades or guaranteed reagents, which were used without further purification. All solutions were prepared with deionized water (18 MΩ Milli-Q) and stored at 4 °C. The ozone generator was model HF-3 (Yinhe Corp., China); the UV-Vis spectrophotometer was model UV 2450 (Shimazu Corp., Japan); the pH meter was model pHS-3C (Leici Corp., China); the ion chromatograph (IC) was model ICS-90 (Dionex Corp., USA); the atomic absorption spectrophotometer (AAS) was model Z-2000 (Hitachi Corp., Japan) and the model of X-ray diffractometer was X' Pert Pro (Panalytical Corp. Holand).

The experimental device is shown in Figure 2-1.

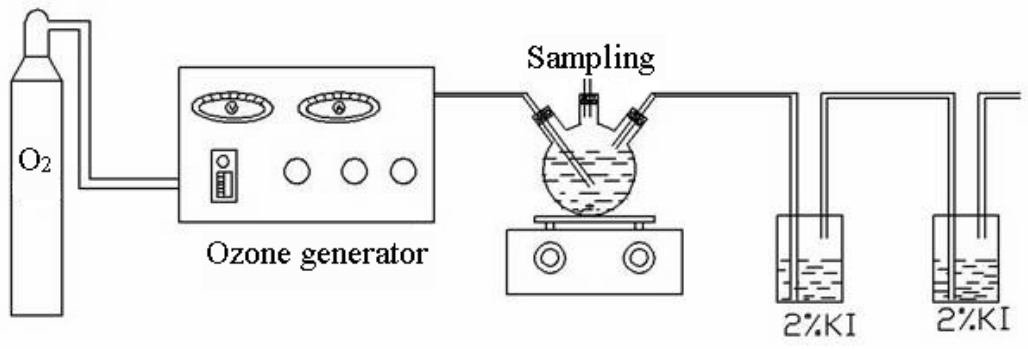


Figure 2-1. Schematic diagram of Ozonation system.

2.2. Analytical Methods

2.2.1. Determination Of Ozone Concentration

Ozone concentrations in gas and aqueous solution were measured by the iodometric titration method and the indigo method [107], respectively, which were based on the following reaction:

$$O_3 + 2KI + H_2O \rightarrow O_2 + I_2 + 2KOH \quad (2\text{-}1)$$

$$I_2 + 2Na_2S_2O_3 \rightarrow 2NaI + Na_2S_4O_6 \quad (2\text{-}2)$$

The concentration of ozone is defined as:

$$C_{O_3} = A_{Na} \times B \times \frac{2400}{V_0} (mg \cdot L^{-1}) \quad (2\text{-}3)$$

C_{O_3} : Ozone concentration in liquid phase, $mg \cdot L^{-1}$;

A_{Na} : The amount of sodium thiosulfate standard solution, mL;

B: The concentration of sodium thiosulfate standard solution, $mol \cdot L^{-1}$;

V_0: Sampling volume of ozone gas, mL;

When the ozone concentration $\geqq$ 3 $mg \cdot L^{-1}$, the precision of the test result is within ±1%.

2.2.2. Determination of Phenol Concentration

The concentration of phenol in aqueous solution was determined by the UV-Vis spectrophotometery at the wavelength of λ=287.5 nm quantitatively [108].

2.2.3. Determination of Oxalic Acid Concentration

Ion chromatography (IC) was employed to detect the concentration of oxalic acid. The analytical conditions were:

Eluent: Na_2CO_3 (12×10^{-3} mol·L^{-1}) and $NaHCO_3$ (5×10^{-3} mol·L^{-1}), with the flow rate of 1.0 mL·min^{-1};
Suppressor current of 60mA,
Column temperature 30 ℃,
Sample size: 1mL.
It turned out that the retention time of oxalic acid ion was 17.6 min.

2.2.4. Determination of Metal Ion Concentration

The Cu(Ⅱ) and Ni(Ⅱ) concentrations in Cu/AC, Ni/AC and various reaction media during the catalytic ozonation were determined by the technique of Atomic Absorption Spectroscopy (AAS).

2.3. Catalyst Preparation and Characterization

2.3.1. Catalyst Preparation

The preparation method for Cu/AC was slightly modified from that reported by Choi et al [109]. AC was firstly washed with ultrapure water and dried at 110℃ overnight. Cu was incorporated into AC via an incipient wetness impregnation method, during which 13.6 g $Cu(NO_3)_3\cdot3H_2O$ was dissolved at 55-60 ℃ with 5 mL ultrapure water and then mixed with 10 g AC for 10 min. For the total incorporation of Cu into AC, the slurry was dried at room temperature for 8 h, followed by drying at 60-70 ℃ using an infrared lamp for 6 h. The mixture was further calcined in a muffle furnace. The temperature was firstly ramped to 150 ℃ for 1 h, and then increased to 300 ℃ and held for 4 h. Finally, it was cooled naturally. Preparation of Ni/AC, accurately weighed 25.48 g Ni $(NO_3)_2\cdot6H_2O$, the remaining steps were the same as the preparation method of Cu / AC.

2.3.2. Catalyst Characterization

2.3.2.1. X-Ray Diffractometer (XRD)

An **X-ray diffractometer** (XRD) (Cu Kα radiation, λ=0.154 06 nm) was employed to observe the crystal structure of AC, Cu/Ac and Ni/Ac at an ambient temperature (X'Pert Pro, Panalytical Corp., Holand).

2.3.2.2. Scanning Electron Microscopy (SEM)

The surface morphologies of AC, Cu/AC and Ni/AC were obtained from a scanning electronic microscope (model JCM-5700 JEOL, JEOL Crop., Japan).

2.3.2.3. Bet Surface Area

The textural properties of AC, Cu/AC and Ni/Ac were determined from the corresponding N_2 adsorption/desorption isotherms obtained at 77 K with an automatic instrument (TriStarⅡ3020, Micromeritics Instrument Corp., US). The samples were previously degassed in N_2 atmosphere at 200 ℃ for 4 h. The surface areas, pore size

distributions and micropore volumes of AC, Cu/AC and Ni/AC were determined by the BET calculation method applied to the adsorption branch of their isotherms.

2.3.2.4. Atomic Absorption Spectrometry (AAS)

The concentration of Cu^{2+} and Ni^{2+} in the reaction solution were determined by AAS.

2.4. Batch Adsorption and Degradation Reaction of Phenol and Oxalic Acid

2.4.1. Absorption Experiments

The initial concentration and volume of phenol were 200 mg/L and 500 mL, which was placed in Flask A, B and C, respectively. The initial pH value of the solutions were all 5.46. Then 0.50 g AC, 0.50 Cu/AC and 0.50 Ni/AC were added into Flask of A, B and C. The flasks were continuously shaken (150 rpm) for 30 mins at 25 °C. At selected time intervals, 5mL sample was collected with glass syringes and filtered through a 0.45 μm membrane filter for analysis. The concentration of phenol was determined by the spectrophotometer.

The initial concentration and volume of oxalic acid were 10 mg/L and 1000 mL; which was placed in Flask A, B and C, respectively. The pH values of the solutions were 3.85 (initial pH value). Then 0.50 g AC, 0.50 Cu/AC and 0.50 Ni/AC were added into Flask A, B and C. The flasks were continuously shaken (150 rpm) for 30 mins at 25 °C. At selected time intervals, 1 mL sample was collected with glass syringes and filtered through a 0.45 μm membrane filter for analysis. The concentration of oxalic acid was determined by IC.

2.4.2. Catalytic Ozonation Experiments

Ozone was produced from pure oxygen which was generated from an ozone generator at a constant inlet ozone concentration of 11.2 mg/L. In each experiment, the initial concentration and volume were 200 mg/L and 500 mL for phenol; and 10 mg/L and 1000 mL for oxalic acid, respectively. In consideration of catalytic effect and the initial concentration of pollutants, AC, Ni/AC or Cu/AC was placed in the reactor, respectively. In the experiments in which ozone was involved, $Na_2S_2SO_3$ solution was added to the sampling tube to quench the residual ozone in the reaction solution. At a predetermined time, samples were first withdrawn and filtered (pore size 0.45 μm) and then the concentrations of phenol, oxalic acid, Cu(Ⅱ) and the pH value of the solution were measured. All the experiments were performed in an agitated glass reactor at an ambient temperature under the same operating conditions. All the glass containers were first soaked in HNO_3 solution overnight, then placed in a sonic bath for 30 min, and finally rinsed with ultrapure water. The residual ozone in the off gas was adsorbed by KI solution. All solutions were prepared with ultrapure water obtained from a Millipore Milli-Q system.

3. RESULTS AND DISCUSSION

3.1. Catalyst Characterization

3.1.1. The Analysis of XRD Patterns

Figure 3-1 shows the XRD patterns for AC, Cu/AC and Ni/AC. It can be seen that Cu/AC has characteristic reflections at 2θ=35.5°, 38.7°, 48.8° and 61.4°, which were corresponding to CuO. The main crystal forms in Ni/AC are NiO and Ni according to the comparison with the standard spectrogram, and the characteristic peak are shown in figure with black dots and point below. The nitrates will exist with in the oxidative forms completely according to the assumption of catalysts preparation. However, there is no elementary substance of Cu in Cu/AC, while it appears the characteristic peak of Ni in Ni/AC, as shown in the Figure 3-1. It probably has two reasons, one is that amount of metal substance added to the nitrates are different. The charge capacity of Ni in Ni/AC is more than that of Cu in Cu/AC based on the calculation, and the more charge capacity and molar concentration of the metal, the more formation of elementary metal substance. The other probable reason is that, according to the research of Maoxiang JING, C deoxidizes NiO to trace elemental Ni because of oxygen inadequacy in short time as a result of lower temperature of nickel nitrate in the preparation of Ni/AC.

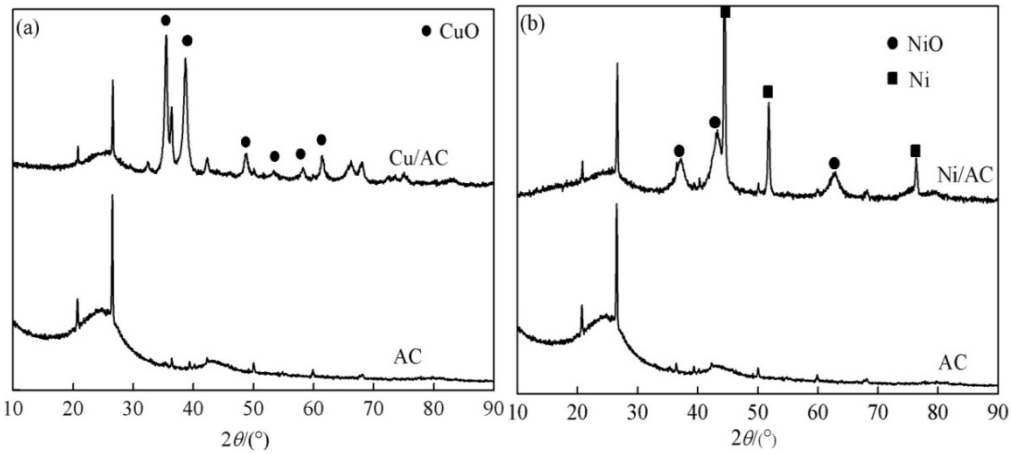


Figure 3-1. XRD patterns of Cu/AC (a) and Ni/AC (b).

Figure 3-1 also shows that all of XRD patterns for AC, Cu/AC and Ni/AC have significant characteristic reflections at 2θ=26.5° which is the typical diffraction peak of disorderly layer carbon [41, 42]. The reason of the existence of disorderly layer carbon is that the structure and permutation of activated carbon is not as completely regular as that of graphite. Its two-dimensional planar structure consists of parallel layers of carbon atoms arranged in hexagon. The parallel layers are not complete orientation to their common vertical axis. The angular displacement between two layers is turbulence. Each layer is irregularly overlapped, forming the disordered structure. As shown in the figure, the diffracted intensities of Cu/AC and Ni/AC are less than that of AC which illustrates the XRD pattern of activated carbon is not changed by the product of CuO and NiO after calcination.

3.1.2. The Analysis of SEM Images

Figure 3-2 and 3-3 displayed the microscopic surface texture of AC, Cu/AC and Ni/AC by scanning electron microscope (SEM) techniques in an enlargement factor of 10^3 and 1.2×10^4.

Figure 3-2 (a) and 3-3 (a) showed that the surface of AC is protuberant rather than flat, which is the macroscopic expression of an increasing of superficial roughness and crystal grain. The superficial area is lager than that of regular and homogeneous ones [43].

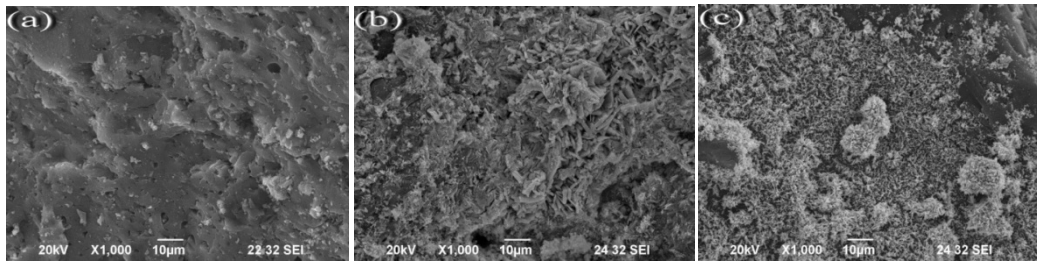


Figure 3-2. SEM images of AC (a), Cu/AC (b) and Ni/AC (c) at a magnification of 10^3.

Figure 3-2 (b) and 3-3 (b) show that the structure of activated carbon has experienced a major change that the surface of Cu/AC is filled with some rod-like structures which are compactly dispersed as a result of the structural change of activated carbon in different temperature or the product of new CuO. Figure 3-2 (c) shows that plenty of NiO was spread evenly on the surface of Ni/AC, and some sections come into conglobation as over concentration. It can be seen from Figure 3-3 (c) that the NiO in Ni/AC present lineage structure and the average diameter is about 300 nm.

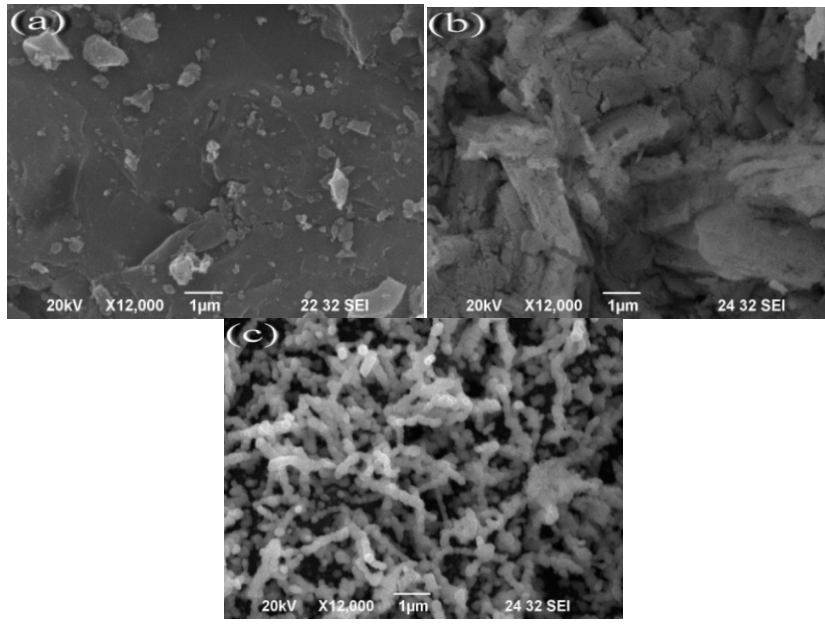


Figure 3-3. SEM images of AC (a), Cu/AC (b) and Ni/AC (c) at a magnification of 1.2×10^4.

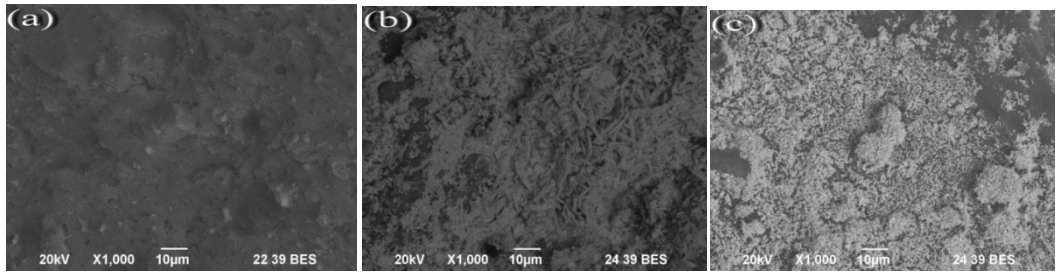


Figure 3-4. BES images of AC (a), Cu/AC (b) and Ni/AC (c) at a magnification of 10^3.

Figure 3-4 shows the back-scattering image (BES) of AC, Cu/AC and Ni/AC, and enlargement factor is 103. The operating principle [44] of backscatter electronography is that the number of the back-scattered electrons varies with the atomic number of various components of samples, therefore, the pixel of light or shade is formed after reception amplification by detector. Besides, only the back-scattered electrons faced the detector could be detected because their trajectories are straight lines, as a result, the images of back-scattered electrons have shadows. Sporadic white dots can be seen from Figure 3-4 (a) which implies extra low impurity; and in Figure 3-4 (b), the surface of Cu/AC is uneven because of the generation of substantial CuO, which also confirmed by the XRD patterns. It can be seen from Figure 3-4 (c) that massive NiO was loaded on the surface of Ni/AC.

3.1.3. The Analysis of BET Images

Figure 3-5 (a) and (b) show the N_2 adsorption-desorption isotherms of AC, Cu/AC and Ni/AC in the temperature of 77 K.

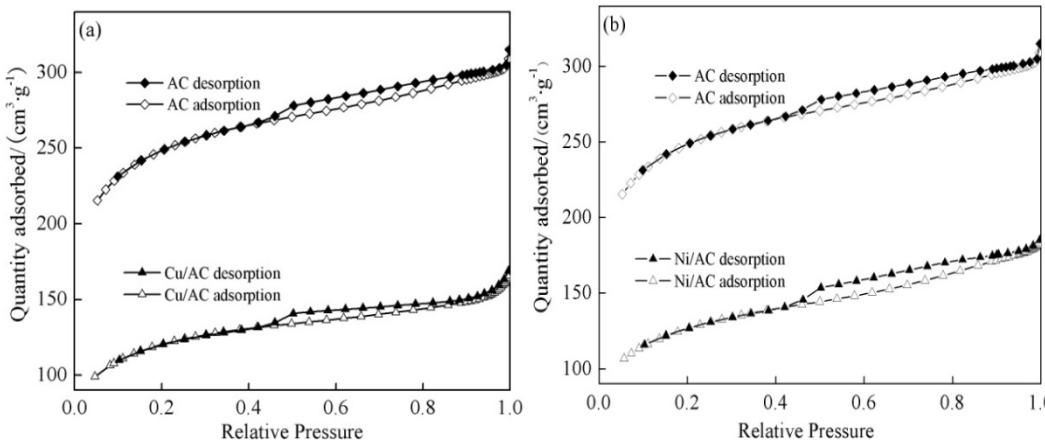


Figure 3-5. N_2 adsorption/desorption isotherms of AC, Cu/AC (a) and AC, Ni/AC (b).

In Figure 3-5, AC, Cu/AC and Ni/AC all expressed in the form of isotherm I (according to the classification of IUPAC). The adsorption plateaus of both Cu/AC and Ni/AC became less than that of AC as the generations of CuO in Cu/AC and NiO in Ni/AC, which illustrate their adsorption capacities reduced significantly and the micropores volume of Cu/AC and Ni/AC are large than that of AC. The adsorption plateau of Ni/AC is a little higher than Cu/AC.

Figure 3-6 (a) and (b) show the distributions of pore size of AC, Cu/AC, AC, and Ni/AC in adsorption.

It can be seen from Figure 3-6 that the peak intensity and peak area of Cu/AC and Ni/AC decreased significantly around 4 nm, which show that specific surface area, pore volume and pore diameter of Cu/AC and Ni/AC reduced markedly with respect to AC.

The BET specific surface area, microporous surface area, appearance area, desorption mean pore size and micropores volume of AC, Cu/AC and Ni/AC are shown in Table 3-1, and the specific surface area of AC, Cu/AC and Ni/AC were 787$m^2 \cdot g^{-1}$, 388 $m^2 \cdot g^{-1}$, 410 $m^2 \cdot g^{-1}$, respectively.

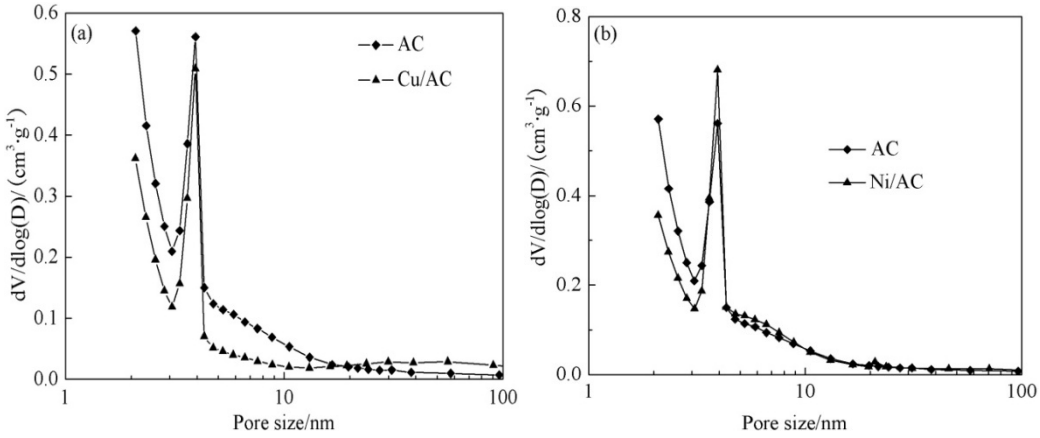


Figure 3-6. BJH pore size distribution plots of AC, Cu/AC (a) and AC, Ni/AC (b).

(dV/dlog(D): desorption pore size differential distribution; V: pore volume; D: pore diameter; BJH: one pore distribution calculation method which take cylindrical pore as model)

Compared to AC, the specific surface area, microporous surface area, appearance area and micropores volume of Cu/AC reduced 50.7%, 62.9%, 34.8% and Ni/AC reduced 62.4%, and 47.9%, 60.6%, 31.0% and 60.7% respectively, while the desorption mean pore size of Cu/AC and Ni/AC increased inordinately compared to AC.

Table 3.1. Surface areas and pore size distributions of AC, Cu/AC and Ni/AC

Sample	S_{BET}/($m^2 \cdot g^{-1}$)	S_m/($m^2 \cdot g^{-1}$)	S_e/($m^2 \cdot g^{-1}$)	V_m/($cm^3 \cdot g^{-1}$)	D/(nm)
AC	787	447	339	0.234	3.38
Cu/AC	388	166	221	0.088	3.62
Ni/AC	410	176	234.4	0.092	3.65

S_{BET}: BET specific surface area; S_m: micropore surface area; S_e: external surface area; V_m: micropore volume; D: average pore diameter.

Table 3-1 shows that the CuO and NiO were distributed in the microporous areas of Cu/AC and Ni/AC, respectively, which is consistent with the results of N_2 adsorption-desorption isotherms and BJH distribution of pore size of Cu/AC and Ni/AC. Meanwhile, the phenomenon that CuO and NiO were distributed in the surfaces of Cu/AC and Ni/AC was

also confirmed, and the loading of metallic oxide decreased the specific surface area significantly, increased the mean pore size slightly.

3.1.4. The Analysis of ASS Results

AAS was used for the determination of soluble Cu^{2+} and Ni^{2+} in Cu/AC and Ni/AC and the results were 0.002mg·L^{-1} and 0.05 mg·L^{-1}, respectively, which shows that the copper in Cu/AC and nickel in Ni/AC are all existed in the form of oxides (CuO or NiO).

3.2. Degradation of Phenol and Oxalic Acid by AC and Catalysts

In order to study the adsorption efficiency of phenol and oxalic acid by AC, Cu/AC and Ni/AC, the experiment condition was set up as follows: the initial concentrations and volumes of phenol and oxalic acid are 200mg·L^{-1}, 500mL and 10mg·L^{-1}, 1000mL, respectively. Meanwhile, the addition of AC, Cu/AC and Ni/AC are all 0.5g in consideration of the catalytic efficiency. The relationship between reaction time and the removal efficiency of phenol and oxalic acid by AC and Cu/AC are shown in Figures 4 (a) and (b), respectively.

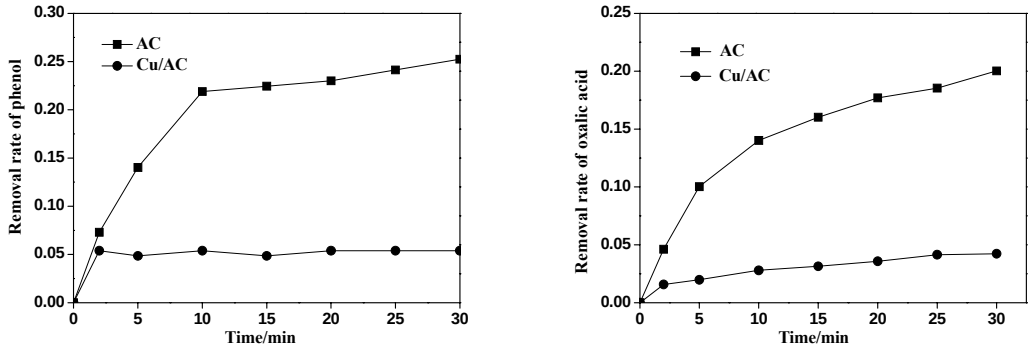


Figure 3-7. Evolution of phenol (a) and oxalic acid (b) concentrations in adsorption systems.

It can be seen from Figure 3-7 (a) and (b) that the proportions of phenol or oxalic acid adsorbed by AC are 25.2% and 20%, while only 5% and 4% for Cu/AC at 30 min. The adsorption of phenol and oxalic acid by AC reached equilibriums at 10 min and 15 min, respectively. While the adsorption capacity of phenol and oxalic acid by Cu/AC was limited, the removal efficiency of pollutants no longer changed after the reaction begins 2 minutes.

Figure 3-8 (a) and (b) show that the relationships between reaction time and the removal efficiency of phenol and oxalic acid by AC and Ni/AC. It can be seen that the adsorption by AC and Ni/AC reached equilibrium at 10 min. The proportions of phenol adsorbed by AC and Ni/AC were 25.2% and 5%, and the adsorption efficiency of oxalic acid by AC was 20%, while only 4% for Ni/AC at 30 min.

The main reason of the different adsorption efficiencies of phenol or oxalic acid between AC and Cu/AC, Ni/AC was mainly that the desultory arrangement of carbon atoms of graphite layers in AC formed many gaps between each another and then larger specific surface area and bigger adsorption capacity [45].

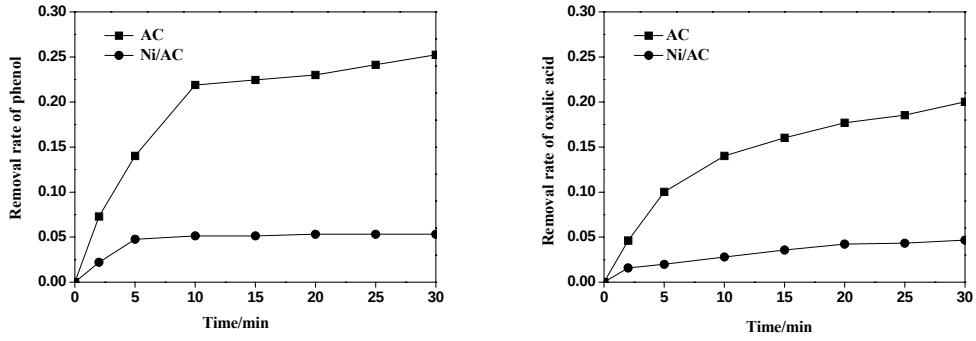


Figure 3-8. Evolution of phenol (a) and oxalic acid (b) concentrations in AC and Ni/AC systems.

The surface character and morphology of active carbon were changed dramatically due to the different calcination temperatures in preparation of catalysts, and the adsorption capacity are weakened significantly as the specific surface areas of Cu/AC and Ni/AC only account for 49% and 52%. Besides, there are plenty of oxygenic and nitrogenous functional groups in the surface of active carbon, in which oxygenic functional groups contain acid group and alkalic group, and alkaline compounds could adsorb low-polar and non-polar substance readily. Great changes have taken place in Chemical and surface structure of catalysts such as superficial base groups, pore volume and pore size distribution after chemical modification, which is confirmed by the images of XRD, SEM and BET. Besides superficial oxides, there are also phenolic hydroxyl groups in active carbon based on some physico-chemical analysis [45]. The increasing numbers of phenolic hydroxyl group vary with the preparation and calcination of catalysts cause the decreasing of adsorption capacity of phenol by AC, and adsorption capacity of hydrophobic organics such as phenol, humic acid and oxalic acid decreases dramatically after oxidized modification. Therefore, the adsorption capacity of phenol and oxalic acid by Cu/AC and Ni/AC is smaller than that of AC, which is in agreement with the findings reported by Faria [17, 18] et al.

3.3. Degradation of Phenol and Oxalic Acid by Ozonation Process

3.3.1. Degradation of Phenol and Oxalic Acid by O_3/Cu/AC and O_3/Ni/AC

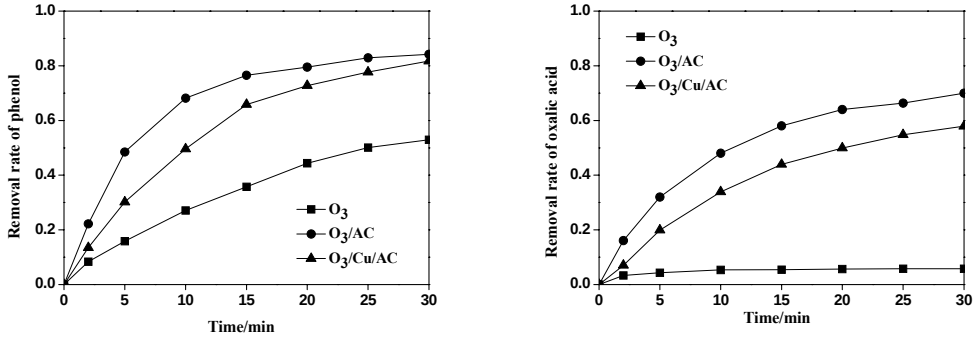


Figure 3-9. Evolution of concentrations of phenol (a) and oxalic acid (b) in O_3, O_3/Cu/AC and O_3/AC systems.

Figure 3-9 (a) and (b) show that the relationship between reaction time and the removal efficiency of phenol and oxalic acid by O_3, O_3/AC and O_3/Cu/AC. It can be seen that the proportions of phenol or oxalic acid adsorbed by O_3 were 53% and 5.8%, respectively, at 30 min. The removal efficiency of phenol and oxalic acid were 84.2% and 70.0%, which were 2% and 12% higher than O_3/AC at 30 min.

Figure 3-10 (a) and (b) show that the relationship between reaction time and the removal efficiency of phenol and oxalic acid by O_3, O_3 /AC and O_3/Ni/AC.

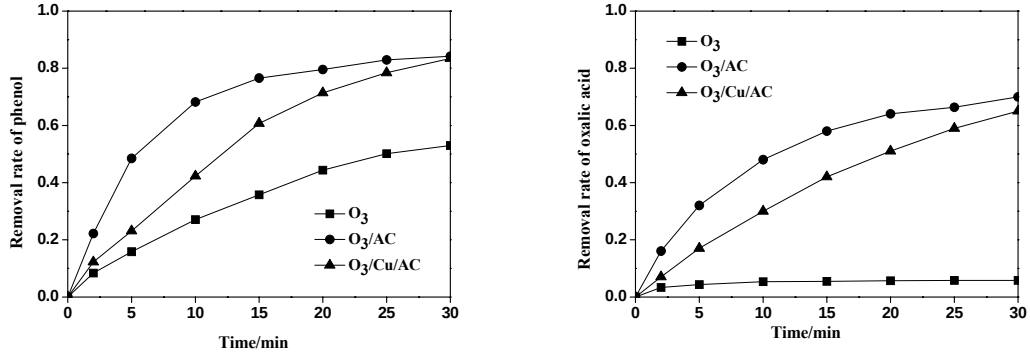


Figure 3-10. Evolution of phenol (a) and oxalic acid (b) concentrations in O_3, O_3/Ni/AC and O_3/AC systems.

It can be seen from Figure 3-10 that the removal efficiencies of phenol and oxalic acid have a great degree improvement after the addition of AC and Ni/AC compared to the single ozonation system. The removal efficiency of phenol and oxalic acid by O_3/Ni/AC were 83.4% and 65.0%, which were 30.4% and 59% higher than O_3 at 30 min. The difference of removal efficiency of phenol and oxalic acid between O_3/AC and O_3/Ni/AC is minor at 30 min, which are 1% and 5%, respectively.

The reason for that the higher removal efficiency of phenol and oxalic acid by O_3 /AC than that by O_3/Cu/AC and O_3/Ni/AC is that bigger reactive surface is provided in ozonation process by AC. Furthermore, the adsorptive capacity of AC outweighs extremely its catalytic capacity. The superficial chemical characteristic have been changed after the loading of metallic oxides as the metals are high-dispersed by carrier [47], and another reason comes from the change in chemical property of metallic oxides. The adsorptive capacity of phenol and oxalic acid has improved 29% and 52% by the addition of Cu/Ni in oxidized system of O_3/Cu/AC. Meanwhile, the rate of improvement is 30.4% and 59% in system of O_3/Ni/AC. The main reason is that more $HO^{\bullet}$ are generated from the decomposition of ozone which is promoted by metallic oxides as the active center in catalysts to enhance the oxidizing ability of the system. The synergistic reaction is formed in heterogeneous reaction among Cu/AC, Ni/AC and O_3. Heterogeneous reaction [47] means the interaction between surface structure of catalysts and adsorptive molecules which go against the elementary reaction steps. The coverage rate of the adsorptive species has been adjusted by the combined action between catalysts and ozone, which results in the rate constant changes of elementary reaction. This observation is in agreement with the findings reported by Khan [47] who prepared the active carbon loaded with chromic collosol which combined with ozonation for the degradation of organics in water. The adsorptive capacity of phenol and oxalic acid by O_3/Cu/AC is lower

than that of O_3/Ni/AC, the possible reason is that the number of NiO molecules in Ni/AC is more than CuO in Cu/AC, which means that when the molar mass is equal, more reaction active centers in Cu/AC are provided than Ni/AC. The opportunity of effective collision with ozone and the generation of $HO^{\bullet}$ which comes from the decomposition of ozone is improved. Then the oxidizing ability of the system will be enhanced.

3.3.2. The Impact of Catalysts Quantity on the Degradation of Phenol and Oxalic Acid

The relationships between reaction time and the removal efficiency of phenol and oxalic acid by catalytic ozonation system in different addition of Cu/AC and Ni/AC were analyzed in order to study the impact of catalysts quantity on degradation. Figure 3-11 (a) and (b) show the relationship between reaction time and the removal efficiency of phenol (a) and oxalic acid (b) in different addition of Cu/AC in the system of O_3/Cu/AC.

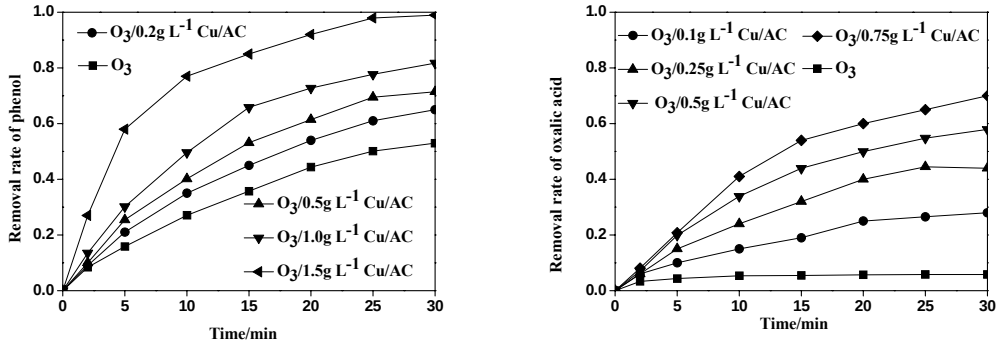


Figure 3-11. Evolution of phenol (a) and oxalic acid (b) concentrations in O_3/Cu/AC system during different dosage of Cu/AC.

It can be seen from Figure 3-11 that the removal efficiency of phenol and oxalic acid by O_3/Cu/AC increased with the increasing addition of Cu/AC. The removal efficiency of phenol by O_3/Cu/AC raised 30% compared to ozone when the usage of Cu/AC was 1.0g·L^{-1}, while the rate of improvement was 47% when the addition of Cu/AC was 1.5g·L^{-1}. The removal efficiency of oxalic acid by ozone was minor, while the proportion was only 5.8% at 30 min. When 0.5g·L^{-1} Cu/AC was added, the removal efficiency of oxalic acid increased nearly 52% than ozonation, and the rate of improvement was 64% when the addition of Cu/AC was 0.75g·L^{-1}.

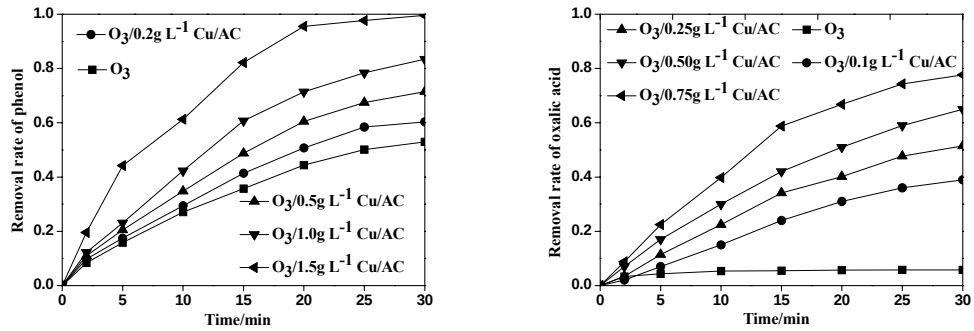


Figure 3-12. Evolution of phenol (a) and oxalic acid (b) concentrations in O_3/Ni/AC system during different dosage of Ni/AC.

It can be seen from Figure 3-12 that the removal efficiencies of both phenol and oxalic acid were increased inordinately with the increase of Ni/AC addition. The removal efficiency of phenol was 83% when the usage of Ni/AC was 1.0 $g \cdot L^{-1}$ in the system of O_3/Ni/AC at 30 min, and the phenol was nearly disappeared when the addition of Cu/AC was 1.5$g \cdot L^{-1}$. The removal efficiency of oxalic acid by ozone was minor, while proportion was only 5.8% at 30 min. When 0.5$g \cdot L^{-1}$ Ni/AC was added in the system of O_3/Ni/AC, the removal efficiency of oxalic acid was 65% which was increased 72% than ozonation.

The reason of lower removal efficiency of oxalic acid by catalytic ozonation is that oxalic acid is the end product of the oxidized removal of organics [48, 49] and the capacity of catalytic ozonation is limited and selective, and some related results are reported [18, 50, 51]. According to the comparison between different addition of catalysts and proportion of absorbed phenol and oxalic acid by catalytic ozonation, the removal efficiency of organics is enhanced greatly with the addition of catalysts and removal efficiency has a positive correlation with quantity. When the addition of catalyst is small, the active sites that can be used in the reaction are less, the collisional opportunities of metallic oxides with ozone reduce which lead to the lower generation of $HO^{\bullet}$ from ozone decomposition. Therefore, the catalytic process will be mainly completed by molecular ozone and the catalytic efficiency will be depressed. However, the active sites, the opportunities and contact area with ozone increased evidently with the increasing addition of catalysts. As a result, the ozone is dispersed evenly, the decomposed efficiency and the number of $HO^{\bullet}$ are increased, which gives rise to the removal efficiencies of phenol and oxalic acid.

3.3.3. The Impact of pH on the Degradation of Phenol and Oxalic Acid

The removal efficiency of phenol and oxalic acid in water by O_3/Cu/AC and O_3/Ni/AC in different values of pH were analyzed, in order to study the impact of pH on the degradation of organics. Figure 3-13 (a) and (b) show the relationship between reaction time and the removal efficiency of phenol and oxalic acid in the system of O_3/Cu/AC.

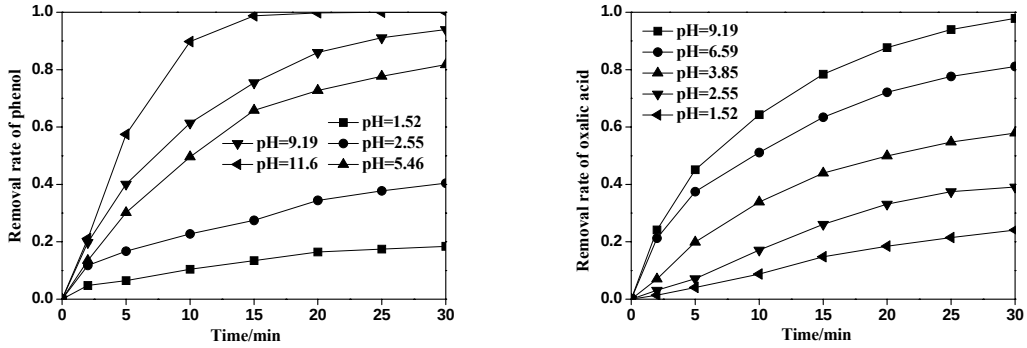


Figure 3-13. Evolution of phenol (a) and oxalic acid (b) concentrations in O_3/Cu/AC system under different initial pH.

It can be seen from Figure 3-13 (a) that the removal efficiency of phenol increased with the increase of the value of pH. The removal efficiency of phenol increased nearly 75% when the value of pH was 1.52 compared with the value of 11.6 at 15 min in the system. The reaction rate with phenol improved rapidly when the pH ranges from 9.16 to 11.6, especially

at 2min to 10min. The reaction rate of phenol decreased dramatically when the value of pH reduced to the acidic area, and the removal efficiency of phenol increased about 40% and 60% when the pH were 1.52 and 2.55 than the background pH of 5.46 at 30 min. As shown in the Figure 3-13 (b), the removal efficiency of oxalic acid increased with the increase of the value of pH. The removal proportion increased 19% compared to the background pH of 3.85 at 30min, while the proportion decreased about 40% when the pH was 1.52.

The relationships between reaction time and the removal efficiency of phenol and oxalic acid in the system of O_3/Ni/AC in different pH were shown in the Figure 3-14 (a) and (b).

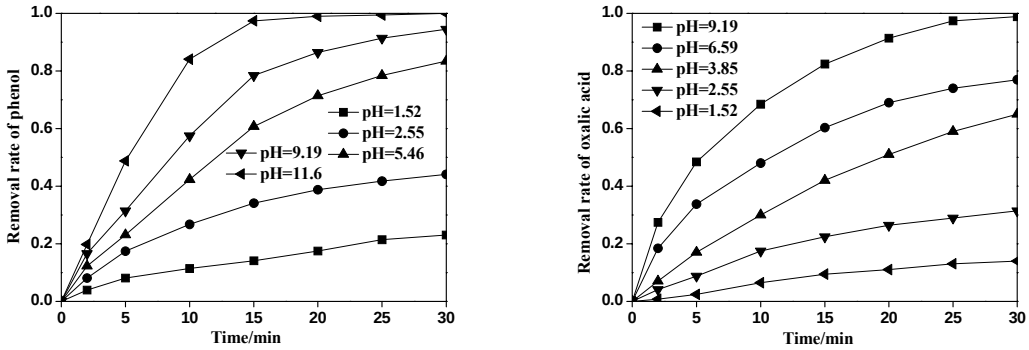


Figure 3-14. Evolution of phenol (a) and oxalic acid (b) concentrations in O_3/Ni/AC system under different initial pH.

It can be seen from Figure 3-14 (a) that the removal efficiency of phenol increased with the increasing of the value of pH in the system of O_3/Ni/AC. The removal efficiency of phenol decreased nearly 60% when the pH was 1.52 at 30 min, compared to the background pH value. When the value of pH increased to 11.6, the removal efficiency of phenol increased significantly and the proportion was nearly 100% at the time of 30 min. Figure 3-14 (b) shows that the removal efficiency of oxalic acid decreased with the reduction of pH value, and increased with the increase of pH. Compared to the background pH value, the removal efficiency of oxalic acid decreased 35% when the pH was 1.52 at 30 min, while the proportion increased 51% when the pH was 9.19.

The removal efficiencies of phenol and oxalic acid have a positive correlation with the value of pH in the system of O_3/Cu/AC and O_3/Ni/AC, which demonstrate that the degradation of phenol and oxalic acid proceed well under basic condition than acidic condition. The reason is that the decomposition of ozone is affected intensively by the value of pH, and there are enormous differences among the decomposition products. The decomposition of ozone follows the pseudo-first order reaction kinetics:

$$-\left(\frac{\mathrm{d}[\mathrm{O}_3]}{\mathrm{d}t}\right)_{\mathrm{pH}} = k'[\mathrm{O}_3] \tag{3-1}$$

Where k' is the pseudo-first order rate constant (min-1) in given pH.

The decomposition of ozone in water is affected intensively by the value of pH. The ozone is decomposed to higher-selective and lower oxidizability molecular ozone under

acidic condition, and the lower-selective and higher oxidizability $HO^{\bullet}$ is generated under basic condition. As a result, the removal efficiencies of phenol and oxalic acid decreased under the condition of acidic pH, while increased dramatically under basic condition in the system of catalytic ozonation.

4. MECHANISMS OF OZONE DEGRADATION OF PHENOL AND OXALIC ACID

In recent years, the advanced oxidation technology of catalytic ozonation attracted widespread attention for a series of advantages. There are more and more researches on the mechanisms of ozone degradation of organics in the aqueous solution. HO• is one of the radicals with the strongest reaction activity and oxidability, E^0=2.33V [48].

$$HO^{\bullet} + H^{+} + e^{-} \rightarrow H_2O \tag{4-1}$$

The reaction rate of HO• with organic molecule is usually $10^6 \sim 10^9\ M^{-1}\ S^{-1}$. It can be shown as type (4-2):

$$-\frac{d[M]}{dt} = k_{OH}[M][HO^{\bullet}] \tag{4-2}$$

After HO• reacted with organic molecular, free radicals would combine disproportionately and form many instable intermediates which will generate superoxide, aldehyde, acid, and H_2O_2 etc further. HO• has no reaction selectivity. It reacts with carbonate, bicarbonate and *t*-BuOH (tert butyl alcohol) rapidly and the reaction rate of HO• with *t*-BuOH is $k_{HO\bullet} = 5 \times 10^8\ M^{-1}\ s^{-1}$. The value is a bit less than that of with organic compounds. That is why the existence of free radicals inhibitors in the aqueous solution may cause free radicals chain reactions. The reactions of HO• and free radicals inhibitors are based on the oxidation removal processes of HO•. The high reactivity of HO• made it possible to react with all types of organics (ethylene, blood fat, aromatic, aliphatic) and inorganics (anion and cation).

4.1. The Effort of *T*-Buoh on the Catalytic Ozonation

It is generally thought that ozone react with organics in water in two ways. One is the direct oxidation of ozone molecules, and the other is the chain reaction of strong oxidant HO• decomposed by ozone. The decomposition of ozone in the water is mainly as HO• ($E°$ = 2.33V), much higher than the ozone $E°$ of 2.07V. The experiment analysis in part 3 showed that during the catalytic ozonation of phenol and oxalic acid, the addition of AC, Cu/AC and Ni/AC favored the removal of phenol and oxalic acid. In order to study in the catalytic ozonation system, whether HO• generated, and whether the activated carbon or a catalyst

promoted the decomposition of HO• by ozone, the addition of tert-butyl alcohol were tested during the testing processes. The different reaction mechanisms of catalytic ozonation were also studied. The reaction between HO• and *t*-BuOH was rapid, $k = 5 \times 10^8\ M^{-1}\ s^{-1}$, while the rapid with ozone is slow, $k = 0.03\ M^{-1}\ s^{-1}$. When added *t*-BuOH to the system, it can capture HO• quickly. Taking this feature, the generation of HO• can be detected accurately and quickly.

4.1.1. The Effort Of T-Buoh On The Catalytic Ozonation Of Phenol And Oxalic Acid

The concentrations of *t*-BuOH in the system of catalytic ozonation of phenol and oxalic acid were $0.20g \cdot L^{-1}$ and $0.050g \cdot L^{-1}$, respectively. Figure 4-1 (a), (b) represented the relationships of the removal rate of phenol and oxalic acid with the reaction time in the systems of O_3, O_3/AC and O_3/Cu/AC under the same condition of pH and TAB.

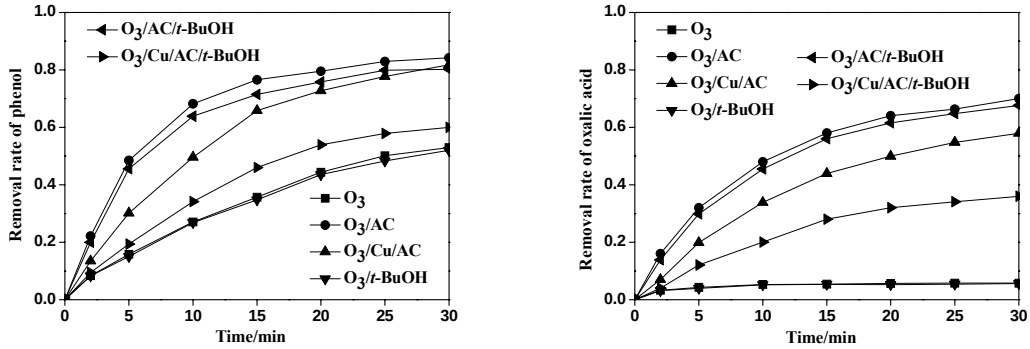


Figure 4-1. Evolution of phenol (a) and oxalic acid (b) concentrations in catalytic ozonation with *t*-BuOH.

Figure 4-1 showed that, after adding *t*-BuOH, the efforts of ozone and O_3/AC on the degradation of phenol and oxalic acid did not change significantly. The removal rates of phenol and oxalic acid decreased by 1%, 4% and 1%, 2% in the systems of ozone and O_3/AC after 30 min. The effort of *t*-BuOH on the removal of phenol and oxalic acid can be neglected. In O_3/Cu/AC system participated by *t*-BuOH, the removal rate of phenol and oxalic acid decreased with the reaction time. After 30min, the removal rate of phenol and oxalic acid decreased nearly 22% compared to the system without *t*-BuOH.

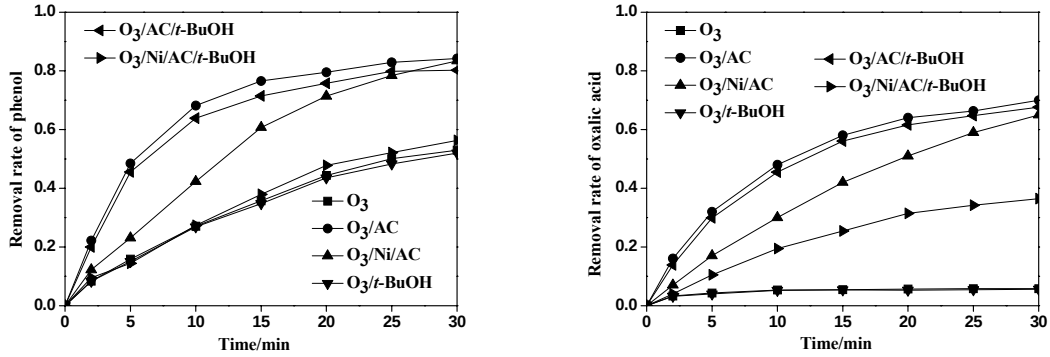


Figure 4-2. Evolution of phenol (a) and oxalic acid (b) concentrations in catalytic ozonation with *t*-BuOH.

Figure 4-2 (a) and (b) represented the relationships of the removal rate of phenol and oxalic acid with the reaction time in the systems of O_3, O_3/AC and O_3/Ni/AC under the same condition of pH and TAB.

Figure 4-2 (a) showed that the efforts of ozone and O_3/AC on the degradation of phenol and oxalic acid did not change significantly after adding *t*-BuOH. In the system of O_3/Ni/AC, the addition of *t*-BuOH weakened the removal of phenol and oxalic acid greatly. After 30 min, the removal rate of phenol and oxalic acid decreased 22% and 29% respectively compared to the system without *t*-BuOH.

It can be seen from the experiment, after the addition of *t*-BuOH, the efforts of ozone and O_3/AC on the removal of phenol and oxalic acid did not change significantly. This is because phenol and oxalic acid were almost removed by ozone molecules in the reaction between ozone and phenol or oxalic acid. While in the reaction between O_3/AC and phenol or oxalic acid, phenol and oxalic acid were removed by the adsorption of ozone molecules and AC. The catalytic effort of AC only decomposed ozone to a small amount of HO•. The reaction constant of *t*-BuOH with HO• is 5×10^8 M^{-1} s^{-1}. As a strong inhibitor of HO•, *t*-BuOH has a strong capture capacity to HO•. The decrease of removal rates of phenol and oxalic acid was contributed to HO•. Certain amount of HO• exist in the system of the combination of catalyst and ozone with phenol and oxalic acid exist. The producing of HO• decomposed by ozone was promoted by Cu/AC and Ni/AC. The oxidative capacity of the system was significantly improved. The degradation of phenol and oxalic acid by O_3/Cu/AC and O_3/Ni/AC followed the mechanism of HO•

4.1.2. The Effort of T-Buoh Concentration on the Catalytic Ozonation Of Phenol and Oxalic Acid

Part 4.1.1 showed the addition of *t*-BuOH reduced the removal rate of phenol and oxalic acid in the O_3/Cu/AC and O_3/Ni/AC systems significantly. In order to investigate the relationship between the added amount of *t*-BuOH and the removal rate of phenol and oxalic acid in the system catalyst combined with ozone, different concentrations of *t*-BuOH were added to reaction systems. Figure 4-3 showed the relationship between the *t*-BuOH concentration and the removal rate of phenol and oxalic acid with the time in the O_3/Cu/AC system under the same pH condition.

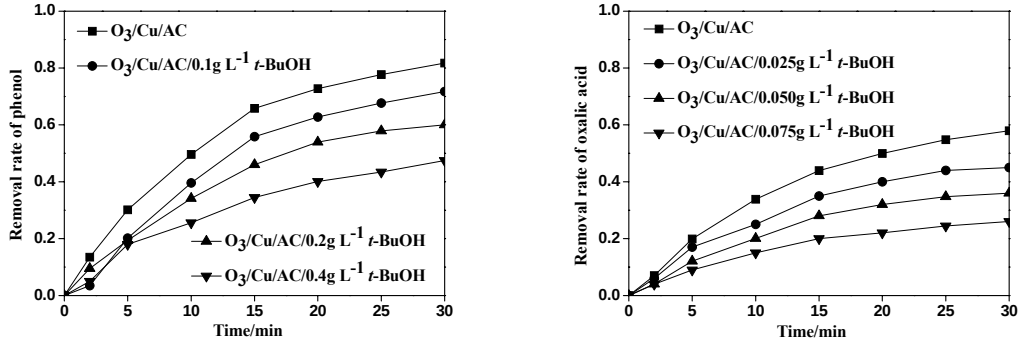


Figure 4-3. Evolution of phenol (a) and oxalic acid (b) concentrations in O_3/Cu/AC system under different dosage of *t*-BuOH.

It can be seen from Figure 4-3, after 30 min, when the concentration of *t*-BuOH were 0.1g • L^{-1}, 0.2g • L^{-1}, and 0.4g • L^{-1}, the removal rate of phenol decreased by 10 %, 21.7% and 34.2%; when the concentration of *t*-BuOH added were 0.025g • L^{-1}, 0.050g • L^{-1}, and 0.075g • L^{-1}, the removal rate of oxalic acid decreased by 12.9%, 21.9% and 31.9% compared to the system without *t*-BuOH.

Figure 4-4 (a) and Figure 4-4 (b) showed the relationship between the *t*-BuOH concentration and the removal rate of phenol and oxalic acid with the time in the O_3/Ni/AC system.

After 30 min, when *t*-BuOH concentration was 0.4g • L^{-1}, the phenol removal rate decreased by 34.2%; when *t*-BuOH concentration was 0.075g • L^{-1}, the oxalic acid removal rate decreased by 31.9%.

Figure 4-4 showed that the removal rate of phenol and oxalic acid declined with the addition of *t*-BuOH. From the effort of *t*-BuOH concentration on the removal of phenol and oxalic acid with the combination of catalyst with ozone, the addition of *t*-BuOH and the decrease of removal rate were positively correlated. This indicates that HO• existed in the O_3/Cu/AC, O_3/Ni/AC systems. The addition of Cu/AC and Ni/AC promoted the production of HO• by ozone. It was found that he degradation reactions follow HO• reaction mechanism.

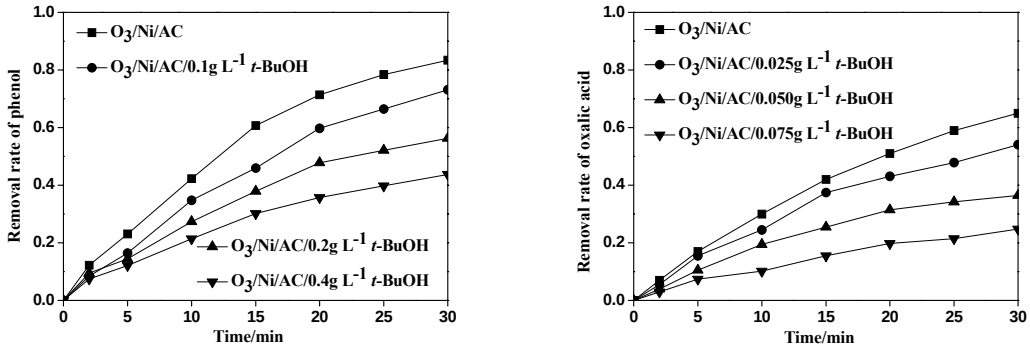


Figure 4-4. Evolution of concentrations of phenol (a) and oxalic acid (b) in O_3/Ni/AC system under different dosage of *t*-BuOH.

4.2. Kinetics of Heterogeneous Catalytic Oxidation

Classical Langmuir-Hinshelwood heterogeneous catalytic reaction kinetics insists that the heterogeneous catalytic reactions happen on the surface of solid catalyst [117]. Firstly, all reactants have to be adsorbed on the catalyst surface. The reaction between adsorbed species and other species is called surface reaction. The product generated on the surface will be desorbed then. In other words, heterogeneous catalysis has three elementary steps: adsorption, surface reaction and desorption.

The degradation of phenol and oxalic acid is accomplished through the heterogeneous reaction. The direct reaction of ozone molecular, an indirect non-selective free radical reaction which happen in the solution system and catalyst surface. According to the dynamics theory of Valdes and Zaror [52], simplified and non-equilibrium reaction mechanism can be expressed as follows:

$$A + O_3 \rightarrow Product \quad -\frac{dC_{A_1}}{dt} = k_1^A C_{O_3} C_A \tag{4-3}$$

$$A + HO^{\bullet} \rightarrow Product \quad -\frac{dC_{A_2}}{dt} = k_2^A C_{HO\bullet} C_A \tag{4-4}$$

$$A + Ar \rightarrow Product \quad -\frac{dC_{A_3}}{dt} = k_3^A C_{Ar} C_A \tag{4-5}$$

$$A + Ar + O_3 \rightarrow Product \quad -\frac{dC_{A_4}}{dt} = k_4^A C_{Ar} C_{O_3} C_A \tag{4-6}$$

$$A + Ar + HO^{\bullet} \rightarrow Product \quad -\frac{dC_{A_5}}{dt} = k_5^A C_{Ar} C_{HO\bullet} C_A \tag{4-7}$$

Where A represents the pollutants (phenol or oxalic acid), Ar represents the surface active centers of activated carbon or catalyst (such as the surface oxygen groups, metal active center, multi-electronic carbon center). The degradation rates of phenol and oxalic acid in the heterogeneous catalytic ozonation are approximately followed first order reaction. The degradation rate of total pollutant A can be expressed by the following:

$$-\frac{dC_{A\ overall}}{dt} = [k_1^A C_{O_3} + k_2^A C_{HO\bullet} + (k_3^A + k_4^A C_{O_3} + k_5^A C_{HO\bullet})C_{Ar}]C_A$$
$$= k_{overall}^A C_A \tag{4-8}$$

Where k_1^A and k_2^A represent the reaction rate constant of O_3 and HO• with phenol in the homogeneous system. k_3^A, k_4^A and k_5^A represent the pollutants degradation reaction constants by adsorption, ozone oxidation and HO• in the non-homogeneous system. In the presence of *t*-BuOH, equations can be amended as follows [47]:

$$-\frac{dC_{A\ overall}}{dt} = [k_1^A C_{O_3} + (k_3^A + k_4^A C_{O_3})C_{Ar}]C_A = k_O^A C_A \tag{4-9}$$

Where $k_{overall}^A$ and k_O^A represent the total reaction constant whthout and with *t*-BuOH. Using the same method, the adsorbed pollutants reaction constant equation can be got

$$-\frac{dC_{A\,ads}}{dt} = k_3^A C_{Ar} C_A = k_{ads}^A C_A \tag{4-10}$$

Using the above equation, the pollutants removal reaction constants of ozone alone, HO• and adsorption in the heterogeneous catalytic ozonation process can be calculated. Where equation (4-10) is obtained by experiment the mechanism of catalytic ozonation of pollutants can be explained by the obtained single rate constant

$$\delta^{ads+O_3} = k_O^A \tag{4-11}$$

$$\delta^{HO^\bullet} = k_{overall}^A - k_O^A \tag{4-12}$$

$$\delta^{ads} = k_{ads}^A \tag{4-13}$$

$$\delta^{O_3} = \delta^{ads+O_3} - \delta^{ads} \tag{4-14}$$

Figure 4-5 (a) and (b) showed the δ^{O_3}, $\delta^{HO^\bullet}$ and δ^{ads} calculated from the test data and above formula in the processed of O_3/AC, O_3/Cu/AC and O_3/Ni/AC.

It can be seen from Figure 4-5, in the oxidation systems of heterogeneous catalytic ozonation of phenol and oxalic acid, the largest proportion of HO• existed in the O_3/Ni/AC reaction system. In the O_3/AC reaction system, the main removal ways were molecular ozone and adsorption. The proportion of HO• in the O_3/Cu/AC system was little less than that of O_3/Ni/AC.

The difference of the two reaction activation energy can be calculated by Arrhenius equation. The effort of activated carbon and catalyst on the reaction activation energy in the catalytic ozonation can be also investigated. After the addition of AC, Cu/AC or Ni/AC, the activation energy of the ozone system changed. It can be obtained by the Arrhenius equation:

$$\frac{k_1}{k_2} = e^{\frac{Ea_2}{RT} - \frac{Ea_1}{RT}} \tag{4-15}$$

After removal of the log on both sides of the equation,

$$Ea_2 - Ea_1 = RT \ln(\frac{k_1}{k_2}) \tag{4-16}$$

As the different reaction rate constants were known, the D-value of the two reaction activation energy can be calculated using Equation 4-16, and then explored the difference between ozonation alone and catalyst ozonation. Figure 4-6 showed the different reaction processes after the removal of adsorption effort. The difference of activation energy between the catalytic reaction and ozone alone was caused by the production of HO•.

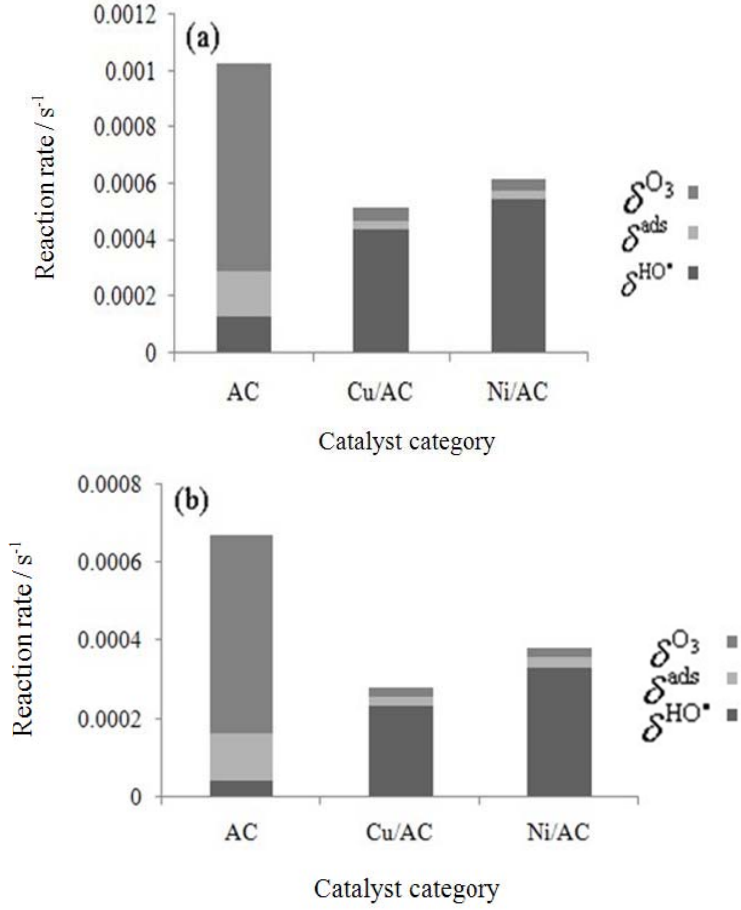


Figure 4-5. Rate constants due to individual contribution of different catalytic ozonation for degradation of phenol (a) and oxalic acid (b).

It can be seen from Figure 4-6, after adding activated carbon to the ozonation of phenol and oxalic acid system, the activation energy decreased by 811J • mol^{-1} and 687J • mol^{-1}. In O_3/Cu/AC system, the activation energy of phenol reduced 7.393KJ • mol^{-1}, the activation energy of oxalic acid reduced 7.6KJ • mol^{-1}. In the Ni/AC combined with ozone to react with phenol and oxalic acid system, activation energy decreased by 7.824KJ • mol^{-1} and 8.055KJ • mol^{-1} than the ozone alone system. Catalyst and reactants produced the unstable intermediate compound, changed the reaction pathway, and reduced the activation energy. This is because the chemical reaction of molecules on a solid surface [122]. The occurrence of molecular deformation, breaking of chemical bonds, atoms rearrangement and other microscopic

process changed the reaction pathway and reduced the activation energy, and thus acted as a catalyst.

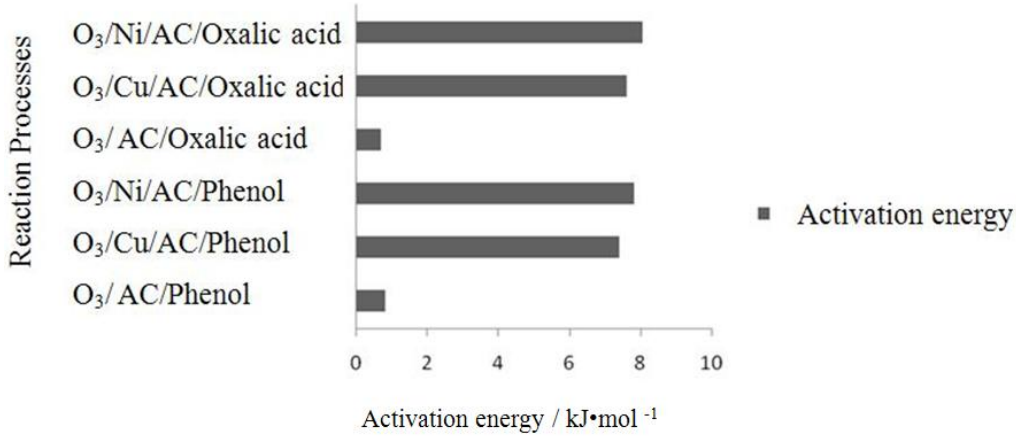


Figure 4-6. The activation energy difference between catalytic ozonation and ozoantion alone.

From the above test results, there are some differences in the degradation mechanisms of phenol and oxalic acid. In O_3/AC system, the degradation of phenol was mainly through molecular ozone and AC adsorption in which HO• took a small proportion. In O_3/Ni/AC and O_3/Cu/AC systems, phenol removal was mainly done by HO•. The ozone molecules and adsorption contributed little in the processes. $\delta^{HO^\bullet}_{O_3/Cu/AC}$ and $\delta^{HO^\bullet}_{O_3/Ni/AC}$ represent the HO• generated reaction constants in the degradation systems of O_3/Cu/AC and O_3/Ni/AC. The calculation showed that, in the heterogeneous catalytic ozonation of phenol and oxalic acid systems, $\delta^{HO^\bullet}_{O_3/Cu/AC}$ and $\delta^{HO^\bullet}_{O_3/Ni/AC}$ decreased by 1.09×10^{-4} s^{-1} and 1.0×10^{-4} s^{-1}, respectively. The small reaction rate constant indicated a small amount of HO• during the reaction. The HO• promoted by Ni/AC was more than that of Cu/AC. In addition, after adding *t*-BuOH, the removal rate of phenol and oxalic acid in O_3/Ni/AC system is about 8% higher than that in O_3/Cu/AC system. The difference of catalysis between Cu/AC and Ni/AC was mainly due to the differences of effective metal active component content and differences in surface properties of catalysts. After calculation, the number of effective metal oxide material molecules of Ni/AC was slightly higher than that of Cu/AC. When added the same dosage of Ni/AC and Cu/AC in the heterogeneous reaction system, the amount of effective metal active component and the surface area of Ni/AC were more than that of Cu/AC 18.8% and 5%, respectively.

The activity of a solid catalyst is often used to characterize the performance of catalyst. During the heterogeneous catalytic ozonation of phenol and oxalic acid processes, Ni/AC had a greater contact area with ozone compared to Cu/AC. The metal oxides molecules had a greater possibility to collide with ozone. There are more reactivity centers in the system and ozone are easier to decompose to HO•. The amount of HO• generated by ozone increases with more conversions and higher conversion rate. There are strong correlation between rate constant and the concentration of active sites, while the active site concentration depends on

the properties of the catalyst. The redox behavior of catalyst is complex and closely related with the catalyst structure and composition. When the metal cluster size decreases, the metal-support interaction becomes stronger. This interaction can change the electronic structure of metal, thus affecting the catalytic activity. In addition, the type of surface structure may cause the reaction rate increases. When the metal clusters increases, the surface atoms contained or the active site becomes more abundant [47]. The BET and pore size distribution results indicated that aperture of Ni/AC is slightly larger than Cu/AC. There are more $HO^{\bullet}$ generated in O_3/Ni/AC system. Therefore, the removal rates of phenol and oxalic acid in O_3/Ni/AC were both higher than in O_3/Cu/AC.

4.3. Comparison of Heterogeneous Catalytic Ozonation Mechanisms

According to the experiment results, the following possible reaction mechanisms of phenol and oxalic acid in O_3/Cu/AC and O_3/Ni/AC systems are proposed [53].

Pollutants were firstly adsorbed on the catalyst surface:

$$A + Ar \leftrightarrow A\text{-}Ar \tag{4-17}$$

Contaminants adsorbed on the metal active center of the catalyst surface:

$$A\text{-}Ar + M\text{-}Ar \leftrightarrow A\text{-}M\text{-}Ar + Ar \tag{4-18}$$

Ozone reaction in the system:

$$O_3 + H_2O \rightarrow 2HO^{\bullet} + O_2 \quad k_2 = 1.1\times10^{-4}\ M^{-1}s^{-1} \tag{4-19}$$

$$O_3 + OH^- \rightarrow O_2^{\bullet-} + HO_2^{\bullet} \quad k_2 = 70\ M^{-1}s^{-1} \tag{4-20}$$

$$O_3 + HO^{\bullet} \rightarrow O_2 + HO_2^{\bullet} \leftrightarrow O_2^{\bullet-} + H^+ \tag{4-21}$$

$$O_3 + HO_2^{\bullet} \leftrightarrow 2O_2 + HO^{\bullet} \quad k_2 = 1.6\times10^{9}\ M^{-1}s^{-1} \tag{4-22}$$

$$2HO_2^{\bullet} \rightarrow O_2 + H_2O_2 \tag{4-23}$$

Pollutants reacted with HO • decomposed by ozone on the catalyst surface in the system:

$$HO^{\bullet} + A\text{-}M\text{-}Ar \leftrightarrow P\text{-}Ar + M\text{-}Ar \tag{4-24}$$

Pollutants intermediates desorped on the catalyst surface, which were represents the pollutants; Ar represents the active centers of catalystl M represents metals contained in the catalyst; P-Ar represent the pollutants reaction intermediates. The possible mechanisms in the processes of degradation of phenol and oxalic acid in O_3/Cu/AC and O_3/Ni/AC systems are: pollutants is adsorbed on the catalyst surface at first; catalyst metal active center was then promoted the decomposition of ozone and generated HO•; HO• reacted with the pollutants on the catalyst surface; the contaminants intermediate eventually desorbed on the catalyst surface.

The differences of catalytic activity [47] were due to the affinity of the catalyst surface, exposure of the crystal surface and the grain size. The catalyst surface structure changes when the two factors. It is because the number of coordination atoms changed and the relative number on the surface changed and the relative proportion of surface atoms also changed. The differences of thermal stability, selectivity, porosity, mechanical strength, and anti-toxic of heterogeneous catalysts lead to different activity of the catalyst and conversion rates. The change of catalyst affinity is due to the change of catalyst surface structure, while the change of surface structure is due to the formation of alloy from catalytic metal or the addition of other improved elements. The BET of catalyst increases with the catalyst dispersion. The ratio of the number of atoms exposed to the surface and the total number of metal atoms is named as metal dispersion on the catalyst carrier. However, the location and property of the surface atoms are different. They can be distributed in the side, angle and platform, which can also be adsorbed atoms. The distribution of different types of surface atoms changed largely with the dispersion. Therefore, the catalytic reaction happening on the catalytic active sites will change with the dispersion for the concentration of active sites. The activity changed greatly with the dispersion of catalyst (structure-sensitive reaction). If more than one reaction happens, the dispersion will also affect the catalyst selectivity.

4.4. The pH Change in the Process of Catalytic Ozonation

Figure 4-7 (a) showed that the final pH was smaller than the initial pH in all reactions ozone participated. This was because the reactions of chain scission and ring opening happened after the phenol oxidized by ozone. Small molecules of organic acids, aldehydes and some esters produced. These small molecules are difficult to be oxidized by ozone further. These acidic molecules accumulated in the reaction system, acidized the solution system. According to other studies [52, 53], phenol will be oxidized to maleic acid, fulvic acid, oxalic acid and formic acid and other substances before complete mineralization. These small molecules increase the acidity of the solution.

Figure 4-7 (b) revealed that pH changed little in the process of oxalic acid oxidized by ozone. It is mainly because oxalic acid is one of the final products of phenol oxidation [54] which is difficult to be oxidized by molecular ozone. Since the oxygen groups and basic groups of activated carbon surface [9] and metal oxide of catalysts were weak alkaline, the pH in the adsorption processes increased gradually. The final pH of phenol oxidized by ozonation is little higher than the ozone alone. In the system of oxalic acid catalytic ozonation, the properties of activated carbon and catalyst in the acid system changed. The combined effort of surface oxygen groups and metal reactive center make the value of pH increased gradually in the catalytic ozonation process.

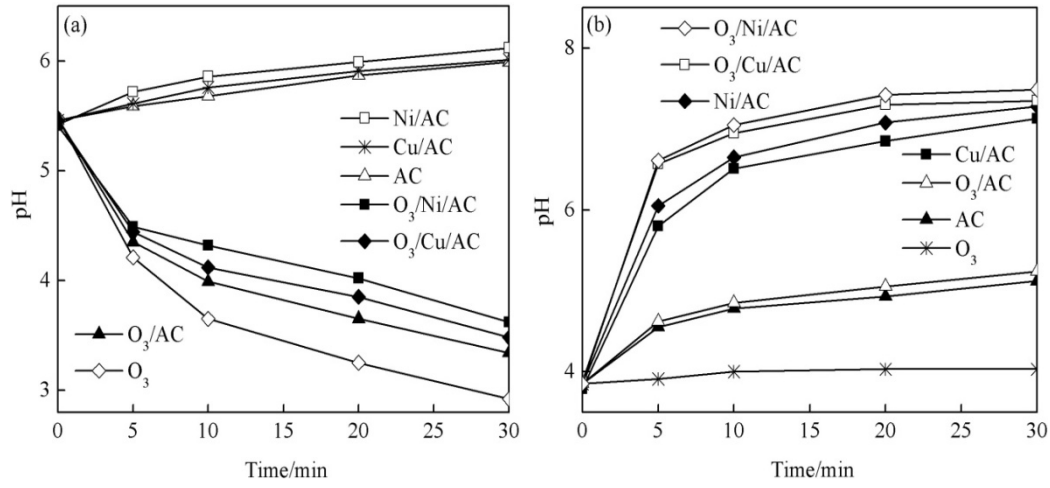


Figure 4-7. Evolution of pH values of phenol (a) and oxalic acid (b) in different reaction processes.

4.5. Chemical Stability of Cu / AC and Ni / AC

To study the chemical stability of Cu/AC and Ni/AC in catalytic ozonation process, the concentration of copper ion and nickel ion in phenol and oxalic acid degradation of O_3/Ni/AC and O_3/Cu/AC systems were measured.

In the reaction of O_3/Cu/AC with phenol or oxalic acid, the maximum precipitation concentration of Cu^{2+} was 4mg • L^{-1}; In the reaction of O_3/Ni/AC with phenol or oxalic acid, the maximum precipitation concentration of Ni^{2+} was 5mg • L^{-1}. The Ni^{2+} precipitation concentration of Ni/AC catalytic ozonation reaction is higher than precipitation of Cu^{2+} precipitation concentration of Cu/AC. It is because there may be trace nickel in the preparation of catalysts, while there were none metal elemental generated in Cu/AC. Therefore in the process of ozone reaction, Ni/AC was more possible to precipitate into metal ions. The precipitation amount of Ni^{2+} was slightly larger than Cu^{2+}. The precipitation percentage of Cu^{2+} and Ni^{2+} is less than 0.5% after calculation. The results showed the high stability of Cu/AC and Ni/AC in the catalytic ozonation processes.

In the reaction of O_3/Cu/AC with phenol and oxalic acid, when reused the fourth time, the removal rate of phenol and oxalic acid decreased by only 2% and 3% compared to the fist time. Similarly, in the reaction of O_3/Ni/AC with phenol and oxalic acid, when it is reused until the fourth time, the removal rates of phenol and oxalic acid decreased by only 3% and 5% compared to the fist time. It showed the reuse of Cu/AC and Ni/AC had little effect on the catalytic activity and stability. It is easy to be recycled with high efficiency.

CONCLUSIONS

The activated carbon loaded of copper and nickel prepared at low temperature were applied to the catalytic ozonation degradation of phenol and oxalate. This study has investigated the catalyst properties, degradation mechanisms and reaction kinetics. The following conclusions were gained:

[1] Copper and nickel exist completely in the form of oxides in catalyst Cu/AC and Ni/AC after burning, which formed in the form of CuO and NiO. The presence of small amounts of elemental Ni in Ni/AC is caused by the low temperature of nickel nitrate during preparation. Lacking of oxygen in a short time, C reduced NiO to a very small amount of Ni metal. After Cu/AC and Ni/AC calcined, activated carbon surface structure changed greatly. Cu/AC surface is filled with uniformly distributed rod-like structure. CuO loaded in the Cu/AC surface, while NiO mainly exists in 300 nm long rod-like structure in the Ni/AC surface.

[2] The N_2 adsorption-desorption isotherms showed that the adsorption platform of Cu/AC and Ni/AC was significantly lower than that of AC. The metal oxides occupied the surface of the catalyst, causing the great decrease of effective absorption area of catalysts. Compared to AC, the specific surface area pore surface area, surface area and pore volume of Cu/AC decreased by 50.7%, 62.9%, 34.8% and 62.4%, while those of Ni/AC reduced by 47.9%, 60.6% 31.0% and 60.7%. The average pore size of Cu/AC and Ni/AC both increased.

[3] After reacted at 30 min, the adsorption rate of phenol and oxalate using Cu/AC and Ni/AC were 5% and 4%, while that of AC was 20%. This is mainly because of the great change of surface functional groups and structure of catalyst active carbon after being calcined. The polar of carbon reduced, so the adsorption capacity of organic declined. The adsorption capacity of active carbon toward phenol, humic acid, oxalic acid and other hydrophobic organics declined greatly after modified oxidation. The removal rate of phenol using ozonation along was 53% at 30 min, and that of oxalic acid was 5.8%. In the system of O_3/AC, the removal of phenol and oxalic acid increased by 31% and 64%, respectively. In the O_3/Cu/AC system, increased by nearly 29% and 52%, and in O_3/Ni/AC system increased by 30.4% and 59%. This was mainly due to the specific surface area of AC was much higher than Cu/AC and Ni/AC. The adsorption of phenol and oxalic acid on unit area was much stronger. The results of catalytic ozonation showed that the degradation of phenol and oxalic acid in O_3/Cu/AC and O_3/Ni/AC systems are catalytic ozonation.

[4] In the catalytic ozonation systems, the catalyst dosage was proportional to the removal rate of phenol and oxalic acid. When the catalyst dosage increased, the reactivity sites of system, the possibility of metal oxides to contact with ozone, the probability of effective collision all increased. The catalyst promoted the ozone to decomposed more HO•. The oxidative capacity of system improved significantly. In O_3/Cu/AC and O_3/Ni/AC systems, the removal rates of phenol and oxalic acid are related to initial solution pH value. They are easier to be degraded in the basic solution than in acid solution. The decomposition of ozone produces mainly HO•.

[5] The reaction rate constant $\delta^{HO^\bullet}_{O_3/Cu/AC}$ is smaller than $\delta^{HO^\bullet}_{O_3/Ni/AC}$, indicating that the HO• promoted by Ni/AC was more than Cu/AC. During the degradation processes of phenol and oxalic acid, the ozone molecules reaction is mainly in the ozone alone system. Ozone molecules, AC adsorption and AC catalysis were mainly in O_3/AC system. The O_3/Cu/AC and O_3/Ni/AC can promote the production of HO• by ozone. The degradation of phenol and oxalate followed the mechanism of HO•. There is a synergistic effect between ozone and catalyst (Cu/AC and Ni/AC).

[6] The degradation mechanism model of phenol and oxalic acid in O_3/Cu/AC and O_3/Ni/AC is mainly: The pollutants are adsorbed on the catalyst surface firstly; catalyst metal active centers promote the production of HO• by ozone; HO• reacts with the pollutant adsorbed on the surface; pollutants desorbed from catalyst surface.

[7] In the O_3, O_3/AC, O_3/Cu/AC and O_3/Ni/AC systems, phenol is oxidized to a series of small acid molecules by O_3 or HO•. The pH of solution is lower. In the AC, Cu/AC and Ni/AC system, the solution pH increased. It is caused by the rich basic groups and oxygen groups on AC surface and metal oxides in catalyst. In O_3, AC, Cu/AC, Ni/AC, O_3/AC, O_3/Cu/AC and O_3/Ni/AC systems, the oxalic acid solution pH increased. This is due to the combination effort of surface oxygen groups and reactive metal centers when AC and catalyst were used in acid systems.

[8] In the reaction of phenol and oxalic acid in O_3/Cu/AC and O_3/Ni/AC systems, the max precipitation percentages of copper ion and nickel ion were less than 0.5%. This indicates that the two catalysts are stable and easy to be recycled.

REFERENCES

[1] Kasprzyk-hordern B, Ziółek M, Nawrocki J. Catalytic ozonation and methods of enhancing molecular ozone reactions in water treatment [J]. Applied Catalysis B: Environmental, 2003, 46(4): 639-669

[2] Bakker, S. H. Ozone depletion, chemistry, and impacts [M]. Hauppauge, N.Y.: Nova Science, 2009: 17-52

[3] Hewes C. G., Davison R. R. Renovation of waste water by ozonation [J]. AIChE Symposium Series, 1973, 69(129): 71-80

[4] Pines D. S., Reckhow D. A. Effect of dissolved cobalt (II) on the ozonation of oxalic acid [J]. Env. Sci. Tech., 2002, 36 (19): 4046-4051

[5] Chen J. W., Hui C., Keller T., Smith G. Catalytic ozonation in aqueous system, AIChE Symposium Series, 1977, 73: 206-212

[6] Fernando J. Beltrán, Francisco J. Rivas, Ramón Montero-de-Espinosa. Catalytic ozonation of oxalic acid in an aqueous TiO_2 slurry reactor [J]. Applied Catalysis B: Environmental, 2002, 39(3): 221-231

[7] Tong S., Liu W., Leng W., Zhang Q., Characteristics of MnO_2 catalytic ozonation of sulfosalicylic acid and propionic acid in water [J]. Chemosphere, 2003, 50(10): 1359-1364

[8] Ernst M., Lurot F., Schorotter J. C. Catalytic ozonation of refractory organic model compounds in aqueous soluiton by alumin oxide [J]. Appl. Catal. B., 2004, 47(1): 15-25

[9] Kasprzyk-Hordern B., Raczyk-Stanisławiak U., Swietlik J., Nawrocki J. Catalytic ozonation of natural organic matter on alumina [J]. Applied Catalysis B: Environmental, 2006, 62(3/4): 345-358

[10] Zhang Tao, Chen Weipeng, Ma Jun, Qiang Zhimin. Minimizing bromate formation with cerium dioxide during ozonation of bromide-containing water [J]. Water Research, 2008, 42(14): 3651-3658

[11] P. C. C. Faria, D. C. M. Monteiro, J. J. M. Órfão, M. F. R. Pereira. Cerium, manganese and cobalt oxides as catalysts for the ozonation of selected organic compounds [J].

Chemosphere, 2009, 74(6): 818-824
[12] Haeryong Jung, Heechul Choi. Catalytic decomposition of ozone and para-Chlorobenzoic acid (*p*-CBA) in the presence of nanosized ZnO [J]. Applied Catalysis B: Environmental, 2006, 66(3/4): 288-294
[13] Zhang Xinyu, Li Xin, Wu Qin. Investigation of the catalytic activity for ozonation on the surface of NiO nano-particles [J]. Chemical Physics Letters, 2009, 479(4/6): 310-315
[14] Zhang Tao, Li Chunjuan, Ma Jun, Tian Hai, Qiang Zhimin.Surface hydroxyl groups of synthetic α-FeOOH in promoting $HO^{\bullet}$ generation from aqueous ozone: Property and activity relationship[J]. Applied Catalysis B: Environmental, 2008, 82(1/2): 131-137
[15] Qu Xianfeng, Zheng Jingtang, Zhang Yanzong. Catalytic ozonation of phenolic wastewater with activated carbon fiber in a fluid bed reactor [J]. Journal of Colloid and Interface Science, 2007, 309(2): 429-434
[16] Fernando J. Beltrán, Francisco J. Rivas, Lidia A. Fernández, Pedro M. Álvarez, Ramón Montero-de-Espinosa. Kinetics of Catalytic Ozonation of Oxalic Acid in Water with Activated Carbon [J]. Ind. Eng. Chem. Res., 2002, 41(25): 6510-6517
[17] P. C. C. Faria, J. J. M. Orfaó, M. F. R. Pereira. Catalytic ozonation of sulfonated aromatic compounds in the presence of activated carbon [J]. Applied Catalysis B: Environmental, 2008, 83(1/2): 150-159
[18] P. C. C. Faria, J. J. M. Orfaó, M. F. R. Pereira. Activated carbon catalytic ozonation of oxamic and oxalic acids [J]. Applied Catalysis B: Environmental, 2008, 79(3): 237-243
[19] A. H. Konsowa, M. E. Ossman, Yongsheng Chen, John C. Crittenden. Decolorization of industrial wastewater by ozonation followed by adsorption on activated carbon [J]. Journal of Hazardous Materials, 2010, 176 (1/3): 181-185
[20] Colin Cooper M., Robbie Burch. An investigation of catalytic ozonation for the oxidation of halocarbons in drinking water preparation [J]. Wat. Res., 1999, 33(18): 3695-3700
[21] Fernando J. Beltrán, Francisco J. Rivas, Ramón Montero-de-Espinosa. Ozone Enhanced Oxidation of Oxalic Acid in Water with Cobalt Catalysts. 2. Heterogeneous Catalytic Ozonation [J]. Ind. Eng. Chem. Res., 2003, 42(14), 3218-3224
[22] Qu Jiuhui, Li Haiyan, Liu Huijuan, He Hong. Ozonation of alachlor catalyzed by Cu/Al_2O_3 in water [J]. Catalysis Today, 2004, 90(3/4): 291-296
[23] Fernando J. Beltrán, Francisco J. Rivas, Ramón Montero-de-Espinosa. Iron type catalysts for the ozonation of oxalic acid in water [J]. Water Research, 2005, 39(15): 3553-3564
[24] M. Stoyanova, P. Konova, P. Nikolov, A. Naydenov, St. Christoskova, D. Mehandjiev. Alumina-supported nickel oxide for ozone decomposition and catalytic ozonation of CO and VOCs [J]. Chemical Engineering Journal, 2006, 122(1/2): 41-46
[25] Yang Li, Hu Chun, Nie Yulun, Qu Jiuhui. Catalytic ozonation of selected pharmaceuticals over mesoporous alumina-supported manganese oxide[J]. Environ. Sci. Technol., 2009, 43(7): 2525-2529
[26] Zhao Lei, Ma Jun, Sun Zhizhong, Zhai Xuedong. Mechanism of influence of initial pH on the degradation of nitrobenzene in aqueous solution by ceramic honeycomb catalytic ozonation [J]. Environmental Science and Technology, 2008, 42(11): 4002-4007
[27] Zhao Lei, Ma Jun, Sun Zhizhong. Oxidation products and pathway of ceramic honeycomb-catalyzed ozonation for the degradation of nitrobenzene in aqueous solution [J]. Applied Catalyst B: Environmental, 2008, 79(3): 244-253

[28] Zhao Lei, Ma Jun, Sun Zhizhong, Zhai Xuedong. Catalytic ozonation for the degradation of nitrobenzene in aqueous solution by ceramic honeycomb supported manganese [J]. Applied Catalyst B: Environmental, 2008, 83(3/4): 256-264

[29] Zhao Lei, Sun Zhizhong, Ma Jun, Liu Huiling. Influencing mechanism of bicarbonate on the catalytic ozonation of nitrobenzene in aqueous solution by ceramic honeycomb supported manganese [J]. Journal of Molecular Catalysis A: Chemical, 2010, 322(1/2): 26-32

[30] Ma Jun, Zhang Tao, Chen Zhonglin, Sui Minghao, Li Xueyan. Pathway of Aqueous Ferric Hydroxide Catalyzed Ozone Decomposition and Ozonation of Trace Nitrobenzen. Environmental Science [J], 2005, 26(2): 78-82

[31] Sui Minghao, Ma Jun, Sheng Li. MnOx/GAC Catalytic Ozonation for Degradation of Nitrobenzene. Modern Chemical Industry [J], 2005, 25(8): 31-37

[32] Faria P, Órfão J, Pereira M. A novel ceria-activated carbon composite for the catalytic ozonation of carboxylic acids [J]. Catalysis Communications, 2008, 9(11/12): 2121-2126

[33] Li Laisheng, Ye Weiying, Zhang Qiuyun, Sun Fengqiang, Lu Ping, Li Xukai. Catalytic ozonation of dimethyl phthalate over cerium supported on activated carbon [J]. Journal of Hazardous Materials, 2009, 170(1): 411-416

[34] Faria P. C. C., Órfão J. J. M. Activated carbon and ceria catalysts applied to the catalytic ozonation of dyes and textile effluents [J]. Applied Catalysis B: Environmental, 2009, 88(3/4): 341-350

[35] Li Xukai, Zhang Qiuyun, Tang Lili, Lu Ping, Sun Fengqiang, Li Laisheng. Catalytic ozonation of *p*-chlorobenzoic acid by activated carbon and nickel supported activated carbon prepared from petroleum coke [J]. Journal of Hazardous Materials, 2009, 163(1): 115-120

[36] Wang Jianbing, Zhou Yunrui, Zhu Wanpeng, He Xuwen. Catalytic ozonation of dimethyl phthalate and chlorination disinfection by-product precursors over Ru/AC [J]. Journal of Hazardous Materials, 2009, 166(1): 502-507

[37] Zhao Weirong. Oxidation of Cationic Red X-GRL Dye by UV, Ozone, and Ozone Combined with UV [D]. Zhengjiang, Zhengjiang University Ph. D Thesis, 2004

[38] Zhang Qinghong, Gao Lian, Guo Jingkun. Effects of calcination on the photocatalytic properties of nanosized TiO_2 powders prepared by $TiCl_4$ hydrolysis [J]. Applied Catalysis B: Environmental, 2000, 26(3): 207-215

[39] Choi H, Al-abed S, Agarwal S, Dionysiou D. Synthesis of reactive nano-Fe/Pd bimetallic system-impregnated activated carbon for the simultaneous adsorption and dechlorination [J]. Chemistry of Materials, 2008, 20(11): 3649-3655

[40] Jing Maoxiang, Shen Xiangqian, Shen Yujun. Preparation of Nanometer Nickel Oxide by the Citrate-Gel Process [J]. Journal of Inorganic Materials, 2004, 19(2): 289-294

[41] Xu C B, Hamilton S, Ghosh M. Hydro-treatment of Athabasca vacuum tower bottoms in supercritical toluene with microporous activated carbons and metal-carbon composite [J]. Fuel, 2009, 88(11): 2097-2105

[42] Rinaldi A, Abdullah N, Ali M, Furche A, Hamid S, Su D S, Schlögl R. Controlling the yield and structure of carbon nanofibers grown on a nickel/activated carbon catalyst [J]. Carbon, 2009, 47(13): 3023-3033

[43] Zhao Lei. Enhancement of Ceramic Honeycomb Catalytic Ozonation by Ultrasound for the Degradation of Organic Compound in Water [D]. Harbin: Harbin Institute of Technology, Ph. D Thesis, 2008

[44] Zhang Qingmin, Xu Pu. Scanning Electron Microscopy and X-ray Microanalysis [M]. Tianjin: Nankai University Press, 1988: 9-17
[45] Zhu Hongfa. Catalyst Preparation and Application of Technology [M]. Beijing: Petroleum Industry Press, 2002: 6-14
[46] Chen Songying, Chen Ping, Li Yongwang, Wang Jianguo. Catalytic Reaction Kinetics [M]. Beijing: Chemical Industry Press, 2007: 76-81
[47] Khan M, Jung J. Ozonation catalyzed by homogeneous and heterogeneous catalysts for degradation of DEHP in aqueous phase [J]. Chemosphere, 2008, 72(4): 690-696
[48] Marcio Pimentel, Nihal Oturan, Marcia Dezotti, Mehmet A. Oturan. Phenol degradation by advanced electrochemical oxidation process electro-Fenton using a carbon felt cathode [J]. Applied Catalysis B: Environmental, 2008, 83(1/2): 140-149
[49] Masato Shiraga, Tomonori Kawabata, Dalin Li, Tetsuya Shishido, Kenji Komaguchi, Tsuneji Sano, Katsuomi Takehira. Memory effect-enhanced catalytic ozonation of aqueous phenol and oxalic acid over supported Cu catalysts derived from hydrotalcite [J]. Applied Clay Science, 2006, 33(3/4): 247-259
[50] Andreozzi R., Insola A., Caprio V., D'Amore M. G. The kinetics of Mn(II)-catalysed ozonation of oxalic acid in aqueous solution [J]. Wat. Res., 1992, 26 (7): 917-921
[51] Liu Zhengqian, Ma Jun, Cui Yuhong. Carbon nanotube supported platinum catalysts for the ozonation of oxalic acid in aqueous solutions [J]. Carbon, 2008, 46(6): 890-897
[52] Khan M, Jung J. Ozonation catalyzed by homogeneous and heterogeneous catalysts for degradation of DEHP in aqueous phase [J]. Chemosphere, 2008, 72(4): 690-696
[53] Valdés H, Zaror C A. Heterogeneous and homogeneous catalytic ozonation of benzothiazole promoted by activated carbon: Kinetic approach [J]. Chemosphere, 2006, 65(7): 1131-1136
[54] Xiao Yanfan, Li Wenbin. Physical Chemistry [M]. Tianjin: Tianjin University Press, 2004: 364-387
[55] Beltrán F. J., Rivas F. J., Montero-de-Espinosa R. Iron type catalysts for the ozonation of oxalic acid in water [J]. Wat. Res., 2005, 39(15): 3553-3564

In: Activated Carbon
Editor: James F. Kwiatkowski
ISBN: 978-1-61209-684-1
©2012 Nova Science Publishers, Inc.

Chapter 3

SURFACE CHEMISTRY OF ACTIVATED CARBONS

Sónia A. C. Carabineiro, M. Fernando R. Pereira, José J. M. Órfão and José L. Figueiredo
Laboratório de Catálise e Materiais (LCM), Laboratório Associado LSRE/LCM,
Faculdade de Engenharia, Universidade do Porto, Rua Dr. Roberto Frias, s/n,
4200-465 Porto, Portugal

ABSTRACT

Activated carbons have a disordered graphitic structure, which has been described as compared to to wrinkled paper sheets. The presence of heteroatoms (such as O, N, H, S, etc) bound to the edges of the graphene layers originates a variety of surface functional groups. Oxygenated functionalities have been most extensively studied, since they are formed spontaneously by exposure of the carbon material to the atmosphere; however, nitrogen, sulfur and phosphorous groups can also be found. The nature and concentration of surface functional groups may be modified by suitable thermal or chemical treatments. Treatments in the gas or liquid phase can be used to increase the concentration of surface groups, while heating under inert atmosphere may be used to selectively remove some of those functionalities. A variety of experimental techniques has been used to characterise functional groups, such as chemical titration methods, temperature-programmed desorption, X-ray photoelectron spectroscopy and infra-red spectroscopy methods. The results obtained by temperature-programmed desorption agree quantitatively with the elemental and proximate analyses of the oxidized materials, and qualitatively with the observations by infra-red spectroscopy. Some applications of functionalised activated carbons in adsorption and catalysis for several reactions are mentioned.

1. INTRODUCTION

1.1. Structure of Activated Carbons

Activated carbons are highly porous materials that can be prepared from several carbon-containing precursors. These materials are prepared by pyrolysis in inert atmosphere,

originating the so-called char, which can be subjected to a process of physical or chemical activation that will increase the porosity [1]. Activated carbons have an interesting structure that is shown in Figure 1.

It is now widely accepted that activated carbons consist of crystallites formed by stacked graphitic planes, randomly oriented, resulting in a disordered structure, similar to wrinkled sheets of paper [2]. The spaces between the graphitic planes of the crystallites create the microporous structure, which has a high internal surface area, providing activated carbons with their remarkable adsorption properties [3-4].

The porous structure depends on the precursor, the activation method and the extent of the activation. For that reason, the total pore volume, the relative fraction of each group of pores (macro, meso or micropores – see Figure 2) and the surface area can vary from sample to sample. The performance of activated carbons depends on their specific surface area, pore volume and pore size distribution.

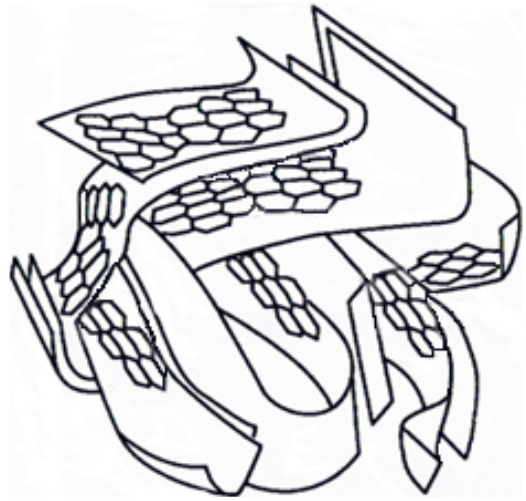


Figure 1. Microstructure of activated carbons (adapted from [2]).

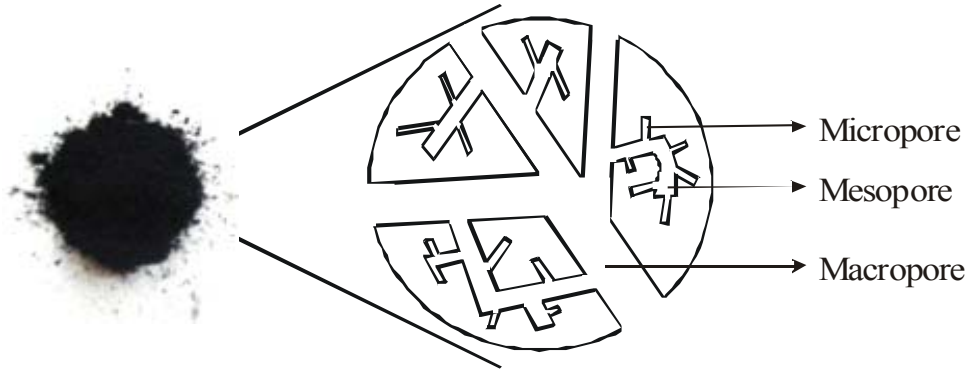


Figure 2. Microstructure of activated carbons showing different kinds of pores (adapted from [2]). The IUPAC classification of pores is based on the pore width or diameter: Micropores (smaller than 2 nm), mesopores (between 2 and 50 nm) and macropores (larger than 50 nm).

1.2. Historical Perspective

The first known use of activated carbon is mentioned in an old egyptian papyrus, dated from 1550 b.C., in a form of carbonised wood (charcoal) [5]. Until the 18th century, several types of carbon made from wood or animal bones were used for purification of liquids. In a typical procedure, a measured quantity of carbon was added to the liquid, mixed, and later separated by filtration or sedimentation. In the 19th century, bone char started to be used by the english sugar industry, for the decolourisation of sugar cane [5]. At that time, several production methods for vegetable carbon started to be patented in the United Kingdom. In the beginning of the 20th century, the first processes for the industrial production of activated carbons were also patented by Norit and Bayer. During the First World War, coconut shells were used to produce activated carbon for gas masks. Ever since, several activation processes were developed, as shown by the near 2000 patents existing all over the world. Activated carbons have the advantages of being cheap, inert, easily produced and thermostable materials [6].

1.3. Preparation of Activated Carbons

Several precursors with high carbon content have been used to obtain chars which can be subsequently activated. There are reports of activated carbons produced from olive [7-14], peach [15-21], cherry [22-30] and apricot stones [31-33], coconut [34-40], and other nut shells [13, 15, 33, 41-65], rice wastes [66-88], cork wastes [89-92], lignite [93-102], anthracite [102-113], fly ashes [114-121], used car tires [43, 122-126], etc. Almost all of these materials are cheap and derive from agricultural, forest or industrial wastes, making their use extremely attractive. There are two main processes of precursor activation: physical (thermal) or chemical [2, 5, 127-128].

Physical activation can be done using steam and/or carbon dioxide, at high temperatures (above 800 ºC) [5, 7-8, 13, 17, 22, 30, 38-39, 43, 48, 50, 54, 56, 81, 89-90, 93-96, 99, 104, 111, 114-115, 124, 129-133]. This process removes some carbon atoms, increasing the size and volume of pores in the char material. Chemical activation can be done with phosphoric acid, potassium or sodium hydroxide, or zinc chloride, at relatively low temperatures [4, 11-12, 14, 16, 20, 25, 27-28, 31, 33, 47, 49-50, 52, 54-55, 57, 59, 62-63, 67, 69, 71-74, 76, 80, 84, 86-89, 91-92, 98, 102, 107-108, 112-113, 120, 123, 126, 134-140]. It is possible to optimise the activation process in order to produce activated carbons with specific characteristics. The choice of the pore sizes are determined by the requirements of the application. Once activated, activated carbons contain pores that can have a surface area of more than 1000 m^2/g (which means that 5 g of this material can have the surface area of a soccer field!).

1.4. Forms of Activated Carbons

Commercial activated carbons can be found in several different forms (Figure 3). The classification is usually made according to the size and shape of carbon particles, which can be in the form of powder, pellets or grains (Figure 3).

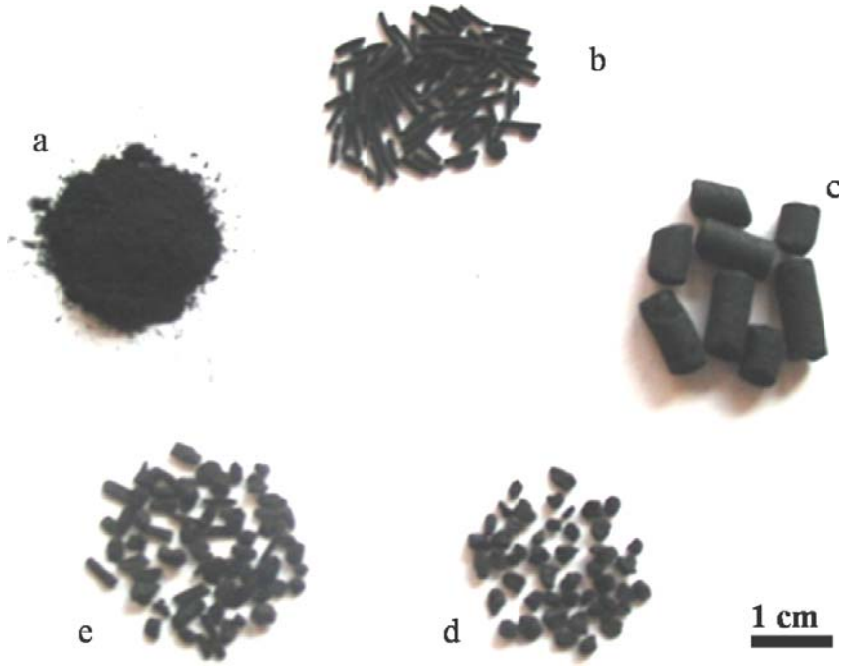


Figure 3. Forms of activated carbon: a) powder, b) pellets, c) extruded, d) and e) granular with different shapes.

The powder consists of pulverized carbon, with a size predominantly less than 0.1 mm, mainly used in liquid phase applications. The grains consists of irregular shaped particles, with sizes ranging from 0.5 to 5 mm. Pellets and extrudates have dimensions varying from 1 to 5 mm width and length sizes from 5 to 10 mm. Both non powdered forms are used in liquid and gas phase applications.

2. SURFACE CHEMISTRY

The presence of heteroatoms (such as O, N, H, S, etc, originating from the precursor used, the activation method, or introduced after treatment) bound to the edges of the graphene layers originates a variety of surface functional groups that have steric, tautomeric and intramolecular hydrogen bond effects since they are close to other different functionalities. Therefore, they are not individual entities, like similar compounds of traditional organic chemistry [141-142].

2.1. Oxygen Surface Groups

Oxygen functionalities are the most important due to their surface properties, and since they can be formed spontaneously by exposure of the carbon material to the atmosphere. There are extensive studies in the literature on the identification and quantification of these groups [2, 19, 34, 40, 133, 138, 140-165]. Once chemisorbed, oxygen can only be removed from the surface as CO and/or CO_2 at temperatures above 120 ºC.

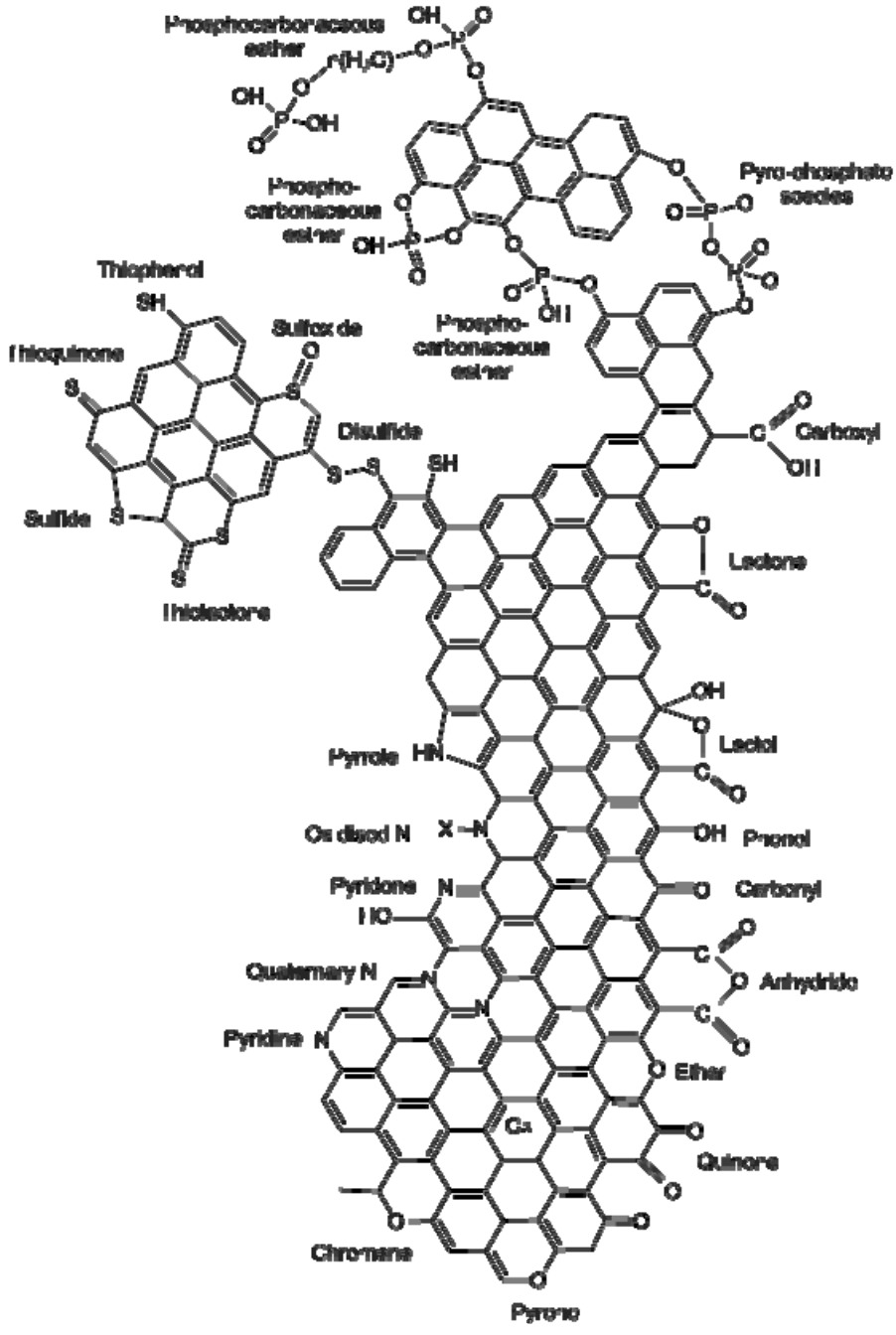


Figure 4. Oxygen, nitrogen, sulfur and phosphorous surface groups found on activated carbon surface.

The unsaturated carbon atoms at the edges of the crystallite basal planes are associated to high concentrations of unpaired electrons, which play a very important role in chemisorption. As activated carbons have a disordered structure (Figure 1), the area of the edges of basal planes is high, resulting in an affinity for oxygen chemisorption. Moreover, the basal planes of microcrystallites can have several imperfections, dislocations and discontinuities, which are also active centres for oxygen chemisorption [141-142], leading to the formation of

oxygen functional groups with variable thermal stability. Oxygen functional groups are not formed exclusively by reaction with oxygen, as they can also result from the reaction with other oxidant gases (such as O_3, N_2O, CO_2, etc) and with oxidising solutions (nitric acid, hydrogen peroxide, etc). The amount and nature of oxygen functional groups, for a given material, will depend on the surface area and the preparation method [144]. Several authors point out different oxygen surface groups (Figure 4), such as: carboxylic acids, carboxylic anhydrides, phenols, lactones, lactols, hydroxyls, carbonyls, quinones and pyrones [40, 128, 133, 138, 140-141, 143, 145-146, 148-169]. In addition, the π-electron density of the carbon basal planes is also considered to be chemically active (Figure 4). Usually, oxygen surface groups are considered either acidic or basic. Acidic surface groups are formed when the carbon surface is exposed to oxygen through reactions with oxidizing agents from solutions or gas phase, at room temperature or higher temperatures. Those oxidation treatments will be described ahead. In contrast, basic groups are formed when the oxidized surface is reduced by heating in an inert or hydrogen atmosphere, at high temperatures. The decomposition of acidic groups creates active sites at the edges of the graphene layers, which can attract oxygen during the cooling stage, in inert atmosphere and after re-exposure to air, forming basic functional groups such as chromene or pyrone [128, 170-172] (Figure 4). Acidic groups include carboxylic acids and anhydrides, lactones or lactols, and phenols, while carbonyl and ether oxygen are neutral or may form basic structures, such as quinone, chromene and pyrone groups (Figure 4). The surface groups, especially those of acidic nature, are responsible for the amphoteric character of activated carbons, which depends on the pH of the aqueous phase. The carbon surface can then have positive or negative charges, as it can be seen in Figure 5. [127, 173]. This Figure also shows the contributions of surface groups and π electrons from basal planes (Ar_π) to the charge developed at the activated carbon surface in aqueous phase. The capacity of the carbon surface to acquire a positive or negative charge varies according to the pH of the aqueous phase. In fact, this capacity depends on the value of pH_{PZC} (point of zero charger), that corresponds to the value of pH at which the activated carbon surface has zero charge (see Section X.4.1.3). Therefore, if the pH_{PZC} of a carbon is larger than the pH of the solution, the surface will have a basic character (positive charge) that will enhance the interaction with anionic species. When the pH of the solution is larger than the carbon pH_{PZC}, the surface will have a negative charge, which will favour the interaction with cationic species.

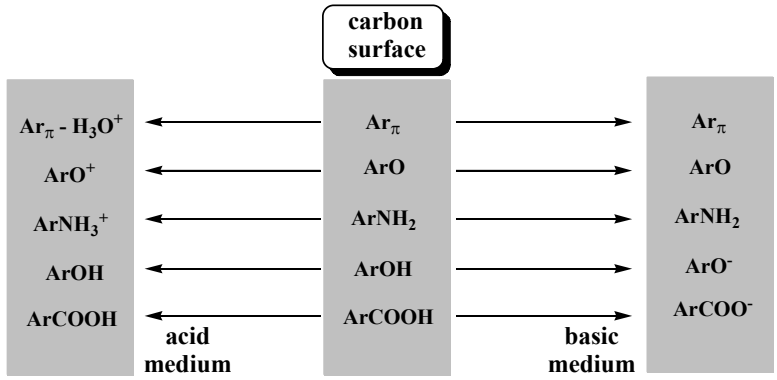


Figure 5. Schematic representation of the features of carbon surface chemistry in aqueous phase (adapted from [127, 173]).

2.2. Nitrogen Groups

Nitrogen functionalities can also be found, although they are not formed spontaneously on carbon surfaces by contact with air (unlike oxygen groups). Usually, the nitrogen content in activated carbons is very small unless it was already present on the carbon precursor (namely carbazole, nitrogen-enriched polymers, acridine, or melamine) or introduced by treatment with nitrogen-containing reagents (e.g., ammonia, urea, melamine, HCN) [128, 169, 174-183].

The type of nitrogen functionalities present on the carbon surface is thus a function of the treatment applied, i.e., the type of precursor and the temperature of the heat treatment. The various nitrogen groups present on the surface of activated carbons are summarized in Figure 4.

2.3. Hydrogen Groups

Hydrogen is usually present on activated carbons as chemisorbed water, as part of other surface groups (like carboxylic acids, phenols, amines), or bonded directly to carbon atoms as a part of aromatic or aliphatic structures.

The carbon–hydrogen bond is very stable but breaks on heating at ~1000 ºC; therefore complete desorption of hydrogen only occurs above that temperature [128].

2.4. Sulfur Groups

Sulfur can be present in activated carbons as the element itself or as sulfur compounds, usually in low amounts. Carbon–sulfur complexes can be extremely stable and might not be removed completely even above 1000 ºC, unless the heating is carried out in a reducing hydrogen atmosphere [128].

Carbon surfaces can be modified through reactions with S-containing compounds such as SO_2 or H_2S, at several temperatures, resulting in the formation of sulfur-containing groups [184-185]. The possible sulfur surface complexes [128, 186] are shown in Figure 4.

2.5. Phosphorous Groups

Phosphorous contained in activated carbons can have its origin in phosphoric acid used as an activation agent in the preparation stage [4, 20, 27, 33, 49-50, 54, 76, 86, 88, 134-135, 139, 187]. Once in the carbon matrix, it can be stable between 500 ºC and 1000 ºC [128] and can be found as red phosphorus and/or in chemically bonded forms, such as –C–P–bonds or –C–O–P–bonds [128, 134, 187-188].

Phosphorous containing species can be formed during the carbonization process at low temperature. Possible phosphorus-containing functionalities [187] are presented in Figure 4.

2.6. Halogenated Groups

Even though there are fewer studies on reactions of *halogens* with activated carbons and consequent formation of carbon–halogen functionalities, in comparison with the work done with oxygen or nitrogen groups, there are some reports in literature showing that the treatment of carbon materials with halogen vapours can originate carbon–halogen complexes [128, 189-190]. Usually, both the reactivity of halogens towards carbon and the stability of carbon–halogen complexes decrease in the following order: chlorine>bromine>iodine [128].

A C–Cl bond can be formed through reaction with *chloride* at high temperature (400-500 ºC). Chloride can be incorporated through addition at the unsaturated sites that are formed due to oxygen removal from the edges of the graphene layers, or else by substitution of this halogen by hydrogen in aliphatic groups at low temperatures, or at the edges of the aromatic platelets at high temperature [128]. Although chlorine–carbon complexes are stable, they can be removed by fusion with NaOH or by heating at 700 ºC in hydrogen. *Bromine* or *iodine* can also form stable halogen–carbon complexes, with a maximum amount at 500 ºC. For aqueous solutions, bromine can occupy the unsaturated sites of the carbon surface; however in vapour phase, partial substitution for hydrogen can also take place [128]. Iodine can also incorporate at the unsaturated edges of carbon surface when in vapour phase but, when in solution, reversible adsorption takes place [191-192].

3. MODIFICATION OF CARBON SURFACE

Both the textural properties and the surface chemistry of activated carbons can be optimized through changes in the activation process. It is possible to prepare carbon materials with different proportions of micro, meso and macropores [127, 193-195], and with different amounts and types of surface groups, as discussed below.

3.1. Introduction of Oxygen Groups

The nature and concentration of surface functional groups may also be modified by suitable thermal or chemical treatments. *Oxidation* in the gas or liquid phase is the most usual method for the introduction of oxygen-containing groups, while heating under inert atmosphere may be used to selectively remove some of these functionalities [40, 133, 138, 140, 143, 145-165, 168, 196-198]. In *gas-phase*, oxygen, ozone, air, or nitrogen oxides can be used as oxidants [30, 102, 128, 152, 165, 168, 199-202]. Although oxidation conditions may vary, it is usually carried out at temperatures between 400 and 500 ºC, with a continuous flow of the oxidant gas. Several oxygen-containing groups are formed, specially carbonyl surface groups and weakly acidic groups like phenols [128, 153]. Oxidation in the *liquid phase* can result in drastic changes in the chemistry of the carbon surface. The most usual oxidizing agents are nitric acid, hydrogen peroxide, hypochlorite, potassium permanganate, sulfuric acid, and sodium and peroxydisulphate, in several concentrations and temperature ranges, depending on the intensity desired [30, 102, 128, 145, 151-153, 155, 157, 165, 168, 174, 180, 198-199, 201, 203-211], since the higher the temperature and the oxidant concentration, the

more oxidized the carbon surface will become. In fact, oxidation at the boiling point with a high concentration of nitric acid can partially destroy the carbon structure, leading to changed in the surface area [40, 168]. This type of treatment usually generates activated carbons with a majority of carboxylic acid groups [40, 128, 153, 168], while treatment with hydrogen peroxide increases the amount of phenols [128]. When nitric acid, nitric oxide or nitrous oxide are used, besides the increase in oxygen content, nitrogen is also incorporated as N-containing groups that probably attach to carbon at the edges of graphene planes [153, 168, 199]. After oxidation, a washing procedure (with distilled water until neutral pH) is needed, in order to remove the excess of oxidant.

3.2. Introduction of Nitrogen Groups

The introduction of *nitrogen* containing functionalities can also be carried out in the gas or liquid phase, using adequate compounds. Ammonia can be used at temperatures between 200 and 1000 ºC [128, 174, 176, 178-179, 181-183, 212]. When the process is carried out in the liquid phase, nitrogen-enriched polymers, acridine, melamine or urea are used. The activated carbon samples can be impregnated with aqueous or alcoholic solutions of the nitrogen precursors and then exposed to heating between 200 and 1000 ºC [128, 172, 213]. Prior oxidation of samples can result in the formation of chemical bonds, usually between the nitrogen-containing precursor and the carbon surface, causing an increase in the nitrogen content [128, 172, 214-215].

3.3. Introduction of Sulfur and Halogenated Groups

The introduction of *sulfur* containing groups to a carbon surface is usually done by heating carbons in the presence of elemental sulfur or hydrogen sulfide, at temperatures varying from 200 to 1000 ºC, which usually generates sulfide formation [128, 184-185].

Halogenation also can be carried out in the gas or liquid phase. In the gas phase, the sample is exposed to gas or vapour halogen from 200 to 400 ºC, the treatment being usually carried out on a reduced carbon surface and resulting in C-halogen bond formation [128, 216-218].

3.4. Selective Removal of Surface Groups

After the above described surface modifications, subsequent heat treatments can be used to selectively decompose some surface functional groups with release of oxides or heteroatom containing gases (such as CO, CO_2, NO, NO_2, H_2S, NH_3), causing possible changes in the surface area and an increase in the basicity [40, 128, 145, 155, 159, 164, 168, 196]. Those treatments can be carried out at temperatures varying from 400 to 900 ºC in a reducing (hydrogen) or inert (nitrogen) atmosphere. Menendez et al. [170] found out that a treatment in hydrogen produces a hydrophobic surface that is stable when re-exposed to air, as surface oxygen is removed and reactive sites are stabilized since they form C–H bonds and the most reactive unsaturated carbon atoms from the edges of graphene layers are gasified. On the

other hand, a treatment in inert atmosphere results in a surface without oxygen groups, that can be prone to reoxidation and formation of new acidic groups [170].

4. CHARACTERISATION OF ACTIVATED CARBONS

The characterisation of the carbon surface can be made by several methods. A brief overview of those techniques is presented in this section. Further details can be found elsewhere [128, 219].

4.1. Textural Characterisation

The *textural characterisation* of activated carbons is usually carried out by the analysis of N_2 adsorption-desorption isotherms obtained at -196 ºC [19, 30, 104, 147, 206, 216, 220-222], which are usually of type I, characteristic of microporous solids [223], as shown in Figure 6. The presence of mesopores can be inferred by a more or less pronounced slope of the isotherm at high relative pressures.

If a hysteresis that is almost parallel to the adsorption curve down to low pressures is found, then slit-shape mesopores are present, as the example shown in Figure 6. The most usual methods for isothermal analysis are the t-method and the Dubinin method. The micropore volume and the mesopore surface area are determined by the t-method using an appropriate standard isotherm. The volume of micropores can be obtained also by the Dubinin method [223]. The Stoeckli equation can be used to calculate the average size of micropores [224].

The total specific surface area is usually determined by the BET method (from Stephen Brunauer, Paul Hugh Emmett and Edward Teller, who first developed it [225]), although it is not the most appropriate parameter for the characterization of microporous solids (but the value is frequently used as a reference in order to compare different samples) [127].

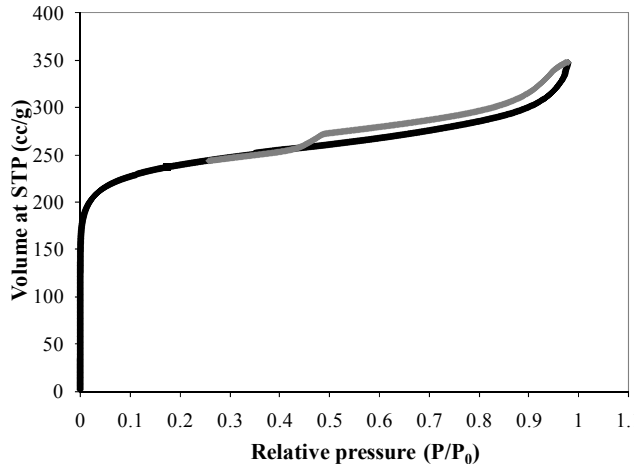


Figure 6. N_2 adsorption-desorption isotherms obtained at -196 ºC for a commercial microporous activated carbon (black – adsorption, grey – desorption).

4.1. Surface Chemistry Characterisation

A variety of experimental techniques has been used to characterize the *surface chemistry* of activated carbons. The most usual techniques will be briefly mentioned below.

4.1.1. Elemental Analysis

Elemental analysis allows the determination of the contents of carbon, hydrogen, nitrogen, and sulfur of activated carbon samples. This technique is carried out by combustion at high temperatures (~1200 ºC) in oxygen. The products formed are then quantified (CO_2, H_2O and SO_2 are generated by oxidation, while nitrogen is obtained by reduction in the presence of Cu). Quite often, the oxygen content is calculated indirectly by difference, but a dedicated method can be used, where O is determined separately. Typical values obtained vary from 70 to 98% of C; 1 to 5% H, 0 to 5% S and 0 to 5% N [31, 90, 128, 140, 157, 161, 221, 226-227]. Analysis of trace elements (coming from the precursor) can be carried out by atomic absorption spectroscopy and inductively coupled plasma spectroscopy, after digestion of samples in an acid solution.

4.1.2. Titrations

The method of selective neutralization or *Boehm titration* consists in neutralizing the oxygen groups according to their acid strength, and has been used often [10, 28, 30, 148, 159, 165, 171, 176, 203, 206-207, 228-233]. Bases are selected according to the pKa values of the corresponding conjugated acids, knowing that a base with one given pKa value for the conjugated acid will only neutralize the surface groups that have lower pKa values. Sodium bicarbonate ($NaHCO_3$, pKa = 6.37), sodium carbonate (Na_2CO_3, pKa = 10.25), sodium hydroxide (NaOH, pKa = 15.74), and sodium ethoxide ($NaOC_2H_5$, pKa = 20.58) are used as bases. $NaHCO_3$ neutralizes carboxylic acids, Na_2CO_3 neutralizes carboxylic acids and lactones, NaOH neutralizes carboxylic acids, lactones, and phenols, whereas $NaOC_2H_5$ reacts with all oxygen species, even extremely weak acids (pKa <20.58). The amount of each groups can then be estimated by difference. Basic groups are titrated with HCl. This method has, however, some drawbacks: The equilibrium times are long, especially for microporous materials; the neighbour functionalities can change the groups properties due to chelation phenomena; and the structure of activated carbons, specially at the edges of graphene layers, changes the properties of groups by resonance [127, 142]. Moreover, classification of all groups as oxygen-containing acids and of all other groups containing nitrogen, sulfur, or phosphorus, can be misinterpreted, since Boehm's titration method is based on the pKa value. Also surface heterogeneity of activated carbons makes it extremely difficult to determine accurately the surface groups based only on their acidic and basic properties [128, 142]. Things can get even more complicated when this method is used to characterize modified samples, since functionalities containing other atoms can also be classified as surface oxide groups. In addition, it has been found that this method only accounts for about 50% of all oxygen present in the samples [166]. A safe way to use this procedure and keep it meaningful is to limit it to the total number of acidic groups, which would include all species neutralized by sodium hydroxide [128, 215]. Direct *potentiometric titration* has also been used by several authors [4, 153, 161, 171, 234-235]. A deconvolution method of the obtained titration curves with a theoretical description of the acid-based dissociation on the surface of activated

carbons can be used, based on the assumption that the studied system consists of acidic sites characterized by their acidity constants (Ka) and that the amount of sites can be described by a continuous pKa distribution. The experimental data can be transformed into a proton-binding isotherm that represents the total amount of protonated sites, which is related to the pKa distribution by an integral equation that can be solved by numerical procedures [128]. Since many groups can yield similar pKa values, the exact classification of species is not possible. However, when the content of heteroatoms is known, this method can show clearly a trend in surface groups and can provide qualitative and quantitative information on the number and strength of the acidic sites of the carbon surface. Some authors compared the Boehm method and the direct potentiometric titration [153, 171, 231]. Usually an acceptable agreement exists between both methods, but for a largely oxygenated carbon surface, some differences can arise [128].

4.1.3. Point of Zero Charge and Isoelectric Point

The pH of an aqueous suspension of an activated carbon sample gives an idea of the average chemistry of the carbon surface. The *determination of the pH corresponding to the zero charge* of the carbon surface (pH_{PZC}) can be carried out by an electrochemical method and corresponds to the pH value where the net surface charge resulting from the adsorption of H^+ and OH^- is zero [127-128]. It can be considered as the pH below which the carbon surface in solution is positively charged, and above which the surface is negatively charged. A simple and fast method to determine pH_{PZC} [226] consists in placing 50 cm^3 of NaCl solution 0.01 M in closed flasks and adjusting the pH of each one to values from 2 to 12 by adding a solution of NaOH or HCl 0.1 M, then adding 0.15 g of the activated carbon sample to analyse, keeping the suspension under stirring, at room temperature for 48 h and measuring the pH after that. The pH_{PZC} is the point where the curve pH_{final} versus $pH_{initial}$ intercepts the line $pH_{final} = pH_{initial}$ (one example is shown in Figure 7). Naturally, acidic activated carbons will have values of pH_{PZC} lower than 7, while basic samples will have pH_{PZC} above that value. Several authors used this method [28-30, 176, 206, 216, 221].

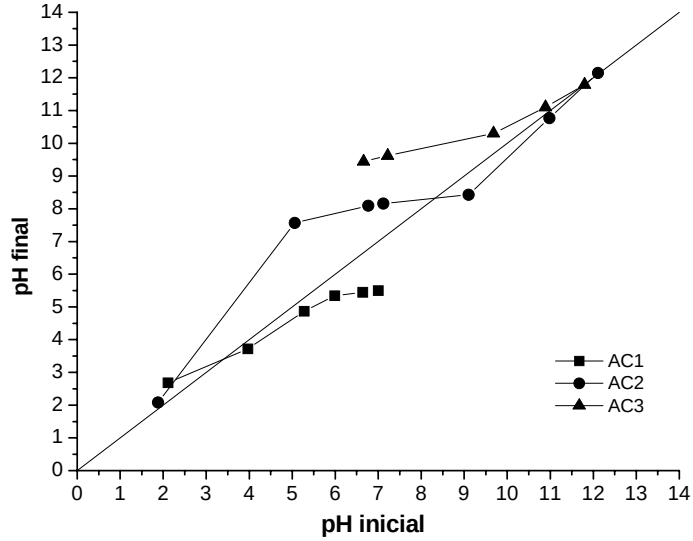


Figure 7. pH_{PZC} determination for different activated carbon samples.

The isoelectric point (pH_{IEP}) is the pH value at which the material carries no electrical charge or the negative and positive charges are equal. It is obtained when an electric field, a pressure gradient, or similar, is used to move the charged particles of colloids in solution using microelectrophoresis or electroosmosis methods [128].

The pH_{PZC}–pH_{IEP} difference is thus a measure of the surface charge distribution of activated carbons. Positive values correspond to more positively charged internal than external particle surfaces (i.e., less acidic external than internal surfaces), and values close to zero corresponding to a more homogeneous distribution of the surface charges [128, 236]. Menéndez and co-workers performed a detailed study of pH_{PZC} and pH_{IEP} for several activated carbons [236-239].

4.1.4. Spectroscopy

Spectroscopic methods, such as *Infrared spectroscopy* are frequently used to qualitatively characterize the surface functionalities of activated carbons, particularly *Fourier transformed infrared analysis* (FTIR) [30, 38, 84, 127-128, 143, 151, 164, 201, 206, 220, 232, 240-242]. However FTIR presents some drawbacks, as a result mainly of the fact that activated carbons are black materials that absorb most energy and are too opaque for direct transmission analysis in the mid-infrared spectral region [127-128].

As in organic chemistry, the assignment of the IR absorption bands and peaks to the different functional groups is made by comparison with the absorption bands of specific organic compounds. In most works published, three bands at ~1750 cm^{-1}, ~1600 cm^{-1} and ~1250 cm^{-1} are usually referred.

The first is attributed to the stretching of the C=O bond in carboxylic acids, anhydrides and lactones, the third to the stretching of C–O in carboxylic acids, anhydrides, phenols, lactones and ethers, and the second to carbonyl/quinone functionalities or to the stretching of C=C in polyaromatic systems [84, 127-128, 143, 151, 164, 201, 220, 240, 242]. Although this technique is not quantitative, it can identify groups created or destroyed on the activated carbon as a result of surface modifications [128].

Other techniques like *diffuse reflectance* (DRIFT) and *photoacustic spectroscopy* (FTIR-PAS) have been used for the characterization of activated carbon surfaces [90, 151, 164, 168, 201, 240, 242-244]. The former shows good sensitivity and high quantitative precision, while the latter eliminates spectral artefacts like baseline shifts due to light scattering [128].

In *X-ray photoelectron spectroscopy* (XPS), a measurement of the kinetic energy of electrons emitted by the atoms when they are submitted to X-rays is obtained. Since the kinetic energy of the electrons dependends on their binding energy, different chemical species can be identified. For each element, there is a characteristic set of peaks at kinetic energies determined by the photon energy and the respective binding energies. This technique is very sensitive for the detection of surface atoms (with the exception of hydrogen), through binding energies of the C1s, N1s, and O1s photoelectrons of surface groups [138, 149, 151, 160, 165, 168, 175, 245-247].

Table 1 shows the position of peaks usually accepted [248-250]. Since the intensity of the peaks is related with the concentration of each element, quantitative analysis is also possible, but only the chemical composition of the few upeermost layers (~10-15 nm deep) is obtained, which might not be representative of the entire sample [127-128, 142]. Moreover, the external surface may be affected by the environment, since activated carbon materials are very reactive towards oxygen and humidity [127].

Table 1. Binding energies (eV) for some species of C1s, O1s and N1s [248-250]

Carbon species (C1s)	Oxygen species (O1s)	Nitrogen species (N1s)
Graphite, aromatic: 284.6	C=O (anhydrides, lactones), phenols, ether: 532.3	CN, NH_2: 399.0-401.0
Aliphatic, C-NH_2: 285.1-285.3	Carbonyls: 531.1	NH_3: 402.0-403.0
Alcohols, phenols, CN: 286.1	C–O (anhydrides, lactones), keto-enol: 533.3	NO_2: ~407
Keto-enol, C-NO_2: 286.4	Carboxylic: 534.2	
Carbonyls: 287.6	H_2O: 536.1	
Carboxylic: 288.1-289.1		
Carbonates, CO_2: 290.6		

In *X-ray fluorescence* (XRF) and *energy-dispersive X-ray spectroscopy* (EDXS) the elements in samples are excited by absorption of the primary beam and emit characteristic X-rays. XRF and EDXS are used to determine the inorganic composition of activated carbons and thus provide information about the relative amounts of elements and their location on the activated carbon surface. [251-253].

Nuclear Magnetic Resonance (NMR) is a spectroscopic technique based on measuring the absorption of electromagnetic radiation by the nuclei of the atoms. This technique can be used to evaluate changes in the surface chemistry of activated carbons. It is based on the determination of ^{13}C NMR spectra, which can give information, by deconvolution, about the aromatic carbon-to-aliphatic carbon ratio in the structure [31, 83, 98, 254-256]. Other nuclei can also be studied like ^{31}P and ^{19}F to give information on groups containing those heteroatoms [128].

In *electron spin resonance spectroscopy* (ESR, also called electron paramagnetic resonance, or EPR) an absorption spectra from transitions induced between spin states is measured from a paramagnetic solid (that has unpaired electron spins), by applying a magnetic field and then supplying electromagnetic energy, usually in the microwave range of frequencies [128]. Activated carbons can behave as semiconductors, due to the π electrons, which can act as charge carriers, so ESR, being sensitive to unpaired electrons (delocalized π electrons and free radicals) can be used in the study of carbon surfaces [257-258]. Some changes in the ESR spectra of carbons after oxidation treatments have been reported, as the formation of surface groups at the edges of carbon atoms caused an increase in conductivity [257]. A significant number of surface sites generated after oxidation of the carbon surface were related to the presence of functional groups (lactones, phenols, and quinones) as new bands on the ESR spectrum were observed [257].

4.1.5. Calorimetry

Calorimetric techniques measure the heat that is generated (exothermic process), consumed (endothermic process) or dissipated by a sample and have been used in the characterisation of activated carbons [12, 139, 146, 148, 176, 222, 259]. In particular, immersion calorimetry measures the energy involved in the interaction of molecules of the immersion liquid with the surface of the activated carbon sample, since this energy depends on the interaction between the solid and the liquid. When the enthalpies of immersion into liquids with different polarities are compared, a picture of the carbon surface chemistry is

obtained, as the surface is made of basal planes and unsaturated sites at the edges of the graphene layers with heteroatom functional groups. Moreover, the affinity of carbon surface to polar and nonpolar liquids is related to its hydrophobic and hydrophilic characteristics, so calorimetric techniques can quantify the carbon hydrophobic and hydrophilic sites by measurements of the preferential heats of adsorption on those probes [128].

In particular, the enthalpy of immersion of activated carbons into water has been related with the amount and nature of their surface oxygen functional groups, as it increases with the surface oxygen level [148, 260-264]. Although calorimetry can only estimate the hydrophobic or hydrophilic character of activated carbons, it can provide useful information about the surface chemistry to complement results obtained by other techniques.

4.1.6. Inverse Gas Chromatography

Inverse gas chromatography (IGC) is a rapid and reliable method for the evaluation of the acid-base character of activated carbons, employing physical adsorption of molecular probes in a chromatographic experiment [132, 203, 230-231]. The amounts of solutes injected are very small, and it is assumed that the adsorption is described by Henry's law. The free energy of adsorption, ΔG^{o}, can be calculated from the retention volume. When both saturated and unsaturated hydrocarbons are used as probe molecules, the difference in the ΔG_{CH2} of alkane and alkene is used to study the effect of the π-bond interactions with electron acceptor sites on the carbon surface [203, 230]. That difference in free energy represents the average number and strength of the acidic centres present on the carbon surface. The more positive (or less negative) it is, the more acidic is the surface of the carbon [128].

The results obtained with activated carbon samples showed good correlation with the data obtained by the Boehm titration method [203, 230-231]. The advantage of the IGC approach is that it provides information about acidity in a nonaqueous environment, and the results are obtained in a rapid and reproducible way.

4.1.7. Electrochemistry

Although *voltammetry* and *polarography* cannot give detailed information about the type of surface groups, good agreement has been reported with the conventional techniques used in the identification of surface functionalities on activated carbons [138, 265]. Cyclic voltammograms of carbon materials after heating at high temperatures and oxidation treatments showed clear evidence of the presence of redox couples on their surfaces, and an attempt to quantify the quinone and hydroquinone groups detected on carbon blacks was made by Kinoshita et al. [266]. The evidence of the presence of quinone groups as electrochemically active species on carbon blacks was provided by polarographic analysis [267].

4.1.8. Temperature-Programmed Desorption

Temperature-programmed desorption (TPD) is a technique which is gaining increased importance for the characterization of activated carbons [40, 126-128, 133, 138, 140, 143, 145-146, 148-152, 154-155, 157-165, 168, 201, 206, 208, 244, 262, 268-270]. It involves heating the sample in an inert carrier gas at a determined heating rate to induce thermal desorption of adsorbed species from the surface. While being heated, the surface groups decompose, releasing various gas compounds at different temperatures, which can be

analyzed by mass spectrometry, infrared spectroscopy, or gas chromatography. Usually, oxygen-containing groups decompose mostly as CO and CO_2 (generally, acid groups desorb as CO_2 while basic groups desorb as CO), while nitrogen functionalities also release NO. H_2O can also be released: a peak at low temperatures is due to the removal of physisorbed water, but a peak at higher temperatures is assigned either to the evolution of water hydrogen-bonded to oxygen complexes, condensation of any phenolic groups, or dehydration reactions of neighbouring carboxylic groups to give carboxylic anhydrides [150].

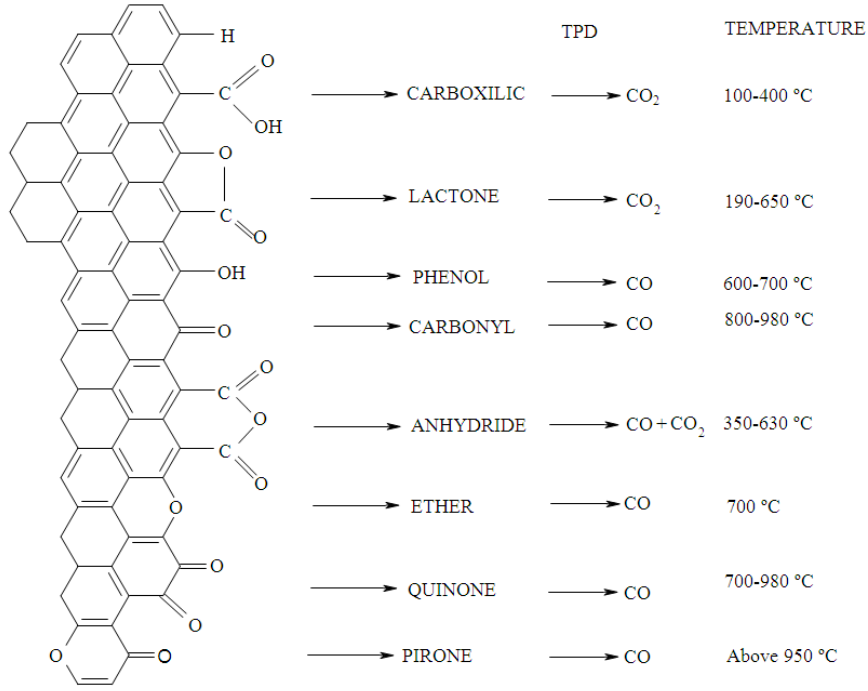


Figure 8. Surface oxygen-containin groups on carbon and their decomposition by TPD (adapted from [127, 168]).

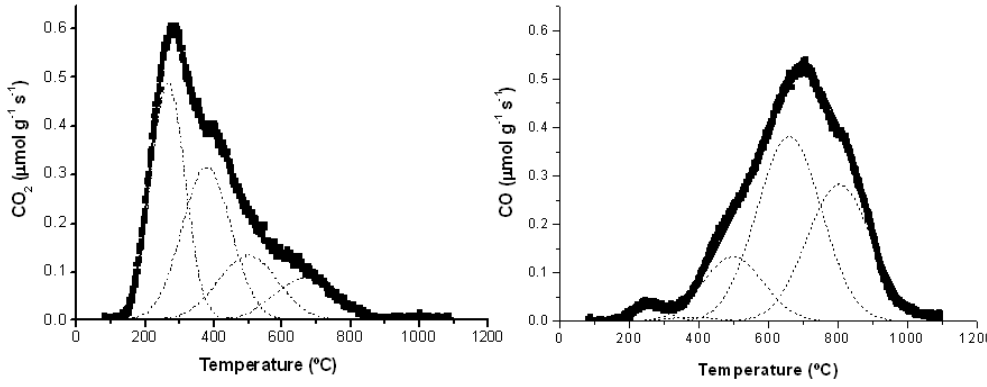


Figure 9. Deconvolution of TPD spectra for an activated carbon treated with nitric acid. CO_2 and CO spectra are shown, where ■ are TPD experimental points, dashed lines are individual peaks obtained by deconvolution and thin lines are the sum of the individual peaks (adapted from [40]).

The results obtained by TPD usually agree quantitatively with other types of analyses [40, 161, 168]. However, the temperature and the way as the different groups decompose has been a subject of several studies, and not all authors are in agreement. The interpretation of TPD spectra is not always easy since some peaks can be broad and not well resolved, although it is possible to observe the existence of different contributions that can be reflected in the presence of more or less pronounced "shoulders".

The groups present on carbon surfaces have a continuous broad distribution of desorption activation energies, due to the interaction with the neighbour groups or with the carbon surface, which cause low resolution of peaks [147]. Nevertheless, TPD still has advantages, namely it is the only method that reflects the total amount of groups present on carbon surfaces, since titration procedures give lower values, XPS give larger values and FTIR is only qualitative.

Figure 8. summarises the temperature ranges corresponding to the evolution of CO and CO_2 upon decomposition of the various types of oxygen functional groups. It is normal to observe larger desorption of CO than CO_2 [40, 152, 168]. Since each peak of the TPD spectra is associated to a characteristic activation energy, numeric deconvolution of curves allows for a better characterization of carbon surface.

A simple deconvolution method can be used to analyse the TPD spectra, allowing for the determination of the amount of each functional group on the surface, by fitting a multiple Gaussian function to the data [40, 152, 168]. An example is shown in Figure 9.

5. APPLICATIONS OF ACTIVATED CARBONS

5.1. Adsorption

The high surface area of activated carbons provides them with high adsorption capacities, hard to achieve with other type of materials [3-4]. Adsorption is the process by which liquid or gaseous molecules are concentrated on solid surfaces (in this case, activated carbons).

Activated carbons have been shown to be efficient in the adsorption of several compounds in the gas or liquid phase, such as volatile organic compounds [6, 50, 92, 259, 271-272], gases like hydrogen [6, 60, 273-277], methane [6, 77, 135-136, 139, 278-282], NO_x [6, 65, 129-131, 137, 270, 283-284], SO_x and H_2S [6, 48, 65, 129-130, 178-179, 284-287], and in water purification [6, 51, 127, 191, 226] through the adsorption of dyes [6, 124, 127, 197-198, 288-289], aromatics [6, 124, 127, 182, 210, 290-297], metals [6, 12, 49, 62, 88, 126-127, 226, 253], etc.

An additional advantage of activated carbons is that, once used, they can also be regenerated, in order to restore their adsorption capacity [6, 19]. That is usually made at temperatures above 800 °C.

The presence of surface groups can affect adsorption. Examples are adsorption of water or alcohols, which is greatly enhanced by the presence of species on the carbon surface, which otherwise is hydrophobic in its nature [298-300].

The adsorption of small organic molecules containing functional groups is also affected by the carbon surface chemistry. Specific studies were done on the adsorption of numerous pollutants, such as heavy metals [301-302], aromatics [207, 233, 295, 302-305], volatile

organic compounds [100], dyes [160, 197-198, 288], amines [306-307], carboxylic acids [141, 308], alcohols [309], etc, where the surface chemistry was shown to influence the adsorption process.

It is generally accepted that the presence of functional groups inhibits adsorption of phenols, creating obstacles for their preferred orientations on the carbon surface. For other polar molecules, functional groups containing oxygen or nitrogen were found to interact favourably with the adsorbate, depending on its chemistry.

In general, surface acidic groups increase the adsorption of bases, while adsorption of organic acids is enhanced by the presence of basic groups [128]. The latter were also found to be fundamental for the adsorption of sulfur dioxide, as they can attract the SO_2 molecules [310-311].

Surface functional groups containing oxygen or sulfur are very important for the desulfurization of liquid fuels [128]. In particular, thiophenic compounds are specifically adsorbed via hydrogen bonding.

Surface groups are also important in the removal of heavy metals from aqueous solutions, as they provide sites for cation-exchange reactions, which is the main mechanism by which those metals are retained on activated carbon surfaces [301, 312]. The removal of heavy metals is also facilitated with sulfonated carbons, due to the strong affinity of sulfur to form complexes with the former [313-315].

5.1. Catalysis

Activated carbons have also been used as catalysts. An overview of several reactions catalysed by activated carbons can be found in Table 2, along with the type of surface chemistry needed. Further details can be found elsewhere [128, 169].

Table 2. Overview of various reactions catalysed by activated carbons and the type of surface chemistry required or nature of the active sites [169]

Reactions	Surface chemistry/active sites
Gas phase Oxidative dehydrogenation	 Quinones
Dehydration of alcohols	Carboxylic acids
Dehydrogenation of alcohols	Lewis acids and basic sites
NO_x reduction (selective catalytic reduction with NH_3)	Acidic surface oxides (carboxylic and lactone) + Basic sites (carbonyls or N5, N6)
NO oxidation	Basic sites
SO_2 oxidation	Basic sites, pyridinic-N6
H_2S oxidation	Basic sites
Dehydrohalogenation	Pyridinic nitrogen sites
Liquid phase Hydrogen peroxide reactions	 Basic sites
Catalytic ozonation	Basic sites
Catalytic wet air oxidation	Basic sites

5.1.1. Oxidative Dehydrogenation of Ethylbenzene and Other Hydrocarbons

The *oxidative dehydrogenation of ethylbenzene* (ODE) using activated carbons as catalysts was first reported by Alkhazov et al. [316]. Subsequent studies were reported attempting to correlate the textural properties of the activated carbon and their activity for ODE [317-319]. Usually deposition of coke blocks small pores. A systematic study on the textural effects was published recently, using activated carbon fibres [320] and activated carbons [269]. The textural effects were found to be only important up to an average of 1.2 nm pore width, as for larger pores sizes, surface chemistry controls catalyst performance. The role of surface chemistry in the ODE was also reported for activated carbons oxidized to different extents [196, 244, 320-321], showing that surface carbonyl/quinone groups are the active sites, in agreement with previous literature [322-323]. The oxidative dehydrogenation of other hydrocarbons over several carbon materials has been explained in similar terms [140, 324-327].

5.1.2. Alcohol Conversion

Alcohol conversion on activated carbon materials has been extensively studied using activated carbon catalysts oxidized to different extents and heat treated at different temperatures [155, 204, 309, 328-331]. It has been shown that alcohol dehydration is controlled by the number, strength and accessibility of the carboxylic acid groups [155, 331].

5.1.3. Removal of NO_x and SO_x

The *removal of sulfur and nitrogen oxides* from gaseous effluents is an important application for activated carbons which combines their remarkable adsorption capacity with their notorious catalytic activity for oxidation and reduction [169].

It was found that the pyridinic groups in activated carbons are the most active for the catalytic oxidation of SO_2 both into SO_3 and H_2SO_4, and a linear correlation between the concentration of these groups and the activity (normalised by the BET surface area) was obtained [177].

The selective catalytic reduction of NO_x with ammonia or urea, producing nitrogen and water, can also be efficiently catalysed by carbon materials at temperatures as low as 30-300 ºC [180, 332]. The active sites involved in the adsorption of NH_3 have been identified as carboxylic acids, lactones and phenols, while NO can be chemisorbed on carbonyl or pyridine surface groups [180, 205].

5.1.4. Oxidation of Organic Compounds

Activated carbons have been used in the *oxidation of organic compounds* in liquid effluents, using air or oxygen (catalytic wet air oxidation) [206, 208, 222, 333-337], ozone [209, 221, 338-343] or hydrogen peroxide [289, 344-345] as oxidants. Basic carbons are the best catalysts and the oxidation of the organic compounds may occur both in the liquid phase (homogeneous reaction) and on the catalyst surface (heterogeneous reaction) [169].

Ozonation processes have been studied in detail, and it has been reported that activated carbons accelerate the decomposition of ozone [346-350]. Both textural and surface chemical properties can influence decomposition. The delocalised π electrons or the oxygen basic surface groups, like chromene and pyrone [221], or the pyrrolic groups [339, 347] have been identified as the active centres for ozone decomposition.

5.1.5. Other Reactions

Several other reactions have been studied using activated carbons as catalysts (Table 3). As their scientific and technical impact is lower than the previously mentioned reactions, a full description will not be made, but just a few examples will be highlighted. One of them is the *catalytic oxidation of Fe(II) in aqueous media*, where the influence of the AC surface chemistry is clearly important [351]. It was shown that Fe^{2+} oxidation without O_2 only occurs with oxidized activated carbons, in the presence of O_2, quinone or chromene surface groups.

Table 3. Examples of reactions catalysed by activated carbons (adapted from [128])

Reaction or process	Reference
Oxidation of Fe(II) in aqueous solution	[351-353]
Esterification of organic acids	[354]
Hydrocracking reactions	[355-360]
Decomposition of dimethyl methylphosphonate	[361]
Decomposition of hydrazine and hydroxylamine	[362-363]
Halogenation and dehalogenation	[364-372]
Selective oxidation	[211, 373-377]
Oxidation of salts	[378]
Synthesis of mesoarylporphyrins	[379]
Oxidative desulfurisation	[380-382]

5.1.6. Existing industrial applications

Activated carbons have industrial applications for the *purification* of a wide range of organic and inorganic compounds like amines, hydrochloric and other mineral acids, amino-acids, glycols, hydrocarbons, and several pharmaceuticals and intermediates [6]. Other applications are in the food industry, mainly in coffee decaffeination and *decolourisation* of various food products, such as sweeteners, like glucose/dextrose and high fructose corn syrup [6]. They are also widely used for *waste water treatment and odour removal* at a number of stages in municipal sewage treatment plants [6]. The urban tap water has often been filtered through swimming pool sized beds of activated carbon. There are also domestic water filters (often found under the kitchen sinks) that contain this material. The air in some public buildings passes through large tanks of activated carbon before being piped into the ventilation system. Also in automotive cabin *air purification* systems, activated carbons can be used to remove odours and pollutants [6]. In addition, activated carbon can be installed on the car fuel tanks to prevent gasoline vapours from escaping into the atmosphere. Activated carbons are very efficient in the removal of volatile organic compounds (VOC) from air and other gases. The very high removal efficiencies, typically greater than 99% at contact times as low as 0.1 s, can meet or even exceed the most strict air quality regulations [6]. The technology is reliable, simple, and has been proven over many years. Activated carbon has also been used industrially for the adsorption of mainly organic compounds, along with some inorganic compounds, such as iodine and mercury. It is also used in industry for the simultaneous removal of SO_2/NO_x from flue gases, acting both as an adsorbent and as a catalyst [169]. Moreover, activated carbon has been used for a long time as a catalyst in the industrial production of sulfur halides and phosgene ($COCl_2$), which is produced by the reaction of carbon monoxide with chlorine) [128, 169]. Finally, the surface chemistry of

carbon has been proven to be crucial in the ink jet industry, where various functional groups are introduced on the surface of carbons in order to increase the adhesion to different types of paper surfaces [128].

CONCLUSION

This chapter shows that activated carbons are very versatile materials that can be prepared from a large variety of precursors, including wastes, and both their texture and surface chemistry can be modified and optimised to make them adequate for the specific purposes. These materials have been already successfully used in several commercially viable chemical processes and in pollution control, including cleaning air space, water and vehicle exhausts. The potential of activated carbons for research is considerable, and upcoming results will certainly lead to even more applications and patents in the future.

REFERENCES

[1] Edwards, IAS. Structure in carbons and carbon forms. In: Marsh, H, editor. *Introduction to Carbon Science*. University of Newcastle upon Tyne: Butterworths; 1989.

[2] Rodríguez-Reinoso, F. Activated carbon: Structure, characterization, preparation and applications. In: Marsh, H, Heintz, U, Rodríguez-Reinoso, F, editors. *Introduction to Carbon Technologies*. Universidad de Alicante; 1997.

[3] Linares-Solano, A. Activated carbons and activated carbon fibers from coal. *Science and Technology of Activated Carbon* (short course). Alicante, Spain, 1994. p. 57-67.

[4] Benaddi, H; Bandosz, TJ; Jagiello, J; Schwarz, JA; Rouzaud, JN; Legras, D; Béguin, F. Surface functionality and porosity of activated carbons obtained from chemical activation of wood. *Carbon*. 2000, 38, 669-674.

[5] Rodríguez-Reinoso, F. Physical activation: Basis and technology. *Science and Technology of Activated Carbon (*short course). Alicante, Spain,1994. p. 36-46.

[6] Carabineiro, SAC. Actieve kool: adsorbeert alle milieuproblemen (Activated carbon: a solution to all environmental problems). *Chemisch Weekblad*. 2003, 99, 15.

[7] Rodríguez-Reinoso, F; Molinas-Sabio, M; González, MT. The use of team and CO_2 as activating agents in the preparation of activated carbons. *Carbon*. 1995, 33, 15-23.

[8] Tlas, M; Olontsev, VF; Elushankov, SL, Procedure for preparation of activated carbon from plant material includes carbonising fruit and/or olive stones in pyrogases medium without oxygen, Patent RU2104925-C1. 1998.

[9] Bacaoui, A; Yaacoubi, A; Dahbi, A; Bennouna, C; Ayele, J; Mazet, M. Activated carbon production from Moroccan olive wastes - Influence of some factors. *Environ. Technol*. 1998, 19, 1203-1212.

[10] El-Sheikh, AH; Newman, AP; Al-Daffaee, HK; Phull, S; Cresswell, N. Characterization of activated carbon prepared from a single cultivar of Jordanian Olive stones by chemical and physicochemical techniques. *J. Anal. Appl. Pyrol*. 2004, 71, 151-164.

[11] Martinez, ML; Torres, MM; Guzman, CA; Maestri, DM. Preparation and characteristics of activated carbon from olive stones and walnut shells. *Ind. Crop. Prod*. 2006, 23, 23-28.

[12] Spahis, N; Addoun, A; Mahmoudi, H; Ghaffour, N. Purification of water by activated carbon prepared from olive stones. *Desalination*. 2008, 222, 519-527.

[13] González, JF; Roman, S; Encinar, JM; Martinez, G. Pyrolysis of various biomass residues and char utilization for the production of activated carbons. *J. Anal. Appl. Pyrol*. 2009, 85, 134-141.

[14] Kutahyali, C; Eral, M. Sorption studies of uranium and thorium on activated carbon prepared from olive stones: Kinetic and thermodynamic aspects. *J. Nucl. Mater*. 2010, 396, 251-256.

[15] Buss, GY; Rodriguez-Reinoso, F; Making granular activated carbon by carbonaceous cellulose material with zinc chloride solution and carbonising, Patent EP329251-A2; ES2042961-A; EP329251-A; AU8929887-A; JP1246117-A; EP329251-B1; DE68908576-E; ES2042961-T3; CA1334192-C. EP329251-A2 EP329251-A, 23 Aug 1989.

[16] Caturla, F; Molina-Sabio, M; Rodríguez-Reinoso, F. Preparation of activated carbon by chemical activation with $ZnCl_2$. *Carbon*. 1991, 29, 999-1007.

[17] Arriagada, R; Garcia, R; Saavedra, G. Activated carbons from eucaliptus-globulus and peach stones. 1. Influence of preparation variables in some textural and adsorption properties. *Bull. Soc. Chil. Quim*. 1995, 40, 119-127.

[18] Vazquez, P; Pizzio, L; Blanco, M; Caceres, C; Thomas, H; Arriagada, R; Bendezu, S; Cid, R; Garcia, R. NiMo(W)-based hydrotreatment catalysts supported on peach stones activated carbon. *Appl. Catal. A: Gen*. 1999, 184, 303-313.

[19] Carabineiro, SAC. Estudos de conversão de NO, N_2O e CO_2 e adsorção/dessorção de SO_2 usando catalisadores binários suportados em carvão activado, Ph.D. Thesis, New University of Lisbon, Portugal; 2001.

[20] Munoz-González, Y; Arriagada-Acuna, R; Soto-Garrido, G; Garcia-Lovera, R. Activated carbons from peach stones and pine sawdust by phosphoric acid activation used in clarification and decolorization processes. *J. Chem. Technol. Biotechnol*. 2009, 84, 39-47.

[21] Maia, DAS; Sapag, K; Toso, JP; Lopez, RH; Azevedo, DCS; Cavalcante, CL; Zgrablich, G. Characterization of activated carbons from peach stones through the mixed geometry model. *Micropor. Mesopor. Mater*. 2010, 134, 181-188.

[22] Gomez-Serrano, V; Piriz-Almeida, F; Duran-Valle, CJ; Pastor-Villegas, J. Formation of oxygen structures by air activation. A study by FT-IR spectroscopy. *Carbon*. 1999, 37, 1517-1528.

[23] Duran-Valle, CJ; Gomez-Corzo, M; Pastor-Villegas, J; Gomez-Serrano, V. Study of cherry stones as raw material in preparation of carbonaceous adsorbents. *J. Anal. Appl. Pyrol.* 2005, 73, 59-67.

[24] Duran-Valle, CJ; Gomez-Corzo, M; Gomez-Serrano, V; Pastor-Villegas, J; Rojas-Cervantes, ML. Preparation of charcoal from cherry stones. *Appl. Surf. Sci*. 2006, 252, 5957-5960.

[25] Olivares-Marin, M; Fernandez-González, C; Macias-Garcia, A; Gomez-Serrano, V. Preparation of activated carbon from cherry stones by chemical activation with $ZnCl_2$. *Appl. Surf. Sci*. 2006, 252, 5967-5971.

[26] Olivares-Marin, M; Fernandez-González, C; Macias-Garcia, A; Gomez-Serrano, V. Preparation of activated carbons from cherry stones by activation with potassium hydroxide. *Appl. Surf. Sci*. 2006, 252, 5980-5983.

[27] Olivares-Marin, M; Fernandez-González, C; Macias-Garcia, A; Gomez-Serrano, V. Porous structure of activated carbon prepared from cherry stones by chemical activation with phosphoric acid. *Energ. Fuels*. 2007, 21, 2942-2949.

[28] Beker, U; Dertli, H; Duranoglu-Gulbayir, D; Cakan, RD. Study of cherry stones as a precursor in the preparation of low cost carbonaceous adsorbent. *Energ. Sources A*. 2010, 32, 1004-1015.

[29] Jaramillo, J; Alvarez, PM; Gomez-Serrano, V. Preparation and ozone-surface modification of activated carbon. Thermal stability of oxygen surface groups. *Appl. Surf. Sci.* 2010, 256, 5232-5236.

[30] Jaramillo, J; Álvarez, PM; Gómez-Serrano, V. Oxidation of activated carbon by dry and wet methods: Surface chemistry and textural modifications. *Fuel Proces. Technol*. 2010, 91, 1768-1775.

[31] Genceli, E; Apak, E; Razvigorova, M; Petrov, N; Minkova, V; Ekinci, E. Preparation, modification, and characterization of pitches from apricot stones. *Fuel Proces. Technol*. 2002, 75, 97-107.

[32] Sentorun-Shalaby, C; Ucak-Astarlioglu, MG; Artok, L; Sarici, C. Preparation and characterization of activated carbons by one-step steam pyrolysis/activation from apricot stones. *Micropor. Mesopor. Mater*. 2006, 88, 126-134.

[33] Soleimani, M; Kaghazchi, T. Agricultural waste conversion to activated carbon by chemical activation with phosphoric acid. *Chem. Eng. Technol*. 2007, 30, 649-654.

[34] Freitas, MMA. Preparação de peneiros moleculares de carbono, Ph.D. Thesis, University of Porto, Portugal; 1998.

[35] Su, W; Zhou, L; Zhou, YP. Preparation of microporous activated carbon from coconut shells without activating agents. *Carbon*. 2003, 41, 861-863.

[36] Wagh, DD; Arabale, GV; Kulkarni, MP; Mulla, IS; Kunjukrishanapillai, V; Vernekar, SP; Jha, RK; Jacob, NE, Preparation of high surface area activated carbon for fabricating fuel cell and ultracapacitor electrode, by treating coconut shell powder with activating agent, drying treated shell powder, and carbonizing powder in inert atmosphere, Patent US2005221981-A1; US7799733-B2. 2005.

[37] Achaw, OW; Afrane, G. The evolution of the pore structure of coconut shells during the preparation of coconut shell-based activated carbons. *Micropor. Mesopor. Mater*. 2008, 112, 284-290.

[38] Yang, K; Peng, J; Srinivasakannan, C; Zhang, L; Xia, H; Duan, X. Preparation of high surface area activated carbon from coconut shells using microwave heating. *Biores. Technol*. 2010, 101,

[39] Yang, KB; Peng, JH; Xia, HY; Zhang, LB; Srinivasakannan, C; Guo, SH. Textural characteristics of activated carbon by single step CO_2 activation from coconut shells. J. Taiwan Inst. *Chem. Eng*. 2010, 41, 367-372.

[40] Figueiredo, JL; Pereira, MFR; Freitas, MMA; Órfão, JJM. Characterization of active sites on carbon catalysts. *Ind. Eng. Chem. Res*,. 2007, 46, 4110-4115.

[41] Aqueous calcined shell powder solutions prepared by heating shells in furnace containing activated carbon, crushing, adding water and separating supernatant liquid, Patent JP52104497-A. 1977.

[42] Li, Z; Cai, F; Li, J; Li, H, Activated carbon preparation from furfural product residue-waste product, to replace wood, coal, nut shells, etc. currently used as starting material, Patent CN8703293-A. 1989.

[43] Merchant, AA; Petrich, MA. Preparation and characterisation of activated carbons from scrap tires, almond shells, and Illinois coal. *Chem. Eng. Commun*. 1992, 118, 251-263.

[44] Mulop, N; Teo, KC; Watkinson, AP. Preparation and characterisation of activated carbon derived from palm oil shells using a fixed bed pyroliser. *Bioproduct. Process*. 1994, 93-99.

[45] Nguyen, C; Do, DD. Preparation of carbon molecular sieves from macadamia nut shells. *Carbon*. 1995, 33, 1717-1725.

[46] Hussein, MZ; Tarmizi, RSH; Zainal, Z; Ibrahim, R; Badri, M. Preparation and characterization of active carbons from oil palm shells. *Carbon*. 1996, 34, 1447-1449.

[47] Ahmadpour, A; Do, DD. The preparation of activated carbon from macadamia nutshell by chemical activation. *Carbon*. 1997, 35, 1723-1732.

[48] Lua, AC; Guo, J. Microporous oil-palm-shell activated carbon prepared by physical activation for gas-phase adsorption. *Langmuir*. 2001, 17, 7112-7117.

[49] Shawabkeh, RA; Rockstraw, DA; Bhada, RK. Copper and strontium adsorption by a novel carbon material manufactured from pecan shells. *Carbon*. 2002, 40, 781-786.

[50] Bansode, RR; Losso, JN; Marshall, WE; Rao, RM; Portier, RJ. Adsorption of volatile organic compounds by pecan shell- and almond shell-based granular activated carbons. *Biores. Technol*. 2003, 90, 175-184.

[51] Sivabalan, R; Rengaraj, S; Arabindoo, B; Murugesan, V. Cashewnut sheath carbon: A new sorbent for defluoridation of water. *Indian J. Chem. Technol*. 2003, 10, 217-222.

[52] Yang, T; Lua, AC. Characteristics of activated carbons prepared from pistachio-nut shells by potassium hydroxide activation. *Micropor. Mesopor. Mater*. 2003, 63, 113-124.

[53] Yang, T; Lua, AC. Characteristics of activated carbons prepared from pistachio-nut shells by physical activation. *J. Colloid Interf. Sci*. 2003, 267, 408-417.

[54] Ng, C; Marshall, WE; Rao, RM; Bansode, RR; Losso, JN. Activated carbon from pecan shell: process description and economic analysis. *Ind. Crop. Prod*. 2003, 17, 209-217.

[55] Lua, AC; Yang, T. Effect of activation temperature on the textural and chemical properties of potassium hydroxide activated carbon prepared from pistachio-nut shell. *J. Colloid Interf. Sci*. 2004, 274, 594-601.

[56] Lua, AC; Yang, T. Effects of vacuum pyrolysis conditions on the characteristics of activated carbons derived from pistachio-nut shells. *J. Colloid Interf. Sci*. 2004, 276, 364-372.

[57] Lua, AC; Yang, T. Characteristics of activated carbon prepared from pistachio-nut shell by zinc chloride activation under nitrogen and vacuum conditions. *J. Colloid Interf. Sci*. 2005, 290, 505-513.

[58] Kim, DH, Preparation method of liquid calcium chloride using shells, Patent KR2004069754-A; KR481286-B. 2005.

[59] Yang, T; Lua, AC. Textural and chemical properties of zinc chloride activated carbons prepared from pistachio-nut shells. *Mater. Chem. Phys*. 2006, 100, 438-444.

[60] Jin, HK, High porous activated carbon for hydrogen storage prepared by dehydrating and activating a mixed powder of nut shells and potassium compounds and preparation method thereof, Patent KR2006034420-A; KR599254-B1. 2007.

[61] Sun, Y; Wei, W; Liu, S; Li, J; Zhao, N, Method for preparing porous solid alkali, involves preparing activated carbon from nut shells, treating, adding in aqueous solution of nitrate, stirring, drying, claiming, heating and keeping in temperature, Patent CN1868592-A; CN100395026-C. 2007.

[62] Kaghazchi, T; Kolur, NA; Soleimani, M. Licorice residue and pistachio-nut shell mixture: A promising precursor for activated carbon. *J. Ind. Eng. Chem*. 2010, 16, 368-374.

[63] Hao, M; Wang, L, Preparation of activated carbon by drying almond shells, screening, soaking in zinc chloride, irradiating in microwave oven, subjecting to pyrolysis oven, subjecting to acid pickling and water washing, drying, grinding, and screening, Patent CN101618871-A. 2010.

[64] Dubois, JL; Plee, D, Use of oil cake, optionally with shells of oilseed plants, preferably non-alimentary for the preparation of active carbon, which is useful as e.g. agent for purification of solid, preferably in food and as agent for purification of water, Patent FR2943048-A1; WO2010103239-A1. 2010.

[65] Sumathi, S; Bhatia, S; Lee, KT; Mohamed, AR. Selection of best impregnated palm shell activated carbon (PSAC) for simultaneous removal of SO_2 and NO_x. *J. Haz. Mater*. 2010, 176, 1093-1096.

[66] Jain, KD; Sharma, MK. Preparation of activated carbon from basmati rice husk. *J. Indian Chem. Soc*. 1971, 48, 1155-and.

[67] Active carbon preparation from rice contaminated with cadmium, Patent JP53026339-A. 1978.

[68] Activated carbon preparation by adding rice bran to crushed coal, carbonising, crushing, sizing and activating, Patent JP2221108-A. 1990.

[69] Usmani, TH; Ahmad, TW; Yousufzai, AHK. Preparation and liquid-phase characterization of granular activated-carbon from rice husk. *Biores. Technol*. 1994, 48, 31-35.

[70] Gu, K; Gu, R; Zhang, T, Preparation of high performance active carbon utilising rice as raw material, Patent CN1110957-A. 1997.

[71] Guo, YP; Yang, SF; Zhao, JZ; Wang, ZC; Zhao, MY. Preparation of active carbon with high specific surface area from rice husks. *Chem. J. Chin. Univ*. 2000, 21, 335-338.

[72] Ju, F; Liu, W, Preparing water glass and by-product active carbon using rice hull ash carbon, Patent CN1229057-A. 2000.

[73] Guo, YP; Yang, SF; Yu, KF; Zhao, JZ; Wang, ZC; Xu, HD. The preparation and mechanism studies of rice husk based porous carbon. *Mater. Chem. Phys*. 2002, 74, 320-323.

[74] Oh, GH; Park, CR. Preparation and characteristics of rice-straw-based porous carbons with high adsorption capacity. *Fuel*. 2002, 81, 327-336.

[75] Kang, AS; Kim, MS; Lim, JB, Preparing method of rice hull activated carbon for electric double layer capacitor, Patent KR2002007458-A; KR348499-B. 2003.

[76] Kennedy, LJ; Vijaya, JJ; Sekaran, G. Effect of two-stage process on the preparation and characterization of porous carbon composite from rice husk by phosphoric acid activation. *Ind. Eng. Chem. Res*,. 2004, 43, 1832-1838.

[77] Balathanigaimani, MS; Kang, HC; Shim, WG; Kim, C; Lee, JW; Moon, H. Preparation of powdered activated carbon from rice husk and its methane adsorption properties. *Korean J. Chem. Eng*. 2006, 23, 663-668.

[78] Suzuki, RM; Andrade, AD; Sousa, JC; Rollemberg, MC. Preparation and characterization of activated carbon from rice bran. *Biores. Technol*. 2007, 98, 1985-1991.

[79] Zheng, X; Lang, G; Zhang, F; Wang, X, Active carbon plate material prepared by rice husk and bamboo wood waste material, Patent CN1868873-A; CN100344535-C. 2007.

[80] Schettino, MA; Freitas, JCC; Cunha, AG; Emmerich, FG; Soares, AB; Silva, PRN. *Preparation and characterization of chemically activated carbon from rice hulls*. Quim. Nova. 2007, 30, 1663-1668.

[81] Deiana, C; Granados, D; Venturini, R; Amaya, A; Sergio, M; Tancredi, N. Activated carbons obtained from rice husk: Influence of leaching on textural parameters. *Ind. Eng. Chem. Res*,. 2008, 47, 4754-4757.

[82] Liou, T-H; Wu, S-J. Characteristics of microporous/mesoporous carbons prepared from rice husk under base- and acid-treated conditions. *J. Haz. Mater*. 2009, 171, 693-703.

[83] Hsu, S-T; Chen, L-C; Lee, C-C; Pan, T-C; You, B-X; Yan, Q-F. Preparation of methacrylic acid-modified rice husk improved by an experimental design and application for paraquat adsorption. *J. Haz. Mater*. 2009, 171, 465-470.

[84] Liou, TH; Wu, SJ. Characteristics of microporous/mesoporous carbons prepared from rice husk under base- and acid-treated conditions. *J. Haz. Mater*. 2009, 171, 693-703.

[85] Hu, Z; Liu, Y; Wang, Z; Ye, F, Co-producing and preparing nanometer silicon dioxide and active carbon by using rice hull ash comprises adding lye to rice hull ash, regulating modulus of silicate, acidifying reaction product, performing activation, and drying, Patent CN101691225-A. 2010.

[86] Chen, G; Li, L; Lin, Q; Li, Z, Preparation of activated carbon from rice hull and straw, by pretreating raw materials, carbonizing, treating with hydrochloric acid or phosphoric acid solution, treating with sodium hydroxide, and sieving, Patent CN101708845-A. 2010.

[87] Uzunova, SA; Uzunov, IM; Vassilev, SV; Alexandrova, AK; Staykov, SG; Angelova, DB. Preparation of low-ash-content porous carbonaceous material from rice husks. *Bulg. Chem. Commun*. 2010, 42, 130-137.

[88] Awwad, NS; Gad, HMH; Ahmad, MI; Aly, HF. Sorption of lanthanum and erbium from aqueous solution by activated carbon prepared from rice husk. *Colloids Surf B Biointerfaces*. 2010, 81, 593-599.

[89] Carrott, PJM; Carrott, M; Lima, RP. Preparation of activated carbon "membranes" by physical and chemical activation of cork. *Carbon*. 1999, 37, 515-517.

[90] Carrott, PJM; Carrott, M; Mourao, PAM; Lima, RP. Preparation of activated carbons from cork by physical activation in carbon dioxide. *Adsorpt. Sci. Technol*. 2003, 21, 669-681.

[91] Carvalho, AP; Cardoso, B; Pires, J; de Carvalho, MB. Preparation of activated carbons from cork waste by chemical activation with KOH. *Carbon*. 2003, 41, 2873-2876.

[92] Cardoso, B; Mestre, AS; Carvalho, AP; Pires, J. Activated carbon derived from cork powder waste by KOH activation: Preparation, characterization, and VOCs adsorption. *Ind. Eng. Chem. Res*,. 2008, 47, 5841-5846.

[93] Activated carbon preparation by burning coal or lignite and then heating with steam, Patent JP48038888-A; JP76007158-B. 1974.

[94] Lakhevich, GD; Proskuryak, VA; Yakovlev, VI, Preparation of carbon-type sorbent by heating mixture of acid tar and lignite and activating with live steam, Patent SU937331-B. 1983.

[95] Karl, A; Walter, E; Kleinschmi, P; Gottschlic, H; Kutz, R; Koth, D, Production of active carbon from brown coal high temperature coke prepared by activating lignite coke with steam while spraying alkali (ne earth) carbonate or hydroxide solution into revolving cylinder furnace, Patent DE3418150-A1; EP164492-A2; US4642304-C1; AU8542490-A; JP60255608-A; ZA8503489-A; US4603119-A; US4642304-A; JP89059970-B; EP164492-B; DE3583894-G. 1985.

[96] Szargan, P; Spindler, H; Mobius, R; Kraft, M; Klose, E; Heschel, W, Prepn. of microporous active carbon from lignite coke|by activation in atmos. contg. steam and carbon di:oxide, limiting heat supply, Patent DD268677-A. 1989.

[97] Karl, A, Activated carbon production by heating freshly mined lignite to high temperature, Patent EP363613-A2; DE3834745-A; JP2153813-A; US5292708-A. 1990.

[98] Toles, C; Rimmer, S; Hower, JC. Production of activated carbons from a washington lignite using phosphoric acid activation. *Carbon*. 1996, 34, 1419-1426.

[99] Chattopadhyaya, G; Macdonald, DG; Bakhshi, NN; Soltan, JS; Dalai, AK. Preparation and characterization of chars and activated carbons from Saskatchewan lignite. *Fuel Proces. Technol*. 2006, 87, 997-1006.

[100] Starck, J; Burg, P; Muller, S; Bimer, J; Furdin, G; Fioux, P; Vix Guterl, C; Begin, D; Faure, P; Azambre, B. The influence of demineralisation and ammoxidation on the adsorption properties of an activated carbon prepared from a Polish lignite. *Carbon*. 2006, 44, 2549-2557.

[101] Havelcova, M; Mizera, J; Sykorova, I; Pekar, M. Sorption of metal ions on lignite and the derived humic substances. *J. Haz. Mater*. 2009, 161, 559-564.

[102] Alcaniz-Monge, J; Perez-Cadenas, M; Lozano-Castello, D. Effect of the pre-oxidation of coals in the preparation of chemically activated carbon pellets. *Energ. Fuels*. 2010, 24, 3385-3393.

[103] Wang, G; Yan, Z; Wang, Z, Preparation of granular activated carbon in black brick kiln by pretreatment of anthracite as raw material, loading into kiln and firing, Patent CN1031514-A. 1990.

[104] Gergova, K; Eser, S; Schobert, HH. Preparation and characterization of activated carbons from anthracite. *Energ. Fuels*. 1993, 7, 661-668.

[105] An, F; Yuan, G, Preparation of coal-base activated carbon by grinding bituminous coal and anthracite, adding coal tar, water, and catalyst, kneading, carburising, and activating, Patent CN1094994-A. 1996.

[106] Daulan, C; Lyubchik, SB; Rouzaud, JN; Beguin, F. Influence of anthracite pretreatment in the preparation of activated carbons. *Fuel*. 1998, 77, 495-502.

[107] Lillo-Rodenas, MA; Lozano-Castello, D; Cazorla-Amoros, D; Linares-Solano, A. Preparation of activated carbons from Spanish anthracite II. Activation by NaOH. *Carbon*. 2001, 39, 751-759.

[108] Lozano-Castello, D; Lillo-Rodenas, MA; Cazorla-Amoros, D; Linares-Solano, A. Preparation of activated carbons from Spanish anthracite I. Activation by KOH. *Carbon*. 2001, 39, 741-749.

[109] Zhang, F, Super-strong decolored activated carbon block preparation from anthracite, Patent CN1309081-A; CN1145584-C. 2002.

[110] Kuznetsov, BN; Chesnokov, NV; Mikova, NM; Drozdov, VA; Shendrik, TG; Lyubchik, SB; Fonseca, IM. Properties of palladium catalysts on carbon supports prepared from chemically modified and activated anthracites. *React. Kinet. Catal. Lett*. 2004, 83, 361-367.

[111] Lyubchik, SB; Galushko, LY; Rego, AM; Tamarkina, YV; Galushko, OL; Fonseca, IM. Intercalation as an approach to the activated carbon preparation from Ukrainian anthracites. *J. Phys. Chem. Solids*. 2004, 65, 127-132.

[112] Li, DY; Zhou, HL; Tian, YJ; Wei, LQ; Wu, XF; Li, WJ; Chen, YF. High-speciric-surface-area activated carbon from anthracite. *Rare Met. Mater. Eng*. 2007, 36, 583-586.

[113] Li, Q; Lv, L; Xiao, R; Xu, S, Preparing activated carbon involves crushing high-carbon material e.g. petrol coke and anthracite, where high-carbon material is mixed with potassium hydroxide to obtain alkali-carbon mixture, Patent CN101700885-A. 2010.

[114] Park, SG, Preparation of activated carbon using fly ash generated in steam power plant and molding method, Patent KR2001083864-A; KR462193-B. 2002.

[115] Caramuscio, P; De Stefano, L; Seggiani, M; Vitolo, S; Narducci, P. Preparation of activated carbons from heavy-oil fly ashes. *Waste Manage*. 2003, 23, 345-351.

[116] Demirbas, A; Arslan, G; Pehlivan, E. Recent studies on activated carbons and fly ashes from Turkish resources. *Energ. Sources A*. 2006, 28, 627-638.

[117] Rubio, B; Izquierdo, MT; Mayoral, MC; Bona, MT; Andres, JM. Unburnt carbon from coal fly ashes as a precursor of activated carbon for nitric oxide removal. *J. Haz. Mater*. 2007, 143, 561-566.

[118] Uddin, MA; Shinozaki, Y; Furusawa, N; Yamada, T; Yamaji, Y; Sasaoka, E. Preparation of activated carbon from asphalt and heavy oil fly ash and coal fly ash by pyrolysis. *J. Anal. Appl. Pyrol*. 2007, 78, 337-342.

[119] Miyake, M; Kimura, Y; Ohashi, T; Matsuda, M. Preparation of activated carbon-zeolite composite materials from coal fly ash. *Micropor. Mesopor. Mater*. 2008, 112, 170-177.

[120] Wu, FC; Wu, PH; Tseng, RL; Juang, RS. Preparation of activated carbons from unburnt coal in bottom ash with KOH activation for liquid-phase adsorption. *J. Environ, Manage*. 2010, 91, 1097-1102.

[121] Rubio, B; Izquierdo, MT. Coal fly ash based carbons for SO_2 removal from flue gases. *Waste Manage*. 2010, 30, 1341-1347.

[122] Ogasawara, S; Kuroda, M; Wakao, N. Preparation of activated carbon by thermal-decomposition of used automotive tires. *Ind. Eng. Chem. Res*,. 1987, 26, 2552-2556.

[123] Teng, HS; Lin, YC; Hsu, LY. Production of activated carbons from pyrolysis of waste tires impregnated with potassium hydroxide. *J. Air Waste Manag. Ass*. 2000, 50, 1940-1946.

[124] Ariyadejwanich, P; Tanthapanichakoon, W; Nakagawa, K; Mukai, SR; Tamon, H. Preparation and characterization of mesoporous activated carbon from waste tires. *Carbon*. 2003, 41, 157-164.

[125] Yuan, CS; Lin, HY; Wu, CH; Liu, MH. Preparation of sulfurized powdered activated carbon from waste tires using an innovative compositive impregnation process. *J. Air Waste Manag. Ass*. 2004, 54, 862-870.

[126] Skodras, G; Diamantopouiou, I; Zabaniotou, A; Stavropoulos, G; Sakellaropoulos, GP. Enhanced mercury adsorption in activated carbons from biomass materials and waste tires. *Fuel Proces. Technol*. 2007, 88, 749-758.

[127] Pereira, MFR; Órfão, JJM; Figueiredo, JL. Les charbons actifs dans le traitement des eaux. Traitement et épuration des eaux industrielles polluées. Procédés membranaires, bioadsorption et oxydation chimique. Presses Universitaires de Franche-Comté; 2007. p. 265-304.

[128] Serp, P; Figueiredo, JL, editors. Carbon Materials for Catalysis. Hoboken, New Jersey: John Wiley and Sons, Inc.; 2009.

[129] Lu, GQ; Do, DD. Preparation of economical sorbents for SO_2 and NO_x removal using coal washery reject. *Carbon*. 1991, 29, 207-213.

[130] Davini, P. SO_2 and NO_x adsorption properties of activated carbons obtained from a pitch containing iron derivatives. *Carbon*. 2001, 39, 2173-2179.

[131] Claudino, A; Soares, JL; Moreira, RFPM; José, HJ. Adsorption equilibrium and breakthrough analysis for NO adsorption on activated carbons at low temperatures. *Carbon*. 2004, 42, 1483-1490.

[132] Diaz, E; Ordonez, S; Vega, A; Coca, J. Comparison of adsorption properties of a chemically activated and a steam-activated carbon, using inverse gas chromatography. *Micropor. Mesopor. Mater*. 2005, 82, 173-181.

[133] Belhachemi, M; Rios, R; Addoun, F; Silvestre-Albero, J; Sepulveda-Escribano, A; Rodriguez-Reinoso, F. Preparation of activated carbon from date pits: Effect of the activation agent and liquid phase oxidation. *J. Anal. Appl. Pyrol*. 2009, 86, 168-172.

[134] Jagtoyen, M; Derbyshire, F. Activated carbons from yellow poplar and white oak by H_3PO_4 activation. *Carbon*. 1998, 36, 1085-1097.

[135] Molina-Sabio, M; Almansa, C; Rodríguez-Reinoso, F. Phosphoric acid activated carbon discs for methane adsorption. *Carbon*. 2003, 41, 2113-2119.

[136] Almansa, C; Molina-Sabio, M; Rodríguez-Reinoso, F. Adsorption of methane into $ZnCl_2$-activated carbon derived discs. *Micropor. Mesopor. Mater*. 2004, 76, 185-191.

[137] Lee, Y-W; Park, J-W; Jun, S-J; Choi, D-K; Yie, J-E. NO_x adsorption-temperature programmed desorption and surface molecular ions distribution by activated carbon with chemical modification. *Carbon*. 2004, 42, 59-69.

[138] Bleda-Martinez, MJ; Lozano-Castello, D; Morallon, E; Cazorla-Amoros, D; Linares-Solano, A. Chemical and electrochemical characterization of porous carbon materials. *Carbon*. 2006, 44, 2642-2651.

[139] Rodríguez-Reinoso, F; Nakagawa, Y; Silvestre-Albero, J; Juárez-Galán, JM; Molina-Sabio, M. Correlation of methane uptake with microporosity and surface area of chemically activated carbons. *Micropor. Mesopor. Mater*. 2008, 115, 603-608.

[140] Gniot, I; Kirszensztejn, P; Kozlowski, M. Oxidative dehydrogenation of isobutane using modified activated carbons as catalysts. *Appl. Catal. A: Gen*. 2009, 362, 67-74.

[141] Boehm, HP. Some aspects of the surface chemistry of carbon blacks and other carbons. *Carbon*. 1994, 32, 759-769.

[142] Leon y Leon, C; Radovic, L. Chemistry and Physics of Carbon. Thrower, PA, editor; Vol. 24; Dekker, M, publisher; New York: 1994.

[143] Moreno-Castilla, C; Ferro-García, MA; Joly, JP; Bautista-Toledo, I; Carrasco-Marín, F; Rivera-Utrilla, J. Activated carbon surface modifications by nitric acid, hydrogen peroxide and ammonium peroxydisulfate treatments. *Langmuir*. 1995, 11, 4386-4392.

[144] Radovic, L; Rodríguez-Reinoso, F. Chemistry and Physics of Carbon. Thrower, PA, editor; Vol. 25; Dekker, M, publisher; New York: 1997.

[145] de la Puente, G; Pis, JJ; Menendez, JA; Grange, P. Thermal stability of oxygenated functions in activated carbons. *J. Anal. Appl. Pyrol*. 1997, 43, 125-138.
[146] Rodríguez-Reinoso, F; Molina-Sabio, M. Textural and chemical characterization of microporous carbons. *Adv. Colloid Interf. Sci*. 1998, 76, 271-294.
[147] Pereira, MFR. Desidrogenação oxidativa do etilbenzeno, Ph.D. Thesis, University of Porto, Portugal; 1998.
[148] López-Ramón, MV; Stoeckli, F; Moreno-Castilla, C; Carrasco-Marín, F. On the characterization of acidic and basic surface sites on carbons by various techniques. *Carbon*. 1999, 37, 1215-1221.
[149] Zhu, ZH; Wang, S; Lu, GQ; Zhang, DK. The role of carbon surface chemistry in N_2O conversion to N_2 over Ni catalyst supported on activated carbon. *Catal. Today*. 1999, 53, 669-681.
[150] Haydar, S; Moreno-Castilla, C; Ferro-García, MA; Carrasco-Marín, F; Rivera-Utrilla, J; Perrard, A; Joly, JP. Regularities in the temperature-programmed desorption spectra of CO_2 and CO from activated carbons. *Carbon*. 2000, 38, 1297-1308.
[151] Moreno-Castilla, C; Lopez-Ramon, MV; Carrasco-Marín, F. Changes in surface chemistry of activated carbons by wet oxidation. *Carbon*. 2000, 38, 1995-2001.
[152] Aksoylu, AE; Freitas, MMA; Pereira, MFR; Figueiredo, JL. The effects of different activated carbon supports and support modifications on the properties of Pt/AC catalysts. *Carbon*. 2001, 39, 175-185.
[153] Salame, II; Bandosz, TJ. Surface chemistry of activated carbons: Combining the results of temperature-programmed desorption, Boehm, and potentiometric titrations. *J. Colloid Interf. Sci*. 2001, 240, 252-258.
[154] Domingo-Garcia, M; Garzon, FJL; Perez-Mendoza, MJ. On the characterization of chemical surface groups of carbon materials. *J. Colloid Interf. Sci*. 2002, 248, 116-122.
[155] Szymanski, GS; Karpinski, Z; Biniak, S; Swiatkowski, A. The effect of the gradual thermal decomposition of surface oxygen species on the chemical and catalytic properties of oxidized activated carbon. *Carbon*. 2002, 40, 2627-2639.
[156] Silva, AR; Vital, J; Figueiredo, JL; Freire, C; de Castro, B. Activated carbons with immobilised manganese(III) salen complexes as heterogeneous catalysts in the epoxidation of olefins: Influence of support and ligand functionalisation on selectivity and reusability. *New J. Chem*. 2003, 27, 1511-1517.
[157] Calvo, L; Gilarranz, MA; Casas, JA; Mohedano, AF; Rodriguez, JJ. Effects of support surface composition on the activity and selectivity of Pd/C catalysts in aqueous-phase hydrodechlorination reactions. *Ind. Eng. Chem. Res*,. 2005, 44, 6661-6667.
[158] Li, JY; Ma, L; Li, XN; Lu, CS; Liu, HZ. Effect of nitric acid, pretreatment on the properties of activated carbon and supported palladium catalysts. *Ind. Eng. Chem. Res,*. 2005, 44, 5478-5482.
[159] Fletcher, AJ; Uygur, Y; Thomas, KM. Role of surface functional groups in the adsorption kinetics of water vapor on microporous activated carbons. *J. Phys. Chem. B*. 2007, 111, 8349-8359.
[160] Wang, SB; Zhu, ZH. Effects of acidic treatment of activated carbons on dye adsorption. *Dyes Pigments*. 2007, 75, 306-314.
[161] Gorgulho, HF; Mesquita, JP; Gonçalves, F; Pereira, MFR; Figueiredo, JL. Characterization of the surface chemistry of carbon materials by potentiometric titrations and temperature-programmed desorption. *Carbon*. 2008, 46, 1544-1555.

[162] Almarri, M; Ma, XL; Song, CS. Role of surface oxygen-containing functional groups in liquid-phase adsorption of nitrogen compounds on carbon-based adsorbents. *Energ. Fuels*. 2009, 23, 3940-3947.

[163] Calvillo, L; Moliner, R; Lazaro, MJ. Modification of the surface chemistry of mesoporous carbons obtained through colloidal silica templates. *Mater. Chem. Phys.* 2009, 118, 249-253.

[164] Kohl, S; Drochner, A; Vogel, H. Quantification of oxygen surface groups on carbon materials via diffuse reflectance FT-IR spectroscopy and temperature programmed desorption. *Catal. Today*. 2010, 150, 67-70.

[165] Wang, L; Zhou, YB; Liu, QF; Guo, Y; Lu, GZ. Effect of surface properties of activated carbon on CO oxidation over supported Wacker-type catalysts. *Catal. Today*. 2010, 153, 184-188.

[166] Boehm, HP. Surface oxides on carbon. *High Temp. High Pressures*. 1990, 22, 275-288.

[167] Ehrburger, P. Characteristics of activated carbon. II. Chemistry. Science and Technology of Activated Carbon (short course). Alicante, Spain1994. p. 25-35.

[168] Figueiredo, JL; Pereira, MFR; Freitas, MMA; Órfão, JJM. Modification of the surface chemistry of activated carbons. *Carbon*. 1999, 37, 1379-1389.

[169] Figueiredo, JL; Pereira, MFR. The role of surface chemistry in catalysis with carbons. *Catal. Today*. 2010, 150, 2-7.

[170] Menéndez, JA; Phillips, J; Xia, B; Radovic, LR. On the modification and characterization of chemical surface properties of activated carbon: In the search of carbons with stable basic properties. *Langmuir*. 1996, 12, 4404-4410.

[171] Contescu, A; Contescu, C; Putyera, K; Schwarz, JA. Surface acidity of carbons characterized by their continuous pK distribution and Boehm titration. *Carbon*. 1997, 35, 83-94.

[172] Strelko, VV; Kuts, VS; Thrower, PA. On the mechanism of possible influence of heteroatoms of nitrogen, boron and phosphorus in a carbon matrix on the catalytic activity of carbons in electron transfer reactions. *Carbon*. 2000, 38, 1499-1503.

[173] Radovic, LR; Moreno-Castilla, C; Rivera-Utrilla, J. Chemistry and Physics of Carbon. Radovic, LR, editor; Vol. 27; Dekker, M, publisher; New York: 2000.

[174] Vinke, P; van der Eijk, M; Verbree, M; Voskamp, AF; van Bekkum, H. Modification of the surfaces of a gasactivated carbon and a chemically activated carbon with nitric acid, hypochlorite, and ammonia. *Carbon*. 1994, 32, 675-686.

[175] Lahaye, J. The chemistry of carbon surfaces. *Fuel*. 1998, 77, 543-547.

[176] Xie, F; Phillips, J; Silva, IF; Palma, MC; Menéndez, JA. Microcalorimetric study of acid sites on ammonia- and acid-pretreated activated carbon. *Carbon*. 2000, 38, 691-700.

[177] Raymundo-Piñero, E; Cazorla-Amorós, D; Linares-Solano, A. The role of different nitrogen functional groups on the removal of SO_2 from flue gases by N-doped activated carbon powders and fibres. *Carbon*. 2003, 41, 1925-1932.

[178] Boudou, JP. Surface chemistry of a viscose-based activated carbon cloth modified by treatment with ammonia and steam. *Carbon*. 2003, 41, 1955-1963.

[179] Boudou, JP; Chehimi, M; Broniek, E; Siemieniewska, T; Bimer, J. Adsorption of H_2S or SO_2 on an activated carbon cloth modified by ammonia treatment. *Carbon*. 2003, 41, 1999-2007.

[180] Szymanski, GS; Grzybek, T; Papp, H. Influence of nitrogen surface functionalities on the catalytic activity of activated carbon in low temperature SCR of NO_x with NH_3. *Catal. Today*. 2004, 90, 51-59.

[181] Przepiórski, J; Skrodzewicz, M; Morawski, AW. High temperature ammonia treatment of activated carbon for enhancement of CO_2 adsorption. *Appl. Surf. Sci*. 2004, 225, 235-242.

[182] Przepiórski, J. Enhanced adsorption of phenol from water by ammonia-treated activated carbon. *J. Haz. Mater*. 2006, 135, 453-456.

[183] Inagaki, N; Narushima, K; Hashimoto, H; Tamura, K. Implantation of amino functionality into amorphous carbon sheet surfaces by NH_3 plasma. *Carbon*. 2007, 45, 797-804.

[184] Feng, W; Borguet, E; Vidic, RD. Sulfurization of carbon surface for vapor phase mercury removal - I: Effect of temperature and sulfurization protocol. *Carbon*. 2006, 44, 2990-2997.

[185] Feng, W; Borguet, E; Vidic, RD. Sulfurization of a carbon surface for vapor phase mercury removal - II: Sulfur forms and mercury uptake. *Carbon*. 2006, 44, 2998-3004.

[186] Chin, HC. Preparation and characterization of carbon-sulfur surface compounds. *Carbon*. 1981, 19, 175-186.

[187] Bourbigot, S; Le Bras, M; Delobel, R; Bréant, P; Trémillon, J-m. Carbonization mechanisms resulting from intumescence-part II. Association with an ethylene terpolymer and the ammonium polyphosphate-pentaerythritol fire retardant system. *Carbon*. 1995, 33, 283-294.

[188] Imamura, R; Matsui, K; Takeda, S; Ozaki, J; Oya, A. A new role for phosphorus in graphitization of phenolic resin. *Carbon*. 1999, 37, 261-267.

[189] Rivin, D; Aron, J. 118. Halogenation of carbon black. *Carbon*. 1965, 3, 358-359.

[190] Tobias, H; Soffer, A. Chemisorption of halogen on carbons-I. Stepwise chlorination and exchange of C-CI with C-H bonds. *Carbon*. 1985, 23, 281-289.

[191] Hill, A; Marsh, H. A study of the adsorption of iodine and acetic acid from aqueous solutions on characterized porous carbons. *Carbon*. 1968, 6, 31-39.

[192] Puri, BR; Bansal, RC. Iodine adsorption method for measuring surface area of carbon blacks. *Carbon*. 1965, 3, 227-230.

[193] Samant, PV; Fernandes, JB; Rangel, CM; Figueiredo, JL. Carbon xerogel supported Pt and Pt-Ni catalysts for electro-oxidation of methanol in basic medium. *Catal. Today*. 2005, 102, 173-176.

[194] Job, N; Pereira, MFR; Lambert, S; Cabiac, A; Delahay, G; Colomer, JF; Marien, J; Figueiredo, JL; Pirard, JP. Highly dispersed platinum catalysts prepared by impregnation of texture-tailored carbon xerogels. *J. Catal*. 2006, 240, 160-171.

[195] Mahata, N; Pereira, MFR; Suarez-Garcia, F; Martinez-Alonso, A; Tascon, JMD; Figueiredo, J. Tuning of texture and surface chemistry of carbon xerogels. *J. Colloid Interf. Sci*. 2008, 324, 150-155.

[196] Pereira, MFR; Órfão, JJM; Figueiredo, JL. Oxidative dehydrogenation of ethylbenzene on activated carbon catalysts. I. Influence of surface chemical groups. *Appl. Catal. A: Gen*. 1999, 184, 153-160.

[197] Pereira, MFR; Soares, SF; Órfão, JJM; Figueiredo, JL. Adsorption of dyes on activated carbons: Influence of surface chemical groups. *Carbon*. 2003, 41, 811-821.

[198] Faria, PCC; Órfão, JJM; Pereira, MFR. Adsorption of anionic and cationic dyes on activated carbons with different surface chemistries. *Water Res*. 2004, 38, 2043-2052.

[199] Silva, IF; Vital, J; Ramos, AM; Valente, H; do Rego, AMB; Reis, MJ. Oxydehydrogenation of cyclohexanol over carbon catalysts. *Carbon*. 1998, 36, 1159-1165.

[200] Silva, AR; Freitas, MMA; Freire, C; de Castro, B; Figueiredo, JL. Heterogenization of a functionalized copper(II) Schiff base complex by direct immobilization onto an oxidized activated carbon. *Langmuir*. 2002, 18, 8017-8024.

[201] Ryczkowski, J; Pasieczna, S; Figueiredo, JL; Pereira, MFR; Borowiecki, T. Characterization of activated carbons by FT-IR/PAS and TPD. *J. Phys*. IV. 2004, 117, 57-63.

[202] Silva, AR; Figueiredo, JL; Freire, C; de Castro, B. Manganese(III) salen complexes anchored onto activated carbon as heterogeneous catalysts for the epoxidation of olefins. *Micropor. Mesopor. Mater*. 2004, 68, 83-89.

[203] Jagiello, J; Bandosz, TJ; Schwarz, JA. Application of inverse gas chromatography at infinite dilution to study the effects of oxidation of activated carbons. *Carbon*. 1992, 30, 63-69.

[204] Moreno-Castilla, C; Carrasco-Marín, F; Parejo-Pérez, C; López Ramón, MV. Dehydration of methanol to dimethyl ether catalyzed by oxidized activated carbons with varying surface acidic character. *Carbon*. 2001, 39, 869-875.

[205] Teng, H; Tu, Y-T; Lai, Y-C; Lin, C-C. Reduction of NO with NH3 over carbon catalysts: The effects of treating carbon with H_2SO_4 and HNO_3. *Carbon*. 2001, 39, 575-582.

[206] Aguilar, C; García, R; Soto-Garrido, G; Arriagada, R. Catalytic wet air oxidation of aqueous ammonia with activated carbon. *Appl. Catal. B: Environ*. 2003, 46, 229-237.

[207] Ania, CO; Parra, JB; Pis, JJ. Oxygen-induced decrease in the equilibrium adsorptive capacities of activated carbons. *Adsorpt. Sci. Technol*. 2004, 22, 337-351.

[208] Quintanilla, A; Casas, JA; Rodríguez, JJ. Catalytic wet air oxidation of phenol with modified activated carbons and Fe/activated carbon catalysts. *Appl. Catal. B: Environ*. 2007, 76, 135-145.

[209] Faria, PCC; Órfão, JJM; Pereira, MFR. Ozonation of aniline promoted by activated carbon. *Chemosphere*. 2007, 67, 809-815.

[210] Faria, PCC; Órfão, JJM; Figueiredo, JL; Pereira, MFR. Adsorption of aromatic compounds from the biodegradation of azo dyes on activated carbon. *Appl. Surf. Sci*. 2008, 254, 3497-3503.

[211] Song, W; Li, Y; Guo, XH; Li, JA; Huang, XM; Shen, WJ. Selective surface modification of activated carbon for enhancing the catalytic performance in hydrogen peroxide production by hydroxylamine oxidation. *J. Mol. Catal. A: Chem*. 2010, 328, 53-59.

[212] Biniak, S; Szymanski, G; Siedlewski, J; Swiatkowski, A. The characterization of activated carbons with oxygen and nitrogen surface groups. *Carbon*. 1997, 35, 1799-1810.

[213] Lahaye, J; Nansé, G; Bagreev, A; Strelko, V. Porous structure and surface chemistry of nitrogen containing carbons from polymers. *Carbon*. 1999, 37, 585-590.

[214] Bagreev, A; Menendez, JA; Dukhno, I; Tarasenko, Y; Bandosz, TJ. Oxidative adsorption of methyl mercaptan on nitrogen-enriched bituminous coal-based activated carbon. *Carbon*. 2005, 43, 208-210.

[215] El-Sayed, Y; Bandosz, TJ. Role of surface oxygen groups in incorporation of nitrogen to activated carbons via ethylmethylamine adsorption. *Langmuir*. 2005, 21, 1282-1289.

[216] Pérez-Cadenas, AF; Maldonado-Hódar, FJ; Moreno-Castilla, C. On the nature of surface acid sites of chlorinated activated carbons. *Carbon*. 2003, 41, 473-478.

[217] Papirer, E; Lacroix, R; Donnet, J-B; Nansé, G; Fioux, P. XPS study of the halogenation of carbon black-Part 2. Chlorination. *Carbon*. 1995, 33, 63-72.

[218] Touhara, H; Okino, F. Property control of carbon materials by fluorination. *Carbon*. 2000, 38, 241-267.

[219] Bandosz, TJ, editor. Activated carbon surfaces in environmental remediation. Oxford, UK: Elsevier; 2006.

[220] Moreno-Castilla, C; Carrasco-Marín, F; Mueden, A. The creation of acid carbon surfaces by treatment with (NH4)2S2O8. *Carbon*. 1997, 35, 1619-1626.

[221] Rivera-Utrilla, J; Sánchez-Polo, M. Ozonation of 1,3,6-naphthalenetrisulphonic acid catalysed by activated carbon in aqueous phase. *Appl. Catal. B: Environ*. 2002, 39, 319-329.

[222] Morales-Torres, S; Silva, AMT; Pérez-Cadenas, AF; Faria, JL; Maldonado-Hódar, FJ; Figueiredo, JL; Carrasco-Marín, F. Wet air oxidation of trinitrophenol with activated carbon catalysts: Effect of textural properties on the mechanism of degradation. *Appl. Catal. B: Envir*on. 2010, 100, 310-317.

[223] Rodríguez-Reinoso, F; Linares-Solano, A. Chemistry and Physics of Carbon. Thrower, PA, editor; Vol. 21; Dekker, M, publisher; New York: 1988.

[224] Stoeckli, HF; Ballerini, L; De Bernardini, S. On the evolution of micropore widths and areas in the course of activation. *Carbon*. 1989, 27, 501-502.

[225] Brunauer, S; Emmett, PH; Teller, E. Adsorption of gases in multimolecular layers. *J. Am. Chem. Soc*. 1938, 60, 309-319.

[226] Rivera-Utrilla, J; Bautista-Toledo, I; Ferro-García, MA; Moreno-Castilla, C. Activated carbon surface modifications by adsorption of bacteria and their effect on aqueous lead adsorption. *J. Chem. Technol. Biotechnol*. 2001, 76, 1209-1215.

[227] Samant, PV; Gonçalves, F; Freitas, MMA; Pereira, MFR; Figueiredo, JL. Surface activation of a polymer based carbon. *Carbon*. 2004, 42, 1321-1325.

[228] Boehm, HP. Eley, DD, Penes, H, Weisz, PB, editors. Vol. 16. New York: Academic Press; 1966.

[229] Boehm, HP. *Functional groups on the surfaces of solids*. Angewandte Chemie International Edition in English. 1966, 5, 533-544.

[230] Jagiello, J; Bandosz, TJ; Schwarz, JA. Inverse gas chromatographic study of activated carbons: The effect of controlled oxidation on microstructure and surface chemical functionality. *J. Colloid Interf. Sci*. 1992, 151, 433-445.

[231] Jagiello, J. Stable numerical solution of the adsorption integral equation using splines. *Langmuir*. 1994, 10, 2778-2785.

[232] Adib, F; Bagreev, A; Bandosz, TJ. Effect of pH and surface chemistry on the mechanism of H_2S removal by activated carbons. *J. Colloid Interf. Sci*. 1999, 216, 360-369.

[233] Salame, II; Bandosz, TJ. Role of surface chemistry in adsorption of phenol on activated carbons. *J. Colloid Interf. Sci*. 2003, 264, 307-312.
[234] Jagiello, J; Bandosz, TJ; Schwarz, JA. Carbon surface characterization in terms of its acidity constant distribution. *Carbon*. 1994, 32, 1026-1028.
[235] Jagiello, J; Bandosz, TJ; Putyera, K; Schwarz, JA. Determination of proton affinity distributions for chemical systems in aqueous environments using a stable numerical solution of the adsorption integral equation. *J. Colloid Interf. Sci*. 1995, 172, 341-346.
[236] Menéndez, JA; Illán-Gómez, MJ; y León, CAL; Radovic, LR. On the difference between the isoelectric point and the point of zero charge of carbons. *Carbon*. 1995, 33, 1655-1657.
[237] Montes-Morán, MA; Menéndez, JA; Fuente, E; Suárez, D. Contribution of the basal planes to carbon basicity: An ab initio study of the $H3O^{+}$–π interaction in cluster models. *J. Phys. Chem. B*. 1998, 102, 5595-5601.
[238] Fuente, E; Menéndez, JA; Suárez, D; Montes-Morán, MA. Basic surface oxides on carbon aaterials: A global view. *Langmuir*. 2003, 19, 3505-3511.
[239] Montes-Morán, MA; Suárez, D; Menéndez, JA; Fuente, E. On the nature of basic sites on carbon surfaces: An overview. *Carbon*. 2004, 42, 1219-1225.
[240] Fanning, PE; Vannice, MA. A DRIFTS study of the formation of surface groups on carbon by oxidation. *Carbon*. 1993, 31, 721-730.
[241] Buczek, B; Biniak, S; Swiatkowski, A. Oxygen distribution within oxidised active carbon granules. *Fuel*. 1999, 78, 1443-1448.
[242] Salame, II; Bandosz, TJ. Comparison of the surface features of two wood-based activated carbons. *Ind. Eng. Chem. Res*,. 2000, 39, 301-306.
[243] Dandekar, A; Baker, RTK; Vannice, MA. Characterization of activated carbon, graphitized carbon fibers and synthetic diamond powder using TPD and DRIFTS. *Carbon*. 1998, 36, 1821-1831.
[244] Pereira, MFR; Órfão, JJM; Figueiredo, JL. Oxidative dehydrogenation of ethylbenzene on activated carbon catalysts 3. Catalyst deactivation. *Appl. Catal. A: Gen*. 2001, 218, 307-318.
[245] Pels, JR; Kapteijn, F; Moulijn, JA; Zhu, Q; Thomas, KM. Evolution of nitrogen functionalities in carbonaceous materials during pyrolysis. *Carbon*. 1995, 33, 1641-1653.
[246] Bradley, RH; Sutherland, I; Sheng, E. Carbon surface: area, porosity, chemistry, and energy. *J. Colloid Interf. Sci*. 1996, 179, 561-569.
[247] Kapteijn, F; Moulijn, JA; Matzner, S; Boehm, HP. The development of nitrogen functionality in model chars during gasification in CO_2 and O_2. *Carbon*. 1999, 37, 1143-1150.
[248] Desimoni, E; Casella, GI; Morone, A; Salvi, AM. XPS determination of oxygen-containing functional groups on carbon-fibre surfaces and the cleaning of these surfaces. *Surf. Interf. Anal*. 1990, 15, 627-634.
[249] Desimoni, E; Casella, GI; Cataldi, TRI; Salvi, AM; Rotunno, T; Di Croce, E. Remarks on the surface characterization of carbon fibres. *Surf. Interf. Anal*. 1992, 18, 623-630.
[250] Zielke, U; Hüttinger, KJ; Hoffman, WP. Surface-oxidized carbon fibers: I. Surface structure and chemistry. *Carbon*. 1996, 34, 983-998.
[251] Hines, D; Bagreev, A; Bandosz, TJ. Surface properties of porous carbon obtained from polystyrene sulfonic acid-based organic salts. *Langmuir*. 2004, 20, 3388-3397.

[252] Ania, CO; Bandosz, TJ. Sodium on the surface of activated carbons as a factor enhancing reactive adsorption of dibenzothiophene. *Energ. Fuels*. 2006, 20, 1076-1080.
[253] Espinoza-Quinones, FR; Modenes, AN; Camera, AS; Stutz, G; Tirao, G; Palacio, SM; Kroumov, AD; Oliveira, AP; Alflen, VL. Application of high resolution X-ray emission spectroscopy on the study of Cr ion adsorption by activated carbon. *Appl. Radiat. Isotopes*. 2010, 68, 2208-2213.
[254] Schmiers, H; Friebel, J; Streubel, P; Hesse, R; Köpsel, R. Change of chemical bonding of nitrogen of polymeric N-heterocyclic compounds during pyrolysis. *Carbon*. 1999, 37, 1965-1978.
[255] Haghseresht, F; Lu, GQ; Whittaker, AK. Carbon structure and porosity of carbonaceous adsorbents in relation to their adsorption properties. *Carbon*. 1999, 37, 1491-1497.
[256] Hu, JZ; Solum, MS; Taylor, CMV; Pugmire, RJ; Grant, DM. Structural determination in carbonaceous solids using advanced solid state NMR techniques. *Energ. Fuels*. 2000, 15, 14-22.
[257] Liu, C-C; Walters, AB; Vannice, MA. Measurement of electrical properties of a carbon black. *Carbon*. 1995, 33, 1699-1708.
[258] Los, S; Duclaux, L; Kempinski, W; Polomska, M. Size effect in the characterization of microporous activated nanostructured carbon. *Micropor. Mesopor. Mater*. 2010, 130, 21-25.
[259] Popescu, M; Joly, JP; Carré, J; Danatoiu, C. Dynamical adsorption and temperature-programmed desorption of VOCs (toluene, butyl acetate and butanol) on activated carbons. *Carbon*. 2003, 41, 739-748.
[260] Barton, SS; Evans, MJB; Harrison, BH. Surface studies on carbon: Water adsorption on polyvinylidene chloride carbon. *J. Colloid Interf. Sci*. 1973, 45, 542-548.
[261] Rodríguez-Reinoso, F; Molina-Sabio, M; González, MT. Effect of oxygen surface groups on the immersion enthalpy of activated carbons in liquids of different polarity. *Langmuir*. 1997, 13, 2354-2358.
[262] Barton, SS; Evans, MJB; Halliop, E; MacDonald, JAF. Acidic and basic sites on the surface of porous carbon. *Carbon*. 1997, 35, 1361-1366.
[263] López-Ramón, MV; Stoeckli, F; Moreno-Castilla, C; Carrasco-Marín, F. Specific and non-specific interactions of water molecules with carbon surfaces from immersion calorimetry. *Carbon*. 2000, 38, 825-829.
[264] Terzyk, AP; Gauden, PA; Furmaniak, S; Wesolowski, RP; Kowalczyk, P. Activated carbon immersed in water-the origin of linear correlation between enthalpy of immersion and oxygen content studied by molecular dynamics simulation. *Phys. Chem. Chem. Phys*. 2010, 12, 10701-10713.
[265] Swiatkowski, A; Pakula, M; Biniak, S; Walczyk, M. Influence of the surface chemistry of modified activated carbon on its electrochemical behaviour in the presence of lead(II) ions. *Carbon*. 2004, 42, 3057-3069.
[266] Kinoshita, K; Bett, JAS. Potentiodynamic analysis of surface oxides on carbon blacks. *Carbon*. 1973, 11, 403-411.
[267] Hallum, JV; Drushel, HV. The organic nature of carbon black surfaces. *J. Phys. Chem*. 1958, 62, 110-117.
[268] Gomes, HT; Figueiredo, JL; Faria, JL; Serp, P; Kalck, P. Carbon-supported iridium catalysts in the catalytic wet air oxidation of carboxylic acids: kinetics and mechanistic interpretation. *J. Mol. Catal. A: Chem*. 2002, 182, 47-60.

[269] Pereira, MFR; Órfão, JJM; Figueiredo, JL. Influence of the textural properties of an activated carbon catalyst on the oxidative dehydrogenation of ethylbenzene. *Colloids Surf. A: Physicochem. Eng. Asp.* 2004, 241, 165-171.

[270] Gao, X; Liu, S; Zhang, Y; Luo, Z; Ni, M; Cen, K. Adsorption and reduction of NO_2 over activated carbon at low temperature. *Fuel Proces. Technol*. 2011, 92, 139-146.

[271] Chiang, HL; Huang, CP; Chiang, PC. The adsorption of benzene and methylethylketone onto activated carbon: thermodynamic aspects. *Chemosphere*. 2002, 46, 143-152.

[272] Lillo-Ródenas, MA; Fletcher, AJ; Thomas, KM; Cazorla-Amorós, D; Linares-Solano, A. Competitive adsorption of a benzene-toluene mixture on activated carbons at low concentration. *Carbon*. 2006, 44, 1455-1463.

[273] Llorens, J; Pera-Titus, M. Influence of surface heterogeneity on hydrogen adsorption on activated carbons. *Colloids Surf. A: Physicochem. Eng. Asp*. 2009, 350, 63-72.

[274] Ahluwalia, RK; Peng, JK. Automotive hydrogen storage system using cryo-adsorption on activated carbon. *Int. J. Hydrogen Energ*. 2009, 34, 5476-5487.

[275] Li, J; Wu, E. Adsorption of hydrogen on porous materials of activated carbon and zeolite NaX crossover critical temperature. *The Journal of Supercritical Fluids*. 2009, 49, 196-202.

[276] Shindo, K; Kondo, T; Arakawa, M; Sakurai, Y. Hydrogen adsorption/desorption properties of mechanically milled activated carbon. *J. Alloy. Compd*. 2003, 359, 267-271.

[277] Hermosilla-Lara, G; Momen, G; Marty, PH; Le Neindre, B; Hassouni, K. Hydrogen storage by adsorption on activated carbon: Investigation of the thermal effects during the charging process. *Int. J. Hydrogen Energ*. 32, 1542-1553.

[278] Jagiello, J; Sanghani, P; Bandosz, TJ; Schwarz, JA. Thermodynamic study of high-pressure adsorption of methane on activated carbons: The effect of oxidation on pore structure and adsorption energy heterogeneity. *Carbon*. 1992, 30, 507-512.

[279] Prasetyo, I; Do, DD. Adsorption rate of methane and carbon dioxide on activated carbon by the semi-batch constant molar flow rate method. *Chem. Eng. Sci*. 1998, 53, 3459-3467.

[280] Zhou, L; Li, M; Sun, Y; Zhou, Y. Effect of moisture in microporous activated carbon on the adsorption of methane. *Carbon*. 2001, 39, 773-776.

[281] Salehi, E; Taghikhani, V; Ghotbi, C; Nemati Lay, E; Shojaei, A. Theoretical and experimental study on the adsorption and desorption of methane by granular activated carbon at 25°C. *J. Nat. Gas Chem*. 2007, 16, 415-422.

[282] Bastos-Neto, M; Canabrava, DV; Torres, AEB; Rodriguez-Castellón, E; Jiménez-López, A; Azevedo, DCS; Cavalcante, JCL. Effects of textural and surface characteristics of microporous activated carbons on the methane adsorption capacity at high pressures. *Appl. Surf. Sci*. 2007, 253, 5721-5725.

[283] Neathery, JK; Rubel, AM; Stencel, JM. Uptake of NO_X by activated carbons: bench-scale and pilot-plant testing. *Carbon*. 1997, 35, 1321-1327.

[284] Lee, Y-W; Kim, H-J; Park, J-W; Choi, B-U; Choi, D-K; Park, J-W. Adsorption and reaction behavior for the simultaneous adsorption of NO-NO_2 and SO_2 on activated carbon impregnated with KOH. *Carbon*. 2003, 41, 1881-1888.

[285] Cal, MP; Strickler, BW; Lizzio, AA. High temperature hydrogen sulfide adsorption on activated carbon: I. Effects of gas composition and metal addition. *Carbon*. 2000, 38, 1757-1765.

[286] Cal, MP; Strickler, BW; Lizzio, AA; Gangwal, SK. High temperature hydrogen sulfide adsorption on activated carbon: II. Effects of gas temperature, gas pressure and sorbent regeneration. *Carbon*. 2000, 38, 1767-1774.

[287] Zhou, AN; Ma, XL; Song, CS. Effects of oxidative modification of carbon surface on the adsorption of sulfur compounds in diesel fuel. *Appl. Catal. B: Environ*. 2009, 87, 190-199.

[288] Órfão, JJM; Silva, AIM; Pereira, JCV; Barata, SA; Fonseca, IM; Faria, PCC; Pereira, MFR. Adsorption of a reactive dye on chemically modified activated carbons-Influence of pH. *J. Colloid Interf. Sci*. 2006, 296, 480-489.

[289] Santos, VP; Pereira, MFR; Faria, PCC; Órfão, JJM. Decolourisation of dye solutions by oxidation with H_2O_2 in the presence of modified activated carbons. *J. Haz. Mater*. 2009, 162, 736-742.

[290] Leng, CC; Pinto, NG. Effects of surface properties of activated carbons on adsorption behavior of selected aromatics. *Carbon*. 1997, 35, 1375-1385.

[291] Radovic, LR; Silva, IF; Ume, JI; Menéndez, JA; Leon y Leon, CA; Scaroni, AW. An experimental and theoretical study of the adsorption of aromatics possessing electron-withdrawing and electron-donating functional groups by chemically modified activated carbons. *Carbon*. 1997, 35, 1339-1348.

[292] Franz, M; Arafat, HA; Pinto, NG. Effect of chemical surface heterogeneity on the adsorption mechanism of dissolved aromatics on activated carbon. *Carbon*. 2000, 38, 1807-1819.

[293] Derylo-Marczewska, A; Goworek, J; Swiatkowski, A; Buczek, B. Influence of differences in porous structure within granules of activated carbon on adsorption of aromatics from aqueous solutions. *Carbon*. 2004, 42, 301-306.

[294] Kawasaki, N; Kinoshita, H; Oue, T; Nakamura, T; Tanada, S. Study on adsorption kinetic of aromatic hydrocarbons onto activated carbon in gaseous flow method. *J. Colloid Interf. Sci*. 2004, 275, 40-43.

[295] Villacanas, F; Pereira, MFR; Órfão, JJM; Figueiredo, JL. Adsorption of simple aromatic compounds on activated carbons. *J. Colloid Interf. Sci.* 2006, 293, 128-136.

[296] Yu, C; Qiu, JS; Sun, YF; Li, XH; Chen, G; Bin Zhao, Z. Adsorption removal of thiophene and dibenzothiophene from oils with activated carbon as adsorbent: effect of surface chemistry. *J. Porous Mater*. 2008, 15, 151-157.

[297] Yu, MX; Li, Z; Ji, QN; Wang, SW; Su, DG; Lin, YS. Effect of thermal oxidation of activated carbon surface on its adsorption towards dibenzothiophene. *Chem. Eng. J.* 2009, 148, 242-247.

[298] Dubinin, MM; Serpinsky, VV. Isotherm equation for water vapor adsorption by microporous carbonaceous adsorbents. *Carbon*. 1981, 19, 402-403.

[299] Brennan, JK; Bandosz, TJ; Thomson, KT; Gubbins, KE. Water in porous carbons. *Colloids Surf. A: Physicochem. Eng. Asp*. 2001, 187-188, 539-568.

[300] Turov, VV; Gun'ko, VM; Leboda, R; Bandosz, TJ; Skubiszewska-Zieba, J; Palijczuk, D; Tomaszewski, W; Zietek, S. Influence of organics on the structure of water adsorbed on activated carbons. *J. Colloid Interf. Sci*. 2002, 253, 23-34.

[301] Bautista-Toledo, I; Rivera-Utrilla, J; Ferro-García, MA; Moreno-Castilla, C. Influence of the oxygen surface complexes of activated carbons on the adsorption of chromium ions from aqueous solutions: Effect of sodium chloride and humic acid. *Carbon*. 1994, 32, 93-100.

[302] Sato, S; Yoshihara, K; Moriyama, K; Machida, M; Tatsumoto, H. Influence of activated carbon surface acidity on adsorption of heavy metal ions and aromatics from aqueous solution. *Appl. Surf. Sci.* 2007, 253, 8554-8559.

[303] Magne, P; Walker Jr, PL. Phenol adsorption on activated carbons: Application to the regeneration of activated carbons polluted with phenol. *Carbon*. 1986, 24, 101-107.

[304] Tessmer, CH; Vidic, RD; Uranowski, LJ. Impact of oxygen-containing surface functional groups on activated carbon adsorption of phenols. *Environ. Sci. Technol*. 1997, 31, 1872-1878.

[305] Karanfil, T; Kilduff, JE. Role of granular activated carbon surface chemistry on the adsorption of organic compounds. 1. Priority pollutants. *Environ. Sci. Technol*. 1999, 33, 3217-3224.

[306] Pérez-Mendoza, M; Domingo-García, M; López-Garzón, FJ. Adsorption of methylamines on carbon materials at zero surface coverage. *Langmuir*. 2000, 16, 7012-7018.

[307] El-Sayed, Y; Bandosz, TJ; Wullens, H; Lodewyckx, P. Adsorption of ethylmethylamine vapor by activated carbon filters. *Ind. Eng. Chem. Res*,. 2006, 45, 1441-1445.

[308] El-Sayed, Y; Bandosz, TJ. Adsorption of valeric acid from aqueous solution onto activated carbons: role of surface basic sites. *J. Colloid Interf. Sci*. 2004, 273, 64-72.

[309] Zawadzki, J; Wisniewski, M; Weber, J; Heintz, O; Azambre, B. IR study of adsorption and decomposition of propan-2-ol on carbon and carbon-supported catalysts. *Carbon*. 2001, 39, 187-192.

[310] Davini, P. Adsorption and desorption of SO_2 on active carbon: The effect of surface basic groups. *Carbon*. 1990, 28, 565-571.

[311] Bagreev, A; Bashkova, S; Bandosz, TJ. Adsorption of SO_2 on activated carbons: the effect of nitrogen functionality and pore sizes. *Langmuir*. 2002, 18, 1257-1264.

[312] Monser, L; Adhoum, N. Modified activated carbon for the removal of copper, zinc, chromium and cyanide from wastewater. *Sep. Purif. Technol*. 2002, 26, 137-146.

[313] Macías-García, A; Gómez-Serrano, V; Alexandre-Franco, MF; Valenzuela-Calahorro, C. Adsorption of cadmium by sulphur dioxide treated activated carbon. *J. Haz. Mater*. 2003, 103, 141-152.

[314] Macías-García, A; Valenzuela-Calahorro, C; Espinosa-Mansilla, A; Bernalte-García, A; Gómez-Serrano, V. Adsorption of Pb^{2+} in aqueous solution by SO_2-treated activated carbon. *Carbon*. 2004, 42, 1755-1764.

[315] Yantasee, W; Lin, YH; Alford, KL; Busche, BJ; Fryxell, GE; Engelhard, MH. Electrophilic aromatic substitutions of amine and sulfonate onto fine-grained activated carbon for aqueous-phase metal ion removal. *Sep. Sci. Technol*. 2004, 39, 3263-3279.

[316] Alkhazov, TG; Lisovskii, AE; Ismailov, YA; Kozharov, AI. *Kinet. Catal*. 1978, 19, 482.

[317] Grunewald, GC; Drago, RS. Oxidative dehydrogenation of ethylbenzene to stykene over carbon-based catalysts. *J. Mol. Catal*. 1990, 58, 227-233.

[318] Guerrero-Ruiz, A; Rodríguez-Ramos, I. Oxydehydrogenation of ethylbenzene to styrene catalyzed by graphites and activated carbons. *Carbon*. 1994, 32, 23-29.

[319] Drago, RS; Jurczyk, K. Oxidative dehydrogenation of ethylbenzene to styrene over carbonaceous catalysts. *Appl. Catal. A: Gen*. 1994, 112, 117-124.

[320] Pereira, MFR; Órfão, JJM; Figueiredo, JL. Oxidative dehydrogenation of ethylbenzene on activated carbon fibers. *Carbon*. 2002, 40, 2393-2401.

[321] Pereira, MFR; Orfão, JJM; Figueiredo, JL. Oxidative dehydrogenation of ethylbenzene on activated carbon catalysts: 2. Kinetic modelling. *Appl. Catal. A: Gen*. 2000, 196, 43-54.

[322] Iwasawa, Y; Nobe, H; Ogasawara, S. Reaction mechanism for styrene synthesis over polynaphthoquinone. *J. Catal*. 1973, 31, 444-449.

[323] Schraut, A; Emig, G; Hofmann, H. Kinetic investigations of the oxydehydrogenation of ethylbenzene. *J. Catal*. 1988, 112, 221-228.

[324] Sui, Z-j; Zhou, J-h; Dai, Y-c; Yuan, W-k. Oxidative dehydrogenation of propane over catalysts based on carbon nanofibers. *Catal. Today*. 2005, 106, 90-94.

[325] Maciá-Agulló, JA; Cazorla-Amorós, D; Linares-Solano, A; Wild, U; Su, DS; Schlögl, R. Oxygen functional groups involved in the styrene production reaction detected by quasi in situ XPS. *Catal. Today*. 2005, 102-103, 248-253.

[326] de Jesús Díaz Velásquez, J; Suárez, LMC; Figueiredo, JL. Oxidative dehydrogenation of isobutane over activated carbon catalysts. *Appl. Catal. A: Gen*. 2006, 311, 51-57.

[327] Zhang, J; Liu, X; Blume, R; Zhang, A; Schlogl, R; Su, DS. Surface-modified carbon nanotubes catalyze oxidative dehydrogenation of n-butane. *Science*. 2008, 322, 73-77.

[328] Szymanski, GS; Rychlicki, G. Importance of oxygen surface groups in catalytic dehydration and dehydrogenation of butan-2-ol promoted by carbon catalysts. *Carbon*. 1991, 29, 489-498.

[329] Szymanski, GS; Rychlicki, G. Catalytic conversion of propan-2-ol on carbon catalysts. *Carbon*. 1993, 31, 247-257.

[330] Szymanski, GS; Rychlicki, G; Terzyk, AP. Catalytic conversion of ethanol on carbon catalysts. *Carbon*. 1994, 32, 265-271.

[331] Carrasco-Marín, F; Mueden, A; Moreno-Castilla, C. Surface-treated activated carbons as catalysts for the dehydration and dehydrogenation reactions of ethanol. *J. Phys. Chem. B*. 1998, 102, 9239-9244.

[332] Wang, Z; Wang, YL; Wang, DJ; Chen, QJ; Qiao, WM; Zhan, LA; Ling, LC. Low-temperature selective catalytic reduction of NO with urea supported on pitch-based spherical activated carbon. *Ind. Eng. Chem. Res*,. 2010, 49, 6317-6322.

[333] Fortuny, A; Font, J; Fabregat, A. Wet air oxidation of phenol using active carbon as catalyst. *Appl. Catal. B: Environ*. 1998, 19, 165-173.

[334] Suarez-Ojeda, ME; Stüber, F; Fortuny, A; Fabregat, A; Carrera, J; Font, J. Catalytic wet air oxidation of substituted phenols using activated carbon as catalyst. *Appl. Catal. B: Environ*. 2005, 58, 105-114.

[335] Santos, A; Yustos, P; Rodriguez, S; Garcia-Ochoa, F. Wet oxidation of phenol, cresols and nitrophenols catalyzed by activated carbon in acid and basic media. *Appl. Catal. B: Environ*. 2006, 65, 269-281.

[336] Ayude, A; Rodriguez, T; Font, J; Fortuny, A; Bengoa, C; Fabregat, A; Stüber, F. Effect of gas feed flow and gas composition modulation on activated carbon performance in phenol wet air oxidation. *Chem. Eng. Sci*. 2007, 62, 7351-7358.

[337] Santos, A; Yustos, P; Rodríguez, S; Garcia-Ochoa, F; de Gracia, M. Decolorization of textile dyes by wet oxidation using activated carbon as catalyst. *Ind. Eng. Chem. Res*,. 2007, 46, 2423-2427.

[338] Beltrán, FJ; Rivas, FJ; Fernández, LA; Álvarez, PM; Montero-de-Espinosa, R. Kinetics of catalytic ozonation of oxalic acid in water with activated carbon. *Ind. Eng. Chem. Res*,. 2002, 41, 6510-6517.

[339] Rivera-Utrilla, J; Sánchez-Polo, M. Ozonation of naphthalenesulphonic acid in the aqueous phase in the presence of basic activated carbons. *Langmuir*. 2004, 20, 9217-9222.

[340] Beltrán, FJ; García-Araya, JF; Giráldez, I. Gallic acid water ozonation using activated carbon. *Appl. Catal. B: Environ*. 2006, 63, 249-259.

[341] Faria, PCC; Órfão, JJM; Pereira, MFR. Activated carbon catalytic ozonation of oxamic and oxalic acids. *Appl. Catal. B: Environ*. 2008, 79, 237-243.

[342] Faria, PCC; Órfão, JJM; Pereira, MFR. Catalytic ozonation of sulfonated aromatic compounds in the presence of activated carbon. *Appl. Catal. B: Environ*. 2008, 83, 150-159.

[343] Faria, PCC; Órfão, JJM; Pereira, MFR. Activated carbon and ceria catalysts applied to the catalytic ozonation of dyes and textile effluents. *Appl. Catal. B: Environ*. 2009, 88, 341-350.

[344] Oliveira, LCA; Silva, CN; Yoshida, MI; Lago, RM. The effect of H_2 treatment on the activity of activated carbon for the oxidation of organic contaminants in water and the H2O2 decomposition. *Carbon*. 2004, 42, 2279-2284.

[345] Georgi, A; Kopinke, F-D. Interaction of adsorption and catalytic reactions in water decontamination processes: Part I. Oxidation of organic contaminants with hydrogen peroxide catalyzed by activated carbon. *Appl. Catal. B: Environ*. 2005, 58, 9-18.

[346] Jans, U; Hoigné, J. Activated carbon and carbon black catalyzed transformation of aqueous ozone into OH-radicals. *Ozone: Sci. Eng.: J. Int. Ozone Ass*. 1998, 20, 67 - 90.

[347] Sánchez-Polo, M; von Gunten, U; Rivera-Utrilla, J. Efficiency of activated carbon to transform ozone into OH radicals: Influence of operational parameters. *Water Res*. 2005, 39, 3189-3198.

[348] Beltrán, FJ; Rivas, J; Álvarez, P; Montero-de-Espinosa, R. Kinetics of heterogeneous catalytic ozone decomposition in water on an activated carbon. *Ozone: Sci. Eng.: J. Int. Ozone Ass*. 2002, 24, 227 -237.

[349] Alvárez, PM; García-Araya, JF; Beltrán, FJ; Giráldez, I; Jaramillo, J; Gómez-Serrano, V. The influence of various factors on aqueous ozone decomposition by granular activated carbons and the development of a mechanistic approach. *Carbon*. 2006, 44, 3102-3112.

[350] Faria, PCC; Órfão, JJM; Pereira, MFR. Ozone decomposition in water catalyzed by activated carbon: Influence of chemical and textural properties. *Ind. Eng. Chem. Res*,. 2006, 45, 2715-2721.

[351] Ahumada, E; Lizama, H; Orellana, F; Suárez, C; Huidobro, A; Sepúlveda-Escribano, A; Rodríguez-Reinoso, F. Catalytic oxidation of Fe(II) by activated carbon in the presence of oxygen.: Effect of the surface oxidation degree on the catalytic activity. *Carbon*. 2002, 40, 2827-2834.

[352] Kuznetsova, NI; Likholobov, VA; Gurrath, M; Boehm, HP. Promotion effect of carbon on the oxidation of ferrous ions by oxygen in the presence of sodium nitrite. *Appl. Catal. A: Gen*. 1995, 128, 41-52.

[353] Ronnholm, MR; Warna, J; Salmi, T; Turunen, I; Luoma, M. Oxidation kinetics of ferrous sulfate over active carbon. *Ind. Eng. Chem. Res*,. 1999, 38, 2607-2614.

[354] Nevskaia, DM; Martín-Aranda, RM. Nitric acid-oxidized carbon for the preparation of esters under ultrasonic activation. *Catal. Lett*. 2003, 87, 143-147.

[355] Farcasiu, M; Smith, C. Modeling coal liquefaction. 1. Decomposition of 4-(1-naphthylmethyl)bibenzyl catalyzed by carbon black. *Energ. Fuels*. 1991, 5, 83-87.
[356] Farcasiu, M; Petrosius, SC; Eldredge, PA; Anderson, RR; Ladner, EP. Modeling coal liquefaction. 3. Catalytic reactions of polyfunctional compounds. *Energ. Fuels*. 1994, 8, 920-924.
[357] Farcasiu, M; Petrosius, SC; Ladner, EP. Hydrodehydroxylation and hydrodehalogenation of substituted polycyclic aromatics using carbon catalysts. *J. Catal*. 1994, 146, 313-316.
[358] Ni, Z-H; Zong, Z-M; Zhang, L-F; Sun, L-B; Liu, Y; Yuan, X-H; Wei, X-Y. Synergic effect of sulfur on activated carbon-catalyzed hydrocracking of di(1-naphthyl)methane. *Energ. Fuels*. 2002, 17, 60-61.
[359] Fukuyama, H; Terai, S; Uchida, M; Cano, JL; Ancheyta, J. Active carbon catalyst for heavy oil upgrading. *Catal. Today*. 2004, 98, 207-215.
[360] Sun, L-B; Zong, Z-M; Kou, J-H; Zhang, L-F; Ni, Z-H; Yu, G-Y; Chen, H; Wei, X-Y; Lee, CW. Activated carbon-catalyzed hydrogenation of polycyclic arenes. *Energ. Fuels*. 2004, 18, 1500-1504.
[361] Cao, L; Suib, SL; Tang, X; Satyapal, S. Thermocatalytic decomposition of dimethyl methylphosphonate on activated carbon. *J. Catal*. 2001, 197, 236-243.
[362] Larsen, JW; Freund, M; Kim, KY; Sidovar, M; Stuart, JL. Mechanism of the carbon catalyzed reduction of nitrobenzene by hydrazine. *Carbon*. 2000, 38, 655-661.
[363] Larsen, JW; Jandzinski, J; Sidovar, M; Stuart, JL. Carbon-catalyzed decompositions of hydrazine and hydroxylamine. *Carbon*. 2001, 39, 473-476.
[364] Anthony Ryan, T; Stacey, MH. A novel reaction catalysed by active carbons: Production of dichloromethane from phosgene and formaldehyde. *Fuel*. 1984, 63, 1101-1106.
[365] Boehm, HP; Mair, G; Stoehr, T; De Rincón, AR; Tereczki, B. Carbon as a catalyst in oxidation reactions and hydrogen halide elimination reactions. *Fuel*. 1984, 63, 1061-1063.
[366] Arends, IWCE; Ophorst, WR; Louw, R; Mulder, P. Gas phase hydrogenolysis mediated by activated carbon: Monosubstituted benzenes. *Carbon*. 1996, 34, 581-588.
[367] Nicoll, G; Francisco, JS. Heterogeneous degradation of carbon tetrachloride: Breaking the carbon−chlorine bond with activated carbon surfaces. *Environ. Sci. Technol*. 1999, 33, 4102-4106.
[368] Gan, J; Megonnell, NE; Yates, SR. Adsorption and catalytic decomposition of methyl bromide and methyl iodide on activated carbons. *Atmos. Environ*. 2001, 35, 941-947.
[369] Santoro, D; Louw, R. Gas phase hydrogenolysis mediated by activated carbon: Substituted chlorobenzenes. *Carbon*. 2001, 39, 2091-2099.
[370] Santoro, D; de Jong, V; Louw, R. Hydrodehalogenation of chlorobenzene on activated carbon and activated carbon supported catalysts. *Chemosphere*. 2003, 50, 1255-1260.
[371] Kastner, JR; Das, KC; Melear, ND. Catalytic oxidation of gaseous reduced sulfur compounds using coal fly ash. *J. Haz. Mater*. 2002, 95, 81-90.
[372] Kastner, JR; Das, KC; Buquoi, Q; Melear, ND. Low temperature catalytic oxidation of hydrogen sulfide and methanethiol using wood and coal fly ash. *Environ. Sci. Technol.* 2003, 37, 2568-2574.
[373] Barkauskas, J; Kareiva, A. Investigation of n-hexane oxidation on the surface of activated charcoal React. *Kinet. Catal. Lett*. 1994, 53, 7-12.

[374] Pinel, C; Landrivon, E; Lini, H; Gallezot, P. Effect of the nature of carbon catalysts on glyphosate synthesis. *J. Catal*. 1999, 182, 515-519.

[375] Pigamo, A; Besson, M; Blanc, B; Gallezot, P; Blackburn, A; Kozynchenko, O; Tennison, S; Crezee, E; Kapteijn, F. Effect of oxygen functional groups on synthetic carbons on liquid phase oxidation of cyclohexanone. *Carbon*. 2002, 40, 1267-1278.

[376] Gauthard, F; Horvath, B; Gallezot, P; Besson, M. Catalytic oxidation with air of cyclododecanone and 3,3,5-trimethylcyclohexanone to the corresponding linear dicarboxylic acids over synthetic carbons. *Appl. Catal. A: Gen*. 2005, 279, 187-193.

[377] Bashkova, S; Baker, FS; Wu, XX; Armstrong, TR; Schwartz, V. Activated carbon catalyst for selective oxidation of hydrogen sulphide: On the influence of pore structure, surface characteristics, and catalytically-active nitrogen. *Carbon*. 2007, 45, 1354-1363.

[378] King, A. Studies in chemisorption on charcoal Part VIII The influence of temperature of activation of charcoal on (a) catalytic oxidation of salts, (b) catalytic decomposition of hydrogen peroxide. *J. Chem. Soc*. 1936, 1688-1692.

[379] Vignaud, Y; Granet, R; Krausz, P. An expeditious, solvent-free synthesis of meso-arylporphyrins using activated charcoal as a catalyst. *J. Porphyr. Phthalocya*. 2006, 10, 937-941.

[380] Yu, G; Lu, S; Chen, H; Zhu, Z. Oxidative desulfurization of diesel fuels with hydrogen peroxide in the presence of activated carbon and formic acid. *Energ. Fuels*. 2004, 19, 447-452.

[381] Yu, G; Lu, S; Chen, H; Zhu, Z. Diesel fuel desulfurization with hydrogen peroxide promoted by formic acid and catalyzed by activated carbon. *Carbon*. 2005, 43, 2285-2294.

[382] Rios, RVRA; Silvestre-Albero, J; Sepúlveda-Escribano, A; Rodríguez-Reinoso, F. Liquid phase removal of propanethiol by activated carbon: Effect of porosity and functionality. *Colloids Surf. A: Physicochem. Eng. Asp*. 2007, 300, 180-190.

In: Activated Carbon
Editor: James F. Kwiatkowski
ISBN: 978-1-61209-684-1
©2012 Nova Science Publishers, Inc.

Chapter 4

ACTIVATED CARBONS AS CATALYST SUPPORTS

M. E. Gálvez, S. Ascaso, A. Boyano, R. Moliner and M. J. Lázaro
Instituto de Carboquímica, CSIC, Miguel Luesma Castán, 4, 50018 Zaragoza, Spain

1. ACTIVATED CARBONS IN CATALYSIS

Among their many interesting applications, activated carbons have been considered over the last decades for their utilization in several processes involving heterogeneous catalytic reactions. In these processes the catalyst increases the reaction rate and controls the selectivity of the reactions involved towards the generation of desired products. Most of these catalysts consist of metals or metallic compounds supported on several materials which role is not only to maintain the catalytic phase in a well dispersed state but also affect the catalytic activity, by means of direct participation in any of the steps of the reaction mechanism, or by favouring the interactions between active phase and support. This participation and their interaction with the active phase make catalyst supports more than just simple active phase carriers.

Some of the properties desirable in a support are its inertness towards unwanted reactions, stability under regeneration and reaction conditions, adequate mechanical properties, tuneable surface area, porosity, and physical form, i.e. the possibility of being manufactured in granulates or conformates of different size and shape to suit different chemical reactor configurations (Moss 1980, Satterfield 1980). Only a few out of a wide range of potential materials totally fulfil this set of desirable properties and combine them in an optimum way. Carbon materials, and particularly activated carbon, are among this list of materials. However, the number of industrial processes using activated carbon as catalyst or catalyst support is still very small (Rodríguez-Reinoso 1998, Rodríguez-Reinoso 1997). The irreproducibility of the results obtained when employing activated carbon supported catalysts has been pointed as the main cause of their poor implementation in the catalyst market in earlier years (Cameron 1990). Since the last decades of the last century until nowadays, research efforts have been directed towards the understanding of the several aspects in the preparation and physical and chemical properties of active carbons that determine their behaviour as catalyst supports. As a result of these studies, activated carbons are being

recognized as unique materials for supporting a catalytically active phase. Moreover, their flexibility in tailoring their properties to specific needs offers incomparable advantages *vis-à-vis* other well known and widely applied catalyst supports.

Rodríguez-Reinoso (Rodríguez-Reinoso 1995a), summarized as follows some of the clearest advantages of activated carbons as catalyst supports:

- They are resistant to acidic or basic media.
- Their structure remains stable even at high temperatures, in comparison to ceramic supports which sinter at temperatures higher than 900ºC.
- Their porous structure can be tailored to obtain the desirable pore-size distribution, once the precursor and preparation method are properly chosen.
- They can be prepared into several physical forms to suit a particular application or reactor design, i.e. granulates, powder, fibres, cloths, pellets, briquettes, monoliths, etc.
- Their chemical properties can be modified to control polarity, hydrophobicity, favour adsorption or interaction with the active phase.
- The active phase can be recovered easily from spent catalysts by simply burning away the carbon support.
- Their low cost in comparison to other supports such as alumina, silica or zeolites.

It should be also mentioned that activated carbon can act as a catalyst itself and has been used in some processes such as the formation of phosgene, sulphuryl chloride and chlorinated alkenes and alkanes, as well as in many oxidation reactions, i.e. H_2S to sulphur, SO_2 to H_2SO_4 or NO to NO_2 (Rodríguez-Reinoso 1995a, H. Jüntgen 1986). Other carbon materials, such as carbon blacks, ordered mesoporous carbons, carbon fibres or carbon molecular sieves, have been considered and used in catalysis in the last years. They posses some features in common with activated carbons and other particular characteristics, such as electrical conductivity or wide pore size distribution, which made their application interesting in certain fields such as electrocatalysis, i.e. as supports for the catalysts employed in fuel cells (Antolini 2009). Still, activated carbons suppose a lower cost option for catalyst preparation, in comparison to these other synthetic carbon materials.

2. Preparation of Activated Carbons and Properties Influencing Their Behaviour as Catalyst Supports

2.1. Preparation of Activated Carbons

Although extensively described in other chapters of this book, a few aspects on activated carbons preparation will be introduced here in order to better understand the influence of preparation process in the final features of these materials determining their behaviour as catalyst supports.

In principle, any material with high carbon content is susceptible of being transformed into an activated carbon (Bansal 1988). Wood and coal are the preferred materials for the manufacture of active carbons. Around one third of the world production of active carbons

comprises coal-origin carbons, this ratio being bigger in both the European Union and United States. Low-rank coals are believed to be, in general, better precursors than anthracite, thus most of the activated carbons of coal origin are prepared from bituminous and sub-bituminous coals (Bansal 1988). Other materials, such as different kind of biomass (Rodríguez-Reinoso 1992), peat, waste lignin, sulphite liquors, and waste from processing of petroleum or lubricating oil industries, have been used as raw materials for the production of active carbons. Lately, activated carbon fibres, cloths and other synthetic carbon materials prepared using different polymeric compounds are also being studied (Castro-Muñiz 2008, Villar-Rodil 2005, Alcañiz-Monge 1998). In general, low ash or low inorganic contents are desirable in raw materials used for the preparation of activated carbons for catalytic applications. High bulk density and high volatile content are important parameters for the selection of the raw material, as they contribute to enhanced strength of the final carbon and allow better control of the yield. Bansal et al. (Bansal 1998), reported a list of raw materials commonly used in the preparation of active carbons, their properties and texture of the carbons obtained. A review of literature shows that the experimental conditions to produce an activated carbon cannot be extrapolated from one given raw material to another. The carbonization conditions, the type of reactor, the gas flow, etc, can lead to different results, and consequently, a specific study must be carried out for any particular material (Bansal 1988, Wigmans 1989).

After the selection and conditioning of the raw material, carbonization, also known as pyrolysis, is the first step in the manufacture of activated carbons. During carbonization, most of the non-carbon elements in the matrix of the raw material, such as hydrogen or oxygen, evolve as volatile gaseous products as a result of the pyrolytic decomposition of the starting material. The residual carbon atoms group themselves into stacks of flat aromatic sheets cross-linked in a random manner. Since the arrangement of these sheets is irregular, it leaves interstices among them, which may become filled or partially blocked with the tars and other decomposition products finally transformed into disorganized carbon (Rodriguez-Reinoso 1998). Carbonization is usually carried out at temperatures below 800ºC and under continuous flow of an inert gas. Heating rate, final temperature, and nature and physical state of the raw material are important parameters that determine the quality and yield of the carbonized product, also known as char (Bansal 1988) (Wigmans 1989).

For bituminous coals carbonization temperatures of 500ºC are needed for an adequate development of porosity. Temperatures higher than 700ºC, temperature at which the carbonization is completed, do not result in a further reactivity of the char in the subsequent activation process (Linares-Solano 1999). Rubio and co-workers (Rubio 1997, Rubio 1998a, Rubio 1998b) also studied the influence of the pyrolysis temperature on the features of the resulting chars and activated carbons, using a sub-bituminous coal with high ash content. They showed that 800ºC was the optimal temperature for maximizing the amount of oxygen functionalities on the carbon surface as well as for porosity development. Heating rate during carbonization has also an influence on the characteristics of the resulting materials. Shchipko and co-workers (Shchipko 1998) found that a fast-pyrolysis favours the formation of meso and macropores, due to the increase of the pressure inside the coal particle as a consequence of higher devolatilization rate in comparison with that of diffusion. Particle size influence was studied by Linares-Solano et al. (Linares-Solano 1999), who reported lower micropore volumes and specific surface areas for the activated carbons obtained after carbonization of the precursor with smaller particle sizes. Residence times in carbonization do not normally exceed 5 hours, being on average of 1 hour. However, for low rank coals, 30 minutes

residence time has been proven to be adequate for obtaining an optimal burn-off and porosity development (Moliner 1994).

Carbonization usually results in products of poorly developed porous structure and low surface area. The goal of the activation stage in the preparation of activated carbons is to enhance the pore volume and enlarge the diameters of the pores which were created during the carbonization process. The irregular arrangement of the aromatic sheets during carbonization leaves free interstices which become totally or partially filled by tars and other decomposition products, finally converted into disorganized carbon. During activation this disorganized carbon is initially removed, exposing the aromatic sheets to the action of the activation agents, which leads to the development of the microporous structure, widening of new and existing pores or formation of large-sized pores. Thus, the extent of burn-off has been generally used as a measure of the degree of activation (Bansal 1988). Activation methods are commonly divided into two main types: chemical and physical activation. In chemical activation carbonization and activation are carried out in a single step by thermal decomposition of the raw material impregnated with certain chemical substances. Physical activation involves gasification of the carbonized material by oxidation under water vapour or carbon dioxide, at temperatures in the range 700-1100ºC.

Chemical activation is carried out normally for raw materials of wood origin. The starting material is impregnated with the chemical agent and then pyrolysed in absence of air at temperatures from 400 to 800ºC. The resulting material is washed to remove the activating agent, which can be recycled. Most widely used chemicals are phosphoric acid, zinc chloride and potassium hydroxide, their common feature is that they are dehydrating agents which influence thermal decomposition inhibiting the formation of tars (Bansal 1988).

Physical activation requires a previous carbonization steps and slightly higher temperatures than chemical activation. Reactions of carbon with steam or CO_2 are endothermic, thus, external heating is required in order to drive the process and maintain an adequate reaction temperature. Activation in the presence of CO_2 involves less energetic reactions than activation with steam and therefore requires higher temperatures. The larger dimension of the CO_2 molecule compared to H_2O results in slower diffusion into the porous structure of the carbonized material, restricted accessibility towards micropores and significantly slower reaction rate (Wigmans 1989). However, it has been generally admitted that steam activation promotes the formation of mesopores in the carbon, whereas in the presence of CO_2 microporosity is preferentially developed. Alcañiz-Monge and co-workers (Alcañiz-Monge 1994), observed that CO_2-activated carbon fibres possessed higher micropore volumes than steam-activated ones, with this latter leading to wider pore size distributions. As a possible reason, they pointed to higher activated diffusion coefficients into narrower pores in the case of CO_2. Walter further discussed this fact, explaining the differences in porous structure development using both activating agents in terms of stronger H_2 inhibition than that of CO, which makes steam activation less uniform (Walker 1996). Alcañiz-Monge et al. (Alcañiz-Monge 1997) refuted the explanation given by Walter, claiming again that CO_2 diffused easier than H_2O inside the microporous structure of the carbonized material. Rodriguez-Reinoso, Molina-Sabio and co-workers (Rodríguez-Reinoso 1995b, Molina-Sabio 1996), reported also enhanced microporosity in CO_2-activated carbons, and claimed that this was due either to the different molecular configuration of CO_2 in comparison to H_2O, or, most probably, to the higher number of surface functional groups introduced upon CO_2 activation that led to a significant reduction in the effective diameter of

the pores, which impeded the access of the activation agent and thus the further enlargement of the pore diameter. Later on, Linares-Solano et al. prepared activated carbons from bituminous coals and reported once again that CO_2 promoted the formation of new micropores in the char, while steam activation results in a general enlargement of the initially microporous structure of the material (Linares-Solano 2000). Heating rate during activation seems not to have a big impact on the features of the resulting material (Gale 1995, Linares-Solano 1999, Shchipko 1998). Wigmans (Wigmans 1989) found inconvenient to activate at temperatures higher than the one used in the previous carbonization step; tars and other decomposition products formed may inhibit the right development of the carbon porosity. Lázaro and co-workers (Lázaro 2007a) reported the structural and textural changes occurred in the pyrolysis and steam activation of a low-rank sub-bituminous coal. For this particular precursor, they found 750ºC to be the optimal activation temperature for gaining a maximal development of surface area and medium size micropores. Higher activation temperatures resulted in higher meso and macropore volumes at the expense of the microporosity of the carbon. Steam content in the gas of 20% and residence time between 2 and 4 hours, corresponding to an optimal burn-off around 25%, led to a proper development of porosity in the carbons.

It is also well known that the surface of activated carbons contains a given number of heteroatoms, such as O, H, N, in the form of functional groups. Although some of these heteroatoms may have their origin in the raw material itself, the considerable amount of unsaturated valences at the edge of the grapheme layers in the structure of activated carbons serve as active sites for oxygen accumulation. In fact, surface oxygen in activated carbons may be responsible of up to 40% of their mass (Walker 1991). Even if the nature of carbon-oxygen structures is not yet precisely understood, it is generally assumed that there may be different types of surface groups, as depicted in Figure 1, namely carboxylic, phenolic, quinone, lactone, carboxylic anhydride and cyclic peroxide (Rodriguez-Reinoso 1997). A detailed description of the analytic techniques for the determination of surface oxygen groups in carbons can be found elsewhere (Boehm 2002).

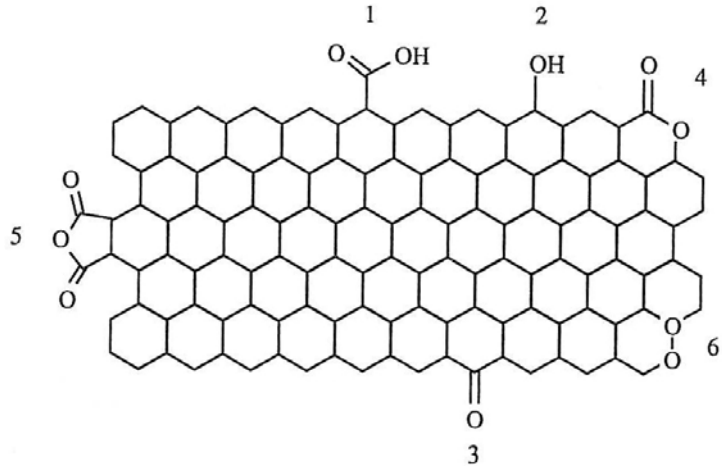


Figure 1. Types of oxygen surface groups in activated carbons: 1) carboxylic acid; 2) phenolic; 3) quinone; 4) lactone; 5) carboxylic anhydride; and 6) cyclic peroxide.

The presence of these functionalities is responsible for activated carbons acid-base character. They can be formed during the activation process (Lázaro 2007b), but it is also possible to adjust their nature and amount by means of different pre-treatments, i.e. reaction with oxidizing gases such as ozone, oxygen, nitrous oxide, nitric oxide, carbon dioxide, etc., or oxidizing solutions, such as nitric acid, sodium hypochlorite, hydrogen peroxide, etc (Park 2008, Barton 1997). Chingombre et al. (Chingombre 2005) studied oxidized porous activated carbons treated with diluted nitric acid for 6 h at 90 °C, producing samples with weakly acidic functional groups. Pradhan et al. (Pradhan 1999) functionalized activated carbons using oxidants like HNO_3, H_2O_2 and a saturated solution of $(NH_4)_2S_2O_8$ in H_2SO_4. According to these authors nitric acid treatment is the most effective one in terms of modifying surface area and porosity of activated carbons. Comparing chemically modified activated carbons using nitric acid and hypochlorite, Vinke et al. (Vinke 1994) stated that nitric acid oxidation is the most effective way of introducing oxygen functionalities, resulting in the highest amount of acidic surface groups, whereas hypochlorite seems to be a much weaker oxidant. Boyano et al. (Boyano 2010) reported that HNO_3 functionalization resulted in the formation of carboxylic acid and lactone groups, whereas funcntionalization by means of H_2O_2 significantly increased the concentration of phenols, carbonyl and quinine groups. Although the main aim of these treatments is the modification of the surface chemical properties, it must be taken into account that they often involve important changes in the textural structure of the activated carbons. In this way, Moreno-Castilla et al. (Moreno-Castilla 1998), Gil et al. (Gil 1997) and Boyano et al. (Boyano 2008a, Boyano 2010), reported loss of surface area and pore enlargement for powder activated carbons, carbon briquettes and carbon coated monoliths subjected to oxidation using nitric acid, oxygen peroxide and sulphuric acid.

2.2. Properties of Activated Carbons Affecting Their Role as Catalyst Supports

The possibility of tailoring both the porous structure and the chemical surface properties of activated carbons, by means of modifying several parameters in their preparation process, offers unique flexibility to obtain a material that suits the conditions required in the catalyst needed for any specific reaction. One can design a proper activated carbon-supported catalyst exploiting the unique virtues of this carbon supports. We summarize herein these fundamental properties, along with some representative examples of their influence in catalyst preparation and behaviour.

2.2.1. Surface Area and Porosity

Due to the large number of studies performed on the preparation of activated carbons and on the modification of their porous structure in order to adjust their adsorptive properties to a certain application, it is possible today to produce carbons of high adsorption capacity and specific molecular sieving effect. All this knowledge can be applied also to the use of activated carbons as catalyst supports. Surface area and pore size distribution influence several crucial parameters during the preparation of the catalyst, determining the interaction between the active phase and the carbon support, as well as the final behaviour of the carbon-supported catalyst. High surface area and well-developed porosity are important for achieving

an adequate dispersion of the active phase. Activated carbons exhibit surface areas much higher than those of other conventional catalyst supports, such as alumina or silica. However, it must be recognized that a substantial portion of this surface area is due to narrow micropores which sometimes may not be available to reactants or to the chemical substances used for the deposition of an active phase.

Many studies report the effect of porosity and surface area on active phase dispersion and catalytic activity. Linares-Solano and co-workers (Linares-Solano 1982) prepared platinum catalysts using a graphitized carbon black (V3G) as support, which was subjected to various degrees of activation in air in order to increase its surface area. They reported that Pt dispersion increased from 0.17 to 0.35 as a result increasing carbon support surface area from 62 to 136 m^2/g. Martín-Guillón et al. (Martín-Guillón 1993) proved that increased surface area, up to 1000 m^2/g, facilitated metal loading as well as contributed to enhanced specific activity of molybdenum activated carbon supported catalysts for the hydrodesulfurization (HDS) process. Similar influence of surface area and porosity was reported for cobalt loaded activated carbons prepared from olive stones and tested for the hydrogenation of CO and CO_2 (Moreno-Castilla 1995). Some more recent results show that porosity can also influence the particle size and distribution of the active phase. Ma et al. (Ma 2010) reported better dispersion of the metals on the surface of activated carbons possessing increased and wider porosity, claiming that a larger number of micropores induced more aggregation of metals and the formation or larger crystallites in Fe-Mo-Cu-K catalysts used in Fischer-Tropsch synthesis. Halttunen and co-workers (Halnttunen 2001) observed a similar influence of activated carbon porosity in the synthesis of Rh supported on activated carbon catalysts, and assigned better distribution of the metal to improved mass transfer during impregnation in the meso- and macroporous structure of the carbon material. It is generally believed that higher surface area and adequate pore size distribution contributing to a better dispersion of the active phase, minimize its sintering during operation and result in enhanced and more reliable catalytic activity (Vissers 1984). Diffusion of reactants and/or products in and out the porous structure of a catalyst may play an important role in its activity. In some cases, high surface area of the carbon support can be detrimental if it is confined in narrow micropores which are not accessible to the reactant molecules (Rodriguez-Reinoso 2009). This fact becomes especially important in processes where large molecules are involved, i.e. liquid-phase reactions (Maia 2008, Barrientos-Ramírez 2010). It has been also reported that the particular shape of pores in activated carbons may influence the active phase dispersion and catalytic activity. The so-called *sink effect* was observed by Laine and co-workers (Laine 1997), who reported a synergetic effect of the activated carbon support in hydrodesulphurization catalysts assigned to the presence of slit-shaped micropores which worked as sulphur sinks promoting the activity of the catalyst.

2.2.2. Surface Chemistry

It is clear that accessible and large surface area and adequate pore size distribution are important features in the preparation of activated carbon supported catalysts. However, these textural properties themselves do not explain many of the properties and behaviour of carbon-supported catalysts (Rodríguez-Reinoso 1995b). Prado-Burguete and co-workers (Prado-Burguete 1991) prepared Pt catalysts using several carbons as supports, including an activated carbon produced from olive stones, and observed that there was not a single carbon property which could be related to metal dispersion. Rodríguez-Reinoso et al. prepared several iron

catalysts supported on activated carbons with different pore size distributions (Rodríguez-Reinoso 1990). They used two different metal precursors: iron nitrate and iron pentacarbonyl, and observed that the access of the metal solution was related not only to the more developed porous structure of some of the carbons, but also to the chemical character of their surface, which determined the interaction with the metal precursor. Common methods for the preparation of activated carbon-supported catalysts are excess solution, incipient wetness impregnation and ion-exchange. All these methods imply contact between the metal precursor and the activated carbon surface, and the effectiveness of this contact will depend both on the solvent used for impregnation and on the acid-base properties of the carbon. Due to the amphoteric nature of activated carbon, at some point its surface will be neutral, corresponding to the isoelectric point. If the surface of the carbon is rich in negatively charged surface functionalities, i.e. deprotonated carboxylic groups, it will attract cations from the solution used for the impregnation. On the other hand, the presence of positively charged groups will attract anions towards the carbon surface (Radovic 1997). Hanika and co-workers (Hanika 1982) showed how the use of different dispersants, i.e. water and acetone, substantially influenced active phase distribution in the preparation of Pt supported on activated carbon pellets. More uniform Pt distribution was achieved when using an acetone solution of chloroplatinic acid. Dun et al. reported that the pH of the impregnating solution had a significant effect on the amount of metal loaded on the carbons they used in the preparation of molybdenum catalysts for Fischer-Tropsch synthesis (Dun 1985). Derbyshire and co-workers attempted to clarify the influence of the surface chemistry of carbon supports, claiming that the increased activity could be related to the presence of nitrogen-containing surface groups which provide preferential sites for the adsorption of Mo species and that, moreover, the affinity between a particular carbon and precursor might depend upon the chemical compatibility of the carbon surface and the precursor used in its impregnation (Derbyshire 1986). Solar et al. (Solar 1991), prepared carbon-supported molybdenum catalysts and found that their activity depended mostly on the pH of the impregnating solution. Later on, de la Puente and Menéndez (de la Puente 1998) added that the presence of oxygen surface groups increases the hydrophilicity of activated carbons, favouring Mo dispersion. The explanation of metal adsorption on activated carbons in terms of the amphoteric characteristics of their surface and the interactions with impregnating solutions of different pHs, has been frequently denoted as “electrostatic” approach (Okhlopkova 2009).

Surface functionalities are thought to act moreover as anchoring sites for the active phase during catalyst preparation. Its presence and concentration may determine not only the dispersion of the active phase but strongly condition its interaction with the support. There is a considerable amount of papers reporting the influence of surface groups on Pt and Pd fixation on activated carbon and other carbon supports. In example, Prago-Burguete et al. (Prado-Burguete 1989) observed that Pt dispersion increased with the amount of surface groups in H_2 and H_2O_2 carbon blacks, not only due to the presence of more acidic functionalities which decreased the hydrophobicity of the carbon support, making its surface more accessible to the impregnating solution, but also to the increase in the interaction between the metal precursor and the support due to Pt fixation on CO complex more stable oxygen surface groups. The sintering resistance increased the same way, fact that was ascribed also to enhanced Pt interaction with the carbon surface, preventing its migration. Kim and co-workers (Kim 1992, Kim 1993) found that Pt uptake, dispersion and resistance towards sintering were also strongly dependant on the amount of surface oxygen groups in

HNO_3 functionalized carbon blacks. Van Dam and Van Bekkum (Van Dam 1991) prepared a set of different pre-oxidized activated carbons and used them as supports in the synthesis of Pt-catalysts. They attempted to clarify the chemistry of Pt adsorption on the carbon surface during catalyst preparation and claimed that an increased amount of carboxylic groups, i.e. increased surface negative charge, resulted in a decrease of Pt dispersion. Something similar was observed by Torres and co-workers (Torres 1997). They reported stronger interaction between Pt and the support for those carbons of lower acidity. Carbons functionalized with weak oxidants, developed acidic sites of moderate strength showed enhanced interactions with the Pt precursor (H_2PtCl_6) during the impregnation and favoured Pt dispersion of the carbon surface, resulting in increased catalytic activity. Later on, Fraga et al. (Fraga 2002) pointed to basic oxygen surface functionalities as Pt-anchoring sites when using H_2PtCl_6 as precursor, in an extension of Van Dam and Van Bekkum model. Palladium dispersion was also found to depend on the extent of activated carbon surface oxidation and on the presence of certain types of surface groups. Suh and Park (Suh 1993) reported increased Pd dispersion when using pre-oxidized activated carbon supports. However, the catalytic activity did not increase proportionally, due probably to more uniform distribution of the metal into the smallest pores. Calvo and co-workers (Calvo 2005) showed the importance of the presence of surface groups such as carboxylic acids, carbonyls and quinones in Pd fixation on oxidized activated carbons. Surface groups were found to contribute to improved selectivity towards the production of cyclohexanol in aqueous-phase hydrodechlorination reactions. Radkevich et al. (Radkevich 2008) prepared functionalized stone-fruit activated carbons and concluded that Pd dispersion increased with strengthened basic properties of the support. Already in the year 1983, Ehrburger and co-workers (Ehrburger 1983) observed that the oxygen complexes associated with the edge carbon atoms on an activated carbon black acted as anchoring sites for Fe particles, ensuring a higher state of dispersion. Since then, there has been a considerable amount of work published on the preparation of activated carbon-based catalysts, reporting the influence of the support surface chemistry on metal dispersion and catalytic activity, using Fe (Quintanilla 2007), Cu (Dandekar 1999, Zhu 2000c, Tseng 2006, Xue 2008), V (Huang 2008, Boyano 2008b) and other transition metals (Calafat 1996) as active phase. Extensive research on V-loaded activated carbons was performed by Lázaro and co-workers, studying as well the use of petroleum coke ashes as V-source (Lázaro 2004, Lázaro 2006a, Lázaro 2008). The authors optimized the features of the activated carbon support, modifying several parameters in their preparation process via steam activation of a low-rank coal (Lázaro 2007a) and observed that apart from adequate surface area and porosity, oxygen surface groups played a decisive role in V fixation on the carbon surface, moreover when petroleum coke ashes were used as the active phase precursor. More basic groups, such as phenolic, were pointed as surface sites for V adsorption, resulting in enhanced support-active phase interactions and increased catalytic activity. Figure 2 shows the NO reduction measured in its selective catalytic reduction (SCR) in the presence of ammonia and O_2 at 150ºC in the presence of several catalysts synthesised using different activated carbon supports and petroleum coke ashes (PCA) as V-source, corresponding to 3% wt V-load. A considerable increase in the activity was observed for the catalyst prepared using the carbon support which possessed the highest amount of surface groups, concretely those decomposing as CO in the temperature programmed desorption (TPD) analyses. Functionalization of the supports by means of HNO_3 pre-treatments yielded higher NO conversions, reaching almost 90% in some cases (Gálvez 2005).

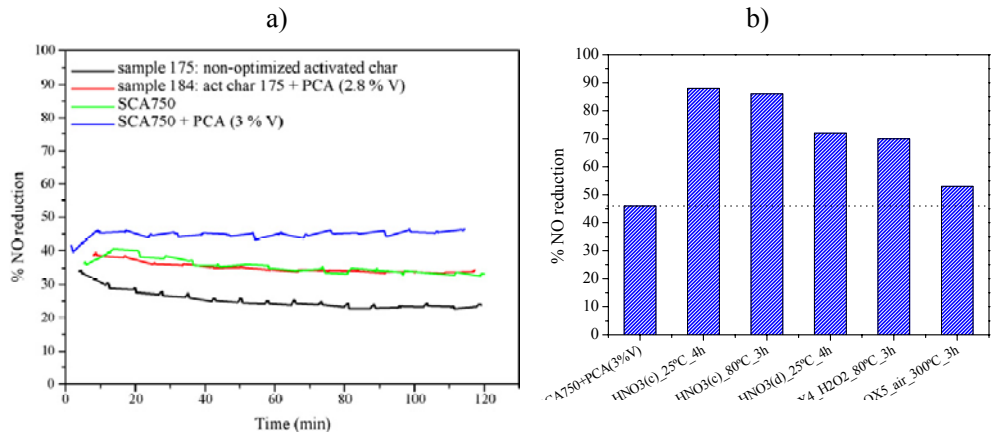


Figure 2. NO reduction at 150ºC in the presence of NH_3 and O_2 measured for a) a series of V-loaded activated carbons, increase in the catalytic activity after optimization of the activation process; and b) catalysts prepared using pre-oxidized carbon supports (Lázaro 2006a, Gálvez 2005).

The studies of Lázaro, Gálvez and co-workers also revealed that the presence of surface functionalities can also be directly involved in the reaction mechanism (Gálvez 2008). Characterization techniques, such as temperature programmed desorption (TPD), ammonia chemisroption, *in-situ* DRIFT spectrometry and transient response analysis allowed the elucidation of the different steps in the mechanism of the selective catalytic reduction of NO in the presence of ammonia and O_2 and over the V-loaded activated carbons assayed. The analysis revealed that ammonia adsorption on the catalyst surface was a key step in the overall reaction mechanism. Furthermore, the authors concluded that ammonia could be adsorbed in two different active sites, metallic centres (V) as well as oxygen surface groups. Oxygen surface groups, most probably carboxylic acids, favour thus ammonia adsorption, acting as a reservoir of ammonium ions, which would then migrate to metallic sites where the reaction takes place. The presence of oxygen surface functionalities can be beneficial, as seen in this last example, or detrimental, as observed in the hindered adsorption of phenol on the surface of acidic activated carbons (Grant 1990, Vidic 1997).

Oxygen surface groups are not the only centres characterizing the catalytic behaviour of activated carbon-supported catalysts. In the case of carbons submitted to heat treatments at high temperatures (1600-220ºC), basicity increases as a consequence of the presence of C_π sites on the basal planes. These sites are thought to maximize the electrostatic attractions between the metal anion and the carbon surface, i.e. C_π-H_3O^+ - $PtCl_6^{2-}$, and minimize the electrostatic repulsions, i.e. COO^- - $PtCl_6^{2-}$, resulting in an increased dispersion (Rodríguez-Reinoso 1998).

2.2.3. Inertness and Stability in Reaction Media

It's clear that the chemical properties of the surface of activated carbons are highly beneficial in several aspects of the preparation of activated carbon-supported catalysts and have a positive impact on active phase dispersion, fixation and catalytic activity. However, an important feature of activated carbons that must be also taken into account is that the active phase-support interactions are generally much weaker than when using other common catalyst support, such as silica, alumina, titania, etc. Thus activated carbon has been

considered as a low reactivity or relatively inert support. This fact implies, in example, that the metallic compound loaded on an activated carbon can be more easily transformed into its catalytically active species, e.g. by means of simple heat treatment under less severe conditions than when using other types of supports (Radovic 1997, Jung 1982). In reaction involving sulphur compounds, the participation of catalyst supports such as alumina, the sulphation of aluminium may cause a detrimental effect on the stability and regeneration of the catalyst (Yoo 1994). On the other hand, Co-Mo HSC catalysts supported on activated carbon Activated carbon supported catalysts are thought to be more resistant to coking (De Beer 1984). Coke deposition is hindered by lower acidity of the surface of activated carbon in comparison to alumina.

Another important issue to be taken into account is the stability of the carbon support under reaction conditions. Grzybek et al. (Grzybek 1999) observed that, for MnO_x supported on activated carbons and under 800 ppm NO, 800 ppm NH_3, 3% O_2 in He, noticeable gasification of the carbon support occurred at temperatures higher than 250ºC. Singoredjo and co-workers (Singoredjo 1990) reported that gasification took place over 200ºC, for Cu-loaded activated carbons, its extent depending on the copper compound used in the preparation of the catalysts. Lázaro et al. (Lázaro 2006a) performed thermogravimetric experiments to asses the gasification of the activated carbon support used in the preparation of vanadium-supported catalysts. Following CO_2 formation with the help of a mass spectrometer and under 1000 ppm NO, 1500 ppm, 3.5% O_2 in Ar, they observed that noticeable carbon gasification started to take place at temperatures higher than 350ºC, at slightly lower temperatures, 250-300ºC, in the case of HNO_3 pre-oxidized carbons, due also to the thermal decomposition of less stable oxygen surface functionalities.

3. Structured Activated Carbon-Based Catalysts: Preparation of Activated Carbon Briquettes and Carbon Coated Monoliths

As explained before in this chapter, activated carbons possess the advantage of being easily manufactured under different shapes and physical forms, adapting their size and geometrical properties to the requirements of any specific application or reactor design. There is a considerable amount of papers dealing with the preparation of activated carbons in the shape of cloths (Such-Basañez 2004, Matatov-Meytal 2002), fibres (Marbán 2003, Marbán 2001a) and monoliths (Gatica 2004, García-Bordejé 2001, García-Bordejé 2002) Two examples of structured carbon-based catalyst, activated carbon briquettes and carbon coated monoliths, are presented herein, paying attention to their preparation procedure, features and catalytic activity on the selective catalytic reduction (SCR) of NO.

3.1. Activated Carbon Briquettes

Briquetting of coal is one of the types of size enlargement by agglomeration that has been traditionally based on the experience and rudimentary tests. The main advantage of the briquetting process step is that the obtained catalyst presents a lower pressure drop when

installed into a system. However, due to the complexity of the shape, there is smaller area exposed to reactant gases and modifications in the porosity or chemistry surface influencing the catalytic activity.

Briquettes can be prepared by means of a pressure procedure with a binder, following several steps: 1) pyrolysis of raw materials, 2) mixing of char and binder agent, 3) briquetting under pressure, and 4) curing in air. The influence of the different briquetting processes has been studied along all steps involved. The pyrolysis or co-pyrolysis of raw materials has a main influence in the mechanical properties. Blesa et al. (Blesa 2001) showed that the briquettes prepared with co-carbonized materials fit better the mechanical resistance than those prepared with blends of materials carbonized separately. Using a pyrolyzed char as the starting material, the binder is expected to act as cement, filling all the interstices between particles and clocking to some extent the pore entrances. Moreover, briquetting under high pressures greatly reduces the void volume between char particles, breaking them in some cases and destroying large pores. The strength, porosity and surface chemical properties of the final briquette will depend on its individual components and their interactions. The catalytic activity of the briquettes, will be consequently, influenced by all these factors. Rubio and Blesa (Rubio 1999, Blesa 2001) and Lázaro et al (Lázaro 2006b) studied the effect of briquetting procedure on the properties of the final product obtained. The main goal of these studies was to use a Spanish coal to obtain briquettes with acceptable mechanical properties and minimum loss of catalytic activity as experienced in its powered form. Especial attention was paid by Rubio and Izquierdo (Rubio 1999) to the influence of binder addition on impact and compressive resistance as well as on surface area and surface chemical properties of the briquettes. In this study, they concluded that the mechanical strength of a series of briquettes made of a low rank coal char and a commercial pitch (with a softening point of 70ºC) depends on the pyrolysis temperature of the parent char and on the pitch content of the briquettes. Using the highest temperature char and an amount of pitch higher than 18% by weight, briquettes exhibited good mechanical resistance, even after the activation process, was obtained. The changes in the textural and physical-chemical features observed in the briquettes with respect to parent chars are related to the changes experienced by the pitch and the char themselves. These changes, in turn, depend on the temperature of carbonization and activation. After the curing and carbonization stage, the briquettes show similar surface areas and lower pore volumes, as well as lower amount of acid functionalities than the parent chars.

The preparation of carbon-based catalytic briquettes was recently studied by Lazaro, Boyano, Gálvez and co-workers (Boyano 2006, Lázaro 2007b, Lázaro 2008, Boyano 2008a, Boyano 2008b, Gálvez 2010). They produced carbon briquettes from a low rank coal which was pyrolysed at 800ºC, blended with a commercial tar pitch and cold pressed at 125 MPa. The obtained cylindrical briquettes (10.5 mm diameter, 13.5 mm height and approximately 1.2 g weight) were then cured in air for 2 h, raising the temperature from ambient to 200ºC, 2ºC/min heating rate. Cured briquettes were further submitted to pyrolysis at 800ºC in N_2 atmosphere and to subsequent activation in the presence either of CO_2 and H_2O, with the aim of obtaining a well developed porous structure. The influence of briquette functionalization by means of liquid phase oxidation using HNO_3 and H_2SO_4 was also studied. Active phase was introduced by means of impregnation using different vanadium precursors, including V obtained from the ashes of a petroleum coke (PCA). Mechanical strength of the catalytic briquettes was evaluated by means of Impact Resistance Index (IRI) and Water Resistance Index (WRI), following the procedure described by Richards (Richards 1990).

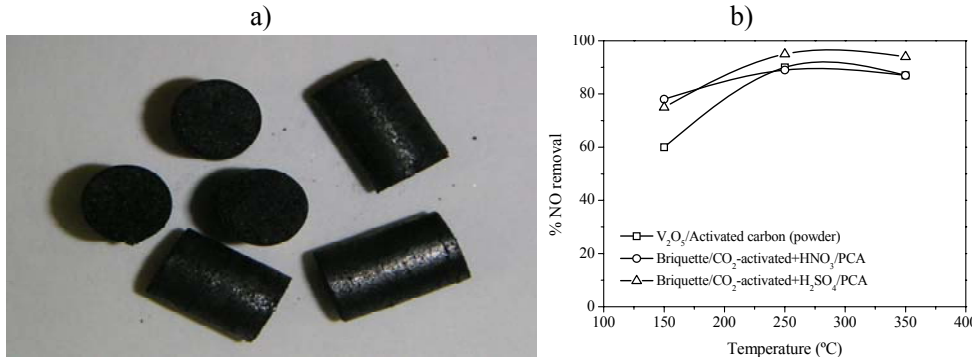


Figure 3. a) Appearance of the catalytic carbon briquettes, and b) NO removal as a function of temperature for the CO_2-activated briquettes loaded with petroleum coke ashes (PCA) and for the powder catalyst prepared with a steam-activated carbon loaded with vanadium pentoxide.

Catalytic, textural, structural and mechanical properties of the carbon briquettes were strongly influenced by the several steps in their preparation procedure. Activation process notably influenced the mechanical properties of the carbon briquettes. IRI increased after activation either with steam or CO_2, with respect to the pyrolysed briquette. Stricter activation conditions led to a decrease in the mechanical strength, in a similar way to what was reported by Rubio et al. (Rubio 1999) and Amaya et al. (Amaya 2007). WRI was mostly affected by the chemical chemistry of the briquettes. According to the mechanism postulated by Ozaki et al. (Ozaki 1997), carboxylic groups avoid to a certain extent the adsorption of water on the external surface of the briquette which retards the formation of cracks and their propagation.

The prepared catalytic briquettes showed significant activity in the selective catalytic reduction (SCR) of NO in the presence of ammonia (60-98% conversion, see Figure 3.b) in a wide range of temperatures (75-350ºC). Activity of the catalytic briquettes was found to depend both on surface area and on the amount of basic oxygen surface functionalities o its surface. An adequate development of porosity seemed necessary to avoid pore blockage, especially after the deposition of the active phase, allowing the diffusion of reactants and products out of the structure of the briquette. The presence of surface functionalities promoted support-active phase interaction resulting in enhanced catalytic activity (Gálvez 2010).

3.2. Carbon-Coated Monoliths

Monolithic structures have been widely used in the last years in many catalytic applications. They were developed during the last decades of the past century for automotive pollution control, as they allow the treatment of large volumes of gases, offer low pressure drop, high geometric surface area and short diffusion lengths, adequate mechanical properties and thermal shock resistance (Heck 2001). In the last years, monolithic reactors have been used also for flue gas cleaning and in combustion processes, as well as in several fine chemistry processes involving three-phase catalytic reactions (Cybulski 1994, Cybulski 1999). In many application fields, cordierite ($2MgO{\cdot}2Al_2O_3{\cdot}5SiO_2$) monoliths are normally used as substrate material, due to its excellent mechanical properties. Low pressure drop in the exhaust system, good thermal shock resistance and refractoriness are some of its most important properties (Tomašić 2007). However, cordierite presents relative low surface area,

which does not allow its direct use for catalytic approaches, and should be thus coated with a material, generally denoted washcoat, which offers adequate porosity and surface area for the accommodation of the catalytic phase. Carbon coating of different supports employing carbon, silicon carbide, alumina or magnesia as fillers which were impregnated with a binder in the so-called coat-mix process was initially considered with the aim of preparing composite carbon and ceramic materials with low residual porosity which could be used e.g. as electrodes (Luhleich 1997). Further on, Vergunst and co-workers considered carbon coated materials for their application in catalytic processes (Vergunst 2001, Vergunst 2002). The method to develop and optimize carbon-coated structured supports was initially developed by Hücke et al. (Hücke 1975). This method makes use of a carbon-yielding compound, such as furfuryl alcohol or furfuryl alcohol/pyrrole mixtures, a pore-forming liquid (polyethylene glycol or methyl ether), and a polymerization catalyst (nitric acid). Furfuryl alcohol polymers are known for their use as starting material in the preparation of carbon molecular sieves (Lafyatis 1990). Polyfurfuryl alcohol shows a high carbon yield (50 wt%) and is therefore suitable as a starting material for carbon coating of monoliths. Using an acidic catalyst, furfuryl alcohol readily polymerizes under ambient conditions (Moreno-Castilla 1980). The polymer mixture can be then used for dip-coating a structured support, followed by solidification of the polymer, carbonization and activation. This dip-coating step consists in dipping the structured material into the liquid polymer blend. Figure 4 shows the different steps in the preparation of the polymer mixture and support impregnation. Vergunst et al. (Vergunst 2002) investigated different preparation methods based in the original Hücke procedure. They employed furfuryl alcohol with or without pyrrole and/or polyethylene glycol monomethyl ether, using nitric acid as catalysts under ambient conditions. The partially polymerized furfuryl alcohol mixtures were used in the dip-coating of cordierite monolithic supports. Samples were first dried, cured in air at 250ºC and finally carbonized in Ar at temperatures between 550 and 900ºC, yielding a carbon layer on the monolithic support. The deposited polymer shrank during carbonization, generating cracks on the layer and resulting in a non-uniform coverage of the monolithic support. They observed that the porous properties of this layer strongly depended on the carbonization conditions applied. Oxidizing treatments prior to carbonization in combination with the use of a pore former (polyethylene glycol) resulted in an enhanced formation of mesopores in the carbon layer. Upon carbonization above a specific temperature, depending on the nature of the polymer, around 700ºC, in the case of poly furfuryl alcohol, the carbon-coated monoliths became electrically conducting.

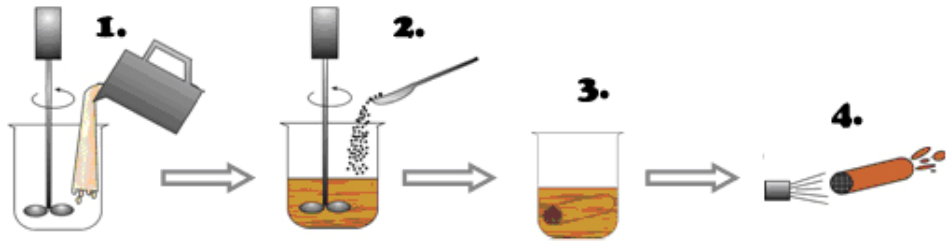


Figure 4. Carbon coating process for ceramic monoliths: 1) preparation of the polymer mixture, 2) addition of pore fillers or pore-forming compounds, 3) monolith dip-coating, and 4) elimination of the excess of the impregnating mixture.

García-Bordejé and co-workers (García-Bordejé 2002) prepared carbon-coated monoliths following a similar method than the one considered by Vergunst et al. (Vergunst 2002). They studied the influence of the carbon precursor (Novolac and Furan resins), the presence of pore fillers (activated carbon), the viscosity of the polymer mixture and the carbonization temperature, with aim of maximizing monolith coverage and mesoporosity of the carbon layer. An optimal viscosity of the polymer mixtures around 0.1 Pa·s was found when using both the Novolac and Furan resins. Carbon yields and porous properties of the deposited carbon layer were different when using the two different resins. Adding activated carbon as filler substantially increased the mesoporosity of the carbon layer, which was mostly microporous in all cases. Valdés-Solís et al. (Valdés-Solís 2001a) prepared carbon–ceramic cellular monoliths by coating a ceramic cellular monolith with a polymeric solution. Phenolic (resol and novolac), furanic resins and polysaccharides (sucrose and dextrose) were studied as carbon precursors. The procedure consisted in substrate impregnation with the polymeric mixture, curing or drying of the impregnated monolith, carbonization (700–1000°C in N_2), and physical (H_2O, 700°C) or chemical ($ZnCl_2$) activation. The addition of this later activation step resulted in a considerable increase in the micropore volume and surface area of the deposited carbon layer. Chemical activation allowed high carbon loads (13% wt.) in a single preparation step. The activated material showed a uniform carbon distribution, good adsorption properties, good electrical conductivity and a high mechanical strength. These same authors assayed the catalytic activity of Mn-loaded carbon-coated monoliths in the low-temperature SCR of NO (Valdés-Solís 2001b, Valdés-Solís 2003). They studied the influence of the textural and chemical properties of the carbon coating in the catalytic behaviour of the monoliths. Best results were obtained when using an steam-activated carbon–ceramic monolith (burn-off degree of 40 % wt.), oxidised with nitric acid (90°C) for 4 h and Na-exchanged prior to impregnation (NO_x reduction: 73% at 150°C and 4000 h^{-1}). Creeze et al. studied the dispersion and distribution of ruthenium on carbon-coated ceramic monolithic catalysts (Creeze 2003). For the preparation of the carbon-coated monoliths, they followed the method developed by García-Bordejé et al. (García-Bordejé 2002), adding a physical activation step (CO2, 850ºC, 14 h, burn-off degree of 40 % wt.) in order to increase the support's surface area. As a consequence of activation, the material presented a wide pore size distribution, including meso/macropores in the region 10-100 nm. However, ruthenium was found to be bond to the carbon surface through weak physisorption forces, being able to migrate upon catalyst drying due to capillary forces and resulting in a non-homogeneous distribution with low dispersion. García-Bordejé and co-workers (García-Bordejé 2004a, García-Bordejé 2004b) prepared carbon-coated cordierite monoliths using Furan resin and polyethylene glycol, which after carbonization and activation with CO_2 at 800ºC, were loaded with vanadium and tested for the SCR of NO in the presence of ammonia. With respect to the preparation of the carbon-coated monoliths, they reported that during pyrolysis the resin yielded the carbon layer, whereas polyethylene glycol helped in the creation of mesoporosity in this layer, and thus, increasing the amount of PEG in the polymer mixture resulted in an increase in the mesopore volume, concretely in the range of narrow mesoporosity (2-5 nm). On the other hand, activation with CO_2 contributed to the formation of new micropores. Upon vanadium addition, by means of equilibrium adsorption using ammonium metavanadate as precursor, they observed that oxygen surface functionalities were crucial for an optimal distribution of the active phase while narrow microporosity (< 0.7 nm) did not contribute to enhance the dispersion of the catalyst. Up to 6% wt. vanadium loading, the catalysts showed

activities comparable to similar SCR catalytic systems reported in the literature, with complete selectivity towards N_2. Increasing vanadium content resulted in less uniform distributions of the active phase. By simulating the influence of the coating thickness on the geometric parameters and conversion, they identified and optimal coating thickness around 30 μm meeting the compromise between activity and pressure drop. Later on, García-Bordejé and co-workers reported the influence of oxidation pre-treatments performed on the carbon-coated honeycomb monoliths (García-Bordejé 2006a), as well as their catalytic behaviour in the SCR of NO in the presence of steam and SO_2 (García-Bordejé 2006b). Using several characterization techniques, such as Fourier transform infrared spectroscopy, X-ray photoelectron spectroscopy and temperature programmed desorption for the determination of the surface oxygen functionalities created upon the different oxidation treatments, they concluded that pre-treating the carbon-coated monoliths at 330ºC in the presence of 10% O_2-Ar, gave rise to the formation of an optimal amount of surface groups resulting in the highest vanadium loading at high dispersion. Vanadium loading did not only depend on the amount of oxygen-containing groups but also on the textural properties of the carbon after the oxidation pre-treatment. When studying the catalytic behaviour of these vanadia-loaded carbon-coated monoliths in the SCR of NO and under the presence of traces of steam and SO_2 they observed that at temperatures higher than 200ºC the catalyst was able to maintain its activity, due to an auto-regenerating mechanism in which ammonium sulphate salts were instantaneously decomposed as long as they were formed and deposited on the catalyst surface. Pérez-Cadenas et al. assayed the performance of Pd and Pt supported on carbon-coated monoliths in hydrogenation reactions, i.e. selective hydrogenation of fatty acid methyl esters (Pérez-Cadenas 2005, Pérez-Cadenas 2006a) and in the catalytic oxidation of benzene, toluene and xylenes (Pérez-Cadenas 2006b, Pérez-Cadenas 2009). They coated cordierite monoliths using polyfurfuryl alcohol following a modified version of the method proposed by García-Bordejé et al. (García-Bordejé 2002). The coated monoliths were carbonized at 350 and 800ºC, subsequently activated in air at 300ºC, and oxidized with H_2O_2 at room temperature. A thin, homogeneous, consistent and good adhering carbon layer was obtained, whose textural and chemical surface properties depended on the preparation procedure. Pd and Pt were loaded by means of equilibrium impregnation using an aqueous solution of the corresponding tetraammine metal (II) nitrates. The metal dispersion was found to be strongly determined by the surface oxygen complexes content. The monolithic catalysts showed high activities both in the hydrogenation and in the oxidation reactions tested. An increase in the selectivity of the hydrogenation reactions was observed when including a previous α-Al_2O_3 coating step of the cordierite monolith, followed by carbon impregnation, resulting in a better distribution of Pd within the carbon layer, higher accessibility and reduced diffusion limitations. Based in the results obtained by García-Bordejé and co-workers (García-Bordejé 2004a, García-Bordejé 2004b, García-Bordejé 2006a, García-Bordejé 2006b) Boyano et al. have recently considered the application of vanadium-loaded carbon-coated cordierite monoliths for the on-board reduction of NO (Boyano 2008b, Lázaro 2008, Boyano 2008c, Boyano 2009, Boyano 2010). Selective catalytic reduction in the presence of urea has been regarded as one of the most promising technologies for the abatement of NO_x from the exhaust gas generated in engines using lean-burn mixtures. Furthermore, carbon-based catalyst offer unique advantages such as being active at much lower temperatures than classical TiO_2-based catalytic systems, and enhanced resistance towards sulphur poisoning. Thus, carbon-coated monoliths seemed a promising support for preparing catalyst for on-

board gas cleaning, and in fact, excellent results had been previously obtained when applying these catalysts in the SCR of NO in the presence of ammonia (García-Bordejé 2006b). In the preparation of the carbon-coated monoliths Boyano and co-workers used a polymeric blend of Furan resin and polyethylene glycol, carbonized the coated monoliths at 700ºC and submitted them to activation with CO_2 at 900ºC. They studied the influence of several oxidation treatments, i.e. using HNO_3, H_2O_2, H_2SO_4, in the textural and surface chemistry features of the carbon layer as well as in vanadium dispersion and catalytic activity. Again, the presence of oxygen surface functionalities was found to be a key issue for achieving an adequate dispersion of the active phase. The influence of the chemical properties of the carbon layer surface became even more important for V-fixation and dispersion when petroleum coke ashes were used as the precursor of the active phase. Regarding textural properties, a slight decrease in surface area was measured, as a result of pore widening caused by the strongest oxidizing agents. Especially important was to asses the adherence and mechanical properties of the carbon coating, moreover after the oxidation pre-treatments. This was done by measuring Young's modulus, elastic deformation and maximum strength of the materials during compressive strength tests, as well as the weight loss of the coated monoliths after being submitted to successive periods of ultrasonic agitation in an acetone bath and after cyclical thermal stress periods at 500ºC and room temperature (Boyano 2009). In comparison to alumina-coated monoliths, carbon-coated monoliths showed good layer adherence, together with higher resistance towards thermal shock and vibration. Indeed, carbon coating resulted in a reinforcement of the cordierite structure. Figure 5 shows two SEM images obtained for the carbon-monoliths. Average layer thicknesses around 800-900 nm were measured. The activity of these vanadium-loaded carbon-coated monoliths in terms of NO conversion was assayed by means of isothermal experiments at different temperatures, under experimental conditions as close as possible to real on board operation, i.e. a GSHV of 34,000 h^{-1} was maintained for all runs. Figure 6. shows the NO conversion measured for a series of catalysts prepared using carbon-coated monoliths submitted to different oxidation pre-treatments. NO conversion reaches in some cases values close to 90%. The catalysts prepared using the carbon-coated monolith pre-treated in diluted nitric acid yielded the best results in this series. XPS measurements evidenced that the diverse amounts of vanadium V^{4+} on the catalysts surface may be responsible for the differences in their activity. At the same time, the presence of V^{4+} seemed to be linked to the concentration of carboxylic acidic groups on the carbon surface, introduced upon functionalization.

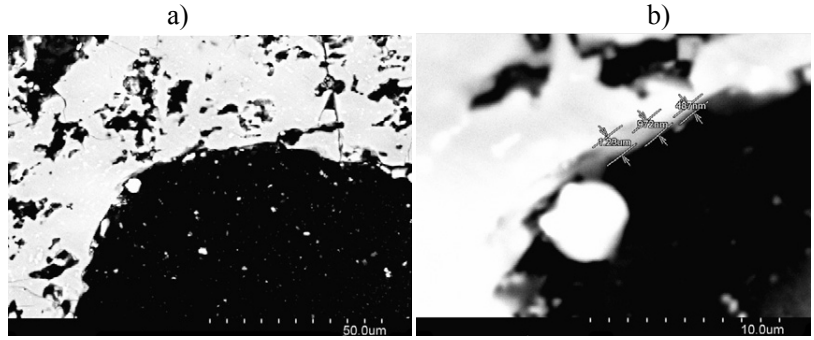


Figure 5. SEM images corresponding to a perpendicular cut of a carbon-coated monoliths. Layer thickness around 500-1200 nm measured in this case (Boyano 2009).

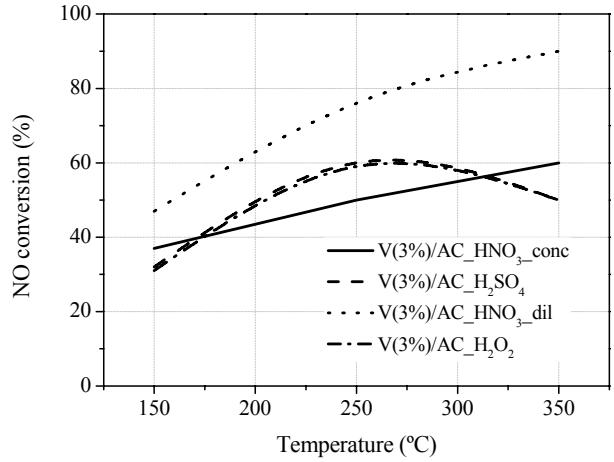


Figure 6. NO conversion for vanadia-loaded carbon-coated monoliths submitted to pre-oxidation treatments using concentrated and diluted HNO_3, H_2SO_4 and H_2O_2.

Structured materials can be also coated by means of in-situ formation of carbon nanofibres. Jarrah and co-workers (Jarrah 2003, Jarrah 2004) deposited carbon nanofibres on the surface of a γ- Al_2O_3 coated cordierite monolithic support. The monolith was first impregnated with nickel compounds and then exposed to a gas mixture containing 50% CH_4 and H_2 in N_2, at a temperature of 570ºC. Carbon fibres formed a homogeneous layer less than 1 μm thick, covering the surface of the channels in the monolith. In a similar way, Ulla et al. (Ulla 2008) grew carbon nanofibres over Co-mordenite coated cordierite monoliths. Recently, Morales-Torres et al. (Morales-Torres 2009) assayed the activity of Pd and Pt catalysts supported on carbon nanofibre coated monoliths for low-temperature combustion of BTX. They reported higher activities for the carbon nanofibre coated monoliths in comparison to alumina coated ones.

4. APPLICATIONS OF ACTIVATED CARBONS AS CATALYST SUPPORTS

Although some examples have been given already along the previous pages of this chapter, herein we aimed to summarize some the most important catalytic applications of activated carbons as supports. Radovic and Sudhakar (Radovic 1997) and, more recently, Rodríguez-Reinoso and Sepúlveda-Escribano (Rodríguez-Reinoso 2009), and Calvino-Casilda et al. (Calvino-Casilda 2010) presented interesting reviews on chemical reactions taking place in the presence of activated carbon-supported catalysts. However, extensive research is being continuously performed towards the investigation of newer and more challenging applications of activated carbons in catalysis.

4.1. Activated Carbon-Supported Catalysts in Oxidation Reactions

Selective oxidation reactions are fundamental in the production of industrial organic chemicals and intermediates used in the manufacture of industrial products and consumer

goods, i.e. the synthesis of fine chemicals and pharmaceuticals normally involves the oxidation of organic functional groups.

Noble metals, such as Au, Pt and Pd, supported on activated carbons have yielded excellent results when applied in the liquid-phase oxidation of alcohols to aldehydes, ketones or carboxylic acids (Korovchenko 2007). In example, Pritchard et al. (Pritchard 2010) have recently reported the preparation of Au-Pd nanocrystalline catalysts supported on activated carbon via a sol-immobilization technique, and explored their use for the direct synthesis of hydrogen peroxide and the oxidation of benzyl alcohol. The different products of the oxidation of benzyl alcohols have important applications in the pharmaceutical industry. Wang and co-workers (Wang 2010) assayed as well the liquid-phase oxidation of benzyl alcohol in the presence of Au and Pd activated carbon-based catalysts. Zhu et al. (Zhu 2010, Zhu 2008) studied the role of activated oxygen species in the oxidation of CO and benzyl alcohol, in the presence of Au-loaded activated carbons. They concluded that oxygen functional groups on the surface of the carbon support are directly involved in the reaction mechanism, through the formation of $Au\text{-}OH^-$ activated metallic sites. The oxidation of glycerol leads to a complex reaction pathway and a large number of products can be obtained. These products are useful intermediates for the synthesis of fine chemicals and are still being obtained by either expensive processes or by an enzymatic way. Glycerol selective oxidation was extensively studied by Prati and co-workers (Porta 2002, Veith 2007, Prati 2007). Demirel-Gülel et al. reported controlled selectivity towards the desired products, i.e. glyceric acid, and high conversions, when adjusting the metal particle size of Au-activated carbon supported catalyst employed in the oxidation of glycerol.

Some important gasoline and diesel fuel additives are also synthesized by means of oxidation reactions, such as the oxidative carbonylation of ethanol for the production of diethyl and dimethyl carbonates, DEC and DMC. The catalysts used in these processes are Wacker-type systems composed of $CuCl_2$ and $PdCl_2$. Zhang and co-workers (Zhang 2007a, Fan 2007) prepared activated carbon-supported $CuCl_2$–$PdCl_2$–KCl–NaOH catalysts and studied their behaviour in the gas-phase oxidative carbonylation of ethanol to diethyl carbonate. This synthesis route was proposed before by Wang et al. (Wang 1998) as an alternative to the phosgene-methanol process and the ester exchange process, making use of toxic raw materials, and to overcome the problems associated to the liquid-phase oxidative carbonylation of methanol. CO oxidation has also been assayed in the presence of activated carbon supported Wacker-type catalysts (Park 2000, Dyakonov 2003).

The use of activated carbons in electrochemical processes, i.e. fuel cells, is also well documented. Carbon blacks are traditionally used for the manufacturing of fuel cell eletrocatalysts. Pt, Ru and Pd are the most commonly metals employed in proton exchange membrane (PEM) fuel cell technologies. The metal load is generally high, around 20% wt. One way for cutting down the metal load and improve the specific performance and durability of the electrocatalyst is to increase its dispersion on the carbon support. Activated carbons offer several advantages in this sense, in comparison to carbon blacks, such as their more developed surface area and the possibility of tailoring its pore volume distribution and surface chemistry. Huang et al. (Huang 2008b) prepared Pt nanoparticles electrocatalysts using an activated carbon fibre with high specific surface area as support. Pt nanoparticles appeared highly and homogeneously dispersed on the surface of the fibres, with an average size of 2.4 nm. The prepared electrocatalysts showed much higher catalytic activity than a commercial Pt/C (E-TEK), in the oxidation of methanol, ethanol and isopropanol. The claimed that the

uniform Pt dispersion and the strong interactions between the metal nanoparticles and the carbon fibres resulted in this enhanced catalytic performance. Naga Mahesh and co-workers (Naga Mahesh 2009) assayed the performance of Pd supported on an activated carbon in a single cell PEM water electrolyser. They obtained acceptable hydrogen yields for 5 to 10% wt. Pt load.

4.2. Activated Carbon-Supported Catalysts in Hydrogenation Reactions

Liquid-phase, or in some cases gas-phase, hydrogenations are an important field of application of activated carbon based catalysts. Hydrogenation of alkanes, alkynes, aromatics, aldehydes, esters, carboxylic acids, nitro groups, nitriles and imides are fundamental steps in the synthesis of fine and industrial chemicals, or in pharmaceutical and agrochemical industries. Activated carbon-supported noble metals or transition metals such as Mo, Ni or V are commonly used in these reactions. In example, cyclohexanone is an important intermediate for manufacture of Nylon-6, and is produced by selective hydrogenation of phenol. Pd/C catalysts are used industrially in a batch process (Dobrovolszky 1982). Recently, Watanabe and Arunajatesan (Watanabe 2010) studied the influence of the support's acidity on the activity of activated carbon supported Pd-catalysts in the selective hydrogenation of phenol. They observed that acid modification of the carbon support, by means of HNO_3 treatment, enriched the electron density of Pd, and enhanced the desorption of the phenoxy species, resulting in improved cyclohexanone selectivity in phenol hydrogenation.

The hydrogenation of simple unsaturated hydrocarbons, such as ethylene, in the presence of activated carbon supported Ni and Ni-Mo catalysts, has been assayed by Matos and Laine (Matos 2003). They reported enhanced tolerance to coke deposition and durability for their Ni and Ni-Mo carbon-based catalysts in comparison to similar alumina supported catalytic systems. Chemicals such as 2-pheylethanol, a compound with bacteriostatic and antifungic properties, frequently used in the formulation of cosmetics or in the manufacture of chemicals, can be synthesized by means of gas-phase hydrogenation of styrene in the presence of carbon-supported Pt and Pd catalysts. Kirm et al. (Kirm 2007, Kirm 2005) observed higher selectivities to 2-phenylethanol for Pt and Pd supported on activated carbon than for the alumina supported catalysts and claimed that the acid-base character of the support has a decisive role in the selectivity of the hydrogenation of styrene, with higher acidity of the alumina support leading to the more substituted alcohol 1-phenylethanol, instead of to 2-phenylethanol.

Pérez-Cárdenas et al. (Pérez-Cadenas 2006b) assayed the hydrogenation of fatty acid methyl esters in the presence of palladium catalysts supported on carbon-coated monoliths. These kind of hydrogenation processes aim to reduce the amount of poly-unsaturated *trans* fats formed during the manufacture of products in food industry, i.e. vegetable oils. The authors identified a strong interplay between the carbon support properties, determined by the carbonization temperature, activation process, surface functionality and microporosity, and the performance of the assayed carbon-based Pd catalysts.

The potential use of activated carbon-based catalysts for the hydrogenation of CO and/or CO_2, i.e. Fischer-Tropsch synthesis, has been widely explored in the last decades (Radovic 1997). Particularly remarkable is the work of Vannice and collaborators who studied the

activity of metal carbonyl clusters and their impact in the selectivity in the Fischer-Tropsch synthesis reactions (Vannice 1981, Martín-Martínez 1989, de Lecea 1990). More recently, Ma and co-workers studied the behaviour of Mo, Fe, Co, Cu supported on activated carbon (Ma 2006a, Ma 2006b, Ma 2007a, Ma 2007b, Ma 2010). Their last results show that the Fischer-Tropsch synthesis activity can be related directly to the textural parameters (surface area) of the catalysts, associated with the relative ease of mass transfer and the relative fraction of metal crystallites present in the wide pores and inversely to the metal crystallite size. The selectivity toward C_{5+} products is related to the the number of basic and neutral functionalities on the surface. On the other hand, high selectivity toward C_1 correlates well to the low pH of the external surface of the support.

4.3. Petroleum Refining Catalyst

Many studies report the use of carbon-supported catalysts in petroleum refinery, concretely, in hydrotreating processes, i.e. hydrodesulphurization (HDS), hydrodenitrogenation (HDN) or hydrodechlorination (HDC). Hydrodesulphurization has acquired a renewed interest in the last years due to the more severe environmental legislation implemented in many countries, requiring sulphur content in diesel fuels to be reduced below 10 ppm by the year 2012 in Europe, Japan and the USA. Activated carbon-supported Co-Mo and Ni-Mo catalysts have shown lower coking propensity, weaker metal-support interaction and higher activity in comparison to alumina supported ones (Vissers 1987, Abosti 1898, Rankel 1993). Metals are normally active in their sulphide form. Calafat et al. (Calafat 1996a) studied the influence of the nature of an HNO_3-treated carbon support on the HDS activity of Mo, Ni, and NiMo catalysts. HDS activity of the catalysts is enhanced by acid treatments of the carbon support. Moreover the synergetic effect for the bimetallic catalysts was only observed when oxygen functional groups were present on the carbon surface $NiMoO_4$-like phase formed during impregnation seemed to be the precursor for the formation of the active sulphide phase over the studied NiMo/C catalysts. Puello-Polo and co-workers (Puello-Polo 2008:, Puello-Polo 2010a, Puello-Polo 2010b) have recently reported that carbides with sulphided surfaces or mixed carbo-sulphide species are the active phase in HDS on Fe-Mo, Co-Mo and Ni-Mo carbide catalysts. The results they obtained further remark the importance of sulphided surface phases in HDS on carbides of transition metal catalysts Lagos et al. (Lagos 2009) examined the effect of the textural and chemical properties of two activated carbons on the activity of carbon-supported Re catalysts for the HDS of dibenzothiophene (DBT). They observed that the presence of oxygen surface groups on the carbons, predominantly of carbonylic and quinone type, played an important role in the dispersion of the Re sulphide species, resulting in enhanced catalytic activity.

Hydrodenitrogenation (HDN) processes convert to hydrocarbons and NH_3 the nitrogen compounds contained in petroleum cuts. Nitrogen removal from petroleum feedstocks is necessary in order to avoid catalyst poisoning during the processing of petroleum distillates. Like in the case of HDS, the catalytic systems most commonly used are alumina-supported Co-Mo and Ni-Mo sulphides. As well, promising results have been obtained when substituting the alumina support by activated carbon (Ledoux 1989:, Vít 1993: Rankel 1993). Calafat et al. (Calafat 1996b) studied the activity of activated carbon-supported Mo and NiMo sulphided catalysts in the HDN of pyridine. A more oxidized support's surface increased the

intrinsic activity of the sulphide active sites where the denitrogenation reaction took place. They claimed that the acidic sites associated to the carbon support may also participate in the denitrogenation reaction. Re-containing catalysts supported on activated carbon have also been considered for the dehydronitrogenation (HDN) of gas oil (Escalona 2003, Escalona 2007). The authors observed that the behaviour for intrinsic HDN activity showed similar trends as those observed for HDS, i.e. higher activity for the carbon-based catalysts in comparison to alumina-based ones, for Re loadings below 0.4 atoms nm^{-2}. Re-activated carbon based catalysts were about twice as selective for HDN than the alumina-supported ones. This increased HDN selectivity of Re sulphide deposited on carbon suggested an additional effect of the carbon support, which might introduce structural and textural modifications of the active phase, more favourable to HDN than HDS.

4.4. Ammonia Synthesis

More than 90% of the world consumption of ammonia, the second largest synthetic chemical product, is manufactured from N_2 and H_2 via the catalytic Haber-Bosch process. Although this reaction is exothermic ($\Delta H^0_{25ºC}$ = -46.2 kJ mol^{-1}) and should occur spontaneously, significant energy input is needed for N_2 to achieve the activated state because of its high dissociation energy (941 kJ mol^{-1}). The use of catalysts lowers the activation energy and effects the reaction in the range of 250-400°C. Supported ruthenium or iron catalysts have been widely studied and applied in the ammonia synthesis process. Activated carbon has been also considered as catalyst support for this particular application. Aika and co-workers presented, already in 1972, some interesting results, obtained using a K-promoted activated carbon-supported Ru catalysts (Aika 1972). They found that the necessary electron transfer between the support and Ru active sites, key process in the formation of N-anionic intermediates, was substantially hindered by the electron-withdrawing nature of activated carbon. However, in the presence of K, once the electron-withdrawal capacity of the carbon was neutralized, the role of the activated carbon support was postulated as a medium for the electron transfer from the alkali to the transition metal sites. Later on, Kowalczyk et al. (Kowalczyk 1996) compared the activity of activated carbon-supported Ru catalysts and fussed iron, observing that the Ru/AC system was less sensitive to ammonia concentration in the reactant gas, as well as to changes in the total pressure. They concluded that ruthenium catalyst supported on carbon can be a valuable alternative for fused iron catalyst, particularly at high conversion degrees and relatively low total pressures in the reactor. This fact was further confirmed by Liang et al. (Liang 2001) which studied K and Ba promoted Ru catalysts supported on an activated carbon fibre, measuring activities about an order of magnitude higher than that of commercial iron catalyst. Zheng and co-workers reported higher activities for alkali promoted Ru catalysts prepared using activated carbons previously submitted to thermal treatments at temperatures from 1600 to 2500ºC (Zheng 2002). Carbon supports with high purity, high electronic conductivity and high surface area are thought to favour the high activity of Ru-based catalysts for ammonia synthesis (Liang 2001). Zheng and co-workers claimed that thermal treatment of activated carbon eliminates the impurities and improves the carbon support resistance to methanation under the conditions of ammonia synthesis. Subsequent mild oxidation of the carbon supports, under 10% O_2 at 450ºC, partially recovered the surface area and porosity lost during the high temperature thermal treatment,

resulting in a better Ru dispersion and enhanced catalytic activity. More recently, Zhu et al. (Zhu 2007) examined the effects of such oxidation treatments on the carbon surface chemistry and pore structure, closely related to Ru dispersion and catalytic activity. Cobalt has also been considered as a promising active metal in the formulation of carbon-supported catalyst for ammonia synthesis. In this way, Raróg-Pilecka et al. (Raróg-Pilecka 2006) studied the use of a graphitized activated carbon as support for K and Ba promoted Fe and Co catalysts. They measured about six times higher surface-based reaction rate (TOF) for Ba-Co/C than for Ba-Fe/C, at low temperature (400 °C) and at high conversion (8% NH_3 in the gas).

4.5. Activated Carbon as a Catalysts or Catalyst Support for Hydrogen Production

The application of carbon materials as catalysts in hydrogen production processes, such as the direct decomposition of methane, has considerably attracted the attention of the scientific community in the last years. Direct decomposition of methane appears as a promising alternative to steam reforming or partial oxidation of methane for the CO_x-free production of hydrogen (Habbas 2010). The thermal decomposition of hydrocarbon fuels into hydrogen and carbon has been extensively reviewed by Muradov (Muradov 1993, Muradov 1998, Muradov 2001a, Muradov 2005a). This process needs the presence of a catalyst and yet one of its most important drawbacks is the catalyst deactivation associated with the carbon build up on the catalyst surface. Muradov (Muradov 2001b) stated that the use of carbon-based catalysts offers several advantages over metal catalysts: (i) there is no need for the regeneration of the catalyst by burning carbon off the catalyst surface, (ii) no contamination of hydrogen with carbon oxides, and (iii) possibility of production of both hydrogen and carbon with minimum CO_2 emissions. Moreover, carbon can be still utilized as a valuable byproduct of the process, thus reducing the net cost of hydrogen production. They evaluated the catalytic activity of a variety of carbon materials of different origin and structure, including a wide range of activated carbons, carbon blacks, graphites, nanostructured carbons and others, towards methane decomposition reaction, observing that although activated carbons were initially more active than carbon blacks, the latter resulted in more sustainable process of methane decomposition (Muradov 2001b, Muradov 2005b). They concluded that the catalytic activity of carbons for methane decomposition reaction was mostly determined by their structural and surface properties. Suelves and co-workers studied the thermal decomposition of methane over carbon materials, including activated carbons (Suelves 2007), as well as the regeneration of the carbon catalysts by means of physical activation (Pinilla 2007). In agreement with what was observed by Muradov and co-workers they claimed that, although initially more active, activated carbon was rapidly deactivated, whereas in the case of carbon black, the process continued until most of the surface was covered by carbon crystallites generated from methane cracking. Carbon surface chemistry and the pore size distribution played an important role on the initial rate conversion of methane and the long term sustainability of the catalyst, respectively. In their attempt of regenerating the deactivated carbon catalysts by means of CO_2 activation, the authors observed that, after three cycles of decomposition/regeneration, most of the carbon sample consisted of the carbon formed during the methane decomposition process, since the initial catalyst was completely gasified. Dominguez, Fidalgo and collaborators (Domínguez 2007, Fidalgo 2008) studied the

study the microwave-assisted pyrolysis of CH_4 over an activated carbon, which acted as both microwave receptor and catalyst. They found that methane conversions were higher under microwave conditions than with conventional heating when the temperature measured was lower than or equal to 800ºC. Steinfeld and co-workers investigated the thermal decomposition of methane in the presence of activated carbon particles and under concentrated solar radiation (Trommer 2004, Maag 2009). Experiments were performed in a solar simulator able to provide 75 kW of continuous radiative power with peak fluxes exceeding 4250 kW/m^2, mostly at visible wavelengths with additional power in the near IR and UV. Different type of powder activated carbons were fed in an entrained CH_4 flow. Carbon particles served simultaneously as efficient radiant absorbers and as reaction sites for the heterogeneous decomposition reaction. Thus, the introduction of carbon particles enhanced considerably the reaction rate with respect to the un-catalysed reaction, by increasing the frequency factor by six orders of magnitude, as a result of the larger specific surface reaction and of the more efficient radiation heat transfer to the reaction sites.

Activated carbon has also been used for supporting an active metal in the preparation of catalysts for methane thermal decomposition. In example, Muradov et al. (Muradov 2006) reported the oxygen-assisted decomposition of methane over activated carbon-supported Fe catalysts. Bai et al. studied both methane decomposition over activated carbons (Bai 2005, Bai 2006a, Bai 2006b) and Ni-doped activated carbons (Bai 2007). At temperatures from 550 to 850ºC, Ni-catalyst showed higher activity in methane decomposition than the activated carbon itself. At 750ºC, the methane decomposition rate and the quality of the carbon material, fibres, formed were found to be optimal in the presence of the catalysts tested. However, the authors observed the formation of Ni_3C species during methane decomposition, which may be another disadvantageous factor for catalyst deactivation. Takehira and co-workers assayed as well Ni supported on carbons, i.e. graphite, activated carbon and carbon nanofibres, as catalysts for methane decomposition (Takehira 2005). They focused their attention on the production and quality of the carbon material obtained out of methane decomposition, rather than on the hydrogen yield, but they observed that pre-treatment of the carbon supports, graphite and nanofibres, with hydrogen peroxide and/or nitric acid increased the interaction between Ni and the carbon surface, resulting in Ni metal particles of smaller size and in higher yields and quality of carbon material in methane decomposition. On the other hand, activated carbon-based catalyst was not influenced to that extent by hydrogen peroxide and nitric acid pre-treatments in comparison to carbon nanofibres and graphite. The authors thus concluded that the properties of the carbon product can be controlled by varying the carbon materials used as catalyst support, their pre-treatment, and hydrocarbon mixture fed as reactant gas.

Activated carbon-based catalysts have been as well proposed for the dry reforming of methane, i.e. in the presence of CO_2. Guerrero-Ruiz et al. compared the activity of silica- and activated carbon-supported Co catalyst, adding MgO as promoter to avoid carbon deposition on the catalysts surface (Guerrero-Ruiz 1994). Bradford and Vannice studied the activity of Ni supported on SiO_2, TiO_2, MgO and activated carbon (Bradford 1996) and measured specific activities, on a turnover frequency basis, in the order: $Ni/TiO_2 > Ni/C > Ni/SiO_2 > Ni/MgO$. Diaz and co-workers (Diaz 2007) reached high methane conversions (up to 40%) at mild reaction conditions, in the presence of activated carbon-based Ni-Ca catalysts. Ca played a co-support role inhibiting the deactivation of the catalyst at prolonged time-on-stream. More recently, Fidalgo et al. (Fidalgo 2010) have studied the influence of the surface chemistry of

the carbon used as support, the drying method (i.e. microwave or conventional drying) and the temperature of the reduction stage, on the Ni particle size, Ni dispersion and final catalytic activity in the dry reforming reaction of a series of carbon-based Ni catalysts. They observed that the presence of oxygen surface functionalities created upon the oxidation treatment of the carbon support favoured the interaction between Ni particles and carbon surface, resulting in a higher Ni dispersion. The modification of the rest of the parameters in the preparation procedure of the catalyst had a deep influence in the final Ni particle size and dispersion. However, Ni particles sintered at reaction temperature (800ºC), and other factors can play a more important role, including the oxidation of the carbon support, which considerably reduced the catalytic activity.

4.6. Environmental Catalysis

Activated carbons have been widely applied in several catalytic processes for the detoxification and decontamination of liquid or gaseous effluents. Worldwide, the each time stricter environmental regulation has forced the introduction of newer and more efficient after-treatment catalytic technologies, in order to bring down the concentrations of the pollutants contained in such effluents under the limits fixed by the present or upcoming legislation. Apart from the excellent properties of activated carbon as an adsorbent, i.e. in volatile organic compounds (VOCs) removal processes or adsorption of several organic pollutants in liquid effluents (Brasquet 1997, Busca 2008), the particular features of activated carbons offer unique advantages for their application as catalyst support, or as a catalyst itself, i.e. in flue or exhaust gas cleaning processes, such as SO_2 and H_2S removal, VOCs and CO oxidation, NO_x selective reduction, or in the treatment of polluted liquid effluents by means of innovative advanced oxidation technologies, such as catalytic wet air oxidation (CWAO).

Sulphur compounds might be present, up to a certain extent, in flue gases generated in the combustion or gasification of fossil fuels, such as coal or natural gas, or in the combustion and gasification of biomass. Fuel processing under gasification conditions results in the transformation of the fuel's sulphur content into H_2S. Hydrogen sulphide is also naturally present in bio and natural gas and in gaseous industrial effluents, such as off-gases of viscose production process or residual gases of Claus plants (Richter 1990). It is of course highly toxic and thus considered as a major air pollutant, but in addition its presence can cause severe catalyst deactivation when further processing, i.e. in integrated gasification combined cycle (IGCC) power plants, hydroprocessing or ammonia synthesis, or directly making use of the gaseous stream, i.e. in electricity generation devices such as fuel cells. Moreover, for some particular applications, the sulphur content must be reduced to low parts per billion (ppb) levels. The conventional ways for H_2S removal include amine aqueous solution, adsorption-clause process, liquid redox process and fixed-bed solid adsorption process which has been widely investigated at higher temperature (300–500°C) (Richter 1990, Wang 2003, Sasaoka 1994). Another method for removal H_2S is its direct oxidation to elemental sulphur, at low temperatures (< 100°C) and in the presence of a catalyst. Activated carbon has been widely studied as a catalyst (Wu 2005, Gardner 2002) or catalyst support (Wang 2006, Bashkova 2007, Bashkova 2009, Chen 2010) in this process. It is claimed that activated carbon plays a dual role, being both a catalyst for the direct oxidation of H_2S by air and as an adsorbent for removing sulphur via chemisorption and keeping it within its pore structure.

The challenge is to avoid SO_2 formation and increase the selectivity of the reaction towards S formation. Impregnation of the active carbon with metal oxides, such as V (Mikhalovsky 1997), or alkali compounds, such as K_2CO_3 (Przepiórski 1999),

NaOH (Bashkova 2009) or Na_2CO_3 (Wang 2006) significantly improved their catalytic performance with respect to raw activated carbons.

Sulphur dioxide, SO_2, is an important air pollutant that causes photochemical smog and acid rain. As an alternative to wet gas cleaning processes, its removal from stack gases can be performed by means of catalytic oxidation to SO_3 and further surface reaction with the steam content in the flue gas to form H_2SO_4. The carbon can be later thermally regenerated recovering an SO_2-rich gas which can be further processed for S production in a Claus plant (Richter 1990, Knoblauch 1981, Olson 2000). More recently, Macías-Pérez et al. (Macías-Pérez 2007, Macías-Pérez 2008a, Macías-Pérez 2008b) have investigated the SO_2 uptake capacity of CaO-loaded activated carbons. Wey et al. (Wey 2003) assayed the activity of a Cu-Ce promoted activated carbon in the SO_2 removal from an incineration flue gas. The same authors (Tseng 2003) studied as well the catalytic activity of carbons loaded with V and Fe-oxides. Rubio and Izquierdo (Rubio 2010) have recently reported results on the activity of coal fly ash based carbons in the SO_2 removal from flue gases. They observed that both the presence of Ca and Fe in the activated carbons, as well as their more developed porous structure, enhanced the catalytic activity in SO_2 oxidation, in the case of the activated carbons prepared using a low rank coal.

Nitrogen oxides, NO_x, removal from a flue gas can also be accomplished in the presence of activated carbon or carbon-supported catalysts. This series of contaminants, namely NO, NO_2 and N_2O, have a huge impact in our environment, as they are known to be partially responsible of acid rain, soil eutrophization and acidification, as well as water nitrification, play an important role in the photochemical reactions occurring in the stratosphere and contribute to ozone formation in the lower layers of our atmosphere (Muzio 1997, Longhurst 1993a, Longhurst 1993b). They are generated in every combustion process making use of a fossil or N-containing fuel and/or, most importantly, when combustion takes place under air atmosphere at high temperatures (> 900ºC), by means of the formation of thermal-NO_x. Most recent environmental legislation sets the emission limits of NO_x to very low concentrations which cannot be met by modifying or optimizing the combustion process, i.e. via the introduction of primary measures. Therefore, after-treatment technologies, most of the time catalytic, need to be applied in order to attain an efficient de-nitrification of stack gases or automotive exhausts. Several approaches have been made concerning the use of activated carbons as catalysts in De-NO_x after-treatment technologies. Activated carbon can act as a NO_x reductant itself, as a catalyst or as a catalyst support, either in the presence or in absence of an external reducing agent. In the processes known as char-consuming reduction of NO_x (Aarna 1997, Suzuki 1994, Illán-Gómez 1993) the reduction of NOx takes place directly by reaction with carbon. The reduction reaction is substantially catalysed in the presence of activated carbon loaded with K, Ca or Fe compounds (Illán-Gómez 1995a, Illán-Gómez 1995b, Illán-Gómez 1995c, Illán-Gómez 1995d). Nitrogen oxide reduction in the presence of a catalyst and a reducing agent is widely known as selective catalytic reduction (SCR). The use of activated carbon or carbon-based catalyst in this process has been widely studied in the last years, as they are able to bring down considerably the optimal reaction temperature for achieving high De-NO_x conversions, in comparison to TiO_2-based catalytic systems. Bergbau-Forschung (Deutsche Montan Technologie) and Mitsui Mining commercialized the

MET-Mitsui-BF process based on the selective reduction in the presence of ammonia over non-doped activated carbons (Knoblauch 1981, Olson 2000). In this process the activated carbon adsorbs first the SO_2 contained in the flue gas, generating sulphates on its surface. Ammonia is then fed and selective reduction of NO_x starts taking place, enhanced by the presence of the sulphated activated carbon surface. The reactions take place at temperatures between 100 and 200ºC, and the spent activated carbon is regenerated by means of heating it up at 400ºC. It has been claimed that in these gas cleaning processes, making use of activated carbon, some other toxic pollutants such as mercury or dioxins, can be simultaneously removed by adsorption on the carbon surface (Olson 2000). The main disadvantage of using non-doped activated carbons is the high residence times and, thus, reactor volume needed for an effective operation, due to their lower catalytic activity. The catalytic activity increases when loading activated carbons with an active phase, such as copper oxides (Teng 2001, Zhu 2000a), iron oxides (Teng 2001), manganese oxides (Grzybek 1998, Grzybek, T, Grzybek 1999, Marbán 2001a, Marbán 2001b) or vanadium oxides (Zhu 2000b, Lázaro 2004, Lázaro 2006a, Lázaro 2008, Gálvez 2005).

Liquid phase applications include catalytic wet air oxidation (CWAO), as a way of converting harmful organic pollutants such as phenolic compounds into innocuous carbon dioxide. This process is currently employed for the treatment of industrial wastewaters. The use of catalyst overcomes the aforementioned costly, high-pressure, energy-intensive conditions of non catalytic WAO. The latest research advances regarding CWAO have been reviewed by Luck (Luck 1996, Luck 1999) and more recently by Bhargava et al. (Bhargava 2006). Solid catalysts bypass the need of a separation step of catalyst and wastewater. Most of the active catalysts proposed for CWAO of phenol are solids containing either noble metals (Pt, Ru) or transition metal cations (Cu, Co, Mn, Fe) as active phase. Frequently, such active phases are supported on alumina or carbon, and may contain ceria additives. In example, Martínez et al. (Martínez 2009) have lately reported results on the activity copper supported on activated carbon as catalyst in the CWAO of methylene blue (MB) and polyvinyl alcohol (PVA) in aqueous phase. Sousa et al. (Sousa 2010) studied the behaviour of pyrolysed and subsequently activated textile acrylic fibres and melamine foams, as catalysts for the wet air oxidation of aniline. The use of these N-enriched carbons improved the rate of aniline removal. Morales-Torres and co-workers (Morales-Torres 2010) demonstrated the feasibility of using non-doped activated carbons as catalysts in the WAO of 2,4,6-trinitrophenol (TNP). Hydrogen peroxide has been used instead of oxygen in WAO processes. Quintanilla et al. (Quintanilla 2010) studied the effect of hydrogen peroxide as radical promoter in the wet air oxidation of phenol over activated carbon catalysts. They found that hydroperoxy radicals, produced by the reaction between hydrogen peroxide and adsorbed oxygen, initiate the reaction on both the carbon surface and in the liquid phase. Surface carbon properties can be thus crucial for attaining high phenol oxidation extents.

REFERENCES

Aarna, I.; Suuberg, E. *Fuel* 1997, *76* 475-491.

Abotsi, G.M.K.; Scaroni, A.W. *Fuel Process. Technol.* 1989, *22*, 107-133.

Aika, K.-I.; Hori, H.; Ozaki, A. *J. Catal.* 1972, *27*, 424-431.

Alcañiz-Monge, J. D.; Cazorla-Amorós, A.; Linares-Solano, A.; Yoshida, A. Oya. *Carbon* 1994, *32*, 1277-1283.

Alcañiz-Monge, J.; Cazorla-Amorós, D.; Linares-Solano, A. *Carbon* 1997, *35*, 1665-1668.

Alcañiz-Monge, J.A.; Cazorla-Amorós, D.; Linares-Solano, A.; Morallón E.; Vázquez J.L. *Carbon* 1998, *36*, 1003-1009.

Amaya, A.; Medero, N.; Tradeci, N.; Silva, H.; Deiana, C.; *Bioresour. Technol.* 2007 *98,* 1635-1641.

Antolini, E. *Appl. Catal. B: Environ* 2009, *88*, 1-24.

Bai, Z., Chen, H., Li, B., Li, W. *Int. J. Hydrogen Energy* 2007, *32*, 32-37.

Bai, Z.; Chen, H.; Li, B.; Li, W. *J. Anal. Appl. Pyrolysis* 2005, *73*, 335-341.

Bai, Z.; Chen, H.; Li, W.; Li, B. *Int. J. Hydrogen Energy* 2006b, *31*, 899-905.

Bai, Z.-Q.; Chen, H.-K.; Li, W.; Li, B.-Q. *J. Fuel Chem. Technol.* 2006a, *34*, 66-70.

Bansal, R.C.; Donnet, S.B.; Stoeckli F. (Eds.), *Manufacture of active carbons*, in Active Carbon, Marcel dekker, New York, 1988.

Barrientos-Ramírez, S.; Montes de Oca-Ramírez, G.; Sepúlveda-Escribano, A.; Pastor-Blas, M.M.; González-Montiel, A.; Rodríguez-Reinoso, F. *Cat. Today* 2010 *150*, 42-48.

Barton, S.S.; Evans, M.J.B.; Halliop, E.; McDonald, J.A.F. *Carbon* 1997, *35,* 1361-1366.

Bashkova, S.; Armstrong, T.R.; Schwartz, V. *Energy and Fuels* 2009, *23*, 1674-1682.

Bashkova, S.; Baker, F.S.; Wu, X.; Armstrong, T.R.; Schwartz, V. *Carbon* 2007, *45*, 1354-1363.

Bhargava, S.K.; Tardio, J.; Prasad, J.; Fo1ger, K.; Akolekar, D.B.; Grocott, S.C. Ind. Eng. Chem. Res. 2006, 45, 1221–1258.

Blesa, M.J.; Fierro, V.; Miranda, J.L.; Moliner, R.; Palacios, J.M. *Fuel Process. Technol.* 2001, *74*, 1-17.

Boehm, H.P. *Carbon* 2002 *40*, 145-149.

Boyano, A.; Gálvez, M.E.; Lázaro, M.J.; Moliner, R. *Carbon* 2006, *44*, 2399–2403.

Boyano, A.; Gálvez, M.E.; Moliner, R.; Lázaro, M.J. *Catalysis Today* 2008b, *137,* 209–214.

Boyano, A.; Gálvez, M.E.; Moliner, R.; Lázaro, M.J. *Fuel* 2008a, *87*, 2058-2068.

Boyano, A.; Herrera, C.; Larrubia, M.A.; Alemany, L.J.; Moliner, R.; Lázaro, M.J. *Chem. Eng. J.* 2010, *160,* 623-633.

Boyano, A.; Lázaro, M.J.; Cristiani, C.; Maldonado-Hódar, F.J.; Forzatti, P.; Moliner, R. *Chem. Eng. J.* 2009, *149,* 173-182.

Boyano, A.; Lombardo, N.; Gálvez, M.E.; Lázaro, M.J.; Moliner, R. *Chem. Eng. J.* 2008c, *144*, 343-351.

Bradford, M.C.J.; Vannice, M.A. *Appl. Catal. A: General* 1996, *142*, 97-122.

Brasquet, C.; Le Cloirec, P. *Carbon* 1997, *35*, 1307-1313.

Busca, G.; Berardinelli, S.; Resini, C.; Arrighi, L. J. Hazard. Mater. 2008, 160, 265-288.

Calafat, A.; Laine, J.; López-Agudo, A. *Catal. Lett.* 1996b, *40*, 229-234.

Calafat, A.; Laine, J.; López-Agudo, A.; Palacios, J.M. *J. Catal*. 1996a, *162*, 20-30.

Calvino-Casilda, V; López-Peinado, A.J.; Durán-Valle, C.J.; Martín-Aranda, R.M. Cat. Rev. Sci. Eng. 2010, 52, 325-380; Harrison, B.; Jenkins, J.W. *Cat. Today* 1990, *7*, 113-137.

Calvo, L.; Gilarranz, M.A.; Casas, J.A.; Mohedano, A.F.; Rodríguez, J.J. *Ind. Eng. Chem. Res.* 2005, *44,* 6661-6667.

Cameron, D.S.; Cooper, S.J.; Dogson, I.L.; Harrison, B.; Jenkins, J.W. *Cat. Today* 1990, *7*, 113-137.

Castro-Muñiz, A.; Martinez-Alonso, A; Tascón, J.M.D. *Microp. Mesop. Mat.* 2008, *114*, 185-192.

Chen, Q.; Wang, Z.; Long, D.; Liu, X.; Zhan, L.; Liang, X.; Qiao, W.; Ling, L. *Ind. Eng. Chem. Res.* 2010, *49*, 3152-3159.

Chingombre, P.; Saha, B.; Wakeman, R.J.; *Carbon* 2005, *43*, 3132.

Creeze, E.; Kooyman, P.J.; Kiersch, J.; Sloof, W.G.; Mul, G.; Kapteijn, F.; Moulijn, J.A. *Cat. Letters* 2003, *90,* 181-186.

Cybulski, A.; Moulijn, J.A. *Catal. Rev. Sci. Eng.* 1994, *36*, 179-270.

Cybulski, A.; Stankiewicz, A.; Edvinsson Albers, R.K.; Moulijn, J.A. *Chem. Eng. Sci.* 1999, *54*, 2351-2358.

Dandekar, A.; Baker, R.T.K.; Vannice, M.A.; *J. Catal.* 1999, *183*, 131-154.

De Beer, V.H.J.; Derbyshire, F.J.; Grook, C.K.; Prins, R.; Scaroni, A.W.; Solar, J.M. *Fuel* 1984, *63,* 1095-1109.

De la Puente, G.; Menéndez, J.A.; *Solid State Ion.* 1998, *112*, 103-111.

de Lecea, C.S.-M.; Linares-Solano, A.; Vannice, M.A. *Carbon* 1990, 28, 467-476.

Derbyshire, F.J.; de Beer, V.H.J.; Abotsi, G.M.K.; Scaroni, A.W.; Solar, J.M.; Skrovanek, D.J. *Appl. Catal.* 1986, *27*, 117-131.

Díaz, K.; García, V.; Matos, J. *Fuel* 2007, *86*, 1337-1344.

Dobrovolszky, M.; Tétényi, P.; Paál, Z. *J. Catal.* 1982, *74*, 31-43.

Domínguez, A.; Fernández, Y.; Pis, J.J.; Menéndez J.A. *Int. J. Hydrogen Energy* 2007, *32*, 4792–4799.

Dun, J.k,; Gulari, E.; Ng, K.Y.S. *Appl. Catal.* 1985, *15*, 247-263.

Dyakonov, A.J. A*ppl. Catal. B: Environ.* 2003, *45*, 257-267.

Ehrburger, P.; Mongilardi, A.; Lahaye, J. J. *Colloid Interface Sci.* 1983, *91,* 151-159.

Escalona, N.; Ojeda, J.; Palacios, J.M.; Yates, M.; Fierro, J.L.G.; Agudo, A.L.; Gil-Llambías, F.J. *Appl. Catal. A: General* 2007, *319*, 218-229.

Escalona, N.; Yates, M.; Ávila, P.; López Agudo, A.; Fierro, J.L.G.; Ojeda, J.; Gil-Llambías, F.J. *Appl. Catal. A: General* 2003, *240*, 151-160.

Fan, M.; Zhang, P.; Ma, X. *Fuel* 2007, *86*, 902-905.

Fan, M.; Zhang, P.; Ma, X. *Fuel* 2007b, *86*, 902-905.

Fidalgo, B.; Fernández, Y.; Domínguez, A.; Pis, J.J.; Menéndez J.A. *J. Anal. Appl. Pyrolysis* 2008, *82*, 158–162.

Fidalgo, B.; Zubizarreta, L.; Bermúdez, J.M.; Arenillas, A.; Menéndez, J.A. *Fuel Process. Technol.* 2010, *91*, 765-769.

Fraga, M.A.; Jordão, E.; Mendes, M.J.; Freitas, M.M.A.; Faria, J.L.; Figueiredo, J.L, *J. Catal.* 2002, *209*, 355-364.

Gale, T.K.; Fletcher, T.H.; Bartholomew, C.H. *Energy and Fuels* 1995, *9*, 513-524.

Gálvez, M.E.; Boyano, A.; Lázaro, M.J.; Moliner, R. *Chem. Eng. J.* 2008, *144*, 10-20.

Gálvez, M.E.; Boyano, A.; Moliner, R.; Lázaro, M.J.; *J. Anal. Appl. Pyrol.* 2010, *88*, 80-90.

Gálvez, M.E.; Lázaro, M.J.; Moliner, R. *Cat. Today* 2005, *102-103*, 142-147.

García-Bordejé, E.; Calvillo, L.; Lázaro, M.J.; Moliner, R. *Appl. Catal. B: Environ.* 2004a, *50,* 235-242.

García-Bordejé, E.; Calvillo, L.; Lázaro, M.J.; Moliner, R. *Ind. Eng. Chem. Res.* 2004b, *43*, 4073-4079.

García-Bordejé, E.; Kapteijn, F.; Moulijn, J.A. *Carbon* 2002, *40*, 1079-1088.

García-Bordejé, E.; Kapteijn, F.; Moulijn, J.A. *Cat. Today* 2001, *69*, 357-363.

García-Bordejé, E.; Lázaro, M.J.; Moliner, R.; Álvarez, P.M.; Gómez-Serrano, V.; Fierro, J.L.G. *Carbon* 2006a, *44*, 407-417.

García-Bordejé, E.; Pinilla, J.L.; Lázaro, M.J.; Moliner, R. *Appl. Catal. B: Environ.* 2006b, *66*, 281-287.

Gardner, T.H.; Berry, D.A.; David Lyons, K.; Beer, S.K.; Freed, A.D. *Fuel* 2002, *81*, 2157-2166.

Gatica, J.M.; Rodríguez-Izquierdo, J.M.; Sánchez, D.; Ania, C.; Parra, J.B.; Vidai, H.; *Carbon* 2004, *42*, 3251-3254.

Gil, A.; de la Puente, G.; Grange, P.,*Microp. Mat.* 1997, *12*, 51-61.

Grant, T.M.; King, C.J. *Ind. Eng. Chem. Res.* 1990*, 29*, 264-271.

Grzybek, T.; Pasel, J.; Papp, H. *Phys. Chem. Chem. Phys.* 1999, *1*, 341-348.

Grzybek, T.; Pasel, J.; Papp*, H. Phys. Chem. Chem. Phys*. 1999, 1, 341-348.

Guerrero-Ruiz, A.; Sepúlveda-Escribano, A.; Rodríguez-Ramos, I. *Cat. Today* 1994, *21*, 545-550.

Habbas, H.F.; Wan Daud, W.M.A. *Int. J. Hydrogen Energy* 2010, *35*, 1160-1190

Halnttunen, M.E.; Niemelä, M.K.; Krause, A.O.I.; Vaara, T.; Vuori, A.I.; *Appl. Cat. A: General* 2001, *205,* 37-49.

Hanika, J.; Machek, V.; Němec, V.; Růžička, V.; Kunz, J. *J. Catal.* 1982 *77*, 248-256.

Heck, R.M.; Gulati, S.; Farrauto, R.J. *Chem. Eng. J.* 2001, *82*, 149-156.

Huang, H.; Ye, D.; Huang, B.; Wei, Z. *Cat. Today* 2008a, *139*, 100-108.

Huang, H.X.; Chen, S.X.; Yuan, C. *J.Power Sources* 2008b, *175*, 166-174.

Hücke, E.E.; *US patent 3859421*, 1975.

Illán-Gómez, M.; Linares-Solano, A.; Radovic, L.R.; Salinas-Martínez de Lecea, C. *Energy and Fuels* 1995a, *9*, 540-548.

Illán-Gómez, M.; Linares-Solano, A.; Radovic, L.R.; Salinas-Martínez de Lecea, C. *Energy and Fuels* 1995b, *9*, 97-103.

Illán-Gómez, M.; Linares-Solano, A.; Radovic, L.R.; Salinas-Martínez de Lecea, C. *Energy and Fuels* 1995c, *9*, 112-118.

Illán-Gómez, M.; Linares-Solano, A.; Salinas-Martínez de Lecea, C. Energy and Fuels 1995d, 9, 976-983.

Jarrah, N.A.; Van Ommen J.G.; Lefferts, L. *Cat. Today* 2003, *79-80*, 29-33.

Jarrah, N.A.; Van Ommen, J.G.; Lefferts, L. J. *Mater. Chem.* 2004, *14,* 1590-1597.

Jung, H.J.; Walker Jr., P.L.; Vannice, M.A.; J. *Catal.* 1982, *75,* 416.

Jüntgen, H. *Fuel* 1986, *65*, 1436-1446.

Kim, K.T.; Chung, J.S.; Lee, K.H.; Kim, Y.G.; Sung, J.Y. *Carbon* 1992, *30*, 467-475.

Kim, K.T.; Kim, Y.G.; Chung, J.S.; *Carbon* 1993, *31*, 1289-1296.

Kirm, I.; Medina, F.; Rodríguez, X.; Cesteros, Y.; Salagre, P.; Sueiras, J.E. *J. Mol. Catal. A: Chem.* 2005, *239*, 215-221.

Kirm, I.; Medina, F.; Sueiras, J.E.; Salagre, P.; Cesteros, Y. *J. Mol. Catal. A: Chem.* 2007, *261*, 98-103.

Klinik, J.; Rogóz, M.; Papp, *H. Chem. Soc. Faraday Trans*. 1998, 94, 2843-2850.
Knoblauch, K.; Richter, E.; Juntgen, H. *Fuel* 1981, *60*, 832-838.
Korovchenko, P.; Donze, C.; Gallezot, P.; Besson, M. Cat. Today 2007, 121, 13-21.
Kowalczyk, Z.; Jodzis, S.; Sentek, J. *Appl. Catal. A: General* 1996, *138*, 83-91.
Lafyatis, D.S.; Tung, J.; Foley, H.C. *Ind. Eng. Chem. Res.* 1990, *30*, 865-873.
Lagos, G., García, R., Agudo, A.L., Yates, M., Fierro, J.L.G., Gil-Llambías, F.J., Escalona, N. *Appl. Catal. A: General* 2009, 358, 26-31.
Laine, J.; Labady, M.; Severino, F.; Yunes, S. *J. Catal.* 1997, *166,* 384-387.
Lázaro, M.J.; Boyano, A.; Gálvez, M.E.; Izquierdo, M.T.; García-Bordejé, E.; Ruiz, C.; Juan, R.; Moliner, R. *Cat. Today* 2008, *137*, 215-221.
Lázaro, M.J.; Boyano, A.; Gálvez, M.E.; Izquierdo, M.T.; Moliner, *R. Cat. Today* 2006b, 119, 175-180.
Lázaro, M.J.; Boyano, A.; Gálvez, M.E.; Izquierdo, M.T.; Moliner, R. *Cat. Today* 2007b, *119,* 175–180.
Lázaro, M.J.; Gálvez, M.E.; Artal, S.; Palacios, J.M.; Moliner, *R. J. Anal. Appl. Pyrolysis* 2007a, 78, 301-315.
Lázaro, M.J.; Gálvez, M.E.; Ruiz, C.; Juan, R.; Moliner, R. *Appl. Catal. B: Environ.* 2006a, *68*, 130-138.
Lázaro, M.J.; Gálvez, M.E.; Suelves, I.; Moliner, R.; Vassilev, S.V.; Braekman-Danheux, C. *Fuel* 2004, *83,* 875-884.
Ledoux, M.J.; Djellouli, B. *J. Catal*. 1989, *115*, 580-590,
Liang, C.; Wei, Z.; Xin, Q.; Li, C. *Appl. Catal. A: General* 2001, *208*, 193-201.
Linares-Solano, A. In Investigación *Técnica del Carbón. Informe nº. 7220-EC/758*. European Comission, 1999.
Linares-Solano, A.; Martín-Guillón, I.; Martínez de Lecea, C. *Fuel* 2000, *79*, 635-643.
Linares-Solano, A.; Rodríguez-Reinoso, F.; Salinas-Martínez de Lecea, C.; Mahajan, O.P.; Walker Jr, P.L. *Carbon* 1982, *20*, 177-184.
llán-Gómez, M.; Linares-Solano, A.; Salinas-Martínez de Lecea, C.; Calo, J.M. *Energy and Fuels* 1993, *7*, 146-154.
Luck, F. *Catal. Today* 1996, 27, 195–202.
Luck, F. *Catal. Today* 1999, 53, 81–91.
Luhleich, H.; Dias, J.; Nickel, H. *Carbon* 1997, *35*, 95-102.
Ma, W.; Kugler, E.L.; Dadyburjor, D.B. *Energy and Fuels* 2007a, *21*, 1832-1842.
Ma, W.; Kugler, E.L.; Dadyburjor, D.B. *Energy and Fuels* 2010, *24*, 4099-4110.
Ma, W.; Kugler, E.L.; Dadyburjor, D.B. *Stud. Surf. Sci. Catal.* 2007b, *163*, 125-140.
Ma, W.; Kugler, E.L.; Wright, J.; Dadyburjor, D.B. *Energy and Fuels* 2006a, *20*, 2299-2307.
Ma, X.; Sun, Q.; Cao, F.; Ying, W.; Fang, D. *J. Natural Gas Chem.* 2006b, *15*, 335-339.
Maag, G., Gutierrez, F.J., Lipinski, W., Steinfeld, A. *ASME International Mechanical Engineering Congress and Exposition* 2009, Proceedings 8, 597-604.
Macías-Pérez, M.C.; Bueno-López, A.; Lillo-Ródenas, M.A.; Salinas-Martínez de Lecea, C.; Linares-Solano, A. *Fuel* 2007, *86*, 677–683.
Macías-Pérez, M.C.; Bueno-López, A.; Lillo-Ródenas, M.A.; Salinas-Martínez de Lecea, C.; Linares-Solano, A. *Fuel* 2008a, *87*, 2544–2550.
Macías-Pérez, M.C.; Bueno-López, A.; Lillo-Ródenas, M.A.; Salinas-Martínez de Lecea, C.; Linares-Solano, A. *Fuel* 2008b, *87*, 3170-3175.

Maia, F.; Silva, R.; Jarrais, B.; Silva, A.R.; Freire, C.; Pereira, M.F.R. *J. Coll. Interf. Sci.* 2008, *328,* 314-323.

Marbán, G.; Antuña, R.; Fuertes, A.B. *Appl. Catal. B: Environ.* 2003, *41,* 323-338.

Marbán, G.; Fuertes, A.B. *Appl. Catal. B: Environ.* 2001, *34,* 55-71.

Marbán, G.; Fuertes, A.B. *Appl. Catal. B: Environ.* 2001b, *34*, 43-53.

Martínez, N.D.; Venturini, R.B.; Soé Silva, H.; González, J.E.; Rodríguez, A.M. *Mat. Research* 2009, *12*, 45-50.

Martín-Guillón, A.; Prado-Burguete, C.; Rodríguez-Reinoso, F. *Carbon* 1993, *31*, 1099-1105.

Martín-Martinez, J.M.; Rodríguez-Reinoso, F.; Vannice, M.A. *Appl. Catal.* 1989, *51*, 93-112.

Matatov-Meytal, Y.; Sheintuch, M. *Appl. Catal. A: General*2002, *231*, 1-16.

Matos, J.; Laine, J. *Appl. Catal. A: General* 2003, *241*, 25-38.

Mikhalovsky, S.V.; Zaitsev, Yu.P. *Carbon* 1997, *35*, 1367-1374.

Molina-Sabio, M.; González, M.T.; Rodríguez-Reinoso, F.; Sepúlveda-Escribano, A. *Carbon* 1996, *34*, 505-509.

Moliner, R.; Ibarra, J.V.; Lázaro, M.J. *Fuel* 1994, *73*, 1214-1220.

Morales-Torres, S.; Pérez-Cadenas, A.F.; Kapteijn, F.; Carrasco-Marín, F.; Maldonado-Hódar, F.J.; Moulijn, J.A. *Appl. Cat. B: Environ* 2009, *89,* 411-419.

Morales-Torres, S.; Silva, A.M.T.; Pérez-Cadenas, A.F.; Faria, J.L.; Maldonado-Hódar, F.J.; Figueiredo, J.L.; Carrasco-Marín, F. *Appl. Catal. B: Environ*. 2010, 100, 310-317.

Moreno-Castilla, C.; Carrasco-Marín, F.; Maldonado-Hódar, F.J.; Rivera-Utrilla, J. *Carbon* 1998, *36*, 145-151.

Moreno-Castilla, C.; Carrasco-Martín, F.; J. *Chem. Soc. Faraday Trans.* 1995, *91*, 3519-3524.

Moreno-Castilla, C.; Mahajan, O.P.; Walker Jr., P.L.; Jung, H.-J. *Carbon* 1980, *18*, 271-276.

Moss, R.L., in Experimental Methods in Catalytic Research*,* Anderson, R.B., and Dawson, P.T. (eds), New York, Academic Press, 1976, *Vol. II*, p. 43.

Muradov, N. *Catal. Commun*. 2001b*, 2*, 89-94.

Muradov, N.; Smith, F.; Huang, C.; T-Raissi, A. *Cat. Today* 2006, *116*, 281-288.

Muradov, N.; Smith, F.; T-Raissi, A. *Cat. Today* 2005b, *102-103*, 225-233.

Muradov, N.Z. *Int. J. Hydrogen Energy* 2001a, *26*, 1165-1175.

Muradov, N.Z., Veziroğlu, T.N. *Int. J. Hydrogen Energy* 2005a, *30*, 225-237.

Muradov; N.Z. *Energy and Fuels* 1998, *12*, 41-48.

Muradov; N.Z. *Int. J. Hydrogen Energy* 1993, *18*, 211-215.

Naga Mahesh, K.; Sarada Prasad, J.; Venkateswer Rao, M.; Himabindu, V.; Yerramilli, A.; Raghunathan Rao, P. *Int. J. Hydrogen Energy* 2009, *34*, 6085-6088.

Okhlopkova, L.B.; *Appl. Catal. A: General* 2009, *355*, 115-122.

Olson, D.G.; Tsuji, K.; Shiraishi, J. *Fuel Process. Technol.* 2000, *65-66*, 393-405.

Ozaki, J.; Nishiyama, Y.; Guy, P.J.; Perry, G.J.; Allardice, D.J. *Fuel Process. Technol.* 1997, *50,* 57-68.

Park, E.D.; Lee, J.S. *J.Catal.* 2000, *196*, 5-15

Park, S.-E.; Sujandi, *Curr. Appl. Phys.* 2008, *8*, 664-668.

Pérez-Cadenas, A.F.; Kapteijn, F.; Moulijn, J.A.; Maldonado-Hódar, F.J.; Carrasco-Marín, F.; Moreno-Castilla, C. *Carbon* 2006b, *44,* 2463-2468.

Pérez-Cadenas, A.F.; Morales-Torres, S.; Maldonado-Hódar, F.J.; Carrasco-Marín, F. *Appl. Cat. A: General* 2009, *366*, 282-287.

Pérez-Cadenas, A.F.; Zieverink, M.M.P.; Kapteijn, F.; Moulijn, *J.A. Cat. Today* 2005 *105,* 623-628.

Pérez-Cadenas, A.F.; Zieverink, M.M.P.; Kapteijn, F.; Moulijn, J.A. *Carbon* 2006a, *44*, 173-176.

Pinilla, J.L.; Suelves, I.; Utrilla, R.; Gálvez, M.E.; Lázaro, M.J.; Moliner, R. *J. Power Sources* 2007, *169*, 103-109.

Porta, F.; Prati, L.; Rossi, M.; Scari, G. *J. Catal.* 2002, *211*, 464-469.

Pradhan, B.K.; Sandle, N.K. *Carbon* 1999, *37*, 1323.

Prado-Burguete, C.; Linares-Solano, A.; Rodríguez-Reinoso, F.; Salinas-Martínez de Lecea, C. *J. Catal.* 1991, *128*, 397-404.

Prado-Burguete, C.; Linares-Solano, A.; Rodríguez-Reinoso, F.; Salinas-Martínez de Lecea, C. *J. Catal.* 1989, *115,* 98-106.

Prati, L.; Villa, A.; Campione, C.; Spontoni, P. *Top. Catal.* 2007, *44*, 319-234.

Pritchard, J.; Kesavan, L.; Piccinini, M.; He, Q.; Tiruvalam, R.; Dimitratos, N.; Lopez-Sanchez, J.A.; Carley, A.F.; Edwards, J.K.; Kiely, C.J.; Hutchings, G.J. *Langmuir* 2010, *26*, 16568-16577.

Przepiórski, J.; Yoshida, S.; Oya, A. *Carbon* 1999, *37*, 1881-1890.

Puello-Polo, E., Brito, J.L. *Cat. Today* 2010b, *149*, 316-320.

Puello-Polo, E.; Gutiérrez-Alejandre, A.; González, G.; Brito, J.L. *Catal. Lett.* 2010a, *135*, 212-218.

Puello-Polo, E.;, Brito, J.L. *J. Molec. Catal. A: Chem.* 2008, *281*, 85-92.

Quintanilla, A.; Casas, J.A.; Rodriguez, J.J. *Appl. Catal. B: Environ*. 2010, *93*, 339-345.

Quintanilla, A.; Casas, J.A.; Rodríguez, J.J. *Appl. Catal. B:Environ.* 2007, *76,* 135-145.

Radkevich, V.Z.; Senko, T.L.; Wilson, Grishenko, L.M.; Zaderko, A.N.; Diyuk, V.Y. *Appl. Catal. A: General* 2008, *335*, 241-251.

Radovic, L.R.; Sudhakar, C., Carbon as catalyst support, in *Introduction to Carbon Technologies*, Ed. H. Marsh, E.A. Heintz, F. Rodríguez-Reinoso, University of Alicante, Secretariado de Publicaciones, Alicante, Spain, 1997.

Rankel, L.A. *Energy and Fuels* 1993, *7*, 937-942.

Raróg-Pilecka, W.; Jedynak-Koczuk, A.; Petryk, J.; Miśkiewicz, E.; Jodzis, S.; Kaszkur, Z.; Kowalczyk, Z. *Appl. Catal. A: General* 2006, *300*, 181-185.

Richards, J. *Fuel Proc. Technol.* 1990, *25*, 321-326.

Richter, E. *Cat. Today* 1990, *7*, 93-112.

Rodríguez-Reinoso F., *Characterization and Applications, in Porosity in Carbons*, Ed. J.W. Patrick, Edward Arnold, London, 1995b.

Rodríguez-Reinoso F.; *Carbon as Catalyst Support, in Porosity in Carbons*, Ed. J.W. Patrick, Edward Arnold, London, 1995a.

Rodríguez-Reinoso, F. Molina-Sabio, M. *Carbon* 1992, *30*, 1111-1118.

Rodriguez-Reinoso, F., *Carbon* 1998, *36*, 159-175.

Rodriguez-Reinoso, F., in *Introduction to Carbon Technologies*, Ed. Marsh, H., Heintz, E.A., Rodríguez-Reinoso, F., University of Alicante, Secretariado de Publicaciones, Alicante, Spain, 1997.

Rodríguez-Reinoso, F.; Salinas-Martínez de Lecea, C.; Sepúlveda-Escribano, A.; López-González, J.D. *Cat. Today* 1990, *7*, 287.

Rodriguez-Reinoso, F.; Sepúlveda-Escribano, A.; Carbon as Catalyst Support, in Carbon Materials for Catalysis, Ed. Serp, P. and Figueiredo, J.L., John Wiley and Sons, New Jersey, 2009.
Rubio, B.; Izquierdo, M.T. *Carbon* 1997, *35*, 1005-1011.
Rubio, B.; Izquierdo, M.T. *Carbon* 1998a, *36*, 263-268.
Rubio, B.; Izquierdo, M.T. *Fuel* 1998b, *77*, 631-637.
Rubio, B.; Izquierdo, M.T. *Waste Manage.* 2010, *30*, 1341-1347.
Rubio, B.; Izquierdo, M.T.; Segura, E.; *Carbon* 1999, *37*, 1833-1841.
Sasaoka, E. *Energy and Fuels* 1994, *8*, 1100–1105.
Satterfield, C.N., *Heterogeneous Catalysis in Practise*, New York, McGraw-Hill, 1980.
Shchipko, M.L.; Kuznestov, B.N. *Fuel* 1998, *77*, 527-532.
Singoredjo, L.; Slagt, M.; Van Wees, J.; Kapteijn, F.; Moulijn, J.A, *Cat. Today* 1990, *7*, 157-165.
Solar, J.M.; Derbyshire, F.J.; de Beer, V.H.J.; Radovic, L.R. J. *Catal.* 1991, *129*, 330-342.
Sousa, J.P.S.; Silva, A.M.T.; Pereira, M.F.R.; Figueiredo, J.L. *Sep. Sci. Technol*. 2010, *45*, 1546-1554.
Such-Basáñez, I.; Román-Martínez, M.C.; De Lecea, C.S.-M. *Carbon* 2004, *42*, 1351-1355.
Suelves, I.; Lázaro, M.J.; Moliner, R.; Pinilla, J.L.; Cubero, H. *Int. J. Hydrogen Energy* 2007, *15*, 3320-3326.
Suh, D.J.; Park, T-J. *Carbon* 1993, *31*, 427-435.
Suzuki, T.; Kyotani, T.; Tomita, A. *Ind. Eng. Chem. Res.* 1994, *33*, 2840-2845.
Takehira, K.; Ohi, T.; Shishido, T.; Kawabata, T.; Takaki, K. *Appl. Catal. A: General* 2005, *283*, 137-145.
Teng, S.; Tu, Y.T.; Lai, Y.C.; Li, C.C. *Carbon* 2001, *39*, 575-582.
Tomašić, V. *Cat. Today* 2007, *119*, 106-113.
Torres, G.C.; Jablonski, E.L.; Baronetti, G.T.; Castro, A.A.; de Miguel, S.R.; Scelza, O.A.; Blanco, M.D.; Peña Jiménez, M.A.; Fierro, J.L.G. *Appl. Catal. A: General* 1997, *161*, 213-226.
Trommer, D; Hirsch, D.; Steinfeld, A. *Int. J. Hydrogen Energy* 2004, *29*, 627-633.
Tseng, H.-H.; Wey, M.-Y. *Chemosphere* 2006, *62*, 756-766.
Tseng, H.-H.; Wey, M.-Y.; Liang, Y.-S.; Chen, K.-H. *Carbon* 2003, *41*, 1079-1085.
Ulla, M.A.; Valera, A.; Ubieto, T.; Latorre, N.; Romeo, E.; Milt, V.G.; Monzón, A. *Cat. Today* 2008, *133-153*, 7-12.
Valdés-Solís, T.; Marbán, G.; Fuertes, A.B. *Appl. Catal. B: Environ.* 2003, *46,* 261-271.
Valdés-Solís, T.; Marbán, G.; Fuertes, A.B. *Cat. Today* 2001b, *69*, 259-264.
Valdés-Solís, T.; Marbán, G.; Fuertes, A.B. *Microp. Mesop. Mat.* 2001a, *43*, 113-126.
Van Dam, H.E.; Van Bekkum, H., J. *Catal.* 1991, *131*, 335-349.
Vannice, M.A.; Walker Jr., P.L.; Jung, H.-J.; Moreno-Castillat, C.; Mahajan, O.P. *Stud. Surf. Sci. Catal.* 1981, *7*, 460-474.
Veith, G.M.; Lupini, A.R.; Pennycook, S.J.; Villa, A.; Prati, L.; Dudney, N.J. *Catal. Today* 2007, *122*, 248-253.
Vergunst, T.; Linders, M.J.G.; Kapteijn, F.; Moulijn, J.A. *Catal Rev Sci Eng* 2001, *43*, 291–314.
Vergunst, Th.; Kapteijn, F.; Moulijn, J.A. *Carbon* 2002, *40*, 1891-1902.
Vidic, R.D.; Tessmer, L.J.; Uranowski, L.J. *Carbon* 1997, *35*, 1349-1359.

Villar-Rodil, S.; Suárez-García, F.; Paredes, J.I.; Martínez-Alonso, A.; Tascón, J.M.D. *Chem. Mater.* 2005, *17*, 5893-5908.

Vinke, P.; Van der Eijik, M.; Verbree, M.; Voskamp, A.F.; Van Bekkum, H.; *Carbon* 1994, *32*, 675.

Vissers, J.P.R.; Lensing T.J.; de Beer, V.H.J.; Prins, R. *Appl. Catal.* 1984, *11,* 21.

Vissers, J.P.R.; Scheffer, B.; de Beer, V.H.J.; Moulijn, J.A.; Prins, R. *J. Catal.* 1987, *105*, 277-284.

Vít, Z. *Fuel* 1993, *72*, 105-107.

Walker Jr, P.L.; Taylor, R.L.; Ranish, J.M. *Carbon* 1991, *29*, 411-421.

Walker, P.L. *Jr. Carbon* 1996, *34*, 1297-1299.

Wang, D.; Villa, A.; Spontoni, P.; Su, D.S.; Prati, L. *Chemistry - A European Journal* 2010, *16*, 10007-10013.

Wang, L.; Cao, B.; Wang, S.; Yuan, Q. *Chem. Eng. J*. 2006, *118*, 133-139.

Wang, R. *Sep. Purif. Technol.* 2003, *31*, 111–121.

Wang, Y.; Zhao, X.; Yuan, B.; Zhang, B.; Cong, J. *Appl. Cat. A: General* 1998, *171*, 255-260.

Watanabe, S.; Arunajatesan, V. *Top. Catal.* 2010, *53*, 1150-1152.

Wey, M.Y.; Fu, C.H.; Tseng, H.H.; Chen, K.H. *Fuel* 2003, *82*, 2285-2290.

Wigmans, T. *Carbon* 1989, *27,* 13-22.

Wu, X.; Schwartz, V.; Overbury, S.H.; Armstrong, T.R. *Energy and Fuels* 2005, *19*, 1774-1782.

Xue, Y.; Lu, G.; Guo, Y.; Guo, Y.; Wang, Y.; Zhang, Z. *Appl. Cat. B: Environ.* 2008, *79*, 262-269.

Yoo, K.S.; Kim, S.D.; Park, S.B. *Ind. Eng. Chem. Res.* 1994, *33*, 1786-1791.

Zhang, Z.; Ma, X.; Zhang, P.; Li, Y.; Wang, S. *J. Molec. Catal. A: Chem*. 2007a, *266*, 202-206.

Zheng, X.; Zhang, S.; Xu, J.; Wei, K. *Carbon* 2002, *40*, 2597-2603.

Zhu, H.; Han, W.; Liu, H. *Catal. Lett.* 2007, *115*, 13-18.

Zhu, J.; Carabineiro, S.A.C.; Shan, D.; Faria, J.L.; Zhu, Y.; Figueiredo, J.L. *J. Catal.* 2010, *247*, 207-214.

Zhu, J.; Figueiredo, J.L.; Faria, J.L. *Catal. Commun.* 2008, *9*, 2395-2397.

Zhu, Z.; Liu, Z.; Liu, S.; Niu, H. *Fuel* 2000b, 79, 651-658.

Zhu, Z.; Liu, Z.; Liu, S.; Niu, H.; Hu, T.; Liu, T.; Xie, Y. *Appl. Catal. B: Environ.* 2000a, *26*, 25-35.

Zhu, Z.H.; Radovic, L.R.; Lu, G.Q. *Carbon* 2000c, *38*, 451-464.

In: Activated Carbon
Editor: James F. Kwiatkowski
ISBN: 978-1-61209-684-1
©2012 Nova Science Publishers, Inc.

Chapter 5

CONVENTIONAL AND NON-CONVENTIONAL THERMAL PROCESSING FOR THE PRODUCTION OF ACTIVATED CARBONS FROM AGRO-INDUSTRIAL WASTES

Leandro S. Oliveira* ***and Adriana S. Franca***
Departamento de Engenharia Mecânica/UFMG
Av. Antônio Carlos, 6627 – 31270-901 – Belo Horizonte, MG – Brasil

ABSTRACT

Adsorption is currently the most prospective technology being used for the removal of organic and inorganic pollutants from waters and wastewaters. Although there are many adsorbents in use, activated carbon is the most widely used adsorbent for the removal of a variety of contaminants from waters. However, there is a major disadvantage associated with it, which is the strict necessity to regenerate the activated carbon, due to its inherent high cost, to allow for further use, thus, imparting additional costs to the adsorption process. Another negative aspect is the loss of adsorption capacity during the regeneration process which restricts its application even further. Although synthetic resins present a longer working life than activated carbons as adsorbents, their use is still costly for they also require regeneration after use. These aspects have greatly stimulated research interests into the production of alternative low-cost adsorbents to replace the costly activated carbons and synthetic resins. Attention has been focused on preparation and use of low-cost adsorbents, which present adequate adsorption capacities and are able to remove unwanted pollutants from contaminated waters without the need for regeneration and, thus, doing so at a low-cost. Industrial wastes and agricultural byproducts are classes of materials that are being considered the most promising precursors for the production of low-cost adsorbents for they are renewable, locally available in large quantities, inexpensive and require little processing to turn them into activated carbons and increase their adsorption capacities toward a specific adsorbate (pollutant). The majority of potential precursor materials being studied is of biological origin and, thus, fit into the categories of carbonaceous or lignocellulosic materials. As

* E-mail:leandro@demec.ufmg.br.Tel:+55-31-34093517.Fax:+55-31-34433783.

such, these materials contain a variety of chemical functional groups at their surfaces (e.g., carboxylic, phenolic, amino and others) and upon thermal and chemical treatment these groups can be manipulated, transforming the material into a more functionally selective activated carbon. These surface modifications will contribute to a variety of adsorption mechanisms, such as chemisorption, complexation, ion exchange and others, depending on the possible spectrum of interactions between adsorbent and adsorbate. Thus, the objective of this essay is to present a critical overview on conventional and non-conventional thermal and chemical treatments that are being employed in the preparation of activated carbons using residues of biological origin as precursors, discussing their effects on both physical and chemical characteristics of the produced adsorbents and on the performance of the prepared activated carbon for the removal of wastewater pollutants.

1. INTRODUCTION

To have a better understanding of the scope of this chapter, it is firstly necessary to present a clear definition of activated carbon (AC). Activated carbon is a highly porous form of carbon, comprised of stacked and extensively cross-linked microcrystalline graphite interspersed with non-graphitic aromatic carbon structures containing heteroatoms all crumpled into a randomly-oriented three-dimensional structure, obtained by the carbonization of carbonaceous materials followed by an activation process, and which is employed strictly for adsorption purposes. A schematic representation of the three-dimensional structure of activated carbons is presented in Figure 1. For a more comprehensive model of porous carbons in which the chemical structure is fully elucidated, including the presence of oxygen heteroatoms, free radicals and dangling bonds, the reader is encouraged to assess the work presented by Bourke et al. (2007).

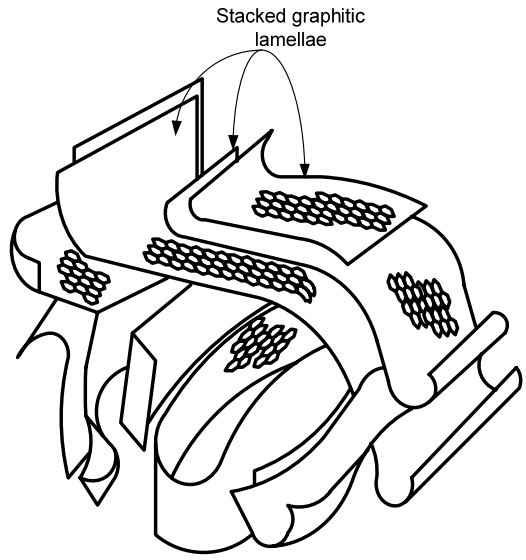


Figure 1. Schematic representation of the internal structure of activated carbons (adapted from Rodríguez-Reinoso and Molina-Sabio, 1998).

The desired porosity in activated carbons is imparted by the activation process to which the precursor carbonaceous material is subjected and the generated network of pores provide internal surface areas that usually range from 200 to over 2000 $m^2 g^{-1}$. The activation process is also responsible for the chemical structure of the internal surface in activated carbons. By varying the activation conditions, not only the final porosity is varied but also the chemical composition of the carbon.

The microscopic structure, characterized by the pore size distribution and its inherent surface area, and the chemical composition of the internal surface area are the main aspects of an activated carbon that contribute to its adsorption performance. Thus, the activation process, which controls these characteristics, is the key issue in defining the adsorption performance of an activated carbon for a specific application. The control of the pore sizes and their respective distribution within the carbon matrix, together with its internal surface chemical composition, leads to a production of a broad range of adsorbents allowing for a wide diversity of adsorbate selectivities (Crittenden and Thomas, 1998). Not only the chemical composition of the internal surface plays a role in the adsorption selectivity of a carbon but also the size and shape of its narrow pores through molecular sieve effects (Rodríguez-Reinoso and Molina-Sabio, 1998).

Depending on the activation process and the specific target application, activated carbons may be produced with a narrow or a wide range of pore sizes (defined by the pore width) which are usually classified into three groups (Rodríguez-Reinoso and Molina-Sabio, 1998): micropores, with width smaller than 2 nm; mesopores, with width greater than 2 and smaller than 50 nm; and macropores, with width greater than 50 nm. Micropores are relevant to the adsorption of small molecules such as gases and solvents, and mesopores are relevant to the adsorption of larger molecules (molecular sizes greater than 2 nm) such as peptides, proteins and a few dyes. Micropores are the ones that contribute the most to the internal surface area, being mostly comprised of slit-shaped spaces between graphitic lamellae and holes (structural defects) in the graphitic structure; whereas meso and macropores, aside from providing an adsorption surface, act as transport pathways for the adsorbates to the interior of the carbon matrix and ultimately to its microporosity. Thus, since the adsorption capacity of an activated carbon depends on the accessibility of the adsorbate molecules to its micro and mesopores, it becomes imperative for an activated carbon to present a well-structured network of interconnected micro, meso and macropores. This desired distribution of pore sizes can be achieved by establishing an adequate set of carbonization/activation conditions for a specific carbonaceous precursor material. At this point, it is noteworthy to point out that division into pore size ranges is just a convention and that the pore structure of any lignocellulosic material is actually comprised of a continuous distribution of pore sizes.

Although microporosity, for the most part, is the characteristic of porous carbons that contributes the most to providing a large adsorptive capacity, the chemical composition of the surface, on the other hand, has been recognized to greatly affect the adsorption performance. Activated carbons usually contain significant amounts of heteroatoms, such as oxygen, hydrogen and nitrogen, chemically bonded to the non-graphitic portion of the structure, mostly at the edge of the basal planes, where unsaturated carbon atoms are present. These bonded heteroatoms constitute functional groups at the surface that, depending on their chemical nature, impart either an acid or a basic character to the carbon, and, consequently, affect hydrophylicity and hydrophobicity of the activated carbon.

Examples of oxygen and nitrogen functional groups on carbon surfaces are presented in Figure 2. At the basal planes of the microstructure, the graphitic portion is strictly non-polar and hydrophobic, favoring interactions of the dispersive-type (e.g., π-π interactions) between the adsorbent and the adsorbate. This is a relevant aspect of activated carbons, for a significant fraction of their total surface is comprised of microcrystalline non-polar graphite surfaces (e.g., up to 71% for heat treatments in the range of 950 to 1050°C; Bourke et al., 2007). Nitrogen surface groups will be naturally present when a nitrogen-containing precursor is used to produce the activated carbon or when the precursor or the activated carbon itself has been reacted with a nitrogenous reagent (Figueiredo and Pereira, 2010).

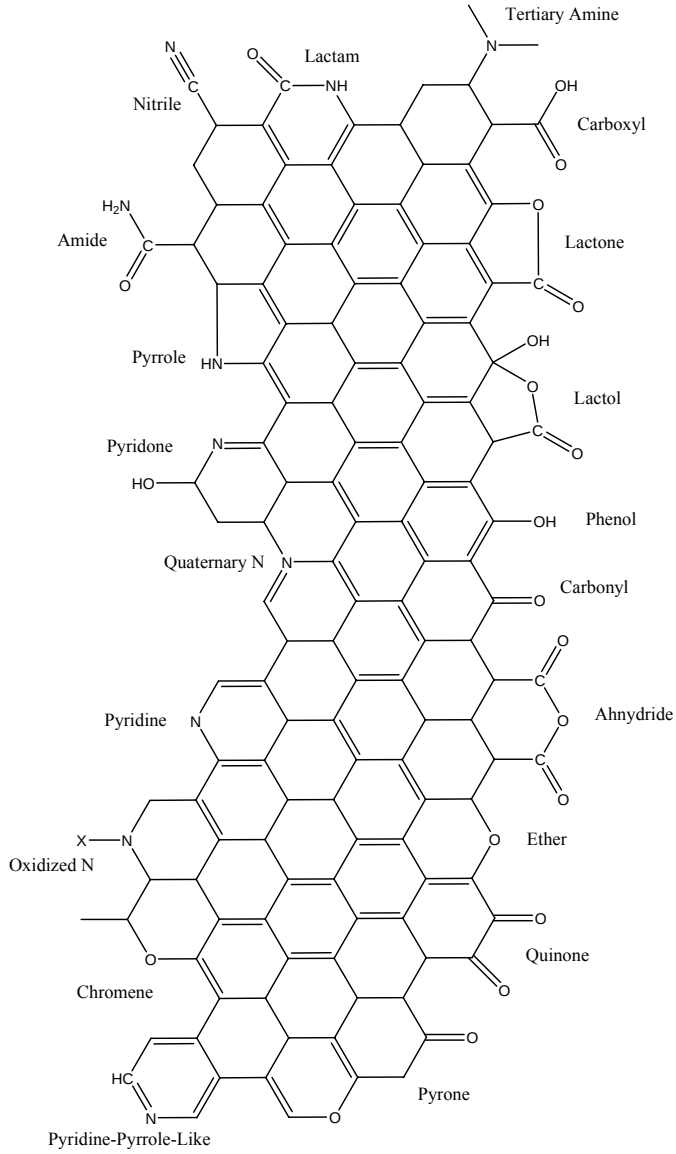


Figure 2. Examples of oxygenated and nitrogenous groups at the surface of carbons (adapted from Daud and Houshamnd, 2010).

Oxygen surface groups play a major role in defining the AC properties such as hydrophylicity/hydrophobicity, surface charge, electron density of the graphitic layers and catalytic activity (Daud and Houshamnd, 2010). The nature and the extent to which oxygenated groups are present at the surface of activated carbons are determined by the chemical composition of the precursor material, including the ash content, and by the temperature and degree of carbonization to which the precursor is subjected to (Bourke et al., 2007). The most common carbon-oxygen functional groups encountered in ACs are carboxyl, carboxyl anhydride, lactone, phenolic hydroxyl, ether, carbonyl, quinine and pyrone-like. Each individual surface oxide presents a distinct thermal stability upon heating and decomposes into either CO_2 or CO, depending on its thermal decomposition temperature. Evolution of CO_2, observed at temperatures below 600°C, is associated with decomposition of acidic oxygenated groups such as carboxylic (decomposition at 100 to 400°C) and carboxylic anhydrides and lactones (decomposition at 400 to 600°C). On the other hand, evolution of CO, observed at temperatures above 600°C, is associated with the thermal decomposition of basic oxygenated groups such as phenolic hydroxyls, carbonyls, quinones, ethers, and pyrone-like structures, with the latter being the most thermally stable carbon-oxygen structure with decomposition temperatures in the range of 900 to 1200°C (Susuki, 1990; Bourke et al., 2007).

Aside from the original content of oxygenated groups in the precursor materials, oxygenated groups can be formed spontaneously at the surface by exposure of the carbon material to gaseous oxygen (e.g., atmospheric air) during the carbonization/activation process or afterwards. Chemisorption of molecular oxygen by the carbon material occurs due to the high concentration of unpaired electrons at the edge of the basal planes of the carbon structure and it increases as the temperature is increased (Rodríguez-Reinoso and Molina-Sabio, 1998). At high temperatures, the oxygen molecules dissociate into atoms that react with the carbon atoms at the surface to form the oxygenated functional groups. The amount of oxygenated groups at the surface of the finished product can be further increased or their respective chemical nature modified by treatments with oxidizing agents such as HNO_3 and H_2O_2. Upon increasing the amount of functional groups at the surface of the carbon, the internal surface area is usually decreased but the carbon adsorption capacity is not necessarily diminished. The easiness with which the surface of a carbon can be altered to increase the amount and to modify the nature of the carbon-oxygen groups is one of its most advantageous characteristics when compared to other adsorbents. Activated carbons, as versatile adsorbents, are widely used for the removal of undesirable (e.g., odor, color and taste) and hazardous (e.g., phenol, heavy metal ions) organic and inorganic compounds from domestic and industrial wastewater, for air purification (e.g., removal of volatile organic compounds, toxic gases), for food decolorization and pharmaceutical purification, and others. Commercial activated carbons have been produced and used mostly in granular (GAC) and powder (PAC) forms, with GACs taking up a large percentage of the carbon market. GACs are considered more versatile than the powdered carbons due to factors such as better regenerability and lower pressure drops in fixed-bed adsorption columns applications (Ahmedna et al., 2000). Recently, they were made available in spherical, fibrous and textile forms which are tailored for specific applications (Bansal and Goyal, 2005). The most common carbonaceous materials that are currently used to produce commercial activated carbon are coal, wood, sawdust, lignite, coal, peat and coconut shells (Marsh and Rodríguez-Reinoso, 2006). Coal-based activated carbons present higher ash content than carbons produced from lignocellulosic materials. However, as

good adsorbents as they have proven to be, activated carbons still present several disadvantages, such as non-selectivity for non-tailored carbons (which is the general case for commercial activated carbon), inefficacy for certain types of sorbates (e.g., dispersive and vat dyes), and the need for expensive non-straightforward regeneration of the saturated carbon which, in general, incur in loss of adsorption capacity (Crini, 2006). However, the major drawback is still their cost (Savova et al., 2001). These disadvantages have spurred a growing interest in cheaper materials and processes that, in turn, has led to extensive research in the use of agricultural and food residues and other wastes (e.g., recycled tires, municipal wastes) as precursor materials for activated carbon production (Dias et al., 2007; Oliveira and Franca, 2008; Sud et al., 2008; Gupta and Suhas 2009; Bhatnagar and Sillanpää, 2010). Agricultural residues, being mostly lignocellulosic materials, present the major advantage of having unique chemical compositions, such as low contents of inorganic materials and relatively high contents of volatile matter, that allow for the controlled manufacturing of activated carbons with well-structured networks of pores and adequate structural strength. Also, these residues present the advantage of being largely available from renewable sources and of presenting low or no cost at all. Lignocellulosic materials, such as sawdust and coconut shells, already constitute the most commonly used precursors in the commercial manufacture of activated carbon, accounting for almost 50% of the total of raw materials used for that purpose (Marsh and Rodríguez-Reinoso, 2006). Thus, the use of more economic and eco-friendly precursor materials such as agricultural residues constitutes a promising alternative not only to promote reductions in the costs of the finished product but also to allow it to be more widely and economically used in the mitigation of current and future environmental problems. The current commercial processes for production of activated carbons are usually carried out in two stages: (i) carbonization of the precursor material at temperatures below 800°C in an inert atmosphere; and (ii) subsequent activation of the carbonized material at temperatures ranging between 800 and 1000°C in an atmosphere of air, CO_2 or steam (Bansal and Goyal, 2005). Sometimes, flue gases, containing large volumes of CO_2, are used as activating agents in industry (Crittenden and Thomas, 1998). Chemical activation with phosphoric acid is also becoming more frequently used (Marsh and Rodríguez-Reinoso, 2006). A diversity of equipments is currently available for the commercial production of activated carbons, with rotary kilns and drums being the most commonly used, followed by multiple-hearth furnaces, and to a lesser extent fluidized beds (Marsh and Rodríguez-Reinoso, 2006). Having presented an overview of activated carbons, their properties and applications, in the next sections we will focus on the description and discussion of conventional and non-conventional thermal processes currently employed and studied for the preparation of activated carbons produced from lignocellulosic residues.

2. CONVENTIONAL THERMAL PROCESSES

The basic process of turning a precursor carbonaceous material into an activated carbon can be carried out in one or more steps, involving the carbonization of the precursor material, followed by the activation of the produced charcoal. The charcoal is, thus, the solid residue of the carbonization of biomass by heat in the absence of air at temperatures above 300°C (Bourke et al., 2007), and can sometimes be used directly as an adsorbent if, in its current

state, it already presents a well-developed accessible microporosity and an adequate chemical makeup at the surface, thus requiring no further processing (activation). The activation is, thus, the process with which the desired physical (texture) and chemical (functionality) properties are attained and it can be either strictly physical or physical/chemical, and occur at low (400 to 600°C) or high (700 to 1000°C) temperatures.

2.1. Physical Activation

Physical activation of a carbonaceous material constitutes a process in which the desired physical characteristics of the activated carbon are developed by a heat treatment of the precursor in a stream of gases, usually carried out in a two-step process. First, the carbonaceous material is carbonized at temperatures ranging from 400 to 800°C in an inert atmosphere (usually nitrogen) to produce the charcoal. In the carbonization process, the least stable bonds within the carbonaceous material structure (e.g., methylene and oxygen bridges between the aromatic layers) are broken and radical components are formed which, upon stabilization by hydrogen additions, lead to the production of volatile compounds. The solid charcoal final structure is, thus, a result of the polymerization and condensation reactions occurring between volatile and non-volatile radical components (Demirbaş, 2001). The volatile compounds are driven-off the transforming carbon and the non-carbon elements (heteroatoms) are mostly removed. The volatile matter content of a lignocellulosic precursor is recognized as one of the key factors in defining the chemical structure of carbonized material (Mészáros et al., 2007). The inorganic compounds (ash content) of the precursor material are sometimes postulated to behave as catalysts for some of the pyrolytic reactions that occur during carbonization. Charcoals produced by carbonization of lignocellulosic materials as previously described are only slightly microporous and, to attain a final product with a well-developed micropore structure, a second heat treatment, with the aid of 'gasifying agents' at temperatures ranging from 600 to 1000°C, is necessary. This second step in the activated carbon preparation process is denominated 'activation' and the most common gasifying agents used to promote the necessary changes in the charcoal structure are carbon dioxide (CO_2), steam or a mixture of them. These agents act as extractants of carbon atoms (Marsh and Rodríguez-Reinoso, 2006) but the general mechanism with which each agent extracts the carbon atoms is different. Molecular oxygen, present in atmospheric air, under high temperatures reacts with carbon atoms in the carbonaceous material surface according to the simplified equations

$$2C_f + O_2 \rightarrow 2CO \quad (1)$$

$$C_f + O_2 \rightarrow CO_2 \quad (2)$$

where C_f describes a carbon atom free from bonding with heteroatoms. These reactions are highly exothermic, making it difficult to control, and, because they occur predominantly at the outside surface, little or no enhancements in microporosity are observed. Thus, oxygen (air) is not commonly used as an activating agent. Carbon dioxide is the preferred gas for physical activation since it can be easily handled and it is largely available in different

degrees of purity. On the other hand, activation with steam presents the advantage of being less expensive than activation with carbon dioxide. Also, because the reactions with both carbon dioxide and steam are endothermic and consequently slow, the activation process with these agents can be more easily controlled (Marsh and Rodríguez-Reinoso, 2006; Ioannidou and Zabaniotou, 2007). The reactions of carbon materials with both CO_2 and steam can be described by

$$C + CO_2 \rightarrow 2CO\ \Delta H = +159\ kJ\ mol^{-1} \quad (3)$$

$$C + H_2O \rightarrow CO + H_2\ \Delta H = +117\ kJ\ mol^{-1} \quad (4)$$

$$C + 2H_2O \rightarrow CO_2 + 2H_2\ \Delta H = +75\ kJ\ mol^{-1} \quad (5)$$

In general, the activation with CO_2 leads to the creation and widening of small micropores, whereas activation with steam only promotes widening of the existing micropores in the char structure (Rodríguez-Reinoso and Molina-Sabio, 1998), thus producing activated carbons with meso- to macropore structures. Regardless of the activating agent being used, there will always be molecular oxygen present in the gases and some burning of the carbon will necessarily occur in accordance with equations (1) and (2).

When talking about activation, the effects of the original chemical structure of the lignocellulosic precursor on the microporous properties of the activated carbon cannot be neglected. Hemicellulose (H), cellulose (C) and lignin (L) are the main constitutive fractions of this type of precursor material in terms of weight and, thus, their thermal decomposition play a major role in the definition of the activated carbon properties upon carbonization and activation. Based on this aspect, Cagnon et al. (2009) studied the effects of H, C and L contents of lignocellulosic precursors on the final burn-off and microporosity properties of their respective activated carbons, produced by physical activation with steam at 800°C. The lignocellulosic precursor materials used were coconut shell, apple pulp, plum pulp and stones, olive stones and a soft wood, and the same experimental conditions were applied for all of them. A synthetic mixture of the three laboratory-grade basic components (H, C and L), in the same proportions as they occur in a natural coconut shell, was also subjected to the same carbonization/activation procedure to better understand the role each of the major components play in developing the final properties of the activated carbon. The major conclusion was that lignin is the most relevant chemical constituent in terms of generating activated carbons with higher carbon yields (less weight loss) and well-structured microporosity. However, the contribution of the other precursor constituents to the final properties of both the chars and their respective activated carbons cannot be neglected. At this point, it is noteworthy to recall that both the chemical constituency of the lignocellulosic precursor material and the process conditions used for the production of its respective activated carbon play a relevant role in the development of the desired properties of the final product. It would be rather interesting to be able to predict the end result of a physical activation process as applied to a specific lignocellulosic precursor, for it would help in the selection of an appropriate set of activation conditions to achieve the desired properties for the final product. However, this cannot be done at present, because a comparison of the results of the various studies devoted to the physical activation of a given precursor is currently precluded by considerable variations in the experimental conditions employed from one work to another. These experimental

conditions such as precursor amount, heating rate, nature and flow rate of the inert gas during the carbonization step, and final temperature of carbonization/activation vary considerably amongst the works presented in the literature. Regardless of this difficulty, an overview of the end result of different pairs of lignocellulosic precursor/activation conditions is worthy to be presented here, for it can allow the narrowing down of the range of activation conditions to be used when studying a specific precursor. Hence, a series of selected pairs of lignocellulosic precursor/activation conditions and their respective outcomes in terms of activated carbon properties are presented in Table 1. It is noteworthy to point out that the literature containing the preparation of activated carbons from lignocellulosic precursors is quite extensive and it would be impossible to cover the most part of it here, thus, we have focused on a few distinctive applications and on more recent literature. More in-depth information on the intrinsic chemical and physical changes occurring during carbonization and physical activation processes can be found in the compelling works of Rodríguez-Reinoso and Molina-Sabio (1998), Marsh and Rodríguez-Reinoso (2006), Mészáros et al. (2007) and Bourke et al. (2007).

Table 1. Lignocellulosic precursor/activation conditions and respective AC properties

Lignocellulosic precursor	Carbonization conditions Gas/ temperature/time	Activation conditions Gas/temperature/time	Porosity Surface area/micropore volume (m^2g^{-1})/(cm^3g^{-1})	Reference
Almond shells	N_2/700 or 800°C/1 h N_2/700 or 800°C/1 h	Steam/800°C/2-4 h CO_2+N_2/800°C/2-4 h	396-673/n.i. 197-560/n.i.	Toles et al. (2000)
Macadamia nut shells	N_2/700°C/2 h	CO_2/800°C/4-20 h	750-1440/0.26-0.51	Wang et al. (2002)
Avocado kernel seeds	N_2/800 or 1000°C/1 h	-	227-452/0.073-0.147	Elizalde-González et al. (2007)
Coconut shells	N_2/400-1000°C/2 h	Steam/750-950°C/0.5-2 h	130-702/0.03-0.35	Li et al. (2008)
Coconut shells	N_2/200-1000°C /2 h	CO_2/750-950°C/2-6 h	613-1700/0.307-0.882	Guo et al. (2009)
Cherry stones	N_2/600°C/2 h N_2/900°C/2 h N_2/900°C/2 h -	air/300°C/3 h CO_2/850°C/2-3 h Steam/850°C/3 h Steam/850°C/3 h	508/0.231 604-731/0.299-0.347 901/0.383 771/0.336	Jaramillo et al. (2009)

Table 1. (Continued)

Lignocellulosic precursor	Carbonization conditions Gas/ temperature/time	Activation conditions Gas/temperature/time	Porosity Surface area/micropore volume (m^2g^{-1})/(cm^3g^{-1})	Reference
Bean pods	-/600°C/10 min	Steam/700°C/1 h	258/0.08	Budinova et al. (2009)
Corncob	N_2/300-800°C/1 h	CO_2/300-800°C/1 h	720-774/0.3351-0.3595	Aworn et al. (2009)
Walnut shells	N_2/600°C/2 h N_2/600°C/2 h	CO_2/850°C/2-3 h Steam/700-900°C/1-2 h	542-1304/0.05-0.21 542-1361/0.04-0.2	González et al. (2009)
Almond shells	N_2/400°C/1 h	CO_2/700 or 800°C/1-7 h	1138/0.49	Nabais et al. (2010)
Olive bagasse	N_2/500°C/n.i.	Steam/750-900°C/0.5-1 h	523-1106/0.1989-0.4012	Demiral et al. (2010)

2.2. Chemical Activation

The chemical activation of charcoals is carried out by means of the impregnation of the carbon structure with an activating agent followed by heat treatment. Chemical activation is considered rather advantageous in regard to physical activation since both the carbonization and activation steps are carried out simultaneously, and it usually occurs at lower temperatures than in physical activation, leads to higher carbon yields, allows better control of the development of microporosity, and promotes a relevant reduction in the mineral content of the activated carbon (Lillo-Ródenas et al., 2003; Ioannidou and Zabaniotou, 2007). Chemical activation not only promotes chemical changes to the charcoal matrix but also physical changes by favoring the creation of pores (by volatilization of organic matter) and, depending on the chemical agent, further enlargement of existing pores, thus increasing the internal surface area and the pore volumes, which are highly desirable properties. In altering the chemical makeup of the charcoal surface, the chemical agent invariably alters the final chemical functionality of the activated carbon surface and, hence, its affinity to specific sorbates. The final pore structure of the activated carbon is not only influenced by the nature of the activating agent used but also by the nature and flow rate of the gas used (carbonizing atmosphere) and by the impregnation degree, usually defined as the ratio between the mass of the chemical agent and the mass of the precursor material.

The general action of an activating chemical agent during the impregnation step can be described as promotion of hydrolysis and simultaneous swelling of the carbon structure, while occupying a volume which inhibits the shrinking of the structure during heat treatment (Mohamed et al., 2010). The most common agents used in chemical activation of lingo-

cellulosic materials are dehydrating agents such as inorganic acids (e.g., H_3PO_4 and H_2SO_4), metal chlorides (e.g., $ZnCl_2$, $FeCl_3$ and $CaCl_2$) and metal hydroxides (e.g., KOH and NaOH), with the most popular among them being H_3PO_4, $ZnCl_2$ and KOH. Different activating mechanisms are proposed for each of these chemical agents during carbonization, with the ultimate effect of the agents on the activated carbon structure being generalized as KOH only promoting a widening of the micropore produced by the carbonization of the precursor, $ZnCl_2$ further developing small mesoporosity, and H_3PO_4 leading to a more heterogeneous pore size distribution (Molina-Sabio and Rodríguez-Reinoso, 2004).

The specific activation mechanisms for both NaOH and KOH are based on the redox reactions between the carbon structure and the metal hydroxides (MeOH, Me = Na or K), according to the general equations (Lillo-Ródenas et al., 2003; Alcañiz-Monge and Illán-Gómez, 2008):

$$4MeOH + C \rightarrow 4Me + CO_2 + 2H_2O \quad (6)$$

$$6MeOH + 2C \rightarrow 2Me + 3H_2 + 2Me_2CO_3 \quad (7)$$

$$4MeOH + (-CH_2) \rightarrow Me_2CO_3 + Me_2O + 3H_2 \quad (8)$$

Activation with KOH was observed by Alcañiz-Monge and Illán-Gómez (2008) to start at lower temperatures than with NaOH. The peak maximum for gas evolution also occurred at lower temperatures for KOH activation. Above a certain temperature (starting at 300°C for KOH and above 600°C for NaOH), the metal hydroxides can either react with the evolved products from the reaction described by equation (6) or decompose (Alcañiz-Monge and Illán-Gómez, 2008):

$$2MeOH + CO_2 \rightarrow Me_2CO_3 + H_2O \quad (9)$$

$$2MeOH \rightarrow Me_2O + H_2O \quad (10)$$

The generated products can also react with the carbon matrix or amongst themselves:

$$Me_2O + CO_2 \rightarrow Me_2CO_3 \quad (11)$$

$$H_2O + C \rightarrow CO + H_2 \quad (12)$$

$$2Me + H_2O \rightarrow Me_2O + H_2 \quad (13)$$

Another activation mechanism that has been observed for both potassium and sodium hydroxide with lignocellulosic materials is metal intercalation (Alcañiz-Monge and Illán-Gómez, 2008). In this mechanism, the metallic potassium or sodium, resulting from the reactions of Me_2O or Me_2CO_3 with carbon

$$Me_2O + C \rightarrow 2Me + CO \quad (14)$$

$$Me_2CO_3 + 2C \rightarrow 2Me + 3CO \quad (15)$$

reacts with the graphitic structures through donation of an electron to the π-electronic network of the carbon to form two types of graphite intercalation compounds, one containing a lamellar carbon structure and the other a disordered structure (Xue and Shen, 2003). At the temperature ranges usually employed in the carbonization/activation of lignocellulosic materials, both metallic potassium and sodium formed in reactions (14) and (15) are susceptible to volatilization for they present boiling points at 759°C and 883°C, respectively. Although metallic potassium has a boiling point in the range of 760°C, Tseng et al. (2008), in their study of activated carbon prepared from corncob at that temperature range, observed that only 17% of the original content of the potassium used as activating agent was lost to the exhaust gas phase and the rest (83%) remained in the final carbon structure, thus, suggesting the predominant occurrence of the reactions described by equations (6) to (13). In the case of NaOH, both Lillo-Ródenas et al. (2003) and Alcañiz-Monge and Illán-Gómez (2008), working respectively with anthracite and coal, have concluded that above 570 ^{o}C NaOH reacts to form Na_2CO_3 which does not present activating activities.

Another factor that influences the development of microporosity during activation with metal hydroxides is the nitrogen gas flow rate. The suggested action for its influence on the activation performance (i.e., attaining higher carbon yield with well-developed porosity) is the physical removal (drag) of the produced H_2O (reaction (6)), which in its vapor form is also an activating agent (steam physical activation), in accordance with equations (4) and (5). The higher the nitrogen flow rate, the faster the removal of H_2O from the reacting medium (Alcañiz-Monge and Illán-Gómez, 2008). Lillo-Ródenas et al. (2003) evaluated the influence of the nature of the gas used on the chemical activation of lignocellulosic materials with NaOH and concluded that nitrogen is the most adequate gas for the activation process and that steam is effective, but the porosity produced in the activated carbons were lower than that with nitrogen for the same activating conditions. They also concluded that CO_2 is not a suitable gas for chemically activating carbons with NaOH, for it does not incur in porosity development. CO_2 will react with NaOH, according with equation (9), and form sodium carbonate which does not act as an activating agent in the presence of this gas and is stable up to temperatures of the order of 850°C.

Nabais et al. (2008) used the coffee bean endocarp, which constituted an industrial residue from the Portuguese coffee industry, to produce activated carbons by means of both physical and chemical activation with carbon dioxide and potassium hydroxide, respectively. Activated carbons with surface areas ranging from 136 to 852 $m^2\ g^{-1}$ were produced. Physical activation with CO_2 produced carbons with smaller surface areas and pore volumes than the chemical activation with KOH. All the AC's produced were very basic in nature with pHs of the point of zero charge greater than 8. CO_2 activation led to the production of samples slightly more basic than KOH activation due to the lower quantity of oxygen functional groups formed. Cardoso et al. (2008) prepared activated carbon using cork powder waste as precursor and using KOH as activating agent. The produced activated carbons presented specific surface areas higher than 1300 $m^2\ g^{-1}$ and microporous volumes higher than 0.5 $cm^3\ g^{-1}$. An increase in activating temperature from 500 to 800 ^{o}C promoted an increase in surface area and in the pore volume for all carbons prepared. An impregnation ratio of 1:1 and a carbonization temperature of 800 ^{o}C provided the best textural properties for the prepared activated carbons.The produced activated carbons compared favorably with commercial

activated carbons in terms of volatile organic compounds adsorption. High surface area activated carbons were prepared by Tongpoothorn et al. (2010) via a simple thermo-chemical activation of Jatropha curcas fruit shell with NaOH as a chemical activating agent. Activated carbons with surface areas of the order of 1873 m^2 g^{-1} and micropore volume of 1.312 cm^3 g^{-1} were obtained for an impregnation ratio of 4:1 NaOH:char and a temperature of 800 ^oC for 2 h.

Regarding $ZnCl_2$, a Lewis acid, although it has been extensively used as an activating agent, little is known about its intrinsic activation mechanism in relation to carbonaceous materials. Only a handful of researchers have tried to infer about the mechanism with which $ZnCl_2$ activates a carbon and a detailed study of this mechanism is yet to be undertaken. Hu and Vansant (1995) proposed that the $ZnCl_2$ activating mechanism be that of catalysis of the removal of hydrogen and oxygen atoms from the carbon matrix in the form of water, which results in charring and aromatization of the carbon skeleton and the creation of a pore structure. In their study on the preparation of activated carbon using elutrilithe (coal waste) as precursor material, they observed that at temperatures higher than 238^oC liquid $ZnCl_2$ is formed, making the agent quite mobile, and at temperatures above 732^oC (its boiling point) it evaporates. Regardless of the temperature, below or above its boiling point, it was concluded that the elutrilithe was activated with $ZnCl_2$, presumably by two distinct activation mechanisms. Activation temperatures lower than 732^oC resulted in a low degree of carbon loss and produced a porous adsorbent with micropores as well as mesopores, whereas activation temperatures higher than 732^oC were favorable to produce highly microporous adsorbents with only a few mesopores.

Caturla et al. (1991) studied the effect of impregnation with $ZnCl_2$ in the activation of peach stones and concluded that the amount of $ZnCl_2$ used for impregnation was the most relevant factor governing the textural properties (specific surface area and micropore size distribution) of the prepared activated carbon. They also tried a combination of chemical activation with $ZnCl_2$ and physical activation with CO_2 and found it to yield a carbon material with high specific surface areas (~3000 m^2g^{-1}) for a 60 to 70% burn off.

In their study on the preparation of activated carbons using macadamia nut shells as precursor materials, Ahmadpour and Do (1997) observed that carbonization time did not have much effect on the weight loss of the $ZnCl_2$-treated shells, whereas BET surface area and pore volume decreased with an increase in the carbonization time. For the KOH-treated shells, all the properties remained relatively constant in the time range investigated. Regarding impregnation ratio, the higher the amount of activating agent the higher was the carbon yield. It was also observed that samples carbonized in the presence of $ZnCl_2$ presented larger micropore half-width and volume than those carbonized in the presence of KOH. The suggested activation mechanisms were that zinc chloride, which is a Lewis acid, promoted Scholl condensation (polymerization) reactions while potassium hydroxide catalyzed carbon oxidation reactions. Valix et al. (2006) prepared activated carbons from bagasse by physical (CO_2) and chemical ($ZnCl_2$, $MgCl_2$ and $CaCl_2$) activation to use them for adsorption of Acid Blue dye. The physical activation of bagasse was carried out by a two-step process invloving first the carbonization of bagasse through the use of a dehydrating agent, sulfuric acid, followed by gasification with carbon dioxide at 900°C. The carbonization/activation of the chemically impregnated fibers was conducted in a furnace at 500°C under nitrogen for 2 h. The effects of impregnation ratio on the carbon textural properties were to increase the surface area with increasing ratio for both $ZnCl_2$ and $CaCl_2$ and did not follow any trend for

$MgCl_2$. An increase in impregnation soaking time incurred in a decrease in surface area for both $ZnCl_2$ and $CaCl_2$ and, again, did not follow any specific trend for $MgCl_2$. All chemically activated carbons presented pore widths larger than 2 nm, thus, fitting in the range of mesopores. In general, the physically activated carbons presented larger surface areas than the chemically activated carbons. The main oxygenated surface groups in the chemically activated carbons were the alcohol-type of groups. In average, if the carbons that were physically activated for long periods of time (longer than 5 hours) are excluded, all physically and chemically activated carbons presented similar adsorption capacities for Acid Blue dye.

Williams and Reed (2006) used a biomass waste in the form of biomass flax fibre, produced as a by-product of the textile industry, to produce activated carbons via both physical and chemical activation. Surface areas of the physically activated carbons attained values up to 840 $m^2 g^{-1}$ and the carbons were of mesoporous structure. Chemical activation using zinc chloride produced high surface area activated carbons up to 2400 $m^2 g^{-1}$ with essentially micropores. By altering the carbonization/activation temperature and impregnation ratio, the surface area and porosity of the carbons were manipulated, allowing for the production of microporous, mesoporous and mixed microporous/mesoporous activated carbons. Activated carbons produced by physical activation presented a nodular and pitted surface morphology whereas activated carbons produced through chemical activation had a smooth surface morphology. Activated carbons were prepared by Önal et al. (2007) using sugar beet bagasse as precursor material by chemical activation with $ZnCl_2$. The influence of activation temperature on the pore structure was investigated. An impregnation ratio of 1:1 was used and the impregnated sample was subjected to activation at temperatures in the range of 400–900^oC, under N_2 flow atmosphere for 1 h. BET surface area of the resulting carbons were in the range of 832 to 1697 $m^2 g^{-1}$. Under the tested experimental conditions, 500^oC was found to be the optimal temperature for producing high surface area carbons with $ZnCl_2$ activation.

Oliveira et al. (2009) used both $ZnCl_2$ and $FeCl_3$ as activating agents to prepare activated carbons from coffee husks, a waste from coffee production. The AC obtained by the activation of the coffee husks presented specific surface areas of 1522, 1374 and 965 $m^2 g^{-1}$, respectively, by using only $ZnCl_2$, a mixture of $ZnCl_2$ and $FeCl_3$, and only $FeCl_3$. The iron salt allowed the preparation of a material with high specific surface area and very small pores, however, with an activation temperature of 280°C, which is far below those employed for other activating agents (including $ZnCl_2$) commonly described in the literature. The adsorption capacity for phenol was higher for the carbon activated with a mixture of $ZnCl_2$ and $FeCl_3$ than it was when either salts were used alone. Coffee residue was used by Boudrahem et al. (2009) as raw material in the preparation of powder activated carbon by the method of chemical activation with zinc chloride. The optimum experimental condition for preparing predominantly microporous activated carbons with high pore surface area (890 $m^2 g^{-1}$) and micropore volume (0.772 $cm^3 g^{-1}$) was an impregnation ratio of 100%. Higher impregnation ratios promoted pore widening, resulting in a mesoporous carbon pore structure.

Moreno-Piraján and Giraldo (2010) prepared activated carbons by pyrolysis of cassava peel in the presence of zinc chloride. Different impregnation ratios (e.g., 40, 70, 110 and 160% wt) were used and the activation was carried out under argon flow by heating to 550^oC with 1 h soaking time. The impregnation ratio had a strong influence on the pore structure of these ACs, with low impregnation ratio leading to essentially microporous ACs, intermediate

impregnation ratios to ACs with wider pore size distribution (from micropores to mesopores), and high impregnation ratios yielding essentially mesoporous carbons with high surface area and pore volume.

The mechanisms for chemical activation of lignocellulosic materials impregnated with H_3PO_4 were extensively studied (Molina-Sabio et al., 1995a; Jagtoyen and Derbyshire, 1998; Fierro et al., 2005; Olivares-Marín et al., 2006) together with the effects of thermal processing parameters (Molina-Sabio et al., 1995b; Girgis et al., 2007) on the final porosity of the resulting activated carbon. Several mechanisms were proposed for the action of H_3PO_4 on the carbon structure of lignocellulosic precursor, including acid catalysis to promote bond cleavage, hydrolysis, dehydration and condensation, and the formation of phosphate linkages (e.g., phosphate and polyphosphate esters) that promote the cross-linking between phosphoric acid and the lignocellulosic biopolymers (mostly cellulose and hemicellulose) (Zuo et al., 2009ab).

In phosphoric acid activation, the dehydration of the lignocellulosic material begins at temperatures lower than those of physical activation. Jagtoyen and Derbyshire (1998) observed that the acid treatment of white oak and yellow poplar promoted the removal of oxygen and hydrogen from the carbon matrix, through elimination of water, at temperatures as low as 75°C. During phosphoric acid activation of lignocellulosic precursors, an overall structural dilation and the concomitant development of microporosity is usually observed for temperatures in the range of 150 to 350°C and a further increase in temperature incurs in mesopore development, mostly through widening of the existing micropores (Molina-Sabio et al., 1995a; Jagtoyen and Derbyshire, 1998). The formation of phosphate ester linkages between cellulose chains is considered to be the major contributor to the dilation of the carbon structure since these linkages are based on the insertion of phosphoric acid molecules in between the cellulose chains, which further separates them. Dilation can be further enhanced by the formation and subsequent insertion of polyphosphates into the structure through ester linkages with cellulose chains, which in turn is considered to be one of the major contributors to the development of mesopores. Jagtoyen and Derbyshire (1998) proposed that the phosphate crosslinks may become bulkier at higher temperatures due to the favored polymerization of the phosphoric acid. These findings were supported by the fact that the mesopore volume was found to increase with an increase in the H_3PO_4 impregnation ratio, i.e., the more H_3PO_4 in the impregnating solution the more of it can be turned into polyphosphates and subsequently incorporated into the carbon structure at higher temperatures (Molina-Sabio et al., 1995a; Jagtoyen and Derbyshire, 1998). The mechanism of incorporation of phosphates and polyphosphates into cellulosic structures proposed by Jagtoyen and Derbyshire (1998) is depicted in Figure 3. At temperatures higher than 450°C, the phosphate ester linkages are thermally unstable and start to breakdown leading to a contraction of the carbon structure. Jagtoyen and Derbyshire (1998) observed that, in the heat treatment of phosphoric acid-impregnated wood at temperatures of the order of 650°C, the overall contraction in the radial direction was only 11% while the overall structure was still dilated relative to the extent of contraction experienced at temperatures lower than 150°C.

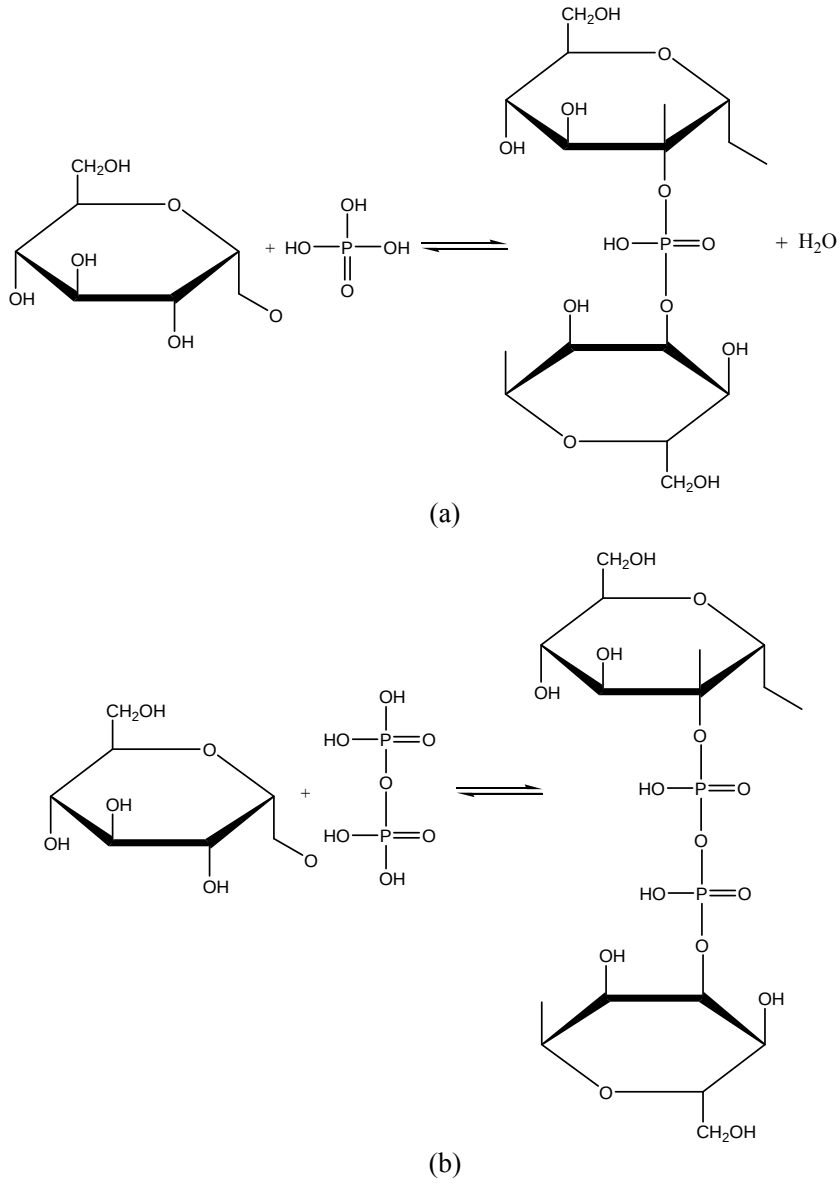


Figure 3. Mechanism of (a) phosphate and (b) polyphosphate ester formation with cellulose (T < 450°C) (Jagtoyen and Derbyshire, 1998).

Jagtoyen and Derbyshire (1998) inferred that, during impregnation and subsequent activation of lignocellulosic materials, the acid will firstly attack lignin and hemicellulose, both amorphous polymers, which are more easily accessible than cellulose. The activation of amorphous polymers produces mostly micropores, whereas the activation of crystalline cellulose produces a more widespread range of pore sizes. Crystalline cellulose was deemed to present a much greater potential for dilation than their amorphous polymer counterparts due to, among other aspects, the fact that it is more prone to higher degrees of esterification with phosphates and polyphosphates. After activation of phosphoric acid-impregnated carbons, it is a common practice to wash the carbon with water to recover the acid. Water

hydrolyzes the phosphate crosslinks and removes the phosphoric acid formed, together with that which was converted to $P_2O_5.xH_2O$ upon high temperature carbonization, leaving behind a vacant space which comprises a micropore with a volume that corresponds to that of the removed phosphoric acid (Molina-Sabio et al., 1995a; Jagtoyen and Derbyshire, 1998). Thus, it can be stated that, aside from its chemical action, phosphoric acid also acts as a template for micropore formation.

A few investigations have been conducted to evaluate the influence of thermal processing parameters on the development of pore structure of activated carbons produced from H_3PO_4-impregnated lignocellulosic materials (Molina-Sabio et al., 1995b; Girgis et al., 2007; Zuo et al., 2009a). The atmosphere used for phosphoric acid activation of lignocellulosic materials, including nitrogen, steam, air, carbon dioxide and a self-generated atmosphere (gaseous pyrolytic products of lignocellulosic material), was demonstrated to have pronounced effects on the physicochemical properties of activated carbons. Molina-Sabio et al. (1995b) prepared activated carbons from H_3PO_4-impregnated peach stones under a flow of nitrogen and of air and evaluated the effect of both gases on yield and density of the final carbon. The carbons produced under nitrogen flow presented higher yields than those prepared under air. When the heat treatment was carried out in the presence of air, the presence of oxygen was deemed to inhibit the aromatization process, reducing the influence of the phosphoric acid in both promoting the development of porosity and reducing the extent of contraction produced during the heat treatment. This resulted in activated carbons with a lower bulk density and micropore volume than those prepared in an inert atmosphere (N_2). At high impregnation ratios, an increase in weight (slightly higher yield) by the carbons heat-treated in air was considered to be due to chemisorbed oxygen since the differences in both micropore volume and bulk density between the air-treated and nitrogen-treated carbons were small. Girgis et al. (2007) studied the effects of different gas atmospheres (e.g., no external gas, nitrogen, carbon dioxide, steam or air) during thermal treatment (500°C for 2 h) of peach stone shells activated by 50% H_3PO_4. All prepared carbons exhibited high surface areas between 1050 and 1400 m^2/g with total pore volumes in the range of 0.57 to 0.69 cm^3/g, confirming the microporous character of all activated carbons derived from peach stone shells under different gaseous atmospheres. Both the air and steam treatments resulted in small pore widening, with enhancement of mesopores and an increase in non-microporous areas from about 50 to 100 m^2/g. In regard to the case of no flow of external gases (base case), the flowing of N_2, CO_2 or steam did not affect much the carbon yield (43.8–46.0% instead of 41.8% for the base case). In case of air, an additional gasification diminished the carbon yield to 30.0%, but with the total specific surface area and the pore volume not being affected, and with the mesopore surface area and volume being increased. Thus, it was concluded that concurrent flow of air stabilized the texture with a small enhanced mesoporosity, which was associated with the generation of oxygenated functional groups on the surface. The effects of the carbonization of volatile pyrolytic products of starting materials on the properties of phosphoric acid-activated carbon were investigated by Zuo et al. (2009a). Activated carbons were prepared from China fir wood impregnated with phosphoric acid in a cylindrical container that was kept in a closed state covered with a lid (the covered case) or in an open state, at a temperature of 475°C. Nitrogen flow was used to drive the air out of the muffle furnace prior to heating. Also, considering that as the mass of starting material increased the depth of the impregnated materials in the container increased, and that consequently the path for the volatiles to escape was extended, a set of experiments was performed using different masses of precursor

material. Both covering the cylindrical container and increasing the mass of precursor material exerted a positive effect on the mesopore development but had little or no effect on micropores in the process of phosphoric acid activation. Based on their findings, Zuo et al. (2009a) proposed that there are two different carbonizations in the process of phosphoric acid activation of lignocellulosic materials: one is the direct carbonization of constituent biopolymers, taking place in the solid state, and the other is the carbonization of volatile pyrolytic components, occurring in the gas phase, with the pores in the latter being predominantly mesopores. The promotion of the carbonization of volatile pyrolytic products, in both the covered case and in the use of increased mass of starting material, was attributed to the fact that they allow more phosphoric acid to remain in a protonated nature, due to the prevention of water escape, and retard the escape of the volatiles from the activating material, i.e., the volatiles had more time to continuously contact the retained phosphoric acid while trying to diffuse out of the activating materials. The enhancement for the covered case was more pronounced than that for the increased mass. The surface chemistry of activated carbons prepared by phosphoric acid activation of fruit stones in an argon atmosphere at various temperatures in the 400–1000°C range and at different acid/precursor impregnation ratios was investigated by Puziy et al. (2005). Phosphoric acid activation applied to fruit stones led to the incorporation of a significant amount of phosphorus in the resulting activated carbon, with the increase in the carbonization temperature leading to an increase in the content of phosphorus. A decrease in phosphorus content was observed above 800°C and was attributed to volatilization of phosphorus-containing compounds, most probably in the form of polyphosphoric acid, phosphorus pentoxide or even as elemental phosphorus. Phosphoric acid-activated carbons from fruit stones contained a relatively high amount of oxygen. Relative to its original composition in the precursor, the oxygen content decreased as the carbonization temperature increased up to 500°C. With further increase of the temperature, the oxygen content increased reaching a maximum at 700–800°C and decreased at higher temperatures. At low temperatures (400–500°C) the carbonaceous material lost a small portion of its oxygen due to dehydrating effect of phosphoric acid. At this stage, the phosphorus content was relatively low, suggesting that the most of retained oxygen was bound to the carbonaceous material. When the carbonization temperature was increased from 600 to 800°C, the oxygen content followed the same temperature dependence as did the phosphorus, suggesting that at higher temperatures the proportion of oxygen bound to phosphorus increased progressively. At the highest temperatures (900–1000°C), a departure of this trend was observed and was attributed to a possible evaporation of phosphorus and/or reduction of pentavalent phosphorus with carbon. Chemical activation of fruit stones with phosphoric acid produced carbons with strongly acidic surface groups that were associated with phosphorus-containing species along with carboxylic and phenolic groups. All prepared activated carbons showed considerable cation exchange capacity, which was attributed to the presence of carboxylic and phenolic groups in addition to the phosphorus-containing surface groups. Yeganeh et al. (2006) studied the effect of the ash content of raw materials on the properties of their respective activated carbons. Activated carbons were prepared from agricultural by-products such as hard shells of apricot stones, almond shells, walnut shells, pistachio shells, rice hulls and residues of liquorices by chemical activation with H_3PO_4 at a carbonization temperature of 400°C for 1 h. The surface area of the activated carbons was observed to depend on the ash content of the precursor material: the higher the ash content, the lower was the surface area. Thus, the samples of rice hulls and residues of liquorices had

the lowest surface areas and the highest surface areas were obtained for activated carbons produced from pistachio shells and apricot stones. The chemical structure of phosphorus species in fruit-stone-based carbons obtained by phosphoric acid activation at 400–1000°C was studied by Puziy et al. (2008) using XPS and solid state 31P-NMR and 13C-NMR. The most abundant and thermally stable phosphorus species in all investigated carbons were phosphate-like structures bound to carbon lattice via C-O-P bonding. Small contributions of phosphonates (C-P-O linkage) were observed in carbons obtained at temperature range of 500–700°C. Phosphorus oxides were observed in carbons prepared at 900°C and elemental phosphorus in carbons activated at 1000°C. Zuo et al. (2009b) studied the effect of the crystallinity of lignocellulosic material on the porosity of phosphoric acid-activated carbons prepared from China fir wood, cotton stalks and corncobs, at a temperature of 475°C. The results showed that decreasing the crystallinity of lignocellulosic material, depending on selection of the precursor material, promoted pore development, especially of mesopores. Excessive impregnation, which is another factor controlling the degree of crystallinity, was detrimental to mesopore development during activation. Impregnation and the selection of parent lignocellulosic material had, thus, a similar effect on developing porosity during phosphoric acid activation. Activated carbons were prepared by Reffas et al. (2010) by the pyrolysis of coffee grounds impregnated by phosphoric acid at 450°C and with different impregnation ratios to study the effect of the amount of phosphoric acid on the chemical composition of the surface of the activated carbon. Low impregnation ratios led to acidic microporous carbons with almost no mesopores and low surface areas. An increase in the impregnation ratio from 60 to 180 wt.%, promoted a reduction from 20 to 13 wt.% in the content of oxygenated surface groups. At impregnation levels as high as 180 wt.%, the acidic surface shifted to neutral because of the decrease in amount of carboxylic and phenol groups and the development of carbonyl surface groups. The effect of chemical reagent (H_3PO_4, KOH, and NaOH), temperature (400°C, 475°C, 550°C), and impregnation ratio (100 %, 150 %, 200 %) on the specific surface area and iodine uptake of the carbons produced from almond, walnut, and pistachio-nut shells and date stones was investigated by Arjmand et al. (2006). Activating the precursors with NaOH and KOH at low temperatures (about 400 °C) under a flow of N_2 produced very fine powdered activated carbons which could not be separated from the contaminants in order to undergo characterization. The low temperature activation of the nutshells and date stones with phosphoric acid resulted in carbons with a highly developed pore network. The acid activation of the raw materials produced carbons with high iodine numbers. The carbons produced from almond shells were mesoporous with surface areas as high as 1500 $m^2\ g^{-1}$. Varying the temperature and the amount of acid caused changes in the pore size distribution rather than influencing the surface area. Sun and Webley (2010) prepared activated carbons from agricultural waste corncob using a variety of different activation strategies and activators. Two different preparation strategies: a two-step activation, in which the alkalis KOH, K_2CO_3, and NaOH were used as activators; and a one-step activation procedure, in which H_3PO_4 50 wt% (with an impregnation ratio of 1 by weight) or $ZnCl_2$ were employed. All carbons presented microporous character, except for the sample that was prepared by one-step phosphoric acid activation, which presented mesoporous character. Among the prepared carbons, the one produced by two-step KOH activation with the aid of ultrasonic treatment during the impregnation process yielded the largest specific surface area and pore volume, which were 3012 $m^2\ g^{-1}$ and 1.7 $cm^3\ g^{-1}$, respectively. All prepared carbons presented a microporous character, except for the one

prepared by one-step phosphorous acid activation, which exhibited hysteresis of a mesoporous carbon.

3. NON-CONVENTIONAL THERMAL PROCESSES

The conventional thermal processes for the preparation of activated carbons from agricultural residues are based in carbonization followed by either physical or chemical activation in convection furnaces at temperatures in the range of 300 to 1000°C, under the flow of inert gases or air. What we call non-conventional thermal processes here are the processes in which the changes in the process with regard to the conventional ones would require a change in the equipment used. Thus, in this section, we will tackle basically the use of microwaves and the carbonization/activation carried out under vaccum.

3.1. Microwaves

Many studies have been carried out on the preparation of AC from various carbonaceous raw materials, using chemical or steam activation under various conditions, and in most of the cases aiming at a careful development of the pore structure (Molina-Sabio and Rodriguez-Reinoso, 2004; Suhas et al., 2007). In many of these studies, the thermal treatments were performed by means of an external heating source such as an electric or convection furnace. In these cases, the thermal energy is supplied to the surface of the raw material and then transferred inside by heat conduction, and therefore it is difficult to achieve a uniform temperature in the material. Moreover, it is necessary to heat and maintain the activation temperature in the activation furnace as well as the reactant, resulting in high energy consumption (Kubota et al., 2009). Microwaves (MW) have been employed as a heat source since the 1940s, with applications in the food and chemical engineering industries (Franca and Oliveira, 2008). The way in which a material will be heated by microwaves will depend on its shape, size, dielectric constant and also on the nature of the microwave equipment used (Bradshaw et al., 1998). The dominant mechanism for dielectric heating is dipolar loss (re-orientation loss), associated to a volumetrically distributed heat source inside the material, due to molecular friction resulting from dipolar rotation of polar solvents and from the conductive migration of dissolved ions. The dipolar rotation is caused by variations of the electrical and magnetic fields in the product, with water being the main source for microwave interactions due to its dipolar nature (Alton, 1998). Heat is thus generated within the material, leading to faster heating rates and shorter processing times compared to conventional heating.

Microwaves have been extensively employed as an alternative heating method and several studies have demonstrated that this technique can be successfully employed in the production of activated carbons (Hirata et al., 2002; Li et al., 2008a; Franca et al., 2010a). Some of the advantages of such technique in comparison to conventional heating for the production of adsorbents are reduced processing time with consequent reduction in energy consumption, reduction or even elimination of the amount of gases employed for the treatment, and more efficient carbonization, given that the heating mechanism is internal and volumetric as opposed to heat transfer from the surface towards the interior in the case of

conventional processing (Franca et al., 2010a). Other advantages include higher heating rates, no direct contact between heating source and the heated materials, possibility of selective heating, precise control of temperature, small equipment size and reduced ammount of waste (Zhang et al., 2009). The main applications of microwave heating in association with activated carbons are related to either (i) the preparation of activated carbons by carbonization and activation of precursor materials (Hirata et al., 2002; Li et al., 2009; Franca et al., 2010ab) or of previously prepared activated carbons (Carrot et al., 2004; Zou et al., 2009; Liu et al., 2010); or to (ii) the regeneration/reactivation of spent activated carbons (Bradshaw et al., 1998; Zhang et al., 2009; Jou et al., 2010). A few studies also deal with the application of microwaves for removal of compounds adsorbed onto the carbon matrix (Li et al., 2008b). A detailed review on application of microwave heating to the production of activated carbons is presented by Yuen and Hameed (2009). Studies on the use of MW for production and regeneration of other types of adsorbents such as carbon nanotubes, alumina, silica and zeolites are also available (Polaert et al., 2010; Han et al., 2010; Wang et al., 2010). The discussion herein presented will focus mainly on AC´s based on agricultural residues.

3.1.1. Preparation of Activated Carbons

The methods of preparation of activated carbons can be classified into two major categories, thermal and chemical activation. Thermal activation involves two stages, namely pyrolysis and activation. In the first stage, suitable carbon-based precursors are pyrolysed (600–800 °C) under an inert atmosphere or reducing gas (N_2, H_2) in order to release volatile components and produce chars with rudimentary pore structures. Subsequently, the resulting chars are subjected to a partial gasification at a higher temperature (usually above 900 °C) with oxidising gases, such as air, steam, CO_2 or their mixtures, to produce activated carbons with well-developed and accessible internal porosities (Crini, 2006; Yuen and Hameed, 2009). Chemical activation procedures, on the other hand, are accomplished in a single stage, with the carbonization and activation steps being carried out simultaneously. The raw material is impregnated with an activating agent (dehydrating, oxidant) and the impregnated material is heat-treated under inert atmosphere. Microwaves have been employed as an alternative heat treatment in both thermal and chemical activation procedures. Some of the thermal activation studies dealing with microwaves have employed domestic type ovens, without the presence of inert or other types of gases (Hirata et al., 2002; Carrot et al., 2004; Franca et al., 2010ab), while others have employed microwave heating under the flow of inert gases such as N_2 (Carrot et al., 2004; Liu et al., 2010) or gases commonly employed in conventional activation such as steam and CO_2 (Li et al., 2009; Yang et al., 2010). In general most studies confirm that (i) microwave activation produces a significant reduction in processing time in comparison with conventional heating, (ii) that the resulting adsorbents are mainly microporous, and (iii) that porosity increases with processing time (Yang et al., 2010). Most characterization studies obtained N_2 adsorption isotherms of type I, characteristic of microporous solids. Nonetheless, pore development seems to be dependent on the precursor material. Nabais and co-workers (2004) reported that microwave treatment under N_2 atmosphere provided reduction in micropore volume and micropore size, when the precursor material was an activated carbon based on acrylic textile fibres. Development of mesopores, on the other hand, will only be effective by the use of a chemical activating agent (Guo and Lua, 2000). Microwave activation has a distinct effect on the chemical characteristics of the adsorbent surface. Some studies report that the adsorbents prepared by microwave activation

present a more acidic characteristic in comparison to the ones obtained by conventional activation, thus being more effective for adsorption of basic dyes (Hirata et al., 2002; Franca et al., 2010; Nunes et al., 2010). This has been attributed to the milder effect of microwaves on the removal of acid groups from the adsorbent surface.

Table 2. Summary overview of recent applications of microwaves as an alternative thermal activation procedure

Precursor material	Microwave processing conditions	Gas flow	Application	Reference
Activated carbon	Power: 1000 W Time: 1.5, 5 and 30 min	Yes, N_2	Adsorbent characterization	Menéndez et al. (1999)
oil palm stone char	Power: 80 to 750 W Time: 5 to 60 min	Yes, CO_2 and N_2	Adsorbent characterization	Guo and Lua (2000)
spent coffee grounds	Power: 500 W Time: 7 to 12 min	No	Removal of dyes: orange II, methylene blue, and gentianviolet	Hirata et al. (2002)
activated carbon fibers	Power: 1000 W Time: 5 to 30 min	Yes, N_2	molecular sieves (adsorption of O_2, N_2, CO_2 and CH_4)	Carrot et al. (2004)
activated carbon fibers	Power: 1000 W Time: 15 min	Yes, N_2	Adsorbent characterization	Nabais et al. (2004)
coconut shells	Power: 60000 W Time: 15 min	Yes, steam	Adsorbent characterization	Li et al. (2009)
coconut shells	Power: 30000 W Time: 15 to 210 min	Yes, steam, CO_2 or both	Adsorbent characterization	Yang et al. (2010)
bamboo-based activated carbon	Power: 200 W Time: 2 to 10 min	Yes, N_2	Adsorbent characterization, removal of dyes: methylene blue.	Liu et al. (2010)
Precursor material	Microwave processing conditions	Gas flow	Application	Reference
defective coffee beans	Power: 800 W Time: 6 min	No	Removal of dyes: methylene blue, malachite green	Franca et al. (2010ab)
Raphanus sativus press cake	Power: 900 W Time: 3 to 5 min	No	Removal of dyes: methylene blue.	Nunes et al. (2010)

As in the case of pore development, such characteristics will also vary depending on the precursor materials. Some studies that employed activated carbons as raw materials have reported that microwave treatment provided an increase in the basic character of the adsorbent, associated with the production of pyrone groups (Nabais et al., 2004; Liu et al., 2010). When activated carbons are submitted to microwave treatments under nitrogen flow, most oxygen-containing groups are removed from the surface of the carbons and thus only a few minutes are required to transform an acidic carbon into a basic carbon with relatively low oxygen content (Menéndez et al., 1999). Also, microwave-treated carbons can undergo re-oxidation upon atmospheric exposure. A summary overview of recent studies involving microwaves as an alternative thermal activation procedure is displayed in Table 2.There are several studies that employed microwaves in chemical activation procedures. When activated carbons were used as raw materials, microwave treatment caused the adsorbent surface to become more reactive with a consequent increase in adsorption capacity (Zou et al., 2009). Microwave-assisted acid activation provides AC's with significant increase in porosity and specific area. The produced adsorbents tend to present a less acidic surface in comparison to the ones obtained by conventional heating, this being attributed to microwaves inducing stronger interactions of surface functional groups with the activating agent (Wang et al., 2005).

Also, microwave radiation energy coupled to chemical activation induces the opening of closed pores in the solid matrix, with consequent increases on total porosity and also on the amount of mesopores.

The produced adsorbents usually exhibit Type IV N_2 adsorption isotherms characteristic of mesoporous materials (Deng et al., 2010), as opposed to type I isotherms reported when microwaves are employed in thermal activation studies.

The activated carbons prepared by microwave-assisted activation employing basic agents such as KOH usually present higher surface area and larger pore volume in comparison to those obtained by conventional heating employing the same type and amount of activating agent. MW heating provides a considerable reduction in activation time and also a decrease in the amount of oxygen containing groups. This is attributed to oxygen containing functional groups being released during MW heating (Ji et al., 2007). Kubota et al. (2009) reported the use of microwaves coupled to KOH activation of phenolic resins provided better development of mesopores in comparison to conventional heating.

A summary overview of recent studies involving microwaves in the production of activated carbons by chemical activation procedures is displayed in Table 3.

Table 3. Overview of applications of MW coupled to chemical activation procedures

Precursor material	Activating agent	MW processing conditions	Application	Reference
Commercial activated carbon	HNO_3	Power: 1000 W Time: 1.5 to 30 min	Adsorbent characterization	Menéndez et al. (1999)
fly ash	HCl	Power: 800 W Time: 2 to 10 min	Removal of basic dyes: methylene blue, crystal violet, and rhodamine B	Wang et al. (2005)

Table 3. (Continued)

Precursor material	Activating agent	MW processing conditions	Application	Reference
tobacco stems	K_2CO_3	Power: 80 to 700 W Time: 5 to 60 min	Adsorbent characterization, adsorption of dyes: methylene blue.	Li et al. (2008a)
mesocarbon microbeads	KOH	Power: 3000 W Time: 10 to 30 min	Adsorbent characterization	Ji et al. (2007)
tea factory waste	H_3PO_4	Power: 900 W Time: 30s	Adsorbent characterization	Yagmur et al. (2008)
phenolic resins	KOH	Power: 260 to 520 W Time: intermittent heating	Adsorbent characterization	Kubota et al. (2009)
wood	$ZnCl_2$	Power: 700 W Time: 1 to 3 min	Adsorbent characterization	Wang et al. (2009)
cotton stalks	$ZnCl_2$	Power: 400 to 560 W Time: 8 to 10 min	Removal of basic dyes: methylene blue	Deng et al. (2009)
commercial activated carbon	HCl	Power: 595 W Time: 5 min	Removal of 2,4-dichlorophenol	Zou et al. (2009)
cotton stalks	H_3PO_4	Power: 400 to 560 W Time: 8 to 10 min	Removal of basic dyes: methylene blue	Deng et al. (2010)
petroleum coke	KOH	Power: 250 W Time: 27 to 37 min	Production of electrodes	He et al. (2010)
Cassia javanica seed gum	Acrylic acid	Power: 160 to 800W Time: 15 to 60 min	Adsorbent characterization, removal of Hg (II)	Singh et al. (2010)
Chitosan	β-cyclodextrin	Power: 160 to 800W Time: 15 to 60 min	Adsorbent characterization, removal of Pb (II)	Sharma and Mishra (2010)

3.1.2. Re-Activation or Regeneration of Spent Activated Carbons

The techniques usually employed for AC regeneration can be divided into thermal, chemical and bioregeneration, with thermal regeneration being the most extensively used. Convetional thermal re-activation is usually accomplished by heating between 800 and 1000 °C under mildly oxidizing atmospheric conditions, either carbon dioxide or steam (Yuen and Hameed, 2009). The application of microwave heating technology to regenerate industrial waste activated carbon has been recently investigated, given the already pointed out technique advantages over conventional heating such as rapid and precise control of the carbon bed temperature, shorter processing time, smaller equipments and energy savings.

Some studies have also concluded that microwave regeneration gives rise to a better performance of the activated carbons in terms of adsorption capacity and rate of adsorption compared to conventional processing (Yuen and Hameed, 2009). Under conventional heating, the adsorption capacity decreases gradually with subsequent regeneration cycles, this being attributed to the partial desorption of adsorbate molecules and the blockage of the porous structure. There is a decrease in micropore volume accompanied by a downward shift to pores of narrower sizes, suggesting that regeneration treatment introduces some molecular sieve effects into the porous structure of the regenerated activated carbon. With microwave heating, on the other hand, despite the slight deterioration of the porous structure of the parent activated carbons, adsorptive capacities after microwave regeneration are unexpectedly high (Ania et al., 2005). For example, Zhang and co-workers (2009) compared microwave and conventional thermal treatmens for reactivation of spent activated carbons employed as catalyst supports in vinyl acetate synthesis. Reactivation experiments were based on the use of a single mode microwave device (800 W, 2450 MHz) and a conventional electric furnace, both operating at the same temperature (1000°C) under steam and CO_2 atmospheres. The activation times ranged from 25 to 45 min and from 90 to 100 min for microwave and conventional heating, respectively. The AC obtained by microwave irradiation under steam atmosphere presented higher adsorption capacities for iodine, methylene blue (MB) and acetate acid. Both microwave-activated adsorbents presented higher BET surface areas and mesoporosity than the ones obtained by conventional heating. The carbons reactivated by steam presented a narrower and more extensive microporosity as well as higher BET than those activated by carbon dioxide for a specific heating equipment. A summary overview of recent studies employing microwaves for regeneration of activated carbons is displayed in Table 4.

Table 4. Summary overview of recent applications of microwaves as an alternative AC regeneration procedure

Precursor material/activating agent	Microwave processing conditions	Gas flow	Application (adsorbate to be removed)	Reference
Coal/steam	Power: 2000 W 850°C	Yes, N_2 and CO_2	phenol	Ania et al. (2004)
Coal/steam; wood/ H_3PO_4	Power: 2000 W 850°C	Yes, N_2	phenol	Ania et al. (2005)
Wood/ H_3PO_4	Power: 2000 W 450 and 850°C	Yes, N_2 and CO_2	salicylic acid	Ania et al. (2007)
Coal/HCl	Power: 700 W Time: 5 min	No	2,4,5-trichlorobiphenyl	Liu et al. (2007)
? (commercial GAC)	Power: 150 W Time: 25 min	Yes, N_2	methy-ethyl-ketone	Tai and Lee (2007)
Coconut shell (commercial GAC)	Power: 400 to 800 W Time: 1 min	No	chlorobenzene	Jou et al. (2010)
Date seeds/ H_3PO_4	Power: 2000 W 850°C, 4 min	Yes, CO_2	2,4-Dinitrophenol	Al-Mutairi (2010)

3.2. Activation under Vacuum

Activated carbons with well-developed pore structures were prepared by Lua and Yang (2005) from pistachio-nut shells by chemical activation using zinc chloride under both nitrogen atmosphere and vacuum conditions. The characteristics of the activated carbons produced under vacuum conditions were better than those produced under nitrogen atmosphere. The optimum experimental conditions for preparing predominantly microporous activated carbons with high pore surface area and micropore volume were an impregnation ratio of 0.75, an activation temperature of 400°C, and a hold time of 1 h. Under these conditions, the surface areas of the carbons activated under nitrogen atmosphere and vacuum conditions were 1635.37 and 1647.16 m^2 g^{-1}, respectively. However, for a predominantly mesoporous activated carbon, the conditions of a $ZnCl_2$ impregnation ratio of 1.5, a furnace temperature of 500 ^{o}C, and a hold time of 2 h led to carbons with a much higher surface area (2527 m^2 g^{-1}). Ismadji et al. (2005) prepared activated carbons by vacuum pyrolysis of the char of teak sawdust. The activated carbon prepared from char obtained by vacuum pyrolysis presented higher surface area and pore volume than that prepared by atmospheric pyrolysis of the char. The surface area and pore volume of activated carbon prepared from vacuum pyrolysis char were 1150 m^2 g^{-1} and 0.43 cm^3 g^{-1}, respectively.

Juan and Ke-Qiang (2009) prepared activated carbons from Chinese fir sawdust by zinc chloride activation under vacuum condition. The electrical furnace system was vacuumed to pressures in the range of 10 to 100 kPa while the temperature was varied from 400 to 600°C. It was observed that the structure of the starting material was kept after activation and that the activated carbon prepared under vacuum exhibited higher values of surface area (up to 1079 m^2 g^{-1}) and total pore volume (up to 0.5665 cm^3 g^{-1}) than those of AC´s obtained under atmospheric pressure. This was attributed to the effect of vacuum condition that reduces oxygen in the system and limits the secondary reaction of the organic vapor. The prepared activated carbon presented well-developed microstructure and high microporosity. The vaccum condition led to lower activation temperatures than in the regular process carried out at atmospheric pressure. Activated carbons were prepared by Juan and Ke-Qiang (2010) from walnut shells by vacuum chemical activation with zinc chloride as the activation agent. The optimum activated carbon was obtained with a system pressure of 30 kPa, an activation temperature of 450°C, and an impregnation ratio of 2.0, and presented a surface area of 1800 m^2 g^{-1} and total pore volume of 1.176 cm^3 g^{-1}.

CONCLUDING REMARKS

The methodologies being currently used in research facilities for the preparation of activated carbons from agricultural residues are practically the same as those being currently used for the commercial production of either powder or granulated ACs, requiring little or no modifications at all to the equipments and processes. In commercial production, the preferred methods are the two-step carbonization/activation procedures in which either steam or CO_2 are used as the physical activating agents or the chemical activation with phosphoric acid. Chemical activation with zinc chloride and KOH are used to a lesser extent in industrial processes. The development of new and improved methods of activation of carbon materials

allows the tunning of the structural, textural, morphological and surface properties of carbon materials suitable to be employed in specific adsorption applications. However, our current knowledge about carbonization and activation processes, as related to the preparation of activated carbons, can only give us clues as how to find a suitable precursor material and a carbonization/activation procedure that will match the desired properties for the final product. Hence, for every agricultural residue envisioned as a potential candidate for precursor material in the preparation of activated carbons, extensive studies should be carried out to find a suitable carbonization/activation procedure that will lead to carbons with the desired textural (porosity) and chemical properties (surface functionality).

Regarding the applications of the ACs produced from agricultural wastes, the final product has been several times proven of equal or sometimes better capacities than the currently available commercial carbons. They were frequently and successfully tested in comparative studies with commercial carbons under the same conditions. A lack of a closer interaction between researchers and the producers of activated carbons might be the prevalent issue precluding the widespread production and application of such types of activated carbons in large scale (Oliveira and Franca, 2008).

The chemical activation methods have been demonstrated to produce activated carbons with better textural and chemical properties at lower temperatures than those used in physical activation processes. However, these methods employ chemical agents that are not environmentally benign and are, therefore, not adequate to be fitted into the concept of "green technology". Thus, activation methods based on environmentally benign activating agents and on reaction conditions milder than those currently employed are highly desirable and a rather interesting opportunity for the development of innovative technology in this area is envisioned. Microwave thermal processing has been demonstrated to produce activated carbons with excellent textural and chemical properties with very low energy input. However, microwaves still present the limitation associated with its restricted penetration in the medium being irradiated which precludes its large scale applications. Carbonization under vaccum has been proposed as an efficient method for lowering the activation temperatures in both physical and chemical activation, but, unless a high-valued product is being sought, the use of vaccum in industrial process is usually avoided for it increases the costs of production.

ACKNOWLEDGMENTS

The authors gratefully acknowledge financial support from the following Brazilian Government Agencies: CNPq and FAPEMIG.

REFERENCES

Ahmadpour, A., Do, D.D. (1997) The preparation of activated carbon from macadamia nutshell by chemical activation, *Carbon* 35, 1723-1732.

Ahmedna, M., Marshall, W.E., Rao, R.M. (2000) Production of granular activated carbons from select agricultural by-products and evaluation of their physical, chemical and adsorption properties, *Bioresource Technology* 71, 113-123.

Alcañiz-Monge, J., Illán-Gómez, M.J. (2008) Modification of activated carbon porosity by pyrolysis under pressure of organic compounds, *Adsorption*, 14, 93-100.

Al-Mutairi, N.Z. (2010) 2,4-Dinitrophenol adsorption by date seeds: Effect of physico-chemical environment and regeneration study, *Desalination*, 250, 892-901.

Alton, W. J. (1998) Microwave pasteurization of liquids, *Society of Manufacturing Engineers*, Paper No. EM98-211.

Ania, C.O., Menendez, J.A., Parra, J.B., Pis, J.J. (2004) Microwave-induced regeneration of activated carbons polluted with phenol. A comparison with conventional thermal regeneration, *Carbon*, 42, 1383-1387.

Ania, C.O., Parra, J.B., Menendez, J.A., Pis, J.J. (2005) Effect of microwave and conventional regeneration on the microporous and mesoporous network and on the adsorptive capacity of activated carbons, *Microporous and Mesoporous Materials*, 85, 7-15.

Ania, C.O., Parra, J.B., Menendez, J.A., Pis, J.J. (2007) Microwave-assisted regeneration of activated carbons loaded with pharmaceuticals, *Water Research*, 41, 3299-3306.

Arjmand, C., Kaghazchi, T., Latifi, S.M., Soleimani, M. (2006) Chemical production of activated carbon from nutshells and date stones, *Chem. Eng. Technol.* 29, 986–991.

Aworn, A. Thiravetyan, P. Nakbanpote, W. (2009) Preparation of CO_2 activated carbon from corncob for monoethylene glycol adsorption, *Colloids and Surfaces A: Physicochemical and Engineering Aspects* 333, 19–25.

Bansal, R.C., Goyal, M. (2005) Activated Carbon Adsorption, Boca Raton: Taylor and Francis.

Bhatnagar, A., Sillanpää, M. (2010) Utilization of agro-industrial and municipal waste materials as potential adsorbents for water treatment—A review, *Chemical Engineering Journal* 157, 277–296.

Boudrahem, F., Aissani-Benissad, F., Aït-Amar, H. (2009) Batch sorption dynamics and equilibrium for the removal of lead ions from aqueous phase using activated carbon developed from coffee residue activated with zinc chloride, *Journal of Environmental Management* 90, 3031–3039.

Bourke, J., Manley-Harris, M., Fushimi, C., Dowaki, K., Nunoura, T., Antal Jr., M.J. (2007) Do all carbonized charcoals have the same chemical structure? 2. A model of the chemical structure of carbonized charcoal, *Ind. Eng. Chem. Res.* 46, 5954-5967.

Bradshaw, S.M., Van Wyk, E.J., De Swardt, J.B. (1998) Microwave heating principles and the application to the regeneration of granular activated carbon, *Journal of The South African Institute of Mining and Metallurgy,* 98, 201-210.

Budinova, T. , Savova, D., Tsyntsarski, B., Ania, C.O., Cabal, B., Parra, J.B. , Petrov, N. (2009) Biomass waste-derived activated carbon for the removal of arsenic and manganese ions from aqueous solutions, *Applied Surface Science* 255, 4650–4657.

Cagnon, B., Py, X., Guillot, A., Stoeckli, F., Chambat, G. (2009) Contributions of hemicellulose, cellulose and lignin to the mass and the porous properties of chars and steam activated carbons from various lignocellulosic precursors, *Bioresource Technology* 100, 292–298.

Cardoso, B., Mestre, A.S., Carvalho, A.P., Pires, J. (2008) Activated Carbon derived from cork powder waste by KOH activation: Preparation, characterization, and VOCs adsorption, *Ind. Eng. Chem. Res.* 47, 5841–5846.

Carrott, P. J. M., Nabais, J. M. V., Ribeiro Carrott, M. M. L., Menendez, J. A. (2004) Microwave heating as a novel method for introducing molecular sieve properties into activated carbon fibres, *Carbon*, 42, 227-229.

Caturla, F., Molina-Sabio, M., Rodríguez-Reinoso, F. (1991) Preparation of activated carbon by chemical activation with $ZnCl_2$, *Carbon* 29, 999-1007.

Crini, G. (2006) Non-conventional low-cost adsorbents for dye removal: A review, *Bioresource Technology* 97, 1061-1085.

Crittenden, B., Thomas, W.J. (1998) Adsorption Technology and Design, London: Elsevier Science and Technology Books.

Daud, W.M.A.W., Houshamnd, A.H. (2010) Textural characteristics, surface chemistry and oxidation of activated carbon, *Journal of Natural Gas Chemistry* 19, 267–279.

Demiral, H., Demiral, İ., Karabacakoğlu, B., Tümsek, F. (2010) Production of activated carbon from olive bagasse by physical activation, *Chemical Engineering Research and Design*, in press, doi:10.1016/j.cherd.2010.05.005.

Demirbaş, A. (2001) Carbonization ranking of selected biomass for charcoal, liquid, and gaseous products, *Energy Conversion and Management* 42, 1229-1238.

Deng, H., Yang, L., Tao, G., Dai, J. (2009) Preparation and characterization of activated carbon from cotton stalk by microwave assisted chemical activation-Application in methylene blue adsorption from aqueous solution, Journal *of Hazardous Materials*, 166, 1514-1521.

Deng, H., Zhang, G., Xu, X., Tao, G., Dai, J. (2010) Optimization of preparation of activated carbon from cotton stalk by microwave assisted phosphoric acid-chemical activation, *Journal of Hazardous Materials*, 182, 217-224.

Dias, J.M., Alvim-Ferraz, M.C.M., Almeida, M.F., Rivera-Utrilla, J., Sánchez-Polo, M. (2007) Waste materials for activated carbon preparation and its use in aqueous-phase treatment: A review, *Journal of Environmental Management* 85, 833–846.

Elizalde-González, M.P., Mattusch, J., Peláez-Cid, A.A., Wennrich, R. (2007) Characterization of adsorbent materials prepared from avocado kernel seeds: Natural, activated and carbonized forms, *J. Anal. Appl. Pyrolysis* 78, 185–193.

Fierro, V., Torné-Fernádez, V., Montané, D., Celzard, A. (2005) Study of the decomposition of Kraft lignin impregnated with orthophosphoric acid, *Thermochim. Acta* 433, 142–148.

Figueiredo, J.L., Pereira, M.F.R. (2010) The role of surface chemistry in catalysis with carbons, *Catalysis Today* 150, 2–7.

Franca, A.S. and Oliveira, L.S. (2008) An Overview of Simulation Studies on Microwave Processing of Food Products. In E. N. Koeffer. (Ed.), *Progress in Food Chemistry*, New York: Nova Publishers, pp. 167-182.

Franca, A.S., Oliveira, L.S., Nunes, A.A., Alves, C.C.O. (2010a) Microwave assisted thermal treatment of defective coffee beans press cake for the production of adsorbents, *Bioresource Technology*, 101, 1068-1074.

Franca, A.S., Oliveira, L.S., Nunes, A.A. (2010b) Malachite green adsorption by a residue-based microwave-activated adsorbent, *Clean - Soil, Air, Water,* 38, 843-849.

Girgis, B.S., Attia, A.A., Fathy, N.A. (2007) Modification in adsorption characteristics of activated carbon produced by H_3PO_4 under flowing gases, *Colloids Surf. A Physicochem. Eng. Asp.* 299, 79–87.

González, J.F., Román, S., González-García, C.M., Nabais, J.M.V., Ortiz, A.L. (2009) Porosity Development in activated carbons prepared from walnut shells by carbon dioxide or steam activation, *Ind. Eng. Chem. Res.* 48, 7474–7481.

Gupta, V.S., Suhas (2009) Application of low-cost adsorbents for dye removal – A review, *Journal of Environmental Management* 90, 2313–2342.

Guo, J., Lua, A.C. (2000) Preparation of activated carbons from oil-palm-stone chars by microwave-induced carbon dioxide activation, *Carbon*, 38, 1985-1993.

Guo, S.-H., Peng, J., Li, W., Yang, K., Zhang, L., Zhang, S., Xia, H. (2009) Effects of CO_2 activation on porous structures of coconut shell-based activated carbons, *Applied Surface Science* 255, 8443–8449.

Han, R., Wang, Y., Sun, Q., Wang, L., Song, J., He, X., Dou, C. (2010) Malachite green adsorption onto natural zeolite and reuse by microwave irradiation, *Journal of Hazardous Materials*, 175, 1056-1061.

He, X., Geng, Y., Qiu, J., Zheng, M., Long, S., Zhang, X. (2010) Effect of activation time on the properties of activated carbons prepared by microwave-assisted activation for electric double layer capacitors, *Carbon*, 48, 1662-1669.

Hirata, M., Kawasaki, N., Nakamura, T., Matsumoto, K., Kabayama, M., Tamura, T., Tanada, S. (2002) Adsorption of Dyes onto Carbonaceous Materials Produced from Coffee Grounds by Microwave Treatment, *Journal of Colloid and Interface Science*, 254, 17-22.

Hu, Z., Vansant, E.F. (1995) A new composite adsorbent produced by chemical activation of elutrilithe with zinc chloride, *Journal of Colloid and Interface Science* 176, 422–431.

Ioannidou, O., Zabaniotou, A. (2007) Agricultural residues as precursors for activated carbon production – A review, *Renewable and Sustainable Energy Reviews* 11, 1966-2005.

Ismadji, S., Sudaryanto, Y., Hartono, S.B., Setiawan, L.E.K., Ayucitra, A. (2005) Activated carbon from char obtained from vacuum pyrolysis of teak sawdust: pore structure development and characterization, *Bioresource Technology* 96, 1364–1369.

Jagtoyen, M., Derbyshire, F. (1998) Activated carbons from yellow poplar and white oak by H_3PO_4 activation, *Carbon* 36, 1085-1097.

Jaramillo, J., Gómez-Serrano, V., Álvarez, P.M. (2009) Enhanced adsorption of metal ions onto functionalized granular activated carbons prepared from cherry stones, *Journal of Hazardous Materials* 161, 670–676.

Ji, Y., Li, T., Zhu, L., Wang, X., Lin, Q. (2007) Preparation of activated carbons by microwave heating KOH activation, *Applied Surface Science*, 254, 506-512.

Jou, C.-J. G., Wu, C.-R. and Lee, C.-L. (2010), Application of microwave energy to treat granular activated carbon contaminated with chlorobenzene, *Environmental Progress and Sustainable Energy*, 29, 272–277.

Juan, Y., Ke-Qiang, Q. (2009) Preparation of activated carbon by chemical activation under vacuum, *Environ. Sci. Technol.* 43, 3385–3390.

Juan, Y., Ke-Qiang, Q. (2010) Preparation of activated carbons from walnut shells via vacuum chemical activation and their application for methylene blue removal, *Chemical Engineering Journal* 165, 209–217.

Kubota, M., Hata, A., Matsuda, H. (2009) Preparation of activated carbon from phenolic resin by KOH chemical activation under microwave heating, *Carbon*, 47, 2805-2811.

Li, W., Yang, K., Peng, J., Zhang, L., Guo, S., Xia, H. (2008) Effects of carbonization temperatures on characteristics of porosity in coconut shell chars and activated carbons derived from carbonized coconut shell chars, *Industrial Crops and Products* 28, 190–198.

Li, W., Zhang, L.-B., Peng, J.-H., Li, N., Zhu, X.-Y. (2008a) Preparation of high surface area activated carbons from tobacco stems with K_2CO_3 activation using microwave radiation, *Industrial Crops and Products*, 27, 341-347.

Li, W., Peng, J., Zhang, L., Zhang, Z., Li, L., Zhang, S., Guo, S. (2008b) Pilot-scale extraction of zinc from the spent catalyst of vinyl acetate synthesis by microwave irradiation, *Hydrometallurgy*, 92, 79-85.

Li, W., Peng, J., Zhang, L., Zhang, L., Yang, K., Xia, H., Zhang, S., Guo, S.-H. (2009) Preparation of activated carbon from coconut shell chars in pilot-scale microwave heating equipment at 60 kW, *Waste Management*, 29, 756-760.

Lillo-Ródenas, M.A., Cazorla-Amorós, D., Linares-Solano, A. (2003) Understanding chemical reactions between carbons and NaOH and KOH. An insight into the chemical activation mechanism, *Carbon* 41, 267–275.

Liu, X., Yu, G., Han, W. (2007) Granular activated carbon adsorption and microwave regeneration for the treatment of 2,4,5-trichlorobiphenyl in simulated soil-washing solution, *Journal of Hazardous Materials*, 147, 746-751.

Liu, Q.-S., Zheng, T., Li, N., Wang, P., Abulikemu, G. (2010) Modification of bamboo-based activated carbon using microwave radiation and its effects on the adsorption of methylene blue, *Applied Surface Science,* 256, 3309-3315.

Lua, A.C., Yang, T. (2005) Characteristics of activated carbon prepared from pistachio-nut shell by zinc chloride activation under nitrogen and vacuum conditions, *Journal of Colloid and Interface Science* 290, 505–513.

Marsh, H., Rodríguez-Reinoso, F. (2006) *Activated Carbon*, Elsevier Science and Technology Books, 536 p.

Menéndez, J. A., Menendez, E. M., Iglesias, M. J., Garcia, A., Pis, J. J. (1999) Modification of the surface chemistry of active carbons by means of microwave-induced treatments, *Carbon*, 37, 1115-1121.

Mészáros, E., Jakab, E. Várhegyi, G., Bourke, J., Manley-Harris, M., Nunoura, T., Antal, M.J., Jr. (2007) Do all carbonized charcoals have the same chemical structure? 1. Implications of thermogravimetry-mass spectrometry measurements, *Ind. Eng. Chem. Res.* 46, 5943-5953.

Mohamed, A.R., Mohammadi, M., Darzi, G.N. (2010) Preparation of carbon molecular sieve from lignocellulosic biomass: A review, *Renewable and Sustainable Energy Reviews* 14, 1591-1599.

Molina-Sabio, M., Rodríguez-Reinoso, F., Caturla, F., Selés, M.J. (1995a) Porosity in granular carbons activated with phosphoric acid, *Carbon* 33, 1105–1113.

Molina-Sabio, M., Caturla, F., Rodríguez-Reinoso, F. (1995b) Influence of the atmosphere used in the carbonization of phosphoric acid impregnated peach stones, *Carbon* 33, 1180–1182.

Molina-Sabio, M. and Rodriguez-Reinoso, F. (2004) Role of chemical activation in the development of carbon porosity, *Colloids and Surfaces A: Physicochemical and Engineering Aspects,* 241, 15-25.

Moreno-Piraján, J.C., Giraldo, L. (2010) Study of activated carbons by pyrolysis of cassava peel in the presence of chloride zinc, *Journal of Analytical and Applied Pyrolysis* 87, 288–290.

Nabais, J.M.V., Carrott, P.J.M., Ribeiro Carrott, M.M.L., Menendez, J.A. (2004) Preparation and modification of activated carbon fibres by microwave heating, *Carbon*, 42, 1315-1320.

Nabais, J.M.V., Carrott, P.J.M., Ribeiro Carrott, M.M.L., Luz, V., Ortiz, A.L. (2008) Influence of preparation conditions in the textural and chemical properties of activated carbons from a novel biomass precursor: The coffee endocarp, *Bioresource Technology* 99, 7224–7231.

Nabais, J.M.V., Laginhas, C.E.C., Carrott, P.J.M., Ribeiro Carrott, M.M.L. (2010) Production of activated carbons from almond shell, *Fuel Processing Technology*, 92, 234-240.

Nunes, D.L., Franca, A.S., Oliveira, L.S. (2010) Use of *Raphanus sativus L.* press cake, a biodiesel processing solid residue, in the production of adsorbents by microwave activation, *Environmental Technology*, DOI: 10.1080/09593330.2010.526965.

Olivares-Marín, M., Fernández-González, C., Macías-García, A., Gómez-Serrano, V. (2006) Thermal behavior of lignocellulosic material in the presence of phosphoric acid. Influence of the acid content in the initial solution, *Carbon* 44, 2347–2350.

Oliveira, L.S., Franca, A.S. (2008) Low-Cost Adsorbents from Agri-Food Wastes In: Food Science and Technology: New Research, Lorenzo V. Greco; Marco N. Bruno (org), Nova Publishers, New York, Chap. 3, p. 171-209.

Oliveira, L.C.A., Pereira, E., Guimaraes, I.R., Vallone, A., Pereira, M., Mesquita, J.P., Sapag, K. (2009) Preparation of activated carbons from coffee husks utilizing $FeCl_3$ and $ZnCl_2$ as activating agents, *Journal of Hazardous Materials* 165, 87–94.

Önal, Y., Akmil-Başar, C., Sarici-Özdemir, Ç., Erdoğan, S. (2007) Textural development of sugar beet bagasse activated with $ZnCl_2$, *Journal of Hazardous Materials* 142, 138–143.

Polaert, I., Estel, L., Huyghe, R., Thomas, M. (2010) Adsorbents regeneration under microwave irradiation for dehydration and volatile organic compounds gas treatment, *Chemical Engineering Journal*, 162, 941-948.

Puziy, A.M., Poddubnaya, O.I., Martínez-Alonso, A., Suárez-Garcia, F., Tascón, J.M.D. (2005) Surface chemistry of phosphorus-containing carbons of lignocellulosic origin, *Carbon* 43, 2857–2868.

Puziy, A.M., Poddubnaya, O.I., Socha, R.P., Gurgul, J., Wisniewski, M., (2008) XPS and NMR studies of phosphoric acid activated carbons, *Carbon* 46, 2113–2123.

Reffas, A., Bernardet, V., Davia, B., Reinert, L., Lehocine, M.B., Dubois, M., Batisse, N., Duclaux, L. (2010) Carbons prepared from coffee grounds by H_3PO_4 activation: Characterization and adsorption of methylene blue and Nylosan Red N-2RBL, *Journal of Hazardous Materials* 175, 779–788.

Rodríguez-Reinoso, F., Molina-Sabio, M. (1998) Textural and chemical characterization of microporous carbons, *Advances in Colloid and Interface Science* 76-77, 271-294.

Savova, D., Apak, E., Ekinci, E., Yardim, F., Petrova, N., Budinova, T., Razvigorova, M., Minkova, V. (2001) Biomass conversion to carbon adsorbents and gas, *Biomass and Bioenergy* 21, 133–142.

Sharma, A.K., Mishra, A.K. (2010) Microwave induced [beta]-cyclodextrin modification of chitosan for lead sorption, *International Journal of Biological Macromolecules*, 47, 410-419.

Singh, V., Singh, S.K., Maurya, S. (2010) Microwave induced poly(acrylic acid) modification of Cassia javanica seed gum for efficient Hg(II) removal from solution, *Chemical Engineering Journal,* 160, 129-137.

Sud, D., Mahajan, G., Kaur, M.P. (2008) Agricultural waste material as potential adsorbent for sequestering heavy metal ions from aqueous solutions – A review, *Bioresource Technology* 99, 6017–6027.

Suhas, Carrott, P.J.M., Ribeiro Carrott, M.M.L. (2007) Lignin - from natural adsorbent to activated carbon: A review, *Bioresource Technology*, 98, 2301-2312.

Sun, Y., Webley, P.A. (2010) Preparation of activated carbons from corncob with large specific surface area by a variety of chemical activators and their application in gas storage, *Chemical Engineering Journal* 162, 883–892.

Susuki, M. (1990) Adsorption Engineering, Elsevier Science Publishers B.V., Amsterdam, The Netherlands.

Tai, H.-S., Lee, C.-L. (2007), Desorption of methy-ethyl-ketone from granular activated carbon with microwave radiation, *Environmental Progress*, 26, 1547-5921.

Toles, C.A., Marshall, W.E., Wartelle, L.H., McAloon, A. (2000) Steam- or carbon dioxide-activated carbons from almond shells: physical, chemical and adsorptive properties and estimated cost of production, *Bioresource Technology* 75, 197-203.

Tongpoothorn, W., Sriuttha, M., Homchan, P., Chanthai, S., Ruangviriyachai, C. (2010) Preparation of activated carbon derived from Jatropha curcas fruit shell by simple thermo-chemical activation and characterization of their physico-chemical properties, *Chemical Engineering Research and Design*, doi:10.1016/j.cherd.2010.06.012.

Tseng, R.L., Tseng, S.K., Wu, F.C.,Hu, C.C., Wang, C.C. (2008) Effects of micropore development on the physicochemical properties of KOH-activated carbons, *Journal of the Chinese Institute of Chemical Engineers* 39, 37–47.

Valix, M., Cheung, W.H., McKay, G. (2006) Roles of the textural and surface chemical properties of activated carbon in the adsorption of acid blue dye, *Langmuir* 22, 4574-4582.

Xue, R., Shen, Z. (2003) Formation of graphite-potassium intercalation compounds during activation of MCMB with KOH, *Carbon* 41, 1851 –1864.

Wang, Z.M., Kanoh, H., Kaneko, K., Lu, G.Q., Do, D. (2002) Structural and surface property changes of macadamia nut-shell char upon activation and high temperature treatment, *Carbon* 40, 1231–1239.

Wang, S., Boyjoo, Y., Choueib, A. (2005) A comparative study of dye removal using fly ash treated by different methods, *Chemosphere*, 60, 1401-1407.

Wang, T., Tan, S., Liang, C. (2009) Preparation and characterization of activated carbon from wood via microwave-induced $ZnCl_2$ activation, *Carbon*, 47, 1880-1883.

Wang, J., Peng, X., Luan, Z., Zhao, C. (2010) Regeneration of carbon nanotubes exhausted with dye reactive red 3BS using microwave irradiation, *Journal of Hazardous Materials*, 178, 1125-1127.

Williams, P.T., Reed, A.R. (2006) Development of activated carbon pore structure via physical and chemical activation of biomass fibre waste, *Biomass and Bioenergy* 30, 144–152.

Yagmur, E., Ozmak, M., Aktas, Z. (2008) A novel method for production of activated carbon from waste tea by chemical activation with microwave energy, *Fuel,* 87, 3278-3285.

Yang, K., Peng, J., Srinivasakannan, C., Zhang, L., Xia, H., Duan, X. (2010) Preparation of high surface area activated carbon from coconut shells using microwave heating, *Bioresource Technology*, 101, 6163-6169.

Yeganeh, M.M., Kaghazchi, T., Soleimani, M. (2006) Effect of Raw Materials on Properties of Activated Carbons, *Chem. Eng. Technol.* 29, 1247–1251.

Yuen, F. K. and Hameed, B.H. (2009) Recent developments in the preparation and regeneration of activated carbons by microwaves, *Advances in Colloid and Interface Science,* 149, 19-27.

Zhang, S., Qu, W., Peng, J., Zhang, L., Ma, X., Zhang, Z., Li, W. (2009) Comparison between microwave and conventional thermal reactivations of spent activated carbon generated from vinyl acetate synthesis, *Desalination*, 249, 247-252.

Zou, X., Wan, X., Shi, H., Wang, D. (2009) Adsorption of 2,4-dichlorophenol from aqueous solution onto microwave modified activated carbon: Kinetics and equilibrium, *Transactions of Tianjin University*, 15, 408 – 414.

Zuo, S., Yang, J., Liu, J., Cai, X. (2009a) Significance of the carbonization of volatile pyrolytic products on the properties of activated carbons from phosphoric acid activation of lignocellulosic material, *Fuel Processing Technology* 90, 994–1001.

Zuo, S., Liu, J., Yang, J., Cai, X. (2009b) Effects of the crystallinity of lignocellulosic material on the porosity of phosphoric acid-activated carbon, *Carbon* 47, 3574 –3584.

In: Activated Carbon
Editor: James F. Kwiatkowski
ISBN: 978-1-61209-684-1
©2012 Nova Science Publishers, Inc.

Chapter 6

ACTIVATED CARBONS: CLASSIFICATIONS, PROPERTIES AND APPLICATIONS

John U. Kennedy Oubagaranadin[1] and Z. V. P. Murthy[2] *

[1] Department of Ceramic and Cement Technology, PDA College of Engineering, Gulbarga 585102, Karnataka, India
[2] Department of Chemical Engineering, S.V. National Institute of Technology, Surat - 395007, Gujarat, India

ABSTRACT

Activated carbons are processed forms of carbon and are one of the most significant adsorbent materials due to their highly developed porosity, large surface area ranging from 500 to 3000 m^2/g, variable characteristics of surface chemistry, and high degree of surface reactivity. Most of the activated carbons are produced by a two-stage process, viz., carbonization followed by activation. The first-stage, carbonization, is to enrich the carbon content and to create an initial porosity and the second-stage, activation process, helps in enhancing the pore structure. Precursors to activated carbons are either of botanical origin (e.g., wood, coconut shells and nut shells) or of degraded and coalified plant matter (e.g., peat, lignite and all ranks of coal). Agricultural by-products are also considered as very important source material for the production of activated carbons as they are renewable and low-cost materials. Utilization of wastes as raw materials in the preparation of activated carbon is an interesting alternative to the expensive commercial activated carbons. Activated carbons may be obtained by physical activation (with steam or gaseous CO_2) or chemical activation by strongly reacting chemicals, such as $ZnCl_2$, H_3PO_4 and alkali-metal hydroxides (NaOH and KOH). Chemically activated carbons have good thermal stability, characteristic porous structure, and large internal surface area and porous volume. Activated carbons are classified in many ways, although a general classification can be made based on their physical characteristics, as powdered activated carbon, granular activated carbon, extruded activated carbon, impregnated carbon, polymer coated carbon and other types, such as cloths and fibers. They are used in specific applications. Powdered activated carbons are added directly to process units,

* E-mail: zvpm2000@yahoo.com, zvpm@ched.svnit.ac.in, Tel.: +91 261 2259571, 2201648 Fax: +91 261 2227334

granulated carbons are used for deodorization and for the separation of components in flow systems, extruded activated carbons are mainly used for gas phase applications, impregnated carbons are used for specific applications in air pollution control and polymer coated carbons are useful for hemoperfusion. Properties of activated carbon are: its specific surface area, iodine index, molasses index, tannin index, methylene blue index, butane index, carbon tetrachloride index, dechlorination half-value length, density, hardness number, ash content, porosity and particle size distribution. The indexes give an idea of the kind of pore a certain carbon has. Activated carbons are used in a wide range of applications that include medicinal uses, gas storage, pollutant and odor removal, gas separations, catalysis, gas purification, metal extraction, water purification, chromatographic separation, chemical purification, trapping mercury, fuel cells and many other applications. Carbon adsorption has numerous applications in industrial processes; such as spill cleanup, groundwater remediation, drinking water filtration, air purification, volatile organic compounds removal, gasoline dispensing operations, and other processes. With the development of technology, the applications of activated carbons keep expanding, with newer applications such as super-capacitors, electrodes, gas storage, and so on. This chapter deals with a short review of preparation of activated carbons from various raw materials reported in published literature in the recent past. In this chapter the various classifications, significance of various properties and applications of activated carbons are treated in detail with cross reference to a number of relevant publications.

1. INTRODUCTION

Activated carbons are the oldest adsorbents known (Hassler, 1963). The term active carbon stands for highly carbonaceous materials consisting mostly of carbon exhibiting large internal surface (Juntgen, 1977). Activated carbons are known to be very effective adsorbents due to their highly developed porosity, large surface area (that can reach 3000m^2/g), variable characteristics of surface chemistry, and high degree of surface reactivity (Bansal et al., 1988; Rodrígues-Reinoso, 1997). These unique characteristics make activated carbons very versatile materials, which have been studied not only as adsorbents, but also as catalysts and catalyst supports used for different purposes; such as the removal of pollutants from gaseous or liquid phases and the purification or recovery of chemicals (Derbyshire et al., 2001). Activated carbons are available in two main forms, viz., powdered activated carbon (PAC) and granular activated carbon (GAC). PAC is comprised of fine particles, less than about 0.2 mm in diameter, and thus presents large external surface area. GAC, on the other hand, is comprised of larger carbon particles, up to about 5 mm in diameter, with smaller external surface areas as compared to PAC. Powdered carbons are applied in a so-called batch-contact treatment; in this measured amounts of carbon and the substance to be treated are mixed and subsequently separated by filtration. With granular carbons, the gas or liquid to be purified is passed continuously through a bed of carbon. Formerly, granular carbons were used primarily in vapor-phase adsorption, but in recent years their use has been extended to liquid-phase applications. GAC can be regenerated, whereas this is often impossible with PAC due to the difficulty of separating the powdered adsorbent from the fluid. Activated carbon is manufactured according to the Ostrejko patents of 1900 and 1901 (Bartell and Sloan, 1929). Various materials like coal, coconut shells, lignite, wood and peat are commonly used for the preparation of activated carbons (Mattson and Mark, 1971). A wide variety of other materials have also been used by many workers as source materials (Aygün et al., 2003; Carrott et al.,

2003; Gupta and Ali, 2002; Juang et al., 2000; Kennedy et al., 2004; Márquez-Montesinos et al., 2001; Razvigorova et al., 1998; Warhurst et al., 1997). The properties of the finished activated carbons are influenced by the source material used and by conditions of activation. Consequently, carbons made by different procedures will be dissimilar in adsorptive properties, and can have diversity in specific utility.

2. METHODS OF TESTING FOR GRANULAR AND POWDERED ACTIVATED CARBONS

The following are the Indian Standards (IS 877:1989) for the testing of granular and powdered activated carbons.

2.1. Moisture

About 10 g of carbon is weighed accurately in a flat-bottomed Petri dish and placed in an electric oven maintained at 110 ± 5°C for about 4 hours. It is then taken out of the oven, covered and cooled in a desiccator and weighed. The procedure of heating, cooling and weighing is continued at half-an-hour intervals until the difference between two consecutive weighing is less than 5 mg. Then the moisture content can be calculated as

$$\text{Moisture content (\% mass)} = X = \frac{100\ (M - M_1)}{M}$$

where, M is the mass (g) of carbon taken for test and M_1 is the mass (g) of carbon after drying.

2.2. Ash

About 2 g of carbon (of known moisture content) is weighed accurately into a porcelain crucible (42 mm top diameter and 35 mm deep). The crucible with its contents is placed in an electric oven maintained at 110 to 120°C for about 4 hours. The crucible is removed from the oven and placed on a nichrome triangle and its content ignited with a flame from a Meker burner for 5 hours. The crucible is cooled in a desiccator and weighed. The above procedure of igniting, cooling and weighing is repeated at half-an-hour intervals until the difference between two consecutive weighings is less than 1 mg.

The preliminary drying of carbon in an oven is desirable, since if the moist sample is ignited then the liberation of moisture can throw a part of the material out of the crucible. An electric muffle furnace may be used with advantage in place of a Meker burner. Place the crucible in the furnace and heat at 1000°C for about 3 hours. Then the ash content can be found as

$$\text{Ash (on dry basis) by mass \%} = \frac{10000\ M_2}{M\ (100\ -\ X)}$$

where, M_2 is the mass (g) of ash content in the carbon taken for test.

2.3. Particle Size

The following Indian Standard (IS) test sieves; 500 μm, 250 μm, 125 μm, 63 μm and 53 μm; are thoroughly cleaned and dried before use. The sieves are nested in order, with 500 μm sieve on top. A 100 g of well mixed carbon powder is weighed accurately and transferred into the top sieve. The sieves are mounted on the mechanical shaker and shaken for 10 minutes. The material retained in each sieve is transferred to separate Petri dishes with the help of camel hair brush. The material collected from each sieve is weighed, and then the top sieve is removed and shaken separately. The sum of percentage of the material retained on each sieve plus the percentage passing through 53 μm IS sieve shall be 100.

2.4. Matter Soluble in Water

About 10 g of carbon of known moisture content is accurately weighed and transferred into a one-liter beaker. A 300 mL of water is added into that beaker and heated to boiling with continuous stirring. The contents are stirred for about 5 minutes after the flame is removed. Then the material is allowed to settle and the supernatant liquid is decanted through a Gooch crucible fitted with an asbestos mat. The above procedure is repeated three times, adding 300 mL of water to the residue in the beaker each time. After the fourth digestion, the volume is concentrated to less than 100 mL. The volume is then made up to 100 mL mark in a volumetric flask. A 50 mL of the concentrate is transferred to a shallow dish and evaporated as far as possible on a water-bath and finally dried in an electric oven maintained at 160±2°C. The dish is covered and cooled in a desiccator and weighed. The above procedure of drying, cooling and weighing is repeated at half-an-hour intervals until the difference between the two consecutive weighings is less than 5 mg. Then,

$$\text{Matter soluble in water (on dry basis), by mass \%} = \frac{20000\ M_3}{M\ (100\ -\ X)}$$

where, M_3 is the mass (g) of dried residue present in the material taken for test.

2.5. Matter Soluble in Acid

About 10 g of carbon of known moisture content is accurately weighed and transfer to a one-liter beaker. A 300 mL of 0.25 N hydrochloric acid is added to that beaker and heated to boiling with continuous stirring. Stirring is continued for about 5 minutes after the flame is removed. Then the material is allowed to settle and the supernatant liquid is decanted through

a Gooch crucible fitted with an asbestos mat into a two-liter beaker. The above procedure is repeated thrice, adding 300 mL of acid to the residue in the beaker each time. After the fourth digestion and decantation, the filtrate is concentrated to less than 100 mL. The volume is then made up to 100 mL mark in a volumetric flask. Exactly 50 mL of the concentrate is transferred to a shallow dish and evaporate to dryness on a water-bath and finally dried in an electric oven maintained at 160±2°C. The dish is covered, cooled in a desiccator and weighed. The above procedure of drying, cooling and weighing is repeated at half-an-hour intervals until the difference between two consecutive weighings is less than 5 mg. A blank is carried out using the same quantity of water and standard hydrochloric acid. Then,

$$\text{Acid soluble matter (on dry basis) by mass \%} = \frac{20000\ (A - B)}{M\ (100\ - X)}$$

where, A is the mass (g) of dried residue and B is the mass (g) of dried residue in the blank.

2.6. pH

About 10 g of the dried material is transferred to a 1000 mL beaker. A 300 mL of freshly boiled and cooled water (adjusted to *p*H 7) is added to that beaker and heated to boiling. Digestion is carried out for 10 minutes and filtered while hot, rejecting the first 20 mL of the filtrate. The filtrate is cooled to room temperature and then its *p*H is determined using glass electrode.

2.7. Iron

A 0.702 g of ferrous ammonium sulphate hexahydrate [$FeSO_4(NH_4)SO_4.6H_2O$] is dissolved in about 100 mL of water containing 10 mL of dilute sulphuric acid (10% *v*/*v*) and diluted to 1000 mL with water in a measuring flask. One milliliter of this solution contains 0.1 mg of iron (as Fe).

The ash from the carbon as obtained in Section *2.2* is transferred to a 150 mL conical flask using 50 mL of dilute hydrochloric acid. The slurry is heated to boiling; then 1 mL of concentrated nitric acid is added and again boiled for about 1 minute. It is then cooled and transferred to a 250 mL volumetric flask. A 20 mL of dilute sulphuric acid is added to this flask and made up to the mark with water. To 5 mL of this solution, a 5 mL of ammonium thiocyanate solution and a 20 mL of iso-amyl alcohol or ether are added in a Nessler cylinder and shaken well.

A control test is carried out in another Nessler cylinder by taking 2 mL of water, 5 mL of ammonium thiocyanate, 20 mL of iso-amyl alcohol or ether, 0.5 mL of dilute sulphuric acid, 2.5 mL of dilute hydrochloric acid and 2 drops of concentrated nitric acid. Standard iron solution is added drop-by-drop with the help of a micro-burette with constant stirring till the intensity of the color is same in both the cylinders. Then,

$$\text{Iron (as Fe) by mass \%} = \frac{0.4 \times V_1}{M}$$

where, V_1 is the volume (mL) of standard iron solution required for matching the color.

2.8. Determination of Decolorizing Power

A 0.15 g of methylene blue is dissolved in 100 mL of water. About 0.1 g of carbon is weighed accurately and transferred to a 50 mL glass stoppered flask. A 10 mL of methylene blue solution is added from a burette and shaken for 5 minutes.

After the first 10 mL are decolorized, then methylene blue solution (1 mL at a time) is added and shaken well till the blue color does not disappear for 5 minutes. Decolorizing power of carbon is expressed in terms of milligrams of methylene blue adsorbed by 1 g of activated carbon. Granular activated carbon for the purpose of this test has to be reduced to 75 μm IS sieve.

$$\text{Decolorizing power} = \frac{15 \times V_2}{10 \times M}$$

where, V_2 is the volume (mL) of methylene blue solution consumed.

2.9. Filtrability

A 200±0.1 g of refined groundnut oil is weighed in a 500 mL beaker. A 10 g of carbon is weighed accurately and added to the oil. The oil is heated to 90°C, mixing thoroughly with a glass rod. Wet filter paper (Whatman No. 1 is suitable) is placed inside a Buchner funnel with a little groundnut oil, taking care to avoid channeling effect.

The water-bath is heated and maintained at 90°C. The content of the beaker is thoroughly mixed and the entire mixture is immediately poured in the Buchner funnel. Vacuum is adjusted to an absolute pressure of 100±10 mm Hg. In another beaker a 200 g of groundnut oil is kept ready (without the material) heated up to 90°C (oil *A*).

As soon as the film of oil on the cake in the Buchner funnel disappears, the second batch of groundnut oil heated to 90°C (oil *B*) is poured into the Buchner funnel over the bed of the previous material. Stop-watch is started as soon as the filtered oil starts flowing from the funnel.

Vacuum is maintained at the absolute pressure of 100±10 mm Hg. The time taken for the oil film of the cake in the Buchner funnel to disappear is noted. At this point the vacuum will also drop. Filterability is then the time in minutes taken by the second batch of oil (oil *B*) to filter through the cake of the material. The filtration is continued till the rate of filtration falls to one drop per 15 seconds. The pump is stopped and the cake from the Buchner funnel is removed for the determination of oil retention as described in Section *2.10.*

2.10. Determination of Oil Retention

About 5 g of the cake obtained in Section *2.9* is weighted accurately on a filter paper (Whatman No. 42 is suitable), rolled and enclosed in a second filter paper folded in such a manner so as to prevent the cake from escaping (the second filter paper is left open at the top to serve as a thimble). A piece of absorbent cotton is placed on the top of the thimble to distribute the solvent evenly over the material. The wrapped material is placed in the Soxhlet extraction apparatus. Approximately 75 mL of the solvent is added into the tared extraction flask before attaching to the tube. A water-bath or electric hot-plate is heated at such a rate that the solvent drops from the condenser on the centre of the thimble at the rate of at least 150 drops per minute. The volume of the solvent is kept fairly constant by adding more solvent to make up the loss due to evaporation. Extraction is continued for 3 hours. The extraction flask is cooled and disconnected. The solvent is evaporated on a steam or water-bath until no odor of it remains. A gentle flow of clean and dry air may be used to facilitate removal of the solvent. The flask is cooled to room temperature, any moisture or dirt from the outside of the flask is removed carefully and then weighed. Heating, cooling and weighing is repeated until the difference between two successive weighings does not exceed 1 mg. The mass of oil retained in the extraction flask is found as

$$\text{Oil retained by carbon (by mass \%)} = \frac{100 \times M_4}{M_5}$$

where, M_4 is the mass (g) of oil retained in the extraction flask and M_5 is the mass (g) of filter cake taken for the determination of oil retention. The determination of oil retention should be done soon after the determination of filterability.

2.11. Hardness

About 50 g of carbon is weighed and transferred to a sieve bottom (pan) with fifteen 12.7 mm diameter and fifteen 9.5 mm diameter smooth steel balls. The pan is covered and shaken on a vibrating machine for 30 minutes. All the material is brushed out on to a 600 μm IS sieve and shaken separately on the vibrating machine for 3 minutes. The material remaining on the sieve is weighed. The hardness number is found as:

$$\text{Hardness number} = \frac{M_6 \times 100}{M}$$

where, M_6 is the mass (g) of material remaining on the sieve.

2.12. Adsorption Capacity for Carbon Tetrachloride

The material (carbon) is dried at 140° to 150°C for 4 hours and cooled in a desiccator. A volume of the dried material (carbon) sufficient to give a tapered column length of 15.0 cm in

the adsorption tube is transferred to the adsorption tube. The tube and the contents are weighted. The adsorption tube is placed in position in the thermostat, which is controlled at about 30°C. Sufficient time is allowed (about 30 minutes) for the material to reach temperature equilibrium with thermostat. An air-flow rate of 150 mL per minute through carbon tetrachloride is maintained. Passing of carbon tetrachloride-air mixture is continued with weighing of the adsorption tube every half-an-hour until no further gain in mass is evident. The gain in mass of carbon tetrachloride in 100 g for the material is recorded as adsorption capacity, which is calculated as

$$\text{Adsorption capacity of carbon (by mass \%)} = \frac{100 \times M_7}{M}$$

where, M_7 is the increase in mass (g) of the material.

2.13. Retentivity Index

Dry air at 30°C is passed through the material, after the measurement of carbon tetrachloride adsorption capacity as in Section *2.12* and weighed to constant mass. Then

$$\text{Retentivity index (by mass \%)} = \frac{M_8 - M_9}{M_8}$$

where, M_8 is the mass of material before passing dry air and M_9 is the mass of material after passing dry air.

2.14. Chloride

A 1.0 g of the sample of activated carbon of particle size less than 212 μm is taken and mixed with 5.0 g of the mixture *A* (containing 1 part by mass of sodium carbonate and 2 parts by mass of light calcined magnesium carbonate) in a porcelain dish. This mixture is covered with another 1.0 g of the mixture *A*. The porcelain dish containing the mixture is kept in a muffle furnace and heated slowly to 400°C and then rapidly to 800°C. The temperature is maintained at 800°C for 1 h. The fused mass is cooled and treated with concentrated nitric acid to dissolve the fused mass and filtered. A 100 mL of silver nitrate solution is added to the filtrate. The excess silver nitrate is titrated with standard ammonium thiocyanate solution using ferric alum solution as indicator. Prior to titration a few drops of nitrobenzene is added for masking the precipitate of silver chloride. The end point is indicated by the appearance of a wine red color. Then

$$\text{Chloride (by mass \%)} = 0.1773\,(100 - V_3 N)$$

where, V_3 is the volume (mL) of ammonium thiocyanate solution used in the titration and N is the concentration of ammonium thiocyanate solution.

2.15. Sulphate

A 1.0 g of activated carbon is taken in a porcelain dish and thoroughly mixed with the mixture *A* (containing 1 part by mass of sodium carbonate and 2 parts by mass of light calcined magnesium carbonate). This mixture is covered with 1.0 g of mixture *A* and placed in a muffle furnace. It is heated slowly to 400°C and then rapidly to 800°C. The temperature is maintained at 800°C for 1 h. It is then cooled and transferred to a 500 mL beaker. A 180 mL of water is added slowly and then 20 mL of concentrated hydrochloric acid is added slowly. The mass is digested on a hot plate for about 30 minutes. It is then filtered with Whatman filter paper (No. 42) and the residue is rejected. The filtrate is neutralized with the addition of concentrated ammonium hydroxide solution followed by 10 mL of barium chloride solution. It is then kept overnight and then filtered. The residue is washed with hot water till it is chlorine free. The residue is taken along with the filter paper in porcelain crucible and ignited at 850°C for 1 h. The residue is cooled and weighed. The sulphate is measured as

$$\text{Sulphate (by mass \%)} = \frac{41.12\, M_{10}}{M}$$

where, M_{10} is the mass in g of the residue.

2.16. Cyanogen Compounds

A 5.0 g of activated carbon is added to a solution of 2 g of tartaric acid in 50 mL of water contained in a distillation flask. The flask is attached to an efficient condenser with the outlet tube dipping below the surface of 10 mL of 1 N sodium hydroxide, and about 25 mL is distilled. To the liquid in the receiver 2 mL of ferrous sulphate solution is added and acidified to litmus paper with hydrochloric acid. The sample shall be considered as having passed the test for cyanogen compounds if no blue color is produced.

3. PREPARATION AND ACTIVATION OF CARBONS

Activated carbons can be prepared from a wide range of carbonaceous raw materials. Commercial activated carbons are produced from coal, wood and coconut shells. However, utilization of agricultural and forestry wastes as raw materials for the production of activated carbons have increased notably in recent years because they are very cheap and readily available. In the literature, a lot of research has been reported on activated carbons from agricultural wastes (Aljundi and Jarrah, 2008; Belhachemi et al., 2009; Li et al., 2008; Patnukao and Pavasant, 2008; Yorgun et al., 2009; Zabaniotou et al., 2008).

Basically, two main steps are involved in the preparation and manufacture of activated carbons, viz., (1) the carbonization of the carbonaceous raw material below 800ºC, in the absence of oxygen, and (2) the activation of the carbonized product (char), which is either physical or chemical.

3.1. Physical Activation

Physical activation is a two-step process. It involves carbonization of a carbonaceous material followed by the activation of the resulting char at elevated temperature in the presence of suitable oxidizing gases; such as carbon dioxide, steam, air or their mixtures. The activation gas is usually CO_2; since it is clean, easy to handle and it facilitates control of the activation process due to the slow reaction rate at temperatures around 800ºC (Zhang et al., 2004). Carbonization temperature range between 400 and 850ºC, and sometimes reaches 1000ºC, and activation temperature range between 600 and 900ºC.

3.2. Chemical Activation

In the chemical activation process the two steps are carried out simultaneously, with the precursor being mixed with chemical activating agents, as dehydrating agents and oxidants. Chemical activation offers several advantages; since it is carried out in a single step, combining carbonization and activation, performed at lower temperatures and therefore resulting in the development of a better porous structure. Besides, a part of the added chemicals (such as zinc salts and phosphoric acid) can be recovered easily (Tsai et al., 1997, 1998; Zhang et al., 2004). However, a two-step process (an admixed method of physical and chemical processes) can be applied (Oh and Park, 2002). The most common chemical agents are $ZnCl_2$, KOH, H_3PO_4 and K_2CO_3. In fact, this method (two-step chemical activation process), gives higher surface area.

3.3. Steam Pyrolysis / Activation

There is also an additional one-step treatment route, denoted as steam-pyrolysis (El-Hendawy et al., 2001; Fan et al., 2004; Girgis et al., 2002; Minkova et al., 2000, 2001; Savova et al., 2001), where the raw material is either heated at moderate temperatures (500 to 700°C) under a flow of pure steam, or heated at 700 to 800ºC under a flow of just steam.

3.4. Waste Materials for the Preparation of Activated Carbons

Activated carbon texture includes a wide range of pores that can be classified according to their width, viz., micropores (<2 nm), mesopores (2 to 50 nm) and macropores (450 nm) (Moreno-Castilla, 2004). In order to increase its adsorption capacity, the pore network should be developed during the preparation of activated carbon by application of adequate physical or chemical treatments. Physical activation is normally made by carbonization followed by activation using steam or CO_2; during carbonization, the material is pyrolyzed to remove non-carbon elements, then activation occurs, at temperatures ranging from 700 to 1100°C, using gases that open and develop the porosity of the carbonized material (Bansal et al., 1988; Rodrígues-Reinoso, 1997). Chemical activation is a one-step method used for the preparation of activated carbon; different chemical activating agents might be used. The chemical agents

help to develop the porosity, by means of dehydration and degradation; the mixture of the chemical and the carbon is then heated at a maximum of around 750°C. The use of a lower temperature, compared to physical activation, is compensated by the interaction between the chemicals and the carbon skeleton. The major advantages of chemical activation are the higher yield, lower temperature of activation (less energy costs), less activation time and, generally, higher development of porosity; among the disadvantages are the activating agents costs and the need to perform an additional washing stage to remove the chemical agent (Maciá-Agulló et al., 2004). To optimize preparation procedures, the parameters normally studied are time of carbonization, temperature and CO_2 / steam flow rate for physical activation; and time of impregnation and impregnation ratio of chemical agents in chemical activation. The characteristics of activated carbon (mainly its surface area) strongly depend on both the raw material and the activation procedure. Consequently, it is not possible to preview which is the activation procedure that yields a product with the highest surface area.

Activated carbons can be prepared from a wide variety of raw materials (Dąbrowski, 2001), which should be abundant and cheap, with high carbon content and low inorganic content; raw materials should be easily activated and should have low degradation by aging (Moreno-Castilla and Rivera-Utrilla, 2001). Coal is the most commonly used precursor, mainly due to its low cost and large supply (Ahmadpour and Do, 1997). The adsorption properties of each type of coal are determined by the nature of the vegetal material and the extent of the physical-chemical changes occurring during coal formation and after its deposition (Ahmedna et al., 2000). A wide variety of activated carbons have been prepared from different waste materials; viz., conventional wastes (from agriculture and wood industry) as well as non-conventional wastes (from municipal and industrial activities) have been used.

3.4.1. Conventional Wastes

Due to their abundance, agricultural wastes have low economic value; additionally, their current deposition creates significant environmental degradation. Agricultural waste is a rich source for the production of activated carbons due to its low ash content and reasonable hardness (Ahmedna et al., 2000); therefore, conversion of agricultural wastes into activated carbon is a promising alternative to solve environmental problems and also to reduce the costs of preparation of activated carbons. There are currently a large number of studies available regarding the use of several agricultural wastes to produce activated carbons. Most of them focus on the use of waste materials of considerable rigidity; such as the shells and/or stones of fruits like nuts, peanuts, olives, dates, almonds, apricots and cherries; however, wastes resulting from the production of cereals; such as rice, coffee, soybean, maize and corn as well as olive cakes, sugar cane and sugar beat bagasse, coir pith, oil-palm shell (from oil-palm processing mills) and various seed wastes were already used. The preparation of activated carbons from these materials has been made using both physical and chemical activation. In a study by Ioannidou and Zabaniotou (2007) an extensive revision regarding the preparation of activated carbons from agricultural residues is made and the effects of different parameters regarding activation procedures are presented. The structure of the raw material tends to strongly influence the best parameters needed to obtain a specific activated carbon. It is possible to obtain activated carbons with different pore texture by varying the activation conditions, therefore, optimizing their production for a specific purpose. High surface areas might be obtained, with values over 2500 m^2/g. Among the revised studies, chemical

activation was the most studied method, namely by using H_3PO_4, KOH, and $ZnCl_2$ as activating agents. Activated carbons prepared from different agricultural wastes have been used for several treatment purposes. There is a considerable amount of studies regarding the use of these materials (many of them considering chemical activation) to remove contaminants from aqueous phase; namely different types of dyes, herbicides, heavy metals and volatile organic compounds. Kadirvelu et al. (2003) showed that activated carbons prepared from agricultural solid wastes removed very significant amounts of different types of dyes, Hg(II) and Ni(II), in shorter time and with better adsorption rates and removal capacities than when applying other methods. Due to their particular porous characteristics, woody materials are very relevant and challenging raw materials to prepare activated carbons, namely for the adsorption of solutes in the liquid phase (Wu and Tseng, 2006). The wood industry is responsible to produce great amounts of woody waste materials that might be recycled to produce activated carbons. Also, several forest residues can be used, additionally contributing to a better forest management and conservation. Many studies were made concerning the recycling of these materials for the production of activated carbon. Woody materials of different types; such as cedar, fir, oak, as well as from tropical trees have already been used. Activation by using either physical or chemical method has been recently studied, namely the use of physical activation proceeded by chemical treatment using for instance H_2O_2 or H_2SO_4 as chemical agents. The use of such pre-treatments mainly influences the surface chemistry of the activated carbon, and lead to the preparation of enhanced adsorbents. Also, compression treatment of sapwood followed by carbonization was studied as a possible way of producing activated carbon, essentially microporous (Abe et al., 2001). The application of activated carbons prepared from woody materials has been made for the removal of contaminants; such as organic compounds, dyes, and heavy metals, from aqueous phase. These materials seem to be very effective in adsorbing heavy metals; such as chromium and copper, being considered potentially good substitutes of the commercial ones.

3.4.2. Non-Conventional Wastes

The economical activities in the modern society gradually created a pattern of mass production, mass consumption as well as mass deposition (Gao et al., 2005). As a consequence, there is an accumulation of several industrial and post-consumer waste products, which by their nature, are difficult or poorly effective to be regenerated into other materials and that more currently end up in incineration plants or landfills. Due to the more restricted environmental standards, limitations on the application of such alternatives are remarkably increasing. The discharge of plastic wastes; such as polyethylene terephthalate (PET) and polyvinyl chloride (PVC); industrial wastes; such as oil combustion residues and fabrics, as well as the discharge of tires, sewage sludges, and fertilizers; represents a serious challenge for waste management strategies. It is, therefore, of main relevance to find alternatives by which such materials can be reused or recycled according to environmentally acceptable procedures (Hayashi et al., 2005). The use of such non-conventional wastes as carbon source for the production of activated carbons might be an efficient alternative for both, adoption of effective waste management practices, and production of low-cost activated carbons. Plastic wastes, various industrial wastes like fly ashes, pitch, and polymeric residues from factories as well as other wastes such as tires and sewage sludge have been used as raw material for activated carbon production. For instance, a waste commercial ion-exchange resin might be used to prepare activated carbon with values of specific surface area and pore

volume suggesting its application in different purposes that might include aqueous-phase treatments (Gun'ko et al., 2005). Also, activated carbon can be successfully prepared from both old newspaper and paper prepared from simulated paper sludge by physical and chemical activation (Okada et al., 2003). Due to the nature of most of the raw materials, such as plastics and polymeric materials, activated carbon fibers are the physical form of activated carbon more commonly prepared. There is quite a great amount of recent studies on the application of activated carbons prepared from non-conventional waste materials for the removal of pollutants from aqueous phases (Gupta et al., 1997a,b, 2000, 2004, 2005; Jain et al., 2003a,b). Among the contaminants that might be removed using these adsorbents are organic compounds of variable nature namely phenol and its derivatives, and different types of dyes and heavy metals such as mercury, nickel, and copper. The use of industrial wastes loaded with chemicals such as organometallics, could even be used to prepare activated carbon with antibacterial activity (Tamai et al., 2001). The prepared activated carbons are expected to be economically viable and the adsorption mechanism is, in several studies, fundamentally dependent on the solution pH. Generally, the adsorbents present good development of both chemical surface and porosity.

4. CLASSIFICATION OF ACTIVATED CARBONS

Activated carbons are complex products which are difficult to classify on the basis of their behavior, surface characteristics and preparation methods. However, some broad classification is made for general purpose based on their physical characteristics.

4.1. Powdered Activated Carbon (PAC)

Traditionally, active carbons are made in particular form as powders or fine granules of less than 1.0 mm in size with an average diameter between 0.15 and 0.25 mm. Thus, they present a large surface-to-volume ratio with a small diffusion distance. PAC is made up of crushed or ground carbon particles, 95 to 100% of which will pass through a designated mesh sieve or sieve. Granular activated carbon (GAC) is defined as the activated carbon being retained on a 50 mesh sieve (0.297 mm) and PAC material as finer material, while ASTM classifies particle sizes corresponding to an 80 mesh sieve (0.177 mm) and smaller as PAC. The PAC is normally mixed with the liquid to be treated and afterwards disposed-of. Due to its small particles, adsorption on PAC is normally very effective, however, and for the same reasons, settling and removal tend to be slower than when GAC is used.

4.2. Granular Activated Carbon (GAC)

Granular activated carbon has a relatively larger particle size compared to powdered activated carbon and consequently, presents a smaller external surface. Diffusion of the adsorbate is thus an important factor. These carbons are therefore preferred for all adsorption of gases and vapors as their rates of diffusion are faster. Granulated carbons are used for

water treatment, deodorization and separation of components of flow system. GAC can be either in the granular form or extruded. GAC is designated by sizes such as 8×20, 20×40, or 8×30 for liquid phase applications and 4×6, 4×8 or 4×10 for vapor phase applications. A 20×40 carbon is made of particles that will pass through a U.S. Standard Mesh Size No. 20 sieve (0.84 mm) (generally specified as 85% passing) but will be retained on a U.S. Standard Mesh Size No. 40 sieve (0.42 mm) (generally specified as 95% retained). American Water Works Association (AWWA) B604 uses the 50 mesh sieve (0.297 mm) as the minimum GAC size. The most popular aqueous phase carbons are the 12×40 and 8×30 sizes because they have a good balance of size, surface area, and head loss characteristics. GAC can be prepared from hard material, such as coconut shells. It is commonly used as column filler for gas or liquid treatments and can be regenerated after use.

4.3. Extruded Activated Carbon (EAC)

Extruded activated carbon combines powdered activated carbon with a binder, which are fused together and extruded into a cylindrical shaped activated carbon block with diameters from 0.8 to 130 mm. These are mainly used for gas phase applications because of their low pressure drop, high mechanical strength and low dust content.

4.4. Impregnated Carbon

Porous carbons containing several types of inorganic impregnants, such as iodine and silver; cations such as Al, Mn, Zn, Fe, Li, and Ca have also been prepared for specific application in air pollution control, especially in museums and galleries. Due to antimicrobial / antiseptic properties, silver loaded activated carbon is used as an adsorbent for purification of domestic water. Drinking water can be obtained from natural water by treating the natural water with a mixture of activated carbon and $Al(OH)_3$, a flocculating agent. Impregnated carbons are also used for the adsorption of H_2S and thiols. Adsorption rates for H_2S as high as 50% by weight have been reported.

4.5. Polymer Coated Carbon

This is a process by which a porous carbon can be coated with a biocompatible polymer to give a smooth and permeable coat without blocking the pores. The resulting carbon is useful for hemoperfusion (a treatment technique in which large volumes of the patient's blood are passed over an adsorbent substance in order to remove toxic substances from the blood).

4.6. Other Types

Activated carbon is also available in special forms such as cloths and fibers. The “carbon cloth” for instance is used in personnel protection for the military.

5. PROPERTIES OF ACTIVATED CARBONS

5.1. Specific Surface Area

A gram of activated carbon can have a surface area in excess of 500 m^2, with 1500 m^2 being readily achievable. The BET surface area of char is important because it may strongly affect the reactivity and combustion behavior of the char. The chars from pyrolysis above 400ºC had a surface area and a high surface area formed (Putun et al., 2005). In the study of Tsai et al. (Tsai et al., 1997, 1998) surface areas were observed to decrease at higher pyrolysis temperature and soaking time. The higher surface areas are probably due to the opening of the restricted pores. The percentage of micropores followed the increase of pyrolysis temperature, but this rate of increase was not as fast as the rate of declination in surface areas. The BET surface areas which calculated in the research of Tsai et al. (1997, 1998) were observed to increase at higher activation temperature, for both KOH and K_2CO_3 series, and the maximum rate of increase in BET surface area occurred between 650 and 700ºC.

5.2. Iodine Index

Iodine number is defined as the milligrams of iodine adsorbed by one gram of carbon when the iodine concentration in the residual filtrate is 0.02 normal. Basically, iodine number is a measure of the iodine adsorbed in the pores and, as such, is an indication of the pore volume available in the activated carbon of interest. Typically, water treatment carbons have iodine numbers ranging from 600 to 1100. Frequently, this parameter is used to determine the degree of exhaustion of a carbon in use. However, this practice should be viewed with caution as chemical interactions with the adsorbate affect the iodine uptake giving false results. Thus, the use of iodine number as a measure of the degree of exhaustion of a carbon bed can only be recommended if it has been shown to be free of chemical interactions with adsorbates and if an experimental correlation between iodine number and the degree of exhaustion has been determined for the particular application.

5.3. Molasses Index

Molasses number is a measure of the degree of decolorization of a standard molasses solution that has been diluted and standardized against standardized activated carbon. It is a measure of the mesopore content of the activated carbon (greater than 20 Å, or larger than 2 nm) by adsorption of molasses from solution. A high molasses number indicates a high adsorption of big molecules (range 95 to 600). Caramel dp (decolorizing performance) is similar to molasses number. Molasses efficiency is reported as a percentage (range 40% to 185%) and parallels molasses number (600 = 185%, 425 = 85%). The European molasses number (range 525 to 110) is inversely related to the North American molasses number. Frequently, this parameter is useful in evaluating a series of active carbons for their rates of adsorption. Given two active carbons with similar pore volumes for adsorption, the one

having the higher molasses number will usually have larger feeder pores resulting in more efficient transfer of adsorbate into the adsorption space.

5.4. Tannin Index

Tannins are a mixture of large and medium size molecules. Carbons with a combination of macropores and mesopores adsorb tannins. The ability of a carbon to adsorb tannins is reported in parts per million concentrations (range 200 ppm to 362 ppm).

5.5. Methylene Blue Index

Some carbons have a mesopore (20 Å to 50 Å, or 2 to 5 nm) structure which adsorbs medium size molecules, such as the dye methylene blue. Methylene blue adsorption is reported in g/100g (range 11 to 28 g/100g).

5.6. Butane Index

The butane index measures the number of grams of butane adsorbed by 100 g of activated carbon. Its value may range from 20 to 80%. Certain standards also refer to the BWC (Butane Working Capacity), a volumetric index that measures the number of grams of butane adsorbed by 100 mL of carbon, with deduction made of the quantity restored by natural desorption. The butane index only estimates adsorption capacity.

5.7. Carbon Tetrachloride Index

Carbon tetrachloride index is the measurement of the porosity of an activated carbon by the adsorption of saturated carbon tetrachloride vapor.

5.8. Dechlorination Half-Value Length

Some carbons are evaluated based on the dechlorination half-value length, which measures the chlorine-removal efficiency of activated carbon. The dechlorination half-value length is the depth of carbon required to reduce the chlorine level of a flowing stream from 5 ppm to 3.5 ppm. A lower half-value length indicates superior performance.

5.9. Density

Higher density provides greater volume activity and normally indicates better quality activated carbon.

5.10. Hardness / Abrasion Number

It is a measure of the activated carbon's resistance to attrition. It is an important indicator of activated carbon to maintain its physical integrity and withstand frictional forces imposed by backwashing, etc. There are large differences in the hardness of activated carbons, depending on the raw material and activity level.

5.11. Ash Content

It reduces the overall activity and the efficiency of reactivation of activated carbon. The metal oxides (Fe_2O_3) can leach out of activated carbon resulting in discoloration. Acid / water soluble ash content is more significant than total ash content. Soluble ash content can be very important for aquarists, as ferric oxide can promote algal growths; a carbon with low soluble ash content should be used for marine, freshwater fish and reef tanks to avoid heavy metal poisoning and excess plant/algal growth.

5.12. Porosity

Both the size and distribution of micropores, mesopores and macropores determine the adsorptive properties of activated carbons. For instance, small pore size will not trap large adsorbate molecules and large pores may not be able to retain small adsorbates, whether they are charged, polar molecules or uncharged, non-polar compounds (Ahmedna et al., 2004). Materials with a greater content of lignin (grape seeds, cherry stones) develop activated carbons with macroporous structure, while raw materials with a higher content of cellulose (apricot stones, almond shells) yield activated carbon with a predominantly microporous structure (Savova et al., 2001).

5.14. Particle Size Distribution

The finer the particle sizes of an activated carbon, the better the access to the surface area and faster the rate of adsorption kinetics. In vapor phase systems this needs to be considered against pressure drop, which will affect energy cost. Careful consideration of particle size distribution can provide significant operating benefits.

6. APPLICATIONS OF ACTIVATED CARBONS

Activated carbon is used in gas purification, gold purification, metal extraction, water purification, medicine, sewage treatment, air filters in gas masks and respirators, filters in compressed air and many other applications. One major industrial application involves use of activated carbon in the metal finishing field. It is very widely employed for purification of

electroplating solutions. Activated carbon treatment removes such impurities and restores plating performance to the desired level.

6.1. Applications and Uses of Agricultural Based Active Carbons

Activated carbons concern many industries as diverse as food processing, pharmaceuticals, chemical, petroleum, mining, nuclear, automobile and vacuum manufacturing, because of their adsorptive properties, which results in their extensive internal pore structure. Such high porosity is a function of both the precursor as well as the scheme of activation (El-Hendawy et al., 2001). The chemical nature of activated carbons significantly influences its adsorptive, electrochemical, catalytic, and other properties. Generally speaking, activated carbons with acidic surface chemical properties are favorable for basic gas adsorption, such as ammonia, while activated carbons with basic surface chemical properties are suitable for acidic gas adsorption, such as sulphur dioxide (Yang and Lua, 2003).

6.1.1. Application in Gas-Phase Adsorption

Activated carbons may be used as adsorbents for air pollution control, as they can effectively treat industrial gas, and indoor air environments (Tsai et al., 1998). Due to their large number of micropores and the high surface area (high adsorption capacities) they can be used as catalysts for gas purification, separation and deodorization. Adsorption by commercial activated carbons offers an efficient technology for removing volatile organic compounds (VOCs) from air pollution sources, owing to their large specific surface areas, high micropore volumes and rapid adsorption capabilities (Yates et al., 2000). Furthermore, several microporous activated carbons from various manufacturers were selected to study the viability of using monolithic adsorption units, capable of regeneration for the purification of effluent gas streams (Yates et al., 2003).

The removal processes for SO_x and NO_x can be designed using activated carbon fiber (ACF) for the environment of busy traffic crossings, parking spaces, and large halls as well as for exhaust gases, such as the flue gas from a power plant, catalyst regeneration for fluidized catalytic cracking (FCC) process, and ventilated gas from motorway tunnels (Mochida et al., 2000). Activated carbons are also used for removing mercury vapors from a gas mixture containing H_2S, O_2 and moisture that is representative of the exhaust gas emissions of the geothermal power plants (Vitolo and Seggiani, 2002).

6.1.2. Application in Liquid-Phase Adsorption

Liquid phase adsorption applies to many purification processes, one of the most relevant has been the wastewater treatment, e.g., by rice husk carbons (Daifullah et al., 2003), the drinking water (Heijman and Hopman, 1999), the industrial effluents purification (Pintar, 2003), simulated heavy metal bearing wastewater (Oubagaranadin et al., 2007; Oubagaranadin and Murthy, 2009) and ground water treatment, e.g., Jordanian olive stones (El-Sheikh et al., 2004). Adsorption of methylene blue has been one of the most important means of assessing removal capacity from the aqueous phase. Phosphoric acid activated carbons are the best in the uptake of methylene blue from aqueous solutions (200 to 400 mg/g) (Girgis et al., 2002). Porous carbons with high surface area and adsorption capacities

for methylene blue and iodine could be obtained from a rice straw precursor (Oh and Park, 2002), particularly by the two-stage method, in which the raw rice straw is carbonized at the first stage and activated with KOH at the subsequent stage. From the one-stage method, porous structure of only moderate performance could be obtained, because the ash-formation makes it difficult to increase the optimum temperature at which micropores can be created. Activated carbons are used for the removal of phenols, phenolic compounds (Dabrowski et al., 2005; Dursun et al., 2005), heavy metals and dyes (Chuah et al., 2005; Ricordel et al., 2001), metal ions (Ho and Ofomaja, 2005; Kadirvelu et al., 2003) and mercury(II) (Namasivayam and Kadirvelu, 1999) from aqueous solutions. Phenolic derivatives belong to a group of common environmental contaminants. Their presence, even at low concentrations, can be an obstacle to the use and/or reuse of water. Phenols cause unpleasant taste and odor of drinking water and can exert negative effects on different biological processes. Phenolic derivatives are widely used as intermediates in the synthesis of plastics, colors, pesticides, insecticides, etc. Degradation of these substances means the appearance of phenol and its derivatives in the environment (Dabrowski et al., 2005). They can also adsorb arsenic (Manju et al., 1998) and trace metals (Ahmedna et al., 2004) from drinking water, or will be used as support for noble metals or as catalysts *per se* in liquid-phase reactions (Besson et al., 2005). Adsorption of acid dyes from aqueous solutions, like acid violet 17 from waste waters, by orange peel carbons (Sivaraj et al., 2001), or acid yellow 36 by rice husk carbons (Malik, 2003), is one of the most efficient methods. Carbons with low dye uptake (30 to 100 mg/g) are those chemically activated with $ZnCl_2$, KOH, steam pyrolyzed or chars (Girgis et al., 2002).

6.1.3. Application in the Remediation of Organics-Pesticides

Activated carbons are very efficient in the adsorption of nitrate and pesticides from surface waters (Aslan and Turkman, 2005; Ayranci and Hoda, 2005; Kouras et al., 1995; Murayama et al., 2003). Pitch-based activated carbon fibers are more effective in the atrazine removal dynamic tests than granular activated carbon if they are highly activated. The rapid adsorption kinetics of the atrazine with the highly activated carbon fibers seems to be the main reason for it having a better performance than granular activated carbon. This means that a fiber-type structure, with micropores directly accessible from the surface, is not enough reason to justify the good efficiency of ACF (Gullon and Font, 2001). Another carbon based material, Nyex 100 (Brown et al., 2004), was also used for the removal of atrazine to low levels (below 1 mg/L).

The feasibility of using activated carbon membranes as the solid phase for an on-line single step extraction-cleanup of fruits and vegetables for multi-residue screening was reported in literature (Sojo et al., 1997). The type of carbon present in these membranes (an acid-washed coconut charcoal) seems to be able to discriminate between compounds containing benzene rings with small substituents from those with bulky substituents. The origin of this selectivity may be due to the presence of active sites on the carbon surface. It is hypothesized that these sites are electron deficient sites, which could be deactivated by exposure to reducing agents, such as ascorbic acid. This is a property that could be exploited in the cleanup of samples for the isolation of compounds such as polyaromatic hydrocarbons (PAHs) and polychlorinated biphenyls (PCBs) from complex matrices such as soils and sediments.

6.1.4. Dye Removal Using Activated Carbons

A wide variety of carbons have been prepared from agricultural wastes; such as bagasse (Raghuvanshi et al., 2005; Valix et al., 2004), coir pith (Kavitha and Namasivayam, 2007; Namasivayam and Kavitha, 2002), banana pith (Namasivayam et al., 1998), date pits (Tan et al., 2008a,b), sago waste (Namasivayam et al., 1998), silk cotton hull (Namasivayam et al., 1998), corncob (Juang et al., 2002), maize cob (Namasivayam et al., 1998), palm kernel shell (Pollard et al., 1992), rice husk (Mohamed, 2004), fruit stones (Aygün et al., 2003), nutshells (Aygün et al., 2003), pinewood (Tseng et al., 2003), sawdust (Malik, 2003), coconut tree sawdust (Namasivayam et al., 1998) and soy hull (Mokhtar et al., 2006) were used for dye removal from aqueous solutions.

The effectiveness of adsorption on commercial activated carbons for the removal of a wide variety of dyes from wastewaters has made them as ideal alternatives to other expensive treatment options (Hameed and Daud, 2008). Commercially available activated carbons are usually derived from natural materials such as wood, coconut shell, lignite or coal, but almost any carbonaceous material may be used as precursor for the preparation of carbon adsorbents (Nasr et al., 2006). Because of its availability and cheapness, coal is the most commonly used precursor for activated carbon production (Carrasco-Marin et al., 1996). The sorption properties of each individual coal are determined by the nature of the original vegetation and the extent of the physical-chemical changes occurring after deposition (Juang et al., 2002). Coal based adsorbents were used by Mohan et al. (2002) for dye removal. However, since coal is not a pure material, it has a variety of surface properties and thus different sorption properties. The ability of activated carbon and different low-cost by-products and waste material as sorbents to remove various reactive dyes from aqueous solutions and wastewaters was investigated by several researchers (Demirbas, 2008; El Nemr et al., 2009; Hameed et al., 2008; Tan et al., 2008a,b).

Juang et al. (2002) reported that the adsorption capacities of activated carbons made from bagasse had very large values of adsorption capacity of dye onto carbon. Hameed and El-Khaiary (2008) showed that the adsorption does not always increase with surface area. Besides the physical structure, the adsorption capacity of a given carbon is strongly influenced by the chemical nature of the surface. The acid and base character of a carbon influences the nature of the dye isotherms. The adsorption is a complicated process depending on several interactions, such as electrostatic and non-electrostatic interactions.

The commercial activated carbon presents several disadvantages (Nasr et al., 2006). It is quite expensive, the higher the quality then greater the cost, non-selective and ineffective against disperse and vat dyes. The regeneration of saturated carbon is also expensive, not straightforward, and results in loss of the adsorbent. The use of carbons based on relatively expensive starting materials is also unjustified for most of pollution control applications (Streat et al., 1995). Activated carbons demonstrate a high capacity for both acid and basic dyes (Aleni and Koumanova, 2005). The effects of various experimental parameters of dye adsorption are initial pH, dye concentration, sorbent dosage, ion strength, and residence time. The inexpensive and readily available adsorbent provides an attractive alternative material for adsorption process. Mahogany sawdust was used to develop an effective carbon adsorbent (Malik, 2004). This adsorbent was employed for the removal of direct dyes from spent textile dyeing wastewater. The results indicate that the Mahogany sawdust carbon could be employed as a low cost alternative to commercial activated carbon in the removal of dyes from wastewater (Malik, 2004). The sorption kinetics and equilibrium of basic dye onto palm

kernel shell activated carbon studies suggested that it could be used as low cost alternatives in wastewater treatment for dye removal (Jumasiah et al., 2005).

6.2. Comparison of Active Carbons

Making a comparison among various waste-issued activated carbons, those obtained from agricultural are much better than those produced by another abundant waste such as used tires. Waste tires (Ariyadejwanich et al., 2003; San Miguel et al., 2001) give high pore volumes. However, using tires as raw material to produce activated carbons, the higher surface area that can be taken is 1260 m^2g (Ogasawara et al., 1987), and somehow it is lower than that obtained from agricultural residues. Generally, they can be used to adsorb phenols, p-chlorophenols, dyes, metals, lead, copper and chromium for the purification of drinking water and water treatment. They are suitable for the separation, storage and catalysis of gaseous species, and air pollution control (flue gas treatment). It was also found that steam-activated carbons have better adsorption capacity for dye (Black 5) and slightly lower phenol adsorption capacity in comparison with commercial carbons (Ariyadejwanich et al., 2003). If the activation is made with CO_2, the capacity for phenol and methylene blue is almost the same to that of the commercial carbons (Helleur et al., 2001). Commercial carbons can be used satisfactory enough, as post treatment in order to adsorb color, nitrate and dissolved organic carbon from drinking water, effluent water (Aslan and Turkman, 2005). Organic pollutants, like different kinds of pesticides, are also being removed by either powdered or granular or fiber activated carbons. Kouras et al. (1995) showed that a particular powdered active carbon produced by CHEMVIRON Company was very effective in cleaning surface waters by the adsorption of dodine. The result was even better when coagulants were used (polyelectrolyte, Al, Fe). The highest removal was observed when 50 mg/L PAC was mixed with ferric chloride (498.2%). Ayranci and Hoda (2005) supported that ACF and especially pitch-based, was more effective in the removal of atrazine than granular activated carbon. In their tests for waste-water purification it turned up that ACF (from Spectra corp.) had very high specific surface area, adsorption capacity and mechanical strength. A new collection method of organic chlorine pesticides in water samples (rainwater, river water, seawater) using an ACF filter (KF-175, TOYOBO) was proposed in the study of Murayama et al. (2003) to be effective and economical as compared to those by the conventional method. Brown et al. (2004), used a novel carbon-based adsorbent material (Nyex 100) for the removal of atrazine to low levels, below 1 mg/L, from aqueous solutions, which regenerated electrochemically, and has the ability to reach three times greater adsorptive capacities than originally achieved. This material does not have internal surface and pores, and it has low cost.

CONCLUSIONS

Activated carbons are the oldest adsorbents known. They are known to be very effective adsorbents due to their highly developed porosity and large surface area. Various materials like coal, coconut shells, lignite, wood and peat are commonly used for the preparation of

activated carbons. Agricultural wastes are a rich source of carbon. A wide variety of carbons have been prepared from agricultural wastes such as bagasse, coir pith, banana pith, date pits, sago waste, silk cotton hull, corncob, maize cob, palm kernel shell, rice husk, bagasse, fruit stones, nutshells, pinewood, sawdust, coconut tree sawdust, coir pith, soy hull etc. They can be used for the removal of various pollutants from aqueous solutions. The use of non-conventional wastes such as polyethylene terephthalate, polyvinyl chloride, oil combustion residues, fabrics, tires, sewage sludges, and fertilizers for the production of activated carbons might be an efficient alternative. The properties of the finished activated carbon are influenced by the source material used and by conditions of activation.

Activated carbons are prepared by the carbonization of the carbonaceous raw material below 800ºC, in the absence of oxygen, and the activation of the carbonized product (char), by either physical or chemical methods. Chemically activated carbons have been found superior to the physically activated carbons.

Activated carbons (i) have a capacity to virtually adsorb any contaminant, (ii) have a large capacity for organic molecules, especially solvents, (iii) can adsorb and retain a wide variety of chemicals at the same time, (iv) work well under a wide range of temperature and humidity conditions, (v) can be used as a carrier of one material to attract and hold or react with another material, and (vi) are inert and safe to handle and use.

Activated carbons are employed in many industries. They may be used as adsorbents for air pollution control and can be used as catalysts for gas purification, separation and deodorization. Activated carbons are also very efficient in the adsorption of nitrate and pesticides from surface waters.

REFERENCES

Abe I, Fukuhara T, Iwasaki S, Yasuda K, Nakagawa K, Iwata Y, Kominami H, Kera Y. 2001. Development of a high density carbonaceous adsorbent from compressed wood. *Carbon* 39, 1485–1490.

Ahmadpour A, Do DD. 1997. The preparation of activated carbon from macadamia nutshell by chemical activation. *Carbon* 35, 1723–1732.

Ahmedna M, Marshall WE, Husseiny AA, Rao RM, Goktepe I. 2004. The use of nutshell carbons in drinking water filters for removal of trace metals. *Water Research* 38, 1062–1068.

Ahmedna M, Marshall WE, Rao RM. 2000. Production of granular activated carbons from select agricultural by-products and evaluation of their physical, chemical and adsorption properties. *Bioresource Technology* 71, 113–123.

Aleni SJ, Koumanova B. 2005. Decolourisation of water/wastewater using adsorption. *Journal of the University of Chemical Technology and Metallurgy* 40, 175–192.

Aljundi IH, Jarrah N. J. 2008. A study of characteristics of activated carbon produced from Jordanian olive cake. *Journal of Analytical and Applied Pyrolysis* 81, 33–36.

Ariyadejwanich P, Tanthapanichakoon W, Nakagawa K, Mukai SR, Tamon H. 2003. Preparation and characterization of mesoporous activated carbon from waste tires. *Carbon* 41, 157–164.

Aslan S, Turkman A. 2005. Combined biological removal of nitrate and pesticides using wheat straw as substrates. *Process Biochemistry* 40, 935–943.

Ayranci E, Hoda N. 2005. Adsorption kinetics and isotherms of pesticides onto activated carbon-cloth. *Chemosphere* 60, 1600–1607.

Aygün A, Yenisoy-Karakaş S, Duman I. 2003. Production of granular activated carbon from fruit stones and nutshells and evaluation of their physical, chemical and adsorption properties. *Microporous and Mesoporous Materials* 66, 189–195.

Bansal RC, Donnet JB, Stoeckli F. 1988. In: *Active Carbon*. Marcel Dekker, New York.

Bartell FE, Sloan CK. 1929. Adsorption by pure carbon from non-aqueous binary systems over the entire concentration range. *Journal of the American Chemical Society* 51, 1643-1656.

Belhachemi M, Rios RVRA, Addoun F, Silvestre-Albero J, Sepulveda-Escribano A, Rodriguez-Reinoso F. J. 2009. Preparation of activated carbon from date pits: Effect of the activation agent and liquid phase oxidation. *Journal of Analytical and Applied Pyrolysis* 86, 168–172.

Besson M, Gallezot P, Perrard A, Pinel C. 2005. Active carbons as catalysts for liquid phase reactions. *Catalysis Today* 102–103, 160–165.

Brown NW, Roberts EPL, Chasiotis A, Cherdron T, Sanghrajka N. 2004. Atrazine removal using adsorption and electrochemical regeneration. *Water Research* 38, 3067–3074.

Carrasco-Marin F, Alvarez-Merino MA, Moreno-Castilla C. 1996. Microporous activated carbons from a bituminous coal. *Fuel* 75, 966–970.

Carrott PJM, Carrott MMLR, Mourão PAM, Lima RP. 2003. Preparation of activated carbons from cork by physical activation in carbon dioxide. *Adsorption Science and Technology* 21, 669–681.

Chuah TG, Jumasiah A, Azni I, Katayon S, Thomas Choong SY. 2005. Rice husk as a potentially low-cost biosorbent for heavy metal and dye removal: an overview. *Desalination* 175, 305–16.

Dąbrowski A. 2001. Adsorption - from theory to practice. *Advances in Colloid and Interface Science* 93, 135–224.

Dabrowski A, Podkoscielny P, Hubicki Z, Barczak M. 2005. Adsorption of phenolic compounds by activated carbon - a critical review. *Chemosphere* 58, 1049–70.

Daifullah AAM, Girgis BS, Gad HMH. 2003. Utilization of agro-residues (rice husk) in small waste water treatment plans. *Materials Letters* 57, 1723–1731.

Demirbas A. 2008. Products from lignicellulosic materials via degradation processes. *Energy Sources Part A 30*, 27–37.

Derbyshire F, Jagtoyen M, Andrews R, Rao A, Martín-Gullón I,Grulke E. 2001. *Carbon Materials in Environmental Applications*. Marcel Decker, New York.

Dursun G, Cicek H, Dursun AY. 2005. Adsorption of phenol from aqueous solution by using carbonised beet pulp. *Journal of Hazardous Materials* 125, 175–182.

El-Hendawy ANA, Samra SE, Girgis BS. 2001. *Adsorption characteristics of activated carbons obtained from corncobs. Colloids and Surfaces A: Physicochemical and Engineering Aspects* 180, 209–221.

El Nemr A, Abdelwahab O, El-Sikaily A, Khaled A. 2009. Removal of direct blue-86 from aqueous solution by new activated carbon developed from orange peel. *Journal of Hazardous Materials* 161, 102–110.

El-Sheikh AH, Newmana AP, Al-Daffaee HK, Phull S, Cresswell N. 2004. Characterization of activated carbon prepared from a single cultivar of Jordanian Olive stones by chemical and physicochemical techniques. *Journal of Analytical and Applied Pyrolysis* 71, 151–64.

Fan M, Marshall W, Daugaard D, Brown RC. 2004. Steam activation of chars produced from oat hulls and corn stover. *Bioresource Technology* 93, 103–107.

Gao NF, Kume S, Watari K. 2005. Zeolite - carbon composites prepared from industrial wastes: (I) Effects of processing parameters. *Materials Science and Engineering A* 399, 216–221.

Girgis BS, Yunis SS, Soliman AM. 2002. Characteristics of activated carbon from peanut hulls in relation to conditions of preparation. *Materials Letters* 57, 164–172.

Gullon MI, Font R. 2001. Dynamic pesticide removal with activated carbon fibers. *Water Research* 35, 516–520.

Gun'ko VM, Leboda R, Skubiszewska-Zieba J, Charmas B, Oleszczuk P. 2005. Carbon adsorbents from waste ion-exchange resins. *Carbon* 43, 1143–1150.

Gupta VK, Ali I. 2002. Adsorbents for water treatment: low cost alternatives to carbon. In: Hubbard, Arthur (Ed.), *Encyclopedia of Surface and Colloid Science*, Vol. 1. Marcel Dekker, New York.

Gupta VK, Ali I, Saini VK, Van Gerven T, Van Der Bruggen B, Vandecasteele C. 2005. Removal of dyes from wastewater using bottom ash. *Industrial and Engineering Chemistry Research* 44, 3655–3664.

Gupta VK, Mohan D, Sharma S, Sharma M. 2000. Removal of basic dyes (rhodamine B and methylene blue) from aqueous solutions using bagasse fly ash. *Separation Science and Technology* 35, 2097–2113.

Gupta VK, Srivastava SK, Mohan D. 1997a. Equilibrium uptake, sorption dynamics, process optimization, and column operations for the removal and recovery of malachite green from wastewater using activated carbon and activated slag. *Industrial and Engineering Chemistry Research* 36, 2207–2218.

Gupta VK, Srivastava SK, Mohan D, Sharma S. 1997b. Design parameters for fixed bed reactors of activated carbon developed from fertilizer waste for the removal of some heavy metal ions. *Waste Management* 17, 517–522.

Gupta VK, Suhas Ali I, Saini VK. 2004. Removal of rhodamine B, fast green, and methylene blue from wastewater using red mud, an aluminum industry waste. *Industrial and Engineering Chemistry Research* 43, 1740–1747.

Hameed BH, Chin LH, Rengaraj S. 2008. Adsorption of 4-chlorophenol onto activated carbon prepared from rattan sawdust. *Desalination* 225, 185–198.

Hameed BH, Daud FBM. 2008. Adsorption studies of basic dye on activated carbon derived from agricultural waste: *Hevea brasiliensis* seed coat. *Chemical Engineering Journal* 139, 48–55.

Hameed BH, El-Khaiary MI. 2008. Batch removal of malachite green from aqueous solutions by adsorption on oil palm trunk fibre: equilibrium isotherms and kinetic studies. *Journal of Hazardous Materials* 154, 237–244.

Hassler JW. 1963. Activated Carbon. *Chemical Publishing Company*, Inc., New York.

Hayashi J, Yamamoto N, Horikawa T, Muroyama K, Gomes VG. 2005. Preparation and characterization of high-specific-surface-area activated carbons from K_2CO_3-treated waste polyurethane. *Journal of Colloid and Interface Science* 281, 437–443.

Heijman SGJ, Hopman R. 1999. Activated carbon filtration in drinking water production: model prediction and new concepts. *Colloids and Surfaces A: Physicochemical and Engineering Aspects* 151, 303–310.

Helleur R, Popovic N, Ikura M, Stanciulescu M, Liu D. 2001. Characterisation and potential applications of pyrolytic char from ablative pyrolysis of used tires. *Journal of Analytical and Applied Pyrolysis* 58–59, 813–824.

Ho YS, Ofomaja AE. 2005. Kinetics and thermodynamics of lead ion sorption on palm kernel fibre from aqueous solution. *Process Biochemistry* 40, 3455–3461.

Ioannidou O, Zabaniotou A. 2007. Agricultural residues as precursors for activated carbon production - a review. Renewable and Sustainable Energy Reviews 11, 1966–2005.

IS 877:1989. Activated carbons, powdered and granular - methods of sampling and test.

Jain AK, Gupta VK, Bhatnagar A, Jain S, Suhas. 2003a. A comparative Assessment of adsorbents prepared from industrial wastes for the removal of cationic dye. *Journal of Indian Chemical Society* 80, 267–270.

Jain AK, Gupta VK, Bhatnagar A, Suhas. 2003b. Utilization of industrial waste products as adsorbents for the removal of dyes. *Journal of Hazardous Materials* 101, 31–42.

Juang R, Wu F, Tseng R. 2000. Mechanism of adsorption of dyes and phenols from water using activated carbons prepared from plum kernels. *Journal of Colloid and Interface Science* 227, 437–444.

Juang RS, Wu FC, Tseng RL. 2002. Characterization and use of activated carbons prepared from bagasses for liquid-phase adsorption. *Colloids and Surfaces A: Physicochemical and Engineering Aspects* 201, 191–199.

Jumasiah A, Chuah TG, Gimbon J, Choong TSY, Azni I. 2005. Adsorption of basic dye onto palm kernel shell activated carbon: sorption equilibrium and kinetics studies. *Desalination* 186, 57–64.

Juntgen H. 1977. New applications for carbonaceous adsorbents. *Carbon* 15, 273-283.

Kadirvelu K, Kavipriya M, Karthika C, Radhika M, Vennilamani N, Pattabhi S. 2003. Utilization of various agricultural wastes for activated carbon preparation and application for the removal of dyes and metal ions from aqueous solutions. *Bioresource Technology* 87, 129–132.

Kavitha D, Namasivayam C. 2007. Experimental and kinetic studies on methylene blue adsorption by coir pith carbon. *Bioresource Technology* 98, 14–21.

Kennedy LJ, Vijaya JJ, Sekaran G. 2004. Effect of two-stage process on the preparation and characterisation of porous carbon composite from rice husk by phosphoric acid activation. *Industrial and Engineering Chemistry Research* 43, 1832–1838.

Kouras A, Zouboulis A, Samara C, Kouimtzis T. 1995. Removal of pesticides from surface waters by combined physicochemical process. Part I: dodine. *Chemosphere* 30, 2307–2315.

Li W, Zhang L, Peng J, Li N, Zhu X. 2008. Preparation of high surface area activated carbons from tobacco stems with K_2CO_3 activation using microwave radiation. *Industrial Crops and Products* 27, 341–347.

Maciá-Agulló JA, Moore BC, Cazorla-Amorós D, Linares-Solano A. 2004. Activation of coal tar pitch carbon fibres: Physical activation vs. chemical activation. *Carbon* 42, 1367–1370.

Malik PK. 2003. Use of activated carbons prepared from sawdust and rice-husk for adsorption of acid dyes: a case study of Acid Yellow 36. *Dyes and Pigments* 56, 239–249.

Malik PK. 2004. Dye removal from wastewater using activated carbon developed from sawdust: adsorption equilibrium and kinetics. *Journal of Hazardous Materials* 113, 81–88.

Manju GN, Raji C, Anirudhan TS. 1998. Evaluation of coconut husk carbon for the removal of arsenic from water. *Water Research* 32, 3062–3070.

Márquez-Montesinos F, Cordero T, Rodríguez-Mirasol J, Rodríguez JJ. 2001. Powdered activated carbons from pinus caribaea sawdust. *Seperation Science and Technology* 36, 3191–3206.

Mattson JS, Mark HB. 1971. *Activated Carbon Surface Chemistry and Adsorption from Solution*. Marcel Dekker, New York.

Minkova V, Marinov SP, Zanzi R, Björnbom E, Budinova T, Stefanova M, Lakov L. 2000. Thermochemical treatment of biomass in a flow of steam or in a mixture of steam and carbon dioxide. *Fuel Processing Technology* 62, 45–52.

Minkova V, Razvigorova M, Bjornbom E, Zanzi R, Budinova T, Petrov N. 2001. Effect of water vapour and biomass nature on the yield and quality of the pyrolysis products from biomass. *Fuel Processing Technology* 70, 53–61.

Mochida I, Korai Y, Shirahama M, Kawano S, Hada T, Seo Y, Yoshikawa M, Yasutake A. 2000. Removal of SO_x and NO_x over activated carbon fibers. *Carbon* 38, 227–239.

Mohamed MM. 2004. Acid dye removal: comparison of surfactant modified mesoporous FSM with activated carbon derived from rice husk. *Journal of Colloid and Interface Science* 272, 28–34.

Mohan SV, Rao NC, Karthikeyan J. 2002. Adsorptive removal of direct azo dye from aqueous phase onto coal based sorbents: a kinetic and mechanistic study. *Journal of Hazardous Materials* 90B, 189–204.

Mokhtar A, Nargess YL, Niyaz MM, Nooshin ST. 2006. Equilibrium and kinetics studies for the adsorption of direct and acid dyes from aqueous solution by soy meal hull. *Journal of Hazardous Materials* 135, 171–179.

Moreno-Castilla C. 2004. Adsorption of organic molecules from aqueous solutions on carbon materials. *Carbon* 42, 83–94.

Moreno-Castilla C, Rivera-Utrilla J. 2001. Carbon materials as adsorbents for the removal of pollutants from the aqueous phase. *Materials Research Society Bulletin* 26, 890–894.

Murayama H, Moriyama N, Mitobe H, Mukai H, Takase Y, Shimizu K, Kitayama Y. 2003. Evaluation of activated carbon fiber filter for sampling of organochlorine pesticides in environmental water samples. *Chemosphere* 52, 825–833.

Namasivayam C, Kadirvelu K. 1999. Uptake of mercury (II) from wastewater by activated carbon from an unwanted agricultural solid by-product: coirpith. *Carbon* 37, 79–84.

Namasivayam C, Kavitha D. 2002. Removal of Congo red from water by adsorption onto activated carbon prepared from coir pith, an agricultural solid waste. *Dyes and Pigments* 54, 47–58.

Namasivayam C, Prabha D, Kumutha M. 1998. Removal of direct red and acid brilliant blue by adsorption onto banana pith. *Bioresource Technology* 64, 77–79.

Nasr MF, Abo El-Ola SM, Ramadan A, Hashem A. 2006. A comparative study between the adsorption behavior of activated carbon fiber and modified alginate. I. Basic dyes adsorption. *Polymer - Plastics Technology and Engineering* 45, 335–340.

Ogasawara S, Mikiya K, Wakao N. 1987. Preparation of activated carbon by thermal decomposition of used automotive tires. *Industrial and Engineering Chemistry Research* 26, 2552–2556.

Oh GH, Park CR. 2002. Preparation and characteristics of rice-straw-based porous carbons with high adsorption capacity. *Fuel* 81, 327–336.

Okada K, Yamamoto N, Kameshima Y, Yasumori A. 2003. Porous properties of activated carbons from waste newspaper prepared by chemical and physical activation. *Journal of Colloid and Interface Science* 262, 179–193.

Oubagaranadin JUK, Sathyamurthy N, Murthy ZVP. 2007. Evaluation of Fuller's earth for the adsorption of mercury from aqueous solutions: A comparative study with activated carbon. *Journal of Hazardous Materials* 142, 165-174.

Oubagaranadin JUK, Murthy ZVP. 2009. Removal of Pb(II) from aqueous solutions by carbons prepared from Salwood (*Shorea robusta*). *European Journal of Wood and Wood Products* 67, 197-206.

Patnukao P, Pavasant P. 2008. Activated carbon from *Eucalyptus camaldulensis Dehn* bark using phosphoric acid activation. *Bioresource Technology* 99, 8540–8543.

Pintar A. 2003. Catalytic processes for the purification of drinking water and industrial effluents. *Catalysis Today* 77, 451–465.

Pollard SJT, Fowler GD, Sollars CJ, Perry R. 1992. Low cost adsorbents for waste and wastewater treatment: a review. *Science of the Total Environment* 116, 31–52.

Putun AE, Ozbay N, Onal EP, Putun E. 2005. Fixed-bed pyrolysis of cotton stalk for liquid and solid products. *Fuel Processing Technology* 86, 1207–1219.

Raghuvanshi SP, Singh R, Kaushik CP. 2005. Kinetics study of methylene blue dye boiadsorption on bagasse. *Applied Ecology and Environmental Research* 2, 35–43.

Razvigorova M, Budinova T, Petrov N, Minkova V. 1998. Purification of water by activated carbons from apricot stones, lignites and anthracite. *Water Research* 32, 2135–2139.

Ricordel S, Taha S, Cisse I, Dorange G. 2001. Heavy metals removal by adsorption onto peanut husks carbon: characterization, kinetic study and modelling. *Seperation and Purification Technology* 24, 389–401.

Rodrígues-Reinoso F. 1997. Introduction to Carbon Technologies. Publicaciones de la Universidad de Alicante, Spain (Chapter 2).

San Miguel G, Fowler GD, Dall-Orso M, Sollars CJ. 2001. Porosity and surface characteristic of activated carbons produced from waste tyre rubber. *Journal of Chemical Technology and Biotechnology* 77, 1–8.

Savova D, Apak E, Ekinci E, Yardim F, Petrova N, Budinova T, Razvigorova M, Minkova V. 2001. Biomass conversion to carbon adsorbents and gas. *Biomass and Bioenergy* 21, 133–142.

Sivaraj R, Namasivayam C, Kadirvelu K. 2001. Orange peel as an adsorbent in the removal of Acid violet 17 (acid dye) from aqueous solutions. *Waste Management* 21, 105–110.

Sojo LE, Brocke A, Fillion J, Price SM. 1997. Application of activated carbon membranes for on-line cleanup of vegetable and fruit extracts in the determination of pesticide multiresidues by gas chromatography with mass selective detection. *Journal of Chromatography* A 78, 141–154.

Streat M, Patrick JM, Pérez MJ. 1995. Sorption of phenol and parachlorophenol from water using conventional and novel activated carbons. *Water Research* 29, 467–472.

Tamai H, Katsu N, Ono K, Yasuda H. 2001. Antibacterial activated carbons prepared from pitch containing organometallics. *Carbon* 39, 1963–1969.

Tan IAW, Ahmad AL, Hameed BH. 2008. Optimization of preparation conditions for activated carbons from coconut husk using response surface methodology. *Chemical Engineering Journal* 137, 462–470.

Tan IAW, Ahmad AL, Hameed BH. 2008. Preparation of activated carbon from coconut husk: optimization study on removal of 2,4,6-trichlorophenol using response surface methodology. *Journal of Hazardous Materials* 153, 709–717.

Tsai WT, Chang CY, Lee SL. 1997. Preparation and characterization of activated carbons from corn cob. *Carbon* 35, 1198–1200.

Tsai WT, Chang CY, Lee SL. 1998. A low cost adsorbent from agricultural waste corn cob by zinc chloride activation. *Bioresource Technology* 64, 211–217.

Tseng RL, Wu FC, Juang RS. 2003. Liquid-phase adsorption of dyes and phenols using pinewood-based activated carbons. *Carbon* 41, 487–495.

Valix M, Cheung WH, McKay G. 2004. Preparation of activated carbon using low temperature carbonisation and physical activation of high ash raw bagasse for acid dye adsorption. *Chemosphere* 56, 493–501.

Vitolo S, Seggiani M. 2002. Mercury removal from geothermal exhaust gas by sulfur-impregnated and virgin activated carbons. *Geothermics* 31, 431–442.

Warhurst AM, McConnachie GL, Pollard SJT. 1997. Characterisation and application of activated carbon produced from moringa oleifera seed husks by single – step steam pyrolysis. *Water Research* 31, 759–766.

Wu FC, Tseng RL. 2006. Preparation of highly porous carbon from fir wood by KOH etching and CO_2 gasification for adsorption of dyes and phenols from water. *Journal of Colloid and Interface Science* 294, 21–30.

Yang T, Lua AC. 2003. Characteristics of activated carbons prepared from pistachio-nut shells by physical activation. *Journal of Colloid and Interface Science* 267, 408–417.

Yates M, Blanco J, Avila P, Martin MP. 2000. Honeycomb monoliths of activated carbons for effluent gas purification. *Microporous and Mesoporous Materials* 37, 201–208.

Yates M, Blanco J, Martin-Luengo MA, Martin MP. 2003. Vapour adsorption capacity of controlled porosity honeycomb monoliths. *Microporous and Mesoporous Materials* 65, 219–231.

Yorgun S, Vural N, Yorgun HD. 2009. Preparation of high-surface area activated carbons from Paulownia wood by $ZnCl_2$ activation. *Microporous and Mesoporous Materials* 122, 189–194.

Zabaniotou A, Stavropoulos G, Skoulou V. 2008. Activated carbon from olive kernels in a two-stage process: Industrial improvement. *Bioresource Technology* 99, 320–326.

Zhang T, Walawender WP, Fan LT, Fan M, Daugaard D, Brown RC. 2004. Preparation of activated carbon from forest and agricultural residues through CO_2 activation. *Chemical Engineering Journal* 105, 53–59.

In: Activated Carbon
Editor: James F. Kwiatkowski
ISBN: 978-1-61209-684-1
©2012 Nova Science Publishers, Inc.

Chapter 7

CARBON NANOFIBERS: SYNTHESIS, TYPES, PROPERTIES AND CHEMICAL ACTIVATION

Vicente Jiménez*, Paula Sánchez, Mª Luz Sánchez, Antonio Nieto-Márquez, José Luís Valverde and Amaya Romero[1]

[1]Facultad de Ciencias Químicas / Escuela Técnica Agrícola
Departamento de Ingeniería Química, Universidad de Castilla-La Mancha,
13071 Ciudad Real, Spain

ABSTRACT

Carbon materials are found in a variety of forms such as graphite, diamond, fullerenes, carbon nanofibers (CNFs), and carbon nanotubes (CNTs). Within the five, the nanostructured carbon materials have sparked an increasing interest for chemists, physicists, and material scientists worldwide. Carbon nanofibers have been recently innovated due to their unique properties, which have generated an interest in applications, including selective adsorption, hydrogen storage, polymer reinforcement and catalysts support.

To produce carbon nanostructures, three main techniques are generally used: arc discharge, laser ablation, and chemical vapor deposition. In general, chemical vapor deposition (CVD) results in carbon nanostructures that have a large diameter range, which can be poorly controlled.

There are mainly three types of carbon nanofibers: the herringbone, in which the graphene layers are stacked obliquely with respect to the fiber axis; the platelet, in which the graphene layers are perpendicular to the fiber axis; and the ribbon, in which the graphene layers are parallel to the growth axis.

High surface area, controlled pore size and pore size distribution are necessary for the application of those materials in a specific end use. Thus, the specific surface area and porosity of carbons nanofibers can be significantly modified by an activation process that removes the most reactive carbon atoms from the structure, increasing the surface area

* Tel.: +34-926295300 ; Fax: +34-926295318; E-mail address : vicente.jimenez@uclm.es

and porosity. The porous texture of the activated carbons depends strongly on both the activation process (chemical or physical) and the nature of the precursor.

It has been shown that some experimental variables have great influences on the porosity of the activated carbons prepared by chemical activation: nature of the metal hydroxide, nature of the inert gas, the mass ratio activating agent/CNFs, activation temperature and time, and the inert gas flow rate during the carbonization.

1. INTRODUCTION

Carbon materials are found in a variety of forms such as graphite, diamond, fullerenes, carbon nanospheres (CNSs), carbon nanofibers (CNFs) and carbon nanotubes (CNTs). It is necessary to note that the term "carbon nanotube" is normally used to refer to a structure with the graphene layers concentric to the tube axis and "carbon nanofiber" is a more general term referring to graphitic structures with other orientations of the graphene layers [1].

The large variety of structures, textures or surface chemistry associated to carbon materials has attracted a big research effort devoted to carbon production [2,3], characterization [4, 5], surface modification [6, 7] and use [8, 9]. In the last decades, the scientific community has attended an exponential increase in patent filings and publications related to these carbon nanomaterials [10]. As an example, the discovery of fullerenes in 1985 meant the Novel Laureate for Curl, Kroto and Smalley [11]. In 1889, Hughes and Chambers [12] reported that carbon filaments can grow from carbon containing gases using a metallic crucible as a catalyst. Robertson [13] was among the first to recognize that the interaction of methane and metal surface led to graphitic carbon at relatively low temperatures. But it was not until 1958 when Hillert and Lange recorded the first images of carbon nanofilaments employing electron transmission microscopy [14]. During almost the entire 20th century, the occurrence of these materials (essentially carbon nanofibers) was considered a nuisance, usually associated to industrial processes, deactivating catalysts and even attacking the reactor walls [15].

It was since the discovery [16] of carbon nanotubes in 1991 by Iijima when a real scientific revolution started, switching from being undesirable compounds to one of the most promising materials in a multitude of applications: manufacture of nanoconductors in electrical circuits, manufacture of composites and catalytic supports, up to its utilization in neurological medicine. Figure 1 shows a typical TEM image of carbon nanofibers.

Carbon nanofibers, the focus of this review, belong to the same family as fullerenes, being graphitic filamentous structures with diameters in the range of 0.4-500 nm, lengths of up to several millimeters and specific surface areas between 10-200 m^2/g. These carbon materials have unique properties, which have generated a huge interest in many applications, including selective adsorption [17], hydrogen storage [18], polymer reinforcement [19] and catalysts support [20]. Although the mechanical/chemical sector has accounted for around 73.5% of total revenues in 2007, other key sectors such as energy and electronics are also very important [21]. In many cases, the problem associated with these structures is that their specific surface area is not very high, a situation that is detrimental for many applications such as those regarding gas and energy storage, both of which are strongly dependent on the remarkable surface and structural properties of such materials. Thus, for example, a good

adsorbent usually has a high specific surface area, which arises from the presence of a reasonable number of micropores and high adsorption capacity [22, 23].

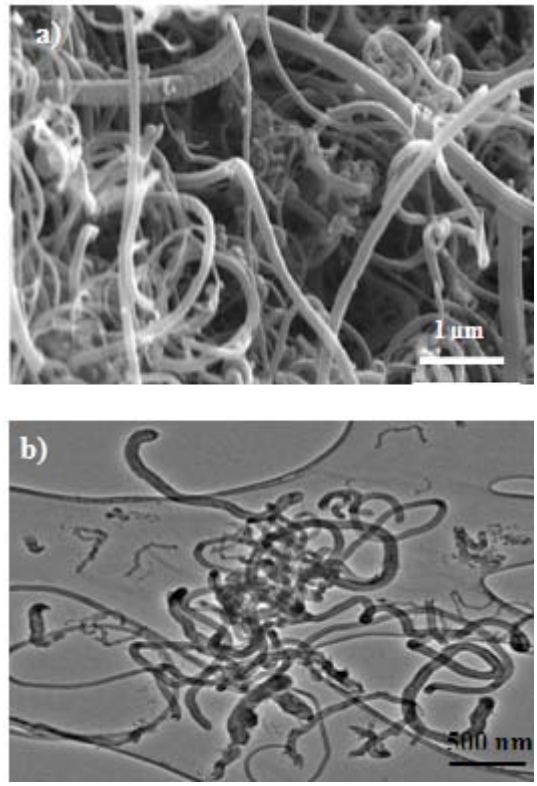


Figure 1. Representative images of carbon nanofibers: a) SEM and b) TEM.

In this regard, the porosity of carbons can be significantly modified by activation processes that remove the most reactive carbon atoms from their structure. There are essentially two different processes for the preparation of activated carbons, the so-called *physical* and *chemical* activation approaches. The great interest of carbon nanofibers in certain industry segments is in part, based on that alternative materials are characterized by their limited performance or much higher unit prices [10] (a good example is the utilization of carbon nanofibers as an alternative to carbon nanotubes for electron emitters in flat panel displays). The main problem associated with CNFs is that the lack of sufficient amount of material limits the development of more practical applications. For this reason, the development of a low cost and high productivity method to synthesize CNFs is of great importance, which would allow for novel applications for these materials [24]. In order to produce carbon nanostructures, three main techniques are generally used: arc discharge, laser ablation and chemical vapor deposition (in the presence of a catalyst). However, scientists are looking for more economic ways to produce these materials. In the laser ablation technique, a high-power laser beam impinges on a volume of carbon-containing feedstock gas (methane or carbon monoxide). Laser ablation produces a small amount of clean nanotubes, whereas arc discharge methods generally produce large quantities of impure materials. In general, chemical vapor deposition (CVD) results in carbon nanostructures that have a large diameter

range, which can be poorly controlled. Nevertheless, this method has the advantage that is comparatively simple, ease of control and low cost [15]. Moreover, CVD is easy to scale up, which favors commercial production [25]. There are mainly three types of carbon nanofibers: the herringbone, in which the graphene layers are stacked obliquely with respect to the fiber axis; the platelet, in which the graphene layers are perpendicular to the fiber axis; and the ribbon, in which the graphene layers are parallel to the growth axis [26, 27]. The morphology of CNFs depends on the temperature used during synthesis process and the catalytic metal and support used [28-30].

2. SYNTHESIS OF CARBON NANOFIBERS

Several methods have been established to synthesize carbon nanomaterials: arc discharge, laser ablation and chemical vapor deposition. As commented above, arc discharge and laser ablation have been employed in the synthesis of structured carbon [31-34] but these methods also produce a significant quantity of undesired by-product, such as carbon soot, that necessitates additional purification steps. Moreover, the associated low yields and high energy requirements have served as the impetus for the development of more efficient carbon production processes. Thus, the chemical vapor deposition (CVD) method has emerged as a promising method for carbon nanostructure synthesis, being able to control the final structure and to produce them in large quantities. Moreover, this method presents a high selectivity, a moderate cost and a feasible scale-up, which favors the commercial production [24, 25, 35, 36]. Another advantage of CVD is the possibility of conducting to a range of nanostructures, such as straight, bent or helical, and with much greater lengths [37]. Moreover, it is also possible to synthesize aligned carbon nanomaterials with high yields using the CVD method [38-40]. The advantages of this method increase if zeolites are applied as catalyst supports [41].

2.1. Arc Discharge Method

In 1992 Thomas Ebbessen y Pullickel Ajayan, from NEC laboratories [31], published the first method to produce macroscopic amounts of carbon nanofibers/nanotubes. This method consists of connecting two graphite rods with diameters between 0.5 and 40 mm to a feeding source with voltage of 20-50 V, these rods are separated by millimeters and then a switch is worked. When a current of 50-120 A appears between the rods under a pressure of 400 torr of helium, the carbon is evaporated in a hot plasm. Then, part of this evaporated carbon is condensed in the form of nanofibers/nanotubes.

The main characteristics of this method are:

- Yields of up to 30% by weight are obtained.
- The main limitation is that the nanofibers formed are generally short (50 microns or less) and are deposited in aleatory forms and sizes, with a wide distribution of diameters. During the process, amorphous carbon and fullerenes are also formed. Therefore, the selectivity is not higher.

The CNFs produced by this technique are typically bound together by strong van der Waals interactions and form tight bundles [42]. The first success in producing substantial amounts of carbon nanostructures by arc-discharge was achieved by Bethune et al. in 1993 [43]. The optimization of carbon nanostructures growth by arc-discarge was achieved by Journet et al. using a carbon anode containing 1.0 at.% of yttrium and 4.2 at.% of nickel as catalysts [44].

2.2. Laser Ablation

A research group from the University of Rice [32] was studying the bombard of a metal with intense pulses of laser to produce metallic molecules when they received the news of the discovery of carbon nanofibers/nanotubes. In their device, they substituted the metal with graphite rods. They produced carbon nanofibers/nanotubes using laser pulses instead of electricity, to generate a hot gas (1200 ºC) of carbon starting from the one that formed the carbon nanofibers/nanotubes. They tested several metal catalysts (Fe, Co, Ni) and they achieved the conditions under which large quantities of single-wall carbon nanotubes were produced. The main characteristics of this method are:

- Yields of up to 70% by weight are obtained
- Single-wall Carbon nanotubes are produced, with a range of diameters that can be controlled by varying the reaction temperature.
- The main disadvantage is the need for very expensive lasers.

The growth of high quality carbon materials at the 1-10 g scale was achieved by Thess et al. [45]. These nanostructures were produced mostly in form of ropes consisting of tens of individual nanotubes closely packed into hexagonal crystals via van der Waals interactons.

2.3. Chemical Vapour Deposition (CVD)

M. Endo, at the University of Pagano [46], introduced, in the carbon nanofibers production, the method of the chemical deposition in phase vapor (CVD). In the method, a substrate is placed inside the reactor which acts as a catalyst (Fe, Co, Ni) forming a thin film from 1 to 50 nm of thickness in an oven of inert atmosphere of helium at low pressure, it warms to 600 ºC and slowly methane, acetylene or ethylene, benzene, etc. gas is added liberating atoms of carbon which are recombined in order to form the carbon nanofibers. Due to the advantage of CVD method commented above, it has been extensively used for the production of carbon nanofibers [46-49]. The growth process involves heating a catalytic material to high temperatures (500-1000 ºC) in a tube furnace under a hydrocarbon flow. The catalytic species are typically transition-metal nanoparticles usually dispersed on a support material, such as porous aluminium oxide with large surface area. The main characteristics of this method are the following:

1. Yields of up to 100% by weight are obtained.

2. The CVD technique is the simplest of the three methods for its application at industrial scale.
3. The main disadvantage of this method is that the nanostructures synthesized can have a lot of defects. Thereby, these carbon nanofibers have only a 10% of the resistance to traction regarding those manufactured by the discharge of electric arch.

The mechanism of formation of carbon nanostructures that has generally been accepted is based on concepts of the vapor-liquid-solid theory developed by Wagner and Ellis [50]. This mechanism has been described more extensively in reviews by de Jong and Geus [24], Dai [42], Trimm [51], Rostrup-Nielsen [52], Bartholomew [53] Rodriguez [54] or Dupuis [55]. It includes hydrocarbon chemisorptions on a metal surface (transition metal), decomposition of the adsorbed hydrocarbon via surface reaction [56], subsequent segregation of surface carbon atoms into the layer near the surface, diffusion of carbon atoms through metal particles and then precipitation on the rare side of the particle [1, 42, 57, 58].

It is not clear at this point of the model which is the driving force for carbon diffusion within the catalytic particle. For some authors, this force is originated by the temperature gradient created in the particle by exothermic decomposition of the hydrocarbon at the exposed front face and endothermic deposition of carbon at the rear faces, which are initially in contact with the support [59, 60]. However, other authors explained the driving force to a concentration gradient [36, 52]. On the other hand, the metal-support interactions are found to play a determinant role for the growth mechanism [59, 61]. Weak interaction yielded tip-growth mode whereas strong interaction lead to base-growth [55].

2.4. Metals and Supports Used for CNF Growth

A large number of papers can be found in literature reporting CNF growth. The most important metals that are generally used to catalyse the growth of graphitic carbon nanofibers are transition metals. Thus, the most common metals are Ni [62-65], Co [41, 65-67], Fe [65, 68-70] or bi-metallic catalyst [71-73]. The special ability of these metals to promote CNF synthesis is associated with their capability to promote the decomposition of carbon precursors (linked to its electronic structure, i. e. overlap of non-filled 3d-orbitals with carbon orbital), the formation of meta-satable carbides, the diffusion of carbons and the formation of graphitic sheet, etc. [74, 75]. Besides, the structure of the filaments grown is strongly dependent on the metal used [76]. The finite solubility for carbon of 3d-metals in a certain temperature range [42] may play an important role in the growth process. Once the hydrocarbon molecules are broken, carbon atoms are believed to diffuse into the catalyst particle, leading to supersaturation of carbon in the metal [55]. Therefore, to understand the catalytic metal effect on the growth of CNFs it is necessary to consider the diffusion coefficient of carbon in bulk Fe, Co or Ni metals, for example (around $0.8x10^{-7}$, $0.2x10^{-7}$ and $1.2x10^{-7}$ cm^2/s, respectively, at 550 ºC) [77]. Thus, fishbone-type structures are usually formed from cobalt catalysts, tubular or ribbon-type and platelet-type from iron catalyst and fishbone-type from nickel catalyst [65]. The size of the catalyst nanoparticles seems to be the determining factor for the diameter of the carbon nanostructures grown on it. Additionally, small nanoparticles catalyse this growth better than the big ones, since they exhibit special electronic properties (and thus catalytic properties) as a consequence of their unusual ratio

surface atom/bulk atom [1]. In order to get CNFs of a given diameter, it is necessary to produce nanoparticles with a controlled size, what can be partially tuned by a proper selection of the preparation method of the catalyst [28, 78]. On the other hand, it has been demonstrated that the interactions between support and metal nanoparticles play an essential role in the whole growth process (affecting both the electronic structure of the nanoparticles as well as their morphology, and in turn, their catalytic properties). Among all of the catalytic supports, the most widely used are silicon or aluminium oxides and graphite [71, 79-81]. However, other supports have also been tested. Li et al. [38] have produced CNFs using iron nanoparticles supported over mesoporous materials; Iwasaki et al. [82] have synthesized CNFs by embedding cobalt nanoparticles in alumina nanoholes. Clay carbon templates were prepared by Barata-Rodrigues [83] for the diameter controlled synthesis of CNFs. De Lucas et al. used Fe-pillared clays [29] and Romero et al. CNFs [30] as an alternative for immobilizing the catalytic metal (Ni), in the synthesis of carbon nanostructures using ethylene as the carbon source. An alternative to prepare and produce nanoparticles of small enough sizes and well dispersed on the support surface in order to get nanostructures with the desired diameters, is to resort to porous supports, such as zeolites. Thus, zeolites used as the hosts to support or encapsulate the catalytic transition metal constitutes an alternative approach to selective and efficient synthesis of CNTs/CNFs. Hernadi et al. [41] first reported the use of zeolites as catalyst supports to synthesize CNTs and the chemical separation of the formed products from catalyst particles. Zeolites, being molecular sieve materials, have had a significant impact due to their high reactive surface area, structural homogeneity, and could be used in potential applications, such as petrochemical research [84] and micro-reactor technology [85].

2.5. Influence of the Hydrocarbon/H_2 Ratio

Several authors have suggested that hydrogen plays a significance role in the formation of CNFs [86, 87]. Thus, it is observed that the weight of solid carbon increases as the hydrocarbon/H_2 ratio decreases until an optimum value (i. e. De Lucas et al. observed the optimum value was 1.85 [28], Jiménez et al. was 4 [23] and Viera et al. was 0.2 [87]) and thereafter, exhibits a steady decline with a further decrease of this ratio. Hydrogen present in the feed could allow the rapid saturation of the valences at the face edges of the graphite planes, preventing the formation of amorphous carbon.

Moreover, the presence of hydrogen also prevents the carbon build-up on the nickel surface, which would ultimately lead to the catalysts' deactivation. However, the hydrogen concentration should be low enough to avoid surface carbon removal during the synthesis, which would lead to a lower CNF yield [28]. On the other hand, when there is no hydrogen in the feed, the catalytic activity could be very little, which is indicative that hydrocarbon would only decompose on metal surfaces in appreciable quantities if hydrogen had been co-adsorbed onto the metal surface [28].

3. TYPES OF CARBON NANOFIBERS

Figure 2 presents the main CNF structures. The type of carbon nanofibers formed depends on the type of metal used as a catalyst [65, 76] (as was explained previously) and, for the same metal, the synthesis temperature [23].

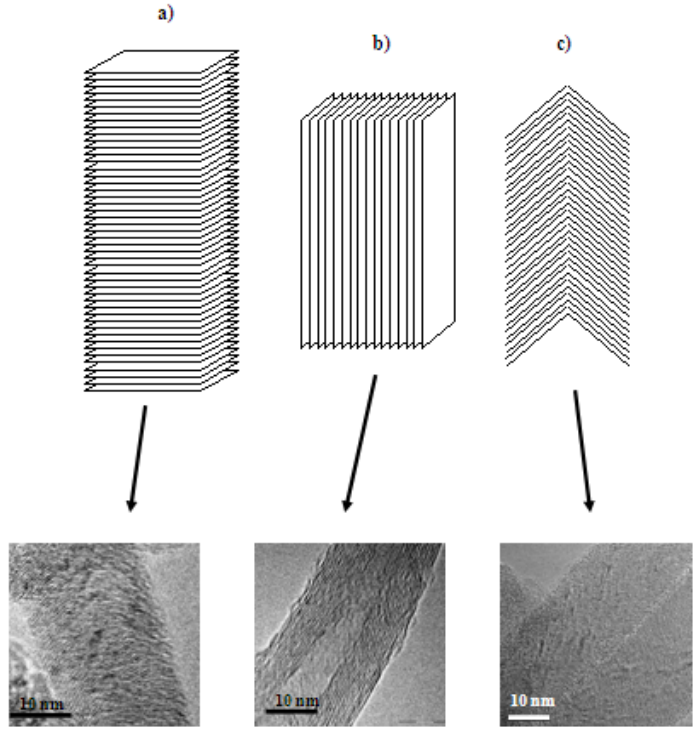


Figure 2. Different structures of carbon nanofibers: a) platelet CNFs, b) tubular/ribbon CNFs and c) fishbone/herringbone CNFs.

Thus, at low temperatures, less-structured carbon nanofibers will be formed: platelet CNFs; at higher temperatures, the most graphitic ones will be produced: ribbon CNFs; and at intermediate temperatures: herringbone CNFs. In platelet CNFs, the graphite layers are stacked parallel to the base and perpendicular to the fiber axis (Figure 2.a), in ribbon CNFs, the carbon atoms precipitate at the side faces of the metal particle, and the graphene layers are aligned parallel to the fiber axis (Figure 2.b). The central region of carbon nanofibers formed by this technique is generally hollow and these structures are commonly referred to as nanotubes.

Finally, Figure 2.c shows the structure that may be considered as an intermediate stacking arrangement between the previous cases. In these types of CNFs, the metal particles adopt a rhombic morphology and the nanofibers are precipitated from a pair of opposite faces to generate a structure in which the graphitic layers are aligned at an angle to the fibers axis; i.e. herringbone or fishbone [88].

Figure 3 shows the representative oxidation profiles (TPO) of CNFs produced at different temperatures and therefore, different types of CNFs. This technique is used to evaluate the graphitic degree of CNFs. It is evident that an increase in the reaction temperature leads to

more crystalline structures (tubular CNFs) [89], while at lower temperatures, mainly platelet CNFs are obtained, which are the least crystalline CNFs. Consequently, CNFs grown at lower temperatures have higher surface areas, more defects and exposed edge planes, and C-H/O-H groups, making them easier to oxidize [90]. While TPO analysis provides an indirect assessment of carbon structural order, the inferred trends find further support in XRD analyses. From XRD, the mean number of grapheme planes in the crystallites (npg), as a measurement of the graphitic character can be obtained. It is calculated using the formula npg = Lc/d_{002} where L_c is the average crystal domain size along a direction perpendicular to the basal planes in a graphitic-type structure, obtained from Scherrer's equation, and d_{002} is the average interlayer spacing obtained from Bragg's equation.

npg values increase with the synthesis temperature, indicating more graphitic carbon materials. At low reaction temperatures, carbon atoms are deposited as highly disordered carbon, usually as long nanofibers emerging from metallic particles. However, at higher temperatures, carbon atoms are deposited as a well-ordered, almost graphitic carbon usually associated with coatings of uniform thickness on metallic particles, also leading to a fast catalyst deactivation. [23, 28-30].

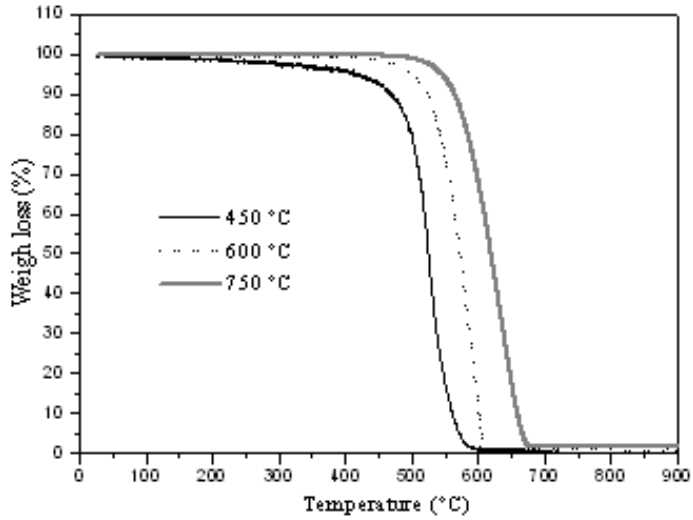


Figure 3. Representative TPO analysis associated with different types of CNFs (Reproduced with permission from Ref. [24]).

Typically, CNFs present type IV isotherms (according to IUPAC classification) characteristic of mesoporous materials. Figure 4 presents representative nitrogen adsorption-desorption isotherm associated with CNFs.

Additionally, these isotherms present a hysteresis loop, commonly related to capillary condensation in laminar mesopores. It is observed that as the operating temperature increases, the specific BET surface area of the deposited carbon decreases. Low specific surface areas of carbonaceous materials are typically assigned to highly ordered graphitic carbon and high specific surface areas with highly disordered carbons [91, 92].

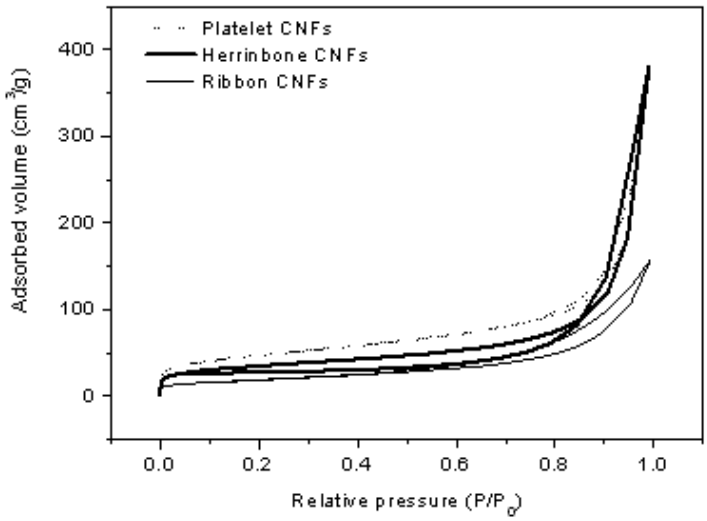


Figure 4. Representative N2 adsorption-desorption isotherms for different types of carbon nanofibers.

Finally, an increase in reaction temperature generates a wide range of CNFs diameters, which is attributed to thermal sintering of the metallic particles. As was previously mentioned, the CNFs diameter is governed by the size of the metal particle [93].

Summarizing, the following graphitic degree order is related to the different types of CNFs: tubular > herringbone > platelet.

4. PROPERTIES AND APPLICATIONS OF CNFS

Carbon nanofibers have unique electronic and mechanical properties, as well as low bulk density. These characteristics qualify these materials for a multitude of applications in different areas like electronics, catalyst support materials, energy storage or polymer additive, among others. Thus, depending on the CNF structure (diameter and chirality) [58, 94], these materials can be either a metal, semiconductor or small-gap semiconductor [95, 96].

Moreover, they present a high hardness (high Young's modulus, about 1.2 TPa) and tensile strength of about a hundred times higher than steel and can tolerate larges strains before mechanical failure [58, 94-96]. Thus, CNFs are appropriate candidates as components of fibers of high hardness, low weight and high electric conductivity [58, 97]. The main characteristics of these materials are:

- CNFs exhibit a high aspect ratio (length to width), that allows a better control of the unidirectional properties of the resulting materials.
- CNFs show a great mechanical resistance and a great flexibility, making them suitable for application as a polymer additive.
- CNFs present a high porosity that makes them good materials for gas storage, adsorption or as catalyst supports.

- CNFs exhibit field effect transistor (FET) behavior at room temperature and have been intensively explored in the recent years for nanoelectronics devices, including transistors and logic devices.

Subsequently, CNFs have been tested in real applications as the preparation of nanocomposites and polymer additive [19, 98-100], selective adsorption/desorption [9, 17, 101, 102] and hydrogen storage [18, 103-105], electronic applications [106-108], fuel cells [109, 110] and catalyst support materials [20, 111-113]. However, their use at a commercial stage is still embryonic.

5. ACTIVATION OF CARBON NANOFIBERS

One problem presented by these materials is the relatively low specific surface area and are essentially mesoporous in nature, which represents a limitation for adsorption, since this is strongly dependent on the remarkable surface and structural properties of such materials. Thus, a good adsorbent usually has a high specific surface area, which arises from the presence of a reasonable number of micropores and high adsorption capacity [21, 22]. Therefore, controlled pore size and pore size distribution are necessary for the application of those materials in a specific end use. In that regard, the specific surface area and porosity of carbons can be modified significantly by an activation process that removes the most reactive carbon atoms from the structure, thus increasing the surface area and porosity. There are essentially two different processes for the preparation of activated carbons, the so-called *physical* and *chemical* activation approaches [2, 114]. The first process involves carbonization of a precursor followed by controlled gasification of the carbonized material and then direct activation of the starting material in the presence of an activating agent such as CO_2 or steam (or a combination of them). In the chemical activation process, the parent carbon material is mixed with an activating agent (i.e. $ZnCl_2$, H_3PO_4, KOH, NaOH) and this is followed by pyrolysis under an inert gas [2, 114]. Chemical activation has been shown to be a very efficient method to obtain carbons with high surface areas and narrow micropore distribution. The most important advantage of chemical activation over physical activation is that the sample is activated at a lower temperature. Other advantages are that higher yields and greater porosity development are obtained and less time is required for the activation process. Key disadvantages of the chemical activation process are the need for a thorough washing step due to the incorporation of impurities arising from the activating agent, which may affect the final chemical properties of the activated carbon [28] and the corrosiveness of the process [2].

It is necessary to highlight that the porous texture of the activated carbons depends strongly on both the activation process and the nature of the precursor. In this regard, the activation of materials with ordered graphitic structure is more difficult than the activation of amorphous carbon [115-117]. Furthermore, the type of the starting carbon nanofibers, i.e. herringbone, tubular or platelet [26, 27, 117] can also influence the pore properties of the final activated material. Table 1 shows the effect of the carbon precursor, chemical agent and activating method in the development of BET surface area. Structured carbon materials, as CNFs, CNSs or graphite, are formed by layers of carbon atoms arranged in planes of

hexagons where these layers are closer than in other carbon materials. Thus, the close graphite layers limit the intercalation of activating agent during the activation process and, therefore, the activation degree will be smaller in comparison with amorphous carbon which has not ordered graphite layers. Due to these advantages exposed above, this work will be focused on the chemical activation.

6. CHEMICAL ACTIVATION OF CARBON NANOFIBERS

Inside the chemical activation method, two well-differentiated performance methods can be distinguished: CNF coating with an activating agent (preliminary CNF coating with anactivating agent and slow evaporation of a saturated KOH aqueous solution) and physics mixture (direct contact between the raw CNFs and the activating agent in the form of mixed powders).

Activating agent coating method is usually recognized to lead to better results [26, 122] in terms of activating agent efficiency and induced microporous properties. Nevertheless, considering both the energetic and time consumptions of the evaporating method, the simplest route of *physical mixing* has been also tested because it could also present some interest for industrial purposes [26].

In both methods, the mixture between the activating agent and CNFs is prepared and then pyrolized at high temperatures. Later, in order to remove the unreacted activation agent, the sample can be washed with distilled water until the neutrality of the solution is obtained or can be washed with hydrochloric acid to remove the residual activating agent and then washed with distilled water until neutrality [2, 123].

On the other hand, most of the studies about chemical activation of carbon material considered different hydroxides as activation agents [2, 119, 123-125] in which solid–solid or solid–liquid reactions involved the hydroxide reduction and carbon oxidation to generate porosity [119, 125-128]. During the reactions, CO, CO_2, and H_2 evolution are observed. A recent study suggests that the chemical activation by hydroxides consists of the overlapping of different redox processes [119, 125, 127, 128] where the hydroxide reduction leads to H_2 and corresponding metal being carbon oxidized to carbonates according to the following global reaction [129]:

$$6\ MOH + 2C \leftrightarrow 2M + 3H_2 + 2M_2CO_3$$

According to Yoon *et al.* [124], the chemical activation of CNFs with KOH is produced in three steps:

1. Selective gasification of grapheme layers by KOH.
2. Formation of ladder-like structure by local the removal or broadening of graphene layers (although fibrous form is maintained).
3. Collapse and rearrangement of graphene layers (fibrous form is destroyed).

On the other hand, Kim *et al.* [130] suggested different mechanisms to the porosity development that are illustrated in Figure 5. As has been reported in several works [23, 28, 114, 123, 130], CNFs have a layered structure. According to the type of pore development, three different mechanisms can be found: *breaking, expansion* and *exfoliation*. *Breaking* is simply the breaking of fibers and the resulting formation of shorter fibers. *Expansion* is the pore opening without demolition of fibrous CNF shape. Finally, *exfoliation* is the co-reaction of the layer separation and the fibers breaking, resulting in the predictable collapse of carbon structures.

In the other hand, it has been shown [2, 115, 116, 119, 123, 124, 131] that some experimental variables have great influence over the final porosity of activated carbons prepared by chemical activation. Thus, the *nature of the protector gas*, the mass ratio *activating agent/carbon material*, the *activation temperature*, the *inert gas flow rate* during the carbonization and the *activation time* are vary important parameters in the final characteristics of the activated materials and they are discussed below.

Table 1. Comparison of BET surface areas obtained by chemical and physical activations with different precursors and chemical agents (m^2/g)

	Chemical activation				Physical activation	
Carbon precursor	Initial BET surface	KOH	$ZnCl_2$	NaOH	CO_2	Reference
Herringbone CNFs	475	1000	-	-	678	[118]
Herringbone CNFs	178	263	-	174	-	[119]
Herringbone CNFs	13	212	-	-	-	[114]
Herringbone CNFs	40	183	-	-	-	[114]
Herringbone CNFs	220	850	-	300	-	[26]
Herringbone CNFs	202	570	-	-	-	[117]
Platelet CNFs	286	786	-	-	-	[117]
Ribbon CNFs	68	310	-	-	-	[117]
CNSs	12	231	-	-	-	[117]
Amorphous carbon	638	2157	-	-	-	[117]
Amorphous carbon	200	836	-	-	664	[120]
Amorphous carbon	10	925	1062	-	705	[121]

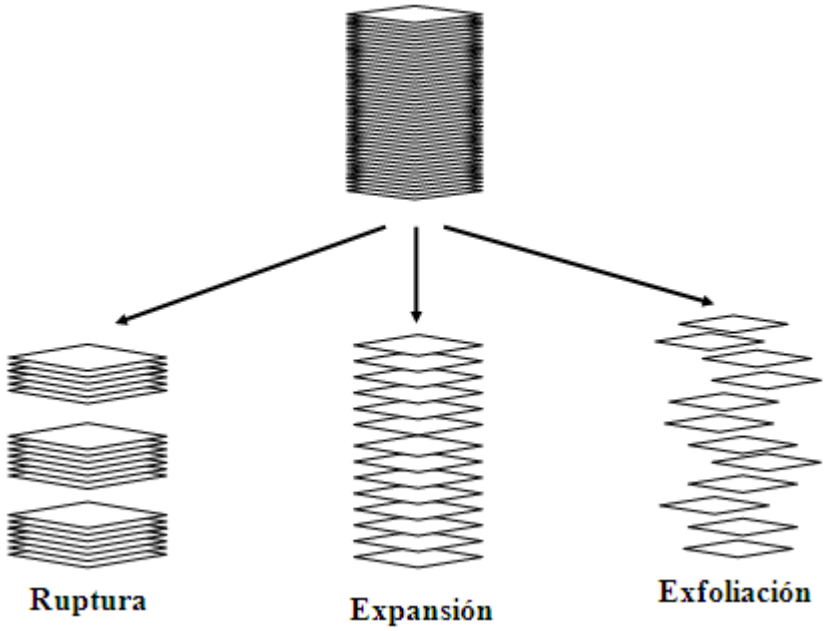


Figure 5. Schematic diagrams of mechanisms of pore development (Reproduced with permission from Ref. [130]).

6.1. Influence of the Protector Gas Nature

During the chemical activation process, an inert gas is used in order to avoid the burning of carbon material and to remove the CO, H_2 and CO_2 formed during the process. Nitrogen is usually used as the protection gas [2, 120, 123, 132], however, Jiménez *et al.* [116] studied the influence of the type of gases during the activation process. Three inert gases, N_2, Ar and He, were studied in order to see their influence on the pore opening behavior of the resulting CNFs. Thus, the best activation results (high BET surface area increase and ultra and supermicropores generation) were obtained using He as the carrier gas. In this work, the activation degree increases in the following order: Ar < N_2 < He. These results were explained attending to the diffusion of the gases evolved during the activation process (basically H_2, CO_2 and CO) in the different inert gases. Thus, the diffusion coefficients of H_2, CO_2 and CO in He, Ar and N_2 were determined [133] being always higher those diffusion coefficients in He than in Ar or N_2. As a consequence, the most efficient removal of evolved gases was obtained using this inert gas [116]. When He is used as the carrier gas, ultramicropores are principally developed. In spite of this, some ultramicropores are widened as the activation process progressed, leading to the formation of both supermicropores and mesopores. On the other hand, when N_2 is used as the carrier gas, the activation process mainly led to a development in the CNF mesoporosity although the microporosity can be also enhanced to a lesser extent. Finally, when Ar is used as the carrier gas, the mesoporosity hardly increased, meaning that the poor CNF activation only gave rise to the microporosity development. Figure 6 clearly illustrate all the porosity changes in the CNFs structures that were commented on before. On the other hand, the degree of crystallinity of the different

activated CNFs is different, which can clearly be observed in Figure 7. d_{002} values increases in the next sequence: Ar < N_2 < He, while the Lc_{002} values increases in opposite order: He < N_2 < Ar. Finally, although an important crystalline nature is lost after activation, CNFs still retained a certain order of the graphite planes [2, 119].

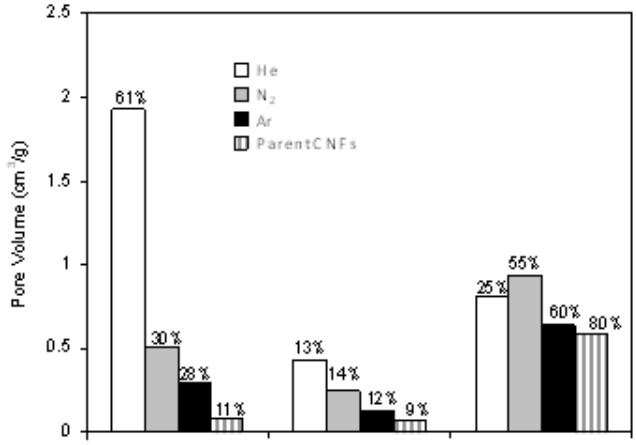


Figure 6. Proportion of ultramicropores, supermicropores and mesopores in CNFs activated using different inert gases (Reproduced with permission from Ref. [116]).

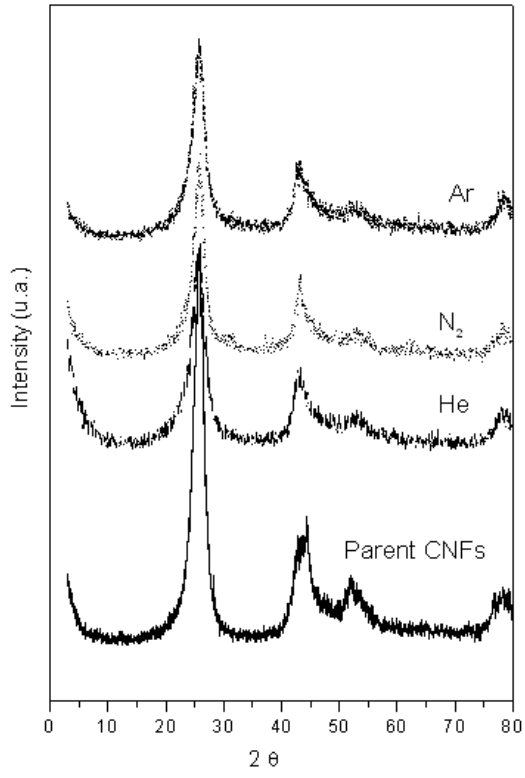


Figure 7. Representative XRD patterns of CNFs activated using different inert/protector gases (Reproduced with permission from Ref. [116]).

6.2. Influence of the Nature of the Metal Hydroxide

The porosity development can be significantly different depending on the chemical reagent used. As it has been demonstrated, depending on the nature of the activating agent used, is possible to control the development of only micropores or both micro and mesopores [134, 135].

Two groups of materials could be considered: *alkali earth hydroxides* of small or moderate size and high melting/boiling point such as $Ba(OH)_2$, $Ca(OH)_2$, and $Mg(OH)_2$ and *alkali hydroxides* such as NaOH, CsOH, RbOH and KOH. The first group of reagents is not active but nevertheless, using the second group of reagents, exceptional activation results were obtained [115].

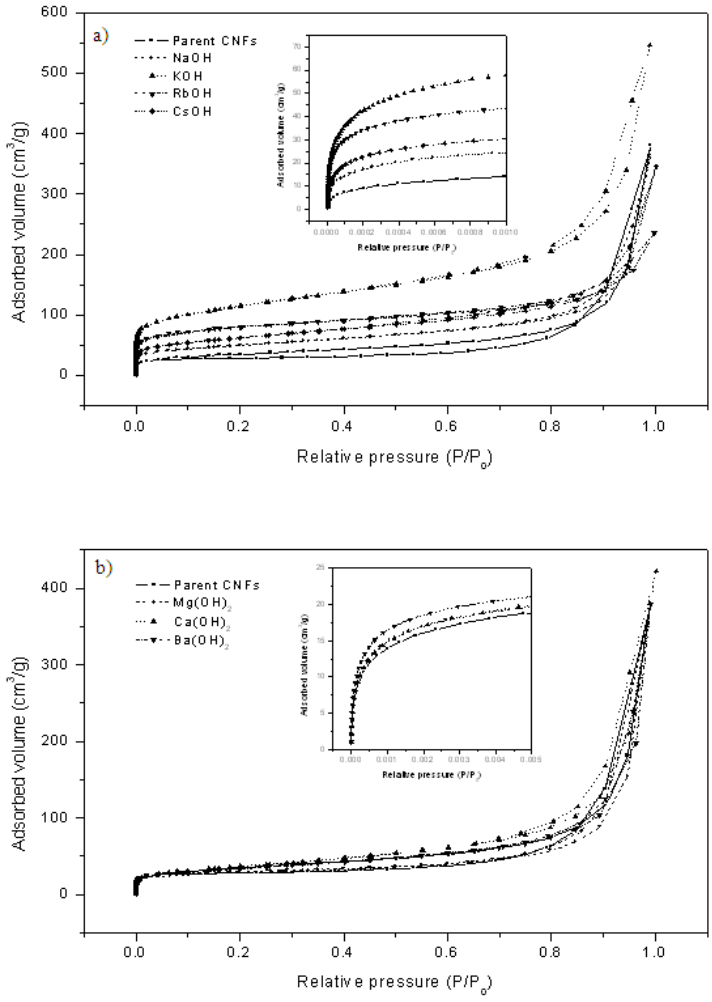


Figure 8. N_2 adsorption-desorption isotherms of CNFs activated using: a) alkali hydroxides, b) alkali earth hydroxides (Reproduced with permission from Ref. [115]).

To illustrate these results in Figure 8, the N_2 isotherms of the activated CNFs using different hydroxides have been shown.

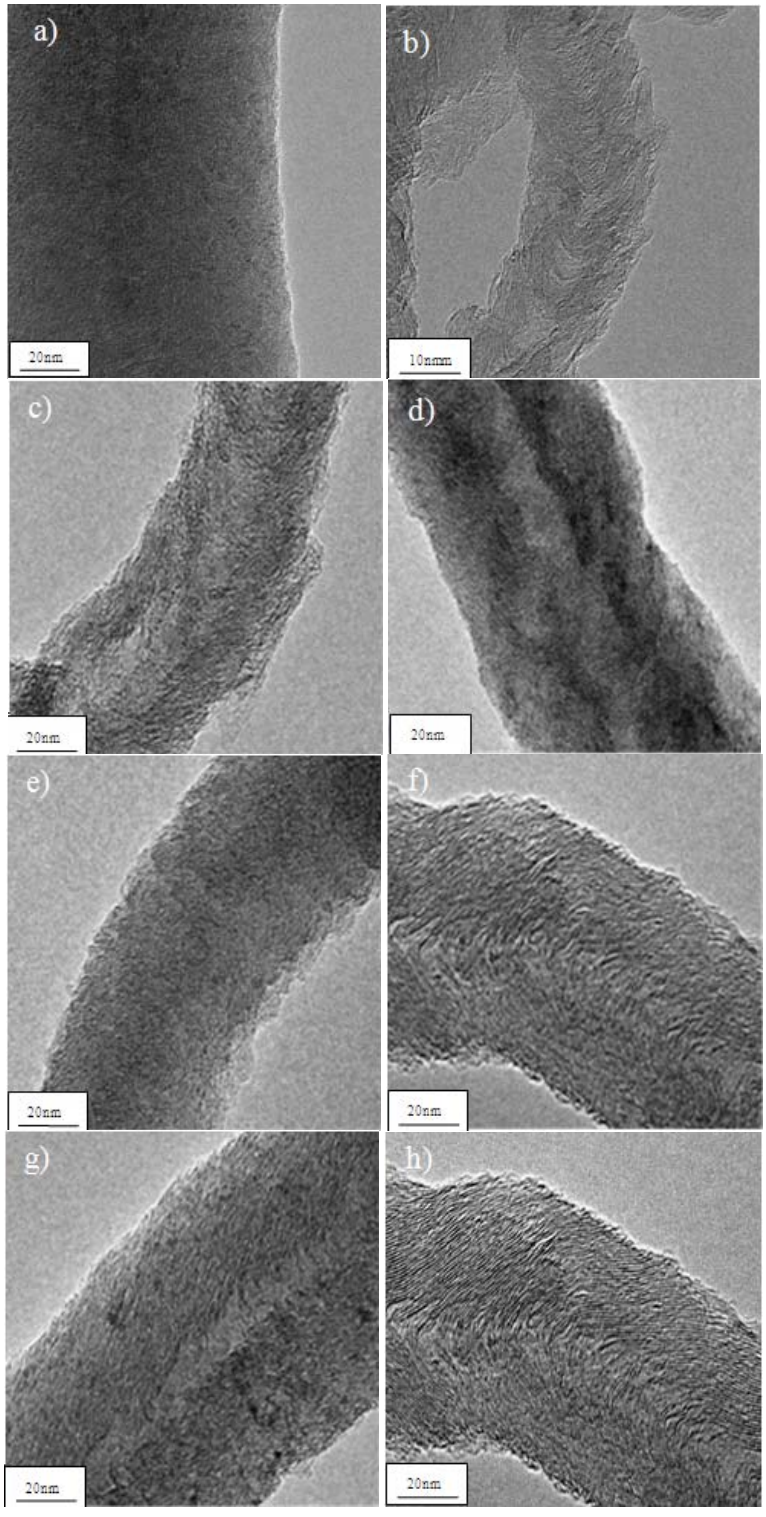


Figure 9. Representative TEM images of: a) raw CNFs and, CNFs activated using b) KOH, c) RbOH, d) CsOH, e) NaOH, f) $Ca(OH)_2$, g) $Mg(OH)_2$, h) $Ba(OH)_2$ (Reproduced with permission from Ref. [115]).

Table 2. Ion size and melting/boiling point of alkali and alkali earth metals

	Na	K	Rb	Cs	Mg	Ca	Ba
Ion size (nm)	0.190	0.266	0.296	0.338	0.130	0.198	0.270
Melting point (ºC)	98	63	39	28	650	842	727
Boiling point (ºC)	883	759	688	671	1090	1527	1870

It can be observed that the isotherms corresponding to activated small using *alkali earth hydroxides* are similar to those of the non-activated materials both in the micropore and the mesopore zone, indicating that the porosity development was negligible. On the contrary, chemical activation using *alkali hydroxides* induced an important increase in N_2 adsorption capacity mainly at low relative pressure indicating microporosity development. Note that in samples activated with KOH, the hysteresis loop of the adsorption-desorption isotherm become wider and shift to higher relative pressure values, indicating that the activated material was evolved toward a structure with larger pore size [134]. On the other hand, an important mesoporosity development only took place when CNFs were activated using KOH.

According Jiménez *et al.*, it is necessary to combine different properties of the *alkali* and *alkali earth* metals present in the hydroxides used as reagent such as boiling point and size (see Table 2) to explain the activation results. According to the proposed activation mechanism commented on before [124], the corresponding *alkaline* or *alkali earth* metal is formed during the activation. Later, this metal is vaporized and intercalated into the CNF nanostructure destroying some graphitic structures (it can be confirmed by the important decrease in the carbon content after activation [136-138]). And thus, producing the pore opening or porosity development of the parent materials [119, 128, 136]. Therefore, activation temperatures higher than the metal boiling point are needed to get the metal vaporization, i.e. Na was the worst activation agent due to its high boiling point, being necessary to increase the activation temperature to get the porosity development [115]. In other cases, the control parameter to get the activation is the metal size, i.e. Cs, having a suitable melting and boiling point, has such a high size that makes its intercalation difficult into the interlayers of the carbon network structure [137]. On the other hand, it has also been investigated by different authors how the porosity development influences the amount and type of oxygen groups (normally in the form of carboxylic, lactonic and phenolic groups) present in the activated carbon nanostructures surface [139]. Thus, it could be confirmed that, at a higher activation degree, the higher the amount of oxygenated groups. The parent CNFs are composed of carbon, hydrogen, and oxygen. After the activation process, carbon content decreases and hydrogen content is approximately kept constant, whereas oxygen content increases (C/O ratio drastically decreases in CNFs with high activation degree) [138]. To illustrate how the activation process midified the carbon material surface in Figure 9, some representative TEM images are shown as an example. Raw fishbone type CNFs were characterized by individual sheets of the graphite-like lattice with exposed surface edges in which a significant amount of defects i.e. two planes coinciding to one, bending planes, plane ends parallel to the fiber axis/or fiber surface [140, 141] were present. After activation, CNFs exhibited the same fishbone type but some structural changes, such as the consumption of particular grapheme parts at constant intervals [26, 124], could be observed.

6.3. Influence of the KOH/CNFs Ratio

According to different authors, it is possible to control the porosity development of a carbon material depending on the KOH/CNFs mass ratio used in the activation process [2, 26, 131, 132, 135]. Thus, it could be possible to develop only the micropore area of a carbon material without changing the mesopore range, or increase both the micro and mesopore area or only decrease the mesopore area depending on the final application of the materials. Results obtained during the study of the KOH/CNFs mass ratio in an activation process have suggested that it is possible to have differentiated two pore opening mechanisms. Thus, while the CNF micropore development could be correlated with the partial opening of graphite layers, the mesopore development could probably be related to other phenomenas such as, breaking of nanofibers or full exfoliation of graphite layers, which can cause different sizes of mesopores according to the extension of the exfoliation process or to even in the collapse of some micropore structures [124]. Jimenez et al. [131] observed that both the surface area and the micropore volume continuously increased with the KOH/CNFs mass ratio, reaching a maximum for a value of KOH/CNFs ratio of 5/1. In respect to the mesoporosity, they observed that a marked increase of mesoporitiy only took place at KOH/CNFs = 4/1, but generally it turned to a decrease in activated materials compared to the non-activated ones. They explained these results in base to the interaction of the initial mesopores (inherent to raw CNFs) with the chemical agent responsible for the activation of generating new micropores [135].

6.4. Influence of the Activation Temperature

The activation temperature is another important parameter in the porosity control of carbon materials and its selection will depend on the final application of the activated material (catalytic support, hydrogen storage, etc). Results obtained by different authors [131, 135, 142] have shown that a high activation temperature (around 900ºC) clearly developed the porosity in the micropore range (mainly ultramicropores). Nevertheless, if an important proportion of mesopores were also required, it would be necessary to carry out the activation process at lower temperatures (around 800-850ºC). These results have been explained taking into consideration that during the activation reaction, K in the metal form must be formed (KOH was always used as the activation agent). Although this metal could be removed from the carbon matrix by evaporation (boiling point of K: 759ºC), a proportion of it could also be intercalated between the graphite layers, which would produce a pore opening since some graphitic structures would be destroyed and micropores and mesopores would be generated [135]. Obviously, a strong interaction K-CNF will produce the generation of new mesopores while a mild interaction will induce only the generation of micropores (in some cases, at the expense of the original mesopores destruction). Summarizing, if the micropore development is desired, a weak interaction between the activating agent and the carbon material would need to be generated by the selection of the appropriate activation temperature. By increasing the value of this parameter, the stronger the K-CNF interaction will be and so mesopores will also be generated. But be careful, because if the reaction temperature exceeds a limit, no new mesopores would be generated and they could even disappear by the interaction with the activating agent (K) generating some new micropores [135].

Influence of the Activation Time

The activation time has been demonstrated to be another control parameter over the porosity in a chemical activation process of carbon materials [124, 131, 132]. As in the case of the activation temperature, obtained results showed how the amount of micropores could be increased by increasing activation times until a maximum is, i.e., 3h. However, for higher activation times i.e., 4 or 5h, the amount of micropores (including both ultramicropores and supermicropores) could decrease while the mesopores could increase [124]. On that basis and according to the activation mechanism already commented on, micropores would be firstly formed during the activation process and then they would be widened into larger micropores and even mesopores. The explanation of these results was given attending to the total activating agent consumption. Thus, it was postulated that the maximum activation degree could be obtained when the activation agent (KOH) was totally exhausted (at a determinate activation time). After that, reforming reactions could take place due to the high temperatures used in the process and, as consequence, some micropores widened to larger mesopores decreasing the surface area and micropore volume but increasing the mesopore volume [132].

6.5. Influence of the Inert Gas Flow Rate

According to different authors, the inert gas flow rate is the most important parameter in the porosity development control of carbon materials [2, 120, 128, 129, 131, 132]. Jiang et al. [132] studied the effect of N_2 flow rate during the CNTs activation and observed that a maximum value of porosity development was reached at 400 ml/min of N_2, and decreased again for higher flow rates values. As far as Jiménez et al. is concerned [131], the maximum porosity development was reached using a He flow rate of 700 ml/min in the activation of fishbone-type CNFs. A further inert gas flow rate increase led to a porosity development decrease. These results have been explained considering the removal of gases evolved during the activation process: a fast removal of gases favors the porosity development and it occurs at elevated flow rates values. As explained before, during the pyrolysis process, K could be formed and it is continuously removed from reaction place (due to the inert gas flow) once its role has been fulfilled. Once K is removed, the equilibrium of the principal reaction of the proposed mechanism ($6KOH + 2C \rightleftarrows 2K + 3H_2 + 2K_2CO_3$) would be displaced to the production of further K, increasing the degree of reaction between CNFs and KOH [2].

On the other hand, H_2O can also be formed during the pyrolysis reaction at high temperatures ($4\ KOH + C \rightleftarrows 4K + CO_2 + 2H_2O$; $4KOH + 2CO_2 \rightleftarrows 2K_2CO_3 + 2H_2O$), which have the ability of penetrating into the solid material and help in the desorption and efficient removal of volatile products from it [128, 129]. Water vapor is moreover a reactive agent, which reacts with the pyrolysis products stabilizing the radicals obtained in the thermal decomposition and thus, increasing the yield of volatiles [143]. As a result, the removal of the $H_2O(v)$ would be against the activation, while the removal of CO, CO_2 and H_2 would favor the activation process. Therefore, a balance between these two removal processes would exist: an inert gas flow rate too high could remove from the reaction place a high amount of H_2O, detrimental of the porous development; a small inert gas flow rate probably would not remove amounts of CO, CO_2 . . . enough, which would also be detrimental in the carbon material activation [120, 132].

CONCLUSION

In the past decades, an exponential increase of researches related to the synthesis and application of carbon nanostructures has taken place which has given rise to an increase in patent filing and publications on these carbon materials.

Carbon nanofibers (CNFs), a novel carbon nanomaterial, are characterized by the stacking of graphene sheets of varying shapes, producing edge sites on the outer wall which could be beneficial for their final application. The unique chemical and physical properties make CNFs exceptional candidates for multiple applications such as selective adsorption, polymer reinforcement, hydrogen storage or catalysts support. Nevertheless, an important problem associated to CNFs is its low surface area and poor (micro) porosity. For this reason, different activation methods (chemical or physical) can be applied to CNFs in order to increase the CNF surface area and to control their porosity.

In this work, it has been reviewed in detail the different types of carbon nanofibers and their synthesis. Three different methods to synthesize CNFs are arc discharge, laser ablation and chemical vapour deposition and they have been discussed emphasizing the last one, the catalytic decomposition of certain hydrocarbons on small metal particles. Fundamental aspects surrounding the CNF growth and a discussion of the key factors which enable one to control their chemical and physical properties have been also commented. Finally, the structural changes produced in the CNFs through chemical activation, with the development of particular pores as a consequence of the selective consumption of graphenes and local broadening of the interspacing between structure units, has been discussed in detail. The influence of different parameters related to the activation process, such as the nature of the metal hydroxide, nature of the inert gas, the mass ratio activating agent/CNFs, activation temperature and time and the inert gas flow rate during the carbonization has been explained.

REFERENCES

[1] De Cheng, Christensen, K. O., Ochoa-Fernández, E., Yu, Z., Totdal, B., Latorre, N., Monzón, A.,Holmen, A. Synthesis of carbon nanofibers: effects of Ni crystal size during methane decomposition. *J. Catal*., 2005, 229, 82-96.

[2] Lozano-Castelló, D., Lillo-Ródenas, M. A., Cazorla-Amorós, D., Linares-Solano, A. Preparation of activated carbons from Spanish anthracite: I. Activation by KOH. *Carbon*, 2001, 39, 741-749.

[3] Rodríguez-Reinoso, F., Molina-Sabio, M., González, M. T. The use of steam and CO_2 as activating agents in the preparation of activated carbons. *Carbon*, 1995, 33, 15-23.

[4] Dandekar, A., Baker, R. T. K., Vannice, M. A. Characterization of activated carbon, graphitized carbon fibers and synthetic diamond powder using TPD and DRIFTS. *Carbon*, 1998, 36, 1821-1831.

[5] Cuesta, A., Dhamelincourt, P., Laureyns, J., Martínez-Alonso, A., Tascón, J. M. D. Raman microprobe studies on carbon materials. *Carbon*, 1994, 32, 1523-1532.

[6] Figueiredo, J. L., Pereira, M. F. R., Freitas, M. M. A., Órfão, J. J. M. Modification of the surface chemistry of activated carbons. *Carbon*, 1999, 37, 1379-1389.

[7] Moreno-Castilla, C., Ferro-García, M. A., Joly, J. P., Bautista-Toledo, J. P., Carrasco-Martín, F., Rivera-Utrilla, J. Activated carbon surface modifications by nitric acid, hydrogen peroxide and ammonium proxydisulfate treatments. *Langmuir*, 1995, 11, 4686-4392.

[8] Cahen, S., Furdin, G., Marêche, J. F., Albiniak, A. Synthesis and characterization of carbon-supported nanoparticles for catalytic applications. *Carbon*, 2008, 46, 511-517.

[9] Gaur, V., Asthana, R., Verma, N. Removal of SO_2 by activated carbon fibers in the presence of O_2 and H_2O. *Carbon*, 2006, 44, 46-60.

[10] Nadarajah, A., Lawrence, J. G., Hughes, T. W. Development and commercialization of vapor grown carbon nanofibers: A review. *Key Eng. Mater*. 2008, 380, 193-206.

[11] Kroto, H. W., Heath, J. R., O'Brien, S. C., Curl, R. F., Smalley, R. E. C60: Buckminsterfullerene. *Nature*, 1985, 318,162–163.

[12] Hughes, T. V., Chambers, C. R. *US Pat*. 1889, 405480.

[13] Robertson, S. D. Graphite formation from low temperature pyrolysis of methane over some transition metal surfaces. *Nature*, 1969, 221, 1044-1046.

[14] Hillert, M., Lange, N. The structure of graphite filaments. *Zeitschr. Kristall*., 1958, 111, 24-34.

[15] De Jong, K. P., Geus, J. W. Carbon nanofibers: catalytic synthesis and applications. *Catal. Rev. Sc. Eng*. 2000, 42, 481-510.

[16] Iijima, S. Helical microtubules of graphitic carbon. *Nature*, 1991, 354, 56-58.

[17] Li, H., Gao, Y., Pan, L., Zhang, Y., Chen, Y., Sun, Z. Electrosorptive desalination by carbon nanotubes and nanofibers electrodes and ionexchange membranes. *Water Res*. 2008, 42, 4923-4928.

[18] Niemann, M. U., Srinivasan, S. S., Phani, A. R., Kumar, A., Goswami, Y. D., Stafanakos, E. K. Nanomaterials for hydrogen storage applications: A review. *J. Nanomater*. 2008, 1, Article no. 950967.

[19] Njuguna, K., Pielichowski, K., Desai, S. Nanofiller-reinforced polymer nanocomposites. *Polym. AdV. Technol*. 2008, 19, 947-959.

[20] Pham-Huu, C., Ledoux, M. J. Carbon nanomaterials with controlled macroscopic shapes as new catalytic materials. *Topics Catal*. 2006, 40, 49-63.

[21] Liu, Q., Ren, W., Chen, Z. G., Yin, L., Li, F., Cong, H., Cheng, H. M. Semiconducting properties of cup-stacked carbon nanotubes. *Carbon* 2009, 47, 731-736.

[22] Ryu, Z., Rong, H., Zheng, J., Wang, M., Zhang, B. Microstructure and chemical analysis of PAN-based activated carbon fibers prepared by different activation methods. *Carbon* 2002, 40, 1144-1147.

[23] Kruk, M., Jaroniec, M., Gadkaree, K. P. Carbon '97, Extended abstract 23rd biennial conference on carbon, Penn State, University Park, USA, 1997, pp. 108–109.

[24] Jiménez, V., Nieto-Márquez, A., Díaz, J. A., Romero, R., Sánchez, P., Valverde, J. L., Romero, A. Pilot plant scale study of the influence of the operating conditions in the production of carbon nanofibers. *Ind. Eng. Chem. Res*. 2009, 48, 8407–8417.

[25] Su, M., Zheng, B., Liu, J. A scalable CVD method for the synthesis of single-walled carbon nanotubes with high catalyst productivity. *Chem. Phys. Lett*. 2000, 322, 321-326.

[26] Luxembourg, D., Py, X., Didion, A., Gadiou, R., Vix-Guterl, C., Flamant, G. Chemical activations of herringbone-type nanofibers. *Micropor. Mesopor. Mater*. 2007, 98, 123-131.

[27] Zhu, Y. A., Sui, Z. J., Zhao, T. J., Dai, Y. C., Cheng, Z. M., Yuan, W. K. Modeling of fishbone-type carbon nanofibers: a theoretical study. *Carbon* 2005, 43, 1694-1699.

[28] De Lucas, A., Garrido, A., Sánchez, P., Romero, A., Valverde, J. L. Growth of carbon nanofibers form Ni/Y zeolite-based catalysts: effects of Ni introduction method, reaction temperature and reaction gas composition. *Ind. Eng. Chem. Res*. 2005, 44, 8225-8236.

[29] De Lucas, A., García, P. B., Garrido, A., Romero, A., Valverde, J. L. Catalytic synthesis of carbon nanofibers with different graphene plane alignments using Ni deposited on iron pillared clays. *Appl. Catal. A: General*, 2006, 301, 123-132.

[30] Romero, A., Garrido, A., Nieto-Márquez, A., De la Osa, A. R., De Lucas, A., Valverde, J. L. The influence of operating conditions on the growth of carbon nanofibers on carbon nanofiber-supporter nickel catalyst. *Appl. Catal. A*, 2007, 319, 246-258.

[31] Ebbesen, T. W., Ajayan, P. M. Large scale synthesis of carbon nanotubes. *Nature*, 1992, 358, 220-222.

[32] Guo, T., Nikolaev, P., Thess, A., Colbert, D. T., Smalley, R. E. Catalytic growth of single-walled nanotubes by lasser vaporization. *Chem. Phys. Lett*., 1995, 243, 49-54.

[33] Glerup, M., Steinmetz, J., Samaille, D., Stephan, O., Enouz, S., Loiseau, A., Roth, S., Bernier, P. Synthesis of N-doped SWNT using the arc-discharge procedure. *Chem. Phys. Lett*., 2004, 387, 193-197.

[34] Zhang, Y., Gu, H., Suenaga, K., Iijima, S. Heterogeneous growth of B-C-N nanotubes by laser ablation. *Chem. Phys. Lett*., 1997, 279, 264-269.

[35] Kneller, J. M., Soto, R. J., Surber, S. E., Pietrab, T., Colomer, J. F., Fonseca, A., Nagry, J. B., Van Tendeloo, G. TEM and Laser-Polarized 129Xe NMR characterization of oxidatively purified carbon nanotubes. *J. Am. Chem. Soc*. 2000, 122, 10591-10597.

[36] Cheng, H. M., Li, S.F., Pan, G., Pan, H. Y., He, L. L., Sun, X., Dresselhaus, M. S. Large-scale and low-cost synthesis of single-walled carbon nanotubes by the catalytic pyrolysis of hydrocarbons. *Appl. Phys. Lett*. 1998, 72, 3282–3284.

[37] Teo, K. B. K., Singh, C., Chhowalla, M., Milne, W. I. *Encyclopedia of nanoscience and nanotechnology*. American Scientific publisher. Stevenson Ranch, CA, 2004, Vol. 10.

[38] Li, W. Z., Xie, S. S., Qian, L. X., Chang, B. H., Zou, B. S., Zhou, W. Y., Zhao, R. A., Wang, G. Large-scale synthesis of aligned carbon nanotubes. *Science*, 1996, 274, 1701-1703.

[39] Fonseca, A., Hernadi, K., Piedigrosso, P., Colomer, J. F., Mukhopadhyay, K., Doome, R., Lazarescu, S., Biro, L. P., Lambin, P., Thiry, P. A., Bernaerts, D., Nagy, J. B. Synthesis of single and multiwall carbon nanotubes over supported catalysts. *Appl. Phys. A,* 1998, 67, 11-22.

[40] Rao, C. N. R., Sen, R., Satishkumar, B. C., Govindaraj, A. Large aligned-nanotube bundles from ferrocene pyrolysis. *Chem. Commun*., 1998, 15, 1525-1526.

[41] Hernadi, K., Fonseca, A., Nagy, J. B., Bernaerts, D., Fudala, A., Lucas, A. A. Catalytic synthesis of carbon nanotubes using zeolite support. *Zeolites*, 1996, 17, 416-423.

[42] Dai., H. Carbon nanotubes: opportunities and challenges. *Surface Sci*., 2002, 500 218-241.

[43] Bethune, D. S., Kiang, C. H., de Vries, M., Gorman, G., Savoy, R., Vazquez, J., Beyers, R. Cobalt-catalysed growth of carbon nanotubes with single-atomic-layer walls. *Nature*, 1993, 363, 605–607.

[44] Journet, C., Maser, W., Bernier, P., Loiseau, A., Delachapelle, M., Lefrant, S., Deniard, P., Lee, R., Fischer, J. Large-scale production of single-walled carbon nanotubes by the electric-arc technique. *Nature*, 1997, 388, 756–758.

[45] Thess, A., Lee, R., Nikolaev, P., Dai, H., Petit, P., Robert, J., Xu, C., Lee, Y., Kim, S., Rinzler, A., Colbert, D., Scuseria, G., Tomanek, D., Fischer, J., Smalley, R. Crystalline ropes of metallic carbon nanotubes. *Science*, 1996, 273, 483–487.

[46] Oberlin, A., Endo, M., Koyama, T. Filamentous growth of carbon through benzene decomposition. *J. Crystal Growth*, 1976, 32, 335-349.

[47] Baker, R.T.K., Kim, M.S., Chambers, A., Park, C., Rodriguez, N. M. The relationship between metal particle morphology and the structural characteristics of carbon deposits. *Stud. Surf. Sci. Catal*., 1997, 111, 99-109.

[48] Helveg, S., Lopez-Cartes, C., Sehested, J., Hansen, P. L., Clausen, B. S., Rostrup-Nielsen, J.R., Abild-Pedersen, F., Nørskov, J. K. Atomic scale imaging of carbon nanofiber gorwth. *Nature*, 2004, 427, 426-429.

[49] See, C. H., Harris, A. T. CaCO3 supported Co-Fe catalysts for carbon nanotube synthesis in fluidized bed reactors. *AIChE J.* 2008, 54, 657-664.

[50] Wagner, R.S., Ellis, W.C. Vapor-liquid-solid mechanism of single crystal growth. *Appl. Phys. Lett*. 1964, 4, 89-90.

[51] Trimm, D. L. The formation and removal of coke from nickel catalyst. *Catal. Rev. Sci. Eng.*, 1977, 16, 155-189.

[52] Rostrup-Nielsen, J. R., Trimm, D. L. Mechanisms of carbon formation on nickel-containing catalysts. *J. Catal*., 1997, 48, 155-165.

[53] Bartholomew, C. H. Carbon deposition in steam reforming and methanation. *Catal. Rev. Sci. Eng*., 1982, 24, 67-112.

[54] Rodríguez, N. M. Review of catalytically Brown carbon nanofibers. *J. Mater. Res*., 1993, 8, 3233-3250.

[55] Dupuis, A. C. The catalyst in the CCVD of carbon nanotubes-a review. *Prog. Mat. Sci*., 2005, 50, 929-961.

[56] Tibbetts, G. G. Why are carbon filaments tubular? *J. Cryst. Growth*, 1984, 66, 632–638.

[57] Poncharal, P., Berge, C., Yi, Y., Wang, Z. L., de Heer, W. A. Room temperature ballistic conduction in carbon nanotubes. *J. Phys. Chem*. B, 2002, 106, 12104–12118.

[58] Dai, H. Carbon nanotubes: synthesis, integration and properties. *Acc. Chem. Res.,* 2002, 35, 1035-1044.

[59] Baker, R. T. K. Catalytic growth of carbon filaments. *Carbon*, 1989, 27, 315–323.

[60] Kanzow, H., Ding, A. Formation mechanism of single-wall carbon nanotubes on liquid–metal particles. *Phys. Rev. B*, 1999, 60, 11180-11186.

[61] Cassel, A. M., Raymakers, A., Kong, J., Dai, H. Large scale CVD synthesis of single-walled carbon nanotubes. *J. Phys. Chem. B*, 1999, 103, 6484–6492.

[62] Wen, J.G., Huang, Z.P., Wang, D.Z., Chen, J.H., Yang, S.X., Ren, Z.F. Growth and characterization of aligned carbon nanotubes from patterned nickel nanodots and uniform thin films. *J. Mater. Res*., 2001, 11, 3246–3253.

[63] Kaatz, F.H., Siegal, M.P., Overmyer, D.L., Provencio, P.P., Jackson, J.L. Diameter control and emission properties of carbon nanotubes grown using chemical vapor deposition. *Mater. Sci. Eng. C*, 2002, 1009, 1–4.

[64] Bai, J.B. Growth of nanotube/nanofiber coils by CVD on an alumina substrate. *Mater. Lett*., 2002, 4212, 1–5.

[65] Romero, A., Garrido, A., Nieto-Márquez, A., Sánchez, P., de Lucas, A., Valverde, J. L. Synthesis and structural characteristics of highly graphitized carbon nanofibers produced from the catalytic decomposition of ethylene: influence of the active metal (Co, Ni, Fe) and the zeolite type support. *Micropor. Mesopor. Mat*., 2008, 110, 318-329.

[66] Lee, C.J., Park, J. Growth and structure of carbon nanotubes produced by thermal chemical vapor deposition. *Carbon*, 2001, 39, 1891–1896.

[67] Penheiro, P., Schouler, M. C., Gadelle, P., Mermoux, M., Dooryhee, E. Effect of hydrogen on the orientation of carbon layers in deposits from the carbon monoxide disproportionation reaction over Co/Al_2O_3 catalysts. *Carbon*, 2000, 1469–1479

[68] Cheng, H. M., Li, F., Sun, X., Brown, S. D. M., Pimenta, M. A., Marucci, A., Dresselhaus, G., Dresselhaus, M. S. Bulk morphology and diameter of SWNTs synthesized by catalytic decomposition of hydrocarbons. *Chem. Phys. Lett*. 1998, 289, 602–610

[69] Nikolaev, P., Bronikowski, M.J., Bradley, R. K., Rohmund, F., Colbert, D. T., Smith, K. A., Smalley, R. E. Gas-phase catalytic growth of SWNTs from CO. *Chem. Phys. Lett*., 1999, 313, 91–97.

[70] Endo, M., Kim, Y. A., Takeda, T., Hong, S. H., Matusita, T., Hayashi, T., Dresselhaus, M. S. Structural characterization of carbon nanofibers obtained by hydrocarbon pyrolysis. *Carbon*, 2001, 39, 2003–2010.

[71] Willems, I., Konya, Z., Colomer, J. F., Tendeloo, G. V., Nataraju, N. I., Fonseca, A., Nagry, J. B. Control of the outer diameter of thin carbon nanotubes synthesized by catalytic decomposition of hydrocarbons. *Chem. Phys. Lett*., 2000, 317, 71–76.

[72] Murakami, Y., Miyauchi, Y., Chiashi, S., Maruyama, S. Characterization of single-walled carbon nanotubes catalytically synthesized from alcohol. *Chem. Phys. Lett*., 2003, 374, 53–58.

[73] Willems, I., Kónya, Z., Colomer, J. F., Van Tendeloo, G., Nagaraju, N., Fonseca, A., Nagy, J. B. Control of the outer diameter of thin carbon nanotubes synthesized by catalytic decomposition of hydrocarbons. *Chem. Phys. Lett*., 2000, 317, 71–76.

[74] Kiang, C.H. Carbon ring and cages in the growth of single-walled carbon nanotubes. *J. Chem. Phys*., 2000, 113, 4763-4766.

[75] Andriotis, A.N., Menon, M., Froudakis, G. Catalytic action of Ni atoms in the formation of carbon nanotubes : a molecular dynamics study. *Phys. Rev. Lett*., 2000, 85, 3193-3196.

[76] Ivanov, V., Fonseca, A., Nagy, J.B., Lucas, A. A., Lambin, P., Bernaerts, D., Zhang, X.B. Catalytic production and purification of nanotubules having fullerene-scale diameters. *Carbon*, 1995, 33, 1727-1738.

[77] Smithells, C.J., Smithells' Metals Reference Book, seventh ed., Butterworth-Heinemann Ltd., 1992.

[78] Park, C., Keane, M.A. Catalyst support effects in the growth of structured carbon from the decomposition of ethylene over nickel. *J. Catal*., 2004, 221, 386-399.

[79] Anderson, P.E., Rodríguez, N.M. Influence of the support on the structural characteristics of carbon nanofibers produced from the metal-catalyzed decomposition of ethylene. *Chem. Mater*., 2000, 12, 823-830.

[80] Hernadi, K., Fonseca, A., Nagy, J.B., Siska, A., Kiricsi, I. Production of nanotubes by the catalytic decomposition of different carbon-containing compounds. *Appl. Catal. A*, 2000, 199, 245-255.

[81] Piedigrosso, P., Kónya, Z., Colomer, J. F., Fonseca, A., van Tenedlo, G., Nagy, J.B. Production of differently shaped multi-wall carbon nanotubes using various cobalt supported catalysts. *Phys. Chem. Chem. Phys*., 2000, 2, 163-170.

[82] Iwasaki, T., Motoi, T., Den, T. Multi-walled carbon nanotubes growth in anodic alumina nanoholes. *Appl. Phys. Lett*., 1999, 75, 2044-2046.

[83] Barata-Rodrigues, P.M., Mays, T.J., Moggridge, G.D. Structured carbon adsorbents from clay, zeolite and mesoporous aluminosilicate templates. *Carbon*, 2003, 41, 2231-2246.

[84] Venuto, P.B. Organic catalysis over zeolites: A perspective on reaction paths within micropores. *Micropor. Mater*., 1994, 2, 297-411.

[85] Armor, J.N. Catalytic reduction of nitrogen oxides with methane in the presence of excess oxygen: A review. *Catal. Today*, 1995, 26, 147-158.

[86] Singh, C., Shaffer, M. S. P., Windle, A. H. Production of controlled architectures of aligned carbon nanotubes by an injection chemical vapor deposition method. *Carbon*, 2003, 41, 359-368.

[87] Vieira, R., Ledoux, M. J., Pham-Huu, C. Synthesis and characterisation of carbon nanofibers with macroscopic shaping formed by catalytic decomposition of C_2H_6/H_2 over nickel catalyst. *Appl. Catal., A,* 2004, 274, 1-8.

[88] Rodríguez, N. M., Chambers, A., Baker, R. T. K. Catalytic engineering of carbon nanostructures. *Langmuir*, 1995, 11, 3862-3866.

[89] Yu, Z., Chen, D., Ronning, M., Totdal, B., Vralstad, T., Ochoa-Fernández, E., Holmen, A. Large-scale synthesis of carbon nanofibers on Ni-Fe-Al hydrotalcite derived catalysts. II: Effect of Ni/Fe composition on CNF synthesis from ethylene and carbon monoxide. *Appl. Catal*. 2008, 338, 147-158.

[90] Bom, D., Andrews, R., Jacques, D., Anthony, J., Chen, B., Meier, M. S., Selegue, J. P. Thermogravimetric analysis of the oxidation of multiwalled carbon nanotubes: Evidence for the role of defect sites in carbon nanotube chemistry. *Nano Lett*. 2002, 2, 615-619.

[91] Park, C., Baker, R. T. K. Catalytic behavior of graphite nanofiber supported nickel particles. 2. The influence of the nanofiber structure. *J. Phys. Chem. B,* 1998, 102, 5168-5177.

[92] Fonseca, A., Hernadi, K., Nagy, J. B., Bernaerts, D., Lucas, A. A. Optimization of catalytic production and purification of buckytubes. *J. Mol. Catal. A: Chem*., 1996, 107, 159-168.

[93] Müller, T. E., Reid, D. G., Hsu, W. K., Hare, J. P., Kroto, H. W., Walton, D. R. M. Synthesis of nanotubes via catalytic pyrolysis of acetylene: A SEM study. *Carbon*, 1997, 35, 951-966.

[94] Dai, H. Controlling nanotube growth. *Phys. World*, 2000, 13, 43-47.

[95] Ebbesen, T. W. Carbon nanotubes. *Ann. Rev. of Mater. Sci*., 1994, 24, 235-264.

[96] Östling, D., Tománek, D., Rosén, A. Electronic structure of single-wall, multi-wall and filled carbon nanotubes. *Phys. Rev. B* 1997, 55, 13980–13988.

[97] Dekker, C. Carbon nanotubes as molecular quantum wires. *Phys. Today*, 1999, 52, 22-28.

[98] Gong, K. P., Zhang, M. N., Yan, Y. M., Su, L., Mao, L. Q., Xiong, Z. X., et al. Sol-gel derived ceramic-carbon nanotubes nanocomposite electrodes: tunable electrode dimension and potential electrochemical applications. *Ana. Chem*. 2004, 76, 6500-6505.

[99] S. Wang, H. M. Bao, P. Y. Yang, G. Chen. Immobilization of trypsin in polyaniline-coated nano-Fe_3O_4/carbon nanotube composite for protein digestion. *Anal. Chim. Acta*. 612 (2) (2008) 182-189.

[100] Pötsche, P., Fornes, T.D., Paul, D.R. Rheological behavior of multi-walled carbon nanotube/polycarbonate composites. *Polymer*, 2002, 43, 3247-3255.

[101] Park, C., Engel, E.S., Crowe, A., Gilbert, T. R., Rodríguez, N.M. Use of carbon nanofibers in the removal of organic solvents from water. *Langmuir*, 2000, 16, 8050-8056.

[102] Nevskaia, D. M., Castillejos-López, E., Guerrero-Ruiz, A., Muñoz, V. Effects of the surface chemistry of carbon materials on the adsorption of phenol-aniline mixures form water. *Carbon*, 2004, 42, 653-665.

[103] Jiménez, V., Sánchez, P., Díaz, J. A., Valverde, J. L., Romero, A. Hydrogen storage capacity on different carbon materials. *Chem. Phys. Lett*., 2010, 485, 152–155

[104] Browning, D. J., Gerrard, M. L. Lakerman, J. B., Mellor, I. M., Mortimer, R. J., Turpin, M. C. Studies into the storage of hydrogen in carbon nanofibers: proposal of a possible reaction mechanism. *Nano. Lett*., 2002, 2, 201–205.

[105] Rzepka, M., Bauer, E., Reichenauer, G., Schliermann, T., Bernhardt, B., Bohmhammel, K., Henneberg, E., Knoll, U., Maneck, H. E., Braue, W. Hydrogen storage capacity of catalytically-grown carbon nanofibers. *J. Phys. Chem. B*, 2005, 109, 14979–14989.

[106] Rao, C.N.R., Novel materials, materials design and synthetic strategies: recent advances and new directions, *J. Mater. Chem*., 1999, 9, 1-14.

[107] Rochefort, A., Salahub, D.R., Avouris, P. Effects of finite length on the electronic structure of carbon nanotubes, *J. Phys. Chem. B,* 1999, 103, 641-646.

[108] Obreja, V. V. N. On the performance of supercapacitors with electrodes based on carbon nanotubes and carbon activated material-a review. *Physica E*., 2008, 40, 2596-2605.

[109] Wang, C., Waje, M., Wang, X., Tang, J. M., Haddon, R. C.,Yan, Y. Proton exchange membrane fuel cells with carbon nanotube-based electrodes. *Nano. Lett*., 2004, 4, 345-348.

[110] Shao, Y., Liu, J., Wang, Y., Lin, Y.. Novel catalyst support materials for PEM fuel cells: current status and future prospects. *J. Mater. Chem*., 2009, 19, 46-59.

[111] Jarrah, N., van Ommen, J. G., Lefferts, L. Development of monolith with a carbon-nanofiber-washcoat as a structured catalyst support in liquid phase. *Catal. Today*, 2003, 79, 29-33.

[112] Centi, G., Perathoner, S. Novel catalyst design for multi-phase reactions. *Catal. Today*, 2003, 79, 3-13.

[113] Nieto-Márquez, A., Gil, S., Romero, A., Valverde, J. L., Gómez-Quero, S., Keane, M. A. Gas phase hydrogenation of nitrobenzene over acid treated structured and amorphous carbon supported Ni catalysts, *Appl. Catal. A: General*, 2009, 363, 188-198.

[114] Merino, C., Soto, P., Vilaplana-Ortego, E., Gomez de Salazar, J. M., Pico, F., Rojo, J. M. Carbon nanofibers and activated carbon nanofibers as electrodes in supercapacitors. *Carbon*, 2005, 43, 551–557.

[115] Jiménez, V., Sánchez, P., De Lucas, A., Valverde, J. L., Romero, A. Influence of the nature of the metal hydroxide in the porosity development of carbon nanofibers. *J. Colloid Interface Sci*., 2009, 336, 226-234

[116] Jiménez, V., Sánchez, P., Valverde, J. L., Romero, A. Influence of the activating agent and the inert gas (type and flow) used in an activation process for the porosity development of carbon nanofibers. *J. Colloid Interface Sci*., 2009, 336, 712-722.

[117] Jiménez, V., Sánchez, P., Valverde, J. L., Romero, A. Effect of the nature the carbon precursor on the physico-chemical characteristics of the resulting activated carbon materials. *Mater. Chem. Phys*., 2010, 124, 223-233.

[118] Blackman, J. M., Patrick, J. W., Arenillas, A., Shi, W., Snape, C. E., Activation of carbon nanofibers for hydrogen storage. *Carbon*, 2006, 44, 1376-1385.

[119] Maciá-Agulló, J. A., Moore, B. C., Cazorla-Amorós, D., Linares-Solano, A. Influence of carbon fibres crystallinities on their chemicals activation by KOH and NaOH. *Micropor. Mesopor. Mater*., 2007, 101, 397-405.

[120] Azargohar, R., Dalai, A. K. Steam and KOH activation of biochar: experimental and modeling studies. *Micropor. Mesopor. Mater*., 2008, 110, 413-421.

[121] Ahmadpour, A., Do, D. D. The preparation of active carbons from coal by chemical and physical activation . *Carbon*, 1996, 34, 471-479.

[122] Py, X., Daguerre, E., Menard, D. Composites of expanded natural graphite and in situ prepared activated carbons. *Carbon*, 2002, 40, 1255–1265.

[123] Lillo-Ródenas, M. A., Lozano-Castelló, M. A., Cazorla-Amorós, D., Linares-Solano, A. Preparation of activated carbons from Spanish anthracite: II. Activation by NaOH . *Carbon*, 2001, 39, 751-759.

[124] Yoon, S., Lim, S., Song, Y., Ota, Y., Qiao, W., Tanaka, A., Mochida, I. KOH activation of carbon nanofibers . *Carbon*, 2004, 42, 1723-1729.

[125] Lillo-Ródenas, M. A., Juan-Juan, J., Cazorla-Amorós, D., Linares-Solano, A. About reaction occurring during chemicals activation with hydroxides. *Carbon*, 2004, 42, 1371-1375.

[126] Díaz-Teran, J., Nevskaia, D. M., Fierro, J. L. G., Lopez-Peinado, A. J., Jerez, A. Study of chemical activation process of a lignocellulosic material with KOH by XPS and XRD. *Micropor. Mesopor. Mater*., 2003, 60, 173-181.

[127] Xue, R., Shen, Z. Formation of graphite-potasium intercalation compounds Turing activation of MCMB with KOH. *Carbon*, 2003, 41, 1862-1864.

[128] Lillo-Ródenas, M. A., Cazorla-Amorós, D., Linares-Solano, A. Understanding chemical reactions between carbons and NaOH and KOH: An insight into the chemical activation mechanism. *Carbon*, 2003, 41, 267-275.

[129] Raymundo-Piñero, E., Azaïs, P., Cacciaguera, T., Cazorla-Amorós, D., Linares-Solano, A., Béguin, F. KOH and NaOH activation mechanisms of multi-walled carbon nanotubes with different structural organization. *Carbon*, 2005, 43, 786-795.

[130] Kim, B., Lee, S., Park, S. A study on pore-opening behaviors of graphite nanofibers by a chemical activation process. *J. Colloid Interf. Sci*., 2007, 306, 454-458.

[131] Jiménez, V., Díaz, J. A., Sánchez, P., Valverde, J. L., Romero, A. Influence of the activation conditions on the porosity development of herringbone carbon nanofibers. *Chem. Eng. J*., 2009, 155, 931-940.

[132] Jiang, Q., Zhao, Y. Effects of activation conditions on BET specific surface area of activated carbon nanotubes. *Micropor. Mesopor. Mater*., 2004, 76, 215-219.

[133] Reid, R. C., Prausnitz, J. M., Poling, B. E., *The properties of gases and liquids*, fourth ed., McGraw-Hill, New York, 1988. pp. 582-584.

[134] Zubizarreta, L., Arenillas, A., Pirard, J. P., Pis, J. J., Job, N. Tailoring the textural properties of activated carbon xerogels by chemical activation with KOH. *Micropor. Mesopor. Mater*. 2008, 115, 480-490.

[135] Niu, J. J., Wang, J. N. Effect of temperature on chemical activation of carbon nanotubes. *Solid State Sci*., 2008, 10, 1189-1193.

[136] Im, J. S., Park, S. J., Kim, T. J., Kim, Y. H., Lee, Y. S. The study of controlling pore size on electrospun carbon nanofibers for hydrogen adsorption. *J. Colloid Interf. Sci*., 2008, 318, 42-49.

[137] Okada, K., Yamamoto, N., Kameshima, Y., Yasumori, A. Porous properties of activated carbons from waste newspaper prepared by chemical and physical activation. *J. Colloid Interface Sci*., 2003, 262, 179-193.

[138] Tseng, R. L. Mesopore control of high surface area NaOH-activated carbon . *J. Colloid Interface Sci*., 2006, 303, 494-502.

[139] Salame, I. I., Bandosz, T. J. Role of surface chemistry in adsorption of phenol on activated carbons . *J. Colloid Interface Sci*., 2003, 264, 307-312.

[140] Rodríguez, N. M., Chambers, A., Baker, R. T. K. Catalytic engineering of carbon nanostructures. *Langmuir*, 1995, 11, 3862-3866.

[141] Toebes, M. L., Van Heeswijk, J. M. P., Bitter, J. H., Van Dillen, A. J., De Jong, K. P. The influence of oxidation on the texture and the number of oxygen-containing surface groups of carbon nanofibers. *Carbon* 2004, 42, 307-315.

[142] Evans, M. J. B., Halliop, E., MacDonald, J. A. F. The production of chemically-activated carbon. *Carbon*, 1999, 37, 269-274.

[143] Minkova, V., Razvigorova, M., Bjornbom, E., Zanzi, R., Dufinova, T., Petrov, N. Effect of water vapor and biomass nature on the yield and quality of the pyrolysis products from biomass. *Fuel Process. Technol*., 2001, 70, 53-61.

In: Activated Carbon
Editor: James F. Kwiatkowski
ISBN: 978-1-61209-684-1
©2012 Nova Science Publishers, Inc.

Chapter 8

ACTIVATED CARBON AS A METAL OXIDE SUPPORT: A REVIEW

A. Barroso-Bogeat, C. Fernández-González, M. Alexandre-Franco and V. Gómez-Serrano*

Departamento de Química Orgánica e Inorgánica,
Universidad de Extremadura (UEx), Badajoz 06071, Spain

ABSTRACT

There is increasing interest in semiconductor oxides supported on activated carbon because of their variety of applications, such as photocatalytic degradation of many pollutants in wastewaters, catalysis of important organic reactions, adsorption of inorganic ions and gas sensors. These oxides include TiO_2, Fe_2O_3, ZnO, SnO_2, WO_3 and Al_2O_3. Because of their applications, these materials have been widely studied and researched, specially the first one. This paper is a critical review of the published reports of the latest investigations for each of these materials. Particular attention is paid to the preparation methods, applications and results of the applications.

INTRODUCTION

Activated carbon is an amorphous carbon material with a highly developed porosity. It is characterized by excellent textural properties (surface area, porosity and porosity distribution) and surface chemistry, which give it a high capacity to adsorb gases, vapours and solutes in solution. Because of these properties, activated carbon is widely used as adsorbent, catalyst and catalyst support.

Activated carbon can be prepared from a variety of carbonaceous materials, such as coal, lignite, peat, different kinds of wood, nutshells, fruit stones and others [1]. It is usually achieved by the well known methods of physical activation and chemical activation [2,3]. The

* Telephone: +34-924-289-300. Fax: +34-924-271-149. E-mail: vgomez@unex.es

former consists of two successive stages of carbonization and activation. At the carbonization stage the raw material is subjected to heat treatment, usually in inert atmosphere, and a char is produced with an incipient porosity. In the activation stage the char is partially gasified in an oxidant atmosphere of steam, carbon dioxide or air. This process results in the activated product, which has a high developed porosity and surface area. By contrast, in the chemical activation method the precursor is first impregnated with the activating agent in aqueous solution and the resulting product is then heated in an inert atmosphere.

Activated carbon can be used directly as a catalyst by itself or as a support of other catalytically active phases, such as metals or metal oxides. Among the advantages of using activated carbon as catalyst support are its chemical inertness, high surface area and porosity as well as the possibility of obtaining activated carbon with tailored porous structure for particular applications. In addition, activated carbon has a high thermal resistance and to the attack by acids and bases, and the catalytic phase is easily recovered by burning the support. Finally, the price of carbon supports is usually lower than for conventional supports, such as alumina or silica.

The main drawbacks of activated carbon as a catalyst support are associated with its use in hydrogenation reactions above 700 K [4] and in reactions in oxygen atmosphere at temperatures above 520 K because of the gasification of carbon atoms to yields methane gas and carbon dioxide, respectively [4,5].

In these applications the main role of activated carbon is to maintain the catalytic phase in a high dispersed state. However, several researches have demonstrated that its role is not only as a support but it can also contribute significantly to catalytic activity [4]. In other words, there may be a synergistic effect on catalytic activity of the material because of the interactions between the activated carbon surface groups and the active phase [6].

In recent years there has been growing interest and research activity in the development of catalysts based on semiconductor metal oxides supported on activated carbon. The reason is that many of these oxides have photocatalytic properties which are very useful in degradation and removal of organic and inorganic pollutants in both liquid and gaseous effluents. These metal oxides include TiO_2, α-Fe_2O_3, ZnO, SnO_2 and WO_3, of which TiO_2 is the most used and researched.

CHARACTERISTICS OF SEMICONDUCTOR OXIDES

Semiconductors are a wide group of crystalline materials characterized by the increase in their electrical conductivity with temperature. The electrical conductivity for these materials is much smaller than for metals and much higher than for insulators [7-9]. Semiconductors with photocatalytic activity are solid metal oxides and sulphides.

Electronic structure of semiconductors can be described by band theory. In these solids the overlap of atomic orbitals is extended throughout the lattice, leading to a large number of molecular orbitals of very close energies. The result is a configuration of bands formed by allowed electronic states [7,10]. The electrons of atoms are distributed in these bands. Between two bands there is an interval of energy, named band gap, where there are no allowed electronic states.

In the field of photocatalysis the bands limiting the gap are the least energetic valence band, and the most energetic conduction band. The valence band is the highest energy band occupied by electrons, whereas the conduction band is the next highest energy band empty of electrons.

In the ground state and temperature 0 K, electrons occupy the electronic states of the bands up to a maximum energy value E_f, called Fermi level. Higher energy electronic states are empty. At temperatures above 0 K, electron transit occurs to higher energy levels than E_f by thermal excitation.

The difference between metals, semiconductors and insulators is established according to the Fermi level position, which is in the conduction band for metals and in the band gap for semiconductors and insulators. The difference between a semiconductor and an insulator is the band gap width, E_g. The gap in semiconductors is small enough to excite electrons from the valence band to the conduction band [8]. This excitation can be thermal, electric or light, the latter being the case of photocatalysis.

Electrical conductivity of a material depends on two factors: the existence of charge carriers and their ability to move in the presence of an electric field. The charge carriers in metals are electrons in the partially filled conduction band, which can move freely through it. However, in semiconductors the charge carriers are electrons that have migrated to conduction band and holes generated in the valence band. When a conductor material is irradiated and absorbs photons of energy above E_g, the transit of electrons from the valence band to the conduction band occurs. This phenomenon is called photoexcitation and for each excited electron a hole in the valence band is generated. Electron-hole pairs are charge carriers with opposite signs and are rapidly recombined (around 30 ns) in absence of an electric field. The excess of energy is usually released as heat, known as non-radiative recombination, or by photon emission, which is radiative recombination [8].

In order to prevent recombination of the electron-hole pairs, an electric field can be applied, to separate the electric charges, or when there are electron and hole acceptors on the semiconductor surface. The latter option is the basis of photocatalytic activity of these materials [8].

Semiconductor materials suitable for photocatalysis are those with a gap similar to the photon energy of visible or UV light, i.e. a value of E_g less than 3.5 eV. Traditional semiconductors such as Si, Ge, GaAs or InP are not suitable for photocatalysis because of their small E_g value and instability against water.

The semiconductor oxides which are most used currently in photocatalysis are the so-called wide band gap semiconductors, as their E_g value is around 3.0 eV. This group includes TiO_2, α-Fe_2O_3, ZnO, SnO_2 and WO_3. Table 1 lists the band gap values for each of these oxides. Because α-Fe_2O_3 has the lowest band gap value, it can be activated by visible light irradiation. Other oxides require more energetic UV radiation to be activated. A particular situation is that of TiO_2.

Both anatase and rutile can absorb UV radiation, but only rutile can absorb radiation near visible light. However, several researches have demonstrated that anatase shows higher photocatalytic activity than rutile, because the position of its conduction band provides greater reducing power than rutile.

Table 1. Band gap values for semiconductor oxides with photocatalytic activity [8,11]

Semiconductor	TiO_2 (rutile)	TiO_2 (anatase)	α-Fe_2O_3	ZnO	SnO_2	WO_3
E_g (eV)	3.0	3.2	2.2	3.35	3.8	2.7

PHOTOCATALYTIC MECHANISM

The above mentioned semiconductor oxides are able to degrade organic and inorganic pollutants by a photocatalytic mechanism. The first step of the mechanism consists of the absorption of sufficiently energetic radiation (visible or UV) by semiconductor oxide particles. The light absorption causes electronic transitions from the valence band to the conduction band, thus generating electron-hole pairs. The electrons (e^-) in conduction band and the holes (h^+) in valence band show a certain oxidizing and reducing capacity, respectively, hence they can participate in redox reactions. In these processes, holes and electrons react with donor or acceptor electron species adsorbed in the semiconductor surface or present in the electrical double layer surrounding the semiconductor particle. Activated carbon with a semiconductor oxide supported on its surface approaches this oxide to the pollutant molecule, thus facilitating its degradation.

In aerated aqueous media, the oxide particles adsorb oxygen and water molecules on their surface, which initiate the redox processes. Firstly, the formation of hydroxyl radicals ($^{\bullet}OH$) takes place through the capture on holes of water molecules or hydroxide ions adsorbed (Eq. (1) y (2)).

$$MO(h^+) + H_2O_{ad} \rightarrow {}^{\bullet}OH + H^+ \quad (1)$$

$$MO(h^+) + {}^-OH_{ad} \rightarrow {}^{\bullet}OH \quad (2)$$

These $^{\bullet}OH$ radicals are highly reactive and have a very short half life. They can also be formed by direct oxidation of pollutant molecules under UV radiation [12]. Then the reduction of adsorbed oxygen occurs by the excited electrons in the conduction band of oxide, thus producing superoxide radicals (O_2^-) (Eq. (3)). After several elementary steps hydrogen peroxide (H_2O_2) is also generated. Moreover, adsorbed oxygen species derived from other available electron acceptors in the aqueous medium can be reduced [12].

$$MO(e^-) + 1/2\ O_{2\ ad} \rightarrow O_2^- \quad (3)$$

Finally, it is worth noting that both $^{\bullet}OH$ radicals and H_2O_2 are highly reactive oxidant species and ultimately responsible for the degradation of organic and inorganic pollutants in aqueous solution.

PREPARATION METHODS

In the preparation of semiconductor oxide catalysts supported on activated carbon different procedures have been used, the most common being impregnation. In this method a determined solution volume of a catalyst precursor is kept in contact with the activated carbon for a certain period of time. The process is carried out at a controlled temperature, with or without stirring. There are two variants of this technique in terms of volume of solution used. If the volume of solution is equal to or less than the pore volume, the method is known as incipient wetness. Conversely, if an excess of precursor solution is used, the technique is called wet impregnation. After a certain period of time, the activated carbon is separated from solution and the excess solvent is removed by drying [13].

In the case of semiconductor oxides, the precursor is usually a metallic salt soluble in aqueous medium. Thus, the adsorption of the metallic ion on the surface of carbon support is achieved. The prepared sample must then be dried and calcined in an inert atmosphere, typically nitrogen gas, to promote the formation of metal oxide on activated carbon surface.

As a precursor, the most used salts are nitrates due to their high solubility in water [14-16]. However, in the case of titanium, tin and tungsten these salts are not commercially available, and so it necessary to resort to others such as tin (II) chloride [17-21] and sodium or ammonium tungstate [22-31]. Preparation of TiO_2 is more complex as described below.

To prepare iron oxide supported on activated carbon the most used precursors are iron (III) nitrate [21,32-49], iron (III) chloride [50-56] and iron (II) sulphate [50-53]. For zinc oxide, salts such as zinc acetate [57-60] and, less frequently, zinc nitrate [61] are used. Aluminium oxide formation on carbon supports has been by far the least studied, aluminium chloride [62] and nitrate [63] being the most common precursors.

Impregnation of carbon support with an aqueous solution of the precursor has the disadvantage that the penetration of the solution into the pores at room temperature is very slow. This is due to the high surface tension of water and largely hydrophobic character of carbon surface [36]. Therefore impregnation is usually carried out by heating and stirring to accelerate the process.

A variant of impregnation method consists of treating the support with a solution of metal carbonyl or alkoxide in *n*-hexane as precursor. This technique has been used to prepare iron and tungsten oxides supported on activated carbon from iron pentacarbonyl [35] and tungsten pentaethoxide [22,27,28,31].

Impregnation method is usually applicable for most of the metal oxides discussed in this chapter, except for TiO_2. Given the large polarizing capacity of the Ti^{4+} cation, due to its high charge and small ionic radius, this ion does not exist as such, but tends to form compounds with a great covalent character, as the TiO_2 itself. For this reason there is no isolated Ti^{4+} ion in solution [64,65]. This problem required the development of different techniques for the preparation of TiO_2 catalysts on different supports. One of the most used and well-known is the sol-gel process. This method involves two major stages. In the first place, the formation of a sol takes place, which consists of a colloidal suspension of solid particles in a liquid phase, through hydrolysis and polymerization reactions of an appropriate precursor, usually metal alkoxides. Then, this sol becomes a semirigid porous gel either by a change in pH, temperature or electrolyte. In order to achieve the cristallinity of the product, the solvent and the residuals in pores must be removed by aging, drying and annealing [13,66]. For TiO_2, the

most used precursors are alkoxides, especially titanium tetraisopropoxide (TTIP) and, to a lesser extent, titanium tetrabutyltitanate (TBOT). Precipitation is one of the simplest and oldest solution-phase synthetic methods. The technique consists of catalyst precursor transformation in another insoluble form through a chemical reaction. Once this precipitated form is deposited on activated carbon, calcination is normally required for its conversion into the corresponding metal oxide. This thermal treatment is carried out in an inert atmosphere as in the impregnation method.

The most used precipitating agent for preparation of metal oxides is hydroxide ion, which is in a basic solution such as NaOH or NH_4OH. Precipitation of metal cations with hydroxide ion leads to the formation of the corresponding metal hydroxides. Their conversion into oxides is easily carried out by drying and aging. This method has been widely used to prepare iron oxide [32-34,50-52,67] and zinc oxide [68] catalysts supported on activated carbon. Iron oxide is usually prepared from a solution of iron (II) sulphate and iron (III) chloride in different molar ratios. However iron compounds, such as hydroxides and oxyhydroxides, which belong to α or γ series, may be formed depending on the precipitation conditions. If a solution of Fe^{2+} and Fe^{3+} cations is used, precipitation with NaOH solution on activated carbon support leads to the formation of four types of compounds: magnetite (Fe_3O_4), maghemite (γ-Fe_2O_3), hematite (α-Fe_2O_3) and goethite (α-FeO(OH)) [51]. Whereas α-FeO(OH) can be turned into α-Fe_2O_3 by direct heating, β- and γ-FeO(OH) provide first γ-Fe_2O_3, which also becomes α-Fe_2O_3 by subsequent heating [69]. Magnetite formation allows its magnetic separation of the adsorbent after application [51]. Another method of general application to load semiconductor oxides supported on activated carbon is Chemical Vapour Deposition (CVD). This technique is widely used in industrial chemical processes to produce high purity solid materials. It is applied in the semiconductor industry to produce thin solid films on this type of material. The technique consists of exposing the substrate to one or more volatile precursors in gaseous phase, in an inert atmosphere. At controlled temperature and pressure, these precursors react or decompose on the substrate surface, thus producing the desired film. During this process volatile by-products are usually generated, which are removed by flowing inert gas. This technique allows solids to be deposited in several forms, such as monocrystalline, polycrystalline, amorphous and epitaxial. Deposited materials include silicon, carbon fibres, nanofibres, filaments and nanotubes, SiO_2, silicon-germanium, tungsten, silicon carbide and nitride, titanium nitride and several others [70-72]. There is a great variety of methods of CVD, which differ in the way of initiation of chemical reaction and process conditions. The choice of one or another method depends on both the type of substrate and precursors used, as well as the required degree of thin film uniformity [12]. For TiO_2 supported on activated carbon, the preferred technique is Metal-Organic Chemical Vapour Deposition (MOCVD). It is characterized by the use of metallo-organic precursors, such as titanium tetra-isopropoxide (TTIP) o $TiCl_4$. In the work of G. Li Puma *et al*. an in-depth discussion is made of the characteristics and advantages of the MOCVD technique for the preparation of TiO_2 photocatalyst supported on activated carbon. In impregnation, precipitation and sol-gel methods for preparing semiconductor oxides on activated carbon support the active phase is mainly spread over the internal surface of the support pores [13,73,74]. This is a serious drawback, since in photocatalysis the active phase must be easily accessible to radiation, which does not occur in the activated carbon pores. This disadvantage can be solved with the application of the MOCVD technique, as described above. The MOCVD preparation method provides the following advantages. First, the active phase is

mostly placed on the outer surface of the support. The active phase has a minimal effect on the porous surface of the support due to the use of gaseous precursors. Moreover, it is possible to eliminate several of the traditional steps in the preparation of these catalysts, such as saturation, drying and reduction. Finally, the properties of the deposited material can be easily controlled [74]. Another method applied to the preparation of metal oxides on activated carbon is the sublimation technique. Basically, it consists of mixing the metal carbonyl with the proper amount of carbon support in a sealed glass tube under vacuum conditions. This system is rotated for a time at an appropriate temperature to achieve the sublimation of the carbonyl on the support. Finally, the assembly is cooled to room temperature. This procedure has been mainly applied to the preparation of tungsten oxide catalysts on activated carbon [22,23,30,31,75] from tungsten hexacarbonyl. It has also been used for iron from $Fe_2(CO)_9$ and $Fe_3(CO)_{12}$. This method is only applied to tungsten and iron because they form stable carbonyls. $W(CO)_6$ is a white solid that sublimates in vacuum, $Fe_2(CO)_9$ forms golden crystals that decompose at 373 K and $Fe_3(CO)_{12}$ is a dark green solid that decomposes at 413 K. A new technique applied in recent years to the synthesis of metal oxides on activated carbon involves the use of supercritical fluids, mainly water and carbon dioxide. A supercritical fluid is any substance which is in conditions of pressure and temperature higher than its critical point. Supercritical fluids can effuse through solids as can gases, and also dissolve such as liquids substances. Therefore they have properties intermediate between those of a liquid and a gas [76]. Supercritical water has been used for the synthesis of iron oxides on activated carbon [36,77,78]. The basis of this method is hydrolysis and dehydration of a metal oxide precursor salt in supercritical water. Supercritical carbon dioxide has also been used in the preparation of titanium dioxide on activated carbon [79]. Application of supercritical fluids to the deposition of metal oxides on carbon supports has the advantage of not using solvents which are toxic or harmful to the environment. Besides, the penetration of precursor in the support porous structure is increased due to the gas-like transport properties and to the very low surface tension of supercritical water [36]. All of the preparation methods outlined above are characterized by the fact that the metal oxide from a suitable precursor is generated in situ on the activated carbon support. However, there is an alternative to these methods which consists of using powder metal oxide to achieve deposition on the carbon support. This technique has been mainly used in the preparation of TiO_2 [80-85] and ZnO [83,86,87] supported on activated carbon, as they are the only two commercially available semiconductor oxides. A very interesting alternative for preparing ZnO catalysts supported on activated carbon consists of starting off with spent catalysts used in the synthesis of vinyl acetate. In this case the zinc acetate adhered to the spent catalyst surface is used as a precursor of ZnO particles. This method has additional advantages such as the abundance and low cost of the spent catalyst used as raw material [59].

APPLICATIONS

Applications of semiconductor metal oxides supported on activated carbon are numerous, the most important ones being those based on catalytic and photocatalytic activity. Most of these oxides are used in heterogeneous catalysis and photocatalysis, which range from degradation reactions of organic pollutants in aqueous solution to organic reactions of

industrial interest such as hydrocarbon isomerization. The second application in importance is the adsorption of certain compounds in gaseous effluents for purification, such as ammonia or carbon monoxide. Without a doubt the most used semiconductor oxide in photocatalysis is titanium dioxide. The reasons for its widespread utilization are the high stability of its chemical structure [12], photostability and reduced gap. In addition, it is not degraded in successive catalytic cycles, therefore it can be reused, and it is a non-toxic and low cost material [91]. Titania exists in three crystalline forms: anatase, rutile and brookite. However, only the first two forms have photocatalytic activity. In many cases it has been found that anatase shows higher photocatalytic activity than rutile. Currently a commercial form of TiO_2 called P-25 is often used, manufactured by the German company Degussa. This material has a high photocatalytic activity and contains around 70 % anatase and 30 % rutile [11,91]. Titania powder degrades pollutant molecules when it is irradiated with UV light. During this process, however, TiO_2 can undergo coagulation due to its interaction with pollutant molecules or the degradation intermediates, thus causing a decrease in photocatalytic activity [12]. This drawback has been solved by supporting TiO_2 on different materials, especially activated carbon. The main application of titania supported on activated carbon is in the purification of indoor and outdoor air and degradation of toxic organic and inorganic pollutants in aqueous solution [12]. The organic species include aromatics (phenol, 4-chlorophenol, 2,4-dinitrophenol, catechol, resorcinol, hydroquinone, *p*-benzoquinone and benzoic acid), dyes (methyl orange, methylene blue, indigo carmine dye and rhodamine 6G), pesticides, paper mill wastewater, alkenes, alcohols, aldehydes and ketones. With regard to inorganic species, the reduction of nitrogen oxides (NO_x) and Cr(VI) species is a main concern. An extensive list of the different organic substrates which can be photodegradated by TiO_2 supported on activated carbon can be found elsewhere [11,12]. Iron oxides supported on activated carbon have been used in degradation reactions of organic compounds in wastewater. This is because they combine the oxidizing power of iron oxides with adsorptive properties of the carbon support [48]. The classic Fenton system consists of iron (II) salts combined with hydrogen peroxide under acidic conditions. This system has been widely used in oxidation and degradation of organic pollutants in water. However, in recent years heterogeneous Fenton systems have been developed, in which the iron (II) cation is replaced by solid materials incorporating iron on their surface, such as iron oxides supported on activated carbon [48,50]. These systems have several advantages, including the possibility of working at a pH value near neutral and of reusing the catalyst [50]. Organic pollutants removed by iron oxides catalysts on activated carbon are varied and range from volatile organic compounds to dyes and pesticides. Some pollutants degraded by this method are phenol [35,43,47,51], methylene blue [48,53], atrazine [50], chloroform [51], chlorobenzene [51] and hydrogen peroxide [45]. Another important application of iron oxide supported on activated carbon is the catalysis of organic reactions of industrial interest, such as Fischer-Tropsch reaction [42], alcohols and amines acylation with carboxylic acids [56], ethylbenzene dehydrogenation [21], NO reduction with CO [44] and benzene hydroxylation [46,49]. Tungsten oxide is a solid of acid character which has a large number of applications in heterogeneous catalysis. In order to improve the efficiency and recovery of tungsten oxide, it is usually supported on different materials, especially activated carbon. Among the applications of these materials are the catalysis of industrial reactions such as hydrotreatment, hydrocracking of heavy fractions from oil, alcohol dehydration, metathesis and isomerization of olefins [23]. It has also been used successfully in the removal of ammonia from air and gaseous effluents [25,89], as well

as the catalytic combustion of volatile organic compounds [29]. Tungsten oxide shows the ability to form a variety of stoichiometric (mainly WO_3 and WO_2) and non- stoichiometric oxides depending on the precursor, type of support, atmosphere and heat treatment temperature [23,29]. The most important tungsten oxide characteristic regarding its applications is the acid character, which is due to the existence of two types of acidic active sites, Brønsted type and Lewis type [23]. Lewis type active sites are a consequence of the existence of unsaturated tungsten atoms which are able to accept electron pairs, whereas the Brønsted type active sites appear because of surface hydroxylation of tungsten oxide particles. The former are important in processes such as the removal of ammonia in gaseous effluents and the latter are involved in the catalysis of reactions such as cracking and isomerization of olefins [23,88]. In order to determine the surface acidity of tungsten oxide catalysts supported on activated carbon several catalytic reactions have been used, such as decomposition of isopropanol. The dehydration of this alcohol is catalyzed only by acid active sites, while dehydrogenation is catalyzed by both acid and basic active sites. Therefore, the dehydration rate provides a measure of total surface acidity, whereas the ratio of dehydrogenation and dehydration rates is an estimation of the total surface basicity of the catalyst. Due to the strongly basic character and to the small size of the ammonia molecule, it is ideal for measuring surface acid sites even within the narrow pores [23]. It has been found that surface acidity of tungsten oxides supported on activated carbon decreases with increasing heat treatment temperature. This fact is due to the loss of acid surface sites of Lewis type, which is caused by the reduction of some tungsten atoms and Brønsted type as a result, in turn, of the loss of surface hydroxyl groups of tungsten oxide particles [23]. A drawback of tungsten oxide catalyst supported on activated carbon is the relatively low gasification temperature, around 400 ºC, when used in an oxidizing atmosphere. It is also important to consider the possibility of tungsten oxide reduction by carbon support around 1123 K [22]. This reaction is thermodynamically favoured at that temperature and leads to the formation of a metal oxide with tungsten in an oxidation state lower than VI or even metallic tungsten (Eq. (4) y (5)) [23]. At higher temperatures it could also lead to the formation of different stoichiometric and non-stoichiometric tungsten carbides.

$$WO_3 + C \rightarrow WO_2 + CO \quad (4)$$

$$WO_3 + 3C \rightarrow W + 3CO \quad (5)$$

The main application of tin (IV) oxide supported on activated carbon is the use in Pressure Swing Adsorption (PSA) systems for hydrogen purification. Currently hydrogen use as an energy source alternative to fossil fuels such as coal, oil and natural gas is being investigated. In this field the PEM (Polymer Electrolyte Membrane) fuel cell has been developed, which obtains electric energy by hydrogen oxidation with oxygen or air, water being the only by-product. The cell electrodes contain a platinum catalyst, which can be poisoned if the concentration of carbon monoxide in the hydrogen flow is above 100 ppm. Therefore, the application of this energy technology requires high purity hydrogen. However, the cheapest production source of hydrogen, steam reforming, produces gas with high carbon monoxide concentrations. Adsorption, and particularly the PSA system, is considered to be one of the best techniques for hydrogen purification by removal of carbon monoxide [18].

It is noteworthy that the presence of a metal such as tin improves the adsorption capacity and affinity of activated carbon toward carbon monoxide. The most important characteristic of SnO_2 is the oxygen deficiency, which gives it *n*-type semiconducting properties. This feature allows it to transfer electrons from conduction band to adsorbed oxygen molecules on its surface to form O_2^- ions and, at higher temperatures, O^- or O^{2-} ions [9,18]. These ionic species adsorbed on SnO_2 surface are responsible for carbon monoxide adsorption and its subsequent oxidation to carbon dioxide. This reaction takes place at room temperature and high pressure by forming a complex [18]. Zinc oxide supported on activated carbon has been used successfully in the adsorption of heavy metals in aqueous solution. ZnO in aqueous media is able to dissociate water molecules in a heterogeneous reaction to create surface hydroxyl groups. These groups, with the surface functional groups of activated carbon, favour the adsorption of toxic heavy metals such as Pb(II), Hg(II), Cd(II), Cu(II) and Cr(VI) [61]. Heavy metals are found in aqueous solution mainly as cationic species and at a relatively acid pH values. In order to promote their adsorption, the total charge of the adsorbent surface must be negative to make possible the solute-adsorbent electrostatic attraction and hence the solute adsorption. This is achieved through the preparation of adsorbents having a low point of zero charge (pH_{PZC}). In this connection it is of note that ZnO supported on activated carbon reduces the point of zero charge with respect to the virgin support, thus promoting the adsorption of heavy metals in aqueous solution [61]. ZnO supported on activated carbon has also been applied in the photocatalytic degradation of organic and inorganic compounds. ZnO is an alternative to TiO_2 supported on activated carbon because their photocatalytic degradation mechanisms are quite similar. Furthermore, ZnO has been proved to be a more efficient metal oxide than TiO_2 in some photocatalytic processes. Treatment of industrial effluents with ZnO is also cheaper than with TiO_2 [59,86]. Accordingly, ZnO supported on activated carbon has been used in the degradation of phenols and its derivatives, such as 4-acetylphenol [86], in aqueous effluents of many chemical industries and dyes in textile effluents, such as acid violet dye [87]. Finally, ZnO supported on activated carbon has been used in the purification and desulfurization of bioethanol. Depending on the starting biomass and the fermentation route used in its preparation, bioethanol can contain different sulphur impurities (e.g. dimethylsulfide) which must be removed. The elimination of sulphur species is carried out traditionally by catalytic hydrodesulphurization, a process which requires large amounts of hydrogen and, therefore, is quite expensive. Adsorption on activated carbon has been shown to be an interesting alternative to the aforesaid process, especially when activated carbon is modified by metal deposition to enhance its adsorption capacity. For adsorptive desulphurization ZnO, in particular, is one of the most suitable metal species due to the strong interaction of zinc with sulphur compounds [92]. Some of the latest studies related to the applications of semiconductor oxides supported on activated carbon are listed in Table 2. For TiO_2 applications a comprehensive recompilation is found elsewhere [12].

Table 2.Some of the latest investigations on semiconductor oxides supported on activated carbon

Raw material	Textural features	Preparation method	Characterization methods	Results	Applications	Comments	References
Hydrocarbon derived granular active carbon	BET surface area: 974 m^2/g Micropore volume: 0.341 cm^3/g Mesopore volume: 0.190 cm^3/g Macropore volume: 0.222 cm^3/g	Impregnation method with an aqueous solution of $Fe(NO_3)_3 \cdot 9H_2O$.	N_2 adsorption-desorption at 77 K Hg porosimetry TXRF Mössbauer spectroscopy	Iron is mainly found as Fe_2O_3. The catalyst is chemically stable and the amount of Fe leached is very low.	Wet air oxidation of phenol at mild conditions (127 ºC and $P(O_2)$ =8 atm.	The oxidation takes place through a heterogeneous mechanism on the catalyst surface. The oxidative coupling of phenol and phenolic compounds is negligible.	[47]
Commercial activated carbon	BET surface area: 880 m^2/g	Impregnation method with an aqueous solution of $Fe(NO_3)_3 \cdot 9H_2O$.	Powder XRD Mösbauer spectroscopy N_2 adsorption-desorption at 77 K Total Fe content measured by AAS XPS SEM	XPS and Mössbauer spectroscopy analysis shows the presence of Fe^{3+}. The iron oxide particles are well-dispersed over the support.	H_2O_2 decomposition Oxidation of methylene blue (MB)	H_2O_2 decomposition takes place by a radical mechanism. MB removal occurs through combined adsorption and oxidation processes. The catalyst is chemically stable and can be reused.	[48]
Activated carbon from coffee used grounds	BET surface area: 950 m^2/g Spongy like texture	Impregnation method with an aqueous solution of $Fe(NO_3)_3 \cdot 9H_2O$.	Powder XRD Mösbauer spectroscopy N_2 adsorption-desorption at 77 K Total Fe content measured by AAS XPS SEM	XPS and Mössbauer spectroscopy analysis shows the presence of Fe^{3+}. The iron oxide particles are well-dispersed over the support.	H_2O_2 decomposition Oxidation of methylene blue	H_2O_2 decomposition takes place by means of a radical mechanism. MB removal occurs through combined adsorption and oxidation processes.	[48]
Commercial activated carbons Norit	BET surface area: 861.5 m^2/g Average pore radius: 11.9 Å Median pore radius: 2.5 Å	Impregnation method with an aqueous solution of $Fe(NO_3)_3 \cdot H_2O$.	XRD N_2 adsorption-desorption at 77 K FE-SEM TPD-MS CO adsorption	Iron is found as Fe_2O_3. The iron oxide is finely dispersed on the AC support. The heat treatment at 600 ºC causes a definite alteration of the nature of surface oxygen groups.	Benzene hydroxylation	The oxygen surface groups have influence on the reaction. Yield of phenol: 20%. There is a synergistic interaction between the oxygen surface groups and the impregnated iron in catalyzing the reaction.	[49]

Table 2. (Continued)

Raw material	Textural features	Preparation method	Characterization methods	Results	Applications	Comments	References
Commercial activated carbon Dinâmica	BET surface area: 666 m^2/g Micropore volume: 0.261 cm^3/g Total pore volume: 0.271 cm^3/g Microporous texture.	Precipitation from an aqueous solution of $FeCl_3$ and $FeSO_4$ with NaOH solution.	Powder XRD FTIR N_2 adsorption-desorption at 77 K SEM	Iron is only found as goethite. The cristallinity increases with the amount of Fe. The iron oxide particles are well-dispersed.	Atrazine oxidation in aqueous medium	The addition of H_2O_2 increases the atrazine removal. The oxidation process consists of two steps: (I) atrazine adsorption and (II) atrazine oxidation. Catalytic activity increases with the iron content.	[50]
Commercial activated carbon pellets	(i) Mesoporous BET surface area: 1370 m^2/g Micropore area: 844.26 m^2/g Total pore volume: 0.694 cm^3/g Micropore volume: 0.390 cm^3/g Pore size: 3.83 nm	Hydrolysis and dehydration of $Fe(NO_3)_3$ in supercritical water. Drying at 50 ºC overnight.	Iron oxide and ash contents determined by calcination at 1273 K for 150 min N_2 adsorption-desorption at 77 K Powder XRD SEM EDS TEM	Iron is mostly found as α-Fe_2O_3. The Fe_2O_3 content increases with immersion time. The specific surface area and total pore volume decrease with immersion time. The pore size does not change.	Volatile organic compounds oxidation		[36,77]
Commercial activated carbon	BET surface area: 933 m^2/g Micropore volume: 0.264 cm^3/g	Precipitation from an aqueous solution of $FeCl_3$ and $FeSO_4$ with NaOH solution.	Powder XRD TG Magnetization measurements Chemical analyses TPR N_2 adsorption at 77 K Mössbauer spectroscopy SEM	The concentration of non-magnetic iron oxides increases with higher activated carbon content. It is mainly formed Fe^{3+} compounds, such as magnetite and maghemite.	Adsorption of volatile organic compounds from aqueous solution (chloroform, phenol, chlorobenzene and drimaren red dye)	The composites show high adsorption capacities for phenol, chlorobenzene, chloroform and drimaren red dye. The iron oxide does not significantly affect the adsorption capacity of activated carbon.	[51]

Raw material	Textural features	Preparation method	Characterization methods	Results	Applications	Comments	References
Commercial activated carbon	BET surface area: 1026 m^2/g Macropore volume: 0.255 cm^3/g Mesopore volume: 0.182 cm^3/g Micropore volume: 0.356 cm^3/g	Precipitation from an aqueous solution of $FeCl_3$ and $FeSO_4$ with NaOH solution.	XRD N_2 adsorption at 77 K SEM XPS	The main phase in the composite is magnetite, maghemite, hematite and goethite. Iron oxides do not affect the surface area and the pore structure of activated carbon.	Removal of arsenic from drinking water.	The composite has more capacity of adsorption arsenic than the virgin activated carbon. Adsorption isotherms of arsenic are described by Langmuir isotherm.	[52]
Polymer-derived carbon.		Polymer impregnation with $Fe(NO_3)_3$ and carbonization.	N_2 adsorption at 77 K Elemental analysis XRD SEM Thermal analysis		Adsorption and oxidation of dibenzo-thiophenes.	Iron oxides participate in the oxidation of adsorbed dibenzothiophenes in larger pores	[38]
Activated carbon from apricot stones.	Surface area: 1060 m^2/g Total pore volume: 0.91 cm^3/g	Impregnation method with different solutions of $Fe(NO_3)_3$: aqueous, methanol, mixed acetone-methanol and ether-methanol.	Fe content by AAS N_2 adsorption at 77 K XPS XRD Magnetic susceptibility Mössbauer spectroscopy	Internal and external surfaces are uniformly distributed in the samples. The methanol medium provides uniform distribution of the iron phase. Iron oxides are in amorphous form.	Reaction of NO reduction by CO.	The catalytic activity decreases in order: water > methanol > ethyl ether > acetone. The catalytic activity increases with treatment temperature for all samples except for that prepared in acetone.	[44]
Commercial activated carbon and activated carbon from spent coffee grounds.	Commercial AC: Surface area: 880 m^2/g Total pore volume: 0.60 cm^3/g AC from spent coffee grounds: Surface area: 950 m^2/g Total pore volume: 0.45 cm^3/g	Impregnation method with an aqueous solution of $Fe(NO_3)_3 \cdot 9H_2O$.	Powder XRD Fe content by AAS N_2 adsorption at 77 K XPS TPR SEM	The treatment of catalysts in hydrogen causes the partial reduction of iron oxides and the formation of magnetite and metallic iron.	H_2O_2 decomposition.	The catalysts were very active for H_2O_2 decomposition and highly stable. Catalyst prepared from spent coffee grounds is more active than that prepared from activated carbon.	[45]

Table 2. (Continued)

Raw material	Textural features	Preparation method	Characterization methods	Results	Applications	Comments	References
Commercial activated carbon		Impregnation method with an aqueous solution of $Fe(NO_3)_3 \cdot 9H_2O$ and iron acetylacetonate.	N_2 adsorption at 77 K XRD SEM Benzene and methanol adsorption	Iron is found as iron oxides on the catalyst surface.	Benzene hydroxylation with H_2O_2.	The transition metals are able to activate the oxidant. The *d* orbital electron density of metal, the surface acidity and hydrophobicity influence the yield of phenol.	[46]
Commercial activated carbon from coconut shell.	Surface area: 1000 m^2/g Mesopore surface area: 186 m^2/g Micropore surface area: 811 m^2/g	Impregnation with an aqueous solution of $Zn(NO_3)_2 \cdot 6H_2O$.	N_2 adsorption at 77 K Measurement of pH_{PZC} Surface functional groups by Boehm method	ZnO supported on activated carbon increases the specific surface area.	Pb(II) adsorption from aqueous solution.	ZnO supported on activated carbon reduces pH_{PZC} and increases Pb(II) removal. Hydroxyl groups are likely responsible for the Pb(II) adsorption.	[61]
Commercial activated carbon.	Surface area: 735.60 m^2/g	Mixing ZnO with activated carbon in an aqueous suspension.	N_2 adsorption at 77 K SEM DRS XRD FT-IR	ZnO particles do not form conglomerates, but are adsorbed on the activated carbon surface.	4-acetylphenol degradation in water.	The efficiency of the photocatalyst is due to the synergetic effect between ZnO and activated carbon. The catalyst is more efficient in solar light, and is stable and reusable.	[86]
Commercial activated carbon	Surface area: 1391 m^2/g Total pore volume: 1.26 cm^3/g Mesopore volume: 1.09 cm^3/g Micropore volume: 0.17 cm^3/g	Impregnation with an aqueous solution of zinc acetate.	N_2 adsorption at 77 K TG XRD		Desulfurization of bioethanol.	Adsorption of dimethylsulfide on ZnO/activated carbon is twice as much as that on activated carbon. The adsorption efficiency is unchanged by impurities.	[92]
Commercial activated carbon		Hydrothermal impregnation with ZnO under mild conditions (T=150 ºC and P=20-30 bars).	N_2 adsorption at 77 K Powder XRD FT-IR SEM		Degradation of acid violet dye.	The decrease in COD values demonstrates the degradation of the organics in the textile effluent.	[87]

Raw material	Textural features	Preparation method	Characterization methods	Results	Applications	Comments	References
Activated carbon from olive stones	Micropore volume: 0.29 cm^3/g Mesopore volume: 0.13 cm^3/g Macropore volume: 0.79 cm^3/g Surface area: 691 m^2/g	Sublimation technique with $W(CO)_6$. Impregnation with an aqueous solution of $(NH_4)_2WO_4$. Impregnation with an *n*-hexane solution of $W(OEt)_5$.	N_2 adsorption at 77 K TPD XRD HRTEM XPS Surface acidity from decomposition of isopropanol	WO_3 particles are formed by thin sheets or films with low cristallinity. $W(CO)_6$ provides the most homogeneous distribution of WO_3 phase.	Decomposition reaction of isopropanol	The catalysts are mainly of acidic character. The total surface acidity follow the order: $W(CO)_6 > W(OEt)_5 > (NH_4)_2WO_4$, the same order as for WO_3 dispersion.	[22]
Activated carbon from almond shells	Surface area: 929 m^2/g Mesopore volume: 0.17 cm^3/g Macropore volume: 0.36 cm^3/g	Impregnation with an aqueous solution of $(NH_4)_2WO_4$. Sublimation technique with $W(CO)_6$.	N_2 adsorption at 77 K Mercury porosimetry TPD XRD XPS Surface acidity from desorption of ammonia and decomposition of isopropanol	The support is able to reduce tungsten oxides to metallic tungsten and react with it to produce tungsten carbides.	Ammonia adsorption. Decomposition reaction of isopropanol	The catalysts are mainly of acidic character. Total surface acidity increases with W content and decreases with treatment temperature.	[23]
Activated carbon from almond shells	Surface area: 929 m^2/g Mesopore volume: 0.17 cm^3/g Macropore volume: 0.36 cm^3/g	Impregnation with an aqueous solution of $(NH_4)_2WO_4$.	N_2 adsorption at 77 K XRD TPD of adsorbed ammonia		Skeletal isomerization of 1-butene	The activity of catalysts does not decrease with reaction time and increases linearly with total surface acidity. By-products from dimerization are not produced. The increase in treatment temperature causes a loss of activity.	[88]
Wood-based carbon	Surface area: 2143 m^2/g Total pore volume: 1.494 cm^3/g Mesopore volume: 0.696 cm^3/g Micropore volume: 0.798 cm^3/g	Impregnation with an aqueous solution of ammonium metatungstate $(NH_4)_6H_2W_{12}O_{40}$.	Surface pH TG N_2 adsorption at 77 K Potentiometric titration FT-IR		Removal of ammonia from air.	Tungsten oxides supported on activated carbon increase NH_3 uptake due to the creation of additional Brønsted centres.	[25]

Table 2. (Continued)

Raw material	Textural features	Preparation method	Characterization methods	Results	Applications	Comments	References
Activated carbon from almond shells	Surface area: 929 m^2/g Mesopore volume: 0.17 cm^3/g Macropore volume: 0.36 cm^3/g	Impregnation with an aqueous solution of $(NH_4)_2WO_4$.	N_2 adsorption at 77 K XRD TPD of adsorbed ammonia		Decomposition reactions of methanol and ethanol.	The activity of catalysts increases linearly with total surface acidity. Activated carbon reduces the acid strength of tungsten oxide particles due to metal oxide- carbon interactions.	[26]
Coconut shell-based activated carbon	Surface area: 1069 m^2/g Total pore volume: 0.55 cm^3/g Mesopore volume: 0.01 cm^3/g Micropore volume: 0.54 cm^3/g	Impregnation with an aqueous solution of ammonium metatungstate $(NH_4)_6H_2W_{12}O_{40}$.	N_2 adsorption at 77 K Potentiometric titration FT-IR XRD TG		Removal of ammonia from air.	Tungsten oxides supported on activated carbon increase surface acidity and NH_3 uptake due to the creation of additional Brønsted centres.	[89]
Activated carbon from almond shells	Surface area: 929 m^2/g Mesopore volume: 0.17 cm^3/g Macropore volume: 0.36 cm^3/g	Impregnation with an aqueous solution of $(NH_4)_2WO_4$.	N_2 adsorption at 77 K Mercury porosimetry Surface acidity from desorption of ammonia and decomposition of isopropanol Powder XRD XPS TG	Catalyst acidity and cristallinity increase with tungsten content. Tungsten oxide is well dispersed on the carbon surface.	Catalytic combustion of toluene.	Formation of nonstoichiometric tungsten oxides favours the toluene oxidation to CO_2. The catalytic behaviour improves with the increase of tungsten content, reaction temperature and contact time.	[29]
Activated carbon from almond shells	Surface area: 929 m^2/g Mesopore volume: 0.17 cm^3/g Macropore volume: 0.36 cm^3/g	Impregnation with an aqueous solution of $(NH_4)_2WO_4$. Sublimation technique with $W(CO)_6$.	N_2 adsorption at 77 K Mercury porosimetry XRD XPS	W particles are sintered with increasing treatment temperature. The proportion of metallic W increases with W content after the treatment in H_2 flow.	Hydrogenation reaction of ethylene.	The catalysts containing WC are much more active than those containing metallic W.	[30]

CONCLUSIONS

The use of semiconductor oxides supported on activated carbon has received increasing interest due to certain advantages of this support, such as its high surface area and porosity, which allows the dispersion of catalytically active phase, chemical inertness and low cost.

There are a variety of preparation methods for semiconductor oxides supported on activated carbon. However, none of them can be generally applied to all of these oxides because of their different features. The choice of a preparation method depends on the semiconductor oxide as well as other factors such as the application, the dispersion degree or the oxide crystalline structure. These materials find their main application in the wastewater purification by the photocatalytic degradation of organic and inorganic compounds. This area mainly includes TiO_2, α-Fe_2O_3 and ZnO supported on activated carbon. Another important application is in the heterogeneous catalysis of numerous organic reactions, especially in the case of WO_3. Finally, SnO_2 has been used in purification systems for gaseous effluents.

REFERENCES

[1] Bansal, R. C.; Doner, J. B. *Active Carbon*. Marcel Dekker: New York, 1998.

[2] Marsh, H; Heintz, E. A.; Rodríguez-Reinoso, F. *Introduction to Carbon Technologies*. Universidad de Alicante: Alicante, 1997.

[3] Jankowska, H.; Swiatkowski, S.; Choma, J. *Active Carbon*. Ellis Horwood: New York, 1991.

[4] Rodríguez-Reinoso, F. The role of carbon materials in heterogeneous catalysis. *Carbon* 1998, *36*, 159-175.

[5] Gómez-Serrano, V.; Piriz-Almeida, F.; Durán-Valle, C. J.; Pastor-Villegas, J. Formation of oxygen structures by air activation. A study by FT-IR spectroscopy. *Carbon* 1999, *37*, 1517-1528.

[6] Choi, J. S.; Kim, T. H.; Choo, K. Y.; Sung, J. S.; Saidutta, M. B.; Ryu, S. O.; Song, S. D.; Ramachandra, B.; Rhee, Y. W. Direct synthesis of phenol from benzene on iron-impregnated activated carbon catalysts. *Appl. Catal. A*. 2005, *290*, 1-8.

[7] Miessler, G. L.; Tarr, D. A. *Inorganic Chemistry*, 3rd ed.; Pearson Education: 2004.

[8] Candal, R. J.; Bilmes, S. A.; M. A. Blesa. Semiconductores con Actividad Fotocatalítica. *In Eliminación de Contaminantes por Fotocatálisis Heterogénea*; CYTED: La Plata, 2001.

[9] Housecroft, C. E.; Sharpe, A.G. *Inorganic Chemistry*, 2nd ed.; Pearson Education: 2005.

[10] Hoffman, R. *Solids and Surfaces: A Chemist's View of Bonding in Extended Structures*. VCH Publishers: New York, 1988.

[11] Mills, A.; Le Hunte, S. An overview of semiconductor photocatalysis. *J. Photochem. and Photobiol. A*. 1997, *108*, 1-35.

[12] Li Puma, G.; Bono, A.; Krishnaiah, D.; Collin, J. G. Preparation of titanium dioxide photocatalyst loaded onto activated carbon support using chemical vapor deposition: A review paper. *J. Hazard. Mater*. 2008, *157*, 209-19.

[13] Schwarz, J. A.; Contescu, C.; Contescu, A. Methods for Preparation of Catalytic Materials. *Chem. Rev*. 1995, *95*, 477-510.

[14] Sharpe, A. G. *Inorganic Chemistry*, 2nd ed.; Logman: New York, 1986.

[15] Douglas, B.E.; Alexander, J. J.*Concepts and Models of Inorganic Chemistry*, 2nd ed.;Wiley: New York, 1983.

[16] Rochow, E. G. *Modern Descriptive Chemistry*. Saunders College Publishing: Philadelphia, 1977.

[17] Iyuke, S. E. Synthesized tin-activated carbon adsorbent for purer and cheaper hydrogen. *Trans. IChemE*. 2001, *79*: Part A.

[18] Iyuke, S. E.; Daud, W. R. W.; Mohamad, A.B.; Kadhum, A.A.H.; Fisal, Z.; Shariff, A. M. Application of Sn-activated carbon in pressure swing adsorption for purification of H_2. *Chem. Eng. Sc*. 2000, *55*, 4745-4755.

[19] Mohamad, A. B.; Iyuke, S.E.; Daud, W.R.W.; Kadhum, A. A. H.; Fisal, Z.; Al-Khatib, M. F.; Shariff, A. M. Adsorption of carbon monoxide on activated carbon-tin ligand. *J. Molec. Struc*. 2000, *550-551*, 511-519.

[20] Al-Khatib, M. F.; Iyuke, S. E.; Mohamad, A. B.; Daud, W. R. W.; Kadhum, A. A. H.; Shariff, A. M.; Yarmo, M. A. The effect of impregnation of activated carbon with $SnCl_2{\cdot}2H_2O$ on its porosity, surface composition, and CO gas adsorption. *Carbon*. 2002, *40*, 1929-1936.

[21] Ikenaga, N.; Tsuruda, T.; Senma, K.; Yamaguchi, T.; Sakurai, Y.; Suzuki, T. Dehydrogenation of Ethylbenzene with Carbon Dioxide Using Activated Carbon-Supported Catalysts. *Ind. Eng. Chem. Res*. 2000, *39*, 1228-1234.

[22] Pérez-Cadenas, A. F.; Moreno-Castilla, C.; Maldonado-Hódar, F. J.; Fierro, J. L. G. Tungsten oxide catalysts supported on activated carbons: effect of tungsten precursor and pretreatment on dispersion, distribution, and surface acidity of catalysts. *J. Catal*. 2003, *217*, 30-37.

[23] Álvarez-Merino, M. A.; Carrasco-Marín, F.; Fierro, J. L. G.; Moreno-Castilla, C. Tungsten catalysts supported on activated carbon. I: preparation and characterization after their heat treatments in inert atmosphere. *J. Catal*. 2000, *192*, 363-373.

[24] Pawelec, B.; Mariscal, R.; Fierro, J. L. G.; Greenwood, A.; Vasudevan, P. T. Carbon-supported tungsten and nickel catalysts for hydrodesulfurization and hydrogenation reactions. *Appl. Catal. A General*. 2001, *206*, 295-307.

[25] Petit, C.; Bandosz, T.J. Role of surface heterogeneity in the removal of ammonia from air on micro/mesoporous activated carbons modified with molybdenum and tungsten oxides. *Micropor. Mesopor. Mater*. 2009, *118*, 61-67.

[26] Moreno-Castilla, C.; Álvarez-Merino, M.A.; Carrasco-Marín, F. Decomposition reactions of methanol and ethanol catalyzed by tungsten oxide supported on activated carbon. *React. Kinet. Catal. Lett*. 2000, *71*, 137-142.

[27] [27] Pérez-Cadenas, A. F.; Maldonado-Hódar, F. J.; Fierro, J. L. G.; Moreno-Castilla, C. Influence of Carbon-Chlorine Surface Complexes on the Properties of Tungsten Oxide Supported on Activated Carbons. 1.Dispersion, Distribution, and Chemical Nature of Metal Oxide Phase. *J. Phys. Chem. B*. 2003, *107*, 4997-5002.

[28] Pérez-Cadenas, A. F.; Maldonado-Hódar, F. J.; Fierro, J. L. G.; Moreno-Castilla, C. Influence of Carbon-Chlorine Surface Complexes on the Properties of Tungsten Oxide Supported on Activated Carbons. 2.Surface Acidity and Skeletal Isomerization of 1-Butene. *J. Phys. Chem. B*. 2003, *107*, 5003-5007.

[29] Álvarez-Merino, M. A.; Ribeiro, M. F.; Silva, J. M.; Carrasco-Marín, F.; Maldonado-Hódar, F. J. Activated Carbon and Tungsten Oxide Supported on Activated Carbon Catalysts for Toluene Catalytic Combustion. *Envirom. Sci. Technol.* 2004, *38*, 4664-4670.

[30] Moreno-Castilla, C.; Álvarez-Merino, M. A.; Carrasco-Marín, F.; Fierro, J. L. G. Tungsten and Tungsten Carbide Supported on Activated Carbon: Surface Structures and Performance for Ethylene Hydrogenation. *Langmuir*. 2001, *17*, 1752-1756.

[31] Moreno-Castilla, C.; Pérez-Cadenas, A. F.; Maldonado-Hódar, F. J.; Carrasco-Marín, F.; Fierro, J. L. G. Influence of carbon-oxygen surface complexes on the surface acidity of tungsten oxide catalysts supported on activated carbons. *Carbon*. 2003, *41*, 1157-1167.

[32] Chen, W.; Parette, R.; Zou, J.; Cannon, F. S.; Dempsey, B. A. Arsenic removal by iron-modified activated carbon. *Wat. Res*. 2007, *41*, 1851-1858.

[33] Uranowski, L. J.; Tessmer, C. H.; Vidic, R. D. The effect of surface metal oxides on activated carbon adsorption of phenolics. *Wat. Res.* 1998, *32*, 1841-1851.

[34] Heisig, C.; Zhang, W.; Oyama, S. T. Decomposition of ozone using carbon-supported metal oxide catalysts. *Appl. Catal. B: Environ*. 1997, *14*, 117-129.

[35] Rey A, Faraldos M, Casas JA, Zazo JA, Bahamonde A, Rodríguez JJ. Catalytic wet peroxide oxidation of phenol over Fe/AC catalysts: Influence of iron precursor and activated carbon surface. *Appl. Catal. B: Environ*. 2009; *86*, 69-77

[36] Xu, C.; Teja, A. S. Supercritical water synthesis and deposition of iron oxide (α-Fe_2O_3) nanoparticles in activated carbon. *J. Supercrit. Fluids*. 2006, *39*, 135-141.

[37] Shimada, H.; Akazawa, T.; Ikenaga, N.; Suzuki, T. Dehydrogenation of isobutene to isobutene with iron-loaded activated carbon catalyst. *Appl. Catal. A General*. 1998, *168*, 243-250.

[38] Seredych, M.; Bandosz, T. J. Adsorption of dibenzothiophenes on activated carbons with copper and iron deposited on their surfaces. *Fuel Process. Technol*. 2010, *91*, 693-701.

[39] Huwe, H.; Fröba, M. Iron (III) oxide nanoparticles within the pore system of mesoporous carbon CMK-1: intra-pore synthesis and characterization. *Micropor. Mesopor. Mater*. 2003, *60*, 151-158.

[40] Minchev, C.; Huwe, H.; Tsoncheva, T.; Paneva, D.; Dimitrov, M.; Mitov, I.; Fröba M. Iron oxide modified mesoporous carbons: Physicochemical and catalytic study. *Micropor. Mesopor. Mater*. 2005, *81*, 333-341.

[41] Huwe, H; Fröba, M. Synthesis and characterization of transition metal and metal oxide nanoparticles inside mesoporous carbon CMK-3. *Carbon*. 2007, *45*, 304-314.

[42] Abbaslou, R. M. M.; Tavassoli, A.; Soltan, J.; Dalai, A. K. Iron catalysts supported on carbon nanotubes for Fischer-Tropsch synthesis: Effect of catalytic site position. *Appl. Catal. A General*. 2009, *367*, 47-52.

[43] Quintanilla, A.; Menéndez, N.; Tornero, J.; Casas, J. A.; Rodríguez, J. J. Surface modification of carbon-supported iron catalyst during the wet air oxidation of phenol: Influence on activity, selectivity and stability. *Appl. Catal. B Environmental.* 2008, *81*, 105-114.

[44] Stoyanova, D.; Nickolov, R.; Khristova, M.; Paneva, D.; Mehandjiev, D. Catalytic activity of Fe/AC, obtained by impregnation of activated carbon in aqueous and non-aqueous media, to neutralize NO. *J. Porous Mater*. 2009, *16*, 1-7.

[45] Castro, C. S.; Oliveira, L. C. A.; Guerreiro, M. C. Effect of Hydrogen Treatment on the Catalytic Activity of iron oxide based materials dispersed over activated carbon: investigations toward hydrogen peroxide decomposition. *Catal. Lett.* 2009, *133*, 41-48.

[46] Choi, J. S.; Kim, T. H.; Choo, K. Y.; Sung, J. S.; Saidutta, M. B.; Song, S. D.; Rhee, Y. W. Transition metals supported on activated carbon as benzene hydroxilation catalysts. *J. Porous Mater*. 2005, *12*, 301-310.

[47] Quintanilla, A.; Casas, J. A.; Zazo, J. A.; Mohedano, A. F.; Rodríguez, J. J. Wet air oxidation of phenol at mild conditions with Fe/activated carbon catalyst. *Appl. Catal. B Environmental*. 2006, *62*, 115-120.

[48] Castro, C. S.; Guerreiro, M. C.; Oliveira, L. C. A, Gonçalves, M.; Anastácio, A. S.; Nazzarro, M. Iron oxide dispersed over activated carbon: Support influence on the oxidation of the model molecule methylene blue. *Appl. Catal. A General*. 2009, *367*, 53-58.

[49] Choi, J. S.; Kim, T. H.; Choo, K. Y.; Sung, J. S.; Saidutta, M. B.; Ryu, S. O.; Song, S. D.; Ramachandra, B.; Rhee, Y. W. Direct synthesis of phenol from benzene on iron-impregnated activated carbon catalysts. *Appl. Catal. A General*. 2005, *290*, 1-8.

[50] Castro, C. S.; Guerreiro, M. C.; Gonçalves, M.; Oliveira, L. C. A.; Anastácio, A. S. Activated carbon/iron oxide composites for the removal of atrazine from aqueous medium. *J. Hazard. Mater*. 2009, *164*, 609-614.

[51] Oliveira, L. C. A.; Rios, R. V. R. A.; Fabris, J. D.; Garg, V.; Sapag, K.; Lago, R. M. Activated carbon / iron oxide magnetic composites for the adsorption of contaminants in water. *Carbon*. 2002, *40*, 2177-2183.

[52] Zhang, Q. L.; Lin, Y. C.; Chen, X.; Gao, N.Y. A method for preparing ferric activated carbon composites adsorbents to remove arsenic from drinking water. *J. Hazard. Mater*. 2007, *148*, 671-678.

[53] Castro, C. S.; Guerreiro, M. C.; Oliveira, L. C. A.; Gonçalves, M. Removal of organic compounds from water by activated carbon impregnated with iron oxide: combined action of adsorption and oxidation in the presence of H_2O_2. *Quimica Nova*. 2009, *32*, 1561-1565.

[54] Fierro, V.; Muñiz, G.; González-Sánchez, G.; Ballinas, M. L.; Celzard, A. Arsenic removal by iron-doped activated carbons prepared by ferric chloride forced hydrolysis. *J. Hazard. Mater*. 2009, *168*, 430-437.

[55] Yang, J. K.; Park, H. J.; Lee, H. D.; Lee, S. M. Removal of Cu(II) by activated carbon impregnated with iron(III). *Colloids Surfaces A Physicochem. Engin. Aspects*. 2009, *337*, 154-158.

[56] Sreedhar, B.; Bhaskar, V.; Sridhar, C.; Srinivas, T.; Kótai, L.; Szentmihályi, K. Acylation of alcohols and amines with carboxylic acids: a first report catalyzed by iron(III) oxide-containing activated carbon. *J. Molec. Catal. A Chemical*. 2003, *191*, 141-147.

[57] Park, N. K.; Lee, Y. J.; Han, G. B.; Ryu, S. O.; Lee, T. J.; Chang, C. H.; Han, G. Y. Synthesis of various zinc oxide nanostructures with zinc acetate and activated carbon by a matrix-assisted method. *Colloids and Surfaces A: Physicochemical and Engineering Aspects*. 2008, *313-314*, 66-71.

[58] Kawaguchi, T.; Nakagawa, J.; Wakasugi, T. Method of preparation of an activated carbon supported zinc acetate catalyst. *Appl. Catal*. 1987, *32*, 23-36.

[59] Zhang, Z.; Niu, H.; Fernández, Y.; Menéndez, J. A.; Peng, J.; Zhang, Z.; Zhang, L.; Duan, X. Effect of temperature on the properties of ZnO/activated carbon composites from spent catalysts containing zinc acetate. *Journal of the Taiwan Institute of Chemcial Engineers*. 2010, *41*, 617-621.

[60] Yao, S.; Li, J.; Shi, Z. Immobilization of TiO_2 nanoparticles on activated carbon fiber and its photodegradation performance for organic pollutants. *Particuol*. 2010, *8*, 272-278.

[61] Kikuchi, Y.; Quian, Q.; Machida, M.; Tatsumoto, H. Effect of ZnO loading to activated carbon on Pb(II) adsorption from aqueous solution. *Carbon*. 2006, *44*, 195-202.

[62] Tchomgui-Kamga, E.; Alonzo, V.; Nanseu-Njiki, C. P.; Audebrand, N.; Ngameni, E.; Darchen, A. Preparation and characterization of charcoals that contain dispersed aluminum oxide as adsorbents for removal of fluoride from drinking water. *Carbon*. 2010, *48*, 333-343.

[63] Leyva-Ramos, R.; Ovalle-Turrubiartes, J.; Sánchez-Castillo, M. A. Adsorption of fluoride from aqueous solution on aluminum-impregnated carbon. *Carbon*. 1999, *37*, 609-617.

[64] Housecroft, C. E.; Sharpe, A. G. *Inorganic Chemistry*, 2nd ed.; Pearson Education: Harlow, Essex, England, 2005.

[65] Chambers, C.; Holliday, A. K. *Modern Inorganic Chemistry*. Butterworth: Chichester, Sussex, England, 1975.

[66] Lalena, J. N.; Cleary, D. A.; Carpenter, E. E.; Dean, N. F. *Inorganic materials synthesis and fabrication*. Wiley: New Jersey, 2008.

[67] Hristovski, K. D.; Westerhoff, P. K.; Möller, T.; Sylvester, P. Effect of synthesis conditions on nano-iron (hydr)oxide impregnated granulated activated carbon. *Chem. Engin. J*. 2009, *146*, 237-243.

[68] Xu, Z.; Li, F.; Zhang, X. Preparation and photocatalytic activity of ZnO/AC composite photocatalyst. *Chin. J. Rare Metals*. 2008, *32*, 493-496.

[69] Wells, A. F. *Structural Inorganic Chemistry*, 3rd ed.; Clarendon Press: London, 1962.

[70] Smith, D. L. *Thin-film deposition: principles and practice*, McGraw-Hill: New York, 1995.

[71] Dobkin, D. M.; Zuraw, M. K. *Principles of chemical vapor deposition*. Kluwer: Dordrecht, The Netherlands, 2003.

[72] Jaeger, R. C. *Film deposition, in: Introduction to microelectronic fabrication. Modular Series on Solid State Devices*, Vol. 5, 2nd ed; Prentice Hall: Upper Saddle River, 2002.

[73] Tryba, B.; Morawski, A. W.; Inagaki, M. Application of TiO_2 mounted activated carbon to the removal of phenol from water. *Appl. Catal. B Environmental*. 2003, *41*, 427-433.

[74] Zhang, X.; Zhou, M.; Lei, L. Preparation of photocatalytic TiO_2 coatings of nanosized particles on activated carbon by AP-MOCVD. *Carbon*. 2005, *43*, 1700-1708.

[75] Álvarez-Merino, M. A.; Joly, J. P.; Carrasco-Marín, F.; Moreno-Castilla, C. Application of ammonia intermittent temperature-programmed desorption to evaluate surface acidity of tungsten oxide supported on activated carbon. *Journal of Colloid and Interface Science*. 2003, *260*, 449-453.

[76] Székely, E. *Supercritical Fluid Extraction*. University of Technology and Economics: Budapest, 2007.

[77] Xu, C.; Teja, A. S. Characteristics of iron oxide/activated carbon nanocomposites prepared using supercritical water. *Appl. Catal. A General*. 2008, *348*, 251-256.

[78] Fan, H.; Xu, Q.; Guo, Y.; Peng, Q.; Hou, Z. Nanoporous ferric oxide prepared with activated carbon template in supercritical carbon dioxide. *Mater. Sc. Engin. A*. 2006, *422*, 272-277.

[79] Tatsuda, N.; Itahara, H.; Setoyama, N.; Fukushima, Y. Preparation of titanium dioxide/activated carbon composites using supercritical carbon dioxide. *Carbon*. 2005, *43*, 2358-2365.

[80] Lu, M. C.; Chen, J. N.; Chang, K. T. Effect of adsorbents coated with titanium dioxide on the photocatalytic degradation of propoxur. *Chemosphere*. 1999, *38*, 617-627.

[81] Cao, X.; Oda, Y.; Shiraishi, F. Photocatalytic and adsorptive treatment of 2,4-dinitrophenol using a TiO_2 film covering activated carbon surface. *Chem. Engin. J*. 2010, *156*, 98-105.

[82] Cao, X.; Shiraishi, F. A mechanism of photocatalytic and adsorptive treatment of 2,4-dinitrophenol on a porous thin film of TiO_2 covering granular activated carbon particles. *Chem. Engin. J*. 2010, *160*, 651-659.

[83] Matos, J.; García-López, E.; Palmisano, L.; García, A.; Marcì, G. Influence of activated carbon in TiO_2 and ZnO mediated photo-assisted degradation of 2-propanol in gas-solid regime. *Appl. Catal. B Environmental*. 2010, *99*, 170-180.

[84] El-Sheikh, A. H.; Newman, A. P.; Al-Daffaee, H.; Phull, S.; Cresswell, N.; York, S. Deposition of anatase on the surface of activated carbon. *Surf. Coat. Technol*. 2004, *187*, 284-292.

[85] Kahn, A.; Mazyck, D. Journal of Undergraduate Research 2002 June, http://www.clas.ufl.edu/jur/200206/papers/paper_khan.html

[86] Sobana, N.; Murugadanandam, M.; Swaminathan, M. Characterization of AC-ZnO catalyst and its photocatalytic activity on 4-acetylphenol degradation. *Catal. Commun*. 2008, *9*, 262-268.

[87] Byrappa, K.; Subramani, A. K.; Ananda, S. Impregnation of ZnO onto activated carbon under hydrothermal conditions and its photocatalytic properties. *J. Mater Sci*. 2006, *41*, 1355-1362.

[88] Álvarez-Merino, M. A.; Carrasco-Marín, F.; Moreno-Castilla, C. Tungsten Catalysts Supported on Activated Carbon. II. Skeletal Isomerization of 1-Butene. *J. Catal*. 2000, *192*, 374-380.

[89] Petit, C.; Bandosz, T. J. Removal of Ammonia from Air on Molybdenum and Tungsten Oxide Modified Activated Carbons. *Environ. Sci. Technol*. 2008, *42*, 3033-3039.

[90] Iyuke, S. E.; Ahmadun, F.-R. Adsorption and solid catalysed reaction between activated carbon impregnated with SnO_2 and CO at ordinary temperature. *Appl. Surf. Sc.* 2002, *187*, 37-44.

[91] Grupo TAR. Anexo I. Uso del dióxido de titanio (TiO_2) como catalizador. www.grupotar.org

[92] Chaichanawong, J.; Yamamoto, T.; Ohmori, T.; Endo, A. Adsorptive desulfurization of bioethanol using activated carbon loaded with zinc oxide. *Chem. Engin. J*. 2010, doi:10.1016/j.cej.2010.09.020.

In: Activated Carbon
Editor: James F. Kwiatkowski
ISBN: 978-1-61209-684-1
©2012 Nova Science Publishers, Inc.

Chapter 9

USING "ACTIVATED CARBON FROM BAGASSE" FOR COLOR REMOVAL

Paitip Thiravetyan*[1] and Parinda Suksabye[2]
[1]Division of Biotechnology, School of Bioresources and Technology, King Mongkut's University of Technology Thonburi, Thakham, Bangkhuntien, Bangkok, Thailand
[2]Department of Environmental Science, Faculty of Science and Technology , Suan Dusit Rajabhat University, Dusit, Bangkok, Thailand

1. INTRODUCTION

Activated carbons have always become interesting materials due to their continuous usages in many areas. These materials have been synthesized from many types of carbonaceous precursors. Formerly, coal has become the major precursor for activated carbon production. Since coal is more valuable to be used for energy generation, people started to study many type of biomass such as coconut shell (Mozammel *et al*., 2002; Daud and Ali, 2004) as the precursors. The utilization of several type of biomass for activated carbon production has a positive impact in reducing organic solid wastes.

One of the potential side products from the industries that can be used for producing derivative products is bagasse, a solid waste from sugar juice extraction process. At present, the common utilization of bagasse is based on its cellulosic content such as for making pulp and particle board. In fact, bagasse is a valuable solid fuel to be combusted in steam boilers. Most of the industries take this advantage and leave minimal excess of bagasse during normal milling season. However, the ash from combustion process still contained high fixed carbon content (60%) and have not yet commercially utilized causing disposal problems. This ash is called 'bagasse bottom ash (BBA)' has high potential in producing activated carbon. In term of BBA, the supply is steady as long as sugar industries still use bagasse for fueling their steam boiler. A sugar industry emits approximately 5.5 kg of fly ash per metric ton of cane processed in the fuel gases from the bagasse combustion. In case of Indonesia with around 2.5

* Corresponding author: E-mail:paitip.thi@kmutt.ac.th

million tons of annual production of cane, 13,750 tons of BBA per year is produced nationwide.

Different types of activated carbons can be produced with specific characteristics depending on the raw material and activation technique used in their production. The manufacture of activated carbons involved two mains steps: the carbonization of carbonaceous raw material, and the physical and/or chemical activation. According to BBA is already a charcoal. Therefore, production of activated carbon from BBA needed only one step by activation BBA by physical and/or chemical activation. The advantage of activated carbon from BBA is it contained mainly mesopores that can use to adsorb large molecules of organic compounds such as textile dyes, melanoidins, various colors from sugar syrup, colors from vegetable oils, etc which the commercial activated carbon from coconut shell cannot adsorb these large molecules. Therefore, BBA activated carbon can be applied to use as an alternative adsorbent in various industries such as sugar and vegetable oils industries.

2. SUGARCANE BAGASSE AND ITS APPLICATION

2.1. Composition of Bagasse

Bagasse is a fibrous residue of cane stalks left over after the crushing and extraction of the juice from the sugar cane. It is a by-product of the sugar industry and is almost completely used by the sugar factories themselves as fuel for the boilers (Pandey et al., 2000). The cellulose and lignin are major contained in sugarcane bagasse (Table 1). In addition, the proximate analysis of sugarcane is shown in Table 1. For the results, the sugarcane bagasse has low ash content and high fixed carbon content. Therefore, it can be developed to be activated carbon.

Table 1. Chemical composition and proximate analysis of sugarcane bagasse (Modified from Kalderis et al., 2008; Garzia –Perez et al., 2002)

Composition	%
Chemical composition	
-Cellulose	43.1
-Hemicellulose	35.8
-Lignin	21.1
Proximate analysis	
-Moisture	6.1
-Ash content	3.3
-Volatile matter	65.9
-Fixed carbon	24.7

2.2. Application of Bagasse

There are many process and products that utilize bagasse as raw material as following:

- *Ethanol:* Bagasse could use for the production of ethanol. However, the ethanol production from bagasse needs its hydrolysis, which requires large quantities of cellulase enzymes for saccharification. As processes for the production of cellulases are presently quite expensive and economically unfeasible, such bioconversion appears unattractive. Thus, much effort would be needed to develop the technology for economical production of saccharifying enzymes and also improve the condition of hydrolysis (Pandey et al., 2000).
- *Fuel and electricity generation:* Normally, almost quantity of the bagasse produced is used by the sugar mills themselves as fuel for boilers, which is necessity-based economical and an efficient application. Furthermore, sugarcane bagasse is also used to generate the electricity for using in sugar mill or sale electricity to independent power producers.
- *Protein-enriched animal feed and enzymes:* One of the significant applications of bagasse has been for the production of protein-enriched cattle feed and enzymes. Although the economy of such processes in submerged fermentation is severely affected by the high cost of product isolation, simultaneous isolation and marketing of cellulases enzymes have made economics to recover somewhat. Similarly, although enzymatic saccharification of cellulose has been demonstrated to be uneconomical, cellulases are increasingly being used for the extraction of fruit juices, starch, and oil from woody materials. These enzymes can be recovered rather easily from fermented matter involving solid-state fermentation of bagasse making this system appropriate for protein enrichment and cellulases production from bagasse (Pandey et al., 2000).
- *Pulp and paper:* Using bagasse for paper production has advantage rather than wood due to reducing deforestation. Furthermore, bagasse requires less bleaching chemicals than wood pulp to achieve a bright, white sheet of paper. Bagasse fibers are well suited for tissue, corrugating medium, newsprint, and writing paper.
- *Adsorbent:* Bagasse can be developed to be an adsorbent for removal of the impurities of wastewater such as heavy metals, dyes from textile wastewater and organic compounds. In addition, it can adsorb the colorant of sugar syrup and the pigments of vegetable oil.

2.3. The Waste “Bagasse Bottom Ash” and its Composition

The bagasse bottom ash is the waste from the boiler of sugar factories due to the fact that sugarcane bagasse is used as fuel in boiler. The properties of bagasse bottom ash are given in Table 2. The proximate analysis is calculated by TGA analyzer. An elemental analyzer determined the contents of C, H, N, O and S in the ultimate analysis. The results indicated that bagasse bottom ash had high fixed carbon and high ash content. In addition, the physical properties of bagasse bottom ash are shown in Table 2.

Table 2. Chemical composition, physical properties and proximate analysis of bagasse bottom ash (Aworn, 2007; Suksabye, 2009)

Composition	%
Proximate analysis(dry basis,wt%)	
- Volatile matter	27.0
- Ash	18.4
- Fixed carbon	54.6
Ultimate analysis (wt%)	
- C	60.83
- H	0.24
- N	0.007
- S	0.00
- O (by difference)	38.86
Physical properties	
Total surface area, S_T ($cm^2\ g^{-1}$)	281.51
Total pore volume, V_T ($cm^3\ g^{-1}$)	0.1840
Average pore diameter, D (Å)	26.14

3. PRODUCTION OF BAGASSE BOTTOM ASH ACTIVATED CARBON

Activated carbon is a process carbon material with a highly developed porous structure and a large internal specific surface area (McKay, 1996). The activated carbon can be produced from many material such as bituminous coal, pistachio shell (Wu et al., 2005) coconut shell (Moazmmel et al., 2002 ; Daud and Ali, 2004), oil-palm shell (Lua et al., 2006) and corncob (Tseng et al., 2006), etc. These adsorbents are used for the purification and separation of liquids and gases. The complex network of pore of activated carbon has been classified into micropore (diameters <2 nm), mesopore (diameters 2-50 nm), and macropore (diameter >50 nm) (Patrick, 1995). The pore size of activated carbons depends on the raw material and activation technique used in their production. The manufacture of activated carbons from materials involves two main steps: carbonization and activation.

– Carbonization

Carbonization involves thermal decomposition of the carbonaceous material, eliminating noncarbon specials and producing a fixed carbon mass and a rudimentary pore structure. The process is usually carried out in rotary kilns or multiple hearth furnance at temperature below 800 °C in a continuous stream of an inert gas. The carbonization is almost complete in the temperature range 400-600 °C. The carbon content of the product, during this process, attains usual value of about 80 %. In the carbonization is generally carried out at a sufficiently fast to minimize the moisture content and the temperature of carbonization significantly influence the rate of pyrolysis of the raw material (Basal et al., 1988).

The carbonaceous material that constitute the basis for the manufacture of activated carbon by steam-gas method must meet certain requirements among which the most important are: (a) low content of volatile matter, (b) high content of element carbon, (c) a definite porosity, and (d) sufficient strength of attrition (Jankowska et al., 1991). The natural

carbonaceous materials do not meet all these requirements simultaneously. However, the product of carbonization has a weakly developed porous structure, surface area and pore volume. Therefore, it should be developed further by activation process.

– Activation

The activation process is to enhance the volume and to enlarge the diameters of the pore which were created during carbonization process and to create some new porosity. The structure of the pores and their pore size distribution are largely predetermined by the nature of the raw material and the history of its carbonization. The activation removes disorganized carbon, exposing the aromatic sheets to the action of activation agents in the first phase and leads to the development to a microporous structure. In the latter phase of the reaction the significant effect is the widening of the existing pores or the formation of the larged-sized pores by the complete burnout of the walls between the adjacent pore. This result is an increase in the transitional pores and macroporosity (Basal et al., 1988), whereas the volume of the micropore was decreased. Thus the extent burn off of the carbon material is a measure of degree of activation. There are two activations: chemical and physical activation

Chemical activation is usually limited to woody precursor. This process involved carbonizing the patent material after impregnation with phosphoric acid, zinc chloride, sulphuric acid, potassium sulphide, carbonates of alkali metals, and metal chorides. The common feature of these compounds is their ability to act as dehydrating agents which influence the pyrolitic decomposition and inhibit tar formation. The temperature range for chemical activation is 400-800 °C (Patrick, 1995). However, chemical activation poses problems such as lack of adequate control over porosity development. In addition, the chemical activation agents are considered hazardous chemicals. Therefore, it is best to avoid if it is possible.

Physical activation is the development of porosity by gasification with and oxidizing gas at 700-1100 °C. Gas are commonly used carbon dioxide, steam and air (Patrick, 1995).

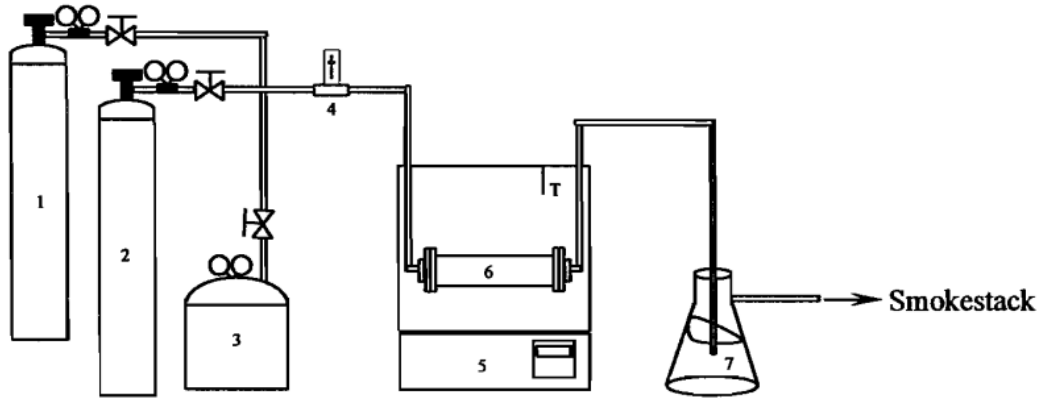
3.1. The Condition Used to Produce Bagasse Bottom Ash Activated Carbon

The bagasse bottom ash is a waste material. It is suitable to produce activated carbon due to low cost, renewable resource and more quantity. In addition, it has high fixed carbon.

Aworn et al. (2008) investigated the preparation of activated carbon obtained from bagasse bottom ash into two steps: carbonization and physical activation (Figure 1). In the carbonization step, a stainless steel tube reactor filled with bagasse bottom ash was carbonized in the muffle furnace at various temperatures from 300 to 800 °C under the flow of N_2 gas at 200 cm^3 min^{-1}. The heating rate was controlled at 20 °C min^{-1}, starting from room temperature (30 °C). Carbonized was held at each temperature for 1 h. The proximate analysis was calculated on a TGA analyzer and was presented in Table 3.

For physical activation step, the activation process was carried out in the muffle furnace by carbon dioxide (CO_2) and steam as activating agents. The flow rate of CO_2 was 200 cm^3 min^{-1}. Steam was generated from a heating pot at a constant rate of 8 g min^{-1} and pressure at 1.5 kg cm^{-2}. The chars of bagasse bottom ash (raw material) at various char temperatures

(300-800 °C) were activated by steam or CO_2 at 300, 400, 500, 600 and 800 °C. The N_2 gas was switched to steam or CO_2 and left until the temperature reached to 800 °C and held time 1 hour (Table 4).



(T) Thermocouples; (1) Nitrogen gas cylinder; (2) Carbon dioxide gas cylinder; (3) Steam generator; (4) Gas flow meter; (5) Muffle furnace; (6) Stainless tube reactor; (7) Gas-water trap.

Figure 1. Schematic diagram of activated carbon production process (Aworn, 2007).

Table 3. Proximate analysis of chars from bagasse bottom ash (Aworn et al., 2008)

Chars of bagasse bottom ash	Proximate analysis (dry basis wt%)		
	Volatile matter	Fixed carbon	Ash
300 °C	18.1	57.5	24.4
400 °C	15.8	59.7	24.5
500 °C	15.4	59.1	25.5
600 °C	15.1	59.0	25.9
800 °C	10.5	607	28.8

3.2. Effect of Activating Temperature / Volatile Matter / Activating Agents for Bagasse Bottom Ash Activated Carbon on Porosity Development

The chars of bagasse bottom ash at various char temperatures (300-800 °C) were activated by steam or CO_2 at 300, 400, 500, 600 and 800 °C. Table 5 shows the BET surface area of bagasse bottom ash activated carbons at various char temperatures under different activating agents. It was found that a higher activation temperature resulted in the decrease of the amount of volatile matter in materials and it was shown that at low-activating temperature led to higher surface area than at high temperature. Theses results indicated that the optimum amount of volatile matter enhanced the highest surface area. As shown in Table 4, the optimum condition for production of bagasse bottom ash activated carbon was activating

temperature of 300 °C and the amount of volatile matter left in this material was 18.1 %. The steam activation was more suitable than CO_2 activation for producing the bagasse bottom ash activated carbon in developing the BET surface area.

Table 4. Comparison of the optimum activated temperature for bagasse bottom ash activated carbon (Aworn et al., 2008)

Sample code	Condition of activation process
BBA-steam -300	Start from char (300 ° C) : N_2 gas was switched to steam at 300 ° C continue up to 800 ° C
BBA-steam-400	Start from char (400 ° C) : N_2 gas was switched to steam at 400 ° C continue up to 800 ° C
BBA-steam-500	Start from char (500 ° C) : N_2 gas was switched to steam at 500 ° C continue up to 800 ° C
BBA-steam-600	Start from char (600 ° C) : N_2 gas was switched to steam at 600 ° C continue up to 800 ° C
BBA-CO_2 -800	Start from char (800 ° C) : N_2 gas was switched to steam at 800 ° C
BBA-CO_2 -300	Start from char (300 ° C) : N_2 gas was switched to steam at 300 ° C continue up to 800 ° C
BBA-CO_2-400	Start from char (400 ° C) : N_2 gas was switched to steam at 400 ° C continue up to 800 ° C
BBA-CO_2-500	Start from char (500 ° C) : N_2 gas was switched to steam at 500 ° C continue up to 800 ° C
BBA-CO_2-600	Start from char (600 ° C) : N_2 gas was switched to steam at 600 ° C continue up to 800 ° C
BBA-CO_2 -800	Start from char (800 ° C) : N_2 gas was switched to steam at 800 ° C

Remark: BBA= bagasse bottom ash

Table 5. The relation of volatile matter and BET surface area of bagasse bottom ash activated carbons by physical activation at various char temperatures (Aworn, et al., 2008)

Activated carbon	Char temperature (°C)	BET surface area (mg^2 g^{-1})		Volatile Matter (%)
		Steam activation	CO_2 activation	
BBA-Y-300	300	595	546	18.1
BBA-Y-400	400	547	517	15.8
BBA-Y-500	500	524	523	15.4
BBA-Y-600	600	513	493	15.1
BBA-Y-800	800	491	467	10.5

Remark: BBA= Bagasse bottom ash; Y= an activating agent (steam or CO_2)

In addition, Aworn et al. (2008) also investigated total pore volume (V_T), mesopore volume (V_{me}), micropore volume (V_{mi}), microporosity (V_{mi}/V_T), mesoporosity (V_{me}/V_T) and average pore diameter (D) for bagasse bottom ash activated carbon by steam activation and CO_2 activation (Table 6). The results presented that the mesoporous by steam activation (V_{me}/V_T = 31.42-33.39 %) is higher than CO_2 activation (V_{me}/V_T =21.40-24.06%). It suggested that the steam activation of bagasse bottom ash has resulted in more improving the mesoporous.

As shown in Table 6, the microporosity and mesoporosity of the commercial activated carbon obtained from coconut shell was 91.29 % (V_{mi}/V_T) and 8.71 % (V_{me}/V_T), respectively. It indicated that the commercial activated carbon obtained from coconut shell had mainly microporous. Whereas the activated carbon obtained from bagasse has higher mesopore volume than the commercial activated carbon obtained from coconut shell. Valix et al. (2004) explained that the high ash content had some metal oxides fill or block some portions of micropore volume which may explain partially the low surface area observed in carbon with high content. This led mesopore volume with high ash content. Furthermore, Aworn et al. (2008) reported that a material which contained a high ash content such as bagasse bottom ash (Table 6) tended to have mesopore volume instead of micropore volume. However, the removal of carbon atom first generates mainly mesopores, the pore enlarging causes a shift from micro to mesoporosity due to the activation occurs mainly on the external surface of the particles. Thus, the porosity and surface area development was increasing the mesopore structure. On the other hand, the less ash content in the material show an increase of porosity and surface area mainly microporous. From the results, if we want to produce the mesopore activated carbon, we will choose feedstock from bagasse bottom ash. Therefore, the activated carbon obtained from bagasse bottom ash is the alternative adsorbent used to adsorb large molecules such as colorant of sugar syrup, melanoidins from food, distilleries and fermentation industries and pigments from vegetable oils.

Table 6. Surface area and pore volume of bagasse bottom by steam activation and CO_2 activation (Aworn et al., 2008)

Activated carbon	S_{BET} ($m^2\ g^{-1}$)	V_T ($cm^3\ g^{-1}$)	V_{me} ($cm^3\ g^{-1}$)	V_{mi} ($cm^3\ g^{-1}$)	D (Å)	V_{me}/V_T (%)	V_{mi}/V_T (%)
BBA-steam-300	595	0.3953	0.1330	0.2653	26.79	33.39	66.61
BBA-steam-800	491	0.353	0.1022	0.2231	26.51	31.42	68.58
BBA-CO_2-300	517	0.3059	0.0736	0.2323	24.34	24.06	75.94
BBA-CO_2-800	467	0.2785	0.0596	0.2189	23.84	21.40	78.60
Commercial activated carbon	924	0.4662	0.0406	0.4256	20.18	8.71	91.29

Remark: S_{BET}=BET surface area, V_T= Total pore volume, V_{me}=Mesopore volume, V_{mi}= Micropore volume, D=Average pore diameter.

4. Application of Bagasse Bottom Ash Activated Carbon in Various Industries

4.1. Removal of Color from Sugar Syrup by Bagasse Bottom Ash Activated Carbon

In the technological process of sugar production the main problem is the separation of non-sucrose compounds. Purified sugar solution, which is to be crystallized, consists of non-

sucrose compounds diluted in water. Colored matters or "colorant" the material causing the color (Carpenter, 1980) as non-sucrose compounds, have the tendency to form inclusions in the sugar crystal or to be adsorbed on the surface. Sugar colorant is unfortunately not one single molecular species. It consists of a wide range of materials each with its own molecular weight (MW), pH sensitivity, charge, and chemical structure. There are many types of sugar colorants such as phenolic, caramel, melamins, alkaline degradation products, melanoidins and polysaccharide complex (Broadhurst, 2002; Mudoga et al., 2008).

The possibility of applied methods for a reduction of non-sucrose compounds in sugarcane syrup such as ultrafiltration (UF) process (Balakrishnan et al., 2000; Durante et al, 2001), ion exchange resins, proposed for sugar syrup decolorization (Pease and Steven, 1999). An ion exchanger resin has been the most commonly used for sugar decolorization. However, high cost of resins, and regeneration and the disposal of the concentrate from the cleaning cycles pose problems in the use of resins. Hence, the search of new low cost adsorbents has attracted a number of investigators. Activated carbons have large surface area. The important roles of them are use as adsorbents for decolorization in sugar cane refining. Activated carbon is produced from bagasse bottom ash, the waste material obtained from the particulate collection devices attached to the flue-gas line of the sugarcane bagasse-fired boilers, is the alternative low-cost adsorbent for decolorization of sugar syrup. The bagasse bottom ash has mainly mesorporous on the surface area. Therefore, it is suitable as an adsorbent to adsorb the large molecular such as colorant of sugar syrup.

4.1.1. Effect of Contact Time for Decolorization of Sugar Syrup by Bagasse Bottom Ash Activated Carbon

Simaratanamongkol (2008) investigated the decolorization of sugar syrup by bagasse bottom ash activated carbon in fixed bed column. The experiment was conducted in the 6 ml size syringes. The 2.5 g of bagasse bottom ash activated carbon was packed in the column. After that, the 50 ml of sugar syrup solution was continuously pumped through packed column with the controlled flow rated at 1.5 ml m^{-1}. The samples were taken at interval time. and the solutions were measured by spectrophotometer at 420 nm. Furthermore, the samples were analyzed for ICUMSA (International Commission for Uniform Methods of Sugar Analysis) (ICUMSA, 1994) color remaining and decolorization efficiency following by Eq. (1) and Eq. (2), respectively:

$$\text{ICUMSA color} = \frac{1000 \times A}{b \cdot c} \tag{1}$$

A = absorbance at 420 nm of the test sample
b = length (cm) of the adsorbing path
c = concentration (g sugar/ml) of the test sample

$$\text{Decolorization efficiency}\,(\%) = \left(1 - \frac{\text{OD}_{420}\ \text{color of permeate}}{\text{OD}_{420}\ \text{color of sugar syrup}}\right) \times 100 \tag{2}$$

An ICUMSA rating is an international unit for expressing the purity of the sugar in solution, and is directly related to the color of the sugar. The lower the ICUMSA build the whiter the sugar. For refined sugar (ICUMSA ≤ 40) that is first grade quality sugar, with the longest time of refining process, ICUMSA in sugar syrup must less than 100 unit. Table 7 shows that sugar can be classified by their color.

Table 7. ICUMSA color acceptable in various type of sugar (Mitr Phol Sugar group, 2007)

Type of Sugar	Color Max. (ICUMSA)
Raw Sugar	1001-2000
Very High Polarization sugar (Golden Granulated Sugar)	1001-1400
White Sugar	100
Refined Sugar	40
Super Refined Sugar	20

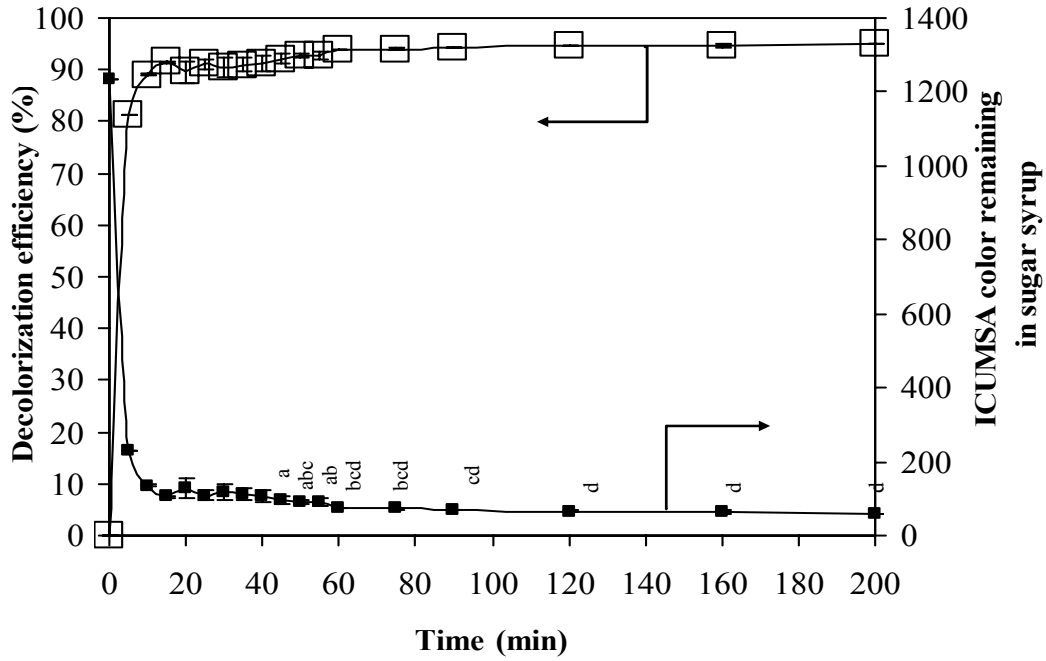


Figure 2. Decolorization efficiency (□) and ICUMSA color remaining (■) of sugar syrup by 5% (w/v) bagasse bottom ash activated carbon at various contact time (Simaratanamongkol, 2008).

The results (Figure 2) showed that sugar syrup had residual color less than 100 ICUMSA at the contact time of 45 min. Statistical analysis of ICUMSA color remaining in sugar syrup after pass bagasse bottom ash activated carbon (BFA-AC) from 45 to 200 minutes showed at contact time from 60 to 200 minutes were in the same group of Duncan Group of The ANOVA procedure. It indicated that the equilibrium time of sugar syrup adsorption by bagasse bottom ash activated carbon is 60 minute. The contact time of 1 hour was selected for all decolorization efficiency study of sugar syrup by bagasse bottom ash activated carbon.

The system pH of sugar syrup was slightly increased to basic when increasing of contact time as shown in Figure 3. However final pH of sugar syrup was nearly acceptable value of pH (7.7-8.3) (Mitr Phol Sugar Specification, 2007). This might be that BFA-AC had weakly basidic performance, resulted in increasing pH property of sugar syrup. The pH of final sugar syrup is important in aspect of it is the effect on the next step in sugar processing. For acidic pH of sugar syrup was the effect on inversion of sucrose and noncrystallizable of sugar brought to low yield of the product. For basidic pH of sugar syrup involve alkaline degradation products, the one sugar colorant (Ahmedna, et al., 1997).

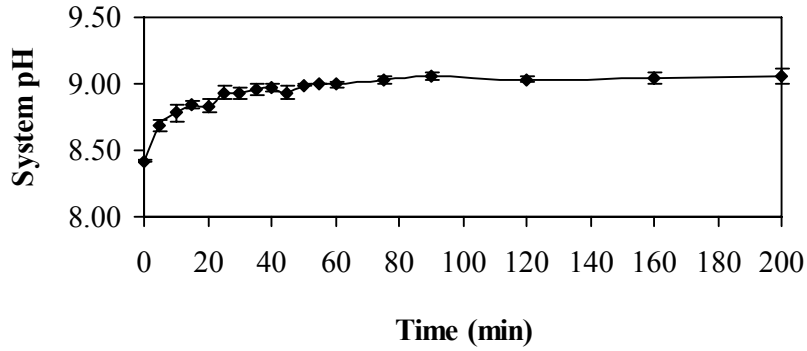


Figure 3. The system pH on the decolorization efficiency of sugar syrup using 5% bagasse bottom ash activated carbon at various contact time (Simaratanamongkol, 2008).

4.1.2. Effect of Adsorbent Dosage for Decolorization of Sugar Syrup by Bagasse Bottom Ash Activated Carbon

Simaratanamongkol (2008) studied the effect of adsorbent dosage of bagasse bottom ash activated carbon (BBA-AC) on decolorization efficiency of sugar syrup in the packed column (contact time 1 hour) (Figure 4).

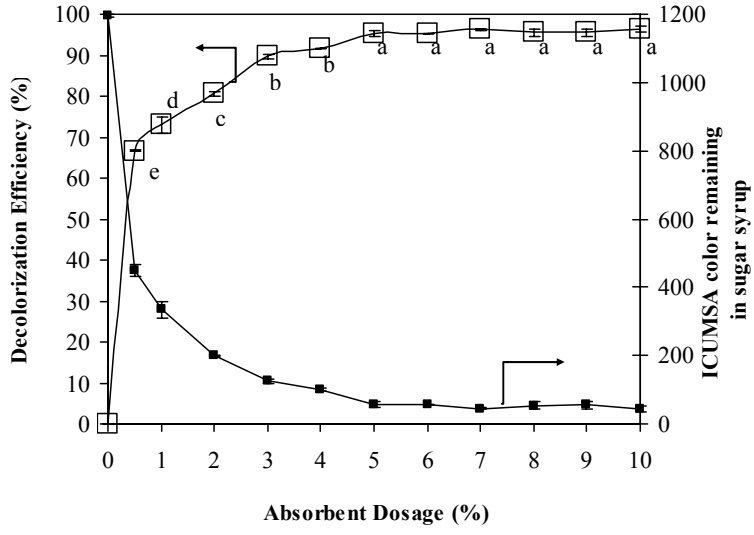


Figure 4. Decolorization efficiency (□) and ICUMSA color remaining (■) of sugar syrup by bagasse bottom ash activated carbon at various adsorbent dosages (Simaratanamongkol, 2008).

The results showed that the percentage of decolorization increased from 66.7 to 96.4% with increase in adsorbent dose from 0.5 to 10% (w/v) and then became almost constant. Statistical analysis of percentage of decolorization at adsorbent dose from 0.5 to 10% (w/v) showed adsorbent dose from 5 to 10% (w/v) were in the same group of Duncan Group of the ANOVA procedure. The best economical adsorbent dosage was chosen to be 5% (w/v). Since bagasse bottom ash activated carbon had the characteristic of absorb sugar syrup within itself so using the lowest adsorbent dosage was enhanced in no lost of sugar syrup in the column.

4.1.3. Comparison Of Decolorization Efficiency With Other Adsorbents

Table 8. Decolorization of sugar syrup by various adsorbents (Simaratanamongkol, 2008)

Adsorbent and dosage	Syrup			Physical properties					
	ICUMSA Remaining (Initial 1233)	Decolorization efficiency (%)	System pH (Initial=7.3)	S_{BET} (m^2g^{-1})	V_T (cm^3g^{-1})	V_{me} (cm^3g^{-1})	V_{mi} (cm^3g^{-1})	D (Å)	V_{me}/V_T (%)
5 % BBA	451.48±3.74	64.75±0.64	6.81±0.03	234.66	0.1601	0.1123	0.0478	27.28	70.14
5% BBA-AC	65.89 ± 9.31	94.42±0.79	8.35±0.03	703.86	0.5375	0.2915	0.2460	30.55	54.23
5%AC (Coconut shell)	972.28± 0.73	22.32±0.71	7.73±0.01	993.00	0.4920	0.0417	0.4503	19.82	8.48

Remark: BBA = Bagasse bottom ash
BBA-AC = Bagasse bottom ash activated carbon
AC = Activated carbon from coconut shell

The bagasse bottom ash (BBA) and commercial activated carbon (AC obtained from coconut shell) were used as adsorbents for decolorization of sugar syrup to compare with bagasse bottom ash activated carbon (BBA-AC) (Table 8). The results indicated that bagasse bottom ash activated carbon had higher decolorization efficiency than the commercial activated carbon (AC) and bagasse bottom ash (BBA). The bagasse bottom ash had higher mesopore volume than commercial activated cabon (Table 8). This result confirmed that pore diameter in the range of mesopore was the significant factor for entrap the large molecular size of chemical compound of sugar colorant. Remaining ICUMSA color in sugar syrup after pass through bagasse bottom ash activated carbon was lower than 100 (acceptable for white sugar). Initial ICUMSA color in sugar syrup is varied depend on quality of cane in each lot.

4.1.4. Mechanism of Bagasse Bottom Ash Activated Carbon in Adsorbing Sugar Syrup

4.1.4.1. FTIR Spectroscopy

FTIR was used to study the functional groups of bagasse bottom ash activated carbon (BBA-AC) before and after decolorization of sugar syrup. After BBA-AC adsorb color from sugar syrup, BBA-AC got peaks of -O-H, -C-H, -C=O, -C-H, -O-H, -O-H, -C-O, -C-O and -O-H at the wavelengths 3254**,** 2924**,** 1650**,** 1435, 1347**,** 1284, 1132, 1006 and 930 cm^{-1}, respectively (Figure 5) . The wave number of BBA-AC after decolorization of sugar syrup

and the wave number of initial sugar syrup were at the same location. Syrup color may be adsorbed only on the surface of BBA-AC, not create chemical bonding.

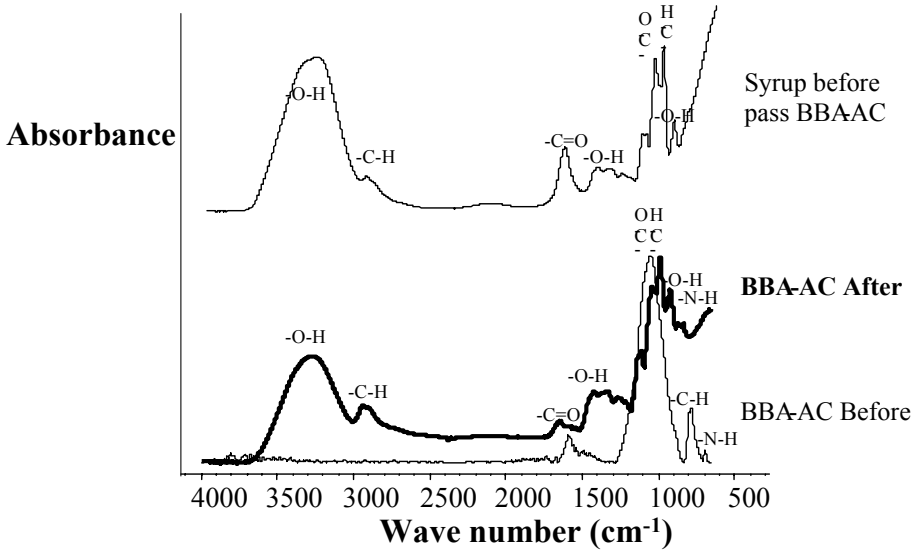


Figure 5. IR spectra of initial sugar syrup, bagasse bottom ash activated carbon (BBA-AC) before and after decolorization of sugar syrup (Simaratanamongkol, 2008).

4.1.4.2. Desorption Studies

Desorption studies were conducted to identify the mechanism of adsorption. Because the properties of colorants in sugar syrup are tended to be polymeric species containing one or several carboxylic acid groups. These "colors" tend to be large organic molecules which have a weakly negative charge (Ahmedna, et al., 2000a; Ahmedna, et al., 2000b; Migo, et al., 1997; Royle, et al., 1998).

Simaratanamongkol (2008) studies the desorption of the color-adsorbed on bagasse bottom ash activated carbon (BBA-AC) by using distilled water followed by 0.5 M NaOH and absolute ethanol as eluents (Table 9).

Water has the highest polarity property among all chemical solvents. Dipole moment, dielectric constant and polarity index of water are 1.85, 80 and 9, respectively (Byers, 2003). Distilled water was selected as an eluent in this study because it could explain the mechanism of adsorption in two ways. First, if distilled water was able to elute sugar colorant out of the column, this polymeric species adsorb on the surface or in the pore of the carbon. If distilled water was able to desorb colors from the matrix, no requirement of chemical bonding. Second, the mechanism of adsorption involved polarity of the adsorbent and adsorbate. Since water has the highest polarity index then it has efficiency to destroy or disturb the system of interaction between chemical colorant compounds and BBA-AC. For dipole moment, dielectric constant and polarity index of ethanol are 1.69, 24.3 and 5.2, respectively (Byers, 2003). This reagent uses for indicate the mechanism involve polarity and solvent perturbation. Sodium hydroxide is completely ionic, containing sodium cations and hydroxide anions. The hydroxide anion makes sodium hydroxide a strong base. This chemical use for explain

electrostatic interaction between functional groups of colorant compounds and surface chemistry of BBA-AC.

As shown in Table 9, distilled water and NaOH could slightly elute syrup color , while BBA-AC is mainly desorbed with absolute ethanol. When integrate data from IR spectra (Figure 5) and desoprtion, it could explain that physical adsorption with differently polarity of colorant involve interaction between syrup color and BBA-AC. Various species of colorant in syrup had versatile properties. Some colorant had high polarity and the others had low polarity. Therefore, the collection of three eluents in this study had efficiency to completely desorb a variety of colorant.

Table 9. The desorption efficiency of sugar color-adsorbed on bagasse bottom ash activated carbon (5% (w/v) of dosage) (Simaratanamongkol, 2008)

Eluents	Desorption efficiency (%) of sugar colorants from BBA-AC
Distilled water	3.78 ± 0.59
0.5M NaOH	10.01 ± 0.77
Absolute ethanol (Purity ≥ 99.9%)	86.2 ± 1.36
Total	100

Remark: BBA-AC = bagasse bottom ash activated carbon

4.1.5. Effect of Recycle Number of Bagasse Bottom Ash Activated Carbon on Decolorization Efficiency of Sugar Syrup

The bagasse bottom ash activated carbon (BBA-AC) was packed in the columns and use as an adsorbent for decolorization of sugar syrup. After adsorption, the color-adsorbed on BBA-AC was regenerated with absolute ethanol and the columns were rinsed with distilled water. The columns were reused again to decolorize color from initial new sugar syrup. The recycle of columns of BBA-AC were repeated. It was found that 5% of BBA-AC (w/v) was able to decolorization of syrup about 3 recycle number in order to get the ICUMSA not higher than 100 (Fig. 6). It meant that to use BBA-AC 16.67 kg can decolorize sugar syrup 1 m^3 and reduced initial ICUMSA from 1233 to less than 100 ICUMSA.

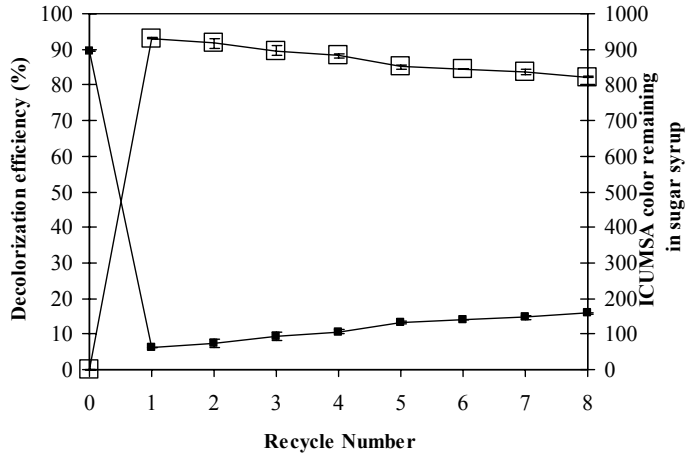


Figure 6. Effect of recycle number of bagasse bottom ash activated carbon (BBA-AC) on decolorization efficiency (□)and ICUMSA color remaining (■) of sugar syrup ((Simaratanamongkol, 2008).

4.2. Removal of Melanoidins from Sugar Syrup by Bagasse Bottom Ash Activated Carbon

The most common colored substances that form during sugar production can be divided in three groups: (a) melanins (b) melanoidins and (c) caramels (Mudoga et al., 2008). Melanoidins, which are also known as Maillard reaction products (Coca et al., 2004) are produced by non-enzymatic browning reactions, which involve the condensation of sugars and amino acids. The structure of melanoidins is poorly defined and is dependent on the nature and concentrations of the parent compounds, and reaction conditions as pH, temperature, heating time and solvent system (Chandra et al., 2008; Yaylayan and Kaminsky, 1998). Therefore, the melanoidins can be used as the model for the colorant in the sugar syrups to study adsorption isotherm, thermodynamic and adsorption mechanism on activated carbon obtained from bagasse bottom ash.

4.2.1. Adsorption Isotherm

Generally, the adsorption isotherm equations used to describe the experimental isotherm data are the langmuir and Freundlich isothems.

- -Langmuir isotherm

The Langmuir assumes monolayer adsorption and the maximum adsorption capacities on an adsorbent surface with homogeneous sites as shown in Eq. (3).

$$\frac{1}{q_e} = \frac{1}{q_{\max}} + \frac{1}{bq_{\max}C_e} \tag{3}$$

where q_e is the amount of adsorbate adsorbed per unit weight of adsorbent at equilibrium (mg g^{-1}), C_e is the residual adsorbate concentration of the liquid phase at equilibrium (mg l^{-1}), $q_{\max}$ is the maximum adsorption capacity (mg g^{-1}) of adsorbate concentration in the solid phase corresponding to complete coverage of available sites, and b is the Langmuir constant, which is related to the energy of adsorption.

Simaratanamongkol and Thiravetyan (2010) investigated the Langmuir isotherm of melanoidin adsorption by bagasse bottom ash activated carbon at various temperatures (5, 25 and 60 °C). The synthetic melanoidin was used as the represent of colorant in sugar syrup.

Synthetic melanoid solution was prepared by method of Bernardo et al. (1997) by mixing 4.5 g (0.025 M) of glucose, 1.88 g (0.025 M) of glycine and 0.42 g (0.005 M) of sodium bicarbonate with 100 ml of distilled water and then heating overnight at 80 °C unit dry. 100 ml of water were then added and dilute solutions of melanoidin in water were prepared. The molecular weight of melanoidin was assumed about 15,000 dalton (Simaratanamongkol and Thiravetyan, 2010).

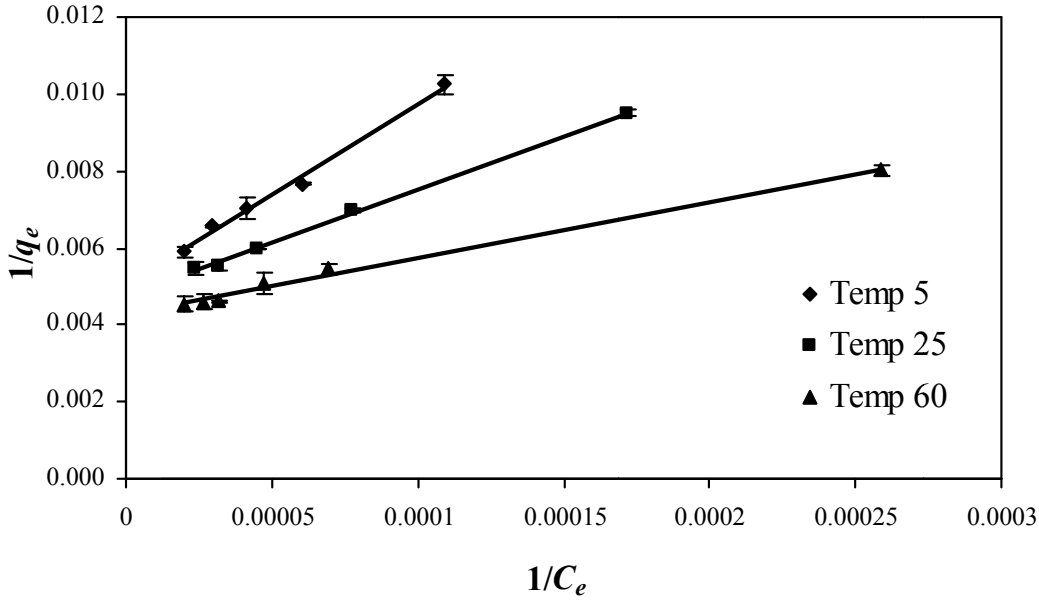


Figure 7. The Langmuir isotherms of synthetic melanoidin colorants by bagasse bottom ash activated carbon at 5, 25 and 60 °C (Simaratanamongkol and Thiravetyan, 2010).

The effect of temperature on the adsorption isotherms of the synthetic melanoidin on BBA–AC are shown in Fig. 7. These isotherms could be fitted using the Langmuir model with correlation coefficients (R^2) all $\geq$0.99. R^2 is used as a measure of the goodness of fit; the closer R^2 approaches 1 the better the fit. The results show that adsorption of the synthetic melanoidin increased with increasing temperature.

The maximum adsorption capacity of bagasse bottom ash activated carbon (BBA–AC) increased from 200 to 232.56 mg g^{-1} as the temperature was increased from 5 °C to 60 °C (Table 10). This was accompanied by a corresponding increase in the b value from 1.05×10^{-4} to 2.95×10^{-4} l mg^{-1}. Thus BBA–AC has a higher affinity for synthetic melanoidin at higher temperature.

Table 10. Langmuir constants for the adsorption of synthetic melanoidin colorants by bagasse bottom ash activated carbon at various temperatures (Simaratanamongkol and Thiravetyan, 2010)

Temperature (°C)	q_{max} (mg g^{-1})	b (l mg^{-1})	R^2
5	200.00	1.05×10^{-4}	0.9920
25	208.33	1.73×10^{-4}	0.9982
60	232.56	2.95×10^{-4}	0.9930

– Freundich isotherm

The Freundlich isotherm describes equilibrium on a heterogeneous surface and does not assume monolayer adsorption:

$$q_e = K_f C_e^{1/n} \tag{4}$$

where K_f and n are the Freundlich constants related to adsorption capacity and intensity, whilst C_e and q_e are the equilibrium concentration of adsorbate and the amount adsorbed at equilibrium, respectively.

The Freundlich constants can be evaluated by linearization of Eq. 5

$$\log q_e = \log K_f + \frac{1}{n} \log C_e \tag{5}$$

Simaratanamongkol and Thiravetyan (2010) also evaluated the Freundlich isothem of melanoidin adsorption by bagasse bottom ash activated carbon at various temperatures (5, 25 and 60 °C). Figure 8 shows the linear plots of log q_e versus log C_e. Values of n and K_f calculated from the slope and interception of Freundlich plots, are listed in Table 11 and R^2 are $\geq$0.9.

The K_f values in Freundlich isotherms are related to the capacity of the adsorbent to bind the adsorbate. In this study, the K_f values increased as the system temperature increased. The results agree with the q_{max} values obtained from the Langmuir isotherm, indicating that the adsorption capacity of BBA–AC increased as the temperature increased.

The n values in Freundlich isotherm are a functional of the strength of adsorption; higher n values indicate higher adsorption capacity. The n values of BBA–AC are between the range 2–10, which represents good adsorption at temperature of 5, 25 and 60 °C.

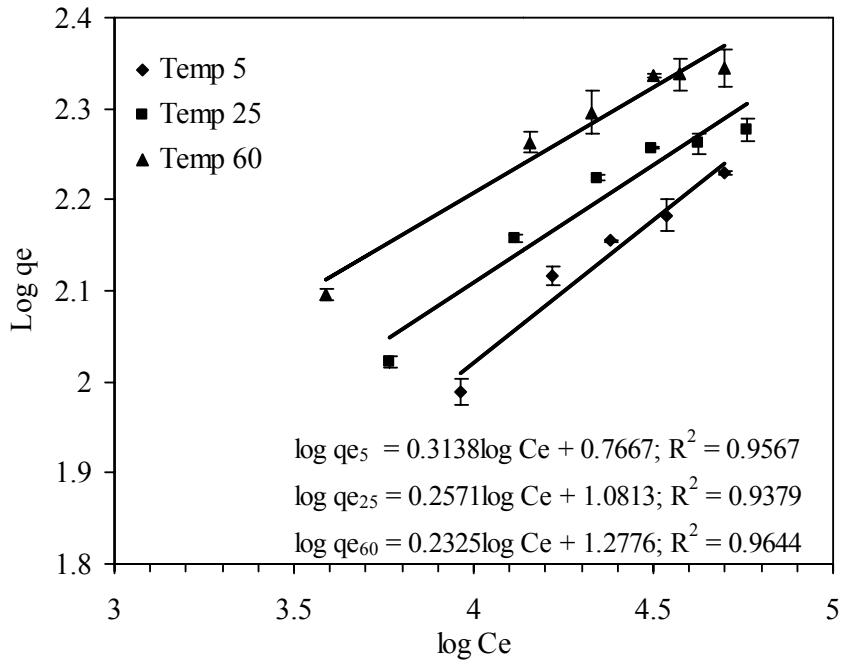


Figure 8. Freundlich isotherm linear plots for the adsorption of synthetic melanoidin colorants by bagasse bottom ash activated carbon at 5, 25 and 60°C (Simaratanamongkol and Thiravetyan,2010).

Table 11. Freundlich isotherm constants for adsorption of synthetic melanoidin colorants by bagasse bottom ash activated carbon (Simaratanamongkol and Thiravetyan, 2010)

Temperature (°C)	K_f (mg^{-1})	n	R^2
5	5.84	3.19	0.9567
25	12.06	3.89	0.9379
60	18.95	4.30	0.9644

4.2.2. Thermodynamic Study

The thermodynamic parameters such as Gibbs free energy change (ΔG), enthalpy change (ΔH) and entropy change (ΔS) for the melanoidin adsorption process can be determined using the following equations:

$$\Delta G = -RT \ln(b) \quad (6)$$

$$\ln(b) = -\Delta H/RT + \text{constant} \quad (7)$$

$$\Delta G = \Delta H - T\Delta S \quad (8)$$

where b is the Langmuir constant related to energy of adsorption, T is the temperature (K) and R is the universal gas constant (8.314 J mol^{-1} K^{-1}) (Barrett et al., 1951; Lippens and de Boer, 1965; Mall et al., 2005). Yaylayan and Kaminsky (1998) separated three polymers in the 10,000–20,000 MW range in the glycine/glucose model system; consequently in this study we have assumed an average molecular weight of 15,000 for the synthetic melanoidin. ΔH was determined graphically from the linear plot of ln b versus $1/T$ (Figure 9), and the values of ΔG and ΔS computed numerically, are presented in Table 12.

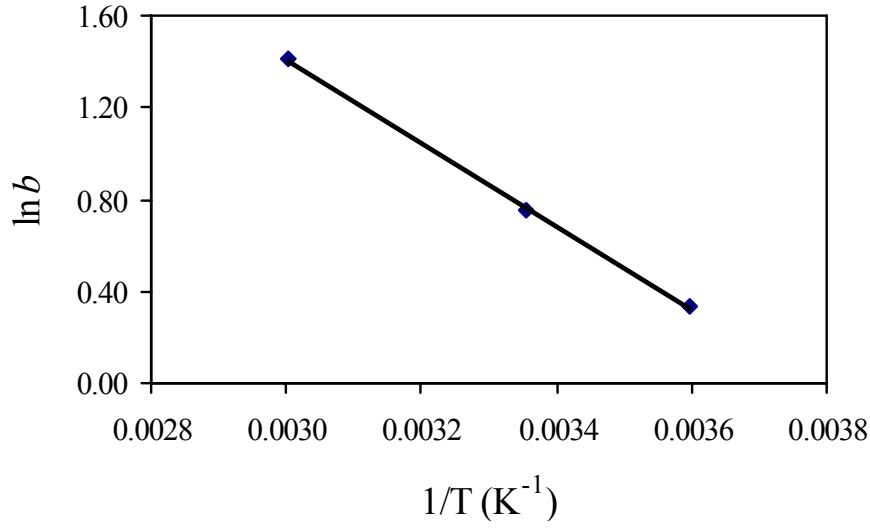


Figure 9. Plot of ln b vs $1/T$ for melanoidin adsorption by bagasse bottom ash activated carbon (Simaratanamongkol and Thiravetyan, 2010).

The positive value of ΔH suggests that the adsorption of melanoidin on BBA–AC is endothermic. The negative value for the Gibbs free energy (ΔG) shows that the adsorption process is spontaneous in nature and that the degree of spontaneity of the reaction increases with increasing temperature (Argun and Dursun, 2008). The positive values of ΔS show the increased randomness at the solid/solution interface during the adsorption process. From this experiment, adsorption process between BBA–AC and melanoidin could occur at room temperature so it was spontaneous in nature. When the environmental temperature increased, the probability of molecule of melanoidin increased for attack each other and movement. Hence, higher adsorption efficiency increased when increasing temperature. This explanation supported endothermic and freedom of molecule of melanoidin for random adsorbed on BBA–AC.

Table 12. Thermodynamic parameters of melanoidin adsorption by bagasse bottom ash activated carbon at various temperatures (Simaratanamongkol and Thiravetyan, 2010)

Temperature (K)	ln *b*	ΔG (kJ mol^{-1})	ΔH (kJ mol^{-1})	ΔS (J mol^{-1}K^{-1})
278	0.3352	-0.7747	15.0766	57.0192
298	0.7536	-1.8670		56.8578
333	1.4103	-3.9045		57.0002

4.2.3. Mechanism of Bagasse Bottom Ash Activated Carbon in Adsorbing Melanoidin

FTIR and desorption studies was studied the mechanism of bagasse bottom ash activated carbon in adsorbing melanoidin.

After BBA-AC adsorb color from melanoidin found BBA-AC got broad band spectrum of 3171 cm^{-1} (NH) and peak of 1390 cm^{-1} (OH) from melanoidin (Figure 10).

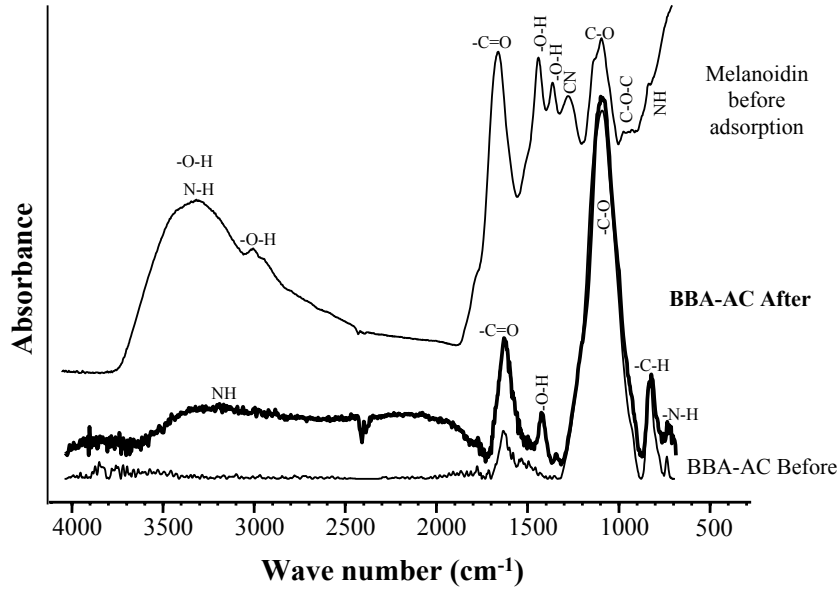


Figure 10. IR spectra of bagasse bottom ash activated carbon (BBA-AC) before and after decolorization of melanoidin (Simaratanamongkol and Thiravetyan, 2010).

This data implied that melanoidin interacted at surface level of BBA-AC like syrup color. Desorption studies of melanodins was also investigated. The results showed that distilled water itself can completely elute (100%) the melanodins on BBA-AC.

From the FTIR and desorption by distilled water, it suggested that the adsorption process involved mainly physical process. In addition, 0.5 M NaOH or absolute ethanol were also able to completely elute the melanoidin adsorbed on BBA-AC. Therefore, it implied that melanoidin might adsorb in mesopore volume of the BBA-AC.

4.3. Removal of Pigments from Vegetable Oils by Bagasse Bottom Ash Activated Carbon

Bleaching operation is a vital step of any vegetable oil refining process. In these steps, the color pigments and unwanted compound such as gums, soaps and pro-oxidant metals are adsorbed on solid material (Nguetnkam, 2008; Kaynak et al, 2004). The color pigments came from chlorophyll, carotenoids and related compounds (Kaynak et al., 2004).

The activated carbon is the one of most commonly adsorbent for decolorization in the vegetable oil bleaching step. The bagasse bottom ash is the waste from the waste of boiler of sugar factories that sugarcane bagasse is used as fuel. There is a high waste quantity of bagasse bottom ash especially in the agricultural country. Bagasse bottom ash is a potential material to produce as an activated carbon for decolorization of vegetable oil because it contented high fixed carbon.

4.3.1. Decolorization Efficiency of Crude Rice Bran Oil by Bagasse Bottom Ash Activated Carbon

Presently, rice bran oil is popular in several countries as a cooking oil and has been growing from the health and nutritional aspects as well as its wide application as an industrial oil (Ghosh, 2007). In the bleaching process of rice bran oil, the color pigment, which carotenoids and chlorophyll, are color pigment present in most of the crude rice bran oil (Manjula and Subramanian, 2009). However, bleaching crude rice bran oil is more difficult than most other vegetable because of the present of high chlorophyll content, products of oxidized tocopherols, and metallic salts of fatty acids (Ghosh, 2007). Chlorophyll is the green pigment molecule in plant cell. Chlorophyll itself is actually not a single molecule but a family of related molecules, designated chlorophyll a, b, c and d. However, chlorophyll-a is the molecule found in all plant cells, and therefore its concentration is what is reported during chlorophyll analysis.

Suksabye (2009) studied the decolorization of crude rice bran oil (after degrumming and neutralization) by bagasse bottom ash activated carbon. It was produced by one step pyrolysis which combined carbonization and activation by steam simultaneously. The bagasse bottom ash (raw material) was carbonized in a muffle furnace with N_2 at 200, 400, 600 and 800 °C and then was continued to activate by steam at 200, 400, 600 and 800 °C. During carbonization, N_2 gas was switched to steam and left until the temperature reached to 800 °C and held time 1 hour (Table 13).

Table 13. Conditions of activation process of bagasse bottom ash by one-step pyrolysis (Suksabye, 2009)

Sample code	Activaton process
BBA-AC-200	Start from raw bagasse bottom ash ; N_2 gas was switched to steam at 200 °C up to 800 °C
BBA-AC- 400	Start from raw bagasse bottom ash ; N_2 gas was switched to steam at 400 °C up to 800 °C
BBA-AC- 600	Start from raw bagasse bottom ash ; N_2 gas was switched to steam at 600 °C up to 800 °C
BBA-AC- 800	Start from raw bagasse bottom ash ; N_2 gas was switched to steam at 800 °C

Table 14 shows the decolorization of crude rice bran oil by various adsorbents in batch experiments. The results found that the BET surface area and total pore volume for bagasse bottom ash activated carbon were increased with increasing activation temperature by steam from 200 to 800 °C. The bagasse bottom ash activated carbon at activation temperature of 800 °C (BBA-AC-800) has the highest decolorization of crude rice bran oil (85.23 ±0.13 %) compared to bagasse bottom ash (BBA), the activated carbon obtained from rice husk (Rice husk–AC), commercial activated carbon from coconut shell (AC) and kaolin at the same conditions (temperature of 90 °C, 10% (w/w) of dosage, contact time of 1 h). Although the commercial activated carbon had higher BET surface area than bagasse bottom ash activated carbon, the decolorization of commercial activated carbon was lower than the bagasse bottom ash activated carbon. This reason is due to the fact that the commercial activated carbon contained lower mesopore volume than bagasse bottom ash activated carbon. The mesopore may mainly involve in absorbing the color of rice bran oil.

Table 14 Decolorization efficiency of rice bran oil by various adsorbents (Suksabye, 2009)

Adsorbents	Decolorization efficiency (%)	Physical properties				
		S_{BET} (m^2g^{-1})	V_T (cm^3g^{-1})	V_{me} (cm^3g^{-1})	V_{mi} (cm^3g^{-1})	D (Å)
BBA	41.94 ± 0.64	281.51	0.1840	0.1267	0.0573	26.14
BBA-AC -200	81.50 ± 0.17	426.35	0.3343	0.1650	0.1693	31.37
BBA-AC -400	82.10 ± 0.13	456.31	0.3605	0.1856	0.1749	31.60
BBA-AC-600	83.39 ± 0.23	507.39	0.4018	0.2141	0.1877	31.67
BBA-AC- 800	85.23± 0.13	615.76	0.4712	0.2516	0.2196	30.61
Rice husk-AC	55.35±0.21	145.59	0.1411	0.1077	0.0334	38.78
Kaolin	78.44±0.18	33.13	0.1373	0.1373	0.0000	16.44
Commercial activated carbon (from coconut shell)	65.54±0.27	959	0.4466	0.0309	0.4157	18.64

4.3.2. Effect of Contact Time for Decolorization of Crude Rice Bran Oil by Bagasse Bottom Ash Activated Carbon

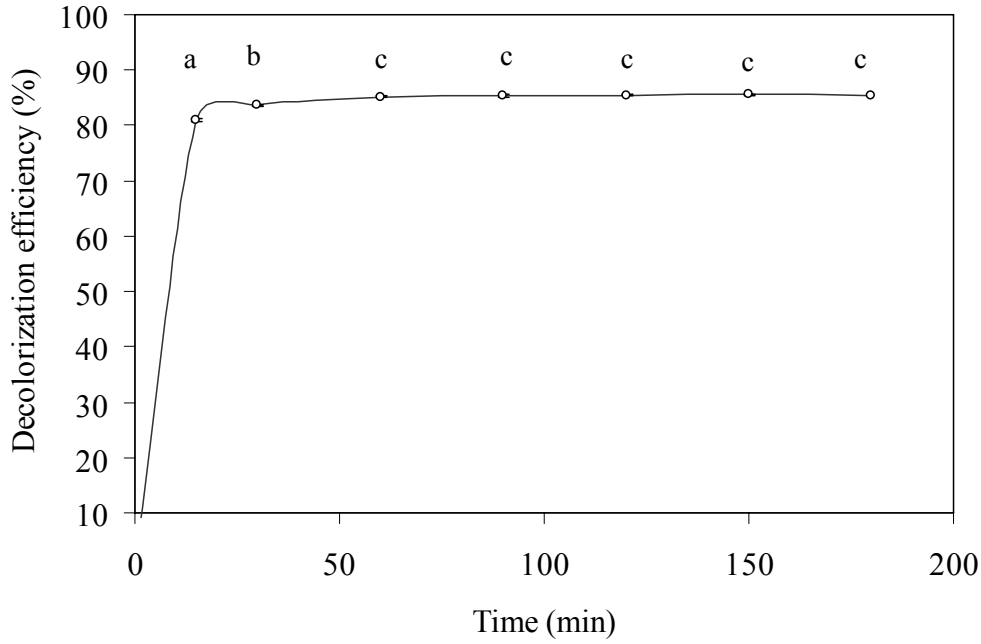


Figure 11. Effect of contact time for decolorization of sugar syrup using bagasse bottom ash activated carbon.

Suksabye (2009) reported that the decolorization efficiency of crude rice bran oil by bagasse bottom ash activated carbon (BBA-AC-800) was rapid within the first 15 minutes (80.94±0.18 %), the later adsorption rate was gradually decreased (Figure 11). The data submitted to analysis of variance and means separation, using Duncan's new multiple range test (DMRT), were not significantly different at $P \leq 0.05$ indicating that the decolorization efficiency of crude rice bran oil from 60 to 180 minutes was not different. This indicated that the decolorization of crude rice bran oil was reached equilibrium at 60 minutes or 1 hour.

4.3.3. Effect of Dosage for Decolorization of Crude Rice Bran Oil Using Bagasse Bottom Ash Activated Carbon

The decolorization efficiency increased with increasing adsorbent dosage from 1 to 12 % (w/w) and then remained constant (Figure 12). The data were submitted to analysis of variance and means separation was performed using Duncan's new multiple range test (DMRT). The results were not significantly different at $P \leq 0.05$ indicating that the decolorization efficiency of crude rice bran oil by bagasse bottom ash from 10 to 12 % (w/w) was not different. This indicated that the optimum dosage for decolorization of crude rice bran oil was 10 % (w/w) at 85.23 ±0.23 %. The increase in the decolorization efficiency with increasing adsorbent dosage is due to the increase in the adsorbent sites.

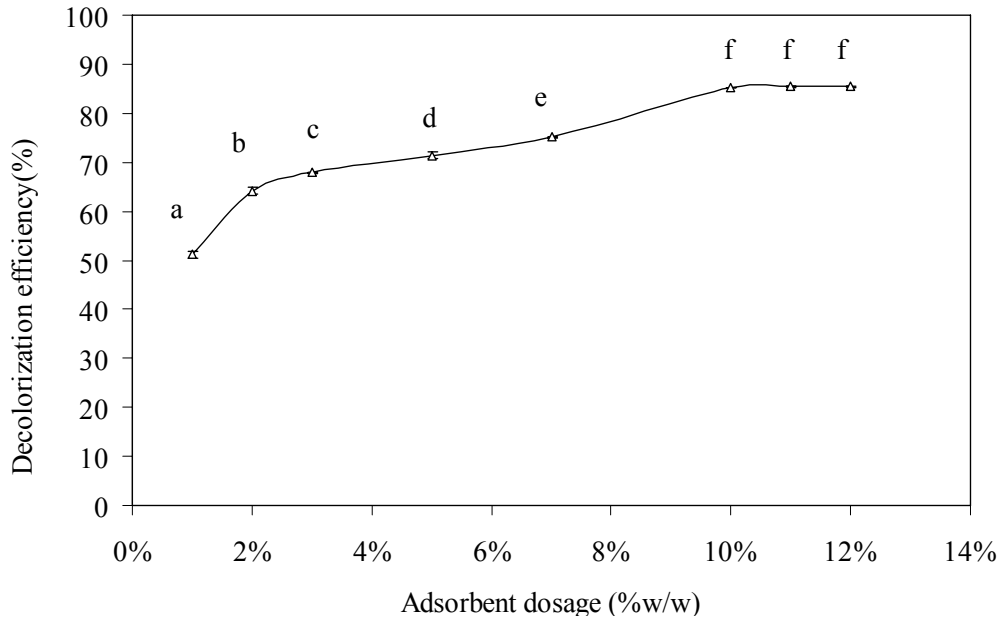


Figure 12. Effect of dosage for decolorization of sugar syrup using bagasse bottom ash activated carbon.

4.3.4. Mechanism of Bagasse Bottom Ash Activated Carbon in Adsorbing Color Pigment of Rice Bran Oil

Suksabye (2009) investigated the mechanism of bagasse bottom ash activated carbon in adsorbing pigment of rice bran oil by FTIR and desoprtion. FTIR was used to study the functional groups of bagasse bottom ash activated carbon before and after decolorization of crude rice bran oil (Figure 13). The FTIR spectrum of bagasse bottom ash activated carbon before decolorization observed at 3424, 1587, 1047 and 765 cm^{-1} corresponds to hydroxyl (O-H), carbonyl (C=O), C-O and amines (N-H) groups. After adsorption, the bagasse bottom ash activated carbon got the spectrum of C-H (2929 cm^{-1}, 2852 cm^{-1}, 1453 cm^{-1}) , C=O (1731 cm^{-1}) and O-H (1364 cm^{-1}) from initial pigment of rice bran oil. This confirmed that the pigment of rice bran oil can adsorb on the bagasse bottom ash activated carbon.

For desorption, 1g of the bagasse bottom ash activated carbon after adsorption of color pigment from crude rice bran oil was used for desorption studies. Desorption experiments were studied using distilled waster followed by 0.5 M NaOH and absolute ethanol as eluents. The results showed that the absolute ethanol is mainly desorbed the pigment of rice bran oil (94.41±1.41%). The distilled water (1.47±0.12 %) and NaOH (5.34 ±0.31 %) can slightly desorb the pigment of rice bran oil. The most of color pigment in the rice bran oil is chlorophyll (Ghosh, 2007). Chlorophyll-*a* ($C_{55}H_{72}MgN_4O_5$) (Sabah, 2007) is the most color pigment in rice bran oil.

High desorption of ethanol, it implied that the chlorophyll-*a* molecules may be adsorbed on the bagasse bottom ash activated carbon by physical adsorption due to the action of Van der Waals forces between the surface of adsorbent and adsorbate. Normally, the chlorophyll-*a* can solute in ethanol. Therefore it is easy to desorb the pigment using ethanol while the chlorophyll–*a* can not be desorbed by distilled water because it is hydrophobic. This is the reason that the desorption efficiency using distilled water was quite low though the

mechanism of color pigment of rice bran oil may interact at the surface adsorbent by Van der Waals forces.

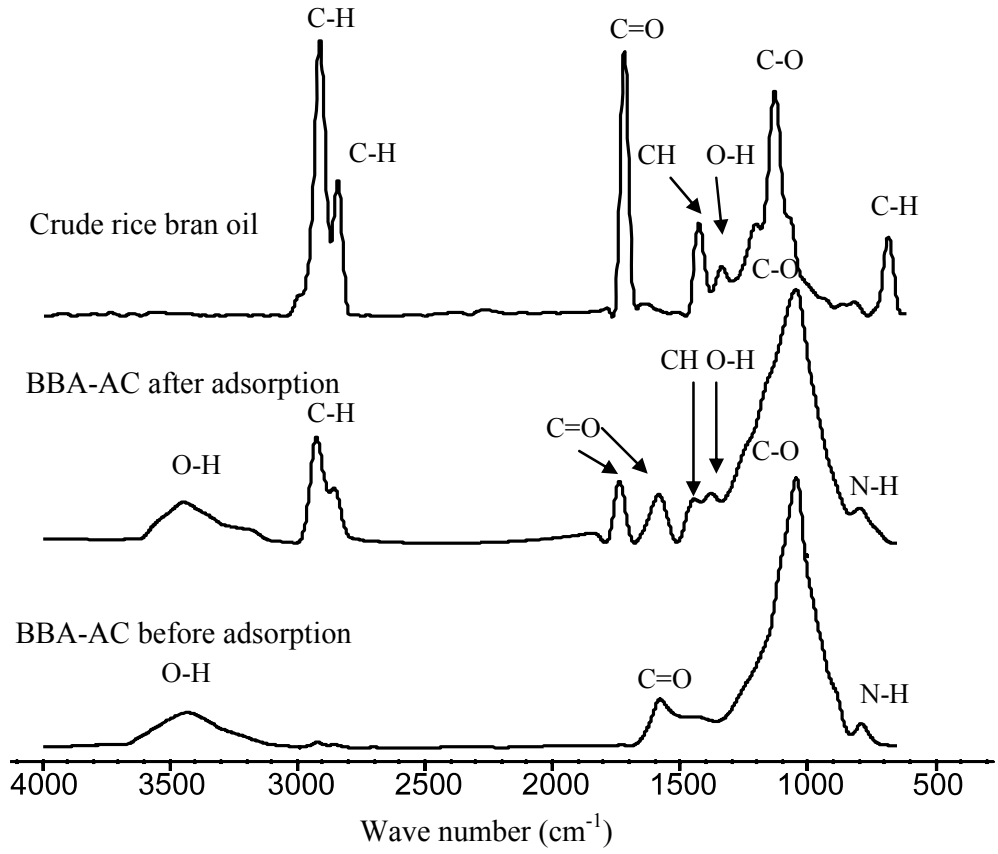


Figure 13. FTIR spectrum of bagasse bottom ash activated carbon before and after pigment adsorption of crude rice bran oil.

From the results of FTIR and desorption studies, it confirmed that the adsorption mechanism of color pigment from rice bran oil was mainly physical adsorption.

CONCLUSIONS

Activated carbon from bagasse bottom ash (BBA-AC) can be produced by one-step pyrolysis. A stainless steel tube reactor filled with raw bagasse bottom ash was carbonized in the muffle furnace at the heating rate of 20 ^{o}C min^{-1} until the temperature reach to 800 ^{o}C under the flow of N_2 gas at 200 cm^3 min^{-1}. The N_2 gas was switched to the steam as an activated agent at 800 ^{o}C . The steam was generated from a heating pot at a constant rate of 8 g min^{-1} and pressure at 1.5 kgcm^{-2}. The activation process at 800 ^{o}C was continued for 1 hour. The BBA-AC obtained from this process had BET surface areas about 615 m^{2}g^{-1} and mesopore volume 0.2516 cm^{2}g^{-1} while the commercial activated carbon (from coconut shell) had BET surface areas about 959 m^{2}g^{-1} and mesopore volume 0.0309 cm^{2}g^{-1}. The advantage

of BBA-AC is adsorbing larger molecules of organic compounds than commercial activated carbon from coconut shell because it contained mainly mesopore volume. BBA-AC is applied to adsorb the colorants of sugar syrup. Sugar syrup generally used resins as adsorbents to adsorb colors but still had some problems about the high cost, regeneration and the disposal of the concentrate from the cleaning cycles of resins. Therefore, BBA-AC might be an alternative adsorbent because the sugar industries already had this bagasse waste themselves. From the study found that bagasse bottom ash activated carbon 16.67 kg can decolorize sugar syrup 1 m^3 and reduced initial ICUMSA from 1233 to less than 100 ICUMSA. The sugar color-adsorbed on BBA-AC can be desorbed by absolute ethanol > 80%. It implied that the mechanism of color-adsorbed on BBA-AC involved mainly physical process. It meant that BBA-AC can be reused 3 recycle number in order to get the ICUMSA not higher that 100. In addition, the BBA-AC was also applied to remove the pigments from vegetable oils industries. Rice bran oil is selected as a representative of vegetable oils in order to remove the pigments. Rice bran oil generally used montmorillonite as a commercial bleaching clay for remove the pigments from rice bran oil. Therefore, BBA-AC is applied to use as an alternative adsorbent instead of montmorillonite in decolorization of crude rice bran oil. The mechanism of BBA-AC in adsorbing color pigments of rice bran oil involved mainly physical adsorption because the pigments-adsorbed on BBA-AC can be mainly desorbed by the absolute ethanol. The disadvantage of BBA-AC in adsorbing vegetable oil is some lost of oil during adsorption. So, the optimum dosage of BBA-AC used is needed to consider.

REFERENCES

Ahmedna, M., Johns, M.M., Clarke, S.J., Marshall, W.E. and Rao, R.M. (1997) Potential of agricultural by-product-based activated carbons for use in raw sugar decolorization. *Journal of the Science of Food and Agriculture, 75*, 117–124.

Ahmedna, M., Marshall, W.E. and Rao, R.M. (2000a). Production of granular activated carbons from select agricultural by-products and evaluation of their physical, chemical and adsorption properties. *Bioresource Technology*, 71, 113 - 123.

Ahmedna, M., Marshall, W.E. and Rao, R.M. (2000b). Surface properties of granular activated carbons from agricultural by-products and their effects on raw sugar decolorization. *Bioresource Technology*, *71,* 103 - 112.

Argun, M.E. and Dursun, S. (2008). A new approach to modification of natural adsorbent for heavy metal adsorption. *Bioresource Technology***,** *99,* 2516-2527.

Aworn, A. (2007). *Preparation of activated carbon obtained from corncob and bagasse bottom ash for ethylene glycol adsorption,* Ph.D. thesis, The Joint of Graduate School of Energy and Environment, King Mongkut's Univesity of Technology Thonburi.

Aworn, A., Thiravetyan, P. and Nakbanpote, W. (2008), Preparation and characteristics of agricultural waste activated carbon by physical activation having micro-and mesopores. *Journal of Analytical and Applied Pyrolysis, 82*, 279-285.

Balakrishnan, M., Dua, M. and Bhagat, J. J. (2000). Effect of operating parameters on sugarcane juice ultrafiltration: Results of a field experience. *Separation and Purification Technology, 19*, 209-220.

Basal, R.C., Donet, J.B. and Stoeckli. F. (1988). *Active Carbon,* Marcel Dekker, New York.

Bernado, E.C, Egashira, R. and Kawasaki, J. (1997). Decolorization of molasses wastewater using activated carbon prepared from cane bagasse. *Carbon, 35(9),* 1217-1221.

Broadhurst, H. A. (2002). *Modeling Adsorption of Cane Sugar Solution Colorant in Packed-Bed Ion Exchangers,* M. S.Thesis, Department of Chemical Engineering, Louisiana State University and Agricultural and Mechanical College, Louisiana.

Byers, J.A. (2003). *Solvent Polarity and Miscibility* [Online], Available: http://www.chemical-ecology.net/java/solvents.htm [2008, October 21].

Carpenter, F. G. (1980) . *Cane Sugar Handbook,* Chen, J. C. P. (Ed.), John Wiley and Sons, Inc., New York.

Chandra, R., Bharagava, R.N. and Rai. V. (2008). Melanoidins as major colourant in sugarcane molasses based distillery effluent and its degradation. *Bioresource Technology, 99 (11),* 4648-4660.

Coca, M., Garcia, M. T., Gonzalez, G., Pena, M. Garcia, J. A. (2004). Study of colored components formed in sugar beet processing. *Food Chemistry*, *86,* 421 - 433.

Daud., W.M.A.W. and Ali., W.S.W. (2004). Comparison on pore development of activated carbon produced from palm shell and coconut shell. *Bioresource Technology, 9*3,63-69.

Durante, R. M. B. O., Santos, E. B. H. and Durante, A. C. (2001) Comparison between diafiltration and concentration operation modes for the determination of permeation coefficients of humic substances through ultrafiltration membranes. *Analytica Chimica Acta, 442,* 155 - 164.

Garcia-Perez, M., Chala, A. and Roy, C. (2002) Vacuum pyrolysis of sugarcane bagasse. *Journal of Analytical and Applied Pyrolysis, 65*, 111-136.

Ghosh, M. (2007). Review on recent trends in rice bran oil processing. Journal of the America Oil Chemist's Society , 84, 315-324.

ICUMSA, 1994, *ICUMSA Methods Book*, ICUMSA Publications Department, Norwich.

Jankowska, H., Swiatkowski, A. and Choma, J. (1991). *Active Carbon*, Ellis Horwood, New York.

Kalderis, D., Koutoulakis, D., Paraskeva, P., Diamadopoulos, E., Otal., E., Olivares del Valle, J. and Fermandez-Pereira, C. (2008). Adsorption of polluting substances on activated carbons prepares from rice husk and sugarcane bagasse. *Chemical Engineering Journal*, *44,* 42-50.

Kaynak, G., Ersoz, M. and Kara, H. (2004). Investigation of the properties of oil at the bleaching unit of an oil refinery. *Journal of Colloid and interface Science, 280,* 131-138.

Lippens, B.C. and de Boer, J.H. (1965). Studies on pore systems in catalysts V. The *t* method. *Journal of Catalysis***,** *4,* 319-323.

Lua, A.C., Lau, F.Y. and Guo, J. (2006). Influence of pyrolysis conditions on pore development of oil-palm shell activated carbon. *Journal of Analytical and Applied Pyrolysis, 76,* 96-102.

Mall, I.D., Srivastava, V.C., Agarwal, N.K. and Mishra, I.M. (2005). Adsorption removal of malachite green dye from aqueous solution by bagasse bottom ash and activated carbon-kinetic study and equilibrium isotherm analyses. *Colloids and Surfaces A: Physicochemical and Engineering Aspects, 264,* 17-28.

Manjula, S. and Subramanian, R. (2009). Simultaneous degumming, dewaxing and decolorizing crude rice bran oil using nonporous membranes. *Separation and Purification Technology, 66,* 223-228.

McKay, G. (1996), *Use of adsorbents for the removal of pollutants fro wastewater*, CRC Press, New York.

Migo, V.P., Rosario, E.J.D. and Matsumura, M. (1997). Flocculation of Melanoidins Induced by Inorganic Ions. *Journal of Fermentation and Bioengineering, 83,* 287 - 291.

Mitr Phol Sugar group . (2007) *Mitr Phol Sugar Specification* [Online], Available: http://www.mitrphol.com/en/04_distribution/01_export_market.php

Mozammel, H. M., Masahiro, O. and Bhattacharya, S. C. (2002). Activated carbon charcoal from coconut shell using $ZnCl_2$ activation. *Biomass and Bioenergy, 22*, 397-400.

Mudoga, H.L., Yucel, H. and Kincal, N.S. (2008). Decolorization of Sugar Syrups Using commercial and sugar beet pulp based activated carbons. *Bioresource Technology, 99,* 3528-3533.

Nguetnkam, J. P., Kamga, R., Villieras, F., Ekodeck, G.E. and Yvon, J. (2008). Assessing the bleaching capacity of some Cameroonian clays on vegetable oils. *Applied Clay Science,* 39, 113-121.

Pandey, A., Garlos, R., Nigam, P. and S. V.T. (2008). Biotechnological potential of agro-industrial residues. I:sugarcane bagasse. *Bioresource Technology*, *74*, 69-80.

Patrick, J.W. (1995). *Porosity in Carbons,* Edward Arnold, Great Britain.

Pease, S. F. W. and Steven, M. (1999) . Process for purifying sugar solutions. *Patent* (US Patent 5,893,947), Advanced Separation Technologies Incorporated (Lakeland, FL), assignee.

Royle, L., Bailey, R.G. and Ames, J.M. (1998). Separation of Maillard Reaction Products from Xylose-glycine and Glucose-glycine Model Systems by Capillary Electrophoresis and Comparison to Reverse Phase HPLC. *Food Chemistry*, 62, 425 - 430.

Sabah, E. (2007). Decolorization of vegetable oils: Adsorption mechanism of chlorophyll-*a* on acid-activated sepiolite. *Journal of colloid and interface science, 310,* 1-7.

Simaratanamongkol, A. (2008). *Production of bagasse bottom ash activated carbon for decolorization of sugar syrup*, M.S thesis, School of Bioresources and Technology, King Mongkut's Univesity of Technology Thonburi.

Simaratanamongkol, A. and Thiravetyan, P.(2010). Decolorization of melanoidin by activated carbon obtained from bagasse bottom ash.. *Journal of Food Engineering, 96,* 14-17.

Suksabye, P. (2009). *Application of bagasse bottom ash activated carbon for decolorization of bleaching process in vegetable industrial*, research report, Suan Dusit Rajabhat University.

Tseng, R.L., Tseng, S.K. and Wu. F.C. (2006).Preparation of high surface area carbons for conrncob with KOH etching plus CO_2 gasification the adsorption of dryer and phenols from waste . *Colloids and Surface A: Physicochemical and Engineering Aspects, 279,* 69-78.

Valix, M., Cheung, W.H. and McKay, G.. (2004). Preparation of activated carbon using low temperature carbonization and physical activation of high ash raw bagasse for acid dye adsorption. *Chemospere, 56,* 493-501.

Wu, F. C., Tseng, R. L. and Hu, C. C. (2005). Comparisons of pore properties and adsorption temperature of KOH-activated and steam-activated carbons. *Microporous and Mesoporous Materials, 80,* 95-106.

Yaylayan, V.A. and Kaminsky, E. (1998). Isolation and structural analysis of Millard polymers: caramel and melanoidin formation in glycine/glucose model system. *Food Chemistry, 63 (3),* 25-31.

In: Activated Carbon
Editor: James F. Kwiatkowski
ISBN: 978-1-61209-684-1
©2012 Nova Science Publishers, Inc.

Chapter 10

USE OF ACTIVATED CARBON AS PRE-SEPARATION AGENT IN NAA OF SELENIUM, COBALT AND IODINE

M. Navarrete* [*] *and T. Martínez
Faculty of Chemistry, Building D, UNAM, 04510 Mexico City, Mexico

ABSTRACT

The position of pre-irradiation separations in neutron activation analysis is shortly discussed. Special attention is given to separations for purification and/or concentration of analyte elements, either complexed or uncomplexed, via sorption on activated carbon. It was shown for a number of trace elements that the blank value introduced due to the use of activated carbon is small or mostly even negligible. The NAA determination via pre-separations based on activated carbon is highlighted for selenium, cobalt and iodine.

INTRODUCTION

Presently, instrumental neutron activation analysis (INAA) has been applied substantially more than neutron activation analysis using of radiochemical separations (RNAA), in spite of the fact that the latter reaches a higher accuracy and sensitivity for a single trace element among many others in a sample. One of the drawbacks of RNAA is imposed by the time needed for post-irradiation chemical separations when dealing with rather short- lived radioisotopes. This may imply a substantial loss of accuracy and sensitivity of the analysis or even an impediment at all to perform RNAA. Pre-concentration of trace elements before irradiation has been used in neutron activation analysis to remove interferences and/or to concentrate the element of interest, to increase the sensitivity of INAA. However, this entails the risk that the procedure followed may add as impurity traces of the analytes to the sample, with the risk of invalidating the analytical outcome. Application of special materials, equipment and procedures may minimise this risk, quite often to negligible levels, but this should be continuously checked with blank samples processed under conditions identical to

[*] E-mail: jmnat33@servidor.unam.mx, fax (525) 56-22-52-32

those for the samples. There are quite a few elements, which react with organic reagents at certain fixed pH values without any need of a carrier, even at extremely low concentrations, to form complexes, which are easily retained by a small filter consisting of activated carbon. Since the carbon is transparent for thermal neutrons and displays no radioactivity after neutron irradiation, it doesn't interfere at all with both irradiation and gamma-spectrum measurement. Table 1. shows the trace-element levels of activated carbon (Merck No. 2186), as determined via INAA, performed by irradiation in a neutron flux of 5x10 [13] cm^{-2} s^{-1} and variable irradiation, cooling and counting times [1]. Assuming a required mass of 50 mg of carbon for concentration of iodine and of complexes of cobalt and selenium, the blank value is calculated to $1x10^{-7}$g for cobalt and to $2x10^{-9}$ g for selenium. For iodine the concentration in carbon was already below the detection limit. These masses may be considered as the background above which determinations can be performed in other experimental conditions, and the results may be treated according the Currie's criteria for statistical variations in gamma-spectrum measurements [2]. In this way, separations established originally as radiochemical separations for several elements [3] have been used as pre-concentration methods for elements, which form short-lived radioisotopes. For instance, ^{60}Co ($t_{1/2}$ = 5.3y) is used for determination of cobalt in INAA and RNAA, which needs much longer irradiation, cooling and counting times than ^{60m}Co ($t_{1/2}$ = 10.5 min), whose activation conditions according to half lives, cross sections (σ = 19 b and 18 b respectively) and target isotopic abundance (both 100% [4]) are still favourable for ^{60m}Co when the cobalt pre-concentration is performed, in spite of the low branching yield (2%) for the gamma-ray of interest [4,5].

Table 1. Trace-element concentrations in commercial activated carbon (Merck No. 2186) as determined via INAA according the following conditions: neutron flux 5x10[13] $n.cm^{-2}.s^{-1}$; irradiation time 1 min or 24 h; decay time and counting time both variable[1]

Element	Concentration in mg/kg
Al	1.13
As	0.3
Br	0.45
Co	2.45
Cr	5.5
Cu	43
Fe	190
Mn	60
Na	80
Sb	0.8
Sc	0.034
Se	0.05
V	0.29
Zn	14
Au	0.38
Hg	0.2

The same applies to selenium, because ^{75}Se ($t_{1/2}$ = 120d) needs much longer irradiation, cooling and counting times than ^{77m}Se ($t_{1/2}$ = 17.5 s), whose irradiation conditions according to half lives, cross sections (σ = 30 b and 22 b respectively) and target isotopic abundances (0.87% and 9% respectively [4]) are quite favourable for ^{77m}Se when selenium pre-concentration is performed [6,7,8,9].

Concerning iodine, ^{128}I ($t_{1/2}$ = 25 min) is the only radioisotope formed by thermal-neutron irradiation of the target isotope ^{127}I (σ = 6.4 b, isotopic abundance 100 % [4]), and therefore pre-concentration of traces has also considerable advantage over INAA and RNAA, because the gamma spectrum is much cleaner, with lower background and dead time, without imposing a requirement of necessarily very quick radiochemical separations [10,11,12].

This paper describes how the organic reagents APDC and Cupferron in combination with activated carbon filters perform notably well in the pre-concentration of traces for thermal-neutron activation analysis of these elements in organic samples.

EXPERIMENTAL

Filters of activated carbon with a mass of 50 mg each are made in the following way. An amount of 1.25 g of activated carbon (Merck No. 2186) is put in a 100 ml beaker equipped with a stirrer on a magnetic plate. To the beaker 25 ml of 2-propanol is added, and while stirring the suspension 1 ml is taken out with a pipette and deposited in a 250-ml vacuum filtration apparatus with a 2.5-cm diameter cellulose filter paper inserted. Each carbon layer is washed with 5 ml of bidistilled water. The propanol and water washings in the Erlenmeyer of the vacuum filtration apparatus are discarded. Filters are now ready for use.

About 500 mg of the sample is dissolved in a Teflon tube of a dissolution bomb (Parr Instruments, 276AC2-T304-092302), with 3-5 ml of ultrapure concentrated HNO_3, shut under pressure and put in an oven at 140-160°C during 3-4 h. Instead, also a microwave dissolution device may be used to dissolve the sample in the same volume of HNO_3 in some minutes. Once the dissolution bomb is cooled overnight or with cold water, the nitric acid sample solution is poured into a beaker, together with the Teflon tube washings and the volume is brought to 50-100 ml with bidistilled water. The pre-separation is performed in three steps.

First, the pH is set to 1-2 by adding dropwise ultrapure concentrated NH_4OH while stirring magnetically. An amount of 25 mg of APDC (Aldrich 14,269-7) is added and stirring is continued for 2-3 min. Subsequently, the solution is filtered through an activated-carbon filter using the vacuum filtration apparatus. The selenium traces are now retained in the carbon filter. The filtered solution is brought back to its original beaker and the filter is washed with 20 ml of an aqueous solution of 0.2 mg APDC/ml at pH 1-2. The filter washing solution is discarded.

As second step, the pH of the original sample solution is set to 4-6 by adding dropwise concentrated NH_4OH while stirring magnetically. When this solution is filtered through a second, fresh carbon filter, iodine traces in the sample are trapped in the filter, which is washed with 20 ml of bidistilled water at pH 4-6. Washing water is discarded. In the third step 25 mg of Cupferron (Aldrich 20,688-1) is added to the filtered solution, while stirring magnetically during 2-3 minutes. The solution is filtered through a third, fresh activated-carbon filter in another vacuum filtration apparatus. The cobalt traces from the sample are

now in this carbon filter, which is washed with 20 ml of aqueous solution 0.2 mg Cupferron/ml at pH 4-6. The carbon filters are removed from the cellulose filter papers by using a small scalpel and tweezers over a clock glass, and put separately into the small containers used for neutron irradiation, by means of a small glass funnel inserted on their tip. Special high-purity Teflon filter papers suitable for neutron irradiation may be used, and wrapped around the carbon filters. Activated carbon filters with the analyte element are now ready for neutron irradiation and are put separately in the rabbits. For the selenium determination, the irradiation time is 17.5 s. The cooling time is as short as possible, about 5 s, to allow ^{38m}Cl to decay. The measurement time is 20 s. Cyclic activation analysis may be used when a fast, automatic, pneumatic transport system from irradiation to detection position is available [13]. For determination of iodine and cobalt the irradiation, cooling and detection times are similar. The irradiation time is 10-25 min, the cooling time 1-5 min, and measurement duration 5-10 min. The thermal neutron fluxes used ranged from 10[11] to 10[14] $cm^{-2}.s^{-1}$. Both NaI(Tl) scintillator detectors and semiconductor detectors have been used.

RESULTS AND DISCUSSION

Filtering efficiency or yields for each element, as a percentage of the traces retained by the carbon filter plus reagent at the pH value set, were obtained by filtering no-carrier-added solutions of longer half-lived radioisotopes of cobalt (^{60}Co), selenium (^{75}Se) and iodine (^{131}I). From the solution, 2 ml is taken before filtering, and counted in a test tube during 1-5 min in a well-type 3"x3" scintillation detector, connected to a PC running the Maestro Program for radioactive detection (activity A). After filtering, 2 ml of the solution is removed and counted in the same way (activity B). The yield as percentage of the elements retained by the filter is then:

Yield (in %) = 100 x (A – B) / A

For the three elements, the yield is on the average 97-99%. In this way, cobalt in blood-serum samples has been measured in relation to vitamin B_{12} [5]. Selenium has been determined in samples of cattle fodder, since selenium is related to the myopathy dyspnoea disease [6], and in human urine samples related to cervical uterine cancer [7,8,9]. Iodine has been measured in cornstarch and dried shrimp flour (unpublished results). The method has also been applied to the reference material BCR 279 (Ulva Lactuca or Sea Lettuce), issued by the Bureau of Reference Materials of the European Union. The results agreed within the statistical variations.

The evident advantages of the pre-concentration of Co and Se traces in activated carbon for neutron activation analysis, are the incomparably shorter irradiation, cooling and counting times, which allows to obtain so many results as practically is wanted, in order to obtain a good mean with a realistic associated standard deviation. It also allows to apply any other criteria for statistical variations in a results set, such as that of Proschan to reject one particular value, which does not belong to the set due to experimental errors or any other reason, as can be statistically demonstrated [14]. For iodine, the same applies as for cobalt and selenium.

The gamma spectra obtained are much cleaner than for almost any other matrix, with a small (<10%) dead time and always with a much lower background than that encountered in normal INAA [10,11,12] . Nevertheless, from a theoretical point of view, if it is calculated K_c, constant of counts/g for the longer-lived radioisotopes ^{60}Co and ^{75}Se, for a set of established experimental conditions[2], larger figures are obtained than those of the shorter-lived radioisotopes ^{60m}Co and ^{77m}Se. This happens because irradiation, cooling and counting times can be established as it is wanted for longer-lived radioisotopes, in a frame of working conditions. On the contrary, unavoidable time limitations are found for short half life ones, mainly related to detection time. But also it is true that this theoretical calculation is quite independent from background and dead time values, which are definitely lowered by the pre-concentration method and shorter lived radioisotopes induced during incomparably shorter irradiation times.

CONCLUSION

The use of blank samples has been almost unnecessary when this method has been applied, because 50 mg of activated carbon (Merck No. 2186) as well as 25 mg of Cupferron (Aldrich, 20688-1) and APDC (Aldrich, 14,269-7), yield a negligible or undetectable mass of Co, Se and I for short irradiation times, when compared with the masses of these elements present in 500 mg of any of the analysed samples, put in solution and filtered before irradiation. However, in order to support this method for Co, Se and I traces pre-concentration, some data about the activities induced in the containers and blank samples are given, as well as how it has been proved in one Reference Material and the standards used. Containers used were the common, plastic polyethylene type, suitable for short neutron irradiation time. Two sizes were used. First one was cylindrical shape, 2 cm height and 2 cm diameter. Second one was about half in volume of the first one, elliptic shape, 1 cm height, 1 cm diameter. Activities induced in both types by thermal neutron irradiation of empty containers were ^{28}Al ($t_{1/2}$=2.28 m, γ rays 1.78 MeV) and ^{41}Ar ($t_{1/2}$=1.83 h, γ rays 1.29 MeV) for irradiation time 2m, cooling time 1 m, detection time 2m, flux about 2x10[12] n. cm^{-2}.s^{-1} in the Triga Mark III reactor of the Nuclear Center of Mexico. When the blank sample of activated carbon (50 mg) plus either APDC (25 mg) or cupferron (25 mg) filtered through it was irradiated in the same type of container, ^{56}Mn ($t_{1/2}$=2.6 h, γ rays 0.847 MeV) appeared together with ^{28}Al and ^{41}Ar under the same irradiation conditions. When empty containers and blank samples were irradiated making use of one pneumatic fast transfer system, ^{110}Ag ($t_{1/2}$=24.6 s, γ rays 0.658 MeV) appeared in empty containers and ^{46m}Sc ($t_{1/2}$=18.7 s, γ rays 0.142 MeV) in blank samples, for irradiation time 17 s, cooling time 3 s, detection time 20 s, 3 cycles, flux about 4.7x10[11] n.cm^{-2}.s^{-1}, in the Reactor Facility of Strasbourg University, France [15]. The method was applied for Se to the Reference Material BCR-279, Ulva Lactuca (Sea Lettuce), issued from the Bureau of Reference Materials of European Union. First, the conventional method of the radiochemical separation proposed was made for Se after irradiation of samples under these conditions: irradiation time 65h, cooling time 3 weeks, detection time 5 hours in one semiconductor detector, flux about 1x10[14] n.cm^{-2}.s^{-1} in the Osiris Nuclear Reactor at CE-Saclay, France. The average set out from 4 determinations was 0.605 ± 0.032 mg/Kg. Second, the pre-concentration of Se traces was

performed, followed by the short irradiation to detect the activity of ^{77m}Se at conditions said in the nuclear reactor of Strasbourg University, France. The average set out from 4 determinations was 0.582 ± 0.030 mg/Kg. The certified concentration of Se in this Reference Material is 0.593 ± 0.032 mg/Kg[15].The standards used in both procedures were the conventional ones, diluted solutions of selenious acid (Aldrich 22 985-7) with known concentrations, absorbed by high purity cellulose (Whatman CF-11) conditioned in pills by pressure an wrapped in aluminium foil (for long irradiation), and the same diluted solutions passed through the activated carbon filters, according the proposed method (for short irradiation)[15]. The peaks of 59 keV (^{60m}Co), 161 keV (^{77m}Se) and 441 keV (^{128}I, X rays from ^{128}Te)[4] appeared neatly in clean gamma spectra with lower background and dead time than in any other possible INAA, and competing in this zone of spectra with those obtained by RNAA, either by comparing to standards or by using the k_0 method. Finally, the fact to put the sample in solution for filtering before irradiation, allows using as much as 500 mg of sample mass, and even more, which improves the sensitivity or capacity to measure lower concentrations. Therefore, the pre-concentration method for Co, Se and I traces seems to be competitive enough comparing either with INAA or RNAA following any of published radiochemical separations.

ACKNOWLEDGMENTS

To the memory of Vincent P. Guinn and George W. Leddicotte, creators and innovators in neutron activation analysis.

REFERENCES

[1] H.A.Van Der Sloot, D. Hoede, S. Zonderhuis, C. Meijer, *Netherlands Energy Research Foundation Report ECN*-80 (1980) 8.
[2] L. A. CURRIE, *Anal. Chem*. 40 (1968) 586.
[3] H.A. Van Der Sloot, G.D. Wals, C.A. Weers, H.A. *Das, Anal. Chem*. 52 (1980) 112.
[4] C.M. Lederer, J.M. Hollander, I. Perlman, *Table of Isotopes*, 6th Ed., Wiley and Sons, New-York (1967) p. 249, 258, 298.
[5] M. Navarrete, L. Cabrera, A. Ley, J. Radioanal. *Nucl. Chem. Lett*. 49 1981) 341.
[6] M. Navarrete, L. Cabrera, N. Deschamps, N. Boscher, G. Revel, J.P. Meyer, *J. Radioanal. Nucl. Che*m. 168 (1993) 15
[7] M. Navarrete, L. Cabrera, T. Martinez, G. Revel, J.P. Meyer, A. Stampfler, *J. Radioanal. Nucl. Chem*. 195 (1995) 91.
[8] M. Navarrete, L. Cabrera, T. Martinez, G. Revel, J.P. Meyer, *J.Radioanal. Nucl. Chem*. 217 (1997) 167.
[9] M. Navarrete, A. Gaudry, L. Cabrera, T. Martinez, Biol. *Trace Elem. Res*. 79 (2001) 97.
[10] R. Rao, A. *Chatt, Anal. Chem.* 63 (1991) 1247.
[11] R. Rao, A. *Chatt, Anal. Chem*. 118 (1993) 1298.
[12] M. Navarrete, A. Gaudry, L. Cabrera, T. Martinez, *J. Radioanal. Nucl. Chem*. 251 (2002) 297.
[13] N.M. Spyrou, *J. Radioanal. Nucl. Chem*. 61 (!981) 215.

[14] F. Proschan, *Am. J. of Phys*. 21 (1953) 520, Prec. Meas. Cal. NBS Sp. Publ. 300-1 (1969) 351.

[15] M. Navarrete, These de Doctorat de l'Université Paris 6, Analyse par Activation du Se dans des echantillons biologiques,en utilisant une méthode de pre-séparation des traces (1992) 41,43.

In: Activated Carbon
Editor: James F. Kwiatkowski
ISBN: 978-1-61209-684-1
©2012 Nova Science Publishers, Inc.

Chapter 11

VIRTUAL POROUS CARBON (VPC) MODELS: APPLICATION IN THE STUDY OF FUNDAMENTAL ACTIVATED CARBON PROPERTIES BY MOLECULAR SIMULATIONS

Artur P. Terzyk[1] *, Sylwester Furmaniak[1], Piotr A. Gauden[1], Peter J. F. Harris[2], Radosław P. Wesołowski[1] and Piotr Kowalczyk[3]

[1] N. Copernicus University, Department of Chemistry, Physicochemistry of Carbon Materials Research Group, Gagarin St. 7, 87-100 Toruń, Poland

[2] Centre for Advanced Microscopy, University of Reading, Whiteknights, Reading RG6 6AF, UK

[3] Nanochemistry Research Institute, Department of Chemistry, Curtin University of Technology, P.O. Box U1987, Perth, 6845 Western Australia, Australia

1. INTRODUCTION

Due to progress in the development of computers, molecular simulations have become the major theoretical technique in chemistry and physics. In the field of activated carbons the so called Virtual Porous Carbon (VPC) models are becoming more and more popular. As stated by Biggs and Buts (who are the authors of this term) "we use the term Virtual Porous Carbon (VPC) to describe computer-based molecular models of nanoporous carbons that go beyond the ubiquitous slit pore model and seek to engage with the geometric, topological and chemical heterogeneity that characterizes almost every form of nanoporous carbon. We differentiate these from the many other complex models that have been proposed for nanoporous carbons since the early 20th century by requiring them to be computer-based and, thus, open to further analysis or use in molecular simulations" [1]. Therefore, the major properties of VPC models are a well defined absolute (geometric) pore size distribution (PSD), as well as known chemical composition of carbon surface layer, exactly known

* E-mail: aterzyk@chem.uni.torun.pl, url:http://www.chem.uni.torun.pl/~aterzyk/ tel.(+48) (056) 611-43-71, fax:(+48) (056) 654-24-77

density etc. It is obvious that a PSD, as well the chemical composition of the carbon surface determine adsorption properties from the gaseous phase as well as from solutions. Because the geometry of pores and the composition of surface layers are hard to determine in the case of real activated carbons we still use more or less trivial approaches (for example one can use the BET model for calculation of surface area or one can assume the slit - like pore geometry to calculate the PSD curve, or use the Boehm's titration method for calculation of surface functionalities concentration). All those properties and characteristics are well known for VPC. Moreover, in contrast to real experiments, we also know carbon ring statistics, the number of edge carbon atoms etc. Therefore using VPC models one can easily and systematically determine the influence of different factors on carbon adsorption properties, and then compare the results with experimental data. In this chapter we review recent progress in the field of simulation of gas and liquid adsorption on VPC models. We will start from two basic older VPC models i.e. the model proposed by Biggs et al. [1-5] and the model proposed by Do et al. [6-9]. Next we will discuss the VPC model proposed, based on HRTEM measurements, by Harris et al. [10-18]. We will show that some empirically observed correlations that were not simply explained become clear if one performs a series of molecular simulations using those VPC models. The same can be stated about the methods of PSD curve calculation, or about the mechanisms of adsorption from liquid phase. We will demonstrate that the application of a simulation technique and VPCs leads to an explanation of the mechanism of phenol adsorption from aqueous solutions on activated carbons. In simulations which agree with the real experiment, introduction of oxygen groups on an activated carbon surface leads to a decrease in phenol adsorption, but because in the simulation we use well defined VPCs we can explain the reason of this decrease. Additionally in this chapter other examples of VPC application will be given and discussed.

2. VPC MODELS OF BIGGS ET AL. AND DO ET AL. AS EXAMPLES

A very interesting model of VPC was proposed in the 90's by Biggs and Agarwal [19-22]. This model is based on hierarchical idea of carbon structure. To check the influence of porosity, pore connectivity or temperature on diffusion of different gases relatively large structures ($100\times100\times100$ nm^3) composed of carbon crystallites were prepared. It can be mentioned here that a similar approach (but used for smaller systems i.e. $4{,}0\times1{,}2\times1{,}2$ nm^3) was proposed by MacElroy et al. [23].

In their studies Biggs and Agarwal [19-22] used activated carbon crystallites composed of five layers and the edge carbon atoms were not saturated with hydrogen. A simulation box was filled with 26 different types of crystallites (chosen from a base) differing in a number of carbon atoms (the maximum number of carbon atoms was equal to 60 in each layer having the size 0.5-1.5 nm). The creation of empty spaces (i.e. pores) in a simulation box was allowed. Moreover the rotation of crystallites was also possible (overlapping atoms were removed from a structure). The authors mentioned a possible application of this structure in the studies of the effects of surface functionalities but the results have not yet been published. In later studies Biggs et al. [1-5,20] tried to check the effect of structural heterogeneity on adsorption/desorption processes (and on energetics) of the following molecules: N_2, CH_4, CF_4

and SF_6. They also studied the diffusion of CH_4, and tried to verify the most popular adsorption theories and equations.

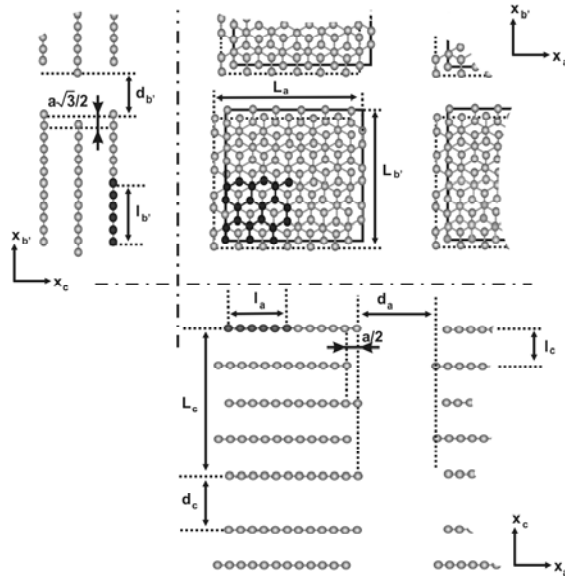


Figure 1. The Biggs model [2]. Reprinted with permission from *M.J. Biggs, A. Buts, D. Williamson, Langmuir, 2004, 20, 5786*. Copyright 2004 American Chemical Society.

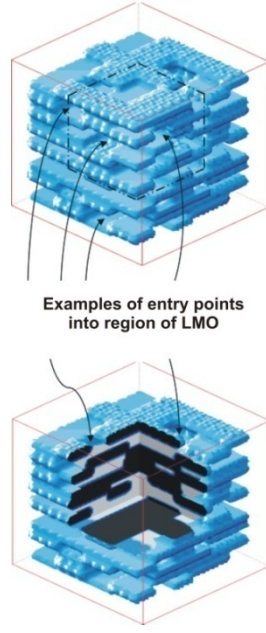


Figure 2. Typical simulation cell of the Biggs model [2]; the structure seen from two perspectives together with isoenergetic surfaces – black colour shows the regions available for an adsorbate, grey – unavailable. Reprinted with permission from *M.J. Biggs, A. Buts, D. Williamson, Langmuir, 2004, 20, 5786*. Copyright 2004 American Chemical Society.

The model proposed earlier [19-22] was slightly modified by Biggs et al. [1-5,19] but without major changes in the fundamental assumptions.

Figure 1 shows a schematic representation of a carbon crystallite together with an explanation of the characteristic parameters i.e.: L_a, L_c and d_{002}. In this case a parallel arrangement of the graphene sheets was assumed. From this figure one can conclude that the LMO (*local molecular order*) of a basic structure is composed of crystallites having the same sizes and arrangement. Therefore, to characterise the arrangement of crystallites the authors introduced a parameter α. Deleting of atoms was also possible and this led to the creation of new pores. In Figure 1 black balls denote the remaining (after the procedure of deleting) carbon atoms seen on a background of a perfect graphene layer. Figure 2 shows some typical structures.

Nonporous fragments of the structure (creating individual crystallites) are composed of parallel graphite fragments having finite sizes (the sizes are not necessary the same). They are in the range: 0.0982-0.1276 nm^2 and contain 1-5 graphene sheets. Both adsorbents do not contain free spaces between crystallites, but they possess different orientation of graphene sheets. The structure of the first adsorbent is "perfect" whereas in the structure of a second the deviation of planes from the equilibrium position is possible (in both directions by $\pm 15^o$). Additionally in Figure 2 the accessibility/inaccessibility of an adsorbent free space was marked using isoenergetic surfaces. In this case the whole cell of the simulation box was isolated. To imitate the changes in porosity, the crystallites were shifted, and the individual areas of LMO were surrounded by a free space forming in this case mesopores (the parameter d describes this distance in three directions). To obtain micropores the starting structures were disturbed by deleting carbon atoms in such a way that the fragments of remaining structures are composed of six - membered carbon rings (a typical fragment having the size described by the two dimensional parameter l is marked in black in Figure 1). The second method leading to the creation of the narrowest pores was by changing parameter α value because this parameter influences the orientation of graphite planes. In addition the authors checked (by changing L, d and l and sometimes α) the influence of graphite stacking (ABA and ABC). The values of the parameters were fixed to mimic experimental values: L_a (0,1-0,4 nm), L_c (1,0-3,0 nm), l (0,5-1,5 nm), d_{002} (0,35-0,65 nm) i α ($\pm 15°$) [19,20,24-27].

The model proposed by Biggs et al. [1-4,28-33] found different application in fundamental studies. Thus for example authors tested the BET concept of surface area [28,29], the properties of DR and DA equations [29,30], the idea of α_s plots [3,28], and the concept of fractal analysis [1,31]. They also studied the methods for determining the PSD and pore-network connectivity of porous carbons [4] as well as studied the diffusion in carbons [1,32,33].

Another very interesting model of carbon black [8,9] and so called "soft" carbons [6-8] was proposed by Do et al. These authors considered graphene planes (forming the external surface of carbon black or pores) with defects [7,8]. These defects were introduced only into the external layer. Figures 3 and 4 show some typical structures i.e. a side-view of a slit like pore and a top view of different types of created defects. It should be mentioned that the major idea of this model originates from the papers published by Seaton et al. [34] and Turner and Quirke [35]. The parameters describing defects were: the percentage of deleted atoms, and the size of created "holes" (R_c, the radius of a sphere which can be fitted to the hole, it was in the range: 0-0.584 nm).

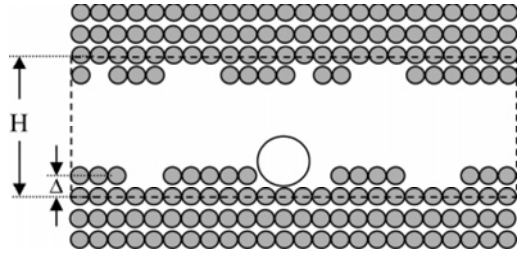


Figure 3. The slit with defects considered by Do et al. [7,8]. Δ - interlayer spacing, H – the distance between undefected carbon layers. Reprinted with permission from *D.D. Do, H.D. Do, J. Phys. Chem. B, 2006, 110, 17531*. Copyright 2006 American Chemical Society.

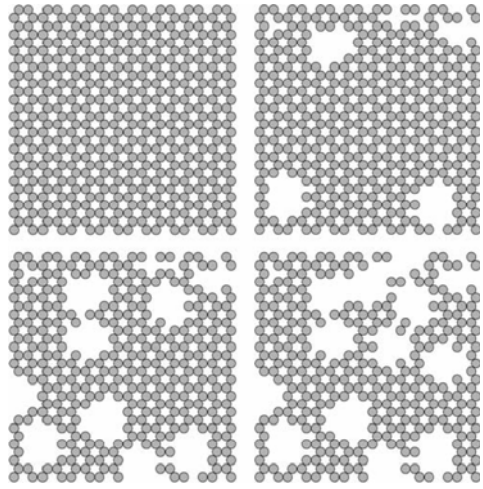


Figure 4. The outer surface of graphitised carbon with the percentage of removed carbon atoms equal to: 0, 10, 20 and 30 % and the effective diameter of „holes" ($2R_c$,) = 0,284 nm [8]. Reprinted with permission from *D.D. Do, H.D. Do, J. Phys. Chem. B, 2006, 110, 17531*.

The first above-mentioned parameter describes the "global" heterogeneity, while the second "local". The authors proposed the following procedure of carbon atom deletion: (i) the random choice of a carbon atom located on the external surface (ii) deletion of atoms included in a circle having assumed radius R_c and a centre located on a previously chosen atom (iii) the calculation of the percentage contents of deleted atoms in a given layer (iv) deletion of next atoms if necessary (and the return to point (i)). Of course some heterogeneity areas can connect as can be observed in Figure 4. The authors studied (using molecular simulations) adsorption of N_2 [9,36,37], Ar [6-9,36], and H_2O [6,37]. They also studied the influence of structural heterogeneity on the adsorption process and on energetics of adsorption, using infinite [8] and finite [9] surfaces, and compared the simulated results with experimental data. The results obtained from this comparison show that this model can be representative for carbon black surface. Authors also proposed so called "accessible pore size distribution" [38] and developed a new method to determine pore size and volume distribution of porous solids having a known atomistic configuration [39]. Lately, based on a VPC model a Monte Carlo integration method to determine accessible volume, accessible surface area and its fractal dimension was also proposed [40].

3. The Model of Harris and Co-Workers

In a series of our studies [41-48] we used a model of activated carbon proposed a few years ago by Harris et al. [10-18]. These authors initiated a series of studies of typical non-graphitizing microporous carbons using high-resolution transmission electron microscopy (HRTEM) in the mid-1990s.

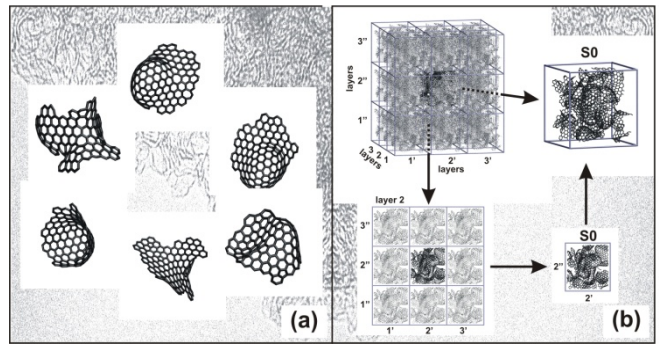


Figure 5. The fragments creating the model of Harris et al. (a). Additionally background shows the HRTEM picture of typical "hard" activated carbon. VPC model is shown in (b) as an isolated structure (named S0) and the same structure applied in simulations under periodic boundary conditions.

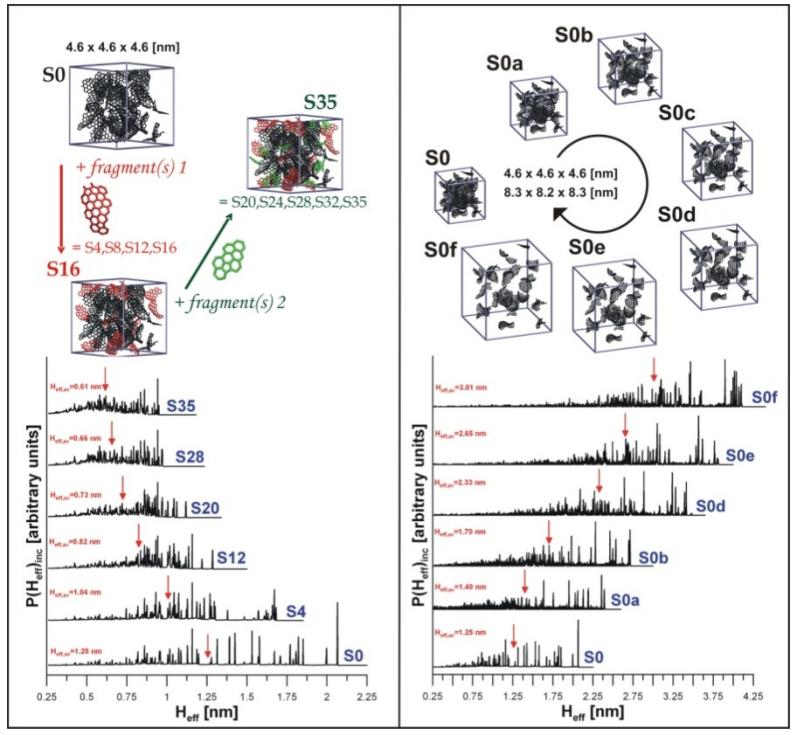


Figure 6. Schematic representation of the methods leading to the systematic changes in porosity of VPC model proposed by Harris et al., together with the typical BG PSD curves. One can observe how easily the porous structure can be changed by adding/deleting or shifting of different fragments.

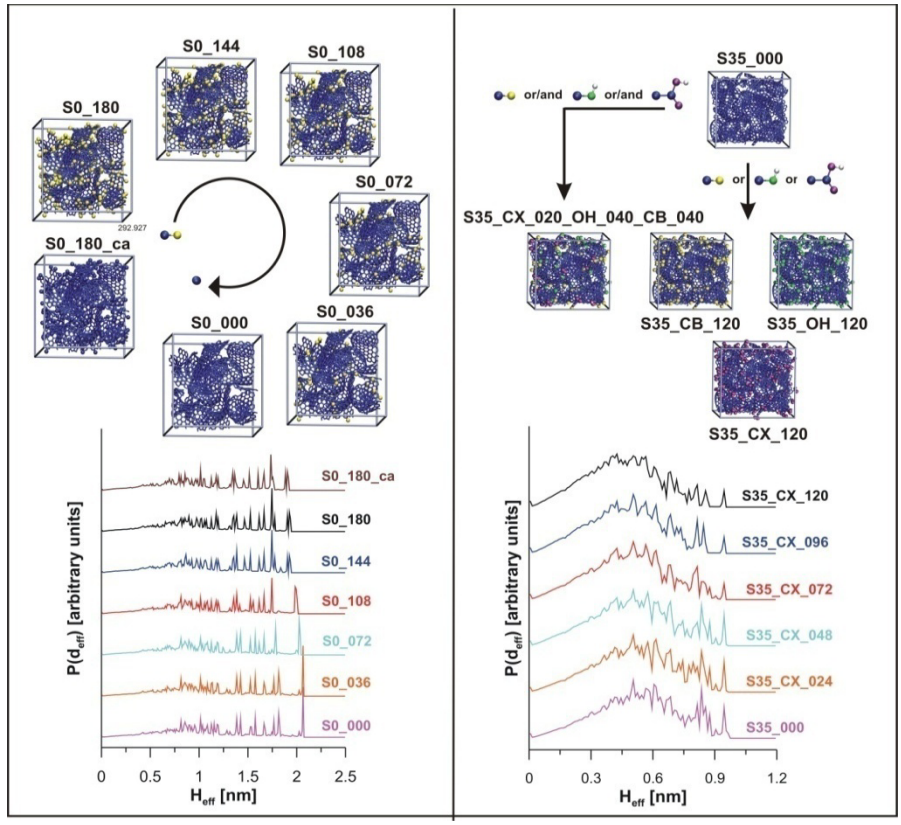


Figure 7. Schematic representation of the virtual oxidation procedure. One can observe that this procedure practically does not change the absolute BG PSD of VPC models.

By careful examination of both freshly prepared and heat-treated carbons, it was concluded that the structure consisted of discrete fragments of curved carbon sheets, in which pentagons and heptagons are dispersed randomly throughout networks of hexagons, as illustrated in Figure 5 [12-15].

This fullerene-like model explains many properties of so-called “hard” synthetic activated carbons, especially their microporosity and high resistance to graphitization. A number of other groups have also found evidence for fullerene-related structures in “conventional” carbons [49-56]. The validity of this model was recently confirmed by quenched MD simulations of different carbon structures by Powles et al. [57], Palmer et al. [58] and Shi [59]. Therefore, we assume that the initial model, proposed by Harris and colleagues, is very close to the true structure of microporous non-graphitizing carbons. Knowing the geometric coordinates of atoms in the simulation box, as the reference method of the PSD calculation, the method proposed by Bhattacharya and Gubbins [60] can be applied. They reported a new technique of fast computation of the PSD of model materials, from knowledge of the molecular coordinates. The PSD is defined as the statistical distribution of the radius of the largest sphere that can be fitted inside a pore of a given point. This method was successfully tested in our recent research for different ideal and defected carbon slit-like pores [42]. Summing up, we know the exact (i.e. geometric) pore size distribution for our VPC model. Next, we can easily change the porosity of our model by

adding/deleting or shifting different carbon fragments. In this way we can easily obtain structures with systematically changed pore size distributions (see Figure 6).

Another advantage of the VPC models is the possibility of changing the chemical structure of the carbon surface. This can be done using the so called "virtual oxidation", recently proposed by us [44]. Thus for example to the attachment of carbonyl oxygen (called "virtual oxidation") is performed in such a way that the oxygen atom and the carbon atom attaching this oxygen (and two nearest neighbours of this carbon atom) lie in the same plane, and the axis of the carbon-oxygen bond is determined by the secant of the C–C–C angle (the oxygen atom from the carbonyl group is attached to the middle C atom). This oxygen atom is placed in such a way that the length of the carbon-oxygen bond is equal to 0.1233 nm [61] and that there are no overlaps between this atom and the remaining fragments of the structure. We introduced the maximum number of surface carbonyl groups which may be introduced in the studied structure. Next subsequent structures were generated by the random removal of the carbonyls from the starting model. Of course a similar procedure can be applied to introduce different groups for example carboxylic ones (see Figure 7) [46].

4. Application of the Harris Model in Simulation of Adsorption from the Gaseous Phase

As was pointed out above since in the case of VPC the structure and a PSD curve are known exactly one can simulate an adsorption isotherm and check the validity of the methods of PSD curve calculation from adsorption data. Recently by using the grand canonical Monte Carlo (GCMC) method, adsorption isotherms of Ar (87 K) were simulated for VPC structures with differing porosity [42]. From simulated isotherms PSD curves were calculated using the Horvath-Kawazoe, Non-Local Density Functional Theory (NLDFT), Nguyen and Do, and Barrett-Joyner-Halenda (BJH) approaches, and compared with those predicted by the BG method. This was the first study in which different methods of calculation of PSDs for carbons from adsorption data could be really verified, since absolute (i.e. true) PSDs are obtained using the BG method. This was also the first study reporting the results of computer simulations of adsorption on fullerene-like carbon models proposed by Harris et al. It was concluded that the density of the initial model proposed by Harris et al. is reasonable, compared to experimental ones, suggesting that the model is a realistic one. The shapes of the Ar isotherms simulated using three analogous VPC models corresponded very well with the pore diameters detected by the BG method.

It was found that the HK model led to the most reliable PSDs in the range of micropores, assuming a fullerene-like carbon structure. The assumption of a slit-like pore shape and the failure to take pore connectivity into account are the two major effects leading to bi-modal PSDs of real activated carbons (the range of mesoporosity is reproduced well). The corrected BJH method with the assumption of a cylindrical meniscus shape recovers relatively well the porosity in the range of mesopores.

In the next paper of this series [41] using a new Monte Carlo simulation algorithm, two types of carbon fragments were gradually placed into the initial structure to increase its microporosity. Thirty six different microporous carbon structures were generated in this way. Using the BG method the micropore size distributions of the obtained carbon models and the

average micropore diameters were calculated. For ten chosen structures, Ar adsorption isotherms (87 K) were simulated *via* the tempering Monte Carlo simulation method. The isotherms obtained in this way were described by widely applied methods of microporous carbon characterisation, i.e. Nguyen and Do, Horvath-Kawazoe, high-resolution α_s plots, adsorption potential distributions and the Dubinin-Astakhov (DA) equation. From simulated isotherms described by the DA equation, the average micropore diameters were calculated using empirical relationships proposed by different authors and they were compared with those obtained from the BG method. It was shown that simulated isotherms described by the widely used methods of microporosity characterisation show typical behaviour, as recorded for real adsorbents. Since the filling pressure for the assembly of slit-like pores is much lower than that for the disordered porous carbon, the average ND micropore diameters correlate linearly with those from the BG model very well. An empirical relationship between the maximum on the APD curve and the average pore diameter is recovered from simulation data, and confirms the above-mentioned differences in the pore-filling pressures for slits and disordered systems. The DA adsorption isotherm equation correctly predicts the maximum amount of adsorption if the studied system is strictly microporous.

Moreover, the simulation data show the validity of the inverse relationship between the characteristic energy of adsorption (E_0) and the average pore diameter (H_{eff}). On the other hand, the assumption of the inverse linear relation between the parameter n and the pore diameter is not correct. Simulated Ar adsorption isotherms described by the DA model also confirm the validity of the empirical relationships proposed in the literature between E_0 and H_{eff}. Among them, the two simplest relations proposed by Stoeckli have almost the same shapes as obtained from the simulation data reported in this study (see Figure 8).

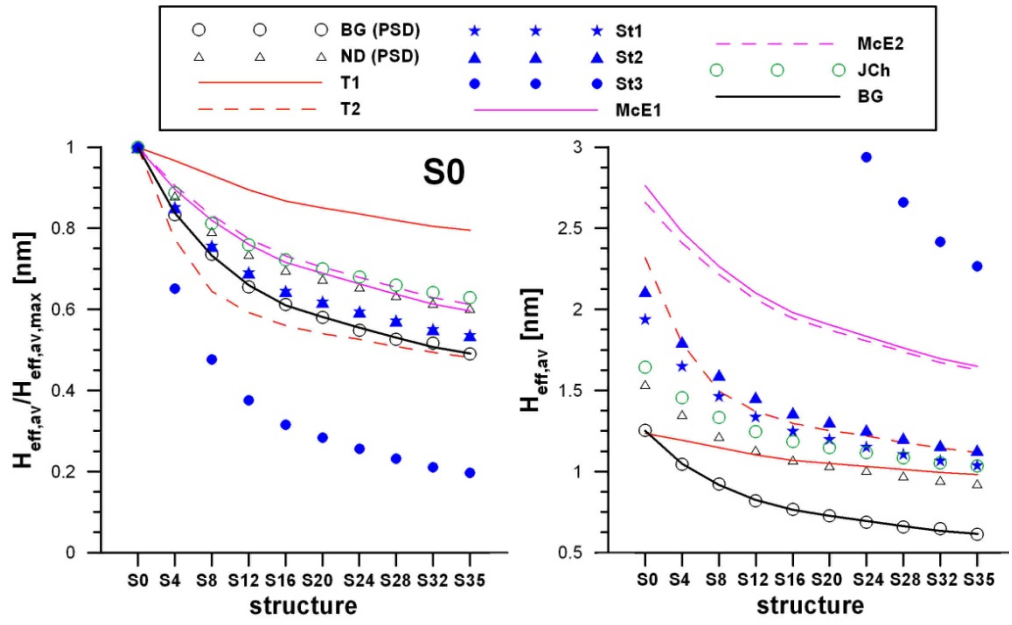


Figure 8. The shapes of relationships between the characteristic energy of adsorption (E_0) and the average pore diameter (H_{eff}) observed from experiment and obtained from molecular simulations on VPC models.

Using also the same model and procedures we studied the applicability of standard methods for describing adsorption data on microporous carbons [43]. In this case two carbon structures were used, one with a small distribution of micropores in the range up to 1 nm, and the other with micropores covering a wide range of porosity.

For both structures, adsorption isotherms of noble gases (from Ne to Xe), carbon tetrachloride and benzene were simulated. The data obtained were considered in terms of Dubinin-Radushkevich plots.

Moreover In addition, for benzene and carbon tetrachloride the temperature invariance of the characteristic curve (TICC) was also studied. We showed that using simulated data some empirical relationships obtained from experiment can be successfully recovered. Next we tested the applicability of Dubinin's related models including the Dubinin-Izotova (DI) [62], Dubinin-Radushkevich-Stoeckli (DRS) [63], and Jaroniec-Choma (JCh) [64] equations.

The results obtained demonstrated the limits and applications of the models studied in the field of carbon porosity characterization. It was concluded that simulation results on the studied models mimic very well the experimental behaviour of real activated carbons fulfilling Gurvich's rule, the empirical correlations developed by Tsunoda [65] or the fundamental relation proposed by Stoeckli and Morell [66] (Figure 9).

We have also shown that the validity of the Chen and Yang [67,68] derivation of the DA model can be confirmed. The TICC condition is fulfilled for the adsorption of benzene and carbon tetrachloride; therefore, one should expect that it should be fulfilled for systems where the dispersion interactions in the adsorbed phase dominate. The DR-plot is more sensitive to changes in the energetic or geometric parameters of adsorbed fluids if the carbon structure is more microporous; however, the deviation from linearity strongly depends on the type of studied adsorbate and the temperature.

For activated carbons having a wide distribution of micropores the DRS model leads to the most realistic PSD, and noble gases or carbon tetrachloride adsorption data should be applied to obtain reliable pore characteristics.

On the other hand, if the studied sample is highly microporous, the JCh model should be preferred and one should apply the data of adsorption of noble gases to obtain the most realistic PSD curve (Figure 10).

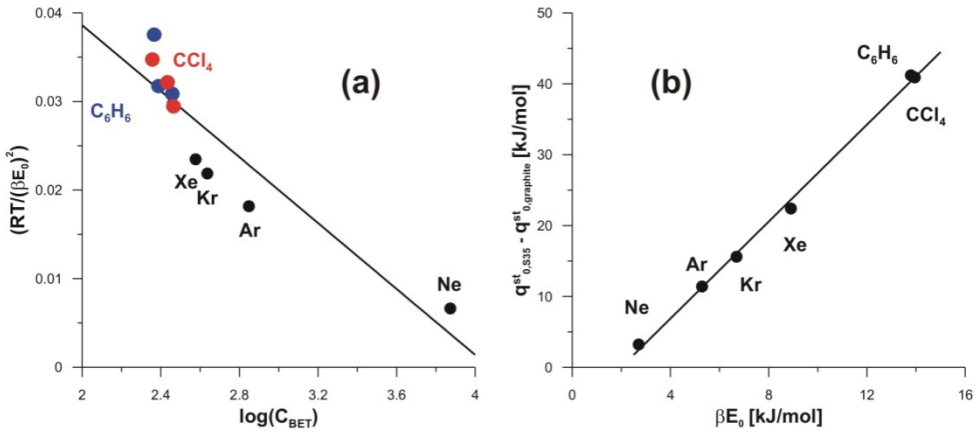


Figure 9. The recovering of Tsunoda (a) and Stoeckli-Morell (b) empirical correlations by molecular simulations on Harris VPCs.

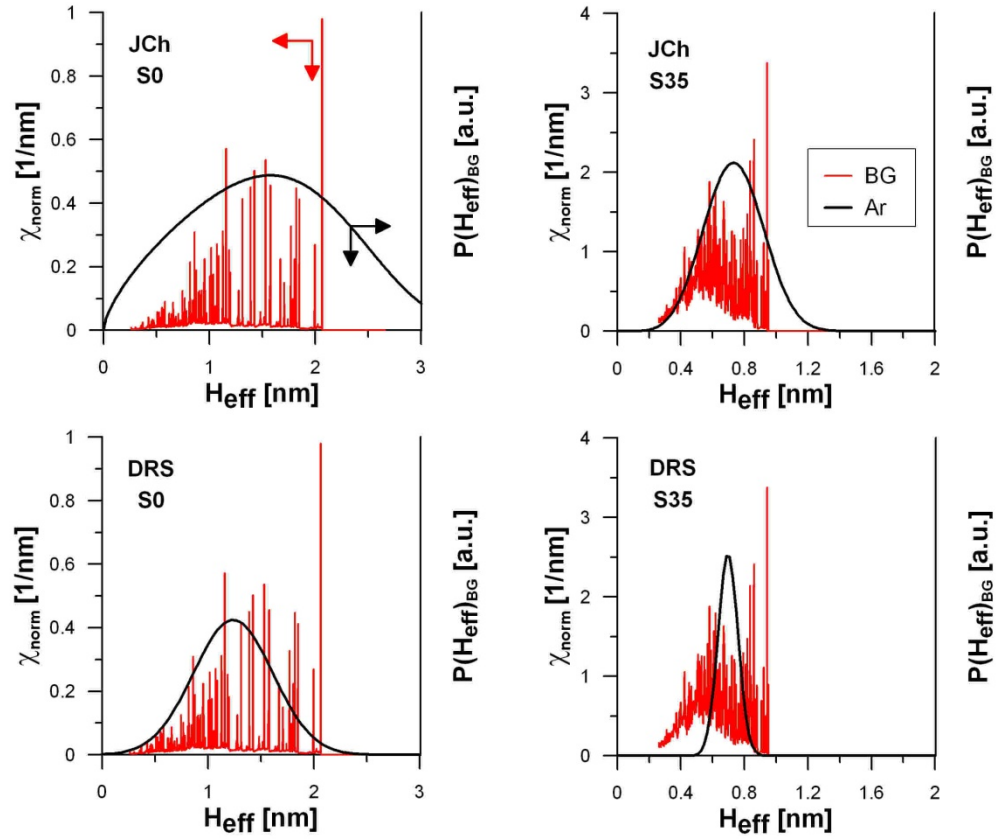


Figure 10. The comparison of PSDs calculated from JCh and DRS models with the absolute PSDs from the BG method for two types of VPC structures.

For the first case the DRS model predicts the average micropore diameter well, and the best results are recorded for Ar adsorption data. On the other hand, if carbon has narrow microporosity both models can be successfully applied for the calculation of the average pore diameters based on noble gases adsorption data.

In the next study using the above-mentioned "virtual oxidation" procedure we tried to check how the oxidation of carbon surface changes the porosity of structure [44]. For real experimental carbons IUPAC recommended the application of Ar adsorption measurements for determination of the PSD curve, since this molecule, being non-polar, is not too "sensitive" to the chemical composition of the surface. On the other hand, for practical reasons, nitrogen adsorption isotherm determination (at the boiling point i.e. 77 K) is also the standard tool applied to determination of the PSD curve. Some authors also suggest using CO_2 measurements at ambient temperature as a fast and standard method of determination of the structural parameters of carbons [69]. This approach is based mainly on experimental findings [70] showing that some pores can be inaccessible for nitrogen due to diffusion restriction. In fact, simulation results of Sweatman and Quirke [71] showed that nitrogen is diffusionally limited in microporous carbons, and that pore connectivity can significantly affect the adsorption of nitrogen at 77 K in carbons. This has important consequences for characterization studies of microporous carbons that employ nitrogen at this temperature. The authors also claimed that measurements of nitrogen adsorption above 90 K and CO_2 above

260 K (but below their respective bulk critical temperatures and up to their respective saturation pressures) will provide more accurate characterization of carbon porosity. There are many different approaches to porosity characterization; however, it has not been established yet, to what extent the application of the three standard molecules (Ar, N_2 and CO_2) can shift the PSD curve for a realistic carbon model, i.e. to what extent the changes in porosity are in fact the changes in porosity and not only the 'apparent' changes caused by the presence of surface groups being able to interact via so called specific interactions. For example, there are many literature reports showing the application of CO_2 for characterization of porosity of chemically modified carbons. After oxidation of the carbon, different oxygen surface functionalities are created. The measurement of the adsorption isotherm on such oxidized materials leads to the PSD curve. The PSD curve of the oxidized sample is often compared with the PSD of the initial one (i.e. before surface modification). But the question arises as to what extent the observed shifts on the PSD curve are due to the changes in porosity and to what extent they are due to the change in the nature of the interactions between an adsorbent and adsorbate (note that we still base this only on an isotherm being the balance between enthalpy and entropy). It seems that many researchers have forgotten the results of some experimental findings showing the strong influence of polarity of carbon dioxide molecule on adsorption properties of modified chemically carbons. For example, Meredith and Park [72] studied adsorption of nitrogen and carbon dioxide on metal impregnated carbons and found a strong influence of polarity of CO_2 on adsorption isotherms. The next important paper showing the influence of carbon surface chemical composition on CO_2 adsorption was published by Park and Kim [73]. They studied the behaviour of carbon modified with HCl and NaOH and their results show small changes in nitrogen adsorption isotherms (leading to similar pore volumes and BET surface areas for virgin and modified adsorbents), however remarkable changes on adsorption isotherms of ammonia and CO_2. Also recently, Samios et al. [74], when studying the applicability of GCMC local isotherms of CO_2 simulated for carbon slit-like pores to a description of experimental data, concluded that the presence of polar sites in the carbon sample considerably affects the calculated optimal PSD, especially at low temperatures. Such polar sites on the internal carbon surface lead to enhanced adsorption, which is more pronounced at low temperature and is interpreted in the PSD analysis as due to extra micropores. They noticed that caution should therefore be exercised when applying the method for the determination of micropore size distribution, and if the existence of polar sites is suspected the use of a non-polar adsorbate (e.g. Ar) may provide a more reliable picture of the micropore structure. Also Tenney and Lastoskie [75], who studied the influence of oxygen on CO_2 adsorption isotherms for different coal models, stated that the electrostatic adsorbate-adsorbent interactions significantly influenced adsorption onto coal-like model surfaces. Increasing the surface density of oxygen containing functional groups generally increased CO_2 adsorption and lowered the pore filling pressure. However, exceptions were noted, and in some cases outwardly small differences between surfaces resulted in very different isotherms. For the coal-like model pores with explicit charge interactions simulated in their study, low-pressure CO_2 uptake was significantly enhanced, and the excess adsorption at the saturation pressure was slightly increased, relative to CO_2 adsorption in comparably sized graphite slit pores. Recently Scherdel and Reichenauer [76], while comparing the structural data for a series of carbons from sucrose obtained from SAXS results with those calculated from adsorption isotherms of Ar, N_2 and CO_2, noticed the differences between porosity parameters from SAXS and from adsorption, especially for CO_2,

concluding that sorption of this molecule includes 'unspecified effects' affecting the results. In their interesting study the authors did not characterize the chemical composition of the studied carbons; therefore, it can be suspected that (as will be shown below) some 'artificial' results obtained from CO_2 data can be caused by the specific interactions of this molecule with surface oxides. To find to what extent the oxidation of carbon can change the absolute porosity (assuming that the oxidation is not destructive for the carbon skeleton) and to what extent this oxidation changes the adsorption isotherms (and the PSDs calculated from those isotherms) of all the above mentioned adsorbates, it was necessary to perform a simulation experiment, since a laboratory experiment is impossible (we do not know a method of determination of the absolute PSD curve for real carbons). This was also possible using the VPCs. We assumed that surface oxidation is not destructive for the carbon skeleton, and that all pores are accessible for the studied molecules (i.e., only the effect of the change of surface chemical composition was studied). The results obtained showed two important things, i.e., oxidation of the carbon surface very slightly changes the absolute porosity (calculated using the BG method); however, PSD curves calculated from simulated isotherms were to a greater or lesser extent affected by the presence of surface oxides. The most reliable results were obtained from Ar adsorption data. Not only was adsorption of this adsorbate practically independent of the presence of surface oxides, but, more importantly, for this molecule one can apply the slit-like model of pores as the first approach to recover the average pore diameter of a real carbon structure. For nitrogen, the effect of carbon surface chemical composition was observed due to the quadrupole moment of this molecule, and this effect shifts the PSD curves compared to Ar (Figure 11).

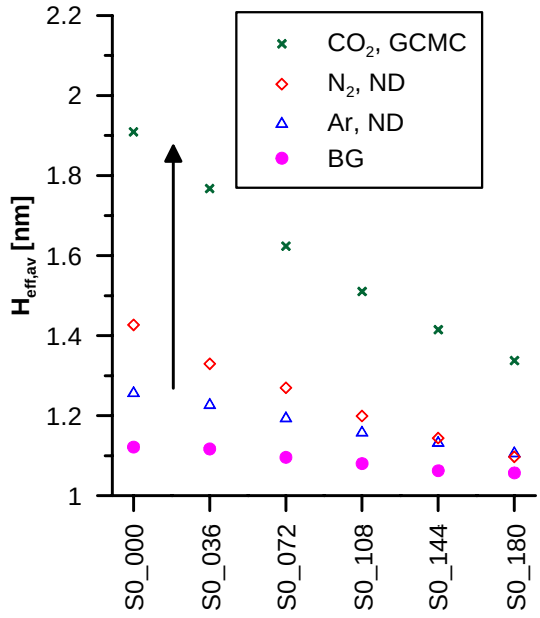


Figure 11. The comparison of absolute average pore diameters (BG method) with those calculated form adsorption data simulated for adsorption of different adsorbates on VPC models (containing different amount of oxygen groups). One can see that the difference between absolute (BG) average pore diameters and the diameters calculated from simulated adsorption data increases with a rise in electric moment of an adsorbate (from Ar up to CO_2).

The largest differences were seen for CO_2, and it was clearly demonstrated that the PSD curves obtained from adsorption isotherms of this molecule contained artificial peaks and the average pore diameter was strongly influenced by the presence of electrostatic adsorbate-adsorbate as well as adsorbate-adsorbent interactions.

In our next paper we extended these studies to VPC containing not only carbonyl but also surface carboxylic and phenolic groups as well as their mixtures [46]. A systematic study of the influence of carbon surface oxidation on the Dubinin-Astakhov equation parameters obtained from the fitting of CO_2 adsorption data was performed. Using GCMC simulations of adsorption on VPC models with differing porosity and containing the most frequently occurring carbon surface functionalities (carboxyls, hydroxyls and carbonyls) and their mixtures we observed a remarkable influence of oxygen on the characteristic energy of adsorption and the heterogeneity parameter of the DA model, while the maximum adsorption was affected to a smaller degree. Since the largest influence was observed for the structures containing surface carboxylic groups (being the most frequently observed in commercial carbons) we concluded that the results of porosity parameters calculated based on fitting of the DA model to experimental CO_2 adsorption data are questionable.

Another application of the VPC model proposed by Harris can be found in [47]. Again using GCMC simulation of methane adsorption we concluded that in a realistic carbon model the optimal pore diameter for methane adsorption is similar to that observed for slit-like carbon micropores (i.e. around 0.8 nm). The Dubinin-Astakhov model described simulated methane adsorption isotherms satisfactorily. The validity of the relation proposed by Amankwah and Schwarz [77] for determining the apparent saturated vapour pressure of supercritical methane was confirmed, and the proposed VPC model leads to realistic (i.e. similar to obtained in experiment) values of the parameter k proposed in this relation. Mild oxidation of carbons leading to creation of surface carbonyl groups increased methane adsorption. The parameters of the DA model as well as k are linearly correlated with the pore diameters and the contents of surface oxygen groups. The empirical Toth and Sips adsorption isotherm equations also described simulated methane data well and even small rise in the value of DC (compared to the DA model) was observed. The constants of the both equations correlated with the pore diameters and oxygen content in VPCs. The heterogeneity parameter t of the Toth model shows an almost linear increase with the number of oxygen surface groups in the carbon structure.

The applicability of the BET model for calculating surface area of activated carbons was also checked by using molecular simulations of adsorption on VPC models [48]. By calculating geometric surface areas for the simple model carbon slit-like pore with increasing width, and by comparison of the obtained values with those for the same systems from the VEGA ZZ package [78,79] (adsorbate-accessible molecular surface), it was shown that the latter methods provide correct values. For the system where a monolayer inside a pore is created the ASA approach (GCMC, Ar, T = 87 K) underestimates the value of surface area for micropores (especially, where only one layer is observed and/or two layers of adsorbed Ar are formed). Therefore, we proposed a modification of this method based on searching the relationship between the pore diameter and the number of layers in a pore. Finally BET; original and modified ASA; and A, B and C-point surface areas were calculated for a series of VPCs using simulated Ar adsorption isotherms (GCMC and T = 87 K). A comparison of the results showed that the BET method underestimates and does not, as usually postulated, overestimate the surface areas of microporous carbons.

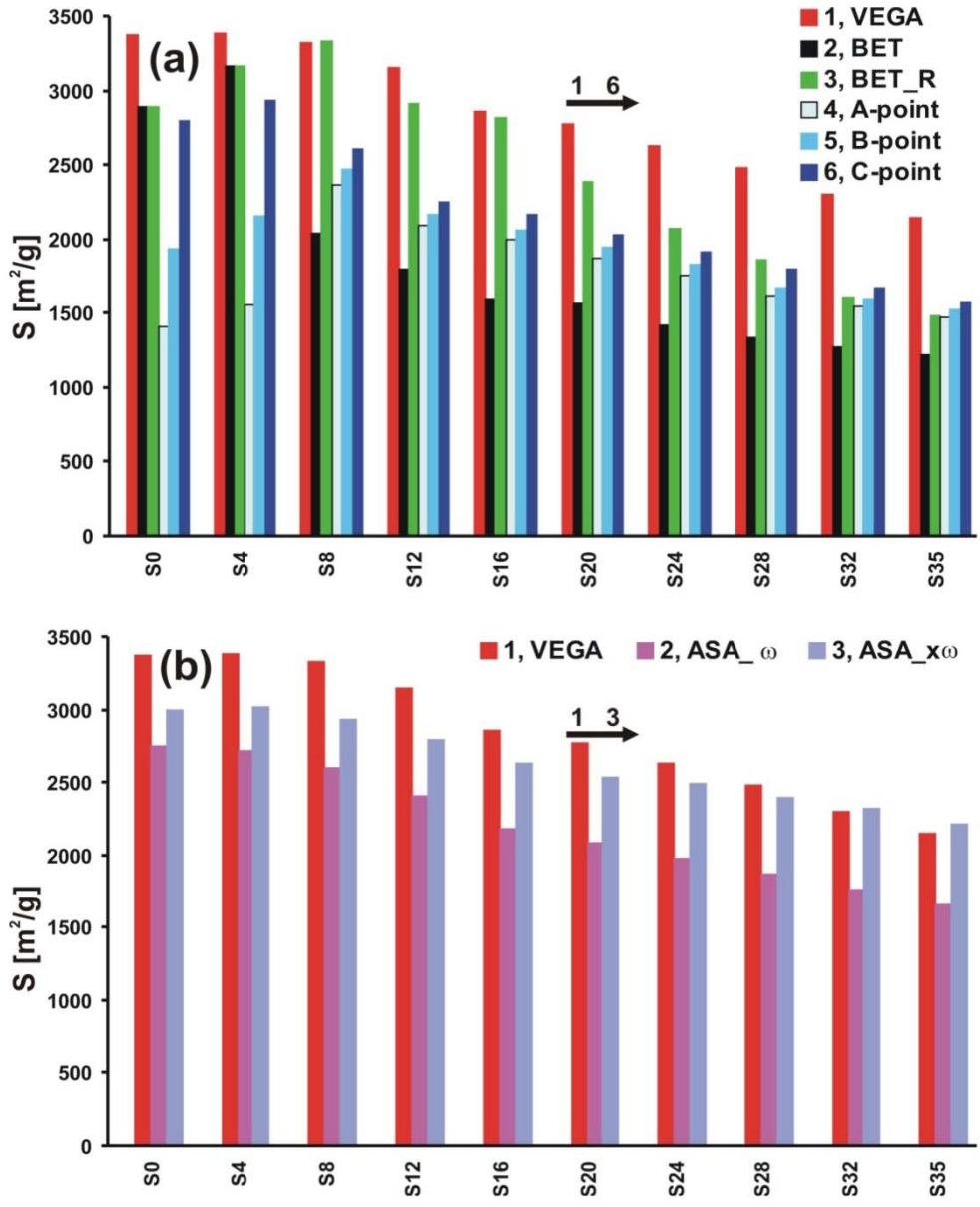


Figure 12. (a) The comparison of surface areas calculated for VPCs models using different methods based on simulated adsorption data with the true (i.e. obtained from the VEGA package) surface area values. Bottom figure (b) shows a modification of the ASA method proposed recently [48].

5. Application of VPC Models in Simulation of Adsorption from Aqueous Solutions

Adsorption of phenol - a common water pollutant - is widely studied because activated carbons are used in water plant stations, filters etc [80]. It has been proved and widely documented by experimental results that carbon surface oxidation, causing the introduction of

oxygen containing surface groups, reduces adsorption of phenol at small equilibrium concentrations [81]. However, there is a never ending debate in literature about the mechanism of this reduction. Two major explanations of this effect were proposed during discussion of experimental data (see [82,83], and references therein). The first postulates that the decrease in phenol adsorption after carbon oxidation is caused by the reduction in the energy of π - π interactions between the carbon matrix and the benzene ring of the phenol molecule. This effect is due to changes in the electron density of carbon after appearance of surface oxygen groups. The second proposed effect is the "pore blocking" postulated by Coughlin and Ezra [84] who suggested, that surface oxygen complexes increase the affinity of water to carbon, and therefore solvent molecules can effectively block some micropores for phenol. We tried to determine the influence of carbon porosity on phenol adsorption and to find an explanation for the decrease in phenol adsorption at low coverages after carbon oxidation [45]. These effects were studied using Molecular Dynamics simulations of phenol adsorption on VPC models. To our knowledge, this was the first paper showing simulation results of phenol adsorption from aqueous solutions on realistic carbon models. Three VPC structures with gradually changed microporosity were created. Next, a different number of surface oxygen groups was introduced. We concluded that an optimal microporous carbon for phenol adsorption should possess the largest possible volume of micropores with diameters around 0.6 nm. Pore blocking causes a decrease in phenol adsorption. Results obtained by us support the idea of Coughlin and Ezra [84] showing that highly hydrogen- bonded water clusters around surface oxygen groups enable the penetration of some micropores by subsequent phenol molecules. The number of phenol molecules interacting with carbon oxygen groups was small at low coverages and this is in agreement with the DFT calculations [85]. Although our simulations take into account only one type of surface groups, we neglect the presence of Lewis basic sites, the chemisorption and/or phenol oxidative coupling; the obtained results recover the regularities observed in real experiments, i.e. a decrease in phenol adsorption with the rise in carbon surface oxidation.

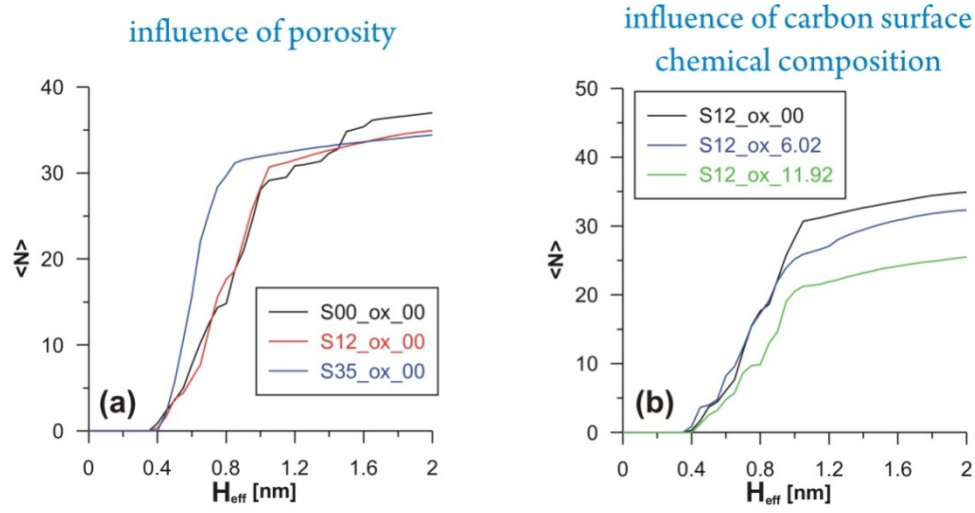


Figure 13. The influence of porosity (a) and chemical composition of carbon surface layer (b) on phenol adsorption on microporous VPC models.

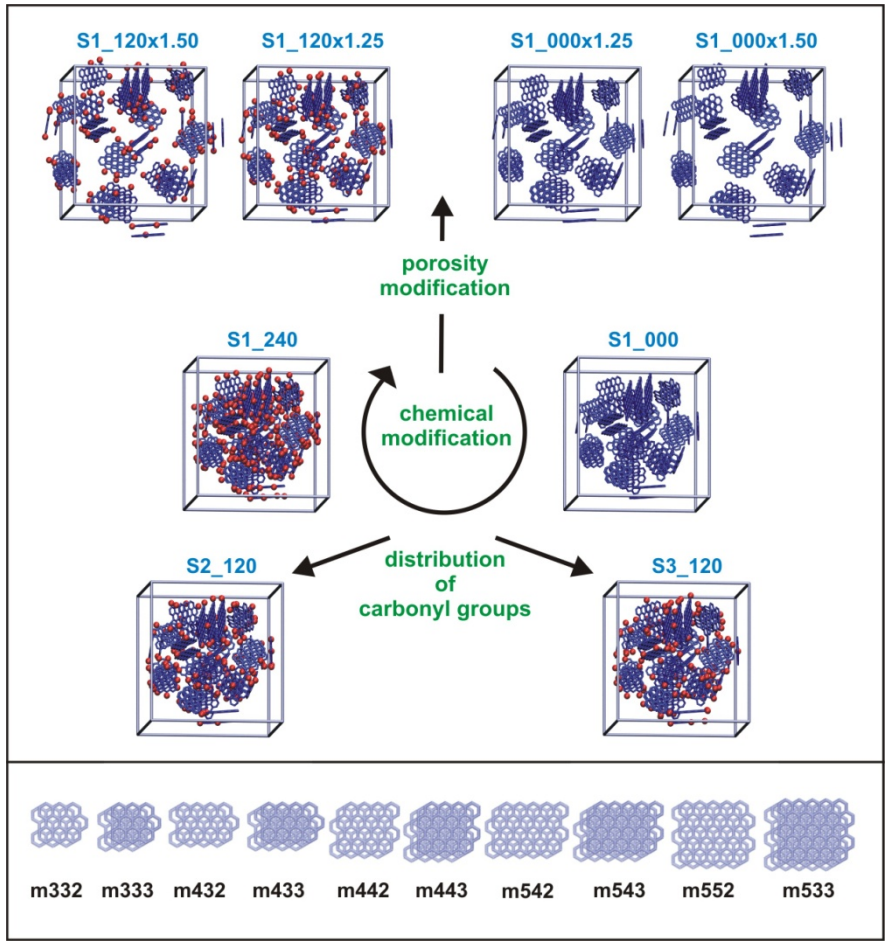


Figure 14. The model of "soft" VPC carbon studied in [86], the procedures of porosity and chemistry of surface modifications and the basis of microcrystallites. Note that some figures (i.e. Figures 5-7 and 14) were created using the VMD program [87,88]).

The first Molecular Dynamics simulation results of activated carbon immersion in water were also reported [86]. However, in this case the VPC model of "soft" carbon was studied. This model is composed of microcrystallites. The procedure of model creation inserts randomly double and triple layered graphene microcrystallites into a simulation box in such a way, that a microporous carbon model is created. The carbon - carbon bond length was assumed as equal to 0.142 nm and the interlayer spacing was fixed as equal to 0.335 nm (since we tried to prepare a model of "soft" carbon both values are the same as observed for graphite). Also like in graphite the centres of benzene rings in each layer are shifted by 1/3 (we assumed ABC stacking of graphene layers). Figure 14 shows applied basis of microcrystallites (the notation m*xyz* is used, where *x* and *y* denote the number of benzene rings in a layer in respective directions, and *z* is the number of layers).

The program generating carbon structure randomly uses one of 10 microcrystallites and introduces it inside the simulation box at random position and with a random angular orientation. This insertion is accepted if there are no overlaps between fragments (i.e. the distance between any carbon atom of the inserted fragment and the fragments just present in

the box is not smaller than 0.34 nm). In this way different structures having progressively changed porosity were created. Moreover In addition we used also the procedure of "virtual oxidation" proposed previously [44-47], introducing carbonyl surface groups into the initial structure.

The influence of surface oxygen content, distribution of groups and micropore diameter on the enthalpy of carbon immersion in water was studied. We performed first Molecular Dynamics simulations of carbon immersional process. The results obtained suggest, that there is small influence of the distribution of surface groups on the enthalpy of immersion value. A linear relation between this enthalpy and the concentration of surface groups was recorded, independently on micropore size distribution and this observation is in accordance with experimental findings. The obtained enthalpy of immersion is also a function of polar surface area, and the ration polar/nonpolar surface area. The latter finding is in accordance with the correlations between XPS results and ΔH_i. The mechanism of the immersional process depends on carbon porosity and the concentration of oxygen on the surface. For unoxidised carbons enthalpy of immersion can be positive if micropores are small however, ΔH_i increases (i.e. is more exothermic) with the rise in the average micropore diameter (Figure 15). The slopes of the relations between enthalpy value and oxygen content are almost the same as for carbons with different porosity therefore the shifts between them are caused by the differences in the energy of water interaction with the starting carbon structure. This is why enthalpy increases with the rise the average micropore diameter. Generally the behaviour of carbon in the immersional process follows the Pratt-Chandler theory of hydrophobicity. We observed the creation of a liquid-vapour interface in the case of strongly hydrophobic systems. This interface however, vanishes with the rise in the number of carbon oxygen functional groups. The density of water approaches the density of bulk with the rise in average micropore diameter. This is also in accordance with Pratt - Chandler mechanism because with the rise in micropore diameter the microcrystallites forming VPC start to behave more independently.

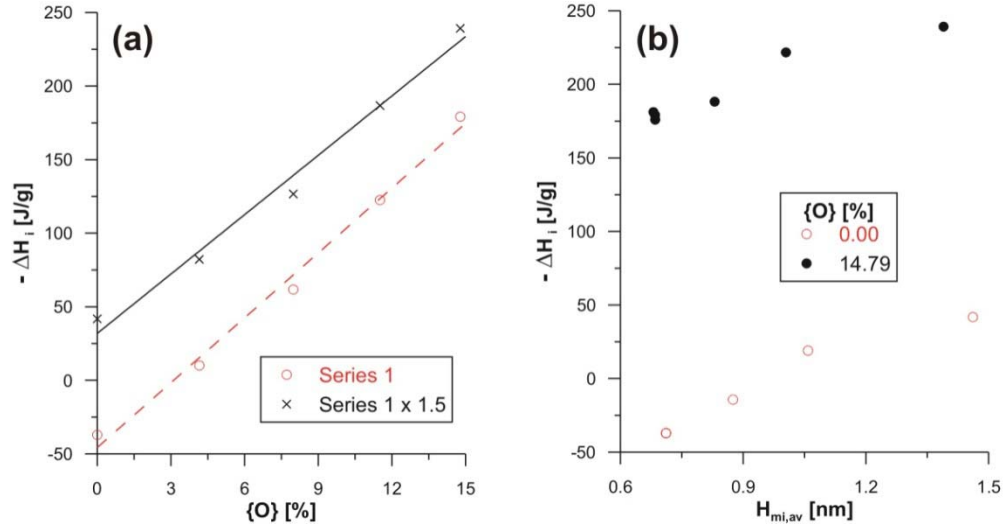


Figure 15. Typical relationships between the enthalpy of carbon immersion in water and the oxygen contents (a), and average pore diameter (b) for two VPC structures.

For such a case a solute can be treated as a system of small microcrystallites and water molecules behaviour approaches the behaviour of bulk water. Analysis of proximal distributions suggested slightly larger accessibility of water to carbonyl groups located on the edges of structures. Also a restriction of accessibility to the surface groups by some water molecules interacting with neighbouring groups is observed. We also observed the effect of limited accessibility to carbon atoms due to presence of carbonyls. The average number of hydrogen bonds calculated per one carbonyl group increases with the average micropore diameter. Therefore in microporous carbons the formation of hydrogen bonds between water and surface groups is strongly restricted. Moreover, the number of created hydrogen bonds between water and carbonyl groups decreases with the rise in the number of those groups. This is caused by the above-mentioned restriction of accessibility to the surface groups by water molecules interacting with neighbouring surface functionalities.

CONCLUSION

Virtual Porous Carbon models are very important in current adsorption science. The results of the studies cited above clearly demonstrate that molecular simulations combined with VPC models provide important and interesting information on adsorption mechanisms. Additionally one can easily check the reality of widely-applied methods in adsorption science. Molecular simulations techniques are now basic tools in science therefore one can expect that interest in the application of VPC models will grow.

ACKNOWLEDGMENT

SF gratefully acknowledges financial support from the Foundation for Polish Science. The chapter was supported by grants N N204 288634 (PG). We acknowledge the use of the computer cluster at Toruń (the Information and Communication Technology Centre of the Nicolaus Copernicus University, Poland) and at Poznań (Supercomputing and Networking Center, Poland).

REFERENCES

[1] Biggs, M.J.; Buts, A. *Mol. Sim.* 2006, 32, 579.
[2] Biggs, M.J.; Buts, A.; Williamson, D. *Langmuir* 2004, 20, 5786.
[3] Biggs, M.J.; Buts, A.; Williamson, D. *Langmuir* 2004, 20, 7123.
[4] Cai, Q.; Buts, A.; Biggs, M.J.; Seaton, N.A. *Langmuir*, 2007, 23, 8430.
[5] Biggs, M.J.; Buts, A.V. In *Proceedings of the International Carbon Conference*, Aberdeen, 2006.
[6] Do, D.D.; Nicholson, D.; Do, H.D. *Appl. Surf. Sci.* 2007, 253, 5580.
[7] Birkett, G.R.; Do, D.D. *Adsorption* 2007, 13, 407.
[8] Do, D.D.; Do, H.D. *J. Phys. Chem. B* 2006, 110, 17531.
[9] Wongkoblap, A.; Do, D.D. *Carbon* 2007, 45, 1527.

[10] Harris, P.J.F. In *Chemistry and Physics of Carbon*; Ed. Radovic, L.R.; Marcel Dekker Inc.: New York, 2003; Vol. 28, p 2.
[11] Harris, P.J.F. In *The Encyclopedia of Materials: Science and Technology*; Eds. Jürgen Buschow, K.H. et al., Elsevier: Oxford, 2001.
[12] Harris, P.J.F.; Tsang, S.C. *Phil. Mag. A* 1997, 76, 667.
[13] Harris, P.J.F. *Int. Mater. Rev.* 1997, 42, 206.
[14] Harris, P.J.F.; Burian, A.; Duber, S. *Phil. Mag. Lett.* 2000, 80, 381.
[15] Harris, P.J.F. *Crit. Rev. Sol. State Matt. Sci.* 2005, 30, 235.
[16] Tsang, S.C.; Harris, P.J.F.; Claridge, J.B.; Green, M.L.H. *J. Chem. Soc., Chem. Comm.* 1993, 90, 1519.
[17] Harris, P.J.F.; Liu, Z.; Suenaga, K. *J. Phys. Condens. Matt.* 2008, 20, 362201.
[18] Harris, P.J.F. In *Carbon Materials – Theory and Practice*; Eds. Terzyk, A.P.; Gauden, P.A.; Kowalczyk, P., Research Signpost, Kerala, 2008; p 1.
[19] Bandosz, T.J.; Biggs, M.J.; Gubbins, K.E.; Hattori, Y.; Iiyama, T.; Kaneko, K.; Pikunic, J.; Thomson, K.T. In *Chemistry and Physics of Carbon*; Ed. Radovic, L.R.; Marcel Dekker Inc.: New York, 2003; Vol. 28, p 97.
[20] Marsh, T.H.; Rodriguez-Reinoso, F. *Activated Carbon*; Elsevier: Amsterdam, 2006.
[21] Biggs, M.; Agarwal, P. *Phys. Rev. A* 1992, 46, 3312.
[22] Biggs, M.; Agarwal, P. *Phys. Rev. E* 1994, 49, 531.
[23] MacElroy, J.M.D.; Friedman, S.P.; Seaton, N.A. *Chem. Eng. Sci.* 1999, 54, 1015.
[24] Inagaki, M. *Tanso* 1985, 122, 144.
[25] Oberlin, A.; Villey, M.; Combaz, A. *Carbon* 1980, 18, 347.
[26] Kaneko, K.; Ishii, C.; Kanoh, H.; Hanzawa, Y.; Setoyama, N.; Suzuki, T. *Adv. Colloid Interf. Sci.* 1998, 76-77, 295.
[27] Rouzaud, J.N.; Clinard, C. *Fuel Process. Technol.* 2002, 77-78, 229.
[28] Biggs, M.J.; Buts, A. In *Proceedings Carbon '02 Conference*; Beijing, 2002; p 16.
[29] Biggs, M.J.; Buts, A. *Proc. AIChE Ann. Meet.* 2002, 930.
[30] Biggs, M.J. *Proc. AIChE Ann. Meet.* 2001, 1640.
[31] Biggs, M.J.; Buts, A. *Proc. AIChE Ann. Meet.* 2003, 17.
[32] Cai, Q.; Biggs, M.J.; Buts, A.V.; Seaton, N.A. In *Proceedings of the International Carbon Conference*; 2006.
[33] Cai, Q.; Buts, A.; Seaton, N.A.; Biggs, M.J. *Chem. Eng. Sci.* 2008, 63, 3319.
[34] Seaton, N.A.; Friedman, S.P.; MacElroy, J.M.D.; Murphy, B.J. *Langmuir* 1997, 13, 1199.
[35] Turner, A.R.; Quirke, N. *Carbon* 1998, 36, 1439.
[36] Herrera, L.F.; Do, D.D. *Adsorption* 2009, 15, 240.
[37] Herrera, L.F.; Do, D.D.; Birkett, G.R. *J. Colloid Interf. Sci.* 2008, 320, 415.
[38] Do, D.D.; Herrera, L.; Fan, C.; Wongkoblap, A.; Nicholson, D. *Adsorption* 2010, 16, 3.
[39] Do, D.D.; Herrera, L.F.; Do, H.D. *J. Colloid Interf. Sci.* 2008, 328, 110.
[40] Herrera, L.; Do, D.D.; Nicholson, D. *J. Colloid Interf. Sci.* 2010, 348, 529.
[41] Terzyk, A.P.; Furmaniak, S.; Gauden, P.A.; Harris, P.J.F.; Włoch, J.; Kowalczyk, P. *J. Phys. Cond. Matt.* 2007, 19, 406208.
[42] Terzyk, A.P.; Furmaniak, S.; Harris, P.J.F.; Gauden, P.A.; Włoch, J.; Kowalczyk, P.; Rychlicki, G. *Phys. Chem. Chem. Phys.* 2007, 9, 5919.
[43] Terzyk, A.P.; Furmaniak, S.; Gauden, P.A.; Harris, P.J.F.; Włoch, J. *J. Phys. Cond. Matt.* 2008, 20, 385212.

[44] Furmaniak, S.; Terzyk, A.P.; Gauden, P.A.; Kowalczyk, P.; Harris, P.J.F. *J. Phys. Cond. Matt.* 2009, 21, 315005.
[45] Terzyk, A.P.; Gauden, P.A.; Furmaniak, S.; Wesołowski, R.P.; Harris, P.J.F. *Phys. Chem. Chem. Phys.* 2010, 12, 812.
[46] Furmaniak, S.; Terzyk, A.P.; Gauden, P.A.; Harris, P.J.F.; Kowalczyk, P. *J. Phys. Cond. Matt.* 2010, 22, 085003.
[47] Terzyk, A.P.; Furmaniak, S.; Wesołowski, R.P.; Gauden, P.A.; Harris, P.J.F. In *Advances in Adsorption Technology*; Eds. Saha, B.B.; Ng, K.C.; Nova Publ:, 2010; ch. 14.
[48] Gauden, P.A.; Terzyk, A.P.; Furmaniak, S.; Harris, P.J.F.; Kowalczyk, P. *Appl. Surf. Sci.* 2010, 256, 5204.
[49] Acharya, M.; Strano, M.S.; Mathews, J.P.; Billinge, S.J.L.; Petkov, V.; Subramoneyk, S.; Foley, H.C. *Phil. Mag. B* 1999, 79, 1499.
[50] Smith, M.A.; Foley, H.C.; Lobo, R.F. *Carbon* 2004, 42, 2041.
[51] Bourgeois, L.N.; Bursill, L.A. *Phil. Mag. A* 1999, 79, 1155.
[52] Goel, A.; Hebgen, P.; Vander Sande, J.B.; Howard, J.B. *Carbon* 2002, 40, 177.
[53] Goel, A.; Howard, J.B.; Vander Sande, J.B. *Carbon* 2004, 42, 1907.
[54] Grieco, W.J.; Howard, J.B.; Rainey, L.C.; Vander Sande, J.B. *Carbon* 2000, 38, 597.
[55] Kumar, A.; Lobo, R.F.; Wagner, N.J. *Carbon* 2005, 43, 3099.
[56] Cataldo, F. *Carbon* 2002, 40, 157.
[57] Powles, R.C.; Marks N.A.; Lau, D.W.M. *Phys. Rev. B* 2009, 79, 075430.
[58] Palmer, J.C.; Llobet, A.; Yeon, S.-H.; Fischer, J.E.; Shi, Y.; Gogotsi, Y.; Gubbins, K.E. *Carbon* 2010, 48, 1116.
[59] Shi, Y. *J. Chem. Phys.* 2008, 128, 234707.
[60] Bhattacharya, S.; Gubbins, K.E. *Langmuir* 2006, 22, 7726.
[61] Jorge, M.; Schumacher, C.; Seaton, N.A. *Langmuir* 2002, 18, 9296.
[62] Izotova, T.I.; Dubinin. M.M. *Zh. Fiz. Chim.* 1965, 39, 2796.
[63] Stoeckli, H.F. *J. Colloid Interf. Sci.* 1986, 59, 521.
[64] Jaroniec, M.; Choma, J. *Mater. Chem. Phys.* 1986, 15, 521.
[65] Tsunoda, R. *J. Colloid Interf. Sci.* 1987, 117, 291.
[66] Stoeckli, F.; Morell, D. *Chimia* 1980, 12, 502.
[67] Chen, S.G.; Yang, R.T. *Langmuir* 1994, 10, 4244.
[68] Chen, S.G.; Yang, R.T. *J. Colloid Interf. Sci.* 1996, 177, 298.
[69] Lozano-Castello, D.; Cazorla-Amoros, D.; Linares-Solano, A. *Carbon* 2004, 42, 1233.
[70] Cazorla-Amoros, D.; Alcaniz-Monge, J.; Linares-Solano, A. *Langmuir* 1996, 12, 2820.
[71] Sweatman, M.B.; Quirke, N. *Langmuir* 2000, 17, 5011.
[72] Meredith, J.M.; Park, C.A. *J. Chem. Eng. Data* 1967, 12, 259.
[73] Park, S.J.; Kim, K.D. *J. Colloid Interf. Sci.* 1999, 212, 186.
[74] Samios, S.; Stubos, A.K.; Papadopoulos, G.K.; Kanellopoulos, N.K.; Rigas, F. *J. Colloid Interf. Sci.* 2002, 224, 272.
[75] Tenney, C.M.; Lastoskie, C.M. *Environ. Prog.* 2006, 25, 343.
[76] Scherdel, C.; Reichenauer, G. *Carbon* 2009, 47, 1102.
[77] Amankwah, K.A.G.; Schwarz, J.A. *Carbon* 1995, 33, 1313
[78] Pedretti, A.; Villa, L.; Vistoli, G. *J. Comput.-Aided Mol. Des.* 2004, 18, 167.
[79] http://www.vegazz.net/.

[80] Dąbrowski, A.; Podkościelny, P.; Hubicki, Z.; Barczak, M. *Chemosphere* 2005, 58, 1049.
[81] Bansal, R.C.; Goyal, M. *Activated Carbon Adsorption*; CRC: Boca Raton, 2005.
[82] Terzyk, A.P. *J. Colloid Interf. Sci.* 2003, 268, 301.
[83] Terzyk, A.P. *J. Colloid Interf. Sci.* 2004, 275, 9.
[84] Coughlin, R.W.; Ezra, F.S. *Environ. Sci. Technol.* 1968, 2, 291.
[85] Efremenko, I.; Sheintuch, M. *Langmuir* 2006, 22, 3614.
[86] Terzyk, A.P.; Gauden, P.A.; Furmaniak, S.; Wesołowski, R.P.; Kowalczyk, P. *Phys. Chem. Chem. Phys.* 2010, 12, 10701.
[87] Humphrey, W.; Dalke, A.; Schulten, K. *J. Mol. Graphics*, 1996, 14, 33.
[88] http://www.ks.uiuc.edu/Research/vmd/.

In: Activated Carbon
Editor: James F. Kwiatkowski
ISBN: 978-1-61209-684-1
©2012 Nova Science Publishers, Inc.

Chapter 12

ACTIVATED CARBONACEOUS MATERIALS BASED ON THERMOSETTING BINDER PRECURSORS

J. Simitzis [*] ***and Z. Ioannou***
National Technical University of Athens, School of Chemical Engineering, Section III: Materials Science and Engineering, Laboratory Unit "Advanced and Composite Materials", 9 Heroon Polytechniou str., Zografou Campus, Athens, 15773, Greece

ABSTRACT

There are many raw materials available for preparing activated carbons which can be divided into two kinds: a) grade low coal (such as peat and lignite), waste pulp solution, waste plastics and various agricultural by-products and b) synthetic resins and fibers. Coal and lignocellulosic materials are the most commonly used starting materials for the production of commercial activated carbons (ACs). The latter are also prepared from various agricultural by-products and polymeric materials because of their low cost and high carbon yield.

The pores in carbon materials play an important role in their functions and characteristics. Glass-like carbon (GC) is prepared by heat-treatment on thermosetting resins in inert atmosphere. They show various unique properties such as great hardness compared with other carbon materials and gas impermeability.

Phenol-formaldehyde resins are being increasingly used to replace pitch as bonding agents for refractory materials. Starting from such precursors, various carbons in the form of fibers, particles, membranes and preforms have been produced. Carbonised phenolic resins are usually highly microporous, with the amount of open micropores passing through a maximum at a carbonisation temperature of 700 to 800 ^{o}C.

Molecular sieving carbon (MSC) or carbon molecular sieves (CMSs) are carbonaceous adsorbents with almost uniform micropores of a few angstroms in diameter having the ability to selectively separate molecules, mainly of a gas mixture. Carbon molecular sieve membrane (CMSM) is usually prepared by carbonisation of polymeric films, which conducts to the formation of a thin carbon layer or thin film of CMS with pores smaller than 1 nm. In order to prepare CMSM, the polymeric precursor needs to

[*] E-mail: simj@chemeng.ntua.gr

have thermosetting property in order to avoid melting when heated and thus retain structure shape during heating and pyrolysis.

Mesoporous carbons, due to their high surface area and periodic arrays of uniform pores, are utilized as catalysis and electrode materials for different purposes such as protection of environment and improvement of energy efficiency. Mesoporous carbons with high surface area, large porosity and fine electric-conductivity have been regarded as an advanced material for many potential applications in nanotechnology. Monomers such as furfuryl alcohol, acrylonitrile, and phenol-aldehyde monomers mixture were usually used as the precursors to prepare mesoporous carbons.

Other carbonaceous forms includes carbon brushes prepared from proper thermosetting resin binder and monolithic activated carbons prepared from resin impregnated expanded graphite, from isotropic fibers or prepared as carbon aerogels. Nanostructured carbon materials are potentially of great technological interest for the development of electronic, catalytic and hydrogen-storage systems.

1. INTRODUCTION

There are many raw materials available for preparing activated carbons which can be divided into two kinds. One includes grade low coal (such as peat and lignite), waste pulp solution, waste plastics and various agricultural by-products and the other one includes synthetic resins and fibers [1]. Although a wide range of carbonaceous precursor materials can be converted into activated carbons (ACs), coal and lignocellulosic materials are the most commonly used starting materials for the production of commercial ACs. Furthermore, there are quite a large number of studies reporting the preparation of ACs from various agricultural by-products and polymeric materials because of their low cost and high carbon yield [2]. The pores in carbonaceous materials play an important role in their functions and characteristics. The precursor materials used and the production conditions applied to convert them to carbonaceous adsorbents strongly influence the structure of the solid products and their properties, mainly their adsorption properties. The carbonaceous adsorbents are distinguished in three types under the aspect of their porous structure: activated carbons, activated cokes and carbon molecular sieves. The latter are characterized by the presence of submicropores with a mean diameter less than 8 Å. In these materials, the adsorption of small molecules is preferred against greater molecules. The activated cokes are similarly characterized by the presence of very narrow micropores and by the increase of their structure to greater pores during the adsorption. As activated carbons are characterized high porous adsorbents with mean diameter of micropores above 8 Å [3]. The term activated carbon in its broadest sense includes a wide range of amorphous carbon-based materials prepared to exhibit a high degree of porosity and an extended interparticulate surface area [4]. There are two major types of carbon molecular sieve materials: coals which occur naturally and polymer carbons which are produced artificially by the heating of polymers (selected thermosetting polymer or copolymer systems) to produce a solid char or coke. The term carbon is used in the generic sense, since these molecular sieves, as well as the other carbonaceous adsorbents, contain other elements. The synthetic polymer carbons are very low in metallic and metal oxide impurities but usually contain some oxygen and hydrogen and sometimes contain nitrogen sulfur and / or chlorine [5]. Carbonaceous adsorbents and especially activated carbon are a type of polymeric carbons (or polymer carbons). Polymeric carbon refers to the carbon solid

residues after pyrolysis of an organic polymer which does not pass through a liquid or tarry state leading to the formation of the new carbon structure based on the initial polymeric structure [6]. Polymeric carbons with basically similar molecular structure may act as powerful adsorbents with enormous available internal surfaces, in the form of activated charcoal, or as effective barriers, impermeable even to helium, in the form of glassy carbon. They can exist as weak, friable charcoals or as some of the strongest and stiffest fibres. They form a distinctive group of materials which need to be differentiated from the soft graphitic carbons. The latter are formed from organic precursors passing into a liquid state above 300 ^{0}C prior to carbonization [6,7]. The different models that have been proposed to describe the porosity in carbons are reviewed in details [8]. Carbonaceous adsorbents are widely used during World War I as a protective material in the gas masks from toxic compounds in the air. Early interest in the development of activated carbons was stimulated by their use in the cane sugar industry and their decolorizing effects on solutions. Many methods were applied for the production of carbonaceous adsorbents and especially carbon molecular sieves, which are nowadays popular in gas separation techniques with commercial interest [9]. The application of adsorption processes with carbonaceous adsorbents gain in increased importance as partial step in the drink water preparation process, tertiary waste water purification and air clear maintenance as well as in gas separation processes. The design and the optimization of the adsorption processes need the knowledge of the interaction of physical-chemical background, experimental investigation and engineering considerations. Generally, the outlet and the result of all adsorption processes mainly depend on the adsorption rate and the adsorption capacity. On one hand, the adsorption kinetic considers the rate of the adsorption rate and its dependence on different parameters and on the other, the adsorption capacity depends on the structure of the adsorbent and the nature of the adsorptive agent based on the theory of equilibrium systems [10]. The adsorbent should exhibit high activity and selectivity. The activity has the meaning of the enrichment degree of the adsorptive molecules in interplay with their adsorption on the adsorbent. The selectivity means the feasibility of selective adsorption of a substance on the adsorbent in relation to one another and attributes to the influence of the energy interaction between adsorbent and adsorptive on one hand and to the influence of the diffusion rate in narrow pores, i.e. molecular sieve effect, on the other [3]. Concerning their application forms, the adsorbents are divided to powder and grains. Granular adsorbents compared to the former can be regenerated more easily after their application in order to re-obtain their adsorption capability [11]. The scope of the present work concerns the carbonaceous adsorbents based on thermosetting resins used alone or in combination with other organic precursor materials. Thermosetting polymers (or thermoset polymers) are cross-linked, three-dimensional network polymers, that cannot be softened and reshaped by heating in opposite to thermoplastic polymers [12].

2. THERMOSETTINGS COMBINED OR NOT WITH OTHER PRECURSORS AND THEIR FORMATION PROCESSING METHODS

The basic criterion for the selection of a precursor material for the production of carbonaceous adsorbents is its carbon (solid) yield after its pyrolysis / carbonization. Organic polymers have been pyrolyzed under the aspect to obtain technical useful solid residues (such

as activated carbons and carbon molecular sieves) since the decades of 1950/1960. Polymers such as phenol-formaldehyde resins, melamine-formaldehyde resins, poly(furfuryl alcohol), poly(vinylidene chloride), polydivinylbenzene, copolymers (e.g. Saran consisting of vinylidene chloride to vinyl chloride units with a ratio of 90:10) took the interest of the researchers [13-16]. In below, the processing methods for precursors based on thermosetting resins combined or not with other organic materials are briefly described.

The method of Bergbau-Forschung (BF), which was developed by Juentgen and his team [17,18], leads to the production of carbon molecular sieves (CMSs) and is applied in industrial scale. In this method stone coal is mixed with pitch (which is a thermoplastic polymer used as binder material and carbon precursor) and is formed under pressure. Then pyrolysis follows and the produced material reacts with hydrocarbons under a thermal process with temperatures above 600 ^{o}C. The diffusion of hydrocarbons in the pores of the produced material takes place and there with their cracking and application leads to the straitening of pores. Such carbon molecular sieves are appropriate in industrial scale for the separation of oxygen and nitrogen from the air. The method developed by Walker and his team [15,19] combines more than one raw material to manufacture composite carbon molecular sieves (C.C.M.S.). This method is based on the coating of the existing granular activated carbon with a layer of microporous carbon which acts as molecular sieve. This layer is created by the impregnation of the existing activated carbon with a polymer (in liquid phase) and then with their carbonization. The produced material presents some advantages in comparison with the polymer carbon sieves, which come from carbonization of polymer materials. Such advantages are the higher adsorption capacity due to the structure of the initial activated carbon which contains. Another method, which was developed by Simitzis and his team [20,21], is based on the mixture of a resin, (i.e. phenol-formaldehyde resin) with a raw material that can be pyrolysed (i.e. agricultural by-products, lignite) following appropriate pyrolysis of the composite material. The originality of the produced material lies in the modification of its pore structure in comparison with activated carbons, which derive from typical raw materials, or carbon molecular sieves, which come from carbonization of polymer materials. These materials present high adsorption capacity exceeding in some cases commercial adsorptive materials [22]. Carbon molecular sieves (CMSs) can be prepared with a variety of ways according to the initial raw materials. Such sieves are formed by a thin microporous carbon layer, which obtained by pyrolysis up to 700°C of a phenolic resin film, deposited on the inner face of a porous alumina tube. The prepared carbon membrane exhibits good separation capabilities towards the separation of gas mixtures such as O_2–N_2, CO_2 –N_2 and CO_2–CH_4 [23]. Moreover, CMSs can be formed from phenol formaldehyde novolac resin by dip coating of an ethanol solution of a phenol formaldehyde novolac resin with addition of a few CMS. Different gases, including H_2, CO_2, O_2, N_2 and CH_4, were selected in order to examine the permeation characteristics of the membranes [24]. Another similar method is described elsewhere [25]. In this method an asymmetric CMS was prepared by coating alcohol solution of novolac phenol-formaldehyde resin containing hexamine on a porous resin support from the same material. Other method, which was used, is the creation of CMS from phenol-formaldehyde resin by an ester-carbonization method [26]. Carbon molecular sieves have also been prepared from polyfurfuralalcohol, polyformaldehyde, polydivinylbenzene and polyacrylonitrile. In every case adsorbents with molecular sieve properties have slit-shaped pores. The slit shape is demonstrated by the selective adsorption of benzene (3.7 Å thick x 7.0 Å wide) and the exclusion of carbon tetrachloride (roughly a 6.0 Å diameter

sphere) [27]. Other methods concerns the production of activated carbon fibers (ACFs) using commercially available phenolic fibres (Kynol^{TM}) or pitch and polyacrylonitrile fibres by proper carbonization. The ACFs are especially interesting since they have a uniform micropore structure, faster adsorption kinetics and a lower pressure drop as compared to granular activated carbons [28,29]. Carbons were prepared from resins synthesised using many derivatives of phenolic precursors which influence the microporosity of the carbon products [30]. Activated carbon binderless monoliths with high consistency and large porosity, synthesised from a mesophase pitch, are investigated as electrodes for supercapacitors [31]. Mesoporous carbons can be prepared from phenol-formaldehyde resin and various mesostructured silicas as nano-templates [32]. Moreover, spherical chars with micro- and mesopores have been obtained from the heating and activation of waste ion-exchange resin Amberjet 1200H and were used for the remediation of waters from toluene [33]. Furthermore, carbons were also prepared from different phenolic resins under the carbonization process. The produced carbons were examined for the different pore sizes and specific surface areas [34,35]. Mesoporous carbons can also derive from the mixtures of phenol-formaldehyde resin as a carbon precursor and ethylene glycol as the pore forming agent. The influence of the mass ratio of the two initial materials in the final carbon material was examined through the pore size distribution and the average pore size [36]. Other carbonaceous materials include carbon brushes which were prepared from the appropriate thermosetting resin. These materials are composed of carbon materials such as graphite, solid lubricant such as MoS_2, a thermosetting resin binder and additive. All materials were mixed, tabletted, dried, milled, sized, molded at different pressures and finally cured at specific temperature [37]. Moreover, monolithic activated carbons were prepared from exfoliated graphite, which was compressed in a specific shape, impregnated with a thermosetting resin and finally carbonized and activated [38]. Nanostructured carbon materials present structures of highly ordered, rigid arrays of nanoporous carbon having uniform but tunable diameters from 6 nm inside to 9 nm outside. These materials are formed by using ordered mesoporous silicas as templare and a high dispersion of platinum nanoparticles [39].

3. PYROLYSIS OF THERMOSETTING POLYMERS AND ACTIVATION OF THEIR CHAR FORMED

When polymers are heated in an inert atmosphere (i.e. under pyrolysis conditions) reactions take place initially within the C-C chain. These intramolecular reactions result in one of three possibilities: (i) the chains degrade into small molecules and the products are evolved as gases leaving little or no carbon behind, e.g. polyethylene or poly(methyl methacrylate), respectively, (ii) the chains collapse to form aromatic lamellae leading to spherulitic liquid crystals (mesophase) at about 400°C and to crystalline anisotropic coke by further heating, e.g. poly(vinyl chloride) and (iii) the chains remain intact and merely coalesce with neighbours, without passing through a plastic state, e.g. poly(vinylidene chloride) which forms a “hard” char [6]. Organic compounds are the main and almost exclusive raw materials for the production of artificial carbons and graphites. Pyrolysis leads to the thermal decomposition of the initial raw material, i.e. thermosetting polymer, producing a carbon material with a rudimentary pore structure. The procedure of pyrolysis takes place in furnaces

with a gradual increase of temperature until 1000°C under a continuous flow of an inert gas, such as nitrogen or argon. The parameters that influence the pyrolysis are the physical and chemical structure of the initial raw material, the heating rate, the final temperature, the residence time, and possibly the total gas pressure when the process take place with pressure [40,41]. The low-temperature stage of pyrolysis, especially below 700°C, has the greatest influence on both the carbon yield and the carbon properties. Even in the simple case of isothermal pyrolytic decomposition, a great number of parallel and sequential reactions occur [41]. In general, when polymers of type (iii) are pyrolysed, the following stages of structural change are noted: I. The precarbonization, by removing of all "loose" molecules such as excess monomer or solvent, II. The carbonization, typically between 300 and 500°C, in which oxygen, nitrogen, chlorine etc. are removed, a rapid weight loss of the polymer occurs, and the result is a loose network of linear conjugated systems which are still isolated electronically from each other, III. The dehydrogenation, between 500 and 1200°C, in which hydrogen is gradually eliminated and the electrical conductivity increases rapidly as separate conjugated systems become interconnected to form a conducting network and IV. The annealing, by heat treatment above 1200°C leading to slightly softer but still remaining relatively hard and amorphous compared to graphite materials [6]. The carbon yield is determined as the ratio of the weight of the carbon residue to the initial weight and the conversion efficiency is the ratio of the weight of carbon (as element) in the residue to the weight of carbon (as element) in the original resin [6]. The carbon yield does not seem to be influenced by whether the polymer is thermoplastic or thermosetting, linear or cross-linked, but whether it is capable of cyclization, ring fusion or chain coalescence at the onset of carbonization. Generally, the resins should have a high degree of aromaticity and high molecular weight. There should be no more than one carbon atom between aromatic rings, because chain scissions will take place leading to volatilization of the fragmented parts [6,41]. Nitrogen should be in the ring structure and not in the chain. Other elements such as sulfur do not affect the stability of the polymer, but do result in lower char yields and low conversion efficiency. All phenolic polymers except those in which the para position is blocked by either a phenyl or methyl group are good char-forming materials. Phenol-furfuraldehyde has a high carbon yield (62%) and conversion efficiency (80%), higher than phenol-formaldehyde (52% and 76%, respectively) [6]. Another class of cross-linked polymers is that of macroreticular (macroporous) polymers, mainly based on styrene (S) / divinylbenzene (DVB) copolymers, which are suitable precursors for carbon production upon pyrolysis (carbon yield of 60% for cross-linked copolymer of S /48% DVB and chlorinated) [27]. The porosity of activated carbons is conditioned, among other factors, by the carbonaceous precursor and the activation method used for its preparation, i.e. the physical (thermal) activation or chemical activation [42]. Therefore, the char formed after the pyrolysis follows an activation process where the volume of the pores will be enhanced and new porosity will be created. Activation process increases the diameter of the existing pores, due to the burnout of the walls between the pores and increases the microporosity of the char, due to the removal of the disorganized carbon and the exposure of the aromatic sheets to the activation agent. Since the extent of the burnoff plays an important role to the diameter of pores, it is generally accepted that a microporous carbon is created when the degree of burnoff is less than 50%, a carbon with all types of pores has a degree of burnoff between 50 and 75% and finally a macroporous carbon is created when the degree of burnoff is more than 75% [40,43]. The use of chemical substances such as zinc chloride, phosphoric acid, potassium or sodium hydroxide as activating agents for the

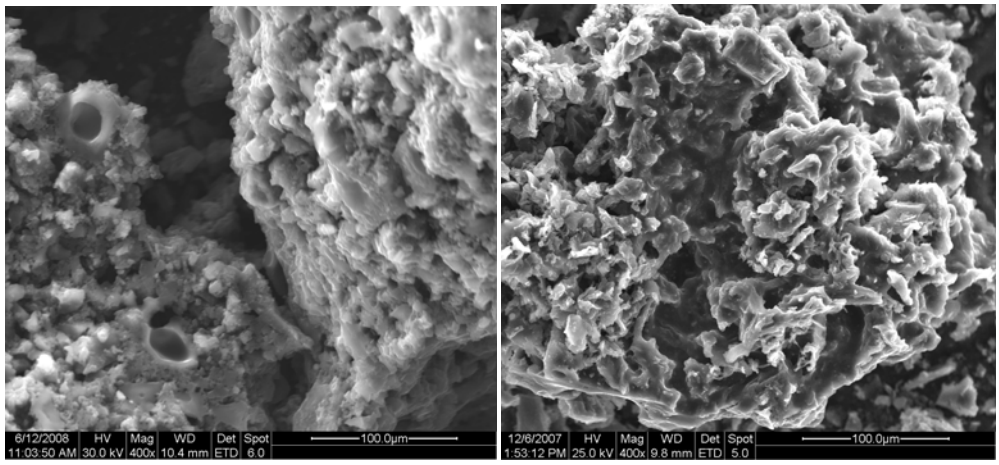
char characterizes the chemical activation while the use of oxidizing gases such as steam, carbon dioxide, air or any mixture of these gases characterizes the physical (thermal) activation. Chemical activation is carried out at temperatures between 400 and 800°C while the respective temperatures for physical activation are higher between 800 and 1100°C [40,44]. Thermosetting polymers such as phenol-formaldehyde resins are used as initial materials for mesoporous carbons of different pore structures [45]. The use of resol type phenol-formaldehyde resin with various mesostructured silicas can be converted into mesoporous carbons of high surface area, large pore size and great pore volume via pyrolysis procedure under nitrogen atmosphere and a heating rate of 10°C. Furthermore, the use of novolac type phenol-formaldehyde resin in the surface of a carbon through the spin coating technique can lead to the creation of carbon molecular sieves (CMSs) via pyrolysis at different temperatures and under vacuum [46]. Other studies concerns the use of novolac type phenol-formaldehyde resin and agricultural by-products, which were used as fillers due to their low cost. Various mixtures of olive stone biomass (OL.B.) and novolac resin (N.R.) were cured with hexamethylenetetramine, pyrolyzed up to 1000°C under nitrogen atmosphere and eventually activated with steam or CO2 [20-22]. Composite materials consisting of N.R./OL.B. show additional cross linkages due to the lignin constituent, compared to N.R. and hence their low temperature pyrolysis differs from that of N.R. and OL.B. The use of N.R. in the initial mixture with OL.B. reduces the weight loss during pyrolysis compared to OL.B. [47]. Many reports have appeared on the development of activated carbon from low cost raw materials. Activated carbons have been prepared from rattan sawdust [48], sugar beet bagasse [49], apricot shell [50], sunflower seed hull [51] , rubber seed coat [52], coconut shell [53], apricot stone shells [54], oil palm fibre [55], bamboo [56], coconut husk [57] e.t.c. Moreover the use of other agricultural by-products such as black gram husk, green gram husk and rice husk [58] are very often. Besides the pyrolysis and the activation of the carbonaceous adsorbents, another process concerns their regeneration. The latter consists of two sequential phenomena, namely the desorption, and if this takes place not fully, the reacrivation. The desorption of the adsorptive agent in the gas phase is achieved by decreasing the pressure alone, in its combination with washing or by heating with simultaneous washing. A desorption in the liquid phase is carried out by the extraction of the adsorptive. In opposite to the regeneration of the granular carbonaceous adsorbents, the adsorbents in powder form can not be regenerated in many cases [10].

4. CHARACTERIZATION AND STRUCTURE OF ACTIVATED CARBONACEOUS MATERIALS

Activated carbonaceous materials are carbons which consist mainly of the carbon element containing also other elements such as hydrogen, oxygen, nitrogen and sulphur. The elemental composition of a typical activated carbon is 88% C, 0.5% H, 0.5% N, 1% S and 6-7% O [59]. The concept of a graphitic ribbon network structure for all polymeric carbons has been introduced, as opposed to the extensive graphitic sheets which must exist in graphitic carbons [6]. The structure of activated carbons is similar to stacks of flat aromatic sheets crosslinked in a random manner. These aromatic sheets contain free radical structures or structures with unpaired electrons which can react with the above heteroatoms (oxygen,

hydrogen, nitrogen, sulphur) creating different types of surface functional groups. Generally, activated carbons are predominantly amorphous materials (nongraphitizable carbonaceous materials) according to x-ray diffraction analysis. The use of thermosetting precursors such as phenolic resins leads after thermal treatment to the formation of the basic macromolecular or polymeric structure of the carbonaceous material losing small molecules as volatile gaseous products and developing cross-linking [40]. The main characteristics of the activated carbonaceous materials are the extended surface area and the high degree of porosity. The two processes that create the high surface area and the large porosity of carbons are the carbonization, which leads to the creation of the macroporous structure of carbons and the activation which leads to the creation of the microporous structure. Raw materials play an important role in the final pore size of the carbonaceous material. The use of coconut shell as precursor for the creation of activated carbons has shown that the produced carbonaceous materials present specific surface area around 380 m^2/g and pore volume for micropores around 0.12 cm^3/g [53]. On the other side the use of digested sewage sludge with coconut husk as precursor leads to activated carbons with a specific surface area around 870 m^2/g [57]. During carbonization the raw materials will be thermally decomposed and the noncarbon species will escape in the form of gases leading to a rudimentary pore structure. Activation results in the opening of the blocked pores, and in the creation of wider pores and more active sites. Activated carbons contain a complex network of pores which can be classified to micropores with a diameter less that 2 nm, mesopores with a diameter between 2 and 50 nm and macropores with a diameter larger than 50 nm. The high values of the surface area of carbons depend on the extended network of micropores where the adsorption takes place, and not to mesopores and macropores which are the passage for the adsorbate to result to the interior micropores [40,59]. The structure of carbon molecular sieves (CMSs) is similar to that of activated carbons containing almost uniform micropores of a few angstroms in diameter (probably less than 0.8 to 1.2 nm) and having the ability to selectively separate molecules, mainly of a gas mixture [60,61]. Carbon molecular sieves which derived from phenol-formaldehyde resin by an esterification method present average pores structure between 0.40 and 0.45 nm and pore volume between 0.18 and 0.22 cm^3/g [60]. Moreover carbon molecular sieve membranes, which derived from a microporous carbon layer over a macroporous carbon substrate, have micropore size around 4.2 Å [46]. Mesoporous carbons, especially from phenol-formaldehyde resin and various mesostructured silicas, present high surface areas from 850 to 1500 m^2/g, large pore size from 2 to 22 nm and great pore volume from 0.65 to 1.15 cm^3/g [32]. Furthermore, the preparation of mesoporous carbons from a polystyrene-based ion-exchange resin by chemical activation with potassium hydroxide has shown specific surface areas between 357 and 1950 m^2/g [62].Moreover, nanostructured carbon materials present structures of highly ordered, rigid arrays of nanoporous carbon having uniform but tunable diameters from 6 nm inside to 9 nm outside. These materials are formed by using ordered mesoporous silicas as templare and a high dispersion of platinum nanoparticles. These nanostructured materials present specific surface areas around 2000 m^2/g according to BET measurements [39]. Besides the physical structure, activated carbons are also influenced by the chemical structure of their surface. Two kinds of chemical species are presented: the chemical species between activated carbons and heteroatoms such as oxygen and hydrogen and the created chemical species due to the variation in the arrangement of electron clouds in the carbon skeleton which results in the creation of unpaired electrons and incompletely saturated valencies which can react with the adsorbate creating a chemical bond.

These heteroatoms can also be derived from the initial raw material of the carbonaceous material such as chlorine, nitrogen or sulphur. The most important role among the different surface functional groups plays the carbon – oxygen surface group in carbons which is also responsible for the acid-base character of carbons. Such chemical groups can be identified through XPS analysis. The most important functional groups in the C 1s region are graphitic carbon, C-OH, C=O, -COOH, CO_3^{2-} with binding energies of 284.6, 286.1, 287.6-288.2, 288.8 and 289.1 eV respectively. In the case of lignocellulosic materials the main components are oxides of silicon, magnesium, calcium, iron, aluminium and sodium. Oxygen surface groups can be created not only through the reaction of carbon with oxygen but also with other oxidizing gases such as ozone, carbon dioxide, nitric oxide e.t.c. or solutions such as nitric acid, sodium hypochlorite e.t.c [40,59]. The characterization of the pore structure of the carbonaceous materials can be made either directly through Hg-porosimetry, BET measurements or indirectry through techniques such as iodine, phenol and methylene blue adsorption [59,63]. The capacity of carbonaceous materials to remove colour can be evaluated through iodine number which is expressed as milligrams of adsorbed iodine per gram of carbonaceous material. This indicates their relative activation level and the surface area available for micropores. A high value of iodine number is an indicator for high surface area of the carbonaceous materials. Except for the iodine number, phenol adsorption provides also information on the adsorptive properties of activated carbonaceous materials. Specifically this method measures the adsorption of phenol in milligrams per gram of carbonaceous material when reducing the original concentration of phenol from 10 to 1 mg/l. Since the molecular size of phenol is around 5 Å this method can be used to characterize the microporosity of activated carbons. The determination of the mesopores and macropores in a carbon can be made through the adsorption of methylene blue which has a molecular size above 15 Å. The methylene blue value is defined as the milligrams of methylene blue adsorbed by one gram of dry adsorbent (carbonaceous material) with a solution of methylene blue at a concentration of 1.0 mg/L [63].



(a) (b)

Figure 1. SEM micrographs of carbonaceous adsorbents. commercial activated carbon, x400, (b) carbonized and activated carbon from precursor composite material of novolac/olive stones, 40/60 % w/w, x400.

Based on such dye tests on one hand and on modified acrylics and acrylic copolymers with defined groups on the other, an appropriate method has been developed to determine the acidic and basic groups of an adsorbent [64,65]. Methylene blue (having electron donor groups) and alizarin yellow (having mainly electron acceptor groups) have been chosen as suitable dyes from aqueous solutions for studying the interactions, according to the concept of electron donor-acceptor (EDA) interaction, between their groups and those of the examined material and for characterizing them. The adsorption of an adsorptive agent (e.g. a dye such as methylene blue) into a carbonaceous material is influenced not only by the pore size distribution of the carbonaceous material but also from its surface chemistry [66]. An overall view of the latter can be obtained based on the electron donor-acceptor (EDA) interactions between the functional groups of the dye and the carbonaceous material, whereas the adsorption of methylene blue indicates the presence of electron-acceptor groups (e.g. COOH) contained in the carbonaceous material.

New materials, which come from cured novolac with hexamethylenetetramine and olive stones biomass were prepared in the laboratory. These materials were carbonized in a furnace up to 1000°C in an inert atmosphere and then activated up to 1000°C in CO_2 atmosphere. The scanning electron micrographs (SEM) of a such material and of a commercial activated carbon are presented in Figure 1.

Figure 1(a) presents a SEM micrograph of the commercial activated carbon. The material shows a compact structure with slots creating an extended degree of pores ranging from 7 to 22 μm. Figure 1(b) shows the surface of the carbonized and activated material (40/60% w.t./w.t. novolac/olive stones). During the activation process, more pores were opened in the structure of the material. The surface of the material presents a web of different pores ranging from 3.7 to 25.9 μm. The shape of the solid mass of commercial material differs from that of the produced one and therefore differ not only the corresponding free passages between the particles but also their pore structure. Furthermore, macroscopically the commercial carbon is more stiff and is difficult in cutting in comparison with the produced material. The adsorbent prepared from 100% olive stone biomass by pyrolysis at 1000°C contained mainly mesopores, with only a few micropores, and for this reason it adsorbed methylene blue but did not practically adsorb from the vapour phase (e.g. pentane, cyclohexane and toluene). The adsorbent prepared from novolac/biomass in the proportion of 20/80 by pyrolysis at 1000°C and subsequently activated contained more micropores, but it also contained mesopores, so that they were able to adsorb both vapours and methylene blue [22].

5. PROPERTIES (MAINLY ADSORPTION PROPERTIES) AND APPLICATIONS

The more important properties of the carbonaceous adsorbents for a technological application are: (1) high adsorption capacity, (2) rapid adsorption kinetics, (3) low reaction feasibility against the regeneration agent and (4) mechanical strength [67].

Carbonaceous materials are widely used for many applications such as separation of gases, recovery of solvents, removal of organic pollutants from drinking water and as catalyst support. Moreover, these materials are important adsorbents in many industrial activities such as the food, pharmaceutical and chemical industries [9].

According to the pore size, microporous activated carbons can be used for gas applications especially gas separations and purification. These carbons have a well developed microporosity to provide a high adsorptive capacity and selectivity for gases and organic vapors. Moreover activated carbons reduce also, through adsorption, the pollutant or toxic gases to very low concentrations. Activated carbons with high degree of micropores are used to remove hydrogen sulphide from natural gas, filter breathing air and remove odor from air conditioning systems and to remove sulphur dioxides from flue gases. Furthermore pressure swing adsorption (PSA) is applied for the separation of gases with the help of activated carbons in the form of carbon molecular sieves. Activated carbons help to separate oxygen from nitrogen from the air, linear from branched hydrocarbons and carbon dioxide from natural gas [9,59].

The contribution of activated carbons to the recovery of solvents from the industry is also very important. The efficiency of activated carbon is high generally 98% of the vapour collected. Operating costs are low. Some of the solvents that are recovered by activated carbons are the following: acetone, benzene, ethanol, ethyl acetate, ethyl ether, isopropanol, methanol, methyl acetate, methyl ethyl ketone, petroleum naphtha, solvent naphtha, tetrachloroethylene, trichloroethylene, toluene and xylene [9].

Mesoporous and macroporous carbons are used primarily for liquid phase applications such as water purification. Specifically, granular and powdered activated carbons were used in batch and continuous operations with the difference that the final solutions with powdered carbons should follow the filtration process in order to remove carbons from the solution. Water purification is the main application of activated carbons in liquid phase applications with the removal of unpleasant taste, odor and organic compounds like chloroform and trihalomethanes from water. Activated carbons are used in many sectors of water industry from potable water to municipal and industrial waste waters which can be purified in a large extent and re-use to the agricultural sector [9].

Activated carbons are also used either as contact catalysts in reactions such as isomerization, polymerization, oxidation and halogenation or as a promoter or carrier for other catalysts. Such examples are the production of phosgene without light, the creation of sulfuryl chloride in the liquid phase, the formation of hydrogen chloride from steam and chlorine, the formation of vinyl chloride from acetylene and hydrogen chloride [9].

Activated carbons find many uses in biochemical studies. They are employed in the preparation of biological products, medicaments, and are appropriate as a tool for the study of biological processes [9].

Carbon molecular sieves are effective for separating gas mixtures such as O_2–N_2 and CO_2–CH_4 and H_2-CH_4 [46,68,69]. Activated carbons are widely used for a number of applications such as separation of gases, recovery of solvents, removal of organic pollutants from drinking water, catalyst support. Activated carbons are important adsorbents in various industrial sectors such as the food, pharmaceutical and chemical industries. Furthermore the demand of activated carbons for confronting environmental pollution is nowadays unexceptionable [62,70,71]. More specifically, mesoporous carbons play an important role in new applications such as catalyst supports, battery electrodes, capacitors, gas storage and biomedical engineering. The high mechanical strength of porous carbons is necessary for some practical applications. Moreover their use in electric double-play capacitors is necessary not only for electric conductivity but also for mechanical strength [71]. Carbon brushes have also applications especially in the motors, where they have excellent commutation ability

[37]. Monolithic activated carbons are used in catalysis, and in gas storage applications [38]. Nanostructured carbon materials are used to the development of electronic, catalytic and hydrogen-storage systems [39]. Carbon nanotubes as both molecular device elements and molecular wires for reading and writing information were developed [72]. The well-ordered nanotubes can also be used as electron field emission arrays [73]. Carbon nanostructures can also be utilized in catalytic engineering [74,75]. Catalytically grown carbon nanofibers are novel materials that are the product of the decomposition of carbon-containing gases over certain metal surfaces [74]. Carbon nanotubes can be used for hydrogen-storage systems since a gas like hydrogen can condense inside the single-walled nanotubes (SWNTs) under conditions that do not induce adsorption within a standard mesoporous activated carbon. The high hydrogen uptake of these materials makes them appropriate as hydrogen storage materials for fuel - cell electric vehicles [76].

REFERENCES

[1] Xuefei, Z.; Shiquan, L.; Hongzhao, L.; Lijuan G. (2009) Preparation and characterization of activated carbon foam from phenolic resin, *J.Environmental Sciences Supplement*, S121-S123.

[2] Park, S.-J.; Jung, W.-Y. (2002) Preparation of activated carbons derived from KOH-impregnated resin, *Carbon*, 40, 2021-2140.

[3] Seewald, H. Technisch verfuegbare Adsorbentien, in Adsorptionsverfahren bei der Gas- und Wasserreinigung, Herausgeber E.Steinmetz, Vortragsveroeffentlichungen Nr.404, Haus der Technik, Vulkan-Verlag Dr.W.Classen, Essen, (1978), S.24-34.

[4] Bansal, R. C.; Donnet, J.-B.; Stoeckli, F. *Active Carbon*, N. York, ST: Marcel Dekker Inc.; 1988; vii.

[5] Walker, Jr. P. L.; Austin, L. G.; Nandi, S. P. *Chemistry and Physics of Carbon: Activated diffusion of gases in molecular sieve materials*. In: P.L. Walker Jr., editor, New York, ST:Marcel Dekker Inc.; vol. 2; (1966); 256-371.

[6] Jenkins, G. M.; Kawamura, K.; *Polymeric Carbons: Carbon Fibre, Glass and Char*, London, New York, ST:Cambridge University Press; 1976; 1,2,11-16,137.

[7] Fitzer, E. *Carbon fibres and their composites*, N. York, ST:Springer-Verlag; 1985; 11.

[8] Marsh, H.; Rodriguez-Reinoso F. *Activated Carbon*, N. York, ST:Elsevier; 2006; 87-137.

[9] Hassler, J. W. *Purification with activated carbon: Industrial, Commercial*, Environmental, New York, ST: Chemical Publishing Co., Inc.; 1974; 3-5,248-250, 274-278.

[10] Jüntgen, H. Adsorptionsverfahren bei der Gas- und Wasserreinigung: Physikalisch-chemische und verfahrenstechnische Grundlagen von Adsorptionsverfahren, In: E.Steinmetz, Herausgeber Vortragsveroeffentlichungen Nr.404, Haus der Technik, Essen, ST: Vulkan-Verlag Dr.W.Classen; 1978; 5-24.

[11] Jüntgen, H., 2nd Intern. Carbon Conference, organized by the German Ceramic Society, Baden-Baden, 27.6.-2.7.1976, Preprints p.1-3.

[12] Seymour, R.B.; Carraher Jr., C.E. *Polymer Chemistry*, New York and Basel, ST: Marcel Dekker Inc.;1981; 2,9.

[13] Winslow, F. H.; Baker, W. O.; Pape, N. R.; Matreyek, W. (1955) Formation and properties of polymer carbon, *J. Polym. Sci*., 16, 101.
[14] Marsh, H.; Wynne-Jones, W.F.K. (1964) The surface properties of carbon –I. The effect of activated diffusion in the determination of surface area, *Carbon*, 1, 269-279.
[15] Lamond, T.G.; Metcalfe, J.E.; Walker Jr, P.L. (1965) 6A Molecular sieve properties of Saran-type carbons, *Carbon*, 3, 50-63.
[16] Fitzer, E.; Schaefer W.; Yamada S. (1969) The formation of glasslike carbon by pyrolysis of polyfurfuryl alcohol and phenolic resin, *Carbon*, 7, 643-648.
[17] Jüntgen, H.; Knoblauch, K.; Harder, K. (1981) Carbon molecular sieves: production from coal and application in gas separation, *Fuel*, 60, 817-822.
[18] Jüntgen, H. (1986) Activated carbon as catalyst support, *Fuel*, 65, 1436-1446.
[19] Walker, Jr. P.L.; Shelef, M. (1967) Carbon dioxide sorption on carbon molecular sieves, *Carbon* 5, 7-11.
[20] Simitzis, J. (1987) Aktivkohle aus Phenolharz mit gepressen Olivenkernen als Fuellstoff, Angew. *Makromolek. Chemie*, 153, 165-176.
[21] Simitzis, J.; Sfyrakis, J. (1994) Activated carbon from lignocellulosic biomass-phenolic resin, *J. Appl. Polym. Sci*., 54, 2091-2099.
[22] Simitzis, J.; Sfyrakis, J.; Faliagas, A. (1995) Characterization of pore structure by porosimetry and sorption on adsorbents produced from novolac – biomass, *Mater. Chem. Phys*., 41, 245-250.
[23] Centeno, T. A.; Fuertes, A. B. (2001) Carbon molecular sieve membranes derived from a phenolic resin supported on porous ceramic tubes, *Separation and Purification Technology*, 25, 379-384.
[24] Zhang, X.; Hu, H.; Zhu, Y.; Zhu, S. (2006) Effect of carbon molecular sieve on phenol formaldehyde novolac resin based carbon membranes, *Separation and Purification Technology*, 52, 261-265.
[25] Wei, W.; Qin, G.; Hu, H.; You, L.; Chen, G. (2007) Preparation of supported carbon molecular sieve membrane from novolac phenol-formaldehyde resin, *Journal of Membrane Science*, 303, 80-85.
[26] Hayashi, J.; Matsuzaki, K.; Hiraumi, T.; Muroyama, K. (1996) Production of molecular sieving carbon from phenol-formaldehyde resin by an ester-carbonization method, *Carbon*, 34(2), 273-281.
[27] Neely, J. W. and Isacoff, E. G. *Carbonaceous Adsorbents for the Treatment of Ground and Surface Waters,* Marcel Dekker Inc., New York and Basel: 1982; 43,46,51.
[28] Daley, M.A.; Mangun, C.L.; DeBarr, J.A.; Riha, S.; Lizzio, A.A.; Donnals, G.L.; Economy, J. (1997) Adsorption of SO_2 onto oxidized and heat-treated activated carbon fibers (ACFS), *Carbon* 35(3), 411-417.
[29] Mangun, C.L.; DeBarr, J.A.; Economy, J. (2001)Adsorption of sulfur dioxide on ammonia-treated activated carbon fibers", *Carbon*, 39, 1689-1696.
[30] Lenghaus, K.; GuangHua Qiao, G.; Solomon, D.H.; Gomez, C.; Rodriguez-Reinoso, F.; Sepulveda-Escribano, A. (2002) Controlling carbon microporosity: the structure of carbons obtained from different phenolic resin precursors, *Carbon* 40, 743-749.
[31] Ruiz, V.; Blanco, C.; Santamaria, R.; Ramos-Fernandez, J.M.; Martinez-Escandell, M.; Sepulveda-Escribano, A.; Rodriguez-Reinoso, F. (2009) An activated carbon monolith as an electrode material for supercapacitors, *Carbon*, 47, 195-200.

[32] Lin, Y.-P.; Lin, H.-P.; Chen, D.-W.; Liu, H.-Y.; Teng, H.; Tang, C.-Y. (2005) Using phenol-formaldehyde resin as carbon source to synthesize mesoporous carbons of different pore structures, *Materials Chemistry and Physics*, 90, 339-343.

[33] Bratek, K.; Bratek, W.; Kulazynski, M. (2002) Carbon adsorbents from waste ion-exchange resin, *Carbon*, 40, 2213-2220.

[34] Lenghaus, K.; Qiao, G. G.; Solomon, D. H.; Gomez, C.; Rodriguez-Reinoso, F.; Sepulveda-Escibano, A.; (2002) Controlling carbon microporosity: the structure of carbons obtained from different phenolic resin precursors, *Carbon*, 40, 743-749.

[35] Nakagawa, K.; Mukai, S. R.; Tumura, K.; Tamon, H. (2007) Mesoporous activated carbons from phenolic resins, Trans IChemE, Part A, *Chemical Engineering Research and Design*, 85(A9), 1331-1337.

[36] Xu, S.; Qiao, G.; Wang, H.; Li, D.; Lu, T. (2008) Preparation of mesoporous carbon derived from mixtures of phenol-formaldehyde resin and ethylene glycol, *Materials Letters* 62, 3716-3718.

[37] Xia, J.-T.; Hu, Z.-L.; Chen, Z.-H.; Ding, G.-Y. (2007) Preparation of carbon brushes with thermosetting resin binder, *Transactions of Nonferrous Metals Society of China*, 17, 1379-1384.

[38] Mareche, J. F.; Begin, D.; Furdin, G.; Puricelli, S.; Pajak, J.; Albiniak, A.; Jasienko-Halat, M.; Siemieniewska, T. (2001) Monolithic activated carbons from resin impregnated expanded graphite, *Carbon*, 39, 771-785.

[39] Joo, S.-H.; Choi, S.-J.; Oh, I.; Kwak, J.; Liu, Z.; Terasaki, O.; Ryoo, R. (2001) Ordered nanoporous arrays of carbon supporting high dispersions of platinum nanoparticles, *Nature*, 412, 169-172.

[40] Bansal R. C., Donnet J.-B., Stoeckli F., (1988) *Active carbon,* N. York, ST: Marcel Dekker Inc.,4-8, 9-15, 27-29.

[41] Fitzer, E.; Mueller, K.; Schaefer, W.; *Chemistry and Physics of Carbon: The Chemistry of the pyrolytic conversion of organic compounds to carbon*, In: P.L. Walker Jr., New York, ST: Marcel Dekker Inc.; vol. 7; (1971); 237-383.

[42] Belhachemi, M.; Rios, R.V.R.A.; Addoun, F.; Silvestre-Albero, J.; Sepulveda-Escribano, A.; Rodriguez-Reinoso, F. (2009) Preparation of activated carbon from date pits: Effect of the activation agent and liquid phase oxidation", *J. Anal. Appl. Pyrolysis*, 86, 168-172.

[43] Dubinin, M. M. and Zaverina, E. D. (1949) Issledovanie adsorbtsii gazov aktivnymi uglyami. *Dokl. Akad. Nauk. SSSR*, 65, 295-298.

[44] Rand, B. and Marsh, H. (1971) The process of activation of carbons by gasification with CO_2-III. *Uniformity of gasification Carbon*, 9, 79-85.

[45] Yen-Po, L.; Hong-Ping, L.; Dong-Wun, C.; Hsin-Yu, L.; Hsisheng, T.; Chin-Yuan, T. (2005) Using phenol–formaldehyde resin as carbon source to synthesize mesoporous carbons of different pore structures, *Materials Chemistry and Physics*, 90, 339–343.

[46] Centeno, T. A. and Fuertes, A. B. (1999) Supported carbon molecular sieve membranes based on a phenolic resin, *Journal of Membrane Science*, 160, 201-211.

[47] Simitzis J. (1994) High temperature pyrolysis of novolac resin biomass composites, *J. Anal. and Appl. Pyrolysis*, 30, 161-171.

[48] Hameed, B.H. and Rahman, A.A. (2008) Removal of phenol from aqueous solutions by adsorption onto activated carbon prepared from biomass material, *Journal of Hazardous Materials*, 160(2-3), 576-581.

[49] Munir, S.; Daood, S.S.; Nimmo, W.; Cunliffe, A.M.; Gibbs, B.M. (2009) Thermal analysis and devolatilization kinetics of cotton stalk, sugar cane bagasse and shea metal under nitrogen and air atmospheres, *Bioresource Technology*, 100, 1413-1418.

[50] Philip, C. A. and Girgis, B. S. (1996) Adsorption Characteristics of microporous carbons from apricot stones activated by phosphoric acid, *J. Chem. Tech. Biotechnol*. 67, 248-254.

[51] Thinakaran, N.; Baskaralingam, P.; Pulikesi, M.; Panneerselvam, P.; Sivanesan, S. (2008) Removal of Acid Violet 17 from aqueous solutions by adsorption onto activated carbon prepared from sunflower seed hull, *J. Hazardous Materials* 151, 316-322.

[52] Rengaraj, S.; Moon, S. H.; Sivabalan, R.; Arabindoo, B.; Murugesan, V. (2002) Removal of phenol from aqueous solution and resin manufacturing industry wastewater using an agriculture waste: rubber seed coat, *J. Hazardous Materials*, 89, 185-196.

[53] Singh, K. P.; Malik, A.; Sinha, S.; Ojha, P. (2008) Liquid-phase adsorption of phenols using activated carbons derived from agricultural waste material, *Journal of Hazardous Materials*, 150, 626-641

[54] Daifullah, A.A.M.; Girgis, B.S. (1998) Removal of some substituted phenols by activated carbon obtained from agricultural waste,*Water Research*, 32, 1169– 1177.

[55] Tan, I.A.W.; Hameed, B.H.; Ahmad, A.L. (2007) Equilibrium and kinetic studies on basic dye adsorption by oil palm fibre activated carbon, *Chemical Engineering Journal*, 127, 111–119.

[56] Hameed, B.H.; Din, A.T.M.; Ahmad, A.L.; (2007) Adsorption of methylene blue onto bamboo-based activated carbon: kinetics and equilibrium studies, *Journal of Hazardous* Materials, 141, 819–825.

[57] Tan, I.A.W.; Ahmad, A.L.; Hameed, B.H. (2008) Adsorption of basic dye on high-surface area activated carbon prepared from coconut husk: equilibrium, kinetic and thermodynamic studies, *Journal of Hazardous Materials*, 154(1–3), 337–346.

[58] Srihari, V.; Das, A. (2008) Comparative studies on adsorptive removal of phenol by three agro-based carbons: Equilibrium and isotherm studies, *Ecotoxicology and Environmental Safety*, 71, 274-283.

[59] Rodriguez-Reinoso F., The encyclopedia of materials : A*ctivated carbon and Adsorption*, ST: Elsevier Science Ltd.; 2001; 22-35.

[60] Hayashi J., Matsuzaki K., Hiraumi T., Muroyama K., (1996) Production of molecular sieving carbon from phenol-formaldeyde resin by an ester-carbonization method, *Carbon* 34(2), 273-281.

[61] Foley, H. C.; Kane, M. S.; Goellner, J. F. (1995) *Access in Nanoporous Materials: New directions with carbogenic molecular sieve materials* In: T. J. Pinnavaia, M. F. Thorpe, editors. Plenum Press, N. York, 39-58.

[62] Park, S.-J. and Jung, W.-Y. (2002) Preparation of activated carbons derived from KOH-impregnated resin, *Carbon*, 40, 2021-2040.

[63] Mikhail, R.S. and Robens, E. *Microstructure and Thermal Analysis of Solid Surfaces*, John Wiley and Sons, Chichester, New York: 1983; 122,123.

[64] Simitzis, J. (1994) Modified polyacrylonitrile for adsorption applications, *Acta Polymer*, 45, 104-109.

[65] Simitzis, J. (1995) Diffussion limited sorption of dyes on modified acrylics and acrylic copolymers, *Polymer*, 36, 1017-1021.

[66] Ahumada, E.; Lizama, H.; Orellana, F.; Suarez, C.; Huidobro, A.; Sepulveda-Escribano, A.; Rodriguez-Reinoso, F. (2002) Catalytic oxidation of Fe(II) by activated carbon in the presence of oxygen. Effect of the surface oxidation degree on the catalytic activity, *Carbon*, 40, 2827-2834.

[67] Klein, J. Reinigung von Abwasser durch adsorptive Verfahren mit integrierter Regeneration in : Adsorptionsverfahren bei der Gas- und Wasserreinigung, Herausgeber E.Steinmetz, Vortragsveroeffentlichungen; Nr.404; Haus der Technik; Vulkan-Verlag Dr.W.Classen; Essen; (1978); 59-69.

[68] Centeno, T. A.; Fuertes, A. B. (2001) Carbon molecular sieve membranes derived from a phenolic resin supported on porous ceramic tubes, *Separation and Purification Technology* 25, 379-384.

[69] Zhang, X.; Hu, H.; Zhu, Y.; Zhu, S. (2006) Effect of carbon molecular sieve on phenol formaldehyde novolac resin based carbon membranes, *Separation and Purification Technology* 52, 261-265.

[70] Hayashi, J.; Uchibayashi, M.; Horikawa, T.; Muroyama, K.; Gomes, V. G. (2002) Synthesizing activated carbons from resins by chemical activation with K_2CO_3, *Carbon*, 40, 2747-2752.

[71] Cai, Q.; Huang, Z.-H.; Kang, F.; Yang, J.-B. (2004) Preparation of activated carbon microspheres from phenolic-resin by supercritical water activation, *Carbon*, 42, 775-783

[72] Rueckes, T.; Kim, K.; Joselevich, E.; Tseng, G. Y.; Cheung, C.-L.; Lieber, C. M. (2000) Carbon Nanotube -Based Nonvolatile Random Access Memory for Molecular Computing, *Science*, 289, 94-97.

[73] Fan, S.; Chapline, M. G.; Franklin, N. R.; Tombler, T. W.; Cassell, A. M.; Dai H. (1999) Self-Oriented Regular Arrays ofCarbon Nanotubes and Their Field Emission Properties, *Science*, 283, 512-514.

[74] Rodriguez, N. M.; Chambers, A.; Baker, R. T. K. (1995) *Catalytic Engineering of Carbon Nanostructures*, Langmuir, 11, 3862-3866.

[75] Planeix, J. M.; Coustel, N.; Coq, B.; Bretons, V.; Kumbhar, P. S.; Dutartre, R.; Geneste, P.; Bernier, P.; Ajayan, P. M. (1994) Application of Carbon Nanotubes as Supports in Heterogeneous Catalysis, *J. Am. Chem. Soc*., 116, 7935-7936.

[76] Dillon, A. C.; Jones, K. M.; Bekkedahl T. A.; Kiang, C. H.; Bethune, D. S.; Heben, M. J. (1997) Storage of hydrogen in single walled carbon nanotubes, *Nature*, 386, 377-379.

In: Activated Carbon
Editors: James F. Kwiatkowski
ISBN: 978-1-61209-684-1
©2012 Nova Science Publishers, Inc.

Chapter 13

PLATINUM CATALYSTS ON ACTIVATED CARBON SUPPORTS PREPARED FROM MONONUCLEAR AND POLYNUCLEAR PRECURSORS: INFLUENCE OF POROUS STRUCTURE OF THE SUPPORT

L. B. Okhlopkova [*] ***and S. Yu. Troitskii***
Boreskov Institute of Catalysis, Novosibirsk 630090, Russia

A number of catalysts have been prepared by adsorption of platinum precursors on activated carbons of different origin followed by reduction in flowing hydrogen. They were characterized by CO chemisorption, TEM and liquid-phase hydrogenation of cyclohexene. Porous structure of the support and the nature of platinum precursor proved to have a profound influence on the properties of catalysts.

The metal dispersion of catalysts prepared from platinum (IV) chloride can be controlled in the range from 10 to 90%. Activity of the catalysts reached a maximum in the range of intermediate metal dispersion, with the limit being dependent on the support used. It has been suggested that a part of the supported metal became inaccessible to the organic substrate due to localization of metal particles in narrow pores of the support.

The extent of blocking proved to be higher for highly dispersed Pt particles and on the supports with smaller pores. An alternative route to preparing supported Pt catalysts is the synthesis of polynuclear hydroxochloride complexes from Pt(II) chloride that is followed by their deposition on carbon.

The catalysts prepared from polynuclear precursor showed high activity even in the range of high metal dispersion and for microporous carbons. Structure of product of Pt(II) chloride hydrolysis was established by means of NMR ^{195}Pt, ^{17}O.

[*] Fax. (+7)-3833-3308056: mila65@catalysis.ru

1. INTRODUCTION

Carbon-supported platinum are the catalyst in a large number of industrial processes with participation of oxygen and/or hydrogen [1, 2]. The metal dispersion in the final catalyst depends on a number of factors, such as a functional coverage of the carbon surface [3, 4], metal precursor [4-6], pore structure of the support [4, 7] and acidity of adsorption solution [8]. The high degree of dispersion of the metal or a very small particle size, that is, in the lower nanometer range of approximately 1-5 nm is quite often insufficient to receive high activity of the catalysts in the transformation of organic substrates. Even though metal particles are well dispersed, those blocked in micropores of the support would not easily interact with large organic molecules. The possibility of losing a great part of the catalytically active surface due to the metal blocking has long been recognized [9]. The structural effect was observed for 1-hexene hydrogenation on Pd supported on activated carbon fiber with small pores (< 1 нм) [10]. The shape selectivity of Pt on carbon-fiber catalysts was demonstrated in the competitive hydrogenation of 1-hexene and cyclohexene and in the parallel dehydrogenation of cyclohexanol to cyclohexanone and phenol [11]. The low activity of the catalysts supported on the carbon-fiber has been explained by a configurational diffusion resistance inside the narrow constrictions that were further blocked by metal atoms. Torres et al. showed in [12] that Pt particles distribution in the porous network could affect the activity of cyclohexane dehydrogenation and nitrobenzene hydrogenation. Job et al. expressed in [13] that the accessible platinum surface depends on the carbon xerogel texture. For the micro-mesoporous supports with small mesopores and micropores blocking of microporosity was detected. Fuente et al. [4] suggested that differences in catalytic conversion and TOF in acetone hydrogenation could be due to the different pore size of the supports. In the support, which has a smaller pore size, part of the metal could be deposited inside the pores and will be not accessible to the large molecules. Analogous explanation was given in [14] for an inconsistency between activity in nitrobenzene hydrogenation (large molecules) and H_2 chemisorption (small molecules). The method of catalyst preparation affecting the Pt distribution in the pore structure has received little attention. Brazi et al. showed in [15] that precipitation deposit of palladium on activated carbon must be preferred to exchange, as the more active catalysts in nitrobenzene hydrogenation were received in the latter case. It was observed by Landau et al. [11] that catalyst washed in water possessed high activity and low selectivity probably owing to back migration of the Pt species to the external surface. As was shown in [16], carbon-supported Pd catalysts prepared by the alkali hydrolysis of palladium chloride were more active than samples impregnating with the H_2PdCl_4 solution. De Miguel et al. observed in [17] that the higher impregnation times during the preparation of platinum on activated carbon felts led to catalysts with Pt mainly deposited inside the pores having lower catalytic activity in nitrobenzene hydrogenation.

To create high active catalysts the blocking of metal particles in the pores of the support has to be avoided. Most of the studies on the blocking effect investigated the unusual low activity in structure insensitive reactions of highly dispersed catalysts rather than factors increasing the accessibility of active metal. The porous structure of the support is a primary factor of appearance of blocking effect [7]. The observed order of activities for catalysts on different carbons corresponded to the narrowing of their pores. This chapter describes the influence of the platinum precursor on the blocking Pt particles in the pores of the support.

Three different commercial activated carbons were used as supports. The catalysts were prepared by adsorption of platinum(IV) chloride and platinum(II) polyhydroxochloride complexes (PHC) followed by reduction in hydrogen flow. To evaluate the degree of particles blocking, the activity in cyclohexene hydrogenation which belongs to structure-insensitive reaction were measured [18]. The dispersion of the catalysts was evaluated by means of transmission electron microscopy (TEM) and CO chemisorption. Furthermore, the structure of mononuclear precursor of PHC was analyzed by ^{195}Pt, ^{17}O NMR.

2. Pt/C Catalysts Prepared from Platinum(IV) Chloride. Effect of Porous Structure of the Support on Metal Dispersion and Activity in Cyclohexene Hydrogenation

AR (from coconut shell, Sutcliffe, England), Sibunit-M (produced industrially in Russia by hydrocarbon pyrolysis followed by gas activation) and Sibunit-SM (differed from Sibunit-M by activation conditions) were used [19]. The supports are marked in the text by corresponding codes: AR, Sib-M and Sib-SM listed in Table 1. All the carbons were subjected to standard treatment. Fractions of carbons 100-200 μm were treated in conc. HCl (at boiling for several weeks) followed by prolonged washing with water in a Soxhlet extractor and outgassing in high vacuum at 570 K. Ash content after such treatment was equal <0.2% for AR, Sib-M and Sib-SM (1.6 , <1% and <1% for untreated AR, Sib-M and Sib-SM, respectively). Data on structural characteristics of the carbons are presented in Table 1. AR is microporous carbon. In the pairs of carbons manufactured from the same precursor, Sib-M proves to have a more developed mesoporosity as compared with Sib-SM. Values of specific surface areas and the volumes of different pores in Table 1 were derived from the t-plots following the methodology of Sing [20].

Table 1. Texture characteristics of the supports (surface area S in m^2/g, pore volumes V in cm^3/g)

Carbon	Origin	L_{pore} [a)]	S_{BET} [b)]	S_{sm+me} [c)]	S_{me} [d)]	V_{total} [e)]	V_{um} [f)]	V_{um+sm} [g)]	V_{me} [h)]
Sib-M	hcs	7.8	412	264	311	0.83	0.01	0	0.83
Sib-SM	hcs	>2[i)]	360	235	96	0.44	0.05	0.16	0.28
AR	coconut	1.0	1140	635	19	0.52	0.26	0.47	0.05

[a)] Mean size of pores (nm).

[b)] From experimental data at p/p_o 0.01-0.15.

[c)] From slope of t-plot at t within 0.2-0.3 nm (p/p_o from 0.01-0.045) corresponds to supermicropores and mesopores.

[d)] From slope of t-plot at t within 0.50-0.63 nm (p/p_o within 0.35-0.57).

[e)] From pore filling at saturation (p/p_o>0.99).

[f)] Volume of the smallest micropores; from the intercept of the ordinate in the back extrapolation of the linear branch of the t-plots at t from 0.2-0.3 nm.

[g)] Volume of all micropores; by back extrapolation of the t-plots at t within 0.50-0.63 nm.

[h)] (V_{total}-V_{um+sm}).

[i)] 5 nm if formally calculated (beyond applicability of Stoeckli equation).

The widths of the micropores, L_{micro}, were estimated from the DR characteristic energy, E_0, following Stoeckli et al. [21]: $L_{micro} = 10.8 / (E_0 - 11.4)$ with E_0 in kJ mol^{-1} and L in nm.

The reaction conditions for cyclohexene hydrogenation in liquid phase were set in order to exclude external and internal diffusion limitations [22]. A static reactor was used, with the stirring of the reaction mixture sufficiently intensive to exclude external diffusion limitations. To minimize internal diffusion limitations, all catalysts were thoroughly ground in a mortar prior to the catalytic runs; a mean particle size of approximately 5 μm was thus established. All the activity data were obtained at 30% conversion of cyclohexene, as it provided a better accuracy of the measurement compared to the initial activity, taking into account a zero-order dependence of the rate on the concentration of organic substrate. The catalysts with different dispersion were prepared from platinum (IV) chloride by varying preparation conditions. In Figure 1, the dependence of activity on CO/Pt of samples prepared with variation of the regimes of adsorption, drying and reduction of the Pt catalysts and acidity of the solution values are presented.

A decrease in the adsorption time from 20 hour to 0.5 hour gives sometimes a decrease of the dispersion, obviously due to retention of the precursor near the external surface of the carbon particles. The most critical parameter is the flow rate of hydrogen during reduction. A higher rate is favorable of a higher metal dispersion, whereas moisture (reduction of wetted samples) has a strong detrimental effect [23]. The low-dispersed catalysts (CO/Pt < 0.2) are catalysts which were taken for reduction in a wet state or, alternatively, were pretreated in He at a high temperature. Electron microscopy confirmed formation of bulky metal particles in these cases (up to 10 nm and even more). The high-temperature treatment in He at 523 K is accompanied by reduction and agglomeration of platinum particles. Pt(II) species stabilized on the carbon surface after impregnation in acid solution and drying are reduced to zerovalent Pt even by thermal treatment of the dried samples with He at 523 K, which is evident from the results of TPR [23]. Autocatalytic reduction is faster than nucleation and thus rapid growth of nuclei on the carbon surface will occur. The resulting clusters are growing during reduction in hydrogen. The large crystallites will grow faster than small crystallites, as the rate of crystallite growth is proportional to its surface area [24]. The solution acidity also has an appreciable influence on the metal dispersion of Pt/C catalysts. Assuming that $PtCl_6^{2-}$ adsorption occurs due to electrostatic force between the ionic metal complex and the charge surface sites on the support, Pt chloride should be adsorbed on the cationic sites of the carbon surface. The low solution pH must favor this process. Acid adding to adsorption solution does increase the dispersion of platinum on active carbons [8].

Data on Figure1 show that the catalytic activity does not correlate with metal dispersion and the catalysts on different supports with the same dispersion of platinum differed in activity. An increase in dispersion of the metal supported on AR and Sib-SM carbons is not accompanied by an increase of the activity. These differences in activity were proved earlier [22] to can not be caused by the impurity factors or diffusion. This fact has been attributed to the blocking of metal particles in the pores of the support which makes the active component inaccessible to relatively large molecules of organic substrates. Such a blocking effect proved to be larger on the supports with smaller pores and for metal particles of high dispersion [7]. It has been just narrow pores and dispersed metal particles which have participated in blocking effect. The activity of the low-dispersed catalysts increased with their dispersion; however, the activity becomes inversely proportional to the dispersion for atomically-dispersed platinum particles (Figure 1).

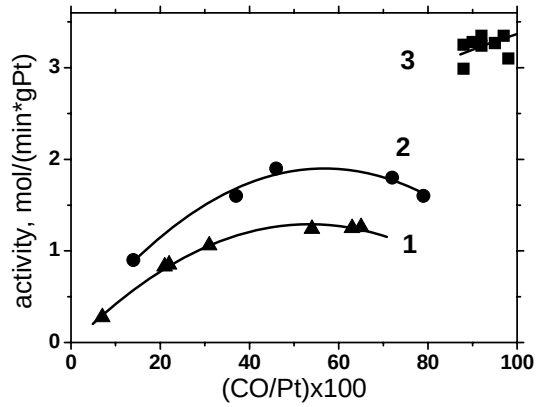


Figure 1. Catalytic activity in cyclohexene hydrogenation vs. apparent dispersion for 1.0 wt. % Pt/C samples with variation of adsorption time (0.5, 24 h), the duration and temperature of drying (300 K in air for 1h, or up to 520 K in He for 2 h), acidity of solution (0.01, 0.02 M NaOH, 0.09 M HCl), the flow rate of hydrogen (30, 200 cm^3/min/g).Carbons: 1 - AR, 2- Sib-SM, 3- Sib-M. Cyclohexene hydrogenation was carried out at 303 K and 1atm.

By a proper choice of the preparation conditions of the catalysts and pretreatments of the carbon surface, it was possible to decrease the blocking of platinum particles [23]. The blocking effect is reduced if the catalysts were prepared by adsorption from basic solution in particular [8]. The bulky particles are formed on the support after adsorption of platinum precursor and its reduction in flowing hydrogen. They can be localized only in wide pores, thus increasing the metal accessibility and weakening the blocking effect. TPR data witnesses for partial reduction of Pt(IV) after impregnation and drying. It was proposed that under basic medium the resultant product of partial reduction and hydrolysis of $PtCl_6^{2-}$ can be Pt(II) polyhydrocoxomplexes. The key factor for the given method of preparation is the concentration of added alkali. After adsorption in highly basic solutions (0.05M NaOH) and reduction in flowing hydrogen, highly dispersed particles are formed; however, a part of the active surface is lost because of the metal blocking.

3. HYDROLYSIS OF Pt(II) COMPLEXES

3.1. Kinetics of Hydrolysis

Literature data on the hydrolysis of Pt(II) are ambiguous, and this process was studied in the presence of background electrolytes and small concentrations of target complexes. The investigation of polynuclear hydrolysis products was limited to the statement of their existence. In this chapter the hydrolysis process of Pt(II) compounds at relatively large concentrations was explored by NMR spectroscopy, measurements of solution pH and optical transmission. ^{195}Pt, ^{17}O , ^{35}Cl, ^{133}Cs NMR spectra were recorded on a MSL-400 Brucker spectrometer at the frequencies of 85.9 MHz, 40.7 MHz, 29.4 MHz and 39.36 MHz, using natural isotope abundance. Chemical shifts (CS) were referenced to external standards, viz. H_2O (^{17}O) and salt solution containing cations in the infinite dilution limit. Concentration of Cl^- was determined by comparison of the amplitudes of ^{35}Cl NMR signals (free induction

decay) of the reference and studied samples, equal sample volumes and identical experimental parameters provided. Pt(II) chloride is kinetically inert, which allows us to study in detail the mechanism of hydrolytic transformations of mononuclear compounds at the initial stages of this process. Bands with δ_{Pt} =1615 and 1152 ppm in initial solutions of K_2PtCl_4 corresponds to $[PtCl_4]^{2-}$ complexes (main component) and $[PtCl_3(H_2O)]^-$. Adding small amount of alkali at ambient temperature has almost no influence on position of this bands but changes ^{17}O NMR spectrum. The band attributed to oxygen in $[PtCl_3(H_2O)]^-$ complexes shifts to downfield (from -86 to -72 ppm referenced to H_2O). These changes reflect a very rapid deprotonating of H_2O in Pt coordination sphere. Increasing alkali concentration (molar ratio $NaOH/K_2PtCl_4$ marked in the text as Z is equal to 2) and heating K_2PtCl_4 solution results in slow hydrolysis of mononuclear chloride complexes and formation of polynuclear hydroxochloride complexes. Bands were referenced to $[PtCl_4]^{2-}$ and $[Pt(OH)_4]^{2-}$ complexes prepared by K_2PtCl_4 heating with excess of HCl and NaOH, respectively. Other compounds were identified by the ratio of integral intensities in the spectra of the coordinated oxygen. The NMR data are summarized in Table 2. They are consistent to literature data [25]. Fig. 2 gives evolution of the Pt(II) concentration during hydrolysis of K_2PtCl_4. Increasing temperature increases the rate of stepwise hydrolysis. It is evident from Fig. 2 that Pt(II) complexes remain for long in its original mononuclear structure. It was difficult to control the heating and stirring of the samples. Nevertheless, total concentration of the complexes is equal to initial platinum concentration. Again, total concentration of individual Pt(II) complexes observed in ^{195}Pt NMR spectra coincides with total platinum concentration measured by the amplitude of free induction decay (curve $\sum_{Pt}$ on Fig. 2-A). This fact demonstrates that all Pt(II) complexes are detected in ^{195}Pt NMR measurements. After kinetics experiments at 308 K the solution was heated to 333 K. Pt concentration sharply decreases within 10 min. NMR signal of $[PtCl_2(OH)_2]^{2-}$ with δ_{Pt} = -859 ppm is simultaneously broadened. On the basis of ^{35}Cl NMR, the complexes undetected by ^{195}Pt NMR contain about 2 Cl^- ions per 1 Pt. This observation suggests that the polynuclear complexes (PHC) contain unsubstituted chloride ligands. The PHC formation is accompanied by the appearance of the two resonance peaks in the ^{133}Cs NMR spectra with δ= -24.3 and -21.7 ppm [26]. When all platinum is converted to PHC, these peaks disappears and new peak with δ= 17.6 ppm is observed. We can assume that there is a formation of compact crystalline structures accompanied by release of Cs^+ into the external solution.

Table 2. Chemical shift (δ) of the Pt(II) complexes in ^{17}O NMR and ^{195}Pt NMR spectra of K_2PtCl_4 solutions

Complex	Nucleus	δ, p.p.m.
$[Pt(OH)_4]^{2-}$	^{17}O	-102
$PtCl_3(OH)]^{2-}$	^{17}O	-72
$[PtCl_3(H_2O)]^-$	^{17}O	-86
$H_2[PtCl_6]$	^{195}Pt	0
$[PtCl_4]^{2-}$	^{195}Pt	-1615
$[PtCl_3(OH)]^{2-}$	^{195}Pt	-1152
$[PtCl_2(OH)_2]^{2-}$	–	-859
$[PtCl_3(OH)]^{2-}$	–	-463
$[Pt(OH)_4]^{2-}$	–	-204

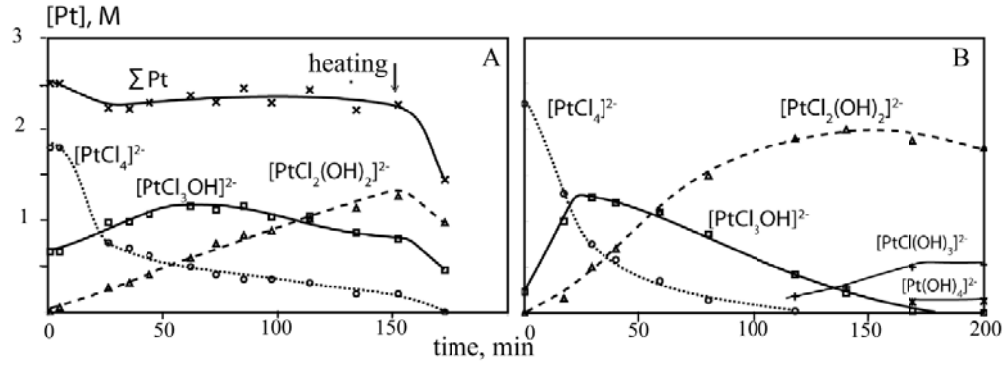


Figure 2. Evolution of hydrolysis products of $K_2[PtCl_4]$ according to ^{195}Pt NMR . Total concentration of Pt(II) 0.25 M, Z=2. A - hydrolysis temperature 308 K; B - hydrolysis temperature 318 K.

3.2. Mechanism of Formation of Pt(II) Polynuclear Complexes

Beginning of the PHC formation can hardly be determined by NMR and UV-spectroscopy. Abrupt increase of the edge absorption at higher wavelengths has been found to occur upon PHC formation. Light transmission is measured at wavelength 650 nm, supplied by the radiation of a laser. The high light intensity from this source makes possible measurements in the solution with very high optical density. Photodiode is used to detect optical signal.

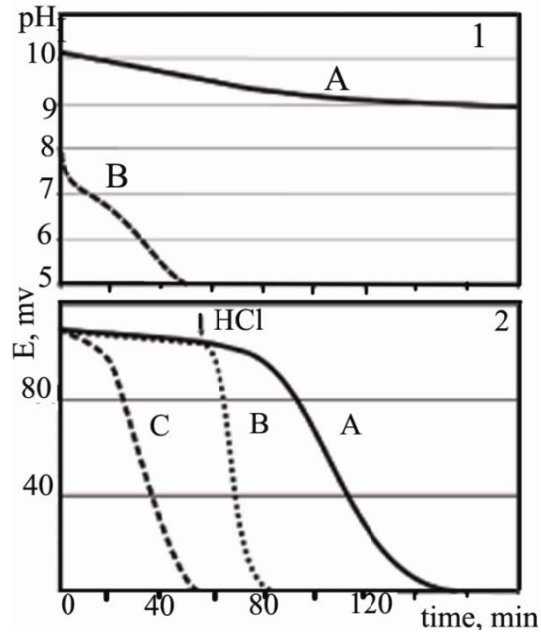


Figure 3. Evolution of pH (1) and photodiode potential (2) in hydrolysis of $K_2[PtCl_4]$. Concentration of Pt(II) 0.005 M, temperature of hydrolysis 328 K. A – without adding HCl, Z=2; B - HCl was added after the 65th min., Z=2; C – without adding HCl, Z=1.

A quantitative analysis of dependence of photodiode potential on solution parameters (particle size, concentration, etc.) does not enter into the scope of the present chapter. Further study is needed to establish the possibility of this method. This method has enabled the dependence of PHC formation on the temperature and acidity of the solution to be studied. Other physical method failed to make this due to their low sensitivity and long time required for measurements. The dependence of photodiode potential and pH on time of hydrolysis is presented in Figure 3. The potential jump is accompanied by gradual blackening solutions and at E ~ 10 mV the solution becomes intensely dark, almost opaque in the layer thickness of 0.5 cm. PHC is not precipitated within one weak.The acidity dependence on time is shown in Figure 3 (1). pH initially decreases from 10.3 to 9.3 (reaction time is about 90 min.) after the addition of alkali (Z=2). On the basis of NMR data on Figure 2, pH decrease indicates the formation of mononuclear hydroxochloride complexes from tetrachloride and aqua trichloride complexes of Pt(II). PHC formation is accompanied by a slight pH decrease (from 9.2 to 8.95 in the time interval from 90 min to 180 min). When all platinum is converted to PHC, acidity slowly increases by about 0.1unit per hour. The following scheme of hydrolysis of platinum (II) complexes can be suggested:

$$[PtCl_4]^{2-} + OH^- \rightarrow [PtCl_3(OH)]^{2-} + Cl^- \quad [1]$$

$$[PtCl_3(OH)]^{2-} + OH^- \rightarrow [PtCl_2(OH)_2]^{2-} + Cl^- \quad [2]$$

$$[PtCl_2(OH)_2]^{2-} + H^+ \leftrightarrow [PtCl_2(OH)\ H_2O]^- \quad [3]$$

$$[PtCl_2(OH)\ H_2O]^- + [PtCl_2(OH)_2]^{2-} \rightarrow [(OH)\ Cl_2Pt\text{-}O\text{-}PtCl_2(H_2O)]^{3-} + H_2O \quad [4]$$

$$[(HO)PtCl_2\text{-}O\text{-}PtCl_2(H_2O)]^{3-} + n[PtCl_2(OH)\ H_2O]^- \rightarrow \quad [5]$$

Stages 1 and 2 describe a stepwise substitution of inner sphere Cl^- ligands for OH^- . Their kinetics at room temperature with an excess of alkali were studied by ^{195}Pt NMR [25]. Li Wu et. al. observed only a slight decrease in the total concentration of Pt in solution and attributed this to hydrolysis of Pt(II) hydroxochloride complexes. Polymerization of the complexes led to some discrepancy between theoretical and experimental data on the concentration of mononuclear hydroxocomplexes. Rate constants were determined with a kinetic equation for successive reactions. A mixture of $[PtCl(OH)_3]^{2-}$ and $[Pt(OH)_4]^{2-}$ doped with $[PtCl_2(OH)_2]^{2-}$ was formed after the 10-day experiment. In the work cited a large excess of alkali inhibited the formation of mononuclear aquocomplexes (reaction 3). In this chapter there is no excess of alkali, as $Pt(OH)_2$ can be obtained at Z=2. Decreasing pH shifted the equilibrium 3 to the right. OH ligands are sufficiently strong complexing agents, which enter into substitution reaction by aquation [27]. Acidification of the solution is necessary for the latter reaction. Hydroxochloride complexes of Pt(II) resulting from hydrolysis are precursors for synthesis of oligomeric chains of PHC. Oligomerization does not occur at high pH values, even though the starting materials are already present in the solution. This led us to conclude that hydroxochloride complexes must be protonated for PHC formation (reaction 3). Reactions 4 and 5 describe the process of nucleation and growth of the chains and are accompanied by a slight decrease of pH (Figure 3(2), A). Detailed mechanism of substitution reaction in square

planar complexes is beyond the purpose of the present chapter. It is not improbable that the reaction 4 proceeds through a elimination of water and PHC grows through the attack of terminal fragment of PHC (-$PtCl_2(OH)$) by $[PtCl_2(OH)H_2O]^-$. The electroneutral protonated complex $[PtCl_2(H_2O)_2]^0$ is more likely to attack the growing chain.

The reactions 1-4 are slightly changed in this case. Main features described by these equations are preserved, namely, synthesis of mononuclear hydroxochloride complexes is accompanied by pH decrease, and the increase of proton concentration allows the formation of aquocomplexes participating in polycondensation. In addition to the above, it has been found that the induction period in the oligomerization reaction at Z=2 decreases with increasing temperature and the concentration of Pt(II). To test the proposed scheme of PHC formation, HCl solution was injected till neutral pH before oligomerization. Fig. 3(2), B shows the evolution of light transmittance. HCl injection results immediately in PHC formation. The more complete the synthesis of monomeric hydroxocomplexes, the more rapid oligomerization after adding HCl. In order to verify the unit of PHC chain -$(PtCl_2O)$-, the hydrolysis product at Z=1 has been studied. For the synthesis of PHC to occur the hydroxocomplex with one OH^- ligand must be present in the solution. $[PtCl_3(H_2O)]^-$ is formed immediately after the dissolution of $K_2[PtCl_4]$, while an increase of pH rapidly results in its deprotonation to $[PtCl_3(OH)]^{2-}$. The PHC would thus be expected to be formed even in acidic solutions after the substitution of one ligand to OH. pH of $K_2[PtCl_4]$ solution increases immediately after adding alkali (pH of 0.005 M solution is equal to 3). Then pH decreases from 7.8 to 5 (Fig. 3(1), C). The PHC starts to form after 20 min. Pause may be attributed to the final formation of complexes with O-ligands, which are structure unit of PHC. To describe the reactions at Z=1 the equation 1 - 5 should be corrected according to the new ligand composition of the solutions:

$$[PtCl_4]^{2-} + OH^- \rightarrow [PtCl_3(OH)]^{2-} + Cl^- \quad [6]$$

$$[PtCl_3(OH)]^{2-} + H_2O \leftrightarrow [PtCl_2(OH)\,H_2O]^- + Cl^- \quad [7]$$

$$[PtCl_3(OH)]^{2-} + [PtCl_2(OH)\,H_2O]^- \rightarrow [Cl_3Pt\text{-}O\text{-}PtCl_2(H_2O)]^{3-} + H_2O \quad [8]$$

$$[Cl_3Pt\text{-}O\text{-}PtCl_2(H_2O)]^{3-} + n[PtCl_2(OH)H_2O]^- \rightarrow$$
$$\rightarrow [PtCl_3\text{ -O- }(PtCl_2O)_n\text{ - }PtCl_2(H_2O)]^{(2n+3)-} + nH^+ + H_2O \quad [9]$$

The release of protons may account for pH decrease during the process of oligomerization (Fig. 3(1), C). Chain breakage can be represented by equations:

$$[PtCl_3\text{ -O- }(PtCl_2O)_n\text{ - }PtCl_2(H_2O)]^{(n+3)-} + Cl^- \rightarrow$$
$$[PtCl_3\text{ -O- }(PtCl_2O)_n\text{ - }PtCl_3]^{(n+4)-} + H_2O \quad [10]$$

When growth of the chain is blocked, the negative charge in the active terminal groups increases. Their reaquation can be sterically and diffusionly hindered, if the potentially active groups are involved in the chain. Thus, Cl^- ions block the chain growth as indicated by appearance of two forms of the cations Cs^+ and by a decrease of the Cl^- concentration in the external solution according to ^{35}Cl NMR spectra [26]. Chloride, aquochloride and

mononuclear hydroxochloride complexes of Pt(II) may also participate in the chain breakage as their concentration is comparable to that of Cl^- ions.

4. Pt/C Catalysts Prepared from the Hydrolysis Products of Chloride Pt(II). Effect of the Molar Ratio $NaOH/K_2PtCl_4$ on Metal Dispersion and Activity in Cyclohexene Hydrogenation

In the case of Sib-SM carbon, a number of catalysts have been prepared with variation of metal precursor. Presented in Figure 4, curve 1 are the data on activities and metal dispersion for Pt catalysts which were prepared from platinum (IV) chloride with variation of the regimes of drying and reduction. An increase in dispersion of the metal is not accompanied by an enhancement of the activity. The samples prepared from product of Pt(II) chloride hydrolysis (Figure 4, curve 2) exhibit higher activity comparing with Pt(IV) chloride in the range of high CO/Pt values. A variation of molar ratio of $NaOH/K_2PtCl_4$ and time of hydrolysis has been undertaken. The activity of the samples with different dispersion linearly increases with CO/Pt uptakes.

The effect of molar ratio $NaOH/K_2PtCl_4$ (Z) on activities of the samples prepared from Pt(II) chloride is shown in Figure 5. The activities of Pt/AR samples increase with increasing $NaOH/K_2PtCl_4$ molar ratio from 0 to 1 (Figure 5, curve 1).

The TEM data on Pt prepared from Pt(II) chloride show an uniform distribution of metal. In this case individual particles in atomically-dispersed state with the size about 1 nm are seen in electron micrographs. The electron micrographs of the Pt particles supported on AR are given on Figure 6-A, as the example of Pt prepared from Pt(II) chloride. The surface average metal particle size is equal to 1.7 nm and calculation by formula $D(\%) = 108/d_s$ (nm) [28] in which d_s indicates surface average size, gives Pt dispersion 62%.

The TEM data indicate that the average particle size of Pt/AR prepared from product of Pt(II) chloride precursor is larger than that of Pt/AR prepared from Pt(II) chloride. As clearly seen from Figure 6-B, Pt particles located on AR have a narrow range size from 2 to 3 nm. The surface average metal particle size is equal to 2.6 nm, and calculation by the above mentioned formula gives Pt dispersion 41%. Hence the increase of activity per mass of metal is not due to increase of metal dispersion. Mononuclear chloride complexes of Pt(II) and Pt(IV) can penetrate into the narrow pores of carbons, resulting in a decrease of metal accessibility. The loss of a great part of the catalytically active surface due to metal blocking appeared to result in the poor catalytic activity.

As shown in Sec. 3.2, platinum (II) chloride is hydrolyzed in alkaline solution forming polyhydroxocomplexes. The oligomeric chains can be localized only in wide pores due to their increased size. Under such circumstances, the accessibility of an active component to organic substrate and the activity of catalysts should increase. The concentration of bulky polyhydroxocomplexes in adsorption solution and metal accessibility is likely to increase with increasing Z from 0 to1.

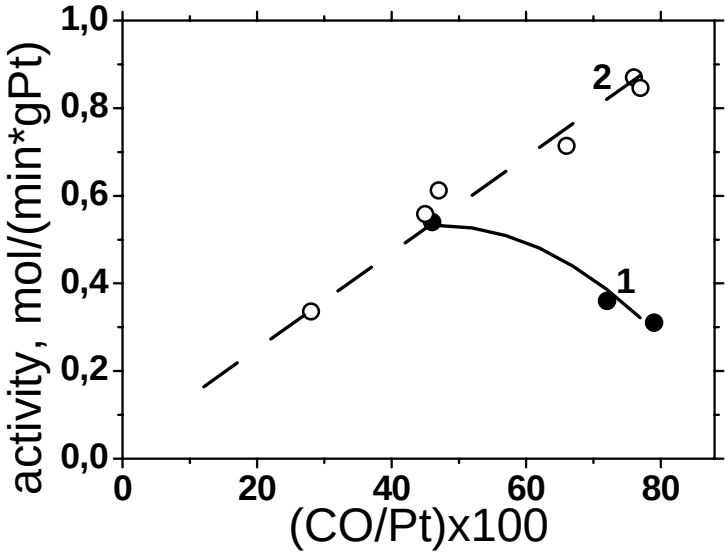


Figure 4. Catalytic activity in cyclohexene hydrogenation vs. apparent dispersion for Pt/Sib-SM samples prepared from different precursor:1 - platinum (IV) chloride with variation of duration and temperature of drying (300 K in air for 20 hour, or up to 523 K in He for 2 hour), mode of heating in hydrogen (step-wise or immediately to 523 K); 2- product of hydrolysis of Pt(II) chloride with variation of Z (1-3), time of hydrolysis (0.2-1 hour). Temperature of hydrolysis 328 K, adsorption time for 24 hour, drying at ambient conditions, step-wise reduction first to 423 K for 1 hour, then to 523 for 1 hour, hydrogen flow rate 200 cm^3/min/g. Cyclohexene hydrogenation was carried out at 273 K and 1 atm.

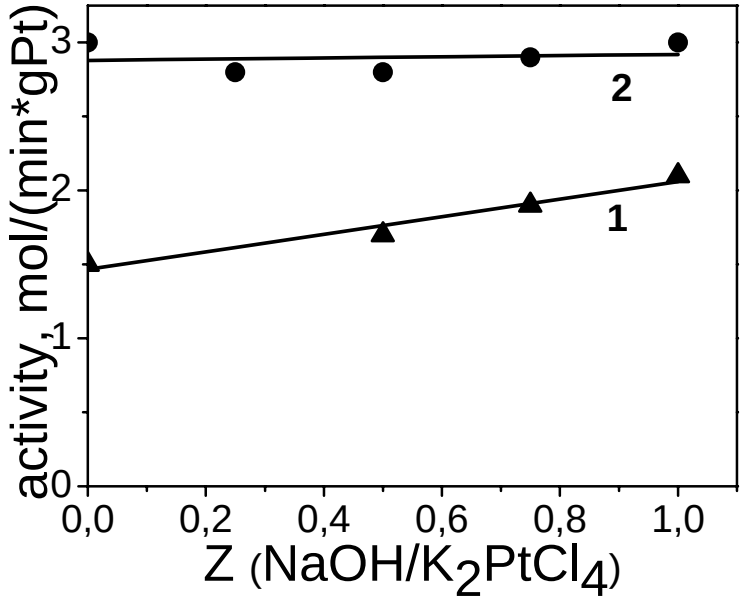


Figure 5. Catalytic activity in cyclohexene hydrogenation vs. molar ratio $NaOH/K_2PtCl_4$. Carbons: 1-AR , 2-Sib-M. Temperature of hydrolysis 328 K, time of hydrolysis 0.3 hour, adsorption time for 24 hour, drying at ambient conditions, step-wise reduction first to 423 K for 1 hour, then to 523 for 1 hour, hydrogen flow rate 200 cm^3/min/g. Cyclohexene hydrogenation was carried out at 303 K, 1 atm.

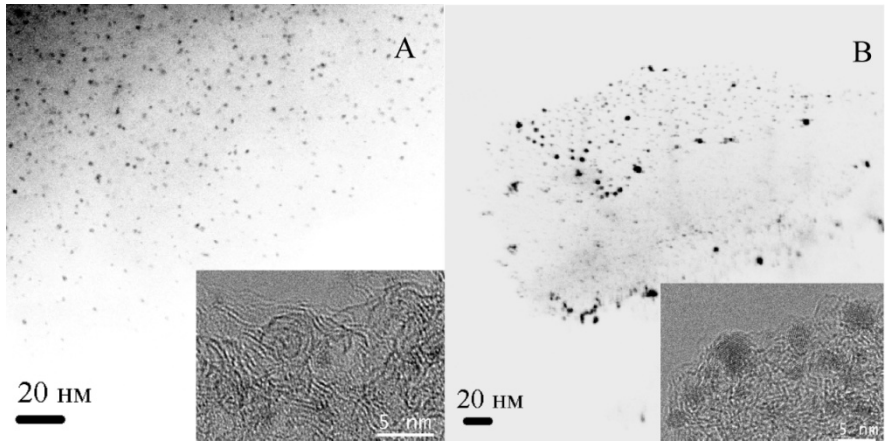


Figure 6. Micrographs of 1.0 wt. % Pt/AR prepared from platinum (II) chloride (A) and product of hydrolysis of Pt(II) chloride (B). Preparation conditions are the same as in Fig. 5.

The effect of NaOH/ K_2PtCl_4 molar ratio on the catalyst activity depends on the support (Figure 5). The differences in catalyst properties are assigned to the influence of the porous structure of the supports. The supports do differ considerably in their porosity, as is clearly seen from L, S and V values in Table 1. The effect of Z proved to be the higher for platinum on AR, which possesses narrow pores. We have thus to assume that the narrower the pores are in the support, the higher is the probability of inaccessibility of the metal particles to the relatively bulky organic substrate in the catalytic process. Table 3 lists data on the activities of the samples prepared from H_2PtCl_6 and product of Pt(II) chloride hydrolysis on different carbons. The catalysts were tested in initial state (IS) and after standard grinding in mortar (GS). Additionally grinding of the Pt catalysts affects the absolute values of activity, whereas it leaves the order of activities for the catalysts on different supports and from different precursor unchanged. Typically, the reaction rates for the additionally crushed and the non-ground catalysts differ by a factor of 1.5-2.5 for catalysts prepared on a <100 μm fraction of the carbons but the difference could reach an order of magnitude for catalysts obtained on coarse-grained supports [22]. The crushed and the non-ground Pt/Sib-M catalysts prepared from H_2PtCl_6 differ in activity by a factor of 3.3, but the ratio of the activities GS/IS falls to 1.8 for product of Pt(II) chloride hydrolysis.

Table 3. Activity in cyclohexene hydrogenation of the catalysts prepared from H_2PtCl_6 and product of K_2PtCl_4 hydrolysis (PHC) on coarse-grained fractions of the carbons and tested both in the initial state (IS) and after the standard grinding (GS)

Precursor	Activity, mol/(min*g Pt)		
	GS	IS	GS/IS
AR			
H_2PtCl_6	2.0	0.5	4.0
PHC	2.1	0.8	2.6
Sib-M			
H_2PtCl_6	2.7	0.9	3.3
PHC	2.8	1.6	1.8

Such a decrease of GS/IS ratio is likely to be caused by an eggshell distribution of active component on the support grain. Electron microscopy witnesses for location of platinum particles on exterior surface of the support grain. The crystallite size and distribution of precious metals on activated carbon catalysts play a key role in achieving high activity and selectivity. This is especially evident in reactions with larger molecules at ambient temperatures and pressures. The eggshell catalyst distribution maximizes the effective utilization of the active component.

CONCLUSION

The present work confirms the substantial influence of the metal precursor on the dispersion and activity in cyclohexene hydrogenation of the Pt/C catalyst. The activity in cyclohexene hydrogenation which is structure-insensitive reaction does not follow the dispersion of the Pt particles located on microporous carbons. Localization of active component in narrow pores makes a part of the supported metal inaccessible to the reagents in the catalytic reaction, thus resulting in a decrease of catalytic activity. The extent of the blocking proves to be larger on the supports with smaller pores and for metal particles of small size. Not only the specific activity but also the activity per total mass of supported metal can become lower at too high dispersions of the metal. The activity increases if the catalysts have been prepared from product of Pt(II) chloride hydrolysis. Bulky polyhydroxocomplexes can be localized only in wide pores, thus increasing the metal accessibility and weakening the blocking effect. The effect of precursor proved to be larger on the supports with smaller pores. The use of different spectroscopic techniques allowed us to study the products and kinetics of alkali hydrolysis of Pt(II) chloride. Increasing pH results in consecutive inner sphere substitution of chloride ligands. Induction period for PHC formation increases with increasing molar ratio of $NaOH/K_2PtCl_4$. For Pt(II) to be completely precipitated in the wide range of Pt(II) concentration (0,01 - 0,2 M), an one mole of OH per mole of Pt(II) must be introduced. The beginning of the PHC formation is hard to observe by NMR and UV-visible spectroscopy, since oligomerization of complexes begins abruptly. Based on the measurements of optical transmission (650 nm) and pH of the solutions, the formation of PHC has been found to be accompanied by the appearance of light-scattering cluster at nearly constant solution acidity.

ACKNOWLEDGMENTS

The author wishes to thank Dr. V.I. Zaikovskii for investigation of the catalysts by TEM and Prof. M.A. Fedotov for his help in NMR experiments.

REFERENCES

[1] Auer, E.; Freund, A.; Pietsch, J.; Tacke, T. *Appl. Catal. A* 1998, 173, 259-271.

[2] Freifelder, M. *Practical Catalytic Hydrogenation*; Wiley-Interscience: New York, NY, 1971.

[3] Yu, X.; Ye, S. J. *Power Sources* 2007, 172, 133-144.

[4] Fuente , A.M.; Pulgar, G.; Gonzalez, F.; Pesquera, C., Blanco, C. *Appl. Catal. A* 2001, 208, 35-46.

[5] Roman-Martinez, M.C.; Cazorla-Amoros, D.; Linares-Solano, A.; Salinas-Martinez de Lecea, C. *Carbon* 1995, 33, 3-13.

[6] Verde, Y.; Alonso, G., Ramos, V., Zhang, H.; Jacobson, A. J.; Keer, A. *Appl. Catal. A* 2004, 277, 201-207.

[7] Okhlopkova, L.B.; Lisitsyn, A.S.; Likholobov, V.A.; Gurrath, M., Boehm, H.P., *Appl. Catal*. A 2000, 204, 229-240.

[8] Okhlopkova, L.B. *Appl. Catal.* A 2009, 355, 115-122.

[9] Radovic, L.R.; Rodriguez-Reinoso, F. In *Chemistry and Physics of Carbon*; Thrower, P.A.; Ed.; vol. 25, Marcel Dekker: New York, NY, 1997; pp. 243-358.

[10] Jin, H.; Park, S.-E.; Lee, J. M.; Ryu, S. K. *Carbon* 1996, 34, 429-432.

[11] Landau, M. V.; Kogan, S.B.; Tavor, D., Herkowitz, M.; Koresh, J. E. *Catal. Today* 1997, 36, 497-510.

[12] Torres, G. C.; Jablonski, E. L.; Baronetti, G. T.; Castro, A. A.; De Miguel, S. R.; Scelza, O. A.; Pena Jimenez, M. D.; Fierro, J. L. G.; *Appl. Catal. A 1997*, 161, 213-226.

[13] Job, N.; Ribeiro Pereira, M. F.; Lambert, S.; Cabiac, A.; Delahay, G.; Colomer, J.-F.; Marien, J., Figueiredo, J. L., Pirard, J.-P. *J. Catal*. 2006, 240, 160-171.

[14] Vilella, I.M.J.; de Miguel, S.R.; Scelza, O.A. *Chem. Eng. J.* 2005, 114, 33-38.

[15] Brazi E., Cordier G., Sauvion G. N. In *New Frontiers in Catalysis*, Proceedings of the 10th International Congress on Catalysis, 19–24 July, 1992; Guczi, L.; Solymosi, F.; Tetenyi, P.; Elsevier: Amsterdam, 1993; pp. 2459-2562.

[16] Suh, D. J.; Park, T.-J; Ihm S.-K. *Ind. Eng. Chem. Res*. 1992, 31, 1849-1856.

[17] De Miguel, S.R.; Viella, Y.I.; Jablonski, E.L.; Scelza, O.A.; Salinas-Martinez de Lecea C.; Linares-Solano, A. *Appl. Catal. A* 2002, 232, 237-246.

[18] Boudart, M. *J. Mol. Catal.* 1985, 30, 27-38.

[19] Surovikin, V.F.; Plaksin, G.V.; Semikolenov, V.A.; Likholobov, V.A.; Tiunova, I.Yu. US Patent 4 978 649, 1989.

[20] Sing, K.S.W., *Carbon* 1989, 27, 5-11.

[21] Stoeckli, H.F.; Rebstein, R.; Ballerini, L. *Carbon* 1990, 28, 907-909.

[22] Okhlopkova, L.B.; Lisitsyn, A.S.; Boehm, H.P.; Likholobov, V.A. *React. Kinet. Catal. Lett*. 2000, 7, 165-171.

[23] Okhlopkova, L.B.; Chuvilin, A.L. *Current Issues in Organic Chemistry; Hadjiivanov*, K.; Valtchev, V.; Mintova, S.; Vayssilov, G., Heron Press: Sofia, 2010, pp. 59-69.

[24] Van Dam, H. E., van Bekkum, H. *J. Catal.* 1991, 131, 335-349.

[25] Li Wu; Schwederski B.E.; Margerum D.W. *Inorg. Chem*. 1990, 29(29), 3578-3584.

[26] Troitskii, S.Yu.; Fedotov, M.A.; Kochubei, D.I.; Novgorodov, B.N.; Chuvilin, A.L.; Likholobov, V.A. *J. Sruct. Chem*.(USSR) 2007, 48(1), 144-149.

[27] Grinberg A.A. *Introduction to the chemistry of complex compounds*; Chemistry: Leningrad, 1971, pp. 457–468.
[28] Anderson, J.R. *Structure of Metallic Catalysts*; Academic Press: London, 1975.

In: Activated Carbon
Editor: James F. Kwiatkowski
ISBN: 978-1-61209-684-1
©2012 Nova Science Publishers, Inc.

Chapter 14

PLANTING SOYBEAN IN CD-, CU-, OR ZN-CONTAMINATED SOILS TO ASSESS ITS FEASIBILITY IN FURTHER PRODUCING BIODIESEL

Hung-Yu Lai [1*], Bo-Ching Chen[1], Hsuen-Li Chen [2], Chih-Jen Lu [2] and Zueng-Sang Chen [3]

[1] Department of Post-Modern Agriculture, MingDao University; No.369, Wenhua Rd., Peetow, Changhua 52345, Taiwan

[2] Department of Environmental Engineering, National Chung-Hsing University; No. 250, Kuo Kuang Rd., Taichung 40227, Taiwan

[3] Department of Agricultural Chemistry, National Taiwan University; No.1, Roosevelt Rd., Taipei 10617, Taiwan

ABSTRACT

There are many farmlands been contaminated with heavy metal (HM) in central Taiwan resulted from the irrigation using river water contaminated with HMs. According to the Soil and Groundwater Pollution Remediation Act (SGWPR Act) of Taiwan, these lands can not planting edible crops until suitable techniques are conducted to decrease the total concentration of HM in soils to conform to the Soil Control Standard (SCS). However, some of the foliar crops still accumulated high concentration of HM in the edible parts even the concentration of HM of the remediated sites is below the SCS. Planting suitable crop species is especially important in this situation and these contaminated sites after remediation can be reused. Soybean, a biomass crop further used to produce biodiesel, seems feasible to plant in the farmlands in this situation. This manuscript reports previous results used pot experiments to investigate the accumulation of HM by various parts of soybean planted in the artificially cadmium- (Cd-), copper- (Cu-), or zinc (Zn-) contaminated soils with different concentrations. The aim is to assess the feasibility of planting soybean in the HM-contaminated soils to produce biodiesel.

Keywords: biodiesel, heavy metal, Soil Control Standard (SCS), soybean.

* E-mail: soil.lai@mdu.edu.tw

1. INTRODUCTION

1.1. Heavy Metal Contamination in Formerly Taiwan (Chen, 1991)

The most famous heavy metal (HM) pollution event was first happened on the paddy farmlands in northern Taiwan irrigated with illegal wastewaters discharges from two chemical plants which produced the stabilizing materials for plastics. The total contaminated area was approximate 100 ha. Soil samples in the two plants were collected and analyzed for the cadmium (Cd) and lead (Pb) in different fractions and 0.1 N HCl extractable concentrations. The root, stem and leaf, hull, and grain (or brown rice) parts of the rice plants and the irrigation water were sampled near the polluted area. The concentration of Cd and Pb in soils most close to the chemical plants were higher relative to other regions and was in the levels of 180 to 378 mg kg^{-1} and 352 to 3,145 mg kg^{-1}, respectively. The Cd predominantly existed in the exchangeable fraction (27-47% of total) and organic matter bounded fraction (28-40% of total). Soil texture affected the distribution of Pb in the contaminated sites and it existed in the order of residual fraction (28-48% of total), free Fe and free Mn fraction (28-31% of total), and exchangeable fraction (16-28% of total).

Analytic results of rice samples show that about 88% of total Cd uptake and 70% of total Pb uptake occurred in the roots. Although the content of Cd in the brown rice is low (ranged from 0.50 to 7.94 mg kg^{-1}), it still exceeded the forward threshold (0.5 mg kg^{-1}) and current threshold (0.4 mg kg^{-1}g) adopted by the Department of Health of Taiwan. The concentration of Pb in the brown rice grown in polluted region is not detectable which indicates that Pb is difficult to transport from root to the brown rice.

1.2. Survey of HMS-Contamination Farmlands in Taiwan

The total area of farmlands in Taiwan is approximately 850,000 ha. Since 1982, four stages of survey have been conducted by the Environmental Protection Administration of Taiwan (Taiwan EPA). The objective is to understand the HM contamination of farmlands in Taiwan (Taiwan EPA, 2010).

- Stage one (1983-1987): Each representative survey unit is 1,600 ha. According to the survey result, more than 300,000 ha of farmlands were contaminated with HMs.
- Stage two (1987-1991): Each representative survey unit is 100 or 25 ha. The results showed that about 50,000 ha of farmlands were contaminated with HMs potentially.
- Stage three (1992-2000): The survey lands were selected according to the results of stage two which have relatively high concentration of HMs in soil. Each representative survey unit was 1.0 ha. There were approximately 950 ha of farmlands been contaminated with HMs. Most of them were located in the central and northern Taiwan and mainly contaminated with chromium (Cr), copper (Cu), and zinc (Zn).
- Stage four (2000 to 2008): This stage was conducted following the Soil and Groundwater Pollution Remediation Act (SGWPR Act) announced in 2000. The control sites or remedial sites were announced based on the criteria Soil Control Standard (SCS) in the SGWPR Act.

Taiwan EPA reported that the areas of contaminated rural soil, which higher than the SCS, based on the results of 319 ha rural soil survey in 2002, were 159 ha of nickel- (Ni-) contaminated soils, 148 ha of Cu-contaminated soils, 127 ha of Cr-contaminated soils, 113 ha of Zn-contaminated soils, 17 ha of Cd-contaminated soils, 4 ha of Pb-contaminated soils, and 0.3 ha of mercury- (Hg-) contaminated soils. Moreover, the total areas of contaminated rural soil were about 251 ha (Taiwan EPA, 2010).

1.3. Remediation of HMs-Contaminated Soils in Taiwan

If the concentrations of contaminants exceed the SCSs the contaminated site is announced as a "control site" according to the SGWPR Act (Taiwan EPA, 2010) (Figure 1). The polluter must then provide a control plans and take necessary actions to avoid the expansion of contaminants. A “remediation site” is announced if the control site posing a threat to public health and environment after going through set assessment procedures. At such time, the polluter will be required to provide a remediation plan to decrease the concentrations of pollutants in the contaminated site to below the SCSs. A flexible remediation target according to risk assessments will be set if there is no way to treat a site to below SCSs due to the limitations of geographic nature, unique character of the pollutant, or remedial technologies. In addition, if the source of contamination is unclear, but pollutant concentrations exceed SCSs, the implementation of control or remedial procedures will be implemented by the proper government authority as the same as described above. According to the SGWPR Act, eight HMs were used as the target contaminants. Total concentrations of arsenic (As), Cr, Cd, Cu, Hg, Ni, Pb, and Zn in soils digested by aqua regia were used as the thresholds in determining contamination. Soil turnover and acid washing were the two most used techniques to decrease the total concentration of HMs in soils in Taiwan.

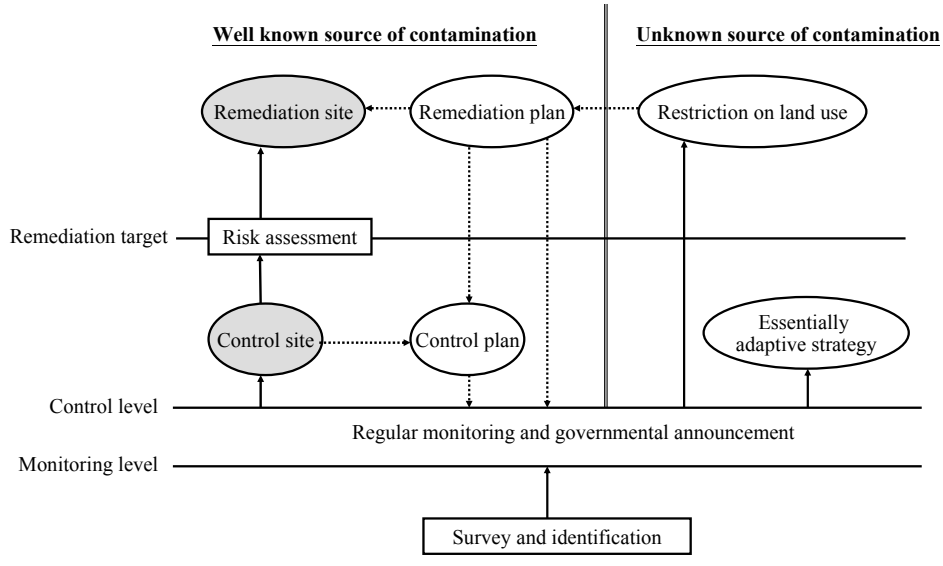


Figure 1. Management and remediation approach for HM-contaminated sites in Taiwan according to SGWPR Act.

Because the soils in upper layer always have lower concentration of HM compared with that in the deeper layer, vertical mixture of them can efficiently reduce the total concentration of HM in soils. Soil turnover with the advantage of lower cost and easy to operation, it was used to treat approximately 250 ha of the HM-contaminated farmlands in Taiwan. However, the farmlands after treating with the two techniques may deficient in organic matters (OMs) and essential nutrients. The HM-contaminated soils after acid washing have lower pH values which are not suitable for the growth of most crops. Suitable practices should be further conducted to adjust the soil pH and to increase the contents of OMs and nutrients

2. ACCUMULATION OF HM BY SOYBEAN GROWN IN HM-CONTAMINATED SOILS

Leafy vegetables are high accumulators compared to non-leafy vegetables (Podlesáková et al., 2001). The bioconcentration factor (BCF is the ratio of shoot HM concentration to soil HM concentration) of Cd of pak choi, a most consumed leafy vegetable in Taiwan, was in the levels of 2.1 to 5.5 (Chen et al., 2010a; Chen et al., 2010b). For lettuce grown in Cd-spiked soils, the BCF values were between 1.9 and 2.2 (Podlesáková et al., 2001). In previous cases, even the total concentration of Cd in farmland was below the SCS (5.0 mg kg^{-1}) of SGWPR Act, some varieties of rice still accumulated more than 0.5 mg Cd kg^{-1} in their brown rice (Römkens et al., 2009). In able to reuse the HM-contaminated farmlands and also to produce non-harmful vegetables, non-leafy vegetable is a better choice. Beans of soybean can further used to produce biodiesel and its agricultural management is mature. Seeds of soybean were sowed in artificially and potted Cd-, Cu, or Zn-contaminated soils to assess their accumulation in different parts, especially for bean.

2.1. Pot Experiment

Soil samples were collected in a HMs-contaminated site in central Taiwan. After air drying, soil samples were ground and screened with stainless steel sieves (10 or 80 mesh). The basic characteristics analyzed namely soil water content (Gardner, 1986), texture (Gee and Bauder, 1986), pH value (Thomas, 1996), organic carbon content (OC) (Nelson and Sommers, 1982), and the total concentration of HMs. Texture of the used soil is silty clay (sand 8.80%, silt 50.9%, clay 40.3%) with slight acidity (pH 6.20) and moderate content of OC (2.52%). Appropriate volume of solutions of $Cd(NO_3)_2{\cdot}4H_2O$, $ZnSO_4{\cdot}7H_2O$, or $CuSO_4$ were added to the soil samples according to their initial concentrations to make their final concentrations (mg kg^{-1}) as Cd-5, Cd-20, Zn-1000, Zn-2000, Cu-200, and Cu-400 (coded as HM-concentration). Approximately 2.5 kg of artificially HM-contaminated soil samples were added in each pot (16 cm diameter and 20 cm height) and sowed five seeds of soybean (*Glycine max* L.). Pot experiment was conducted in the phytotron (day/night = 30 ℃/25 ℃) located in MingDao University with three replicates. Water content of soil was controlled at 50-70% of field capacity by weighting and adding DI water every 2-3 days. Soybeans were sampled after growing for 75 days, separated into different parts (root, shoot, pod, and bean) and rinsed with DI water. After oven drying at 65 ℃ for 72 hours, plant tissues were digested

by mixture solution of concentrated $HNO_3/HClO_4$ (v/v = 87/13). Soil samples after pot experiment were collected, air dried, ground, and then passed through stainless steels (10 or 100 mesh). Soil samples passed through a 100 mesh sieve were digested by aqua regia to determine their total concentrations of HMs. The available concentrations of HMs in soils pass through 10 mesh stainless sieves were extracted by 0.1 M HCl or DI water. The concentrations of Cd, Cu, or Zn in the digestant or extracting solutions were determined with a flame atomic absorption spectrometer (FAAS; Perkin Elmer AAnlyst 200).

2.2. Accumulation of HM by Soybean

The target concentrations of Cd, Cu, and Zn in artificially spiked soils were set according to the SCSs of SGWPR Act. After pot experiment, the total and extractable concentrations of Cd, Cu, and Zn in soils are shown in Table 1. Except for Zn, the final concentrations of HMs in soils were in the levels of 85-125% to the target concentration. Approximately 70-100% of the spiked HMs can be extracted by 0.1 M HCl.

Table 1. Concentration of Cd, Cu, or Zn in soils digested by aqua regia or extract by 0.1 M HCl and deionized water (DI water)

	Concentration in soil (mg kg^{-1})		
	Aqua regia	0.1 M HCl	DI water
	Cd		
CK	0.80±0.26	0.50±0.09	ND*
Cd-5	6.27±0.36	4.87±0.07	ND
Cd-20	19.4±0.5	18.9±0.2	0.02±0.03
	Cu		
CK	50.0±0.8	47.0±2.5	ND
Cu-200	210±13	151±5	ND
Cu-400	340±10	258±9	0.05±0.05
	Zn		
CK	202±2	94.8±1.4	0.07±0.05
Zn-1000	1271±41	884±19	19.9±2.0
Zn-2000	3,135±166	2,583±81	480±79

* ND: not detectable

Similar to that reported by Jung and Thornton (1996), the accumulation of Cd in the different parts of soybean increased when the Cd concentrations in soils increased. Different parts of soybean accumulated less than 3.0 mg kg^{-1} in Cd-CK because of the low Cd concentration in soil (0.80±0.26 mg kg^{-1}). However, the Cd concentrations were in the levels of 9.0 to 220 mg kg^{-1} in the treatment of Cd-20 (Figure 2). The Cd concentration accumulated in the different parts of soybean was in the decreasing order of root, shoot, pod, and bean. Roots of soybean accumulated more than 4-fold of Cd concentration compared with shoots, pod, and beans. Experimental result shows that the soybean did not accumulated Cd in its bean when growing in Cd-5 (6.27±0.36 mg Cd kg^{-1}). Planting soybean in Cd-5 will not produce Cd-contained beans and the other parts can accumulate more than 5.0 mg kg^{-1}.

The shoots of soybean can remove Cd from contaminated soils and the produced beans can be used to produce biodiesel when it is planted in soils contain less than 6.0 mg Cd kg^{-1}.

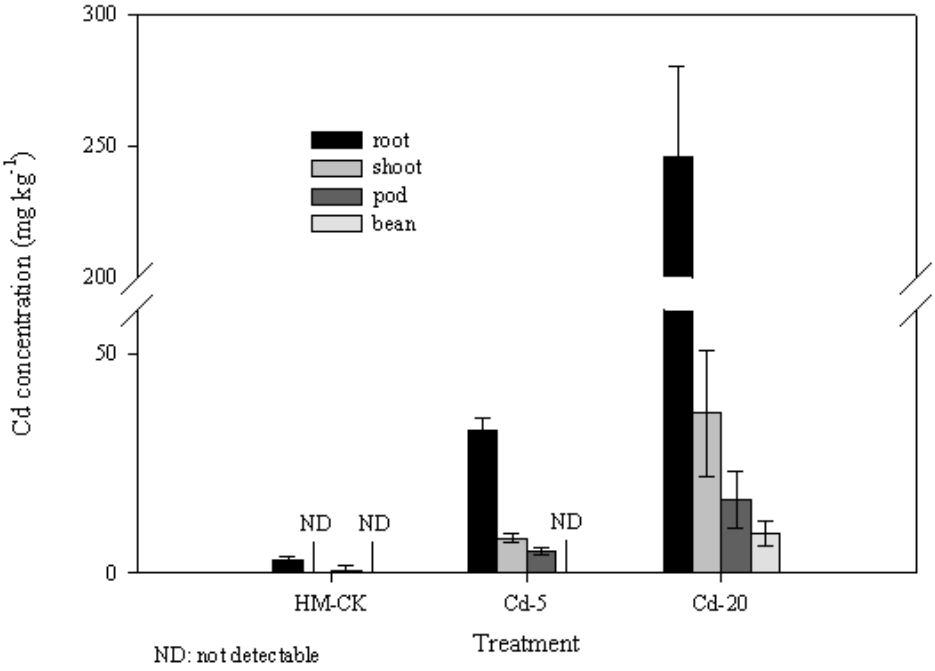


Figure 2. The accumulation of Cd by various parts of soybean grown in artificially Cd-contaminated soils with different concentrations (Replicated (n) = 3).

Similar to the experimental result of Cd, roots of soybean accumulated higher concentrations of Cu compared with other parts (Figure 3). Copper is an essential element for health of the plants and for the nutrient supply to animals. Its content in plant shoots did not often exceed 20 mg kg^{-1}, which is often considered to indicate the threshold of exceed contents (Kabata-Pendias and Pendias, 2001). Less than 25 mg Cu kg^{-1} was accumulated in the bean of soybean, but were not detectable in the shoot and pod for most of the treatments. The experimental result is in agreement with the foregoing reference. Because the total Zn concentration in Zn-2000 was 1.6-fold higher than the target concentration, seeds of soybean after sowing did not germinate at all. In the treatment of Zn-1000, roots of soybean accumulated the highest concentration of Zn compared with other parts (Figure 4). The concentrations of Zn in the roots, shoots, and pod were in the levels of 900-2,200 mg kg^{-1}, which is more than three times of that in the beans. The toxic critical concentration of Zn in the plants is reported to be 150-200 mg kg^{-1} for sensitive plants and 300-400 mg kg^{-1} for young barley and oats. However, the critical concentration of Zn in roots tissues is mulch higher because Zn is immobilized in cell walls (Kabata-Pendias and Pendias, 2001). Experimental result of this study is in agreement with foregoing reference and the Zn concentration in roots is 1.3-fold than that in the shoots. The toxic critical concentration of Zn in the shoot of soybean may higher than 1,500 mg kg^{-1} because no toxic symptom was observed during pot experiment.

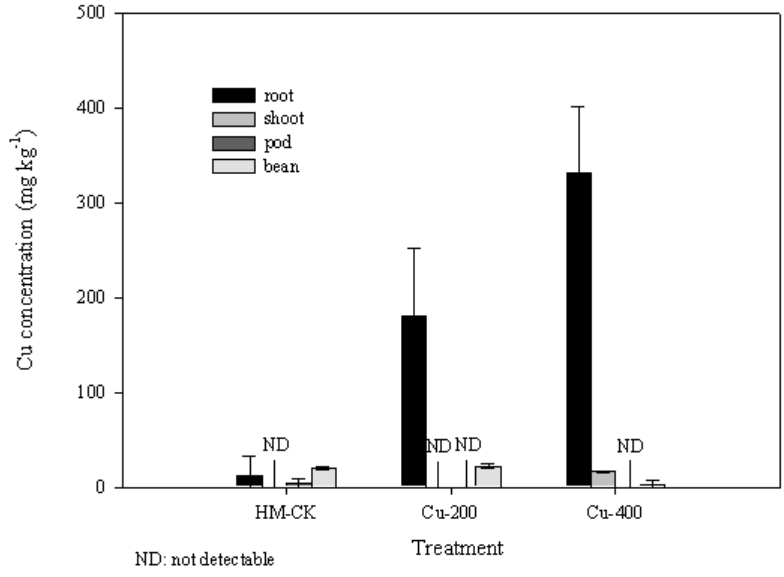


Figure 3. The accumulation of Cu by various parts of soybean grown in artificially Cu-contaminated soils with different concentrations (Replicated (n) = 3).

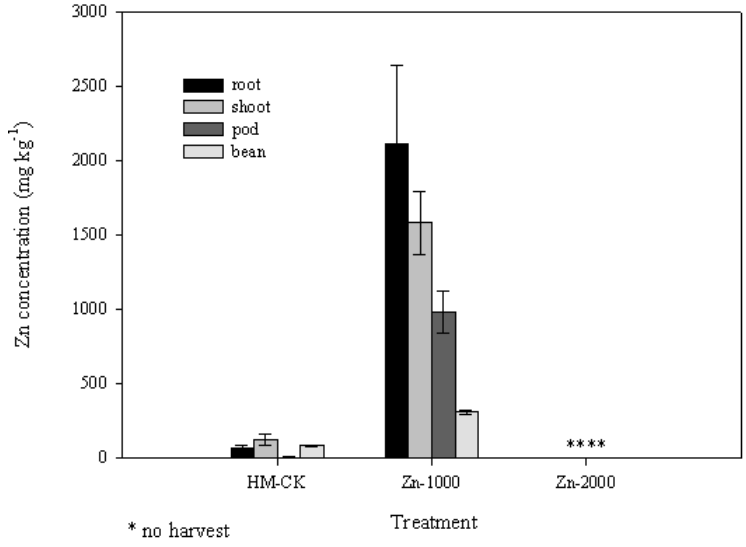


Figure 4. The accumulation of Zn by various parts of soybean grown in artificially Zn-contaminated soils with different concentrations (Replicated (n) = 3).

2.3. Bioconcentration Factor of HM of Soybean

Bioconcentration factor (BCF), as described as equation [1], was used as an indicator to assess the accumulation capacity of the different parts of soybean grown in contaminated soils. The soils treatments used to calculate the BCF values include Cd-5, Cd-20, Cu-200, Cu-400, and Zn-1000. HM-CK and Zn-2000 were not used in the calculation because of the lower concentration of HMs in CK and plants died, respectively.

$$BCF = \frac{\text{Concentrat ion of HM in plants}}{\text{Concentrat ion of HM in soils}} \quad [1]$$

Except for root, similar BCF values were found for Cd and Zn (Figure 5). The translocation of Cd and Zn within plant was faster than Cu, in which its BCF was less than 0.06 and can be neglected except for root. Many researchers reported that Cd was transferred more easily from soil to the tissues of vegetables than other HMs (Wang et al., 2003; Zheng et al., 2007), with translocation decreasing in the order Cd > Zn > Pb > Cu > Cr > Ni (Li et al., 2010). The experimental result of this study is in agreement with the foregoing literatures. For the same HM, the roots of soybean have higher BCF compared with other parts and their values were mostly all more than unity, especially in Cd-5 (BCF = 5.18) and Cd-20 (BCF = 11.1). In relative to other parts, bean of soybean had the lowest BCF, which were all less than 0.24 excluding the highest value (0.47) in Cd-20. Experimental result is in agreement to the experimental result of Murakami et al. (2007) who planted two cultivars of soybean in potted Cd-contaminated soils with total concentration ranged from 0.83 to 4.29 mg kg^{-1}. Lavado (2006) reported that the Cd concentration in beans and leaves of soybean when growing in the soil with 1.25 mg Cd kg^{-1} was 0.11 and 0.20 mg kg^{-1}, respectively. The BCF of bean and leave was only 0.09 and 0.16, respectively. Roots of two cultivars of soybean accumulated higher concentration of Cd compared with shoots, their BCF values for roots and shoots was in the levels of 2.40-4.14 and 0.56-3.66, respectively.

A hyperaccumulator is a plant that can accumulate higher than 100 mg Cd kg^{-1}, or 1,000 mg kg^{-1} for Cu, or 10,000 mg kg^{-1} for Zn (Brooks et al., 1977; Reeves, 1992). The translocation factor (TF; the ratio of HM concentration in the shoot to that in the root) and BCF should greater than unity (Sun et al., 2009). The soybean used in this study accumulated more than 100 mg Cd kg^{-1} in the roots and its BCF of shoots were more than unity. Even so, it still can not be regarded as a Cd hyperaccumulator because of its lower TF values.

3. Effect of Application of Amendments on the Accumulation of HM By Soybean

The application of OM can efficiently improve the soil conditions and thus the growth of plants. Biosolid (BS), which is enriched in OM, was applied to Cd-contaminated soils as an amendment to test its effect on the accumulation of Cd. The following experiment result is excerpted partially from our previous research (Chen et al., 2010a) and reorganized.

3.1. Pot Experiment

The surface soils (0-20 cm) of a contaminated site in central Taiwan were sampled and used for the pot experiment. Biosolid was sampled from a wasted sludge tank of a domestic wastewater treatment plant. Soils and BS were air dried, ground, and passed through a 10 mesh sieve before analysis. Solution of $Cd(NO_3)_2 \cdot 4H_2O$ was artificially added to the soils to make their final total concentration (mg kg^{-1}) as Cd-CK, Cd-3, and Cd-5 (coded as HM-concentration).

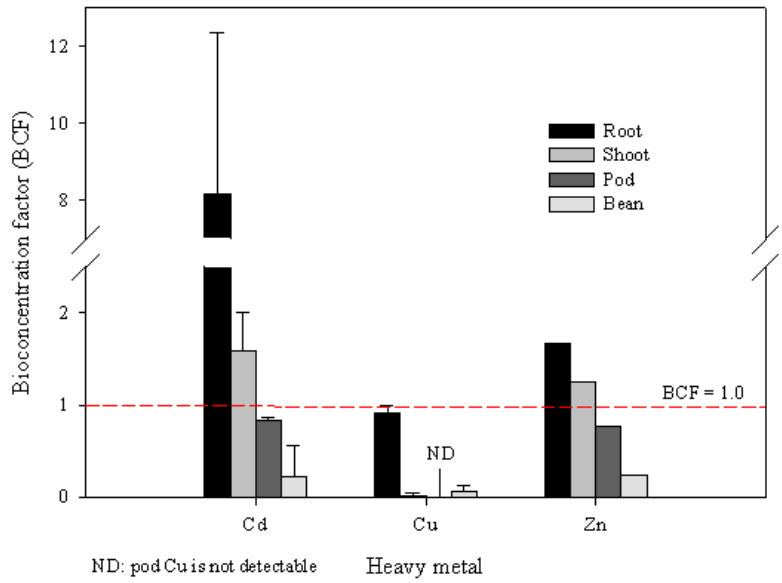


Figure 5. The bioconcentration factor (BCF) of Cd, Cu, and Zn by various parts of soybean grown in artificially contaminated soils (Replicated (n) = 3).

BS was homogenously mixed with artificially Cd-contaminated soils and then 3.0 kg of mixture (5% of BS) was added in each pot (16 cm diameter and 20 cm height). Ten seeds of soybean (*Leichardt* species) were sowed in each pot and all pots were then placed in a greenhouse (day/night = 30 ℃/25 ℃) with four replicates. Soil water content during experiment was controlled in the levels of 50-70% of field capacity by adding DI water every 3-4 days. Soybeans were harvested after growing for 90 days and separated into beans, pod, and shoots. The plant tissues were rinsed and oven dried at 65℃ for 72 hours, weighted, ground, and digested using H_2SO_4/H_2O_2 method (Harmon and Lajtha, 1999). Soil samples after pot experiment were collected, air dried, ground, and digested by aqua regia. The Cd concentrations in the digestant of plants and soils were determined with a FAAS (Hitachi 180-30).

3.2. Effect of BS on the Accumulation of Cd

The texture of the tested soil was silty clay (sand 8.80%, silt 50.9%, clay 40.3%) with moderate CEC (13.2±0.4 $cmol_{(+)}$ kg^{-1}) and water content (2.98±0.48%). The soil pH values were in the levels of 5.9 to 6.7. The total concentration of Cd of Cd-CK, Cd-3, and Cd-5 was 1.02±0.32, 2.94±0.54, and 5.28±0.92 mg kg^{-1}, respectively. Figure 6 shows the Cd concentration in the shoots, pod, and beans of soybean grown in Cd-contaminated soils amended with or without BS. In agreement with that reported by Jung and Thornton (1996), the accumulation of Cd in the shoots and pod of soybean increased with the increasing of spiked Cd concentrations in soils. The Cd concentrations in the various parts of soybean grown in Cd-CK were not detectable because of the lower Cd concentration in soils. The accumulation of Cd by different parts of soybean grown in Cd-3 and Cd-5 is in the decreasing order of shoot, pod, and bean. Soybeans accumulated higher concentrations of Cd in its shoot,

but were all less than 10 mg kg^{-1} and have large variation possible resulted from the soil pH (ranged from 5.9 to 6.7).

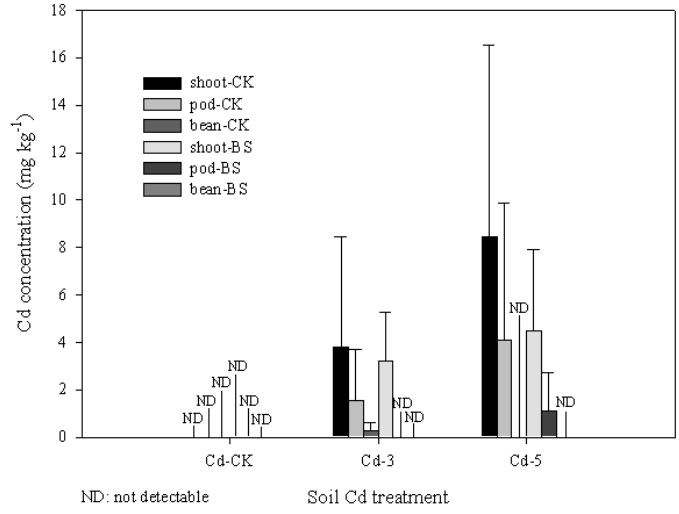


Figure 6. Effect of applying biosolid (BS) on the Cd concentration in the shoots, pod, and beans of soybean grown in artificially Cd-contaminated soils (Replicates (n) = 4).

Beans only accumulated low concentration of Cd (0.25±0.35 mg kg^{-1}) in their beans in the treatment of Cd-3. For other treatments, beans did not accumulated Cd even amended with BS.

3.3. Bioconcentration Factor of Cd of Soybean

After growing in Cd-contaminated soils for 90 days, the BCF values of Cd of various parts of soybean is shown in Figure 7. The shoots of soybean had higher BCF in relative to other parts and some of them were more than unity (dotted line in Figure 7). There was no significant effect of applying BS on the BCF. The BCF of *Brassica rapa* grown in the artificially Cd-contaminated soils was in the levels of 1.9 to 2.2 (Chen et al., 2010b). For lettuce grown in Cd-spiked soils, the BCF values were between 1.9 and 2.2 (Podlesáková et al., 2001). Various parts of soybean and especially the bean had lower BCF compared with leafy vegetables which revealed that soybean is a safer crop when planting in the Cd-contaminated soils.

CONCLUSION

The accumulation of Cd, Cu, and Zn by different parts of soybean grown in artificially spiked soils was investigated using pot experiments. The roots and shoots of soybean accumulated higher concentration of HMs compared with other parts. Even so, the Cd concentration accumulated in the beans of soybean was not detectable for most of the treatments. Planting soybeans in Cd-contaminated soils with total concentration less than

5 mg kg^{-1} seems to be feasible because their bean did not accumulate considerable concentration of Cd. These HMs-contaminated soils can be reused and the following procreative beans can be further used to produce biodiesel. More researches should be conducted from yield and quality of soybean oil and biodiesel to assess its feasibility.

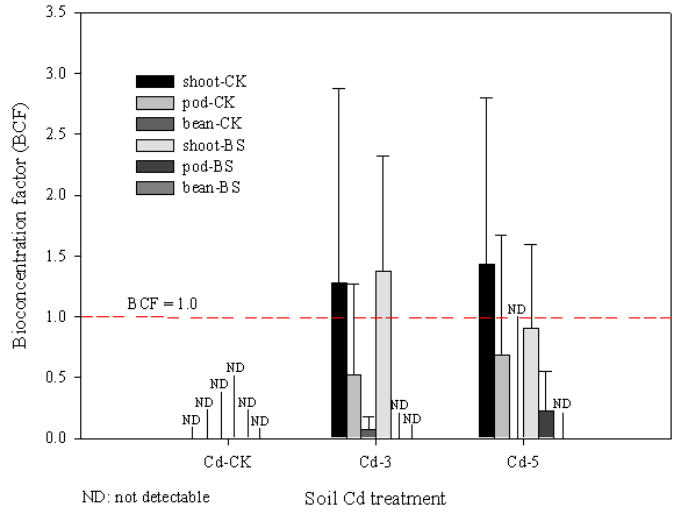


Figure 7. Effect of applying biosolid (BS) on the bioconcentration factor (BCF) of Cd in the shoots, pod, and beans of soybean grown in artificially Cd-contaminated soils (Replicates (n) = 4).

REFERENCES

Brooks, R.R., Lee, J., Reeves, R.D. and Jaffré, T. 1977. Detection of nickeliferous rocks by analysis of herbarium specimens of indicator plants. *J. Geochem. Explor*. 7, 49-77.

Chen, H.L., Lu, C.J. and Lai, H.Y. 2010a. Amendments of activated carbon and biosolid on the growth and cadmium uptake of soybean grown in potted Cd-contaminated soils. *Water Air Soil Poll.* 209, 307-314.

Chen, H.L., Lai, H.Y., Wang, S.M., Kuo, Y.C. and Lu, C.J. 2010b. Effect of biosolid and the Cd/Pb interaction on the growth and Cd accumulation of *Brassica rapa.* grown in the Cd-contaminated soils. *Water Air Soil Poll*. 206, 385-394.

Chen, Z.S. 1991. Cadmium and lead contamination of soils near plastic stabilizing materials producing plants in northern Taiwan. *Water Air Soil Poll*. 57-58, 745-754.

Gardner, W.H. 1986. Water content. In: Klute, A., Campbell, G.S., Nielsen, D.R., Jackson, R.D. and Mortland, M.M., editors. *Methods of Soil Analysis*, Part 1, Physical and mineralogical methods, Second edition. WI, USA: ASA. Inc. and SSSA. Inc.; p. 493-544.

Gee, G.W. and Bauder, J.W. 1986. Particle-size analysis. In: Klute, A., Campbell, G.S., Nielsen, D.R., Jackson, R.D. and Mortland, M.M., editors. *Methods of Soil Analysis*, Part 1, Physical and mineralogical methods, Second edition. WI, USA: ASA. Inc. and SSSA. Inc.; p. 383-412.

Harmon, M.E. and Lajtha, K. 1999. Analysis of detritus and organic horizons for mineral and organic constitutes. In: Robertson, G.P., Coleman, D.C., Bledsoe, C.S. and Sollins, P.,

editors. *Standard Soil Methods for Long-term Ecological Research*. NY, USA: Oxford University Press, Inc.; p. 143-165.

Jung, M.C. and Thornton, I. 1996. Heavy metal contamination of soils and plants in the vicinity of a lead-zinc mine, Korea. *Appl*. *Geochem*. 11, 53-59.

Kabata-Pendias, A. and Pendias, H. 2001. *Trace Element in Soils and Plants*, 3rd edition. FL, USA: CRC Press.

Lavado, R.S. 2006. Concentration of potentially toxic elements in field crops grown near and far cities of the Pamaps (Argentina). *J. Environ. Manage*. 80, 116-119.

Li, Q.S., Cai, S.S., Mo, C.H., Chu, B., Peng, L.H. and Yang, F.B. 2010. Toxic effects of heavy metals and their accumulation in vegetables grown in a saline soil. *Ecotox. Environ. Safe*. 73, 84-88.

Muralami, M., Ae, N., and Ishikawa, S. 2007. Phytoextraction of cadmium by rice (*Oryza sativa* L.), soybean (*Glycine max* (L.) Merr.), and maize (*Zea mays* L.). *Environ. Pollut*. 145, 96-103.

Nelson, D.W. and Sommers, L.E. 1996. Total carbon, organic carbon, and organic matter. In: Page, A.L., Sparks, D.L., Helmke, P.A., Loeppert, R.H., Soltanpour, P.N., Tabatabai, M.A., Johnston, C.T. and Sumner, M.E., editors. *Methods of Soil Analysis*, Part 3, Chemical methods. WI, USA: ASA. Inc. and SSSA. Inc.; p. 961-1010.

Podlesáková, E., Nemecek, J. and Vácha, R. 2001. Mobility and bioavailability of trace elements in soils. In: Iskander, I.K. and Kirkham, M.B., editors. *Trace Elements in Soils*. FL, USA: Lewis Publisher; p. 21-41.

Reeves, R.D. 1992. Hyperaccumulation of nickel by serpentine plants. In: Baker, A.J.M., Proctor, J. and Reeve, R.D., editors. *The vegetation of ultramafic (Serpentine) soils*. Andover, UK: Intercept Ltd.; p. 253-277.

Römkens, P.F., Guo, H.Y., Chu, C.L., Liu, T.S., Chiang, C.F. and Koopmans, G.F. 2009. Prediction of cadmium uptake by brown rice and derivation of soil-plant transfer models to improve soil protection guidelines. *Environ. Pollut*. 157, 2435-2444.

Sun, Y.B., Zhou, Q.X., Wang, L. and Liu, W.T. 2009. Cadmium tolerance and accumulation characteristics of *Bidens Pilosa* L. as a potential Cd-hyperaccumulator. *J. Hazard. Mater*. 161, 808-814.

Taiwan EPA (Environmental Protection Administration of Taiwan). 2010. Status of soil pollution and groundwater pollution in Taiwan. Taiwan EPA website: http://sgw.epa.gov.tw/public/En/index.htm

Thomas, G.W. 1996. Soil pH and soil Acidity. In: Page, A.L., Sparks, D.L., Helmke, P.A., Loeppert, R.H., Soltanpour, P.N., Tabatabai, M.A., Johnston, C.T. and Sumner, M.E., editors. *Methods of Soil Analysis*, Part 3, Chemical methods. WI, USA: ASA. Inc. and SSSA. Inc.; p. 475-490.

Wang, C.X., Mo, Z., Wang, H., Wang, Z.J. and Cao, Z.H. 2003. The transportation, time-dependent distribution of heavy metals in paddy crops. *Chemosphere* 50, 717-723.

Zheng, N., Wang, Q.C. and Zheng, D.M. 2007. Health risk of Hg, Pb, Cd, Zn, and Cu to the inhabitants around Huludao Zinc Plant in China via consumption of vegetables. *Sci. Total Environ*. 383, 81-89.

In: Activated Carbon
Editor: James F. Kwiatkowski
ISBN: 978-1-61209-684-1
©2012 Nova Science Publishers, Inc.

Chapter 15

ADSORPTIVE REMOVAL OF RESIDUAL SULFUR COMPOUNDS IN COMMERCIAL FUEL OIL BY MEANS OF BIOMASS-DERIVED ACTIVATED CARBONS

Seiji Kumagai*

Department of Machine Intelligence and Systems Engineering, Akita Prefectural Univeristy, 84-4 Tsuchiya-aza-ebinokuchi, Yurihonjo, 015-0055, Akita, Japan

ABSTRACT

Micro- and mesoporous granular rice husk activated carbon (RHAC) and microporous granular coconut shell activated carbon (CSAC) were evaluated as adsorptive desulfurization agents to remove residual sulfur in forms of benzothiophenes (BTs) and dibenzothiophenes (DBTs) in commercial kerosene. Fixed-bed flow desufurization tests were conducted, providing the breakthrough curves for BTs and DBTs. The adsorption isotherms for BTs and DBTs were also obtained in a batch-mode, correlating with the results of the fixed-bed flow test. RHAC and CSAC are found to be useful to remove BTs and DBTs. RHAC showed a lower selectivity for DBTs and a higher selectivity for BTs than CSAC did. A larger adsorption capacity of DBTs in volume basis was observed on CSAC, which was attributed to its higher bed density, higher carbon content and larger volume of ultramicropores. Although RHAC had lower carbon content and smaller volume of ultramicropores, it showed a larger adsorption capacity of BTs and acceptable adsorption capacity of DBTs in volume basis. This was explained by a larger volume of mesopores contributing to efficient transportation of BTs and DBTs towards their adsorption sites of ultramicropores.

1. INTRODUCTION

Because the reduction of the sulfur levels in liquid hydrocarbon fuels is connected to environmental conservation, much effort during the past decade has been devoted to the ultra

* Tel/Fax: +81-184-27-2128, E-mail: kumagai@akita-pu.ac.jp

deep desulfurization of liquid fuels. In addition to being used for transportation, liquid hydrocarbon fuels are a promising energy source for fuel cells due to their high energy density, availability, and safe transportation and storage [Song, 2002]. Catalytic hydrodesulfurization (HDS) at high temperature and pressure has become the generally accepted method for attaining the ultra deep desulfurization of liquid hydrocarbon fuels. CoMo, NiMo, and NiW catalysts using different supports (Al_2O_3, TiO_2, Al_2O_3-TiO_2, HY zeolite, carbon, etc.) in the HDS process have been studied for producing liquid hydrocarbon fuels with low sulfur levels [Kabe, 1993; Mochida, 1996; Whitehurst, 1998; Farag, 1999; Song, 2003]. However, catalytic HDS is not appropriate for further ultra deep desulfurization (0.1-10 mass ppm-S) because of the necessary use of more high-cost hydrogen and larger reactor volume, as well as undesirable changes in the fuel properties. Fuel cells require very low sulfur levels of less than 0.1 mass ppm-S to prevent the reforming and generation catalysts from being poisoned [Jayne, 2005]. Sulfur removal in the range of <10 mass ppm-S in liquid hydrocarbon fuels is now becoming an important research subject. In Japan, commercial kerosene is a promising hydrogen source of stationary fuel cells for domestic use, because it can be readily purchased at filling stations or delivered to homes. Benzothiophenes (BTs) and dibenzothiophenes (DBTs) contained in fuel oils such as kerosene and diesel oil are refractory poly-aromatic sulfur compounds. In particular, alkyl-substituted DBTs, i.e., 4-methyldibenzothiophene (4-MDBT) and 4,6-dimethyldibenzothiophene (4,6-DMDBT), are highly refractory [Macaud, 2000]. Adsorptive desulfurization using activated carbons (ACs) have been proposed for the efficient removal of BTs and DBTs from fuel oils [Zhou, 2006]. Activated carbons (ACs), catalyst-loaded ACs and activated carbon fiber have been studied as promising materials for adsorptive desulfurization [Ma, 2002; Sano, 2005; Ania, 2006]. Safe operational procedures under atmospheric pressure and ambient temperature, elimination of the need for large reactor volume, the minor impact on fuel properties, and the lower-cost of operation are principal advantages of adsorptive desulfurization using ACs. It was demonstrated that ACs with a specific pore structure could be used for the efficient and selective removal of DBTs from commercial kerosene [Kumagai, 2009]. ACs made from agricultural waste of rice husk (RH), which were with a composite micro-mesoporous structure, were shown to be promising for the removal of DBTs from commercial kerosene. ACs made from agricultural waste are now very profitable in view of cost and environmental friendliness. In the present study, two types of biomass-based ACs were tested to provide useful knowledge regarding the efective removal of BTs and DBTs from commercial kerosene in Japan. The granular RH-based AC (RHAC) produced in a laboratory and the purchased granular coconut-shell AC (CSAC) were tested in fixed-bed flow tests and batch-mode adsorption tests.

2. EXPERIMENTAL METHODS

2.1. Preparation of AC Samples

RHAC was produced from rice husk and beet sugar in a laboratory. The used RH was Koshihikari rice harvested in Toyooka, Iwata City, Japan in autumn 2004. The beet sugar was a commercial product supplied from the Hokuren Agriculture Cooperative Association

(Hokkaido, Japan). The fabrication process of the RHAC via the two-step activation process is shown in Figure 1. Commercially available CSAC (GW10/32; Kuraray Chemical, Japan) was purchased. The granule size of both the ACs was adjusted to 1-2 mm using sieves. The samples were not subjected to washing.

2.2. Material Characterizations

Nitrogen adsorption-desorption isotherms at -196 °C of the samples were obtained using a gas adsorption analyzer (Autosorb-3B; Quantachrome Instruments Inc., USA). The BET supecific surface area (S_{BET}) is based on the BET theory and was calculated using the volume of N_2 adsorbed at relative pressures of 0.05-0.1. The liquid N_2 volume in relation to the N_2 volume adsorbed at a relative pressure of 0.99 was determined as the total pore volume (V_t). Microporosity in ACs was essentially slit-shaped [Albornoz, 1999; Marsh, 2006]. The formation of micropore in lignocellulosic raw materials such as wood, coconut shell, etc., probably arose from a certain mechanism involving the transformation of the lignocellulose to carbon polyhexagon sheets (graphenes) [Albornoz, 1999]. Slit-shaped pores were assumed for microporosity produced in carbonaceous structures in the ACs. Micropores were distinguished as either ultramicropores (width $\leq$ 0.7 nm) or supermicropores (0.7 < width $\leq$ 2.0 nm), in accordance with [Rouquerol, 1999]. The pore size distribution was evaluated using density functional theory (DFT). The DFT software developed by Quantachrome Instruments Inc. (version 1.62) was used to obtain the pore size distribution. The ultramicropores volume (V_u), the supermicropores volume (V_s), and the mesopores volume (V_m) were obtained using these pore size distribution data. DFT method is applicable to the whole range of micro- and mesopores using a single numerical data reduction [ISO, 2007], which was suitable to the pore size analysis of the micro- and mesoporous ACs. The ash content of the samples (0.1 g) was precisely determined from the residual ash after incineration at 800 °C for 1 h in air (100 cm^3/min) using a thermogravimetric analyzer (TGA-51; Shimadzu Corp., Japan). A CHN/S analyzer (2400 I; Perkin Elmer Inc., USA) was used to determine the hydrogen, carbon, nitrogen and sulfur content of the samples. The oxygen content excluding that in the ash was determined via the mass minus the hydrogen, carbon, nitrogen, sulfur, and ash. Because extra oxygen might be added with inorganic matters during the ashing, the oxygen content might have error. All samples were dried at 105 °C for 3 h prior to analyses. It was verified beforehand that the above periods were sufficient to yield a constant weight on drying. The surface appearance and elemental distribution at the surfaces of the samples were observed by using a scanning electron microscope (SEM) and energy-dispersive X-ray analyzer (EDX) (SEM-EDX Integration System; Hitachi, Ltd., Japan).

2.3. Quantification of Sulfur Compounds in Commercial Kerosene

The sulfur compounds in commercial kerosene were distinguished as either BTs or DBTs. A definition of BTs and DBTs was shown in Figure 2. BTs were defined as sulfur compounds of which molecular mass were less than 4-MDBT. It should be noted that dibenzothiophene (DBT) was categolized to be BTs. DBTs were 4-MDBT and double-aromatic sulfur compounds of which molecular mass was larger than that of 4-MDBT, such

as 4,6-DMDBT. A gas chromatograph-inductively coupled plasma mass spectrometer (GC-ICP-MS) was used to identify and quantify BTs and DBTs in the kerosene.

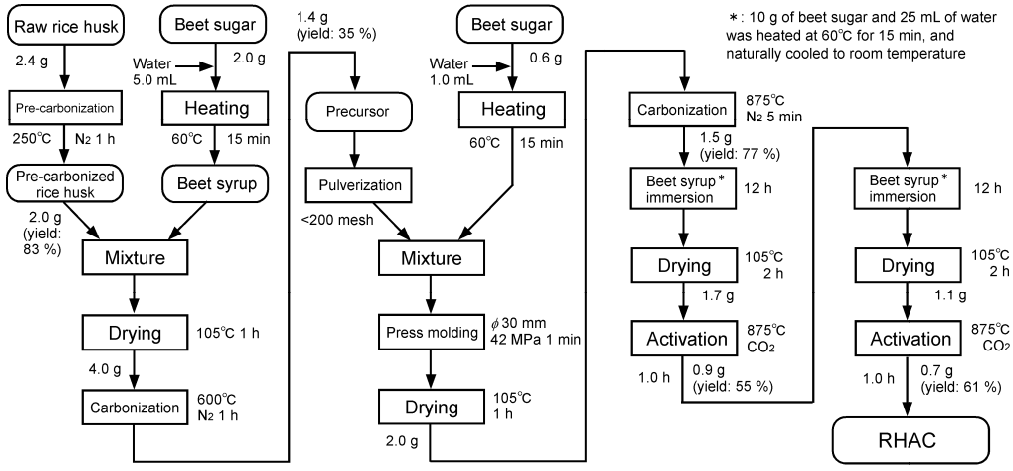


Figure 1. A process to fabricate rice husk activated carbons (RHACs).

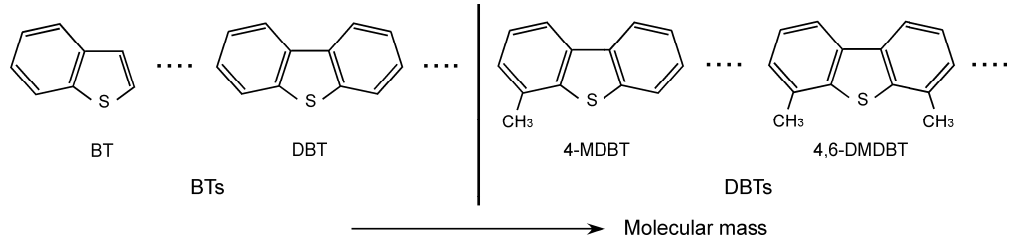


Figure 2. A definition of BTs and DBTs.

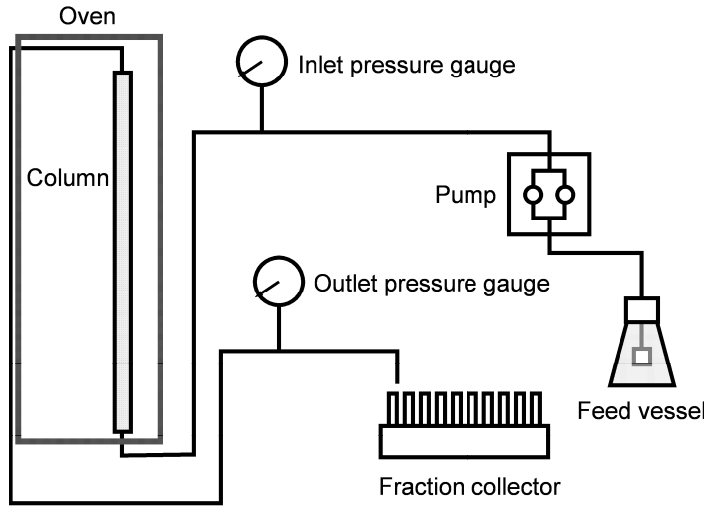


Figure 3. Schematic diagram of the fixed-bed flow desulfurization test.

2.4. Desulfurization Tests

Commercial kerosene produced in 2004 was injected to the cylindrical column filled with the AC sample (length: 150 mm, volume: 13.5 cm^3). Figure 3 shows the schematic diagram of the fixed-bed flow desulfurization test. The sample was dried at 130 °C in ambient air for 3 h prior to the fixed-bed flowing test. The flow-rate of kerosene was adjusted at 1.0 cm^3/min and the ambient temperature was set to be 25 °C. Bed density was measured based on the mass of the sample filled in the used fixed-bed column and the column volume. The effluent kerosene was collected using a fraction collector. The batch-mode adsorption test was also conducted by immersing the AC sample into commercial kerosene produced in 2007. The sample was dried at 130 °C in ambient air for 3 h prior to batch adsorption test. Different masses of the AC samples were immersed in 15.0 g of kerosene in 30 cm^3 glass vessel at 10 °C for 240 h. The kerosene was not stirred during immersion. The adsorption time of 240 h was confirmed to be sufficient to reach equilibrium adsorption.

3. Result and Discussion

Typical nitrogen adsorption-desorption isotherms of the RHAC and CSAC at -196 °C are shown in Figure 4. The sharp knees at relative pressure of <0.1 were observed for both the samples, which are typical to micropore system. A gradual increase in the isotherm slope at relative pressures of >0.1 and a hysteresis loop at a high relative pressure, indicating the existence of mesopores, were also observed for the RHAC. The hysteresis loops had no sharp knees, meaning that mesopores having specific sizes were absent. CSAC showed a modest increase at relative pressures of >0.1 and a slight hysteresis loop at a high relative pressure. The isotherms of RHAC and CSAC belong to the type IV and type I classified by IUPAC [Sing, 1985], respectively.

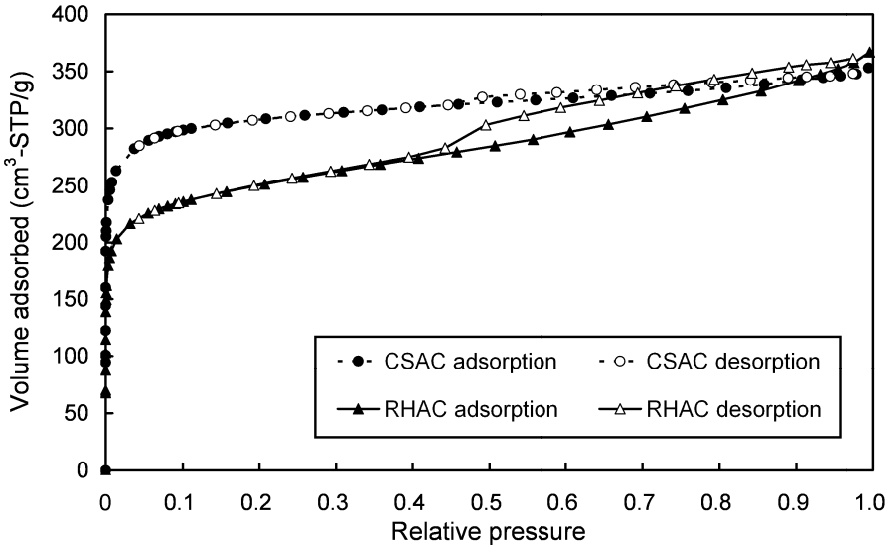


Figure 4. Typical nitrogen adsorption-desorption isotherms of RHAC and CSAC at -196 °C.

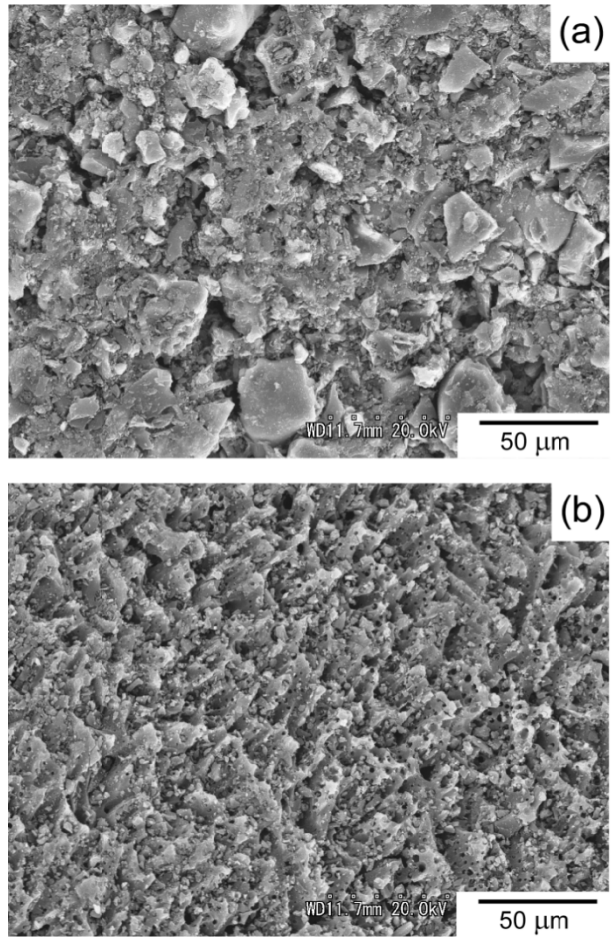


Figure 5. SEM photos of the surfaces of RHAC and CSAC. (a) RHAC, (b) CSAC.

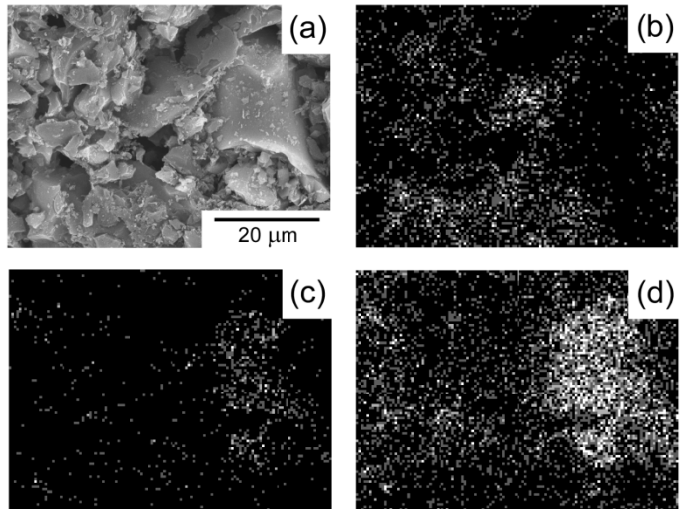


Figure 6. Elemental distributions at the surface of RHAC. (a) SEM photo, (b) C, (c) O, (d) Si.

Table 1. Textural parameters of RHAC and CSAC

Sample	S_{BET} (m^2/g)	V_t (cm^3/g)	V_u (cm^3/g)	V_s (cm^3/g)	V_m (cm^3/g)
RHAC	943	0.56	0.15	0.17	0.19
CSAC	1169	0.56	0.21	0.22	0.06

Data are average of 15 measuemrents for RHAC and 5 measurements for CSAC

Table 2. Composition of RHAC and CSAC

Sample	C (mass%)	H (mass%)	N (mass%)	S (mass%)	Ash (mass%)	O* (mass%)
RHAC	58.6	0	0.6	0	36.8	4.0
CSAC	94.1	0.4	0.3	0.1	0.5	4.6

Data are result of four separate measurements.

* Oxygen content except for that in ash was calculated as: O=100–(Ash+H+C+N+S).

Table 3. Adsorption capacity of BTs and DBTs on RHAC and CSAC at the time of 480 min in the fixed-bed flow test

	Sample	BTs	DBTs
Adsorption capacity in unit mass (mg-S/g-Ads)	RHAC	0.09	0.15
	CSAC	0.01	0.12
Adsorption capacity in unit bed volume (mg-S/cm^3-Bed)	RHAC	0.03	0.05
	CSAC	0.01	0.06
Bed density (g/cm^3)	RHAC	0.36	
	CSAC	0.51	

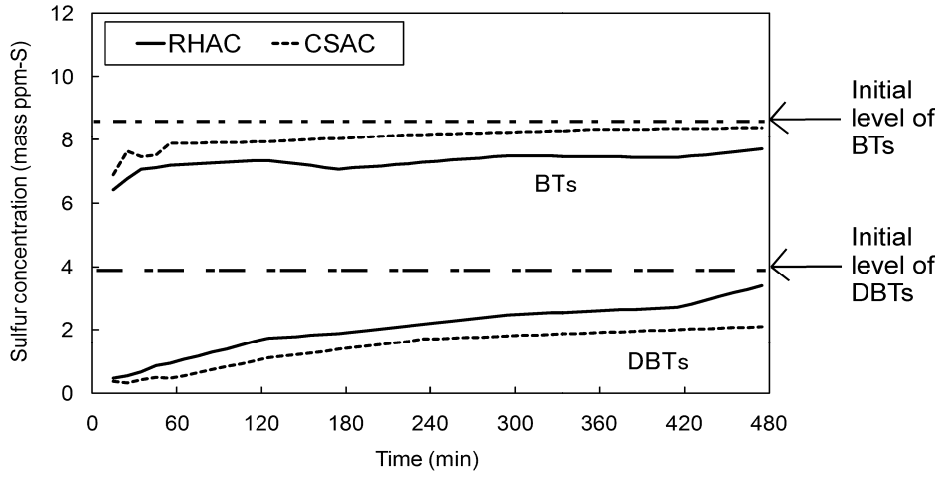


Figure 7. Breakthrough curves of RHAC and CSAC for BTs and DBTs in fixed-bed flow tests using commercial kerosene produced in 2004. Concentrations of BTs and DBTs in the untreated commercial kerosene were 8.5 and 3.9 mass ppm-S, respectively.

A similar level of nitrogen uptake at the relative pressure of 0.99 was observed for both the samples, indicating that both the samples had comparable V_t. The isotherm observation

indicated that a combined system of micropores ane mesopores was developed in RHAC, while micropores were dominantly developed in CSAC. Table 1 shows the textural parameters of RHAC and CSAC, obtained using the above isotherms and the DFT method. Although both the sample had a comparable V_t, RHAC allowing a dominant development of micropores showed a larger volume of micropores (V_u and V_s) and S_{BET} than CSAC did. RHAC in which a combined system of micrpores and mesopores was developed showed a large V_m, which was 3 times-greater than that of CSAC. The above results suggest that CSAC has a micro- and mesoporous structure, while RHAC has a microporous structure.

The elemental compositions of RHAC and CSAC are shown in Table 2. Higher carbon and hydrogen contents were observed in CSAC than in RHAC. The much higher ash content of RHAC was attributed to the intrinsic silica component in natural RHs. A developed mesoporosity in RHAC was attributed to the silica component.The surface appearance of RHAC and CSAC was observed by SEM and shown in Figure 5. It was found that the RHAC consisted of aggregated grains at 5-30 μm which were attributed to pulverization of carbonized RH and to carbonization of beet syrup used as a binder. Many swell with small hole at a few μm were observed on CSAC. Such the surface structure was produced by a gas (steam) activation process.

The elemental distributions of C, O and Si at the surface of RHAC were observed using a SEM-EDX system (see Figure 6). The regions in which O and Si were detected overlapped each other. It was found that the regions in which C was detected did not overlap the Si- and O-regions. It is important to note that C was not highly dispersed in the other elements. Silica-rich or carbon-rich grains at 5-30 μm were aggregated at the surface of RHAC.

The breakthrough curves of RHAC and CSAC for BTs and DBTs in the fixed-bed flow tests are shown in Figure 7. The concentrations of BTs and DBTs in the first effluent kerosene treated by RHAC were respectively 6.4 and 0.5 mass ppm-S, while those by CSAC were respectively 6.9 and 0.4 mass ppm-S. BTs concentration of RHAC was maintained to be ~7 mass ppm-S at >60 min. That of CSAC was also maintained to be ~8 mass ppm-S, which was higher than that of RHAC. DBTs concentrations of both the samples were found to increase with the treated kerosene. DBTs concentration of CSAC was lower than that of RHAC.

Table 3 shows the adsorption capacities of BTs and DBTs in unit mass and volume at the time of 480 min. The adsorption capacity in unit volume was calculated using the data of the measured bed density. Larger adsorption capacities in unit mass of both BTs and DBTs were observed on RHAC than on CSAC. However, a larger adsorption capacity of DBTs in unit volume appeared on CSAC than on RHAC, which was related to higher bed density of CSAC.

The adsorption isotherms of RHAC and CSAC for BTs and DBTs in the batch-mode desulfurization tests are shown in Figure 8. At the lower equilibrium concentration of DBTs (<0.2 mass ppm-S), RHAC and CSAC showed a similar level of DBTs adsorption capacity. At the higher concentration of DBTs, a larger capacity was observed on CSAC than on RHAC, which was more pronounced in volume basis.

For the BTs adsorption, RHAC showed a larger adsorption capacity at any concentrations in both mass and volume basis. The adsorption isotherms in volume basis are consistent with the result of the fixed-bed flow tests.

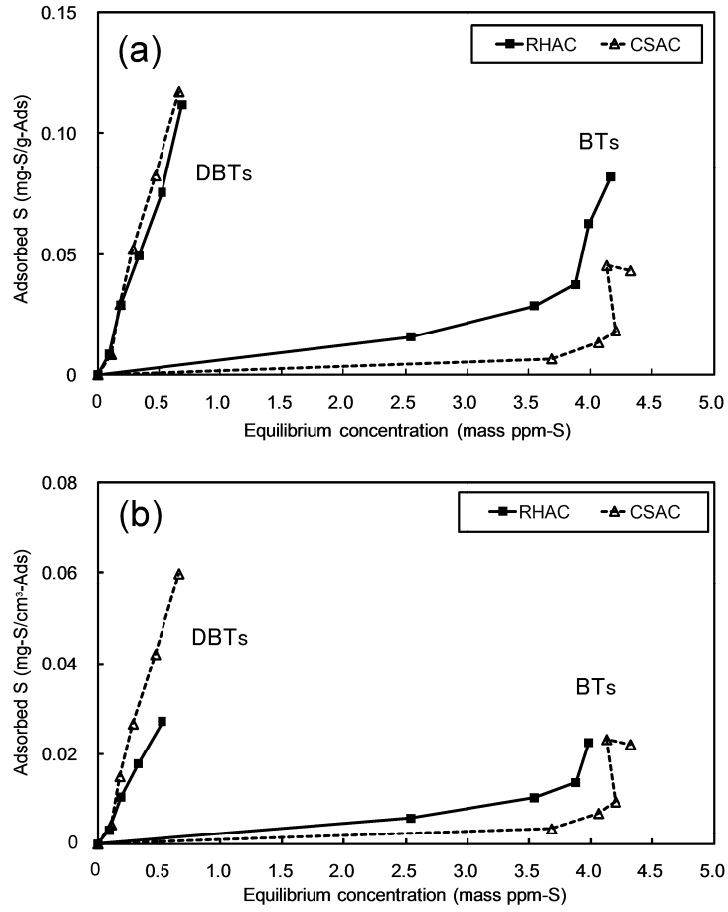


Figure 8. Adsorption isotherms of RHAC and CSAC for BTs and DBTs in batch adsorptive desulfurization tests with the use of commercial kerosene produced in 2007. (a) mass basis, (b) volume basis. Concentrations of BTs and DBTs in the untreated commercial kerosene were 4.5 and 1.2 mass ppm-S, respectively.

The mechanisms have been proposed to explain the adsorption of poly aromatic compounds on ACs. One mechanism is the dispersion interaction mechanism including the π-electron overlap between benzene rings and active sites on the AC surface [Dowaidara, 2007]. The mechanism of DBTs adsorption on a catalyst was studied [Meille, 1999]. They pointed out that π electrons in the aromatic rings participate in the DBTs adsorption mechanism. DBTs include two aromatic rings and BTs include one aromatic ring, indicating that higher affinity with the ACs was expected on DBTs than on BTs. Pore-filling is also major mechanism. The volume of micropores with a width of <0.7 nm (defined as ultramicropores in the present study) governed the amount of DBT adsorbed in n-hexane, and the adsorption capacity was linearly related to the volume of these pores [Ania, 2005]. The size of 4,6-DMDBT molecule was reported to be 0.63 nm [Zhou, 2006]. DBTs with a planar structure can enter slit-shaped ultramicropores. The interaction between π electrons on graphene sheets with slit-shaped pores in ACs and π electrons in DBTs further promotes entry of DBTs parallel to the wall surface of ultramicropores. Therefore, the predominant adsorption sites of DBTs in ACs are deemed to be ultramicropores. It was stated that, for

DBT and 4,6-DMDBT, methyl group at the aromatic ring enhances the negative electrostatic potential on the two sides of the molecular plane because methyl group is an electron donor to the aromatic rings [Kim, 2006]. The increased electrostatic potential is likely to enhance the π-π interaction between the graphene sheets in ultramicropore and the aromatic rings of BTs and DBTs. The mechanisms of the π-π interaction and the ultramicrpore-filling are consistent with the higher-selectivity of RHAC and CSAC for DBTs than for BTs. A higher-selectivity for DBTs and a lower-selectivity for BTs were observed on CSAC in the fixed-bed flow and the batch adsorption desulfurization tests. The compositional analysis revealed that much higher carbon content was observed on CSAC than on RHAC. The higher carbon content is likely to enhance the π-π interaction between the graphene sheets and the aromatic rings. DBTs have a stronger π-π interaction resulting from more aromatic rings and alkyl-substitution, supporting the higher-selectivity of CSAC for DBTs. Low dispersibility of carbon, producing silica-rich or carbon-rich aggregated grains at the surface, was also related to the lower selectivity of RHAC for DBTs. In addition to this, despite the lower carbon content and the smaller volume of ultramicropores, RHAC showed a larger BTs adsorption capacity and an acceptable DBTs adsorption capacity when compared with CSAC. Ania et al mentioned that mesopores in ACs controlled the kinetics of the DBT adsorption process [Ania, 2005]. It was stated that, at low sulfur content (< a few mass ppm-S), the DBTs adsorption sites in ultramicropores might not be fully filled. In such the condition, mesopores play a role of pathways to efficiently lead DBTs into ultramicropores, and the volume of mesopores affects the DBTs adsorption capacity [Kumagai, 2009]. The textural analysis indicated that RHAC had 3-fold larger mesopore volumes. It is supposed that a larger volume of mesopores in RHAC compensated for the reduced carbon content and ultramicropore volume.

CONCLUSIONS

Results of the fixed-bed flow tests and batch-mode adsorption tests showed that RHAC and CSAC were useful to remove aromatic sulfur compounds from kerosene. RHAC showed a lower selectivity for DBTs and a higher selectivity for BTs than CSAC. A larger adsorption capacity of DBTs in volume basis was observed on CSAC, which was attributed to its higher bed density, higher carbon content and larger volume of ultramicropores.

Although RHAC had lower bed density, lower carbon content and smaller volume of ultramicropores, a larger adsorption capacity of BTs and acceptable adsorption capacity of DBTs in volume basis appeared on RHAC. This was explained by a larger volume of mesopores contributing to efficient transportation of BTs and DBTs towards their adsorption sites of ultramicropores.

ACKNOWLEDGMENT

This research was supported in part by the Industrial Technology Research Grant Program in 2006 of the New Energy and Industrial Technology Development Organization (NEDO) of Japan.

REFERENCES

Albornoz A., Labady M., Lopez M., Laine J. Evidence for the Formation of Slit Mesopores in Activated Carbon, *J. Mater. Sci. Lett*, 18, 1999-2000, 1999.

Ania C. O., Bandosz T. J. Importance of Structural and Chemical Heterogenecity of Activated Carbon Surfaces for Adsorption of Dibenzothiophene, *Langmuir*, 21, 7752-7759, 2005.

Ania C. O., Bandosz T. J. Metal-loaded Polystyrene-based Activated Carbon as Dibenzothiophene Removal Media via Reactive Adsorption, *Carbon*, 44, 2404-2412, 2006.

Dowaidara A. M., El-Shahawib M. S., Ashourc I. Adsorption of Polycyclic Aromatic Hydrocarbons onto Activated Carbon from Non-Aqueous Media: 1. The Influence of the Organic Solvent Polarity, *Sep. Sci. Tech*, 42, 3609-3622, 2007.

Farag H, Whitehurst D. D., Sakanishi K., Mochida I. Carbon versus Alumina as a Support for Co-Mo Catalysts Reactivity towards HDS of Dibenzothiophene and Diesel Fuel. *Catal. Today*, 50, 9-17, 1999.

International Organization for Standardization (ISO). ISO 15901-3, Pore Size Distribution and Porosity of Solid Materials by Mercury Porosimetry and Gas Adsorption - Part 3: Analysis of Micropores by Gas Adsorption, 2007.

Jayne D., Zhang Y., Haji S., Erkey C. Dynamics of Removal of Organosulfur Compounds from Diesel by Adsorption of Carbon Aerogels for Fuel Cell Applications, *Int. J. Hydrogen. Energ*, 30, 1287-1293, 2005.

Kabe T., Ishihara A., Zhang Q. Deep Desulfurization of Light Oil. Part 2: Hydrodesulfurization of Dibenzothiophene, 4-methyldibenzothiophene 4, 6-dimethyl-dibenzothiophene, *Appl. Catal. A.-Gen*, 97, L1-9, 1993.

Kim J. H., Ma X., Zhou A., Song C. Ultra-deep Desulfurization and Denitrogenation of Diesel Fuel by Selective Adsorption over Three Different Adsorbents: A Study on Adsorptive Selectivity and Mechanism, *Catal. Today*, 11, 74-83, 2006.

Kumagai S., Shimizu Y., Toida Y., Enda Y. Removal of Dibenzothiophenes in Kerosene by Adsorption on Rice Husk Activated Carbon, *Fuel*, 88, 1975-1982, 2009.

Ma X., Sun L., Song C. A New Approach to Deep Desulfurization of Gasoline, Diesel and Jet Fuel by Selective Adsorption for Ultra-clean Fuels and for Fuel Cell Applications, *Catal. Today*, 77, 107-116, 2002.

Macaud M., Milenkovic A., Schulz E., Lemaire M., Vrinat M. Hydrodesulfurization of Alkyldibenzothiophenes: Evidence of Highly Unreactive Aromatic Sulfur Compounds, *J. Catal*, 193, 255-263, 2000.

Marsh H., Rodriguez-Reinoso F. *Activated Carbon*, Elsevier Ltd., Oxford, UK, 2006.

Meille V., Schulz E., Lemaire M., Vrinat M. Hydrodesulfurization of 4-methyl-dibenzothiophene: A Detailed Mechanistic Study, *Appl. Catal. A.-Gen*, 187, 179-186, 1999.

Mochida I., Sakanishi K., Ma X., Nagao S., Isoda T. Deep Hydrodesulfurization of Diesel Fuel: Design of Reduction Process and Catalysts, *Catal. Today*, 29, 185-189, 1996.

Sano Y., Sugahara K., Choi K. H., Korai Y., Mochida I. Two-step Adsorption Process for Deep Desulfurization of Diesel Oil, *Fuel*, 84, 903-910, 2005.

Rouquerol F., Rouquerol J., Sing K. S. W. *Adsorption by Powders and Porous Solids*, Academic Press, London, 1999, pp. 219-228.

Sing K. S. W., Everett D. H., Haul R. A. W., Moscou L., Pierotti R. A., Rouquerol J., Siemieniewska T. Reporting Physisorption Data for Gas/Solid Systems, *Pure Appl. Chem*, 57, 603-619, 1985.

Song C. Fuel Processing for Low-temperature and High-Temperature Fuel Cells. Challenge and Opportunities for Sustainable Development in the 21st Century, *Catal. Today*, 77, 17-49, 2002.

Song C, Ma X. New Design Approaches to Ultra-clean Diesel Fuels by Deep Desulfurization and Deep Dearomatization, *Appl. Catal. B.-Environ*, 41, 207-238, 2003.

Whitehurst D. D., Farag H., Nagamatsu T., Sakanishi K., Mochida I. Assesment of Limitations and Potentials for Improvement in Deep Desulfurization through Detailed Kinetic Analysis of Mechanistic Pathways. *Catal. Today*, 45, 299-305, 1998.

Zhou A, Ma X. and Song C. Liquid-phase Adsorption of Multi-ring Thiophenic Sulfur Compounds on Carbon Materials with Different Surface Properties, *J. Phys. Chem. B*, 110, 4699-4707, 2006.

In: Activated Carbon
Editors: James F. Kwiatkowski
ISBN: 978-1-61209-684-1
©2012 Nova Science Publishers, Inc.

Chapter 16

COMBINATION OF OZONE AND ACTIVATED CARBON FOR WATER AND WASTEWATER TREATMENT

F. J. Beltrán and P. M. Álvarez
Departamento de Ingeniería Química y Química Física,
Universidad de Extremadura, Badajoz, Spain

1. INTRODUCTION

One the major problems wastewater and drinking water treatment plants, (WWTPs and DWTPs, respectively) will likely have to face in the near future is the removal of emergent contaminants coming from the abundant use of pharmaceutical and personal care products (PPCPs). These compounds, as well as others already catalogued as priority pollutants, are usually encountered in influents and effluents of WWTPs (Halling-Sorensen et al., 1998, Ternes, 1998; Gómez et al., 2007, Joss et al., 2004, Segura et al., 2007) and even of DWTPs (Stakelberg et al., 2004, Jones et al., 2005) at low but potentially hazardous concentrations for humans and other living beings. It has been clearly established that many of these pollutants go through the classical primary and secondary treatments in water plants without being properly removed and only most costly tertiary treatments technologies are able to completely remove them from water. Among these treatments chemical oxidation, particularly advanced chemical oxidation (ACO), and activated carbon adsorption processes (ACAPs) present high efficiency to remove these pollutants. Also, among ACO processes, those involving ozone have already shown their applicability in this field (Ikehata et al., 2008).

The use of activated carbon as adsorbent in water treatment dates back from the 19th century and today ACAPs are considered as the most cost-effective methods for removal of a number of pollutants from water and wastewater. Thus, adsorption onto activated carbon has been designated as best available technology for the adsorption of many synthetic chemicals from water and wastewater by the United States Environmental Protection Agency (USEPA) and the European Union. Today about two thirds of the activated carbon world production at industrial scale is marketed for the removal of pollutants from water and wastewater streams (Cooney, 1999). Its usefulness derives mainly from their textural and chemical properties (high surface area per mass which is provided with large micropore and mesopore volumes

and different surface functional groups). Activated carbons can be modeled as a set of defective hexagonal carbon layer planes crosslinked to aliphatic bridging groups where heteroatoms are incorporated. These heteroatoms give the character of the functional groups typically found in aromatic compounds (Yang, 2003). In the adsorption process the adsorbates are fixed on the carbon surface by physical interactions (i.e., electrostatic and dispersive forces) and/or chemical bonds (i.e., chemisorption). In the water treatment field, activated carbon is extensively used as adsorbent in a wide variety of physical forms such as granular, powdered, fibers, nanotubes, etc. In DWTPs is used to remove taste and odor compounds, synthetic organic chemicals and natural organic matter in order to control the formation of some disinfection by-products (DBPs). In WWTPs activated carbon is mainly used in granular form to remove specific organic micropollutants. Nevertheless, specific activated carbon grades can be prepared with other particular purposes in water treatment. In water treatment, adsorption of organics on activated carbon is a complex process where both water and the organics are simultaneously adsorbed to different extents. There are already excellent works published on the activated carbon adsorption of organics from water, including large compilations of adsorption isotherms of priority pollutants such as pesticides, phenols and chlorinated organic compounds (Faust and Aly, 1987). Main general properties of activated carbons as adsorbents are their capability to act without being previously dried, which is one of the reasons of their application in water treatment, their high adsorption capacity for non-polar and weakly polar organic molecules and their low heat of adsorption compared to those of other adsorbents. As catalysts, activated carbons can act in many different gas and liquid reactions processes such as oxidative dehydrogenation, dehydration and dehydrogenation of alcohols and NO_x reduction (gas phase) or hydrogen peroxide, ozone and wet air oxidation reactions (liquid phase) where their surface chemistry play a key role (Figueiredo and Pereira, 2010).

Ozone is a powerful oxidant and disinfectant gas that, as activated carbon, started to be applied in water treatment in the 19th century although then only as disinfectant. However, its use declined during the first decades of the 20th century due to chlorine advantages and lack of knowledge of ozone chemistry. It was not until the end of the seventies of the past century when ozone application in water rose, especially due to its reaction with precursors of DBPs (i.e., trihalomethane compounds) (Langlais et al., 1991). Years later, knowledge of the ozone chemistry and kinetics of the processes it undergoes in water also increased and ozone advanced oxidation processes commenced to be considered as an important tertiary treatment method to remove priority pollutants (pesticides, polynuclear aromatic hydrocarbons, etc) from water (Glaze et al., 1987). Nowdays, it is well known that ozone reacts with organic matter in water through two different ways, the so-called direct and indirect reactions. Direct reactions are mainly cycloaddition reactions (Criegge mechanism) to double or triple carbon bonds and electrophilic substitution reactions on nucleophilic points (Bailey, 1958, von Gunten, 2003) while indirect reactions develop through hydroxyl radicals coming from ozone reactions with substances called promoters or initiators (Staehelin and Hoigné, 1985). Hydroxyl radicals are more powerful oxidant species than ozone itself and they are able to react in an unselective way with organic and inorganic matter present in water. In fact, rate constants of the reactions between these free radicals and most of the species in water are around 10^7-10^{10} $M^{-1}s^{-1}$ (Buxton et al., 1988). First initiators to be studied were hydrogen peroxide and UVC radiation that decompose ozone through fast reactions to yield hydroxyl radicals (Staehelin and Hoigné, 1982, Peyton and Glaze, 1988, Beltrán, 2003). Hydrogen

peroxide, particularly, constitutes a key agent of many advanced oxidation processes and also for the activated carbon-ozone reactions (see later). Among initiators, catalysts of different nature (metals or metal oxides on supported materials, perovskites, etc, are lately subject of study in a process called catalytic or photocatalytic ozonation depending on the absence or presence of some radiation source (UVC, UVA, solar radiation, etc) (Legube and Vel Leitner, 1999, Kasprzyk-Hordern et al., 2003, Agustina et al., 2005, Beltrán, 2008). These catalysts (and radiation, in some cases) trigger the ozone decomposition into hydroxyl radicals favoring the indirect way of oxidation which is particularly important when refractory compounds to direct ozonation are present in water (Beltrán et al., 2004). Activated carbons are one of the possible catalysts to improve the indirect way of ozonation though, so far, the mechanism of this process is not yet well understood. Ozone and activated carbon are currently applied in water treatment not only as single processes but as a consecutive process which is normally called biological activated carbon process (BACP), constituted by ozonation followed by activated carbon filtration. Also, they can be simultaneously used in a catalytic ozonation process where activated carbon accelerates the decomposition of ozone in hydroxyl radicals usually through hydrogen peroxide formation. This latter process is presently at research and development level. Then, in this chapter these two processes are reviewed. In addition, since ozone strongly reacts with some functional groups of the activated carbon surface, the study of the effects of these interactions and how to take advantage of them to produce activated carbons with special adsorptive properties is also presented. Finally, this chapter also deals with the activated carbon regeneration process with ozone, a step that is also subject of research due to the high reactivity of ozone at ambient conditions compared to other more costly energetic methods for activated carbon regeneration.

2. FUNCTIONALIZATION OF ACTIVATED CARBONS WITH OZONE TO ENHANCE ITS ADSORPTION PROPERTIES

2.1. Methods to Modify the Activated Carbon Surface

As stated before, activated carbon is recognized as an effective adsorbent for the removal of a variety of organic and inorganic materials from water and wastewater. Its adsorptive properties are given by its great surface area, typically ranged from 500 to 2000 m^2/g; well-developed internal porosity with pores of different shapes and sizes (micropores with a pore width of less than 2 nm; mesopores with widths from 2 to 50 nm; and macropores with a pore width larger than 50 nm) and a broad range of surface functional groups, mainly oxygen groups such as carboxyl, carbonyl, phenol, lactone or quinone types (León y León and Radovic, 1994). In addition, activated carbons contain variable amounts of mineral matter (ash content) depending on the nature of the raw material used as precursor. Figure 1 shows the chemical structures of some typical oxygen functionalities on the surface of activated carbon.

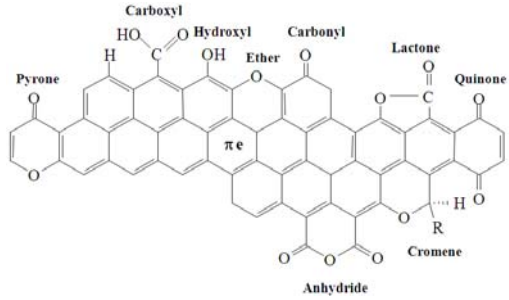


Figure 1. Some types of surface oxygen groups on activated carbons.

Adsorption from aqueous solution is a complex process that generally involves electrostatic and non electrostatic interactions. The electrostatic interactions, attractive and repulsive, are due to charges on the surface of the activated carbon and the ionic state of the adsorbates. The non-electrostatic interactions can be due to van der Waals forces and hydrophobic interactions. The factors that might influence these interactions, and therefore the adsorption process, are not only activated carbon properties such as surface area, pore volume, pore-size distribution and type and concentration of surface functional groups, but also properties of solutes (molecular structure and size, solubility and competitiveness between solutes) and process conditions such as pH, ionic strength and temperature. Although the surface area of an activated carbon is usually considered as the most important property in the adsorption process, in many instances the adsorption capacity is not directly related to this property but to the pore size distribution, which determines the accessibility of a given adsorbate to the microporous structure. In addition, the surface chemistry, which is mainly given by the presence or absence of surface oxygen groups, determines the surface charge of the activated carbon, its hydrophobic character and the electronic density of the graphene layers, thus affecting the adsorption process to some extent. In fact, the adsorption of some compounds (e.g., phenols) is controlled by the surface chemistry rather than by physical properties (Terzyk, 2003). Activated carbons are produced from a variety of solid carbonaceous materials (e.g., wood, lignite and coals, lignocellulosic materials, etc.) by physical and chemical activation methods. Physical activation, also known as thermal activation, usually consists of a carbonization of the raw material (char formation) followed by an activation, where the char produced is gasified with an oxidizing agent, usually steam. In the chemical activation method, the raw material is first impregnated with a chemical agent (e.g., phosphoric acid, zinc chloride) and thermally treated thereafter. Both, the nature of the precursor and the activation process conditions determine the final properties of the activated carbon which influence the adsorption process. While a number of commercial grades of activated carbons are today prepared by these conventional activation methods and marketed for water treatment applications, research on activated carbon modification is gaining interest in order to tailor its physical (i.e., textural) and chemical surface properties to develop its affinity for specific inorganic and organic species present in water. In this line, a number of methods are currently being researched, including those that make use of oxidizing agents such as nitric acid, hydrogen peroxide, peroxidisulphate, ozone or oxygen plasma to generate surface oxygen groups (Gu et al., 2009; Jaramillo et al., 2010a). In some of these cases, a thermal treatment in nitrogen or hydrogen follows the oxidation step to increase carbon basicity (Pereira et al., 2010). Other methods are aimed at fixing heteroatoms other than

oxygen on the carbon surface such as nitrogen, sulfur, phosphorous, halogens or boron (Bandosz and Ania, 2006). In this chapter the research on the modification of activated carbon by ozone treatments is reviewed.

2.2. Functionalization of Activated Carbon with Ozone

Mechanism and Kinetics of Reaction

The reactivity between ozone and carbon materials has been known since long (Papirer et al., 1967; Deitz and Bitner 1972; Deitz and Bitner 1973). Ozone owing to its great reactivity towards aromatic and unsaturated structures can react selectively with functional groups on the surface of activated carbons. In addition, ozone can decompose into free radicals species with high oxidizing capacity, including the hydroxyl radical (HO·), which can react with organic functionalities on activated carbons in an unselectively way (Papirer et al., 1967). Deitz and Bitner (1973) suggested that gaseous ozone is chemisorbed at ambient temperature on the activated carbon surface, rather than being physically adsorbed. These authors considered two different types of adsorption centers: centers C^1_n where the abstraction of an oxygen atom takes place and C^2_n centers where ozone is added to form an ozonide according to the Criegge's mechanism:

$$O_3 + C^1_n \rightleftarrows C^1_n \cdot O(ads) + O_2(ads) \quad [1]$$

$$O_3 + C^2_n \rightleftarrows C^2_n \cdot O_3(ads) \quad [2]$$

$C{\cdot}O_{(ads)}$ and $C{\cdot}O_{3(ads)}$ stand for different types of oxygen surface groups. Although there is not clear evidence about this, it is thought that centers C^1_n are sites on the activated carbon surface such as basic oxygen complexes (e.g., quinone, cromene and pyrone-like groups) (Montes-Morán et al., 1994) and mineral matter of the carbon (Heisig et al., 1997). Centers C^2_n are believed to be olefins and phenolic surface groups which are able to suffer ozone cycloaddition (Bailey, 1982; Mawhinney and Yates, 2001). The products of reactions [1] and [2] can undergo further surface changes to be gasified yielding gaseous CO and CO_2 and leaving stable oxygen-containing groups on the carbon surface (reactions [3] to [5]):

$$C^2_n \cdot O_3(ads) \rightleftarrows C^2_{n-1} \cdot O(ads) + CO_2 \quad [3]$$

$$C'_n \cdot O(ads) + O_3 \rightleftarrows C'_n \cdot O_3(ads) + O_2 \quad [4]$$

$$C'_n \cdot O_3(ads) \rightleftarrows C'_{n-1} \cdot O(ads) + CO \quad [5]$$

In addition to the non-catalytic mechanism outlined above, it has been suggested that gaseous ozone may also decompose catalytically into oxygen over activated carbon (Subrahmanyan et al., 2005). Álvarez et al. (2008), in a study with activated carbons of different textural and chemical surface properties, confirmed the coexistence of both catalytic and non-catalytic routes of ozone decomposition over activated carbon. From a kinetic point of view, the reactivity between ozone and activated carbon surface has been successfully explained by the first-order kinetic equation [6] that accounts for activated carbon deactivation (Álvarez et al., 2008):

$$-r_{O3} = (k_1 \cdot a_1 + k_2 \cdot a_2) \cdot C_{O3} \cdot \eta \qquad [6]$$

where a_1 and a_2 are activity functions (i.e., rate of ozone removal with used activated carbon divided by the rate of ozone removal with fresh activated carbon) related to the two mechanisms of ozone reaction. The effect of internal diffusion resistance to ozone mass transfer is given by the internal effectiveness factor, η, which represents the ratio between the actual rate of ozone removal for a whole activated carbon particle and the rate evaluated at the outer surface of an activated carbon particle (Levenspiel, 1972). Deactivation is attributed to the removal of basic sites and fixation of acidic surface oxygen functionalities on the activated carbon during ozonation. Reactivation can be achieved by thermal treatment at high temperature (850-1000ºC). Activity decay functions can be used to describe a_1 and a_2 as follows:

$$-\frac{da_1}{dt} = k_{d1} \cdot a_1 \cdot C_{O3} \cdot \eta \qquad [7]$$

$$-\frac{da_2}{dt} = k_{d1} \cdot a_2 \qquad [8]$$

Main variables affecting the kinetics of the activated carbon-gaseous ozone reaction are temperature (positive effect up to reach the temperature of thermal ozone decomposition), humidity (negative effect because of pore blockage by water) and properties of the GAC. Properties of GAC that favors the reaction rate are surface area, volume of large pores (meso- and macropores), concentration of basic surface functional groups and ash content. The kinetics and mechanism of the reaction between aqueous ozone and activated carbon surfaces has also been subject of research (Beltrán et al., 2002b; Sánchez-Polo and Rivera-Utrilla, 2003; Guiza et al., 2004; Sánchez-Polo et al., 2005; Álvarez et al., 2006; Faria et al., 2006; Dehouli et al., 2010). Although the activated carbon surface is oxidized by aqueous ozone, this process is much slower than oxidation with gaseous ozone due to the low solubility of ozone in water. The reaction mechanism is not yet clearly elucidated. However, a feasible explanation considers the formation of surface free radicals and other intermediates such as hydrogen peroxide. These can further react with organic compounds in water or decompose in the surface of the activated carbon to yield acidic oxygen groups (Álvarez et al., 2006).

Textural and Chemical Surface Changes

Considerable research has been devoted to the identification of surface oxygen groups generated by means of ozonation of carbon materials. Not only works with activated carbons but also with other carbonaceous materials such as chars (Gómez-Serrano et al., 2002a; Gómez-Serrano et al., 2002b; Kawamoto et al., 2005), carbon blacks (Bradley et al., 1995; Mul et al., 1998), carbon fibers (Fu et al., 1998; Ko et al., 2001; Khokhlova and Semenova, 2008) or carbon nanotubes (Cataldo, 2008) among others have been reported. Table 1 shows a compilation of studies on the modification of activated carbons with ozone. In most of the works listed in Table 1 it was observed that, regardless of the characteristics of the activated carbon used as raw material, the ozone treatment led to an increase of oxygen functionalities on the surface of the activated carbon. These surface groups have been identified by a number of techniques such as FTIR spectroscopy, XPS, TPD, TG-DTG or titration methods and, as a general rule, acidic groups such as carboxylic, phenolic, lactone and carbonyl groups were identified. However, basic groups, such as chromere and pyrone-like groups decreased in concentration or even completely disappeared with the ozonation treatment. As a rough estimation taken from the works of Valdes et al. (2002) and Álvarez et al. (2005), 1 mmol of ozone led to the fixation of 16 μeq/g of acidic sites and removal of 3.2 μeq/g of basic sites on GAC Filtrasorb 400. These figures vary from one activated carbon to another and they also depend on the pre-treatment applied to the activated carbon. Nevertheless, as a general observation, the point of zero charge (PZC) of activated carbons decreases with the ozone treatment, because of the fixation of strong acidic functions such as carboxylic acids. Regarding textural properties, applied at huge doses, ozone leads to a drastic decrease of surface area of the activated carbon as a result of destruction of microporosity. However, at mild conditions, ozone does not destroy porosity and it is possible to obtain activated carbons with well developed non-polar microporosity and acidic hydrophilic external surface area (Jaramillo et al., 2009; Jaramillo et al., 2010b). They can be regarded as dual activated carbons as can adsorb organic compounds on the internal microstructure and cations on their external surface area. Although most of the works listed in Figure 1 do not study the effect of temperature on the ozonation process, being the experiments carried out at room temperature, it has been shown that temperature affects the textural and chemical changes produced by ozone. Thus, the effect of ozonation temperature was investigated by Considine et al. (2001) and Álvarez et al. (2005), who found that at room temperature carboxylic acids were the main surface functionalities generated while a more even distribution of carboxylic, hydroxyl, and carbonyl groups was observed at 100ºC. Moreover at this higher temperature a gasifying effect of ozone is produced thus developing porosity on the activated carbon.

Table 1. Works on modification of activated carbon with gaseous ozone

Activated carbon	Reactor, conditions	Main features	Reference
ACs obtained from coal and coffee grounds	Glass tube reactor O_3 mass flow rate: 0.23 mg/min; Reaction time: 1 h; AC weight : 100 mg; Room temperature	Loss of micropore volume as a result of AC ozonation. Water vapour adsorption isotherms did not change considerably after AC modification.	Tsunoda et al., 1998

Table 1. (Continued)

Activated carbon	Reactor, conditions	Main features	Reference
Microporous AC obtained by activation of coconut shells with steam	Fluidized bed reactor O_3 mass flow rate: 0.6 mg/min; Reaction time: 1-3 h; AC weight : 0.5 g; Temperature: 150-250ºC	No significant modification of textural properties of AC but increase of oxygen content from 3.1% to 8.4%. Loss of adsorption capacity for 2-methylisoborneol from aqueous solution.	Considine et al., 2001
Powdered AC (KBB-type, Norit Corp.)	In situ FTIR cell O_3 mass: 26 mg; Reaction time: up to 6 h; Temperature: 300 K	Carboxylic acids were identified as main oxygen functionalities on the AC surface after oxidation.	Mawhinney and Yates, 2001
Granular AC (Filtrasorb 400, Calgon Carbon Corp)	Fixed bed reactor O_3 mass flow rate: 76 mg/min; Reaction time: 10-120 min; AC weight : 2 g; Room temperature	Loss of surface area and volume of micropores but increase in the volume of mesopores and external surface. Increase in oxygen content and decrease in the PZC as a result of the formation of lactone, carbonyl and carboxyl-type groups.	Valdés et al., 2002
Granular AC (Filtrasorb 400, Calgon Carbon Corp)	Fixed bed reactor O_3 mass flow rate: 76 mg/min; Reaction time: 10-120 min; AC weight : 2 g; Room temperature	The adsorption capacity and affinity of the AC for Cd(II) increased with ozonation. The opposite was observed for Hg(II).	Sánchez-Polo and Rivera-Utrilla, 2002
Granular AC (Filtrasorb 400, Calgon Carbon Corp)	Fixed bed reactor O3 mass flow rate: 76 mg/min; Reaction time: 10-120 min; AC weight : 2 g; Room temperature	The AC adsorption capacity for naphthalenesulphonic acids sharply decreased as the number of electron-withdrawing groups on the AC surface increased with the ozonation treatment	Rivera-Utrilla and Sánchez-Polo, 2002
Granular AC produced from coconut shells (Kowa Cosmos Company)	Fixed bed reactor O3 mass flow rate: 100 mg/min; Reaction time: 30 min; AC weight : 0.5 g; Room temperature	AC samples were pre-treated with aqueous NaOH. Increases of the concentration of surface phenolic and carboxylic groups were observed after ozonation.	Chiang et al., 2002a
Granular AC produced from coconut shells (Kowa Cosmos Company)	Fixed bed reactor O3 mass flow rate: 100 mg/min; Reaction time: 30 min; AC weight : 0.5 g; Room temperature	Surface area and micropore volume of AC increased as a result of AC ozonation. Increases of surface oxygen groups (phenolic and carboxylic) were also observed.	Chiang et al., 2002b

Activated carbon	Reactor, conditions	Main features	Reference
Granular AC (Filtrasorb 400, Calgon Carbon Corp)	Fixed bed reactor O3 mass flow rate: 76 mg/min; Reaction time: 10-120 min; AC weight : 2 g; Room temperature	The adsorption capacity and affinity of the AC for Cr(III) increased with ozonation.	Rivera-Utrilla and Sánchez-Polo, 2003
Granular ACs (Filtrasorb 400 and AQO40, Cehmviron Carbon)	Fixed bed reactor O_3 mass flow rate: 16.6 mg/min; Reaction time: 15 min; AC weight : 0.25 g; Temperature: 25ºC and 100ºC	No great textural but chemical changes were observed. Drastic increase of acidic surface oxygen groups and decrease of PZC. AC ozonation had a negative impact on adsorption capacity for phenolic compounds	Álvarez et al., 2005
Granular AC obtained from coconut shells (Nacalai Tesque)	Glass flask reactor O_3 mass flow rate: 15-35 mg/min; Reaction time: 2 h; AC weight : 1 g; Room temperature	Increase of AC porosity and the O/C ratio after ozonation	Kawamoto et al., 2005
Granular AC (Dong-Yang Carbon Co)	Fixed bed reactor O_3 mass flow rate: 6 g/h; Reaction time: 1-4 h; AC weight : 2 g; Room temperature	Ozonation for a long time produced drastic loss of surface area and microporostiy. Main functional groups fixed on the AC surface by means of ozonation were identified as carbonyl and ether structures. Ozonated carbon was more efficient than the untreated material for the removal of ammonia	Park and Jim, 2005
Granular AC (Filtrasorb 400, Calgon Carbon Corp)	Fixed bed reactor O_3 mass flow rate: 5g/h; Reaction time: 1 h; AC weight : 2 g; Temperature: 298 K	Increase of acidic sites and decreases of basis sites, surface areas and PZC A significant reduction in the carbon adsorption capacity of benzothiazole was observed after ozonation.	Valdés and Zaror, 2006
Granular ACs with different physical and chemical characteristics	Fixed bed and expanded bed reactors O_3 mass flow rate: 0.5-1.25 g/h; Reaction time: 15 min; AC weight : 0.25-1.5 g; Temperature: 298-473 K	Increase of acidic surface oxygen groups and decrease of basic surface groups. Ozonation kinetics followed a first-order law with deactivation.	Álvarez et al., 2008
Granular AC (CarboTechAC GmbH)	Fixed bed reactor inside an IR spectrometer Reaction time: 3 h; AC weight : 200 mg; Temperature: 60ºC	Formation of carbonyl, carboxylic, lactone and anhydride surface groups by ozonation.	Kohl et al., 2009

Table 1. (Continued)

Activated carbon	Reactor, conditions	Main features	Reference
Granular AC obtained from cherry stones	Fluidized bed reactor O_3 mass flow rate: 0.75 g/h; Reaction time: 1 h; AC weight : 10 g; Room temperature	No great textural changes but formation of acidic surface oxygen groups and decrease of PZC. Functionalized AC showed good adsorption capacity for aqueous Cu(II) and Co(II).	Jaramillo et al., 2009
Granular AC obtained from cherry stones	Fluidized bed reactor O_3 mass flow rate: 0.75 g/h; Reaction time: 1 h; AC weight : 10 g; Room temperature	Compared with other dry and wet oxidation methods, oxidation of AC at 100 °C in ozone was proved as a promising method to increase the content of acidic oxygen surface groups without greatly destroying microporosity and with a significant mesoporosity development	Jaramillo et al., 2010b
Granular AC obtained from cherry stones	Fluidized bed reactor O_3 mass flow rate: 0.75 g/h; Reaction time: 1 h; AC weight : 10 g; Room temperature	The type and concentration of oxygen groups on the AC surface and, therefore, its acidic-basic character of AC can be controlled by ozonation followed by thermal treatment.	Jaramillo et al., 2010b

Adsorptive Properties of Ozonated Activated Carbons

A few works reported in the recent literature have been devoted to study the adsorption of specific organic and inorganic compounds from aqueous solution on ozonated carbons (Considine et al., 1991; Sánchez-Polo and Rivera-Utrilla, 2002; Rivera-Utrilla and Sánchez-Polo, 2002; Rivera-Utrilla and Sánchez-Polo, 2003; Álvarez et al., 2005; Park and Jim, 2005; Valdés et al., 2006; Jaramillo et al., 2009). Some of these works were carried out using aromatic compounds as adsorbates, including phenol, p-nitrophenol, p-chlorophenol, naphthalenesulphonic acids and benzothiazole. In all of these cases it was found that activated carbons lost adsorption capacity as a result of the ozonation. Adsorption of aromatic compounds onto activated carbon is governed by dispersive forces between the π electrons of the aromatic ring of the molecule and π electrons distributed on the graphene layers of the activated carbon. The formation of acidic oxygen groups by ozonation, such as carboxylic acids, which has electron-withdrawing nature, weakens dispersive interactions and, therefore, decreases the adsorption capacity to some extent. On the other hand, the adsorption of ions such as Co(II), Cu(II), Cd(II) and Cr(III) was enhanced by treating activated carbons with ozone. The functionalization of activated carbon with ozone brings about a drastic decrease of its pH_{PZC}. The pH_{PZC} can be defined as the aqueous pH at which the net surface charge of the activated carbon is zero. According to this, if the pH is lower than the pH_{PZC} of the solid, this would be negatively charged. Conversely, if the pH_{PZC} of the carbon is lower than the aqueous pH the charge on its surface would be positive. Thus, at near neutral pH, ozonated

activated carbons show a negatively charged surface with ability to electrostatically attract positively charges species.

3. Effects of Ozonation on Subsequent Activated Carbon Filtration: The BAC Process

Activated carbon filters in drinking water constitute one of the recommended processes in a drinking water treatment plant (DWTP) since both non biodegradable and biodegradable dissolved organic carbon, NBDOC and BDOC, respectively, are removed in these units. When the activated carbons filters are initially operating the main process they carry out is adsorption or removal of the NBDOC but as long as the operation time increases biological activity commences and elimination of BDOC can be more important. For example, data from some DWTP indicate that after five months of operation removal of BDOC in activated carbon filters becomes more important than removal of NBDOC, that is, removal by only adsorption mechanisms (Langlais et al., 1981). According to Sontheimer (1988) the biological activity in activated carbons filters starts to be important after 5-20 days of operation. Formation of bacteria colonies in activated carbon filters has been shown through different analytical techniques such as the electronic microscope (Lafrance et al., 1983) or feeding some specific constituents for microorganisms such as triphosphate adenosine (Bourbigot et al. 1981). Contribution of bacteria in activated carbons filters has been confirmed by measurements of dissolved oxygen consumption or carbon dioxide formation (Sontheimer et al., 1977). Previous studies have also confirmed that bacteria removes a fraction of DOC (10%) and increases activated carbon regeneration, thus, increasing filter life (De Laat et al., 1991). Very recently, Yapsakli and Çecen (2010) studied the nitrification process on activated carbon filters both thermally and chemically treated and with raw water (Ömerli reservoir in Istambul) or preozonated water. They identified a series of nitrifying bacteria to improve biodegradation. They observed better performance of thermally treated activated carbon and not too many differences between biodegradation of raw or preozonated water. However, in a second work (Chapsakli et al., 2010), the authors reported that the type of feed water played a more important role than activated carbon pretreatment with respect to the nature of nitrifying bacteria and that ozonation increase gave rise to more different types of ammonia-oxidizing bacteria than non-ozonated raw water. The use of ozonation before activated filters is also a common operation in DWTP since ozone, due to its high reactivity, reduces high molecular weight compounds to lower molecular weight oxygenated organic compounds, that is, it enhances the BDOC of the water (Urfer et al., 1997, Volk et al., 1993). As a result, biological activity in activated carbon filters is enhanced and, hence, filter life time is augmented. The net result is that the water effluent from activated carbon beds has lower BDOC than the influent water to these filters when it comes from an ozonation step. For example, very recently Treguer et al. (2010) studied the influence of ozone on the biodegradability of water treated in three 14 L hollow fiber membrane bioreactors containing fluidized activated carbon (PAC Picasorb 16) of a DWTP with water and PAC residence times being 40 min and 40 days, respectively. Without ozone pretreatment, residual DOC was mainly constituted by NBDOC but ozonation (0.3-1 mg O_3/mgDOC) increased the BDOC fraction of DOC and reduced aromaticity yielding organic compounds of smaller size. Curiously enough the

authors also observed that activated carbon first removed BDOC. However, preozonation can alter the adsorption of organic molecules on activated carbon filters since ozone increases the hydrophilicity of the ozonated effluent. As a result, the adsorption capacity of activated carbon can be reduced. Nonetheless, the decrease of molecular weight of organics after ozonation makes the corresponding molecules more accessible to activated carbon pores. Then, the ozone dose is an important parameter to control the ratio of NBDOC and BDOC reaching the activated carbon filters and the performance of these units. Thus, low ozone doses allow partial breaking of NBDOC into BDOC that could not be enough to benefit the biological process in the activated carbon. In this case, activated carbon filters act as adsorption units. However, a high ozone dose can make filters to act entirely as biological step with deterioration of the adsorption process. From existing bibliographic data (Langlais et al., 1981) it is well known that there is an optimum ozone dose beyond which the BDOC does not increase. This ozone dose will depend on the type of water and further bed contact time on the activated carbon filters. According to Sontheimer (1988) an optimum ozone dose would be around 0.5 mg O_3/mgC. The combination of ozone and activated carbon in a sequential process has also been addressed to the study of specific compounds removal. Among the compounds or to better say, pollutants studied, one can highlight THMs, bromate, pharmaceuticals, dyes, etc. Examples of the use of ozone followed by activated carbon filters from recent works (late three years) are given next. Thus, Xie et al. (2007) have reported results on bromate and trihalomethane formation potential, THMFP, from Yellow river water treated in a DWTP with ozone, bioceramic filtration, coagulation, particle separation, rapid sand filtration and two parallel activated carbon filters, one with fresh activated carbon and a second one with 1.5 year operation BAC. They compared the evolution of bromate, THMFP, TOC and UV radiation absorbance. They observed THMFP increased after ozonation but reduced after AC filtration with fresh AC working better. They also observed similar results for bromate. Then, at the conditions they applied the adsorption process was more important than the biological one on the activated carbon filter. Konsowa et al. (2010) have studied the removal of wastewater containing direct dyes in a sequential ozone-activated carbon process. Samples were first ozonated in a Plexi-glass semibatch bubble column (10 cm i.d. 50 cm height) and then treated for 30 min with activated carbon (Norit NRS CARGON GA, 0.5-2.5 mm, 975 m^2/g) in a well agitated slurry tank charged with the ozonated water. The main aim of the work, this time, was to reduce TOC content of the influent water. Thus, complete decolorization is achieved after ozonation in between 10 and 45 min depending on the experimental conditions (gas flow rate, ozone concentration, dye concentration, pH) but TOC is reduced only about 10%. The use of activated carbon leads to a further 37% TOC reduction. No data is given about the mechanism of mineralization on activated carbon. In another work, Vieno et al. (2007) observed the changes of some pharmaceutical compounds (fluoroquinolones, beta-blockers, antiepilectic drugs, etc) in a river from a sewage effluent. They used a DWT pilot plant consisting of coagulation, rapid sand filtration, ozonation and two stage GAC filtration and UV disinfection. They observed physical operations before ozonation hardly reduced 13% the pharmaceutical compounds present in the water while ozone was very effective. However, hydrophilic compounds such as ciprofloxacin or atenolol were not completely removed after the whole process. The combination ozone-BAC, however, should be conveniently coupled with the rest of operations to optimum performance of the treatment plant. For example, Marda et al., (2008) also studied treatment of river water in a real DWTP where activated carbon was implemented after ozonation. They observed a

sudden reduction of monochloramine formation due to biological activity on AC filters. The problem was solved by changing the free chlorine and ammonia injection points and filter backwashing. Therefore, the combination ozone-BAC eventually improved the performance of the treatment plant. In studying river water influent to a DWTP, Huerta-Fontela et al., (2008) detected the presence of different illicit drugs such as cocaine, amphetamine, methamphetamine and MDMA (ecstasy) at ng/L level. Also, nicotine, caffeine and their metabolites were found at the μg/L level. They found the sequence ozone-activated carbon removes 100% cocaine, 88% MDMA, 72% benzoylecgonine and 63% cotinine. They also applied postchlorination. After the whole process, only caffeine and two metabolites: cotinine and benzoylecgonine persisted. In a series of works (Reungoat et al., 2010ab; Macova et al., 2010) the effect of ozonation and activated carbon filtration on the removal of pharmaceutical compounds from a sewage wastewater was studied and their biological activity was monitored. Data were obtained from a full reclamation plant where 85 compounds were followed. The plant had a series of conventional operation units with coagulation-floculation (aluminium sulphate), dissolved air flotation and sand filtration (6 m^3/m^2h), main ozonation (5 mg/L ozone dose and 15 min contact time) and activated carbon filtration (18 min contact time) as main steps for pollutant removal and decrease of biological activity. Main ozonation decreased the level of non-specific toxicity and other specific toxic modes of action. Thus, from the five toxicity modes measured, after ozone and activated carbon processes only two remained positive for water samples: the vibrio fishery (non-specific toxicity) and Ah-receptor (dioxin-like effects) assays. In any case, positive response to these assays was much lower than that of influent wastewater (79 and 64% decrease of the response, respectively). As far as specific pharmaceutical removal is concerned the combined process also allowed significant reductions for all compounds. Only gabapentin and roxythromycin remained in water at concentrations above their limit of quantification (0.01 μg/L).

Not only specific compounds but general parameters such as natural organic matter, NOM, have been study to check the performance of GAC or BAC processes with a preozonation step. NOM is the main source of organic carbon in surface waters and the precursor of disinfection products (i.e. THMs) and problems associated to odor and taste. However, it is also the origin of microorganism formation on activated carbon surface. In this sense, NOM facilitates the life of activated carbon filters if the water contains BDOC. Yapsakli et al. (2009) studied the influence of ozone on the NOM adsorption-desorption capacity of some activated carbons. They found pH_{PZC} of activated carbons also played a main role, with basic activated carbons recommended to increase the adsorption capacity for all conditions tested which was attributed to the electrostatic attractions between GAC and the negatively charged NOM. Regarding the effect of preozonation they reported the existence of optimum ozone doses (2 mgO_3/mgDOC) to improve the biodegradability of the water. Also, they concluded that choosing an activated carbon that provides a high desorption of biodegradable organics is the best option to improve the BAC process. This is because desorption of biodegradable organics will result in increase adsorption capacity of BAC for non biodegradable organics. In another work, Lou et al., (2009) also treated the problem of THMs together to that of haloacetic acids (HAAC) and assimilable organic carbon (AOC) from a polluted river. AOC in finished water is the main responsible of bacteria regrowth in water distribution systems. Then, this parameter must be kept below some critical value. In this case, not only THMs and HAACs removal was improved by the combined system but also the AOC. For the latter the presence of BAC was fundamental since this process allowed

AOC concentrations in the treated water below the maximum permissible world level (50 μg acetate-C/L).

Wastewater from some processes such as reverse osmosis (RO) has also been studied with ozone and BAC as pretreatment steps of electrolytic brine recovery processes. Thus, Lee et al. (2009) applied ozone and activated carbon to a RO brine concentrated wastewater of very low biodegradability (BOD<2 mg/L, BOD/TOC<0.13). From batch experiments, the authors observed an increase of biodegradability of the wastewater (between 4.3 and 5.4 after 10 min ozone contact with 3 to 10 mg/L ozone dosage, respectively). In a lab scale integrated ozone-BAC-membrane electrolytic process with 6 mgO_3/L dosage and 20 min contact time and a BAC column of 60 min of empty bed contact time (EBCT), the authors measured the molecular weight distribution of organics in the RO wastewater and confirmed the breakdown of complex molecules after ozonation. They also observed 70% and 90% TOC and COD reductions, respectively, after the ozone-BAC process. BDOC was fully retained in BAC filters since effluent BOD was lower than 2 mg/L. In addition, the ozone-BAC process allowed keeping fouling of the membrane electrolytic process under control.

4. Activated Carbon Catalytic Ozonation in Water

Activated carbons are one of the solid materials used as catalysts to improve the ozonation of organic compounds in water. As a matter of fact, this process is one of the most studied OAOP during the last two decades and has already being the subject of some review works (Beltrán, 2008). In this chapter, this latter review is continued from 2007 to present the state of the art of this process. Thus, according to what literature reports works on activated carbon catalytic ozonation mainly deal with the study of operating variables, type of carbon materials used (granular, powdered, fiber, cloth, multiwalled nanotubes activated carbons, etc), activated carbon combined with other catalysts (mainly metals), nature of water to be treated (pollutants in ultrapure, drinking water or wastewater) mechanism, kinetics and modeling of the process. Table 2 gives a list of principal woks published on these aspects since 2007.

Table 2. Works on activated carbon ozonation processes

Compounds, Activated carbon type	Reactor, conditions	Main features	Reference
4 dyes and 2 biological effluents Norit GAC 1240Plus pH_{PZC}=9.7, S_{BET}=972 m^2/g, Size: 0.8-1,1mm	2.5 i.d., 30 cm height GAC bed acrylic column. Liquid residence time: 7.36 min Semicontinuous operation C_{O3g}=50 mg/L, pH 7	Adsorption Breakthrough curves. Decoloration at 436, 525, 620 nm TOC removal in ozone, AC adsorption and AOAC Better process: AOAC	Soares et al., 2007

Compounds, Activated carbon type	Reactor, conditions	Main features	Reference
Azo dyes, Fluka GAC S_{BET}=1600 m^2/g, Size: 2.5 mm	1L semibatch slurry reactor 100 mg/L azo dye, 28 mg/min ozone dose, pH=6	Removal of dyes and mineralization. O3/GAC leads to 50% TOC removal. Ions release to the water. Optimum GAC/organic ratio	Gül and Erbatur, 2007
Phenol, AC Fiber: S_{BET}=749 m^2/g,	3x50 cm Pyrex AC fluidized bed reactor, C_{O3g}=9.8 mg/L, 100 mg/L phenol	Phenol and COD removal. No diffusion limitations. 4 reuse of ACF without loss of activity. Increase of acidic surface oxygen groups. Changes in volume of micro and mesopores	Qu et al., 2007
Naphthalensulfonic acids Sorbo GAC, pH_{PZC}=12.1 S_{BET}=1182 m^2/g, Size: 0.5-0.8 mm UV/H2O2 also studied	2L batch or semibacth slurry reactors and Merry-go-round photoreactor TNN 15/32 Heraeus low and medium pressure Hg lamps	Non effective UV radiation Direct and HO reaction rate constants and 254 nm quantum yields determined. Use of photosensitizers. AOAC better than single processes to remove surfactants	Sánchez-Polo et al., 2007
Industrial pharmaceutical wastewater Yixin GAC Size: 1.5 mm	Batch and 6.5x50 cm GAC bed semibatch ozone reactor (280 g GAC). 10911 mg/L COD, pH=10	pH 12, in less than 30 min ozone and GAC single processes remove <40% COD while O3/GAC removed 86% COD Basic pH: catalytic ozonation takes place Acid pH: Adsorption-O3 AC regeneration predominates	Lei et al., 2007
Polyphenol moixture of gallic and syringic acids and tyrosol P110 Hydrafin AC pH_{PZC}=10.4, S_{BET}=967 m^2/g, Size: 1-1.6 mm	750 cm3 semibatch slurry reactor pH 2.5 and 5	Removal of TOC and individual phenolics Saturated carboxylic acids intermediates. Lower ozone consumption with O3/GAC Effect of pH	Giráldez et al., 2007
Oxalic and oxamic acids Norit GAC 1240 Plus virgin (909 m2/g, pH_{PZC}=8.5) and HNO3 treated (827 m2/g, pH_{PZC}=3), Size: 100-300 μm	1L semibatch slurry reactor 350 mg AC, pH 3 to 7	Adsorption kinetics. In 60 min: 60% oxamic acid removed with O3/AC while 20% from ozone and <5% with GAC. T.butanol does not affect at pH 3 but it does at pH 7. Chemically treated AC is worst	Faria et al., 2008a

Table 2. (Continued)

Compounds, Activated carbon type	Reactor, conditions	Main features	Reference
Polyphenol mixture of gallic and syringic acids and tyrosol P110 Hydrafin AC pH_{PZC}=10.4, S_{BET}=967 m^2/g, Size: 1-1.6 mm	750 cm3 semibatch slurry reactor pH 2.5 and 5	Determination of rate constant and stoichiometric ratio of ozone reactions. Kinetics regarding TOC. Mass transfer and chemical reactions accounted for	Beltrán et al., 2008
Oxalic acid. Carbon nanotubes (CNT): 10-20 nm, 5-15 μm length, 117 m2/g BET, pH_{PHZ}=6.13. , PAC with <5μm. 763 m2/g, pH_{PZC}=8.38 1%Pt/AC and Pt/CNT	1L semibatch slurry reactor. 20 mg/min O3, 100 mg/L catalyst, pH 3	30 min: 95% oxalic acid removal with Pt/CNT/O3 and 60-70% removal with Pt/AC/O3, AC/O3. CNT/O3 TOC increase in water due to carbon ozonation. Effect of catalyst preparation method. t-butanol effect. 5 reuse cycles of catalyst. Mechanism proposed and importance of Pt redox couple. No Pt leaching	Liu et al., 2008
Di2ethylhexylphthalate (DEHP) Norit GAC 830. Untreated GAC and O3 GAC treated. Me/AC (Me:Cr, Co, Fe, Mn)	1.5 L (7.5x35 cm) semibatch slurry column. pH 4, 7, 10 and 11. DEHP=300 μM	Cr/AC/O3 worst than AC/O3 likely due to Cr leaching. Basic SOG favours ozonation	Hammad-Khan and Jung, 2008
Benzene sulfonic and sulfonilic acid. Norit GAC 1240 Plus virgin (909 m2/g, pH_{PZC}=8.5) and HNO3 treated (827 m2/g, pH_{PZC}=3), Size: 100-300 μm	1L semibatch slurry reactor 350 mg AC, pH 3 to 7	O3/AC(virgin) leads to best results in organic and TOC removal. Intermediates acids evolution. Different t-butanol effect depending on pH and organics ozonation	Faria et al., 2008b
4 nitroimidazoles Three ACs: Sorbo: pH_{PZC}=9, 1225 m2/g Merck: pH_{PZC}=7.7, 1301m2/g, Petroleum coke: pH_{PZC}=8, 1261 m2/g 0.45-1 mm	Batch slurry reactor. 0.25-0.5 g/L AC. Ultrapure, surface and urban wastewater used	O3/GAC leads to toxicity reduction(Lumistox system) Increase of TOC and organics removal with O3/GAC. Rate constants determination. Intermediate detection. Influence of the water matrix	Sánchez-Polo et al., 2008
Dyes and humic acids as THM precursors. 63-297 μm AC	200 mL semibatch slurry washing bottles	Good dye removal for the three systems. O3/GAC better process to remove THMFP	Kawasaki et al., 2008

Compounds, Activated carbon type	Reactor, conditions	Main features	Reference
Pulp bleaching effluent GAC: 600 m2/g, 0.5-1.6 mm Also used Fe(II) and Mn(II) for ozone catalysts	1.5 L bubble slurry column. K_La=0.03 s^{-1}. 2900 mg/Lh O3, pH 7 and 10 1150 mg/L COD, 130 mg/L BOD	Comparisons of homogeneous (Fe(II)/O3 or Mn(II)/O3) and heterogeneous (GAC/O3) catalytic ozonations. COD and UVA absorption evolution. 20 and 40% TOC removal increase with GAC/O3 after 20 and 60 min, respectively. 5 Cycles of GAC reuse. GAc regeneration.	Balcioglu and Moral (2008)
Humic substances (HS) (Sigma-Aldrich) PAC from Merck 455 m2/g	7x40 cm semibatch slurry bubble column. 300 mg/L HS. pH 4, 10 and 12	Determination of apparent first order rate constant with pH. Positive effect of PAC amount increase. Artificial neural network application for kinetic modelling	Oguz et al., 2008
Sodiumdodecyl-benzenesulfonate (SDBS). Sorbo carbons: pH_{PZC} 12.1, 1225 m2/g. GAC (0.5-0.8 mm) and PAC (0.05-0.08 mm)	1L batch slurry ozone reactor	Effects of NOM (gallic acid and humic acid) on SDBS removal. Promoters and initiators of ozone decomposition. Mechanism proposed. H2O2/O3, GAC/O3 and PAC/O3 studied	Rivera-Utrilla et al., 2008
pNitrofenol and Simulatedwastewatr Yixin GAC 653 m2/g, pH_{PZC}=6.72,	Semibatch ozone slurry reactor, pH 4-10, pNP=1 g/L, WW: 1560 mg/L COD and 733 mg/L TOC.	Catalytic ozonation mainly at basic pH. Positive effect of t-butanol specially pH 10. In 30 min: 90% COD removal in GAC/O3 and 70% COD removal in GAC. Biodegradability increase after GAC/O3. Mechanism pathways	Gu et al., 2008
Aniline, sulfanilic acid, azo dyes Norit 1240 Plus GAC Me/O3 (Me:Ce, Mn, Co) and MeO/GAC/O3	Semibacth slurry reactor	Characterizacion of catalyst Double metal oxide catalyst 90%TOC removal in 240 min, 85% TOC removal with Ce(5%)/GAC/O3 in 180 min.	Faria et al., 2009a
pNitrophenol Yixin GAC 653 m2/g, pH_{PZC}=6.72 AC modified with non-thermal plasma	6x50 cm pyrex glass semibatch slurry reactor. 1.5 g/L pNP, 5 g/L GAC	AC characterization. Changes in S_{BET} and micro and mesopore distribution. Adsorption isotherms. pH 10 better performance of modified GAC/O3: 70% TOC removal	Gu et al., 2009

Table 2. (Continued)

Compounds, Activated carbon type	Reactor, conditions	Main features	Reference
Methylene blue GAC/O3 and TiO2/GAC/O3	3.2x35 cm semibatch slurry bubble column	Removal of colour and COD. In 210 min: 58, 72, 86% COD removal with O3, GAC/O3and TiO2/GAC/O3, resp. In 40 min: 88, 95 and 100% colour removal with O3,GAC/O3 and TiO2/GAC/O3, resp.	Zhang et al., 2009
SDBS Sorbo-Norit AC pH_{PZC} 12.1, 1225 m2/g. GAC (0.5-0.8 mm) and PAC (0.05-0.08 mm). Other oxidants: MnO_4^-, ClO_2, ClO^-	1L batch slurry ozone reactor	Only GAC/O3 and PAC/O3 give good results. Conventional did not work. No toxicity in ozone processes. PAC/O3 performs better than GAC/O3 for SDBS removal but similar for TOC removal	Méndez-Díaz et al., 2009
Azo and anthraquinone dyes Norit 1240 Plus GAC AC/O3, CeO2/AC/O3, CeO2/O3 systems	1L semibatch slurry reactor Dye: 50 or 300 mg/L, 350 mg/L catalyst, pH 5-6 Use of influent and effluent of biological step for two textile wastewaters	Composite material / O3 leads to best results of TOC removal. 3 cycles reuse catalyst keeps activity. Reaction pathways.	Faria et al., 2009b
pChlorobenzoic acid (PCBA) AC from petroleum coke: 1619 m2/g AC/O3 and Ni/AC/O3 systems	1.4 L semibatch slurry reactor. 100 mg/L PCBA, 5 g catalyst. pH 4.3	With Ni/Ac/O3 total PCBA removal. In 60 min: 60, 43 and 30% TOC removal with Ni/AC/O3, AC/O3 and O3, resp. Demineralized AC performs worst	Li et al., 2009a
Diclofenal (DCF) Three ACs: P110 Hydraffin(pH_{PZC}9.72) Darco12-20 (pH_{PZC}= 6.35) and GMI 2000 (pH_{PZC}=9.23). 1-1.25 mm	5x30 cm semibatch ozone reactor followed by 3x3 cm packed AC fixed bed column. Water recirculation rate: 2 L/h, DCF: 10^{-4} M, C_{O3g}=20 mg/L	Ecotoxicity test with Daphnia Magna. Equilibrium isotherms. Mineralization. Ozone consumption. H2O3 formation. GAC/O3 performs better. Kinetics: external diffusion controls	Beltrán et al., 2009a

Compounds, Activated carbon type	Reactor, conditions	Main features	Reference
Bisphenol A (BPA) Lurgi AC, 972 m2/g	1L semibatch slurry photoreactor. Low pressure Hg lamp (254 nm) $4.5x10^{-6}$ Einstein/Ls TiO_2 Degussa P25 C_{O3g}=30 mg/L	Comparison of processes: O_3, O_3/UVC, O_3/TiO_2/UVC, AC/O_3/UVC, etc Ecomomic considerations AC addition improves TOC removal (100% TOC removed in 20 min)	Rivas et al., 2009
17β-estradiol AC: size: 63-297 μm O_3 treated and untreated AC	Semibatch slurring gas washing bottles 60 min treatment time	Effects of ozone on AC No difference with both ozone treated and untreated AC but reduction of treatment time whehn using O_3/AC	Kawasaki et al., 2009
Diclofenac DCF P110 Hydraffin PAC	Semibatch slurry ozone reactor. PAC=1 g/L, TOC=15 mg/L. C_{O3g}=20-40 mg/L	TOC reduction Kinetic modelling. Important of intermediates as inhibitors or promoters of ozone decomposition in HO radicals	Beltrán et al., 2009b
Two dyes and oxalic acid Mesoporous AC (MAC) from Silica and carbon xerogels Chemical and thermal treatments 0.1-0.3 mm size	1 L semibatch slurry mechanically agitated reactor. C_{O3g}=50 mg/L. Dye: 100 mg/L or Oxalic acid: 10^{-3}M 350 mg MAC	MAC characterization (pH_{PZC}, Mesoporosity and Microporosity, BET surface).More basic MAC after HNO3 and thermal treatments. MAC from silica template presents higher mesoporosity. Ozone Dye removal rate independent on MAC presence. TOC removal rate improves with MAC/O_3. Adsorption is < 20% TOC removal. Basic MAC, high mesoporosity perform better	Orge et al., 2009
17α-Ethynylestradiol ETE Three ACs: P110 Hydraffin(pH_{PZC}9.72) Darco12-20 (pH_{PZC}= 6.35) and GMI 2000 (pH_{PZC}=9.23). 1-1.25 mm	5x30 cm semibatch ozone reactor followed by 3x3 cm packed AC fixed bed column. Water recirculation rate: 2 L/h, ETE: 10^{-4} M, C_{O3g}=20 mg/L	Ecotoxicity with Daphnia Magna. Three 60 min AC reuse show constant activity. Rapid direct reaction ETE-O_3. 90% TOC removal with AC/O_3. Effects of pH (pH 9 worst results). Basic AC performs better	Beltrán et al., 2009c

Table 2. (Continued)

Compounds, Activated carbon type	Reactor, conditions	Main features	Reference
Sulphamethoxazol SMX Three ACs as in previous reference Also Perovskite/O_3 system	The same as in previous reference in this table	Comparison between catalytic ozone processes. Isotherms studies. SMX reacts very fast with O_3 alone. Saturated carboxylic acids and H_2O_2 as intermed. O_3 consumption and TOC reduction. Kinetics	Beltrán et al., 2009d
Phenol in saline wastewater Merck GAC, 0.5 mm size	250 mL semibatch slurry reactor. 0-50 g/L NaCl, 0-25 g/L GAC. Phenol: 1,2 g/L. pH 2, 8 and 10. 2600 mg/L COD	Best performance at pH 8. Nearly 100% Phenol removal in < 5 min with AC/O_3 against 50% with O_3. Nearly 85% COD removal in 20 min. T-butanol effect	Moussavi et al., 2009
Dimethylphthalate (DMTP) Norit GAC 1240 Plus CeO and CeO/AC (522 m2/g)	1.4 L semibatch slurry reactor. pH 5, DMTP: 30 mg/L. 2 g cat.	22, 48 and 68% TOC removal in 60 min with O_3, AC/O_3 and CeO/AC/O_3. Demineralized AC works worst. T-butanol inhibits DMTP removal rate. Catalytic activity keeps after 780 min	Li et al., 2009b
Aniline, Sulfanilic acid, Benzenesulfonic Norit GAC 1240 Plus CeO and CeO/AC	1L semibatch slurry reactor $C_M=10^{-3}$M. 350 mg catal. C_{O3g}=50 mg/L	Evolution of saturated acid intermed. And ions (NH_4^+, NO_3^-, $SO_4^=$). Different compound degradation rates depending on the process. As a whole CeO/AC better catalyst	Faria et al., 2009c
Phenol Calgon AC: 0.6-2.3 mm size, 1060 m2/g BET. Carbokarn AC: 0.4-1.7 mm size, 1154 m2/g BET	3.16x45 cm height co-current upward flow three phase fluidized reactor Phenol: 10 mg/L. AC: 5 g	Comparison of processes AC/O3 removes completely phenol and 80% TOC	Charintpanitkul et al., 2010
Tinidazole TNZ Merck AC: 0.45-1 mm size, 1301 m2/g BET. pH_{PZC}=7.7	Batch slurry (0.25-0.5 g/L) and continuous AC bed fixed reactor (2g AC)	Toxicity reduction. TOC removal. Intermediates. Influence of water matrix. Lack of O_3 at fixed bed column negatively affects TNZ removal	Rivera-Utrilla et al., 2010

Compounds, Activated carbon type	Reactor, conditions	Main features	Reference
Phenol Carbon cryogel beads (CCB) of different S_{BET}. CCB also pretreated with $(NH_4)_2S_2O_8$. Also AC beads	200 mL semibatch ozone reactor. Phenol: 200-400 mg/L. 0.5 g adsorbent	Equilib.Isotherm:Freundlich Apparent first order kinetics CCB better with O_3 Pore size effect. Both CCB and ACB lose activity after reuse	Chaichana wong et al., 2010
2,4-Dichlorophenol (2,4D) and nitrobenzene (NB) Two Pica AC 1000-1300 m2/g. Microporous 0.9-1.7 nm	2L semibatch slurry reactor AC: 1g/L, NB:250-1879 µg/L 2,4D: 1534 µg/L	O_3 diffusion more important than S_{BET} on O_3 decomposition on AC. For 2,4D AC/O_3 has no advantage compared to O_3 For NB, AC/O_3 performs better. Intermediates detected	Merle et al., 2010
Pica 150 AC: 630 m2/g, pH_{PZC}=2.2. Picaflo AC: 840 m2/g, pH_{PZC}=2.6	1.5L batch slurry reactor 10-30ºC	Ozone decomposition on AC. First order kinetics. Effect of textural and chemical properties of ACs. Acid groups favour O_3 decomposition.	Dehouli et al., 2010
Methyl Orange (MO) TiO_2/ACFiber. 41.9% TiO_2 coated. 803 m2/g S_{BET}	400 mL Pulse discharge glass slurry reactor with O_2 bubbling. Intensive radiation (200-1000 nm). pH 6.1; MO: 80 mg/L. 0.25 g TiO_2/ACF	Ozone is formed in the process. There is adsorption and photocat. Ozonation. Increase of anatase/rutile ratio with temp. Catalyst activity keeps after reuse if pulse discharge is on	Zhang et al., 2010

In the following sections, highlights of these aspects are dealt with. First of all, however, it should be reminded that activated carbons are not really catalysts of ozone processes in water. A more exact definition of the role of activated carbon when simultaneously applied with ozone in water is as initiator of ozone decomposition since activated carbon undergoes during ozonation some sort of consumption (the reactions of ozone with some oxygen surface groups), although in a very negligible way, to yield active species, something that is not common to any catalyst that keeps its weight. However, especially in ozone kinetic studies activated carbons are considered as catalysts and kinetic equations of gas-liquid-solid catalytic reactions are usually applied to explain the rate of ozonation (see later).

Comparison with Single Ozonation and Adsorption Processes

First step that most of research works on this subject is to show comparative results of activated carbon ozonation with the so called blank treatment processes, that is, with ozonation alone or single ozonation and single adsorption. It is evident that these comparisons have first to be made in order to assess the combined process is better than the single ones. The results obtained from this comparison, however, are highly dependent on the nature and concentration of the chemical (or water pollutant in our case) to be treated. Thus, many

pollutants that present functional groups with nucleophilic positions (aromatic rings with substituting groups that activate the electrophilic reactions such as phenols, amines, etc) react very fast with ozone through the direct way and addition of activated carbon in these cases do not represent any improvement of their removal rate but some increment due to the adsorption process, that is, the combined process is the sum of single processes as far as removal rates of compounds is concerned. However, this happens when the concentration of the organic compound is high enough so that the kinetic regime of ozonation can be catalogued as fast (Beltrán, 2004). In this case, ozone consumption takes place in the proximity of the water interface through fast direct reactions with the organics. As a consequence, ozone does not reach the surface of activated carbon so as it is not possible any ozone surface catalytic reaction progresses. An example of this situation is seen in the work of Beltrán et al., (2009a) that deals with the activated carbon ozonation of diclofenac, (DCF), a non-esteroidal antiflammatory drug used as analgesic. DCF reacts very fast with ozone through the direct way since the rate constant of this reaction is 10^6 $M^{-1}s^{-1}$ as Huber et al (2003) reported. For this concentration, the Hatta number of the ozone-DCF reaction is higher than 3, that is, the kinetic regime is fast (Charpentier, 1981). As authors observed activated carbon adsorption alone leads to nearly complete DCF removal in about 20 minutes while total elimination of DCF is reached with ozone alone in 10 min. The combined process also removes 100% DCF but in about 6 min. However, the mechanism of DCF removal in the combined process cannot be due to any heterogeneous catalytic reaction but to the sum of the combined direct ozonation and adsorption mechanisms. In fact, as stated above, for any surface reaction taking place on the activated carbon, dissolved ozone should be present in water which is not the case during the activated carbon ozonation of DCF because of ozone consumption in the gas-water film layer. Thus, while DCF is present in water at appreciable concentration, needed for the ozone-DCF reaction to be of fast kinetic regime (Beltrán, 2004), dissolved ozone is not detected in bulk water. This situation can be observed in other works where the concentration of the pollutants is high and the direct reaction with ozone is fast (Beltrán et al., 2009d, Merle et al., 2009). On the other hand, if the concentration of the organic compound is low enough so that the kinetic regime of the ozone-organic reaction is catalogued of slow both direct ozone reaction and catalytic reactions can compete. In this case, dissolved ozone will diffuse through the water film close to the gas-water interfase and reach the bulk water. Then, two parallel mechanisms develop: the direct ozone reaction with the organics in bulk water and the ozone diffusion through the water-activated carbon film layer to reach the activated carbon surface where ozone would undergo surface reactions. Also, if the organic compound present in water does not react very fast with ozone through the direct way (the rate constant of the reaction is very low) which happens with third, fourth, etc, intermediates of direct ozonation of DCF and other organics of complex molecule, then ozone surface reactions on the activated carbons are the predominant mechanism and hydroxyl radical oxidation takes place. Among these intermediates are saturated carboxylic acids such as oxalic acid, one of the very end final products of many ozonation processes. A way of confirming these mechanisms is following the total organic carbon (TOC) or concentrations of ozone refractory intermediates during the ozone activated carbon and ozone processes. Thus, Beltrán et al (2009a) also observed that single ozonation hardly reaches 40% TOC removal while activated carbon ozonation leads to 85 to 95% TOC removal after 120 minutes. During the process, refractory saturated carboxylic acids such as oxalic acid or pyruvic acid are formed. Since these compounds do not react with ozone (the rate constants of their direct ozone reactions

are lower than 1 $M^{-1}s^{-1}$ as Hoigné and Bader (1983) reported) their removal can only be due to hydroxyl radical reactions, that is, to the indirect way of ozonation. While the indirect way of ozonation in the ozone single process is only due to the decomposition of ozone in water catalyzed by hydroxyl ions and hydrogen peroxide formed (Staehelin and Hoigné, 1982, 1985), during the activated carbon ozone process, the indirect way must be due to some other contributing reactions. These reactions are the ozone reactions at the activated carbon surface as presented later. In another work (Beltrán et al., 2009d), on the other hand, results of the single ozonation and activated carbon ozonation of sulfamethoxazole (SMX), a sulfonamide type synthetic antibiotic compound, are reported. SMX is another pharmaceutical compound that reacts very fast with ozone. In addition, in the work quoted, concentration of SMX was high enough so that the kinetic regime was fast and then dissolved ozone was not detected in bulk water until total SMX disappearance. Then, SMX was removed through direct way of ozonation in both processes (single and activated carbon ozonation). SMX removal rate in this case was observed to be practically independent on the presence of activated carbon. Also, unsaturated intermediates (their presence deduced from the evolution of 254 nm absorbance) behaved in a similar way to that of SMX. When these compounds (SMX and unsaturated intermediates) disappear dissolved ozone started to be accumulated in water. From this time, and, especially in the case activated carbon was present, other intermediates, pyruvic and oxalic acids, that accumulated in water as a result of SMX and first unsaturated intermediate oxidations, commenced to disappear. It is evident that removal of these compounds is due to hydroxyl radical reactions and that these reactions are likely due to both ozone decomposition in bulk water and on the activated carbon surface. Then, catalytic reactions are responsible to mineralization of water.

Another important intermediate in ozonation processes is hydrogen peroxide. This compound plays a key role in ozone processes when compounds present are eliminated through the indirect way. First of all, hydrogen peroxide is the main initiator of ozone decomposition in single ozonation. It is formed in the hydroxyl ion ozone decomposition reaction (Staehelin and Hogné, 1982):

$$O_3 + OH^- \xrightarrow{k=70\,M^{-1}s^{-1}} HO_2^- + O_2 \qquad [9]$$

Then, in a subsequent step, the ionic form of hydrogen peroxide reacts fast with ozone to yield free radicals:

$$HO_2^- + O_3 \xrightarrow{k=2{,}8\times10^6\,M^{-1}s^{-1}} HO_2\cdot + O_3^- \qquad [10]$$

It should be highlighted that ozone only reacts with the dissociating form of hydrogen peroxide so that pH of water is an important variable that affects the hydrogen peroxide species distribution (ionic and non-ionic forms) through equilibrium [11]:

$$H_2O_2 \xleftrightarrow{pK=11{,}8} HO_2^- + H^+ \qquad [11]$$

When ozone reacts, through the direct way, with many aromatic compounds or compounds with double carbon bonds the aromatic ring or double carbon bond is broken through cycloaddition reactions, and hydrogen peroxide is also formed. For example, reactions of ozone with the pharmaceutical compounds, as those cited above, develop through this type of mechanism yielding hydrogen peroxide in the case of the ozonation of SMX and DCF. However, when activated carbon is present another mechanism of hydrogen peroxide formation also develops this time from the ozone reactions at the surface of the activated carbon (Giráldez et al., 2007). This was confirmed during the activated carbon ozonation of gallic acid, a polyphenolic acid compound that reacts very fast with ozone. Confirmation was also made once the polyphenolic compound and unsaturated intermediates were removed. At that reaction time, addition of activated carbon gave rise to an increase of hydrogen peroxide concentration (Beltrán et al., 2006). Then, this additional formation of hydrogen peroxide was undoubtedly due to the ozone action on the activated carbon surface, likely through reactions with surface oxygen groups of basic nature such as pyrone and chromene groups (Álvarez et al., 2006) that contains nucleophilic centers where ozone can attack through addition reactions. Beltrán et al. (2009d) compared the hydrogen peroxide concentration-time profile from single and activated carbon ozonations of SMX and observed similar trends, that is, hydrogen peroxide concentration increases since the start of ozonation, reaches a maximum value and then decreases with time. However, the maximum concentration is higher during the activated carbon process what indicates different routes of hydrogen peroxide formation in this process or the development of ozone surface reactions. It is believed that the higher concentration of hydrogen peroxide observed in the activated carbon ozone process triggered the formation of hydroxyl radicals and the rate of disappearance of refractory intermediates, such as pyruvic acid, or end products, such as oxalic acid. Thus, authors reported that after 6 minutes reaction, in the single ozone process pyruvic acid concentration starts to slightly diminish and oxalic acid concentration accumulation in water continues. On the contrary, in the activated carbon ozone process, both carboxylic acid concentrations are decreasing in a significant way. Here, the synergism between ozone and activated carbon was clearly observed.

Operating Variables Affecting the ACO Process

Another important aspect that many research works on water activated carbon ozonation of organics cover is the study of the influence of operating variables. These are mainly pH, concentrations of ozone and organic compounds and mass of activated carbon added. There are also other variables such as presence of other substances in the water matrix (i.e. wastewater), presence of hydroxyl radical inhibitors such as t-butanol or metals on the activated carbon surface, or the form activated carbon is used (fiber, granular, powdered, etc) that will be treated in a following section (see also Table 2). From the variables cited, pH is likely the most important one affecting any ozone process as can be deduced from reactions [7] to [9]. Also, pH plays a key role in activated carbon ozone processes because it also affects the surface charge distribution on the activated carbon once that is positively or negatively charged depending on the water pH be lower or higher than the pH_{PZC} of the activated carbon. As a consequence, the electrostatic or even chemical interactions between surface oxygen groups of activated carbons and adsorbates, especially when these are dissociating compounds and the ozone decomposition in free radicals, are altered. While studying the pH effect on activated carbon ozone processes it is usually observed a decrease

of oxidation rate (TOC removal decrease) when increasing pH which is the contrary situation of that observed in the same ozone process without activated carbon, that is, in single ozonation. For example, this situation develops during the ozonation of a mixture of phenolic compounds in the absence and presence of activated carbon (Giráldez et al., 2007). In this work, TOC remaining in water at a given time in single ozonation of these polyphenolic mixtures decreases with the increasing pH which is in clear concordance with reactions [9] to [11]. However, in the presence of activated carbon, the opposite situation develops, that is, TOC decreases if pH also decreases. Here some discussion is needed to explain these results. First, when pH is increased ionic forms of the organic acids (both initials and intermediates) are more important than non-ionic forms because pH is approaching the pK values of their corresponding equilibrium in water. Second, also when pH is increased, the activated carbons start to be negatively charged because of pH is also approaching the pH_{PZC} value. The net result is that adsorption of organic acids diminish when pH is increased. Then, in the activated carbon ozone process, the increase of TOC reduction when pH decreases, cannot be attributed to any organic adsorption step. On the other hand, hydrogen peroxide formation was reported to increase. Therefore, only adsorption of ozone on the carbon surface can be the reason of the increasing TOC reduction in the activated carbon ozone process. Adsorption of ozone on the carbon surface has already been confirmed in works where the ozone decomposition is followed (Dehouli et al., 2010). Ozone adsorption step is likely favored at low pH values where some chemisorption reactions that generate hydrogen peroxide and then hydroxyl radicals develop (Beltrán et al., 2006, Chand et al., 2010):

$$O_3 + AC \overset{H_2O}{\longleftrightarrow} H_2O_2 - AC \qquad [12]$$

$$H_2O_2 - AC + O_3 - AC \leftrightarrow AC - HO\cdot + AC \qquad [13]$$

Once hydroxyl radicals are formed they react with non-adsorbed organic compounds through the indirect way of ozonation. These reactions likely develop in bulk water as some authors report (Hans and Hoigné, 1999) and experiments in the presence of t-butanol seems to confirm as shown below.

As far as concentration of ozone, organic compounds and mass of activated carbon is concerned, literature also reports many works dealing with the study of the effect of these variables (see Table 2). In many cases, a first order kinetics is found that explain the decrease of organic concentration during the activated carbon ozone process and then, the increase of initial organic concentration leads to increases of their removal rates. A similar situation applied when the ozone concentration effect is studied (Beltrán et al., 2006b). Also, the effect of activated carbon concentration is positive on the removal rate of organics in the activated carbon ozone process as shown in some works (Beltrán et al., 2006b).

Effect of Inhibitors of the Indirect Way of Ozonation

Hydroxyl radicals unselectively react with most substances present in water but products of these reactions are not always the same. Thus, many of these reactions produce peroxyl

radicals that eventually give rise to the superoxide ion radical, $O_2^{\cdot-}$, while others not. When ozone is also present it reacts with the superoxide ion radical generating the ozonide ion radical, $O_3^{\cdot-}$, which is subsequently transformed in another hydroxyl radical. The net result is that the consumption of one hydroxyl radical by reacting with this type of substances eventually leads to another hydroxyl radical via the superoxide ion radical when ozone is present. These substances are called promoters of the ozone decomposition since they propagate the chain mechanism. These reactions are (Staehelin and Hoigné, 1985):

$$OH\cdot + P \overset{\square}{\leftrightarrow} PO_2\cdot \overset{\square\square}{\rightarrow\rightarrow} O_2^{\cdot-} \cdot \qquad [14]$$

$$O_2^{\cdot-} \cdot + O_3 \overset{\square}{\rightarrow} O_3^{\cdot-} \cdot + O_2 \qquad [15]$$

$$O_3^{\cdot-}. + H^+ \overset{\square}{\rightarrow} HO_3\cdot \overset{\square}{\rightarrow} HO\cdot + O_2 \qquad [16]$$

where P represents a promoter of the decomposition of ozone. On the other hand, those reactions between substances and hydroxyl radicals that do not lead to the superoxide ion radical are really termination reactions of the chain mechanism, and in ozone processes these substances are called inhibitors or scavengers because the net result is the elimination of one hydroxyl radical. The reactions are:

$$OH\cdot + S \overset{\square}{\rightarrow} Non\ active\ radicals \qquad [17]$$

where S represents the scavenger substance. t-Butanol is a typical example of inhibitor of hydroxyl radicals in ozonation processes and it is very used to check whether or not the indirect way of ozonation is taking place. In many activated carbon ozonation processes (Lei et al., 2007, Faria et al., 2008b, Gu et al., 2008, Moussavi et al.,2009, see also Table 2), t-butanol has been used to confirm the reactions of contaminants with hydroxyl radicals. Thus, addition of t-butanol leads to a decrease of the contaminant removal rate when the indirect ozonation is the main way of oxidation since t-butanol takes most of hydroxyl radicals present in the water. However, one problem derives from the possible adsorption of t-butanol on the activated carbon surface. If adsorption takes place some active centers on the activated carbon surface would be occupied limiting the capacity of adsorption for ozone and/or products and the oxidation rate would also reduce. Likely, t-butanol does not adsorb or slightly adsorbs on activated carbons as has been shown in some works (Beltrán et al., 2002, Álvarez et al., 2006) and the decrease observed in the oxidation rate can be attributed to t-butanol hydroxyl radical scavenging. It should also be highlighted that t-butanol when added to ozonation systems alter the surface tension of water bubbles and the specific interfacial area of bubbles is increased (Tizaoui et al., 2009). As a consequence, the rate of ozonation also increases since more ozone molecules per volume and time are absorbed. This could rise to an increase of the ozonation rate. These circumstances make t-butanol be questioned as a true scavenger of

hydroxyl radicals in any ozonation process where ozone is fed as a gas. The problem can be solved, however, by carrying out ozone reactions (or activated carbon ozone reactions) in batch reactors, that is, from the mixture of aqueous solutions containing the contaminant, t-butanol and activated carbon with another one containing dissolved ozone. In this way the effect of ozone mass transfer would be eliminated. In any case, when the reduction of the ozonation rate is observed the development of the indirect way of ozonation can be confirmed in one activated carbon ozone process.

Effect of the Water Matrix

Most of research works on activated carbon ozonation of pollutants, however, are carried out in ultrapure water where model substances (the pollutants) are added. However, in practical cases, the pollutants are dissolved in water that also contains other substances that can compete for both ozone and hydroxyl radicals. This situation is especially important when the pollutants to be removed are in an industrial or municipal wastewater. The latter, municipal wastewaters, are of special importance since literature reports the presence of many pharmaceutical compounds both in the influent and effluents of the WWTP which means that primary and secondary treatments are not able to completely remove these substances from water (see start of introduction). Working with wastewater gives a real idea about the efficacy of any oxidizing system as activated carbon ozonation because of the possible presence of scavengers of hydroxyl radicals and ozone fast reacting compounds. Thus, activated carbon catalytic ozonation not only has been applied to aqueous solutions of organics prepared from ultrapure, distilled or deionized water but also with waters from different sources such as wastewater from biological treatments of WWTP (Soares et al., 2007), pharmaceutical industry (Lei et al., 2007), pulp bleaching (Balcioglu and Moral, 2008) or simply wastewater prepared in the laboratory (Gu et al., 2008). One particular case was the work of Moussavi et al (2009) where phenol was treated in saline wastewater with NaCl concentrations up to 25 g/L. In all cases, the synergetic ozone-activated carbon effect was shown to improve the organic removal rate. Also, natural waters were treated to study the effect of activated carbon catalytic ozonation on the removal of THMFP (Kawasaki et al., 2008). In another work, Alvarez et al (2009) reported results on changes of TOC with time of a WWTP effluent subjected to single ozonation, single activated carbon adsorption and granular activated carbon ozonation with the activated carbon used up to three times. This effluent initially contained 171 mg/L TOC, 522 mg/L COD and 150 mg/L BOD and showed a high 254 nm absorbance. The values of these parameters indicate that primary and secondary treatments did not perform appropriately and that a tertiary treatment was also needed. The authors reported that after 2 hours treatment single ozonation and single adsorption lead to 20 and 40% TOC reduction while the combined systems reached about 60% when 5 g AC were used. Another important fact is that catalytic activity was kept constant after three reuses of the AC. In spite of the positive effect of the combined ozonation no definitive conclusion could be established about the possible reasons of these results, that is, the following question remains: were the results obtained due to any catalytic reaction or to the additional effect of ozonation plus adsorption?. However, the constant activity of activated carbon after three consecutive runs suggests some catalytic activity developed on the surface, other way the activated carbon (that becomes saturated after its first use during 2 hours reaction) could not work properly in the two following runs.

Effect of the Presence of Metals on the Activated Carbon Surface

There already many works on metal catalytic ozonation of contaminants in water (see beginning of section 4) since the possibility metals, at different oxidation state, have to be combined with ozone and constitute couple redox systems that can enhance the ozonation rate of pollutants in water. One possibility is the use of activated carbon as supported material of metals or their oxides. In this way the adsorption capacity of organics is enhaced and hydroxyl radical reactions can be triggered at the carbon surface where ozone reacts to yield hydrogen peroxide. This kind of catalytic system has been used in many works where metals such as Ce, Cr, Co, Fe, Mn, Pt (Hammad-Khan and Jung, 2008, Faria et al., 2008, Lin et al., 2008) or metal oxides such as TiO2 (Zhang et al., 2009, 2010) or CeO (Li et al., 2009ab, Faria et al.,2009) have been supported on activated carbons. The importance of metals at trace level in activated carbons has also been shown. For example, Li et al. (2009) reported that demineralized or metal-free activated carbon leads to poor TOC removal that original activated carbon with metal traces to remove p-chlorobenzoic acid from water in an activated carbon ozone process.

Effect of Activated Carbon Form of Use

Different types of activated carbon forms have been investigated as ozone catalysts for removal of pollutants. The most used form is in granular shape of different size but also powdered activated carbon to eliminate mass transfer resistance in kinetic studies (Beltrán et al., 2006b, 2009b, .Méndez-Díaz et al., 2009), activated carbon cloths (Chand et al., 2010) (ACC) or activated carbon fibers have also been used. For example, Chand et al. (2010) use ACC to enhance the elimination of phenol. They first investigated the effect of the presence of hydrogen peroxide and reported the positive action of hydrogen peroxide to decompose on hydroxyl radicals on the activated carbon surface especially at acid pH. They studied the effect of the combined ozone-ACC process observing 70% TOC reduction at pH 9 when ozone is fed as step-wise, specifically, after three 15 min cycles of ozone addition. Activated carbon fibers, on the other hand, present a higher BET surface and micropore volume compared to granular activated carbon (Qu et al., 2007; Zhang et al., 2010). The physical presentation of activated carbons is intimately related to the way of preparation. For example, activated carbons beads have been prepared from carbon cryogels to develop macro and mesoporosity that also facilitates mass transfer rates of organics (Chaichanawong et al., 2010).

Types of Reactors on Activated Carbon Ozonation Studies

Most of the works on activated carbon ozonation are carried out in semibatch or batch slurry reactors where ozone is continuously fed as a gas or added in an aqueous solution, respectively, and known amounts of GAC or PAC have also been charged (see Table 1). However, in some case, fluidized or fixed bed reactors have also been used (Soares et al., 2007, Qu et al., 2007, Charintpanitkul et al., 2009, Rivera-Utrilla, 2010). In some other works, an ozone reactor was connected to an activated carbon bed and the water was passed in recycling mode (Beltrán et al., 2009a,c). Within this latter approach direct contact of ozone gas and activated carbon was avoided limiting the surface oxygen group reactions with ozone. In another work, Zhang et al., (2010) used a pulse discharge reactor where ozone was

produced in situ and its action was combined with radiation and activated carbon fibers present in the medium.

Toxicity Studies

Due to the potential hazardous character of many organic treated in the activated carbon ozonation studies in some of these works toxicity of raw and treated samples was followed through different methods. For example, Beltrán et al. (2009a,c) determined the ecotoxicity of samples from diclofenac and 17α-ethynylstradiol with *Daphnia Magna* and Méndez-Díaz et al. (2009) and Rivera-Utrilla (2010) used *Vibrio Fischeri* bacteria to establish the toxicity, via luminescence methods, of untreated and treated water containing the sodium dodecylbenzenesulphonate surfactant and tinidazole (a model compound of nitroimidazole antibiotics), respectively. In these works significant reduction of toxicity in treated samples are observed.

Activity of Activated Carbons

The reuse of activated carbons to show the activity to catalyzed ozone reactions has also been the subject of many works. As a whole, the same amount of activated carbon was used in a series of ozone experiments to follow the variation of TOC or concentration of some organics. For example, Balcioglu and Moral (2008) observed that exhausted activated carbon could be regenerated after repeated use in an ozone reactor where bleaching pulp wastewater was treated. In this work, the efficiency of regeneration was determined by following COD and color parameters. Rivas et al. (2009) treated bisphenol A (BPA) with different oxidizing systems involving activated carbon and ozone ($AC/O_3/UVC$, $AC/O_3/UVC/TiO_2$). They carried out up to six consecutive runs with fresh BPA solutions and the same amount of catalyst. They observed 100% TOC removal in the first cycle ($AC/O_3/UVC$) in about 25 min although at higher reaction times some TOC appearance in water was observed likely due to leaching of carbon impurities or release of organics from the ozone reactions with the surface oxygen groups of the carbon surface. However, after the third reuse AC stabilization was reached and the system was able to remove again 90% TOC in about 20 min. It is highlighted that AC losses after each reuse gradually decreased from about 15% in the first use to 3% in the following reuses.

Mechanism and Kinetics (Ozone Decomposition, Ozone-AC-Organic Reactions)

Although most of the works already published on activated carbon ozonation deals with the effect of operating variables, some of them also deal with the mechanism and kinetics of the system. Thus, both the kinetics of ozone decomposition in the presence of activated carbon and that of the activated carbon ozonation of some pollutants have already reported (Beltrán et al., 2002, Dehouli et al., 2010).

a) Mechanism and kinetics of ozone decomposition in water in the presence of activated carbon

In a previous work, this research group studied this subject (Beltrán et al, 2002). Basically, the presence of activated carbon accelerates the ozone disappearance rate from water. When using a Gallaquim Gmi (12x40 US size) activated carbon, Beltrán et al., (2002)

observed that pH greatly affected the ozone decomposition rate. Thus, the increasing pH leads to an increase of the ozone decomposition rate constant although the increase was very smooth for pH lower than 6. At higher pH, the increase was significant. Also, for any pH value, the ozone decomposition rate constant in the presence of activated carbon was higher than that in the absence of the adsorbent. The authors proposed a mechanism of reactions involving adsorption, surface reaction and desorption steps in addition to the classical ozone decomposition mechanism of Staehelin and Hoigné (1985). LHHW kinetic equations were deduced from the mechanism and fitted to the experimental results. Participation of hydroxyl radicals was also proposed. In another work, Dehouli et al., (2010) also studied the ozone decomposition kinetics on activated carbons of acid character. They reported first order kinetics and the importance of acid groups on the process.

b) Mechanism and kinetics of activated carbon ozonation of organics in water

Works on the mechanism and kinetics of activated carbon ozonation of organics in water are also reported in literature (Table 2). Both aspects, mechanism and kinetics, depend on the kinetic regime of the direct reactions between ozone and the organics present in water. Thus, two possible situations can be considered: the first one that develops when the direct reactions are fast and dissolved ozone does not reach the bulk water and a second one, when the direct reactions are slow and dissolved ozone reaches not only bulk water but can diffuse to also reach the activated carbon surface. In this second case, ozone catalytic surface reactions can take place. Both cases can be illustrated following the concepts of the film theory (Beltrán, 2004) as shown in Figures 2. and 3.

Figure 2. shows the case when organic removal is due to the sum of both single ozonation (through direct fast ozone reaction) and single adsorption on the activated carbon surface. As it is shown in Figure 2, due the very fast kinetic regime of ozonation, ozone is consumed in the film layer close to the water-interface, so that no ozone reaches the bulk water, hence decomposition of ozone on the carbon surface is not possible although organics can be adsorbed.

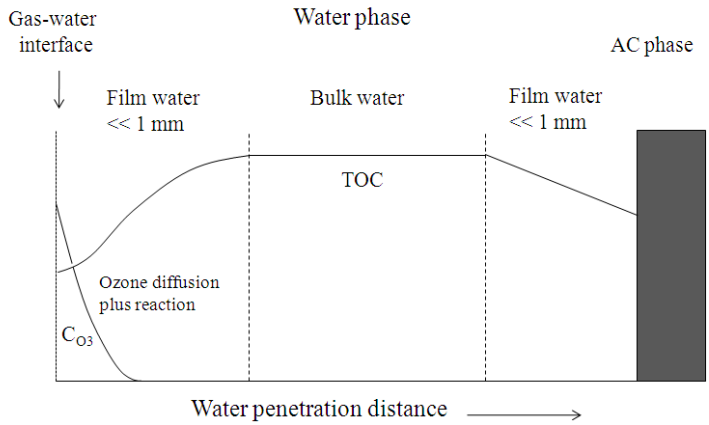


Figure 2. Concentration profiles of ozone and organic compound in activated carbon catalytic ozonation. Fast kinetic regime of ozone absorption.

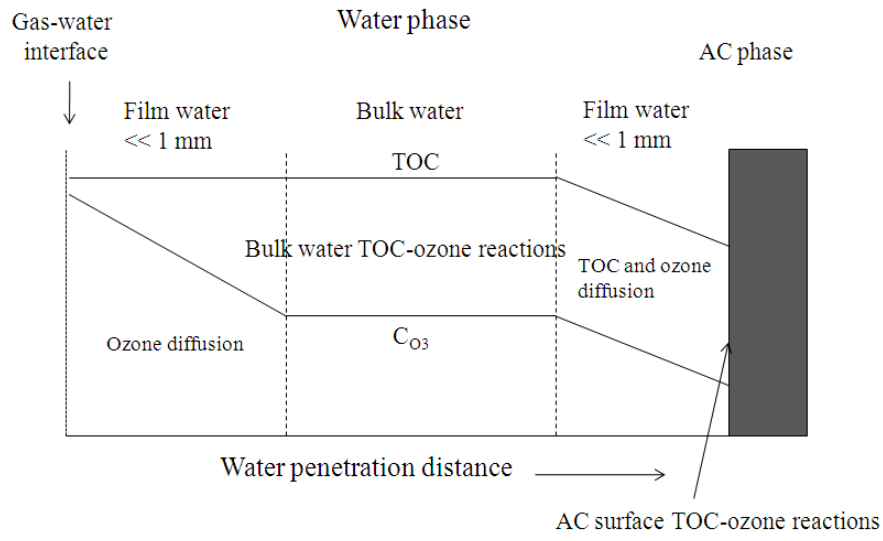


Figure 3. Concentration profiles of ozone and organic compound in activated carbon catalytic ozonation. Slow kinetic regime of ozone absorption.

Figure 3, on the contrary, shows the case when direct ozone reactions are slow. Now, dissolved ozone reaches the bulk water and then can also diffuse to reach the surface of the activated carbon where it can decompose through catalytic reactions yielding hydrogen peroxide, hydroxyl radicals, etc, that can attack the organics whether they are adsorbed or not. In this latter case, an advanced oxidation process takes place. Also, possible ozone-organic reactions in the bulk water can develop.

The kinetics of organic removal when direct ozone reactions are the way of oxidation corresponds to that of fast kinetic regime of ozone absorption that, in many cases, follows kinetic equation [18] (Beltrán, 2004):

$$N_{O3} = k_L a \frac{C_{O3g} RT}{He} Ha \qquad [18]$$

where N_{O3} is the ozonation rate, k_La the mass transfer coefficient, C_{O3g} the ozone concentration in the gas, T, the temperature, R and He the gas perfect and Henry constants, respectively, and Ha the Hatta number, defined as (Beltrán, 2004):

$$Ha = \frac{\sqrt{k D_{O3} C_M}}{k_L} \qquad [19]$$

k, D_{O3}, C_M and k_L being the rate constant of the M-ozone direct reaction, the ozone diffusivity, the concentration of M and the individual mass transfer coefficient, respectively. In a perfectly mixed semibatch ozone reactor, where the organics M are initially charged, the mass balance of M is:

$$-\frac{dC_M}{dt} = zN_{O3} \qquad [20]$$

where z is the stoichiometric ratio of the M-ozone direct reaction. Combination of equations [18] and [20], separation of variables and integration allows the rate constant of the direct reaction be determined provided the other parameters are known. This mechanism and kinetics apply when the Hatta numbers of the M-ozone reactions are higher than 3. If activated carbon is also present an additional term on the right side of equation [20], due to adsorption kinetics, could be added. In activated carbon ozonation processes, when compounds treated follow this mechanism (i.e. SMX, DCF, etc) equations [18] and [20] can be used to determine the rate constant of the direct M-ozone reaction from activated carbon free ozonation experiments. For example, Beltrán et al., (2009e) determined the direct rate constant of the reaction between SMX and ozone with this procedure.

When the organics present in water are refractory to ozonation, that is, their direct reactions with ozone are slow (Hatta numbers lower than 3), the mechanism of Figure 3. applies. Thus, the reaction rate of M can be derived from a LHHW mechanism of reactions involving adsorption, surface reaction, desorption, and reactions of the classical ozone decomposition mechanism in activated carbon free water, that is, removal of M can be due to two contributions, possible direct reaction with ozone, of negligible importance in most of cases, and reactions with hydroxyl radicals both on the activated carbon surface or in bulk water. Notice that contribution of organic adsorption is considered in the LHHW mechanism. Due to the complexity of the mechanism it is usually assumed that the organic compound is removed through two parallel second order reactions, the direct M-ozone reaction in bulk water and the surface catalyzed reaction. To solve this case, the kinetics of gas-liquid-solid catalytic reaction accompanied with homogeneous reaction (the direct ozone reaction in our case) is applied (Chaudhari and Ramachandran, 1980) as equation [21] indicates:

$$N_{O3} = \frac{\frac{C_{O3g}RT}{He}}{\frac{1}{k_L a} + \frac{1}{kC_M + \frac{1}{\frac{1}{w}\left[\frac{1}{k_c a_p} + \frac{1}{\eta k_s C_M}\right]}}} \qquad [21]$$

where w is the concentration of activated carbon or catalyst, k_c and a_p the liquid-solid mass transfer coefficient and specific external surface area of the catalyst, η the internal effectiveness factor of the catalytic reaction that accounts for possible mass transfer limitations inside the catalytic pores and k_s the rate constant of the catalytic reaction. Equation [21] holds if the Hatta number of the direct M-ozone reaction is lower than 3, that is, when this reaction follows the slow kinetic regime of ozone absorption. Combination of equations [20] and [21], integration or its numerical solution allows the determination of the heterogeneous catalytic rate constant, k_s, provided the rest of parameters are known. According to this the M-ozone direct rate constant has to be known. Likely, equations [20] and [21] can also be used for this purpose by fitting the experimental results of activated carbon free ozonation or single ozonation. For example, this procedure was applied in a previous paper (Beltrán et al., 2006b) where the activated carbon ozonation of succinic acid

was studied. Succinic acid reacts slowly with ozone so as the Hatta number of the reaction is first assumed to be lower than 3. Since no activated carbon is present, equation [21] reduces to:

$$N_{O3} = \frac{\frac{C_{Osg} RT}{He}}{\frac{1}{k_L a} + \frac{1}{kC_M}} \qquad [22]$$

Equation [22] can also be simplified if mass transfer resistance due to the liquid film layer close to the gas-water interface ($1/k_La$) is negligible. In any case, whether or not this simplification holds, combination of equations [20] and [22], integration of the resulting equation and fitting to the experimental results of single ozonation of succinic acid allowed the rate constant k be determined. The following step is the simplification of equation [21]. This can be accomplished checking the importance of mass transfer resistances of the process: the external liquid solid, $1/k_ca_c$ and internal or inside the pores, $1/\eta k_sC_M$. These resistances are highly dependent on the hydrodynamic conditions (agitation speed in the case an agitated semibatch reactor is used), size and density of catalyst, adsorbate effective diffusivity, etc. Some criteria as those of Weisz-Prater (1954) and Mears (1971) can be used to check the importance of these resistances. For example, in the activated carbon ozonation of succinic acid, internal mass transfer resistance was observed to be negligible as Weisz-Prater criteria confirmed. Then, in equation [21] the internal effectiveness factor can be considered as unity and with this simplification and a numerical method the catalytic rate constant, k_s, was determined. In some cases and also due to the complexity of the system, equations [20] and [21] are applied to the activated carbon ozonation of TOC. For example, Beltrán et al. (2009a) studied the kinetics of activated carbon ozonation of DCF by using TOC as surrogate parameter to follow the concentration of organic matter in water. They applied equations [20] and [21] to the experimental results once DCF and first fast ozone reacting compounds have disappeared, that is, when the mechanism of Figure 3. holds. In this study, however, they checked that external mass transfer resistance controlled the process rate so that the internal resistance $1/\eta k_sC_M$ was unimportant compared to $1/k_ca_c$. Thus, in their work only the mass transfer coefficient k_c could be determined and not the catalytic rate constant, k_s. This can be determined, instead, by reducing the size of the activated carbon. Thus, in another paper, the authors (Beltrán et al., 2009b) used powdered activated carbon to study the process modeling as is shown in the following section. In this way the rate constant can be determined since mass transfer resistances are negligible ($1/k_ca_c$ very low and $\eta=1$).

c) Kinetic modeling of ACOP

As far as our knowledge is concerned literature only reports two works on rigorous kinetic modeling of ACOP. These works refer to the ACOP of DCF and SMX (Beltrán et al., 2009b, 2010). The works first established the conditions for the mass transfer resistances be negligible (gas flow rate, powdered activated carbon, etc) and then proposed a complex mechanism of reactions involving adsorption, surface reactions where hydrogen peroxide and hydroxyl radicals were generated and homogeneous free radical reactions. The study was addressed to predict the TOC evolution in the water, that is, mineralization. Two TOCs were

considered, corresponding to compounds that adsorb on the carbon surface (the initial organic and first intermediates), TOC_1, and that from lower molecular weight and more polar intermediates that do not adsorb on the carbon surface, TOC_2. The sum of both TOCs was the actual TOC of the process. The model was based on the mass balance equations of main species: Both TOCs, ozone in gas and water, hydrogen peroxide and hydroxyl radicals. For the latter, however, the steady state approximation was applied and the following equation was used:

$$C_{OH} = \frac{1}{k_{IC}IC + \omega k_{HO} TOC_2}[r_{iH} + r_{iC}] \quad [23]$$

where IC represents the inorganic carbon or the concentration of bicarbonate-carbonate ions formed as a results of mineralization that act as scavenger of hydroxyl radicals, k_{IC}, the rate constant of this hydroxyl radical reaction, k_{HO} the rate constant of the reactions between compounds forming TOC_2 and hydroxyl radicals, r_{iH} and r_{iC} which are the rate of initiation reactions to generate hydroxyl radicals from bulk and surface catalytic reactions, respectively, that depend on the concentrations of ozone, hydrogen peroxide and activated carbon and ω a parameter that represents the fraction of TOC_2 that acts as scavenger of hydroxyl radicals that varies from 0 (start of ACOP) to 1 (advanced reaction times). Beltrán et al (2009b) while solving the kinetic model observed that calculated TOC results when TOC_2 was considered promoter (ω=0) or scavenger (ω=1) of hydroxyl radicals at any reaction time significantly differ from the experimental TOC values. Experimental and calculated results are close when considering TOC_2 as partly scavenger at any reaction time (ω=0.4) which suggests that along the ozone process intermediates formed change with time to initially be promoters and progressively be scavengers. Thus, when ω is assumed to follow a time function, beginning as zero and finalizing as 1 the experimental and calculated results agree which confirms above assumption.

For the future works, identification as many intermediates as possible are required to refine the kinetic model by introducing actual rate data of the reactions between ozone, hydroxyl radicals and detected intermediates. Also, knowledge of the promoter or scavenger nature of these intermediates will be needed in order to check the kinetic models.

5. REGENERATION OF ACTIVATED CARBON WITH OZONE

Most of the water treatment processes of adsorption with activated carbon operate in columns where a flow of contaminated water goes through the activated carbon bed. After a time of operation the activated carbon losses capacity to remove the pollutants because its pores are already filled with them and the process became inefficient. The activated carbon bed must be then replaced.

The economics of the adsorption process greatly depends on the reuse of the activated carbon. There are several well-established methods for the regeneration of spent AC that can be classified in various groups: thermal regeneration, regeneration with solvents, wet and supercritical oxidation regeneration, chemical regeneration and biological regeneration

(Menéndez-Díaz and Martín Gullón, 2005). Thermal regeneration is the most widely used method. However, this method is high energy-consuming as temperature must be kept above 800ºC. In addition, considerable amount of carbon is usually lost by attrition, burn-off and washout. Regeneration with solvents requires further purification of the solvent so it is not a recommended method unless a valuable product is recovered. Chemical methods as wet and supercritical oxidation are also expensive as large investment in high-pressure equipment is necessary. Biological regeneration is the cheaper method but it requires the sorbed species to be readily biodegradable. Because of these limitations, finding new regeneration methods or improving the existing ones attracts the interest of researchers.

The use of ozone in water and wastewater treatment plants is growing fast. Owing to its high oxidant power ozone can react with species adsorbed onto activated carbon, thus removing them from the surface in a novel regeneration method. Reaction may take place directly or through free radicals that arise from ozone decomposition over the carbon surface. Potential benefits of the method would be: (1) oxidation can be carried out at ambient temperature and pressure conditions; (2) it can be easily combined with adsorption and carried out in situ, making cycles of adsorption-regeneration in the own water treatment plant.

Álvarez et al., (2004) applied the method to regenerate spent activated carbons exhausted with phenol. It was found that phenol was adsorbed onto the activated carbon by physical forces (physisorption) and chemical forces (chemisorptions). While thermal regeneration was not able to remove chemical adsorbed phenol as charred products were retained on the carbon surface, ozone-regeneration could eliminate both physically and chemical adsorbed phenol, restoring most of the activated carbon surface. However, a limitation of the method was that the dose of ozone had to be tightly controlled. If too much ozone is used, in addition to the removal of phenol, some oxygen surface groups are formed from the interaction between ozone and the carbon surface itself. Resultant acidic groups played a negative role on the recovery of the adsorption capacity for phenol.

Lately Valdés et al. (2006) used the method to regenerate activated carbons saturated with benzothiazole. These authors found that extended gaseous ozonation of the exhausted activated carbon led to the effective destruction of the adsorbate by oxidation reactions. Oxidation of benzothiazole adsorbed on activated carbon seemed to occur via both direct reaction with ozone molecules, and by oxygen radical species generated by catalytic ozone decomposition on metallic surface sites.

Álvarez et al. (2009) compared the efficiency of a catalytic ozonation system using a granular activated carbon as catalyst and a sequential adsorption-ozone regeneration process to remove gallic acid from an aqueous stream. Ozone regeneration showed about 90% regeneration efficiency but this figure progressively decreased with the adsorption-regeneration cycles.

CONCLUSION

Main conclusions from this work are:

Ozone can be used as a chemical agent to modify textural and chemical properties of activated carbons in order to tailor its surface for adsorption processes. As a result of

functionalization with ozone, acidic surface groups are fixed on the carbon surface, thus providing a more hydrophilic surface.

Ozone while introducing oxygen in many organic complex molecules producing more biodegradable substances of lower molecular weight favors the development of biological activity on the activated carbon surface, which is called biological activated carbon operation.

Ozonation just before activated carbon filtration enlarges the half life of the filters since they receive organics of less polar and hydrophobic character, then breakthrough curves need more time to reach high concentrations at the filter outlet.

The simultaneous use of ozone and activated carbon, that is catalytic ozonation, improves TOC removal rates due to the increase of free radical reactions that can develop either on the activated carbon surface or in bulk water.

As a negative point, the activated carbon surface deteriorates due to direct reactions of ozone with some surface oxygen groups, mainly, of basic character. Then, rigorously speaking, activated carbon is not a catalyst but a promoter of ozone decomposition to yield entities of higher oxidizing power.

Nonetheless the kinetics of activated carbon ozonation of organics in water can be studied by applying the rate equations of gas-liquid-catalytic reactions. Depending on the activated carbon particle size, the process is controlled by external diffusion to AC particles (when in granular form, d>0,1 mm) or by chemical reactions (when in powder form, d_p<0,01 mm). However, surface reactions do not take place when ozone is consumed by fast direct reactions with organics in the proximity of the gas-water interfase.

When the process is chemically controlled, kinetic models can be established to predict the performance of the ACOP in terms of TOC removal, hydrogen peroxide formation and ozone gas and water concentrations at reactor outlet. In this sense, the variable ozone decomposition promoting and inhibiting character of organics constituting TOC is fundamental for the kinetic model to give accurate results.

Regeneration of activated carbons with ozone can be considered as a feasible method to recover adsorption characteristics of spent activated carbons. The efficiency of the method greatly depends on the type of compounds adsorbed, characteristics of the activated carbon and dose of ozone applied.

ACKNOWLEDGMENTS

Authors thank the CICYT (MICINN of Spain) and European Feder Funds for their support in accomplishing many of the works quoted in this paper and this paper itself, through projects: CTQ2006/04745, CTQ2009/13459/C05/05 and CSD2006/0044.

REFERENCES

Agustina, T.E.; Ang, H.M.; Vareek, V.K. *J. Photochem. Photobiol. C. Photochem. Rev*. 2005, 6, 264-273.

Álvarez, P.M.; Beltrán, F.J.; Gómez-Serrano, V.; Jaramillo, J.; Rodríguez, *E.M. Water Res*. 2004, 38, 2155-2165.

Álvarez, P.M.; García-Araya, F.J.; Beltrán, F.J.; Masa, F.J.; Medina, *F. J. Colloids Interf. Sci*. 2005, 283, 503-512.

Álvarez, P.M.; García-Araya, J.F.; Beltrán, F.J.; Giráldez, I.; Jaramillo, J.; Gómez-Serrano, V. *Carbon*. 2006, 44, 3102-3112.

Álvarez, P.M.; Masa, F.J.; Jaramillo, J.; Beltrán, F.J.; Gómez-Serrano, V. *Ind. Eng. Chem. Res.* 2008, 47,2545-2553.

Álvarez, P.M.; Beltrán, F.J.; Masa, F.J. Pocostales, P. *Appl. Catal. B. Environ*. 2009, 92, 393-400.

Bailey, P.S. *Chem Rev*., 1958, 58, 925-1010.

Balcioglu, I.A. Moral, Ç.K. *J Adv Oxid Technol*. 2008, 11, 543-550.

Bandosz, T.J.; Ania, C.O. Surface chemistry of activated carbons and its characterization. In: Bandosz, T.J., editor. *Activated carbon surfaces in environmental remediation*. New York. Elsevier, 2006; 159-229.

Beltrán, F.J.; Rivas, F.J.; Fernández, L.A.; Álvarez, P. Montero de Espinosa, R. *Ind. Eng. Chem. Res.* 2002a, 41, 6510-6517.

Beltrán, F.J.; Álvarez, P.; Rivas, F.J.; Montero-de-Espinosa, R. *Ozone Sci. Eng*. 2002b, 24, 227-237.

Beltrán, F.J. Ozone-UV radiation-Hydrogen peroxide oxidation technologies In: Tarr, M., editor. *Chemical degradation methods for wastes and pollutants. Environmental and Industrial Applications*. NewYork: Marcel Dekker, Inc.; 2003; 1-74.

Beltrán, F.J. *Ozone reaction kinetics for water and wastewater systems*. First edition. Boca Ratón, FL; Lewis Publ. 2004.

Beltrán, F.J.; García-Araya, J.F.; Giráldez, I. *Appl. Catal. B. Environ*. 2006a, 63, 249-259.

Beltrán, F.J.; García-Araya, J.F.; Giráldez, I.; Masa, *F.J. Ind. Eng. Chem. Res*. 2006b, 45, 3015-3021.

Beltrán, F.J. Ozone and solid catalysts for the treatment of water pollutants In: A. Gil y S.A. Korill: editors. *Recent research developments in Environmental Technology*. Kerela, India: Transworld research network; 2008; 1-30.

Beltrán, F.J.; Giráldez, I.; García-Araya, *J.F. Ind. Eng. Chem. Res*. 2008, 47, 1058-1065.

Beltrán, F.J.; Pocostales, P.; Alvarez, P.; Oropesa, A. *J. Haz. Mat*. 2009a, 163, 768-776.

Beltrán, F.J.; Pocostales, P.; Alvarez, P.; Jaramillo, J. *J. Haz. Mat*. 2009b, 169, 532-538.

Beltrán, F.J.; Pocostales, P.; Alvarez, P.; Aguinaco, A. *Ozone Sci. Eng*. 2009c, 31, 422-427.

Beltrán, F.J.; Pocostales, P.; Alvarez, P.; López-Piñeiro, F. *Appl. Catal. B. Environ*. 2009d, 92, 262-270.

Beltrán, F.J.; Aguinaco, A.; García-Araya, J.F. *Water Res*. 2009e, 43, 1359-1369.

Bourbigot, M.M.; Lheritier, R.; Benezet-Toulze, M. *Tech. Sci. Munic*. 1981, 12, 639-648. Bradley, R.H.; Sutherland, I.; Sheng, *E. J. Chem. Soc. Faraday Trans.* 1995*,* 91, 3201-3207.

Buxton, G.V.; Greenstock, C.L.; Helman, W.P.; Ross, A,B. *J. Phys. Chem. Ref. Data*. 1988, 17, 513-886.

Cataldo, F. Fullerenes, *Nanotubes and Carbon Nanostructures*. 2008, 16, 1-17.

Chaichanawong, J.; Yamamoto, T.; Ohmori, T. *J. Haz. Mat*. 2010, 175, 673-679.

Chand, R.; Molina, R.; Johnson, I.; Hans, A.; Bremner, D.H. *Water Sci. Technol*. 2010, 61, 2817-2823.

Charinpanitkul, T.; Limsuwan, P.; Chalotorn, C.; Sano, N.; Yamamoto, T.; Tongpram, P.; Wongsarivej, P.; Soottitantawat, A.; Tanthapanichakoon, W. *J. Ind. Eng. Chem*. 2010, 16, 91-95.

Charpentier, J.C. Mass Transfer Rates in Gas Liquid Absorbers and Reactors, In: Drew, T.B.; Cokelet, G.R.; Hoopes, J.W.; Vermeulen, T. *Advances in Chemical Engineering*. New York: Academic Press; 1991. Vol 11, 3-133.

Chaudhari, R.V.; Ramachandran, P.A. *AIChE J.* 1980, 26, 177-201.

Chiang, H.L.; Huang, C.P.; Chiang, P.C. *Chemosphere*. 2002a, 47, 257-265

Chiang, H.L.; Chiang, P.C.; Huang, C.P. *Chemosphere*. 2002b, 47, 267-275.

Considine, R.; Denoyel, R.; Pendleton, P.; Schumann, R.; Wong, S.H. *Colloids and Surfaces A: Physicochemical and Engineering Aspects*. 2001, 179, 271-280.

Cooney, D.O. *Adsorption design for wastewater treatment*. Lewis Publisher: Boca Ratón. 1999.

Dehouli, H.; Chedeville, O.; Cagnon, B.; Caqueret, V.; Porte, C. *Desalination*. 2010, 254, 12-16.

Deitz, V.R.; Bitner, J.L. *Carbon* 1972, 10, 145-154.

Deitz, V.R.; Bitner, J.L. *Carbon* 1973, 11, 393-398.

De Laat, J.; Doré, M.; Mallevialle, *J. Water Res*. 1991, 25, 151-164.

Faria, P.C.C.; Orfao, J.J.M.; Pereira, M.F.R. *Ind. Eng. Chem. Res*. 2006, 45, 2715-2721.

Faria, P.C.C.; Orfao, J.J.M.; Pereira, M.F.R. *Appl. Catal. B. Environ*. 2008a, 79, 237-243.

Faria, P.C.C.; Orfao, J.J.M.; Pereira, M.F.R. *Appl. Catal. B. Environ*. 2008b, 83, 150-159.

Faria, P.C.C.; Monteiro, D.C.M.; Orfao, J.J.M.; Pereira, M.F.R. *Chemosphere*. 2009a, 74, 818-824.

Faria, P.C.C.; Orfao, J.J.M.; Pereira, M.F.R. *Appl. Catal. B. Environ*. 2009b, 88, 341-350.

Faria, P.C.C.; Orfao, J.J.M.; Pereira, M.F.R. *Catal. Letters*. 2009c, 127, 195-203.

Faust, S.D.; Aly, O.M. *Adsorption processes for water and wastewater treatment*. Boston, MA: Butterworths, 1987.

Figuereido, J.L.; Pereira, M.F.R. *Catal. Today*. 2010, 150, 2-7.

Fu, X.; Lu, W.; Chung, D.D.L. *Carbon*. 1998, 9, 1337-1345.

Giráldez, I.; García-Araya, J.F.; Beltrán, *F.J. Ind. Eng. Chem. Res*. 2007, 46, 8241-8247.

Glaze, W.H.; Kang, J.W.; Chapin, D.H. *Ozone Sci. Eng*. 1987, 9, 335-342.

Gómez, M.J.; Martínez Bueno, M.J.; Lacorte, S.; Fernández-Alba, A.R.; Agüera, A. *Chemosphere*. 2007, 66, 993-1002.

Gómez-Serrano, V.; Álvarez, P.M.; Jaramillo, J.; Beltrán, F.J. *Carbon*. 2002a, 40, 513-522.

Gómez-Serrano, V.; Álvarez, P.M.; Jaramillo, J.; Beltrán, F.J. *Carbon*. 2002b, 40, 523-529.

Gül, S.; Özcan, O.; Erbatur, O. *Dyes and Pigments*. 2007, 75, 426-431.

Gu, L.; Zhang, X.; Lei, L. *Ind. Eng. Chem. Res*. 2008, 47, 6809-6815.

Gu, L.; Zhang, X.; Lei, L.; Zhang, Y. *Micropor. Mesopor. Mat*. 2009, 119, 237-244.

Guiza, M.; Ouederni, A.; Ratel, A. *Ozone Sci. Eng*. 2004, 26, 299-307.

Halling-Sorensen, B.; Nielsen, S.N.; Lanzky, P.F.; Ingerslev, F.; Holten-Lützhoft, H.C.; Jorgensen, S.E. *Chemosphere*. 1998, 357-393.

Hammad-Khan, M.; Jung, J.Y. *Chemosphere*. 2008, 72, 690-696.

Heisig, C.; Zhang, W.M.; Oyama, S.T. *Appl. Catal. B. Environ*. 1997, 14, 117-129.

Hoigné, J.; Bader, H. *Water Res*. 1983, 17, 185-194.

Hubert, M.M.; Canonica, S.; Park, G.Y.; von Gunten, U. *Environ Sci. Technol*. 2003, 37, 1016-1024.

Huerta-Fontela, M.; Galceran, M.T.; Ventura, F. *Environ Sci. Technol*. 2008, 42, 6809-6816.
Ikehata, K.; El-Din, M.G.; Snyder, S.A. *Ozone Sci. Eng*. 2008, 30, 21-26.
Jans, U.; Hoigné, *J. Ozone Sci. Eng*. 1998, 20, 67-89.
Jaramillo, J.; Gómez-Serrano, V.; Álvarez, P.M. *J. Hazard. Mat.* 2009, 161, 670-676.
Jaramillo, J.; Álvarez, P.M.; Gómez-Serrano, V. *Fuel Proc. Technol*. 2010a, 91, 1768-1775.
Jaramillo, J.; Álvarez, P.M.; Gómez-Serrano, V. *Appl. Surf. Sci*. 2010b, 256, 5232-5236.
Jones, O.A.; Lester, J.N.; Voulvoulis, N. *Trends in Biotechnol*. 2005, 23, 163-167.
Joss, A.; Andersen, H.; Ternes, T.; Richle, P.R.; Siegrist, H. *Environ. Sci. Technol*. 2004, 38, 3047-3055.
Kasprzyk-Hordern B.; Ziolek, M.; Nawrocki, *J. Appl. Catal. B. Environ*. 2003, 46, 639-669, 2003.
Kawamoto, K.; Ishimaru, K.; Imamura, Y. *Journal of Wood Science*. 2005, 51, 66-72.
Kawasaki, N.; Ogata, F.; Yamaguchi, I.; Fujii, *A. J Oleo Sci*. 2008, 57, 391-396.
Kawasaki, N.; Ogata, F.; Yamaguchi, I.; Tominaga, *H. J Oleo Sci*. 2009, 58, 261-266.
Khokhlova, G.P.; Semenova, S.A. *Soil Fuel Chem*. 2008, 42, 54-59.
Ko, K.R.; Ryu, S.K.; Park, S.J. *Carbon*. 2001, 42, 1864-1867.
Konsowa, A.H.; Ossman, M.E.; Chen, Y.; Crittenden, *J.C. J. Haz. Mat*. 2010, 176, 181-185.
Lafrance, P.; Mazet, M.; Villesot, D. *Water Res*. 1983, 17, 1467-1470.
Langlais, B.; Reckhow, D.A.; Brink, D.R. *Ozone in water treatment*: *Application and Engineering*. Lewis Publ: Chelsea, MI. 1991.
Lee, L.Y.; Ng, H.Y.; Ong, S.L.; Hu, J.Y.; Tao, G.; Kekre, K.; Viswanath, B.; Lay, W.; Seah, H. *Water Res*. 2009, 43, 3948-3955.
Legube, B.; Karpel Vel Leitner, N.; *Catal. Today*. 1999, 53, 61-72.
Lei, L.; Gu, L.; Zhang, X.; Su, Y. *Appl. Catal. A. General*. 2007, 327, 287-294.
Leon y León, C..; Radovic, L.R. *Chemistry and Physics of Carbon*. Marcel Dekker: New York. 1994.
Levenspiel, O. *Chemical Reaction Engineering*. 2nd Ed. Wiley:new York. 1972.
Li, X.; Zhang, Q.; Tang, L.; Lu, P.; Sun, F.; Li, L. *J. Haz. Mat*. 2009a, 163, 115-120.
Li, L.; Ye, W.; Zhang, Q.; Sun, F.; Lu, P.; Li, X. *J. Haz. Mat*. 2009b, 170, 411-416.
Liu, Z.Q.; Ma, J.; Cui, Y.H. *Carbon*. 2008, 46, 890-897.
Lou, J.C.; Chang, T.W.; Huang, C.E. *J. Haz. Mat*. 2009, 172, 1365-1371.
Mawhinney, D.B.; Yates, J.T. *Carbon*. 2001, 39, 1167-1173.
Macova, M.; Escher, B.I.; Reungoat, J.; Carswell, S.; Chue, K.L.; Keller, J.; Mueller, J.F. *Water Res*. 2010, 44, 477-492.
Marda, S.; Kim, D.I.; Kim, M.J.; Gordy, J.; Pierpont, S.; Gianatasio, J.; Amirtharajah, A.; Kim, J.H. *J. Am. Water Works Assoc*. 2008, 100, 117-128.
Mears, D.E. *Ind. Eng. Chem. Proc. Des. Dev*. 1971, 10, 541-547.
Menéndez-Díaz,J.A.; Martín-Gullón, I. Types of carbón adsorbents and their production In: Bandosz, T.J., editor. *Activated carbon surfaces in environmental remediation*. New York. Elsevier, 2006; 1-48.
Méndez-Díaz, J.D.; Sánchez-Polo, M.; Rivera-Utrilla, J.; Bautista-Toledo, M.I. *Water Res*. 2009, 43, 1621-1629.
Merle, T.; Pic, J.S.; Manero, M.H.; Debellefontaine, *H. Water Sci. Technol*. 2009, 60, 2921-2928.
Merle, T.; Pic, J.S.; Manero, M.H.; Mathé, S.; Debellefontaine, *H. Catal. Today*. 2010, 151, 166-172.

Montes-Morán, M.A.; Suárez, D.; Menéndez, J.A.; Fuente, E. *Carbon*. 2004, 42, 1219-1225.
Moussavi, G.; Khavanin, A.; Alizadeh, *R. J. Haz. Mat*. 2009, 171, 175-181.
Mul, G. ; Neeft,J.P.A. ; Kapteijn, F.; Moulijn, *J.A. Carbon*. 1998, 36, 1269-1276.
Oguz, E.; Tortum, A.; Keskinler, *B. J. Haz. Mat*. 2008, 157, 455-463.
Orge, C.A.; Sousa, J.P.S.; Gonçalves, F.; Freire, C.; Orfao, J.J.M.; Pereira, M.F.R. *Catal Letters*. 2009, 132, 1-9.
Papirer, E.; Donnet, J.B.; Schutz, A. *Carbon*. 1967, 5, 113-125.
Park, S.J.; Jin, S.Y. *J. Colloid. Interface Sci*. 2005, 286, 417-419.
Pereira, L.; Pereira, R.; Pereira, M.F.R.; van der Zee, F.P.; Cervantes, F.J.; Alves, M.M. *J. Haz. Mat*. 2010, 183, 931-939.
Peyton, G.R.; Glaze, W.H. *Environ. Sci. Technol*. 1988, 22, 761-767.
Qu, X.; Zheng, J.; Zhang, Y. *J. Colloid. Interf. Sci*. 2007, 309, 429-434.
Reungoat, J.; Macova, M.; Carswell, S.; Escher, B.I.; Mueller, J.F.; Gernjak, W.; Keller, J; *Water Rec. Reuse*. 2010a, 37, 69-72.
Reungoat, J.; Macova, M.; Carswell, S.; Escher, B.I.; Mueller, J.F.; Gernjak, W.; Keller, *J Water Res*.. 2010b, 44, 625-637.
Rivas, F.J.; Encinas, A.; Acedo, B.; Beltrán, F.J. *J. Chem. Technol. Biotechnol*. 2009, 84, 589-594.
Rivera-Utrilla, J.; Sánchez-Polo, M. *Carbon* 2002, 40, 2685-2691.
Rivera-Utrilla, J.; Sánchez-Polo, M. *Water Res*. 2003, 37, 3335-3340.
Rivera-Utrilla, J.; Sánchez-Polo, M.; Méndez-Díaz, J.D.; Ferro-García, M.A.; Bautista-Toledo, M.I. *J. Colloid. Interf. Sci*. 2008, 325, 432-439.
Rivera-Utrilla, J.; Sánchez-Polo, M.; Prados-Joya, G.; Méndez-Díaz, J.D.; Ferro-García, M.A.; Bautista-Toledo, *M.I. J Haz Mat*. 2010, 174, 880-886.
Sánchez-Polo, M; Rivera-Utrilla, *J. Environ. Sci. Technol*. 2002, 36, 3850-3854.
Sánchez-Polo, M.; Rivera-Utrilla, *J. Carbon*. 2003, 41, 303-307.
Sánchez-Polo, M.; von Gunten, U.; Rivera-Utrilla, J. *Water Res.* 2005, 39, 3189-3198.
Sánchez-Polo, M.; Rivera-Utrilla, J.; Méndez-Díaz, J.D.; Canonica, S.; von Gunten, U. *Chemosphere*. 2007, 68, 1814-1820.
Sánchez-Polo, M.; Rivera-Utrilla, J.; Prados-Joya, G.; Ferro-García, M.A.; Bautista-Toledo, I. *Water Res*. 2008, 42, 4163-4171.
Segura, P.A.; García, A.; Lajeunesse, A.; Ghosh, D.; Gagnon, C.; Sauvé, S. *J. Environ. Monitoring*. 2007, 9, 307-313.
Soares O.S.G.P.; Faria, P.C.C.; Orfao, J.J.M.; Pereira, M.F.R. *Separ. Sci. Technol*. 2007, 42, 1477-1492.
Sontheimer, H.; Heilker, E.; Jekel, M.; Nolte, H.; Vollmer, F.H. *J. Am. Water Works Assoc*. 1977, 70, 393-396.
Sontheimer, H. *Activated carbon for water treatment*. Denver, CO: AWWA Research Foundation. 1988.
Staehelin, S.; Hoigné, *J. Environ. Sci. Technol*. 1982, 16, 666-681.
Staehelin, S.; Hoigné, *J. Environ. Sci. Technol*. 1985, 19, 1206-1212.
Stackelberg, P.E.; Furlong, E.T.; Meyer, M.T.; Zaugg, S.D.; Henderson, A.K.; Reissman, D.B. *Sci. Total Environ*. 2004, 329, 99-113.
Subrahmanyam, C.; Bulushev, D.A.; Minsker, L.K. *Appl. Catal. B: Environ*. 2005, 61, 98-106.
Ternes,T.A. *Water Res*. 1998, 32, 3245-3252.

Terzyk, A.P. J. *Colloid Interf. Sci*. 2003, 268, 301-329.
Tizaoui, C.; Grima, N.M.; Derdar, M.Z., *Chem. Eng. Sci*. 2009, 64, 4375-4382.
Treguer, R.; Tatin, R.; Couvert, A.; Wolbert, D.; Tazi-Pain, A. *Water Res*. 2010, 44, 781-788.
Tsunoda, R.; Ozawa, T.; Ando J. J. *Colloid. Interf. Sci*. 1998, 205, 265-270.
Urfer, D.; Huck, P.M.; Booth, S. ; Coffey, B. *J. Am. Water Works Assoc*. 1997, 89, 83-92.
Valdés, H.; Sánchez-Polo, M.; Rivera-Utrilla,J.; Zaror, C.A. Langmuir. 2002, 18, 2111-2116.
Vieno, N.M.; Härkki, H.; Tuhkanen, T.; Kronberg, L. *Environ. Sci. Technol*. 2007, 41, 5077-5084.
Volk, C.; Renner, C.; Roche, P.; Paillard, H.; Joret, J.C. Ozone Sci Eng. 1993, 15, 389-394.
von Gunten, U. *Water Res*. 2003, 37, 1443-1467.
Weisz, P.B.; Prater, C.D. *Adv. Catal*. 1954, 6, 143-196.
Xie, S.G.; Shi, D.W.; Wen, D.H.; Wang, R.; Xi, D.L. *Biomedical Environ. Sci*. 2007, 20, 217-225.
Yang, R.T. Adsorbents: Fundamentals and applications. Hoboken, NJ: Wiley-Interscience. 2003.
Yapsakli, K.; Çeçen, F.; Aktäs, Ö.; Can, Z.S. *Environ. Eng. Sci*. 2009, 26, 489-500.
Yapsakli, K.; Çeçen, F. *Process Biochem*. 2010, 45, 355-362.
Yapsakli, K.; Mertoglu, B.; Çeçen, F. *Process Biochem*. 2010, 45, 1543-1549.
Zhang, J.; Lee, K.H.; Cui, L.; Jeong, T.S. *J. Ind. Eng. Chem*. 2009, 15, 185-189.
Zhang, Y.; Deng, S.; Sun, B.; Xiao, H.; Li, L.; Yang, G.; Hui, Q.; Wu, J.; Zheng, J. *J. Colloid. Interf. Sci.* 2010, 347, 260-266.

In: Activated Carbon
Editor: James F. Kwiatkowski
ISBN: 978-1-61209-684-1
©2012 Nova Science Publishers, Inc.

Chapter 17

STRATEGIES FOR OPTIMIZING THE DEVELOPMENT OF CELLULOSE-BASED ACTIVATED CARBON CLOTHS BY THE CHEMICAL ACTIVATION PROCESS

M. E. Ramos[1,2], P. R. Bonelli[1,2] and A. L. Cukierman*[1,2,3]

[1] Programa de Investigación y Desarrollo de Fuentes Alternativas de Materias Primas y Energía (PINMATE) - Depto. de Industrias, Facultad de Ciencias Exactas y Naturales, Universidad de Buenos Aires, Ciudad Universitaria, Buenos Aires, Argentina
[2] Consejo Nacional de Investigaciones Científicas y Técnicas (CONICET), Buenos Aires, Argentina
[3] Cátedra de Farmacotecnia II. Depto. de Tecnología Farmacéutica, Facultad de Farmacia y Bioquímica, Universidad de Buenos Aires, Buenos Aires, Argentina

ABSTRACT

The present chapter deals with strategies for optimizing the development of activated carbon cloths (ACC) through the chemical activation process with ortho-phosphoric acid solutions, as activating reagent, focusing on two unexplored cellulosic fabrics as precursors, denim and lyocell. The latter is a novel form of regenerated cellulose manufactured from wood pulp by an environmentally-friendly process, and is commercialized through the brand Tencel®. The influence of main variables involved in the chemical activation process, acid concentration (5-15 %wt), temperature (600-950 ºC), thermal treatment time (0-3 h), and N_2 flow rate (100-300 mL min^{-1}), on yield and physico-chemical characteristics of the resulting ACC is examined. Characterization of the ACC is carried out by elemental analysis, total acidity determination, X-ray diffraction, N_2 (77 K) adsorption, and scanning electronic microscopy. Phosphoric acid impregnation of the precursors occasions significant modifications in their thermal behavior, as evidenced from dynamic thermogravimetic analysis of untreated and impregnated samples. It leads to shift thermal degradation onset and maximum rate to

* Cátedra de Farmacotecnia II. Depto. de Tecnología Farmacéutica, Facultad de Farmacia y Bioquímica, Universidad de Buenos Aires. Junín 956. (C1113AAD) Buenos Aires, Argentina. E-mail: analea@di.fcen.uba.ar; anacuki@ffyb.uba.ar

lower temperatures, and to increase residual weight fractions, their intensity depending upon the precursor and acid concentration. Despite substantial changes taking place during the activation process, all the ACC preserve the original structure of the fabrics and integrity of the constituting fibres. Process conditions affect appreciably elemental composition, crystalline structure, surface chemistry and textural properties of the resulting ACC. In particular, activation of denim demonstrates to promote formation of acidic functional groups on the surface of the resulting ACC, as evidenced from enhancement of total acidity. The effect of these functionalities, which are relevant to the potential use of ACC for toxic metals uptake from wastewater, is verified from assays involving Zn(II) ions removal from model dilute solutions. Among the process variables, the thermal treatment temperature exerts a key role on the development of the ACC. For both precursors, increasing the temperature leads to ACC of higher specific surface area and total pore volume, although at the expense of lower yields. Nevertheless, the Tencel-based ACC show a more pronounced development of porosity than those obtained from denim. At the highest temperature investigated (950 °C) and for the same acid concentration (10 wt%), keeping otherwise constant conditions, maximum values of 2011 m^2/g and 0.67 cm^3/g characterize the ACC developed from Tencel, whereas the ACC obtained from denim show maximum surface area and total pore volume of 1055 m^2/g and 0.53 cm^3/g, respectively. Moreover, although all the ACC are essentially microporous, those derived from Tencel show a pronounced development of a fairly narrow microporosity, suggesting that they are potentially suited for gaseous effluents treatment. Prolongation of the thermal treatment time induces an enhanced development of porous structures for the Tencel-based ACC, whereas increase of the gas flow rate leads to the opposite effect. The latter might be due to the relatively less oxidative activation atmosphere generated as a consequence of shorter residence times of the volatile compounds released. Overall, present results contribute to the tailoring of cellulose-based activated carbon cloths in terms of desired properties and/or specific end uses through the strategic selection of main variables involved in the chemical activation process.

1. INTRODUCTION

Activated carbon cloths (ACC) have attracted growing attention in recent years because they offer several technological advantages in comparison with the traditional powder or granular forms of widespread use in several different applications. These advantages, related to the small diameter of the fibres constituting ACC, include faster adsorption/desorption rates, higher efficiency, and larger capacity for adsorption due to the higher surface area and pore volume of the ACC. In particular, micropores (< 2 nm) of ACC are directly connected to the external surface area, reducing diffusional resistance which leads to lower pressure drops in flow units. Activated carbon cloths are light materials, that can be arranged in different stable configurations, and provide a contiguous carbon form ideally suited for electrical and electrochemical applications. Moreover, Joule effect heating of ACC offers additional benefits in terms of desorption for their *in situ* regeneration in VOCs treatment processes (Rouquerol et al., 1999; Rodríguez Reinoso, 2002; Subrenat et al., 2003; Marsh and Rodríguez-Reinoso, 2006; Linares-Solano and Cazorla-Amorós, 2008; Badalyan et al., 2010).

Owing to comparative advantages, activated carbon cloths are promoting a new conception in equipment design and the field of potential applications has been increasingly investigated in the last years, even though involving commercial samples in most cases.

Either untreated or modified ACC have been explored as catalyst or catalyst/bio-catalyst support (Matatov-Meytal and Sheintuch, 2002; Matatov-Meytal, 2005; Perrard et al., 2007; Biniwalea and Ichikawa, 2007; Tien et al., 2008; Xu et al., 2008; Naranjo et al., 2010), and as electrode materials (Lu and Zheng, 2001; Isaev et al., 2003; Babel and Jurewicz, 2004; Sivakumar et al., 2005; Lewandowski et al., 2010). They have also been examined for abatement of gaseous and liquid pollutants (Faur Brasquet et al., 2002; Ayranci and Hoda, 2004; Ayranci et al., 2005; Ayranci and Duman, 2005; 2006; Subrenat and Le Cloirec, 2006; López Ramón et al., 2007; Afkhami et al., 2007; 2008; Tsai et al., 2008; Yao et al., 2009; Ayranci and Duman, 2010; Pastrana Martínez et al., 2009; 2010; Boulinguiez and Le Cloirec, 2010; Goyal et al., 2010; Huang and Su, 2010; Moreno-Castilla et al., 2010), as well as for separation and purification of biomolecules (Shen et al., 2008). Other applications investigated include gas storage and separation, H_2 recovery and purification, and sour gas sweetening (Carrott et al., 2004; Shao et al., 2007; Kunowsky et al., 2008; Zubizarreta et al., 2009).

As for the traditional forms, ACC can be obtained by the so-called physical and chemical activation processes. The latter leads to activated carbons with well-developed pore structure in higher yield and at relatively lower temperatures than physical activation. Moreover, the activating agent alters the course of pyrolysis, leading to a considerable increase in mechanical strength, which is especially relevant to ACC (Rodríguez Reinoso, 2002).

Activated carbon cloths are generally made from natural and synthetic polymeric precursors, such as cellulose, regenerated cellulose (mainly, viscous rayon), polyacrylonitrile (PAN), pitch, polyimides, aramid and phenolic-based fabrics (Pastor et al., 1999; You et al., 2000; Rodríguez Reinoso et al., 2000a; 2000b; Huidobro et al., 2001; Carrott et al., 2001; Wu et al., 2004; Williams et al., 2004; Valente Nabais et al., 2005; Boudou et al., 2006; Zhang et al., 2008). The precursor material selected together with processing parameters play an important role in physico-chemical, mechanical, and electrical properties of the ACC (Ramos et al., 2007; 2008). However, despite recognized advantages, use of ACC is still limited due to their relatively higher cost in comparison with conventional activated carbons. Accordingly, exploration of novel textiles as starting materials and the strategies adopted for the activation processes are relevant to the development and sustainable production of ACC with specific properties, in order to contribute to extend their use in current and new applications.

Within this context, the present chapter deals with the optimization of activation strategies to attain ACC with particular characteristics in terms of desired applications. For this purpose, the effect of main experimental variables involved in the chemical activation process on yield and physico-chemical characteristics of the resulting activated carbon cloths are investigated, focussing on two novel cellulosic textiles as precursors, denim and lyocell (Tencel®), for their development. Although different cellulosic textiles as ACC precursors have been investigated, denim and Tencel® have been unexplored earlier for this purpose, with the exception of our own previous works (Ramos et al., 2007; 2008; 2009, 2010). Denim is a very popular textile, widely known due to its strength and durability. In turn, Tencel® is the brand name for a recently improved fabric from a fiber generically called lyocell. Lyocell is a natural, man-made fiber produced in an environmentally-friendly process from wood pulp, that has become popular in clothing. As a result of the controlled and regular structure of nano-fibrils, new functional properties can be introduced to Tencel® fabrics. Compared to

cotton and viscose fibers, higher strength (specially when wet) and higher modulus are two of the major physical benefits of lyocell fibers.

2. EXPERIMENTAL SECTION

2.1. Materials

Denim and Tencel® fabrics, kindly provided by Santista Textile Group (Buenos Aires, Argentina), were mainly used for ACC development. Physical characteristics and elemental compositions of both precursors are reported in Table I. The latter were determined with a Carlo Erba EA 1108 elemental analyzer.

Table I. Characteristics and elemental compositions (dry basis) of the precursors employed for development of the activated carbon cloths

Precursor	Specific mass (g/m^2)	Warp (yarn/cm)	Weft (yarn/cm)	C (%)	H (%)	N (%)	S (%)	O* (%)
Tencel	200	39	24	42.4	5.9	0.2	0.5	51.0
Denim	457	26	19	43.2	6.2	0.3	0.0	50.2

*Calculated by difference

2.2. Preparation of the Activated Carbon Cloths

Strips of each cellulosic fabric (10 cm x 10 cm) used as precursor, previously dried and weighted, were impregnated with H_3PO_4 acid (analytical grade) solutions of concentration in the range of 5-30 wt % at 60-100 °C for 30 min. Impregnation ratios were calculated as mass of phosphoric acid/mass of dried precursor.

Then, the impregnated samples were thermally treated in a tubular stainless steel reactor of horizontal configuration under a N_2 flow (100 mL min^{-1}), externally heated by an electric furnace. They were heated at 5 ºC min^{-1} up to different final temperatures between 600 °C and 970 °C. Once the desired final temperature was attained, it was held for 1 h. In order to improve mechanical resistance of the ACC, an isothermal step of 40 min at 270 °C was included in the thermal schedule, following the proposal by Pastor et al. (1999). Afterward, the resulting cloths were cooled under N_2 flow and rinsed thoroughly with distilled hot water until the wash water had a neutral pH. They were dried until constant weight.

For the sake of comparison, blank samples, namely, carbon cloths using the precursors soaked only in distilled water (acid-free samples), were also prepared. Furthermore, in order to explore the effect of N_2 flow and of the thermal treatment time at the final temperature, some ACC were obtained from Tencel with 10 wt% H_3PO_4 acid solution at 800 °C, by varying the N_2 flow in the range 100 – 300 mL min^{-1} or the time between 0 and 2 hours. Likewise, the effect of employing more drastic conditions on characteristics of the resulting ACC was examined. For this purpose, ACC from denim were developed using the precursor soaked with a 10 wt% acid concentration solution and thermally treated at 950 °C for 3 h.

Duplicates of the samples were at least prepared in all cases. Further details of the equipment and procedure used may be found elsewhere (Ramos et al., 2007; 2008). Yields were calculated from weight differences.

2.2. Thermogravimetric Measurements of the Untreated and Impregnated Precursors

In order to gain insight into the behaviour of the textiles employed as precursors upon activation, measurements by non-isothermal thermogravimetric analysis (TGA) were conducted for raw and impregnated samples of denim and Tencel. They were carried out on a Netzsch STA 409 thermal analyzer equipped with a data acquisition system, operating under N_2 flow (100 mL min^{-1}). The impregnated samples were obtained by treatment with 10 wt% phosphoric acid solutions prior to TGA analysis. The samples (~10 mg) were placed in the thermobalance, and heated from room temperature up to 800 ºC using a heating rate of 10 ºC min^{-1}. Besides, measurements were also performed for samples of Tencel previously impregnated with phosphoric acid solutions of concentration in the range 5-30 wt%, in order to obtain additional information about the effect of the acid concentration used in the impregnation stage on the precursor's behaviour during thermal treatment.

2.3. Characterization of the Activated Carbon Cloths

Elemental composition of the derived ACC was determined using a Carlo Erba EA 1108 elemental analyzer. No evidence for the presence of sulfur was found. Ash content was assessed according to standard ASTM D5142-04. The total content of acidic surface oxygen functional groups of some ACC was also assessed by titration of the samples with a 0.1 N sodium hydroxide solution following a conventional procedure (Rangel-Mendez and Streat, 2002).

Besides, accounting for the reported effect of the surface chemistry on metal adsorption performance of conventional activated carbons (Basso et al., 2002; De Celis et al., 2009), the influence of the total acidity of selected denim-derived ACC was further explored by carrying out some measurements of Zn[II] ion adsorption from dilute solutions, under fixed, pre-established equilibrium conditions. For this purpose, those ACC samples showing maximum and minimum contents of acidic surface groups and a blank were used. The uptake of Zn[II] ions was determined by contacting a weighed amount of each sample (0.1 g) to 5 mL of a zinc nitrate (analytical grade) solution (20 ppm) in capped glass flasks. They were kept in a shaker. Adsorption assays were carried out at room temperature and pH 3. The contact time and other conditions were selected on the basis of preliminary experiments, which demonstrated that equilibrium was attained in 48 h. After this period, the solution was filtered and concentrations of the Zn[II] ions remaining were determined by spectrophotometry measurements at λ = 510 nm using dithizone as colorimetric reagent at pH 5.5 (Sandell, 1959).

Porosity development of the ACC was evaluated from the adsorption isotherms of nitrogen at 77 K using a Micromeritics Gemini 2360 instrument and/or CE Instruments

Sorptomatic 1990. The isotherms were determined on the samples prior outgassed under helium flow at 120 °C up to constant weight when using the former, whereas they were treated under vacuum for the latter. The Brunauer-Emmett-Teller (BET) model was applied to fit all the isotherms and to evaluate the specific surface area (S_{BET}) of the samples, following the conventional procedure. Total pore volumes (ν_T) were estimated from the amount of N_2 adsorbed at the highest relative pressure, near unity. Mean pore radius (r_{av}) was calculated in the usual way ($r_{av} = 2V_t/S_{BET}$) (Allen, 1997).

N_2 isotherms were analyzed by the α_S method using published standard data in order to obtain the external surface area (A_S) and micropore volume (ν_S). In some cases, they were additionally analyzed by means of the Dubinin-Radushkevich (DR) equation in order to obtain the DR micropore volume (ν_0), characteristic energy (E_0) and the mean pore width (L_0). The latter parameter was estimated from the relationship (Stoeckli et al., 1990):

$$L_0 = 10.8/(E_0 - 11.4)$$

Surface morphology of the raw precursors and derived ACC were examined by scanning electron microscopy (SEM) with a Philips XL-30 Microscope. Before the measurements, all the samples were attached to mounting stubs, dried under vacuum, and sputter coated with Au–Pd (Ramos et al., 2007; 2008).

X-ray diffraction was also applied to some ACC in order to investigate possible changes in the internal structure of the fibres, as a result of the activation process. X-ray diffractograms were measured on a Philips PW1510 instrument using Cu Kα and Ni filter (λ = 0.1542 nm) at 40 kV and 30 mA. Intensity of X-rays was measured with a scintillation counter for a range of dispersion angles (2θ) comprised between 3º and 60º and acquisition velocity of 1 º/min.

Estimates of the interplanar spacing (d_{002}) were calculated from the position of the (002) peak in the corresponding XRD diffractograms by applying the Bragg's law:

$$d_{002} = \frac{\lambda}{2\, sen\, \theta_{002}}$$

where λ is the wave-length of X rays and θ, the Bragg's angle. Mean crystallite dimensions, height (L_c) and width (L_a), were obtained from XRD patterns by applying the Debye-Scherrer equation, which takes the following forms for carbon materials:

$$L_c = \frac{0.9\, \lambda}{\beta \cos \theta_{002}}$$

$$L_a = \frac{1.94\, \lambda}{\beta \cos \theta_{10}}$$

with β equal to the peak width at half height corrected for instrumental broadening (Carrott et al., 2001).

3. RESULTS AND DISCUSSION

3.1. Thermal Degradation Behaviour of the Pristine and Impregnated Precursors

Figures 1 and 2 illustrate comparatively typical representative thermogravimetric (TG) curves and thermal degradation rate profiles determined for the denim and lyocell precursors, pristine and impregnated with 10 wt% phosphoric acid solutions, respectively. The reaction rate profiles were obtained by differentiation of the weight fraction—time curves for each sample (not shown), as a function of the temperature. Weight fractions (w) are given by the ratio between the instantaneous and initial sample masses, respectively. Main features of the TG curves are summarized in Table II. They include values of T_{onset} (temperature of the initial decomposition of the sample), T_f (temperature at which weight fractions remained almost constant), w_{800} (weight fraction at 800 °C), T_{peak} (temperature at which degradation rates attained a maximum), and $(-dw/dt)_{peak}$ (maximum degradation rate).

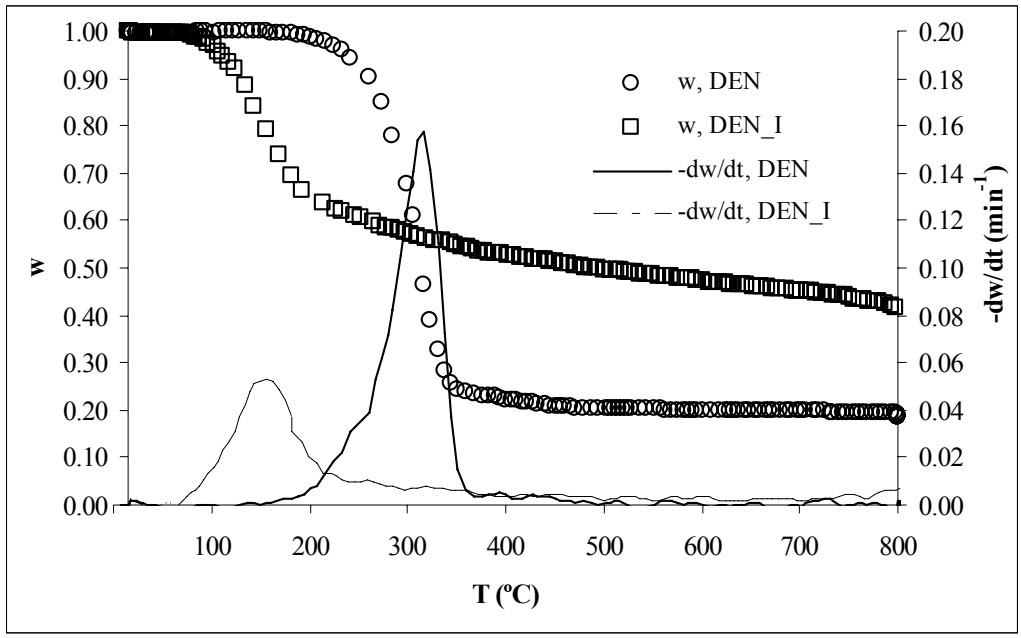


Figure 1. Thermogravimetric curves and reaction rate profiles for thermal degradation of pristine denim (DEN) and of 10 wt% acid-treated denim (DEN_I) under flowing N_2: variation of weight fraction (w) and degradation rate (−dw/dt) with temperature (T).

As seen in Figures 1 and 2, noticeable differences in TG curves and rates profiles arise for the non-impregnated precursors and the acid-treated samples. Acid impregnation leads to degradation of the precursors at lower temperatures compared to that of the pristine fabrics. Thermal degradation of the raw denim and Tencel® begins at around 190 ºC and 230 ºC, respectively, proceeds through sharp weight losses from these temperatures up to 360 ºC, and remains nearly constant at higher temperatures.

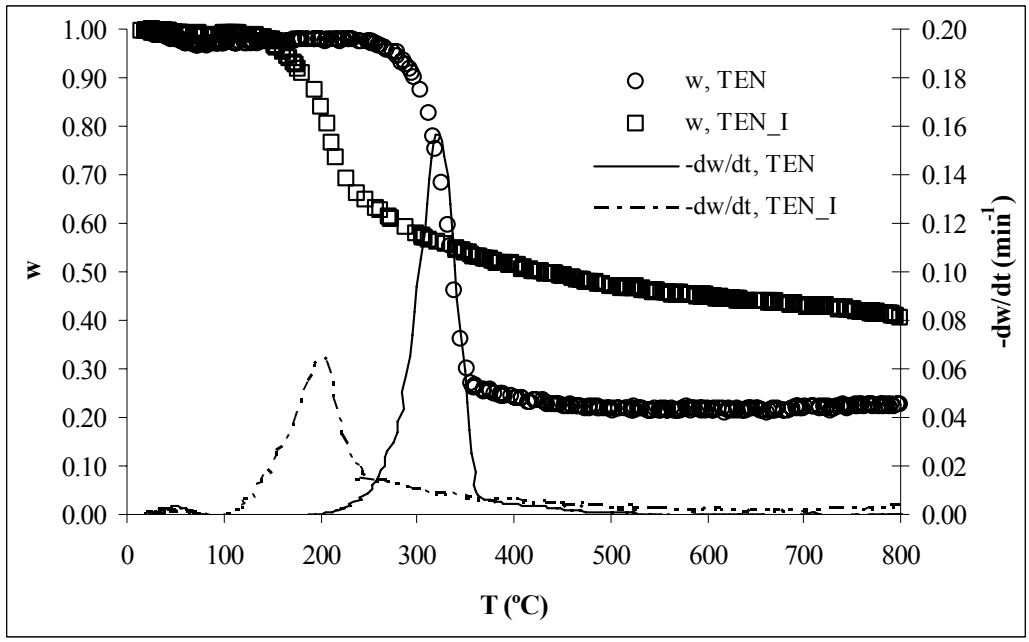


Figure 2. Thermogravimetric curves and reaction rate profiles for thermal degradation of pristine Tencel® (TEN) and of 10 wt% acid-treated Tencel (TEN_I) under flowing N_2: variation of weight fraction (w) and degradation rate (−dw/dt) with temperature (T).

Table II. Characteristic parameters of thermogravimetric curves and thermal degradation profiles for untreated denim (DEN) and Tencel (TEN) and for the same fabrics impregnated with 10%wt phosphoric acid solutions (DEN_I, TEN_I)

Precursor	T_{onset} (ºC)	T_f (ºC)	w_{800}	T_{peak} (ºC)	$(-dw/dt)_{peak}$ (min^{-1})
DEN	189	358	0.19	314	0.16
DEN_I	82	-	0.41	162	0.05
TEN	230	361	0.24	330	0.19
TEN_I	116	-	0.41	205	0.06

For the acid-treated precursors, thermal degradation takes place steadily almost throughout the whole range of temperatures, including the low temperature region (< 250 ºC) where no weight losses for the untreated samples are detected. Lower weight fractions are attained for the untreated precursors than for the acid-treated ones in the range ~ 380–800 ºC. In turn, degradation rates for pristine denim and Tencel achieve a sharp maximum at 314 °C and 330 ºC, respectively, whereas the maximum rates for the corresponding acid-treated precursors take place at considerably lower temperatures (162 ºC and 205 ºC) and show lower values than the former ones (Table II). Differences in the thermal degradation behaviour between the acid-treated precursors may be attributed to different impregnation ratios, although the same acid concentration was used, and to the inherent nature of the fabric precursor, which could affect interactions between the reactive agent and the polymer constituting the fibres during the impregnation stage.

The behavior is similar to that reported for the thermal degradation of other untreated and phosphoric acid impregnated materials used as precursors for preparing conventional forms of activated carbons (Vernersson et al., 2002; Basso and Cukierman, 2005). It may be related to changes in physicochemical properties of the precursor promoted by the acid, affecting markedly its thermal behaviour (Pandey and Nair, 1974; Gurudatt and Tripathi, 1998). Seemingly, the acid promotes bond-cleavage reactions that favor formation of aromatic compounds at lower temperatures in comparison with degradation of the precursors in the absence of the chemical reagent (Benaddi et al., 1998; Jagtoyen and Derbyshire, 1998). Likewise, modifications in the structure of the precursors caused by incorporation of the acid could also favour cross-linking reactions, decreasing losses of volatile compounds and leading to higher weight fractions for the acid-treated samples (Blanco Castro et al., 2000; Puziy et al., 2002b).

Furthermore, Figures 3 and 4 show thermogravimetric curves and thermal degradation rates for Tencel impregnated with phosphoric acid solutions of different concentrations as a function of temperature. For comparative purposes, results for the precursor treated with distilled water (acid-free sample), designated as TEN-BR, as well as those for the raw precursor and samples treated with 10 wt% acid solution are included in the same figures.

As may be appreciated in Figures 3 and 4, impregnation of the Tencel precursor with distilled water (TEN-BR) does not induce important changes in the thermal behavior compared with that for the untreated precursor (TEN). The degradation rate attains a maximum at ~ 325 - 330 ºC.

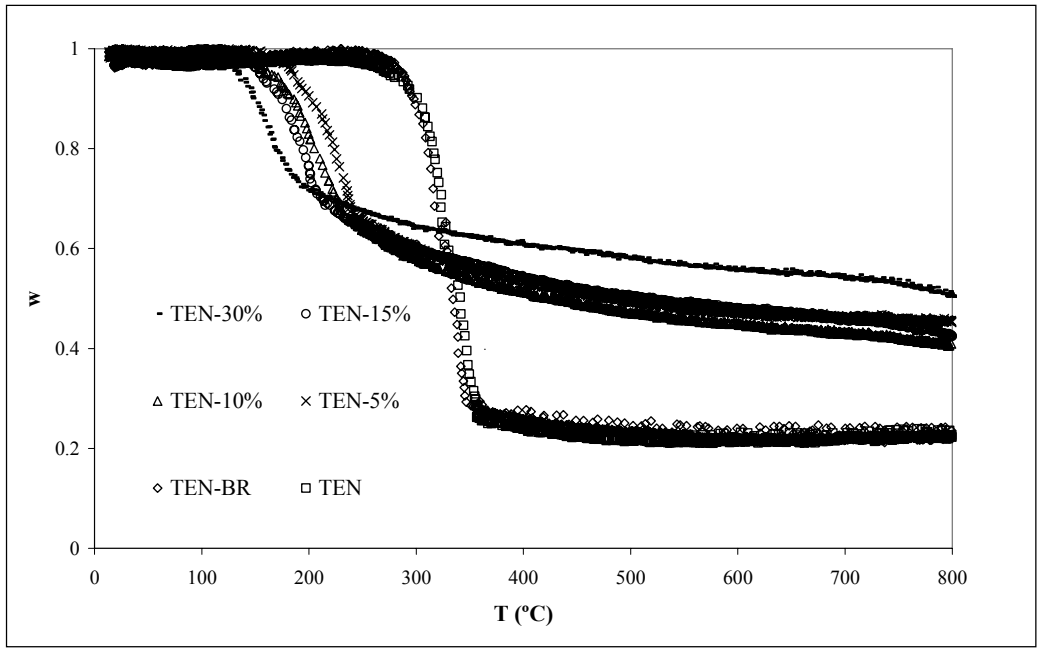


Figure 3. Effect of phosphoric acid concentration on TG curves for thermal degradation of pristine and impregnated Tencel.

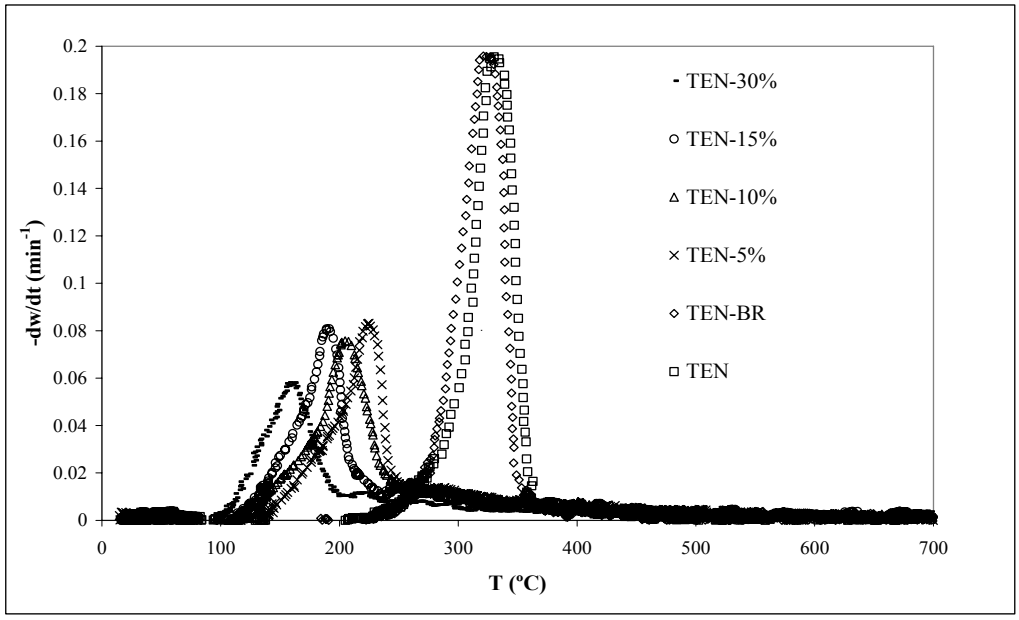


Figure 4. Effect of phosphoric acid concentration on reaction rate profiles for thermal degradation of pristine and impregnated Tencel.

As discussed earlier, treatment of the precursor with phosphoric acid solutions modifies its behavior, with thermal decomposition taking place at lower temperatures. Thermal degradation of Tencel impregnated with solutions of different acid concentrations mainly occurs in the temperature range between 100 and 250 ºC, even though it proceeds in less extension overall the whole temperature range. By contrast, degradation for pristine and water-treated Tencel takes place in the range between ~ 250 and 360 ºC. The results also indicate that concentration of the acid solution employed in the impregnation stage alters the magnitude of the modifications which take place in the thermal behavior of the impregnated precursor (Figures 3 and 4). Thermal decomposition of the precursor starts at lower temperatures as higher the concentration of phosphoric acid. The maximum degradation rate occurs at 227 ºC for the precursor treated with H_3PO_4 acid solution of 5 wt%, and at 156 ºC when the acid concentration is increased to 30 wt%.

3.2. Effect of the Acid Concentration and Thermal Treatment Temperature on Yield snd Physico-Chemical Characteristics of Activated Carbon Cloths

Figure 5 illustrates the effect of the final thermal treatment temperature on yield for ACC developed from denim and Tencel impregnated with 10 wt% phosphoric acid solution by employing the same otherwise process variables. As expected, increasing the temperature induces a progressive decrease in yield for the ACC arising from both precursors due to the larger release of volatile compounds. The trend is more pronounced for those derived from Tencel. Lower yields attained for the ACC derived from this precursor suggest a larger release of volatiles during the thermal treatment stage. The results also highlight the relevance of the nature inherent to the fabric used as precursor for ACC development. Noticeable

differences could be associated with the composition, internal order of the fibres, as well as with acid uptake and interaction with the acid during the impregnation stage.

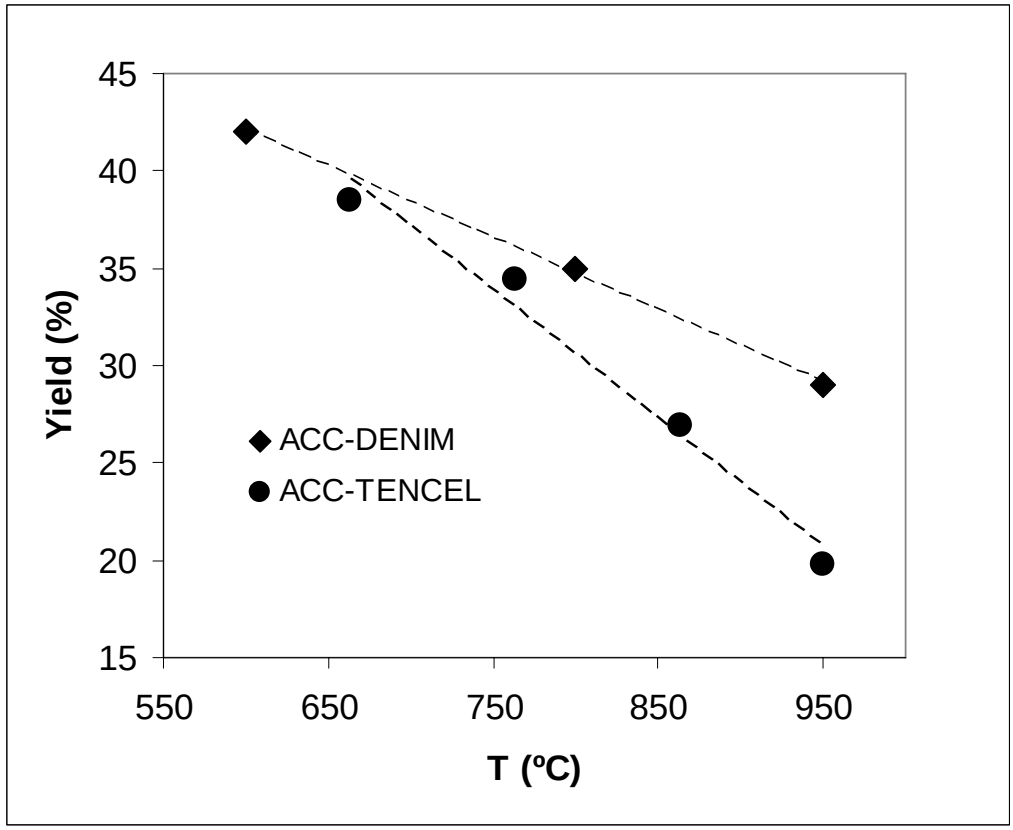


Figure 5. Effect of the final thermal treatment temperature on yield for the ACC developed from denim and Tencel with 10 wt% H_3PO_4 acid solution.

The effect of the phosphoric acid concentration used in the impregnation stage on yield is exemplified in Figure 6 for the ACC developed from denim at a final thermal treatment temperature of 800 °C. Yields for the ACC are higher than that determined for the cloth sample resulting from the acid-free precursor, in agreement with TG results (Figure 1). As mentioned earlier, this arises from modifications brought about by the impregnation reagent which drastically alters the thermal behaviour of the precursor, owing to reduction in volatile compounds loss.

The results in Figure 6 also indicate that, in the range of acid concentrations investigated for the denim precursor, increasing the acid concentration leads to higher yields, likely because of the enhanced retention of volatiles in the precursor's structure. Moreover, higher concentration of phosphoric acid may favour larger amounts of phosphorus compounds retained in the ACC. Present values are similar to those earlier reported in the literature for other cellulosic precursors (Huidobro et al., 2001).

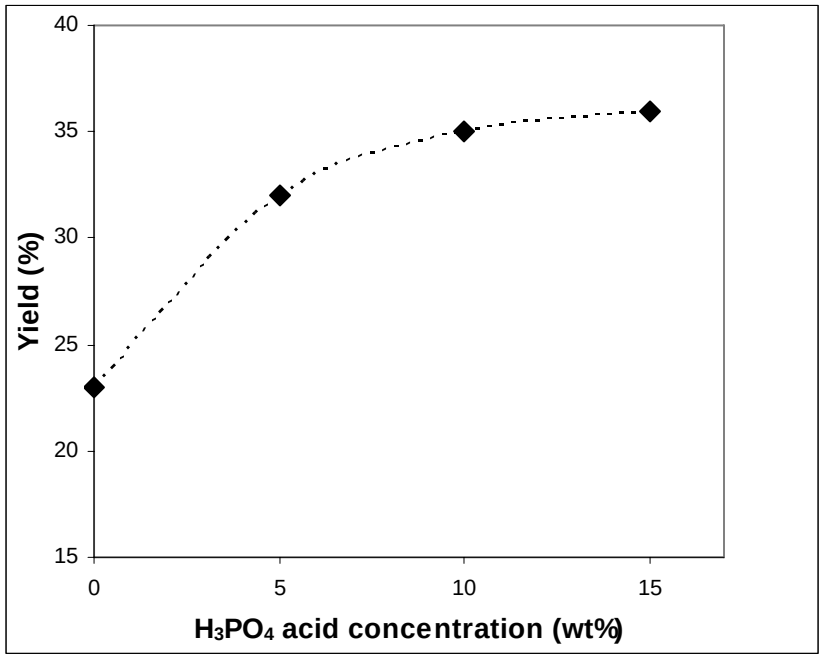


Figure 6. Effect of acid concentration on yield for the ACC developed from denim at 800 °C.

Table II reports elemental compositions, ash contents, and total acidity for the ACC obtained from denim for different phosphoric acid concentrations and final thermal treatment temperatures. The reported results are average values of triplicate determinations, where the standard error does not exceed 5%.

Table III. Effect of the final thermal treatment temperature and concentration of the acid solution on elemental composition (dry-ash free basis), ash content (dry basis) and total acidity of the denim-based ACC

T (ºC)	800	800	800	800	600	950
H_3PO_4 concentration (wt%)	0	5	10	15	10	10
C (wt%)	90.7	85.2	88.0	85.7	77.1	89.0
H (wt%)	0.9	0.7	0.7	0.7	1.2	0.5
N (wt%)	0.8	0.8	0.8	0.6	0.6	0.5
O* (wt%)	7.6	13.4	10.5	13.0	21.1	10.0
Ash (wt%)	2.1	4.9	3.6	4.2	5.6	4.3
Total acidity (mmol/g)	0.15	0.75	0.59	0.80	1.00	0.48

*Calculated by difference

The results in Table III for T = 800 ºC indicate a similar trend for elemental oxygen, ash content, and total acidity of the denim-based ACC when varying H_3PO_4 acid concentration. It suggests that oxygen may be introduced from phosphoric acid, and some phosphorus oxygen surface groups should be responsible for the acidity of the ACC (Puziy et al., 2002a). At 800 °C, increasing the acid concentration leads to ACC with a minimum acidity for 10 wt % acid concentration.

Likewise, the samples obtained from denim with 10 wt% acid concentration at growing temperatures exhibit progressively lower oxygen content and total acidity, and higher %C. In addition, as seen in Figure 7 for the ACC derived from Tencel using the same acid concentration, similar trends are also found for the contents of major elements with temperature raise. Increase in %C is accompanied by decreases in contents of oxygen and hydrogen, as temperature increases. Changes in elemental composition may be attributed to release of volatile compounds, leading to carbon enrichment due to an aromatization process, which is favored at higher temperatures. Tencel-derived ACC present almost negligible amounts of nitrogen (lower than 0.1 wt%).

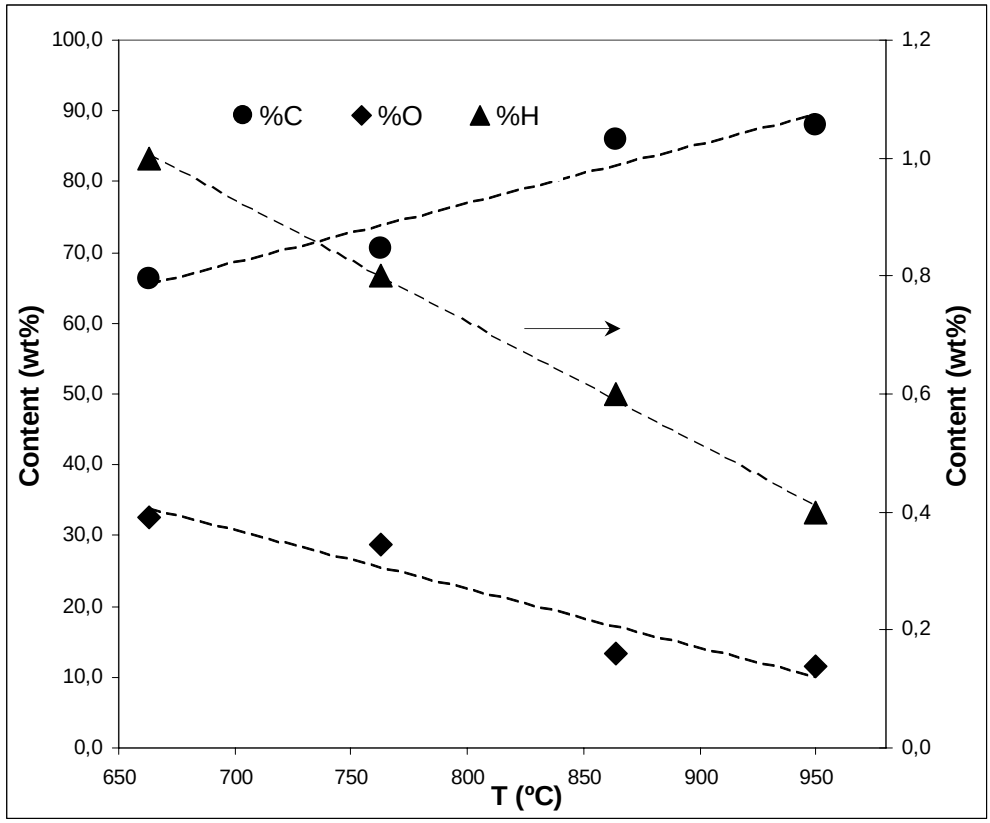


Figure 7. Effect of the final thermal treatment temperature on contents of elemental carbon, oxygen and hydrogen for the ACC developed from Tencel with 10 wt% H_3PO_4 acid solution.

The behavior may also be related to porosity development. A greater porosity involves larger loss of volatile compounds, leading to a decrease in the amount of oxygen groups present on the surface of the ACC, that in turn are responsible for the total acidity. The trend agrees with that found for the specific surface area of the ACC obtained for the same conditions, as discussed below.

The data in Table III also indicate that H_3PO_4 acid activation modifies the surface chemistry of the precursor, promoting development of acidic surface functional groups, as revealed by the increase in the total acidity of all the ACC compared to that for the acid-free sample. These functionalities involve carboxylic groups, phenols, lactones, and others surface

acidic groups formed during carbonization due to the incorporation of the activating agent in the carbon residue (Boehm, 2002; De Celis et al., 2009). Since the ACC were not subjected to any further oxidative treatment and decomposition of most acidic oxygen-containing groups reportedly starts at temperatures considerably lower than the final temperatures used in the thermal treatment stage (Polovina et al., 1997), acidic properties of the ACC appear to be related to the presence of phosphorus-oxygen surface groups formed during the thermal treatment (Puziy et al., 2002a).

From an applicability viewpoint, total acidity of carbon sorbents is important in relation to their potentialities for liquid-phase adsorption of inorganic and organic polar molecules, particularly for wastewater treatment. Dissociation or polarization of these groups reportedly provides anionic characteristics to the surface of the carbons immersed in aqueous solutions, favoring their behavior as cationic exchangers (Basso et al., 2002; Boehm, 2002). In this sense, Figure 8 shows results for Zn[II] ion adsorption on two selected denim-based ACC with maximum and minimum total acidity, and the blank sample (BR-D). The selected activated cloths were obtained with a 10 wt% acid concentration at final temperatures of 600 ºC and 950 °C. They are respectively labeled as ACC-D600 and ACC-D950.

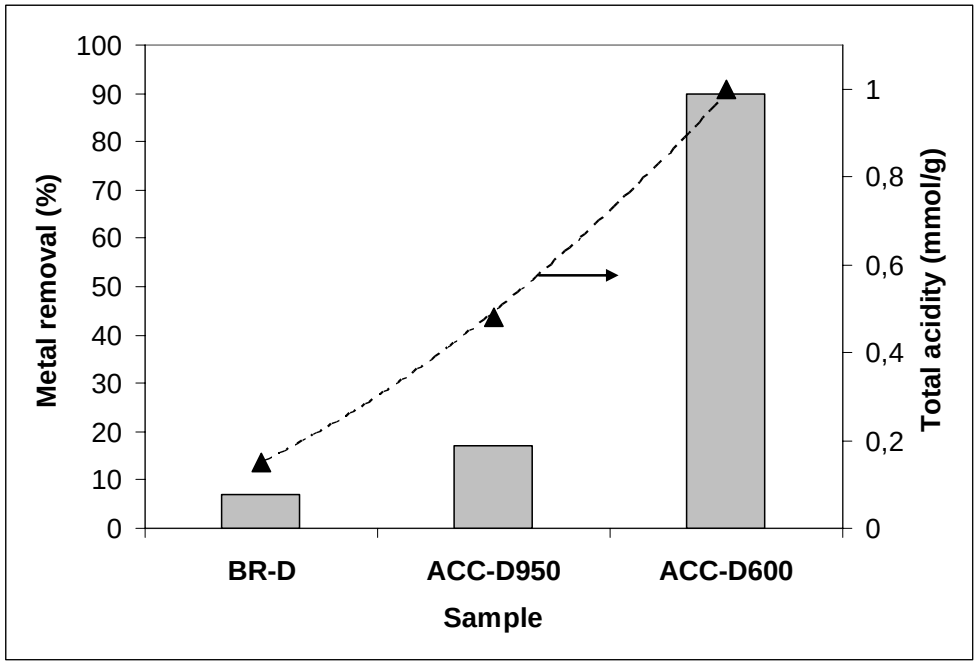


Figure 8. Zn[II] ion adsorption onto denim-based ACC obtained with 10 wt% H_3PO_4 acid solution at 600 ºC (ACC-D600) and 950 ºC (ACC-D950), and onto the blank (BR-D), and relation with total molar acidity of the samples.

As shown in Figure 8, ACC-D600 possessing maximum total acidity (1 mmol/g) presents the highest zinc adsorption (90%). This sample, however, shows the poorest porosity development, as discussed below. It is similar to that determined for the blank with a total acidity of 0.15 mmol/g, in turn exhibiting the lowest Zn[II] ion uptake (7%). ACC-D950 with a relatively low total acidity (0.48 mmol/g) and the best surface properties also demonstrates

a poor effectiveness in Zn[II] ion capture, only attaining 17%. The found trend agrees with results reported for the adsorption of various metallic ions on conventional activated carbons (De Celis et al., 2009) and on some commercial ACC (Rangel-Mendez and Streat, 2002; Afkhami et al., 2008) Accordingly, present results highlight the relevance of the acidic oxygen surface groups on the denim-based ACC in connection with their behavior as cationic exchangers. They also point to the potentialities of the samples obtained at 600 ºC for the removal of metal ions from wastewater.

On the other hand, some representative N_2 adsorption/desorption isotherms are shown in Figure 9 as an example. They correspond to ACC developed from Tencel with 10 wt% phosphoric acid solution and thermally treated at different temperatures. Amounts of N_2 adsorbed per sample mass unit (n_{ads}) are represented as a function of the relative pressure (P/P_0), where P is the equilibrium pressure, and P_0, the saturation pressure of the adsorbate at −196 °C.

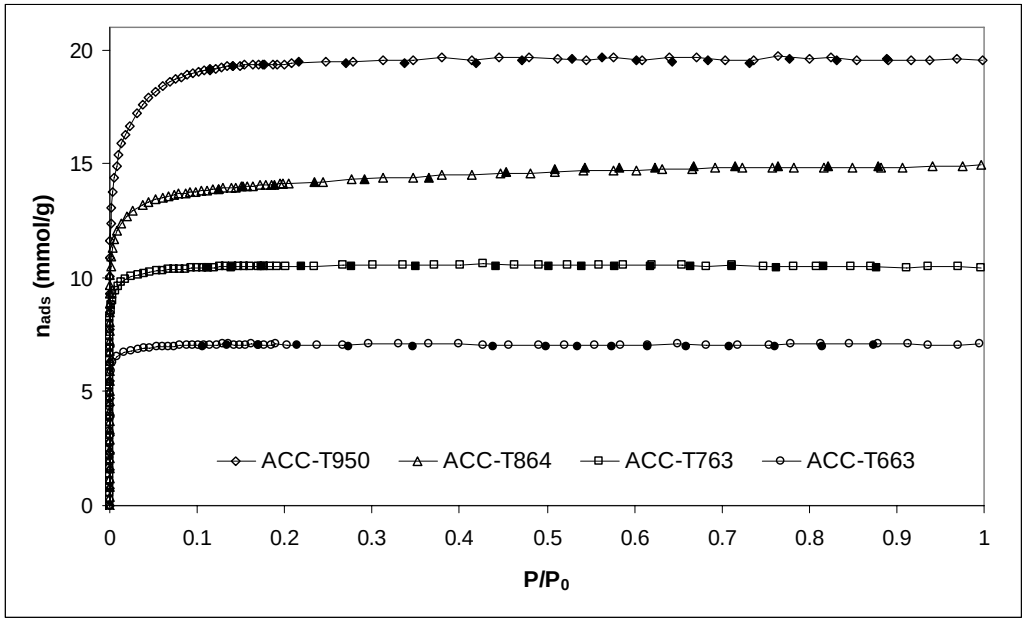


Figure 9. N_2 adsorption/desorption isotherms for ACC samples obtained from Tencel with 10 wt% phosphoric acid solution at different final thermal treatment temperatures.

As seen in Figure 9, all the isotherms are reversible and show a plateau over wide ranges of the relative pressure. They are characteristic of Type I isotherms according to the IUPAC classification, pointing to essentially microporous materials. Only the isotherm for sample ACC-T864 presents a slight slope in the multilayer region. Besides, Figure 9 shows that N_2 adsorption capacity of the ACC increases markedly with increase in the final temperature used for their development. Likewise, the knee of the isotherms becomes more rounded as temperature increases, pointing to an increase in mean pore width (Carrott et al., 2001).

The effect of the final thermal treatment temperature on BET surface area and total pore volume for the ACC developed from both precursors is comparatively illustrated in Figure 10. As may be appreciated, increasing the thermal treatment temperature leads to ACC of higher specific surface area and total pore volume for both precursors. Nevertheless, those developed

from Tencel attain higher values than the denim-based ACC. At the highest temperature (950 ºC) of the investigated range, a maximum value of 2011 m^2/g and total pore volume of 0.67 cm^3/g characterize the ACC derived from Tencel, whereas the ACC obtained from denim show a maximum surface area of 1055 m^2/g and total pore volume of 0.53 cm^3/g. The inverse trend is found for ACC yield, as already shown in Figure 5. Yields of ~ 20% and 29% are attained for ACC developed from Tencel and denim at 950 ºC, respectively, in agreement with the greater development of porosity for the samples obtained from the former.

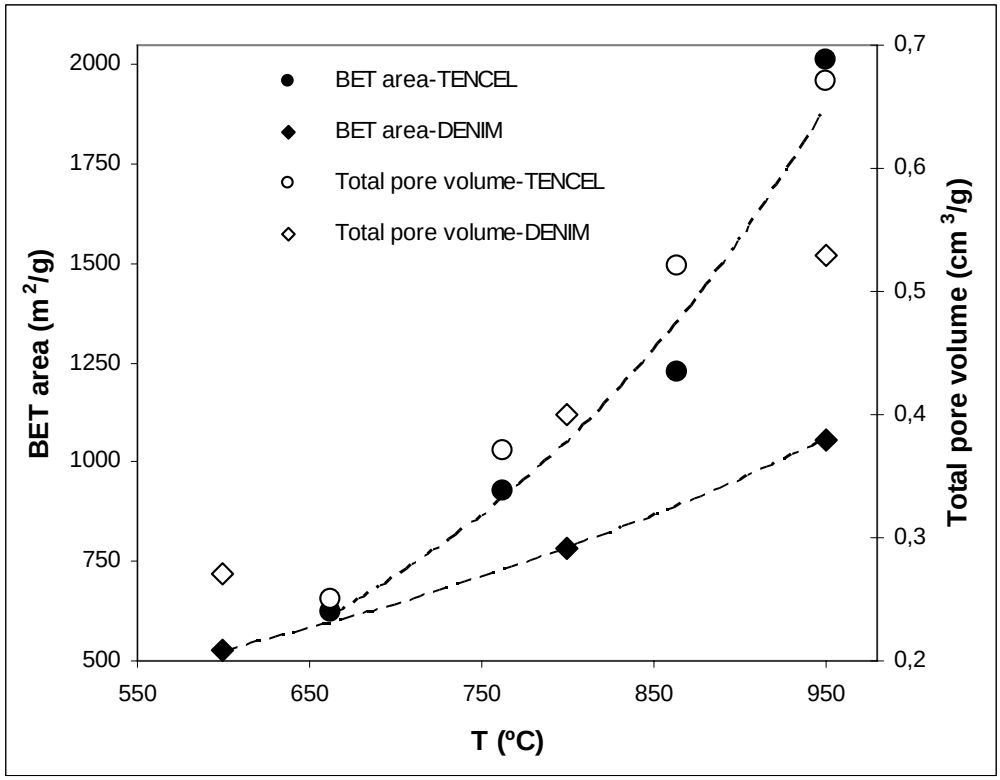


Figure 10. Effect of the final thermal treatment temperature on BET surface area and total pore volume for the ACC developed from denim and Tencel with 10 wt% H_3PO_4 acid solution.

Table IV reports representative results of textural parameters additionally calculated from N_2 adsorption isotherms by applying the α_S method and DR equation, for the ACC obtained from Tencel at different thermal treatment temperatures. In all cases, the DR plots corresponding to the isotherms were found to give good linearity over the relative pressure range between 10^{-5} and 2×10^{-2}, and the α_S plots were linear from relative pressures above about 0.3. Comparison of micropore volumes evaluated by these two methods with total pore volumes, as directly determined from the corresponding isotherms at the highest relative pressure, is shown in Figure 11.

Table IV. Textural parameters calculated by applying the αs and DR methods to N_2 adsorption isotherms for the ACC obtained from TENCEL at different thermal treatment temperatures

T (ºC)	A_S (m^2/g)	v_S (cm^3/g)	v_0 (cm^3/g)	E_0 (kJ/mol)	L_0 (nm)
663	2.1	0.24	0.25	29.9	0.59
763	0.6	0.37	0.37	28.1	0.65
864	10.8	0.51	0.48	24.2	0.84
950	1.6	0.67	0.64	21.3	1.09

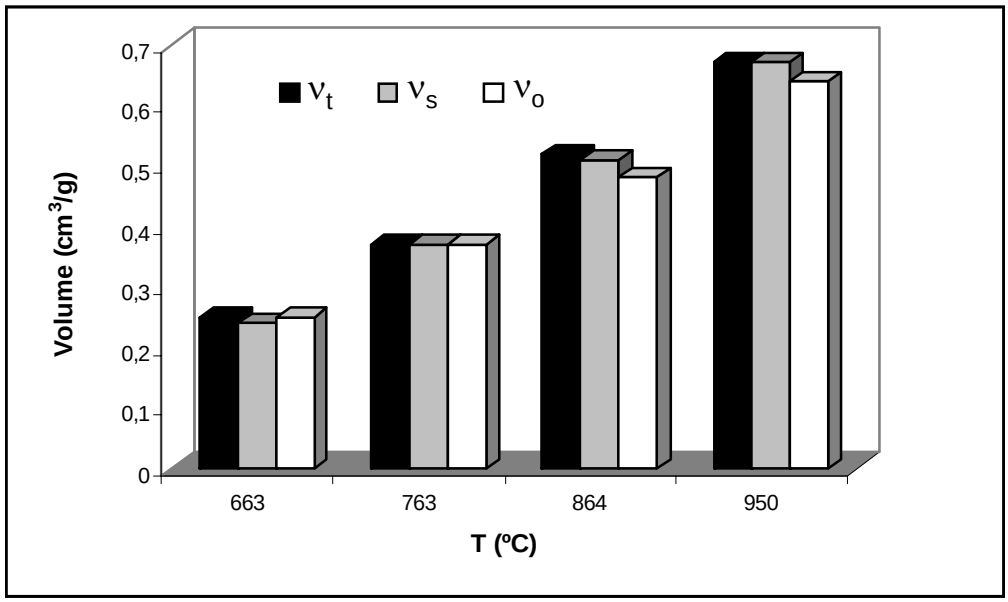


Figure 11. Effect of the thermal treatment temperature on total pore volume and micropore volumes calculated by the α_S and DR methods, for the ACC developed from Tencel with 10 wt% H_3PO_4 acid solution.

As may be appreciated in Figure 11, the corresponding values of v_s and v_o are in close agreement for all the samples, indicating the presence of fairly narrow micropores only. This is confirmed by L_o values (Table IV). They are all lower than 1.1 nm. Nevertheless, these values varying from 0.59 nm up to 1.09 nm in the range of temperatures investigated point to an increase in mean micropore width as the thermal treatment temperature is increased. Likewise, the external surface area (A_S) of the all samples are very low (<11 m^2 g^{-1}), also confirming a negligible development of mesopores. All these characteristics make Tencel-based ACC potentially appropriate for their use in gaseous effluents treatment, i.e. for the adsorption of VOCs in low concentrations in ambient air environments (Ramos et al., 2010).

SEM images of the surfaces of the pristine fabrics used as precursors and of some representative ACC are shown in Figures 12 and 13. Figures 12 (a) and 12 (b) illustrate typical SEM micrographs (magnification of 600x) of the surfaces of denim and of an ACC prepared from this fabric using 10 wt% acid concentration at 950 ºC. Despite substantial

changes taking place upon activation, comparison of parts (a) and (b) of Figure 12 attests that the precursor's original morphology and fibers integrity in the ACC are well preserved.

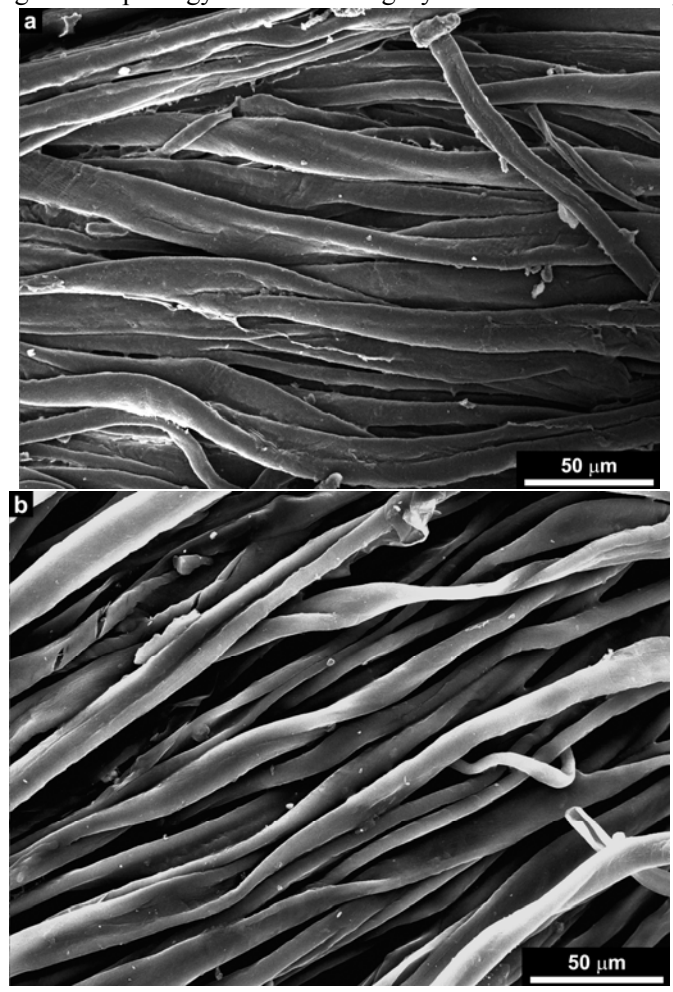


Figure 12. SEM micrographs (magnification of 600x) for: a) pristine denim; b) ACC developed from denim with 10 wt% H_3PO_4 acid solution at 950ºC.

Likewise, Figure 13 (a-c) illustrates SEM images for the surface of pristine Tencel (at 600x) and of an ACC obtained using 10 wt% acid concentration and a thermal treatment temperature of 800 ºC, at two different magnifications (600x and 6000x). As may be appreciated from Figures 13a and 13b, morphology and integrity of the precursor are retained in the Tencel-derived ACC. Nevertheless, certain shrinkage arises attributable to the thermal treatment, as inferred from the relative reduction in the width of the fibers. Compared to the pristine precursor, the fiber's width is found to decrease from 11 μm to 8 μm after the thermal treatment stage. Values are close to those reported in the literature for activated carbon fibers prepared from viscous rayon (Brasquet et al., 2000). It may also be observed that the surface of the ACC results completely smooth and no hole or pore is visualized even at a magnification of 6000x (Figure 13c). Besides, all the ACC developed from both precursors show a good physical appearance looking flexible and relatively strong, except for those

derived from the acid-free precursors and of some samples obtained with phosphoric acid solutions of excessively high acid concentration (i.e. 50 wt%) (Ramos et al., 2007; 2008).

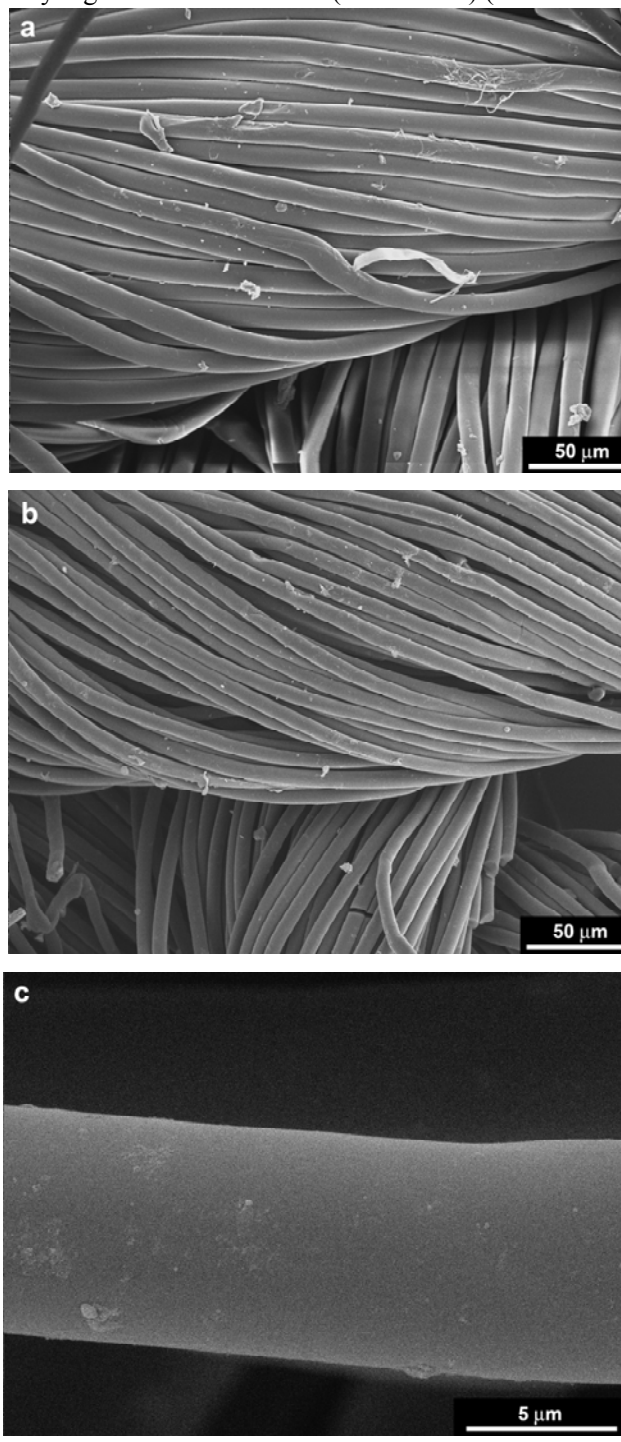


Figure 13. SEM micrographs of: a) pristine Tencel (600x); b) and c) ACC developed from Tencel with 10 wt% H_3PO_4 acid solution at 800 ºC (magnifications of 600x and 6000x, respectively).

The influence of the acid concentration on textural parameters characterizing the ACC obtained from denim at 800 ºC is illustrated in Figure 14. As seen in the figure, the ACC obtained with 10 wt% acid concentration show a maximum BET surface area. The trend indicates that a progressive development of porosity takes place as more acid is incorporated into the precursor, presumably due to dilation of the cross-linked structure, up to a limit above which reduction in porosity development occurs. It might be due to pores collapse occasioned by the larger excess of acid, likely as a consequence of intensified dilation (Jagtoyen and Derbyshire, 1998; Blanco Castro et al., 2000; Vernersson et al., 2002). The results in Figure 14 also show that variations of the total pore volume and micropore volume with the acid concentration follow the same trends as the specific surface area.

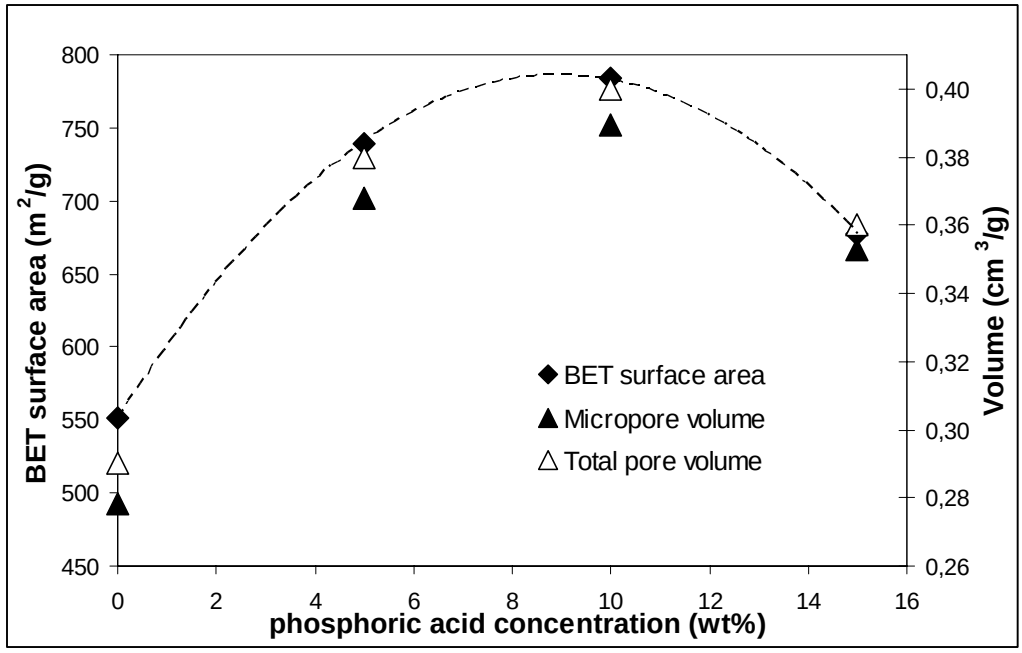


Figure 14. Effect of phosphoric acid concentration on BET surface area, total pore volume, and micropore volume for the activated carbon cloths prepared at a final thermal treatment temperature of 800 °C.

In turn, Figure 15 exemplifies the influence of phosphoric acid solution concentration on BET surface area and yield for the ACC obtained from Tencel at a thermal treatment temperature of 950 ºC.

The results in Figure 15 indicate that impregnation of Tencel with solutions of higher acid concentration leads to a steady enhancement in porosity development for the derived ACC. Although the trend differs from that for the denim-based ACC which attain maximum values for 10 wt% acid concentration (Figure 14), it should be taken into account that the results correspond to a lower temperature. Yields follow in general terms a decrease trend with acid concentration in the range 5-30 wt%. For the highest acid concentration (30 wt%), the ACC attain a BET surface area of ~ 2800 m^2/g but at the expense of a low yield (8 %). Comparison of results (Figures 10 and 15) for Tencel-based ACC reveals that the thermal

treatment temperature exerts a more pronounced effect on porosity development than the acid concentration.

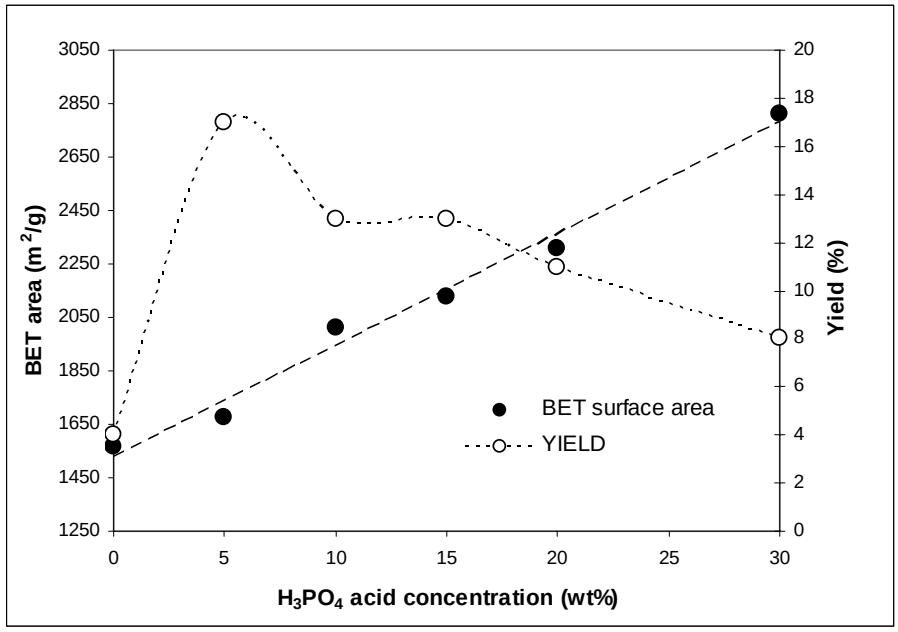


Figure 15. Effect of H_3PO_4 acid concentration on BET surface area and yield for the ACC developed from Tencel at 950 ºC.

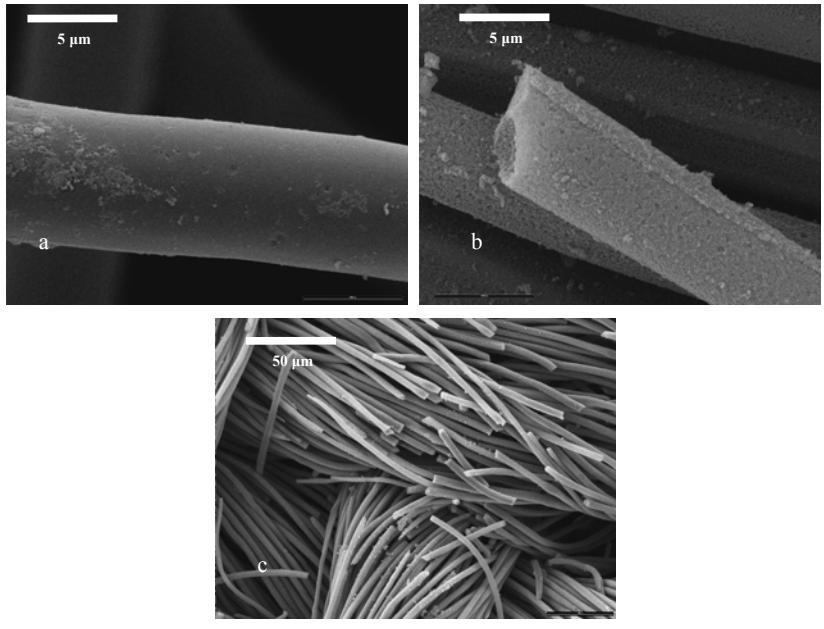


Figure 16. SEM micrographs of: a) ACC prepared from Tencel with 10 wt% H_3PO_4 acid solution at 950 ºC (magnification 6000x); b) acid-free cloth prepared at 950 ºC (magnification 6000x); c) acid-free cloth prepared at 950 ºC (magnification 600x).

In order to visualize the effect of acid impregnation on the surface of the resulting ACC, Figure 16 (a-c) displays comparatively SEM images obtained for the ACC developed from Tencel with 10 wt% phosphoric solution at 950 ºC and for the cloth arising from treatment of the precursor with distilled water at the same temperature, namely an acid-free sample, at two different magnifications.

As may be observed in part (c) of Figure 16, the acid-free cloth clearly evidences a noticeable breakage of the fibres, leading to ACC with a fragile and brittle appearance. Similar results (not shown) were found for blank samples obtained from denim. The images in Figure 16 highlight the fundamental role of the impregnation agent on the final structure of the ACC. It hinders excessive release of volatile compounds and favors cross-linking reactions, thus contributing to preserve the constituent fibres of the resulting cloths. The ACC obtained from Tencel by chemical activation with H_3PO_4 acid show a smooth surface, with some isolated holes (Figure 16.a). By contrast, the acid-free cloth exhibits a rough surface with several defects and holes (Figure 16.b), pointing to the development of a meso-, macroporous structure, which is reflected in a higher average pore radius.

On the other hand, the effect of the final thermal treatment temperature on the crystalline structure of the fibres constituting the ACC is exemplified for those samples developed by activation of denim with 10 wt% phosphoric acid solution at different final temperatures kept for 1 h. For the sake of comparison, ACC developed from denim using more drastic conditions are also examined. In the latter case, the thermal treatment stage was carried out at the highest final temperature (950 ºC) for 3 h. Figures 17 and 18 show XRD patterns for the denim precursor and the ACC derived at different experimental conditions, respectively.

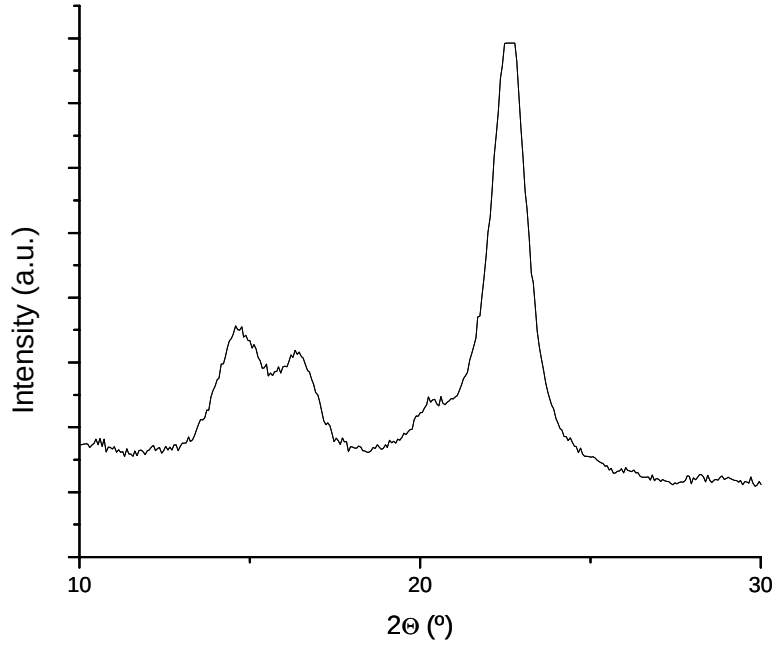


Figure 17. XRD pattern for the denim fabric used as precursor.

In Figure 17, two overlapped peaks at 2θ ~ 14.6º and 16.4 º, and a sharp peak at 2θ ~ 22.7 º with a shoulder at 20.5 º may be observed. The diffractogram for denim agrees with

others reported in the literature for virgin cellulose. The peak at 2θ ~ 22º is due to reflections from the (002) plane, while the overlapped peaks between ~ 15º and 17º characterize cellulose and correspond to (101) and (10-1) planes (Frisoni et al., 2001; Reddy and Yang, 2007).

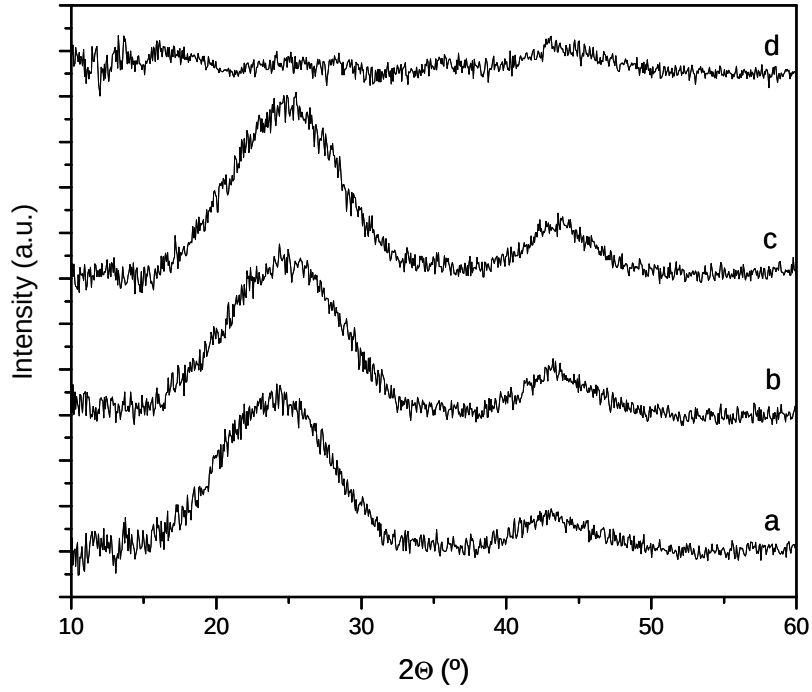


Figura 18. XRD patterns for the ACC obtained from denim using 10 wt% phosphoric acid solution, and thermally treated at: a) 600 º C for 1 h, b) 800 ºC for 1 h, c) 950 ºC for 1 h, and d) 950 ºC for 3 h.

Comparison of the results in Figures 17 and 18 reveals that impregnation and thermal treatment stages involved in the activation process lead to significant changes in the crystalline structure of the denim precursor. The results are in agreement with those reported in the literature, pointing to the disappearance of the crystalline structure of cellulose for temperatures lower than 400 ºC (Gurudatt and Tripathi, 1998).

Representative XRD patterns for the ACC in Figure 18 (a-c) show peaks at 2θ ~ 25º and 2θ ~ 42º, that are characteristic of activated carbons. They are due to reflections from the (002) and (10) planes, respectively, confirming the turbostratic structure of the fibres. The (002) peak vanishes for the ACC developed in more drastic conditions, 950 ºC for 3 hours (Figure 18-d.). The behavior agrees with that reported for ACC developed from viscous rayon by impregnation with H_3PO_4 acid solutions and activated in CO_2 atmosphere. Lack of (002) peak should be due to the small thickness of micro-crystalline units, pointing to an essentially amorphous structure (Kumar et al., 1997; Gurudatt and Tripathi, 1998). Enhancement in internal disorder is accompanied by a significant increase of the specific surface area of the ACC obtained in the most severe conditions (950 °C, 3 h), with this sample attaining BET surface area of 2531 m^2/g.

Structural characteristic parameters calculated from the XRD patterns for the ACC developed from denim using phosphoric acid solution (10 wt%) and different final treatment

temperatures maintained for 1 h are listed in Table V. Parameters for the ACC obtained at 950 ºC for 3 h are not reported since their calculation was not possible. BET surface area values of the ACC are also included in the same table.

Table V. Effect of the final thermal treatment temperature on structural parameters of the ACC developed from denim with 10 wt% H_3PO_4 acid solution keeping the temperature for 1 h

T (ºC)	d_{002} (nm)	L_c (nm)	L_a (nm)	S_{BET} (m^2/g)
600	0.370	1.10	3.70	525
800	0.362	1.05	3.69	784
950	0.359	1.08	3.07	1055

The d_{002} value is traditionally used to estimate the graphitization degree of carbons. In general, growing disorder is reflected in increased values of d_{002} (Liu et al., 2007). Results in Table V reveal that d_{002} values (~ 0.36 – 0.37 nm) are higher than the value for graphite (d_{002} = 0.335 nm), attributable to the turbostratic nature of activated carbon (Carrott et al., 2001). The slightly lower d_{002} value observed in the table at 950 °C points to a slight enhancement in the internal order of the fibres as the thermal treatment temperatures increases.

With regard to the crystallite dimensions, it should be taken into account that values of L_c and L_a are not exactly equal to the height and width of the crystallites, but they can be used as convenient relative estimates of these quantities. Likely, the true crystallite size is slightly greater than the calculated values (Carrott et al., 2001).

As seen in Table V, L_c values are almost constant for the ACC developed from denim at the different final treatment temperatures. It may be mentioned that the Tencel-based ACC show a similar trend. Although increase in thermal treatment temperature should lead to enhancement in internal order of the fibres, the effect might be counterbalanced by porous development, which could explain practically unchanged L_c values. Carrott et al. (2001) also observed that the L_c value for activated carbon fibres (ACFs) derived from acrylic fibres remained almost invariable for a particular range of yields. Likewise, the results in Table V indicate that L_a values decrease as the final thermal treatment temperature increases to 950 ºC. In comparison with results reported for the acrylic fibres-based ACFs, all the values of L_a and L_c calculated for the ACC derived from denim are lower suggesting a lower structural order for the latter.

L_c values for the Tencel-based ACC are similar to those developed from denim, but d_{002} values for the latter are lower. Accordingly, the trend points to a greater number of parallel graphitic layers in crystallite units for the denim-derived ACC, indicating a greater cristallinity degree, which is consistent with their relatively lower porosity development.

3.3. Effect of the Nitrogen Flow and Thermal Treatment Time on Yield and Porous Development of the Activated Carbon Cloths

In order to examine the effect of the nitrogen flow rate used in the thermal treatment stage on yield and porous structure development of the activated carbon cloths, samples

employing Tencel as precursor were prepared by varying the gas flow rate in the range 100-300 mL/min. H_3PO_4 acid solution of 10 %wt concentration and final thermal treatment temperature of 800 ºC maintained for 1 h were employed in all cases. Yield and textural parameters, the latter evaluated from the corresponding N_2 adsorption isotherms, as a function of the gas flow rate are shown in Figures 18 and 19.

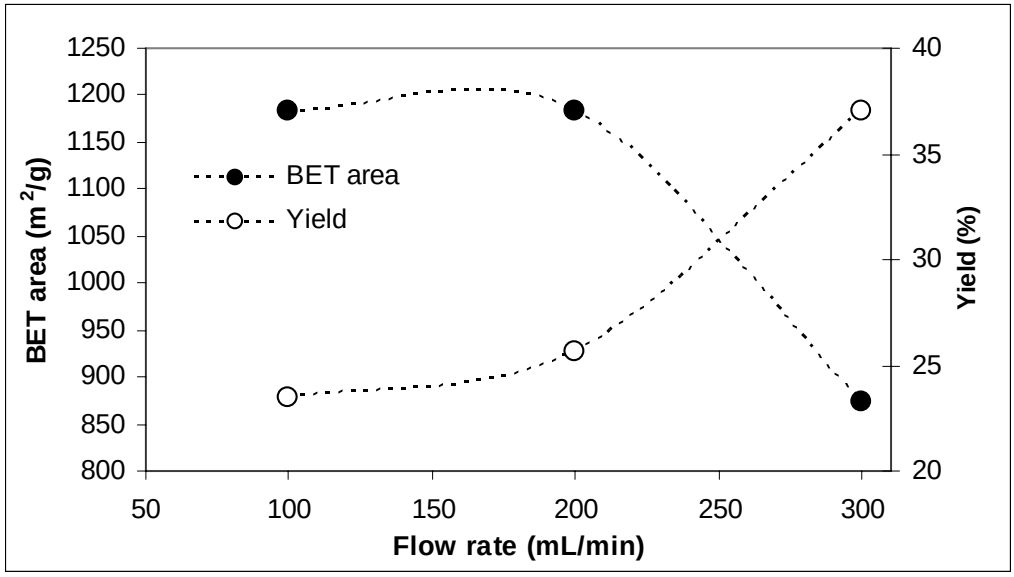


Figure 18. Effect of N_2 flow rate used in the thermal treatment stage on BET surface area and yield for the ACC obtained from Tencel with 10 wt% H_3PO_4 acid solution at 800ºC.

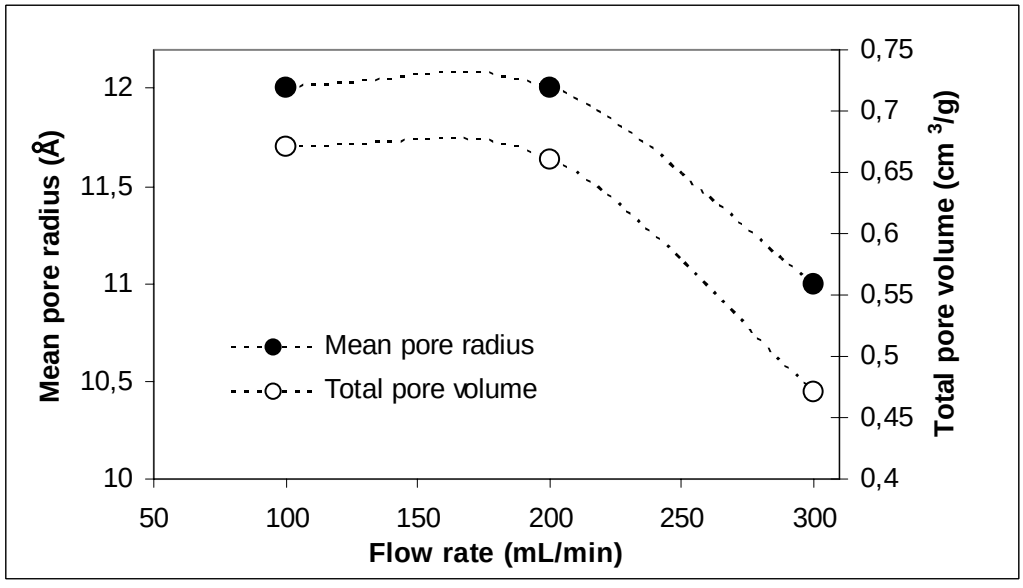


Figure 19. Effect of N_2 flow rate used in the thermal treatment stage on mean pore radius and total pore volume of the ACC obtained from Tencel with 10 wt% H_3PO_4 acid solution and at T = 800ºC.

The results indicate that increasing N_2 flow rate from 100 to 200 mL/min does not lead to significant modifications in porosity development, as inferred from the calculated textural parameters. In opposition, increase in N_2 flow rate to 300 mL/min induces to decrease BET surface area, likely due to variations in the generated activation atmosphere. As the gas flow rate increases, volatile compounds released during the thermal treatment, whose nature is slightly oxidant, remain in the reactor for a shorter time, thus generating a relatively less oxidative atmosphere. Accordingly, ACC with less developed porous structures, as revealed by lower values of S_{BET} and v_T, and higher yield are obtained. Besides, increase of the gas flow rate to 300 mL/min yields more microporous ACC, as revealed by the decrease in the estimated mean pore radius.

The effect of the thermal treatment time at the final temperature on the development of the porous structure of the ACC was also investigated. For this purpose, samples were prepared with H_3PO_4 acid solution of 10 %wt concentration, N_2 flow rate of 100 mL/min, and thermal treatment temperature of 800 ºC, by varying the time at the final temperature between 0 and 2 hours. Yield and textural parameters, evaluated from the corresponding adsorption isotherms, as a function of time are illustrated in Figures 20 and 21.

Time prolongation promotes increases in the BET surface area and total pore volume, slightly decreasing process yield. The results suggest that longer times could intensify formation and release of volatile compounds, which lead to porous structure development. Time prolongation could therefore favor reactions which might induce creation and/or widening of pores, as reflected in textural parameters of the ACC. Nevertheless, the results indicate that prolongation of the thermal treatment time from 1 h to 2 h has almost no influence on pore width, as revealed by constant values of mean pore radius of the resulting ACC (Figure 21).

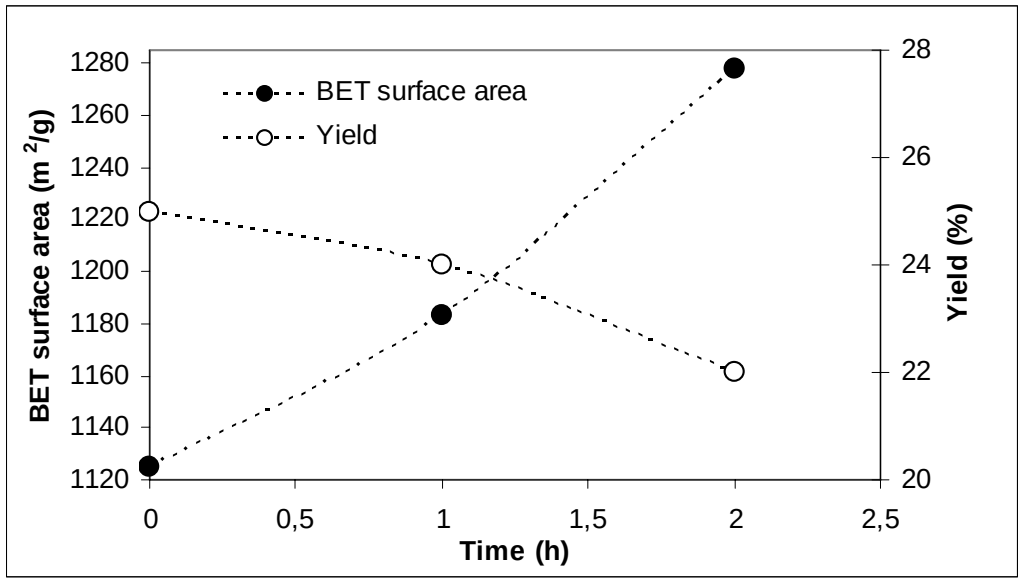


Figure 20. Effect of thermal treatment time on BET surface area and yield of the ACC obtained from Tencel at 800ºC.

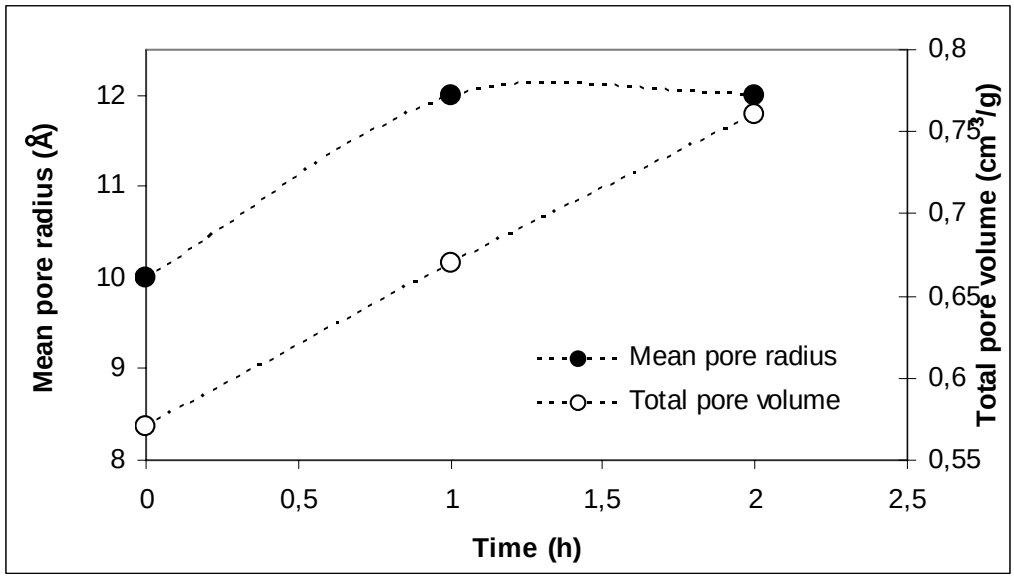


Figure 21. Effect of thermal treatment time on mean pore radius and total pore volume of ACC obtained from Tencel at 800ºC.

CONCLUSIONS

The phosphoric acid activation process has been examined focusing on two novel cellulosic precursors, denim and Tencel®, in an attempt to establish optimal strategies for the development and application of the resulting activated carbon cloths (ACC). For this purpose, the effect of main process variables on yield and physico-chemical properties of the ACC has been investigated.

Impregnation of the fabrics used as precursors with phosphoric acid leads to significant modifications in their thermal behavior, increasing yield and shifting thermal degradation onset and maximum rates to lower temperatures compared to the untreated precursors. They may be attributed to alterations in physico-chemical properties of the precursors occasioned by the acid, that promote cross-linking reactions inducing an enhanced retention of volatiles in the precursors' structure. Changes intensity depends on the inherent nature of the fabric precursor, which could affect interactions between the reactive agent and the constituting fibres during the impregnation stage, and on the acid concentration. Thermal decomposition onset and maximum rates occur at lower temperatures as higher the phosphoric acid concentration.

Despite substantial changes taking place during impregnation and further thermal treatment of both precursors, the developed ACC preserve the original structure of the fabrics as well as integrity of the constituting fibres for almost all the experimental conditions investigated. Acid-free cloths, namely blank samples, arising from both precursors show fibres breakage, thus evidencing the crucial role of the chemical reagent in the development of ACC with well-preserved integrity of the fibres.

Phosphoric acid activation modifies elemental composition, crystalline structure, and surface chemistry of the fabric precursors. Modifications are found strongly dependent on the conditions employed. In particular, as shown for the denim-based ACC, the process promotes formation of acidic oxygen functional groups on the surface of the derived ACC. Those ACC with the highest total acidity (1 mmol/g) but with relatively scarce development of porosity exhibit a good performance in metallic cations removal from dilute aqueous solutions, pointing to their potential use in tertiary treatment of water polluted with metal species. These results also highlight the dominance of the surface chemistry of the activated carbon cloths over porous structures characteristics, in connection with their behavior as cationic exchangers.

Among the investigated variables, the thermal treatment temperature exerts a key role on the development of ACC. For both precursors, increasing the temperature leads to ACC of higher specific surface area and total pore volume. Nevertheless, those obtained from Tencel attain higher values than the denim-based ACC. At the highest temperature (950 ºC) of the investigated range and for the same acid concentration (10 wt%), maximum values of 2011 m^2/g and 0.67 cm^3/g characterize the ACC derived from Tencel, whereas the ACC obtained from denim show a maximum surface area of 1055 m^2/g and total pore volume of 0.53 cm^3/g. The inverse trend is found for ACC yield, attaining values of ~ 20% and 29%, respectively. Furthermore, the activated carbon cloths developed from both precursors show predominantly microporous structures, although those obtained from Tencel show higher micropore volumes and fairly narrow microporosity. These characteristics make Tencel-based ACC potentially suited for their use in gaseous effluents treatment, i.e. for the adsorption of VOCs from air environments.

Regarding the influence of the flow rate involved in the thermal treatment stage, modifications in porosity development of the ACC from Tencel are significant only when the N_2 flow rate is increased three times. The behavior could be related to the generation of a less oxidative atmosphere as a consequence of the shorter residence time of the volatile compounds released, leading to ACC with less developed porous structures and higher yields. On the contrary, prolongation of the thermal treatment time induces an enhanced development of ACC porous structures, presumably because it favors reactions which promote creation and/or widening of pores, even though at the expense of lower yields.

Overall, phosphoric acid activation of both cellulosic textiles used as starting materials may be employed for the manufacture of good quality activated carbon cloths. Their physico-chemical properties may be conveniently optimized in terms of desired characteristics and/or specific end uses, through the strategic selection of main variables involved in the activation process.

ACKNOWLEDGMENTS

Financial support from Consejo Nacional de Investigaciones Científicas y Técnicas - CONICET (Project PIP 0183), Universidad de Buenos Aires-UBA (Project B041), and Agencia Nacional de Promoción Científica y Tecnológica-ANPCYT-FONCYT (Project PICT 2131) from Argentina is gratefully acknowledged.

REFERENCES

Afkhami, A., Madrakian, T., Karimi, Z. 2007. The effect of acid treatment of carbon cloth on the adsorption of nitrite and nitrate ions. *Journal of Hazardous Materials* 144, 427-431.

Afkhami, A., Madrakian, T., Amini, A., Karimi, Z. 2008. Effect of the impregnation of carbon cloth with ethylenediaminetetraacetic acid on its adsorption capacity for the adsorption of several metal ions. *Journal of Hazardous Materials* 150, 408-412.

Allen T. *Particle size measurement*. Volume 2: Surface area and pore size determination. Fifth edition. Chapman and Hall, London, UK, 1997.

Ayranci, E., Hoda, N., 2004. Adsorption of bentazon and propanil from aqueous solutions at the high area activated carbon-cloth. *Chemosphere* 57, 755-762.

Ayranci E., Hoda N., Bayram E. 2005. Adsorption of benzoic acid onto high specific area activated carbon cloth. *Journal of Colloid and Interface Science* 284, 83-88.

Ayranci, E., Duman, O. 2005. Adsorption behaviors of some phenolic compounds onto high specific area activated carbon cloth. *Journal of Hazardous Materials* 124, 125-132.

Ayranci E., Duman O. 2006. Adsorption of aromatic acids onto high area activated carbon cloth in relation to wastewater purification. *Journal of Hazardous Materials* 136, 542-552.

Ayranci, E., Duman, O. 2010. Structural effects on the interactions of benzene and naphthalene sulfonates with activated carbon cloth during adsorption from aqueous solutions. *Chemical Engineering Journal* 156, 70-76.

Babel, K., Jurewicz, K., 2004. KOH activated carbon fabrics as supercapacitor material. *J. Physics and Chemistry of Solids* 65, 275-280.

Badalyan, R. Bromball, P. Pendleton, W. Skinner. 2010. An assessment of activated carbon cloth microporosity change due to chemical activation. *Carbon* 48, 1004-1011.

Basso, M.C., Cerrella, E.G., Cukierman, A.L. 2002. Activated carbons developed from a rapidly renewable biosource for removal of cadmium (II) and nickel (II) ions from dilute aqueous solutions. *Ind. Eng. Chem. Res*. 41, 180-189.

Basso, M.C., Cukierman, A.L. 2005. *Arundo donax*-based activated carbons for aqueous-phase adsorption of volatile organic compounds. *Ind. Eng. Chem. Res*. 44, 2091-2100.

Benaddi H., Legras D., Rouzaud J. N., Beguin F. 1998. Influence of the atmosphere in the chemical activation of wood by phosphoric acid. *Carbon* 36, 306-309.

Biniwale R.B., Ichikawa M. 2007. Thermal imaging of catalyst surface during catalytic dehydrogenation of cyclohexane under spray-pulsed conditions. *Chem. Eng. Sci.* 62, 7370-7377.

Blanco Castro J., Bonelli P., Cerrella G., Cukierman A. L. 2000. Phosphoric acid activation of agricultural residues and bagasse from sugar cane: influence of the experimental conditions on adsorption characteristics of activated carbons. *Ind. Eng. Chem. Res*. 39, 4166-4172.

Boehm H. P. 2002. Surface oxides on carbon and their analysis: a critical assessment. *Carbon* 40, 145-149.

Boudou, J.P. 2003. Surface chemistry of a viscose-based activated carbon cloth modified by treatment with ammonia and steam. *Carbon* 41, 1955-1963.

Boudou J.P., Parent Ph., Suarez-García F., Villar-Rodil S., Martínez-Alonso A., Tascón J.M.D. 2006. Nitrogen in aramid-based activated carbon fibers by TPD, XPS and XANES. *Carbon* 44, 2452-2462.

Boulinguiez, B., Le Cloirec., P. 2010. Adsorption on activated carbons of five selected volatile organic compounds present in biogas: Comparison of granular and fiber cloth materials. *Energy and Fuels* 24, 4756-4765.

Brasquet, C., Rousseau, B., Estrade-Szwarckopf, H., Le Cloirec, P. 2000. Observation of activated carbon fibres with SEM and AFM correlation with adsorption data in aqueous solution. *Carbon* 38, 407–422.

Carrott P. J. M., Nabais J. M. V., Ribeiro Carrott M. M. L., Pajares J. A. 2001. Preparation of activated carbon fibres from acrylic textile fibres. *Carbon* 39, 1543-1555.

Carrott, P. J. M.; Nabais, J. M. V.; Ribeiro Carrott, M. M. L.; Menéndez, J. A. 2004. Microwave heating as a novel method for introducing molecular sieve properties into activated carbon fibres. *Carbon* 42, 227-229.

De Celis, J., Amadeo, N.E., Cukierman, A.L. 2009. *In situ* modification of activated carbons developed from a native invasive wood on removal of trace toxic metals from wastewater. *Journal of Hazardous Materials* 161, 217-223.

Faur-Brasquet C., Reddad Z., Kadirvelu K., Le Cloirec P. 2002. Modeling the adsorption of metal ions (Cu^{2+}, Ni^{2+}, Pb^{2+}) onto ACCs using surface complexation models. *Applied Surface Science* 196, 356-365.

Frisoni, G., Baiardo, M. Scandola, M. 2001. Natural cellulose fibers: Heterogeneous acetylation kinetics and biodegradation behavior. *Biomacromolecules* 2, 476-482.

Goyal, M., Dhawan, R., Bhagat, M. 2010. Adsorption of gallic acid from aqueous solution using fixed bed activated carbon columns. *Separation Science and Technology* 45, 1265-1274.

Gurudatt K., Tripathi V. S. 1998. Studies on changes in morphology during carbonization and activation of pretreated viscose rayon fabrics. *Carbon* 36, 1371-1377.

Huang, C.-C., Su, Y.-J. 2010. Removal of copper ions from wastewater by adsorption/electrosorption on modified activated carbon cloths. *Journal of Hazardous Materials* 175, 477-483.

Huidobro, A., Pastor, A.C., Rodríguez Reinoso, F. 2001. Preparation of activated carbon cloth from viscous rayon. Part IV: Chemical activation. *Carbon* 39, 389-398.

Isaev I., Salitra G., Soffer A., Cohen Y. S., Aurbach D., Fischer J. 2003. A new approach for the preparation of anodes for Li-ion batteries based on activated hard carbon cloth with pore design. *Journal of Power Sources* 119-121, 28-33.

Jagtoyen, M.; Derbyshire, F. 1998. Activated carbons from yellow poplar and white oak by H_3PO_4 activation. *Carbon* 36, 1085-1097.

Kumar, K., Saxena, R.K., Kothari, R., Suri, D.K., Kaushik, N.K., Bohra, J.N. 1997. Correlation between adsorption and x-ray diffraction studies on viscose rayon based activated carbon cloth. *Carbon* 35, 1842-1844.

Kunowsky M., Weinberger B., Lamari Darkrim F., Suárez-García F., Cazorla-Amorós D., Linares-Solano A. 2008. Impact of the carbonisation temperature on the activation of carbon fibres and their application for hydrogen storage. *International Journal of Hydrogen Energy* 33, 3091-3095.

Lewandowski A., Olejniczak A., Galinski M., Stepniak I. 2010. Performance of carbon–carbon supercapacitors based on organic, aqueous and ionic liquid electrolytes. *Journal of Power Sources* 195, 5814-5819.

Linares-Solano, A., Cazorla-Amorós, D. 2008. Adsorption on activated carbon fibers. In: E.J. Bottani, J.M.D. Tascón (Eds.), *Adsorption by Carbons*, Elsevier, Oxford, UK. Chapter 17, 431-449.

Liu, C., Dong, W., Song, J., Liu, L. 2007. Evolution of microstructure and properties of phenolic fibers during carbonization. *Materials Science and Engineering A* 459, 347-354.

López-Ramón, M.V., Fontecha-Cámara, M.A., Alvarez-Merino, M.A., Moreno-Castilla, C. 2007. Removal of diuron and amitrole from water under static and dynamic conditions using activated carbons in form of fibers, cloth, and grains. *Water Research* 41, 2865-2870.

Lu A-H., Zheng J-T. 2001. Study of microstructure of high-surface-area polyacrylonitrile activated carbon fibers. *J. of Colloid and Interface Sci*. 236, 369-374.

Marsh H., Rodríguez Reinoso F. *Activated carbon*. Elsevier, 2006.

Matatov-Meytal, Y., Sheintuch, M. 2002. Catalytic fibers and cloths. *Applied Catalysis A: General* 231, 1-16.

Matatov-Meytal, U.I. 2005. Radial-flow reactor packed with a catalytic cloth: Nitrate reduction in hydrogen-saturated water. *Ind. Eng. Chem. Res.* 44, 9575-9580.

Moreno-Castilla, C., Álvarez-Merino, M.A., Pastrana-Martínez, L.M., López-Ramón, M.V. 2010. Adsorption mechanisms of metal cations from water on an oxidized carbon surface. *J. Colloid and Interface Science* 345, 461-466.

Naranjo, J.C., Córdoba, A., Giraldo, L., García, V.S., Moreno-Piraján, J.C. 2010. Lipase supported on granular activated carbon and activated carbon cloth as a catalyst in the synthesis of bio-diesel fuel. *Journal of Molecular Catalysis B: Enzymatic* 66, 166-171.

Pandey S. N., Nair P. 1974. Effect of phosphoric acid treatment on physical and chemical properties of cotton fiber. *Textile Res. J*. 44, 927-933.

Pastor, A. C.; Rodríguez-Reinoso, F.; Marsh, H.; Martínez, M. A. 1999. Preparation of activated carbon cloths from viscous rayon. Part I. Carbonization procedures. *Carbon* 37, 1275-1283.

Pastrana-Martínez L. M., López-Ramón M. V., Moreno-Castilla C. 2009. Adsorption and thermal desorption of the herbicide fluroxypyr on activated carbon fibers and cloth at different pH values. *J. of Colloid Interface Sci*. 331, 2-7.

Pastrana-Martínez, L.M., López-Ramón, M.V., Fontecha-Cámara M.A., Moreno-Castilla, C. 2010. Batch and column adsorption of herbicide fluroxypyr on different types of activated carbons from water with varied degrees of hardness and alkalinity. *Water Research* 44, 879-885.

Perrard, A., Gallezot, P., Joly, J-P., Durand, R., Baljou, C., Coq, B., Trens, P. 2007. Highly efficient metal catalysts supported on activated carbon cloths: A catalytic application for the hydrogenation of D-glucose to D-sorbitol. *Applied Catalysis A: General* 331, 100-104.

Polovina, M., Babić, B., Kaluderović, B., Dekanski, A. 1997. Surface characterization of oxidized activated carbon cloth. *Carbon* 35, 1047-1052.

Puziy A. M., Poddubnaya O. I., Martínez-Alonso A., Suárez-García F., Tascón J. M. D. 2002a. Synthetic carbons activated with phosphoric acid I. Surface chemistry and ion binding properties, *Carbon*, 40, 1493-1505.

Puziy A. M., Poddubnaya O. I., Martínez-Alonso A., Suárez-García F., Tascón J. M. D. 2002b. Synthetic carbons activated with phosphoric acid II. Porous structure, *Carbon*, 40, 1507-1519.

Ramos, M.E., González, J., Bonelli, P.R., Cukierman, A.L. 2007. Effect of process conditions on physicochemical and electrical characteristics of denim-based activated carbon cloths. *Ind. Eng. Chem. Res*. 46, 1167-1173.

Ramos, M.E., Bonelli, P.R., Cukierman, A.L. 2008. Physico-chemical and electrical properties of activated carbon cloths. Effect of inherent nature of the fabric precursor. *Colloids and Surfaces A: Physicochemical and Engineering Aspects* 324, 86-92.

Ramos, M.E., Bonelli, P.R., Cukierman, A.L., Ribeiro Carrott, M.M.L., Carrott, P.J.M. 2009. Influence of thermal treatment conditions on porosity development and mechanical properties of activated carbon cloths from a novel nanofibre-made fabric. *Materials Chemistry and Physics* 116, 310-314.

Ramos, M.E, Bonelli, P.R., Cukierman, A.L., Ribeiro Carrott, M.M.L., Carrott, P.J.M. 2010. Adsorption of volatile organic compounds onto activated carbon cloths derived from a novel regenerated cellulosic precursor. *Journal of Hazardous Materials* 177, 175-182.

Rangel-Mendez J. R., Streat M. 2002. Adsorption of cadmium by activated carbon cloth: influence of surface oxidation and solution pH. *Water Research* 36, 1244-1252.

Reddy, N., Yang, Y. 2007. Preparation and characterization of long natural. cellulose fibers from wheat straw. *J. Agric. Food Chem*. 55, 8570-8575.

Rodríguez-Reinoso, F. 2002. Production and application of activated carbon. In *Handbook of Porous Solids,* Wiley - VCH, 1766-1827.

Rodríguez-Reinoso, F.; Pastor, A. C.; Marsh, H.; Martínez, M. A. 2000a. Preparation of activated cloth form viscous rayon. Part II: Physical activation process. *Carbon* 38, 379-395.

Rodríguez-Reinoso, F.; Pastor, A. C.; Marsh, H.; Huidobro, A. 2000b. Preparation of activated carbon cloth from viscous rayon. Part III. Effect of carbonization on CO_2 activation. *Carbon* 38, 397-406.

Rouquerol, F., Rouquerol, J., Sing, K., 1999. Properties of some novel adsorbents. In: *Adsorption by Powders and Porous Solids*, Academic Press, London UK. Chapter 12, 401-438.

Sandell, E. B. Colorimetric determination of traces of metals, 3rd ed. New York, Willey *Interscience*. 1959, 442.

Shao X., Wang W., Zhang X. 2007. Experimental measurements and computer simulation of methane adsorption on previous activated carbon fibers. *Carbon* 45, 188-195.

Shen W., Wang H., Guan R., Li Z. 2008. Surface modification of activated carbon fiber and its adsorption for vitamin B1 and folic acid. *Colloids and Surfaces A: Physicochemical and Engineering Aspects* 331, 263-267.

Sivakumar C., Nian J. N., Teng H. 2005. Poly (o-toluidine) for carbon fabric electrode modification to enhance the electrochemical capacitance and conductivity. *Journal of Power Sources* 144, 295-301.

Stoeckli H. F., Rebstein P., Ballerini L. 1990. On the assessment of microporosity in active carbons, a comparison of theoretical and experimental data. *Carbon* 28, 907-916.

Subrenat, A., Bellettre, J., Le Cloirec, P. 2003. 3-D numerical simulations of flows in a cylindrical pleated filter packed with activated carbon cloth. *Chem. Eng. Science* 58, 4965-4973.

Subrenat, A.; Le Cloirec, P. 2006. Volatile organic compound (VOC) removal by adsorption onto activated carbon fiber cloth and electrothermal desorption: an industrial application. *Chemical Engineering Communications* 193, 478-486.

Tien P. D., Satoh T., Miura M., Nomura M. 2008. Continuous hydrogen evolution from cyclohexanes over platinum catalysts supported on activated carbon fibers. *Fuel Processing Technology*. 89, 415-418.

Tsai J.-H., Chiang H.-M., Huang G.-Y., Chiang H.-L. 2008. Adsorption characteristics of acetone, choloform and acetonitrile on sludge-derived adsorbent, commecial granular activated carbon and activated carbon fibres. *Journal of Hazardous Materials* 154, 1183-1191.

Valente Nabais, J.M., Carrott, P.J.M., Ribeiro Carrott, M.M.L. 2005. From commercial textile fibres to activated carbon fibres: Chemical transformations. *Mater. Chem. Phys* 93, 100-108.

Vernersson T., Bonelli P. R., Cerrella E. G., Cukierman A. L. 2002. *Arundo* cane as a precursor for activated carbons preparation by phosphoric acid activation. *Bioresource Technol*. 83, 95-104.

Wu M., Zha Q., Qiu J., Guo Y., Shang H., Yuan A. 2004. Preparation and characterization of porous carbons from PAN-based preoxidized cloth by KOH activation. *Carbon* 42, 205-210.

Williams, P. T.; Reed, A. R. 2004. High grade activated carbon matting derived from the chemical activation and pyrolysis of natural fibre textile waste. *J. Anal. Appl. Pyrolysis* 71, 971-986.

Wu, M., Zha, Q., Qiu, J., Guo, Y., Shang H., Yuan, A. 2004. Preparation and characterization of porous carbons from PAN-based preoxidized cloth by KOH activation. *Carbon* 42, 205-210.

Xu D., Huang Z.-H., Kang F., Inagaki M., Ko T.-H. 2008. Effect of heat treatment on adsorption performance and photocatalytic activity of TiO_2-mounted activated carbon cloths. *Catal. Today* 139, 64–68.

Yao, M., Zhang, Q., Hand, D.W., Perram, D.L., Taylor, R. 2009. Investigation of the treatability of the primary indoor volatile organic compounds on activated carbon fiber cloths at typical indoor concentrations. *Journal of the Air and Waste Management Association* 59, 882-890.

You, S. Y.; Park, Y. H.; Park, C. R. 2000. Preparation and properties of activated carbon fabric from acrylic fabric waste. *Carbon* 38, 1453-1460.

Zhang S.-J., Feng H.-M., Wang J.-P., Yu H.-Q. 2008. Structure evolution and optimization in the fabrication of PVA-based activated carbon fibres. *J. Colloids Interface Sci*. 321, 96-102.

Zubizarreta L., Arenillas A., Pis J.J. 2009. Carbon materials for H_2 storage. *Int. Journal of Hydrogen Energy* 34, 4575-4581.

In: Activated Carbon
Editor: James F. Kwiatkowski
ISBN: 978-1-61209-684-1
©2012 Nova Science Publishers, Inc.

Chapter 18

SELF ASSEMBLED ORDERED MESOPOROUS CARBON: SYNTHESIS, CHARACTERIZATION AND APPLICATIONS

Dipendu Saha[1] and Shuguang Deng*[*2]
[1]Carbon Materials Group, Material Science and Technology Division,
Oak Ridge National Laboratory, TN, US
[2]Chemical Engineering Department, New Mexico State University
Las Cruces, NM, US

ABSTRACT

Controlled and ordered mesoporosity in carbon-based materials has gained a lots interests and applications in the present technology. Conventionally, ordered mesoporous carbon was nanocasted by doping a suitable inorganic scaffold or template (mostly silica) with an organic carbon precursor followed by carbonization at high temperature. Due to the presence of several associated drawbacks of the nanocasting method, different researchers attempted to insert mesoporosity in carbon based materials without employing any inorganic scaffold. In this so called "soft template" or self-assembly process, an organic block copolymer has been employed as a structure dictating agent and a phenol-formaldehyde type of resin as carbon source held together by hydrogen bonding or occasionally by with an external cross-linking agent. During carbonization, the resin converted to pure carbon where as the copolymer decomposes from the system leaving its contribution as the monitor of the structure of porosity in the resultant carbon. Pluronic P123, Pluronic F127 or polystyrene-*block*-ploy(4-vinylpyridine) are most common structure dictating copolymers where as phenol, resorcinol or phloroglucinol-formaldehyde resins are most widely used as a suitable source of carbon precursors. Literature value revels that these ordered mesoporous carbon possesses the BET specific surface area in the range of 280-1300 m^2/g based on the reagents and synthesis procedures. Depending on the processing and aging conditions, the morphology of OMC can be tuned within monolith, fiber or sheets in order to meet the specific demands of the applications.

* sdeng@nmsu.edu

1. INTRODUCTION

Porous carbon materials have received a great deal of interests in today's technology as it finds its widest applications in the numerous fields of gas adsorption and separation, catalysis support, water purification or electrical double layer capacitors which are few to mention [1-3]. Insertion of porosity in carbonaceous material itself was advantageous because of the several inherent properties of carbon including hydrophobicity and chemically inertness in nature, low density, high thermal and electrical conductivity, mechanical stability, bio-compatibility, chemical stability under non-oxidizing conditions, inexpensive and wide variety of precursors resulting in high surface area and large pore volume [4,5]. According to International union of pure and applied chemistry (IUPAC), the porous carbon materials can be divided in to three divisions based on their pore size; microporous (pore size < 20 Å), mesoporous (pore size within 20 to 500 Å) or macroporous (pore size > 500 Å). Figure 1 shows the range of pores in some common carbon materials. Ordered microporous and mesoporous carbon are the examples of almost perfectly shaped microporous and mesoporous carbon respectively. Most of the activated carbon materials and carbon nanotubes have the pore size distribution within micro and mesoporous region which are popularly called as bimodal pore size distribution. Quite similarly, carbon foam has the pore size distribution within mesoporous and macroporous regions.

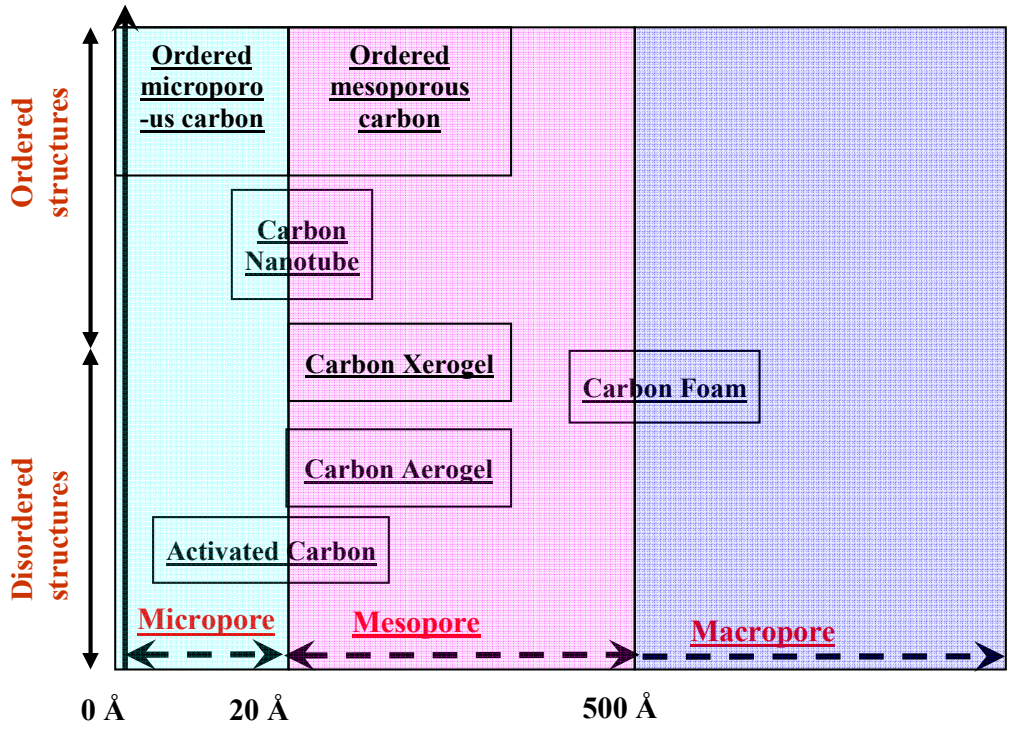


Figure 1. Different carbon structures with their pore sizes.

Traditionally, all the porous carbon synthesized was all disordered structures. Few traditionally employed porous carbon synthesis methods were mentioned below [1]

i. Physical activation, chemical activation or combination of both [6-10]
ii. Catalytic activation of carbon precursor by employing metallic salts or organometallic compounds [11-13]
iii. Carbonization of polymer blends consisting of carbonizable polymer or pyrolizable polymer [14-17]
iv. Carbonization of polymer aerogel synthesized supercritical drying conditions [18-20].

Despite the well-know synthesis process of disordered porous carbons, synthesis of ordered porous carbon was quite challenging from the very early period. Over the past decades, inorganic and engineering designed hard templates came to the research field to fabricate the ordered pores within the carbon structures [1]. Within few years, along with the micropores, there are some growing interests observed in the research fields of mesoporous carbon owing to its typical applications in several technological sectors. Despite the ubiquitous presence of mesoporosity in different kinds of carbon including activated carbon, carbon Aerogel or xerogel, the insertion of ordered mesoporosity also remained quite intriguing to the researchers. In the 1986, the Knox et al. [21] established the first step towards the fabrication of ordered carbon by employing an inorganic mold or template. Several years later, in 1999, Ryoo et al. [22] demonstrated that ordered mesoporosity in the carbon materials can successfully imparted by utilizing a silica mold, more commonly known as 'hard template' with sucrose as the carbon precursor; where the resultant carbon becomes the structural 'negative' of the template mold [23].

There are three strategic steps towards the formation of OMC by hard template method [1]; (i) the fabrication of the hard template like silica/surfactant composites, (ii) removal of surfactant by calcination or solvent extraction (iii) Generation of catalytic sites on the inner wall of mesostructures for polymerization of carbon precursor (iv) doping a suitable carbon precursor on the hard template (v) polymerization of carbon precursor (vi) carbonization of precursor and (vii) leaching of the hard template to achieve the pure OMC. After this pioneering step of synthesizing ordered carbon structure, numerous research works were published with similar technique by varying the template mold, carbon precursor or even the carbonization conditions. A wide spectrum of carbon precursors, including phenol-formaldehyde [24-28], resorcinol-formaldehyde [29-33], acetonitrile [34], polypyrol [35], furfuryl alcohol [36-39], ethylene [40], propylene [24], petroleum pitch [41-43] and several aromatic precursors [44,45] were employed to synthesize ordered mesoporosity in the carbon along with mesoporous silica and aluminosilica [46-47], colloidal particles [48-53] or colloidal crystals [24,33] as the hard templates. Tuning of external of morphology of carbon were also observed in the literature, including powders, films, membranes, spheres, rods, cubes, tetrapods, fibers, nanowires or monoliths [39,24, 42,34, 54-57].

There are several drawbacks of synthesizing ordered mesoporous carbons by hard templating methods. The entire procedure is definitely extremely tedious involving several number of steps and lengths of time that makes this process difficult to commercialize. It involves the usage some toxic chemicals, like hydrofluoric acid which makes this process even more sensitive and safety concerned to be implemented in to reality. The other drawbacks of synthesizing ordered mesoporous carbons are possibility of structural collapse during graphitization, difficulty in making monolithic structures and absence of any real pores. The alternating method of synthesizing ordered mesoporous carbon is by employing a

suitable surfactant as organic template and a carbon precursor held together by hydrogen bonds. Under carbonization, the carbon precursor converts to carbon skeleton where as removal of surfactant gives rise ordered mesostructured pores.

2. SYNTHESIS

The original concept of synthesizing self-assembled porous structures came from the solvent evaporation induced self-assembly method (EISA) [58-78] in which highly ordered mesoprous polymers were synthesized by employing amphiphilic triblock copolymers as organic templates and resol (phenol-formaldehyde resin) as the precursor. The general principle of synthesis ordered mesoporous carbon is quite similar to that of EISA; the cross-linking of thermosetting polymeric resins within the presence of some nonionic surfactants, typically, amphiphilic block copolymers with the help of hydrogen bonding followed by removal of copolymer and subsequent carbonization. The key role of the block copolymer is to dictate the ordered structure of resins or carbon after the carbonization step which is very similar to that of silica or zeolites for the hard template based carbons. These block co-polymers tunes the fine control of the porosity in terms of pore size and distribution by the self assembly of varieties of structures as a consequence of repulsive interactions between the covalently bonded blocks [79], typically in the form of spherical, cylindrical, lamellar or gyroidal structures [80-82]. These block copolymers can be removed thermally at a moderate temperature leaving behind the thermosetting resins that can be pyrolized to give ordered mesostructured carbon.

The self assembled micelles that form with the polymer molecules in a solvent provides basis of organic or soft template of the porous polymer or carbon due to which polymer based soft template method is also referred to as “micelles templating” [83]. The types of triblock or diblock type of copolymers ([A]-[B] or [A]-[B]-[C] type) that are employed to synthesize ordered mesoporous carbon are not widely varied as observed in the literature. Pluronic F127 is one type of triblock copolymer that was used quite frequently in order to create the ordered mesostructures [84-86]. Patented and sold by BASF, Pluronic F127 has the molecular formula of $[(PEO)_{106}(PPO)_{70}(PEO)_{106}]$ with average molecular weight 12600, where as PEO and PPO stands for polyethylene oxide and polypropylene oxide respectively. Pluronic P123 is another type triblock copolymer sold by BASF and used by few researchers to synthesis ordered mesoporous carbon [85, 87, 88]. It has the molecular formula $[(PEO)_{20}(PPO)_{70}(PEO)_{20}]$ and average molecular weight 5750. Two other low molecular weight triblock copolymers Pluronic 17R4 $[(PPO)_{19}(PEO)_{33}(PPO)_{19}]$, average molecular weight 2650 and Pluronic 25R4 $[(PPO)_{14}(PEO)_{23}(PPO)_{14}]$ were also employed as a soft template to synthesis ordered porous polymer [83], however, the identity of the resultant porous carbon structure was not reported. Pluronic F108 $[(PPO)_{132}(PEO)_{50}(PPO)_{132}]$, M_W=14600 was incorporated as surfactant in some of mesostructure synthesis. All of these triblock nonionic surfactants are composed of hydrophilic polyethylene oxide group(s) terminated by hydrophobic polypropylene oxide group(s) that help to form the micelles in the organic phase. Amongst the diblock copolymers, spolystyrene-*block*-poly-4-vinylpyridene (PS-*block*-P4VP, average molecular weights: $M_{n,PS}$=40,000, $M_{n,P4VP}$=5600) which was originally employed to generate hierarchical structures, was also employed by Kosonen et al

[79] and Liang et al. [86] as the organic template to generate ordered mesostructure in carbon. Cetyltrimethylammonium bromide (Figure 2) (CTAB) is the only surfactant that is not a block copolymer but employed to synthesize ordered tunable mesostructured carbon by Lee et al. [89].

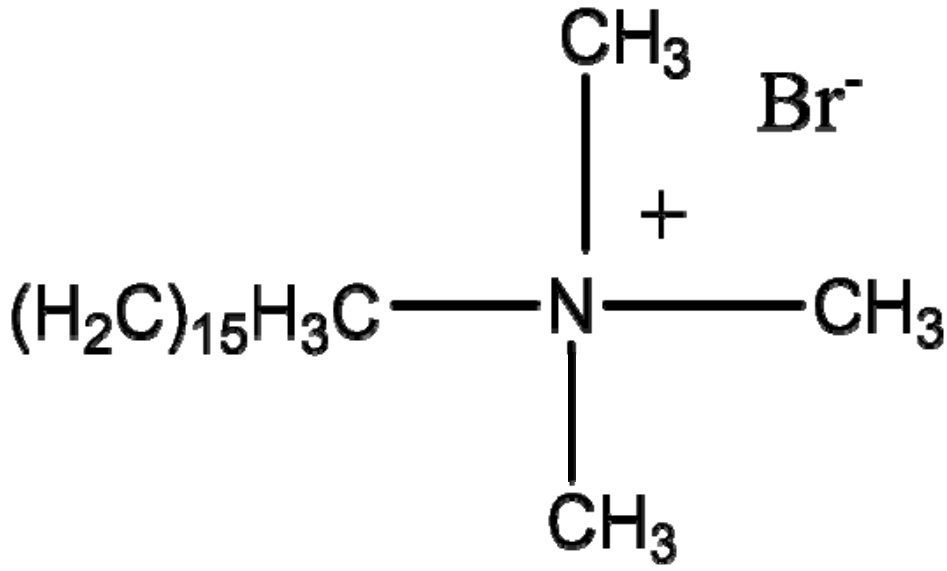


Figure 2. Cetyltrimethylammonium bromide (CTAB).

The carbon precursors that are employed to synthesize the ordered mesostructured polymer or the carbon are phenolic type of resins, typically formed by the condensation reactions between phenolic compounds and formaldehyde. The key reason for incorporating phenolic resins is that there forms a very strong hydrogen bond between hydrogen atom of hydroxyl group of phenolic compound and oxygen atom of the surfactants (block copolymers) or nitrogen atom in the case of PS-block-P4VP copolymer (Figure 3) thus helping to the build the fundamental basis of self assembly. It is observed that this hydrogen bond is quite strong to preserve the self-assembly during the curing of the polymer or during the carbonization. The resins that were successfully used as the carbon precursor during the self assembly are phenol, resorcinol and phloroglucinol along with formaldehyde as co-component of the polymerized structure (Figure 4(a), (b) and (c)). Generally, it is observed that with the increase in hydroxyl group density in the phenolic compounds (phenol → resorcinol → phloroglucinol), the time of polymerization becomes shorter. It was observed that for phenols, the polymerization took place two to three weeks at ambient temperature; the time was shortened to one week to few days for resorcinol. In the case of phloroglucinol, the polymerization was amazingly shrunk to 40 minutes to few hours under the same conditions. The another impact of increasing the number of hydroxyl groups is that stronger hydrogen bonds are formed between precursor and structure dictating agent thereby enhancing the basic driving forces of self-assembly. An example of hydrogen bonding between the surfactant (pluronic) and organic precursor (phenol-formaldehyde) is shown in figure 5. Jang et al. [83] employed polyacrylonitrile (PAN) as a carbon precursor; however, the authors did not proceed to the further step to pyrolize the mesoporous polymer to generate carbon structures.

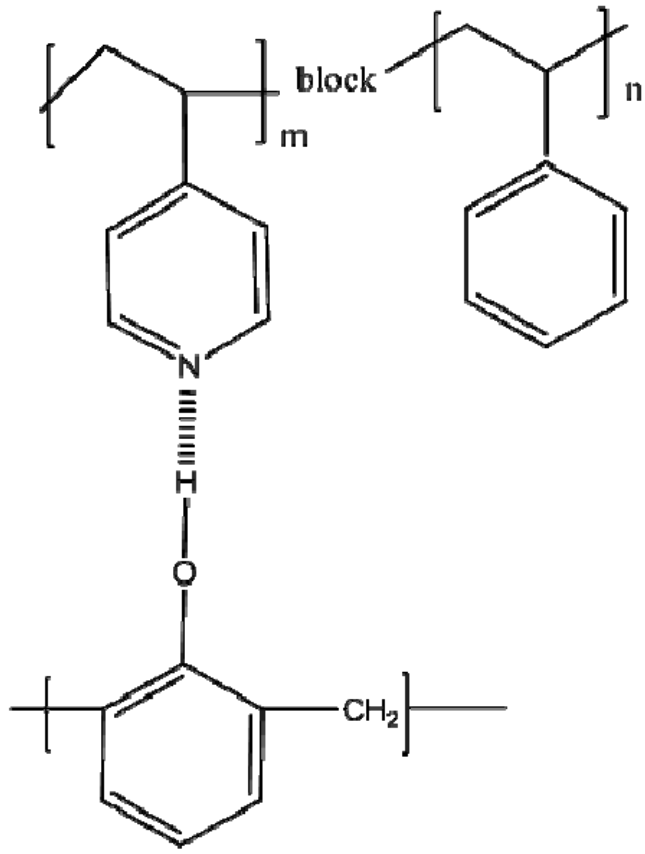


Figure 3. Polystyrene-*block*-poly-4-vinylpyridene (PS-*block*-P4VP) hydrogen bonded with precursor.

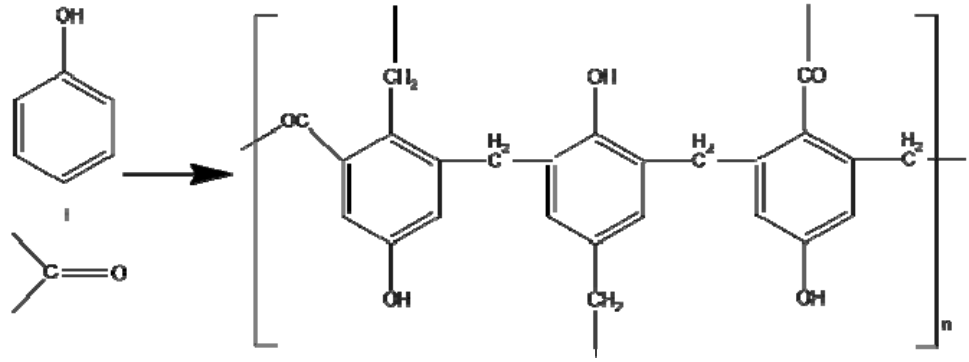


Figure 4(a). Phenol-formaldehyde resin.

The processing conditions including polymerization, curing or carbonization is quite well varied in the different author's work. The condensation between phenolic compounds and formaldehyde takes place in the presence of acid (HCl) or base (NaOH or Na_2CO_3) as the catalyst. For most of the cases, the polymerization reaction between the phenolic compound and formaldehyde takes place without external cross-linking agent, however, on rare occasions, the authors employed external cross-linking agent, hexamethenetetramine

(HMTA) to facilitate the phenol-formaldehyde condensation reaction [79]. Tanaka et al. [84] employed tryethylorthoacetate during the polymerization reaction; the exact role of this substance is not mentioned explicitly, however, they believe it probably provided a favorable condition to maintain the periodic mesostructure. Jang et al. [83] employed azobisbutylonitrile (AIBN) as an initiator to polymerize the acrylonitrile the presence of surfactant. The solvent to dissolve the constituents also observed to vary in different reports; these are N,N-dimethylformamide (DMF), tetrahydrofuran (THF), N-methyl pyrrolidone (NMP), ethanol, water or ethanol-water mixture. The carbonization conditions also seem to vary from 420°C to 900°C for different initial constituents and processing conditions. The synthesis parameters are summarized in short in table 1.

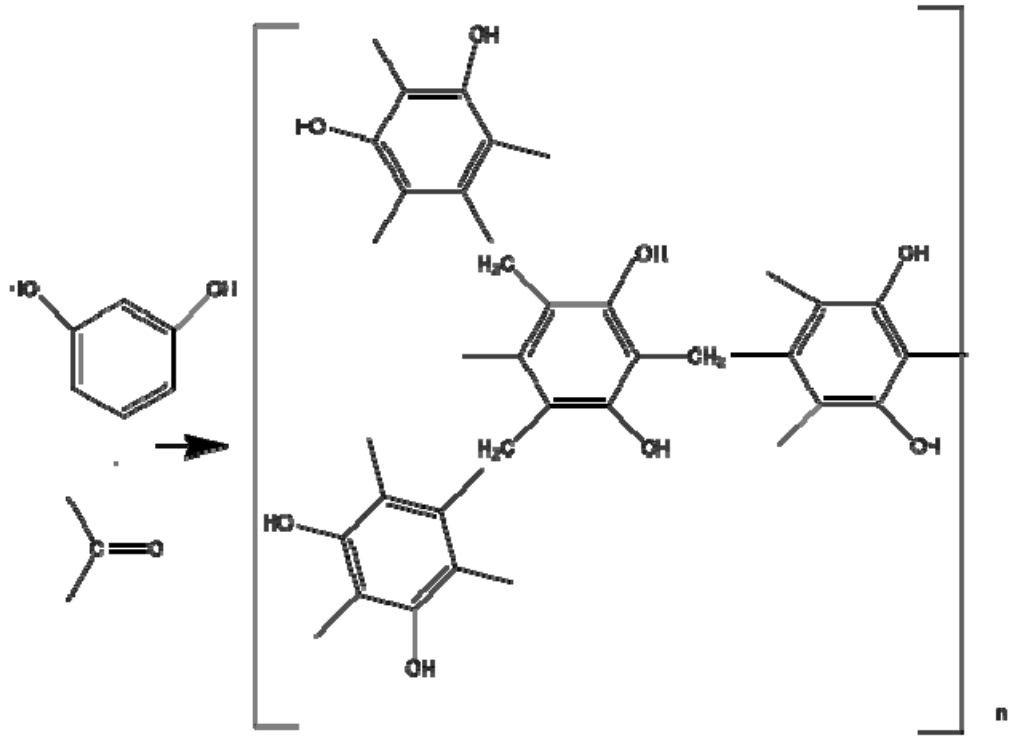


Figure 4(b). Resorcinol-formaldehyde resin.

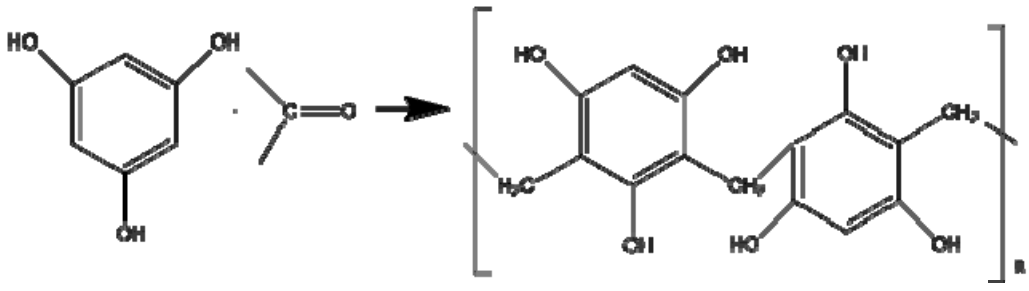


Figure 4(c). Resorcinol-formaldehyde resin.

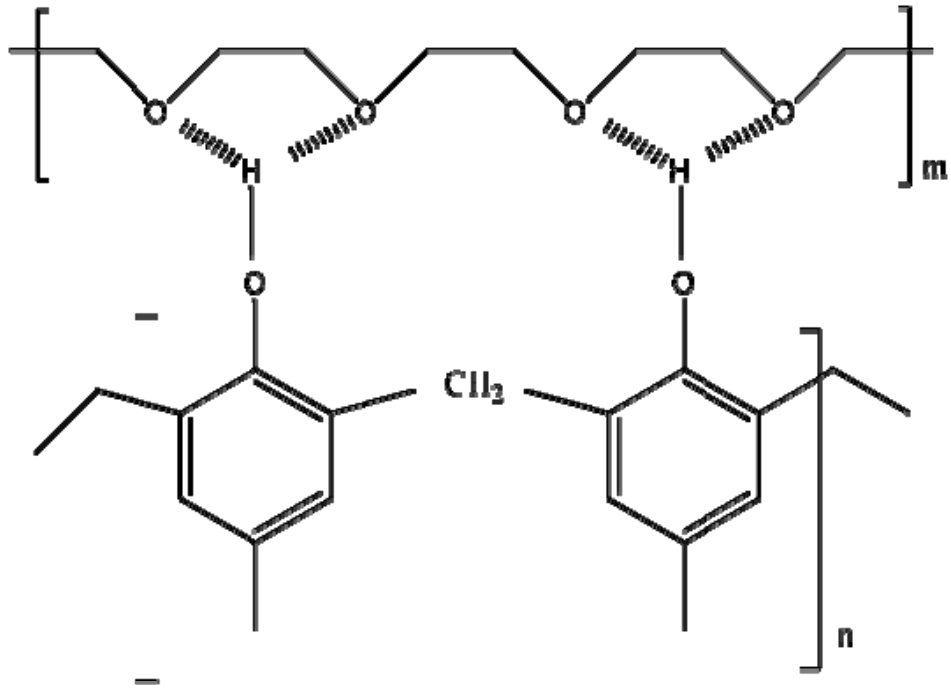


Figure 5. Self-Assembly of phenol-formaldehyde resin with block copolymer.

Table 1.

Polymer precursor	Surfactant type	Molar stoichiometry
Hexagonal FDU-15	Pluronic F127 or P123	Phenol/formaldehyde/NaOH/F127: 1:2:0.1:0.01-0.015 Phenol/formaldehyde/NaOH/P123: 1:2:0.1: 0.007-0.016
Cubic FDU-16 ($Im\bar{3}n$ symmetry)	Pluronic F127 or F108	Phenol/formaldehyde/NaOH/F127: 1:2:0.1:0.003-0.008 Phenol/formaldehyde/NaOH/F108: 1:2:0.1:0.005-0.010
Cubic FDU-16 ($Ia\bar{3}d$ symmetry)	Pluronic P123	Phenol/formaldehyde/NaOH/P123: 1:2:0.1:0.0.018-0.019
Lamellar mesostructure	Pluronic P123	Phenol/formaldehyde/NaOH/P123: 1:2:0.1:0.0.022-0.027

In another work, Meng et al. [65], reported a thorough methodology of reproducible synthesis of a series of highly ordered mesostructured carbon by varying the ratio of carbon precursor (resol) and surfactant (F127, F108 or P123) at the time of synthesis. They observed that adding small amount of oxygen during carbonization increases the specific surface area probably caused by the local activation. They also demonstrated a new method of sulfuric acid aided extraction to remove surfactant from as-synthesized polymers. Table 2 shows the variation of synthesis parameters to achieve different geometrical symmetries in ordered mesoporous polymer precursor and Figure 6 shows the phase diagram as-synthesized initial polymers with surfactant ratio.

Table 2.

Surfactant	Precursor	Solvent	Curing/ Crosslinking Agent	Curing/ polymerization Conditions	Carbonization Conditions	Species (Carbon) Name	Reference
polystyrene-*block*-poly-4-vinylpyridene (PS-*block*-P4VP)	Phenol-formaldehyde resin	THF	HMTA	100°C/2 hour, 150°C/2hour, 190°C/2 hour	420°C with 1°C/minute ramp rate	None	[22]
Pluronic F127	Resorcinol-Formaldehyde resin	Ethanol + Water	TEOA	90°C for 5 hour	400°C for 3 hours with ramp rate 1°C/min followed by 300 and 600°C for 3 hours.	COU-1	[27]
Pluronic F127 Pluronic P123	Phenol-formaldehyde resin	Ethanol	None	100°C for 24 hours	700-1400°C/5 hours with 1°C/min ramp rate, held at 200, 350, 500°C for 2 hours.	C-FDU-15(a) C-FDU-16(b)	[28]
Pluronic P123	Phenol-formaldehyde resin	Water	None	64°C for 120 hours and 72°C for 42 hours.	700°C for two hours with ramp rate 1.5°C/min	C-FDU-15	[30]
Pluronic F127	Phloroglucinol-formaldehyde resin	Ethanol +Water	None	None	100°C to 400°C 5°C/min, 400°C-850°C for 5°C/min, held at 850°C for 2 hours.	None	[29]
Polystyrene-*block*-poly-4-vinylpyridene (PS-*block*-P4VP)	Resorcinol-formaldehyde	DMF	None	100°C for 4 hours.	800°C by 1°C/min	None	[31]
Pluronic 17R4 and Pluronic 25R4	Polyacrylonitrile (PAN)	NMP	AIBN	110°C/24 hours	Not carbonized	None	[26]
CTAB	Resorcinol-formaldehyde resin	Water	None	None	1000°C for 3 hours	None	[32]

THF: Tetrahydrofuran
HTMA: hexamethenetetramine
TEOA: tryethylorthoacetate
DMF: N,N dimethylformamide
NMP: N-methyl pyrrolidone
AIBN: azobisbutylonitrile
CTAB: Cetyltrimethylammonium bromide

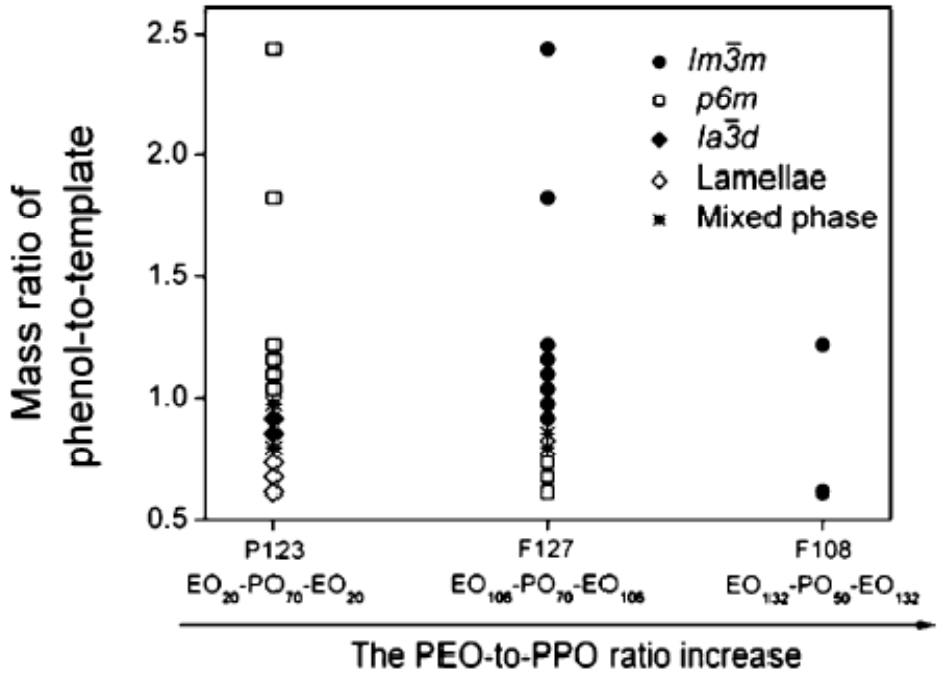


Figure 6. Phase diagram as-synthesized initial polymers with surfactant ratio, reproduced from the publication of Meng et al. [65] with permission from American Chemical Society, 2006.

Generally, the external morphology of mesostructured carbon phase was not deliberately varied in most of the research reports. However, Dai et al. [86] engineered the ordered mesoporous carbon in the form of monolith, fiber or film by altering processing conditions of the precursor polymer before subjecting to carbonization. For monolith, initial polymer was stirred overnight followed by curing at 100°C, also overnight. In order to prepare carbon fibers, the polymer solution was separated by centrifuge followed by charging to fiber drawing machine and passing the extruder. The carbon films were obtained by spin coating the polymer on a substrate followed by curing at 100°C overnight.

The similar research group synthesized different other morphological materials based on ordered mesoporous carbon, including carbon membrane [90], mesoporous nicro and nanowires [91] graphitic mesoporous fuel cell support [92]. Despite the fact that microporous gas separating membrane was quite extensively studied in literature, mesoporous membrane was quite limited in literature [93-94]. In the previous work, Hou et al. [95] inserted the ethanolic solution of F127/phloroglucinol/formaldehyde on the membrane substrate via tape-casting technique followed by drying and curing at room temperature and 80°C respectively. Carbonization of the parent polymer was performed in 400°C for 2 hours with ramp rate 1°C/minute followed by reheating at 850°C for another two hours with 5°C/min. In following years, the same research group made another attempt to synthesize gas separating mesoporous carbon membrane, but incorporating a cross-linking agent, HMTA to the system in the ratio of 1.2 wt.% in order to prevent the cracking in the membrane structure. In a typical synthesis procedure of mesoporous carbon based membrane, phlorolucinol-formaldehyde-F127 system was dissolved in an acidic ethanol solution containing 1.2 wt.% HMTA. Upon removing the

air-bubble from the mixture, it is loaded on the hydrophilic Myler via tape-casting method resulting in a thin film of parent polymer on the substrate. The film was first cured at room temperature overnight and then at 80°C for 24 hours to complete cross-linking. After that it is separated from the substrate, it is cut to the desired sizes and carbonized by putting the piece within two pieces carbon paper and sandwiched between quartz strips in order to maintain the flat-sheet morphology. The width of membrane is around 42 μm.

In order to synthesize the graphitic mesoporous carbon based fuel cell support, the parent polymer was fabricated in the similar fashion from pluronic F 127/phloroglucinol/ formaldehyde system with acid catalyst. After polymer is separated from the ethanol-water system, it is cast as a thin film on the 15 cm diameter petri dish and carbonized under flow 850°C with 1°C/min ramp rate and keeping at 850°C for 2 hours. After carbonization, the sample was graphitized heating at 2600°C for one hour under helium flow. The graphitized sample contains the core width around 9 nm.

Rodriguez et al. reported tubular mesoporous carbon structure by incorporation of block copolymer/carbohydrate mixture on to the porous alumina [96]. Yu et al. [97] reported the synthesis of disordered mesoporous carbon nanorod by the usage of sacrificial silica templates. Cott et al. [98] successfully synthesized mesoporous carbon nanowires by inserting xylene/CO_2 mixture by supercritical deposition within iron-containing mesoporous silica inside porous alumina followed by template removal by etching with hydrofluoric acid. Steinhart et al. [91] reported the a direct template based synthesis of hybrid membranes containing mesoporous carbon inside porous alumina matrix by incorporation solvent free precursor mixture within alumina support that avoiding the macroscopic phase separation and hydrodynamic instability during solvent evaporation. After polymer solution synthesized from phloroglucinol/F127/formaldehyde system (as described earlier) gets phase separated from solvent, it is isolated from the mixture by centrifuge, air-dried and spread on to the self-ordered porous alumina with pore diameter of 400 and 60 nm which results in infiltration of the pores by the viscous polymer. The resultant substance is carbonized at 500°C where porous alumina matrix retains its entity and the carbon naowires receive high aspect ratio and defect free structure. Absence of solvent also provides a great help to minimize the inevitable shrinkage during the carbonization procedures.

Metal-doping on ordered mesostructured carbons synthesized by self-assembly approach was demonstrated by Shanahan et al. [92] and Saha and Deng [99]. Shanahan et al. used *ex-situ* approach in which the OMC sample was infiltrated with chloroplatinic acid (H_2PtCl_6)/acetone solution by ultrasonication followed by reduction of precursor at 150°C under H_2 flow. Saha and Deng employed in-situ approach where acetylacetonates of Pd. Pt, Ni and Ru were dissolved in to the initial precursor solution that gave rise to the corresponding metal nano-particles under heat flow at the same time when the precursors are subjected to carbonization.

3. CHARACTERIZATION

The pore texture of ordered mesostructured carbon varied quite widely with carbon precursors, organic templates and processing conditions. In general, the polymers that generated by the condensation between mostly phenolic resins and formaldehyde did not

show any measurable porosity or quite poor level porosity if there is no structure dictating organic templates were employed. This observation quite well establishes the importance of templates in creating the porosity. When the micelles form hydrogen bonding with carbon precursor and self assemble within the solvent to the generated polymers, mesoporosity was generated within the structure. However, in most of the self assembled polymers, the porosity could not be detected until the template is removed from the structure as it may block the pore space. Removal of template with careful heat treatment opens up the pore space and thus be detected by the gas adsorption of microscopic imaging techniques. Due to the very typical micelles distribution within the solvent, the pores are of typical mesoporous in nature (2- 50 nm). However, in several ordered mesoporous carbon materials, a very narrow distribution of micropores is also observed that are generated by carbonization of the precursor itself and thus generated on the mesopore wall of the resultant carbon matrix. Some conventional activation technique, like CO_2 or alkali activation may also generate micropores within the mesostructured carbon. The generation of pores is schematically described in Figure 7.

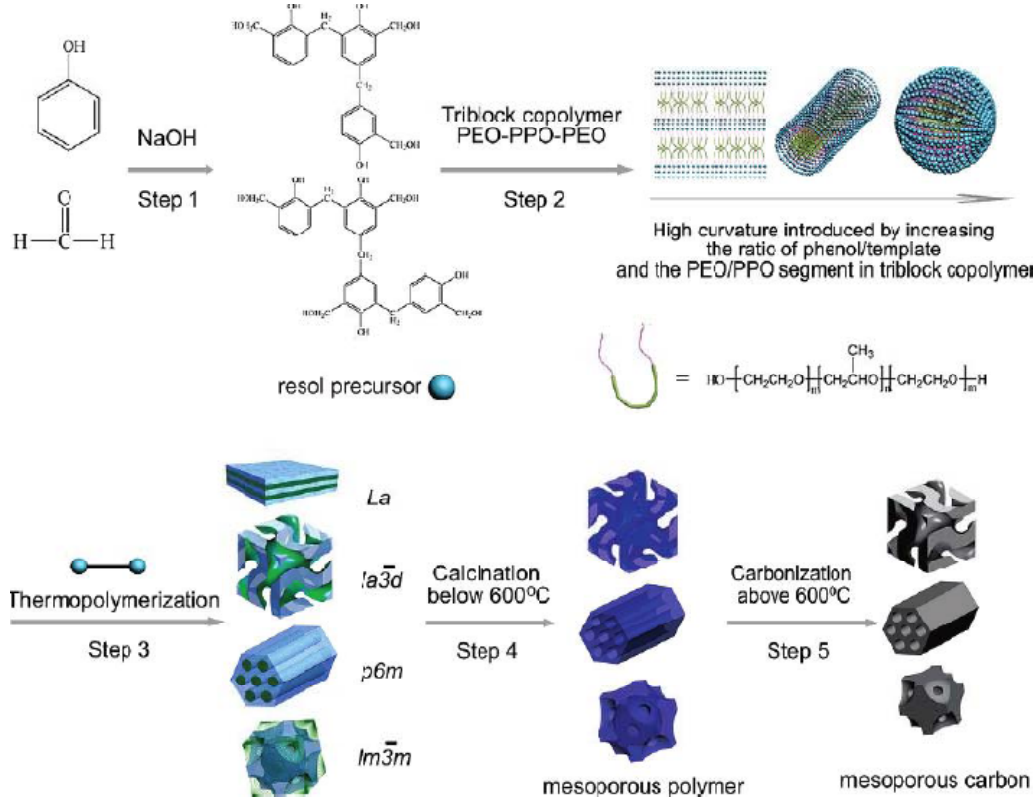


Figure 7. Different stages of ordered mesoporous carbon synthesis by self-assembly. Reproduced from the publication of Meng *et al.* [65] with permission from American Chemical Society, 2006.

Due to the presence of mesopores, all OMCs exhibit type-IV isotherm (according to IUPAC classifications) with hysteresis loop in the nitrogen adsorption-desorption plot during pore texture analysis. In the nitrogen adsorption desorption plot of F127/phloroglucinol/ formaldehyde OMCs by Liang and Dai [86], highest nitrogen adsorption was performed by phloroglucinol based OMC followed by fiber, film and resorcinol based monolith. Despite the

less periodic structure in monolith, it demonstrated more N_2 adsorption but less Bet surface area. The pore width and pore volume of the mesoporous carbon were most commonly measured by Barrent-Joyner-Halenda (BJH) method, however, Zhang et al. [87] employed Kruck-Jaroniec-Sayari model [100] to estimate the porosity. The BET specific surface area membranes synthesized by ordered mesoporous carbons appeared to be much less than the bulk carbon. In the work of Hou et al. [95], the BET surface area was 332.1 m^2/g with a mesoporous range of 5-9 nm. In another work published by same research group for HMTA induced crack-free mesoporous membrane, BET surface area varied between 429 and 334 m^2/g for thick (42 μm) and thin (18 μm) membranes with mesopore widths of 6.4 and 5.7 nm. The same surface area decreased from 420 m^2/g to 190 m^2/g when mesoporous carbon based fuel cell catalysis support was graphitized at an elevated temperature of 2600°C. The lowering of specific surface area and pore volume were also observed in the Saha and Deng [99] where OMC was doped with Pd, Pt, Ni and Ru nanoparticles, which was attributed to the coverage of available pores by metal nanoparticles. The nitrogen adsorption-desorption plots of pure and metal-doped OMCs were shown in Figure 8. The pore width and pore volume of different species of ordered mesoporous carbon are reported in Table 3.

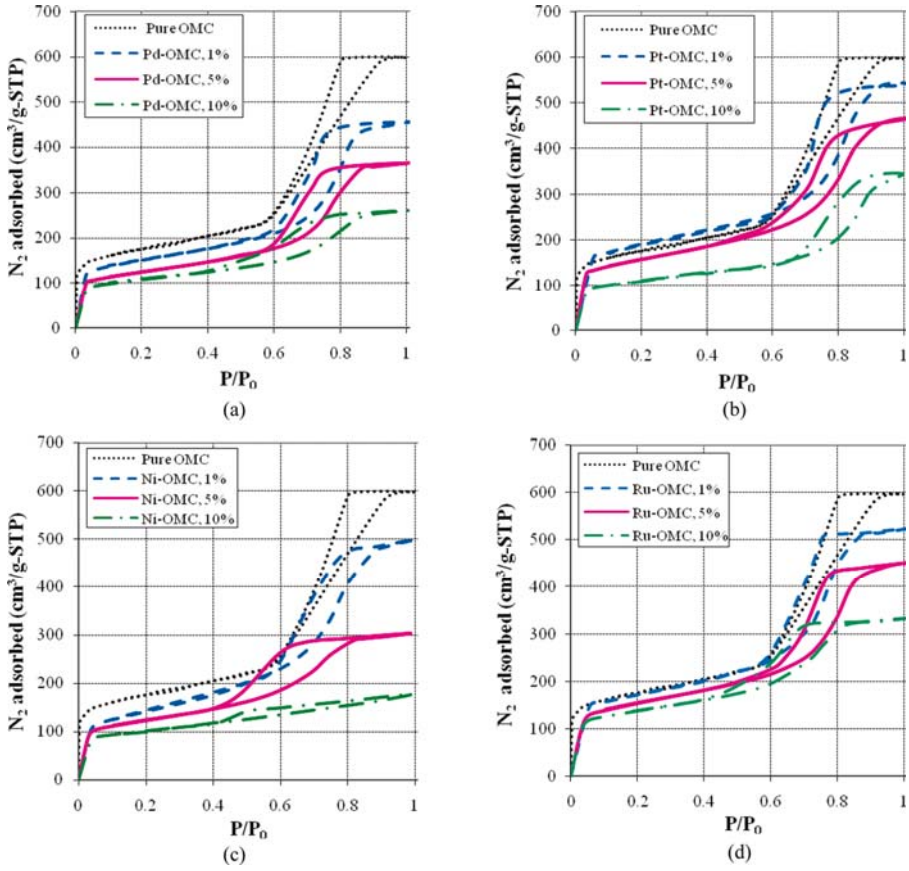


Figure 8. Nitrogen adsorption-desorption isotherms on pure and metal-doped ordered mesoporous carbons at 77 K. (a) Pd-dopedOMC; (b) Pt-doped OMC; (c) Ni-doped OMC; (d) Ru-doped OMC. Reproduced from the publication of Saha and Deng [99] with permission from American Chemical Society, 2009.

Table 3.

Sample name	Unit cell parameter a[a] (nm)	BET surface area[b] (m^2/g)	Micropore area[c] (m^2/g)	Pore size[d] (nm)	Pore volume (cm^3/g)	Wall thickness (nm)[c]	Molar ratio of C:H:O
As-made FDU-16	19.0 (18.4)	-	-	-	-	-	
FDU-16-350N	16.9 (16.2)	460	230	6.6	0.34	8.0	
FDU-16-400N	16.1 (15.3)	670	370	6.1	0.47	7.8	4.4:2.7:1
FDU-16-500	14.6 (14.0)	660	360	4.9	0.42	7.7	
FDU-16-600	13.9 (13.4)	580	400	4.3	0.36	7.7	8.3:2:1
FDU-16-600N	14.5 (14.3)	690	420	4.9	0.44	7.6	
FDU-16-700	13.0 (12.4)	690	480	3.8	0.37	7.5	
FDU-16-800	13.0 (12.5)	820	510	3.8	0.47	7.5	8.6:2:1
FDU-16-800N	13.1 (12.9)	760	510	3.8	0.43	7.5	
FDU-16-900	12.9 (12.4)	740	510	3.8	0.41	7.4	
FDU-16-1200	12.7 (12.3)	990	670	3.8	0.54	7.2	15.4:2:1
FDU-16-1200N	12.8 (12.4)	1490	720	3.8	0.85	7.3	
FDU-16-1400	12.6 (12.1)	990	660	3.5	0.54	7.4	
As-made FDU-16 (F108)	19.0 (17.8)						
FDU-16-600 (F108)	12.2 (12.2)	610		2.8	0.32	7.8	
As-made FDU-15	15.9 (15.4)						
FDU-15-350	13.1 (13.2)	430	120	5.4	0.40	7.7	7.0:5.4:1
FDU-15-350N	14.0 (13.5)	640	240	7.1	0.65	6.9	
FDU-15-400	12.2 (11.5)	510	180	4.9	0.41	7.3	
FDU-15-400N	13.4 (12.1)	630	290	6.6	0.59	6.8	
FDU-15-500	11.1 (10.5)	670	340	3.8	0.42	7.3	
FDU-15-600	10.4 (10.1)	590	300	3.1	0.34	7.3	8.2:2.9:1
FDU-15-600N	11.2 (11.1)	750	380	4.9	0.55	6.3	
FDU-15-700	10.0 (9.6)	750	430	3.1	0.42	6.9	
FDU-15-800	9.9 (9.4)	720	410	3.1	0.40	6.8	12.3:2.4:1
FDU-15-800N	10.6 (10.0)	900	510	4.3	0.66	6.3	
FDU-15-900	9. (9.4)	650	360	3.1	0.37	6.6	
FDU-15-1200	9.8 (9.7)	730	430	2.8	0.42	7.0	16.6:1.7:1
FDU-15-1200N	9.8 (9.5)	1060	590	3.1	0.59	6.7	
FDU-15-1400	10.1 (9.5)	690	440	2.8	0.61	7.3	
H2SO4 treated FDU-15	15.7 (15.0)	140	0	7.4	0.26	8.3	
As made FDU-15 (P123)	13.4 (13.4)						
FDU-15-800 (P123)	8.7 (8.7)	870	440	2.6	0.47	6.1	
As made FDU-14	30.0 (26.0)						
FDU-14-350	23.5 (22.8)	130	0	3.1	0.1	6.1	6.6:5.7:1
FDU-14-350N	24.0 (22.8)	280	64	3.9	0.23	5.8	
FDU-14-600	20.0 (18.4)	630	370	2.3	0.32	5.4	
FDU-14-800	20.0 (18.1)	690	470	2.0	0.34	5.5	

[a] Calculated from SAXS results; data in parentheses are calculated from XRD results. [b] Calculated by the BJH model from sorption data in a relative pressure range from 0.04 to 0.2. [c] Calculated by the *V-t* method. [d] Calculated by the BJH model from the adsorption branches of the isotherms. [e] Calculated by the formulas h) [$(\sqrt{3}/2)$](a - D), $h = a - D$, and h) (a/3.0919) - (D/2) for FDU-16, FDU-15, and FDU-14, respectively, where a represents the unit cell parameter and D represents the pore diameter determined by the BJH model. Reproduced from the publication of Meng et al. [65] with permission from American Chemical Society, 2006

The dependence of specific area with structure, stoichiometry and carbonization temperature is very prominent in the literature. As described by several researchers, lamellar structure exhibits lowest surface area probably due to the partial collapse of the adjacent wall of the consecutive pores. The effect of carbonization temperature on specific surface area is quite prominent in the work of Tanaka et al. [84]; BET surface area increased from 624 to 1354 m^2/g with increase in temperature from 400 to 800^oC, though surface area became constant after 600^oC, suggesting the completion of carbonization at that temperature. Variation of specific surface area with the surfactant concentration is quite explicit in the work of Jhang and Bae [83], although they did not polymerize the resultant precursor to achieve mesostructured carbon. In the second work of Meng et al. [65], a series of ordered mesostructured carbon was synthesized by EISF strategy with the help of varying initial constituents and carbonization conditions. The pore textural properties along with the unit cell parameters and elemental (C,H and O) ratios of these OMCs are revealed in details Table 2.

The structural geometry of ordered mesoporous carbon strongly depends on the stoichiometry of the initial ingredients and the processing environments, including curing and carbonization conditions. The structural geometry can be revealed by small angle x-ray scattering (SAXS), x-ray diffraction (XRD) and electron microscopy which includes scanning electron microscopy (SEM) and transmission electron microscopy (TEM).

Amongst the mesoporous periodic solids, nanostructured silica materials were most popularly synthesized and characterized. The major structural homologues are 2D hexagonal ($P6m$) [101], 3D cubic or bicontinuous ($Ia\bar{3}d$, $\mathrm{Im}\bar{3}n$, $P\mathrm{m}\bar{3}n$) [102-104], 3-D hexagonal [$P6_3/mmc$) [103], tetragonal (P_4/mmm and $P4_2/mnm$ [102] and lamellar, though the distinct periodical structures cannot be found in lamellar frameworks. It was observed that F127 type of surfactant generally gives rise to hexagonal or cubic geometry where as P123 mostly provides lamellar type of structure. However, it is also argued that the distinct periodic structure within organic template based materials is not as frequent as that of inorganic one, most probably, the thermal instability generated from noncovalently bonded frameworks restricted the fine structures to be maintained in the final products [85]. C-FDU which was prepared from F127 surfactant and phenol-formaldehyde resin, showed well-resolved XRD peaks giving rise to hexagonal geometry similar to that of SBA-15 thereby suggesting that *p6m* geometry is reserved and mesostructure is thermally stable at nitrogen atmosphere. TEM imaging of C-FDU-15 also demonstrated well-ordered hexagonal arrays of mesopores with 1D channels. The cell parameter estimated from TEM imaging is around 11.5 nm which is in agreement with that of calculated from XRD patterns.

C-FDU-16 is the OMC generated after calcination of FDU-16 which is the polymer composed of pluronic P 123 and phenol-formaldehyde resin [85]. The XRD pattern of C-FDU-16 showed seven diffraction peaks that can indexed as the reflections from (110), (200), (211), (220), (310), (322) and (321) planes with space geometry of body centered cubic ($\mathrm{Im}\bar{3}m$). The lattice parameter is calculated as 16 nm with shrinkage of 11.6 % from the parent polymer. The TEM imaging also confirmed cubic ($\mathrm{Im}\bar{3}m$) mesostructure along with the cell parameter of 15.9 nm that is almost same that calculated from XRD data.

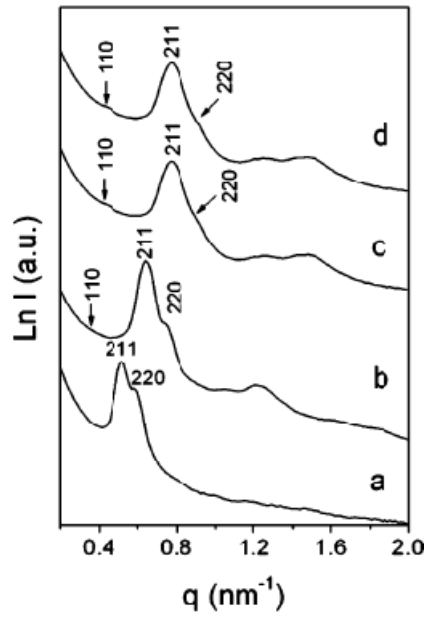


Figure 9 (a). SAXS patterns of the bicontinuous mesostructure FDU-14 prepared by using triblock copolymer P123 as a template via the EISA method: as-made FDU-14 (a) and those calcined at 350 °C under 2.4% O_2/ N_2 atmosphere (FDU-14-350N; b), at 600 °C under Ar (FDU-14-600; c), and at 800 °C under Ar (FD-14-800; d). Reproduced from the publication of Meng *et al.* [65] with permission from American Chemical Society, 2006.

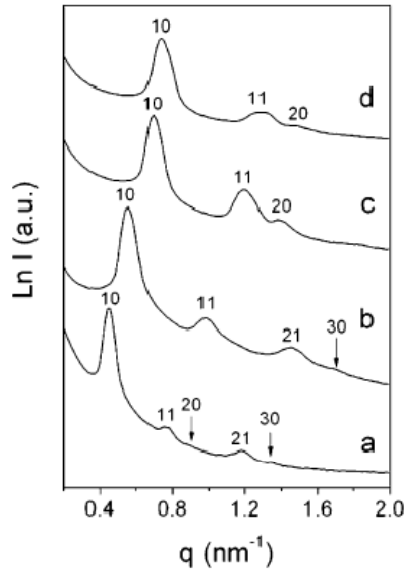


Figure 9 (b). SAXS patterns of mesoporous materials FDU-15 prepared by using F127 as a template via the EISA method: as-made FDU-15 (a), that calcined at 350 °C (FDU-15-350; b), that calcined at 600 °C (FDU-15-600; c), and that calcinced at 1200 °C (FDU-15-1200; d) under Ar. Reproduced from the publication of Meng *et al.* [65] with permission from American Chemical Society, 2006.

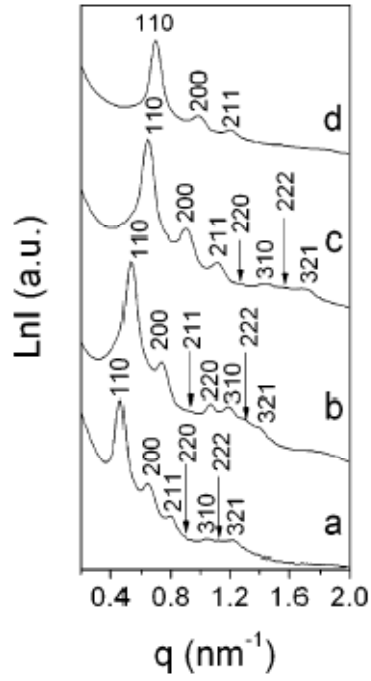


Figure 9(c). SAXS patterns of mesoporous materials FDU-16: as-made FDU- 16 (a), that calcined at 350 °C under 2.4%O2/N2 (FDU-16-350N; b), that calcined at 600 °C under Ar (FDU-16-600; c), and that calcinced at 1200 °C under Ar (FDU-16-1200; d). Reproduced from the publication of Meng *et al.* [65] with permission from American Chemical Society, 2006.

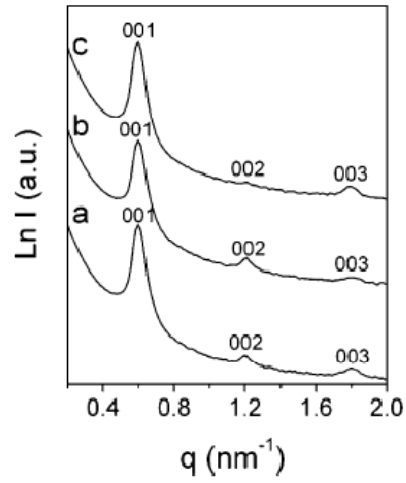


Figure 9(d). SAXS patterns of as-made lamellar mesostructure with P123/ phenol molar ratios of 0.022:1 (a), 0.025:1 (b), and 0.027:1 (c). Reproduced from the publication of Meng *et al.* [65] with permission from American Chemical Society, 2006.

Zhang et al. [87] reported the bicontinious cubic mesostructure of $Ia\bar{3}d$ symmetry of C-FDU-14 with resol as precursor and pluronic P 123 as structure dictating surfactant. After template removal, four distinct peaks of FDU-14, originated from (211), (220), (420) and

(332) reflections, give rise to $Ia\bar{3}d$ geometry which is also supported from SAXS data. A weak reflection from (110) could be indexed to $I4_132$ symmetry which can be attributed to the minor structural defect in the morphology. The lattice parameters of as-synthesized FDU-14, FDU-14 and C-FDU-14 can be calculated as 23, 19 and 15.4 nm respectively suggesting 17.4 % shrinkage after template removal and 18.9 % after carbonization. The TEM image of FDU-14 and C-FDU-14 also suggests the ordered structure with $Ia\bar{3}d$ symmetry.

Meng et al. [65] reproduced the different varieties of FDU-14, 15 and 16 by altering the weight ratios of carbon precursors (resol), triblock copolymers (pluronic F127, F108 and P123) and carbonization conditions. The SAXS patterns are shown in figure 9(a), (b), (c) and (d) where are as the TEM images are represented in figure 10(a), (b) and (c) respectively.

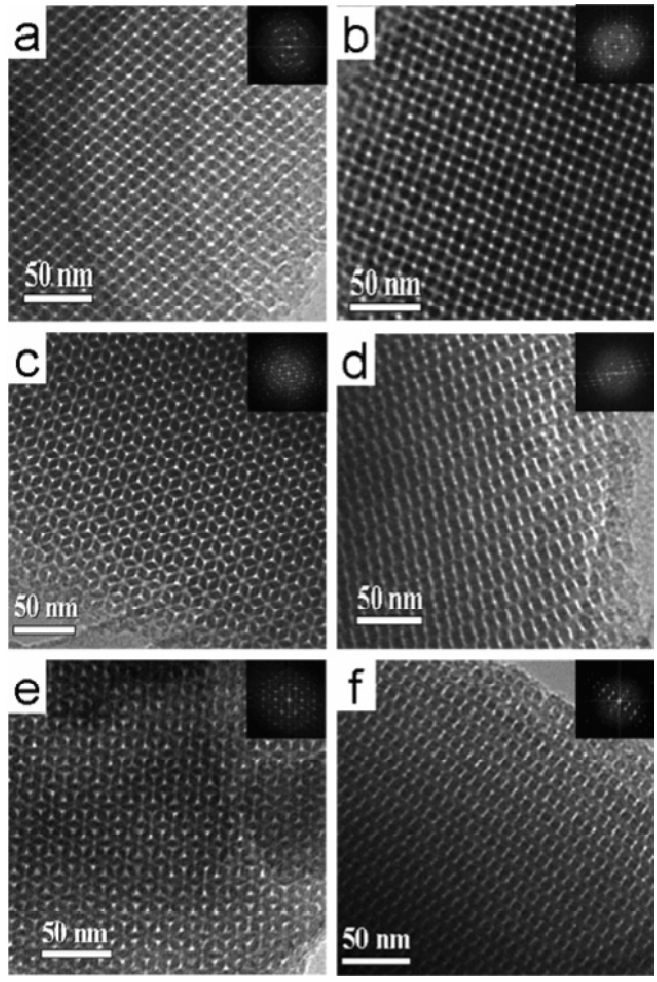


Figure 10 (a). TEM images of mesoporous materials FDU-14 prepared by using triblock copolymer P123 as a template via the EISA method: that calcined at 350 °C under N2 (FDU-14 350N; a-d) and calcined FDU-14 at 600 °C (e, f) under Ar (FDU-14-600), viewed along the [531] (a), [100] (b), [111] (c, e), and [311] (d, f) directions. The insets are the corresponding FFT diffractograms. Reproduced from the publication of Meng et al. [65] with permission from American Chemical Society, 2006.

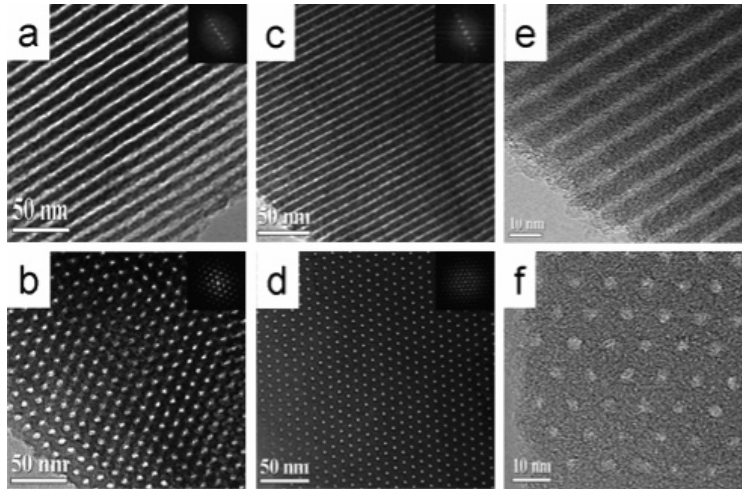


Figure 10(b).TEM images (a-d) and HRTEM images (e, f) of mesoporous materials FDU-15 prepared by using F127 as a template via the EISA method after calcination at 350 °C (FDU-15 350; a, b) and at 1200 °C (FDU-15-1200; c-f) under an Ar atmosphere, viewed from the [110] (a, c,e) and [001] (b, d, f) directions. The insets are the corresponding FFT diffractograms. Reproduced from the publication of Meng et al. [65] with permission from American Chemical Society, 2006.

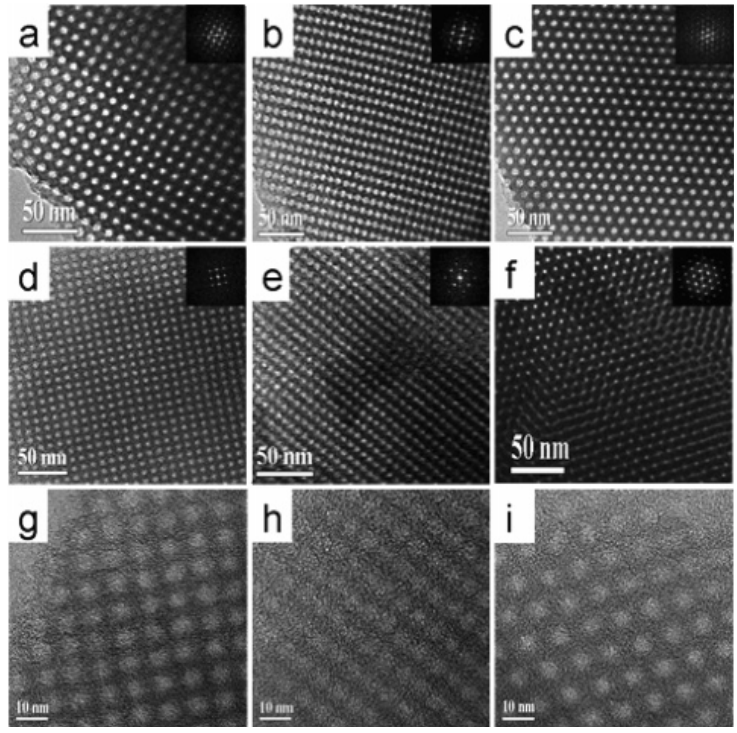


Figure 10 (c). TEM images (a-f) and HRTEM images (g-i) of mesoporous materials FDU-16 prepared by using F127 as a template via the EISA method after calcination at 350 °C under 2.4% O_2/N_2 (FDU-16-350N) (a-c) and at 1200 °C under Ar (FDU-16-1200; d-i), viewed along the [100] (a, d, g), [110] (b, e, h), and [111] (c, f, i) directions. The insets are the corresponding fast Fourier transform (FFT) diffractograms. Reproduced from the publication of Meng et al. [65] with permission from American Chemical Society, 2006.

The structural shift with the change in amphiphilic surfactant is quite explicit in the work of Kosonen et al.[79] the authors varied the concentration of PS-*block*-P4VP from 10 to 70% with 10% increment in every intermediate region and it was observed that four different structures were observed in the resultant species. At the surfactant concentration 20%, spherical morphology was obtained as observed in the TEM imaging. At the next stage of 30% concentration, worm-like structure was obtained with the periodicity of 50 nm. A cylindrical morphology was obtained at 40% surfactant concentration with periodicity and cylinder diameter of 50 nm and 30 nm respectively. The morphology was again changed to lamellar type at the higher concentration of 60%. It was argued that spherical matrix was most difficult to empty during the carbonization because the degraded the polymer residues found less room to escape from the closed matrix was most difficult to "microtome" for TEM imaging because of their extreme fragile nature. Despite well defined SAXS peaks in the polymers before carbonizations, most of the peaks disappeared after the operation, most probably caused by the increased local variations in periodicities when initial chemical bonds are broken and newer ones are formed during carbonization.

FE-SEM imaging provided a strong evidence of periodical mesostructure of ordered mesoporous carbon (COU-1) synthesized by Tanaka et al. [84] from resorcinol-formaldehyde system. Hexagonally arranged pores revealed the lattice spacing and pore diameter of 7.5 and 6.2 nm. The XRD patterns showed that d-spacing shortened from 9.2 to 7.0 nm after carbonization with characteristic peals at $2\theta = 25$ and 45° that are characteristics of graphite matrix. However, the SEM images of the monolithic membrane (Figure 11) synthesized by Huo et al. [95] could not produce any ordered structure.

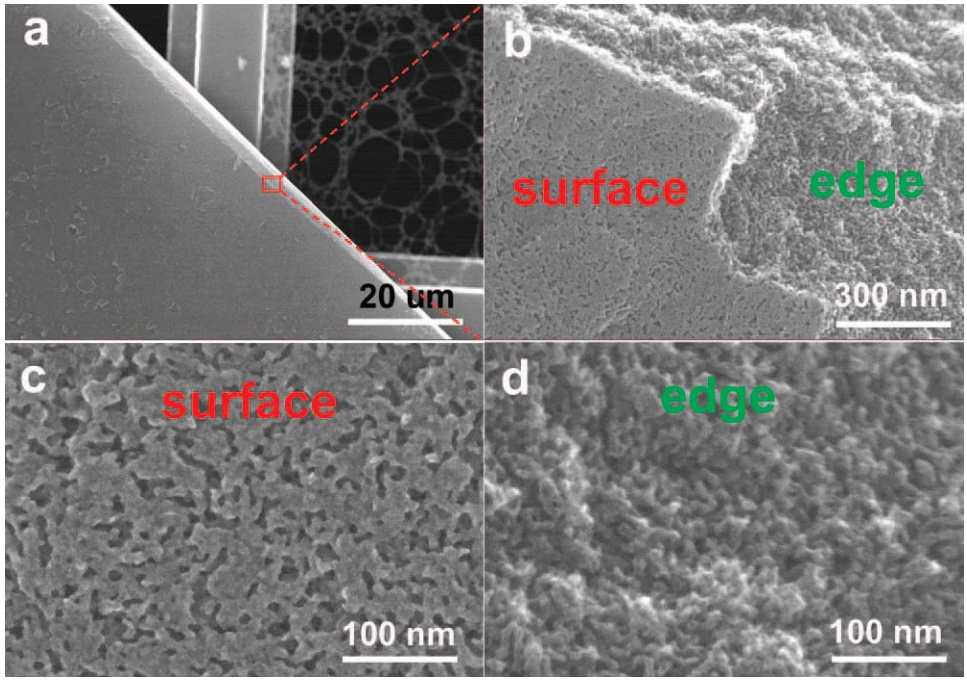


Figure 11. SEM images of a mesoporous carbon membrane at low (a) and high (b, c, d) magnifications. Reproduced from the publication of Hou *et al.* [95] with permission from American Chemical Society, 2008.

Dark-field TEM imaging revealed the well defined periodic structure of fibrous type mesoporous carbon in the work of Liang and Dai [86]. From the high resolution SEM imaging, it was also observed that monolithic type of carbon does not possess any particular type of structure, rather a worm-like structure similar to that of synthesized by Kosonen et al. [79] with surfactant ratio 30 % is noticed. But, film or fibrous type of carbon OMC gave rise to quite well defined periodic structure; it was claimed that spin coating and fiber extrusion technique provided a shear force in the carbon precursor that helped to maintain ordered structure in the resultant carbon species. X-ray diffraction pattern of fiber type of carbon also confirmed the hexagonal mesostructure within its matrix. Ordered graphitic ribbons were confirmed in the work of Saha and Deng [106] who synthesized OMC in the similar process of Liang and Dai [86].

The chemical nature of ordered mesoporous carbon including presence of functional groups and elemental composition were determined by Fourier transformed infra-red spectra (FT-IR), NMR and elemental analysis. The most common observation made by FT-IR and NMR is the disappearance of functional groups that belonged to the amphiphilic surfactants after template removal but remnant of hydroxyl groups from the phenolic resins. Kosonen et al. [79] performed the FT-IR of the all the samples in the regions of 2700-3700 cm^{-1}. All the phenolic OH groups containing samples showed the peak at 3430 cm^{-1} and a shoulder at 3500 cm^{-1} corresponding to stretching bands of hydrogen and free hydroxyl groups respectively. The stretching bands of OH did not disappear in the pyrolized samples, indicating the presence of OH groups in the carbon, but disappearance of peaks in the region of 3100 cm^{-1} to 2800 cm^{-1} that belonged to the surfactant clearly indicating the complete removal of the organic template.

Decomposition of block copolymer were revealed in the work of Meng et al. [85] with help of solid-state ^{13}C NMR. Two forms of ordered mesostructured carbon C-FDU-15 and C-FDU-16 that they synthesized also proved to lose the organic template but retained the periodic nature. Elemental analysis revealed the C/H/O ratio in the parent polymers, FDU-15 and FDU-16 to be 1:0.8:0.15 (C:77.97%, H:5.20%, O:16.8%) and 1:0.7:0.2 (C:75.1%, H: 4.36%, O: 20.5%) which provide quite good proximity of highly cross-linked phenolic resins.

Some typical FT-IR and solid state ^{13}C NMR of parent polymer are shown in figure 12 and 13 from the work of Zhang *et al.* [87] who synthesized ordered mesoporous carbon and the parent polymer, named as C-FDU-14 and FDU-14 respectively. In the figures, 'as-synthesized FDU-14' designates the polymer with surfactant, but 'FDU-14' indicates polymers after treating at 350°C when the surfactants are removed. Similar to the previous studies, complete removal of signals from triblock copolymer is observed where as the signals from phenolic resins are noticed to remain intact. Surfactant removed polymer FDU-14 contains the C/H/O mole ratio of 6.5:4.3:1 (C: 78.1%, H: 4.3%, O: 16.1%) and corresponding carbon C-FDU-14 contains C: 92.1%, H:1.9% and O: 6.0%). Liang et al. [88] reported the FT-IR spectra of PS-*block*-P4VP and PS-*block*-P4VP-resocinol system. It was observed that characteristics stretching modes of P4VP block at 993, 1415 and 1597 cm^{-1} were shifted to 1007, 1419 and 1602 cm^{-1} for P4VP-resorcinol system that is consistent with hydrogen bonding interactions between pyridine groups and resorcinol molecules [105].

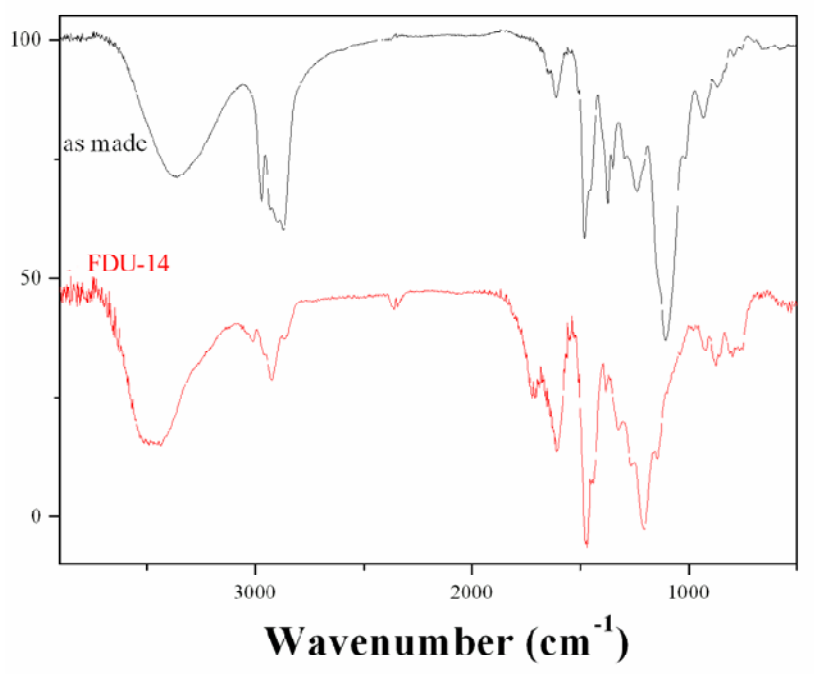


Figure 12. FTIR spectra of as-made FDU-14 and FDU-14. The spectra were recorded with KBr pellets using a Nicolet Fourier transform infrared spectrometer (Avatar-360). Reproduced from the publication of Zhang et al. [87] with permission from American Chemical Society, 2005.

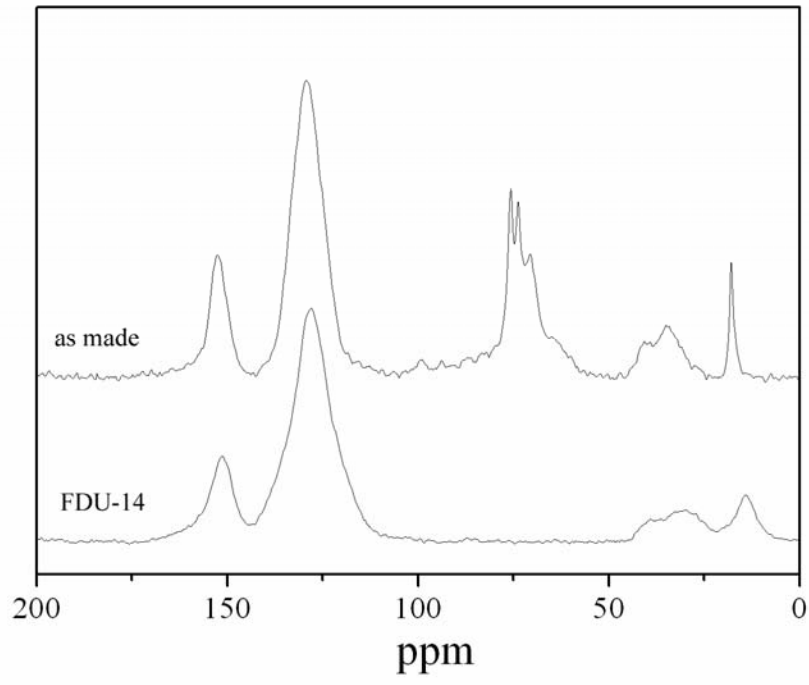


Figure 13. 13C solid-state NMR spectra of as-made FDU-14 and FDU-14. The spectra were recorded on a Bruker DSX300 spectrometer. Reproduced from the publication of Zhang et al. [87] with permission from American Chemical Society, 2005.

Raman spectroscopy is most widely used for determining state of graphitization of any carbonaceous material. A perfect and single graphite crystal gives only one vibrational mode at 1580 cm^{-1}, which is called G band. For disordered carbons, two additional bands are observed due to the loss of symmetry in the structure, which are D and D' lines in the range of 1340 and 1610 cm^{-1}. Some disordered carbon also shows a 2D overtone with a Raman shift of 2700cm^{-1}. Unlike ordered mesoporous carbons synthesized by hard template method, characterization by Raman spectroscopy is not widely observed in soft template based ordered mesostructured carbons. Meng et al. [65] reported the Raman spectra of C-FDU-15 and C-FDU-16 by He-Ne 632.8 nm wavelength laser source and the G band and D lines appeared at 1587 and 1330 cm^{-1} for both types of carbons. Shanahan et al. [92] reported G band and D line for graphitic mesoporous fuel cell support appeared at 596 and 1330 cm^{-1}. Saha et al. [106] and Saha and Deng [99] also reported the Raman bands of OMC and metal-doped OMC; in their work, the G band and D lines appeared in the range of 1565-1595 and 1290-1300 cm^{-1} respectively and did not shift the position with metal doping except for ruthenium. Meng et al. [65] reported the Raman spectra of C-FDU-16 (Figure 14) where G band and D lines appeared in the regions of 1600 and 1330 cm^{-1}.

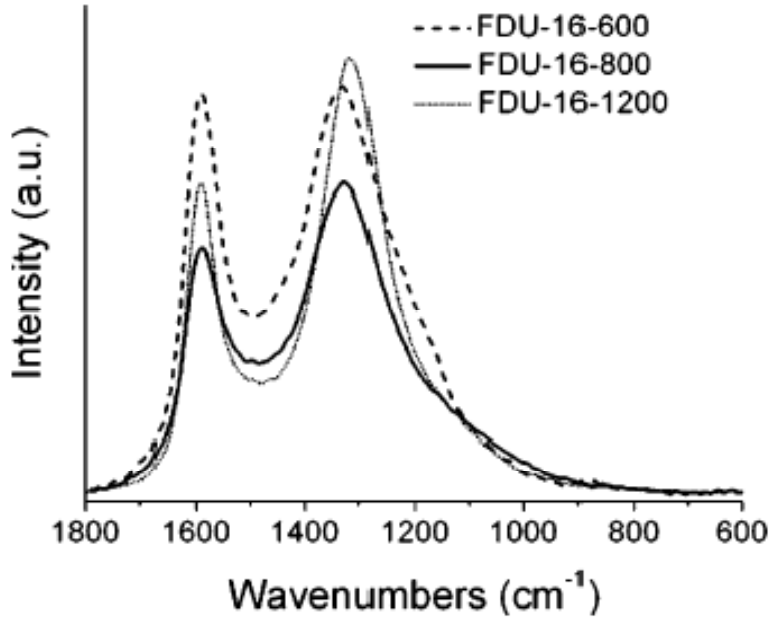


Figure 14. Raman spectra of FDU-16 prepared by using triblock copolymer F127 as a template via the EISA method after calcination at 600 °C (dashed line), 800 °C (solid line), and 1200 °C (dotted line) under Ar. Reproduced from the publication of Meng et al. [65] with permission from American Chemical Society, 2006.

4. APPLICATIONS

In present day's technology, there are several applications of ordered mesoporous carbons including capacitors/supercapacitors [107-109], catalysis support [110-112], fuel cell,

membranes, chemical sensors [113-114] or sorbents [115-117]. However, due to limited number of attempts to synthesize ordered mesostructured carbon by soft template or self assembly, not all the applications have been validated or reported with soft template approach. The applications which have been successfully reported with self-assembled ordered mesoporous carbon are membranes, fuel cell support and hydrogen sorption by doping transitions metals on to it.

As larger molecules receive more restrictions while passing through the pores, size based selectively of membranes could be easily verified and this effect was verified by Hou et al. [15] who reported the molecular sieving effect of mesoporous carbon synthesized by F127 template and phloroglucinol as carbon precursor. The incorporated anilinium ion Rhodamine B for the permeation experiment and it was observed that anilinium has higher selectively (α = 56.9) over Rhodamine B. The permeability of anilinium and Rhodamine B was reported to be as $1.38X10^{-8}$ and $5.39X10^{-10}$ cm^2/s respectively. It was concluded that

The similar research group reported the gas separating membranes composed of ordered mesoporous carbons synthesized by similar constituents except using hexamythelenetetramine (HMTA) as cross-linking agent to prevent cracks on the surface. Membranes with two different thickness were generated (42 μm and 18 μm) by varying the polymer concentration of the casting solution or the casting parameters, such as slit size. The gases that are tested fir this membrane are He, CO_2, O_2, N_2 and C_3H_6 and it was observed that almost all the gases demonstrated high flux, in the order of $\sim10^{-7}$ $mols^{-1}m^{-2}Pa^{-1}$. Restricted permeation of helium and enhanced permeation of CO_2 and C_3H_6 was observed. The restricted permeation of He within the membrane could be caused by the limited diffusion within very narrow micropores (<3 Å) and was reported for mesoporous carbon based membranes [16-dai carbon]. Very high selectivity of C_3H_6 over N_2 is also observed. It is reported that the presence of microporosity (0.1 cc/g) is accountable for the favorable transport of CO_2 and C_3H_6 within the surface etched membrane. The detailed transport parameters are shown in Table. 4.

Table 4.

Membrane	Gas Permeability ($mols^{-1}m^{-2}Pa^{-1}$)					Selectivity of
	He	CO_2	O_2	N_2	C_3H_6	C_3H_6/N_2
Thick (42 μm)	6.02	3.74	2.73	2.98	10.5	3.52
Thin (18 μm)	18.3	10.1	9.40	9.87	21.9	2.22

Shanan et al. [92] fabricated fuel cell support from the ordered mesoporous carbon synthesized by pluronic F127 as template and phloroglucinol as carbon source followed by graphitization at 2600°C. Platinum nanoparticles were dispersed on this support by treating it with chloroplatinic acid/acetone solution. The performance of platinum doped graphitized ordered mesoporous carbon (Pt/GMPC) was compared with commercial Vulcan Pt/XC-72. It was observed that, after Pt addition, corrosion current increases by more than orders of magnitude for Pt/XC-72 but by a single order of magnitude for Pt/GMPC; the corrosion current for Pt/GMPC is 96% less than the Pt/XC-72. The active platinum surface area of both he species was measured by cyclic voltametry and these are 86.6 and 58.3 m^2/gPt for Pt/GMPC and Pt/XC-72 respectively. Comparing the theoretical surface area with measured surface area, the platinum utilization of Pt/GMPC and Pt/XC-72 was calculated as 68 and 46

% respectively. During the course of experiment, Pt/XC-72 lost 39% of catalytic surface area while Pt/GMPC lost only 14% of catalytic surface area resulting indicating the fact that platinum doped ordered mesoporous carbon possesses pore durability than platinum Vulcan carbon samples which probably arise from the graphitic nature of the mesoporous carbon.

Because of its very high power density and relatively high energy density compared to conventional capacitors, electrical double layer capacitor (EDLC) or supercapacitor finds its extensive applications in numerous fields of electrical vehicles, digital telecommunication systems and uninterruptable power supplies for computers and pulsed-laser generators [23]. Two inherent factors that EDLCs possess are very high surface area of the capacitance medium and very thin electrical double layer compared to conventional capacitors. As capacitance values increase with the increase in both overlapping surface area and decrease electrical layer separation, EDLCs provide several times higher specific capacitance compared to conventional ones. As most of the activated porous carbon materials contain micropores, majority of the porous carbons are not suitable for EDLC applications because narrower pores do not provide sufficient space for the many electrolytes to accumulate within the pores and also narrow pores provide the resistance of free movement of the electrolyte ions within the pores.

Despite other forms of mesoporous carbons synthesized by conventional hard template method have studied extensively for electric double layer capacitor applications, OMCs synthesized self assembly were not studied in details except for Hou et al. [95] who employed mesoporous membranes synthesized by the self assembly of phloroglucinol/formaldehyde and F127 for cyclic voltametry experiments to measure specific capacitance. A series of cyclic voltagramms were generated by slow scan (1 mV/s) and fast scan (10 mV/s) using three different electrolytes, sodium chloride (NaCl), magnesium chloride (MgCl) and tetrahydroxyammonium chloride (THACl). It was reported that size effect was important for both electrochemically aided diffusion and eletrosorption process. This size exclusion effect was the key contributing factor for electrical double layer capacitance values of Na^+, Mg^+ and THA^+, at the potentials ranging from negative values to point of zero charge (PZC), corresponding to specific capacitance values of 86.7, 73.1 and 50.0 F/g respectively.

Saha et al [106] and Saha and Deng [99] utilized ordered mesoporous carbon for the hydrogen adsorption experiments. In the first work, Saha et al. [106] synthesized ordered mesoporous carbon from the similar procedures employed by Liang et al. [86], however without any curing steps. The hydrogen adsorption amounts at ambient pressure and temperatures 77 K, 194.5 K and 298 K was 1.27, 0.47 and 0.024 wt.% respectively. Kinetic measurements at 77 k and 194.5 K revealed the diffusion time constants of H_2 within OMC were $8X10^{-6}$ cm^2/s and $1X10^{-5}$ m^2/s respectively. The heat of adsorption amounts were 3.5 to 5 kJ/mol within the adsorption loading of 0.25 to 0.45 kJ/mol.

Saha and Deng [99] doped platinum, palladium, ruthenium and nickel on to ordered mesoporous carbon by *in-situ* technique, in which acetylacetonates of corresponding metal are mixed wit the initial precursors so that the acetylacetonates were thermally cracked to give metal nanopaticles during the carbonizations. The metal contents were varied within1, 5 and10 wt.% to see effect of metal doping on hydrogen uptake at ambient temperature. It was reported that metal doping for all the metals increased the hydrogen uptake amount by possible spill-over phenomenon and chemisorption on metal surface. Increase in metal contents also increased the uptake amount except for Ni doping which showed the reverse effect that is possibly caused by poor metal-carbon contacts. The highest adsorption amount

at ambient pressure was shown by 1% Ni doped OMC, around 0.1 wt.%. High pressure adsorption experiment at 300 bar pressure for 1 % Ni doped and 10 % Pd, Pt and Ru carbon demonstrated that, similar to low pressure hydrogen adsorption, 1 wt.% Ni doped OMC also experience highest adsorption (2.14 wt.%) followed by Pt, Pd and Ru doped carbon. The high pressure adsorption isotherms are shown in Figure 15.

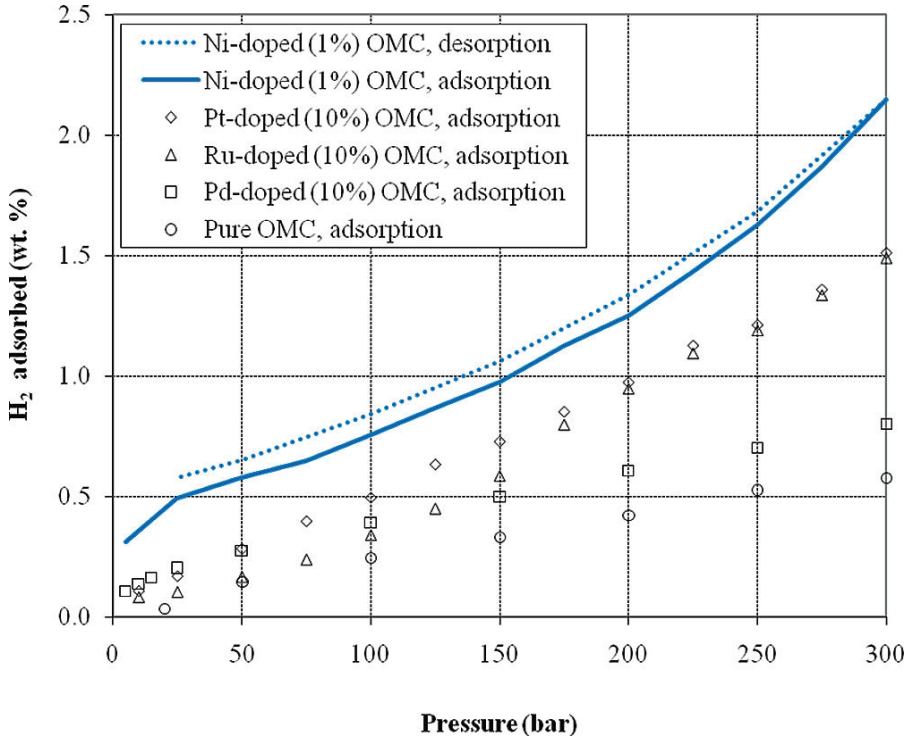


Figure 15. High pressure hydrogen adsorption (300 bar, 298 K) on 1 % Ni and 10 % Pd, Pt and Ru doped ordered mesoporous carbon, reproduced from the publication of Saha and Deng [99] with permission from American Chemical Society, 2009.

REFERENCES

[1] Lee, J.; Kim, J.; Hyeon, T.*; Adv Mater* 2006, 18, 2073-2094.
[2] F. Rodriguez-Reinoso, in *Introduction in Carbon Technology* (Eds: H. Marsh, E. A. Heintz, F. Rodriguez-Reinoso), Universidad de Alicante, Secretariado de publicationes, Alicante, Spain 1997, p. 35.
[3] Patrick, J.W. in *Porosity in Carbons: Characterization and Applications*, Edward Arnold, London, UK 1995.
[4] Ryoo, R.; Joo, S. H. ; Jun, S. *J. Phys. Chem*. B 1999, 103, 7743-7746.
[5] Jun, S.; Joo, S.H.; Ryoo, R.; Kruk, M.; Jaroniec, M.; Liu, Z.; Ohsuna, T.; Terasaki, O. *J. Am. Chem. Soc*. 2000, 122, 1071-10713.
[6] Hu, Z.; Srinivasan, M.P. Ni, Y. *Adv. Mater*. 2000, 12, 62-65.
[7] Zou, Y.; Han, B.-X. *Energy Fuels* 2001, 15, 1383-1386.

[8] Ahmadpour, A.; Do, D.D.; *Carbon* 1996, 34, 471-479.
[9] Zhang, T.Y.; Walawender, W.P.; Fan, L.T.; Fan, M.; Daugaard, D.; Brown, R.C. *Chem. Eng. J*. 2004, 105, 53-59..
[10] Yang, T.; Lua, A.C. *J. Colloid Interface Sci.* 2003, 267, 408-417.
[11] Marsh, H; Rand, B. *Carbon* 1971, 9, 63-72.
[12] Tamai, H.; Kakii, T.; Hirota, Y.; Kummamoto, T.; Yasuda, H. *Chem. Mater*. 1996, 8, 454-462..
[13] Oya, A.; Yoshida, S.; Alcaniz-Monge, J.; Linares-Soleno, A. *Carbon* 1995, 33, 1085-1090.
[14] Patel, N.; Okabe, K.; Oya, A. *Carbon* 2002, 40, 315-320.
[15] Ozaki, J.; Endo, N.; Ohizumi, W.; Igarashi, K.; Nakahara, M.; Oya, A. Car*b*on 1997, 35, 1031-1033.
[16] Oya, A.; Kasahara, N.*Carbon* 2000, 38, 1141-1144.
[17] Alcaniz-Monge, J.; Cazorla-Amores, D.; Linares-Solano, A.; Oya, A.; Sakamoto, A.; Hoshi, K. *Carbon* 1997, 35, 1079-1087.
[18] Pekala, R.W. *J. Mater. Sci*. 1989, 24, 3221.
[19] Pekala, R.W.; Alviso, C.T.; Kong, F.M.; Hulsey, S.S. *J. Non-Cryst. Solids* 1992, 145, 90-98.
[20] Pekala, R.W.; Schaefer, D.W. *Macromolecules* 1993, 26, 5487-5493.
[21] Knox, J.H.; Kaur, B.; Millward, G.R. *J. Chromatogr*. 1986, 352, 3-25.
[22] Ryoo, R.; Joo, S.H.; Jun, S. *J. Phys. Chem. B* 1999, 103, 7743-7746.
[23] Stein ; Wang, Z.; Fierke, M.A. *Adv Mater* 2009, 21, 265-293.
[24] Zakhidov, A.A.; Baughman, R.H.; Iqbal, Z.; Cui, C.; Khayrullin, I.; Dantas, O.; Marti, J.; Ralchenko, V.G.*Science* 1998, 282, 897.
[25] Lee, J.; Sohn, K.; Hyeon, T. *J. Am. Chem. Soc*. 2001, 123, 5146-5147.
[26] Meng, Y.; Gu, D.; Zhang, F.; Shi, Y.; Yang, H.; Li, Z.; Yu, C.; Tu, B.; Zhao, D. *Angew. Chem. Int. Ed.* 2005, 44, 7053-7059.
[27] Zhou, L.; Li, H.; Yu, C.; Zhou, X.; Tang, J.; Meng, Y.; Xia, Y.; Zhao, D. *Carbon* 2006, 44, 1601-604.
[28] Kosonen, H.; Valkama, S.; Nykanen, A.; Toivanen, M.; ten Brinke, G.; Ruokolainen, J.; Ikkala, O.*Adv. Mater*. 2006, 18, 201-205.
[29] Lin, C.; Ritter, J.A.; *Carbon* 1997, 35, 1271-1278.
[30] Lee, K.T.; Oh, S.M. *Chem. Commun*. 2002, 2722-2723.
[31] Zanto, E.J.; Al-Muhtaseb, S.A.; Ritter, J.A.; *Ind. Eng. Chem. Res*. 2002, 41, 3151-3162.
[32] Al-Muhtaseb, S.A.; Ritter, J.A.; *Adv. Mater*. 2003, 15, 101-114.
[33] Lee, K.T.; Lytle, J.C.; Ergang, N.S.; Oh, S.M.; Stein, A. *Adv. Funct. Mater*. 2005, 15, 547-556.
[34] Xia, Y.; Mokaya, R.; *Chem. Mater*. 2005, 17, 1553-1554.
[35] Yang, C.-M.; Weidenthaler, C.; Spliethoff, B.; Mayanna, M.; Schueth, F. *Chem. Mater.* 2005, 17, 355-358.
[36] Kruk, M.; Jaroniec, M.; Ryoo, R.; Joo, S.H. *J. Phys. Chem. B* 2000, 104, 7960-7968.
[37] Lee, J.; Sohn, K.; Hyeon, T. *Chem. Commun*. 2002, 2674-2675.
[38] Lu, A.-H. ; Li, W.-C. ;. Schmidt, W.; Schueth, F. *Microporous Mesoporous Mater.* 2005, 80, 117-128.
[39] Wang, X. Bozhilov, K.N.; Feng, P. *Chem. Mater*. 2006, 18, 6373-6381.
[40] Yang, Z.; Xia, Y.; Sun, X.; Mokaya, R.; *J. Phys. Chem. B* 2006, 110, 18424-18431.

[41]Kim, T.-W. ; Park, I.-S.; Ryoo, R.; *Angew. Chem. Int. Ed.* 2003, 42, 4375-4379.
[42]Yang, H.; Yan, Y.; Liu, Y.; Zhang, F.; Zhang, R.; Meng, Y.; Li, M.; Xie, S.; Tu, B.; Zhao, D. *J. Phys. Chem.* B 2004, 108, 17320-17328.
[43]Gierszal, K.P.; Kim, T.W.; Ryoo, R.; Jaroniec, M. *J. Phys. Chem*. B 2005, 109, 23263-23268.
[44]Kim, C.H.; Lee, D.-K.; Pinnavaia, T. J. *Langmuir* 2004, 20, 5157-5159.
[45]Xia, Y.; Mokaya, R. *Adv. Mater*. 2004, 16, 886-891.
[46]Ryoo, R.; Joo, S.H.; Kruk, M.; Jaroniec, M. *Adv. Mater.* 2001, 13, 677-681.
[47]Yang, H.; Zhao, D.; *J. Mater. Chem*. 2005, 15, 1217-1231.
[48]Li, Z.; Jaroniec, M.; *J. Am. Chem. Soc.* 2001, 123, 9208.
[49]Li, Z.; Jaroniec, M. *J. Phys. Chem. B* 2004, 108, 824-826.
[50]Gierszal, K.P.; Jaroniec, M. *J. Am. Chem*. Soc. 2006, 128, 10026-10027.
[51]Qiao, W.M.; Song, Y.; Hong, S.H.; Lim, S.Y.; Yoon, S.H.; Korai, Y.; Mochida, I. *Langmuir* 2006, 22, 3791-3797.
[52][52] Yoon, S.B.; Sohn, K.; Kim, J.Y.; Shin, C.-H. ; Yu, J.-S.; Hyeon, T. *Adv. Mater.* 2002, 14, 19.-21
[53][53] Kim, M.; Yoon, S. B.; Sohn, V.; Kim, .Y.; Shin, C.-H.; Hyeon, T.; Yu, J.-S. *Microporous Mesoporous Mater*. 2003, 63, 1-9.
[54][54] Wang, Z.; Li, F.; Stein, A..; *Nano Lett*. 2007, 7, 3223-3226.
[55]Steinhart, M.; Liang, C.; Lynn, G.W.; Goesele, U.; Dai, S. *Chem.Mater*. 2007, 19, 2383-2385.
[56]Wang, Z.; Li, F.; Ergang, N.S.; Stein, A. *Chem. Mater*. 2006, 18, 5543-5553.
[57]Wang, Z.; Stein, A. *Chem. Mater*. 2008, 20, 1029-1040.
[58]Liu, Y.F.; Ganguli, R.; Drewin, C.A.; Anderson, M.T.; Brinker, C.J.; Gong, W.L.; Gio, Y.X.; Soyez, H.; Dunn, B.; Hunag, M.H.; Zink, J.I. *Nature* 1997, 389, 364-368.
[59]Brinker, C.J.; Lu, Y.; Sellinger A.; Fan, H. *Adv Mater* 1999, 11, 579-585.
[60]Yu, K.; Hurd, A.J.; Eisenburg, A.; Brinker, C.J. *Langmuir*, 2001, 17, 7961-7965.
[61]Soller-llia, G.J.A.A.; Louis, A.; Sanchez, C. *Chem Mater* 2002, 14, 750-759.
[62]Bore, M.T.; Rathod, S.B.; Ward, T.L.; Datye, A.K. *Langmuir* 2003, 19, 26-264.
[63]Groso, D.; Cagnoi, F.; Soller-llia, G.J.A.A.;Crepaldi, E.L.; Amenitsch, H.; Brunet-Bruneau, A.; Bourgeois, Sanchez, C. *Adv. Funct Mater* 2004, 14, 309-322.
[64]Gibaud, A.; Grosso, D.; Smarsly. B.; Baptiste, A.; Barduau, J.F>; Bobonneau, F.; Doshi, D.A; Chen, Z.; Brinker, C.J.; Sanchez, C. *J Phys CHem B* 2003, 107, 6114-6118.
[65]Meng, Y.; Gu, D.; Zhang, F.; Shi, Y.; Cheng, L.; Feng, D.; Wu, Z.; Chen, Z.; Wan, Y.; Stein, A.; Zhao, D. *Chem Mater* 2006, 18, 4447-4464.
[66]Patarin, J.; Labeau, B.; Zana, R. *Current opinion in colloid and interface science* 2002, 7, 107-115.
[67]Anderson, N.; Kronberg, B.; Corkery, R.; Alberius, P. *Langmuir* 2007, 23, 1459-1464.
[68]Etienne, M.; Walcarius, A. *Electrochem Commun* 2005, 7, 1449-1456.
[69]] Liu, K.; Zhang, M.; Shi, K.; Fu, H. *Mater Lett* 2005, 59, 3308-3310.
[70]Doshi, D.A.; Gibaud, A.; Goletto, V.; Lu, M.; Gerung, H.; Ocko, B.; Han, S.M.; Brinker, C.J. *J Am Soc* 2003, 125, 11646-11655.
[71]Jiang X.; Brinker, C.J. *J Am Soc* 2006, 128, 4512-4513.
[72]Brezesinski, T.; Groenewolt, M.; Gibaud, A.; Pinna, N.; Antonietti, M.; Smarsly, B. *Adv Mater* 2006, 18, 2260-2263.

[73] Fan, H.; Reed, R.; Baer, T.; Lopez, G.P.; Brinker, C.J. *Microporous Mesoporous* Mater 2001, 44, 625-637.
[74] Hampsey, J.E.; Arsenault, S.; Hu, Q.; Lu, Y. *Chem mater* 2005, 17, 2475-2480.
[75] Garnweitner, G.; Smarsley, B.; Assinl, R.; Ruland, W.; Bond, E.; Brinker, C. J. *J Am Soc* 2003,125,5626-5627.
[76] Fan, H.; Lu, Y.; Stump.; Reed, S.T.; Baer, T.; Schunk, R.; Perez-Luna, V.; Lopez, G.P.; Brinker, C.J. *Nature*, 2000, 405, 56-60.
[77] Urade, V.N.; Bollman, L.; Kowalski, J.D.; Tate, M.P.; Hillhouse, H.W. *Languir* 007, 23, 4268-4278.
[78] Zhang, X.; Liu, C.; Wu, W.; Wang, *J. Mater Lett* 2006, 60, 2086-2089.
[79] Kosonen, H.; Valkama, S.; Nykanen, A.; Toivanen, M.; Brinke, G.T.; Ruokolainen, J.; Ikkala, O. *Adv Mater* 2006, 18, 201-205.
[80] Bates, F.S.; Fredrickson, G.H.; *Annu Rev Phys Chem* 1990, 41, 525.
[81] Hamley, I.W.; *The physics of block copolymers,* Oxford Univesity Press, Oxford, UK 1998.
[82] Muthukumar, M.; Ober, C.K.; Thomas, E.L.; *Science* 1998, 280, 557.
[83] Jang J.; Bae, J. *Chem Commun* 2005, 1200-1202.
[84] Tanaka, S.; Nishiyama, N.; Egashira, Y.; Ueyama, K. *Chem Commun* 2005, 2125-2127.
[85] Meng, Y.; Gu, D.; Zhang, F.; Shi Y.; Yanf, H.; Li, Z.; YU, C.; TU, B.; Zhao, D. *Angew Chem Intl Ed* 2005, 44, 7053-7059.
[86] Linag. C.; Dai, S.; *J Am Chem Soc* 2006, 128, 5316-5317.
[87] Zhang, F.; Meng, Y.; Gu, D.; yan, Y.; Yu, C.; Tu, Bo.; Zhao, D. *J Am Chem Soc* 2005, 127, 13508-13509.
[88] Linag C.; Hong, K.; Guiochon, A.; Mays, J.W.; Dai, S. *Angew Chem Int Ed* 2004, 43, 5785, 5789.
[89] Lee, K.T.; Oh, M. *Chem Commun* 2002, 2722-2723.
[90] Wang, X.; Zhu, Q.; Mahurin, M.; Liang C.; Dai, S. *Carbon* 2010, 48, 557-570.
[91] Steinhart, M.; Liang, C.; Lynn, G.W.; Gosele, U.; Dai, S. *Chem. Mater*. 19, 2007, 19, 2383-2385.
[92] Shanahan, P.V.; Xu, L.; Liang, C.; Waje, M.; Dai, S.; Yan, Y.S. *J. Power Sources* 2008, 185, 423-427.
[93] Hatori, H.; Kobayashi, T.; hanzaya, Y.; yamanda, Y.; Iimuma, Y.; Kimura, T.; Shiraishi, M. *J. Appl. Polymer Sci*. 2001,79, 836.
[94] Shah, T.N.; Foley, H.C.; Zydney, A.L.; *J. Membrane Sci* 2007, 295, 40-49.
[95] Hou, C.-H.; Wang, X.; Liang, C.; Yiacoumi, S.; Tsouris, C.; Dai, S. *J. Phys Chem B* 2008, 112, 8563-8570.
[96] Rodriguez, A.T.; Chen, M.; Chen, Z.; Brinker, C.J.; Fan, H.J.; *J. Am Soc.* 2006, 128, 9276-9277.
[97] Yu, C.-Z.; Fan, J.; Tian, B.; Zhao, D.-Y.; Stucky, G.D.; *Adv. Mater*. 2002, 14, 1742-1745.
[98] Cott, D.J.; Petkov, N.; Michael, A.; Morris, M.A.; Platschek.; B.; Bei, T.; Holmes, J.D.; *J. Am. Soc.* 2006, 128, 3920-3921.
[99] Saha, D.; Deng, S.; *Langmuir*, 2009, 25, 12550-12560.
[100] Kruk, M.; Jaroniec, F.Q.; Sayari, A. *Langmuir*, 1997 13, 6267-6273.
[101] Zhao, D.Y.; Feng, J.L.; Hio, Q.S.; Melosh, N.; Fredrickson, G.H.; Chmelka, B.F; Stucky, G.D. *Science* 1998, 279, 548-552.

[102] Sakamato, Y.; Kim, T.W.; Ryoo, R.; Teasaki, O. *Angew. Chem. Intl. Ed.* 2004, 42, 5231-5234.
[103] Zhao, D.Y.; Huo, Q.S.; Feng, J.L.; Chmelka, B.F.; Stucky, G. *J. Am. Chem. Soc*. 1998, 120, 6024-6036.
[104] Huo, Q.S.; Margolese, D.I.; Ciesla, U; Feng, P.Y.; Gier, T.E.; Sieger, P.; Leon, R.; Petroff, P.M.; Schulth, F.; Stucky, G.D. *Nature*, 1994, 368, 317-321.
[105] Ikkala, O.T.; Ruokolainen, J.; ten Brinke, G.; Torkkeli, M.; Serimaa, R.; *macromolecules* 1995, 28, 7088-7094.
[106] Saha, D.; Wei, Z.; Velluri, S.H; Deng, S. *J. Porous Media* 2010, 13, 39-50.
[107] J. Lee, S. Yoon, T. Hyeon, S. M. Oh, K. B. Kim, *Chem. Commun*. 1999, 2177.
[108] T. Hyeon, S. M. Oh, J. Lee, S. Yoon, *Mater. Res. Soc. Symp. Proc*. 2000, 593, 193.
[109] J. H. Jang, S. Han, T. Hyeon, S. M. Oh, *J. Power Sources* 2003, 123, 79.
[110] T. Harada, S. Ikeda, M. Miyazaki, T. Sakata, H. Mori, M. Matsumura, *J. Mol. Catal*. A 2007, 268, 59.
[111] J.-H. Zhou, J.-P. He, Y.-J. Ji, W.-J. Dang, X.-L. Liu, G.-W. Zhao, C.-X. Zhang, J.-S. Zhao, Q.-B. Fu, H.-P. Hu, *Electrochim*. Acta 2007, 52, 4691.
[112] K.-I. Min, J.-S. Choi, Y.-M. Chung, W.-S. Ahn, R. Ryoo, P. K. Lim, *Appl. Catal.* A 2008, 337, 97.
[113] D. Lee, J. Lee, J. Kim, J. Kim, H. B. Na, B. Kim, C.-H. Shin, J. H. Kwak, A. Dohnalkova, J. W. Grate, T. Hyeon, H.-S. Kim, *Adv. Mater*. 2005, 17, 2828.
[114] C. Z. Lai, M. M. Joyer,M. A. Fierke, N. D. Petkovich, A. Stein, P. Buhlmann, *J. Solid State Electrochem*. 2008, DOI 10.1007/s10008-008- 0579-2.
[115] S. Zhu, X. Wang, W. Huang, D. Yan, H. Wang, D. Zhang, *J. Mater. Res*. 2006, 21, 2847.
[116] A. Vinu, C. Streb, V. Murugesan, M. Hartmann, *J. Phys. Chem*. B 2003, 107, 8297
[117] A. Vinu, M. Miyahara, V. Sivamurugan, T. Mori, K. Ariga, *J. Mater. Chem.* 2005, 15, 5122

INDEX

A

abatement, 184, 477
Abraham, 86
absorption spectra, 138
absorption spectroscopy, 2, 135
abstraction, 437
access, 173, 176, 255
accessibility, 61, 143, 172, 184, 207, 358, 373, 394, 397, 402, 405, 436
accommodation, 182
accounting, 210, 479
acetaldehyde, 67
acetic acid, 24, 55, 156
acetone, 66, 176, 185, 309, 387, 394, 507, 519, 532
acetonitrile, 507, 511
acetylation, 504
acetylene gas, 56
ACF, vii, 1, 4, 17, 24, 30, 31, 32, 33, 34, 35, 36, 38, 39, 41, 256, 257, 259, 447, 453
acrylic acid, 20, 236
acrylonitrile, xii, 378, 515
activation energy, 114, 115, 116, 141, 190
active centers, 106, 113, 118, 121, 458
active phase carriers, viii, 169
active site, 20, 37, 59, 107, 116, 118, 130, 142, 143, 147, 173, 178, 190, 257, 305, 384, 429
activity level, 255
acylation, 304
adaptability, 27
adaptation, 54
additives, 187, 195
adenosine, 443
adhesion, 70, 145
adhesives, 2, 18, 20
adjustment, 27
advanced chemical oxidation (ACO), xiii, 433
advancements, 53
adverse effects, 18, 69, 73
aerogels, xii, 378
aesthetic, 22
AFM, 59, 60, 504
aggregation, 69, 71, 175
agricultural byproducts, viii, 205
agricultural sector, 387
agriculture, 25, 249, 391
AIBN, 515, 517
air quality, 144
alcohols, 141, 142, 187, 304, 316, 434
aldehydes, 118, 187, 188, 304
algorithm, 362
alkali-metal hydroxides, ix, 239
alkalinity, 505
alkane, 139
alkenes, 170, 304
alkylation, 54
almonds, 249
alters, 160, 214, 477, 484, 485
aluminium, 48, 179, 271, 273, 301, 352, 385, 445
aluminum oxide, 317
ambient air, 425, 491
amine, 163, 193
amines, 131, 142, 144, 304, 316, 341, 454
amino, ix, 144, 156, 206, 333
amino acid, 333
amino acids, 333
ammonia, 21, 27, 49, 131, 143, 155, 156, 157, 177, 178, 181, 183, 190, 193, 195, 256, 304, 311, 312, 314, 317, 366, 389, 441, 443, 503
ammonium, 23, 34, 55, 153, 156, 178, 183, 243, 246, 247, 288, 301, 311, 312
amorphous polymers, 220
amplitude, 398
analgesic, 454
anatase, 62, 66, 67, 299, 300, 304, 318, 453
anchoring, 176
aniline, 57, 157, 195, 293
annealing, 37, 301, 382
ANOVA, 328, 330

antibiotic, 455
apoptosis, 70, 72, 73, 74
aqueous solutions, xi, 13, 14, 18, 19, 20, 21, 24, 25, 26, 31, 32, 36, 37, 52, 55, 58, 64, 132, 142, 156, 162, 232, 237, 256, 258, 259, 260, 262, 263, 264, 265, 356, 370, 386, 390, 391, 459, 488, 502, 503
aqueous suspension, 67, 136, 310
Argentina, 420, 475, 478, 502
argon, 3, 47, 51, 67, 218, 222, 382
aromatic compounds, 28, 157, 162, 165, 429, 434, 442, 456, 483
aromatic hydrocarbons, 22, 46, 53, 56, 162, 434
aromatic rings, 382, 429, 454
aromatics, 27, 29, 141, 162, 163, 166, 188, 304
Arrhenius equation, 114
arsenic, 232, 257, 264, 309, 316, 411
asbestos, 242, 243
ascorbic acid, 257
aspiration, 72
ASS, 103
assessment, 275, 411, 503, 506
assessment procedures, 411
atomic force, 59
attachment, 362
authority, 411

B

BAC, 444, 445, 446
Bac Pro, 443
Bacillus subtilis, 56
bacteria, 18, 40, 53, 56, 64, 66, 158, 443, 445, 461
bacterial pathogens, 53
bacteriostatic, 188
band gap, 63, 298, 299
barium, 54, 247
barriers, 379
base, xi, xiv, 12, 32, 52, 53, 69, 95, 104, 135, 139, 150, 151, 155, 157, 158, 159, 163, 164, 174, 176, 179, 180, 188, 192, 221, 225, 258, 259, 272, 274, 285, 288, 331, 355, 356, 366, 385, 422, 476, 503, 507, 509, 514
basicity, 133, 159, 178, 305, 436
batteries, 25, 52, 66, 504
behaviors, 294, 503
Beijing, 374
bending, 284
benefits, 64, 255, 467, 476, 478
benign, 231
benzene, 23, 25, 26, 28, 56, 57, 66, 161, 184, 257, 271, 290, 304, 313, 316, 364, 370, 371, 380, 387, 429, 503
benzothiophenes (BTs), xiii, 421
BET model, xi, 356, 368
bias, 32, 50
bicarbonate, 95, 109, 135, 333, 466
binding energies, 15, 137, 385
binding energy, 137
bioavailability, 40, 420
biocompatibility, 74
bioconversion, 321
biodegradability, 443, 445, 446
biodegradation, 18, 40, 58, 157, 443, 504
biodiesel, xiii, 236, 409, 412, 414, 419
biogas, 504
biological activity, 18, 443, 468
biological processes, 257, 387
biomass, x, xiii, 146, 152, 171, 193, 210, 218, 233, 235, 236, 237, 264, 295, 306, 319, 383, 386, 389, 390, 409, 422
biomass materials, 152
biomedical applications, 2
biomolecules, 51, 477
biopolymers, 219, 222
biosensors, 51
bisphenol, 22, 461
Bisphenol A (BPA), 451
bleaching, 321, 338, 343, 344, 345, 449, 459, 461
blends, 180, 511
blood, 69, 71, 72, 109, 252, 350
body weight, 71
boilers, 27, 319, 320, 321, 327
bonding, xii, xiv, 20, 42, 142, 160, 211, 223, 331, 377, 509, 512, 513, 520, 529
bonds, 42, 53, 115, 131, 133, 156, 206, 211, 373, 434, 456, 512, 513, 528
bone, 70, 127
bone marrow, 70
bones, 127
botanical origin, ix, 239
branching, 348
breakdown, 219, 446
breathing, 387
Britain, 345
bromine, 132
burn, 4, 5, 7, 39, 172, 173, 183, 212, 217, 323, 467
burnout, 323, 382
butyl ether, 29
by-products, ix, xi, 95, 222, 231, 239, 258, 260, 302, 343, 377, 378, 380, 383, 434

C

cadmium, xiii, 52, 56, 57, 149, 163, 409, 410, 419, 420, 503, 506
caffeine, 445

calcination temperature, 104
calcium, 46, 148, 385
calorimetry, 138, 139, 160
cancer, 21, 350
candidates, 52, 53, 276, 287
cane sugar, 379
capillary, 183, 275
carbides, 189, 272, 305, 311
carbohydrate, 519
carboxyl, 53, 209, 435, 440
carboxylic groups, 140, 176, 177, 181, 368, 440, 487
carcinogen, 21, 22
carotenoids, 338
case study, 264
casting, 518, 532
chemisorption, ix, xii, 35, 129, 167, 193, 206, 370, 393, 394, 395, 434, 457, 533
China, 76, 93, 95, 221, 390, 420
chirality, 276
chitosan, 35, 55, 236
Chitosan, 55, 228
chlorinated hydrocarbons, 64
chlorination, 58, 156
chlorine, 132, 144, 166, 247, 254, 259, 378, 382, 385, 387, 434, 445
chlorobenzene, 29, 166, 229, 234, 304, 308
chloroform, 25, 28, 36, 304, 308, 387
chlorophyll, 338, 341, 345
chromatography, 96, 139, 140, 153, 157, 265
chromium, 26, 31, 35, 36, 57, 162, 163, 250, 259, 410
classes, viii, 205
classification, ix, 101, 126, 127, 135, 239, 251, 275, 489
cleaning, 4, 145, 159, 181, 185, 193, 194, 195, 259, 327, 343
cleanup, ix, 240, 257, 265
cleavage, 219, 483
clothing, 477
cluster model, 159
clusters, 47, 117, 189, 370, 396
coagulation process, 61
coalified plant matter, ix, 239
coatings, 18, 275, 317
cobalt, xi, 36, 44, 49, 71, 72, 175, 272, 292, 347, 348, 349, 350
cocaine, 445
coconut shell activated carbon (CSAC), xiii, 421
coffee, 9, 144, 216, 218, 223, 226, 232, 233, 236, 249, 307, 309, 439
coke, 9, 95, 143, 151, 152, 177, 180, 181, 185, 188, 228, 290, 378, 381, 448, 450
color, iv, 32, 36, 94, 209, 243, 244, 246, 247, 259, 327, 328, 329, 330, 331, 332, 337, 338, 339, 341, 342, 343, 461
combined effect, 95
combustion, 25, 27, 29, 31, 49, 84, 135, 181, 186, 193, 194, 250, 253, 260, 305, 312, 319
combustion processes, 181
community, 191, 268
comparative advantage, 476
compatibility, 176, 510
competition, 20, 26
competitiveness, 436
compilation, 439
complement, 139
complexity, 180, 464, 465
compression, 250
computation, 361
computer, xi, 355, 362, 373, 506
computer simulations, 362
conception, 476
concordance, 457
condensation, 10, 140, 211, 217, 219, 275, 333, 513, 514, 519
conditioning, 171, 387
conduction, 44, 63, 64, 68, 69, 224, 290, 299, 300, 306
conductivity, xii, 30, 31, 32, 42, 44, 59, 69, 138, 170, 183, 190, 276, 298, 299, 378, 382, 387, 506, 510
conductor, 299
conductors, 43, 44
conference, 288
configuration, 68, 172, 298, 359, 478
Congo, 264
Congress, iv, 199, 406
connectivity, 356, 358, 362, 365
conservation, 250, 421
constant rate, 323, 342
constituents, 26, 28, 212, 443, 515, 523, 532
construction, 1, 51
consumer goods, 187
consumption, 2, 19, 20, 27, 31, 190, 224, 250, 284, 286, 287, 420, 443, 447, 450, 452, 453, 454, 458
contact time, 7, 18, 19, 20, 21, 22, 25, 26, 31, 32, 37, 144, 312, 328, 329, 339, 340, 444, 446, 479
containers, 98, 350, 351
contaminant, 260, 458
contaminated water, viii, 22, 30, 31, 53, 205, 466
contamination, 12, 58, 191, 410, 411, 419, 420
convention, 207, 225
conversion degrees, 190
conversion rate, 116, 118
COOH, 57, 61, 385, 386
cooking, 338

cooling, 130, 241, 242, 243, 245, 348, 349, 350, 351
coordination, 118, 398
copolymer, xiv, 378, 382, 509, 512, 513, 516, 519, 524, 526, 529, 531
copolymers, xv, 380, 382, 386, 391, 509, 512, 513, 526, 537
copper, vii, xiii, 35, 36, 38, 39, 43, 44, 46, 50, 57, 59, 93, 95, 103, 119, 121, 157, 163, 179, 195, 250, 251, 259, 315, 409, 410, 504
copper oxide-loaded activated carbon (CuO/AC), vii, 93
correlation, 107, 108, 116, 139, 143, 160, 253, 334, 504
correlation coefficient, 334
correlations, xi, 356, 364, 372
corrosion, 9, 27, 532
cosmetics, 69, 188
cotinine, 445
cotton, 9, 11, 22, 223, 228, 233, 245, 258, 260, 265, 391, 478, 505
covering, 186, 222, 318, 364
cracks, 181, 182, 532
creosote, 40
cristallinity, 301, 308, 311, 312, 498
critical value, 445
crop, xiii, 409, 418
crops, xiii, 409, 412, 420
cross-linked polymers, 382
cross-linking reaction, 483, 496, 501
crown, 24, 36
crude oil, 40
crystal growth, 290
crystal structure, 44, 97
crystalline, xiv, 220, 275, 281, 298, 304, 313, 381, 398, 476, 496, 497, 502
crystallinity, 223, 238, 280
crystallites, 126, 175, 189, 191, 275, 356, 358, 396, 498
crystals, 271, 303, 381, 511
cubic boron nitride, 42
cultivars, 416
culture, 74
culture medium, 74
cure, 62
CVD, x, 44, 45, 48, 49, 50, 51, 55, 56, 57, 65, 66, 67, 267, 269, 270, 271, 272, 288, 290, 302
cyanide, 24, 35, 163
cyanosis, 21
cycles, 32, 33, 35, 41, 59, 69, 191, 229, 304, 327, 343, 351, 448, 450, 460, 467
cyclohexanol, 157, 177, 394
cyclohexanone, 167, 188, 394
cytoplasm, 73
cytotoxicity, 71, 73, 74

D

damages, iv
DBP, 19
decay, 348, 350, 398, 438
decontamination, 37, 58, 165, 193
deconvolution, 135, 138, 140, 141
deduction, 254
defect site, 292
defects, 44, 53, 207, 272, 275, 284, 358, 359, 496
deficiency, 306
deforestation, 321
deformation, 43, 115, 185
degradation rate, 36, 40, 41, 94, 113, 452, 481, 482, 483, 484
degree of crystallinity, 223, 280
degumming, 344
Degussa, 66, 304, 451
dehydration, 9, 10, 140, 143, 164, 219, 236, 249, 303, 304, 308, 434
density functional theory, 423
deposition, x, xii, 39, 44, 48, 64, 65, 70, 143, 175, 179, 181, 188, 192, 249, 250, 258, 267, 269, 270, 271, 272, 287, 290, 291, 292, 303, 306, 313, 315, 317, 393, 519
deposits, 23, 290, 291
deprivation, 70
depth, 213, 221, 254, 302
derivatives, 57, 153, 251, 257, 306, 381
destruction, 7, 10, 64, 285, 439, 467
detachment, 20
detectable, 25, 410, 413, 414, 417, 418
detection, 51, 69, 137, 265, 348, 350, 351, 448
detergents, 18, 20
detoxification, 193
deviation, 350, 358, 364
DFT, 370, 423, 428
dibenzothiophenes (DBTs), xiii, 421, 422
dielectric constant, 224, 331
diesel fuel, 162, 167, 187, 189, 505
diffraction, xiv, 99, 384, 475, 480, 504, 523, 529
diffuse reflectance, 137, 155
diffusivity, 463, 465
digestion, 135, 242, 243, 293
dilation, 219, 220, 494
dimerization, 311
dimethylformamide, 55, 515, 517
dioxin, 22, 52, 53, 445
discharges, 410
discs, 153
disinfection, 19, 26, 53, 94, 95, 434, 444, 445

disorder, 497, 498
disordered systems, 363
dispersion, xii, 53, 65, 72, 118, 175, 176, 178, 183, 187, 189, 191, 193, 311, 313, 314, 364, 381, 384, 393, 394, 395, 396, 397, 402, 403, 405, 429, 480
displacement, 99
dissociation, 48, 135, 190
dissolved oxygen, 443
distillation, 247
distilled water, 8, 55, 59, 133, 278, 331, 332, 333, 338, 341, 478, 483, 496
diversity, 207, 210, 241
DMF, 515, 517
DOC, 20, 23, 443
DOI, 236, 538
dominance, 502
donors, 53
doping, xiv, 34, 41, 67, 509, 511, 519, 531, 532, 533
dosage, 21, 22, 25, 26, 33, 40, 71, 74, 106, 111, 112, 116, 120, 258, 329, 330, 332, 339, 340, 341, 343, 446
drawing, 518
drinking water, x, xiii, 13, 21, 22, 26, 57, 94, 240, 256, 259, 260, 263, 265, 309, 316, 317, 386, 387, 433, 443, 446
DRS, 310, 364, 365
drug delivery, 69
drugs, 18, 444
drying, 37, 68, 97, 147, 149, 150, 183, 193, 241, 242, 243, 301, 302, 396, 397, 402, 403, 412, 423, 511, 518
durability, 187, 188, 477, 533
dyeing, 22, 258
dyes, 22, 35, 54, 55, 58, 62, 64, 141, 142, 156, 157, 164, 165, 207, 210, 226, 227, 228, 250, 251, 257, 258, 259, 262, 263, 264, 265, 266, 304, 306, 320, 321, 386, 391, 444, 446, 447, 449, 450, 451

E

ecology, 344
economics, 321, 466
ecstasy, 445
editors, 145, 153, 158, 391, 419, 420, 469
effluent, 40, 256, 259, 266, 310, 344, 425, 428, 443, 446, 449, 450, 459
effluents, xiii, xiv, 20, 21, 31, 40, 54, 143, 165, 193, 256, 265, 298, 304, 306, 313, 433, 446, 459, 476, 491, 502
elastic deformation, 185
electric charge, 299
electric conductivity, 276, 387
electric current, 43
electric field, 137, 299
electrical conductivity, 31, 42, 59, 170, 183, 298, 382, 510
electrical properties, vii, 1, 43, 64, 160, 477, 506
electricity, 193, 271, 321
electrocatalysis, 170
electrocatalyst, 187
electrochemical water treatment processes, vii, 1, 62
electrodes, x, 32, 44, 45, 46, 51, 59, 60, 61, 62, 68, 182, 228, 240, 288, 293, 305, 381, 387
electrolysis, 51, 59
electrolyte, 31, 32, 59, 67, 68, 301, 533
electromagnetic, 138
electron, 42, 43, 52, 53, 58, 59, 63, 64, 68, 69, 71, 100, 130, 138, 139, 155, 162, 188, 190, 209, 216, 257, 268, 269, 299, 300, 305, 310, 360, 370, 384, 386, 388, 395, 402, 423, 429, 440, 442, 480, 523
electron microscopy, 360, 395, 480, 523
electron pairs, 305
electron paramagnetic resonance, 138
electronic structure, 117, 272, 293
electrons, 61, 63, 64, 68, 69, 101, 129, 137, 138, 143, 209, 298, 299, 300, 306, 383, 429, 442
electroplating, 36, 256
electroreduction, 30, 32
elucidation, 178
emission, 22, 41, 43, 50, 52, 160, 194, 290, 299, 388
emitters, 2, 42, 52, 269
endocrine, 22
endothelial cells, 74
endothermic, 6, 7, 17, 18, 21, 25, 26, 138, 172, 212, 272, 337
energy, x, xii, 2, 4, 10, 11, 14, 16, 17, 20, 21, 27, 31, 43, 44, 51, 61, 63, 69, 114, 115, 116, 137, 138, 139, 141, 159, 161, 190, 195, 224, 227, 228, 231, 234, 237, 249, 255, 268, 270, 276, 298, 299, 305, 319, 333, 336, 337, 363, 368, 370, 372, 378, 379, 396, 422, 423, 467, 480, 533
energy consumption, 20, 27, 31, 224
energy density, 422, 533
energy efficiency, xii, 378
energy input, 190, 231
engineering, 23, 52, 69, 224, 292, 295, 379, 387, 511
England, 317, 395
enlargement, 100, 101, 173, 174, 179, 214
entropy, 17, 21, 336, 366
enzyme, 25
enzymes, 321
EPA, 410, 411, 420
epithelial cells, 71
EPR, 138
equipment, 49, 224, 225, 229, 235, 347, 467, 476, 479

erbium, 150
erythrocytes, 71
ESR, 138
ESR spectra, 138
ester, 187, 219, 220, 380, 389, 391
etching, 266, 345, 519
ethanol, 49, 50, 55, 61, 65, 68, 164, 187, 309, 312, 314, 321, 331, 332, 338, 341, 343, 380, 387, 515, 518, 519
ethers, 2, 24, 36, 137, 209
ethyl acetate, 387
ethyl alcohol, 62
ethylene, 36, 55, 109, 156, 188, 226, 227, 228, 229, 254, 271, 273, 291, 292, 312, 343, 381, 390, 511
ethylene glycol, 343, 381, 390
Europe, 189
European Union, 171, 350, 351, 433
evaporation, 6, 46, 47, 222, 245, 278, 285, 512, 519
evidence, 53, 72, 139, 361, 437, 479, 528
evolution, 140, 141, 147, 158, 209, 215, 278, 398, 401, 444, 448, 449, 455, 465, 507
excitation, 43, 299
exclusion, 380, 533
experimental condition, 171, 185, 212, 218, 230, 348, 351, 444, 496, 501, 503
experimental design, 30, 150
explosives, 25
exposure, viii, 69, 70, 71, 72, 73, 74, 118, 125, 128, 130, 209, 227, 257, 382
extraction, ix, 39, 52, 54, 57, 235, 240, 245, 255, 257, 319, 320, 321, 383, 511, 516
extracts, 211, 265
extruded activated carbon, ix, 239
extrusion, 529

F

fabrication, 68, 317, 423, 507, 511
Fabrication, 49
factories, 250, 320, 321, 338
farmland, 412
fat, 109
fatty acids, 338
feedstock, 46, 269, 326
fermentation, 306, 321, 326
Fermi level, 299
ferrous ion, 33, 165
fertilizers, 21, 25, 250, 260
FFT, 526, 527
fiber, x, xv, 49, 256, 257, 259, 264, 265, 267, 270, 274, 284, 317, 394, 422, 443, 446, 456, 477, 492, 504, 505, 506, 507, 509, 518, 520, 529
fibrosis, 71
field crops, 420
fields of filtration, vii, 1
filament, 49, 50, 67, 74
fillers, 52, 182, 183, 383
film formation, 53
films, xii, 35, 43, 50, 290, 302, 311, 377, 511, 518
filters, 23, 27, 36, 53, 77, 144, 163, 255, 260, 349, 350, 352, 369, 443, 445, 446, 468
filtration, vii, x, 1, 2, 35, 127, 240, 244, 263, 349, 387, 435, 444, 468
financial, 231, 373
financial support, 231, 373
fires, 25
Fischer-Tropsch synthesis, 175, 176, 188, 315
fish, 27, 255
fixation, 176, 178, 185, 438, 439
fixed bed reactors, 262, 460
flame, 241, 242, 413
flexibility, 41, 170, 174, 276
flocculation, 12, 20
flotation, 445
flour, 350
flue gas, 22, 23, 31, 33, 144, 152, 155, 181, 193, 194, 210, 256, 259, 387
fluid, 39, 240, 303
fluid extract, 39
fluidized bed, 37, 40, 49, 65, 210, 290, 447
fluorescence, 138
fluoroquinolones, 444
foams, 54, 195
folic acid, 506
food, 9, 25, 27, 144, 149, 188, 209, 224, 256, 326, 386, 387
food chain, 25
food industry, 144, 188
food products, 144
force, 59, 272, 396, 529
forest fire, 25
forest management, 250
formula, 114, 275, 402, 512
fouling, 18, 446
fractal analysis, 358
fractal dimension, 359
fragments, 358, 360, 361, 362, 371
France, 351
free energy, 16, 17, 21, 139, 336, 337
free radicals, 109, 138, 206, 434, 437, 438, 455, 456, 467
freedom, 337
freshwater, 255
friction, 224
fructose, 144
fruits, 249, 257

FTIR, 137, 141, 308, 330, 337, 338, 341, 342, 439, 440, 530
FTIR spectroscopy, 439
fuel cell, ix, 69, 147, 170, 187, 193, 240, 277, 293, 305, 422, 518, 519, 521, 531, 532
fullerene, 41, 73, 291, 361, 362
functionalization, 53, 59, 72, 174, 180, 185, 442, 468
fusion, 132, 382

G

gas diffusion, 59
gas sensors, x, 51, 297
gasification, 6, 7, 8, 10, 12, 47, 159, 172, 179, 193, 217, 221, 225, 266, 277, 278, 298, 305, 323, 345, 390
gel, 12, 33, 65, 66, 67, 68, 94, 293, 301, 302
gene therapy, 69
geometry, xi, 64, 146, 356, 523, 526
germanium, 302
Germany, 88
glucose, 144, 333, 336, 345, 505
glutathione, 71, 72
glycerol, 187
glycine, 333, 336, 345
glycol, 182, 183, 232, 343, 381, 390
gold nanoparticles, 39
grades, 95, 434, 436
grain size, 118
grants, 373
granular activated carbon, ix, 146, 148, 151, 161, 163, 165, 231, 232, 234, 237, 239, 240, 257, 259, 260, 261, 318, 343, 380, 459, 460, 467, 505, 507
granulated activated carbon (GAC), vii, 1
granules, 30, 159, 162, 251
graphene sheet, 53, 287, 358, 429
greenhouse, 417
groundnut oil, 244
groundwater, x, 22, 240, 420
growth, x, 19, 24, 48, 51, 53, 71, 255, 267, 270, 271, 272, 287, 289, 290, 291, 292, 396, 400, 401, 412, 416, 419
growth mechanism, 272
growth time, 48
Guangzhou, 93
guidelines, 420

H

hair, 41, 242
halogen, 132, 133, 156
halogenation, 158, 387
halogens, 132, 437
hardness, ix, xii, 42, 43, 240, 245, 249, 255, 276, 377, 505
hazardous waste, 28
hazards, 18, 21
HE, 86
health, 18, 21, 22, 25, 28, 36, 69, 72, 338, 411, 414
health effects, 22, 28
health problems, 36
health risks, 25, 69
heat transfer, 192, 224
heating rate, 4, 6, 8, 12, 139, 180, 213, 224, 225, 323, 342, 382, 479
heavy metals, 18, 25, 64, 141, 142, 250, 251, 257, 306, 321, 420
heavy oil, 152, 166
height, 24, 180, 351, 412, 417, 444, 446, 452, 480, 498
helium, 45, 46, 47, 270, 271, 379, 480, 519, 532
hemicellulose, 219, 220, 232
herbicide, 23, 24, 505
heterogeneity, xi, 135, 161, 162, 314, 355, 356, 359, 368
heterogeneous catalysis, 94, 112, 303, 313
heterogeneous catalytic reactions, viii, 112, 169
heterogeneous systems, 16
hexachlorobenzene, 22
hexane, 166, 301, 311, 429
history, 77, 323
homes, 422
homogeneity, 273
HRTEM, xi, 311, 356, 360, 527
human, 12, 18, 21, 27, 41, 58, 69, 70, 73, 74, 350
human body, 18
human health, 69
humidity, 28, 36, 137, 260, 438
hybrid, 18, 28, 35, 59, 61, 64, 65, 66, 67, 68, 69, 519
hydrazine, 144, 166
hydrocarbons, 22, 27, 28, 40, 46, 51, 53, 56, 64, 139, 143, 144, 162, 188, 189, 257, 287, 289, 291, 380, 387, 434
hydrocracking, 166, 304
hydrofluoric acid, 511, 519
hydrogen bonds, 373, 512, 513
hydrogen chloride, 387
hydrogen cyanide, 35
hydrogen peroxide, 58, 59, 130, 132, 143, 153, 157, 165, 167, 174, 187, 192, 195, 288, 300, 304, 316, 434, 436, 438, 455, 456, 457, 460, 463, 465, 466, 468
hydrogenation, xii, 166, 175, 184, 188, 293, 298, 314, 393, 394, 395, 396, 397, 403, 404, 405, 505

hydrolysis, xii, 214, 219, 301, 303, 316, 321, 393, 394, 397, 399, 400, 401, 402, 403, 404, 405
hydrophilicity, 176, 444
hydrophobicity, 24, 170, 176, 207, 209, 310, 372, 510
hydroquinone, 139, 304
hydroxyl groups, 104, 305, 306, 513, 529
hygiene, 70
hysteresis, 134, 224, 275, 284, 425, 520
hysteresis loop, 275, 284, 425, 520

I

ideal, 52, 94, 258, 305, 361
identification, 128, 139, 439, 466
identity, 512
illumination, 65
image, 101, 268, 526
images, 59, 60, 61, 100, 101, 104, 185, 268, 269, 283, 284, 491, 492, 496, 526, 527, 528
immersion, 138, 139, 160, 308, 371, 372, 425
immobilization, 39, 157, 187
immune response, 71
immune system, 21
improvements, 40
impurities, 27, 69, 72, 73, 190, 256, 277, 306, 310, 321, 378, 461
in vitro, 71, 73
incubator, 14
India, 239, 469
indium, 68
Indonesia, 319
induction, 397, 401
induction period, 401
industrial chemicals, 58, 188
industrial sectors, 387
industrial wastes, vii, 127, 250, 262, 263
Industrial wastes, viii, 205
inflammation, 71, 72
inflammatory responses, 72
infrared spectroscopy, 140, 184
infra-red spectroscopy methods, viii, 125
ingestion, 20
ingredients, 523
inhibition, 71, 172
inhibitor, 25, 35, 111, 458
initial state, 404
initiation, 302, 466
injury, iv, 71
inorganic pollutants, viii, 30, 205, 298, 300, 304
insecticide, 25
insertion, 219, 371, 511
insulators, 44, 298, 299
integration, 290, 359, 464, 465
integrity, xiv, 255, 476, 492, 501
interface, 12, 17, 20, 21, 64, 67, 337, 344, 345, 372, 454, 462, 465, 536
internalization, 73
interphase, 65
inversion, 329
investment, 467
iodine, ix, xi, 2, 132, 144, 156, 223, 229, 240, 252, 253, 257, 347, 348, 349, 350, 385
IR spectra, 331, 332, 337, 529
IR spectroscopy, 146, 155, 313
Iran, 1, 75
iridium, 160
iron, 40, 46, 49, 57, 71, 72, 73, 74, 153, 175, 190, 195, 218, 243, 244, 272, 289, 301, 302, 304, 307, 308, 309, 310, 313, 315, 316, 317, 385, 519
irradiation, xi, 40, 41, 47, 48, 64, 65, 67, 68, 69, 229, 234, 235, 236, 237, 299, 347, 348, 349, 350, 351
irrigation, xii, 409, 410
islands, 49
isobutane, 153, 164
isolation, 257, 321
isomerization, 304, 311, 387
isotherms, xiii, 24, 25, 26, 30, 97, 101, 102, 120, 134, 225, 227, 258, 261, 262, 275, 276, 282, 284, 309, 334, 335, 362, 363, 364, 366, 368, 421, 423, 425, 428, 429, 434, 439, 449, 450, 480, 489, 490, 491, 499, 500, 521, 522, 534
isotope, 349, 397
isotropic fibers, xii, 378
issues, 69

J

Japan, 95, 97, 189, 421, 422, 423, 430

K

KBr, 530
keratinocytes, 74
kerosene, xiii, 421, 422, 423, 425, 427, 428, 429, 430
ketones, 2, 187, 304
kidney, 70, 74
kinetic equations, 453, 462
kinetic model, 13, 21, 22, 24, 25, 30, 449, 465, 466, 468
kinetic studies, 13, 30, 31, 33, 262, 263, 391, 453, 460
kinetics, 18, 20, 21, 24, 25, 30, 36, 95, 108, 112, 119, 154, 160, 165, 255, 257, 258, 261, 263, 264, 381, 386, 391, 398, 400, 405, 430, 434, 438, 441, 446,

447, 453, 457, 461, 462, 463, 464, 465, 468, 469, 504
knees, 425
KOH, ix, 7, 9, 10, 12, 150, 151, 152, 161, 215, 216, 217, 223, 227, 228, 230, 232, 234, 235, 237, 239, 248, 250, 253, 257, 266, 277, 278, 279, 282, 283, 284, 285, 286, 287, 294, 295, 345, 388, 391, 503, 507
Korea, 420

L

laminar, 275
landfills, 23, 27, 39, 250
lanthanum, 150
laser ablation, x, 44, 47, 48, 267, 269, 270, 287, 289
lasers, 271
lattice parameters, 526
lattices, 42
leaching, 23, 150, 448, 461, 511
lead, 3, 10, 22, 25, 37, 52, 57, 58, 107, 118, 145, 158, 160, 171, 211, 231, 232, 236, 250, 259, 263, 272, 273, 278, 305, 366, 383, 410, 419, 420, 430, 458, 459, 497, 498, 500
leakage, 29
legislation, 189, 193, 194
Lewis acids, 142
liberation, 241
life cycle, 69
ligand, 95, 154, 314, 401
light, 22, 52, 62, 63, 64, 65, 66, 67, 68, 69, 101, 137, 246, 247, 299, 300, 304, 310, 387, 399, 401, 405, 476
light scattering, 137
light transmittance, 401
lignin, 171, 212, 220, 232, 233, 255, 320, 383
lignite, ix, xi, 127, 150, 151, 209, 239, 240, 258, 259, 297, 377, 378, 380, 436
lignocellulosic materials, ix, xi, 4, 205, 209, 211, 215, 216, 219, 220, 221, 377, 378, 385, 436
linear dependence, 44
liquid crystals, 381
liquid fuels, 142, 422
liquid phase, viii, xi, 27, 94, 96, 125, 128, 132, 133, 141, 143, 153, 167, 180, 195, 240, 250, 252, 261, 293, 301, 333, 356, 380, 383, 387, 390, 396, 434
liquids, 3, 127, 138, 160, 232, 295, 303, 322
lithium, 52
liver, 70, 72
localization, xii, 73, 393
Louisiana, 344
low temperatures, vii, 3, 43, 44, 93, 127, 132, 140, 153, 193, 222, 268, 274, 366
low-cost adsorbents, viii, 205, 233, 234
lubricating oil, 171
luminescence, 461
Luo, v, 83, 86, 90, 91, 93, 161
lymph, 69

M

macromolecules, 538
macrophages, 73
macropores, 2, 30, 126, 132, 171, 183, 207, 248, 254, 255, 384, 435, 438
magnesium, 246, 247, 385, 533
magnet, 55
magnetic composites, 316
magnetic field, 138, 224
magnitude, 190, 192, 404, 484, 532
Maillard reaction, 333
mainstream smoke, 56
majority, ix, 58, 133, 205, 533
man, 477
management, 250, 412
manganese, 154, 195, 232
manipulation, 70
Manju, 257, 264
manufacturing, 25, 26, 69, 187, 210, 256, 391
marketing, 321
marrow, 70
masking, 246
materials science, 2
matrix, 43, 62, 65, 94, 131, 155, 171, 207, 214, 215, 217, 219, 225, 227, 285, 316, 331, 351, 370, 448, 452, 456, 519, 520, 528, 529
matter, iv, ix, 4, 19, 53, 56, 62, 94, 210, 211, 214, 239, 243, 320, 321, 322, 324, 325, 410, 420, 434, 435, 437, 445, 446, 465
measurement, 137, 246, 254, 275, 348, 350, 366, 396, 503
measurements, xi, 2, 43, 44, 68, 71, 139, 185, 235, 308, 348, 356, 365, 384, 397, 399, 400, 405, 427, 443, 479, 480, 506, 533
mechanical properties, 4, 42, 43, 169, 180, 181, 185, 276, 506
media, 27, 54, 97, 144, 164, 170, 300, 306, 315
medical, 69
medicine, 255, 268
melt, 5
melting, xii, 62, 282, 284, 378
membrane permeability, 73
membranes, xii, 18, 53, 150, 257, 265, 288, 344, 377, 380, 384, 389, 390, 392, 511, 519, 521, 532, 533
memory, 352

mercury, ix, 22, 23, 29, 31, 37, 66, 68, 144, 152, 156, 195, 240, 251, 256, 257, 264, 265, 411
Mercury, 23, 38, 266, 311, 312, 431
mesoporosity, xiv, 183, 215, 221, 229, 280, 284, 285, 325, 326, 362, 395, 428, 442, 451, 460, 509, 511, 520
Mesoporous carbons, xii, 378, 381, 384
mesoporous materials, 227, 273, 275, 524, 525, 526, 527
metabolites, 445
meter, 95
methacrylic acid, 150
methanol, 156, 157, 187, 309, 310, 312, 314, 387
methodology, 12, 266, 395, 516
methyl group, 382, 430
methyl methacrylate, 381
methylene blue, ix, 2, 34, 55, 62, 66, 67, 68, 195, 226, 227, 228, 229, 233, 234, 235, 236, 240, 244, 254, 256, 259, 262, 263, 265, 304, 307, 316, 385, 386, 391
Mexico, 347, 351, 509
mice, 71, 72
microcrystalline, 206, 208
microgravity, 84
micronucleus, 71
microorganism, 445
microorganisms, 1, 27, 443
microporous materials, 135, 489
microscope, 97, 100, 423, 443
microscopy, xiv, 59, 268, 396, 405, 475, 523
microspheres, 54, 392
microstructure, 158, 208, 230, 439, 505
microtome, 528
microwave heating, 11, 147, 225, 228, 229, 234, 235, 236, 237
microwave radiation, 11, 227, 235, 237, 263
microwaves, 40, 224, 225, 226, 227, 229, 231, 238
migration, 176, 224, 394
military, 252
milligrams, 244, 253, 385
mineralization, 37, 62, 94, 95, 118, 444, 447, 455, 465, 466
missions, 191
mixing, 20, 27, 34, 66, 180, 244, 278, 303, 333
MMA, 147, 154, 155, 157, 158
MOCVD, 302, 317
model system, 336, 345
modelling, 164, 265, 449, 451
models, vii, xi, 13, 14, 16, 21, 24, 30, 36, 159, 355, 361, 362, 363, 364, 365, 366, 367, 368, 369, 370, 373, 379, 420, 466, 468, 504
modern society, 250
modifications, ix, xiv, 133, 137, 147, 153, 154, 158, 180, 190, 206, 230, 288, 371, 475, 483, 484, 485, 500, 501, 502
modulus, 42, 43, 150, 185, 276, 478
moisture, 36, 41, 161, 241, 242, 245, 256, 322, 396
moisture content, 41, 241, 242, 322
molar ratios, 302, 525
molasses, ix, 2, 240, 253, 344
mold, 511
molds, 64
mole, 405, 529
molecular dynamics, 160, 291
molecular mass, 423
molecular oxygen, 63, 65, 209, 212
Molecular sieving carbon (MSC), xii, 377
molecular structure, 379, 436
molecular weight, 17, 54, 327, 333, 336, 382, 443, 446, 466, 468, 512
molecular weight distribution, 446
molybdenum, 175, 176, 314
monolayer, 14, 16, 333, 334, 368
monomers, xii, 378
mordenite, 186
morphology, vii, xv, 93, 104, 218, 270, 273, 274, 290, 291, 480, 492, 504, 509, 511, 518, 519, 526, 528
mortality, 74
multiwalled carbon nanotubes, 292
museums, 252
myopathy, 350

N

Na^+, 533
Na2SO4, 60, 68
NaCl, 22, 32, 136, 452, 459, 533
nanocomposites, 68, 277, 288, 317
nanocrystals, 67
nanodots, 290
nanoelectronics, 277
nanofibers, x, 45, 46, 48, 49, 164, 267, 268, 269, 270, 271, 272, 274, 275, 276, 277, 285, 287, 288, 289, 290, 291, 292, 293, 294, 295, 388
nanoindentation, 43
nanomaterials, 42, 65, 66, 68, 69, 70, 268, 270, 288
nanomedicine, 69
nanometer, 54, 69, 150, 394
nanometers, 41, 42
nanoparticles, 38, 39, 46, 50, 54, 56, 57, 67, 68, 74, 187, 271, 272, 288, 315, 317, 381, 384, 390, 521, 532
nanorods, 66, 67
nanostructured materials, 384

nanostructures, x, 42, 267, 269, 270, 271, 272, 284, 287, 292, 295, 316, 388
Nanostructures, 392, 469
nanotechnology, xii, 90, 289, 378
nanotube, 42, 44, 48, 51, 52, 53, 67, 268, 289, 290, 292, 293
nanowires, 511, 518, 519
NaOH catalyst, 187
naphthalene, 40, 56, 503
natural gas, 193, 305, 387
Nd, 48
necrosis, 70, 73
negative effects, 257
neglect, 370
nervous system, 69
Netherlands, 237, 317, 352
network polymers, 379
neural network, 22, 449
neuroblastoma, 74
neurons, 22
neutral, 26, 55, 59, 130, 133, 176, 189, 223, 304, 401, 442, 478
neutron activation analysis, xi, 347, 349, 350, 352
neutrons, 348
neutrophils, 72
New York, iv
NH2, 138
nickel, vii, 36, 44, 46, 49, 52, 57, 93, 95, 99, 103, 119, 120, 121, 186, 251, 271, 272, 273, 289, 290, 291, 292, 314, 411, 420, 503, 533
nickel oxide-loaded activated carbon (NiO/AC), vii, 93
nicotine, 56, 445
nitrates, 21, 99, 184, 301
nitric oxide, 133, 152, 174, 385
nitrification, 194, 443
nitrifying bacteria, 443
nitrite, 21, 165, 503
nitrobenzene, 29, 166, 246, 293, 394, 453
nitrous oxide, 133, 174
NMR, xii, 138, 160, 223, 236, 289, 393, 395, 397, 398, 399, 400, 401, 405, 529, 530
noble gases, 364, 365
noble metals, 188, 195, 257
nonionic surfactants, 39, 512
non-polar, 104, 208, 255, 366, 434, 439
North America, 253
novel materials, 388
Nuclear Magnetic Resonance, 138
nucleation, 396, 400
nuclei, 138, 396
nucleus, 73
nuisance, 268
nutrient, 40, 70, 414
nutrients, 39, 412

O

obstacles, 142
OH, 26, 49, 58, 61, 63, 65, 84, 136, 165, 187, 252, 282, 283, 300, 302, 337, 385, 398, 400, 401, 405, 529
oil, 4, 5, 12, 25, 39, 40, 55, 68, 148, 149, 152, 166, 171, 190, 226, 234, 244, 245, 249, 250, 260, 262, 304, 305, 321, 322, 338, 339, 340, 341, 342, 343, 344, 352, 383, 391, 412, 419, 422
oil samples, 412
oilseed, 149
olefins, 154, 157, 304, 437
oligomerization, 401, 405
operations, x, 240, 262, 387, 444
opportunities, 107, 289
optical activity, 68
optical density, 399
optical properties, 42, 43, 69
optimization, 178, 262, 266, 271, 379, 477, 507
ores, 30, 378
organ, 49, 70, 72, 511
organic chemicals, 186, 434
organic compounds, x, 20, 22, 23, 26, 57, 58, 63, 65, 109, 137, 141, 142, 143, 144, 148, 163, 193, 209, 217, 232, 236, 240, 250, 251, 256, 304, 308, 316, 320, 321, 343, 387, 390, 434, 438, 439, 443, 446, 456, 457, 503, 504, 506, 507
organic matter, 19, 53, 56, 63, 94, 214, 410, 412, 420, 434, 445, 465
organic solvents, 94, 293
organism, 1
organs, 72
originality, 380
osmosis, 446
overlap, 272, 298, 428, 429
ox, 136, 154, 208, 209, 218, 221, 284, 356, 361, 371, 443, 456
oxalate, 119, 120
oxidability, 109

P

paints, 18, 20
palladium, 49, 152, 154, 188, 394, 533
palm oil, 148
PAN, 288, 477, 507, 513, 517
parallel, x, 42, 99, 134, 267, 270, 274, 284, 358, 382, 394, 429, 444, 454, 464, 498

participants, 63
particle morphology, 290
pasteurization, 232
patents, 127, 145, 240
pathogens, 53
pathways, 207, 430, 449, 450
PCA, 177, 180, 181
PCBs, 22, 257
PCP, 40
peat, ix, xi, 26, 171, 209, 239, 240, 259, 297, 377, 378
peptides, 207
periodicity, 528
peripheral nervous system, 69
permeability, 73, 532
permeation, 344, 380, 532
permission, 3, 6, 11, 19, 28, 45, 47, 51, 60, 61, 70, 275, 280, 281, 282, 283, 357, 359, 518, 520, 521, 522, 524, 525, 526, 527, 528, 530, 531, 534
permit, 53
peroxide, 58, 59, 130, 133, 142, 143, 153, 157, 165, 167, 173, 174, 187, 192, 195, 288, 300, 304, 315, 316, 434, 435, 436, 438, 455, 456, 457, 460, 463, 466, 468, 469
personal care products (PPCPs), xiii, 58, 433
Perth, 355
PES, 18
pesticide, 20, 262, 265
PET, 35, 250
petroleum, 9, 33, 95, 171, 177, 180, 181, 185, 189, 228, 256, 387, 450, 511
Petroleum, 9, 189, 448
petroleum distillates, 189
pharmaceutical, xiii, 9, 187, 188, 209, 386, 387, 433, 444, 447, 455, 456, 459
pharmaceuticals, 24, 26, 58, 144, 187, 232, 256, 444
phase diagram, 516
phase transitions, 43
Philadelphia, 314
phonons, 44
phosphate, 9, 25, 219, 220, 221, 223
phosphates, 219, 220
phosphorous, viii, 125, 129, 224, 437
phosphorus, 131, 135, 155, 156, 222, 236, 485, 486, 488
photocatalysis, vii, 1, 62, 63, 299, 302, 303, 313
photocatalysts, 35, 63, 64, 65
photocatalytic degradation, x, 28, 35, 37, 58, 65, 67, 297, 306, 313, 318
photodegradation, 64, 317
photoelectron spectroscopy, viii, 125, 137, 184
photolithography, 21
photoluminescence, 43
photons, 63, 299
photosynthesis, 22
physical characteristics, ix, 211, 239, 251
physical interaction, 434
physical properties, 287, 321, 322, 436
physical structure, 70, 258, 384
physicochemical properties, 221, 237, 483
physics, xi, 44, 278, 355, 537
pinus, 264
pitch, xii, 33, 153, 164, 180, 250, 259, 263, 266, 377, 380, 477, 511
pith, 249, 258, 260, 263, 264
plants, xiii, 1, 20, 24, 27, 53, 58, 144, 149, 193, 250, 256, 410, 414, 415, 416, 417, 419, 420, 433, 467
plasma membrane, 73
plastics, xi, 2, 251, 257, 377, 378, 410
platelets, 132
platform, 118, 120
platinum, xii, 46, 68, 156, 175, 305, 381, 384, 390, 393, 394, 396, 397, 398, 400, 402, 403, 404, 405, 507, 532, 533
Platinum, vi, 68, 393, 395, 532
PM, 77, 78, 79, 84, 85, 86, 91, 147, 164, 165
poison, 25
Poland, 355, 373
polar, 31, 104, 120, 139, 142, 208, 224, 255, 366, 372, 434, 439, 466, 468, 488
polarity, 160, 170, 331, 332, 366
polarization, 31, 32, 488
polyimides, 477
polynuclear complexes, 398
polyphosphates, 219, 220
polypropylene, 59, 512
polysaccharide, 327
polystyrene, xv, 159, 384, 509, 517
polyurethane, 54, 262
polyurethane foam, 54
polyvinyl alcohol, 18, 43, 46, 67, 195
polyvinyl chloride, 250, 260
population, 40
pore size distribution (PSD), xi, 355
porous materials, 40, 125, 161
Portugal, 125, 146, 147, 154
positive correlation, 107, 108
potassium, 57, 127, 132, 147, 148, 152, 172, 215, 216, 217, 237, 323, 382, 384
powdered activated carbon (PAC), vii, 1, 240
power plants, 193, 256
precipitation, 119, 121, 272, 302, 394
preservation, 39
preservative, 35
pressure gradient, 137
prevention, 53, 222

principles, 232, 317
probability, 120, 337, 404
probe, 139
producers, 231, 321
proliferation, 74
promoter, 46, 192, 195, 387, 458, 466, 468
propagation, 181
propane, 164
propylene, 56, 511
protection, xii, 35, 36, 53, 252, 280, 378, 420
proteins, 207
protons, 39, 401
PTFE, 58, 59, 60, 61, 62
public health, 411
pulp, xi, xiii, 25, 71, 212, 261, 319, 321, 345, 377, 378, 459, 461, 475, 477
pulse discharge, 453, 460
purification, ix, xi, 12, 13, 47, 53, 69, 95, 127, 141, 144, 149, 209, 240, 252, 255, 256, 259, 260, 265, 266, 270, 291, 292, 304, 305, 306, 313, 314, 322, 347, 379, 387, 467, 477, 503, 510
purity, 44, 45, 46, 47, 49, 65, 72, 74, 190, 212, 302, 305, 328, 350, 352
PVA, 18, 19, 43, 195, 507
PVC, 250

Q

quality control, 77
quanta, 63
quantification, 128, 445
quantization, 44
quantum yields, 447
quartz, 49, 519
quinone, 130, 137, 139, 143, 144, 173, 189, 435, 437
quinones, 130, 138, 177, 209

R

radiation, 9, 11, 66, 97, 138, 192, 227, 235, 237, 263, 299, 300, 302, 399, 434, 444, 447, 453, 461, 469
radical mechanism, 307
radical reactions, 455, 460, 465, 468
radical structures, 383
radicals, vii, 19, 58, 59, 63, 65, 93, 109, 138, 165, 195, 206, 286, 300, 434, 437, 438, 451, 455, 456, 457, 458, 459, 460, 462, 463, 464, 465, 466, 467
radio, 48, 49, 50
radioisotope, 349
radius, 301, 307, 358, 359, 361, 480, 496, 499, 500, 501
Raman spectra, 531
Raman spectroscopy, 43, 531
ramp, 517, 518, 519
rape, 255
rape seed, 255
raw materials, ix, xi, 68, 150, 171, 172, 180, 187, 210, 222, 224, 227, 239, 247, 249, 250, 251, 255, 377, 378, 380, 381, 384, 423
reactant, 47, 175, 180, 190, 192, 224
reactants, 94, 112, 115, 175, 181
reaction mechanism, viii, 94, 95, 110, 112, 117, 169, 178, 187, 293, 438
reactive oxygen, 74
reactive sites, 133
reactivity, ix, 53, 94, 109, 116, 120, 132, 171, 179, 239, 240, 253, 435, 437, 438, 443
reading, 388
reagents, xv, 58, 59, 95, 131, 282, 348, 349, 405, 509
reality, 373, 511
recall, 212
reception, 3, 101
recombination, 69, 299
recommendations, iv
recovery, 9, 27, 39, 62, 72, 240, 262, 304, 386, 387, 446, 467, 477
recovery process, 62, 446
recovery processes, 62, 446
recycling, 94, 250, 460
red mud, 262
refractory organic pollutants, vii, 93
regenerate, viii, 28, 40, 205, 228, 467
regression, 14, 72
regrowth, 445
regulations, 144
reinforcement, x, 43, 185, 267, 268, 287
relevance, 250, 484, 489
remediation, vii, x, xiii, 1, 2, 12, 17, 30, 34, 39, 40, 53, 58, 63, 158, 240, 381, 409, 411, 469, 471
reparation, 148, 149, 150, 152, 233, 263, 379, 448
requirements, 127, 179, 270, 322
research facilities, 230
researchers, xiv, 12, 20, 22, 24, 27, 28, 30, 32, 37, 40, 59, 65, 94, 95, 217, 231, 258, 366, 380, 416, 467, 509, 511, 512, 523
residuals, 301
residues, ix, 69, 146, 206, 210, 222, 224, 225, 230, 234, 249, 250, 259, 260, 261, 263, 266, 345, 379, 503, 528
resins, viii, xi, xv, 20, 183, 205, 227, 228, 262, 327, 343, 377, 378, 380, 381, 382, 384, 390, 392, 509, 512, 513, 519, 529
resistance, 19, 27, 55, 176, 180, 181, 184, 190, 255, 272, 276, 298, 361, 394, 438, 460, 465, 476, 478, 533

resols, 164
resolution, 141, 160, 360, 363, 529
resorcinol, xv, 57, 304, 509, 511, 513, 520, 528, 529
resources, 152
response, 12, 59, 71, 72, 73, 74, 178, 266, 445
restrictions, 94, 532
retention volume, 139
reusability, 154
rice husk, xiii, 149, 150, 256, 258, 260, 261, 263, 264, 339, 344, 383, 421, 422, 424
rice husk activated carbon (RHAC), xiii, 421
rights, iv
rings, 257, 358, 371, 382, 429, 454
risk, 347, 411, 420
risk assessment, 411
risks, 25, 69
rods, 44, 48, 270, 271, 511
Romanus, 82
room temperature, 24, 25, 44, 48, 55, 60, 65, 67, 68, 97, 130, 136, 184, 243, 245, 277, 301, 303, 306, 323, 337, 400, 439, 479, 518
root, 410, 412, 413, 416
roots, 410, 414, 416, 418
roughness, 100
routes, 70, 438, 456
rubber, 3, 27, 265, 383, 391
Russia, 393, 395
ruthenium, 36, 38, 183, 190, 531, 533
rutile, 66, 67, 299, 300, 304, 453

S

safety, 27, 511
salinity, 26
salts, 21, 49, 51, 94, 144, 159, 167, 184, 218, 248, 301, 304, 338, 511
saturation, 16, 48, 273, 303, 366, 395, 489
savings, 228
sawdust, 3, 146, 209, 230, 234, 258, 260, 262, 264, 383
scanning electron microscopy, 480, 523
scanning electronic microscope, 97
scattering, 101, 137, 405, 523
scavengers, 458, 459, 466
science, 2, 34, 345, 373, 536
scope, 206, 379, 400
security, 53, 94
sedimentation, 127
sediments, 18, 257
seed, 228, 236, 249, 262, 266, 383, 391
segregation, 272
selectivity, viii, xiii, 24, 94, 109, 118, 154, 169, 177, 184, 187, 188, 189, 190, 194, 207, 210, 257, 270, 315, 379, 387, 394, 405, 421, 430, 532
selenium, xi, 347, 348, 349, 350
self-assembly, xiv, 509, 512, 513, 519, 520
SEM micrographs, 385, 491, 492, 493, 495
semiconductor, x, 62, 63, 65, 68, 276, 297, 298, 299, 300, 301, 302, 303, 306, 307, 313, 350, 351
semiconductors, 63, 138, 298, 299
sensitivity, 52, 68, 137, 327, 347, 352, 400
sensors, x, 52, 297, 532
serum, 72, 73, 74, 350
services, iv
sewage, 144, 250, 255, 260, 384, 444
shade, 101
shape, xii, 127, 134, 169, 175, 179, 180, 207, 224, 279, 351, 362, 378, 380, 386, 394, 460
shear, 42, 529
shear deformation, 43
shock, 27, 181, 185
shoot, 412, 413, 414, 416, 417
shoots, 414, 416, 417, 418
showing, 14, 126, 132, 143, 365, 370, 479
shrimp, 350
side effects, vii, 1
signals, 397, 529
signs, 299
silica, xiv, 12, 33, 54, 94, 155, 170, 175, 178, 192, 225, 298, 428, 430, 451, 509, 511, 512, 519, 523
silicon, 49, 50, 150, 182, 273, 302, 385
silk, 258, 260
silver, 36, 246, 252
simulation, xi, 160, 356, 357, 358, 361, 362, 363, 364, 365, 368, 370, 371, 506
simulations, xi, 355, 359, 360, 361, 362, 363, 364, 368, 370, 372, 373, 506
single walled carbon nanotubes, 392
sintering, 175, 176, 276
SiO2, 39, 192, 302
skeleton, 9, 10, 217, 249, 367, 384, 512
skin, 20
slag, 262
sludge, 27, 250, 384, 416, 507
smog, 194
smooth muscle, 71
smooth muscle cells, 71
soccer, 127
society, 250
sodium, 23, 24, 32, 36, 54, 55, 56, 57, 67, 68, 72, 96, 127, 132, 135, 150, 162, 165, 174, 215, 216, 246, 247, 301, 331, 333, 382, 385, 461, 479, 533
sodium hydroxide, 32, 36, 127, 135, 150, 215, 247, 331, 382, 479

software, 423
Soil and Groundwater Pollution Remediation Act (SGWPR Act), xiii, 409, 410
Soil Control Standard (SCS), xiii, 409, 410
soil pollution, 420
sol-gel, 66, 301, 302
solid matrix, 227
solid phase, 54, 64, 257, 333
solid state, 160, 222, 529
solid surfaces, 141
solid waste, x, 250, 264, 319
solidification, 53, 182
solubility, 61, 94, 272, 301, 436, 438
solvent molecules, 370
solvents, 94, 207, 224, 260, 293, 303, 344, 386, 387, 466
sorption, xi, 16, 25, 52, 53, 232, 236, 258, 262, 263, 347, 367, 389, 391, 522, 532
sorption kinetics, 258
sorption process, 25
South Africa, 232
sowing, 414
Soxhlet extractor, 395
soybeans, 418
Spain, 145, 169, 201, 265, 267, 297, 433, 468, 534
spectrophotometry, 31, 479
spectroscopic techniques, 405
spectroscopy, viii, 2, 43, 125, 135, 137, 138, 140, 146, 155, 160, 184, 307, 308, 309, 313, 397, 399, 405, 439, 531
spin, 49, 138, 383, 518, 529
spleen, 69, 71, 72
spontaneity, 337
stability, ix, 18, 21, 33, 39, 42, 52, 59, 63, 64, 68, 94, 95, 118, 119, 130, 132, 147, 154, 169, 179, 209, 239, 304, 315, 382, 510
stabilization, 211, 461
stack gas, 194
standard deviation, 350
standard error, 486
starch, 321
state, viii, 61, 62, 94, 160, 169, 171, 177, 190, 211, 221, 298, 299, 305, 321, 379, 381, 396, 402, 404, 436, 446, 460, 466, 529, 530, 531
states, 43, 138, 298, 299
statistics, xi, 356
steel, 42, 49, 245, 276, 323, 342, 412, 478
stoichiometry, 516, 523
storage, ix, x, xii, 2, 29, 52, 55, 69, 148, 161, 237, 240, 259, 267, 268, 276, 277, 285, 287, 288, 293, 294, 378, 387, 422, 477, 504, 507
stress, 43, 70, 72, 73, 74, 185
stretching, 137, 529
strong interaction, 52, 188, 272, 285, 306
strontium, 54, 148
styrene, 57, 163, 164, 188, 382
subsistence, 58
substitutes, 250
substitution, 132, 400, 401, 405, 430, 434
substitution reaction, 400, 434
substitutions, 163
substrate, xii, 35, 48, 49, 50, 62, 181, 183, 271, 290, 302, 384, 393, 396, 402, 404, 518
substrates, 49, 63, 261, 304, 394, 396
sucrose, 183, 326, 327, 329, 366, 511
sugar beet, 218, 236, 344, 345, 383
sugar industry, 127, 319, 320, 379
sugar mills, 321
sugarcane, 320, 321, 327, 338, 343, 344, 345
sulfate, 33, 55, 67, 68, 95, 165
sulfonamide, 455
sulfur, viii, xiii, 27, 31, 36, 38, 125, 129, 131, 133, 135, 142, 143, 144, 156, 162, 166, 266, 378, 382, 389, 421, 423, 430, 437, 479
sulfur dioxide, 142, 389
sulfuric acid, 57, 132, 217, 516
sulphur, 163, 170, 175, 179, 184, 189, 193, 256, 306, 383, 387
Sun, 75, 80, 82, 83, 86, 88, 89, 149, 161, 162, 166, 199, 223, 234, 237, 288, 289, 291, 416, 420, 431, 471, 473, 535
superconductivity, 43
surfactant, 21, 23, 39, 54, 57, 66, 73, 80, 264, 461, 511, 512, 513, 515, 516, 518, 523, 525, 528, 529
surfactants, 29, 39, 56, 64, 447, 512, 513, 529
susceptibility, 309
suspensions, 73, 74
sustainability, 191
swelling, 214
SWNTs, 291, 388
symmetry, 516, 525, 531
synergistic effect, 37, 120, 298

T

Taiwan, xii, 23, 75, 77, 147, 317, 409, 410, 411, 412, 416, 419, 420
tanks, 29, 144, 255
tannins, 254
tar, 10, 56, 151, 180, 263, 323
target, 48, 64, 70, 74, 207, 348, 349, 397, 411, 413, 414
techniques, viii, x, xiii, 2, 40, 44, 47, 58, 61, 94, 100, 125, 134, 135, 137, 138, 139, 145, 154, 160, 173, 178, 184, 228, 262, 267, 269, 301, 305, 373, 379, 385, 405, 409, 411, 412, 439, 443, 520

technologies, xiii, 184, 433, 469
technology, viii, x, xiv, 11, 23, 34, 39, 69, 94, 109, 144, 145, 205, 228, 231, 240, 256, 273, 305, 321, 433, 509, 510, 531
tensile strength, 276
tension, 301, 303, 458
test data, 114
testing, 43, 110, 161, 241
tetrahydrofuran, 515
textiles, 26, 477, 479, 502
textural character, 134
textural effects, 143
texture, x, 100, 145, 156, 171, 211, 221, 248, 249, 268, 277, 295, 307, 308, 394, 410, 412, 417, 519, 520
TGA, 321, 323, 423, 479
Thailand, 319
therapy, 69
thermosetting resins, xii, 377, 379, 380, 512
thin films, 43, 290
thorium, 146
tin, 68, 301, 305, 306, 314
tin oxide, 68
tissue, 69, 321
titanate, 50, 54
titania, 178, 304
titanium, 54, 66, 67, 301, 302, 304, 313, 318
titanium isopropoxide, 67
tobacco, 228, 235, 263
tocopherols, 338
toluene, 26, 28, 29, 33, 46, 56, 57, 66, 160, 161, 184, 312, 381, 386, 387
total revenue, 268
toxic effect, 71
toxic gases, 209, 387
toxic metals, xiv, 476, 504
toxic substances, 252
toxicity, 9, 20, 21, 26, 42, 58, 63, 69, 72, 73, 74, 445, 448, 450, 461
trace elements, xi, 135, 347, 420
traits, 34
transformation, 165, 193, 302, 394, 423
transformations, 63, 398, 507
transistor, 277
transition metal, 48, 50, 177, 188, 189, 190, 195, 272, 288, 310, 315
translocation, 416
transmission, 137, 268, 360, 395, 397, 399, 405, 523
transmission electron microscopy, 360, 395, 523
transport, 43, 69, 207, 303, 350, 410, 532
transportation, xiii, 420, 421, 422, 430
trypsin, 293
tungsten, 45, 301, 302, 304, 311, 312, 314, 315, 317
tungsten carbide, 305, 311
tunneling, 43
turbulence, 99
turnover, 192, 411, 412

U

uniform, xii, 11, 14, 49, 50, 172, 176, 177, 182, 183, 188, 224, 275, 290, 309, 377, 378, 381, 384, 402
universal gas constant, 16, 17, 336
uranium, 146
urban, 40, 58, 144, 448
urea, 49, 67, 131, 133, 143, 164, 184
urine, 350
uterine cancer, 350

V

vacuum, 148, 230, 234, 235, 244, 256, 303, 349, 383, 395, 480
valence, 63, 64, 68, 299, 300
vanadium, 179, 180, 181, 183, 195
vapor, x, 37, 44, 48, 65, 66, 154, 156, 162, 163, 216, 230, 240, 252, 254, 255, 267, 269, 270, 271, 272, 286, 288, 290, 291, 292, 295, 313, 317
vapor-liquid-solid, 272
variables, x, xiii, 4, 6, 8, 10, 12, 48, 146, 268, 279, 438, 446, 456, 457, 461, 464, 475, 477, 484, 501, 502
variations, 62, 212, 224, 348, 350, 494, 500, 528
varieties, 51, 412, 512, 526
vegetable oil, 40, 188, 320, 321, 326, 338, 343, 345
vegetables, 257, 412, 416, 418, 420
vegetation, 258, 420
vehicles, 29, 388, 533
velocity, 480
ventilation, 144
vibration, 185
vinyl chloride, 380, 381, 387
vinylidene chloride, 380, 381
Virtual Porous Carbon (VPC) models, vii, xi, 355
viruses, 64
viscose, 155, 193, 478, 503, 504
viscosity, 183
vitamin B1, 350, 506
vitamin B12, 350
volatile organic compounds, x, 57, 141, 142, 144, 148, 193, 209, 217, 236, 240, 250, 256, 304, 308, 503, 504, 506, 507
volatilization, 214, 216, 222, 382

W

Washington, 88
wave number, 331
wavelengths, 192, 330, 399
weak interaction, 285
web, 44, 50, 77, 386
weight loss, 185, 212, 217, 382, 481, 482
weight ratio, 67, 526
Western Australia, 355
wetness impregnation method, vii, 93, 97
white oak, 153, 219, 234, 504
wide band gap, 299
wires, 43, 52, 292, 388
withdrawal, 190
witnesses, 397, 405
wood, ix, xiii, 3, 4, 5, 9, 25, 35, 40, 127, 145, 148, 150, 159, 166, 172, 209, 212, 219, 221, 228, 229, 237, 239, 240, 247, 249, 250, 258, 259, 260, 266, 297, 321, 423, 436, 475, 477, 503, 504
wood waste, 150
wool, 22
workers, 35, 137, 171, 172, 175, 176, 178, 179, 180, 182, 183, 186, 187, 188, 189, 190, 191, 192, 195, 225, 229, 240
working conditions, 48, 351
World War I, 379
worldwide, x, 267

X

xenon, 66, 67

Y

yarn, 478
yttrium, 48, 271

Z

zeolites, 12, 33, 40, 170, 225, 270, 273, 292, 512
zinc, xiii, 56, 57, 127, 146, 148, 149, 163, 172, 217, 218, 230, 232, 234, 235, 248, 266, 301, 302, 306, 310, 316, 317, 318, 323, 382, 409, 410, 420, 436, 479, 488
zinc oxide, 301, 302, 316, 318
ZnO, x, 38, 63, 67, 68, 297, 298, 299, 300, 303, 306, 310, 313, 317, 318
zooplankton, 21